THE 6th INDONESIA INTERNATIONAL

GEOTHERMAL

CONVENTION & EXHIBITION 2018

6 - 8 SEPTEMBER 2018

JAKARTA CONVENTION CENTER

EMPOWERING GEOTHERMAL FOR INDONESIA'S ENERGY SUSTAINABILITY

PROCEEDING BOOK

Hosted by

Indonesian Geothermal Association

Supported by

Organized by

EMPOWERING GEOTHERMAL FOR INDONESIA'S ENERGY SUSTAINABILITY

Proceeding

The 6th Indonesia International Geothermal Convention & Exhibition (IIGCE) 2018

6 - 8 September 2018, Cendrawasih Hall - Jakarta Convention Center

Editor:

Abadi Poernomo
Aquardi Suminar
Suryantini
Lestari Apriani
Doddy Astra
Milki Fabian Moningka

Reviewer:

Ali Ashat
Aquardi Suminar
A. Fanani Akbar
Boyke Bratakusuma
Doddy Astra
Hendra Yu Tonsa
Hilman
Imam Baru Rahardjo
Khasani
Novi Ganefianto
Ruly Husni
Suryantini
Uum Komarudin
Yodha Nusiaputra
Yunus Daud

Indonesian Geothermal Association

2019

EMPOWERING GEOTHERMAL FOR INDONESIA'S ENERGY SUSTAINABILITY

6 - 8 September 2018, Cendrawasih Hall - Jakarta Convention Center

COMMITTEE

ADVISOR
Rida Mulyana

STEERING COMMITTEE
Ida Nuryatin Finahari
Riki F. Ibrahim
Tohari Hadiat
Prijandaru Effendi
Abadi Poernomo
Sanusi Satar
Tafif Azimudin
Paul Mustakim
Ahmad Yuniarto
Ali Mundakir
Heribertus Dwiyudha
Eka Satria
Ronny Hendrawan

CHAIRMAN
M. Ikbal Nur

VICE CHAIRMAN
Yudistian Yunis

SECRETARIAT
Endang I
Sudarwo
Andry Susanto
Rachma Nilamsuri
Vanny Widiana
Hera Fitria Zein

TREASURY
Nisriyanto
M. Ikbal Nur

MARKETING & FUND RAISING
Mukawi Djumadin
Idham
Zaldy
Win Sukardi
Manthovani
Rully Subakat

PUBLICATION/ OPENING CLOSING
Ifnaldi Sikumbang
Gladis Gladis Sondakh
Siska Tan
Muhammad Faradhy
Leila Rima
Esti Hayati

TECHNICAL PAPER
Doddy Astra
Uum Kamarudin
Imam B. Raharjo
Ali Ashat
Suryantini
Khasani
Boyke Bratakusuma
Aquardi Suminar
Yunus Daud
Hendra Yu Tonsa
Yodha Nusiaputra
Ruly Husni
A. Fanani Akbar
Nofi Ganefianto
Hilman

PROTOCOL & GOVERNMENT RELATION
Ismoyo Argo
Agdya Pratami Putri
Rangga Wirapasa
Fachry Singka
Reza Arsyad
Sentot Yulianugroho
Syahrini
Zulhendri
Wisnu Subroto
Murdiono
Irfansyah Alam
Arga Surawidjaja

CONVENTION & PRE-CONFERENCE WORKSHOP
Amin Hartoni
Intan
Toni Widiatmoko
Novianto
Supremelehaq Taqwin
Jene Lokasthiti Az

PHOTO COMPETITION
Yulnofrins
Noor Faiz
Agus Suprianto
Syaiful Hidayat

FIELD TRIP
Istiawan
Randy
Puguh

SPEAKERS

- ***Sri Mulyani Indrawati***, *Minister of Finance of the Republic of Indonesia*
- ***HE Trevor Matheson***, *New Zealand's Ambassador to Indonesia*
- ***Rida Mulyana***, *Director General of New Renewable Energy and Energy Conservation. Represented by* ***Ida Nuryatin Finahari*** *(Director of Geothermal)*
- ***Sigit Hardwinarto***, *Director General of Forestry and Environmental Planning*
- ***Ali Mundakir***, *President Director PT Pertamina Geothermal Energy*
- ***Qomaruzzaman***, *Marketing Director PT Rekayasa Industri*
- ***Alexander Richter***, *President of IGA*
- ***Ann Robertson-Tait***, *Senior Geologist and Business Development Manager, GeothermEx, Inc.*
- ***Greg Ussher***, *Jacobs Engineering*
- ***Dennis Preston***, *Aecom Ltd.*
- ***Hardiv Situmeang***, *Member of Indonesia National Research Council (DRN)*
- ***Yuichiro Yoi***, *Unit Head for Indonesia,Infrastructure Finance Division 2, Private Sector Operations Department, Asian Development Bank*
- ***Peter Johansen***, *Senior Energy Specialist/ Task Team Leader World Bank*
- ***Agus Subagyo***, *Pemda Wonosobo*
- ***Arie Sujito***, *UGM*
- ***Heru Prasetyo***, *School of Business Management ITB*

Published by:
Asosiasi Panasbumi Indonesia (API)
2019

ISBN 978-602-52132-1-2

Sanksi Pelanggaran Pasal 72 Undang-Undang Nomor 19 Tahun 2002 Tentang HAK CIPTA

1. Barangsiapa dengan sengaja dan tanpa hak melakukan perbuatan sebagaimana dimaksud dalam Pasal 2 ayat (1) atau Pasal 49 ayat (1) dan ayat (2) dipidana dengan pidana penjara masing-masing paling singkat 1 (satu) bulan dan/atau denda paling sedikit Rp. 1.000.000,00 (satu juta rupiah), atau pidana penjara paling lama 7 (tujuh) tahun dan/atau denda paling banyak Rp. 5.000.000.000,00 (lima miliar rupiah).
2. Barangsiapa dengan sengaja menyiarkan, memamerkan, mengedarkan, atau menjual kepada umum suatu Ciptaan atau barang hasil pelanggaran Hak Cipta atau Hak Terkait sebagaimana dimaksud pada ayat (1) dipidana dengan pidana penjara paling lama 5 (lima) tahun dan/atau denda paling banyak Rp. 500.000.000,00 (lima ratus juta rupiah).

FOREWORD

To advance knowledge and capacity of its geothermal community, Indonesian Geothermal Association (INAGA) conducted the 18th Annual Scientific Gathering (PIT - Pertemuan Ilmiah Tahunan) in conjunction with the Annual Indonesian International Geothermal Convention & Exhibition (IIGCE) 2018.

The 6th IIGCE 2018 was held successfully on September 6th - 8th, 2018 at the Jakarta Convention Center and attended by more than 1000 people around the globe. The 6th IIGCE 2018 is a continuous success of the annual events that have been held since 2013.

This year, the Committee of PIT as part of the 6th IIGCE event, has received 206 abstracts and 167 papers with various topics focusing on Earth Science, Engineering, General, Resources Management and Special Topics. Papers were presented in the Technical Papers Session during the 2 (two) days convention.

By this opportunity, I would like to express my gratitude and appreciation to the Technical Paper Committee, the Chair person of Technical Paper Presentation, Authors, Presenters and all parties who have made the 2018 Technical Papers Session successful.

I believe that the content and the quality of all papers, with various interesting topics, were great and excellent. Therefore, on behalf of INAGA, I have the pleasure to share these papers for our geothermal community.

Yours truly,

Prijandaru Effendi
President of INAGA

CONTENTS

Committee ii
Speakers iii
Foreword v

EARTH SCIENCES 1
ENGINEERING 231
GENERAL 401
RESOURCES AND MANAGEMENT 505
SOCIAL, POLITICS, ECONOMICS, AND COMMUNITY 511

EARTH SCIENCES

ACID WARM SPRINGS AROUND GOU INELIKA VOLCANO, FLORES: FINDING AN EARLY GEOTHERMAL CLUE THROUGH SIMPLE CHEMISTRY INTERPRETATION 1
Anna Yushantarti

STUDY OF A RELATIONSHIP RESISTIVITY GRADIENT VS TEMPERATURE GRADIENT 9
Sayogi Sudarman

GEOHAZARD ASSESSMENT FOR GEOTHERMAL AREA APPLICATION IN INDONESIA: A STRUCTURED GUIDELINE 13
Budi Kristianto, Widhiyaksa Saveedra, Dorman P. Purba, and Daniel W. Adityatama

THE GEOLOGY AND GEOTHERMAL SYSTEMS OF THE MINAHASA DISTRICT, NORTH SULAWESI 23
Muhammad Sidqi and Pri Utami

HYDROTHERMAL ALTERATION MINERALOGY OF WELL MTB A, SOKORIA GEOTHERMAL FIELD, FLORES, INDONESIA 31
Haris Siagian, Dhani Sanjaya, Birean Sagala, and Jul Rafli

THE IMPORTANCE OF PREDICTING AND EVALUATING FAULT INTERSECTIONS IN EXPLORATION AND DEVELOPMENT DRILLING AT SORIK MARAPI GEOTHERMAL FIELD 41
R. Hendry, R. Hidayat , A.C. Licup, Jr., V.R. Chandra, S. Nasution, and X.L. Omac

SOKORIA GEOTHERMAL EXPLORATION DRILLING UPDATE, ENDE, EAST NUSA TENGGARA, FLORES, INDONESIA 53
Dhani Sanjaya, Haris Siagian, Jul Rafli, and Birean Sagala

SUBSURFACE HYDROTHERMAL ALTERATION IN UMBUL-TELOMOYO GEOTHERMAL FIELD, CENTRAL JAVA 61
Hiskia Ulinuha Annisa, Niniek Rina Herdianita, and Dudi Hermawan

SUBSURFACE STRATIGRAPHY AND HYDROTHERMAL ALTERATION MINERALOGY OF WELL E HULULAIS GEOTHERMAL FIELD, BENGKULU, INDONESIA 69
Putra, I. D. Nusantara and V. D. M.

HYDROTHERMAL SYSTEM CHARACTERISTICS USING GEOLOGY AND GEOCHEMISTRY METHODS: A GEOTHERMAL DESKTOP STUDY IN BORNEO ISLAND 77
Meilani, Niniek Rina Herdianita, and Andri Eko Ari Wibowo

CHARACTERISTICS OF HYDROTHERMAL ALTERATION IN EASTERN PART OF PATUHA GEOTHERMAL FIELD, WEST JAVA, INDONESIA 89
F. Pratiwi, K. Yonezu, A. Harijoko, K. Watanabe, Elfina, and M. I. Nurpratama

PROPOSED SLIMHOLE EXPLORATION DRILLING PROGRAM FOR GEUREUDONG GEOTHERMAL FIELD 95
Budi Kristianto, Bridget Lynne, and Jane Brotheridge

THEORETICAL ASSESSMENT OF VP AND VS FOR VOLCANIC ROCKS IN GEOTHERMAL FIELDS 109
D. Mendrofa, S. Mulyani, and D. Juandi

GEOTECHNICAL ASSESSMENT USING ELECTRICAL RESISTIVITY TOMOGRAPHY. CASE STUDY: MARGABAYUR 119
J T Napitupulu, B Ikhsan, J S Meliala, and R A Anwar

PERMEABILITY DISTRIBUTION IN CALDERA SYSTEM OF THE LUMUT BALAI GEOTHERMAL FIELD 125
Sapto Trianggo Nurseto, R.A. Julia Satriani, and Mochamad Husni Thamrin

EXPLORATION ACTIVITIES TO REDUCE UNCERTAINTIES OF A BLIND GEOTHERMAL PROSPECT. CASE STUDY: GEOTHERMAL PROSPECT "X" AT INDONESIA 133
Khalif Rahman, Wisnu Subroto, and Riki Irfan

GEOTHERMOMETER ANALYSIS TO DETERMINE GEOTHERMAL RESERVOIR TEMPERATURE OF PANDAN MOUNTAIN AS POTENTIAL ENERGY OF EAST JAVA 139
Munif Nur Faizin and Laksono Prabowo

COMBINATION OF SPECTRAL ANALYSIS AND MOVING AVERAGE METHOD TOWARD RESIDUAL GRAVITY ANOMALY PROFILE TO DETERMINE BASEMENT STRUCTURE 145
Wahyu Noor Ichwan, Agus Sulistyo, Fitrianita, Fikri Fahmi, Wambra Aswo Nuqramadha, and Yunus Daud

APPLYING AVERAGING METHOD TO SOLVE UNREALISTIC TDEM DATA RESULT STATIC SHIFT CORRECTION IN MT DATA 151
Agus Sulistyo, Fikri Fahmi, Diajeng Liati, Fitrianita, Wambra Aswo N, and Yunus Daud

MATRIX PERMEABILITY CONTRIBUTION IN X-1 EXPLORATION WELL 157
Hendy Sujarmaitanto, Ricsen Halomoan, and Timbul H. Silitonga

MICRO SEISMIC STUDY IN PATUHA GEOTHERMAL FIELD 163
Akhmad Fanani Akbar, Reza Jamil Fajri, Chevy Iskandar, Randy Wijaya Atmaja, Elfina, and Andri Dian Nugraha

BUILDING A 3D EARTH MODEL OF SILANGKITANG GEOTHERMAL FIELD, NORTH SUMATRA, INDONESIA 171
Drestanta Yudha Satya, Yoshio Soeda, Peter Drakos, Doddy Astra, and Enrique Manuel Lima Lobato

FLUID CHEMISTRY CHARACTERISTIC OF NAMORA I LANGIT, A GEOTHERMAL SYSTEM WITHIN THE GREAT SUMATERA FAULT 179
Christovik Simatupang, Koji Matsuda, Elisabeth Easley, and Doddy Astra

ASSESSING THE IMPACT OF FAULTS AND FRACTURES ON PERMEABILITY BASED ON BOREHOLE DATA IN ULUBELU GEOTHERMAL FIELD, LAMPUNG, INDONESIA 187
Muhammad Tajul Arifin, Imam Muhammad Prasetyo, Graniko Reza Pratama, Mochamad Husni Thamrin, and Hary Koestono

UPDATED LITHOLOGICAL AND TEMPERATURE MODEL IN SORIK MARAPI GEOTHERMAL FIELD, INDONESIA 197
S. Mulyani, Z.F. Sarmiento, A.C. Licup, Jr., V.R. Chandra, R. Hendry, S. Nasution, R. Hidayat, P.P. Sari, Jhonny , and D. Juandi

COMPARISON BETWEEN AUTOMATIC LINEAMENTS EXTRACTION AND MANUAL LINEAMENTS EXTRACTION METHODS FOR GENERATING FAULT AND FRACTURE DENSITY MAP: A CASE STUDY FROM CANDI UMBUL TELOMOYO GEOTHERMAL FIELD, MAGELANG, CENTRAL JAVA 207
Albertus Ivan and Jason

HYDROTHERMAL ALTERATION CHARACTERISTIC OF CEMENT CONSTRUCTION CHANGES: A CASE STUDY OF BUKIT KASIH GEOTOURISM AREA 213
Listiana Alifia Nurlaely, I Wayan Warmada, and Ilham Dharmawan Putra

SIMULATING GROUND THERMAL ANOMALY UNDER CONDITIONS OF DENSE VEGETATION BASED ON LAB AND FIELD MEASUREMENTS TO SUPPORT THERMAL INFRARED REMOTE SENSING TECHNIQUES 219
Asep Saepuloh, Suryantini, Christoph Hecker, and Robert Hewson

MULTI-SOURCE REMOTE SENSING DATA ANALYSIS FOR GEOTHERMAL TARGETING ON FLORES ISLAND 223
Christoph Hecker, Robert Hewson, Agung Setianto, Asep Saepuloh, and Freek D. van der Meer

ENGINEERING

HYBRID DRILL BIT IMPROVES DRILLING EFFICIENCY IN GEOTHERMAL APPLICATION IN LUMUT BALAI FIELD, INDONESIA 231
Fakhri Ade Andika, Mada Amatori Sutan, and Widoyo Krisnanto

GEOTHERMAL DRILLING CORROSION PROBLEM ROOTS RELATED WITH DRILLING FLUIDS 237
Ariya Dwinanto, Ashadi, Yudi Hartono, Haris Siagian, Gilang Kharisma, and Joni Sofian

UTILISING TOUGH2 SIMULATOR TO MANAGE THE LIMITATION OF CURRENT ANALYTICAL METHOD IN GEOTHERMAL PRESSURE TRANSIENT ANALYSIS 243
Daniel W. Adityatama, Nadira O. Wisesa, Dorman P. Purba, and Eylem Kaya

GEOTHERMAL WELL TESTING USING A NEW ATMOSPHERIC SEPARATOR AND METERING SYSTEM IN SARULLA, NORTH SUMATERA, INDONESIA 253
Elisabeth Easley, Nurlianto Sadji, and Winahyu Setyo Utami

NEW TECHNIQUES FOR ACID BRINE CORROSION CONTROL IN GEOTHERMAL WELLS 259
Paul von Hirtz, Elisabeth Easley, Russell Kunzman, and Darrell Gallup

FIELD EXPERIMENTS OF DRILLING GEOTHERMAL WELLS USING PDC BITS IN JAPAN 273
Hiroyuki Imaizumi, Tetsuji Ohno, Hirokazu Karasawa, Kuniyuki Miyazaki, Eko Akhmadi, Masahiro Yano, Yosuke Miyashita, Naoto Yamada, Tetsuomi Miyamoto, Masatoshi Tsuzuki, Satoshi Kubo, and Yasuyuki Hishi

BEST PRACTICE FOR MASTER VALVE CHANGE 2017 CAMPAIGN IN GEOTHERMAL INDUSTRIES 283
Ramadhan Primantara Harmanto, Paulus Panggabean, and Sigit Winarno

SUCCESSFUL OPERATION OF CLEAN OUT WELL WITH HWU AT WAYANG WINDU 293
Ridha Budi Nugraha, Redha Bhawika Putra, and Mulyadi

UPDATING CONCEPTUAL MODEL USING NUMERICAL MODELLING FOR GEOTHERMAL GREEN FIELD PROSPECT AREA IN ATADEI, EAST NUSA TENGGARA, INDONESIA 299
Marchel Christian Supijo, Akbar Dwi Wahyono, Ade Lesmana, Abdul Hadi Harahap, Sutopo, Heru Berian, and Welly Prabata

AERATED DRILLING OPTIMIZATION FOR 12-1/4" HOLE SECTION 311
Tunjung Wicaksana Ranukusuma

ENHANCING PERMEABILITY OF NO-TOTAL-LOSS-CIRCULATION WELL BY POWER WASH: CASE STUDY ON TULEHU GEOTHERMAL FIELD 319
Tony Widiatmoro, Miman Afiff, Hendra Y. T. Tondang, and Yudistian Yunis

SILICA SCALE CONTROL IN GEOTHERMAL BOTTOMING CYCLE PLANTS BY pH-MODIFICATION AND THERMAL QUENCHING 327
Paul von Hirtz and Darrell Gallup

3D NATURAL STATE MODEL OF SILERI GEOTHERMAL SYSTEM, DIENG GEOTHERMAL FIELD, INDONESIA 345
Rheza Akbar Dewantara, Khasani, and Ruly Husnie Ridwan

DRILLING RISK IN GEOTHERMAL WELL 353
Jul Rafli, Birean Sagala, Haris Siagian, and Dhani Sanjaya

THE EFFECTS OF FRACTURE INTENSITY IN DRILLING BIT PERFORMANCE THROUGHOUT DEVELOPMENT PHASE OF HULULAIS GEOTHERMAL FIELD 359
Fatah Gunawan, Graniko Reza Pratama, Freddy Haryo Armanto, and Widoyo Krisnanto

PRODUCTION IMPROVEMENT THROUGH SCALE REMOVAL BY JETWASH KAMOJANG GEOTHERMAL FIELD 367
Sabda Indrakusuma Nugroho, Sendy Hendriana, Fernando Pasaribu, and Marihot SP. Silaban

WELL TRAJECTORY PLANNING ISSUES IN GEOTHERMAL DEVELOPMENT FIELD 373
Tommy Souvanir, Redha Bhawika Putra, Edyson Purba, and Ajie Soeryo Koesherbowo

WASTE HEAT RECOVERY USING THERMOELECTRIC GENERATOR FOR POWER GENERATION 381
Hendra Ardi Kurniawan, Hafid Suharyadi, and A. Djumarma Wirakusumah

RESOLVING THE SHIFTING OF PRESSURE, TEMPERATURE AND SPINNER DATASET USING GEOSTATISTICAL PREDICTION DATA METHODS : IN CASE OF SINGLE ERROR DATA RECORDED TOOLS 387
Erwandi Yanto, Fadiel Evan Marastio, Benedict Amandus Hananto, and Ristio Efendi

NUMERICAL INVESTIGATION FOR ESTIMATION OF ROCK TEMPERATURE IN ENHANCED GEOTHERMAL SYSTEM 393
Muhammad Qarinur, Hideaki Yasuhara, and Naoki Kinoshita

GENERAL

LAND ACQUISITION PROCESS AND CHALLENGES IN GEOTHERMAL EXPLORATION PROJECT IN INDONESIA 401
Dorman P. Purba, Daniel W. Adityatama, Satria P. Hasymi, and Vicky R. Chandra

DRILLING MANPOWER AND EQUIPMENT TRANSFER FROM PETROLEUM TO GEOTHERMAL INDUSTRY: A PRELIMINARY STUDY ON SKILL ASSESSMENT 407
Mukhamad F. Umam, Dorman P. Purba, Daniel W. Adityatama, and Bart Van Campen

GEOTHERMAL DRILLING IN INDONESIA: A REVIEW OF DRILLING OPERATION, EVALUATION OF WELL COST AND WELL CAPACITY 417
Eko Hari Purwanto, Eko Suwarno, R. Fitrah Lukman, and Budi Herdiyanto

EVALUATION OF TAX ALLOWANCE INCENTIVE IMPACT TO THE GEOTHERMAL PROJECT IN INDONESIA 425
Pratama, A.R. and Hendra, R.

INSTITUTIONALIZED PUBLIC-PRIVATE PARTNERSHIP FOR GEOTHERMAL DEVELOPMENT IN INDONESIA: PRELIMINARY APPROACH OF PLN INITIATIVE 435
Yodha Yudhistra N., Suardi Nur, Hendra Y. T. Tondang, and Yudistian Yunis

A DECADE OF THE WORLD BANK ENGAGEMENT IN INDONESIA GEOTHERMAL SECTOR 443
Muchsin Chasani Abdul Qadir

AN EXAMINATION OF THE POTENTIAL OF PUBLIC PRIVATE PARTNERSHIPS (PPPS) TO STIMULATE THE DEVELOPMENT OF GEOTHERMAL ENERGY IN INDONESIA: CONCEPT AND ANALYSIS METHODS 447
Suardi Nur, Dr. Ariel Bergmann, and Prof. Bruce Burton

ENERGY CONSULTING AND USAGE OF SUSTAINABLE ENERGY IN HARZ 455
Syouma Hikmahtiar

GEOTHERMAL MENTORING PROGRAM – EMPOWERING WOMEN IN THE INDUSTRY 463
Jane Brotheridge, Jane Bydder, Andy Blair, and Riki Ibrahim

MOBILE EVAPORATOR FOR WATER BASED MUD GEOTHERMAL DRILLING 469
Lely Fitriyani

ANALYSIS OF RISK MITIGATION STRATEGIES 475
Ari Ingimundarson and Thorsteinn Sigmarsson

IDENTIFICATION OF GEOTHERMAL ENERGY POTENTIAL USING 4G METHOD (GEOGRAPHY, GEOLOGY, GEOPHYSICS, GEOCHEMISTRY) IN TELOMOYO MOUNTAIN COMPLEX, CENTRAL JAVA 483
Alfath Zain, Aulia Umami, Desi Kiswiranti, and Fadhil

THE APPLICATION OF GREEN ENERGY CONCEPT IN BUKIT DAUN GREENFIELD IN BENGKULU PROVINCE TO PROVIDE ELECTRICITY NEEDED IN THE AREA 489
Syayidu Guntur Ma'arif, Revanza Adirama Anwar, Jeffri Sembiring Meliala, and Timbul H Silitonga

THE ROLE OF PRELIMINARY DATA QUALITY ASSURANCE IN REDUCING GEOTHERMAL EXPLORATION RISK IN INDONESIA 495
Hevy Julia Umbara, Herry Gunawan, and Triyono Hadi

RESOURCES AND MANAGEMENT

THE URGENCY OF PROPER GEOTHERMAL RESERVOIR MANAGEMENT IN INDONESIA – A LITERATURE REVIEW 505
Yuniar Zhafira Abdillah and Qanitah

SOCIAL, POLITICS, ECONOMICS, AND COMMUNITY

FRAMINGHAM'S SCORE IMPROVEMENT OF GEOTHERMAL EMPLOYEES AT DARAJAT THROUGH HEALTH PROMOTION AND HEALTH COMPETITION PROGRAM 511
Muhyidin and Indra Rohim

UPDATED LITHOLOGICAL AND TEMPERATURE MODEL IN SORIK MARAPI GEOTHERMAL FIELD, INDONESIA 517
S. Mulyani, Z.F. Sarmiento, A.C. Licup, Jr., V.R. Chandra, R. Hendry, S. Nasution, R. Hidayat, P.P. Sari, Jhonny, and D. Juandi

GEOTHERMAL POLICY OF INDONESIA: CHRONOLOGY, EFFECTIVENESS, AND THE LATEST CONDITION 527
Desy Caesary, Eko Hari Purwanto, Seo Young Song, Huieun Yu, and Myung Jin Nam

SEEKING THROUGH THE POTENTIAL OF GEO-TOURISM AT IJEN, EAST JAVA, INDONESIA FOR FURTHER DEVELOPMENT 537
Dhara Adhnandya Kumara, Farhan, Faris Maulana Yunus, Haidar Firdaus Avicienna, and Yunus Daud

COMPARISON BETWEEN AUTOMATIC LINEAMENTS EXTRACTION AND MANUAL LINEAMENTS EXTRACTION METHODS FOR GENERATING FAULT AND FRACTURE DENSITY MAP: A CASE STUDY FROM CANDI UMBUL TELOMOYO GEOTHERMAL FIELD, MAGELANG, CENTRAL JAVA 545
Albertus Ivan and Jason

OPPORTUNITY AND CHALLENGES OF CLEAN DEVELOPMENT MECHANISM GEOTHERMAL PROJECTS IN INDONESIA TO CONTRIBUTE IN NATIONAL EMISSION REDUCTION 551
Muhyidin

NUMERICAL INVESTIGATION FOR ESTIMATION OF ROCK TEMPERATURE IN ENHANCED GEOTHERMAL SYSTEM 559
Muhammad Qarinur, Hideaki Yasuhara, and Naoki Kinoshita

HYDROTHERMAL ALTERATION CHARACTERISTIC OF CEMENT CONSTRUCTION CHANGES: A CASE STUDY OF BUKIT KASIH GEOTOURISM AREA 567
Listiana Alifia Nurlaely, I Wayan Warmada, and Ilham Dharmawan Putra



Earth Sciences



ACID WARM SPRINGS AROUND GOU INELIKA VOLCANO, FLORES: FINDING AN EARLY GEOTHERMAL CLUE THROUGH SIMPLE CHEMISTRY INTERPRETATION

Anna Yushantarti

Center for Mineral, Coal, and Geothermal Resources, Geologycal Agency, MEMR
Jl. Soekarno-Hatta No. 444 Bandung 40254 West Java
Email: anna.yushantarti@esdm.go.id / untuk.anna@gmail.com

ABSTRACT

Gou Inelika volcano is located at Bajawa, Ngada Regency, NTT, Flores. The last phreatic eruption is in 2001, a good indication for the heat source for a geothermal system. The manifestations are only warm springs, cold acid crater water, and cold alteration. Several acid warm springs (Gou, Tukapela, Piga, and Mengeruda warm springs) less than 50°C are discovered around it. They are acid sulphate, acid sulphate-chloride type and immature waters. The neutral warm springs (Loa-Mata Kota, Ae Bulu), bicarbonate type are less than 50°C also manifested at north-east. The upflow-outflow zone, reservoir temperature estimation will be discussed in this paper.

Keywords: Acid warm spring, manifestation, geochemistry geothermal, Inelika Volcano

INTRODUCTION

Promoting geothermal development, Indonesia government has been established Flores as geothermal island by a decision of MEMR No. 2268/2017. Flores island has about 18 geothermal areas, resources of 418 MWe, reserves of 476 MWe, and installed of 12.5 MWe (Geologycal Agency, 2017). Gou Inelika-Mengeruda is one of geothermal area in Flores, located at Bajawa, Ngada Regency, about ± 15 km northwest from Mataloko geothermal field. The nearest geothermal area from Gou Inelika are Nage and Mataloko. One of the surface geothermal investigations is geochemical method which is to understand the characteristic of geothermal fluids that represent their geological setting and the geothermal system. This paper only focus on simple geochemical interpretation about surface manifestation at Gou Inelika geothermal area based on geochemical data investigation on February-March 2018.

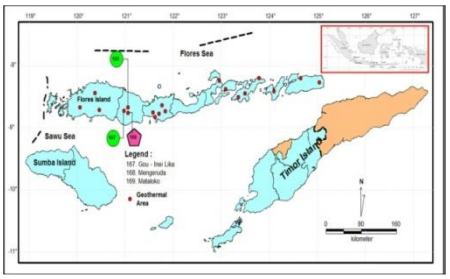


Figure 1: Map Location of Gou Inelika Area

BACKGROUND GEOLOGY

Muraoka et. al, 2005 explained that the Flores volcanoes and geothermal prospects forms a part of the eastern Sunda arc. Bajawa-Ngada regency has several active volcanoes such as Inelika, Ineria, and Ebulobo and several geothermal manifestations such as Gou Inelika-Mengeruda, Mataloko, and Nage. These geothermal areas are in quarternary volcanic areas, set at Bajawa rift zone volcanic rocks which is contained about 60 monogenetic breccia cones volcanoes along NNW-SSE trending zone, and consisted of calc-alkaline andesite which is very homogeneous. The origin of each cone volcanoe most probably is correlated with dike-filling from magmatic fluids event at depth. Inelika volcanoe has the last eruption on January 2001 which is a small phreato-magmatic eruption and formed a fissure at the surface. This could be described that the upper tip of the dike reached very shallow-depth near the surface, so this area has the small heat source, but numerous, and very active at Bajawa rift zone. The consequence is the good geothermal potency because of the favorable heat source and has similar hydrological setting.

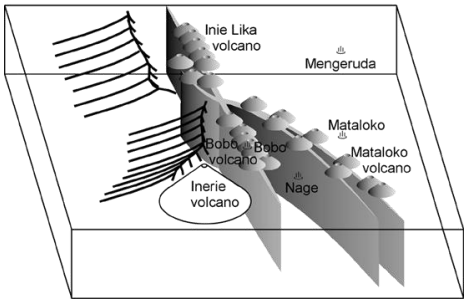


Figure 2: The Illustration of dikes conection beneath Bajawa Cinder Cone Complex (Muraoka et al, 2002 in Muraoka, et al, 2005)

The Lithology of Gou-Inelika geothermal area (figure 3) consist of tertiary rock (Pumice flow deposit, siltstone and sandstone) and quartenary rock (pyroclastics and lava, and debris avalanche deposits). It is associated with caldera structures, volcanic fractures, and faults. The NE-SW structure probably controlled Gou-Inelika-Mengeruda warm springs.

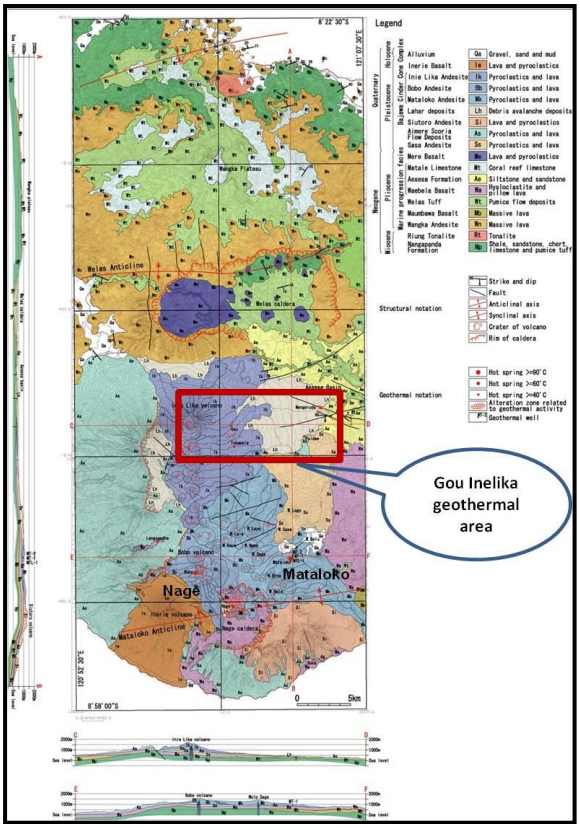


Figure 3: Geological Map of Central Flores (Muaroka et. al, 2005)

MANIFESTATIONS

Unlike Mataloko and Nage geothermal area which have fumarole, steaming ground, and hot springs, Gou-Inelika geothermal area only has warm springs, cold acid crater water, and cold alteration, eventhough it is in volcanic quaternary of high terrrain Inelika.

The distribution of surface manifestation is given in figure 9 and table 1. They are distributed along on high altitude for crater water (1486 asl) until low altitude (235 asl) and could be clustered into 5 (five) group, i.e.: Gou, Tukapela, Piga, Mengeruda, and neutral warm springs (Loa-Mata Kota-Ae Bulu). It is consisted of thermal manifestation (acid warm springs and neutral warm springs) and non thermal manifestation (cold acid crater water and cold alteration).

Gou Manifestation

It is consisted of cold acid crater water of Wolo Wawo Muda at high altitude (1486 asl) and acid warm springs Gou-1, Gou-2, and Gou-3 on lower altitude (757 asl) which are manifested at lava rock. The acid cold crater water of Wolo Wawo Muda has very shallow depth, temperature of 21,1 ^{o}C, no steam gases, but the odour of H_2S is very strong, ph 3,16, conductivity of 1154 µS/cm, and large alteration around it. The physical characteristics of Gou are the temperature of 37-46^{o}C at ambient temperature of 26,5^{o}C, low pH 1,88-2,82, 0,5 l/s of flow rate, conductivity of 1.780 µS/cm (Gou-1), and conductivity of 7.200-7.400 µS/cm (Gou-2&Gou-3), clear, having alteration around it, and having surface gas concentration of Gou-2 of H_2S 8 ppm and CO_2 300 ppm.



Figure 4: Photos of Gou Geothermal Manifestation (Cold Acid Crater water Wolo Wawo Muda, Acid warm springs Gou-1, Gou-2, and Gou-3)

Tukapela Manifestation

It is at altitude of 743 asl consisted of cold alteration Menge and Turamuri and acid warm springs Tukapela-1 & Tukapela-2, which are manifested at lava rock. The physical characteristics of Tukapela are the temperature of 47-48^{o}C at ambient temperature of 24,3^{o}C, low pH 1,83, 0,5 l/s of flow rate, and conductivity of 8.280-8.720 µS/cm, not continuous bubble, clear, and having alteration around it, and having surface gas concentration of Tukapela-1 of H_2S 60 ppm, CO_2 1000 ppm, dan CO 10 ppm.

The cold alteration Menge-2 is on altitude of 924 asl, having the temperature of 24,9 ^{o}C at ambient temperature of 24,3^{o}C, and having H_2S >60 ppm and CO_2 1000ppm which is measured about 3 cm above the alteration.



Figure 5: Photos of Tukapela Geothermal Manifestation (Acid warm springs of Tukapela-1 and Tukapela-2, Cold Alteration of Menge and Turamuri)

Piga Manifestation

It is consisted acid warm springs Piga-1, Piga-2, and Piga-3 which are manifested at lava rock on altitude of 393 asl. The physical characteristics of Piga are the temperature of 36-39ºC at ambient temperature of 27,7ºC, low pH 2,63-2,76, 20 l/s of Piga-1 flow rate, conductivity of 2660 µS/cm, clear, and slightly smell of sulphur.



Figure 6: Photos of Piga Geothermal Manifestation (Acid warm springs of Piga-1, Piga-2, and Piga-3)

Mengeruda Manifestation

It is consisted of acid warm springs Mengeruda-1, Mengeruda-2, and Mengeruda-3 on lower altitude (340 asl) which are manifested at lava rock. The physical characteristics of Mengeruda are the temperature of 40-41ºC at ambient temperature of 27,9ºC, low pH 2,85, of flow rate 100 l/s (Mengeruda-3), flow rate of 10 l/s (Mengeruda-1 and Mengeruda-2), conductivity of 1200-1400 µS/cm, clear, and slightly smell of sulphur, and having CO_2 500 ppm for surface gas concentration of Mengeruda-1.



Figure 7: Photos of Mengeruda Geothermal Manifestation (Acid warm springs of Mengeruda-1, Mengeruda-2, and Mengeruda-3)

Neutral Warm spring Manifestation (Loa-Mata Kota-Ae Bulu)

It is consisted of neutral warm springs Loa, Mata Kota, and Ae Bulu on lower altitude (235 asl) which are manifested at lava rock and very diluted similar with the cold water. The physical characteristics are the temperature of 37-43ºC at ambient temperature of 25,5ºC, neutral pH 7,23, 0,8 l/s of flow rate, conductivity of 1.780 µS/cm (Gou-1), and conductivity of 292-381 µS/cm, clear, and having surface gas concentration of CO_2 300 ppm (Loa).



Figure 8: Photos of Neutral Geothermal Manifestation (Neutral warm springs of Loa, Mata Kota, and Ae Bulu)

RESULT AND DISCUSSION

Fluids Chemistry

Fluids chemistry of the geothermal manifestation can give the clue about the origin of the geothermal fluids, the flow path, and the degree of fluid-rock interaction. Gou Inelika thermal manifestation only has temperature less than 50ºC and exhibits at moderate altitude (757 asl) until the lower ones (235 asl) and. Higher conductivity (7.200-8.700 µS/cm) for acid warm springs (Gou-2, Gou-3, Tukapela-1, and Tukapela-2) and moderate conductivity (1200-2600 µS/cm) for the others acid warm springs, and more dilute for the neutral-lower altitude ones (292-381 µS/cm).

The ion balance for neutral warm springs and acid warm spring of Piga-2 is between -5% until 5 %. The others acid warm springs (Gou, Tukapela, Mengeruda, and Piga-1) have ion balance more than 5%. The result of water analysis shows that all waters only have moderate concentration of SiO_2, SO_4^{-2}, Cl^-, and HCO_3^-.

Based on the sulfate and chloride concentrations (Figure 10), they can be divided into 4 groups: group A (Tukapela-2, low pH of 1,83, higher Chloride); group B (Tukapela-1, Gou-2, and Gou-3, low pH 1,82-1,97), group C (Gou-1, Piga, and Mengeruda, pH 2,63-2,83), and group D (neutral warm springs of Loa, Mata Kota, and Ae Bulu, pH 7,12-7,32).

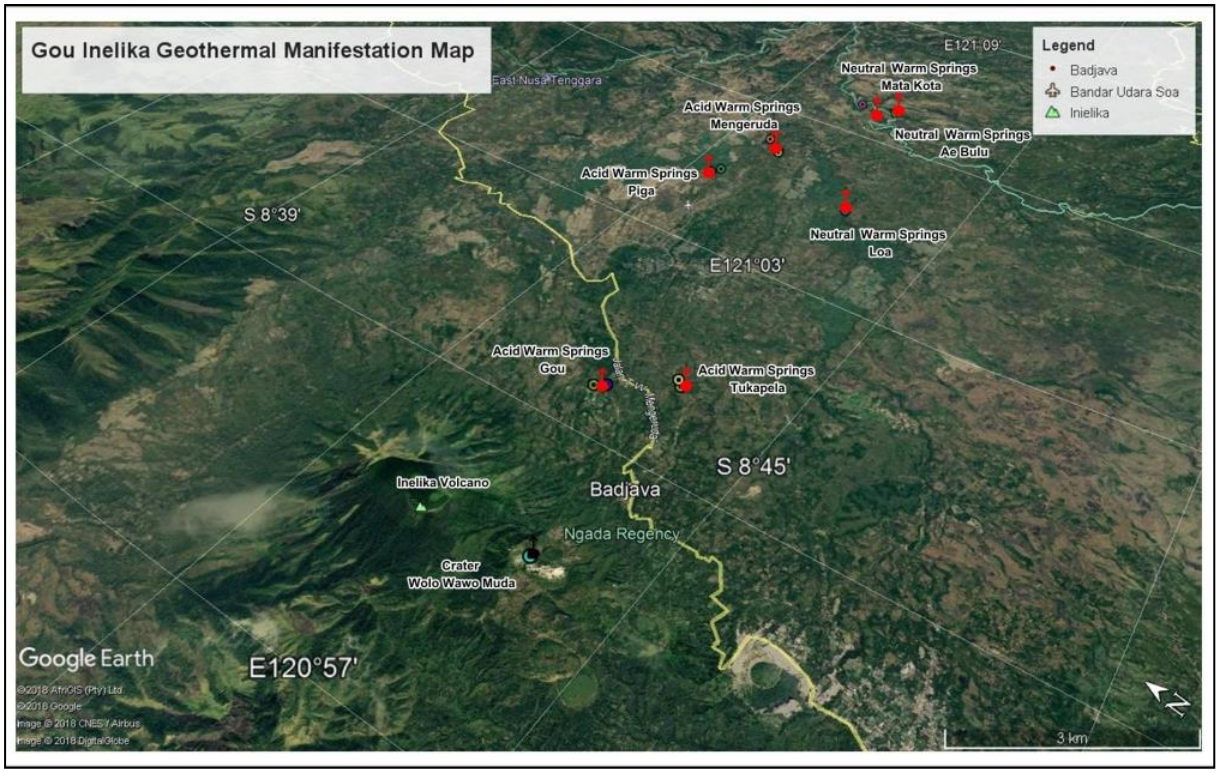


Figure 9: Map of Geothermal Manifestation Distribution of Gou Inelika Geothermal Area

Table 1: Data of Geothermal Manifestation Gou Inelika Geothermal Area

No.	Group of Manifestation	Name of Manifestation/ Sampel	Coordinat			Temperature of Manifestation (°C)	Temperature of Air (°C)	pH	Conductivity (µS/cm)	Flow Rate (l/detik)	Etcetera
			X	Y	Z						
1	Gou Manifestation	Cold Acid Crater Water of Wolo Wawo Muda	277266	9033490	1486	21,1	21,8	3,16	1154	-	Ngoranale village, Bajawa Utara
2		Acid Warmspring Gou-1	280858	9035149	737	37	26,5	2,82	1780	0,5	Gou village, Bajawa Utara
3		Acid Warmspring Gou-2	280988	9034975	749	46	26,7	1,97	7.400	0,5	
4		Acid Warmspring Gou-3	280993	9034975	757	45,9	26,7	1,88	7210	0,5	
5	Tukapela Manifestation	Acid Warmspring Tukapela-1	281671	9033968	743	47,3	23,1	1,82	8280	0,5	Turamuri village, Bajawa Utara
6		Acid Warmspring Tukapela-2	281793	9034088	753	48,3	23,1	1,83	8720	0,5	
7		Cold Alteration of Turamuri	281341	9034320	778	25,8	25,3	Strong smell of gases			
8		Cold Alteration of Menge	279950	9033388	924	24,9	24,3	H2S >60 ppm and CO2 1000ppm.			Menge village, Bajawa Utara,
9	Piga Manifestation	Acid Warmspring of Piga-1	287818	9037029	393	39,2	27,4	2,63	2630	20	Piga village, Soa
10		Acid Warmspring of Piga-2	287610	9037150	387	37	27,4	2,66	2660	1	
11		Acid Warmspring of Piga-3	287741	9036768	387	36,3	27,4	2,76	2560	0,5	
12	Mengeruda Manifestation	Acid Warmspring of Mengeruda-1	289152	9036389	353	41,4	28,9	2,86	1474	10	Mengeruda village, Soa
13		Acid Warmspring of Mengeruda-2	289139	9036390	340	40	27,9	2,84	1283	10	
14		Acid Warmspring of Mengeruda- 3	289515	9036812	321	41,4	27,9	2,85	1402	100	
15	Neutral pH manifestation	Neutral warmspring of Loa	288085	9034226	361	43	25,5	7,23	292	0,5	Loa village, Soa
16		Neutral warmspring of Mata Kota	292149	9035883	235	37,3	29,2	7,12	381	0,8	Mengeruda village, Soa
17		Neutral warmspring of Ae Bulu	292237	9035107	244	39,3	28,9	7,32	372	0,8	Mengeruda village, Soa
18	Cold Spring	Col spring of Seso	284030	9036674	-	25,7	24	7,04	197	-	Seso village, Soa It was taken from the tub shelter

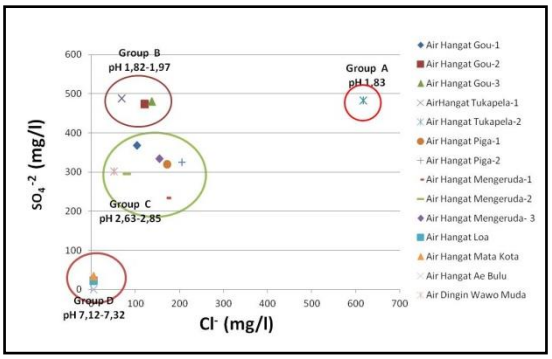


Figure 10: Diagram of SO_4^{-2} vs Cl^- in the samples of Gou Inelika Manifestation

Group A and B which are pH less than 2 (1,82-1,88) have SiO_2 (179-197 mg/l) and SO_4 (472-487mg/l), their concentration little bit higher rather than group C (SiO_2 (124-132 mg/l) & SO_4 (294-367mg/l)) and group D (SiO_2 (110-117 mg/l) & SO_4 (0-33mg/l)). All acid thermal waters (A, B, and C) have intermediate Cl concentration (80-617 mg/l), Ca (92-210 mg/l), and Mg (31-61 mg/l). Only group D has HCO_3 (238-311 mg/l), while group A, B, and C do not have HCO_3. Concentration of Na for all groups are similar (29-83 mg/l) and lower compared with geothermal waters commonly. The non thermal manifestation of acid crater water Wolo Wawo Muda has only high concentration for SO_4 (300 mg/l) and Ca (152 mg/l) while the others have low concentration. It seems that the water of crater Wolo Wawo Muda is from surface waters and cloudy because of being saturated with volcanic gases and dissolved with altered rocks.

Based on ternary plot of relative Cl-SO_4-HCO_3 (Figure 11), all acid waters plotted on SO_4-Cl axis (acid sulphate-chloride type, known as volcanic waters) and all neutral waters (Ae Bulu, Mata Kota, and Loa) plotted on corner of HCO_3. Only Tukapela-1 tend to be closed to Cl zone or relative Cl-SO_4 where the concentration of Cl is more dominant than sulphate.

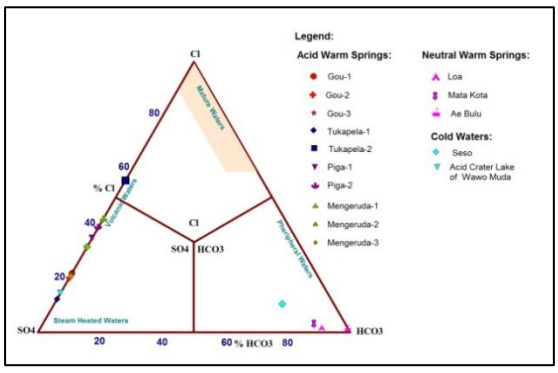


Figure 11: Diagram Type of Gou Inelika Geothermal Waters.

Nicholson (1993) explained that Acid sulphate-chloride waters could be derived from several other processes: a) near surface discharge and oxidation of H_2S into SO_4 in chloride water. b) near-surface condensation of volcanic gases into meteoric waters. c) condensation of magmatic vapor at depth. d) passage of chloride fluids through sulphate bearing sequences or lithologies containing native sulphur.
It is commonly accepted that acid springs formed via uptake of magmatic vapor (or magmatic fluid) occur mainly in active volanic-magmatic-hydrothermal systems or crater lakes such as the Mirravalles geothermal system in Costa Rica (Marini in Guo et al 2014), El Chichon crater lake in Mexico (Armienta in Guo et al 2014). They are located on high volcanic terrain, represent high SO_4, low flow rate, medium temperature. the Cl/SO_4 ratio is relatively low assumed to be an upflow of volcanic gases (especially H_2S) oxidized on the way up to the surface with oxygen at a shallow level.

So, group A, B, and C could be derived from reservoir fluids which has been a lot of mixed or only shallow ground waters that mixed with magmatic gases only. They have Al (25-143 mg/l) and Fe (12-28 mg/l) concentration little bit higher because of the dissolution of altered rocks at shallow levels or near the surface, resulting the waters will be not genuine from the deeper origin. The distance of Piga-Mengeruda (321 asl) from Gou-Tukapela (778 asl) is about 8 km, and from Crater Wolo Wawo Muda (1400 asl) is about 12 km. The Piga-Mengeruda still be dominated by sulphate concentration, could be an outflow from Gou-Inelika could be considered aquifer mobility because of the structure.
The Ae Bulu, Mata Kota, dan Loa have bicarbonate type, which usually shows characteristic of surface waters or associated with CO_2 gas condensation into shallow aquifer or mixing with shallow groundwater. This is confirmed by the CO_2 concentration at Loa reach about 300 ppm at 10 cm from the surface of Loa. The low concentration of Cl (5 mg/l), B (0,22-1,31 mg/l), and As (0-0,1 mg/l), so they could be only shallow groundwaters which is heated by steam from geothermal fluids of Gou-Inelika.

The diagram on a relative concentration of Na-K-Mg represent the degree of fluid rock interaction. The group A, B, C, and D are located in an immature water and interpreted that shallow meteoric water were much involved in hydrothermal processes near the surface (figure 12). They are highly mixed by shallow cold groundwater during their ascent and changed a lot in chemical composition, result in their immature waters. In contrast to acid warm springs, group A, B, and C, plot immature waters environment, could be affected by their interactions with primary or altered rocks at shallow levels to different extents, which will be not equal with their original waters. Thus such water is usually not in equilibrium condition and not useful for prediction of subsurface properties.

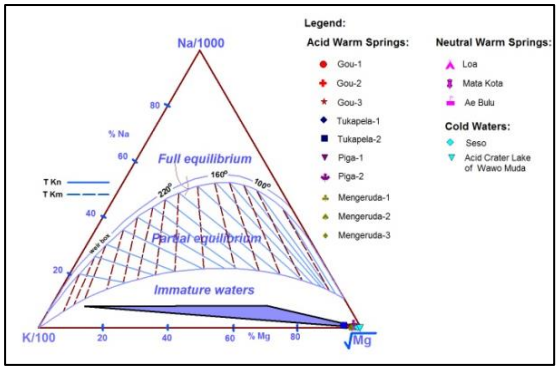


Figure 12: Diagram of Na-K-Mg of Gou Inelika Geothermal Waters

The figure 13 shows equilibration status through cation ratio (normalized Na/K versus Ca/Mg, Giggenbach, 1988) plot of the acid warm springs and neutral warm springs at Gou. This could be confirmed that all waters are not equilibrated. It shows that dilution and mixing of magmatic fluids with meteoric waters all exhibit similar Na/K and Ca/Mg rations for acid warm springs thus indicating their composition by acid dissolution of volcanic rocks (basaltic rock as the diagram shows). The SO_4 and Ca suggesting that composition of thermal waters have possibly been influenced by the leaching of pyroclastic rocks containing gypsum and/or anhydrite. Most Indonesian strato-volcanoes discharge gasses which originate from mantle wedge melts together with large discharges of CO_2 gasses of crustal rock origin (Halldorsson et al, 2013 in Hochstein et al, 2015), this condition could be the triger for disturbing the gas equilibrium, so resulting the unequilibrated condition of the manifestation (Hochstein, 2015).

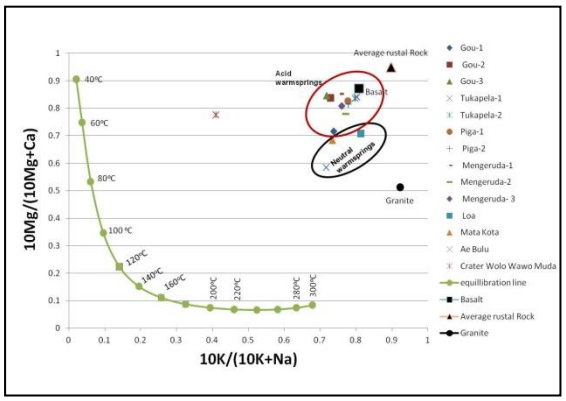


Figure 13: Cation ratio plot of thermal waters Gou Inelika Geothermal Area

Fournier (1977) suggest Chloride-enthalpy mixing diagram to give clue mixing condition. In many places all the hot-spring waters that reach the surface are mixed waters or have re-equilibrated. Figure 14 shows Gou Inelika the mixing trends among all the thermal waters (assumption: the silica is from quartz solubility), that most data points fall between the mixing lines. These waters are probably mixed waters of different depth and different temperatures. Tukapela-2 is the most probably the least diluted while sample Mengeruda the most diluted by cold water. The water of the crater Wolo Wawo Muda do not fall on this mixing trend, indicating that it is not affected by the same process, could be produced by mixing with a different cold water end member.

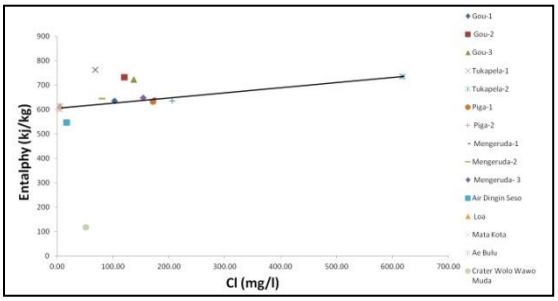


Figure 14: Chloride-entalphy mixing of Gou Inelika Geothermal Area

Isotopic composition of ^{18}O dan ^{2}H

Commonly, geothermal fluids will have process enrichment of isotopic oxigen-18 from their origin of meteoric waters (Craig, 1963 in Nicholson, 1993). All isotopic data Gou Inelika are compared with Bajawa meteoric line (Nasution, et al, 2000) $\delta D = 8{,}58\ \delta^{18}O + 19{,}8$ and with the global meteoric line. They show the significant of water-rocks interaction if compared with the Bajawa meteoric line, but not with isotopic of Seso cold water. This could be a hypothesis that there is no significant fluids-rocks interaction in Gou Inelika thermal waters because it is only formed by magmatic absorption into shallow ground waters. This equal with the result of water analysis that could be representing shallow ground water, so they only steam heated waters and could be affected by evaporation process.

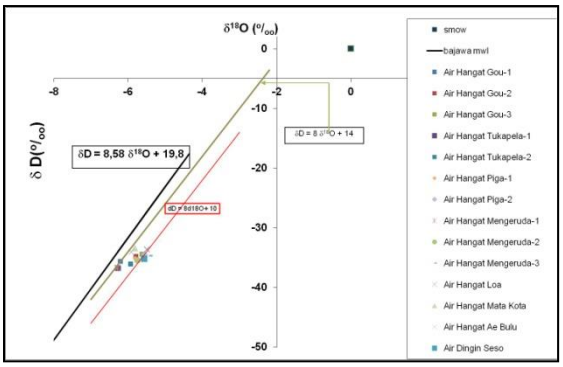


Figure 15: Isotopic diagram of Gou Inelika Geothermal Area

Reservoir Temperature

Since the cation compositions are un-equilibrated (figure 12 & 13), so cation-based geothermometry cannot be applied using these thermal springs. The SiO_2 concentrations (figure 16) are not controlled by quartz and chalcedony solubility, so silica quartz and chalcedony geothermometry could be slightly not representative also. The reservoir temperature is considered with the geological setting of Gou

Inelika which are the phreatic eruption in 2001, only acid warm springs and neutral warm springs, cold alteration with high gasses of H_2S >60 ppm, CO_2>4000ppm, and CO 50 ppm, so it could have medium to slightly high reservoir temperature (comparing with Mataloko and Nage which have high temperature).

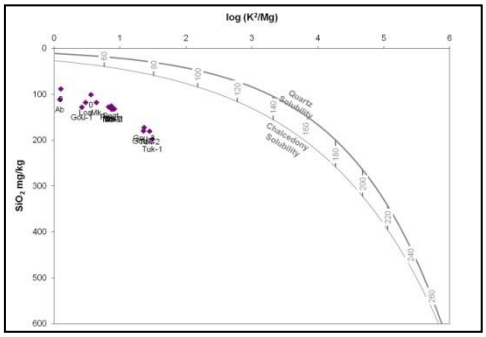


Figure 16: The Silica Solubility Diagram of Gou Inelika Geothermal Area

Takahashi et al (2000) explained that Gou Inelika acid thermal springs are similar in Rank B volcanic geothermal resources areas in Japan and derived from mixing relatively low temperature volcanic gases containing hydrogen sulfide gases, interestial waters in acid alteration zone and meteoric/ subsurface/stream waters. This can be an indication that Gou may be not so prospective compared with Mataloko and Nage.

The Geothermal System

There was an informal discussion delivered a doubt question wether the geothermal system of Gou Inelika already exist or not. Since the concept of geothermal system is a concept of heat energy in hot waters, steam, and rocks (Geothermal Indonesia Law No 21/2014), so the evidence of heat source is very clear at Gou Inelika. This could be concluded that there is a geothermal system at Gou Inelika, but type of the system could be variated depends on the classification.

According to Moeck (2013), Gou Inelika would like to be considered into Extrusive Magmatic Geothermal play type, where it is described by a shallow, intense heat source in the form of a young magma chamber (the heat is from Gou Inelika magma chamber). The others could be considered as volcanic geothermal systems which is hosted by 'volcanic system' whose heat transfer is associated with the production of magmatic fluids, pyroclastics, and lava flows from discharge centres near conduit and eruption craters (Hochstein et al, 2015). Acid geothermal springs formed via direct absorption of magmatic vapor (HCl, H_2S, CO_2, etc) and also mixing the chloride acid fluids of reservoir by infiltrating meteoric waters are ussually from hydrothermal systems located in active volcanic areas with very shallow magma heat sources where acid magmatic fluids may be only partially neutralized, and characterized by little bit higher of Chloride and Sulphate concentration (Giggenbach et al 1990 in Guo et al, 2014).

The upflow is at Gou-Tukapela (higher altitude) and the outflow is at Piga-Mengeruda (lower altitude), eventhough there is no fumarole, no hot springs, and no neutral chloride manifestation discovered at this area. It could be the possibility that there is no much mineral of feldspar and mica in the reservoir which could neutralize acidic fluids resulting the interaction of magmatic gasses and meteoric water at depth. The acid considerations should be calculated careful if it will be developed and according to Takahashi et al (2000) Gou Inelika may be not so prospective compared with Mataloko and Nage.

CONCLUSION

There are several clues for geothermal system of Gou Inelika: the heat from magma chamber of Gou Inelika (phreatic eruption in 2001), several acid sulphate-chloride type of warm springs (Gou, Tukapela, Piga, and Mengeruda), neutral bicarbonate of warm springs (Loa, Mata Kota, and Ae Bulu), cold acid crater waters, and cold alteration. They are immature waters and far for being equilibrated water-rock interaction, indicating their composition by acid dissolution of volcanic rocks. The reservoir temperature is considered with the geological setting of Gou Inelika which are the phreatic eruption in 2001, so it could have medium to slightly high reservoir temperature (comparing with Mataloko and Nage which have high temperature). According to the altitudes and concentration of waters, Gou-Tukapela is the upflow zone and Piga-Mengeruda-Loa is the outflow zone. There should be a geophysic data covering Gou until Mengeruda to find out the subsurface data clearly, wether Gou and Mengeruda could be fix being one system or not.

REFERENCES

Fournier, RO., 1977: Chemical geothermometers and mixing models for geothermal system. Geothermics, 5, 41-50

Geologycal Agency, Center for Mineral, Coal, and Geothermal Resources (2017), Geothermal Area Distribution Map and Its Potential in Indonesia December 2017, Bandung,

Giggenbach, W.F. (1988), Geothermal Solute Equilibria, derivation of Na-K-Mg-Ca indicators, Geochimica Cosmochim. Acta, 32, 2749-2765

Giggenbach, W.F. (1991), Chemical techniques in geothermal exploration. In: D'Amore, F. (coordinator), Application of geochemistry in geothermal reservoir development, UNITAR/UNDP, Rome, 119-142

Guo, Q., Liu, M., Li, J., Zhang, X., and Wang, Y. (2014), Acid hot springs discharged from the Rehai hydrothermal system of the Tengchong volcanic area (China): formed via magmatic fluid absorption or geothermal steam heating?, Bulletin of Volcanology, Berlin, 76:868, (doi:10.1007/s00445-014-0868-9)

Hochstein, M.P. and Sudarman, S. (2015), Indonesian Volcanic Geothermal Systems, Proceedings World Geothermal Congress, Melbourne-Australia, 1-11

Nicholson, K. (1993), Geothermal Fluids Chemistry and Exploration Techniques, Springer-Verlag, Germany.

Moeck, I. (2013), Classification of geothermal plays according to geological habitats, IGA Academy Report 0101.

Muraoka, H., Nasution, A., Simanjuntak, J., Dwipa, S., Takahashi, T., Takahashi, H., Matsuda, K., dan Sueyoshi, Y. (2005), Geology and Geothermal Systems in the Bajawa Volcanic Rift Zone, Flores, Eastern Indonesia. Proceedings World Geothermal Congress, Turkey, 1-13.

Nasution, A., et al, (2000), The Geology and Geochemistry of Mataloko-Nage-Bobo Geothermal Areas, Central Flores, Indonesia, Proceedings World Geothermal Congress, Kyushu-Tohoku, Japan, 2165-2171

Takahashi, M., et al, (2000), Geochemistry of Hot Spring Waters at bajawa Area, Central Flores, Nusa tenggara Timur, Indonesia, Proceedings World Geothermal Congress, Kyushu-Tohoku, Japan, 1807-1813

Undang-Undang Republik Indonesia No. 21/2014 Tentang Panas Bumi

STUDY OF A RELATIONSHIP RESISTIVITY GRADIENT VS TEMPERATURE GRADIENT

Sayogi Sudarman[1,2]

[1] Post Graduate Geothermal Exploration, University of Indonesia
[2] Dewan Pakar Asosiasi Panasbumi Indonesia
Email: ssudarman3@yahoo.com

ABSTRACT

The empirical relationship of resistivity and temperature given by Arrhenus has been expanded in this study in terms of vertical gradients. This relationship is hold when temperature T is the dominant factor cause of resistivity variations. Sounding electrical data of DC-Schlumberger, magneto-telluric (MT) and CSMAT (control source audio magneto-telluric) may be used for calculating the vertical resistivity gradients. This gradient appears to provide better prospect boundary delineation than the apparent resistivity (i.e high T zone), particularly for the diffuse and paleo resistivity prospect. The data from Wayang-Windu geothermal field, W. Java (DC-Schlumberger and some drill holes) and from Citaman-Gn. Karang, Banten (MT and an exploration well) have been used as the examples for this study.

Keywords: Resistivity gradient, MT, CSMAT, temperature gradient.

INTRODUCTION

Background

Mapping the real boundary of the geothermal prospect, i.e the upflow zone, that has diffuse low apparent resistivity or paleo resistivity anomaly is mostly inaccurate. Most of the diffuse anomaly is related to the prospect that geologically located inside a graben structure (e.g Sumatra, Gorontalo, Palu) or surrounded by sedimentary rocks (e.g Gn. Ciremai). This because in both systems can also be filled by a mixing of saturated clayed formation and hydrothermal clay alteration. While the paleo resistivity may related to the paleo alteration that can occur at the boundary area of the geothermal field.

Shallow temperature gradient drilled down to 300 – 500m depth (even deeper) is commonly used to check the diffuse out flow like structure or paleo resistivity. This drilling method is obviously costly, and because of that the resistivity sounding data of DC-Schlumberger and of MT (magneto telluric) has been expanded in the interpretation not just for developing resistivity structure but also in terms of resistivity gradient (RG) analysis.

Principal assumption and driven the formula to be used, plus examples of drilled field application are described in this paper to test the validity of RG.

Objective of the Study

The objective of this study is to make better delineation of the geothermal prospect boundary, that has diffuse apparent resistivity anomaly and/or paleo resistivity. And, also to assist a mapping of temperature gradient for those prospects that has limited gradient hole data.

THEORY AND ASSUMPTION

Geothermal reservoir in general consists of three (3) layers, which are (from top down, Figure 1):

1. resistive fresh rocks overburden layer that frequently permeable filled by convective fresh water which give no temperature gradient.
2. homogenous impermeable conductive clay cap alteration, consisting of argillitic minerals and has relatively high temperature gradient. This clay cap layer may include recent and paleo alteration, and frequently the extension of the layer is used for delineating the prospect boundary.
3. resistive substratum of prophylitic permeable reservoir formation which mostly consisting of convective hydrothermal fluids and almost no temperature gradient.

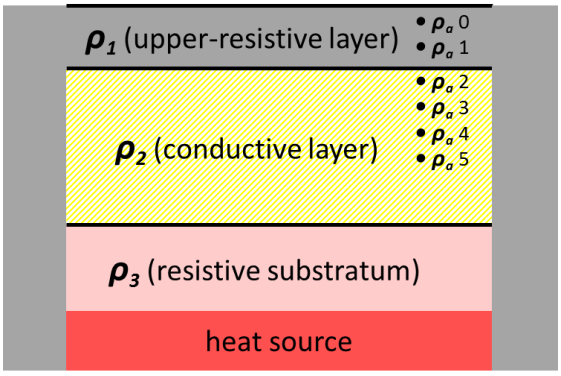


Figure 1: Simplified of resistivity layer of geothermal reservoir

The three layers can be distinguished from a resistivity sounding data, e.g DC-Schlumberger, magnetotellurics MT or control source audio magnetotellurics CSAMT in form of resistivity structures.

It is known that the resistivity (rho, ρ) of porous rocks is controlled by four (4) parameters, i.e porosity, salinity, clay content and temperature. In homogeneous impermeable clay cap, it is assumed that temperature is the major control to the resistivity changes with depth, compared to the 3 other parameters that assumed to be remain constant, i.e porosity, salinity, clay content. Using this assumption, an Arrhenus empirical formula which discussed below has been applied for this study.

BASIC EMPRICAL FORMULA

Here is the basic Arrhenus empirical formula that has been used, i.e:

$$\rho T = \rho o \exp^{\wedge} (\varepsilon/KT) \quad (1)$$

where: ρT, ρo is a resistivity at T and zerodegree K
exp = exponential
ε = activation energy
K = Boltzmann constant
T = temperature in degree Kelvin.

In another format the equation can be changed into:

$$\ln \rho T = \ln \rho o + \varepsilon/KT \quad (2)$$

To see the relationship between resistivity and thermal gradient, Equation 2 has to be partially differentiated to the z axis, and it becomes:

$$1/\rho T \, \partial\rho T/\partial z = 0 - \varepsilon/KT^{\wedge}2 \, \partial T/\partial z \quad (3)$$

substitute ∂ to Δ, then Equation (3) becomes (3a)

$$1/\rho T \, (\Delta\rho T/\Delta z) = - \varepsilon/KT^{\wedge}2 \, (\Delta T/\Delta z) \quad (3a)$$

where: (ΔρT/Δz) = resistivity gradient (Ohm.m/m)
(ΔT/Δz) = thermal gradient (°C/m)
ρT = ρcT true resistivity of the conductive clay cap (Ohm.m).

It is seen from Equation 3a that the relationship of resistivity gradient to thermal gradient is linear, i.e high resistivity gradient will also relatively give a high thermal gradient.

APPLICATION TO THE FIELD SOUNDING DATA

As mention above, the positive thermal gradient is found only at impermeable layer which in geothermal prospecting is composed of clay alteration. This type of alteration has low resistivity, therefore, call conductive layer. This layer can be recognized from descending segment of Q type sounding curve, either in DC or EM methods (i.e DC-Schlumberger, MT and CSAMT). In DC-Schlumberger the sounding curve will be in form of log ρa (Ohm.m) versus log AB/2 (m) while in MT or CSAMT it will be in form of log ρa (Ohm.m) versus log t (time, second) or log f (frequency, Hz).

Figure 2 shows an example of descending Q type DC-Schlumberger sounding curve, with a slope of resistivity gradient 'b' that can be obtained from power regression equation, e.g log ρa = a + b log AB/2 for DC-Schlumberger, or log ρa = a + b log t (or f) for MT or CSAMT sounding. The 'b' value than divided by true resistivity of the conductive layer (ρc) which can be obtained from theoretical curve matching or 1D modeling.

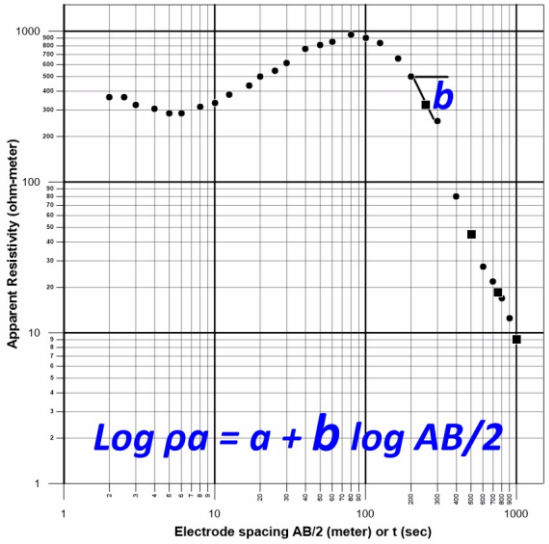


Figure 2: Example of descending DC-Schlumberger curve (Q type) and 'b' resistivity gradient value. Apparent resistivity at AB/2 = 250, 500, 750, 1000m of the mapping data is re-plotted (black square).

CASE STUDY

Two type of resistivity data has been used for this study, i.e DC-Schlumberger and magneto-tellurics which will be applied and discussed at 2 drilled geothermal prospects, i.e Wayang Windu and Citaman-Karang (Banten).

DC-Schlumberger: Sounding and Mapping Data (Wayang-Windu)

The Wayang-Windu prospect is a gentle mature dacitic twin peak with fumarole and alteration found at the saddle between Gn. Wayang and Gn. Windu and at the South flank of Gn. Windu (Hochstein, 2018). A condensed travertine manifestation forming a mini stalactite and stalagmite structure exposes at the South foothill of Gn. Windu. Most of the flat area at West and East slope consists of relatively thick porous soil which saturated with a mixing of cold and bicarbonate hot water.

Intensive DC-Schlumberger measurement including mapping and sounding has been done by Pertamina Geothermal Division in 1986 (Figure 3). The objective of the survey is to delineate the prospect boundary and the subsurface structure. The mapping was used a-4 sampling rate, i.e 250m, 500, 750 and 1000m, which can be called as a mini sounding. The aim of this mini sounding is to have good data control and at the same time to have a possibility to calculate its resistivity gradient (RG) in each measurement station.

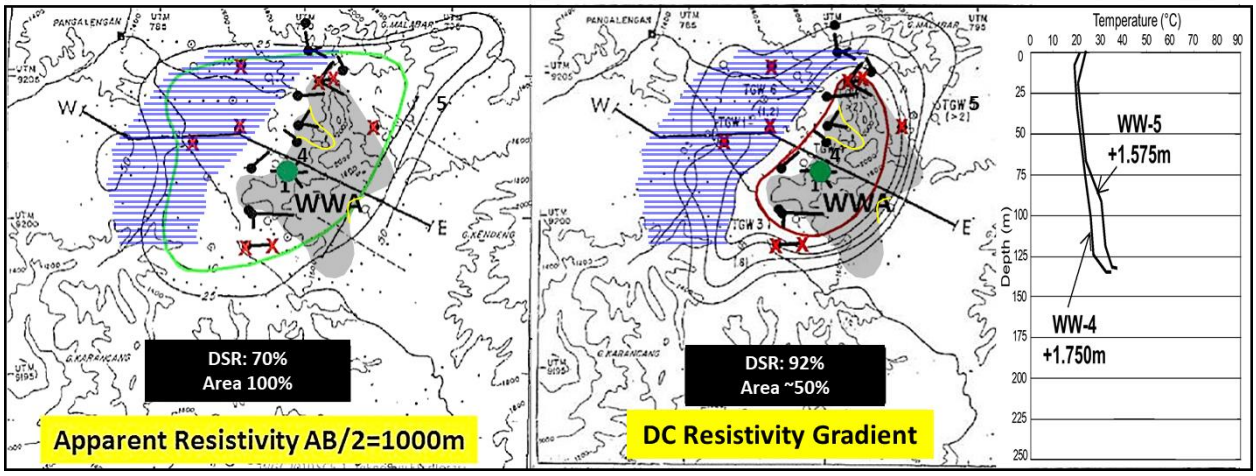


*Figure 3: Map of Wayang Windu field (modified from Sudarman et al, IPA 1986)**:** app. Resistivity, RG and TG profile. Grey shadow = mature WW lava formation, blue strip area = paleo resistivity (< 1 °C/10m), dot cross (red) is dry hole, black dot is productive well.*

A broader DC low apparent resistivity anomaly of AB/2=1000m, spread over the flat terrain at West part of the prospect that has thick porous soil (Figure 3 left), while the high resistivity gradient anomaly (RG) mostly occurs at the elevated fumarolic area (Figure 3 right). The size of RG area is about half the low apparent resistivity area (<10 Ohm.m) which is commonly used for determination the prospect boundary.

Prior to undertake deep exploration holes, some thermal gradient holes (TGH) have been drilled down to maximum 300m depth to understand the cause of low apparent and high RG anomalies discussed above. It shows that the low anomalies (either apparent or RG) at the W flat terrain is associated with low thermal gradient (TG, < 1°C/10m). But not for low apparent anomaly at the elevated E side that has high RG. This area has high TG (S. Sudarman et al, IPA 1986) and, therefore, has been used by Pertamina Geothermal Division as a criteria for selecting the first vertical discovery exploration well WWD-1 at well pad A, drilled in February 1991.

In 1994, the Wayang-Windu prospect was developed under a JOC (Joint Operation Contract) scheme between Pertamina and Magma Nusantara Limited (MNL). Since then, MNL has taken the whole responsibility of the field development including the drilling program and its execution. It is seen in Figure 3 that several deep holes (except WWD-1) were drilled outside the high RG anomaly (Figure 3 right) but still inside low apparent resistivity anomaly (Figure 3 left). These wells are mostly unproductive (marked by cross red) and it gives an indication that a drilling success ratio (DSR) is higher when refer to the RG map, i.e 92% instead of 70% if referring to conventional apparent resistivity map, AB/2 = 1000m.

MT Sounding and DC Mapping Data (Citaman-Karang, Banten)

Figure 4 shows a composite map of the Citaman-Karang area. It is seen that this prospect is located on the South foothill of young fumarolic strato volcano Gn. Karang. The fumarole occurs inside an E-W depression structure of Karang and alteration found at N area of interpreted gravity fault GF, outside of the depression. Bicarbonate hot springs with travertine deposit occur at Citaman area, at the foot hill of Gn. Karang. The prospect is composed of volcanic rocks at the N part and sedimentary rocks at about 2 km S of the hot springs area. General trending of fault structures in this prospect is NW-SE (red line).

A deep exploration bore hole BTN-1 has been drilled, located about 2.5 km N of the hot springs area and has an elevation of about 100m higher (Figure 4). This well was sited inside a-5 Ohm.m resistivity contour of DC-Schlumberger, AB/2 = 1000m. The RG has not yet been studied when drilling was programmed and drilled that resulting dry hole due to low T at the bottom hole, i.e 140°C at total depth of 2500m.

Mapping of low apparent resistivity from both, DC (AB/2 = 1000m) and magneto-tellurics (MT at 1 second), and RG from MT data have been made (Figure 4). It is difficult to recognize the outflow structure from this apparent resistivity map, but not for the RG map since RG is indirectly representing the TG, i.e higher RG means high TG or otherwise. It is seen at Figure 4 that the dry hole BTN-1 due to low bottom hole temperature (BHT) is associated with a low (lobe) RG structure. From this RG map, an upflow zone can be expected to be associated with the East-West Karang depression that has higher RG value and gradually reduces toward the East area forming a tongue structure that died out at the Citaman bicarbonate hot springs area at the South.

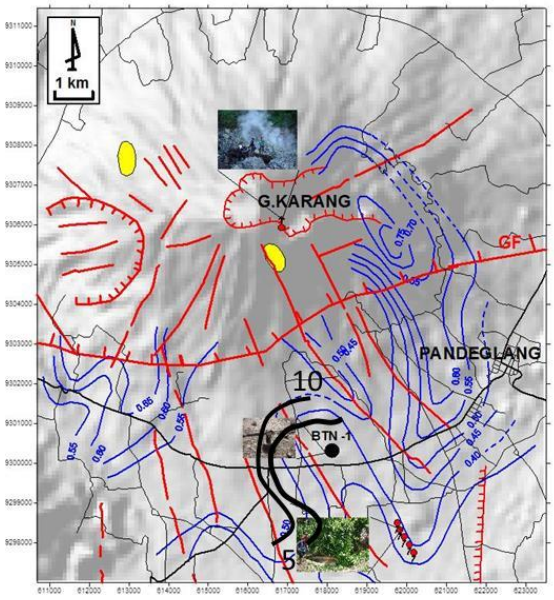


Figure 4: A composite map at Citaman-Karang, Banten: low apparent resistivity DC (black thick line) compared to MT RG anomaly (blue contour line), correlated with manifestation and bore hole location BTN-1. Yellow is alteration rocks, GF is a gravity fault.

DISCUSSION AND CONCLUSIONS

From this 2 case studies, it can be concluded that RG (DC and/or MT) and TG is useful to map the high T zone, correcting the prospect boundary, mapping a paleo resistivity area and clarify the outflow structure.

This because RG is linearly equal to TG (assuming T is a major controlled to resistivity measurement), in other word high RG means high TG, otherwise.

In a case of Wayang-Windu, RG and controlled by deep drilling data shows that the size of the prospect has reduced by half due to paleo resistivity at DC apparent resistivity AB/2 = 1000m. At Wayang Windu geothermal field, combining both data RG and TG has proved to increase a drilling success ratio up to 92%.

At Citaman-Karang area, it proves that the BTN-1 (140oC at TD=2500m) is located at an outflow structure that coming from high RG up flow zone located at Karang fumarolic depression. The previously apparent resistivity map either DC or MT cannot clearly track this structure.

REFERENCES

Hochstein, M, P, March. (2018), Visiting Lecture to the Indonesian Campus (ITB, UNPAD, UI and USAKTI) and to the State Geothermal Developers (PGE, PLN and GeoDipa)

Sudarman S, Restu Pujianto and Bambang Budiharjo. (1986), The Gn. Wayang Windu Area in West Java, the 15th Indonesian Petroleum Association Convention

GEOHAZARD ASSESSMENT FOR GEOTHERMAL AREA APPLICATION IN INDONESIA: A STRUCTURED GUIDELINE

Budi Kristianto, Widhiyaksa Saveedra, Dorman P. Purba, and Daniel W. Adityatama

University of Auckland
Email: bkri045@aucklanduni.ac.nz

ABSTRACT

Indonesian geology that is formed by a complex of tectonic plate settings, subduction processes and lies along the Pacific Ring of Fire are not only give a vast geothermal energy potential but also high risk of geohazard that could occurs during geothermal exploration and development activities. Failure in identifying risks of geohazard in early phase of geothermal development plan might cause some problems and catastrophic events such as damages on bridge, well pad and road access, skewed pipeline, production injection well leaks or broken, impairment of power plant facilities, and following cessation of electricity production. Moreover these events also could impact the nature or environment surrounding the field and results fatality or loss of human lives. Therefore, it is very critical to have a well - structured and comprehensive method as a guide to identify and mitigate the geohazard risks. The aim of this study is to establish a simple yet structured method in identify and mitigate geohazard in a geothermal prospect area since the early phase of exploration project and continue to keep monitoring the field during the development. Several literatures, author's previous studies and records about various possible geohazard cases that have and possibly happen in Indonesia geothermal area are reviewed in this study, such as landslides that related with climate and slope stability condition, it is very common in typical geothermal area with mostly high relief terrain such as in Indonesia and Philippine. Additionally, related with landslide risks in geothermal field, the presence of altered ground and the hydrothermal alteration processes are also adding more problem to the existing field facilities including road, steamline and well pad planning in some particular area near thermal manifestation. This hydrothermal alteration or water rocks reaction process are responsible to changes the chemistry and physical characteristics of the rocks that passed by the high temperature hydrothermal fluids that in reality is our ultimate target when exploiting geothermal field. Another geohazard risk in geothermal field that will be discussed in this paper is earthquakes, active fault, flood, subsidence and eruption risks which related with volcanic, phreatic, phreatomagmatic and hydrothermal processes.
This geohazards risk, mitigation plan and guidance is expected to be able to assist geothermal operators or developer in Indonesia to get an understanding regarding the potential of geohazards risks in a geothermal area since the early phase, thus will make the exploration and development geothermal safer in the future. Some examples of mitigation plans and studies will also be presented in this paper as the list of best practices from some experienced geothermal company in Indonesia and worldwide.

Keywords: Geothermal, geology, geohazard, earthquake, hydrothermal eruption, Salak, Suoh

INTRODUCTION

Hochstein and Sudarman (2015) identified the two groups of Indonesian volcanic geothermal systems that defined by using fluid analyses and volcanic (terrain) settings. The larger group includes geothermal systems that are hosted by young strato-volcanoes and other smaller group includes steeply dipping 'volcanic feeder (plug-type) systems standing in moderate terrain. These two types of geothermal systems asserted that all geothermal fields and prospects in Indonesia are associated with volcanoes and located in the high terrain which is steep and prone to landslides event compare with flat area.

Additionally, it is common in Indonesia that in the adjacent of a geothermal field there are some active volcanic centers and that geothermal areas are enclosed within seismically active zones (Utami, 2010). Volcanic hazard, earthquake and other hazards indirectly related or even unrelated to geothermal activity may also affect a geothermal field.

Geothermal systems itself are dynamic. Their thermal and hydrological structures (and hence the thermal manifestations) to some extent, also affected by the history i.e. natural and artificial changes that has been experienced by the systems.
Based on that condition it is understandable that there are plenty of geohazards in geothermal field which could occurs during exploration or development of the field. Understanding such structures is important when planning construction works on top of a geothermal system because they are directly related to the distribution of the hazard-prone sites and the sites that bear technical difficulties for construction.

Indonesia Geothermal Development

Geothermal resources in Indonesia are known as the largest in the world, with around 40 percent of the

total geothermal resources worldwide located in this country. In order to utilize this enormous energy potential, the government of Indonesia has strengthened its efforts to encourage geothermal power development. The government has target to reach the goal of 7,100 MW in geothermal power generation capacity in Indonesia by 2025.

With installed capacity of currently 1,808.5 MW, this seems to be a rather ambitious goal and would need adding 1,000 MW per year from today until 2025 (Wahjosoedibjo & Madjedi, 2018).

Geothermal Development Challenges

Based on literature study and author experiences in geothermal industry, there are some popular geothermal development challenges in Indonesia. It is recognised by all parties including government but is also hard to overcome and tackle these issues. Firstly, related with the location of geothermal resources which in Indonesia mostly located in the high relief volcanic terrain area which difficult to access and have geohazards problem of landslides and volcanic eruption.

Additionally, there is lack of high quality geoscientific data which crucial to preliminary geothermal potential assessment and to locate available resources. These challenges then followed by there are no standard on the exploration procedures especially for drilling strategy.

Financial issues also deter investment in geothermal development by private companies due to the high up-front cost of preliminary resource exploration. Lastly, an uncertain political and regulatory environment creates uncertainty for geothermal investors.

Study Objectives

The study of geohazard assessment in geothermal field is crucial to finding better management for every geologic hazard that continually threatens some geothermal field in Indonesia from the exploration to the development period. Based on historical data from several developed field, the effects of these hazards have cost EDC in Philippine about USD $6.8 Million annually from 2006 to 2011 alone, in the form of disrupted operations, lost revenues and cost of slope stability program (Marasigan & Olivar, 2015). Similar damaged condition that need high restoration cost also happens in Indonesia for example in Wayang Windu field due to massive landslides event in 2015 befell around the steam pipeline and settlement area which make it worst due to fatality were recorded from this event (Figure 1), and also in Salak and Darajat field based on author's experiences. However, the published information regarding these sensitive issues was hard to find due to company preferences.



Figure 1: Photo of Wayang Windu landslide in 2015 (H Yuhendar, 2016)

The key to effectively addressing the risks inherent to these hazards is timely access to information to aid engineers and management to make decisions that will minimize, if not totally eliminate, these risks. Eventually the study aims to reduce the vulnerability of the geothermal facilities, inhabited structures, roadways and local communities to natural disasters that potentially occurs in geothermal field.

METHOD

The study utilized any geohazards in geothermal field information (published) mostly from news, article, literature data and author's experiences during geothermal exploration and development project in Indonesia.

The geohazard definition and analysis for each cases and examples are elaborate thoroughly to generate a guideline or standard to conduct the geohazard assessment during each geothermal project phases. Figure 2 shows the project flowchart.

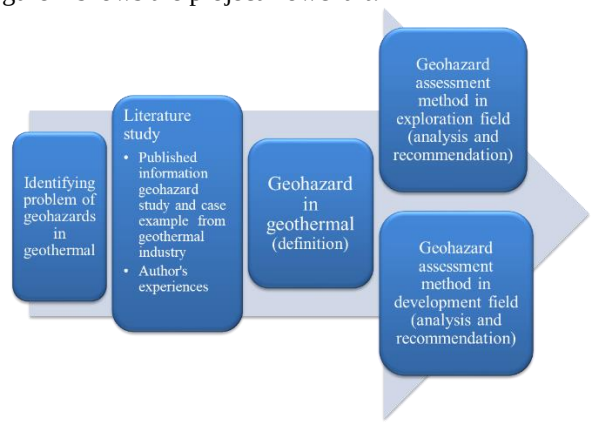


Figure 2: Geothermal geohazard assessment project flowchart

GEOHAZARD IN GEOTHERMAL

The United Nations International Strategy Disaster Reduction (2009) defines hazard as an "unsafe phenomenon, substance, human activity, or condition that may cause loss of life, injury or other health impacts, property damage, loss of livelihoods and services, social and economic disruption, or environmental damage".

Hazards that were present in the geothermal field were grouped into three major classifications. The summary of hazards can be seen in the Table 1 below. Most of the geohazards in the table could occur in both unexploited and exploited field. However, in exploited field the landslide and subsidence are more prone to take place and causing problems for the geothermal facility and assets.

Table 1. List summary of geohazards and possible occurring in the geothermal field

No	Hazards in Geothermal		Possible occurring in field
1	Seismic hazards	Earthquake	Unexploited – exploited
		Active Fault	Unexploited – exploited
2	Mass wasting and Mass loss	Landslides	The possibility is higher in exploited field
		Rock falls	The possibility is higher in exploited field
		Subsidence	Occurs in exploited field
3	Eruption hazards	Hydrothermal eruption	Unexploited – exploited
		Phreatic eruption	Unexploited – exploited
		Volcanic eruption	Unexploited – exploited

Earthquakes

An earthquake is a sudden, rapid shaking of the earth caused by the release of energy stored in rocks. Earthquake is occurs as fault movements. This is a phenomenon that involves two adjacent rock masses moving in opposite directions to each other along a certain plane (a fault plane). The energy of strain accumulated by plate motion in the rock mass is released in the form of a seismic wave. This is due to abrupt faulting. (The Headquarters for Earthquake Research Promotion, 2014).

In Indonesia, the highest potential geothermal area that could impact by earthquake is the geothermal area that situated along the Great Sumatran Fault (GSF) area. In fact most of giant geothermal prospects are located along that area and the prospect is strongly related with the structural tectonic system of GSF (**Figure 3**). Earthquake shaking in geothermal area may cause loss of life and destruction of property. In a strong earthquake the ground shakes violently. Buildings, power plant, road, break the well, pipeline, well pad may fall or sink into the soil. Rocks and soil may move downhill at a rapid rate (landslide).

Moreover, there is also a correlation between seismicity and eruption activity. This will discussed more in the eruption part.

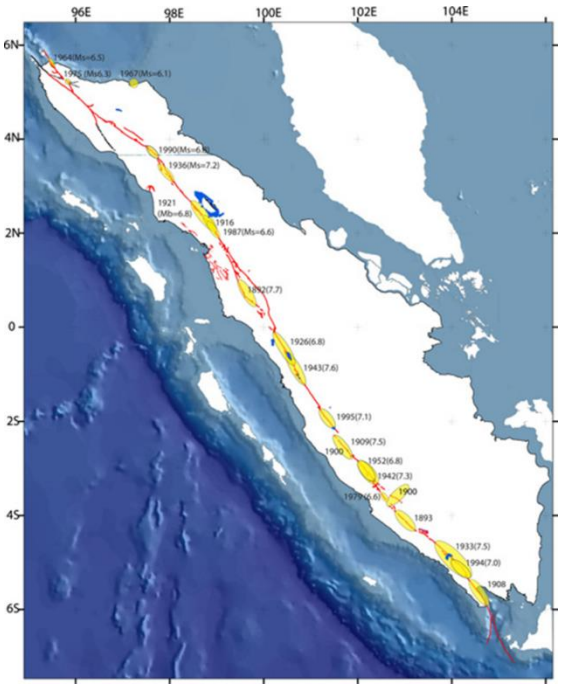


Figure 3: Historical major earthquakes along the Great Sumatran Fault (GSF) since 1892, the yellow ellipsoids indicate fault segments that were ruptured during earthquakes. Numbers indicate years of occurrences and number in brackets are earthquake magnitudes

Active Fault

An active fault is a fault that has repeatedly experienced fault movements in the past and is still deemed to be a source fault of future earthquakes. If a large earthquake occurs inside a continental plate, the fault displacement can reach the ground surface and deform geological layers and geographical features. The deformations caused by repetitive fault movements such as these form characteristic geographies. These can include dislocations along mountain ridges, dislocations along valley faults, and continuous cliff formations. This phenomenon can also impact to geothermal field development with relatively similar impact with earthquake.

Landslides

Landslide is the most common hazard that occurs in the geothermal field. The main contributing factors to the landslides in geothermal field are the steep slopes, high rainfall, and high porosity, loosely consolidated near-surface rocks. During periods of heavy rain the soil has the tendency to become over-saturated with water, triggering slope failure that can lead to soil creep or landslide depending on the nature of the underlying soil.

In 2003 due to the prolonged intense rainfall, the Salak geothermal field experienced a series of landslides and debris flows that disrupted the production facilities capability to provide and control steam to PLN Power Plants Units 1, 2, & 3.

At that time the landslide caused severe pipeline damages and releases of brine, condensate and steam, blocked access roads to well sites and created hazardous conditions at numerous operational locations. This event resulted shut down operations for about 3 months in Salak geothermal field which also lead to lot of detriment and budget to restore the stability problem (Kristianto et al, (2013)).

Based on the soil investigation and geological assessment in that area, the hydrothermal processes have altered the tuffaceous soils into high plasticity, soft to firm clay which is an expansive or reactive soil due to the presence of montmorillonite (smectite) minerals. The material is usually stable in an undisturbed condition, but it becomes very sensitive to water in a disturbed condition (see Figure 4).

Rock falls

Rock slope instabilities, in particular rock fall occurrences, are a common hazard along the rock cuts in mountainous steep terrain area where geothermal field located. This geohazard can cause delays, damage, injury, and possible death to geothermal workers.

Rock falls are generally initiated by some climatic or biological event that causes a change in the forces acting on a rock. These events may include pore pressure increases due to rainfall infiltration, erosion of surrounding material during heavy rain storms, chemical degradation or weathering of the rock, root growth or in an active construction environment, the potential for mechanical initiation of a rock fall will probably be one or two orders of magnitude higher than the climatic and biological initiating events described above.

Subsidence

Subsidence defined as the down motion of the ground surface. It can occur in a wide range of area as an impact of big production of mass and volume of saturation from the geothermal reservoir (Sektiawan et al (2016).

In developed geothermal field, the massive large fluid volume production and lack of injections could leads to the decrease of pore pressure inside reservoir. This decline disturbs the pressure stability and overburden pressure compresses the pores. It results the drop in ground surface. Astisiasari et al (2017) described some subsidence examples in geothermal field around the world. From Wairakei in New Zealand, the subsidence rate 10m over 30km2 areas from the leveling data that gathered on 1956 – 1971.

Meanwhile in Indonesia, Salak field severe 16 cm subsidence in 15 years (1994 – 2008), Wayang Windu 8 cm subsidence in 17 years (1995 – 2012), and Kamojang around 6 cm subsidence from the data 2006 – 2007. The decrease in ground surface level induces a devastating effect in the construction of some facilities, such as building, pipeline, canal, and river.

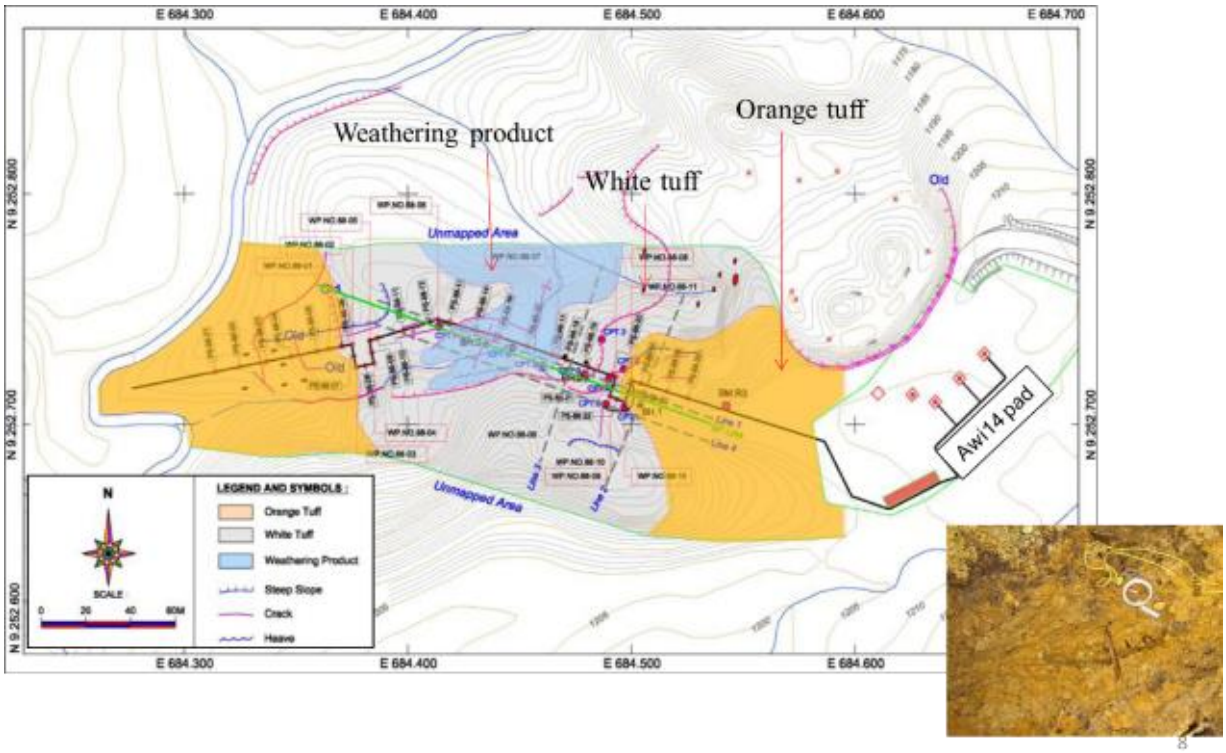


Figure 4: Detail geological mapping result during geotechnical investigation for landslide event in Salak geothermal field (Kristianto et al, (2013)).

Hydrothermal Eruption

Eruption hazard type that most likely occurs in geothermal field is hydrothermal eruption. It is common in both exploited and unexploited geothermal systems with varies in scale and frequency. Lawless and Browne (2001) stated hydrothermal eruptions is an eruption ejecting some consolidated and unconsolidated materials with energy derives solely from heat loss and abrupt changes of phase in a convecting hydrothermal system. This type of eruption is more likely to occurs in geothermal field due to do not require any direct input of either mass or energy derived from a magma and thus differ from both phreatic and phreatomagmatic eruptions.

Many hydrothermal eruptions in a hot water field start very close to the ground surface and result from the rapid formation of steam mainly due to a sudden pressure changing. This steam provides the hydrostatic energy to brecciate, lift and eject fragments of the host rocks. The most definite product of hydrothermal eruption is hydrothermal breccia.

First example of hydrothermal eruption in unexploited field is from the Ohineraki thermal area in the northern part of the Mokai field in 1996. Another example from New Zealand is at Ngatamariki field which occurred in 1948 and produced a crater about 10 m in diameter.

From Indonesia, some large eruptions occurred from three adjacent craters at the Dieng field, Java, in 1979. These occurred prior to power production from the field and resulted in large loss of life (142 persons), which was caused by the accompanying gas release. Most people died located more than a kilometer from the craters. The largest crater also emitted a lahar that flowed further than 3 km. Several earthquakes in Dieng occurred between one and three hours before the eruption (Lawless & Browne, 2001).

Another example is from Suoh exploration area. Hydrothermal eruptions were reported occurred immediately after the Feb 15th 1994 (M 6.8) Liwa earthquake. The focal depth of the earthquake was 23 km and occurred near the SFZ with movement of Kumering fault section through to the Semangko fault section (Natawidjaja & Triyoso , 2007)). Eye witnesses report two simultaneous eruptions at Kalibata Keramikan and Kalibata Atas with mud, rock, soil and hot water erupted to a height of 40-50 m and 50-60 m respectively. The condition prior to these eruptions there were fewer thermal features and activity was less intense in this area.

Case from the exploited field, hydrothermal eruptions have occurred at both Wairakei and Tauhara and these events were undoubtedly a consequence of the exploitation of these hydrologically linked systems. Two eruptions occurred in the Tauhara field at the Taupo Pony Club, in 1974 and 1981, 7 km from the Wairakei Power Station (Lawless & Browne, 2001).

Phreatic - Phreatomagmatic Eruption

In USGS definition, this type of eruptions is steam-driven explosions that occur when water beneath the ground or on the surface is heated by magma, lava, hot rocks, or new volcanic deposits. The intense heat of such material (as high as 1,170 ° C for basaltic lava) may cause water to boil and flash to steam, thereby generating an explosion of steam, water, ash, blocks, and bombs. The water can be from groundwater, hydrothermal systems, surface runoff, a lake or the sea.

Phreatic eruption does not included magma as the eruption product meanwhile the phreatomagmatic does have magma juvenile as ejected products from subsurface and high pressurized processes.

The example event of phreatic - phreatomagmatic eruption was from Suoh exploration geothermal field. This high geothermal prospective field was experienced massive hydrothermal eruption in 1933 two weeks after series of major Liwa earthquakes (M 7.5).

From Stehn (1934) after the earthquake, Suoh basin violently erupted with explosions heard up to 600 km away with fine “ash” falling on the city of Kota Agung 50 km away. Prior to these eruptions, several hot springs depositing sinter and fumaroles existed in the area in smaller portion. Field work carried out by Stehn six days after the first eruptions revealed an observed area of complete devastation covering 35 km^2. Figure 5 showing the illustration of eruption’s scale from Suoh depression in 1933. The explosions could still be heard from Koelatoengkai 510km (Sumatra) and Keboemen 660km (Java).

Volcanic eruption

A volcanic eruption occurs when magma hot materials are thrown out of a volcano. Eruptions can come from side branches or from the top of the volcano. Some eruptions are comes as huge explosions that throw out enormous amounts of rock and volcanic ash and kill many people. Some are quiet outflows of hot lava.

This type of eruption is not common in geothermal field due to different ages between volcanic and hydrothermal systems. Additional information, related with geothermal drilling in volcanic area, there have been numbers of research drilling programs that attempted to drill directly into the active parts of the volcano, such as the conduit at Unzen or the flanks of Kilauea/ Mauna Loa. Neither of these drilling programs had any effect on the eruptive activity at the respective volcanoes (Klemetti, 2018)

Based on the list of hazards and examples above, it is appears that these geohazards could cause very significant problems for geothermal development. It will impact people, facilities and environment, causing huge amount of losses and supplementary cost for area stabilization and restoration.

GEOHAZARD ASSESSMENT METHOD

There are some methods and assessments that recommend to be conducted to mitigate the geohazards and minimize the impacts. From this study, the geohazard assessment method is divided into two types regarding the period of execution, as follow (**Table 2**):

1. Geohazard assessment method that conduct in the geothermal early phase or exploration stage (unexploited field)
2. Geohazard assessment method conduct during the development and production of geothermal field (known as geohazards monitoring program)

Geohazard Assessment in Exploration Field

As mentioned in previous chapter, the geohazards that likely occurs in the unexploited geothermal field or during exploration phase is that related with natural geological processes. For example: Earthquake and active fault that linked to tectonic processes and eruption hazards that correlated with volcanic magmatic and hydrothermal processes.
Some method and hazard assessment that could be conduct during exploration stages is:

- Literature study, records of geohazards in the area
- Aerial remote sensing data analysis
- Map geological structure for surface fault area
- Volcanic mapping, map location for all possible young eruption (volcanic cone, crater, etc.)
- Surface thermal manifestation mapping, map the possible crater of hydrothermal or phreatic eruption
- Landslide susceptible area mapping

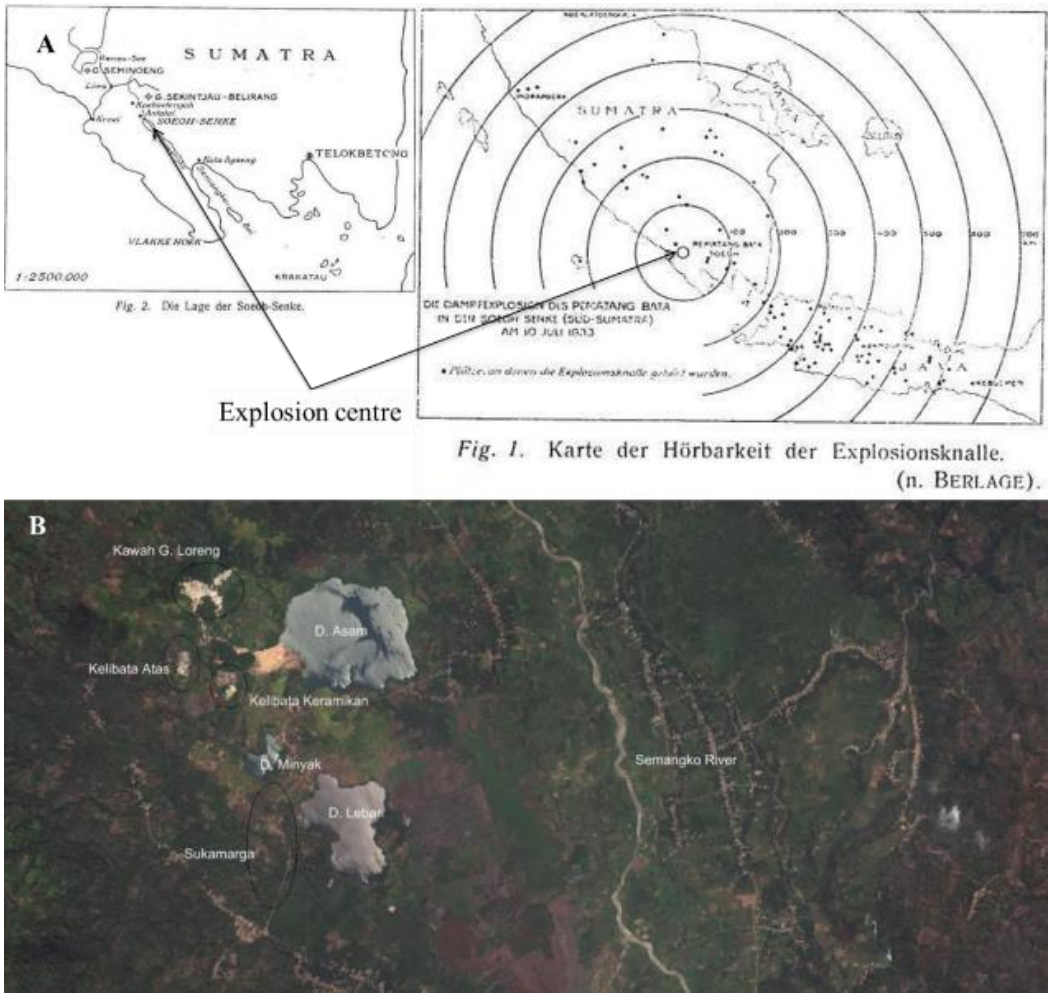


Figure 5: (A) The map showing outermost locations, where the explosions could still be heard, Koelatoengkai 510km (Sumatra) and Keboemen 660km (Java) distance from explosion center (Soeoh Senke) from Stehn (1934) (B) Map of Suoh depression current time. All the lakes were created after the 1933 eruptions (source: Google earth).

Table 2. Two types of geohazards assessment in geothermal field

No	Geohazard assessment method in exploration field	Geohazard assessment method in development field
1	Literature study, Historical geohazards data in the area (Earthquake, landslide, eruption)	Landslide area mapping and routine monitoring on historical landslide area
2	Aerial remote sensing surface data analysis	Checking rainfall data from BMKG
3	Surface geological mapping and geological structure analysis	Installment of tiltmeter or inclinometer in the areas which has frequent landslide record
4	Volcanic mapping, map location for all possible young eruption (volcanic cone, crater, etc.)	Precision leveling survey for subsidence
5	Surface thermal manifestation mapping, map the possible crater of hydrothermal or phreatic eruption	Seismograph
6	Preliminary Landslide susceptible area mapping during the exploration surveys	Drone monitoring can be utilized to monitor the inaccessible areas
7		Integrated GIS geohazard mapping

The assessments mentioned above can utilize surface geological mapping result and aerial remote sensing data, including google earth image. Additional data can be from Volcanology Board Indonesia for example map of volcanic hazard and earthquake historical data.

The earthquake and active fault hazard is assesses using structural mapping including excavating fault traces. This method is useful for estimating the probability of fault activity in the future. By undertaking the mapping project and excavations, the scientist can find out the scale and interval of earthquakes in the past.
The mapping of surface thermal manifestation completed with eruption product sampling analysis is needed to assess the potential area for eruption, divide the craters based on eruption type for example hydrothermal eruption, phreatic and phreatomagmatic eruption. And also predict the possible eruption magnitude that possibly reoccurs in the future.

Landslide area mapping in unexploited geothermal field will produce the classification of high, medium and low landslide susceptibility area.

The information from above assessment during geothermal exploration period will help on the next drilling project planning and steam field design. Road access and well pad need to consider the mapping results and select the safest area for construction, similarly for power plant and pipeline designs.

Geohazard Assessment in Development Field

The most common geohazards that appear in the development field is landslides and rock falls. When the natural condition start to get alteration by several engineering construction which also change the stability of the slope.

The geothermal area is located in the steep slopes area. When the rain season comes, the heavy rainfall can trigger the landslide more especially around high porosity, unconsolidated surface rocks

The method and hazard assessment that conduct during development stage is:

- Landslide area mapping and routine monitoring on historical landslide area
- Checking rainfall data from BMKG
- Installment of tiltmeter or inclinometer in the areas which has frequent landslide record
- Precision leveling survey for subsidence
- Seismograph
- Drone monitoring can be utilized to monitor the inaccessible areas, for example intense thermal manifestation area, instable ground, active crater, etc.
- GIS geohazard map can be developed using data of slope stability, surface lithology, surface structure, land use map, drainage pattern, and historical of landslides.

The GIS geohazard mapping will produce more comprehensive and more valid classification of hazard susceptibility area especially landslide (Figure 6 shows the example of GIS geohazard map result from EDC Philippine). The information from those assessments will help on the project planning in the future. Additionally, the good monitoring management, integration of methods and several surveys will reduce the risk of hazards and the other effects related to it. This discussion output can be used as a guide for minimizing impact in the geothermal field in general.

RESULT AND DISCUSSION

It is clear that although Indonesia has an abundant geothermal potential, it is also accompanied by high geohazard risks due to its geological setting. Natural geological hazards such as earthquakes and eruptions (hydrothermal, phreatic and volcanic) may occur and harm the developed geothermal field or even the unexploited geothermal prospect areas. A detailed and well-structured geological mapping, which consists of geological structures, eruption centers, volcano stratigraphy and thermal manifestations, is the best method to reduce the risk from natural geological hazard. Moreover, reviewing map of volcanic hazard and volcanic activity and earthquake history data from Volcanology Board Indonesia will also help to minimize the risk.

At the development stage, geothermal fields might suffer more geohazards such as landslides, subsidence, rock falls and all other natural geohazards. Integration between geological, slope stability and GIS map with rainfall data might be the best tool to reduce the landslide risk within the fields. Furthermore, tiltmeter and inclinometer should be installed to monitor the landslide prone area. Drone is one of the most recent technologies that can help to survey the remote area where it is inaccessible.

Geohazard assessment is an essential step in exploration stage, so the risk that might be occurred caused by geohazard can be minimized. Methods that are mentioned above are simple, easy and relatively more affordable compared to the risk in the future, particularly the financial risk, since developing geothermal in Indonesia needs outrageously high capital cost.

Therefore, geohazard study needs to become a mandatory evaluation at the exploration stage, before the geothermal prospect area is exploited further. Government may conduct a strict regulation regarding this geohazard assessment in order to attract the investor to develop geothermal prospect area and reducing the loss, e.g. financial, human lives, and nature environment.

ACKNOWLEDGEMENT

This research study was raised and conducted during the program of Master Energy in Engineering Science Department, University of Auckland 2017-2018. We want to thanks to LPDP and MFAT New Zealand ASEAN Scholarship for the financial assistance.

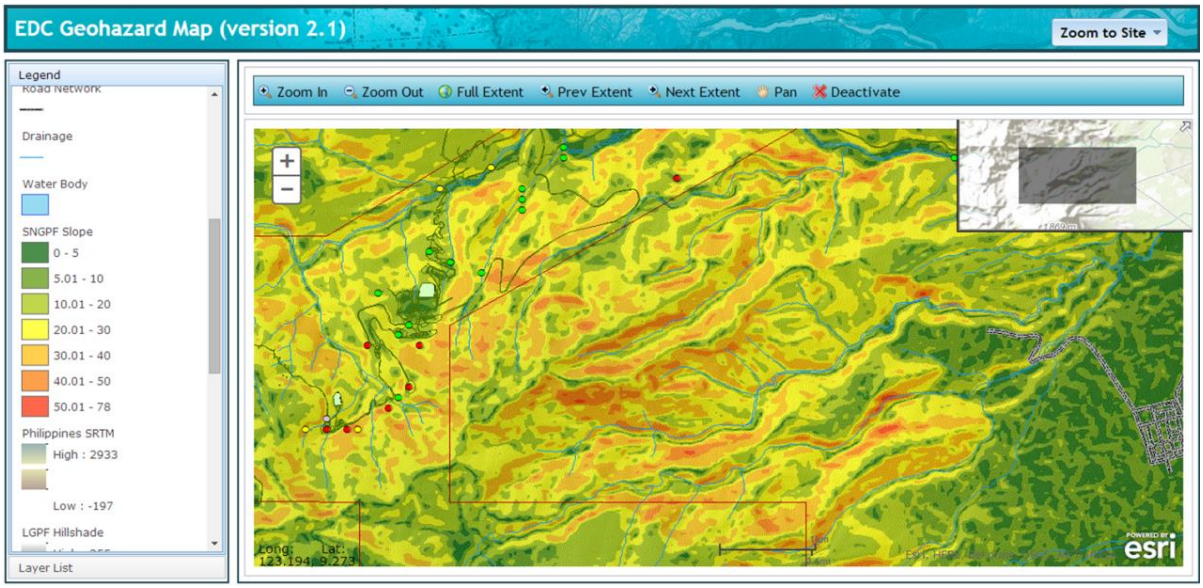


Figure 6: The example of GIS geohazard mapping from EDC Geothermal Philippine, this map produce comprehensive classification of hazard susceptibility area especially landslide (Marasigan & Olivar, 2015)

REFERENCES

Astisiasari, Van Westen, C., & Jetten, V. (2017), "Basic Overview Towards the Assessment of Landslide and Subsidence Risks along a Geothermal Pipeline Network". 6th ITB International Geothermal Workshop. Bandung.

H Yuhendar, A. W. (2016), "Slope stability analysis of landslide in Wayang Windu Geothermal Field, Pangalengan, West Java Province, Indonesia". Jakarta.

Hochstein, M., & Sudarman, S. (2015), "Indonesian Volcanic Geothermal Systems". World Geothermal Congress 2015. Melbourne, Australia.

Klemetti, E. (2018, July 12), "Could geothermal drilling cause an eruption?", Retrieved July 12, 2018, from Big Think: https://bigthink.com/eruptions/could-geothermal-drilling-cause-an-eruption

Kristianto, B., Gunderson , R., & Gunawan, A. (2013), "Geological Engineering for Hazard Assessment of Pad Awi-14, Salak Field, West Java, Indonesia". 13th Indonesia International Geothermal Convention & Exhibition 2013. Jakarta.

Lawless, J., & Browne, P. (2001), "Hydrothermal Eruptions Mechanisms and Implications for Prediction". New Zealand Geothermal Workshop 2001. New Zealand.

Marasigan , R., & Olivar, R. (2015), "Distributing Access to Geohazard Information Using Web GIS for EDC Geothermal Field Sites". Proceedings World Geothermal Congress 2015. Melbourne.

Natawidjaja, D., & Triyoso , W. (2007), "The Sumatran fault Zone – From Source to Hazard". Journal Earthquake and Tsunami Vol. 1.

Sektiawan, A., Prasetyo, G., & Patera, D. (2016), "Subsidence: Causes, Effects, and Mitigations in Geothermal Field". 5th ITB International Geothermal Workshop . Bandung.

Stehn, C. (1934), "Die Semivulkanischen Explosionen des Pematang Bata in der Soeoh-Senke", (Süd Sumatra) im Jahre 1933. No information.

The Headquarters for Earthquake Research Promotion. (2014), "Understanding Earthquakes". Japan: Secretariat Division of the Headquarters for Earthquake Research Promotion.

Utami, P. (2010), "High-Temperature Geothermal Area and Its Challenges for Civil Engineering Works". Development of Geotechnical Engineering in Civil Works and Geo-Environment, (pp. 1-2). Yogtakarta.

Wahjosoedibjo, A., & Madjedi, H. (2018), "Indonesia's Geothermal Development: Where is it Going?", 43rd Workshop on Geothermal Reservoir Engineering, (pp. 1-2). Stanford, California.

THE GEOLOGY AND GEOTHERMAL SYSTEMS OF THE MINAHASA DISTRICT, NORTH SULAWESI

Muhammad Sidqi and Pri Utami

Dept of Geological Engineering and Geothermal Research Center,
Faculty of Engineering, Gadjah Mada University
Jalan Grafika 2 Yogyakarta 55281
Email: sidqi.muhammadms@gmail.com, p.utami@ugm.ac.id

ABSTRACT

The Minahasa district is situated in a volcanic field of the north arm of Sulawesi comprising parts of the Sangihe volcanic arc, at the elevation range of from 687 m asl (Lake Tondano) to 1784 m asl (the summit of Mt. Soputan). The district has geothermal potential contained in several types of system. The economically developed geothermal potential for power generation is located in the Tompaso Field. The field is managed in a total project by PT Pertamina Geothermal Energy (PGE). This paper presents the results of our geological fieldwork aiming to better understand the geological framework of the geothermal systems in the Minahasa district and the association of the volcanoes with the occurence of different types of geothermal system. In general, the history of volcanism in Minahasa district - known from our field geological mapping and other relevant information - started since the volcanic activity of Mt. Kawatak, followed by the volcanic eruptions of Tondano, and later by eruptions forming many volcanic cones (e.g. Rindengan, Lengkoan, Wawona, Wowok, Matatumbak, Pinasuan, Luuk, Kanonang, etc.), Sempu volcanic dome, and Mt. Soputan that is still active. Consequently, geothermal systems with different degrees of "maturity" may occur in the Minahasa district. The low-relief terrain within the remnant of the Tondano Caldera is occupied by a hydrothermal system characterized by the discharge of boiling and near-boiling neutral-pH chloride hot springs in Tempang, Toraget, and Karumenga villages. The inferred volcanic-hydrothermal type system manifests in the form of solfataras with significant sulfur deposition, and steam-heated, acidic hot springs in Kanonang village (Bukit Kasih). It occurs in the high-relief terrain of the Rindengan volcanic complex. Effusive and explosive activities of Mt. Soputan show the existence of a hazardous, magmatic-geothermal system. The result of this study shall be followed up by more detailed work to quantitatively constrain the timing of volcanism and hydrothermal activities. When combined with the results of detailed analysis of the subsurface geoscientific data from the Tompaso geothermal field it will be a very good support to construct the development strategy of the geothermal potential in Minahasa.

Keywords: Minahasa district, North Sulawesi, geology, geothermal system.

INTRODUCTION

This paper present the results of our geological fieldwork aiming to better understand the geological framework of the Minahasa district and the association of the volcanoes with the occurence of different types of geothermal system. The geological fieldwork covered the mapping of volcanic rock units, the geological structures and volcanic features, as well as geothermal manifestations. It was also supported by remote sensing interpretation, and rock and minerals analyses, namely petrography and X-ray diffractometry.

FIELD OVERVIEW

Minahasa district is located about 60 km south of Manado, the Capital of North Sulawesi Province, at the elevations ranging from 687 m asl (Lake Tondano) to 1784 m asl (the summit of Mt. Soputan). The district has geothermal potential contained in several type of system. The economically developed geothermal potential for power generation is located in the Tompaso Field (Figure 1). Currently, the Geothermal Working Area (Wilayah Kerja Panas Bumi/ WKP) Lahendong – Tompaso managed by PT. PGE has 120 MWe installed capacity 2017. Until now, 14 wells have been drilled in Tompaso field to supplay the steam to the 2X20 MWe power plants. Tompaso field is expected to be further developed.

REGIONAL SETTING

Minahasa district is situated in a volcanic field of the north arm of Sulawesi comprising parts of the Sangihe volcanic arc (Hamilton, 1979). The volcanic arc is NE-SW trending, consisting of Mts. Ambang, Soputan, Lokon, Mahawu, Tangkoko. Ruang, Karangetang, and Mt. Awu, and extending to the volcanic islands in the north (Hamilton, 1979,

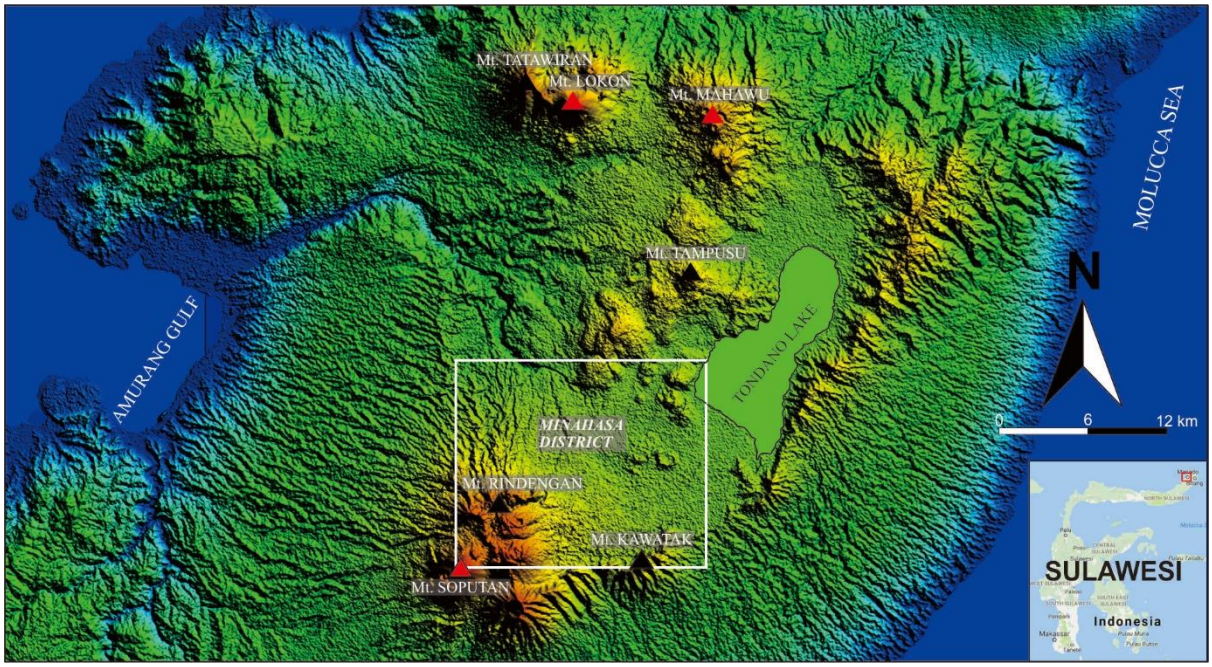


Figure 1. Location of Tompaso field at the northern arm of Sulawesi (modified from ASTER Global Digital Elevation Model of North Sulawesi).

; Kusumadinata, 1979). Verbeek (1908) and Kamerling (1925), cited from Ganda and Sunaryo (1982, in Utami, 2011), stated that the oldest known volcanic activity took place in the Lembeyan volcanic complex. The remnants of its volcanoes can be seen at the east of Lake Tondano (Effendi, 1976). According to Effendi (1976) the Lembeyan volcanic complex was active in Miocene, producing breccia, lava, and tuff.

The prominent volcanic structure in the area is the Tondano Caldera. Lécuyer et al. (1997) stated that Tondano Caldera is of tectonic controlled - caldera type with a size of 20X10 km^2, and formed by two eruption episodes. The first episode is characterized by the white rhyodacitic ignimbrites, the "Domato tuffs", and associated with formation of the older caldera rim. The second one is characterized by grey dacitic ignimbrite, the "Teras tuffs", and associated with formation of the younger caldera rim. The first eruption episode is assumed to take places in Pliocene because the ignimbrites lie on upper Miocene volcanic deposits. According to Kusumadinata (1979) the Tondano Lake occupies the caldera depression. The recent volcanism in Minahasa are marked by the activities of Mts. Soputan, Lokon, and Mahawu.

GEOMORPHOLOGY

In general, the topography of Minahasa district can be divided into high-relief terrain and low-relief terrain. Based on their morphogenetic, the identified morphological units are:

a. **Monogenetic Volcanic Cone**: Mts. Kanonang, Semelenduk, Sinopi, Matatumbak, Kokopit, Luuk, Wowok, Umeh, and Pinasuan.
b. **Volcanic Dome**: Mt.Sempu.
c. **Poligenetic Volcanic Cone:** Mt. Soputan and its parasitic eruption center (Mt. Aesoput), Mts. Kawatak, Rindengan, and Wawona.
d. **Volcanic Plateau**: the low-relief terrain around Tompaso and Langowan villages associated with the Tondano Caldera depression.
e. **Fluvial Plain**: the low-relief terrain at the southern and western sides of the Tondano Lake. This unit is formed by fluvial processes with the Tondano Lake as the local level of erosion.

VOLCANIC STRATIGRAPHY

The rock units in Minahasa area are dominated by Quaternary volcanic rocks (tuf, lava, bom, lapilli, and volcanic ash) and fluvial-lacustrine deposits that lie on Tertiary volcanic rocks (breccia, lava, and tuff) (Effendi and Bawono, 1997). Ganda and Sunaryo (1982, in Utami, 2011) stated that volcanic history of Minahasa can be divided into three episodes of volcanism, namely the Pre-Tondano, Tondano, and post-Tondano. Based on our observations on the spatial association between the volcanic products and eruption center, volcanic stratigraphy of Minahasa district can be divided into 28 volcanic sub-units (scale 1:75000) as shown in Minahasa district geological map (Figure 2).

Pre-Tondano unit

Consists of an autoclastic breccia, andesitic lava, and tuff that mapped into Kawatak autoclastic breccia and tuff and Maimbeng andesite lava formation on the southern and western part of Minahasa district.

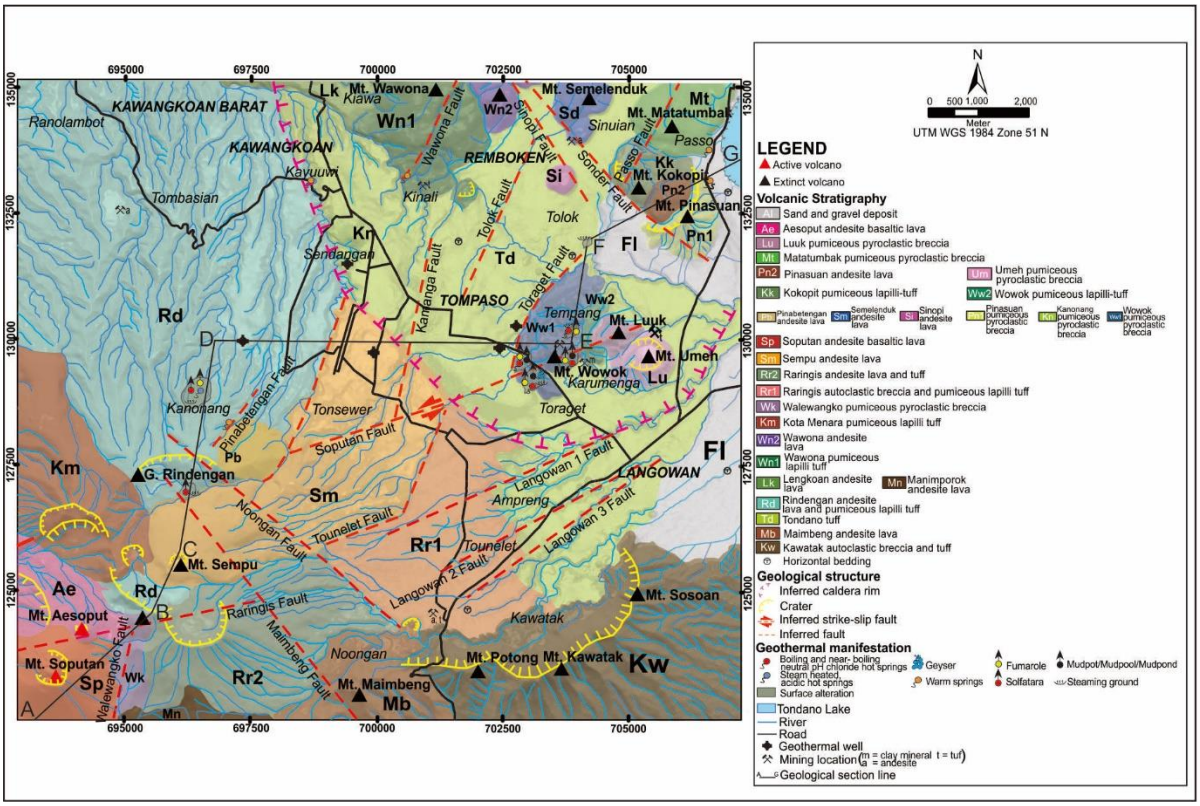


Figure 2. Geologic map of the Minahasa District showing the lithologies, geological structures, and thermal manifestations. Cross-section line for Figure 4 (A-B-C-D-E-F-G) is indicated.

Tondano unit

Characterized by Tondano tuff formation produced by Tondano eruptions. The Tondano tuff formation is consist of pumiceous tuff and lapilli-tuff. Based on K/Ar dates of pumiceous lapilli tuff from Toulimembet believed to represent the product of the Tondano eruptions by PT. Gondwana (1988) cited on Utami (2011), have an age of 0.871 ± 0.097 Ma or Lower Pleistocene. The formation is occupied the low-terrain area of Minahasa district.

Post-Tondano unit

Consists of pyroclastic rock (tuff, lapilli-tuff, and pyroclastic breccia) and andesite lava mapped into Rindengan andesite lava and pumiceous lapilli tuff, Lengkoan andesite lava. Manimporok andesite lava, Wawona pumiceous lapilli-tuff, Wawona andesite lava, Kota Menara pumiceous lapilli-tuff, Walewangko pumiceous lapilli-tuff, Raringis autoclastic breccia and pumiceous lapilli-tuff, Raringis andesite lava and tuff, Sempu andesite lava, Soputan andesite basaltic lava, Pinabetengan andesite lava, Semelenduk andesite lava, Sinopi andesite lava, Pinasuan pumiceous pyroclastic breccia, Kanonang pumiceous pyroclastic breccia, Wowok pumiceous pyroclastic breccia, Kokopit pumiceous lapilli-tuff breccia, Wowok pumiceous lapilli-tuff, Pinasuan andesitic lava, Umeh pumiceous pyroclastic breccia, Matatumbak pumiceous pyroclastic breccia, Luuk pumiceous lapilli-tuff, Aesoput basaltic andesite lava, and alluvial deposit.

Based on K/Ar age dating of andesite lava believed to represent the product of the Manimporok eruptions, the age of the Post- Tondano unit is 0.41 Ma or Middle Pleistocene (PT. Gondwana,1988, in Utami, 2011).

EPISODES OF VOLCANISM

The volcanic history of Minahasa district as revealed by our work integrated with the results of the previous workers, i.e., Ganda and Sunaryo (1982) and Lécuyer et al. (1997), is shaped by three episodes of volcanism, namely the Pre-Tondano, Tondano, and Post-Tondano.

The oldest known volcanic activity on Pre-Tondano episode is the volcanic activity of Mt. Kawatak, followed by the activity of Mt. Maimbeng. These were followed by the eruptions which produced the Tondano Caldera (Tondano episode).

The Post-Tondano episode was caharacterized by explosive and effusive eruptions forming the volcanic cones of Rindengan, Lengkoan, Wawona, Kota Menara, Walewangko, Raringis, Pinabetengan, Semelenduk, Sinopi, Pinasuan, Kanonang, Wowok, Kokopit, Umeh, Matatumbak, and Luuk, Sempu volcanic dome, and the active Soputan volcano with its parasitic eruption center, Mt. Aesoput.

These three episodes of volcanism give consequence of the occurrence of geothermal systems with

different degrees of "maturity" in the Minahasa district.

GEOTHERMAL MANIFESTATIONS

The thermal manifestations in the Minahasa district consist of boiling and near-boiling neutral-pH chloride hot springs (with or without silica sinter), and the steam-heated type manifestations. The neutral-pH hot springs (T = 70 – 90° C) manifestations are spatially associated with fumaroles ($T_{discharge}$ = 60 - 80° C), altered and steaming ground (T = 60 - 85° C at 40 cm depth), mudpots, mudpools, and mudpond.

The neutral-pH, chloride fluid type manifestations occur at Toraget, Tempang, and Karumenga villages. A geyser (T = 82 - 86° C) discharges intermittently at the Toraget village. The steam-heated type manifestations consist of fumarole (T= 70 - 90° C), solfataras (T ~ 96° C) with significant amount of sulfur deposit, acidic hot springs (T ~ 95 °), and altered, steaming ground (T = 70 - 90° C at 40 cm depth). These steam-heated and solfataric-type manifestations occur at Kanonang Village (Bukit Kasih thermal area) and on the flanks of Mt. Rindengan and Mt. Sempu. Steaming and altered ground also occur at Tolok village.

Several warm springs (T = 40 - 50° C) discharge at Pinabetengan, Kayuuwi, Kinali, and Passo villages. The common minerals found on the altered ground are kaolinite, residual silica, sulfur, alunite, aluminium sulfate, and in places, iron oxide.

GEOTHERMAL SYSTEMS

The emergence of geothermal systems in the Minahasa district is thought to take place after the formation of the Tondano Caldera.

The inferred time of the emergence of the geothermal systems in Minahasa district within the framework of the known geologic history of the north arm of Sulawesi region is shown on a diagram in Figure 3. Based on geothermal systems conceptual model by Hochstein and Browne (2000), at least three types of geothermal systems occur in the Minahasa district (Figure 4). These are:

a.Hydrothermal system
b.Volcanic-hydrothermal system
c.Magmatic geothermal system

a. Hydrothermal System

Hydrothermal-type geothermal system occupies the low-relief terrain inside the Tondano Caldera. It is characterized by the discharge of boiling and near-boiling neutral-pH chloride hot springs in Tempang, Toraget, and Karumenga villages. These manifestations mark the location of the upflow zone. Utami (2011) interpreted that rain started to provide adequate recharge fluid for the hydrothermal systems in Minahasa since 31 to 33 ka. This interpretation is based on the integration of paleoclimate data of Lake Tondano and surrounding by Dam et al. (2001) and the coupled atmosphere – ocean general circulation model by Bush and Philander (1997).

b. Volcanic-Hydrothermal System

This system occupies the high-relief terrain of the Rindengan volcanic complex at the western part of the Minahasa district. The volcanic-hydrothermal systems manifests in the form of solfataras with significant amount of sulfur deposit, fumarole, and acidic hot spring at Kanonang village (Bukit Kasih). The presence of the solfataric-type discharges suggest that the system may have some contribution of volcanic waters. The Kanonang thermal area is inferred to be the marker of the upflow zone of this type of system. However, further research such as gas geochemistry need to be conducted to prove or disprove this interpretation.

c. Magmatic Geothermal System

The hazardous, magmatic-type geothermal system is hosted by the Mt. Soputan active volcano. The heat and mass transfer from of this type of system is characterised by the explosive and effusive volcanic activities of Mt. Soputan and the Aesoput parasitic eruption center. Some solfataras discharge around the eruption vent.

CONCLUDING REMARKS

This paper shows that a comprehensive geological fieldwork covering geomorphology, stratigraphy, structural geology, and observation of thermal manifestation can guide us to discover the variety of geothermal types in a volcanic complex. Geological fieldwork using the concepts of volcanology and its relationship with the occurrences of geothermal systems can contribute in prioritizing the location for geothermal development in a large volcanic terrain.

The result of this study shall be followed up by more detailed work to quantitatively constrain the timing of volcanism and hydrothermal activities. When combined with the results of detailed analysis of the subsurface geoscientific data from the Tompaso geothermal field it will be an important knowledge to support the construction of the development strategy of the geothermal potential in Minahasa.

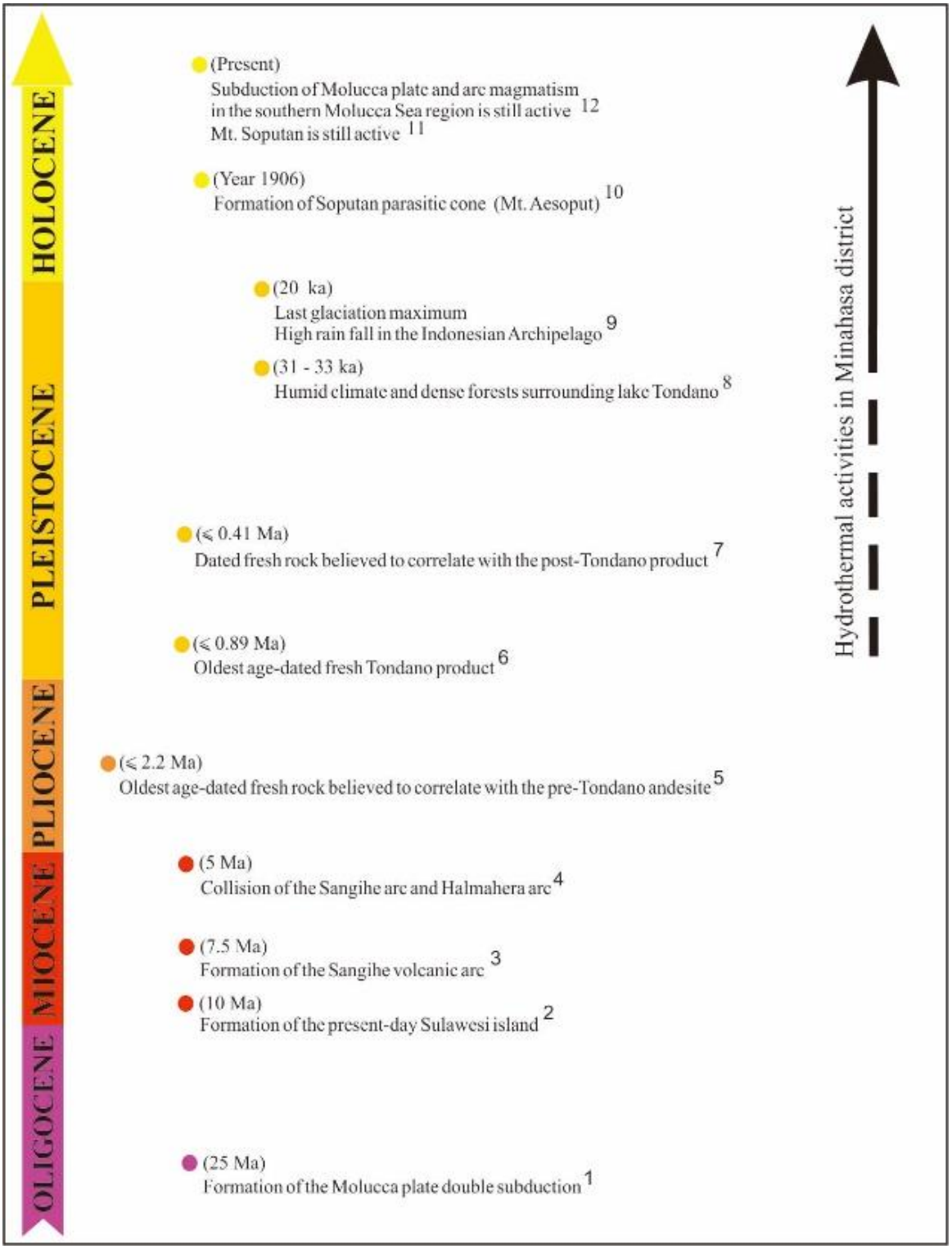


Figure 3. Diagram showing the inferred time of the emergence of the geothermal systems in the Minahasa district within the framework of the known geologic history of the north arm of Sulawesi region. References: 1 = Hall (1995), 2 = Hall (1997 in Utami, 2011), 3 = Pubellier et al. (1991), 4 = Hall (1995), 5 – 7 = PT. Gondwana (1988, in Utami, 2011), 8 = Dam et al., (2001, in Utami, 2011), 9 = Bush and Philander (1999, in Utami, 2011), and 10, 11 = vsi.esdm.go.id, 12 = Macpherson (2003, in Utami, 2011).

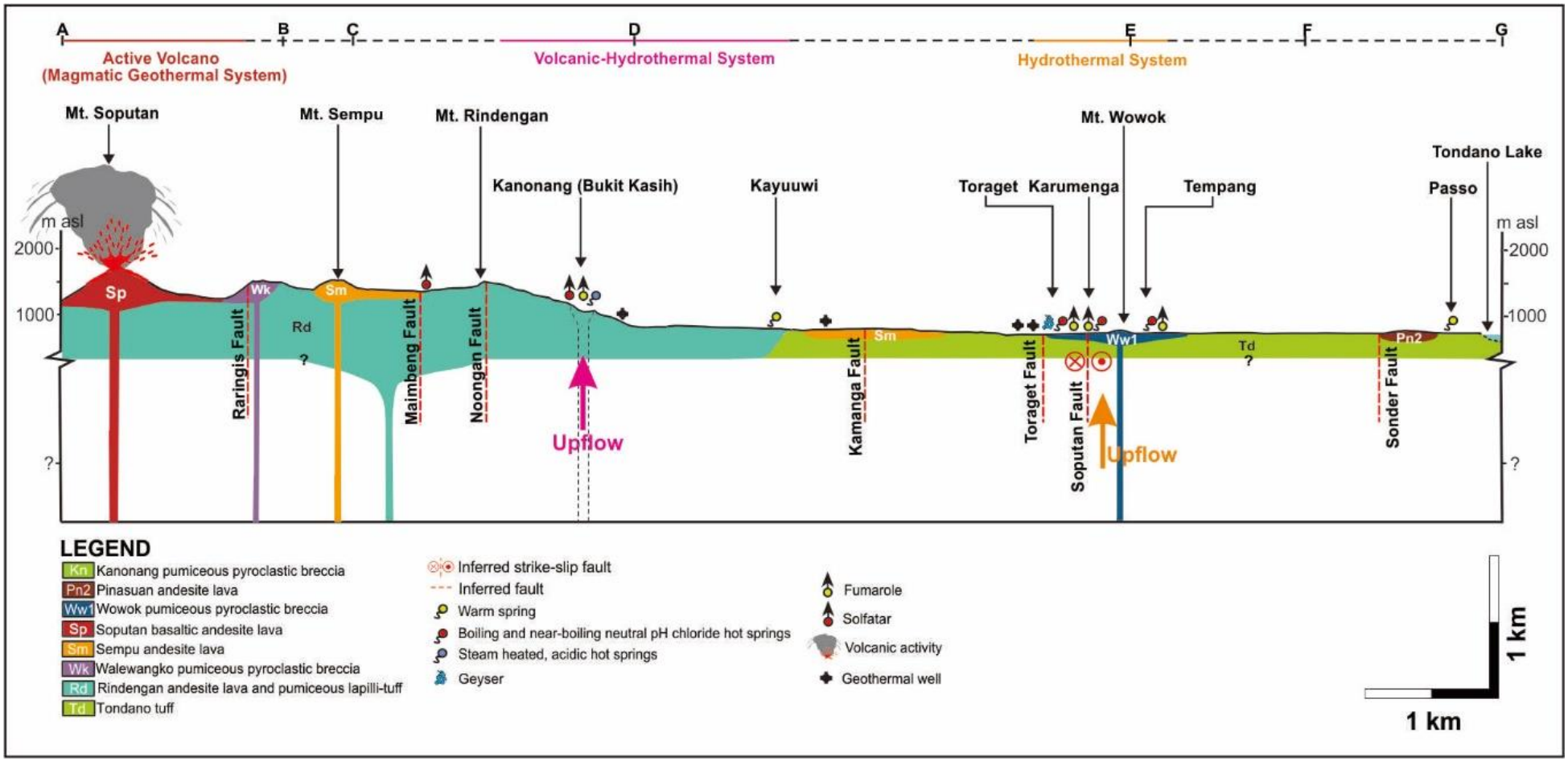


Figure 4. Conceptual model of geothermal systems in the Minahasa District.

ACKNOWLEDGEMENTS

The authors thank UGM – NZAID CaRED Program and Geothermal Research Center for partially funding this research. We sincerely thank PT. PGE Area Lahendong for the permission to access the Lahendong-Tompaso geothermal working area, and PT. PGE Area Kamojang for providing the facilities for the X-ray diffractometry analysis (XRD). Dr. S.H. Sarundajang kindly provided the first author a shelter in his Kawangkoan residence during the fieldwork session.

REFERENCES

Effendi, A.C., and Bawono, S.S., 1997, "Peta Geologi Lembar Manado, Sulawesi Utara, skala 1:250000", Pusat Studi Geologi, Bandung.

Hall, R., 1995, "Plate Tectonic Reconstructions of the Indonesian Region", Indonesia, 24th Indonesian Petroleum Association Association Annual Convention Proceedings, Jakarta.

Hamilton, W., 1979, "Tectonics of the Indonesia Region", Geological Survey Professional Paper, Washington.

Hochstein, M.P., and Browne, P.R.L., 2000, Surface Manifestations of Geothermal Systems With Volcanic Heat Sources, in Sigurdsson, H., Houghton, B., McNutt, S.R., Rymer, H., dan Stix, J., 2000, Encyclopedia of Volcanoes, Academic Press, San Diego.

Kusumadinata, K., 1979, "Data Dasar Gunungapi Indonesia", Direktorat Vulkanologi, Bandung.

Lécuyer, F., Bellier, O., Gourgaud, A., Vincent, P.M., 1997, "Tectonique active du Nord-Est de Sulawesi (Indonesie) et controle structural de la caldeira de Tondano", Academie des science Paris, Elsevier, Paris.

Pubellier, M., Spadea P., Pouclet, A., Solidum, R., Desprairies A., Cambray H., 1991, "Correlations of Tephras in Celebes and Sulu Sea Basins: Constraints on Geodynamics", Proceedings of the Ocean Drilling Program, Scientific Results, Vol. 124, Texas.

Utami, 2011, "Hydrothermal Alteration and the Evolution of the Lahendong Geothermal Sistem, North Sulawesi, Indonesia", Ph.D. Thesis, The University of Auckland.

Internet Resource:
http://www.vsi.esdm.go.id

HYDROTHERMAL ALTERATION MINERALOGY OF WELL MTB A, SOKORIA GEOTHERMAL FIELD, FLORES, INDONESIA

Haris Siagian, Dhani Sanjaya, Birean Sagala, and Jul Rafli

Geoscience Department, PT Sokoria Geothermal Indonesia – A project of KS Orka Renewables Pte Ltd
Recapital Building 5th Floor, Jl Adityawarman Kav 55, Jakarta Selatan 12160
Email: haris.siagian@ksorka.com

ABSTRACT

Sokoria geothermal prospect is located at Flores Island in East Nusa Tenggara Province, Indonesia. The preliminary geoscientific survey (geology, geochemistry and geophysics) and additional MT resistivity survey were completed in 2016. KS-Orka carried out advance MT resistivity survey to get better understanding of the Sokoria geothermal system and to provide assistance for well targeting. Geologically, the main prospect is consisting of quaternary rock of breccia, andesite and tuff. The Sokoria prospect is situated within the large collapse features and Lowongopolo Fault as a major fault trends NNE to SSW then divided onto several fault segments. Four of the exploration well namely Pad A was spudded in lately 2017. Generally, the wells encountered interstratified of tuff, breccia and andesite. The rocks may part of the Mutubusa, Kelinabe and Old Sokoria products. The alteration minerals are smectite, chlorite, illite, quartz, calcite, anhydrite and epidote. There are 3 (three) types of alteration identified, which are: argillic, phyllic, and propylitic. The permeability evidence was marked by the deposition of alteration minerals in veins, such as quartz, pyrite, chlorite, calcite and epidote. Those minerals coincide with the presence of circulation losses during drilling, increased of partial circulation losses and total circulation losses experienced around from -150 m MSL and -350 m MSL.

Keywords: Sokoria, alteration, well MTB A

INTRODUCTION

Sokoria is the second geothermal field of KS-Orka project in Indonesia to being developed for electricity generation, which is currently still in the exploration stage. The Flores island has two developed geothermal fields where are also close to Sokoria geothermal field, namely Ulumbu and Mataloko (PT. PLN, 1995). The late Quaternary volcanism is located on the south side of Flores with eight active volcanoes over the 500 km length (West to East) including Keli Mutu volcano which Sokoria geothermal project is located (Harvey et al., 1989). The appearance of fumaroles at moderate to high elevations and association with active volcanoes are the main indicators for the presence of high quality geothermal systems.

High temperature hydrothermal system is likely centered beneath the Keli Mutu volcano with a vapor-core system is suspected based on geologic and geochemistry assessments, a well target on the flanks of the volcano is recommended. The acid system is separated from the neutral system by an impermeable rind of anhydrite and silica deposition that reduces permeability where the incompatible neutral and acid fluids mix. The Lowongopolo Fault appears to segregate fluid into a more acid influenced area to the east and a less acid influenced area to the west. It is also possible that a probably separate resource exists to the east but the geochemistry and discontinuous claycap would make such a target high risk.



Figure 1: The map shows location of Sokoria near with Mataloko and Ulumbu geothermal fields.

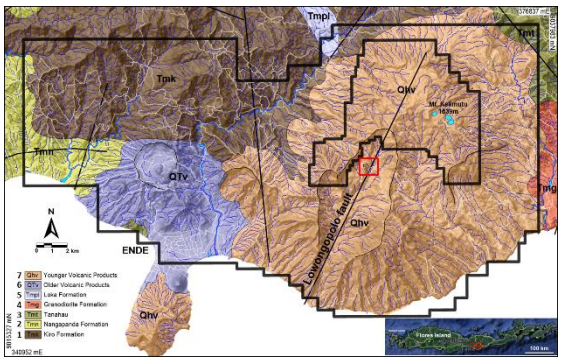


Figure 2: Sokoria concession area (black line) and wellpad area (red line) overlay on regional geology (Suwarna, 1989).

Four exploration wells have been drilled since lately 2017. The wells are encountered the three-rock formation which are Mutubusa volcanic, Kelinabe volcanic and Old Sokoria volcanic products. The average depth of the directional wells drilled is about 1925 mMD to 2072 mMD. The last wells in this prospect are big-bore wells. Subsurface hydrothermal alteration such as alteration mineralogy, alteration zone, feed zone and paragenesis will be discussed in this paper. Until this

paper is published, still waiting for laboratory analysis of XRD and petrography.

SURFACE GEOLOGY

The geology and the formation of the Sokoria geothermal prospect generally can be explained as follows. There are three groups of formation, from oldest to younger; Old Sokoria Volcanic, Kelinabe Volcanic and Mutubusa Volcanic. The surface formations are composed of predominantly andesitic lava flows and associated pyroclastic and lahar deposits. Those rocks well exposed along roads cut to wellpad area and surrounding inside of rim caldera collapse area (Robertus et al., 2007).

Surface hydrothermal alteration zones are also appeared such as Mutubusa fumarole area, on a long road cut nearby gradient well and along road cut on the way from Loworia river to Namulaka village or east part of inside rim caldera collapse. The alteration zones spread out irregularly from SW to SE direction extending about 2000 meters long. This alteration zone is characterized by intensive argillization, where fumarole (acidic steam heated fluids, up to 97 °C) and warm spring (34 °C) neutral pH are distributed. In addition, a number of alteration minerals such as sulfur quartz, pyrites and clay minerals are identified.

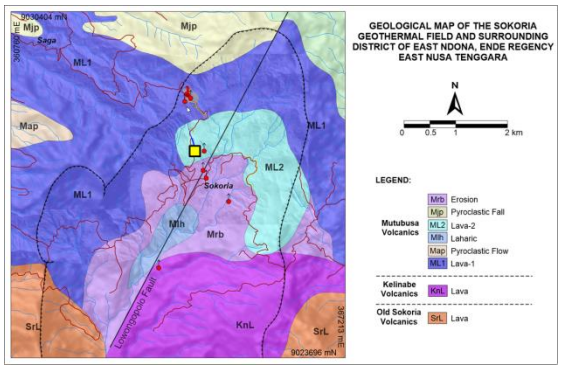


Figure 3: Location wellpad MTB A (yellow) inside rim caldera collapse and near Lowongopolo fault, overlay on geologic map of Sokoria

EXPLORATION ACTIVITY

The geology of Sokoria Geothermal Prospect consists of the quaternary rock volcanic with predominantly andesitic lava flows and associated pyroclastic and lahar deposits, which is especially found in near southwest section of Keli Mutu volcanic complex.

The study area is also characterized by structurally controlled large collapsed features, that elongates NE-SW with fault scarp in the SW is inferred to be a relict caldera structure of the oldest volcanic in Sokoria. The collapse sector coincides with the trace of a major fault which runs NNE-SSW from the coast passing through Sokoria and stretches further N-NE beyond the concession area. This structure termed Lowongopolo fault apparently controls Lowo Ria - the main river system in Sokoria. The Lowongopolo fault zone is actually segmented and has several conjugate fractures or splays. The main trace of this fault exhibits normal displacement. The northern segments have splays that appear to have cut and displaced relatively smaller WNW-ESE to E-W trending structures in a left-lateral motion. The observed cross cutting relationship suggests that NNE-SSW to NE-SW structures are relatively younger. Permeability along this fault is manifested by the presence of several thermal springs and altered grounds located along or adjacent to its trace.

Based on the integrated data among the geological, geochemistry and geophysics data from CGG Electromagnetics (2016), the Sokoria geothermal system is belong to the hot water dominated system. The movement of hydrothermal fluid is mainly controlled by the NNW-SSE and NNE-SSW fault pattern with the top of the reservoir about ≥ 850 m depth.

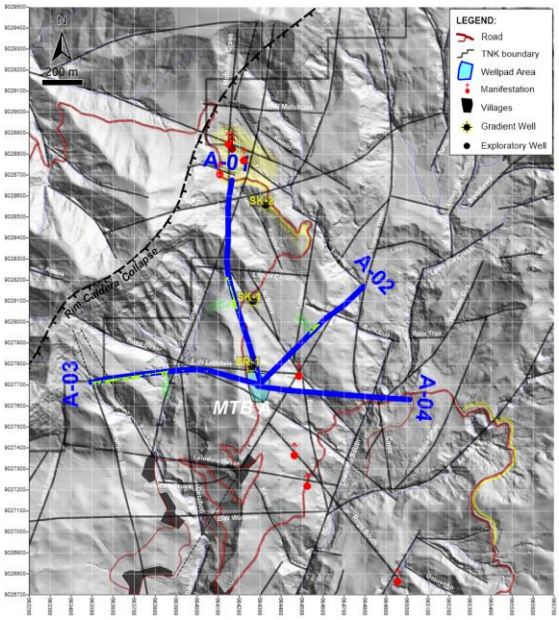


Figure 4: Four wells at MTB A wellpad overlay on detail geologic structure.

Four exploration wells were drilled in the location. The result of four drilled wells is used to give a better picture of the direction of the geothermal system, temperature distribution and permeability of prospect. The difference of the temperature distribution and the permeability of the wells is generally displayed through the drilling data such as mineral distribution, vertical distribution of the clay minerals, P and T profile and the well test (Filtech Energy Drilling, 2016).

The result of the drilling of MTB A wellpad and the concept of the drilling target trending around inside

rim caldera collapse and near Lowongopolo fault. The lineament pattern along manifestation appearance with conductive layer opened relative to NW offers the priority target for developing the prospect.

BOREHOLE GEOLOGY

Lithology

Generally, the geology of the well is composed of interstratified rocks among andesite, tuff breccia, lithic and crystal tuff. In the depth ranging of near surface to about 600 – 700 mVD, the formation is observed as dominantly tuff breccia interstratified by andesite lava and lithic tuff. Below 700 mVD, the formation consists of altered lithic tuff interstratified by altered crystal lithic tuff and small unit of tuff breccia.

Lithologic Column	Rock Unit and Type	Thickness (m)	Age (Ma)	Geothermal Significance
	Mutubusa volcanic: interlayered lava & pyroclastic, consist of lithic tuff, tuff breccia, andesite, dacite and rare basalt	700	Not yet determinated, Holocene	Cap Rock
	Kelinabe volcanic: dominantly pyroclastic altered, consist of lithic tuff and crystal lithic tuff	300-500	0.36 (K-Ar)*, Late Pleistocene to Early Holocene *Abbott & Chamalaun, 1978; 1981	Shallow Reservoir
	Old Sokoria volcanic: contact of altered pyroclastic rocks, consist of lithic tuff – tuff breccia, andesite breccia altered	≥ 700	Not yet determinated, Pleistocene	Deep Reservoir

Figure 5: Simplified subsurface stratigraphy of the Sokoria geothermal field.

These rock units are part of the Mutubusa volcanic formation in the upper part and Kelinabe volcanic formation in the below part and then some part as reservoir rock. The Old Sokoria volcanic formation as the main reservoir rock with characterized by altered lithic tuff interstratified by altered andesite tuff breccia and few altered andesite. So far it is also very important to be a rock reservoir near the exploration target.

Primary Mineral

Based on the rock formation of the well, the rocks unit in the prospect is composed of interstratified rocks among andesite, tuff breccia, lithic and crystal tuff. Some depth was recognized the appearance of andesite tuff breccia. Some alteration minerals were observed as replacement of primary rocks and minerals. Started at depth of 120 mVD, chlorite commonly replaces glass in the andesite and tuff breccia. Plagioclase is altered to quartz, calcite and smectite observed at depth of 300 mVD. Started at depth of 1000 mVD, plagioclase is replaced to epidote. Pyroxene is altered to chlorite at depth of 400 mVD and at depth of about 1000 mVD pyroxene is replaced by epidote.

Hydrothermal Alteration Mineral

The formation of hydrothermal minerals is affected by temperature, pressure, parent rock types, reservoir permeability, fluid composition and duration of activity (Browne, 1978). The alteration minerals observed are smectite, chlorite, illite, quartz, calcite, anhydrite, and epidote (figure 8 to 11). The hydrothermal alteration mineralogy of the well is explained as follows:

Chlorite. Chlorite is found started at depth of 120 mVD and increasing from 400 mVD. Commonly replace plagioclase as phenocryst, then replace plagioclase and glass as matrix.

Quartz. Quartz increased from 700 mVD. Commonly, it is found as replacement of glass matrix in tuff, feldspar and filling in the vein of andesite and tuff breccia.

Calcite. Calcite is found continuously started at shallow depth to total depth (TD), increasing around 400 – 900 mVD. Calcite is commonly replacing plagioclase as phenocryst, sometimes filling as veinlets.

Smectite. Smectite is difficult to identified by microscopic, physically high swell clay content with high MeB index (figure 6). Smectite increasing around 200 – 400 mVD.

Illite. Illite is found continuously started after decreased of smectite clay, increasing from 550 – 600 mVD to total depth (TD). Illite is commonly speck form and replacing plagioclase.

Anhydrite. Anhydrite is observed uncontinously in the well started at 900 mVD, according to rock pH analysis have normal pH 7-8. Anhydrite is commonly found as replacement of phenocryst and sometimes filling vein and observed coincide with appearance of sulphide minerals.
Epidote. Epidote appears as r
eplacement of plagioclase and as vein fillings. The relict epidote observed near surface at 228 mVD. Epidote is observed and increased from 1000 - 1100 mVD as replacement and vein fillings, but slightly different in existence at well A-03 at depth 1200 mVD.

Pyrite. Pyrite increased from 700 – 800 mVD. Pyrite is commonly disseminated, cubical form and as veining.

Alteration Zones

Four well currently drilled on wellpad MTB A Sokoria have provided an overview of the state of a commercial reservoir temperature, typical high temperature geothermal system. This has impact on the existence of alteration mineral assemblage, from surface to around 700 mVD encountered low

temperature hydrothermal alteration with typical Argillic, and then more deeply encountered typical Phyllic alteration as a transition zone between Argillic type to a high temperature hydrothermal alteration typical Propylitic which is expected as a reservoir section with a commercial temperature.

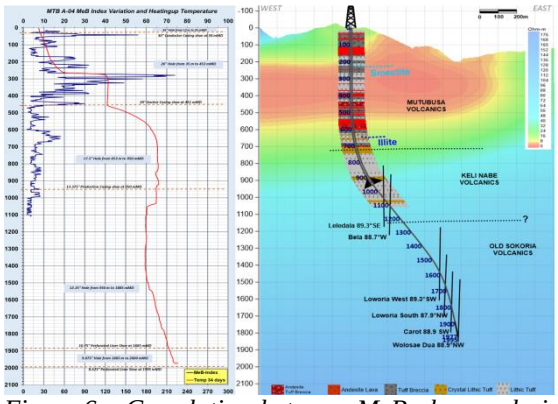


Figure 6: Correlation between MeB clay analysis with heating-up temperature and low resistive layer MTB A-04 well.

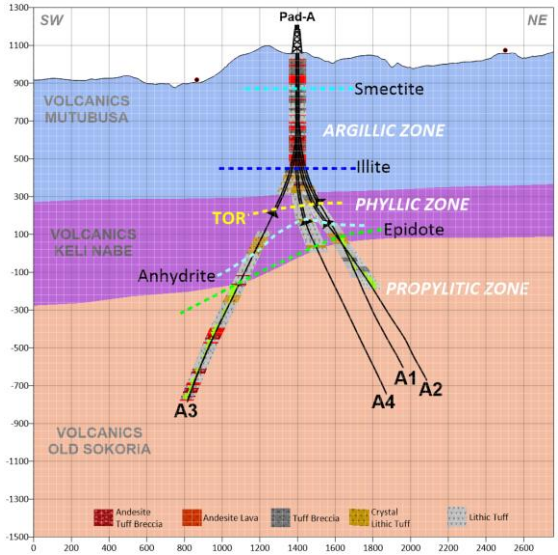


Figure 7: Well profile showing alteration-mineralization type and geologic stratigraphy.

Phyllic alteration. Transition zone which Phyllic alteration assemblage characterized by dominant illite with increasing pyrite and quartz, then appearance of anhydrite as main distinguishing with Argillic type. The anhydrite mineral normally abundant in permeable zone especially where acid and neutral fluids mix. The presence of anhydrite mineral indicated environment of formation is slightly acid with pH ranges from 5 – 6. Phyllic alteration zone was intercepted at depth in ranges of around 600 – 1100 mVD with average thickness is 500 m.

Propylitic alteration. Occurring at reservoir section, typical Propylitic alteration mineral assemblage develops and characterized by appearing of epidote minerals, increasing chlorite coincide with appearance of quartz, calcite, pyrite, illite and anhydrite. The propylitic zone is expected a commercial high temperature reservoir zone as a target in exploration drilling campaign. The increasing epidote mineral identified from cutting in A-01 well is shallower at depth of 1000 mVD, A-02 well is at depth of 1150 mVD, A-03 well is deeper at depth of 1220 mVD, but it is not appeared at well A-04 due to TLC. The appearance of mineral epidote is a high temperature diagnostic mineral >220°C (Lagat after Reyes, 2010) common used to estimate temperature of a formation at depth. Therefore, estimation of temperature at the bottom of the well is ≥230°C. Zonation of alteration mineral assemblages is shown geological well profile in figure 8.

Feed Zones

The identification of the permeability during drilling is usually marked by the encountered of total circulation loss and drilling break, then commonly associated with fracture, fault, joint, formation contact, etc. It is also observed by the appearance of some alteration mineral that commonly fillings in the veins or vesicles such as quartz, anhydrite, pyrite, calcite and epidote.

The permeability zone identification during drilling and after drilling is also important to identify the presence of permeable zone, such as the pressure and temperature survey, spinner survey, completion test, etc.

Common minerals in this well that found as fillings in veins are quartz, calcite, anhydrite, chlorite, epidote and calcite. These minerals are associated with lava and pyroclastic formation. Veining commonly develop below ≥1000 mVD after intersect reservoir zone, typically brecciated and sheared with milky and drussy textures of quartz.

Based on the drilling result, the permeability indication in the well is marked by encountered partial circulation losses started around 500 mVD and total circulation losses that started from 1150 mVD. The target is interpreted to have correlation with the geological structure trending relative North to South that created some permeability as flow path for geothermal fluid.

Paragenesis

The depositional mineral is important to recognize in order to understand the series of formation of mineral in geothermal system then to describe the history of the field. The paragenesis in the well is commonly found as replacement and veins fillings. Successive stages of mineralization process such as replacement or precipitation reflect the paleo-geothermal, present hydrothermal activities and environmental conditions where the water rock

interaction occurs. Every field has different character and sequence. The sequences could vary from single to very complex series.

In well MTB A Sokoria, the paragenesis is analyzed in some depth of cutting sample through microscopic analysis. The alteration mineral depositional sequence of the well was observed as follows: low temperature of smectite clay was found earlier, then altered to chlorite with relict epidote at depth around 200 – 400 mVD. Illite, quartz and pyrite mineral ware increased and observed round 600 – 1100 mVD. Some depth of well also shows that appearance of anhydrite and first epidote around 900 mVD.

CONCLUSIONS

- The Sokoria Geothermal systems is liquid dominated reservoir, with top of reservoir around ≥850 mVD.
- There is limited data for the analysis of hydrothermal alteration in detail, requiring petrography and XRD analysis for further research
- The alteration minerals that observed in the well are smectite, chlorite, illite, quartz, pyrite, anhydrite and epidote.
- The hydrothermal alteration zones are divided by three zones which are argillic alteration zone near surface to 400 – 500 mVD and propylitic alteration zone occurs from around 1000 mVD then deeper at relative Southwest prospect area.
- The minerals indicating as good permeability in the well appearance of epidote and coincide with increasing of quartz, chlorite, illite, calcite.

REFERENCES

Browne, P.R.L. (1978), "Hydrothermal alteration in active geothermal systems," *Annual Review of Earth and Planetary Sciences 6*, 229-250.

CGG Electromagnetics and PT Tunggal Buana Utama. (2016), "3D Modeling of Magnetotelluric (MT) Survey in Sokoria East Nusa Tenggara, Indonesia," KS-Orka Company internal report.

Filtech Energy Drilling Corp. (2016), "Due Diligence: Sokoria Geothermal Prospect, Indonesia," KS-Orka Company internal report.

Gunderson, R., Cumming, W., Astra, D., Harvey, C.C. (2000), "Analysis of Smectite Clays in Geothermal Drill Cuttings by The Methylene Blue Method: for Well Site Geothermometry and Resistivity Sounding Correlation," *Proceedings World Geothermal Congress, Japan*.

Harvey, C.C., Gunderson, E.B., Johnstone, R.D., Christyono. (1998), "Sokoria, East Indonesia: A Classic Volcano-Hosted Hydrothermal System," *Proceedings 20th New Zealand Geothermal Workshop*.

Harvey, C.C., Gunderson, R., Cumming, W. (2000), "Methylene Blue Adsorption: A Real Time Rig Geologist Tool for Estimating Geothermal Reservoir Temperatures and Forecasting Drillhole Stability Problems," *New Zealand Geothermal Workshop*.

Lagat, J. (2010), "Hydrothermal Alteration Mineralogy in Geothermal Fields with Case Examples from Olkaria Domes Geothermal Field, Kenya," *Short Course V on Exploration for Geothermal Resources, UNU-GTP, GDC and KenGen, Kenya*.

PT PLN (PERSERO). (1995), "Studi Geosains PLTP Mini Sokoria, Ende, Flores, NTT", Laporan Akhir, Volume 2.

Robertus, S.L.S, Rezky, Y., Munandar, A., Suparman (2007), "Geologi dan Ubahan Hidrotermal Sumur Eksplorasi SR-1 Lapangan Panas Bumi Sokoria-Mutubusa, Ende, Nusa Tenggara Timur," *Proceeding Pemaparan Hasil Kegiatan Lapangan dan Non Lapangan Tahun 2007 di Pusat Sumber Daya Geologi, Bandung*.

Suwarna, N., Santosa, S. and Koesoemadinata, S. (1989), "Geological map of the Ende quadrangle, East Nusatenggara". Geological Research and Development Centre, Bandung.

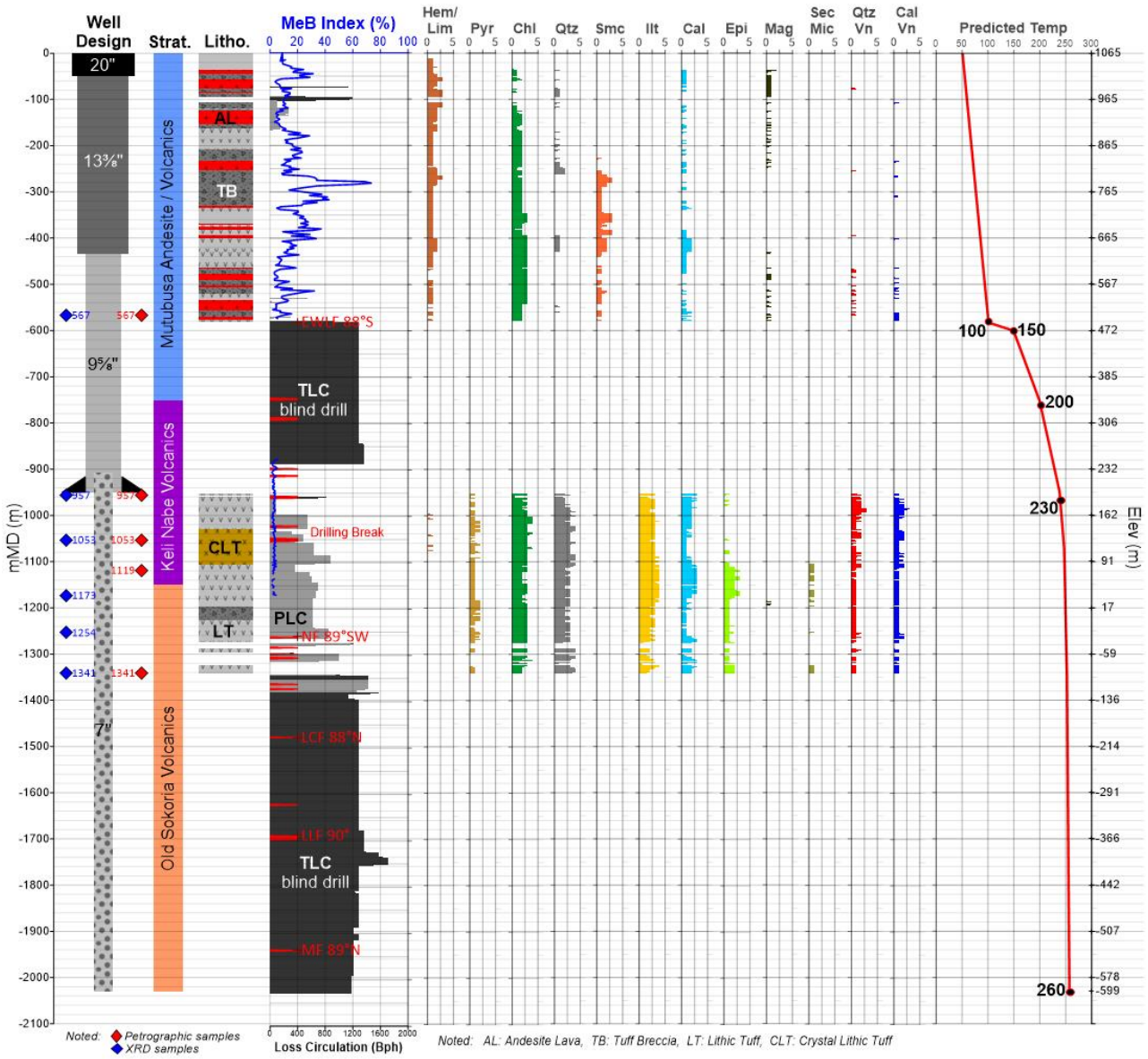


Figure 8: Composite log of MTB A-01 showing lithology, loss circulation, MeB graph and alteration mineral.

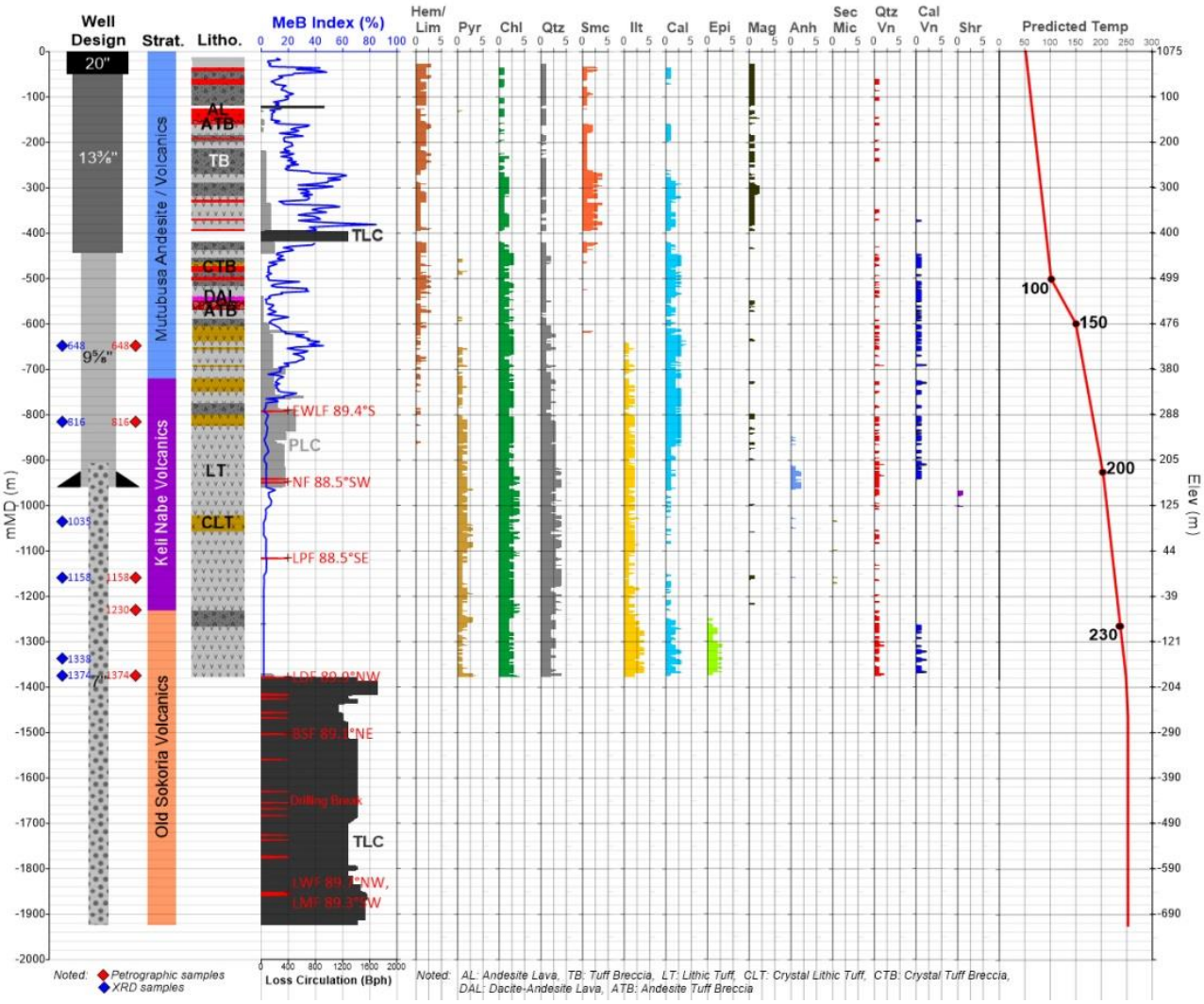


Figure 9: Composite log of MTB A-02 showing lithology, loss circulation, MeB graph and alteration mineral.

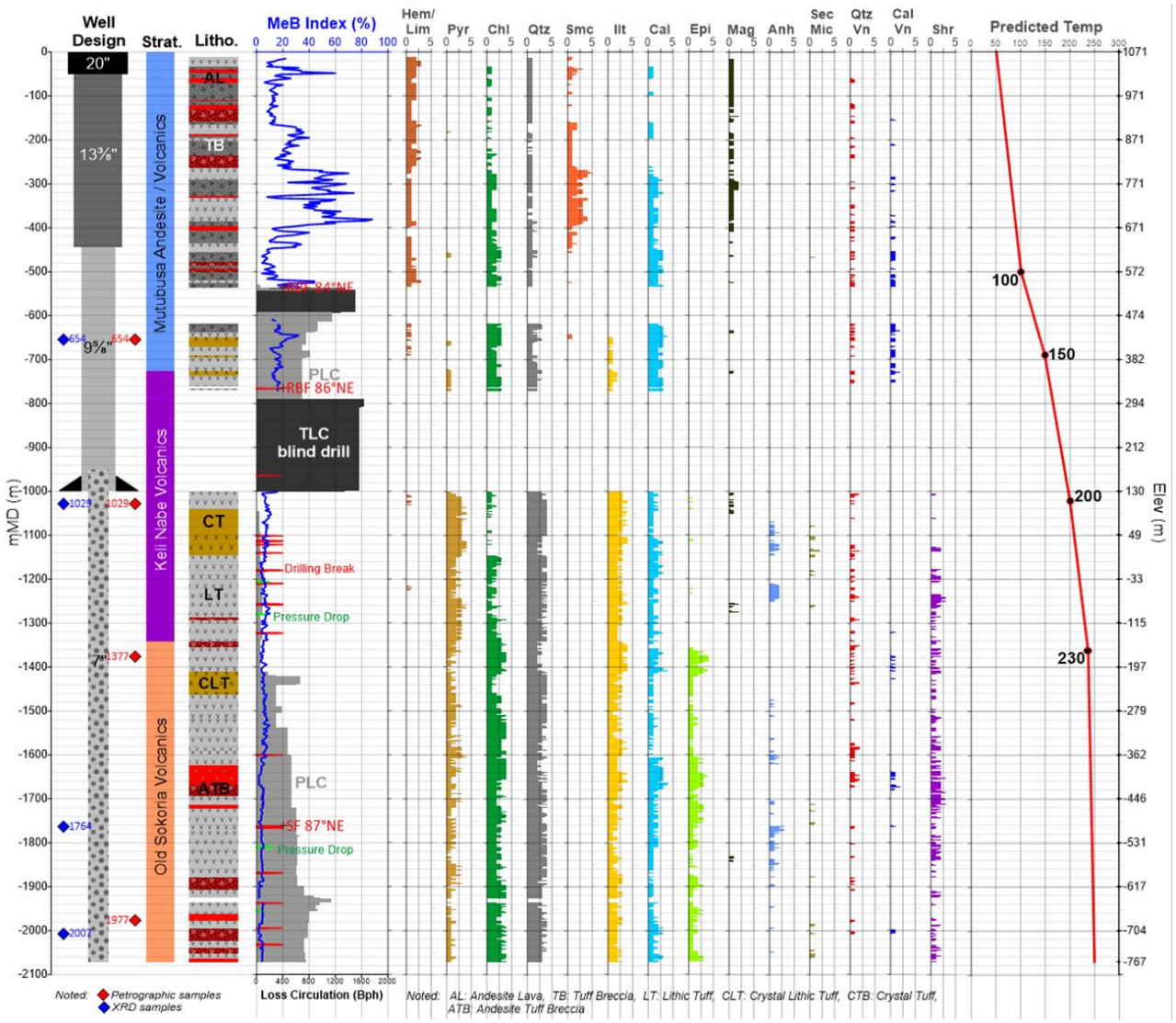


Figure 10: Composite log of MTB A-03 showing lithology, loss circulation, MeB graph and alteration mineral.

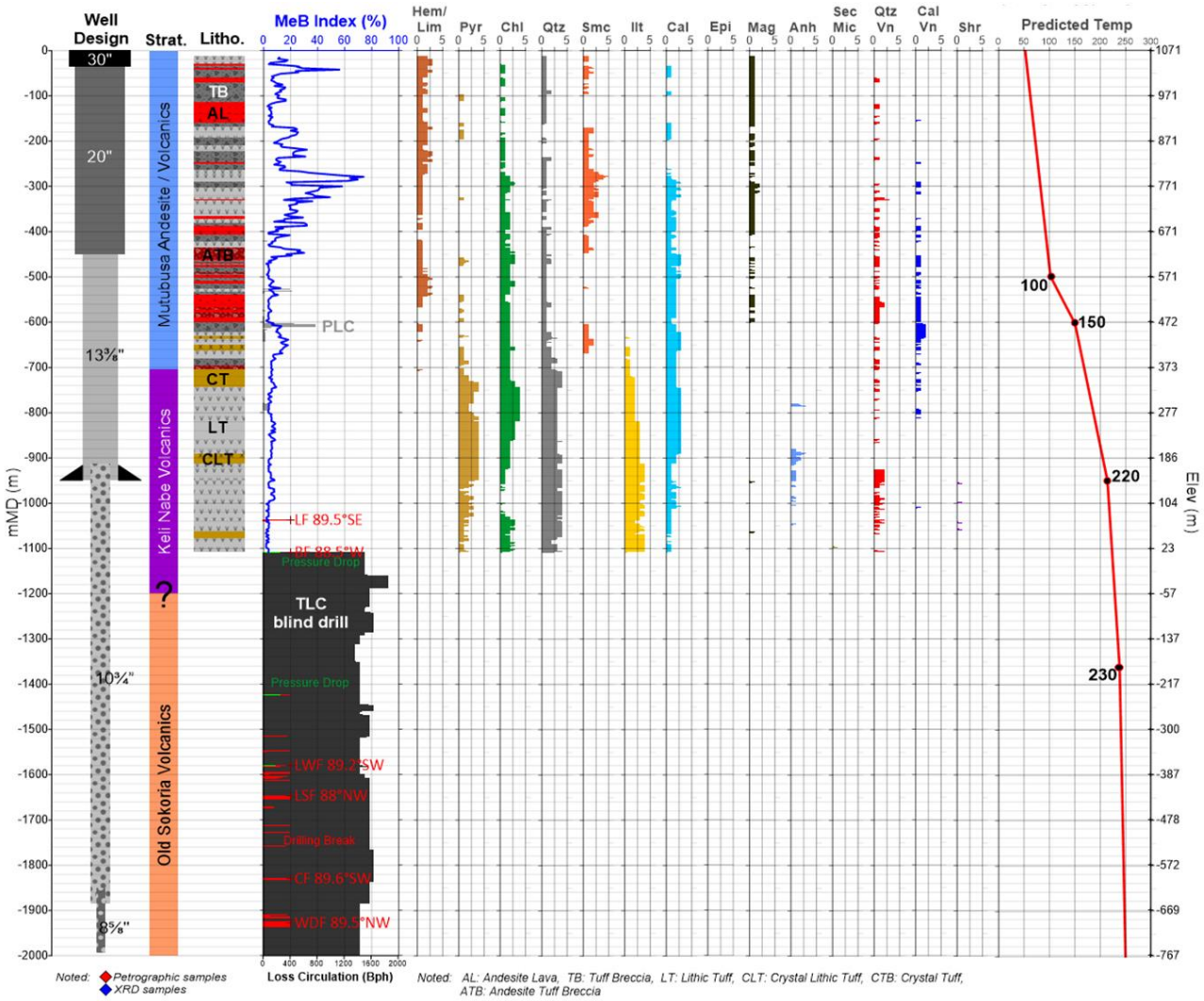


Figure 11: Composite log of MTB A-04 showing lithology, loss circulation, MeB graph and alteration mineral.

THE IMPORTANCE OF PREDICTING AND EVALUATING FAULT INTERSECTIONS IN EXPLORATION AND DEVELOPMENT DRILLING AT SORIK MARAPI GEOTHERMAL FIELD

R. Hendry[1], R. Hidayat[1] , A.C. Licup, Jr.[1], V.R. Chandra[1], S. Nasution[1], and X.L. Omac[2]

[1]PT Sorik Marapi Geothermal Power
[2] Filtech Energy Drilling Company
Email: ridha.hendry@ksorka.com; ryan.hidayat@ksorka.com; armando.licup@ksorka.com; vicky.chandra@ksorka.com; syukri.nasution@ksorka.com; omac.xl@gmail.com

ABSTRACT

Permeability is one of the essential elements of geothermal systems. Thus a clear understanding of permeability is of utmost importance for a successful exploration and development drilling and resource management. In general, the permeability in andesitic volcano-hosted geothermal fields – which are prevalent in Indonesia - are associated with major fault networks. On this regard, comprehensive fault analysis is required for good well trajectory planning and make important decisions during drilling. A good structural analysis is necessary in evaluating reservoir processes during production. One of powerful methods that can be used for fault evaluation is the aerial mapping technique. This exploration method had been used to identify and analyze fault lineaments at the Sorik Marapi Geothermal Project (SMGP). The aerial map used for delineating the faults in SMGP is the Light Detection and Ranging (LiDAR) surface analysis.

LiDAR had been used in Sorik Marapi Geothermal Field that covers 4 potential resource areas - Sibanggor, Roburan, South Sampuraga and Sampuraga sectors. Geological structure mapping through LIDAR analysis was performed to identify surface structural lineaments.

The resulting structural map is the primary basis to estimate well-fault intersections used in designing well trajectories and preparing geological prognosis. During drilling, the fault intersection can be interpreted through megascopic analyses of drill cutting samples and evaluation of drilling parameters. The on-site well-fault intersection evaluation by the geologist is an essential factor in assessment of hole condition and making crucial drilling decisions, especially is pinpointing casing points. After well completion, a detailed fault intersection analysis to establish fault attributes is performed by comparing with the result of completion test, heat-up and flowing downhole measurements.

Comparison between the predicted fault intersection using LiDAR analysis and actual well data (i.e., geology, drilling and well measurements) shows reasonable consistency and has contributed significantly to the success of exploration and development drilling in SMGP. The fault information will also be relevant for the future reservoir management to help explain the reservoir processes during steam production and reinjection of separated waters.

Keywords; Sorik Marapi, exploration, drilling

INTRODUCTION

The Sorik Marapi Geothermal Field is located about 650 km south-southeast of Medan, the capital city of North Sumatra province (Figure 1) and situated within the administrative area of Mandailing Natal district. Sorik Marapi Geothermal Power (PT.SMGP) was awarded with the geothermal concession that covers an area of approximately 629 $km^{2.}$ The Sorik Marapi geothermal area is recognized throgh the existence of surface manifestations such as fumaroles and hot springs. The thermal area lies within a depression zone which is a part of pull-apart basin caused by the displacement of Sumatran Fault Zone. The geothermal field is hosted by networks of criss-crossing synthetic and antithetic geological structures. Thus the challenge of drilling production wells in Sorik Marapi lies on intercepting permeable structures at depth. The purpose of this paper is to discuss the importance of predicting and evaluating fault intersections particularly in Sibanggor area - the focus of the initial phase of geothermal power development.



Figure 1. Concession Boundary of Sorik Marapi Geothermal Project

Regional Geology

In General, the Sorik Marapi geothermal area is a part of Western Bukit Barisan volcanic range which extends along the length of Sumatran island. This zone forms a volcanic range separated by graben from the late Mesozoic meta-volacanics and meta-sedimentary which was covered by volcanic sediment of Miocene age. It was then overlain by the quaternary volcanic rocks made up of andestitic to dacitic pyroclastics and lava.

The active Sumatra fault zone runs through the whole length of Sumatra, within the Bukit Barisan, from Banda Aceh to the Sunda Strait, and is paralleled by a line of quaternary volcanoes. The overall shape of Sumatran Fault is sinusoidal, the northern half of which is gently concaved to SW, whereas the southern half is concaved to NE. In Sorik Marapi, there is an irregularity in the fault geometry termed "bifurcation". The Bifurcation started near Sibual-buali and Lubuk Raya towards the Southeast into two principal active strands (Figure 2). The two strands are separated from each other (*Natawidjaja, 2000*). The western branch of bifurcation does not rejoin the eastern branch which continued toward the southeast of Sumatra.

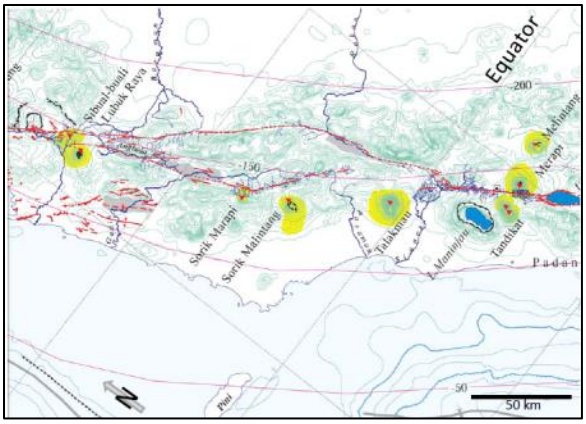


Figure 2. *Map of the Sumatran Fault Zone (In red) in the vicinity of Sorik Marapi Volcanic craters and cones are shown in yellow. Contours in red are the top the Benioff-Wadati zone. Detail from Sieh& Natawidjaja,2000*

The Sibanggor area of Sorik Marapi geothermal field lies at the center of the western branch of Sumatran fault. About 11 wells have been drilled toward to Sumatran fault of western branch. The wells were drilled with the objectives of attaining permeabilites, lithology of reservoir and understand the hydrothermal system that developed in interest area.

Stratigraphy

The stratigraphic unit in Sorik Marapi consists of three (3) formations, from oldest to youngest are (1) Sibanggor Formation, (2) Roburan Volcanics and (3) Sorik Volcanics (Figure 3). Sibangor Formation is the oldest stratigraphic unit ever encountered by wells in Sorik Marapi, but the source of this formation is still uncertain. However, it is possible that an old ancestral caldera situated west of Sorik Marapi volcano could be the eruptive source of this volcanic formation. The formation are generally intensively altered with hardly distinguishable original composition and fabrics, normally in cryptocrystalline texture and microcrystalline matrix. This unit is medium hard to hard because of prevalent silicification. The silica in groundmass is intergrown with calcite and chlorite in rare amounts. The rocks of this formation are often fragmented with variable size of clasts laid in tuffacious matrix (Figure 4). The second unit is Raburan Volcanics which consists of mesocratic to leucocratic dacitic volcanics with cryptocrystalline and ghost porphyritic texture. This volcanic unit consisted mostly of weak to intensely altered, porphyritic and crystalline dacite lavas with primary muscovite. This unit overlained by the Sorik Volcanics composed of unconsolidated lava fragments

and andesitic-dacitic pyroclastics with sizes ranging from pebbles to boulders from the active Sorik Marapi Volcano. This transposes to weakly altered lavas and tephra which host discrete layers of aquifers.

Hydrothermal alteration

The alteration minerals showed alteration signatures produced largely by neutral pH fluids and followed by a general prograde sequence. The capping mechanism of geothermal system in SMGP was composed of clay minerals, amorphous calcite, and massive amorphous quartz. The clay zone was identified in this well consists of smectite, illite, interlayered clay of Smectite – Chlorite and Smectite – Illite but mostly dominated by smectite clay. The reservoir is characterized by epidote – Illite - Semi-drussy Quartz minerals association. Appearance of these minerals usually below 1000m marked the existence of the top of reservoir. Below that zone, the alteration assemblage is composed of illite-epidote-quartz-calcite minerals with some secondary muscovite as indication of high temperature reservoir and signature of neutral fluid environment. Towards bottom, the presence of high temperature minerals like crystalline epidote, secondary muscovite, secondary biotite, common illite and semi-drussy quartz indicate reservoir temperature of more than 250°C.

Hydrogeological Model of the Field

The hydrological model of Sorik Marapi geothermal system has evolved with the drilling of more wells and acquisition of new subsurface data. It becomes more apparent that the Sorik Marapi geothermal system is characterized by a single heat source as opposed to multiple heat source previously envisaged. A resource assessment conducted by FEDCO (2017, Fig. 5) and the 3D subsurface modelling of SMGP (Licup, et al., 2017, Fig. 6) showed that a resistive core – which usually represents the upflow zone – is located west of the Resource Area 1 just beneath the eastern flank of Sorik Marapi volcano. However, MT stations at the west of the concession area are too sparse to clearly define the extent and geometry of the resource.

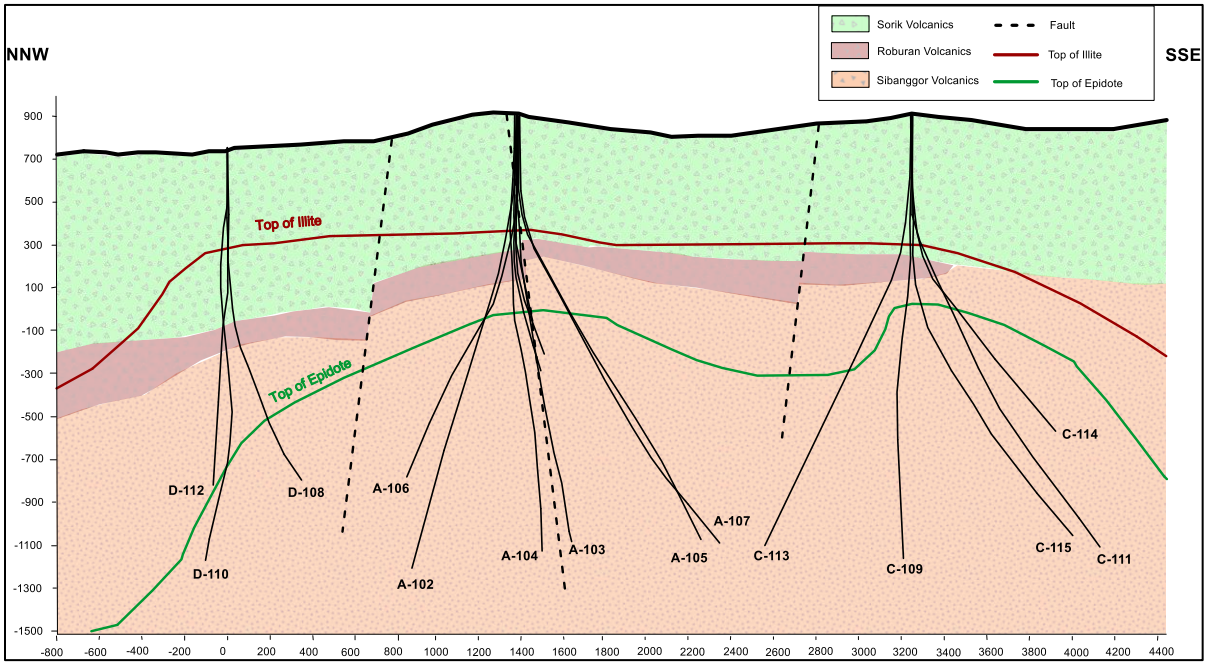


Figure 3, stratigraphy section from pad D to Pad C with the section trend is from NNW – SSE

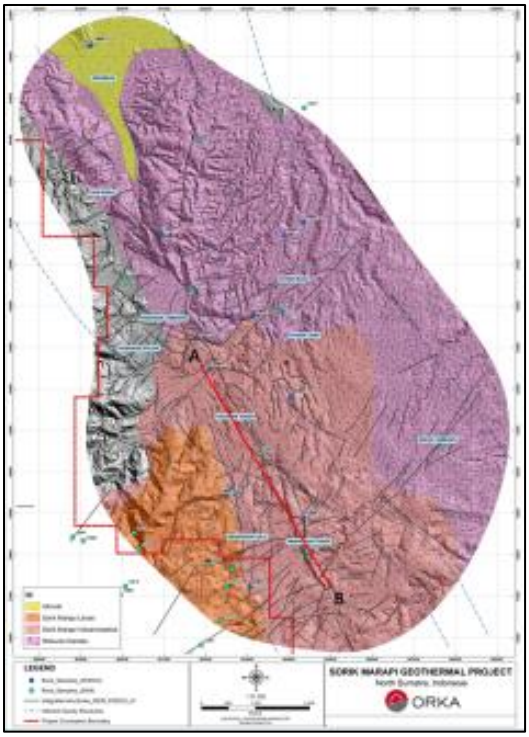


Figure 4. Geological Map of the Sorik Marapi Geothermal Field

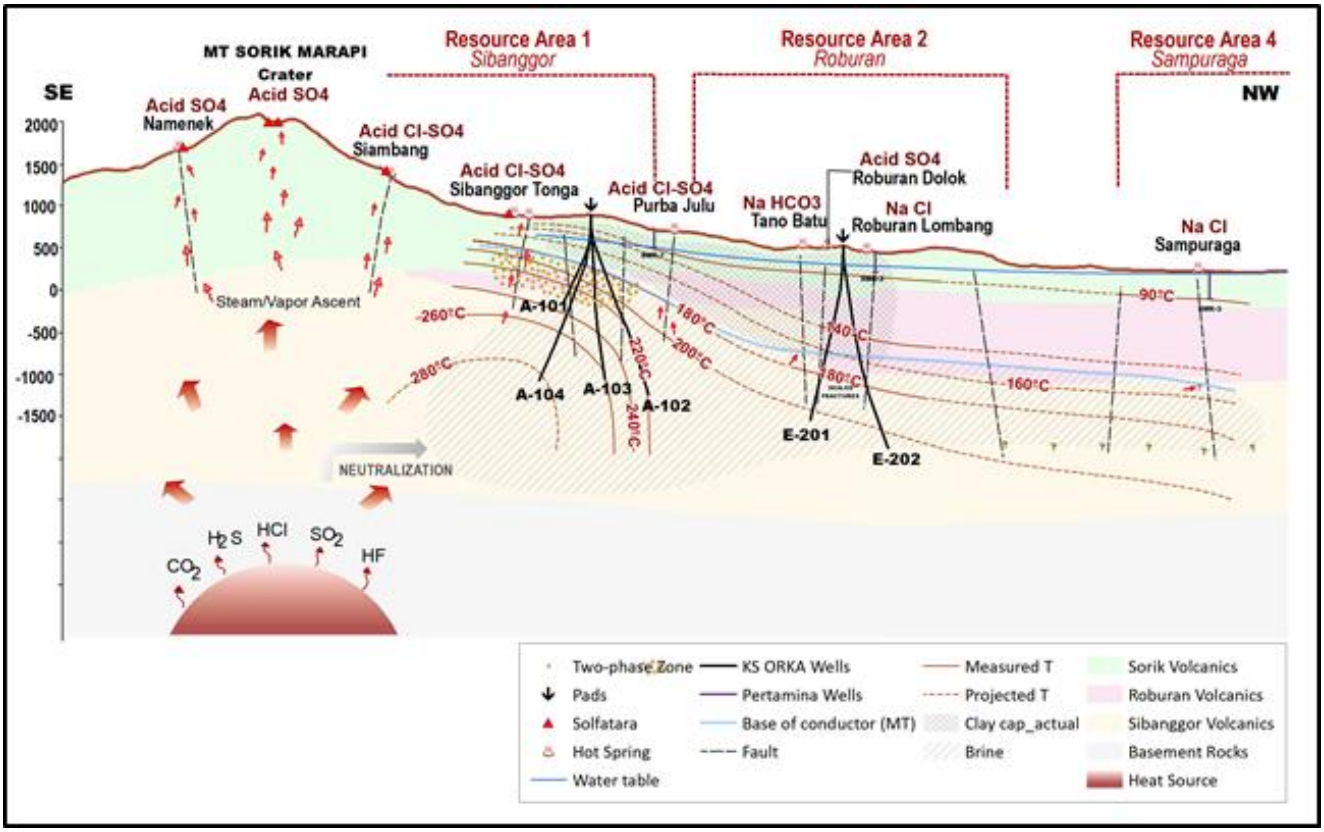


Figure 5 Updated Conceptual Model of the Sorik Marapi Geothermal Project, after FEDCO (2017)

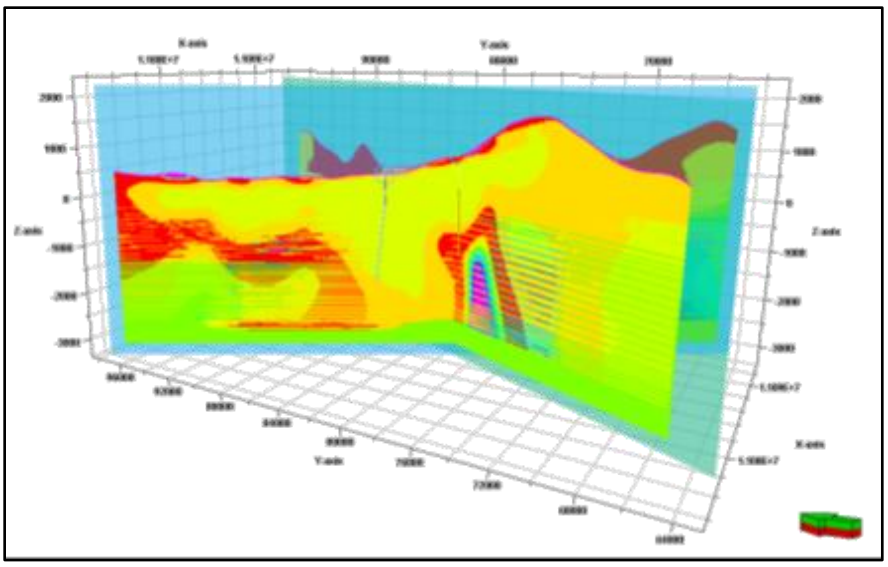


Figure 6. 3D Temperature model based on points data with temperature attributes extracted from resistivity data, adopted from Licup, et. al. (2017)

THE LIDAR AND METHODOLOGY

The evaluation of geological structures at Sorik Marapi geothermal was performed using terrain analysis on existing LiDAR remote sensing data, this is a simple method used to delineate the faults.

The LiDAR data package of SMGP includes a Digital Surface Model (DSM), Digital Terrain Model (DTM), topographic contour lines and ortho photos with horizontal resolutions of 1m x 1m per grid unit. These high resolution images are processed using ArcGIS spatial analyst tools and functions to extract various representations with increased clarity of geomorphological features that may suggest fault control.

Constructed Digital Elevation Models (DEM) were utilized to generate several other images like standard and multi-directional hillshades as well as slope and aspect maps. These enhanced images emphasize terrain features such as deep valleys, ridges, depressions/sag ponds, scarps, offset streams and other subtle linear patterns which are otherwise unremarkable from the original data. The resulting maps are then thoroughly examined for structural signatures. Faults/lineaments are delineated and subsequently digitized. Then, the preliminary map is generated. Figure 7, shows the flowchart of the different processes employed in analyzing and interpreting imageries to enable delineation of more geologic structures and update the structural map of SMGP.

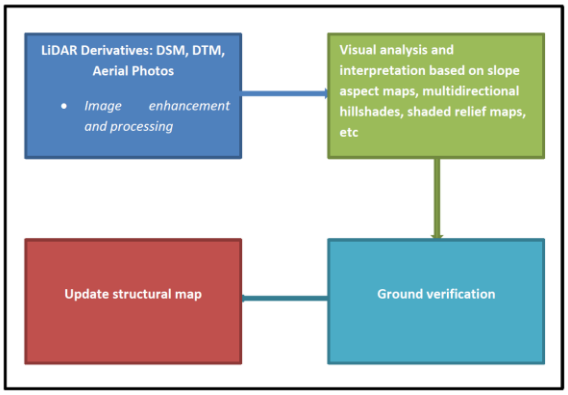


Figure 7. SMGP LiDAR analysis and interpretation flowchart

LiDAR Image Enhancement and Processing

The structural lineament identification involves various algorithms of Data Elevation Model (DEM) consisting of the following;

a) **Slope Map** (Figure 8A) shows the steepness of a surface, computed as the maximum rate of change in elevation between that location and its surroundings. It is expressed weither in degree or percent rise and with classes represented by gradation of color hues. The map shows the slope class values of 10 for flat areas, 20 for low slope areas, 30 for medium slope areas, 40 for high slope areas and >40 for nearly vertical surfaces.

b) **Aspect Grid** (Figure 8B) shows the orientation of the slope measured clockwise from 0° to 360°, where 1 - 22.5 being north, 22.5 - 67.5 northeast, 67.5 – 112.5 east, 112.5 – 157.5 southeast, 157.5

– 202.5 south, 205.5 – 247.5 southwest, 247.5 – 292.5 west and 292.5 – 337.5 northwest. This is created to aid in determination of the general direction of inclined surfaces.

c) **Aspect-Slope Grid** (Figure 8C) is produced by combining re-classed slope map and re-classed aspect grid to produce an image that simultaneously displays both the slope values and their corresponding orientation. This allows for easier perception of possibly fault-controlled linear patterns as well as assistance in determination of dip directions. Appropriate colors are assigned through a scheme that uses hue range to represent aspect categories (e.g., red, yellow, blue, *etc*) while the slope steepness are symbolized by color saturation (or brilliance of color), i.e., the steeper slopes are brighter.

d) **Hillshade Models** (Figure 9) are also generated and used as base maps for structural interpretation. Topography is illuminated from specified directions with azimuth from 0-360° and constant altitude of 45° above the horizon. The relative position of the sun creates shadows which highlight differently oriented linear features and sharpens edges. For this study, hillshades with hypothetical sun direction positioned at 45°, 135°, 270° and 315° azimuths.

e) **Multi-directional Hillshade Model** (Figure 10) apply oblique illumination on all surface from six different light source directions resulting to an excellent representation of relief and topography. This provides a 3-D image of the earth's surface and helps to clearly define geological structures.

The resulting images were thoroughly examined, compared and analyzed for any indications of faulting. Hillshade models were used as base maps for actual delineation of faults/lineaments while dip directions were inferred from visual analysis and interpretation of the shadow directions complemented by the use of slope and aspect maps.

Manual delineation of faults and lineaments ensued based on image interpretation followed by digitization to produce the lineament vector map. Faults are also categorized as Major or Minor depending on its surface extent with degree of confidence classified as Low, Moderate and High based on clarity of observed evidences for faulted surfaces (Figure 11). Ground truthing of LiDAR based structural interpretations is necessary to verify fault attitudes and augment the level of confidence in selecting desirable well-fault targets and prognosticating subsurface fault intersections

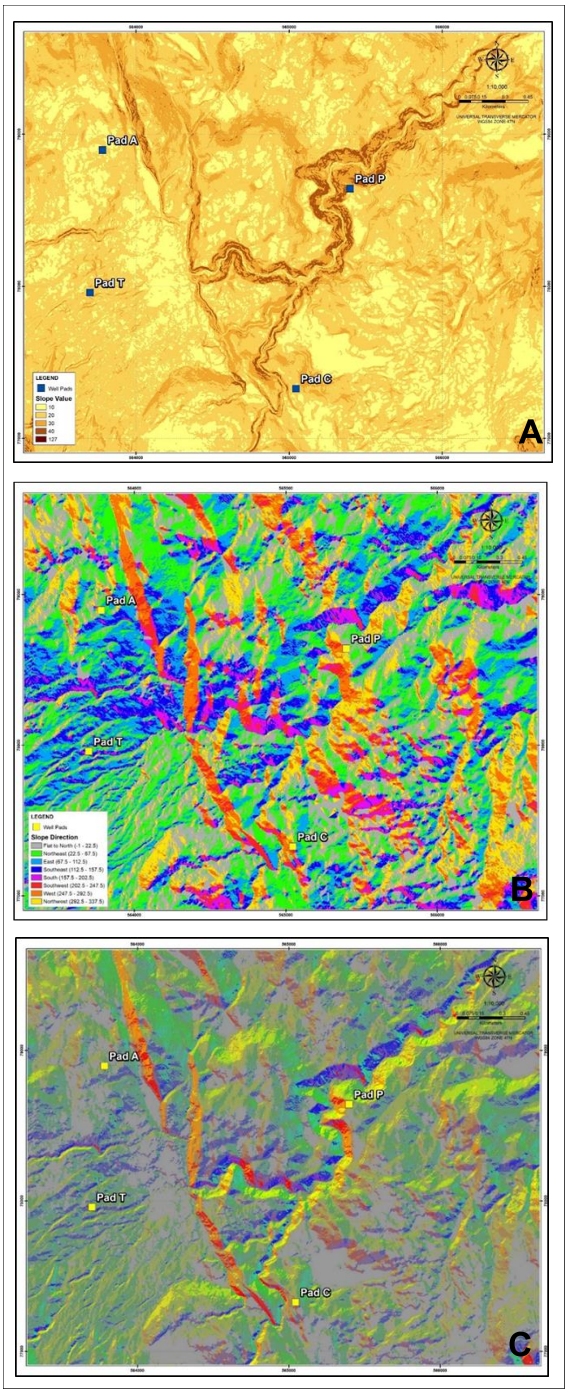


Figure 8. A. Slope map ; B showing linear patterns and general dip direction of slopes; C. Combined aspect –slope map and the general dip direction

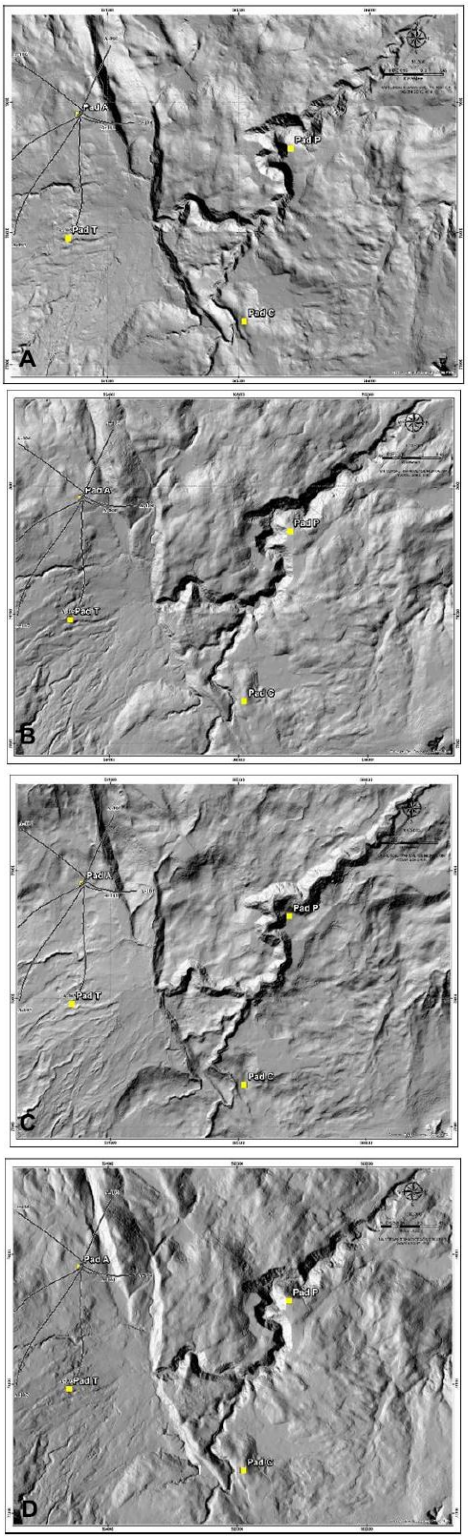


Figure 9. Generated hillshades with A) 45º B) 315º C) 135º dan D) 270º.

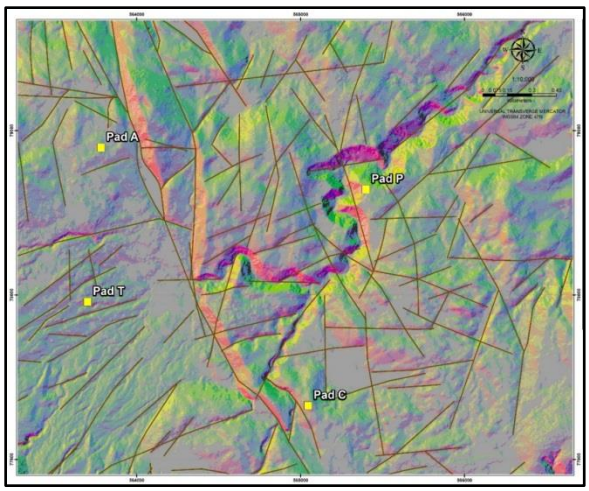


Figure 10, The aspect-slope map with interpreted structures

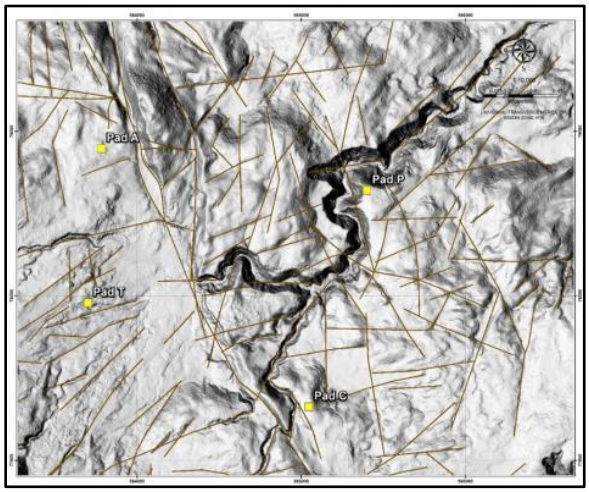


Figure 11. Faults and lineaments delineated from the hillshade analysis

Subsurface correlation

Prediction of the location of faults before and during drilling is important to anticipate the loss zones and pinpoint setting depths of casings. The results of structural analysis are used to estimate the depths of fault intersection. Figure 12 and 13are an illustration of well-fault intersections used in the prognosis of well C-xxx in Sorik Marapi while calculated depths of fault intercepts are shown in table 1. During drilling, the welltrack will continue to be updated based on the directional surveys and the actual fault dips are fine-tuned based on drilling evidences such as circulation losses, drilling breaks and unaccountable pump pressure drops and geological indications such as drussy quartz, acicular epidote, calcite or adularia.

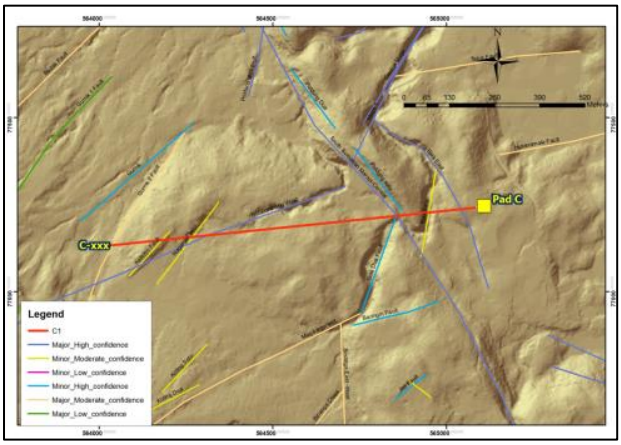


Figure 12. map of cxxx with the targeting fault

Table 1.Estimation depth table of fault intersections

PROJECTED FAULT INTERSECTIONS

Fault	Dip (°)	Depth of Intersection			Remarks
		mMD	mVD	mThrow	
Biak East	85°SW	600.0	594.30	50.72	High Confidence Major Fault
	90°	720.0	701.83	103.63	To be cased off
Biak Satu	85°SE	690.0	675.87	88.58	Medium Confidence Minor Fault
	90°	780.0	751.94	136.61	To be cased off
South Sumatran Marapi-Central	90°	1000.0	934.33	259.63	High Confidence Major Fault
	85°SW	1220.0	1116.72	382.65	Open for production
Hutalumbang West	85°SE	1100.0	1017.23	315.55	High Confidence Major Fault
	90°	1645.0	1469.06	620.31	Open for production
Nagargar Satu	85°SE	1675.0	1493.93	637.09	Medium Confidence Minor Fault
	90°	1995.0	1759.22	816.63	Open for production
Kaleren	85°SE	1755.0	1560.25	681.82	Medium Confidence Minor Fault
	90°	2120.0	1862.85	885.93	Open for production
Gumik 2	85°NW	2405.0	2099.13	1045.30	Medium Confidence Major Fault
	90°	2500.0	2177.88	1098.42	Open for production

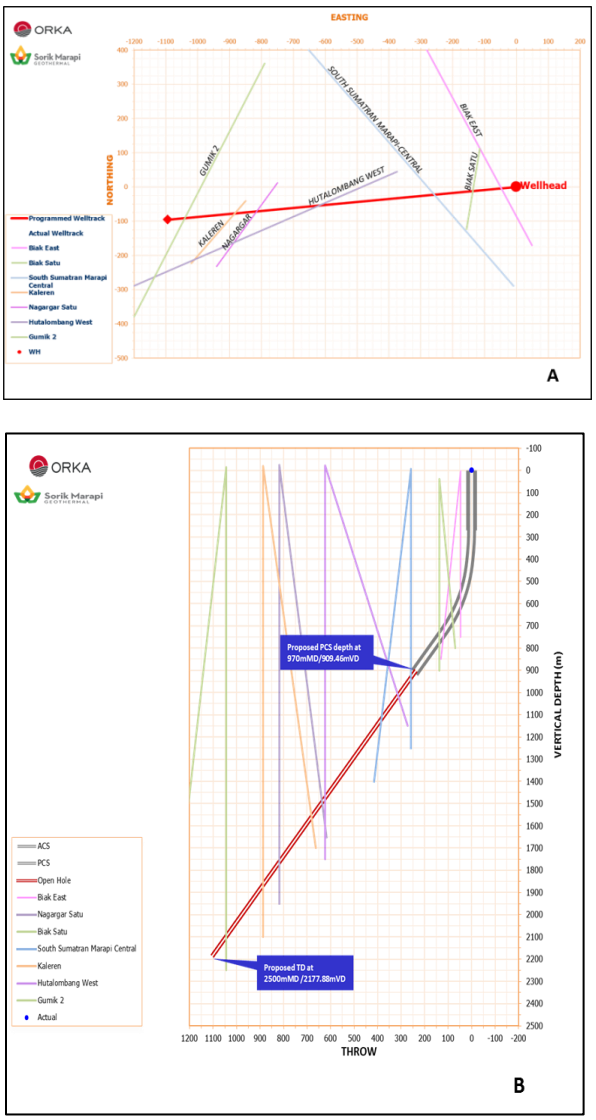


Figure 13. A) is map view and B) is cross section of fault targeting toward cxxx well

Figure 14 shows map and cross section that were updated when the drilling has been completed. Table 2 is the summary of geological evidences which have been correlated with drilling indicators, completion test, mineralogical data and interpreted permeability control.

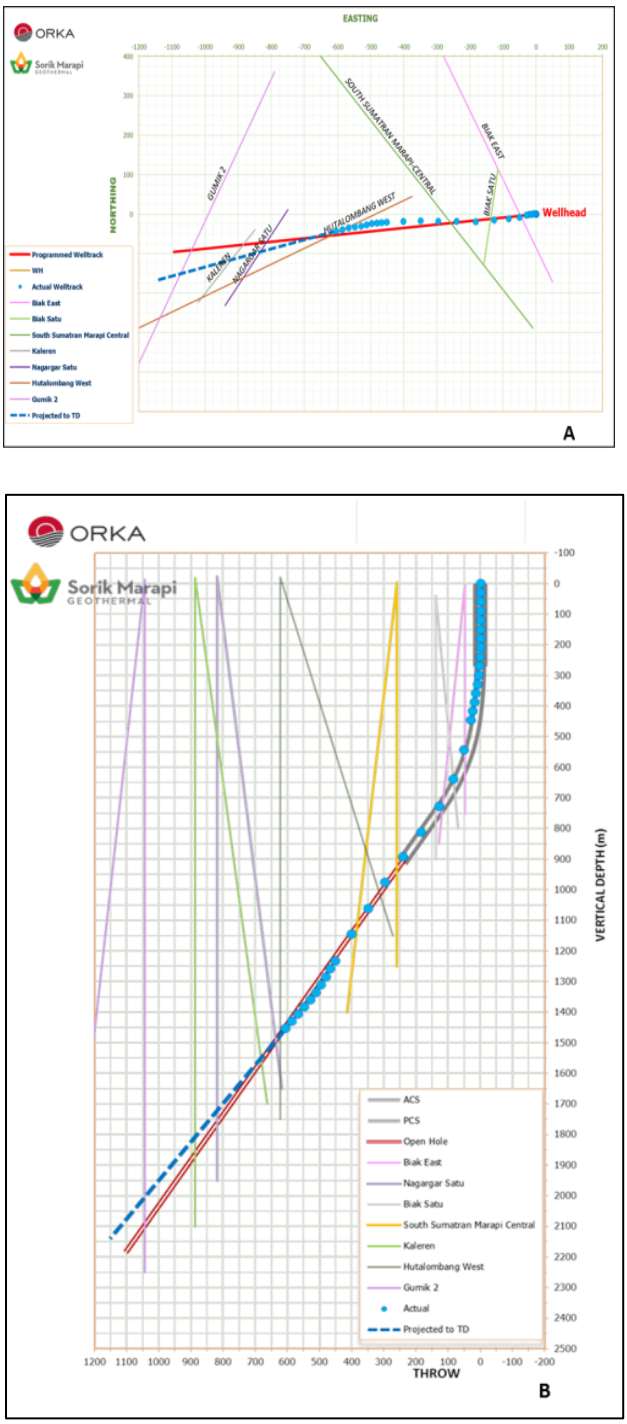


Figure 14. A)map and B) cross section view which updated during drilling

***T**able 2. Summary of geological, drilling and completion test data and interpreted permeability controls*

Depth		Indicators			Interpreted permeability Control	Prgnosis		Remark
from	To	Geology	Drilling	Completion Test		Dips	Depth	
600	678	Increased calcite, illite in weak amount	PLC		Biak East Fault 86° dip	85 SW	600	Cased off
						90	720	
723	786	Reccurent occurance of ubhedral to euhedral crystal of quartz			Biak SatuFault	85 SE	690	
						90	780	
1215	1338	Common subhedral to euhedral crystal quartz, common crystal epidote and wairakite	Drilling Break		South Sumatra Marapi Central	90	1000	Open for production
						85°SW	1220	
1610	1687	Common vein minerals and occurrence of subhedral to euhedral crystal of quartz, incipient-crystal epidote and secondary biotite	PLC to TLC		Hutalombang West Fault at dip 90°	85 SE	1100	
						90	1645	
1880	2078		Drilling break, TLC		Intersection Nagargar Satu Fault at dip 89.1° NE and kaleren Fault at dip 88°NW	85 SE	1675	
						90	1995	
						85 SE	1755	
						90	2120	
2520	2530		Drilling break, TLC		Gumik 2 Fault 89° dip	85 NW	2405	
						90	2500	

CORRELATION OF STRUCTURES WITH PERMEABILITY

C-xxx was designed to intersect and prove permeability associated with major SW-NE and NNW-SSE and minor NE trending structures located Southwest of PAD C. The well intercepted four structures which includes Hutalombang West Fault, Nagara Satu Fault, Kaleren Fault and Gumik 2 Fault. The depths of permeable zones in C-xxx were interpreted based on geological and drilling data. At least six permeable zones were identified as discussed below.

600 mMD to 678mMD (593.02 to 665.25 mVD)

This permeable zone is indicated by the occurrence of subhedral to euhedral crystals of quartz and anhedral calcite. It is associated with Biak East Fault (90°). Based on prognosis well will intersect Biak East Fault at 600 mMD/594.3 mTVD at dip 85°SW and at 720 mMD/701.83 mVD at dip 90°. Partial loss of circulation of 400 to 600 BPH was encountered at 630 mMD which have been sealed off using LCM because formation temperature is still low, so it is not yet feasible to become a production zone. This permeable zone finally cemented to avoid cold water breakthrough.

723 mMD to 786 mMD (705.25 mVD to 759.04 mVD)

This possible permeable zone is indicated by occurrence of subhedral to euhedral quartz, abundant illite and amorphous calcite. It is most likely associated with the foot wall of Biak Satu fault (88-89°SE). Based on prognosis well will intersect Biak Satu Fault at 690 mMD/675.87 mTV at dip 85°SE and at 780 mMD/751.94 mVD at dip 90°. However during drilling there was no circulation loss observed. It is possible that the existence of permeable fractures lined with the subhedral crystals of quartz could have been overprinted by massive silica and calcite deposits that reduced the permeability of this zone.

1251mMD to 1338 mMD (1145.88 mVD to 1221.15mVD)

This possible permeable zone is indicated by drilling breaks and the occurrence of subhedral to euhedral crystals of quartz, common crystalline epidote and

wairakite . It is most likely associated with the foot wall of South Sumatran Marapi-Central Fault (85°-87°SE). Base on prognosis well should intersect South Sumatran Marapi-Central Fault at 1000 mMD/934.33 mTV at dip 90° and at 1220 mMD/1116.72 mVD at dip 85°SW. However during drilling there was no circulation loss observed. This is consistent with other wells drilled in SMGP that intersected this major structure, which can be explained by the compressive stress that produced this fault that makes it generally impervious.

1601mMD to 1735mMD (1437.73mVD to 1544.06mVD)

This permeable zone occured at interval depth 1305 - 1630 mMD, cuttings are composed of euhedral quartz crystals, moderate incipient epidote and secondary biotite. This is most likely related to Hutalombang West Fault (90°) intersection. According to prognosis The well will intersect Hutalombang West Fault at 1100 mMD/1017.23 mTV at dip 85°SE and at 1645 mMD/1469.06 mVD at dip 90°. Partial loss of circulation of 500 to 600BPH was encountered at 1601 mMD and became total loss circulation at depth 1735 mMD with loss rate 1578-2000 BPH.

1880mMD to 2078mMD (1664.71 mVD to 1837.86mVD)

This minor permeable zone is indicated by drilling break at 1881mMD, 1905 mMD, 1995 mMD,2069-2070 mMD and 2078-2078 mMD. It is most likely associated with intersection of Nagara Satu Fault (89.1°NE) and Kaleren (88°NW). Prognosis projected intersection of Nagargar Satu fault at 1675 mMD/1493.93 mVD at dip 85°SE and at 1995 mMD/1759.22 mVD at dip 90°, Kaleren Fault intersected at 1775 mMD/ 2120 mVD at dip 85°SE and 2120 mMD/1862.85 mVD at dip 90°. Static total loss of circulation ranges from 1300 to 1640 BPH.

2520 to 2530 mMD (2251.83 mVD to 2261.53 mVD)

This Major permeable zone is indicated by drilling break at 2523 mMD and 2527 mMD, also increased of loss rate up to 2900 BPH. It is most likely associated with intersection of Gumik 2 Fault (90°). The prognosticated depth of intersection with Gumik 2 Fault is at 2500 mMD/2177.88 mVD at dip 90°.

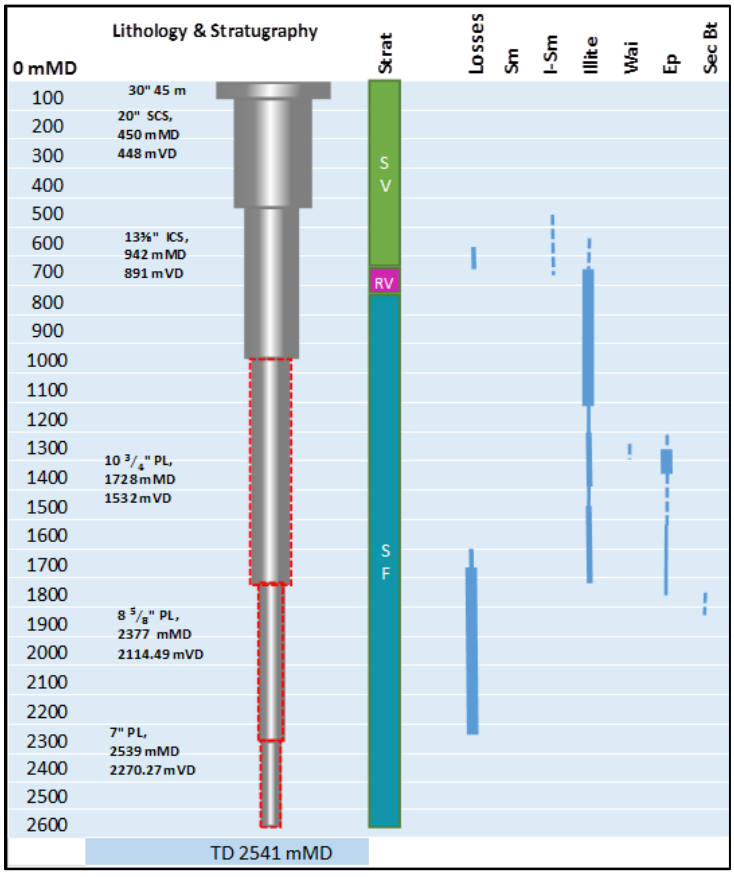


Figure 15. Simplified diagram showing the lithology, key alteration mineral C-xxx based on site megascopic analysis

CONCLUSION

This study has demonstrated the importance of predicting and evaluating well-fault intersections. The obtain an excellent structural map, it is important that a good Data Elevation Model (DEM) such as LiDAR must be acquired. During the exploration phase, the LiDAR images must be thoroughly examined, compared and analyzed for any indications of faulting. Hillshade models can be used as base maps for actual delineation of faults/lineaments while dip directions will be inferred from visual analysis and interpretation of the shadow directions complemented by the use of slope and aspect maps. The structures which resulted from LiDAR analysis should be verified through ground checking or detailed structural mapping. The result of surface structural studies will be the main basis in preparing well trajectory and geological prognosis of the first few wells in the geothermal field.

During drilling, the wellsite geologist should closely monitor and should be able to update well-fault intersections to assist in making important drilling decisions and help the drilling personnel in formulating solutions to hole problems.

After well completion, evaluation of well-fault intersections can be used in preparing well model, update the conceptual hydrological model and development strategy. A good understanding of well-fault intersections will also be important in analyzing well communications which can be used as basis for a better resource management.

REFERENCES

Hendri, R. and Hidayat, R. (2018), "Final Geological Report of Pad C," *PT Sorik Marapi Geothermal Power,"* Internal Assessment Report.

Hochwimmer, A. and Ussher, G., 2011. "Exploration Scientific Assessment and Well Targeting Summary, *Sorik Marapi Geothermal Project*, Internal report.

Licup. A. C. (2018), "Evaluation of pad P Structural Targets for the Reinjection Requirements, 15-25. *PT Sorik Marapi Geothermal Power,"* Internal Assessment Report.

Licup. A. C. et al, (2017), "Sorik Marapi Geothermal Power Plant Notice of Resources Confirmation," *PT Sorik Marapi Geothermal Power*. Internal Assessment Report.

Mulyani. S, Licup. A.C et al, (2017), "Geothermal 3D Subsurface Modeling - A Case Study of Sorik Marapi Geothermal Field", Proceeding of IIGCE 2017.

Sieh, K. Natawidjadja, D., (2000), "Neothectonics of the Sumatra Fault, Indonesia",. Journal of Geophysical Reserch. 105, 28, 295-28, 326.

Suryantini. And Wibowo, H, (2010), "Application of Fault and Fracture Density Method for Geothermal Exploration in Non-Volcanic Geothermal System a Case Study in Sulawesi-Indonesia", *Proceedings of World Geothermal Congress 2010.*

SOKORIA GEOTHERMAL EXPLORATION DRILLING UPDATE, ENDE, EAST NUSA TENGGARA, FLORES, INDONESIA

Dhani Sanjaya, Haris Siagian, Jul Rafli, and Birean Sagala

Geoscience Department, PT Sokoria Geothermal Indonesia – A project of KS Orka Renewables Pte Ltd
Recapital Building 5th Floor, Jl Adityawarman Kav 55, Jakarta Selatan 12160
Email: Dhani.sanjaya@ksorka.com

ABSTRACT

Four production wells were drilled during drilling campaign from November 2017 until June 2018 with the objective to prove the power generating potential of Sokoria, to establish the subsurface geology of the reservoir, its capping mechanism, thermal gradient and chemistry of deep fluids, and to intersect and test the attendant permeabilities of West, North West and North East side developed fault.

Three rock formations are identified, from the oldest to youngest are Old Sokoria Volcanics, Kelinabe Volcanics, and Mutubusa Volcanics. All the unit formations consist of alternating volcanic breccia, lava and tuff with different sources and degree of hydrothermal alteration and mineralization. Alteration minerals observed are smectite, chlorite, illite, quartz, calcite, anhydrite, and epidote. The presence, distribution and intensity of secondary minerals determines the alteration zone of Sokoria field are Argillic zones (200-500mVD), Phyllic zone (500-850mVD), and Propylitic alteration (below 850mVD).

Integration of MeB index data and presence of secondary minerals also suggest top of reservoir occur at around 850 mVD, as indicate by decreasing of MeB value and apperaring of illite minerals as the hole goes deeper. Increasing of vein, silica, calcite and chlorite minerals and in conjunction with several drilling parameters such as drilling break and loss circulation indicates that the well was intersecting fractures and fault zone.Three of four drilled wells intersected productive EW, NW-SE, NE-SW trending faults which gives good permeability of the well. Occurrence of high temperature alteration minerals such as epidote, illite, chlorite, quartz and anhydrite suggest that formation temperature exceed 220°C.

Keywords: Sokoria, drilling

INTRODUCTION

Sokoria geothermal field is located around 30 km to North East side from Ende Regency, East Nusa Tenggara, Indonesia (Figure 1).

The Sokoria area has been the topic of several Indonesian government sponsored geoscientific studies since the prospect was first explored in the early 1970's. It was identified as second to Ulumbu in potential for geothermal development potential on the Island of Flores (GENZL, 1995). This study was followed on by a NZ Ministry of Foreign Affairs and Trade (MFAT) sponsored exploration program by GENZL in 1997. The results of this program are reported in a comprehensive GENZL report to MFAT (Harvey et al, 1998a) and in a brief conference paper (Harvey et al, 1998b).

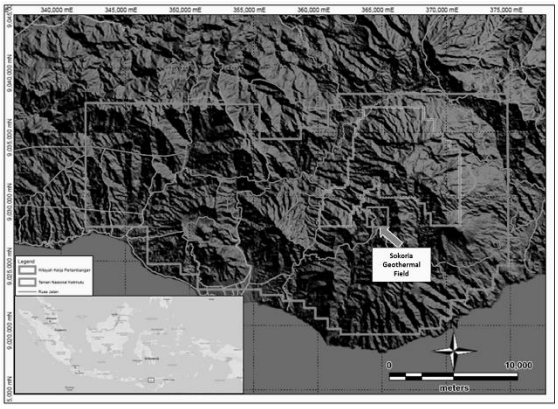


Figure 1: Location Map of Sokoria Geothermal Field, Ende, East Nusa Tenggara

Another study was done by several Indonesian government. PLN was done surface geoscience study including geological mapping and geochemistry sampling on 1995 followed by two thermal gradient wells (SK-1 and SK-2) conducted by Geological Research and Development Centre on 2004. The two temperature gradient wells SK-1 and SK-2 gave confidence to Geological Research and Development Centre to drill SR-1 exploration well on 2006 – 2007, this well reach total depth of 532.96 m from the proposed target depth of 800 m.

REGIONAL GEOLOGY

The Sokoria Prospect is on the southern flank of the Quaternary Kelimutu Volcanic Complex which covers an area of between 300 and 400 km2, extending inland 23 km from the SW coast as shown in Figure 2 The volcanic rocks are predominantly andesite with subordinate dacite. A number of eruptive centres have been identified. On the volcano's flanks the rocks are an inter – fingering sequence of lavas and pyroclastic rocks. There are a number of large collapse features identified within the complex, one which encompasses the immediate Sokoria area. A large fault, the Lowongolopolo

Fault, crosses the complex from the NNE to SSW, passing directly through the Sokoria area.

The volcano has undergone a series of eruptive phases, followed by periods of structural collapse and possible caldera formation, with subsequent filling of the collapse features by later eruptions. Four major phases of eruptive activity are recognised. The oldest is Tertiary age andesite exposed on the volcano's lower slopes. This was followed by construction of the early Quaternary Sokoria andesitic volcano in the north-western part of the complex, which subsequently collapsed forming a caldera. Activity then moved to the Kelibara volcano in the south-eastern part of the complex, with andesite lavas and pyroclastic rocks infilling the earlier collapse features. The last phase has been centred on the Kelimutu volcano, whose acid crater lakes reflect active fumarolic activity from the volcano. Kelimutu last erupted 43 years ago in 1968.

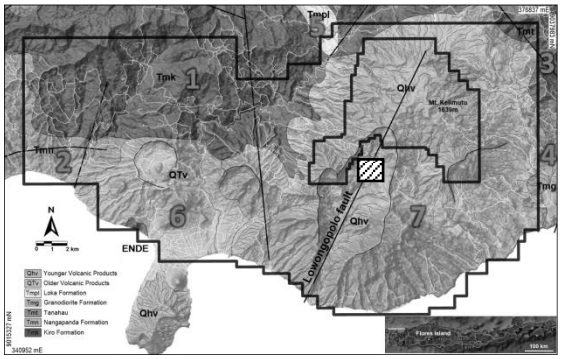


Figure 2: Sokoria concession area (black line) and wellpad area (shade box).

Miocene volcanics, sedimentary and intrusive rocks surround the Kelimutu Volcanic Complex on the northern and eastern sides, and presumably underlie it. Although andesitic lithologies dominate the central volcanic complex, dacite to rhyolite lavas and pyroclastic rocks are found in the northeast and may underlie the complex in this quadrant. The sediments are dominated by limestones and sandstones which commonly have a tuffaceous component. A 10 km diameter granodiorite body intrudes Miocene rocks to the east of the complex.

PRE-DRILLING ASSESSMENT

Combined geological, geophysical and geochemical data shows the Sokoria geothermal system is belong to the hot water dominated system. The movement of hydrothermal fluid is mainly controlled by the NNW-SSE and NNE-SSW fault pattern.

Resistivity map at 750m slicing from 3D MT inversion (SGI MT study, Figure 3) shows conductive zone (red) and it's interpreted as capping mechanism of thermal fluid in this area. The conductive area is divided in two zones by resistive layer (light green) included Northwest sector and Southeast sector. There is thinning of conductive layer to north side of the area that indicates up flow zone to the north.

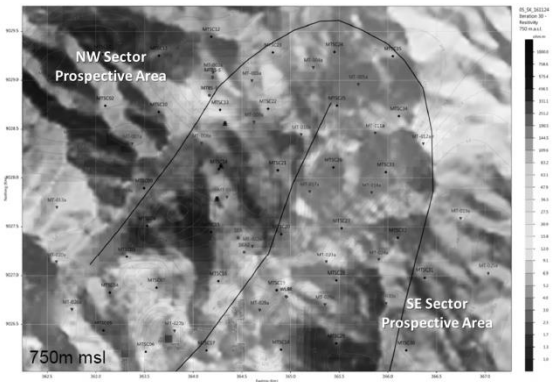


Figure 3: Resistivity map at 750 m slicing, 3D MT inversion

Structural analysis was conducted using LiDAR image to determine the development of fault in surrounding area for well targeting. There are total of 108 structures/lineaments were drawn from the LiDAR image interpretation, All interpreted faults/lineaments are categorized as either Major or Minor Fault targets, mainly based on its length on map. Each structure drawn was further ascribed with level of confidence ranked as Low, Moderate and High based on perceived geomorphic expressions these lineament (Figure 4).

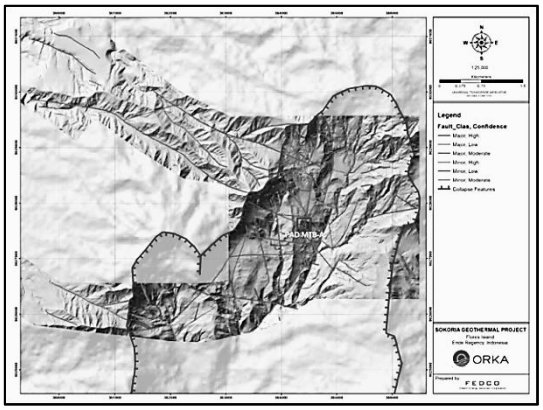


Figure 4: Structural Map of Sokoria (Fedco 2017) and MTB-A Wellpad location

In particular, the Lowongolopolo Fault and its splays are attractive structural targets due to its impressive surface expressions and good indications of permeability, which seemingly controls the occurrence of most surface thermal manifestations in Sokoria.

Integration between 3D MT modelling and structural analysis resulting in 4 well targeting for pad A (Figure 5).

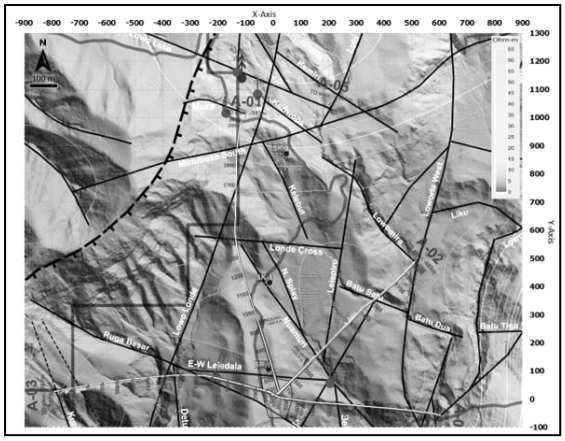


Figure 5: Well targeting MTB A Wellpad, Sokoria Geothermal Field

EXPLORATION DRILLING UPDATE

Four drilled wells on Wellpad MTB A (MTB A-01, A-02, A-03 and A-04) have penetrated a broad sequence of andesitic pyroclastic and lavas rocks that form part of the Mutubusa volcanics, Keli Nabe Volcanics, and Old Sokoria Volcanic.

Megascopic analyses of the drill cuttings collected from all wells showed alteration signatures produced largely by neutral pH fluids and followed a general prograde sequence. MeB test analysis data suggest the clay zone as cap rock appears at interval 200-500mMD while the absence of clay-semectite at interval below 850mMD. Formation temperatures are estimated based on mineral silica, quartz, chlorite, epidote, anhydrite and illite showing temperature exceed 220°C. Several drilling break and loss circulation encountered while drilling was indicate the permeable zone from fault intersection.

Stratigraphy

Based on rock cutting description three stratigraphic units are identified from the youngest to oldest are (Table 1),

- Mutubusa Volcanics.
- Kelinabe Volcanics
- Old Sokoria Volcanics,

All the stratigraphic units consist of volcanic breccia, lava and tuff with different sources and mineralization that distinguish the stratigraphic units from one to other (Figure 6).

Mutubusa Volcanics

The thickness of this formation is around 700m. From surface down to about 700 mVD, all wells in pad A encountered fresh pyroclastic & lava, rock units consist of andesite lava, tuff breccia, lithic tuff, with moderate hard – hard hardness.

Lava unit characterized by andesite aphanitic to porphyritic, phenocrysts consist of plagioclase, pyroxene, hornblend and biotite, embedded in microcrystalline plagioclase groundmass. This volcanic layer is the collective product of various eruption episodes of Mt. Mutubusa that probably occurred during quaternary period.

The middle and lower section of Mutubusa volcanins is altered to smectite clays and other low degree alteration minerals which sealed fissures and vugs and effectively prevent the ascent of the geothermal fluids to the surface. This implies that this stratigraphic unit forms part of the capping mechanism to the geothermal reservoir at depth.

Table 1: Stratigraphy of Sokoria from drilled wells

Depth mMD (mVD)	Formation Description
Surface – 700 mVD MUTUBUSA VOLCANICS	Fresh lava & pyroclastic are near surface, rock units consist of andesite lava - tuff breccia - lithic tuff, with hardness is moderate hard – hard. The Mutubusa volcanics formation dominantly interlayered lava & Pyroclastic. Pyroclastic fragment consist of lithic tuff, andesite, dacite and rare basalt, sub-angular to angular, weak to moderate altered. Lava unit is characterized by aphanitic andesite, partialy amygdaloid texture, phenocrysts consist of moderately mafic crystals, embedded in micro-crystalline groundmass of plagioclase and mafic, minor to moderate chlorite, weakly altered.
700 – 1100 mVD KELI NABE VOLCANICS	Kelinabe formation dominantly pyroclastic altered. Rock unit consist of lithic tuff and crystal lithic tuff characterized by fragmental with andesitic rock fragment, moderate-strong altered. Moderate chlorite as replacement groundmass of andesite lithic, moderate calcite replacement and veinlets, moderate illite set in chlorite groundmass.
1100m – 1800? mVD OLD SOKORIA VOLCANICS	The old Sokoria volcanics characterized by contact of altered pyroclastic rocks, consist of lithic tuff – tuff breccia, andesite altered brecciated, moderate to strong alteration dominated by silica and chlorite, slightly increasing of epidote minerals.

Keli Nabe Volcanics

The Kelinabe formation is dominated by altered pyroclastic. Consist of lithic tuff, crystal lithic tuff and tuff breccia, The upper section of this formation composed by moderate to strong altered pyroclastic characterized by greenish gray and light gray and white clast, very fine grained, fragmental with andesitic rock fragment, composed by plagioclase, biotite, and pyroxene, mostly already altered to chlorite, silica and calcite. Moderate abundant chlorite, quartz and calcite replacing plagioclase and glass, minor to moderate silica replacement and veinlets, moderately abundant calcite replacement and veinlets, rare illite, rare pyrite in very fine grained cubic form, rare hematite in few interval.

Lower section of this formation characterized by lithic tuff with light gray to greenish with white chips, moderate hard to hard, fragmental, strong alteration, composed by abundant to moderate chlorite replacement, minor to abundant silica replacement with amorphous form, rare to minor fine grained pyrite set in silica and chlorite groundmass, rare to moderate illite, and rare calcite.

Old Sokoria Volcanics

The thick undifferentiated pile of highly altered volcanic rocks encountered by drilled well below 1100 - 1200 mVD is tentatively named Old Sokoria Volcanics which is deemed to be more appropriate nomenclature. The eruption center source of this stratigraphic unit is still uncertain, however, it is possible that an old ancestral caldera located in center of Sokoria be the source of this volcanic formation. The rocks belonging to this formation are generally intensely altered with hardly distinguishable original composition and fabrics.

The old Sokoria volcanic characterized by contact of altered pyroclastic rocks consist of lithic tuff – tuff breccia and altered andesite. Hard due to intense silicification. In upper section silica is intergrown with moderate chlorite and moderate quartz, and abundant widespread of illite, silicification become more intense to depth, first epidote also observed in this formation ranging from 1100 to 1200 mVD, become more intense to depth in minor to moderate abundant amount. The intensity of alteration, presence of high temperature secondary minerals and existence of open fractures indicate that this volcanic formation is acting as the main host for the geothermal reservoir.

Hydrothermal Alteration Zones

The formation of hydrothermal minerals is affected by temperature, pressure, parent rock types, reservoir permeability, fluid composition and duration of activity (Browne, 1978). From drilling cutting alteration minerals observed are smectite, chlorite, illite, quartz, calcite, anhydrite, and epidote.

Chlorite. Commonly shows as a replacement of plagioclase phenocryst, then replace plagioclase and glass as matrix. It started observed from depth 120 mVD and increasing from 400 mVD.
Quartz. Quartz increased from 700 mVD. Commonly, it is found as replacement of glass matrix in tuff, feldspar and filling in the vein of andesite and tuff breccia.
Calcite. Calcite is found continuously started at shallow depth to total depth (TD), increasing around 400 – 900 mVD. Calcite is commonly replacing plagioclase as phenocryst, sometimes filling as veinlets.
Smectite. Smectite is difficult to identified by microscopic, physically high swell clay content with high MeB index (figure 6). Smectite increasing around 200 – 400 mVD.
Illite. Illite is found continuously started after decreased of smectite clay, increasing from 550 – 600 mVD to total depth (TD). Illite is commonly speck form and replacing plagioclase.
Anhydrite. Anhydrite is observed uncontinously in the well started at 900 mVD, according to rock pH analysis have normal pH 7-8. Anhydrite is commonly found as replacement of phenocryst and sometimes filling vein and observed coincide with appearance of sulphide minerals.
Epidote. Epidote appears as replacement of plagioclase and as vein fillings. The relict epidote observed near surface at 228 mVD. The first Epidote occurrence commonly observed at 850mVD then increased and become continuesly occurring from 1000 - 1100 mVD as replacement and vein fillings.
Pyrite. Pyrite increased from 700 – 800 mVD. Pyrite is commonly disseminated, cubical form and as veining.

Based on the cutting description of secondary minerals occurrence and intensity, three alteration zones were defined as below (Figure 7).

Argillic alteration

Argillic alteration zone is dominated by smectite minerals with swell clay content ≥ 30% (figure 7). This zone is marked by appearance of moderate to abundant smectite, then rare amount of quartz and calcite. The bottom of this zone is characterized by the appearance of increased chlorite and smectite decreased to depth. Argillic alteration zone is identified around 200 – 500 mVD, with average thickness is 300 m and significantly thinner toward fumarole is about 200 m, due to up-doming claycap impact increasing upflow temperature.

Phyllic alteration.

Transition zone which Phyllic alteration assemblage characterized by dominant illite with increasing pyrite and quartz, as main distinguishing with Argillic type. Phyllic alteration zone was intercepted at depth in ranges of around 500 – 850 mVD with average thickness is 350 m.

Propylitic alteration.

Occurring at reservoir section, typical Propylitic alteration mineral assemblage develops and characterized by appearing of epidote minerals, increasing chlorite coincide with appearance of quartz, calcite, pyrite, illite and anhydrite. The propylitic zone is expected a commercial high temperature reservoir zone as a target in exploration drilling campaign. The anhydrite mineral normally abundant in permeable zone especially where acid and neutral fluids mix. The presence of anhydrite mineral indicated environment of formation is slightly acid with pH ranges from 5 – 6.. First occurrence of epidote at well MTB A-01 and MTB

A-02 are found at 850-950 mVD then increasing and continues ranging from 1000-1100mVD. The appearance of mineral epidote indicates high temperature with predicted temperature mineral >220°C (Lagat after Reyes, 2010).

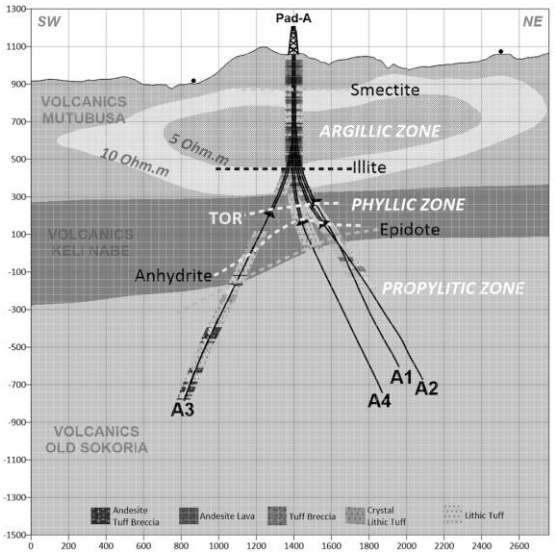


Figure 6: Well profile showing alteration-mineralization type and geologic stratigraphy.

Top Of Reservoir

Determination of the top of reservoir in Sokoria geothermal wells are using The methylene blue (MeB) method and hydrothermal alteration minerals analysis from drill cutting every 3m interval. MeB test is a quick and cheap method to provide estimates of smectite clay content in geothermal well cuttings, and a fast method to determine the location of the top of reservoir such that the production casing can be set at the optimum depth.

Composite MeB data profile showing spike trend at shallow interval around 30-50 mVD, 170-200 mVD, 215-230 mVD and showing the peak of smectite content around interval 250-370 mVD, below this interval smectite content decreasing to minor amount then no longer present below 700 mVD, analysis of cuttings returns indicates values consistently less than 10, and mostly ranging around 3-8.

Another method used to determine the top of reservoir is analysis of secondary minerals from drill cutting. Since epidote indicates high temperature minerals >220°C, the occurrence and observation of this minerals is useful to determine the top of reservoir. From drilled wells the first trace of incipient epidote started occurring ranging around 850 – 950 mVD then become clearer and continuous from 1000 – 1100 mVD indicate high temperature reservoir.

MeB test data and analysis of secondary minerals suggest that top of reservoir most likely occurs at 850 mVD characterize by low value of MeB index (3-5) and the occurrence of epidote starting from 850mVD (Figure 7). This also confirmed by conductivity map from 3D MT modelling of Sokoria (Figure 3).

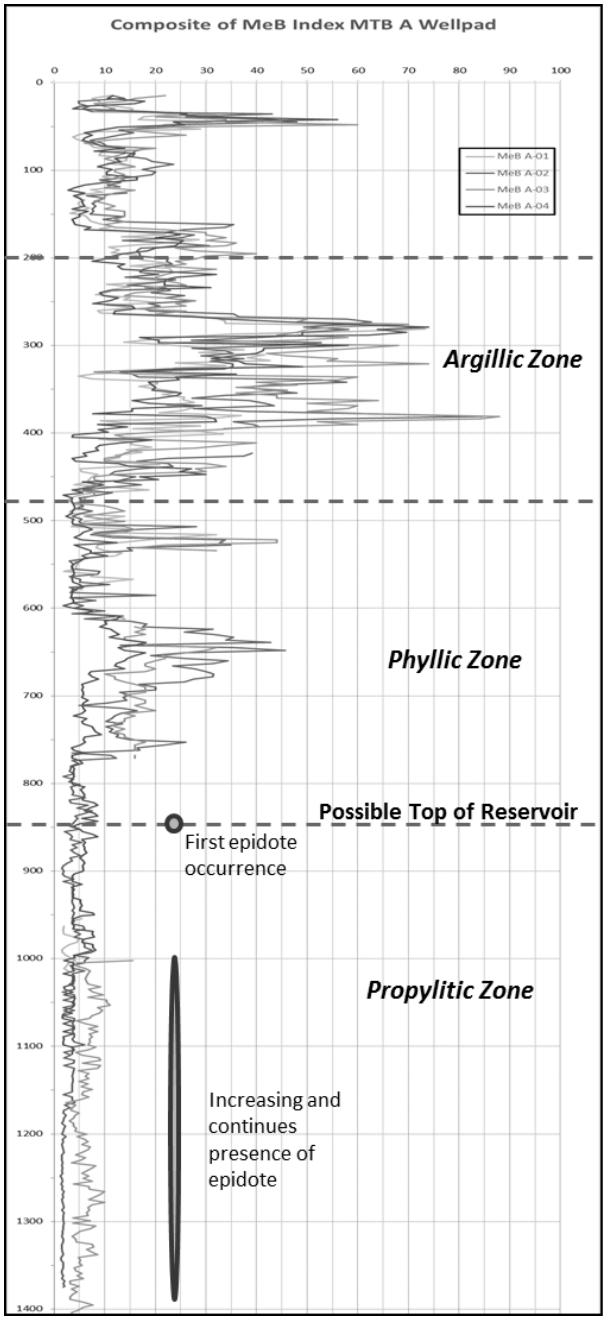


Figure 7: Composite MeB index and alteration zone of Sokoria MTB A Wellpad

Structure and Permeability

All wells in Pad A is designated to intersect the fault developed in north, north east, east and west part of Pad A area.

Based on lidar and structural analysis Pad A well targets aim to intersect major antithetic structures trending NNE-SSW, NW-SE and N-S which are

interpreted to be tensional in nature and most likely have good attendant permeability.

Increasing vein, silica, calcite and chlorite content on cutting sample and several drilling parameters such as drilling break and loss circulation indicates that the well was intersecting fractures and fault zone targeted which give the well permeability to flow the hot fluid for production.

Drilling data from 4 wells drilled confirm that fault with NNE-SSW, NW-SE trending fault is appear to have good permeability. Strike-dip, permeability and type of fault below total loss depth interval is hard to identify due to limitation of data after total loss circulation.

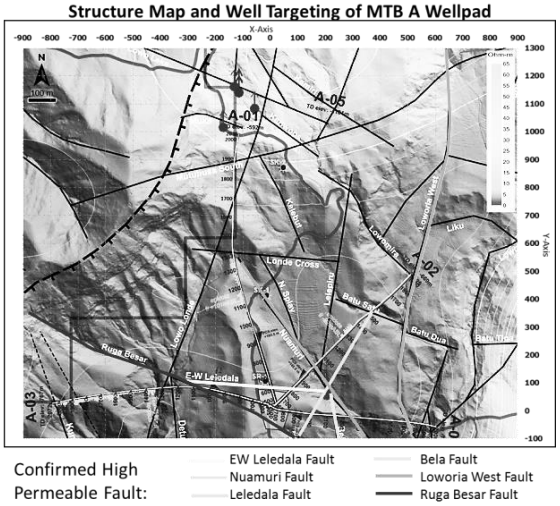


Figure 8: Structure maps shows confirmed high permeable fault

Drilling parameter data, cutting description and spinner data from completion test confirm permeability of the fault intersect by four wells as following (Figure 8):

1. E-W Trending EW Leledala Fault (MTB A-01, MTB A-02)
2. NW-SE Trending Nuamuri Fault (MTB A-01)
3. NE-SW Trending Leledala Fault (MTB A-02)
4. NW-SE Trending Bela Fault (MTB A-04)
5. NNE-SSW Trending Loworia West Fault (MTB A-04)
6. WNW-ESE Trending Ruga Besar Fault (MTB A-03)

Estimated Temperature

The key hydrothermal alteration minerals from drill cuttings analysis every 3 m interval from drilled wells consist of smectite, intense silicification, chlorite, Illite, quartz, calcite, and epidote. Predicted temperature are made base on distribution and association of hydrothermal minerals (Table 2), the integration with MeB data then confirm predicted temperature from cutting description (Figure 9).

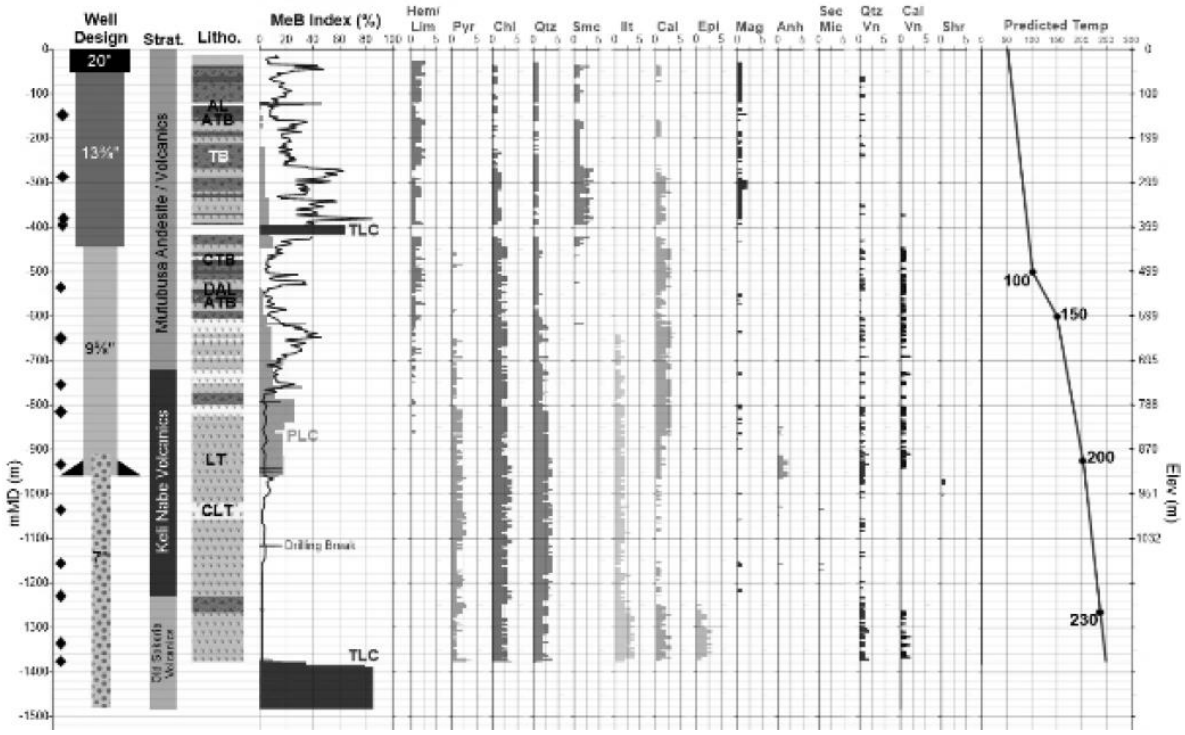


Figure 9: Simplified diagram showing the lithology, key alteration mineral and predicted temperature in MTB A-02 base on site microscopic analysis

Table 2: Hydrothermal alteration and mineral assembly of drilled wells in Sokoria Geothermal Area

DEPTH (mMD)	ALTERATION & MINERAL ASSEMBLY	PREDICT. TEMP(°C)
Surface - 400	Fresh to moderate alteration, dominated by oxide, chlorite are widespread in rare to weak amount, weak silicification, weak to moderate of smectite, intermittent of weak calcite, magnetite also observe in a few interval with rare to weak amount, quartz veining observed in part.	Ambient to <100
400 – 550	Moderate alteration, oxide observed minor to moderate, weak to moderate chlorite are widespread, silicification prevalent, pyrite embedded in groundmass with rare amount, smectite decreased weak to rare, weak to moderate calcite set in groundmass and as veining, quartz veining appearance in tuff breccia and lithic tuff.	100 - 150
550 – 850	Moderate to strong alteration, moderate to strong calcite as the most dominant alteration product replacing groundmass and formed as vein deposits, moderate to strong silica replacing groundmass and in part drussy form. Chlorite is moderate to strong. Illite present in rare to moderate amount as tiny specks in groundmass. Sulphide mineral appearance disseminated fine grain cubical pyrite rare to moderate and increased to depth. Fe-hydroxides are rare to moderate and decreased to depth. Magnetite spotted with rare amount. Anhydrite is nil to rare.	150 -220
Below 850	Primary minerals could not be identified due to strong alteration. Silicification is prevalent intergrown with moderate amorphous chlorite. Illite is widespread in weak to moderate amounts. Rare to weak calcite embedded in groundmass. Weak to moderate pyrite embedded in silicified groundmass. Magnetite spotted with rare amount. Anhydrite is rare to weak. Rare to minor amount of epidote become increasing to moderate abundant amount and continue appear below interval 1000mVD	> 220

CONCLUSIONS

- Based on rock cutting description and combined with regional geology data, three stratigraphic units are identified from the youngest to oldest are,
    - Mutubusa Volcanics.
    - Kelinabe Volcanics
    - Old Sokoria Volcanics
- The hydrothermal alteration zones are argillic alteration zone near surface to 400 – 500 mVD, phyllic zone from 500 to 850 mVD and propylitic alteration zone occurs from around 850 – 1000 mVD then deeper at relative Southwest prospect area.
- MeB analysis data shows smectite content decreasing with depth below 700 – 750 mVD, secondary minerals shows the first trace of incipient epidote started occurring ranging around 850 – 950 mVD then become clearer and continuous from 1000 – 1100 mVD indicates top of reservoir most likely occurring around 850 - 950 mVD
- Drilling data from 4 wells drilled intersect productive fault as follows:
    - E-W Trending EW Leledala Fault (MTB A-01, MTB A-02)
    - NW-SE Trending Nuamuri Fault (MTB A-01)
    - NE-SW Trending Leledala Fault (MTB A-02
    - NW-SE Trending Bela Fault (MTB A-04)
    - NNE-SSW Trending Loworia West Fault (MTB A-04)
    - WNW-ESE Trending Ruga Besar Fault (MTB A-03)

  Drilling parameter data, cutting description and spinner data from completion test confirm permeability of the fault
- Appearance of high temperature diagnostic minerals epidote, anhydrite suggest the temperature of reservoir reach above 220°C

REFERENCES

CGG Electromagnetics and PT Tunggal Buana Utama. (2016), 3D Modeling of Magnetotelluric (MT) Survey in Sokoria East Nusa Tenggara, Indonesia, *KS Orka internal report.*

FEDCO. (2016), Due Diligence Study Report on Sokoria Geothermal Prospect. *KS Orka internal report.*

FEDCO. (2017), Sokoria Lidar Analysis and Interpretation. *KS Orka internal report.*

Fredy N., and S. Dirasutisna. (1991), Laporan Geologi Panas Bumi Daerah Mutubasa, Ende Flores- Nusa Tenggara Timur. Geological Research and Development Centre, Bandung

Gunderson, R., Cumming, W., Astra, D., Harvey, C.C. (2000), "Analysis of Smectite Clays in Geothermal Drill Cuttings by The Methylene

Blue Method: for Well Site Geothermometry and Resistivity Sounding Correlation," *Proceedings World Geothermal Congress, Japan,* 2000.

Harvey, C.C, Gunderson, E.B., Johnstone, R.D., Christyono. (1998), "Sokoria, East Indonesia: A Classic Volcano-Hosted Hydrothermal System," *Proceedings 20th New Zealand Geothermal Workshop,* 1998

Harvey, C., Anderson, E., Johnstone, R. and Christyono. (2000). Co-Existing Volcanism and Hydrothermal Activity at Kelimutu, Flores Island, Eastern Indonesia. Proceedings World Geothermal Congress 2000, Kyushu - Tohoku, Japan, 28 May-10 June, 2000, 1-6.

Harvey, C.C., Gunderson, R., Cumming, W. (2000), "Methylene Blue Adsorption: A Real Time Rig Geologist Tool for Estimating Geothermal Reservoir Temperatures and Forecasting Drillhole Stability Problems," *New Zealand Geothermal Workshop,* 2000.

Panax Geothermal. (2012), Feasibility study for a 20 MW development at the Sokoria Geothermal Resource, Flores, Indonesia. Internal report.

PT PLN (PERSERO). (1995), "Studi Geosains PLTP Mini Sokoria, Ende, Flores, NTT", Laporan Akhir, Volume 2.

Robertus, S.L.S, Rezky, Y., Munandar, A., Suparman. (2007), "Geologi dan Ubahan Hidrotermal Sumur Eksplorasi SR-1 Lapangan Panas Bumi Sokoria-Mutubusa, Ende, Nusa Tenggara Timur," *Proceeding Pemaparan Hasil Kegiatan Lapangan dan Non Lapangan Tahun 2007*. Geological Research and Development Centre, Bandung.

Suwarna, N., Santosa, S. and Koesoemadinata, S. (1989), Geological map of the Ende quadrangle, East Nusatenggara. Geological Research and Development Centre, Bandung.

SUBSURFACE HYDROTHERMAL ALTERATION IN UMBUL-TELOMOYO GEOTHERMAL FIELD, CENTRAL JAVA

Hiskia Ulinuha Annisa[1], Niniek Rina Herdianita[1], and Dudi Hermawan[2]

[1] Geological Engineering, Institute of Teknologi Bandung (ITB)
[2]Centre of Mineral, Coal and Geothermal Resources, Bandung (PSDMBP)
Email: hiskia.annisa@gmail.com

ABSTRACT

Umbul-Telomoyo geothermal field is located in Quarter of Mount Telomoyo, Central Java. Cl-Li-B diagram described that this geothermal system consists of two different reservoirs and it is supported by Magnetotellurik survey (MT). Temperature estimation of Candi Dukuh at 215-230°C, while Candi Umbul reservoir at 240-250°C. Geothermal reserve is speculated 92 MWe which is feasible to further development.

This study utilazed are petrography analysis, XRD and fluid inclusions, which aim to determine rock permeability, temperature changes and ancient hydrothermal fluid. The collected samples come from coring data of CTL-1 and CTL-2 wells. Both of those wells about 700 meters in depth on each.

Litology of CTL-1 and CTL-2 wells were generally dominated by Telomoyo volcanic's product, lava and pyroclastic rocks. It has altered from in various range intensity such from low up to high. In general, in the research area is divided into two assemblages of minerals, namely acidic minerals and neutral minerals. Acidic minerals were located in shallow areas at 0 - 500 meters in depth characterized by clay minerals such as kaolinite, smectite, associated with quartz, calcite, anhydrite, siderite, gypsum, hematite, pyrite and alunite. Neutral minerals were located at a depth of 500 - 700 meters characterized by epidote and illite and associated with chlorite, calcite and anhydrite.

Paleotemperature shown by the presence of alteration minerals was 120-330°C and homogenization temperature reached at 325°C. However, the current temperature is shown by well temperature in a depth 0-700 meters at 20-99°C. This is indicates the cooling process in the research area.

Keywords : alteration, fluid inclusion, geothermal system, Telomoyo, vulkanic rock

INTRODUCTION

The geothermal field of Umbul-Telomoyo is considered a geothermal prospect area in Central Java, Indonesia, about 50 km south of Semarang, the capital of Central Java. The mainfestation appears at two area, in Ungaran and Magelang city. In Ungaran city, there are two manifestation, namely Candi Dukuh-1 and Candi Dukuh-2 hot spring, whereas in Magelang city, there are two manifestation, Candi Umbul and Pakis Dadu hot spring.

In 2010, Centre of Mineral, Coal and Geothermal Resources (PSDMBP) also carried out geology, geochemical and geophysical survey. The research provided an estimation of the potential geothermal reserve in the Umbul-Telomoyo area around ± 92 MWe which was included in the potential of geothermal energy in an unexpected reserve class. On the other side, in 2016, PSDMBP drilled the CTL-1 and CTL-2 wells at 702.6 and 703.4 meters depth. The lithologies of CTL-1 and CTL-2 were product of Telomoyo volcanic activity in which formed lava and pyroclastic rocks. It altered from weak to very strong intensity (Figure.1).

GEOLOGY

The stratigraphy of researce area consist of volcanic rocks such as lava and pyroclastic from Ungaran, Telomoyo, Andong and Merbabu products. The research area consists of 17 lithological units, i.e from the oldest to the youngest these are sedimentary rock, Ungaran Lava-1, Telomoyo Lava-1, Telomoyo Pyroclastic Flow-1, Telomoyo Lava-2, Telomoyo Pyroclastic Flow-2, Telomoyo Pyroclastic Fall, Andong Lava, Telomoyo Lava-3, Ungaran Lava-2, Merbabu Lava-1, Merbabu Pyroclastic Flow, Telomoyo Kolluvium, Merbabu Lava-2, Merbabu Pyroclastic Fall, and Merbabu Lahar (Figure. 2)

Structural geology found in research area are :

a) Three rims of the caldera impacted to subsidence that created the depression zone.
b) Volcanic structure such SW-NE normal fault was formed by the activity of Telomoyo Mount. This structure also caused the discharge of manifestations of Candi Umbul and Pakis Dadu.
c) The tectonic structures such as strike-slip faults were relatively N-S and NW-SE which was the regional structure and partly covered by younger rocks. Some of these structures were reactivated and influenced the occurance of manifestations of Candi Dukuh.

LITHOLOGY

The main lithology in wells CTL-1 and CTL-2 were identified by analyzing of coring which are tuff, andesite and breccia. Pyroclastic breccia was generally gray, fragments composed of andesite, afanitic, less than 5 cm in size, with angular shape embedded in tuff base mass and gray glass masses, open packing, poor sorting, green and moderate porosity. While black andesite lava, afanitic, consists of plagioclase, mineral mafic, glass vulcanic and compact. Tuff had physical characteristic such as grayish, grain size gray ash, good sorting, closed pack, medium porosity and brittle. The rocks came through the intensity of mineral changes from weak to very strong. These rock are identified and confirmed by megascopis and petrography analysis.

HYDROTHERMAL ALTERATION

Hydrothermal Alteration Mineral

Hydrothermal alteration is seen as change in mineralogy, texture and chemistry of rocks due to thermal and environmental changes facilitated by geothermal fluid. The intensity of changes also depends on texture and time. The factore that control alteration in geothermal systems are temperature, rock type, permeablity, fluid composition and the duration of fluid-rock interactions (Reyes, 2000).

In Umbul-Telomoyo geothermal field, hydrothermal alteration minerals appear both as replacement of the primary minerals, as well as filling vugs and fractures, replacement and leaching or dissolution. Replacement textures record interactions between fluids and the host rock. The paragenesis of the space-fill minerals was used to infer the sequence of chemical and physical changes that occured in the circulating fluids. The distribution and abundance of the hydrothermal minerals were obtained from the petrographic and XRD analysis of coring samples taken at different depths.

The main hydrothermal minerals in Umbul-Telomoyo fields are clay minerals (illite, chlorite, kaolinite, and smectite), calcite, anhydrite, and secondary quartz. In addition minor amounts of epidote, gypsum, zeolite, pyrite, alunite, and hematite are present. The distribution of hydrothermal minerals in CTL-1 and CTL-2 wells are shown in Figure. 3 and Figure. 4. Below is a description of the hydrothermal alteration minerals encountered in the Umbul-Telomoyo wells.

Clay Minerals (Smectite, Illite, Chlorite and Kaolinite)

Clay minerals presented on various depth on sample of CTL-1 and CTL-2 wells. Clay minerals commonly altered plagioclase phenocryst and groundmass of volcanic glass. Clay minerals identified by X-Ray diffraction (XRD). They are kaolinite, smectite, and illite.

Chlorite was found to have a brownish green colour, which characterizes chlorite having a rich content of the Mg element. The deeper the depth of the well, the presence of chlorite found more and more.

Secondary Quartz Minerals

Quartz is colourless to white in colour and occurs in euhedral to subhedral crystals. Replacement of minerals that form quartz occurs in every depth. Quartz was generally present associated with calcite and anhydrite. It was formed as a change of plagioclase. It also changed the groundmass as a result of silicification. Quartz that fill the veins and cavities were commonly found through direct precipitation or replacement processes.

Carbonate Minerals

Carbonate minerals consisted of calcite and siderite. Calcite was found in almost every depth. Calcite was present altered the groundmass of the glass and replaced plagioclase phenocryst. Calcite that filled the veins and cavities, after quartz or anhydrite. While, siderite was found in shallow depths (0 - 450 m) and is more common in CTL-1 well. Siderite altered hornblende.

Sulfate Minerals

Sulfate minerals consisted of anhydrite and gypsum. As with quartz and calcite, anhydrite was also found in almost every depth. Anhydrite was present altered of plagioclase, groundmass, and filled the veins and cavities. Meanwhile, gypsum was found in shallow depths and filled cavities. It was present as a vein that replaces calcite. The presence of calcite and anhydrite minerals indicated that fluids contained considerable CO_2 and SO_4.

Calc-silicate Minerals

Calc-silicate minerals consisted of epidote and zeolite. Epidote was formed at high temperatures and in environmental conditions with a neutral pH. Epidote was found in relatively deep depths, with little abundance. It was always appeared with calcite. Early epidote occured at >490 m, which was used to identified as top of reservoir. While, zeolite was found in CTL-1 wells, with little abundance (<5%). Zeolites present altered glass minerals.

Other Minerals

There were various minerals may also appear e.g. pyrite, hematite, and alunite.

Pyrite appeared as an opaque mineral formed in shallow to the deepest depths. Pyrite replaced pyroxene, anhydrite and vein fill.

Hematite was formed due to the oxidation process. This mineral existed as a basic mass with considerable abundance. Hematite altered plagioclase and volcanic glass.

Alunite present filled the veins and cavities associated with quartz. In the study area, alunite formed in shallow depths (<300 m).

Paragenesis of Hydrothermal Minerals

According to Browne (1991), direct deposition is one type of hydrothermal alteration. In the corring of CTL-1 and CTL-2 wells are found to be quite a lot of cross-cutting veins and cavities. This cross-cutting can show the paragenesis of the hydrothermal alteration mineral. Minerals found to form veins and cavities are quartz, calcite, anhydrite, chlorite, pyrite, epidote, clay mineral, hematite, and alunite. The most commonly found minerals as vein and cavity fillers are quartz, calcite and anhydrite.

An early episode is characterised by simple quartz veining, a middle episode by many stages of mineralisation with more diverse mineralogy, incluidng quartz, calcite, anhydrite, chlorite, and gypsum. The latest episode was characterised by deposition of pyrite.

PALEOTEMPERATURE AND WELLS TEMPERATURE

Paleotemperatur is a temperature in the past conditions obtained from the estimated temperature of alteration mineral formation and homogenization temperature of fluid inclusions. As for the well temperature is the temperature measured after the drilling. These wells are interpreted as temperatures under current conditions.

Paleotemperature

The range of hydrothermal alteration mineral temperature in CTL-1 and CTL-2 wells can be known from the distribution of alteration mineral temperature found in the research area. Estimation of alteration mineral formation temperature based on Reyes (1990) at depth 0-490 meter range from 120-180°C. At this depth it is interpreted as a caprock zone characterized by clay minerals (smectite and kaolinite), which are associated with minerals of calcite, anhydrite, quartz, siderite, gypsum, and alunite. While at a depth of 490-700 meters the estimated temperature of alteration mineral formation ranges from 240-330°C, with characterized by epidote associated with illite and chlorite and interpreted as a reservoir zone.

While from the homogenization temperature data of fluid inclusion in Umbul-Telomoyo field sample was measured to determine the formation temperatures during entrapment. This inclusion is hosted by calcite vein at 403 m in CTL-2 well. The fluid inclusion was analyzed amounted to 12 primary inclusions measuring 5-24 μm. The trapped fluid is liquid rich with V/L ratio of 0,2-0,5.

Paleotemperatures of fluid inclusion data are known from homogenizing temperatures (Th). This temperature is known from the heating process, so the inclusion of a two phase fluid is transformed into a single phase. From the analysis conducted, homogenisation temperature (Th) obtained at a depth of 403 meters, is 325ºC (Figure. 5)

In addition to know the value of homogenization temperature (Th) can also know the evolution of the fluid that occurs is by using data melting temperature (Tm) and then obtained salinity value. From the data of the average value of melting temperature (Tm) obtained is -0.78ºC, while for the average salinity value is 1.39 wt% NaCl equiv. Then the salinity values are generated with the homogenization temperature (Th) (Figure. 6). Trends in salinity values against the Th values can illustrate fluid processes occurring in the study area (Wilkinson, 2001). By comparing Figure. 7 with Wilkinson (2001) diagram it can be seen that the process that occurs in the research area is based on the value of Tm in the fluid inclusion analysis that is mixing with the surface fluid.

From the data of alteration mineral temperature range and homogenesization temperature (Th) values were found at a depth of 403 meters with the discovery of fluid inclusions. From alteration mineral data obtained temperature value around 160-180°C, while the data of fluid inclusion obtained temperature 325°C. This temperature change is indicated by heating.

Well Temperature

The measurement of logging temperature in CTL-1 well was obtained the number of 151, 494 and 700 meters of depth formation at 37.25ºC, 70.43°C and 91.23ºC respectively. The CTL-1 well thermal gradient is 9.6°C/100 meters until 700 meters depth.

Whereas, in the CTL-2 well, measurement of temperature logging obtained temperature value of formation at depth of 149, 501 and 700 meter equal to 35,66°C, 73,21°C and 99,12°C respectively. Therefore, the CTL-2 well thermal gradient at a depth of 700 meters is 11.2°C/100 meters.

From the correlation of the drilling temperature data between CTL-1 and CTL-2 wells indicates that both wells have interaction of hot fluid with rocks so that the temperature rise in the south toward to the CTL-2 well which is probably continuously toward the peak of Mount Telomoyo. This proves that the heat source that forms the Umbul-Telomoyo geothermal system is associated with the recent volcanic activity of Mount Telomoyo.

COMPARISON OF TEMPERATURE DATA

By comparing the past and present conditions, in the study area has been changed temperature in the caprock and the reservoir zone. Temperature of

current condisition was known from geothermometer data for temperature in reservoir and thermal gradient data (CTL-1 and CTL-2 wells) for temperature in caprock. While past condition temperature was obtained from the range of hydrothermall alteration temperature.

Table 1. Temperature changes in the past and present

TEMPERATURE		
ZONE	**PAST**	**NOW**
Caprock	120 – 180°C	36 – 193°C
Reservoir	260 – 330°C	215 – 250°C

Based on Table.1, the hydrothermal minerals indicate mostly higher temperatures than those now measured. Caprock and reservoir indicated cooling process. Lowering temperature may be caused :

1. The influence of cold water circulation at the drilling wells, so that the fluid becomes colder, or
2. The mixing with cold water that is located not far from the wells, or
3. The influence of meteoric water which is seen in Mg content of the chemical mainifestation of hot spring.

CONCLUSION

1. The geothermal system of Umbul-Telomoyo belongs to a volcanic complex system that is heavily associated with Telemoyo complex activities. The geological structure of the study area is dominated by some relatively NE-SW and NW-SE trending fault structures that are predicted to facilitate the release of hot springs in the study area. In this system there are two reservoirs located in NE and SW of the research area. The reservoir layer is estimated at depths > 1500 meters.
2. Alteration minerals in CTL-1 and CTL-2 wells were dominated by clay minerals, quartz, calcite and anhydrite. There were also mineral gypsum, epidote, siderite, hematite and pyrite.
3. In the research area has changed the temperature in the capcrock zone and reservoir zone. the hydrothermal minerals indicate mostly higher temperatures than those now measured. Caprock and reservoir indicated cooling process.

REFERENCES

Herdianita, N. R (2012): The Evolution of The Derajat Geothermal System, West Java, Indonesia. Dissertation, Univerity of Auckland.

Pusat Sumber Daya Mineral, Batubara dan Panasbumi (2010): Penyelidikan Terpadu Daerah Panasbumi Candi Umbul Telomoyo, Provinsi Jawa Tengah

Pusat Sumber Daya Mineral, Batubara dan Panasbumi (2016): Landaian Suhu sumur CTL-1 Daerah Panas Bumi Umbul-Telomoyo Kabupaten Semarang. Provinsi Jawa Tengah.

Pusat Sumber Daya Mineral, Batubara dan Panasbumi (2016): Landaian Suhu sumur CTL-2 Daerah Panas Bumi Umbul-Telomoyo Kabupaten Semarang. Provinsi Jawa Tengah.

Reyes, A. G., (1990): Petrology of Philippine Geothermal Systems and The Application of Alteration Mineralogy To Their Assessment. Journal of Volcanology and Geothermal Research, 43, p.279-309

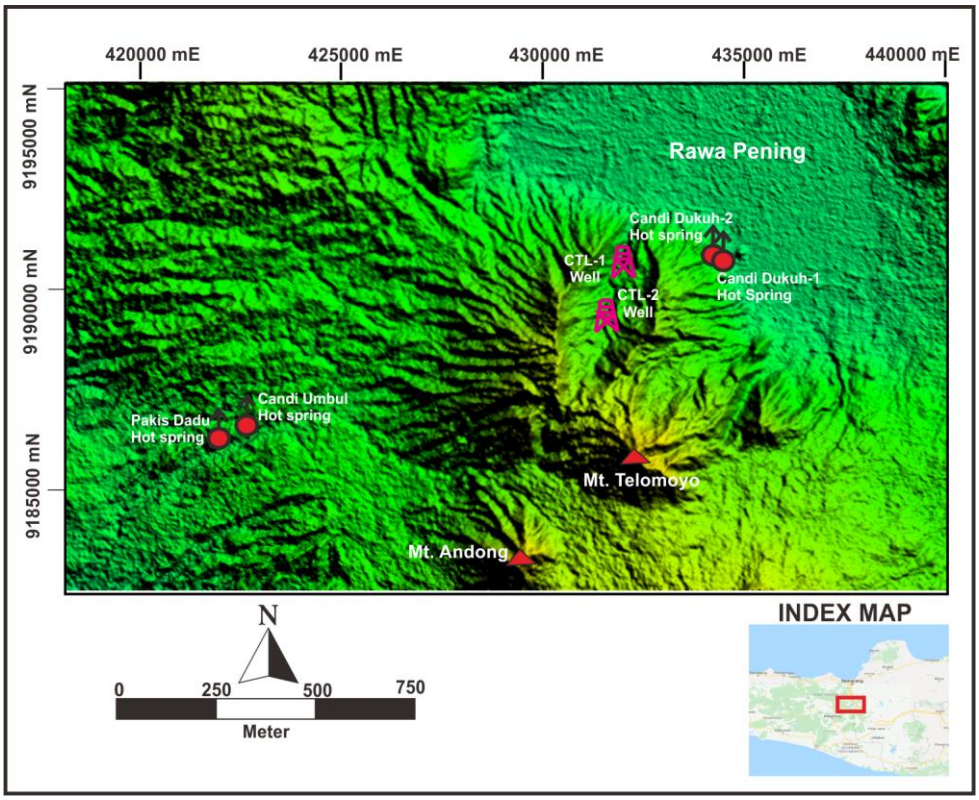


Figure 1. Location of Research Area

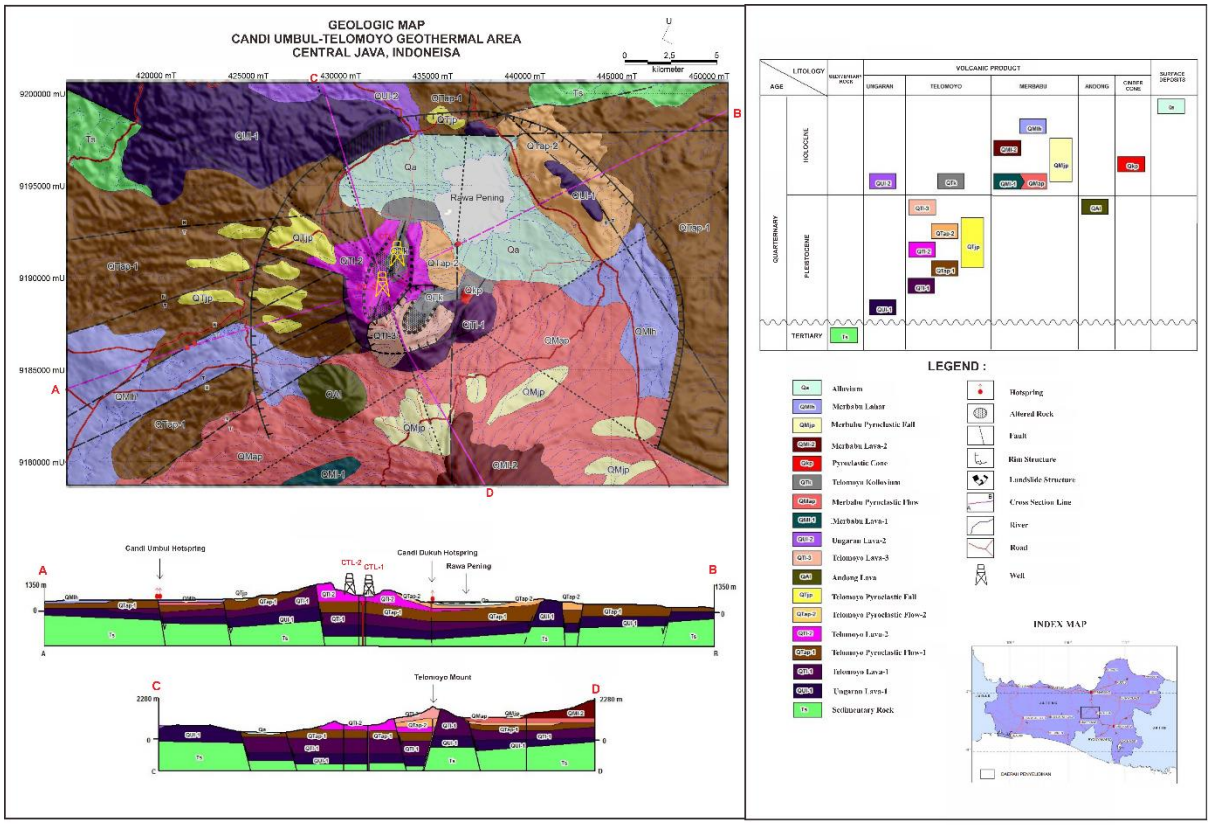


Figure 2. Geologycal Maps in Umbul Telomoyo (PSDMBP, 2010)

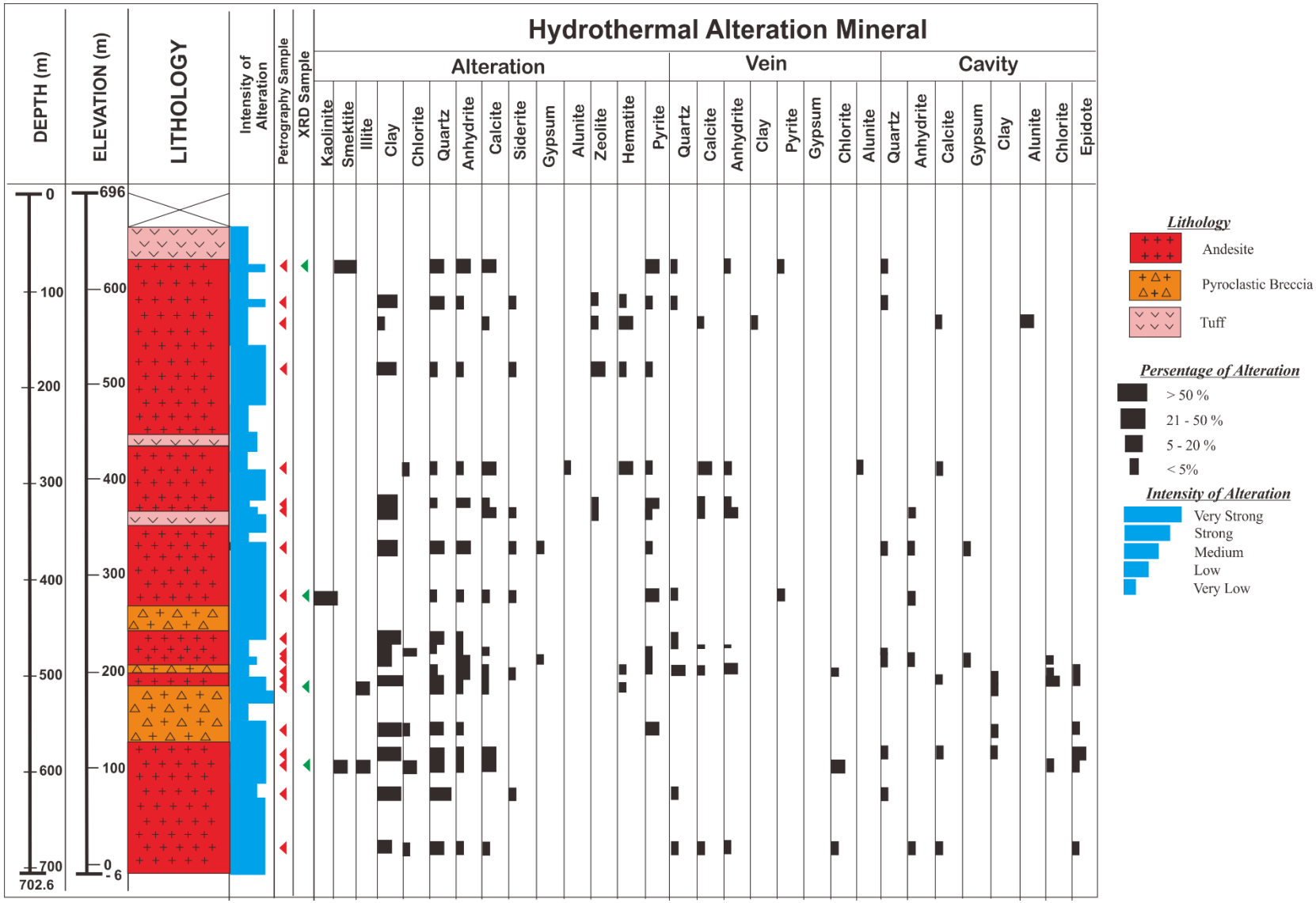


Figure 3. The Distribution of Hydrothermal Minerals in CTL-1 Well.

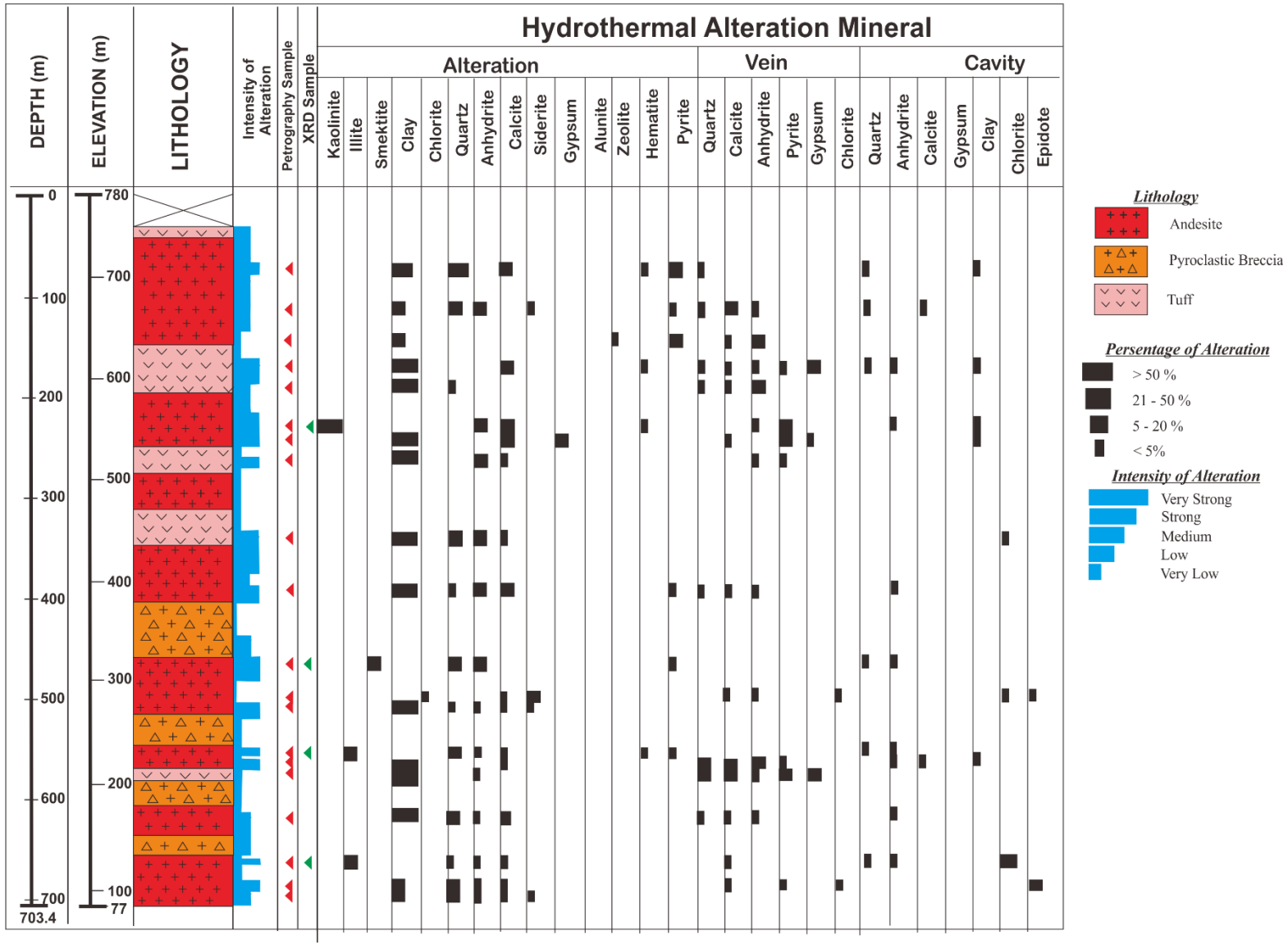


Figure 4. The Distribution of Hydrothermal Minerals in CTL-2 Well.

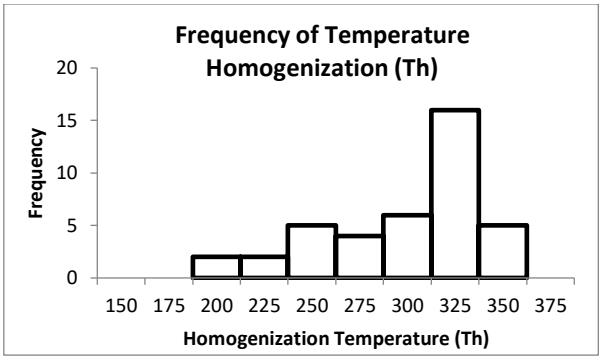


Figure 5. Graph of Homogenization Temperature (Th) to Frequency

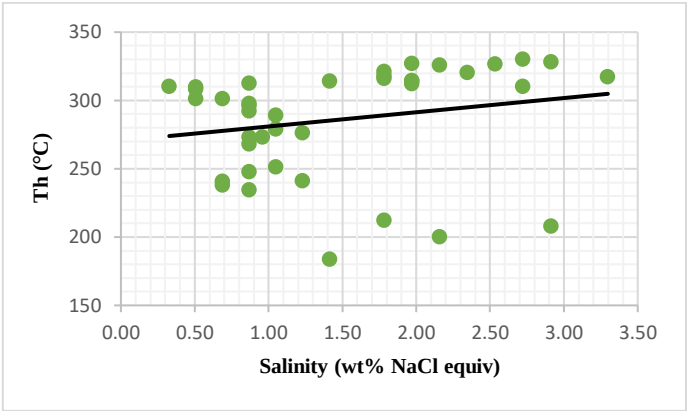


Figure 6. Graph of Trends in Salinity to Th Value.

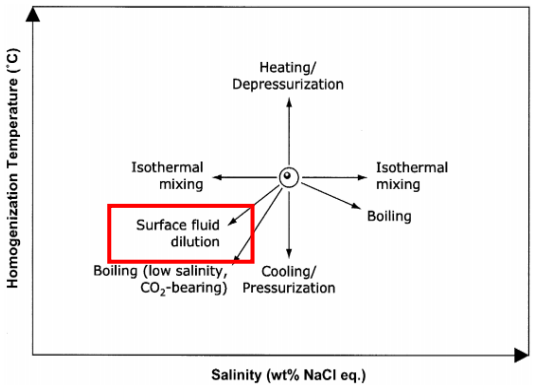


Figure 7. A Diagram Showing The Variation of Fluid Evolution Process from Salinity and Homogenization Temperature (Th) values based on Wilkinson (2001).

SUBSURFACE STRATIGRAPHY AND HYDROTHERMAL ALTERATION MINERALOGY OF WELL E HULULAIS GEOTHERMAL FIELD, BENGKULU, INDONESIA

Putra, I. D.[1] and Nusantara, V. D. M.[2]

[1]Geological Engineering Departement, Faculty of Engineering, University of Gadjah Mada
[2]Pertamina Geothermal Energy
Grafika St.2 Bulaksumur, Sinduadi, Mlati, Sinduadi, Sleman, D.I. Yogyakarta 55284 and Skyline Building, M.H. Thamrin Street, Jakarta
Email: ilham.dharmawan.p@mail.ugm.ac.id

ABSTRACT

Research area is located in Hululais geothermal area, Lebong District, Bengkulu, Indonesia. Pertamina Geothermal Energy (PT PGE) drilled 2941 m depth exploration well in 2017, named by Well HLS E. This research is intended to know the subsurface stratigraphy and hydrothermal alteration mineralogy from HLS E. Twelve (12) cuttings and six (6) cores samples are collected from various depths to be observed through megascopic observation, thin section, X-ray diffraction (XRD), and fluid inclusion combined with methylene blue titration (MBT), lost circulation, and rate of penetration (ROP) data from drilling activity. The results derived from the observations show that there are ±26 stratigraphic layers, predominantly consist of unconsolidated volcanic materials, andesite, tuff breccia, and andesite breccia. There are three (3) zones of alteration, the smectite zone (<200^{O}C) at 84-552 m depth, illite-chlorite zone (220 – 250^{O} C) at 552 – 975 m depth, and epidote zone (220–350^{O} C) at 975 - 2941 m depth. Smectite zone is characterized by the presence of smectite, calcite, chlorites, and secondary quartz. Illite-chlorite zone is characterized by the presence of illite, chlorite, and anhydrite. Epidote zone is characterized by the presence of epidote, anhydrite, illite, calcite, garnet, and secondary quartz. There are two geothermal zone generated in this study, the cap rock and reservoir zone. Cap rock zone is characterized by high percentage of clay minerals, such as smectite, chlorite and illite, and reservoir zone is mainly characterized by the presence of epidote showing increasingly-growth crystal which has relations with increased depth. The study concluded that, Hululais geothermal field has unique characters, as the geothermal system could be classified as a high temperature system, liquid dominated system, and neutral pH fluid, followed by good of both primary and secondary permeability system.

Keywords: Hululais, Subsurface stratigraphy, Hydrothermal Alteration, High Temperature, Liquid Dominated, Neutral pH fluid

INTRODUCTION

Indonesia is a country that have several conditions to develop geothermal systems. The conjunction of three tectonic plates of Eurasia, Indo-Australia, and Pacific has created such conditions of volcanic chain as the parts of world's ring of fire (Verstappen, 2010). This conditions later produced some of geological potentials, one of it is geothermal energy. Some of previously research concluded that there are 40% potential of world geothermal energy can be found in Indonesia, but only little percentage (about 5%) of geothermal energy in Indonesia has been utilized (Rozak et al., 2015). Hululais geothermal field is administratively located at Lebong District, In Bengkulu Province. Kamah et al., (2015) stated that this field could be developed further because of it promising potentials, where 10 – 20 MW of electricity potential are proven by the drilled exploration wells done by PT PGE. This research is intended to supports the exploration activity done by PGE by revealing the subsurface stratigraphy and subsurface hydrothermal alteration mineralogy from well HLS E. through the information of subsurface stratigraphy and hydrothermal alteration, the plans of field development could be achieved.

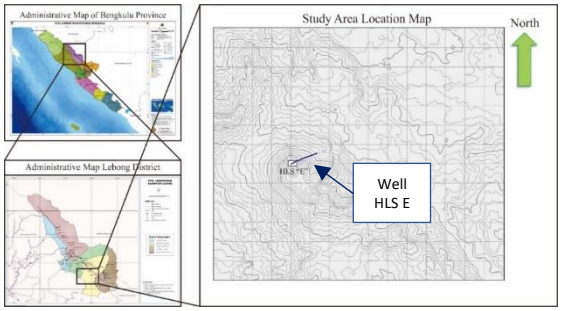


Figure 1: Research area location, administratively (modificated from Kamah et al., 2015).

GEOLOGY

Some researchers conducted studies to reveals the geological conditions of Hululais geothermal field. Physiographically, Hululais geothermal field is located in the volcanic zone of Mt. Bukit Barisan and Sumatran great-dextral fault, as can be seen in figure 2.

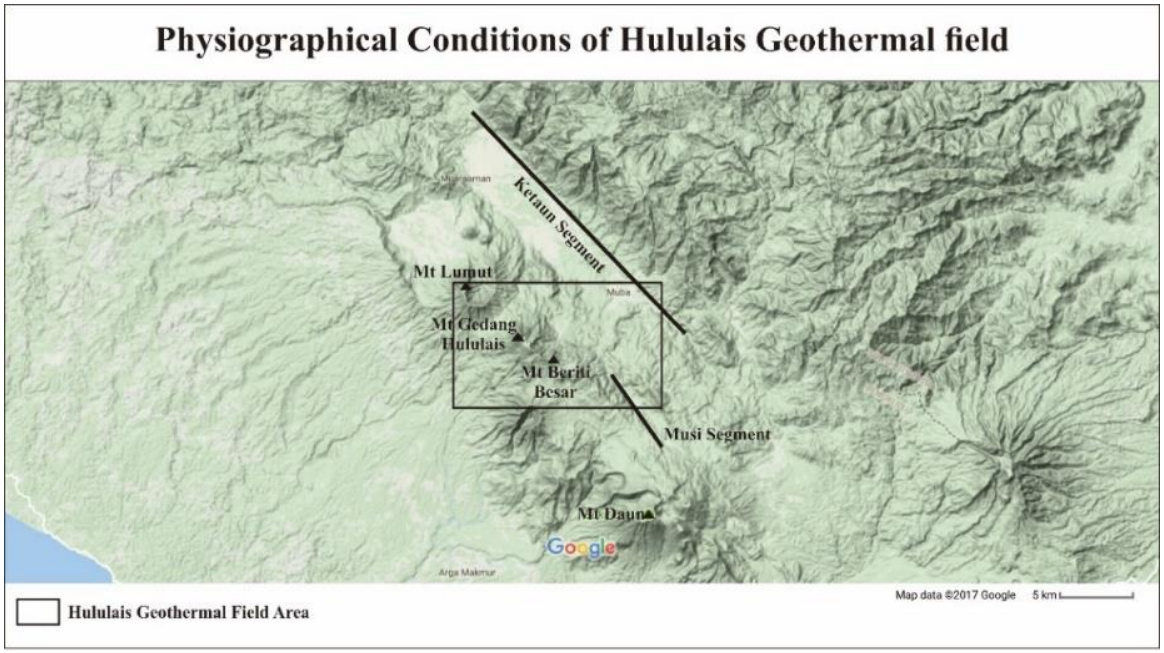


Figure 2: Physiographical conditions of Hululais geothermal field, located on Bukit Barisan volcanic zone and dextral great sumatran fault system (modified from Google earth Landsat image, based on Gafoer et al., (1992), Muraoka et al., (2010) and Juanda et al (2015))

The lithology of research area consist of volcanic rock unit of andesite and basalt, volcanic rock unit of rhyolite and andesite, and Hulusimpang Formation (Gafoer et al., 1992). The condition of subsurface stratigraphy also has been investigated by Nusantara et al., (2016) from several exploration wells of A1, E1 and C1 (see figure 4). that there are several lithology units that construct the Hululais geothermal field, those are andesite, basaltic andesite, andesite breccia, tuff breccia, and metasediment as basement rock. Heat source also expected came from diorite and granodiorite intrusions. The structures that present in the study area also has been investigated by Budiardjo et al., (2010) and Kamah et al., (2015) that there are two main orientation of structural orientation in the research area, the NW – SE and the NE – SW orientations (see figure 2). Early fault formations have characteristics of horizontal fault with Northeast dipping, meanwhile the later fault formations have characteristics of normal fault with Northwest dipping. This NW – SE fault orientation is believed control the secondary permeability of Hululais geothermal field (Kamah et al., 2015).

GOALS AND METHODS

Several drill cuttings and cores have been collected from various depth in HLS E well to be prepared for megascopic observation, petrographic analyses, X-Ray Diffraction (XRD) analyses, and fluid inclusions. Several drilling data also have been used to be combined with previous analysis, such as Methylene blue dye test (MBT), rate of penetration (ROP), and Loss circulation data.

The observation has been done in Pertamina Geothermal Energy (PT PGE) and Kamojang Geothermal Information Center (GIC), where about 35 thin sections and 24 XRD samples from various depth were prepared and analyzed (see table 1.)

Petrographic and XRD observation to identify rocks and minerals will be done based on standard terminology from previous research, i.e. Barker (2014) for petrography and Chen (1973) for XRD.

This research is intended to reveal the conditions of well HLS E, which are subsurface stratigraphy, hydrothermal alteration mineralogy, and its implication to assume subsurface conditions such as temperature, geothermal zone, permeability, fluid acidity, and others.

RESULTS

Subsurface stratigraphy

Observation to reveal the subsurface stratigraphy are conducted through megascopic and petrographic combined with rate of penetration (ROP) data has resulted in at least four (4) unit of lithology that construct the well HLS E, they are unconsolidated volcanic materials, andesite, andesite breccia, and tuff breccia as can be seen in figure 3.

Unconsolidated Volcanic Materials

Unconsolidated Volcanic Materials are found at depth of 0 m (surface) to 49 m of the borehole. This unit consists of rocks lithic of aphanitic Andesite, porphyry andesite, porphyry basalt, and tuff. This rock unit found as unaltered materials, only little

signs of alteration are found. ROP analysis shows the value of 7.0 – 22.8 minutes to drill one meter of the borehole when penetrating this unconsolidated volcanic material. This unit remained unaltered (see figure 3).

Table 1. Analyzed cutting and cores from various depth of the well HLS E and the methods used.

Cut-tings	Cores	XRD	Fluid Inclu-sion
48 m	2175,6A m	251 m	1050 m
249 m	2175,6B m	351 m	1451 m
351 m	2175,6C m	552 m	
552 m	2175,7A m	651 m	
652 m	2175,7B m	750 m	
750 m	2175,7C m	951 m	
951 m		1050 m	
1050 m		1152 m	
1152 m		1250 m	
1250 m		1352 m	
1352 m		1451 m	
1451 m			

Altered Andesite

Altered andesite is found in the various depth of well HLS E and recognized when only one type of cutting is found, and showing fine gray – blackish gray fine minerals in megascopic observation. In petrographic observation, andesite show porphyro-aphanitic texture and interlocking minerals, where plagioclase and pyroxene present as phenocryst, meanwhile plagioclase microlites and volcanic glass present as groundmass. Some andesite also found in trachytic texture indicate as andesite lavas. Petrographic observation also could distinguish the altered cutting clearly, as several cuttings are altered by replacement of primary minerals into secondary minerals such as smectite, calcite, chlorite, illite, epidote, and others, or direct deposition of secondary minerals from the precipitation of hydrothermal fluid, produces secondary quartz, calcite, anhydrite, and pyrites/ opaque minerals. ROP analysis shows the value of 6.1 – 30 minutes to drill one meter of the borehole when penetrating this altered andesite unit. In the depth of ±1472 m and so on, cuttings are not found (total loss circulation) expected due to the presence of fractured andesite that identified from core samples in 2175 m depth (see figure 3).

Altered Tuff Breccia

Tuff breccia in mainly found at the depth of 372 – 452 meters as interbedded rock unit between andesite and andesite breccia units. Tuff breccia is recognized through megascopic observation where tuff breccia is showing characteristics of sticky and washout, that made thin section couldn't cover the observation (see figure 3).

Altered Andesite Breccia

Andesite breccia is found in various depth of HLS E borehole and recognized when there are more than one types of cutting were found, crystalline rock (i.e andesite) as fragments, and non-crystalline rock (i.e. tuff) as matrix. Altered andesite breccia can be clearly seen through petrographic observation, where cuttings are mainly replaced into secondary minerals such as smectite, calcite, chlorite, illite, epidote and others or deposition of secondary minerals, such as secondary quartz, calcite, anhydrites, and pyrites/ opaque minerals. ROP data show value of 1,3 to 33 minutes to drill one meter when penetrating andesite breccia units, high values are expected as drilling process of andesite breccia with andesite fragment supported, meanwhile low values are expected as drilling process of andesite breccia with matrix supported conditions (see figure 3).

Structures

Investigation of loss circulation zone found that partial loss circulation (PLC) and total loss circulation (TLC) are exist. Fluid loss value of > 0 to < 20 bpm is classified as PLC and fluid loss value of > 20 bpm is classified ad TLC.

PLC zone are identified well's depth of 79 – 122 m, 136 – 153 m, 162 – 168 m, 176 – 210 m, 587 – 588 m, 619 m, 647 m, 696 m, 1208 – 1209 m, 1394 – 1407, 1407 – 1419 m, 1424 – 1445 m, and 1458 – 1474 m. TLC zone are identified at borehole depth of 49 – 75 m, 168 – 176 m, 453 – 508 m, 1474 – 2941 m.

Fault presence and fracture could be inferred as causes of the presence of loss circulation zone in Hululais (Kamah et al., 2015 and Budiardjo., 2010). In this study, the observation of cores thin sections from 2175,6 and 2175,7 m depth show that TLC zones are present due to fractured rock, and also could be associated with fault zone as well.

Hydrothermal Alteration

Observation to reveal the subsurface hydrothermal alteration using megascopic, petrographic, XRD, and fluid inclusion combined with MBT data has resulted that there are several hydrothermal alteration minerals identified, they are hematite, smectite, chlorite, illite, anhydrite, alunite, pyrophyllite, epidote, garnet, calcite, and secondary quartz (tridymite, cristobalite, and quartz).

Several primary minerals found in this analyses are plagioclase, pyroxene, primary quartz, and volcanic glass. Plagioclase and pyroxene are found altered into any kinds of minerals, such as calcite, illite, secondary quartz, chlorite, smectite, and epidote.

Volcanic glass also found altered into any kind of secondary minerals, such as such as calcite, illite, secondary quartz, chlorite, smectite, and epidote.

Smectite is found from the surface to depth of 552 meters. First occurrence of illite is found at 552 m depth. First occurrence of Epidote is found at 975 m depth. Hydrothermal alteration such as secondary quartz, anhydrite, calcite, and pyrite are found as direct deposition minerals in the matrix of veins identified from petrographic analyses. Epidote is found as a replacement mineral of plagioclase, and volcanic glass as well as direct deposition in fractured andesite where epidote showing yellow pistachio and has high birefringence. Garnet is found in petrographic analyses at borehole depth 2175.7 m showing high relief and isotropic characteristic.

Alteration intensity (AI) has been investigated through petrographic observation using point counting method showing various AI values that based on Browne (1984) intensity of alteration classification. Surface to 84 m is found as unaltered volcanic materials (AI=0). Later, in the depth of 85 – 1472 m, alteration intensity found ranged from 0.25 to 0.60, where the high AI is followed by the presence of secondary permeability or partial loss-circulation zone. At borehole depth of 1472 m – 2941, AI is observed through cores thin section that showed AI values of 0.6 – 0.7.

Fluid inclusion study also reveals the subsurface temperature and salinity of the hydrothermal fluids of HLS E borehole. Temperature measurement at 1050 m depth show mean value of 245.8^{O} C, modus of 250 – 255^{O} C and salinity of 1,7 – 2,0 % Wt NaCl. Temperature measurement at 1451 borehole depth show mean value of 259O C, modus 250 – 260O C, and salinity of 1.7 – 2.0% Wt NaCl. Fluid inclusion study showing the temperature as inferred from petrographic and XRD study.

DISCUSSIONS

The data obtained of Borehole stratigraphy and Hydrothermal alteration have been used to determine the characteristics of geothermal system of well HLS E, also to identify the geothermal zones. Based on the presence of identified hydrothermal alteration minerals, three (3) zone of hydrothermal alteration could be constructed, the smectite zone, illite-chlorite zone, and epidote zone.

Hydrothermal Alteration Zones

The smectite zone indicate low temperature zone that characterized by the presence of smectite minerals which has temperature of <200^{O} C (Reyes, 1990). This zone was found in the depth of 84 – 975 meter and characterized mainly by the high percentage of smectite minerals identified from MBT data and XRD analyses. Moreover, the other mineral characterized the smectite zone are calcite, chlorite, and secondary quartz.

The illite-chlorite zone was identified through the first occurrence of illite in 552 m depth which replacing the presence of smectite mineral that end in 552 m depth, and present together with chlorite, secondary quartz and anhydrite minerals. This zone extends until 975 m depth, and ended where first occurrence of incipient epidote minerals present. Based on (Reyes, 1990), the temperature of this zone was expected about 220 – 250^{O} C.

The epidote zone indicate high temperature zone. This zone was found in the depth of 975 – 2941 meter and characterized mainly by the presence of epidote minerals that showing increasingly-growth crystal, together with illite, anhydrite, calcite, secondary quartz and chlorite minerals. Based on Reyes (1990), this temperature of incipient epidote to epidote type 3 is expected about 200 – 350^{O} C, but by the presence of other mineral, such as illite, the temperature of this zone is expected ranged from 220 to 350^{O} C. The first occurrence of epidote was analyzed through megascopic observation in the borehole depth of 975 meter as incipient epidote and in depth of 2175.7 meter of borehole depth epidote is found as growth long hexagonal-shaped crystals. Moreover, the presence of garnet minerals in 2175.7 m depth also shows that the lower part this zone can be classified as very high temperature geothermal zone

Geothermal Zone

Three (3) geothermal zone are identified in this study, the cap rock zone, transition zone and the reservoir zone. Based on Browne (1984), cap rock zone can be characterized by the presence of clay minerals and carbonates, i.e. smectite, meanwhile reservoir zone can be characterized by epidote, chlorite, calcite, ±pyrite, and ±illite. In this study, cap rock zone are found associated with smectite zone where smectite mineral abundantly found in 200 – 552 m depth, transition zone is characterized by first occurrence of illite mineral in 552 m depth until 975 m depth, where top of reservoir zone is taken by identifying the first occurrence of epidote (incipient epidote) in 975 m depth.

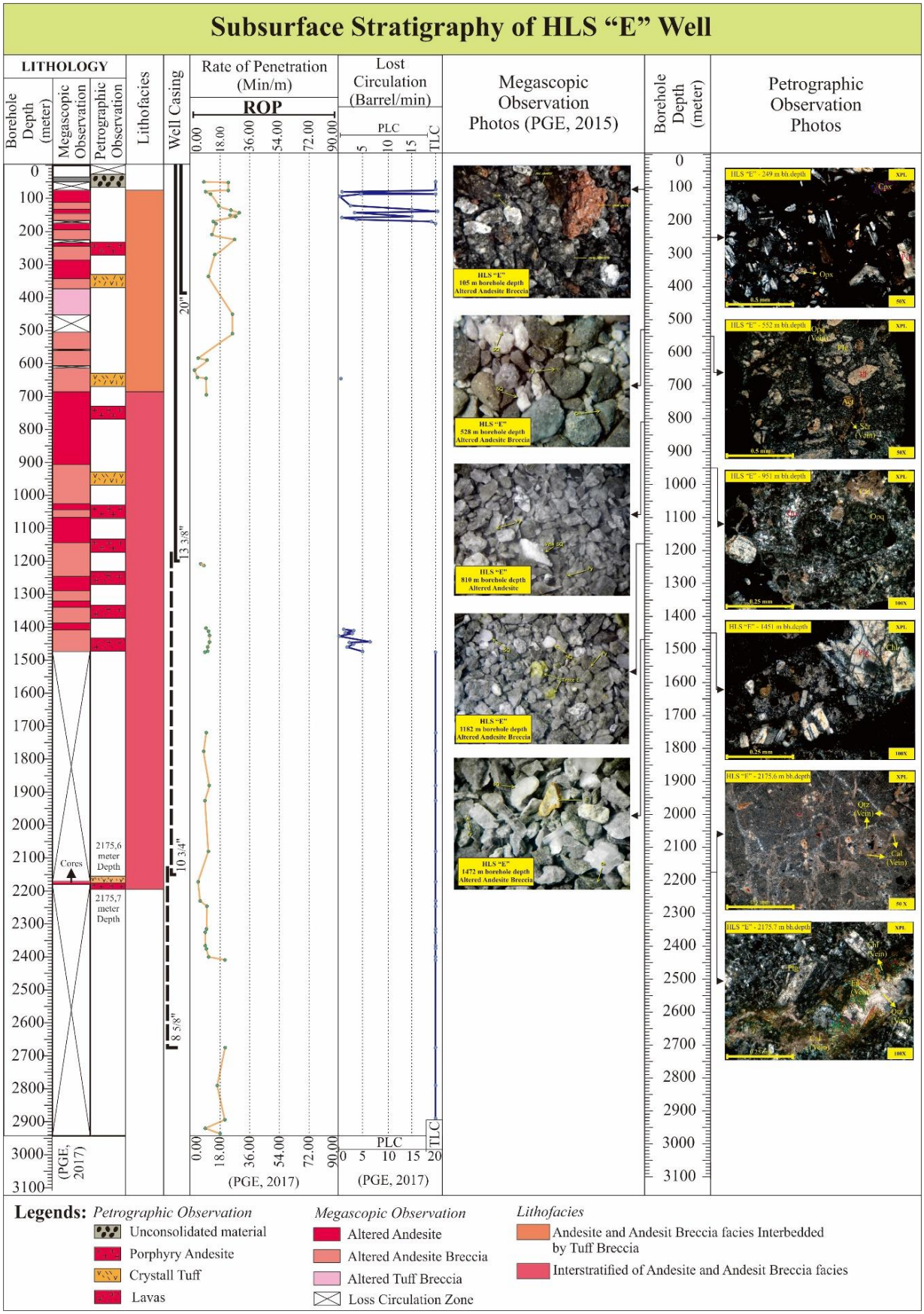


Figure 3: Subsurface stratigraphy log of well HLS E

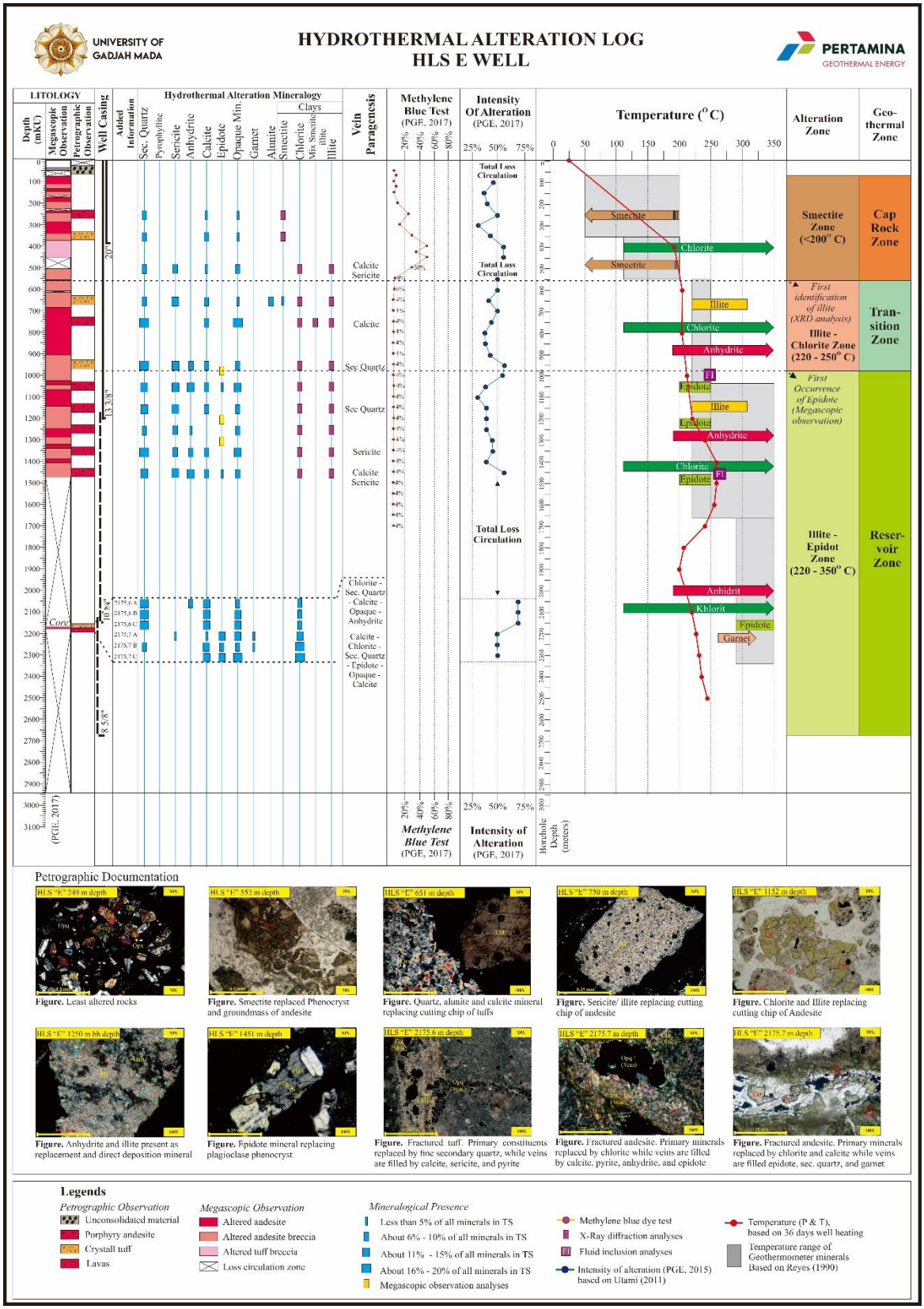


Figure 4: Hydrothermal alteration log of well HLS E

Hydrothermal Alteration

The presence of epidote, which has temperature range of 200 – 350^{O} C (Reyes, 1990) and temperature measurement from fluid inclusion resulted 245.8 at 1050 m and 259 at 1451 m depth gave indication of high temperature geothermal system, which is characterized by temperature more than 225^{O} C of geothermal system (Hocstein, 1990, in Lee 1996). Hululais geothermal system could be classified as high temperature geothermal system.

The presence of certain hydrothermal alteration minerals such as abundant secondary quartz, calcite, anhydrite, and pyrites which appear as direct deposition mineral from precipitation of liquid phase showing that Hululais geothermal system is classified as liquid dominated system (Nicholson, 1993).

Hydrothermal alteration assemblages such as secondary quartz, calcite, illite, epidote, smectite, and anhydrite could be used as indication of neutral pH geothermal fluid (Reyes, 1990), which mean that Hululais geothermal system mainly is a neutral pH fluid systems, except in the depth around 651 meters, where alunite and pyrophyllite is present as assemblages of acid fluid alteration minerals.

High intensity of alteration associated with certain hydrothermal alteration minerals such as secondary quartz, anhydrite, pyrite, could indicate good primary permeability (Reyes, 1990). In This study, high intensity of alteration associated with good permeability mineral indicators are found at almost all depth of the borehole, except at the surface to depth of 84 meter where unconsolidated volcanic materials are deposited. The presence of PLC and TLC zone also that present can be related with the presence of fault or fractures of rocks. From petrographic observation Fractures are observed from cores samples from depth of 2175.6 m and 2175.7 m. Those conditions later could indicate both good primary and secondary permeability of well HLS E.

CONCLUSIONS

There are four lithology units found in well HLS E, unconsolidated volcanic materials, andesite, andesite breccia, and tuff breccia. Several hydrothermal alteration minerals are also present, such as hematite, smectite, illite, chlorite, anhydrite, secondary quartz, calcite, alunite, pyrophyllite, epidote, and garnet. This hydrothermal alteration minerals can be classified into three alteration zone, they are smectite, illite, and epidote hydrothermal alteration zone.

Three geothermal zones are identified in this study, they are cap rock zone, associated with smectite zone, transition zone associated with illite-chlorite zone, and reservoir zone which associated with epidote zone.

Hululais geothermal system is classified as a liquid dominated geothermal systems, high temperature systems (>225^{O} C), and neutral pH fluid systems. Liquid dominated system is characterized by the presence secondary quartz, calcite, and anhydrite as the product of direct deposition. High temperature system is characterized by the presence of high temperature hydrothermal alteration minerals, i.e. epidote and fluid inclusion study. Neutral pH fluid system is characterized by hydrothermal alteration minerals assemblages of smectite, illite, secondary quartz, epidote, and anhydrite.

Hululais geothermal system shows the indication of good primary and secondary permeability, characterized by good permeability indicator minerals and loss circulation zone of borehole.

ACKNOWLEDGEMENT

The authors would like to say thanks to Pertamina Geothermal Energy (PT PGE) for practical work opportunity and permission to using various data, as well as to prepare and analyze it. We also would like to say Thank you to Mr. Eben Ezer Siahaan for the supports before and after practical work, Ms. Baiq Lolla Riandari, Mr. Jujun Juansyah, Mr. Asep, and Mr. Agus in Geothermal Information Center (GIC) Kamojang for the hard work in preparation of the raw data and precious experiences.

REFERENCES

Barker A. J., (2014), *A Key for Identification of Rock-forming Minerals in Thin-Section*, London: CRC Press, 1st ed, 181p

Browne, P.R.L., (1984), *Lectures On Geothermal Geology And Petrology*, Lecture note, Iceland UNU GTP

Budiardjo, B., Hantono, J., Agus, H., and Nugroho., (2010), *Geochemical Characterization of Thermal Waters in Hululauis Geothermal Prospect*, Jakarta, Geothermal Division Of Pertamina

Chen, P.Y., (1977), *Table of Key Lines in X-Ray Powder Diffraction Patterns of Minerals in Clays and Associated Rocks*, Authority of the State of Indiana, Indiana

Gafoer, S, Amin, T. C., and Pardede, (1992), *Geological Map of The Bengkulu Quadrangle, Sumatra*, Geological Research and Development Centre

Hochstein M., P., Sudarman S., (1993), Geothermal Resources of sumatra, *Journal of Geothermics*, **22** (3), pp 181 – 200

Juanda, A. A., Wardhani D. K. W., and Raharjo, I. B., (2015), *Microearthquake (MEQ) Investigation Reveals the Sumatran Fault System in Hululais Geothermal Field*, Bengkulu, Indonesia, Proceedings World Geothermal Congress 2015

Koestono, H., Prasetyo, I.M., and Nusantara, V.D.M., Thamrin, M.H., Kamah, M.Y., (2015), Hydrothermal Alteration Mineralogy of Well HLS-C, Hululais Geothermal Field, Bengkulu, Indonesia, *Proceedings of World Geothermal Congress*, 2015, Melbourne.

Lee, K.C., (1996), Classification Of Geothermal Resources - An Engineering Approach, *Proceedings of twenty-first workshop on geothermal reservoir engineering*, Stanford University

Muraoka, H., Takahashi, M., Sundoro, H., Dwipa, S., Soeda Y., Momita, M., and Shimada, K., (2010), *Geothermal system constrained by the Sumatran Fault and Its Pull-Apart Basins in Sumatra, Western Indonesia*, Proceedings of World Geothermal Congress

Nicholson, K., (1993), *Geothermal Fluids : Chemistry and Exploration Techniques*, United States of America, Springer Publisher, 1st ed. 242 h

Nusantara, V. D. M., Prasetyo I. M., Thamrin M. H., and Siahaan, E. E., (2016), Integrated Petrology Analysis, A Guide to Successful Exploration in Hululais Field, *Proceedings of The 4th Indonesia International Geothermal Convention & Exhibition 2016*

Reyes, A. G., (1990), Petrology of Philippine geothermal systems and the application of alteration mineralogy to their assessment, *Journal of Volcanology and Geothermal Research*, **43**, p 279-309

Rozak, K., Rahayu, D., and Bramantio, D., (2015), Development of Geothermal in Indonesia – PGE, Melbourne, Australia, *Proceeding of World Geothermal Congress 2015*

Thompson, A.J.B. and Thompson, J.F.H., (1996), *Atlas of Alteration: A Field and Petrographic Guide to Hydrothermal Alteration Minerals*, Alpine Press Limited, Vancouver

HYDROTHERMAL SYSTEM CHARACTERISTICS USING GEOLOGY AND GEOCHEMISTRY METHODS: A GEOTHERMAL DESKTOP STUDY IN BORNEO ISLAND

Meilani[1], Niniek Rina Herdianita[1], and Andri Eko Ari Wibowo[2]

[1]Institut Teknologi Bandung
[2]Pusat Sumber Daya Mineral, Batubara, dan Panasbumi
Ganesha St. no.10-12, Bandung City
E-mail: meilani@students.itb.ac.id

ABSTRACT

Borneo Island has several geothermal prospect areas which are classified into non-volcanic geothermal. Non-volcanic geothermal doesn't have a correlation with volcanic activity and presents in outer of Quarter volcanic line. There was a previous study being conducted as preliminary study, but further research is necessary to assess the characteristics of hydrothermal system and develop enhanced geothermal system in Indonesia. Ten geothermal fields were classified to four cluster by tectonic setting. The regional geology of research area is sited on Kutai Basin, Tarakan Basin, Melawi basin, and Meratus Mountain. There are numerous hot spring manifestasions with temperatures ranging from 38 to 85.8 °C and neutral pH ranging 6–8, which contain bicarbonate, chloride-bicarbonate, and sulphate fluids. The fluids characteristics in Borneo non-volcanic system are controlled by reservoir lithology, rock intrusion, and geological structure. The result of this study shows that the characteristic of geothermal reservoirs in Borneo come from geopressured and deep-seated aquifer system, except the heat source at Sajau area which originate from Tertiary intrusion-hosted. In addition, the subsurface temperature in Borneo geothermal areas is classified into low enthalpy to medium enthalpy, hence direct use and indirect use with binary system can be applied.

Keywords: borneo, deep-seated aquifer, geo-pressured, intrusion-hosted, non-volcanic.

INTRODUCTION

Borneo has been known as fossil fuel source in Indonesia. However, the other side of this island has several prospects of geothermal, included non-volcanic system. Non-volcanic geothermal doesn't correlate with volcanic activity and present in outer of Quarter volcanic line. There was a previous study being conducted as preliminary study, but further research is necessary to assess the characteristics of hydrothermal system and to develop enhanced geothermal system in Indonesia.
Other factors that control non-volcanic geothermal come from geopressured, deep-seated aquifer, and intrusion (Stimac et al., 2000).

Research Area

Ten geothermal fields has been classified to four cluster by tectonic setting (Figures 1). The regional geology of research area is sited on Kutai Basin, Tarakan Basin, Melawi Basin, and Meratus Mountain and various location of research area as showed in Table 1.

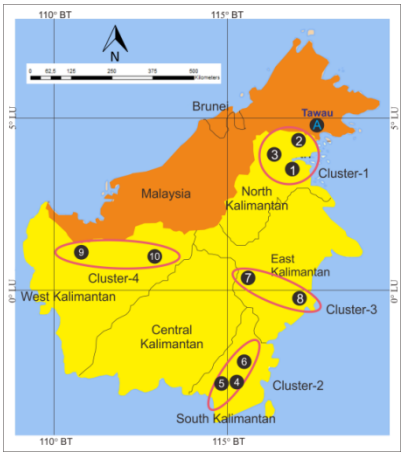


Figure 1: Research area map in four cluster by tectonic setting.

Table 1: Geothermal field location in Borneo.

Cluster	No.	Site	Regency	Province
1	1	Sajau	Bulungan	North Borneo
	2	Sebakis	Nunukan	
	3	Semolon	Malinau	
		Mengkuasar		
2	4	Tanuhi	Hulu Sungai Selatan	South Borneo
		Batubini		
	5	Lokbahan		
	6	Hantakan dan Pembakulan	Hulu Sungai Tengah	
3	7	Sungai Batuq	Mahakam Hulu	East Borneo
	8	Dondang	Kutai Kartanegara	
4	9	Sape	Sanggau	West Borneo
	10	Nanga Dua	Kapuas Hulu	

Regional geology

Borneo is the second biggest island in Southeast Asian, placed at 7° NL to 4° 202 NL and 108° 532 EL to 119° 222 EL with 743,330 km^2 area. Physiographically, Borneo is bordered by South China Sea in northern and west part, Makassar Strait in eastern part, and Java Sea in southern part. Regional geology of Borneo (Figure 2) is described by Darman and Sidi (2000):

- Tarakan Basin is found in the northeast Borneo and formed as Paleogene basin. The stratigraphy arranges in Tarakan Basin (Ellen, 2008) on research area are Sembakung Formation (Early–Middle Eocene) and Sajau Formation (Pliocene–Pleistocene).
- Kutai Basin is the largest and deepest basin, with 165,000 km2 area and 12,000-14,000 meters depth. Formed as Neogene basin. The stratigraphy arranges on research area (Doust and Noble, 2008) are Balikpapan (Middle–Late Miocene) and Kampung Baru Formation (Pliocene).
- Melawi Basin overlays melange and granite as basement rock on the southwest Borneo. This basin was formed as Paleogene basin. Two locations were defined in Lembar Sanggau (Supriatna, et al.,1993) and Putussibau (Pieters, et al., 1993).

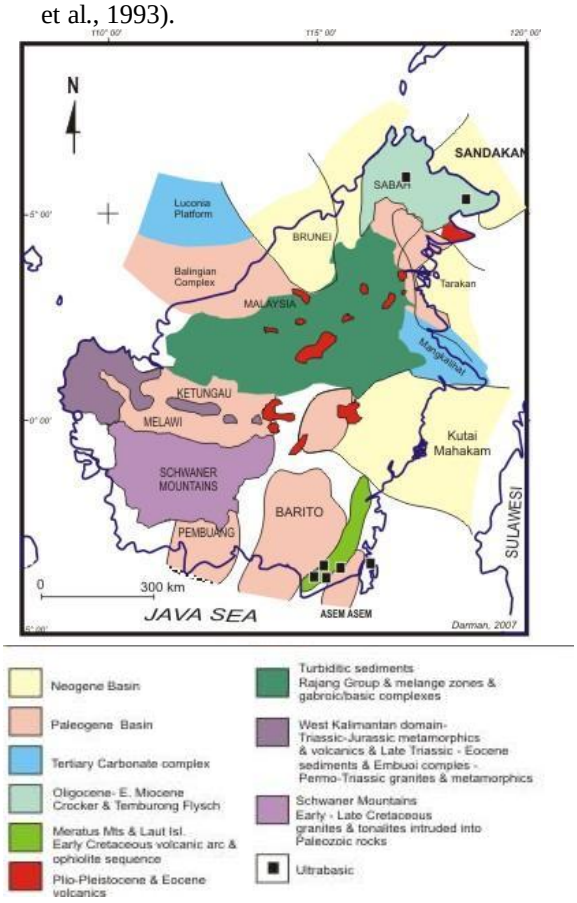


Figure 2: Tectonic setting of Borneo. (From various souce in Darman & Sidi ,2000).

- Meratus Mountain is a volcanic arc and ophiolite sequence, that exist since Cretaceous age. The stratigraphy arranges Meratus (Wakita, et al., 1998) from older to younger as mention: Meratus Complex (ophiolite, melange, and chert), Haruyan Formation (basaltic–andesitic volcanic rocks), Pitap Formation (sandstone, siltstone, conglomerate, and limestone locality), Tanjung Formation (sandstone, claystone, and intercalation with coal).

Geology of North Borneo

Sajau geothermal area is located on Bulungan regency, North Borneo. Regionally, it included to Tarakan Basin. Old to young stratigraphies consist of variety of rocks, those are calcareous claystone, limestone, claystone sandstone, claystone, conglomerate, sandstone, and alluvium (Wibowo et al., 2015) in Figure 3. Geological structures according to lineaments of fault and fracture have major stress NW–SE. Gunungsari normal fault with NW–SE trend had facilitated the appearing of Sajau spring and had altered the rocks.

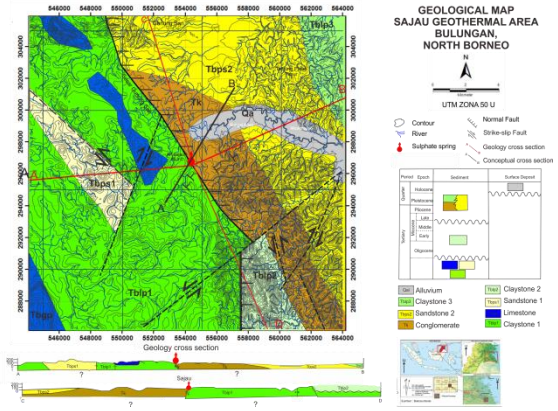


Figure 3: Geological map of Sajau (Wibowo et al., 2015).

Sebakis geothermal area is located on Nunukan regency, North Borneo. Old to young stratigraphies are sandstone interfingering with limestone, claystone, sandstone, and alluvium (PSDMBP, 2011). Geological structures observed in Sebakis area are normal fault with NW–SE. It controls the Sebakis spring (Figure 4)

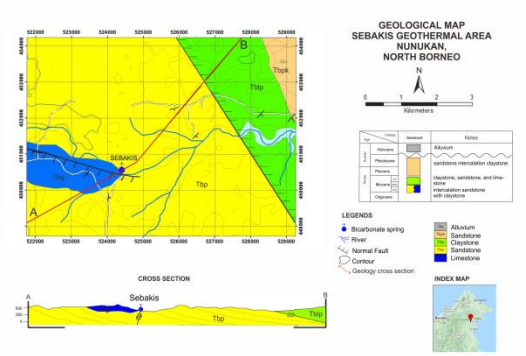


Figure 4: Geological map of Sebakis (PSDMBP, 2011).

Semolon and Mengkuasar geothermal areas are located in Malinau regency, North Borneo. The lithology of Semolon is consists by two sediment rocks, those are sandstone and alluvium. While, 20 km far on that place, Mengkuasar geothermal field is consists more variety lithologies. From old to young stratigraphies are sandstone 1, sandstone int. claystone, sandstone 2, basalt lava, and alluvium (PSDMBP, 2011). NW–SE normal fault also the main factors which controlled the manifestations (Figure 5)

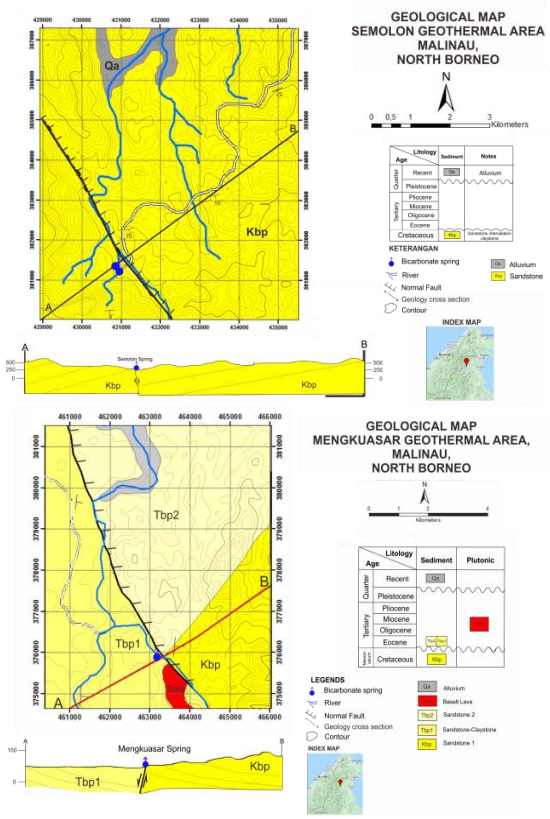


Figure 5: Geological map of Semolon (upper)-Mengkuasar (lower) (PSDMBP, 2011).

Geology of South Borneo

Kandangan geothermal system has five prospect areas. Batubini–Lokbahan–Tanuhi is located in Hulu Sungai Selatan regency, South Borneo (Figure 6). Old to young stratigraphies are granite, limestone 1, sandstone 1, basalt lava, sandstone 2, limestone 2, sandstone 3, and alluvium (PSDMBP, 2010a).

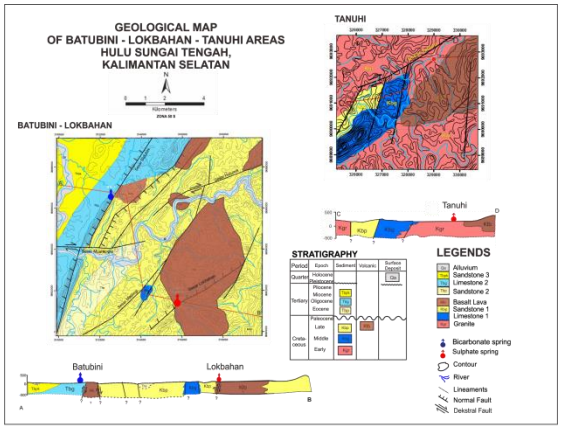


Figure 6: Geological map of Batubini–Lokbahan–Tanuhi (PSDMBP, 2010a).

On the other side, Hantakan–Pembakulan is located in Hulu Sungai Tengah and the stratigraphies are granite, limestone 1, sandstone 1, basalt lava, and sandstone 2 (PSDMBP, 2010a). The structures of geology shows two patterns, (1) NE–SW trend similar with Meratus subduction trend and (2) NW–SE parallel to Adang Fault (Figure 7).

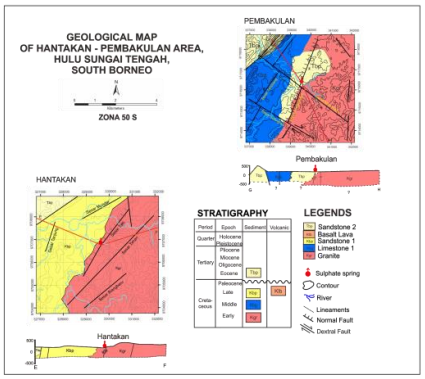


Figure 7: Geological map of Hantakan–Pembakulan (PSDMBP, 2010a).

Geology of East Borneo

Sungai Batuq is located in Mahakam Hulu regency, East Borneo. Old to young stratigraphies are sandstone, claystone, lava, and alluvium (Mulyadi and Munandar, 2014). Sungai Batuq has two structures trend, normal fault with NE-SW trend is cutted by sinistral fault which control the manifestation (Figure 8).

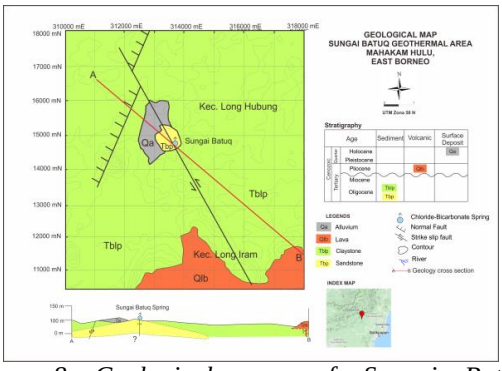


Figure 8: Geological map of Sungai Batuq (Mulyadi and Munandar, 2014).

Dondang is located in Kutai Kartanegara regency, East Borneo. Old to young stratigraphies are classified into 4 unit, those are sandstone–claystone, granite, sandstone, and alluvium (Mulyadi and Munandar, 2014). First geological structures is normal fault in NW–SE trend and being separated by sinistral fault (Figure 9).

Geology of West Borneo

Sape is located in Sanggau regency, West Borneo. Divided to three litologies from old to young, those are marble, sandstone, and claystone (Figure 10). As observation shows, normal faults with NE–SW trend has created graben area (PSDMBP, 2010b).

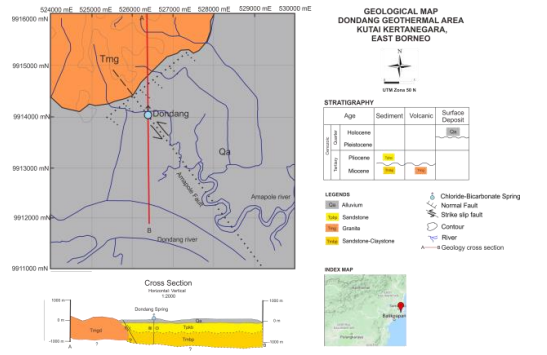


Figure 9: Geological map of Dondang (Mulyadi and Munandar, 2014).

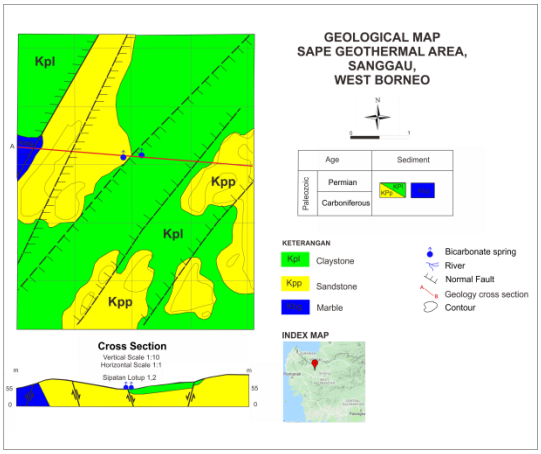


Figure 10: Geological map of Sape (PSDMBP, 2010b).

Nanga Dua is located in Kapuas Hulu regency, West Borneo. Divided to three litologies from old to young, those are shale, granodiorite, and diorite (Figure 11). As observation results, the faults are combine between E–W, NE–SW, and NW–SE faults (PSDMBP, 2010b).

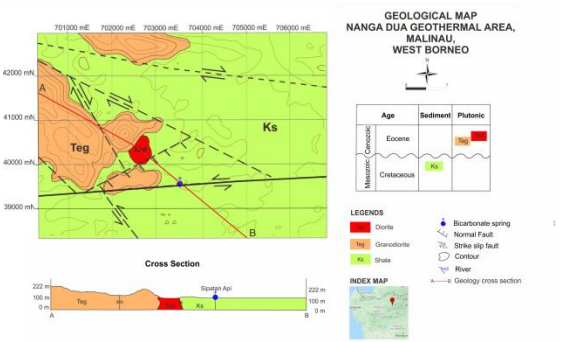


Figure 11: Geological map of Nanga Dua (PSDMBP, 2010b).

Objective

The objective of the research is to comprehend the characteristic of hydrothermal system in Borneo. The purposes of this paper are:

1. Determine the characteristics of geothermal reservoir in Borneo
2. Determine conceptual model of geothermal system in Borneo.

THEORETICAL BASIC

On average, the temperature of the Earth increases about 30˚C/km above the mean surface ambient temperature. However, most geothermal exploration and utilization occurs where the gradient is higher, and thus where drilling is shallower and less costly. These shallow depth geothermal resources occur due to: (1) intrusion of molten rock (magma) from depth (2) high surface heat flow, due to a thin crust and high temperature gradient; (3) thermal blanketing of deep rocks by thick formation of such rocks as shale whose thermal conductivity is low; (4) ascension of groundwater that has circulated to depths of several kilometers and that has been heated by normal temperature gradient; and. (5) anomalous heating of shallow rock by decay of radioactive elements, perhaps augmented by thermal blanketing (Wright, 1998).

Tawau geothermal area is located in Sabah, Malaysia. This location could be a reference for Borneo geothermal system. Tawau system has a range of estimated temperature around 180–220°C. The volcanic mountains have been built up by Miocene to Late Pleistocene andesitic, basaltic, and dacitic volcanic rocks. This area is an extinct volcanic system and has well-developed with good potential for high structural permeability.

DATA

Secondary data from PSDMBP covered geological and geochemical in 10 locations were analyzed. Analysis of geochemistry are chemistry and physics fluid, estimate reservoir temperature, stable isotop. All geochemical data were combined with geology data, resulting in interpretation of conceptual model and characteristics of hydrothermal system.

RESULT AND DISCUSSION

The geochemical results of thermal springs were analyzed and plotted by using ternary diagrams. Isotope and geothermometer also been analyzed on ten locations, as conclude:

North Borneo Geothermal System

Analysis on four locations have been conducted, those are Sajau, Sebakis, and Semolon-Mengkuasar. Based on the diagram Cl-HCO3-SO4, it is shown that Sajau hot spring has chloride-bicarbonate water with neutral pH. The type of water indicated that fluid comes directly from the reservoir and carried out some dissolved chemical compounds which represent the reservoir and interaction between hot fluids with rocks at depth. On the other hand, Sebakis and Semolon-Mengkuasar contains icarbonate waters with neutral pH. The hot fluid might mix with groundwater fluid. There are no fumaroles manifestations, but there are silica sinter at Sajau and travertine deposits in Semolon-Mengkuasar. Silica sinter could be deposited in fluid

with temperature above 175°C and more than 380 ppm SiO2 (Sismanto and Helda, 2012).

Diagram of Na-K-Mg represents partial equilibrium in Sajau location, which indicates there are several time for fluid have interacted with rocks and exchange the soluble. In different areas, Sebakis and Semolon-Mengkuasar were located in immature zone. It might be caused by the balancing between rock and fluid haven't reached yet, and the fluid may mix with groundwater or meteoric water.

The diagram of Cl-Li-B on each areas have their own reservoir. These geochemical data are interpreted as follow – the hydrothermal system that feeds those springs appears to rise from a deep upwelling reservoir. In Sajau reservoir, the characteristics are sediment rock with high organic composition, as described in gas geochemical data, whereas CH4 level has reached 90% (Wibowo et al., 2015). Since, the temperature from Na-K geothermometer by Fournier and Giggenbach give the temperature between 180-200°C. In Sebakis area, the reservoir is considered to be a sedimentary rock, as proven by the regional geology, the location included to sedimentary area. The temperature is ranging from 120-140°C with Na-K geothermometer. The same thing is founded in Semolon-Mengkuasar areas, which is located nearly with Kuching High zone and have sedimentary rock reservoir. So that an estimation of temperature for those locations are 140-160°C. The differences of range are caused by the composition of constituents as measured by the Na-K geothermometer. The boron contents are attributed to the depth of water circulation on surrounding sedimentary rock, which range 34-36 ppm in Sajau, 2 ppm in Sebakis, and 5-26 ppm in Semolon-Mengkuasar.

From the isotope and geochemical data obtained, it shown that the origin of thermal waters in Sajau are deep sedimentary basins (Figure 12), with δ18-O shows significant shift of up to 2 - 4‰ VSMOW; one of the processes involved for the significant enrichment in isotopic and chloride contents in Sajau hot springs are the temperature of hot fluid and the composition of sedimentary basins as reservoir. The $\delta^{18}O$ is about -3‰ VSMOW and the δD is about -35‰ VSMOW. The samples from river and rainfall show local meteoric water line equation $\delta D = 8\ \delta^{18}O+11$ (R^2 = 0,94). Sebakis and Mengkuasar doesn't have any isotope measurement, besides Semolon isotope explains that the source of the fluid is from meteoric water (Figure 13). The $\delta^{18}O$ is about -7‰ VSMOW and the δD is about -43‰ VSMOW. Semolon hot spring isotop is plotted in Sajau local meteoric water line as reference, and that's why we have immature water at Semolon, also at Sebakis and Mengkuasar, if assumed the fluid composition is same with Semolon because the geochemical and geological factors have been look alike.

All the manifestations appear in structures area. In Sajau area, the structures allow to open the permeability, so that the fluid from deep reservoir could be migrated to upper surface. While, in Sebakis and Semolon-Mengkuasar areas, these fracture systems are important as to allow the geothermal systems to be recharged from the meteoric waters. It is assumed that the meteoric recharge has happened through the fractures systems, faults, or joints.

The only one geophysics method is applied in Sajau geothermal area, whereas there are four locations who have high temperatures (58-85°C). Using Audio Magnetotelluric (AMT) method, it is indicated that the approximate of subsurface lithology (Zarkasyi and Risdianto, 2015). On the central to the west of Sajau manifestations, the resistivity is ranging from 0 to 20 ohm.m. It is interpreted as the alteration from hot fluid and also has altered the conglomerate rock and been classified into the caprock. The caprock is found until 1000 m depth, so the estimated reservoir should be under that layer. On the east part of hotsprings, they figured out the higher value of resistivity 20-60 ohm.m and combined with gravity method, the measurement describes high anomaly of density found along NW-SE structures of manifestations. Temporary estimation of the heat source in this location correlates with intrusion, but further detailed exploration and drilling hole are necessary to figure out the heat source and reservoir.

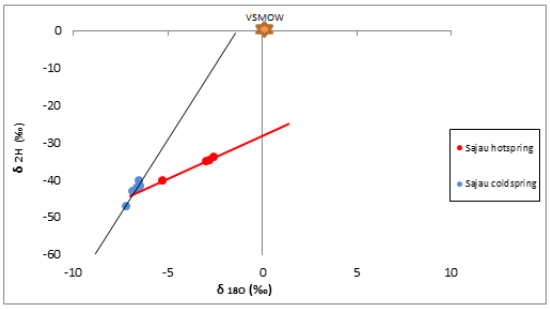


Figure 12: The stable isotope value for Sajau area (Wibowo et al., 2010).

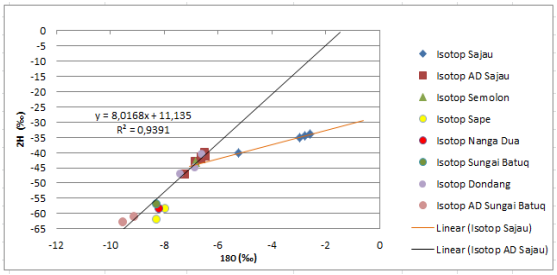


Figure 13: The stable isotope value for five locations in Borneo (Wibowo et al., 2010; PSDMBP, 2010b; PSDMBP, 2011).

South Borneo Geothermal System

Kandangan geothermal system is located in South Borneo and composed by three different locations or can be divided to five locations manifestations. Those are Batubini, Lokbahan, Tanuhi, Hantakan, and Pembakulan.

From Cl-HCO3-SO4 diagram, shows sulphate water with neutral pH in all locations, exclude Batubini has bicarbonate water. The sulphate water with neutral pH, indicated that the hot fluid occurrence in lithology with pyrite minerals abundance, also suggest the rock deposition in reducing environment below an oxygen – minimum zone (Byeres, 1977 in Sikumbang, 1986) isn't coming from magmatic activities. Sulphide addition to waters may be accomplished by alteration of sulphide minerals. Oppositely, the bicarbonate water in Batubini may come from the source of reservoir lithology and having a fluid-rock interactions, since the hotspring is also located in limestone lithology .

Diagram of Na-K-Mg represents partial equilibrium in Lokbahan, Tanuhi, and Hantakan. Therefore, the exchange of rock and fluid constituents have reached the equilibrium. The immature water is found in Pembakulan and Batubini. It might be caused by the fluid mix with meteoric water or leaching with surrounding rocks.

From Cl-Li-B diagram and combine with estimation of lithology reservoir, there are three reservoirs at Kandangan geothermal areas. First reservoir for three manifestations is in Pembakulan-Hantakan-Tanuhi, second reservoir is for Lokbahan manifestations, and the last reservoir is interpreted from bicarbonate rock, has become the components of geothermal system in Batubini.

The estimation of temperature reservoir from Na-K (Fournier) geothermometer in three reservoirs are 110-130°C. With two igneous reservoir and one sedimentary reservoir. All the manifestations appear in structures area.

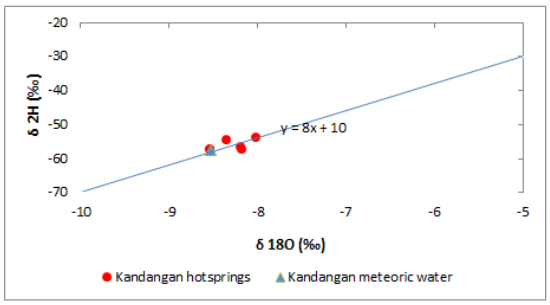


Figure 14: The stable isotope value for Kandangan area (PSDMBP, 2010a).

The results of isotope analysis explains that the origin of thermal waters in Kandangan areas are meteoric waters (Figure 14). Plotting isotope precisely in Global Meteoric Oceanic Water (GMOW) in line equation $\delta D = 8\ \delta^{18}O+10$. The $\delta^{18}O$ is about -8‰ VSMOW and the δD is about -55‰ VSMOW. Meteoric water acts as a source of hot fluid, through the structures coming down to the reservoir depth and has been heated by gradient geothermal.

East Borneo Geothermal System

Assessment of two locations has been done, those are Sungai Batuq and Dondang. Based on Cl-HCO3-SO4 diagram, shows chloride-bicarbonate water in those locations. This type of water indicated that fluid may come directly from the reservoir and diluted with groundwater as appear in high Mg compositions (>5 ppm).

Diagram of Na-K-Mg represents partial equilibrium in Sungai Batuq. Thus, the exchange of rock and fluid constituents have reached the equilibrium until they mix with groundwater. The immature water is found in Dondang. It might be caused by the fluid mix with meteoric water.

According to Cl-Li-B diagram, Sungai Batuq and Dondang has their own reservoir. From regional geology, it is estimated that the reservoir is a sedimentary rock. The estimation of temperature reservoir of both locations, from Na-K (Fournier) geothermometer are 100-120°C. Most of the samples are plotted near Cl corner. The high Cl concentration in the thermal spring are due to the interaction between fluids and rock in sedimentary basin. The boron contents are attributed to the depth of water circulation on surrounding sedimentary rock.

The results of isotope analysis explains that the origin of thermal waters in Sungai Batuq and Dondang areas are meteoric waters (Figure 13). Plotting isotope in Sajau Local Meteoric Water in line equation $\delta D = 8\ \delta^{18}O+11$ (R^2=0,94). The $\delta^{18}O$ is about -8‰ VSMOW and the δD is about -57‰ VSMOW. Meteoric water as a source of hot fluid, through the structures coming down to the reservoir depth and been heating by gradient geothermal.

West Borneo Geothermal System

The geochemical results of thermal springs were analyzed and plotted by using ternary diagrams (Figure 15). Sipatan lotup (hotspring in Sape area) and Sipatan Api (hotspring in Nanga Dua area) are bicarbonate water with neutral pH and electrical conductivities range 941-1155 µs/cm.

All manifestations located in immature water, near Mg corner, because some mixture with cold groundwater. It is actually difficult to estimate the reservoir temperature when it is plotted near the Mg corner. Since most of the water are considered immature water, geothermometer didn't yielding

meaningful equilibration temperatures but still all subsurface temperatures are suggested as reservoir temperature, and drilling may confirm the exact temperature. The estimated temperature using Na-K (Fournier) geothermometer are 160-180°C.

The plot of δD and $\delta^{18}O$ composition of the fluid sources in the study area are shown in Figure 13, which indicates the fluid from meteoric waters. The hotsprings water are plotted in the regression line of Sajau Local Meteoric Water Line (LMWL). The $\delta^{18}O$ is about -8‰ VSMOW and the δD is about -58‰ VSMOW.

CONCEPTUAL MODEL

Isotope composition from all locations can be seen on Table 2. Source of fluid on Sajau origins from deep sedimentary basin. While on other areas may origin from meteoric water, because they're plotted in LMWL. In Sungai Batuq, Sape, and Nanga Dua areas show the heavier isotope because some fluid-rock interactions.

Estimations temperature, kind of lithology, and depth of reservoir can be seen on Table 3. The estimation of depth have obtained from gradient geothermal asumption based on literature reference and gradient geothermal in Tawau location. More comprehensive exploration such as heat flow survey and drilling is needed to be organized. Gradient geothermal classification based on tectonic setting which have been acrossed by Plio-Plistocene volcanic. If it is accrosed by volcanic line, the gradient geothermal is 10°C, and the opposite is 8°C.

North Borneo Geothermal System

Sajau geothermal is approximated associates with plutonic intrusions, estimated in Miocene-Pliocene age. This things have been strengthen by gravity anomaly which gives information that there are high anomaly density of rock around manifestations, along the normal fault. Resistivity methode also declares that there is clay-cap until 1000m depth, may origin from the alteration of conglomerate rock.

Partially mature waters with a Na^+-Cl^- composition were rezognized in all Sajau manifestations, suggesting that a deep hydrothermal reservoir hosted in sedimentary rock represents the main hydrothermal fluid source. Reservoir is beneath the manifestations with temperature 180-200°C. Assesment of lithology reservoir in Sajau is sandstone in 1000-1200 m depth. Gradient geothermal asumption on North areas are 10°C/100 m.

Other locations on North Borneo, Sebakis, Semolon, and Mengkuasar also located nearly with Tarakan Basin. It is possible that the manifestations are controlled from geopressured, with thickness of sediment variable. The hydrothermal reservoirs are mainly recharged by meteoric water. The structures opened the permeability way and meteoric water could be heated when it is mobilized to the subsurface. The temperature ranging from 120-140°C in the reservoir of sandstone on 800-1000 m.

South Borneo Geothermal System

Kandangan geothermal system is related with geological structure and deep-seated geothermal reservoir. Meteoric water is the source for hydrothermal reservoir and have acummulated in plutonic (granite), volcanic (basalt), and sediment (limestone) lithologies. However, geochemical data didn't give a characteristics of magmatic environment, although the manifestations exist in old volcanic arc in subduction zone.

The area is an extinct volcanic system in Cretaceous age and the heat source is come from gradient geothermal with deep-seated reservoir. Gradient geothermal asumption on Kandangan are 8°C/100 m with temperature reservoir 110-130°C in depth 900-1200 m.

East Borneo Geothermal System

Geopressured resources are found when there is an impermeable layer of sedimentary cap rock that traps a geothermal reservoir. In these instances the weight of the sediment layer and the lack of permeability increases the pressure inside of the reservoir.

Sungai Batuq and Dondang which locate in Kutai Basin has geopressured system. Isotopically, the reservoir are mainly rechared by meteoric water and didn't come from oceanic water. In addition, Cl composition just ranging from 660 to 730 ppm.

In Dondang area, there are granite intrusions, which should be proven by further exploration. Radioactivity from young igneous intrusion may gives some heating energy, collectively with heat resulted from sediment pressure. The estimated temperature is 100-120°C in sandstone lithology, on 550-800 m and 600-900 m deep of reservoir.

West Borneo Geothermal System

Sape and Nanga Dua locations sited on Melawi Basin and related with geopressured system too.The hydrothermal reservoir has 160-180°C temperature. Sape geothermal system hosted in Permo-Carbon sandstone reservoir. Furthermore, Nanga Dua reservoir hosted in Eocene claystone intercalation sandstone. This system doesn't have any correlation with radioactive, since the geochemical and geological data doesn't show the significances of them. But, further radioactive survey is needed to be conducted.

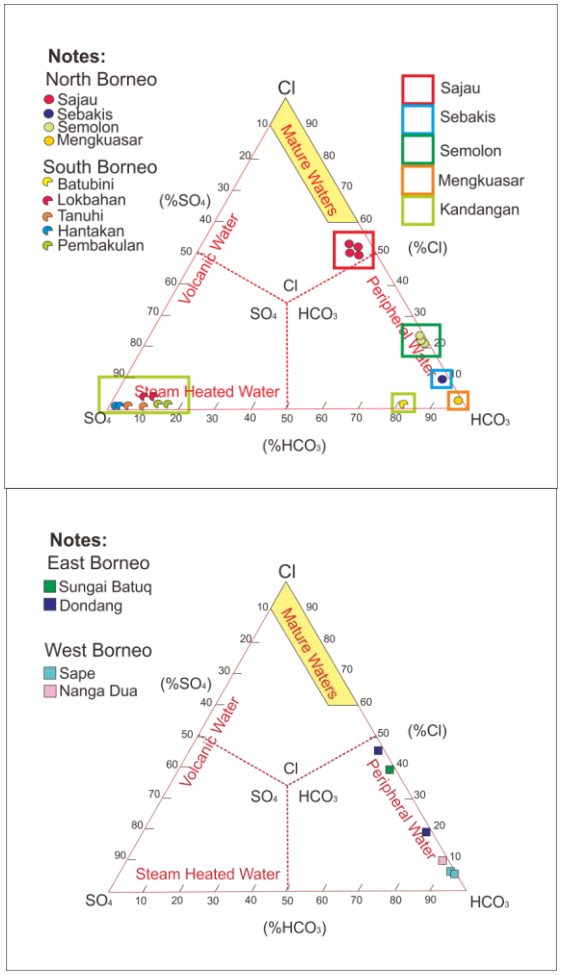


Figure 15: Triangular plot of main anions for hot springs of Borneo.

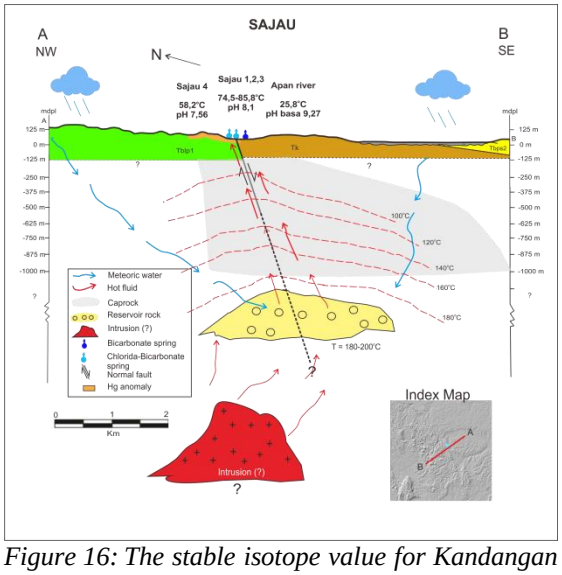


Figure 16: The stable isotope value for Kandangan area (PSDMBP, 2010a).

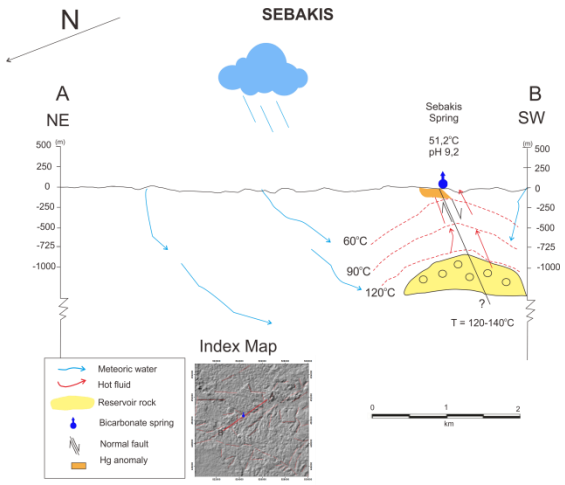


Figure 17: The stable isotope value for Kandangan area (PSDMBP, 2010a).

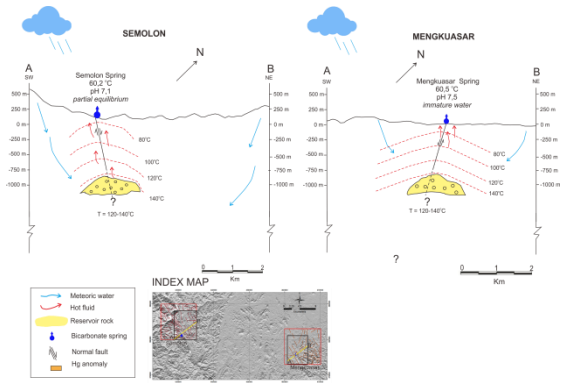


Figure 18: The stable isotope value for Kandangan area (PSDMBP, 2010a).

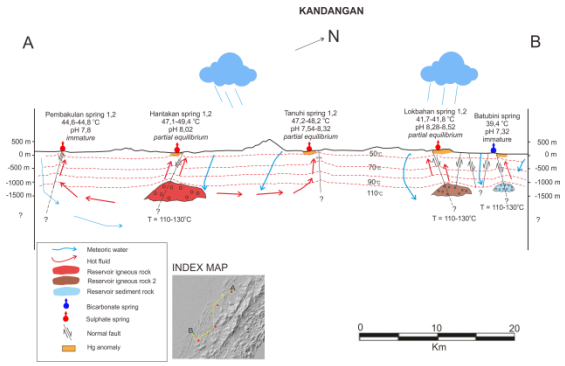


Figure 19: The stable isotope value for Kandangan area (PSDMBP, 2010a).

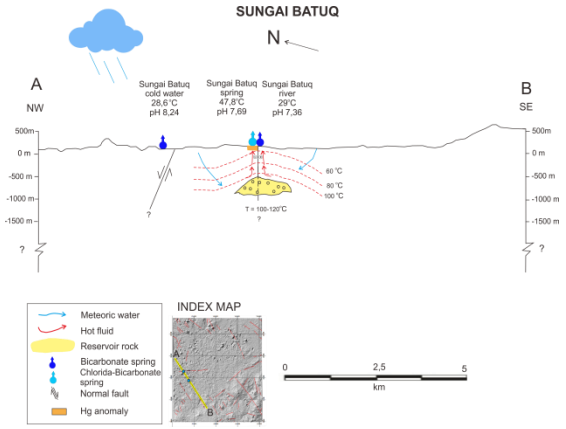


Figure 20: The stable isotope value for Kandangan area (PSDMBP, 2010a).

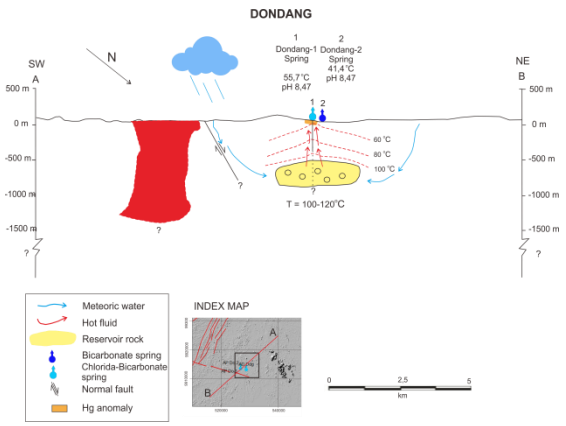


Figure 21: The stable isotope value for Kandangan area (PSDMBP, 2010a).

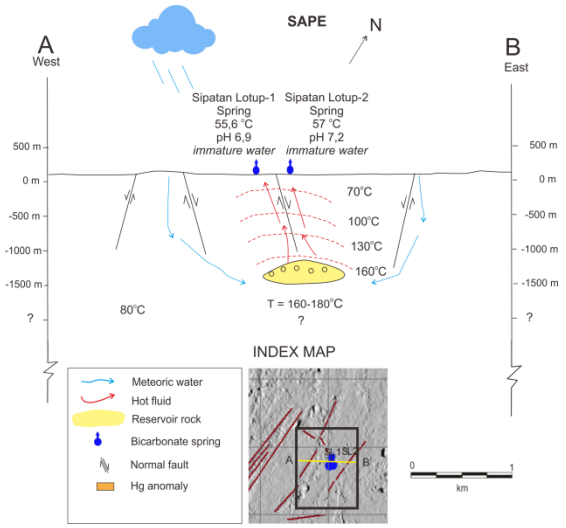


Figure 22: The stable isotope value for Kandangan area (PSDMBP, 2010a).

Table 2: Isotopic composition of the hotspring in Borneo

Sample ID	$\delta^{18}O$ (‰)	δD (‰)
Sajau 1	-2,7747	-34,589
Sajau 2	-2,9727	-35,149
Sajau 3	-2,5943	-33,876
Sajau 4	-5,2531	-40,21
AP Tanuhi-1	-8,18	-57,4
AP Lokbahan-1	-8,19	-56,7
AP Hantakan-1	-8,01	-54,1
AP Pembakulan-1	-8,36	-54,6
Semolon	-6,8361	-43,052
Sungai Batuq	-8,28	-56,8
Dondang-1	-6,84	-45,15
Dondang-2	-7,38	-47,23
Sipatan Lotup 1	-8,27	-62
Sipatan Lotup 2	-7,96	-58,3
Sipatan Api	-8,18	-58,3

CONCLUSIONS

Geothermal in Borneo has ten prospects areas. Details geology and geochemical properties of hydrothermal waters were explored and several conclusions can be drawn as:

(1) The characteristics of geothermal reservoir in Borneo divided to three type, those are geopressured, deep-seated reservoir, and intrusion.

(2) The hydrothermal reservoir located in Tarakan Basin, Kutai Basin, and Melawi Basin is hosted in sedimentary rocks, except in Mt. Meratus locations, it is hosted in igneous and sedimentary rocks. The reservoir is likely opened by secondary permeability such as normal fault or strike-slip fault.

(3) Source of fluid on Sajau origins from deep sedimentary basin. While on other areas may origin from meteoric water.

(4) According to the conceptual model, water geothermometry using Na-K (Fournier) suggested that Borneo geothermal system has low to medium entalphy.

ACKNOWLEDGEMENT

Thank you for PSDMBPB for equipping geochemical and geology data, Dr. Niniek Rina Herdianita and Andri Eko Ari Wibowo who guides writers analyzing paper.

REFERENCES

Anderson, D. N. and Lund, J. W. (1979), "Direct Utilization of Geothermal Energy: A Technical Handbook," *Special Report Geothermal Resources Councis Davis, CA*, **7.**

Bebout, D. G., Gavenda, V. J., and Gregory, A. R. (1978), "Geothermal Resources of Wilcox Group, Texas Gulf Coast," *U.S. Dept. of Energy*, **1,** 82.

Darman, H. and Sidi, H. (2000), "An Outline of The Geology of Indonesia*," Ikatan Ahli Geologi Indonesia.*

Doust, H. and Noble, R. A. (2008), "Petroleum Systems of Indonesia," *Marine and Petroleum Geology*, **25(2)**, 103-129.

Ellen, H., Husni, M. N, Sukanta, U., Abimanyu, R., Feriyanto, and Herdiyan, T. (2008), "Middle Miocene Meliat Formation in the Tarakan Island, Regional Implications for Deep Exploration Opportunity," *Proceedings of Indonesian Petroleum Association 32nd Annual Convention, Jakarta*, **1.**

Fournier, R.O. (1979), "A revised equation for the Na/K geothermometer," *Geothermal Resources Council*, Trans, **3**, 221-224.

GeothermEx (2014), "Apas Kiri Geothermal Project, Sabah, Malaysia – Assessment of Exploration Data and Conceptual Model, Resource Capacity Estimate, Drilling Sites and Targets," *Unpublished Letter Report*, prepared by GeothermEx.

Mulyadi, Eddy and Munandar, Arif. (2014), "Survei pendahuluan daerah panasbumi Kabupaten Mahakam Hulu dan Kabupaten Kutai Kartanegara, Provinsi Kalimantan Timur," *Pusat Sumber Daya Geologi, Bandung.*

Pieters, P.E., Surono, and Noya, Y. (1993), "Peta Geologi Lembar Putussibau, Kalimantan, skala 1: 250.000," *Pusat Penelitian dan Pengembangan Geologi, Bandung*.

Stimac, J., Goff, F., and Goff, C. J. (2000), "Intrusion-related Geothermal Systems, " *The Encyclopedia of Volcanoes,* **2,** 799 – 822.

Supriatna, S., Margono, U., Sutrisno, K. F. D., Langford, R. P., and Trail, D. S. (1993), "Peta Geologi Lembar Sanggau, Kalimantan skala 1:250.000," *Pusat Penelitian dan Pengembangan Geologi, Bandung*.

Tim Survei Pendahuluan PSDMBP. (2010a), "Laporan akhir survei pendahuluan geologi dan geokimia daerah panasbumi Kandangan, Provinsi Kalimantan Selatan," *Pusat Sumber Daya Geologi, Bandung.*

Tim Survei Pendahuluan PSDMBP. (2010b), "Laporan akhir survei pendahuluan geologi dan geokimia daerah panasbumi Kabupaten Sanggau dan Kapuas Hulu, Provinsi Kalimantan Barat," *Pusat Sumber Daya Geologi, Bandung.*

Tim Survei Pendahuluan PSDMBP. (2011), "Laporan penyelidikan pendahuluan geologi dan geokimia panasbumi Kabupaten Nunukan, Bulungan dan Malinau, Provinsi Kalimantan Utara," *Pusat Sumber Daya Geologi, Bandung.*

Wakita, K., Miyazaki, K., Zulkarnain, I., Sopaheluwakan, J., and Sanyoto, P. (1998), "Tectonic Implications of New Age Data for The Meratus Complex of South Kalimantan, Indonesia," *Island Arc*, **7**, 202-222.

White, D. E., Buffler, L. J. P., and Truesdell, A. H., (1971), "Vapor-Dominated Hydrothermal Systems Compared with Hot-Water Systems," *Economic Geology*, **66**, 75-97.

Wibowo, A. E. A., Hadi, M. N., and Suwarno. (2015), "Laporan survei terpadu geologi dan geokimia daerah panasbumi Sajau, Kabupaten Bulungan, Provinsi Kalimantan Utara," *Pusat Sumber Daya Geologi, Bandung.*

Wright, M. (1998), "Nature of Geothermal Resources, in Geothermal Direct-Use Engineering and Design Guidebook," edited by John W. Lund, *Geo-Heat Center*, Klamath Falls, OR, 27-69.

Zarkasyi, A. and Risdianto, D. (2015): Survei gaya berat dan AMT daerah panasbumi Sajau, Bulungan, Provinsi Kalimantan Utara, *Pusat Sumber Daya Geologi, Bandung.*

Table 3: Reservoir temperature and depth estimation

No.	Location	Cluster	Temperature (°C) (Na-K Fournier)	Depth (m)	Estimation of Rocks	Estimation of Gradient Geothermal (°C/100m)
1	Sajau	1	180-200	1000-1200	Sandstone	10
2	Sebakis		120-140	800-1000	Sandstone	10
3	Semolon		120-140	800-1000	Sandstone	10
4	Mengkuasar			800-1000	Sandstone	10
5	Batu Bini	2	110-130	1000-1200	Limestone	8
6	Lokbahan		110-130	1000-1200	Basalt Lava	8
7	Tanuhi		110-130	900-1100	Granite	8
8	Hantakan		110-130	900-1100	Granite	8
9	Pembakulan		110-130	900-1100	Granite	8
10	Sungai Batuq	3	100-120	600-900	Sandstone	8
11	Dondang		100-120	550-800	Sandstone	8
12	Sape	4	160-180	1200-1400	Sandstone	8
13	Nanga Dua		160-180	1400-1600	Shale intercalation Sandstone	8

CHARACTERISTICS OF HYDROTHERMAL ALTERATION IN EASTERN PART OF PATUHA GEOTHERMAL FIELD, WEST JAVA, INDONESIA

F. Pratiwi [1], K. Yonezu[1], A. Harijoko[2], K. Watanabe[1], Elfina[3], and M. I. Nurpratama[3]

[1]Department of Earth Resources Engineering, Kyushu University, Fukuoka 819-0395, Japan
[2]Departement of Geological Engineering, Gadjah Mada University, Yogyakarta 55281, Indonesia
[3]PT Geo Dipa Energi (Persero)
Email: fadiah@mine.kyushu-u.ac.jp

ABSTRACT

The Patuha Geothermal System is a vapor-dominated system located within the Patuha Volcanic Complex in West Java, Indonesia. Total potential of this field is estimated around 400 MW. The purpose of this paper are to investigate the distribution of hydrothermal minerals in eastern part of the Patuha Geothermal Field and deduce thermal change within the system. In total around 200 cutting samples from four wells were used in this study. The rocks encountered by the four wells consist of pyroclastic rocks and andesitic lavas, intruded by microdiorite. From top to down, subsurface hydrothermal alteration can be grouped into four alteration zones, comprising of: kaolinite-cristobalite, clay, epidote, and epidote-actinolite zones. The alteration minerals found at shallow level formed by rock interaction with acid fluids, while those preset at deeper level resulted from interaction with near-neutral fluids. In addition, the temperature suggested from hydrothermal alteration minerals and homogenization temperature of fluid inclusions are higher than down-hole measured temperature. This difference indicates cooling of the system since the identified alteration assemblages and indicated fluid inclusions formed.

Keywords: Hydrothermal alteration, Patuha Geothermal Field.

INTRODUCTION

The Patuha Geothermal System is one of great interest for electric generation in Java Island. It is located in West Java, around 40 km southeast of Bandung (Figure 1). There are several other geothermal systems near Patuha, e.g. Wayang-Windu, Darajat, Kamojang, and Karaha-Talaga-Bodas to the east, Salak and Awi Bengkok to the northwest of Patuha (Hochstein and Sudarman, 2008). This field is estimated to have potential output of 400 MW (Layman and Soemarinda, 2003). Initial exploration of Patuha was accomplished during 1983-1989, including reconnaissance of thermal manifestations, geological mapping, geophysical investigations, and geochemical survey. From 1996 to early 1998, extensive exploration and development was undertaken, however it was suspended in 1998 due to financial issues. Presently, Patuha Geothermal Field is operated by PT. Geo Dipa Energi. It has one active geothermal power plant with a capacity of 60 MW. In the future, PT. Geo Dipa Energi plans to develop this field by building two further geothermal power plants with a capacity of 55 MW for each unit (PT. Geo Dipa Energi, 2016).

The exploration and development of geothermal fields requires comprehensive understanding of the geological and geothermal setting of the system. This paper aims to describe the subsurface hydrothermal alteration of the system and their distribution. Hydrothermal alteration mineralogy is closely related to temperature, permeability, and fluid composition, which is important aspects in geothermal system. Thus, the identification of hydrothermal minerals and their distribution will help to deduce condition and change within the system.

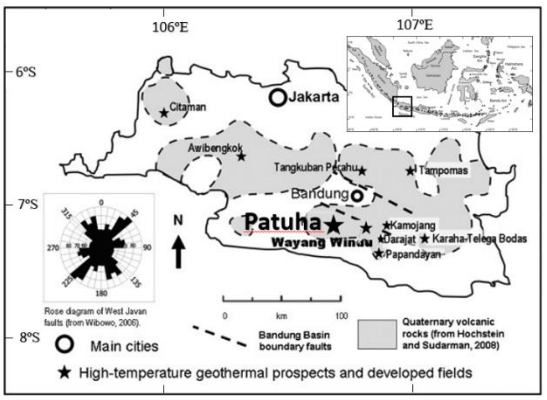


Figure 1: Location of the Patuha Geothermal System (Bogie, Kusumah and Wisnandary 2008). Inset picture shows location of West Java in Indonesia Archipelago (Hall 2002)

GEOLOGICAL SETTING

The Patuha Geothermal system is located in the Patuha Volcanic Complex, situated at an elevation of 1700-2400 meters above sea level. This volcanic complex lies within the Sunda Volcanic Arc, West Java. Sunda Volcanic Arc was formed by subduction in which the Indian-Australian plate is subducting beneath the Eurasian plate. The plate convergent along this subduction can be divided into two parts, western and eastern parts. The western part on Sumatra has oblique subduction and eastern part on Java, Bali, and Sumbawa has frontal

subduction. Thus, West Java can be considered the transitional zone between oblique and frontal subduction (Hall, 2012; Fauzi, et al. 2015).

The volcano-magmatic arc in West Java was developed since early Tertiary (Atmadja, et al. 1994). The Patuha Geothermal System is associated with andesitic lavas and pyroclastic rocks of late Pliocene to Quaternary age. Nearby peaks in this area include North Patuha (2414 m), South Patuha (2390 m), Urug (2201 m) and Walang (2414 m). There is no historical report of eruption in this area (Layman and Soemarinda, 2003).

Patuha area is mostly covered by volcanic products from Mount Patuha and Mount Kendeng (Figure 2). Mount Patuha Volcanic Unit covers the central and south-western part of the area. It consists of vesicular and massive pyroxene andesite lavas and lahar. Volcanic products of Mount Kendeng consts of lava flows intercalated with laharic deposits of andesite breccia and tuff breccia. It covers the northen and eastern part of the area.

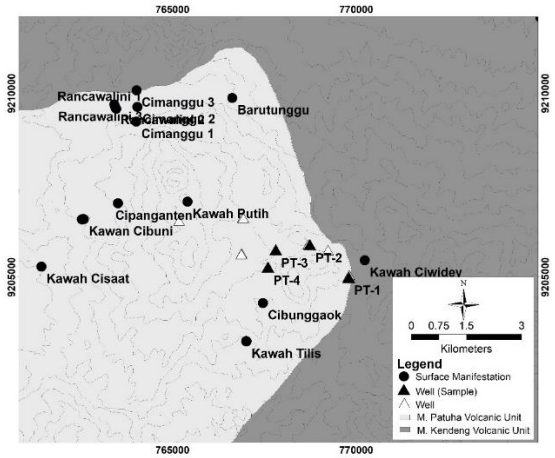


Figure 2: Geological Map of Patuha Area (Edited from Koesmono, Kusnama and Suwarna, 1996).

SAMPLES AND ANALYTICAL METHODS

In total around 200 rock cuttings from four wells were examined in laboratory. The samples first examined using binocular microscope. Samples then measured using X-Ray Diffraction to analyzed bulk and clay mineralogy. Selected samples were made into thin section to observe the alteration mineralogy. Quartz, calcite, and anhydrite grains were selected for fluid inclusion microthermometry.

RESULTS

Lithology

Subsurface lithologies were identified from megascopic and petrographic analysis of the rock cuttings. The rocks mostly comprise of repetitive sequence of pyroclastic rocks and andesite lavas at shallow depth, and andesite lavas and microdiorite at depth. The rocks encountered from four wells are divided into four lithological units: Tuff A, Andesite Hornblende, Tuff B, and Andesite Complex Units.

Tuff A Unit

This unit is encountered at well PT-4 from surface to 777m depth. Intense weathering is observed at the upper part of this unit. This unit consist of lithic tuff and crystalline tuff, interbedded with andesite lavas. Sometimes crystalline tuff shows eutaxitic microtexture interpreted as welded tuff. The appearance of welded tuff and mud clasts in this unit differing this unit with tuff unit encountered in well PT-1 and PT-2.

Andesite Hornblende Unit

Andesite hornblende unit is encountered at PT-2 and PT-3 from surface to 378m and 627m depth respectively, but absent at well PT-1 and PT-4. This unit consists of andesite lava with abundance hornblende phenocryst. This unit is weathered near surface and gradually becomes less weathered downward.

Tuff B Unit

This unit consisting of lithic tuff, crystalline tuff with andesite lava interbedded. This unit is encountered in PT-1 and PT-2 from surface to 402m depth, and 378m to 628 m depth respectively, but absent in PT-3 and PT-4.

Andesite Complex Unit

This unit consist of andesite porphyry and microdiorite. It has thin layer of crystalline tuff at depth around 800m in PT-1 and PT-2 and 900m at PT-3. The andesite porphyry differ with andesite hornblende based on its composition. This unit has lesser amount or does not have hornblende phenocrysts. The microdiorite has phaneritic texture, which observed clearly under microscope. This unit is the deepest unit penetrated by all the wells.

Subsurface Hydrothermal Alteration

Four alteration zones have been recognized based on the distribution of hydrothermal minerals, consisting of: kaolinite-cristobalite, clay, epidote, and epidote-actinolite zones. The distribution of the alteration zones is presented in Figure 3.

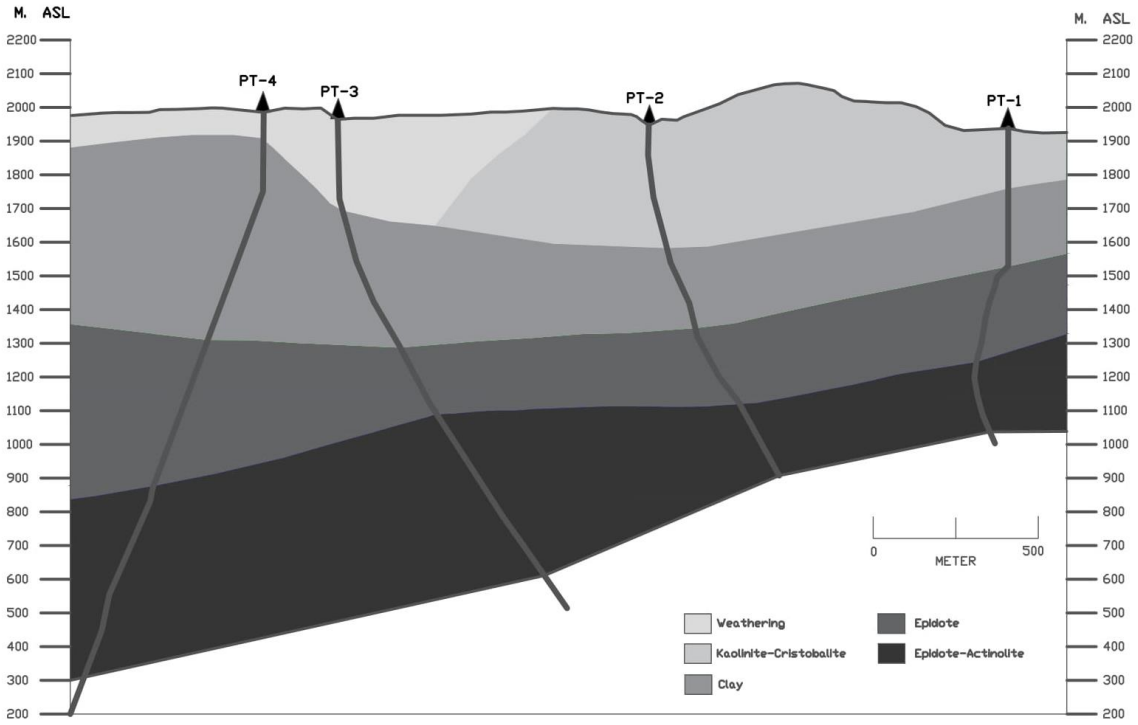


Figure 3: Distribution of the subsurface hydrothermal alteration zone from well in the eastern part of Patuha.

Kaolinite-Cristobalite Zone

The upper part of PT-1 and PT-2 is the kaolinite-cristobalite zone. This zone is characterized by the presence of kaolinite and cristobalite, other alteration minerals present include: quartz, pyrite, halloysite, calcite, anhydrite, and alunite. Meanwhile, at the upper part of PT-3 and PT-4 consist of weathered rocks without kaolinite-cristobalite zone.

Clay Zone

The clay zone is present below the kaolinite-cristobalite zone. This upper boundary of this zone is characterized by last appearance of cristobalite at PT-1 and PT-2 and first appearance of smectite at PT-3 and PT-4. This zone is characterized by the presence of smectite and other clay mineral (kaolinite, chlorite, and illite). Other alteration minerals appear in this zone are; quartz, pyrite, calcite, anhydrite, tourmaline, titanite, ankerite, and siderite.

Epidote Zone

Below the clay zone is the epidote zone. The first appearance of epidote is defined as upper boundary of this zone. This zone is characterized by the presence of epidote, chlorite and illite. Smectite still observed at this zone at PT-1, PT-3 and PT-4. The other minerals are quartz, calcite, anhydrite, pyrite, and zeolites. Prehnite and titanite occasionally found in some samples. The association of epidote, and chlorite, indicate the formation temperature is more than 240º C, with a neutral-pH condition.

Epidote-Actinolite Zone

The epidote-actinolite zone marks the bottom part of the wells. The upper boundary of this zone is distinguished by the appearance of actinolite. This zone is characterized by the appearance of epidote, actinolite, chlorite, and illite. The other minerals are quartz, calcite anhydrite, and pyrite. Chlorite/smectite, illite/smectite, zoisite, prehite, pumpeyllite, wairakite and other zeolites appear occasionally in some of the samples. At PT-3, smectite can be found until the upper part of this zone. The association of actinolite, epidote, and chlorite, indicate the formation temperature is more than 280º, with neutral-pH condition.

Fluid Inclusion MIcrothermometry

Due to the condition of the samples, fluid inclusion microthermometry were measured from random crystal grains found in the rock cuttings. Measurement made on primary and pseudosecondary fluid inclusion hosted by quartz (PT-1 and PT-3), calcite (PT-2), and anhydrite (PT-3 and PT-4) crystal.

Table 1: Result of fluid inclusion microthermometry.

Well	Mineral	Total	Th (ºC) (mode)	NaCl (wt.%)
PT-1 (903m)	Quartz	19	210-220	0.9-1.2
			250-260	0.9-1.2
PT-2 (1062m)	Calcite	29	237-239	0.9-1.2
PT-3 (1311m)	Quartz	16	265-275	0.9-1.9
	Anhydrite	7		
PT-4 (1203m)	Anhydrite	23	235-240	1.4-1.9

DISCUSSIONS

Hydrothermal alteration minerals are formed as a result of interaction between hydrothermal fluids and rocks. This process is significantly controlled by temperature and fluid composition. Thus, the identified hydrothermal alteration minerals could indicate temperature and thermal fluid composition. Acid alteration was found near the surface at PT-1 and PT-2. Kaolinite, cristobalite, alunite, and anhydrite minerals represent this acid alteration. The near surface acid alteration is likely to be formed by steam-heated acid-sulfate waters. (Nicholson, 1993). Acid sulfate are waters usually found in the condensation zone, where H2S gas condensed into shallow groundwater then produce acid sulfate. This condensation zone is interpreted to have developed below Kawah Ciwidey, located near wells PT-1 and PT-2 (Figure 2).

The clay zone, which is characterized by smectite mineral and other clay minerals, is interpreted as the clay cap of the system that act as impermeable barrier to trap the fluid in reservoir. While the epidote and epidote-actinolite zone may represent the reservoir.

Some hydrothermal alteration mineral has limited temperature stability, which can be used to predict the temperature when alteration minerals were formed. A comparison between measured temperature, alteration mineral temperature, and homogenization temperature may explain the temperature change in the system. The temperature indicator mineral used in this study are illite, epidote, actinolite, and smectite. The formation of smectite generally occurs below 180ºC, illite occurs generally above 220ºC, poorly crystalline epidote starts to form around 200ºC and normally stable above 240ºC, and actinolite stable at temperatures above 280ºC (Reyes, 1990).

From all the wells, the relationship between the fluid inclusion micro-thermometry, current measured temperature, and alteration mineral temperature, shows that the geothermal system has experienced cooling (Figure 4).

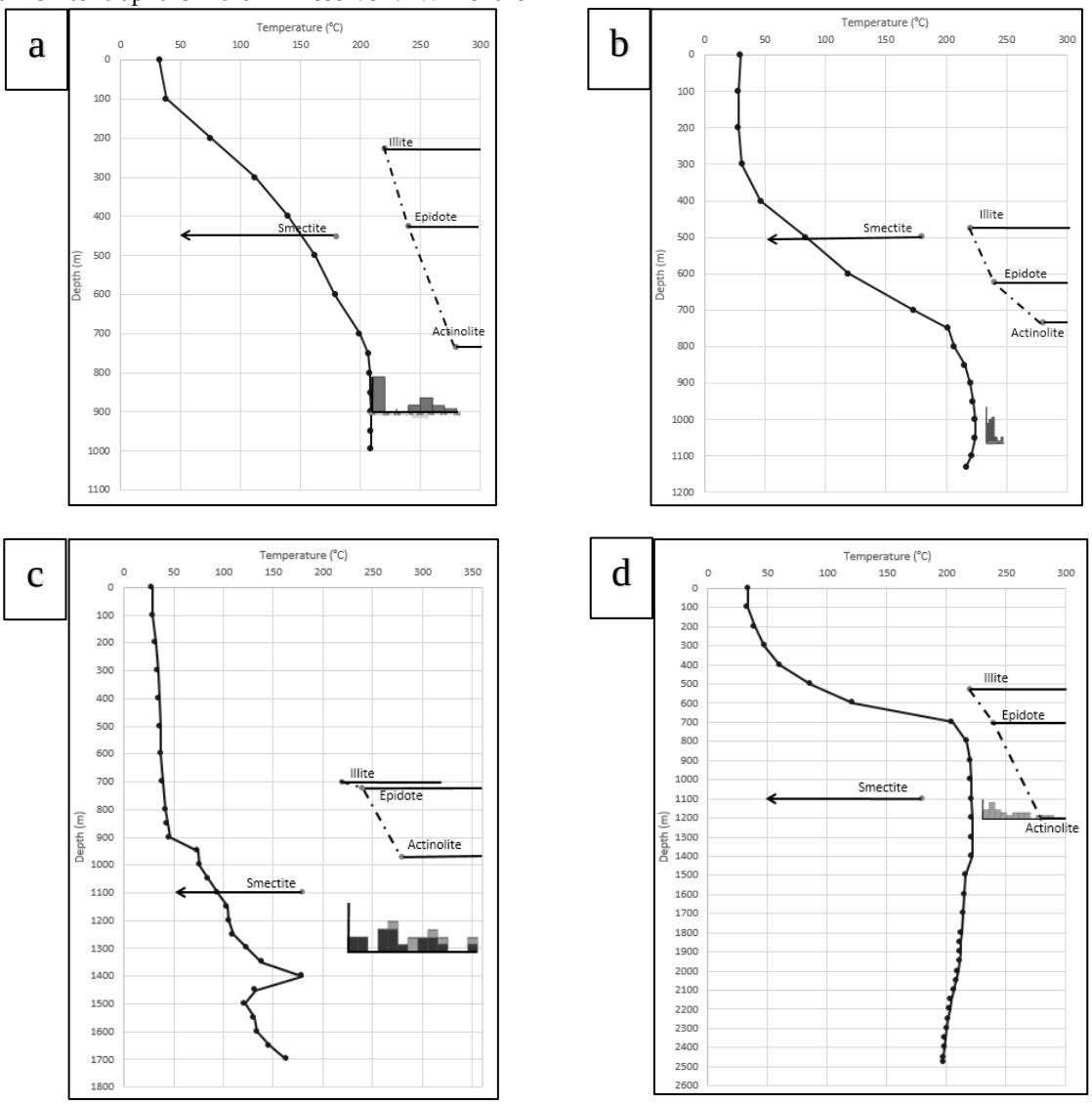


Figure 4: Plot of correlation between measured temperature, interpreted hydrothermal alteration mineral, and fluid inclusion microthermometry at (a) PT-1, (b) T-2, (c) PT-3, and (d) PT-4

Illite, epidote, and actinolite was observed where the current measured temperature is lower than their thermal stability temperature. Homogenization temperature measured from fluid inclusion also shows that fluid inclusion trapped at temperature higher than the current measured temperature. This indicates that the mineral formed when system was hotter than in the present condition.

The relationship between smectite with illite, epidote and actinolite may also support the cooling of the system. The distribution of first appearance of illite, epidote, and actinolite shows progressive heating from low to high temperature mineral with depth. However, in PT-1, PT-3, and PT-4, the deepest occurrence of smectite is below the first occurrence of epidote, and in PT-2 below the first occurrence of illite. Smectite, illite, and epidote has different stable temperature the first one below 180ºC and the later more than 220ºC and 240ºC, these mineral cannot be in equilibrium. It is interpreted that smectite formed later after illite, epidote, and actinolite.

First occurrences of actinolite in PT-1, PT-2, and PT-3 is coincident with the sudden change of thermal gradient, however in PT-4 the change of thermal gradient is coincident with first occurrence of epidote. Comparing the last occurrence of smectite to measured temperature, the last occurrence of smectite at PT-1, PT-2, and PT-3 appears at a measured temperature below 180ºC. In contrast to other wells in PT-4, last appearance of smectite occurs at a measured temperature of 225ºC, which is higher than its thermal stability. This evidence may give rise to the possibility of recent heating in this part of the system, but smectite has not yet changed to a higher stable temperature mineral.

Based on the information provided above, the changes of the thermal regime at Patuha is proposed. The geothermal system is hotter when the system was first initiated. Then, the system experienced cooling which allowed formation of smectite at a deeper part of the system, hence smectite found together with higher temperature minerals (illite, epidote, and actinolite) at PT-1 to PT-4. Followed by recent heating occurring locally at the west side of the research area (PT-4) after the cooling process, which is explained by the occurrence of deepest smectite at temperatures higher than its stability temperature.

ACKNOWLEDGMENTS

We are grateful to PT. Geo Dipa Energi for their kindly help providing the rock cutting samples used in this research and for giving permission to publish this paper. This study was supported by LPDP (Lembaga Pengelola Dana Pendidikan) through Beasiswa Pendidikan Indonesia.

REFERENCES

Atmadja, R. Soeria, R. C. Maury, H. Bellon, H. Pringgoprawiro, M. Polve, and B. Priadi. (1994), "Tertiary magmatic belts in Java." *Journal of Southeast Asian Earth Sciences* 9, no. 1-2: 13-27.

Bogie, Ian, Yudi Indra Kusumah, and Merry C. Wisnandary. (2008), "Overview of the Wayang Windu geothermal field, West Java, Indonesia." *Geothermics* 37, no. 3: 347-365.

Fauzi, Ahmad, Haryadi Permana, Sri Indarto, and E. Z. Gaffar. (2005), "Regional Structure Control on Geothermal Systems in West Java, Indonesia ." *Proceedings World Geothermal Congress.* Melbourne.

Hall, Robert. (2002), "Cenozoic geological and plate tectonic evolution of SE Asia and the SW Pacific: computer-based reconstructions, model and animations." *Journal of Asian Earth Science* 20, no. 4: 353-431.

Hochstein, M. P., and S. Soedarman. (2008), "History of geothermal exploration in Indonesia from 1970 to 2000." *Geothermics* 37: 220-266.

Koesmono, M., Kusnama, and M. Suwarna. (1996), "Geological Map of The Sindangbarang and Bandarwaru, Quadrangles, Java." Geological Research and Development Centre.

Layman, Erik B., and Sukusen Soemarinda. (2003), "The Patuha Vapor Dominated Resource West Java, Indonesia." *Proceedings 28th Workshop on Geothermal Reservoir Engineering 2003.* Stanford, California.

Nicholson, Keith. (1993), "*Geothermal Fluids, Chemistry and Exploration Techniques"*. Berlin: Springer-Verlag.

PT. Geo Dipa Energi. (2016), "*Lapangan Existing: Bisnis Kami: Geo Dipa Energi"*. November 7. http://geodipa.co.id/bisnis-kami/lapangan-existing/.

Reyes, Agnes G. (1990), "Petrology of Philippine geothermal systems and the application of alteration mineralogy to their assesment." *Journal of Volcanology and Geothermal Research, Volume 43*: 279-309.

PROPOSED SLIMHOLE EXPLORATION DRILLING PROGRAM FOR GEUREUDONG GEOTHERMAL FIELD

Budi Kristianto[1], Bridget Lynne[1], and Jane Brotheridge[2]

[1]University of Auckland, New Zealand
[2]Geoscience at Jacobs Engineering Group, New Zealand
Email: bkri045@aucklanduni.ac.nz

ABSTRACT

Geureudong geothermal field is currently at an intermediate exploration phase. During this period even though the data and conceptual model are already established but the uncertainty of possible success (or failure) and possible resource discovery is still huge. Hence, to reduce the uncertainty before spending another massive amount of investment for drilling commercial wells using standard holes, then exploration drilling strategy using slimhole wells is proposed in this project. Exploration slimhole wells is preferred in this project to test the proposed conceptual model, to prove the resource in Geureudong geothermal field and delineate the prospect area for future development strategies, as the cost is cheaper and simpler (compare with standard big hole). The proposed conceptual model interpretation shows Wih Pesam and Pepanji areas as two geothermal prospects in Geureudong. Wih Pesam is located in the northwestern area while Pepanji situated in the south part of Mount Geureudong. Based on low resistivity distribution from geophysics data which shows wide distribution toward NW, combined with interpretation from image, structural geology map and surface thermal manifestation, Wih Pesam is defined as the largest geothermal prospect in Geureudong. There is a similar conclusion based on developed conceptual models from all evaluators, Geureudong geothermal prospect has high potential for producing steam and hot geothermal fluid possibly more than 100MWe, however this estimation of potential capacity is need to be proved by exploration drilling. Total minimum 6 slimhole wells are recommended to drill the resource for prospect in Geureudong. All the wells that will be drilled in these prospective areas are proposed to have total depth approximately 2000 meter to test deeper part of geothermal system, with relative far distance between wells to understand broader area extension and delineate the prospect for geothermal exploitation strategies.

Keywords: Geothermal, geology, exploration, geureudong, drilling, slimhole

INTRODUCTION

Geureudong geothermal prospect is located in the Nanggroe Aceh Darussalam province, which is within the Bener Meriah and Central Aceh regencies. It is approximately 350 km southeast of Banda Aceh, the capital of Aceh. The trips to Geureudong will pass two adjacent geothermal fields inside the Aceh Province named Seulawah Agam and Puet Sagoe (Figure 1).

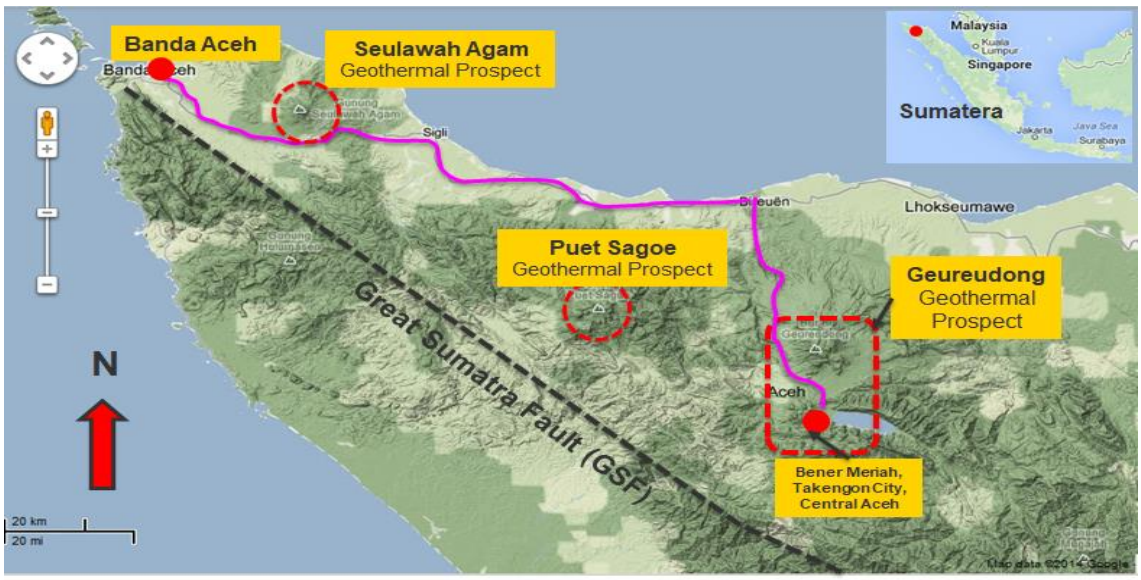


Figure 1: Geureudong project location and the access from Banda Aceh's capital city of Nanggroe Aceh Darussalam, Indonesia, passing two other geothermal prospect areas, Seulawah Agam and Peut Sagoe (Modified from Google Earth, 2018)

Indonesia Geothermal Development

Geothermal resources in Indonesia are known as the largest in the world, with around 40 percent of total geothermal resources worldwide located in this country. In order to utilize this enormous energy potential, the government of Indonesia has strengthened its efforts to encourage geothermal power development. The government has target to reach the goal of 7,100 MW in geothermal power generation capacity in Indonesia by 2025.

With installed capacity of currently 1,808.5 MW, this seems to be a rather very ambitious goal and would need adding 1,000 MW per year from today until 2025 (Wahjosoedibjo & Madjedi, 2018).

Geothermal Development Challenges

Based on literature study and author experiences in geothermal industry, there are some geothermal development challenges in Indonesia. Firstly, related with the location of geothermal resources where mostly located in the protected forest, national park and high relief volcanic terrain area which need permission, relatively difficult to access and have geohazards problem of landslides and volcanic eruption.

Additionally most of the geothermal prospects is have lack of high quality geoscientific data which crucial to preliminary geothermal potential assessment and to locate available resources. This challenges followed by there is no standard on the exploration procedures especially for exploration drilling strategy.

Financial issues also deter investment in geothermal development by private companies due to the high up-front cost of preliminary resource exploration. Lastly, an uncertain political and regulatory environment creates uncertainty for geothermal investors.

Study Objectives

The study objectives are mainly to optimise the existing exploration data which currently belong to government after preliminary survey area relinquishment process from Chevron in 2016. Other objective is to develop a newly proposed conceptual model of the geothermal system at Geureudong based on author's interpretation and construct exploration drilling strategy that fit with the resource evaluation results.

It is acknowledged that the exploration and the development of geothermal reservoirs for this area are very important. Geothermal power will provide a renewable source of base load energy, which will support the national grid from Sumatra system.

METHOD

The study will utilize geoscientific data from last 3G survey that were conducted by previous evaluator Chevron in 2013 – 2014. The conceptual model and exploration drilling target developed comprehensively by integrating all available geoscientific data meanwhile the selection of slimhole wells are based on decision making processes which consider all data available, evaluation results and level of confidence for each interpretation.

GEUREUDONG CONCEPTUAL MODEL

Building geothermal resource conceptual models to support assessments of well targets and resource capacity is a widely recommended geothermal industry best practice (Cumming, 2016). From the integration and analysis of all geoscientific information (3G), the conceptual model is developed and presented as a map view and cross section with several descriptions for several conceptual model basic elements. This project will specifically evaluate the Geureudong geothermal system as one of prospective geothermal areas in Indonesia, discuss the particular prospect location with regard to the whole concession areas, and determine the size of the geothermal resource in this location. The conceptual model will also be used as basis to build interpretation that will assist in targeting the exploratory wells for this project's goal.

Mount Geureudong geothermal prospect is interpreted as a volcanic hosted distributed permeability conceptual model type. The description of each geothermal system's elements is as follows:

- ✓ Liquid level – the water level for the surrounding prospect area is interpreted to be related to hot spring manifestations. In the north of the area the liquid level is around +900m elevation (Wih Pesam springs), meanwhile in the south it is around +1200m elevation (Uning Bertih hot springs).
- ✓ Isotherms – the basis of isothermal temperature values for the conceptual model comes from geochemistry analysis. The temperature reservoir in Geureudong is based on the solute geothermometer analysis and interpretation Na – K – Mg ternary diagram from Wih Pesam spring which shows the projected temperature of around 240 °C (Chevron, 2014 and Directorate of Geothermal, 2017). The other spring samples indicate immature waters and cannot be used to predict the subsurface or reservoir temperature.
- ✓ Upflow zone(s) – the upflow in Wih Pesam area is based on the integration of geoscientific data especially MT TDEM data possibly located beneath the upper slopes of the main

volcanic area of Geureudong, whereas in Pepanji the upflow is possibly in the north of Pepanji hot springs. The old crater volcanic structures from geology data is also considered for this interpretation.

- ✓ Outflow zone(s) – for Wih Pesam prospect, based on the interpretation of MT TDEM profile and geochemistry model, the hydrothermal fluids likely flow to the NW and outflow is heading to Wih Pesam Springs. Meanwhile for the Pepanji prospect the fluid outflow is interpreted towards the south or southwest area.
- ✓ Clay cap – clay cap distribution based on the map of low resistivity data is observed around Wih Pesam northwest of Geureudong and around Pepanji in the southeast, with all the clay cap distribution located around thermal manifestation occurrences and linked with the potential geothermal system in Geureudong volcano. Wih Pesam area has the largest interpreted clay distribution in Mount Geureudong.
- ✓ Younger volcanic rocks – based on geology, rock stratigraphy and volcanic structure analysis, the existence of younger volcanic activities and its products in Geureudong prospects are related with the quaternary eruption of Silih Nara, Geureudong, Pepanji and Burni Telong volcanoes (Figure 2). The volcanic products that originated from those volcanoes have potential as main reservoir rocks in this field with the rock age around 0.03 to 0.24Ma based on magmatic Zircon U-Pb dating (Lai, 2015). This age is relatively well-matched with the common reservoir rocks ages from other geothermal fields in Indonesia which have already proven to be productive reservoirs.



Figure 2: Photograph of Burni Telong Volcano, the youngest volcanic features in Geureudong field. The structures consist of a lava dome and open rim crater (Chevron, 2014)

- ✓ Heat source – Wih Pesam's heat sources based on interpretation of geophysics, map geology and volcanic structures are possibly located beneath the upper slopes of Mount Geureudong where the old crater feature exists, whilst in Pepanji the heat source is interpreted as deep magma associated with Quaternary eruptions at the young Pepanji and Burni Telong volcanos north of Pepanji springs.
- ✓ Deep fractures for permeability – Possibly related with fracture systems within and along the major fault N-S and NW-SE orientation that developed in this prospect area. Other deep permeability fractures are related with some volcanic rock formation that can mediate fracture permeability.
- ✓ Boiling zones, steam caps, mixing zones and zones of gas loss – this information related to subsurface reservoir condition will be answered once completion drilling data available.

The map view of the conceptual model interpretation shows Wih Pesam and Pepanji areas as two geothermal prospects in Geureudong. Wih Pesam is located in the North part of contract area while Pepanji situated in the southern part of Mount Geureudong. Based on low resistivity distribution from geophysics data which shows wide distribution toward NW, combined with interpretation from image analysis, surface geological mapping, structural map (volcanic and tectonic) and surface thermal manifestation data; Wih Pesam is defined as the largest size of geothermal prospect in Geureudong with the total prospective size of potential resources in an optimistic scenario or (P10) of about 20 km^2, meanwhile the P50 size is 15 km^2 and the minimum estimation (P90) is 10 km^2 (Figure 3).

The P10 size is determined based on low resistivity distribution from MT TDEM data only with some data limitation toward south or Geureudong summit area, on the other hand P50 and P90 are determined using a combination all of geoscientific data, for example clear distinction features of volcanic structures, fault systems, potential heat source locations, thermal manifestation types and position or distance with regards to potential heat source.

Wih Pesam prospect area is interpreted with conceivable upflow and heat source positioned possibly beneath the upper slopes of Mount Geureudong where the old crater feature exists, as shown in the map. In this area the geothermal fluids likely flow to the NW and outflows to the Wih Pesam Springs with the active NW-SE faults as a conduit to the surface.

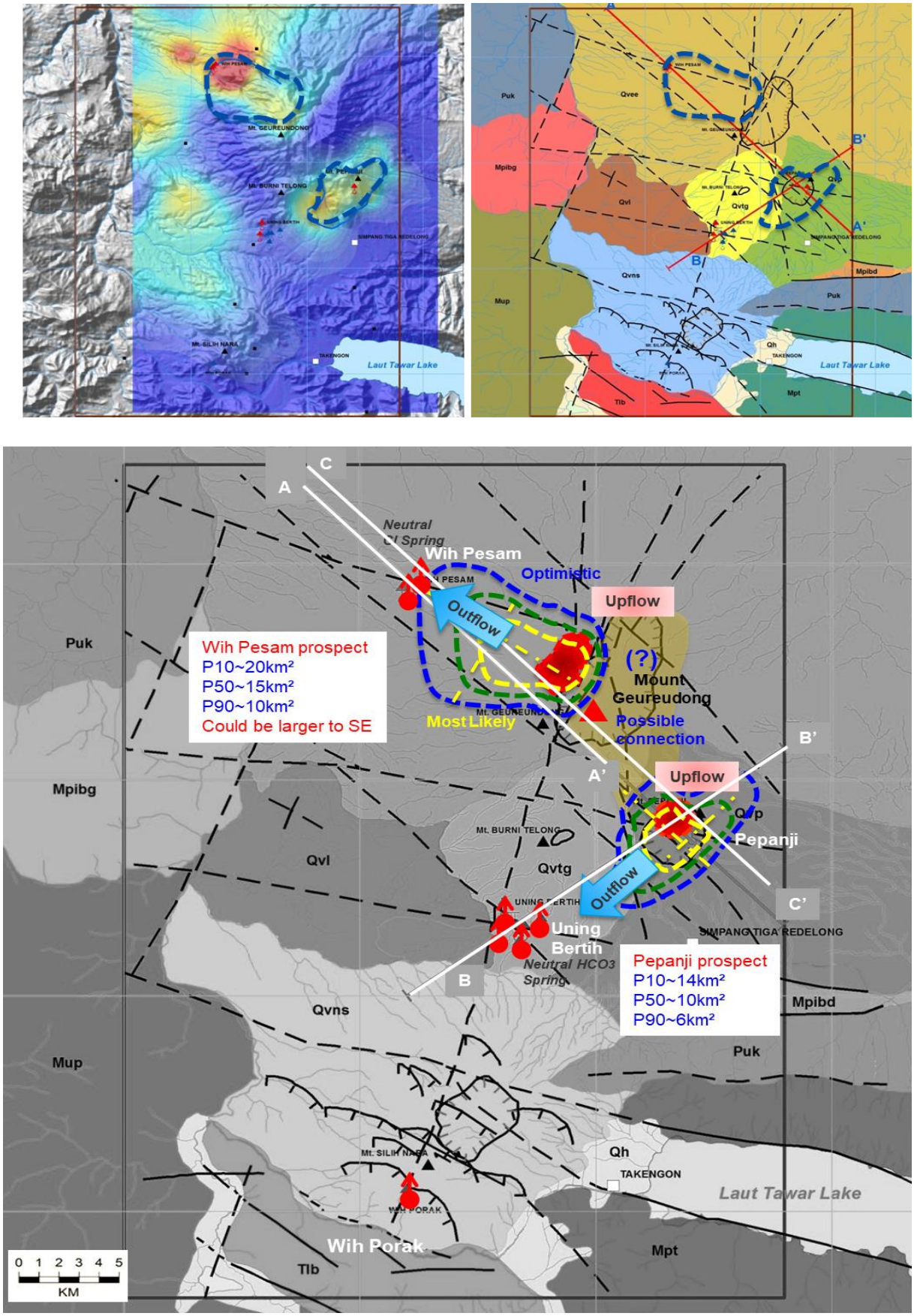


Figure 3: Map of geothermal conceptual model in Geureudong based on current interpretation of all geoscientific data especially low resistivity distribution and surface geology map (upper maps). The two possible prospects located in Wih Pesam and Pepanji (P10 – P50 – P90), the dashed blue, green and yellow area. The red area is interpreted upflow (lower map) (Modified from Chevron, 2014)

Another prospect location is at Pepanji area in the southeast Geureudong where the possible main upflow is from the north of Pepanji thermal manifestation toward the main volcano area. The size of geothermal prospect resources in Pepanji is defined due to a wide distribution of low resistivity towards the south and southwest Geureudong, combined with information from geology, alteration maps, volcanic structures (crater) and distribution of thermal manifestation area, the estimation size for P10, P50 and P90 is about 14km^2, 10km^2 and 6km^2. The heat source of the geothermal system is interpreted as deep magma associated with Quaternary volcanic eruptions at Pepanji and Burni Telong which morphologically act as younger volcanic cones of Mount Geureudong.

Related with permeability, based on the conceptual model interpretation as shown in the map, the major fault systems have orientation N-S and NW-SE. The fault structures and fractures system in this andesitic volcanic geothermal prospect is assumed to be highly responsible for permeable entry in the depth of geothermal reservoir production. Moreover the existence of quaternary volcanic products which have brittle characteristics is expected to be good media for the formation of fractures; these two parameters will reflect relatively low risk permeability in this prospect area. In addition to that, in the southern prospect (Pepanji and Uning Bertih) the superimposition of the two youngest dextral faults interpreted in this area with trending NW-SE and E-W, possibly constructed an extensional zone which indicates higher permeability and hence accountable to control geothermal system and created the outflow patterns to the Southwest area, or Uning Bertih hotsprings location.

Interpretation from the conceptual model cross section for Wih Pesam prospect shows the quaternary volcanic products (Geureudong, Silih Nara and Pepanji) area becomes the potential main reservoir rocks in this prospect area, meanwhile the other deeper possible reservoir rocks consist of the pre tertiary basement metasediments from Kluet formation and intrusion of Granite Bergang. Upflow and highest temperature location were possibly related with Geureudong main volcano and sited around old volcanic features. None of the existing surface thermal manifestation represents upflow (no fumaroles or boiling chloride springs).

The Isotherm contour is constructed based on interpretation of low resistivity data which represent smectite clay (Argillic zone) and having a temperature of approximately 70 to 150°C, meanwhile the base of clay cap signifies the high temperature clay (Illite) which has an estimated temperature of about 200-220°C. The other important isotherm contour is related with the predicted depth of the reservoir zone which has a projected temperature of around 240 and 250°C, based on geothermometry analysis (geochemistry data). The elevation of Top of Reservoir (ToR) based on the expected isotherm contour is possibly situated at +500 meter above sea level elevations, meanwhile the thickness of the reservoir is based on the cross section of approximately 1350 - 1500 meter maximum due to the potential of shallow basement formation below the reservoir zone.

The Pepanji prospect conceptual model is shows possible reservoir rocks are from Geureudong and Pepanji quaternary volcanoes and additionally the upper part of metasediments Kluet and granites Biden formation. The upflow and heat source are possibly related with the young Pepanji and Burni Telong volcanic centers and meanwhile the thickness of the reservoir based on the cross section is approximately 1000 - 1500 meters.

Additional interpretation is occurs regarding the potential connection system between Wih Pesam and Pepanji. However, the uncertainty is still huge due to limitation of geoscientific data around those inaccessible Geureudong summit areas. The recommendation for future evaluation is to revisit the areas where additional thermal features could possibly exist and further help constrain the resource. Another recommendation for the next detailed survey is to conduct additional MT – TDEM point survey around inaccessible summit areas and also measurement with closer spacing (1 km) at the most interesting areas.

GEUREUDONG EXPLORATION DRILLING STRATEGY

The conceptual model and resource estimation from both previous and current evaluators yielded similar conclusion that this prospect has high potential for producing steam and hot geothermal fluid, possibly around 150MWe. This calculation is actually based on the median value (P50) or best estimate scenario, in other words there is a potential of greater capacity in Geureudong geothermal field that might exist and needs to be proved during exploration drilling.

Proposed Exploration Well for Geureudong

Geureudong prospect is currently at intermediate exploration stages. During this period, even though the conceptual model and resource estimation are already established but the uncertainty of possible success (or failure) and possible resource discovery is still huge. Therefore, to reduce the project risks then exploration drilling strategy using slimhole wells is proposed in this project. Exploration slimhole wells is preferred for testing the developed conceptual model, to prove the resource in Geureudong geothermal field and delineate the prospect area for future development strategies, as the cost is cheaper and simpler (compare with a standard big hole).

Apart from the advantage of low budget, this slimhole technology reduces the environmental impact during field exploration and resource assessment activity. Wells with diameter less than 6 inches (152.4 mm) are defined as slimholes (Kruszewski et al 2017). Slim well technology is actually adopted from established techniques of deep-water wells, mineral exploration and geotechnical investigations. This type of well is definitely less costly than standard production size holes as cost is minimised for the rig preparation (road and pad construction), number of crews, drilling fluids, cementing, casing and tubing. This drilling technology can also be easily applied in remote areas, where helicopter-portable rigs can be used.

Currently in Indonesia, the most common geothermal exploration is involve drilling directly with standard or big production hole size and then continued with extensive flow tests as completion procedure. Some examples of this scenario from some exploration field e.g. Muara Laboh, Rantau Dedap (operated by Supreme Energy), Sorik Marapi (KS ORKA), and Baturaden Guci (SAE). This method is considered very expensive and puts severe impact on the surrounding environment. Furthermore prior the drilling itself, this strategy also need a massive expense for civil works (well pad and road access to the drilling locations), especially when the location of the exploration wells is remote and around high terrain areas, which is very common in volcanic hosted geothermal fields like in Indonesia. After the drilling, if the wells turn out to be not productive or not commercial e.g. small production, low temperature, low pressure, tight permeability and acid fluid presence, definitely it will lead to huge problem. In other words, very expensive geothermal wells are drilled with not sufficient reservoir knowledge and very high financial risk in this stage. Thus the proposed exploration drilling with slimhole method is more recommended in this project.

Decision Making Processes

The slimhole well drilling strategy is proposed to answer the question if potential commercial reservoir for geothermal field exists in Geureudong, which consists of a commercial reservoir temperature, commercial permeability and fluid chemistry. Once the slimhole exploration wells have discovered the geothermal prospect in Geureudong, then the resource uncertainty can be answered, for example:

- ✓ Uncertainty of reservoir area: the scenario is to put the well that penetrates the center of reservoir zone (P90 area), the other greater area (P50) and at the edge of area P10. This also known as delineation wells with aim to clearly test the extent of the reservoir in Geureudong field.
- ✓ Uncertainty of reservoir thickness: the slimhole well penetration will be to the deepest part of the reservoir or possible depth of basement rock in Geureudong field.
- ✓ Uncertainty of reservoir temperature: the slimhole drilling target will be toward the area of convective upflow or near the resistivity apex in the base of clay cap and heat source to test the possible highest temperature in Geureudong reservoir. Meanwhile drilling other slimhole wells in other directions is to understand the hydrothermal flow direction in each prospect. Generally the reservoir temperature target is greater than 230°C.
- ✓ Uncertainty of reservoir permeability: the wells proposed to be drilled in in the most permeable area consisting of fault structures (extensional fault and intersection of faults), fractured formations, old craters or the place where fluids can pass through the rocks, hence the convective heat can be established within the reservoir depth zone. It is suggested to avoid drilling into formations with low permeability that potentially appears in the reservoir depth.
- ✓ Uncertain reservoir fluid chemistry: exploration wells using slimhole in Geureudong also have the target of answering the uncertainty about the existence of producible fluid chemistry, the well will be drilled toward the area which has geothermal fluid with the characterization of high temperature, neutral benign fluids, low gas, and no scaling issue.

Figure 4 shows the flow chart of decision making processes when selecting slimhole wells as the preferred exploration drilling strategy in Geureudong geothermal field. Starting from exploration 3G data that was interpreted and used to construct the new resource conceptual model, the assessment basically resulted that high potential geothermal reserves is being available in Geureudong. However, based on comprehensive interpretation and consideration of all available data, it concluded that the level of confidence for that resource estimation is at medium level.

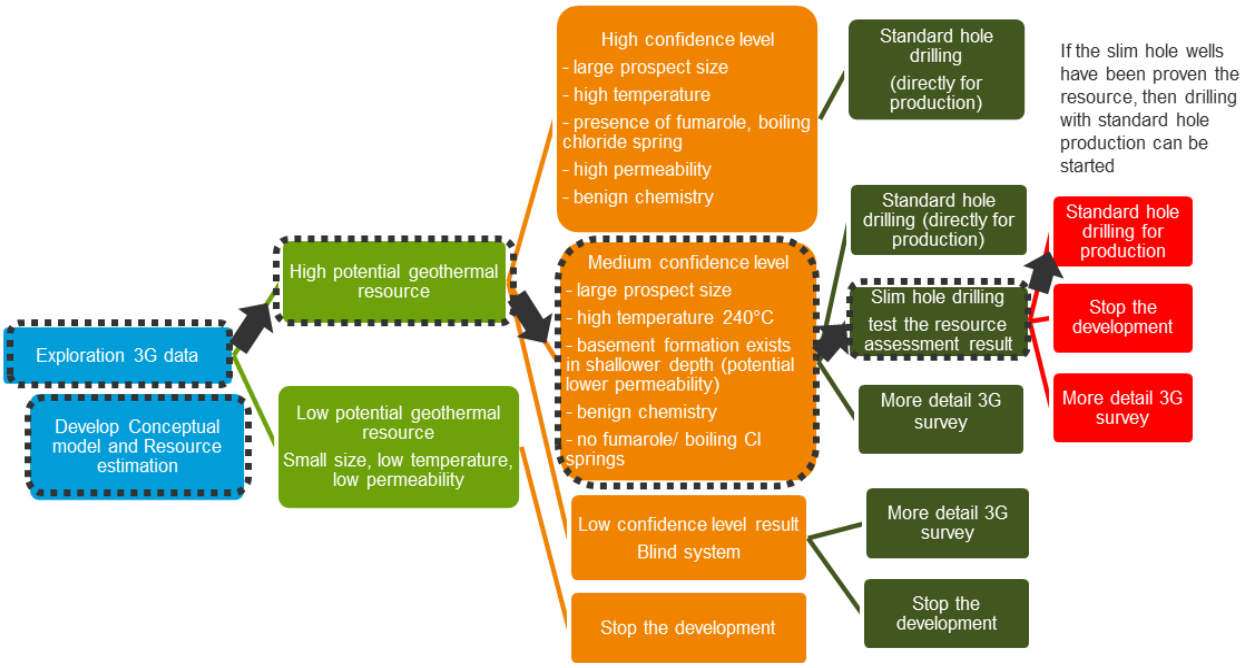


Figure 4: The flowchart of simplified decision making processes when selecting slimhole wells as the preferred exploration drilling strategy in Geureudong geothermal field (Modified from Coopersmith (2000))

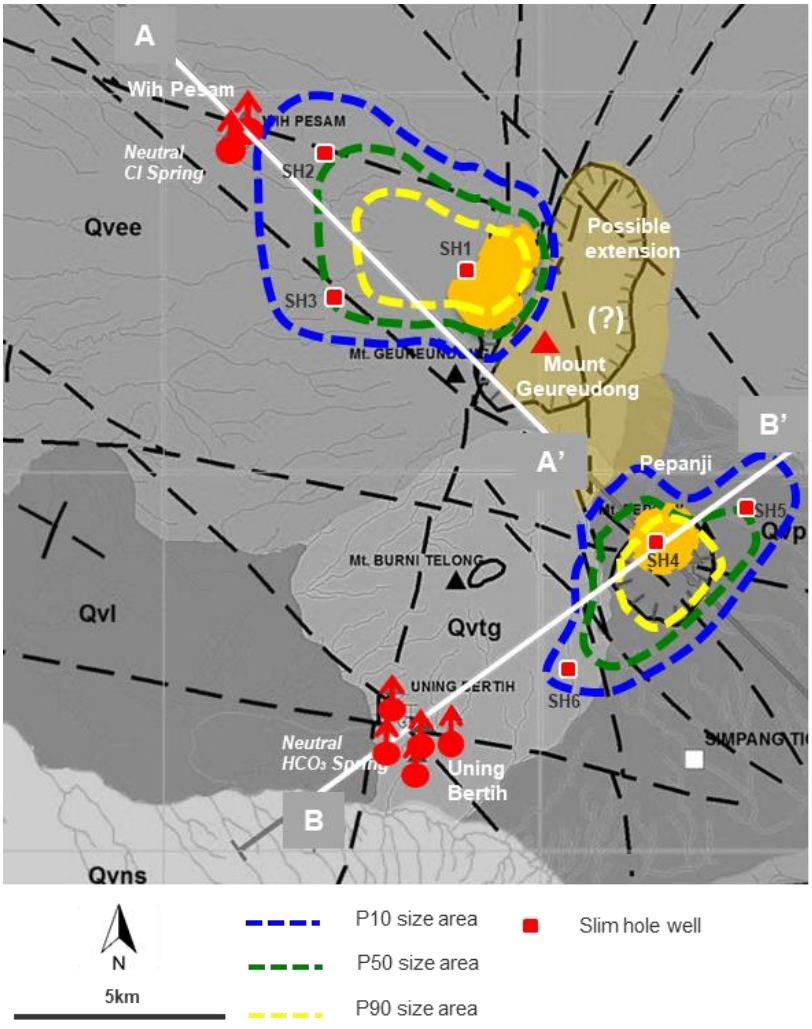


Figure 5: Map view of the proposed exploration slimhole drilling plan for both prospects Wih Pesam and Pepanji in Geureudong geothermal field (Modified from Chevron, 2014)

The new prospect assessment for resource size is already using P50 number which actually the median number, the high temperature 240°C came from a liquid geothermometer at Wih Pesam hotsprings which has high quality of sampling data but within partial equilibrium conditions. In terms of permeability, there is potential of a lower permeability reservoir due to shallow basement formation. Those numbers of considerations then used to determine the slimhole strategy as the preferable exploration wells in this stage. Sooner or later if the existence of a producible geothermal reservoir area is proven by slimhole wells then the real production holes using bigger wells can be applied to exploit both prospects in Geureudong.

Three slimhole wells are recommended to be drilled for proving the resource for each of prospect at Wih Pesam and Pepanji. All the wells that will be drilled in these prospective areas are proposed to have a total depth of approximately 1700 to 2000 meters to test the deeper parts of the geothermal system, with a relatively wide distance between the wells to understand the extent of the broader area and delineate the prospect for future development strategies. The locations for the slimhole exploration for Wih Pesam and Pepanji are shown in the map view Figure 5.

Wih Pesam Exploration Target

Wih Pesam as the largest geothermal prospect in the Geureudong field is becomes the first priority for geothermal field exploration and development. The slimhole for the Wih Pesam area focusses on the three areas. SH1, SH2 and SH3 (see Figure 5).

The slimhole exploration drilling program focuses on the highest location for steam production that possibly exists within the main upflow areas and also tests the reservoir boundary surrounding the prospect. The cross section in Figure 6 illustrates all three slimhole wells located inside P90, P50 and P10 reserves areas in Wih Pesam prospect.

SH1 (Slimhole 1)

Well SH1 is the first proposed slimhole well to drill and test geothermal resource in Geureudong geothermal field. This well is targeted inside P90 or the most likely area reservoir in Wih Pesam. The pad is placed upward nearby an old crater area where an interpreted upflow based on the current conceptual model is located. The slimhole well that is planned to be drilled in this area is to test for the highest production and highest temperature zones in Wih Pesam system.

It is proposed to drill well SH1 vertically with a total depth of a minimum 2000 meters to reach the deep part of the geothermal system. For a higher confidence result the well is targeted to drill toward the young volcanic structures of Geureudong with the location on top of a potential upflow or heat source beneath Mount Geureudong. Meanwhile with regard to permeability, this well's goal is to drill around the N-S splays fault, and toward the possible extensional fault zone around it. The assumption is that the fault movement can trigger the development of a fractured rock system within the convective high temperature reservoir zone in this area. Furthermore, related to fluid chemistry this area also has neutral pH reservoir water which good for production.

Based on cross section of Figure 6, it illustrates the surface ground of SH1 located at approximately +1800m above sea level. This well is expected to drill through ~700 meter thick of clay cap and penetrate the top of reservoir (ToR) depth around +400 meters above sea level. The reservoir thickness for the production zone is around ~1350-1500 meter thick.

SH2 (Slimhole 2)

The plan for this slimhole well is to be positioned in between the hotsprings and SH1, to test the northernmost reservoir boundary near the neutral chloride hotsprings at Wih Pesam. The proposal is to drill the slimhole with a total depth of 1700 meters using a vertical drilling technique around the geothermal outflow direction. The cellar ground level of this slim well is at an elevation +800 m, with a possible thickness clay cap around ~700 meters. The top of reservoir is projected to be encountered around 0 sea levels, and the reservoir thickness for the potential production zone is ~1100 meters thick (Figure 6). For testing the production permeability, this slim well's goal is to drill around a NW-SE major fault that is potentially linked with alteration ground and thermal manifestation occurrence at Wih Pesam.

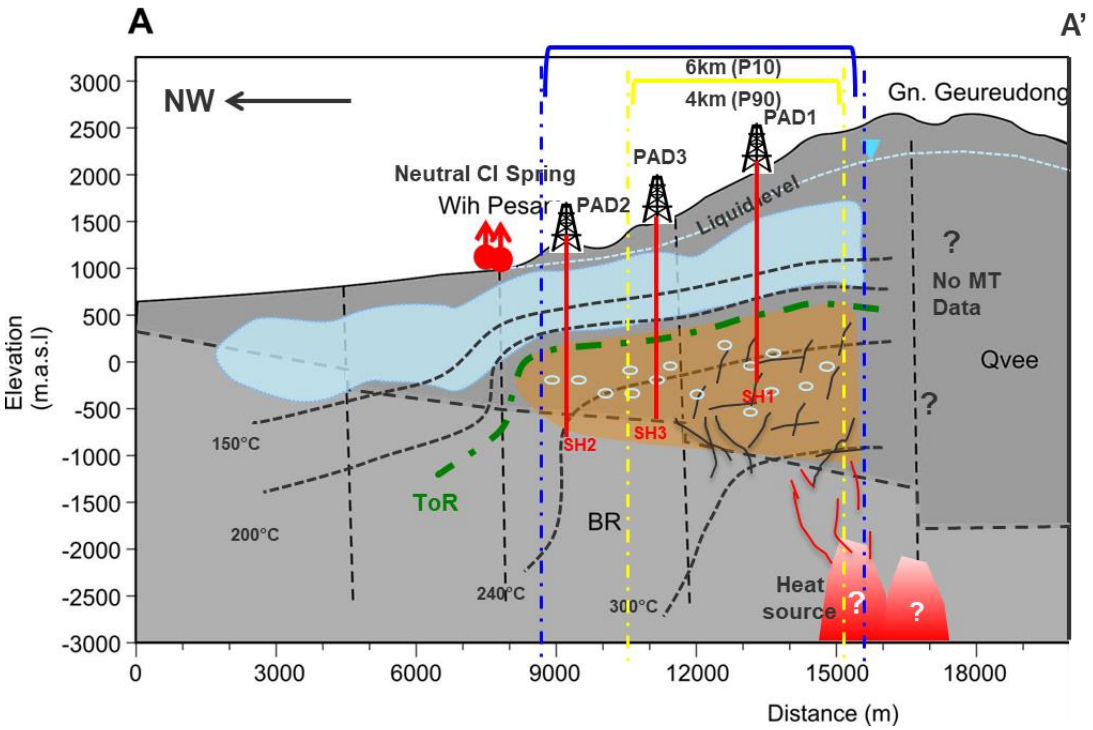


Figure 6: Slimhole exploration drilling target in Wih Pesam (Modified from Chevron, 2014)

SH3 (Slimhole 3)

The SH3 pad is to be located in the edge of P50 area near the West reservoir boundary of Wih Pesam. Similar to the SH2 this slimhole well is proposed to test the reservoir margin and potential extension toward the western area. The slimhole is proposed to a total depth of 1700 meters vertically around the geothermal outflow direction. The ground surface is at elevation +1300 m, with a possible thickness clay cap of around ~700 meters. The top of reservoir is projected to be encountered around +100 meter above sea level, and the reservoir thickness for the potential production zone is ~1350 meters thick (Figure 6). Another NW-SE fault is a target for this well as the potential reservoir border for the southern Wih Pesam prospect. This information related with reservoir boundary then can be a reliable basis for the next appraisal or production drilling plans.

All the proposed slim well exploration drilling within the Wih Pesam prospect is predicted to encounter young volcanic rock products from Geureudong volcano as highly potential fractured reservoir rocks. However, based on the cross section, the upper part of the basement formation, which consists of Pre Tertiary metasediments and Granite formation, also has the possibility to become the reservoir rocks within this zone which potentially lessen the permeability. As mentioned previously, the plan for deep drilling targets within this zone will help to answer this uncertainty.

In addition to that, both slimholes which have reservoir boundary targets (SH2 and SH3) are also important wells to bring information about the possible outer reservoir and to map the potential candidate area for injection wells. Actually the location of the injection wells needs to be further from prospect location and at a lower elevation considering the easier access and to lessen the potential risk of injection breakthrough.

Pepanji Exploration Target

Pepanji prospect is located in the southern area of Geureudong geothermal field. This prospect becomes the second priority for development as it has a smaller prospect size, based on current resource capacity assessment. In terms of possible reservoir temperature, there is no surface thermal feature that could indicated a deep reservoir condition within this prospect, thus the uncertainty and risk for resource temperature in this area is relatively bigger compared with Wih Pesam prospect.

However, similar to Wih Pesam prospect, the slimhole drilling program in Pepanji also focuses on steam production that possibly exists within main interpreted upflow areas and also checks the reservoir boundary extension surrounding Pepanji prospect. The slimhole drilling in Pepanji is focused on the three areas of SH4, SH5 and SH6 (see Map view Figure 5). The cross section in Figure 7 illustrates three slimholes that are located inside P90, P50 and P10 reserve areas in Pepanji.

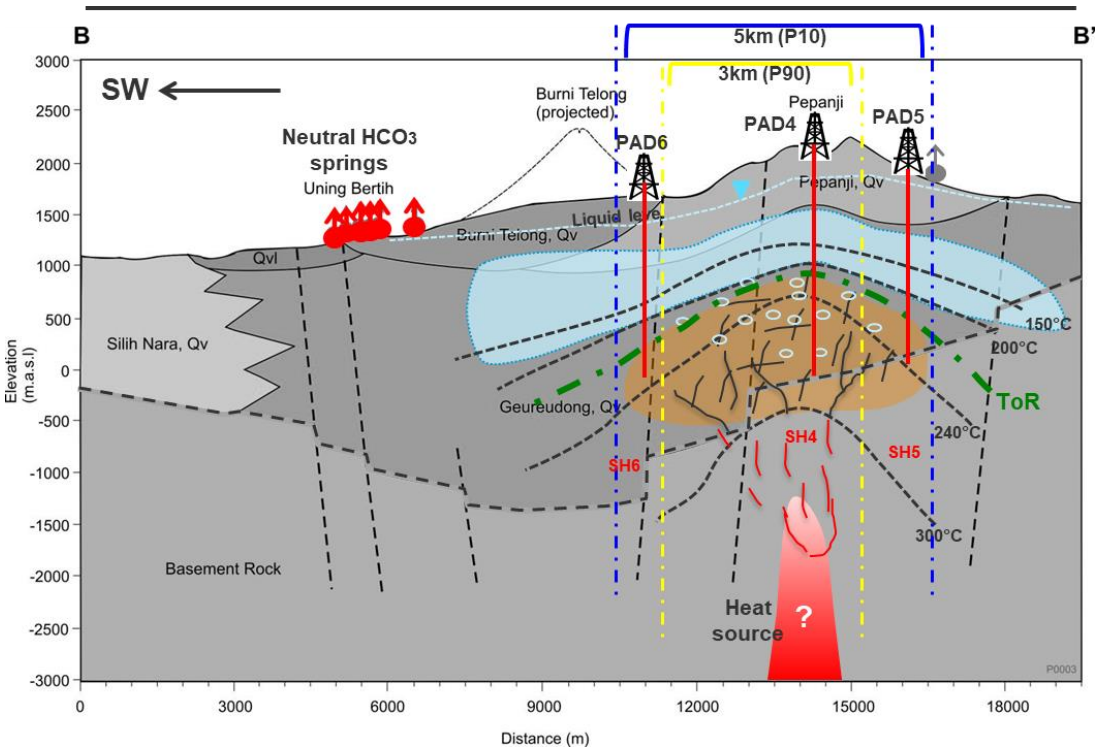


Figure 7: Slimhole exploration drilling target in Pepanji (Modified from Chevron, 2014)

SH4 (Slimhole 4)

Slimhole well SH4 proposed to drill in Pepanji as the first well to test the geothermal resource in this particular prospect area. The pad is located inside P90 area of Pepanji prospect and plan to drill into a total depth of 2000 meters using a vertical well precisely on the possible heat source location beneath the young Pepanji volcanic cone. This well is expected to encounter the highest production and highest temperature in the reservoir of Pepanji. With regard to permeability, this well is targeted to drill toward the NW-SE major fault and possible fault conjunction zone which could develop into significant permeable or fracture networks in this zone. Furthermore, this area also has neutral pH reservoir water which good for production.

In the detailed plan, the surface ground of well SH4 is located at approximately 1700 meters above sea level. This well is expected to drill to ~500-700 meters thick of clay cap and penetrate the top of the reservoir (ToR) at around +800 meters above sea level elevations. The thickness of the fractured reservoir for the potential productive zone is around 1350-1500 meters thick (see Figure 7).

SH5 (Slimhole 5)

This slimhole well, SH5, is located in the P10 area NE of Pepanji prospect to test the reservoir extension surrounding that location. The slimhole is proposed to be drilled with total depth ~1700 meters using a vertical drilling around a geothermal outflow direction. The cellar ground level of this slim well is at elevation +1500 meters, with a possible thickness clay cap of around ~800 meters. The top of the reservoir in this area is projected to be encountered at around +500 meters above sea level, and the reservoir thickness for the potential production zone is ~1000 meters thick. For testing the production permeability, there is no interpreted fault that can be targeted for a permeable feed zone within this area. However, it is assumed that permeability also could develop from a fracture system since this area is mainly constructed by young volcanic products from Pepanji volcano. Additionally, as is presented in Figure 7 the low permeable basement formation could be identified at a shallower depth within this zone due to the uplift tectonic process.

SH6 (Slimhole 6)

SH6 is located in the P10 area precisely in the middle between possible heat sources of Pepanji old crater and the dilute bicarbonate springs at Uning Bertih which is interpreted as an outflow. This slim well is targeted to test the SW reservoir margin and potential extension of Pepanji prospect. The slimhole is proposed to drill with a total depth of ~1700 meters vertically into the area of the main geothermal outflow direction. The ground surface for this well is at an elevation +1400 meters, with a possible thickness clay cap of around ~1000 meters. The top of the reservoir is projected to be encountered around +200 meters above sea level, and the reservoir thickness for the potential production zone is ~1000 meters thick.

In the Pepanji prospect, all proposed slim well exploration drilling is predicted to encounter two or three series of young volcanic rock products from Pepanji, Burni Telong and Geureudong main volcano. Those Quaternary volcanic products are assumed to be highly potential fractured reservoir

rocks. However, still based on cross section, the upper part of basement formation, which consists of relatively tight permeability metasediments and Granite formation, also has the potential to turn into reservoir rocks within this zone which potentially lessen the permeability.
Similar to Wih Pesam prospect, both slimholes which have reservoir boundary targets in Pepanji (SH5 and SH6) are also important wells for understanding the possible outer reservoir condition. This type of information related to reservoir boundaries and potential extensions can then be a reliable basis for the next appraisal or production drilling plan.

Slimhole Well Design in Geureudong Field

Kruszewski et al, (2017) mentioned two different methods of drilling slim wells which are coring and rotary drilling (conventional) method. Wireline coring is a common method. It provides high quality core samples that can be used further for evaluation of reservoir conditions. Because of the smaller hole diameter (from 2 to 6 inches) with corresponding core diameter (from 1 to 4 inches) and significantly smaller rigs, it can be easily applied to slim wells. The main disadvantage of the coring method is the longer drilling time; especially in geothermal fields with dominant igneous volcanic rock and metamorphic rock formations. The most favorable method is a combination of coring and the rotary method. It is very attractive for areas with softer formations at the beginning of drilling and relatively harder formations in the deeper depths of the reservoir. In summary, the geological characteristics of the chosen area should be thoroughly evaluated to select the best drilling method for slim wells.

Similar to the standard or production hole well design, drilling with slimholes also utilizes casing and liner as standard best practices in drilling. The design criteria and guidelines for high-temperature geothermal wells have been described in New Zealand Code of Practice from (New Zealand Standard, Code of Practices for Deep Geothermal Wells, 1991) and the recent update from 2015). The main purposes of casing and liners in high-temperature wells are as follows:

- ✓ Preventing a hole collapse caused by loose formation material
- ✓ Anchorage security and support of drilling operations
- ✓ Containing well fluids and withstanding pressures imposed on casing
- ✓ Preventing contamination of fresh underground water
- ✓ Countering circulation losses during drilling
- ✓ Protecting the well from corrosion, erosion and fracturing.

Using the subsurface data and geological information in Wih Pesam prospect, a suggested slimhole well design is developed for Well SH1 and is generally applicable for all slimhole plans within Geureudong geothermal field (Figure 8).

The ground level of cellar pad SH1 well is at ~+1800 elevation. The 9-5/8" rotary bit will start drilling the hole section down to ~30m, and after the drilling reaches a target depth, casing with a diameter 6-5/8" will be set to seal the shallow and near surface water level to protect the well from cold water incursion. All parts of this section will be cemented to surface as a surface conductor.
Next section uses the 6" tricone bit to rotary drill this intermediate hole down to 600m; this section will start to drill into clay cap zone. After drilling reaches a target depth, a 4½" anchor casing will be used primarily to isolate the shallow water from contamination and to isolate shallow loose formation areas to avoid drilling problems from here to deeper section. This zone also provides an anchorage for the wellhead and seals off zones of shallow loss of drilling fluid.

The next section is drilling using a core barrel bit 3-7/8". This hole section is one of the critical parts for geothermal exploration drilling. Thus some detail and a comprehensive analysis of all available subsurface and well data is crucial to be assessed during drilling as a basis for every decision including the time to keep and stop drilling to the approximate depth of the reservoir target. This section is important as a safe conduit for the reservoir fluid to the surface, to protect shallow formations from deep reservoir pressure and to isolate shallow cool water from degrading the temperature of the reservoir fluids. This last cemented section will drill deep to ~1300m or the estimated depth of the top of the reservoir (ToR). For the Wih Pesam area the ToR depth is at +500m elevation.

Different from the standard hole, during drilling the slimhole using HQ core barrels, the cut rocks will not return to the surface, however a full core sample is available as the replacement data for further analysis. Petrographic analysis for this core sample is one of the most important sources of data for geologists in geothermal exploration. Hence a good understanding about descriptions of mineral geothermometry and its characterization is needed. The minerals that could be a good indicators for high temperature zones common in Indonesia's geothermal fields for example are; Epidote, Actinolite, Wairakite, Prehnite etc. This information related with the confirmation of the Top of Reservoir depth around this area will be used as the most reliable justification for planning a production hole section when using standard hole drilling in the future.

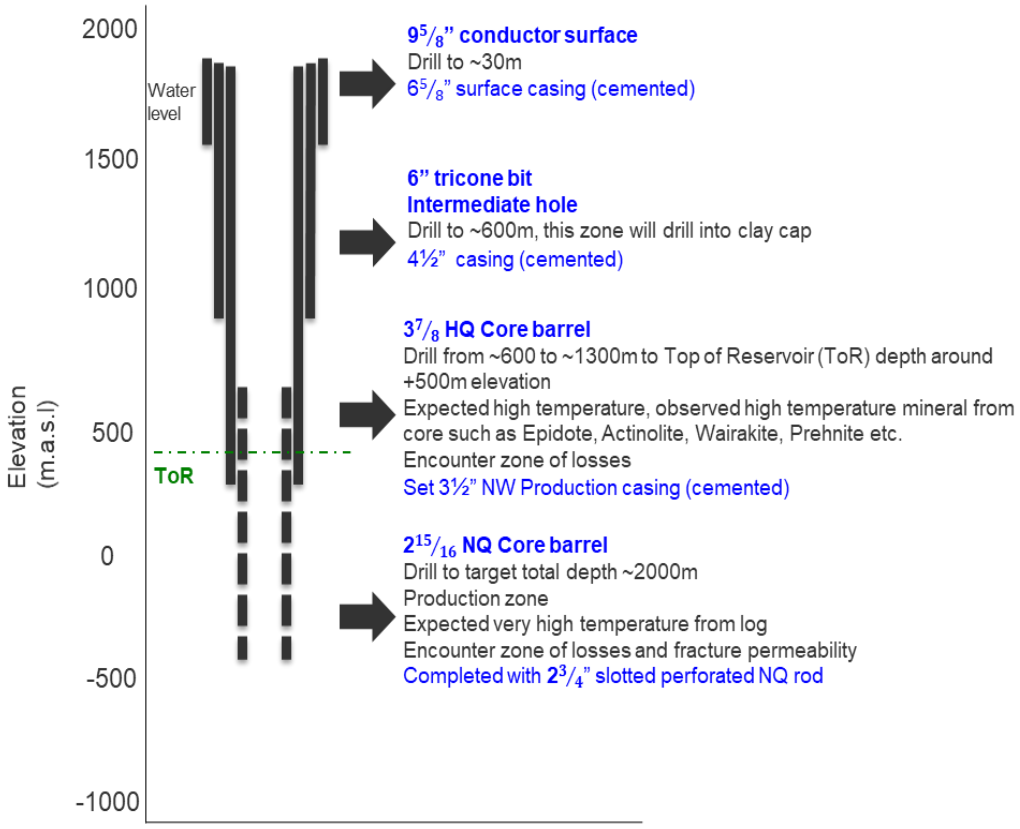


Figure 8: Proposed slimhole well design for Well SH1 and generally applicable for all slimhole plans within Geureudong geothermal field (modified from Nielson & Garg (2016))

Furthermore, when drilling into this important section, there is also a potential of misinterpreting the drilling data. Similarly to the possible remnant geothermal systems that appear in geophysics data (low resistivity interpretation), it is also possible to find a relic geothermal system which might occur and is shown by the relic mineral geothermometry that is observed from the drill core samples. The high temperature mineral geothermometry, as mentioned before, could be detected in the upper depths or in cooler reservoir zones and are absolutely not representative of current reservoir conditions which are possibly located deeper. Thus more thorough well data analysis and crosschecking with well temperatures is needed when planning the next drilling stages using production holes.

The final section of SH1 is drilling inside a reservoir zone using the smallest 2-15/16" NQ core barrel bit. The drilling target is to a total depth ~2000 m to test longer production zones and the possible bottom of the reservoir. Drilling into this section will encounter very high convective reservoir temperature zone, a high possibility of facing the zone of losses and drilling into formations with highly fracture permeability. Therefore, an anticipation of several drilling problem needs to be considered, especially related to potential tight holes, stuck pipes, or steam kicks, etc. The completion of this section uses a 2-3/4" slotted perforated liner. This liner is primarily run to prevent the reservoir wellbore from collapsing and blocking the well flow path for production (see Figure 8).

This proposed slimhole well design for SH1 is also applicable for the other slimhole wells SH2, SH3, SH4, SH5 and SH6. The difference is the possible depth to target for each hole section. This is due to each slimhole having a different surface ground level and predicted depth of subsurface condition regarding clay cap thickness, top of reservoir, reservoir thickness and bottom of reservoir.

SUMMARY AND CONCLUSION

As discussed in previous chapter, Geureudong geothermal field is currently at intermediate exploration stages, with the evaluation of geoscientific data shows the resource conceptual model and capacity estimations from all evaluators are summarize in similar conclusion, that Geureudong geothermal field has high potential for producing steam and hot geothermal fluid from both prospects at Wih Pesam and Pepanji.

Even though this field has the high potential to become a commercial geothermal power plant in Indonesia, all the stakeholders need to understand that at this exploration stage the uncertainty and possibility of failure for developing this prospect is still remain. Author believes the variations in

resource estimation values are just an uncertainty in numbers until an exploration drilling program has been conducted in this particular prospective area, to test and prove the resource exists beneath Geureudong volcano complex.

The exploration drilling will help to reduce the uncertainties and answer all the questions that in an exploration phase are really difficult to answer thoroughly due to limitations of data, for example, related to the uncertainty of reservoir size, temperature, permeability and fluid chemistry that are strongly related to the definition of a producible geothermal reservoir.

Due the fact that there is still a large portion of uncertainty within the exploration phase of Geureudong geothermal project, then exploration drilling using slimhole wells is preferred based on this project. Bear in mind that an exploration phase means the period of finding the information at the most complete level about the resource and the potential risks. It is better not to mix it up with exploitation or production purposes. Unfortunately, that is what actually happens currently in the geothermal business, especially in Indonesia.

Based on this study, six slimhole wells are proposed to test and prove the resource capacity and deep subsurface condition in the Geureudong geothermal prospect. For Wih Pesam prospect the slimhole is consists of SH1, SH2 and SH3 meanwhile the Pepanji prospect will be tested by SH4, SH5 and SH6.

The proposed slim well exploration drilling SH1 and SH4 within the Wih Pesam and Pepanji prospects is expected to test the potential of highest production and highest temperature areas. This slimhole drilling target will be toward the area of convective upflow or near the resistivity apex in the base of clay cap and heat source in Geureudong reservoir.

Meanwhile other slimhole wells (SH2, SH3, SH5 and SH6) are also important wells to understand the hydrothermal flow direction and delineate boundary in each prospect. Those wells are also vital to bring information about the possible outer reservoir and to map the potential candidate area for injection wells.

The slimhole well drilling strategy is aim to answer the question if potential commercial reservoir for geothermal field exists in Geureudong, which consists of a commercial reservoir temperature, permeability and fluid chemistry. Once the slimhole exploration wells have discovered the geothermal prospect in Geureudong, then the resource uncertainty can be answered and then the real production holes using bigger wells can be applied to exploit both prospects in Geureudong.

ACKNOWLEDGEMENT

This research study is a part of author's thesis during the program of Master Energy in Engineering Science Department, University of Auckland 2017-2018. Author wants to thanks to MFAT New Zealand ASEAN Scholarship for the financial assistance, and also the Directorate of Geothermal Indonesia (EBTKE) who give the authorization to make use of the exploration data from Geureudong geothermal field. From this paper, I would like to express my great appreciation to both agencies.

REFERENCES

Chevron Geothermal Indonesia. (2014), "Exploration Report: Geology Geophysics Geochemistry Data from Geureudong Geothermal Field". Jakarta: Chevron Unpublished Report.

Coopersmith, E., Graham , D., McVean, J., & Storaune, E. (2000), "Making Decisions in the Oil and Gas Industry". Oilfield Review Schlumberger.

Cumming, W. (2016), "Resource Conceptual Models of Volcano Hosted Geothermal Reservoirs for Exploration Well Targeting and Resource Capacity Assessment: Construction, Pitfalls and Challenges". GRC Transactions Vol 40.

Directorate of Geothermal, D., & Ministry of Energy Resources and Mineral. (2017), "Geothermal Potential in Indonesia Chapter 1". Jakarta: Directorate of Geothermal.

Kruszewski , M., Thorhallsson, S., Assadi, M., & Śliwa, T. (2017), "Slim Hole Well Casing Design for High Temperature Geothermal Exploration and Reservoir Assessment". AGH Drilling Oil and Gas Vol 34.

Lai, Y. (2015). Miocene to Recent migration of arc volcanism in NW Sumatra. Department of Geosciences, National Taiwan University.

New Zealand Standard. (2015), "Code of Practice for Deep Geothermal Wells". Wellington: Standards New Zealand.

New Zealand Standard. (1991), "Code of Practices for Deep Geothermal Wells". Wellington: Standards Association of New Zealand.

Nielson, D., & Garg, S. (2016), "Slim Hole Reservoir Characterization for Risk Reduction". PROCEEDINGS, 41st Workshop on Geothermal Reservoir Engineering. California: Standford University.

Wahjosoedibjo, A., & Madjedi, H. (2018), "Indonesia's Geothermal Development: Where is it Going?".

THEORETICAL ASSESSMENT OF VP AND VS FOR VOLCANIC ROCKS IN GEOTHERMAL FIELDS

D. Mendrofa[1], S. Mulyani[2], and D. Juandi[2]

[1]Star Energy Geothermal
[2]Schlumberger
Email: dntq@starenergy.id; smulyani@slb.com; djuandi@slb.com

ABSTRACT

There have been many studies in utilizing non-seismic measurement for geothermal field. Gravity and Magnetotelluric are commonly acquired for exploring geothermal prospects in many green fields as well as other geophysical survey like time lapse microearthquakes applied for monitoring steam flow extracted from an established geothermal reservoir.

This study offers an initial thought to consider new approach of how non-seismic measurement can be dealing with petrophysical property of steam saturated rocks of geothermal reservoir. A geophysical interpretation usually comes up when most of these kinds of measurements are usually related to represented number of rock property by averaging porosity matrix, fracture porosity and saturating fluid as part of low resolution property. Matrix itself is composed with various minerals and commonly are grouped in petrophysical group used for numerical modeling.

This time particularly, a theoretical approach will be presented here to define how elastic waves like Vp or Vs propagate through steam saturated rocks which filled in to pore system of matrix and flowing through pore throats and interconnect the pore throat thru fracture system.

Gassmann and Wyllie equation are examined in this study to check reliability of using these approaches which usually works well in consolidated sedimented rocks in Oil and Gas fields. The worries may arise when testing both approaches for complex carbonates that possess less compressible grains. However, volcanic rocks in geothermal may be different as homogeneity criteria is met with the fact of minimum transport as igneous rock rapidly coagulated while erupting from an explosive volcano. This study gives an initial assessment and hopefully give better understanding to refine petrophysical meaning behind Vp and Vs especially observed for geothermal reservoir.

Keywords: empirical approach, compressional wave (Vp), shear wave (Vs), Gassmann, geothermal

BACKGROUND STUDY

Reservoir assessment for geothermal field are using many methods and data from geophysics measurement or petrophysics analysis of rock data. But, there is no many studies about analytical relationship between those geophysical data against petrophysical property for altered rocks in geothermal field. One of common geophysics data used in geothermal case is rock velocity. There are two kinds of rock velocities, primary velocity or compressional wave (Vp) and secondary velocity or shear wave (Vs). Petrophysics parameter that usually related with the velocities are rock porosity, density, elastic modulus and water saturation.

Nowadays there is only empirical approach used for describing correlation between them. Based on those method, understanding the observed correlation is important to get the values range of petrophysics parameter at geothermal field by using known geophysics data (Vp and Vs)

OBJECTIVES

The objectives of this study are providing initial assessment, to see the relationship between Vp/Vs with petrophysical property. The results are range of geophysics and petrophysics numbers from rocks at geothermal field.

Another benefit from this project is to be used as reference for further study that related with analysis in geothermal reservoir based on geophysics data. Proven correlation between those parameters could also increasing the level of confidence and reducing the uncertainty, while using the combination of multidiscipline data during interpretation process.

In the future, more studies to see the relationship between other geophysics data with petrophysics parameter are expected. So, advance method of analysis by using those data can be done, and the usage of available geophysics or petrophysics data will be optimized. Finally, the geothermal operator can get more information about subsurface condition in their field.

BACKGROUND THEORY

To deliver this study, there are several theories related about geophysics parameter (Vp and Vs) and lithology characterization at geothermal field.

Empirical Approach for Elastic Wave

Elastic wave (Vp and Vs) of rocks have been explained by Gassmann equation. This technique is by far the most widely used to calculate rocks velocity changes due to different fluid saturations in reservoir. Gassmann's formulation use simple input parameters that typically directly measured from well data or assumed based on rock type.

This equation was established by using fundamental elastic theory based on elastic modulus of the minerals. The Gassmann model estimates the elastic properties of a porous rock at one fluid state, then it used to predict the properties for another fluid state. This technique called "fluid substitution" or "fluid replacement" that important for seismic rock physics analysis (Gassmann, 1951).

A static model of porous rock has been developed by Gassmann to predict the velocities if rocks are saturated with one fluid, from velocities if rocks are saturated with different second fluid, and vice versa. The result said that changing of pore fluid can influence velocity of elastic waves because of changing elastic moduli and changing density. Those parameters can be described as equation:

$$\rho = (1 - \emptyset)\rho s + \emptyset \,.\rho fl \qquad (1.1)$$

$$\mu\, dry = \mu \text{ sat} = \mu \qquad (1.2)$$

$$k\, sat = k\, dry + \frac{(1 - \frac{kdry}{ks})^2}{\frac{\emptyset}{kfl} + \frac{1-\emptyset}{ks} - \frac{kdry}{ks^2}} \qquad (1.3)$$

Density total (ρ) is influenced by rock porosity ($\emptyset$), density of solid (ρs) and density of fluid ($\rho\, fl$) as shown at equation (1.1). Shear modulus (μ) is independent on the fluid type, so the dry ($\mu\, dry$) and saturated ($\mu\, sat$) value are equal which shown at equation (1.2). While compressional bulk modulus (k) is strongly dependent on fluid compressional modulus (k fl), follows equation (1.3). The principle used to derive that equation can be explained by using Figure 1.1 (Schon, 2011).

Based on that figure there are two condition of rock under compression condition. At dry state, the deformation behavior is influenced by the rock skeleton moduli (bulk and shear modulus), where:

$$\text{k dry} = \text{k and } \mu \text{ dry} = \mu \qquad (1.4)$$

At fluid saturated state, the behavior of deformation is characterized by effective of two moduli as well. But, the bulk modulus in this case is result of combined effect from rock skeleton, solid component and the fluid. The bulk modulus of saturated rock is greater than the dry rock, while shear modulus is same because the fluid does not contribute for it (Mavko et all, 1998).

$$\text{k sat} > \text{k dry} = \text{k and } \mu \text{ sat} = \mu \text{ dry} = \mu \qquad (1.5)$$

Parameters of density, porosity, bulk modulus and shear modulus then used to derive the formula of compressional wave (Vp) and shear wave (Vs) as shown by equation 1.6 and 1.7. Both equation will be used during this study as main reference.

$$Vp = \sqrt{\frac{k + \frac{4}{3}\mu}{\rho}} = \sqrt{\frac{kdry + (1 - \frac{kdry}{ks})^2}{\frac{\emptyset}{kw} + \frac{1-\emptyset}{ks} - \frac{kdry}{ks^2}} + \frac{4}{3}\mu} \qquad (1.6)$$

$$Vs = \sqrt{\frac{\mu}{\rho}} = \sqrt{\frac{\mu\, dry}{(1-\emptyset)\rho + \emptyset.\rho fl}} \qquad (1.7)$$

In this case there are some assumption used for the derivation of Gassmann equation, such as:

1. The porous material assumed as isotropic, elastic, monomineral & homogeneous thing.
2. Pore space in the rock is well connected and in pressure equilibrium.
3. Medium is a closed system without pore fluid movement across boundaries.
4. There is no chemical interaction between fluids and rock, so shear modulus always remains constant.

Most of those assumption are not valid for the real condition in the nature or subsurface. However, Gassmann equation usually applied successfully for sedimentary rock as hydrocarbon reservoir analysis. The real challenges for this equation it to be applied at volcanic rock at geothermal reservoir analysis.

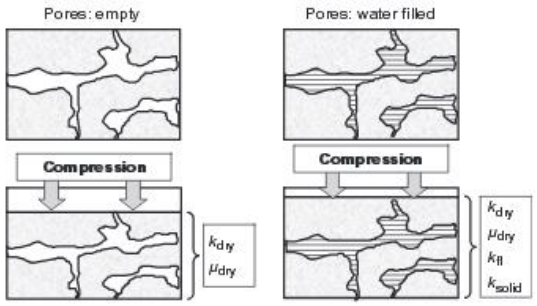


Figure 1.1 Rock model used to derive Gassmann equation. Left is dry and right side is fluid-saturated porous rock under the compression (Schon, 2011).

According to the results of laboratory experiments on volcanic rock specimens towards gas saturation (Sg), wave response of volcanic rocks is seriously affected by its internal structure (Liu, Z. & Zhao,J., 2015). Generally the P-wave velocity decreases with increasing of gas saturation, while the S-wave velocity is barely changes. The Vp/Vs ratio

decreases with increasing of gas saturation. The Vp/Vs ratios of different volcanic rocks are vary, but the general rule is that the Vp/Vs ratio at Sg=0% is greater than that at Sg=100%. But, the ratio doesn't work well when used to identify a reservoir that produces both water and gas.

Lithology in Geothermal Area

Geothermal system that closely related with magmatic system are consist of volcanic rocks as the main lithology. That rocks can be classified based on their specific character such as composition, texture and structures. Each volcanic rock not only has unique chemical composition, but also specific number of physical properties. Below are some examples of volcanic rocks based on its texture and the physical characterization (Gonzales et all, 2007).

Basaltic lava flows

Lava flow is a volcanic extrusive product from the flow of lava on the surface until it cools or the volcanic emission stops. The morphology, length and thickness of deposit depend on the magma's composition and topography. This lithology usually clearly affected by vertical columnar joints.

The variation of dry density for basaltic lava is around 15 - 31 kN/m^3 with average 23 - 28 kN/ m^3. The influence of mineral composition and vascularity in density also influence the uniaxial compressive strength, with values between 25 and 160 MPa, and more frequent values are 40-80 MPa. The vesicular basalts may reach less than 40 MPa, while the massive basalts present usually present more than 80 MPa.

Dykes and other intrusive structures

Dykes can be generally defined as discordant magmatic intrusion along faults, fractures or fissures. It has planar structures, generally vertical or sub-vertical. Horizontal magmatic intrusion which concordant with the neighboring formations is called *sill*. Plugs are the filling up of volcanic conduits which is scoria cones, that has cylindrical shape and can be affected by columnar jointing.

Pyroclastic deposits

Pyroclasts are fragmental rocks ejected from volcanic vents during explosive eruptions. Deposition and accumulation of these solid fragments form volcanic cones or layered deposits, depending on some factors such as: their extent and distribution on the density and size of fragments, height of the eruptive column, wind regime and topography. Based on their genesis, pyroclastic deposits can be classified as pyroclastic flow, surge and fall. According the size of fragments, those pyroclasts are classified into: bombs or blocks (grain size >64mm), lapilli (2–64mm) and ash (<2mm). Scoria, is a general term for a porous, dark and glassy pyroclasts of basaltic composition, while pumice is a broad term for a light color, highly vesicular, low-density with acid composition.

Geomechanical properties of pyroclastic deposits, that can't be considered as rock depends mainly on the grain size and shape, sorting, packing degree, porosity, mineralogical composition and strength, compaction degree of the deposit, etc. Based on lithological observation at certain area, pyroclastic fall deposits have particle specific weight around 22.5–25.0 kN/m^3, dry density between 8 and 15 kN/m3, cohesion ranges of values is 0–0.1MPa, friction angle varies around 30◦–45◦ and uniaxial compressive strength less than 5 MPa. Porosity values in pyroclastic fall deposits can reach 45–65%, with cohesion values are 0.13–0.17 MPa.

Tuffs

Tuff can be defined as a pyroclastic rock that formed by lithification process of lapilli and ash deposits. Depending on the composition of these lapilli and ash fragments, tuffs can be classified as basic or acid. When tuff is formed by pyroclastic fall deposits, the fragments are compacted and consolidated during post-sedimentary process. This lithology generally present massive structure, with few discontinuities and low fracture degree. Most of tuff deposits are composed by fine-grained debris with fragments of pumice or lithic of volcanic rock.

Grain size of tuffs generally is lapilli (2–64 mm), with physic characteristic such as dry density is less than 10 - 25 kN/m^3, specifically 8 - 18 kN/m^3 for poorly compacted deposits and more than 20 kN/m^3 for well-compacted deposits. The density of rock is influenced by mineral composition, where basaltic tuff has higher values than the acid tuffs. The uniaxial strength for saturated rocks usually decreases 30% than the dry rocks. The cohesion value is less than 1 MPa, with friction angle 30◦–50◦, and Young's modulus ranges from 0.1 to 22 GPa for dry and saturated tuffs.

Ignimbrites

Ignimbrites formed from pyroclastic flows or flows of lapilli and ash fragments. This lithology is considered as welded pyroclastic flow deposits that related to its deposition at temperatures higher than 400°–550°C, with foliation and joint structure that exist due to cooling process. Dry density for these rocks varies between 13 – 20 kN/m^3. The uniaxial strength for this lithology is varies between 15 to 70 MPa and being more than 5 MPa for weathered rocks. Value of cohesion in weathered ignimbrites is usually less than 0.1 MPa, and 2 MPa for fresh rocks. While the friction angle is varying between 27°-38° for weathered and fresh rock.

Agglomerates

Agglomerates are heterogeneous compacted rocks that formed by large heterometric fragments,

rounded for some cases, in a micro-agglomerate coarse-grain matrix. They can be formed by pyroclastic flows or mechanical avalanche such as debris flow or mud flow, which have sandy or clay matrix characterization due to crushing process of the mobilized material. In case the fragments are mainly angular and large size, the agglomerate material is named as volcanic breccia.

Dry density for this rock depends on the composition of the blocks, the compaction degree and porosity of the deposits. When fragments of pumice are predominant, agglomerates have small density which is less than 10 kN/m^3, while for basaltic blocks values is similar with the density of basaltic lava flow. Generally, the density has variation value between 12-28 kN/m^3. Uniaxial compressive strength is related to density and composition. Higher values correspond to basic composition agglomerates, and lower values to felsic or acid composition agglomerates. The usual interval is between 0.5 and 25 MPa, and values more than 15 MPa correspond to basaltic agglomerates. The cohesion and friction angle in this rock are vary from 0.03 - 0.4 MPa, and cohesion value 25◦ - 42◦. For Young's modulus values, are vary between 0.1 and 3 GPa.

METHODS

There are two main methods used in this study, they are by using literature as reference and manual calculation to get final results. Basically, all of parameters provided by the literature study were used as input in gasman equation to calculate Vp/Vs. All calculation done in Ms. Excel, with all results shown as tables and scatter charts.

Literature Study

For this study, we use a geothermal field as reference that named geothermal field X. From this field, we got the information about kinds of lithology units, percentage or fraction of each unit, and its porosity average values.

There are five types of lithology found in geothermal field X, they are lava basaltic, lava andesitic, pyroclastic with minor andesitic, pyroclastic with minor basaltic, and intrusion of microdiorite. In the next discussion, those lithologies are called as unit lithology I, II, III, IV and V (Table 2.1).

Fraction of Lithology

Percentage of existing lithology units that formed geothermal field X are vary between 0.1% to 63.1% (Table 2.2). This information show that one lithology unit is more dominated than the others. Big percentage of this unit lithology will give biggest impact to the physical properties or rocks represent the mix lithology of the field. These value of fraction is used to define assumed mixture of rock.

Table 2.1: List of lithology units from geothermal field X that used as project reference.

Lithology	Unit Lithology
Lava Basaltic	I
Lava Andesitic	II
Pyroclastic With Minor Andesitic	III
Pyroclastic With Minor Basaltic	IV
Intrusion Microdiorite	V

Table 2.2. List of fraction values represent each lithology units from geothermal field X

Unit Lithology	Fraction
I	0.1
II	63.1
III	1.8
IV	22
V	13

Porosity of Lithology

Other information that known from geothermal field X is the porosity ranges value for each lithology units. Overall the porosity of matrix from existing lithology units is around 0.02 - 0.40, as shown at Table 2.3 below.

Table 2.3: Ranges value of matrix porosity for each lithology units from geothermal field X

Lithology Unit	Porosity (%)	Porosity Min	Porosity Max
I	0.2-13	0.02	0.13
II	0.2-13	0.02	0.13
III	0.44-24	0.044	0.24
IV	0.44-24	0.044	0.24
V	0.5-40	0.05	0.4

To get the total porosity ranges value from all of lithology units, total porosity for each unit is calculated by using its fraction, then being sum up as explain at equation (2.1).

$$\emptyset\, mix = \sum_{i=1}^{n} \emptyset n \;.\; fn \qquad (2.1)$$

Calculation result for the total porosity of rocks mixture from all lithology units is classified based on porosity data used. The total porosity of rock mixture based on minimum value from all lithology units is 0.03. For total porosity of rock mixture based on maximum value from all lithology units is 0.19.

Density of Lithology

Based on the known lithology units, literature study has been done to find the range values of density for each of them. The reference of literature that used are (Telford et all, 1990) for unit I and II, (Gonzales et all, 2007) for unit III and IV, (Lama & Vutukuri, 1978) for unit V. For each lithology unit, the

maximum and minimum values of density are listed (Table 2.4).

Table 2.4: Density values for all lithology units from geothermal field X based on literature study of several references.

Lithology Unit	Density (Kg/m^3)	Max (Kg/m^3)	Min (Kg/m^3)
I	2700-3300	2700	3300
II	2400-2800	2400	2800
III	816-1530	816	1530
IV	1734–1938	1734	1938
V	2721-2960	2721	2960

Similar with the porosity, total density ranges value from all of lithology units can be calculated by using multiplication with its fraction, then being sum up. The equation that being used is below.

$$\rho\ mix = \sum_{i=1}^{n} \rho n\ .\ fn \qquad (2.2)$$

The calculation results by using that formula for the total density of rocks mixture from all lithology units is classified based on their density data used. The total density of rock mixture based on minimum value from all lithology units is 2267.0 Kg/m^3. And total porosity of rock mixture based on maximum value from all lithology units is 2608.8 Kg/m^3.

Generate Function

Main objective for this step is to get the value of bulk compressional modulus and shear modulus based on density data. To get the formula that show the correlation between those parameters, some cross plot was created based on the available data of rock forming minerals density, compressional and shear modulus (Schon, 2011) as shown in Table 2.5.

Table 2.5: List of rock forming minerals density (ρ), compressional modulus (k), and shear modulus (μ) values (Schon, 2011).

Minerals	ρ (Kg/m3)	k (Gpa)	μ (Gpa)
Quartz	2560	37	44
Hornblende	3124	87	43
Olivine	3320	130	80
Forsterite	3224	129.6	81
Garnet almandin	4180	176.3	95.2
Garnet zircon	4560	19.8	19.7
Epidote	3400	106.5	61.1
Pyroxene-diopside	3310	111.2	63.7
Pyroxene-augite	3260	94.1	57
Feldspar	2620	37.5	15
Anorthite	2760	84	40
Albite	2630	55	29.5
Orthoclase	2570	46.8	27.3
Nepheline	2620	45.5	31.5
Biotite	3050	51	27
Muscovite	2790	52	32
Kaolinite	1580	1.5	1.4
Clay	2580	20.9	6.85
Chlorite		95.3	11.4
Illite		39.4	11.7
Kaolinite		37.9	14.8
Calcite	2712	73	32
Dolomite	2860	94	46
Siderite	3960	123.7	51
Aragonite	2930	47	38.5
Anhydrite	2970	55	30
Barite	4500	54.9	23.7
Pyrite	5010	143	128
Fluorite	3180	86.4	41.8
Sylvite	1990	17.4	9.4

Density vs Bulk Modulus

To get the value of bulk modulus (k) from density value (ρ) a cross plot is created with density as x-axis and bulk modulus as y-axis. The cross plot can be seen at Appendix 1.

In this case, some heavy minerals are being removed from the cross plot because of their special characteristic (out layer) such as pyrite, barite and garnet zircon. The final cross plot is used to generate the logarithmic function, that will be used for the next step calculation.

$$y = 0.7209e^{0.0015x} \qquad (2.3)$$

Where y refers to compressional bulk modulus (Gpa) and x refers to density (Kg/m^3)

Bulk Modulus vs Shear Modulus

To get the value of shear modulus (μ) from compressional bulk modulus value (k) a cross plot is created with bulk modulus as x-axis and shear modulus as y-axis. The cross plot can be seen at Appendix 2. The final cross plot is used to generate the polynomial (3rd order) function, that will be used for the next step calculation.

$$y = -7E\text{-}06x3 + 0.0036x2 + 0.161x + 9.0141 \qquad (2.4)$$

Where y refers to shear bulk modulus (Gpa) and x refers to compressional bulk modulus (Gpa)

Modulus Calculation

Based on the equation generated at previous step, the value of compressional bulk and shear modulus is

being calculated by using minimum and maximum parameters for each of them.

Bulk Modulus

Refer to equation 2.3 the minimum compressional bulk modulus with the minimum density value of rock mixture is 21.61 Gpa. By using the same equation, with maximum density value of rock mixture, the maximum value of compressional bulk modulus is 36.09 Gpa.

Shear Modulus

Result by referring the equation 2.4 the minimum shear modulus with the minimum compressional bulk value from step (C.1) is 14.10Gpa. By using the same equation, with maximum compressional bulk value of rock got from step (C.1), the maximum value of shear modulus is 19.18 Gpa.

Velocities Calculation

For compressional and shear wave (Vp and Vs) calculation, the Gassmann equation (1.6) and (1.7) are being used. In this case, there are some assumption to be applied for equation, such as water saturation is zero (Sw=0) due to dry condition, value of water bulk modulus is 2.2 (Gpa) based on reference (Schon, 2011), so the bulk compressional modulus (k) fluids equal with (k) water and (k) dry is equal with (k) matrix.

The value of Vp and Vs are calculated both for minimum and maximum parameters. The result shown at table 2.6 as below.

Table 2.6: Calculation results for compressional wave (Vp) and shear wave (Vs) with minimum and maximum parameters.

Velocities	Min (m/s^1)	Max (m/s^1)
Vp	4258	5174
Vs	2515	2887

Comparison of Velocities Calculation

Last value to be calculated is the comparison between velocities value (Vp/Vs). The minimum value come from the comparison of minimum Vp over the minimum value of Vs, which is 1.693. And the maximum value of Vp/Vs was come from the comparison of maximum Vp over the maximum value of Vs, with result number 1.792.

Basically, those results can be used to model the density of a reservoir at a given reservoir condition (e.g., pressure, temperature, porosity, mineral type, and water salinity) and pore fluid saturation such as 100% water saturation. Since the seismic velocities of an isotropic material can be estimated using known rock moduli and density (Kumar, 2006).

RESULTS

Based on the literature study and calculation by using gasman formula, ranges value of petrophysic and geophysics parameters in geothermal field assessment can be seen at table 5.1 as below.

Table 5.1: Summaries of all physics parameters range values from literature and calculation as results from this study.

Parameters	Min. Value	Max. Value
Porosity (%)	3.00	19.13
Density (Kg/m^3)	2267	2609
Bulk Modulus (Gpa)	21.61	36.09
Shear Modulus (Gpa)	14.10	19.18
Compressional Wave (m/s^1)	4528	5174
Shear Wave (m/s^1)	2515	2887
Velocity comparison (Vp/Vs)	1.69	1.79

DISCUSSION

Results of this study can be used to understand general values of petrophysic and geophysics values of lithology in geothermal area. However, more studies should be done to validate and follow up that final result.

The next study should use real data from measurement at geothermal field X, instead of using data from other geothermal fields at literature. Calibration by using geophysics measurement data is necessary to see the deviation between manual calculation result of Vp/Vs and processing results from software application. Finally, the accurate Vp/Vs values can be used to see its sensitivity toward fluid condition in geothermal reservoir.

CONCLUSSION

Primary velocity (Vp) of volcanic rocks in geothermal field X varies from 4528-5174 m/s^2. Secondary velocity (Vs) of that lithology are 2515-2887. The range values of Vp/Vs is relatively small, which is between 1.69-1.79.

REFERENCES

Andrew, A., (2018)," *Densities of common rocks and minerals,*"ThoughtCo, May 6.2018, thoughtco.com/densities-of-common-rocks-and-minerals-1439119.

Gassmann, F., (1951),"*Elastic waves through a packing of spheres.*" Geophysics 16, 673-685.

González, L.I., Hijazo, M., Ferrer and Seisdedos, J. (2007),"*Geomechanical characterization of volcanic materials in Tenerife, Volcanic Rocks,"* Malheiro & Nunes (Eds).

Kumar, D. (2006), "*A Tutorial on Gassmann Fluid Substitution: Formulation, Algorithm and Matlab Code,"* Geohorizons, January 2006 /6.

Lama, R.D. and Vutukuri, V.S. (1978)," *Handbook on Mechanical Properties of Rocks*." 2nd Edition, Trans Tech Publications, Switzerland.

Liu, Z. and Zhao, J. (2015)," *An Experimental Study of Velocity-Saturation Relationships in Volcanic Rocks,"* Petroleum Engineering Journal, 8 page 142-152.

Mavko, G., Mukerji, T., Dvorkin, J., (1998)," *The Rock Physics Handbook."* Cambridge University Press.

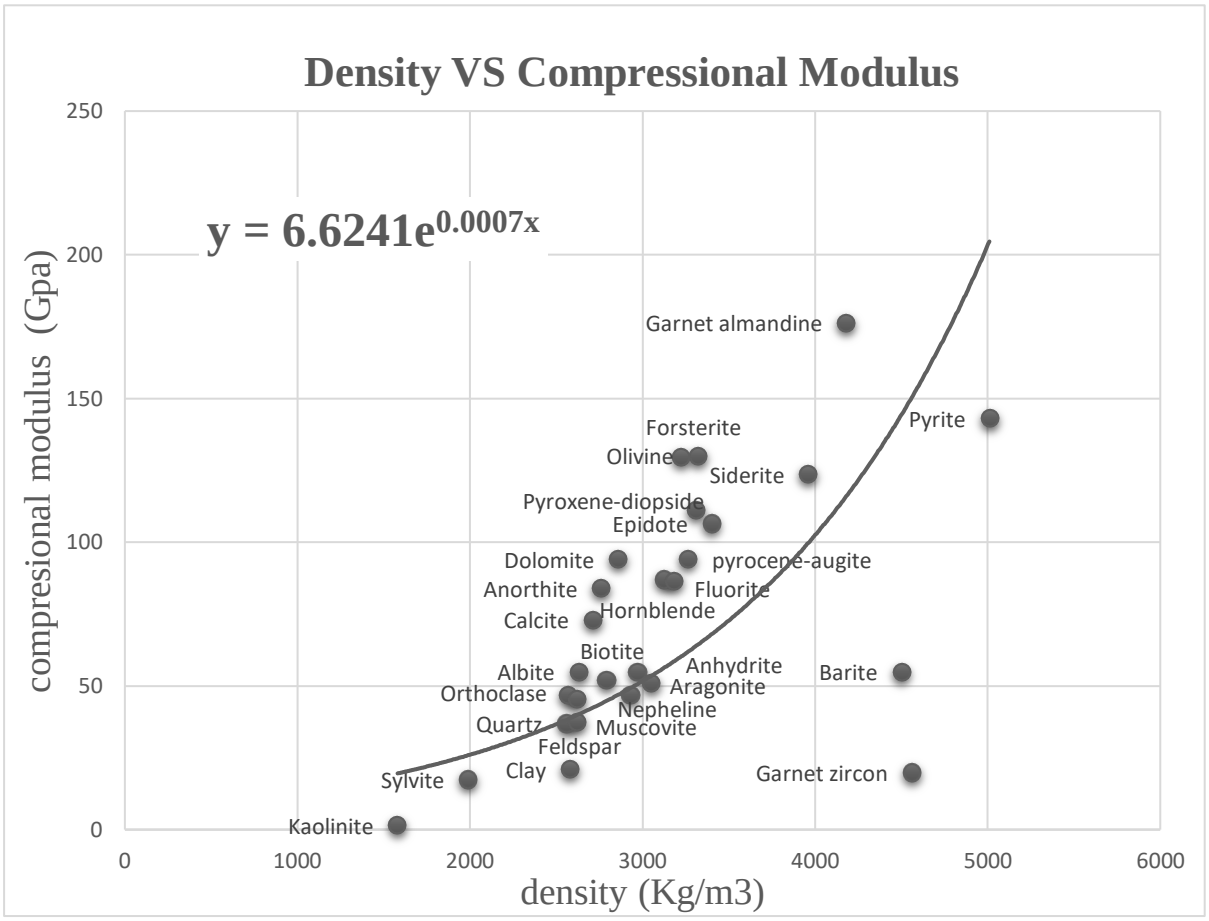
Reynolds, J. M. (1997),"*An introduction to Applied and environmental geophysics,"* Jhon Wiley and Son Ltd. England.

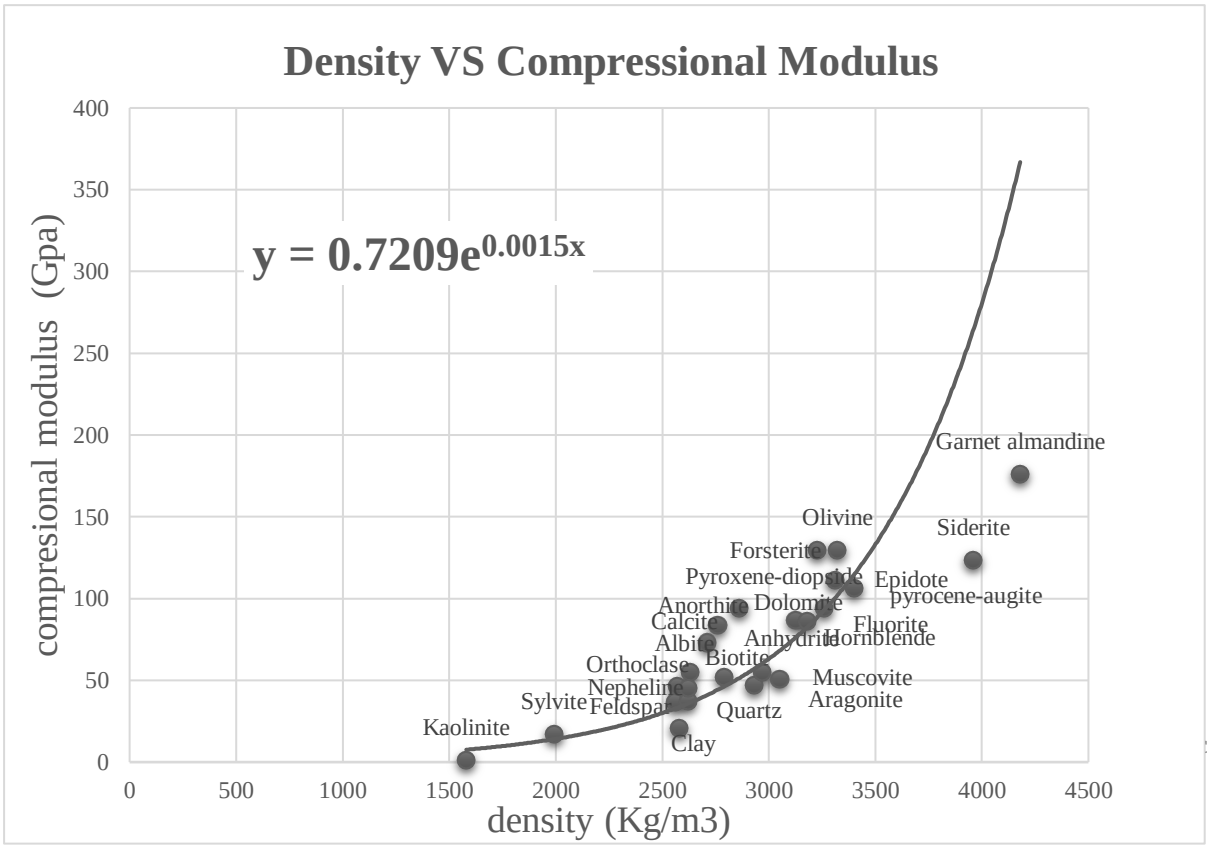
Schön, J.H. (2011)," *Handbook of Petroleum Exploration and Production, 8 Physical Properties of Rocks A Workbook*," Elsevier, Amsterdam. Page 208-210.

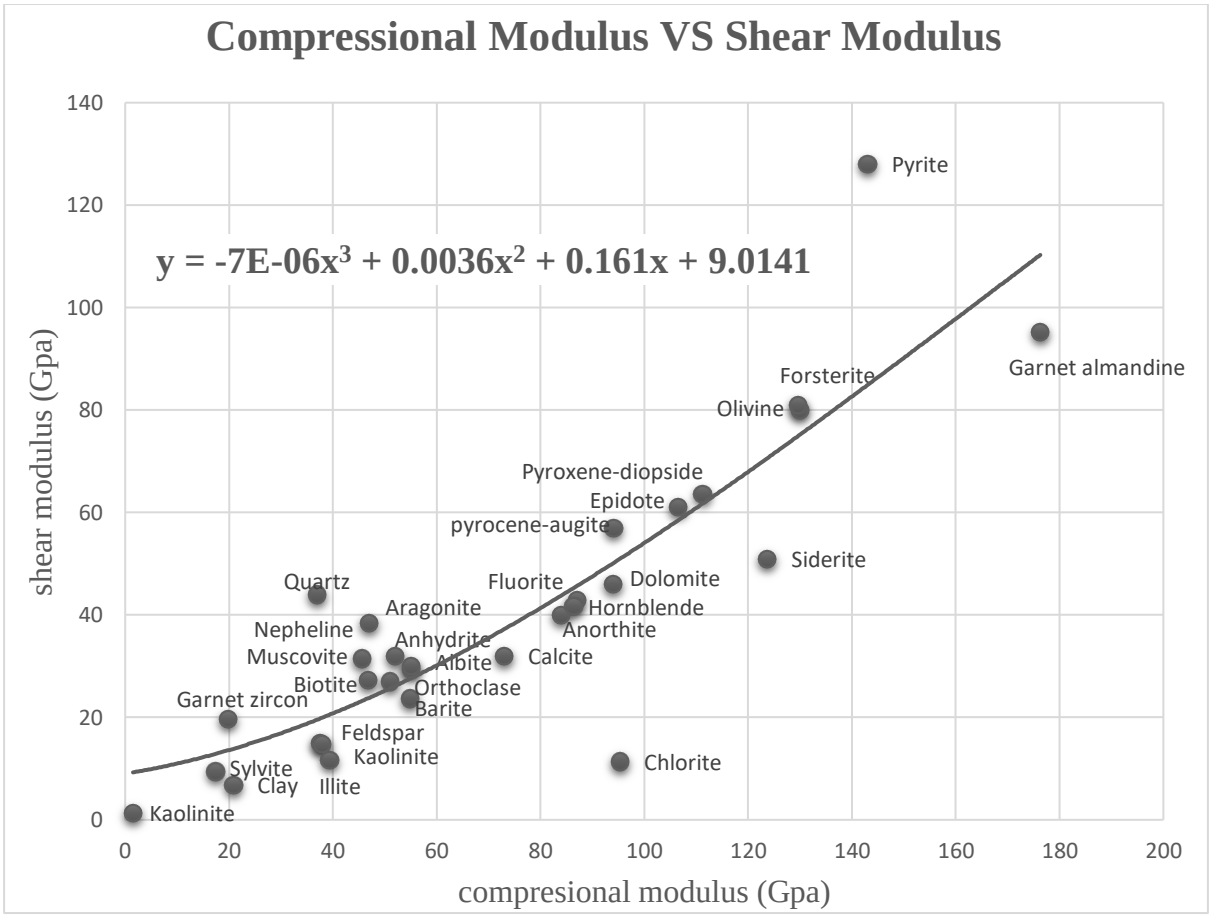
Telford, W.M., Geldart, L.P., Sheriff, R.E. (1990)," *Applied geophysics*," [electronic resource] - 2nd ed.

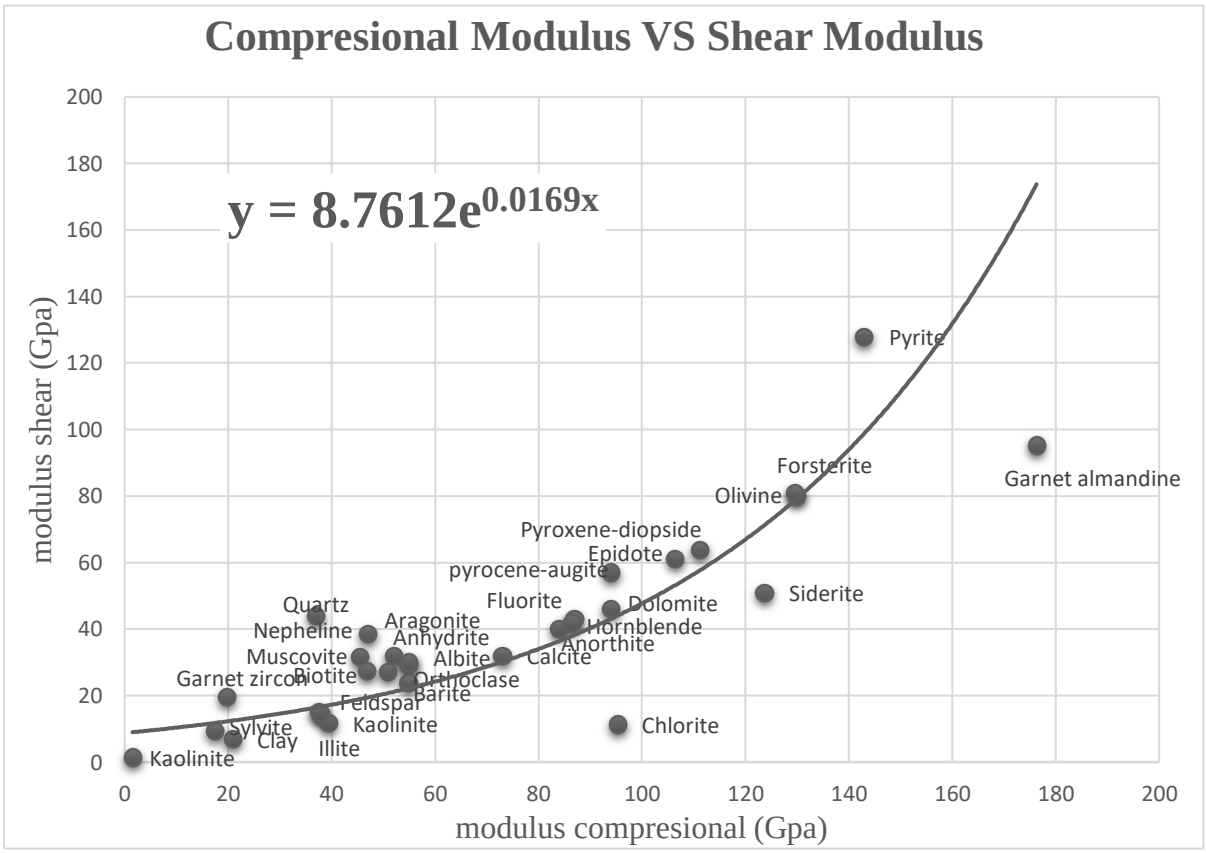
www.petrowiki.org/index.php?title=*Gassmann%27s_equation_for_fluid_substitution*&printable=yes#Overview.

Appendix 1.
Cross plot density vs
compressional bulk modulus before (above) and after (below) moving the heavy minerals with its equation.






Compressional Modulus VS Shear Modulus
y = -7E-06x3 + 0.0036x2 + 0.161x + 9.0141
shear modulus (Gpa)
compresional modulus (Gpa)
Pyrite
Garnet almandine
Forsterite
Olivine
Pyroxene-diopside
Epidote
pyrocene-augite
Siderite
Quartz
Fluorite
Dolomite
Hornblende
Aragonite
Nepheline
Anorthite
Anhydrite
Muscovite
Albite
Calcite
Biotite
Orthoclase
Garnet zircon
Barite
Feldspar
Kaolinite
Sylvite
Chlorite
Clay
Illite
Kaolinite


Compresional Modulus VS Shear Modulus
y = 8.7612e0.0169x
modulus shear (Gpa)
modulus compresional (Gpa)
Pyrite
Garnet almandine
Forsterite
Olivine
Pyroxene-diopside
Epidote
pyrocene-augite
Siderite
Quartz
Fluorite
Dolomite
Hornblende
Aragonite
Nepheline
Anorthite
Anhydrite
Muscovite
Albite
Calcite
Biotite
Orthoclase
Garnet zircon
Barite
Feldspar
Kaolinite
Sylvite
Chlorite
Clay
Illite
Kaolinite

GEOTECHNICAL ASSESSMENT USING ELECTRICAL RESISTIVITY TOMOGRAPHY. CASE STUDY: MARGABAYUR

J T Napitupulu, B Ikhsan, J S Meliala, and R A Anwar

Pertamina Geothermal Energy
Menara Cakrawala 19th Floor, MH Thamrin Street No.9, Jakarta
Email: julius.timothy@pertamina.com

ABSTRACT

Margabayur is a geothermal prospect located in South Sumatra, between Barisan Mountain Range and Southern part of Sumatra Back-Arc Basin. Due to step-over structure, the geothermal system is heavily controlled by pull-apart basin as the main permeable zone. The aforementioned conditions leave Margabayur into having a steep topography and relatively soft soils which is prone to landslide, thus increasing the geohazard potential. *Electrical Resistivity Tomography* and *Self Potential* surveys were conducted to image the lithology beneath proposed location of *Cluster A*, *Cluster B* and *Access Road*. Twelve 300m-lines were performed using more than two configurations on each run, including *Wenner*, *Schlumberger*, and *Dipole-dipole*. Tomographs show that Margabayur is mostly composed by pyroclastic rocks. There are also several portions of altered rocks, which must be treated carefully in infrastructure development due to its unstable nature. Several structures such as *fracturing* and *upflow* could also be interpreted by combining resistivity and self-potential data. Based on this study, we could propose a new location for *cellars* with proper basement and without any sliding planes nearby.

Keywords: Geotechnical assessment, electrical resistivity tomography, Margabayur.

INTRODUCTION

Located in South Sumatra, Margabayur is a prospect located within the Lumut Balai GWA owned by Pertamina Geothermal Energy. The nearest village to Margabayur is the Lawang Agung village, whose residents earn a living from coffee plantations. There are no adequate power grid, thus electricity have been produced from a mini turbine connected to the nearest river. As in general, Margabayur composed mostly by volcanic rocks and has a steep slope, thus a good shallow layer interpretation is needed as the basis for infrastructure development. *Electrical Resistivity Tomography* and *Self Potential* as geophysical methods that read the resistivity value of subsurface rocks was used to interpret the type and layering of soils beneath the proposed location of Clusters and Access Road in Margabayur. The results will be used for geotechnical feasibility assessment based on 4 factors: slope, environment, geology, and hydrogeology conditions (Pioquinto and Caranto, 2005).

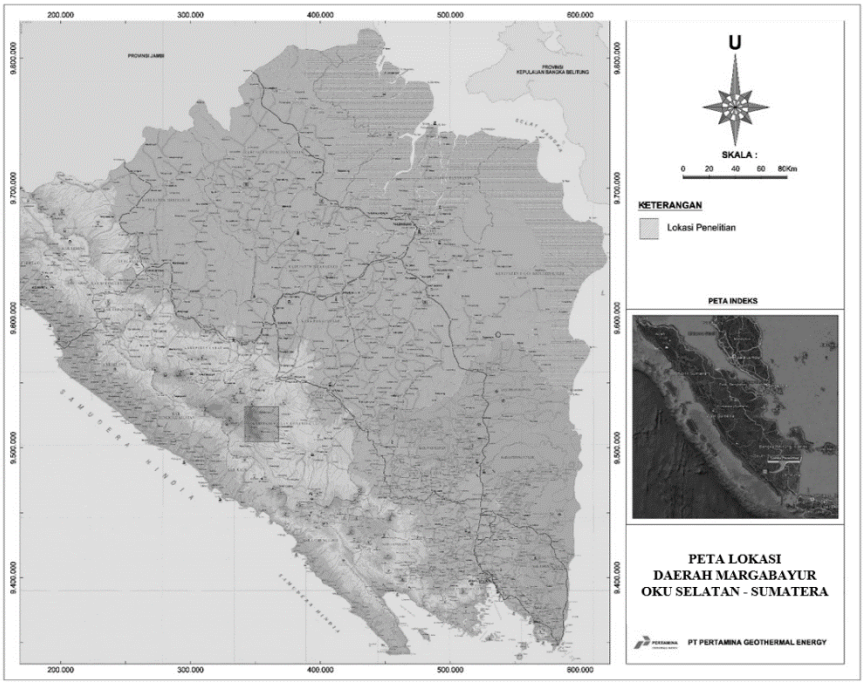


Figure 1. Location of Margabayur

GEOLOGY

Physiographically, Margabayur lies in the conjunction between Bukit Barisan and the South Sumatran Basin which is a part of Sumatran Back Arc Basin (Darman and Sidi, 2000).

Geomorphology

Margabayur's morphology is grouped into volcanic hills, volcanic cones, and alluvium plains. Morphology of volcanic hills with weak-tempered terrain occupy most of the study area. The volcanic cone is presented as G.Ringgit (+2128m), G.Pangeran (+1174m), G.Gajah (+1472m), G.Cabut (+1851m) and G.Besar (+1920m) (Sulistjo et al., 2018). The alluvium plain is located along Luas River's basin.

Stratigraphy

Stratigraphy of research area can be divided into several units based on its characteristics. The stratigraphy of Margabayur (LKFT UGM, 2011) includes:

- G. Kubupangkul Andesitic Breccia. This unit consists of andesitic breccia intercalated with siltstone and andesitic lava. This unit is distributed in the northeastern part of study area. It was produced by volcanic activities of G. Kubupangkul.
- G. Cabut Andesite. It consists of andesitic lava and andesitic breccia. The outcrop is found alongside the rivers in Desa Lawang Agung such as Air Sakiri, Air Keninngan, Air Bayur, and Air Lahan. This unit is a product of volcanic activity from G. Cabut which produces andesitic breccia by pyroclastic deposit and andesitic lava by non-explosive eruption

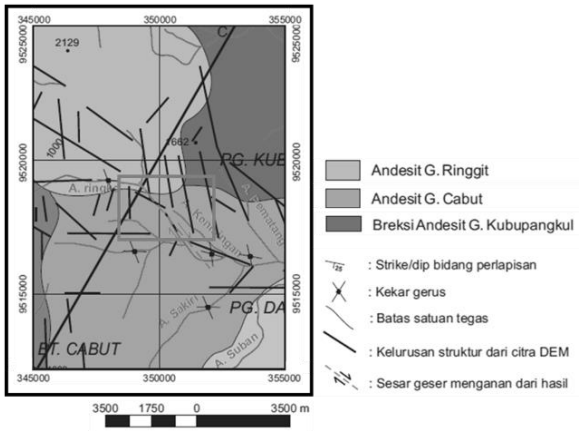


Figure 2. Geological Unit of Margabayur

- G. Ringgit Andesite Unit is the youngest unit in the study area, which was deposited conformably above G. Besar Andesite Unit from Quartenery. It consistes of andesitic lava, tuff, tuff lapili, tuff breccia, and dominated by andesitic lava. The outcrop of andesitic lava and tuff breccia are partially altered, and high-moderately weathered

Geological Structure

Most of the faults have northwest–southeast (NW-SE) trend controlled by the Sumatran Fault, but there are also several other structures with southwest-northeast (SW-NE) trend, defined as the antithetics. Step-over phenomenon between Musi Segment and Ketahun Segment forms a pull-apart structures which is interpreted as the permeable zones where the geothermal hot water circulates onto the surface, forming a geothermal manifestasion along Air Lahan.

METHODS

The *geoelectrical* method is based on measuring the medium's resistivity value by injecting electric current to the medium. The resistivity of a material indicates the material's ability to conduct an electric current (Johnson, 2003).

Resistance (Ohm) is the result of *geoelectric* measurement, which is based on Ohm's Law formulated by:

$$R = \frac{V}{I} \quad (1)$$

where V is the potential difference (volts) and I is the injected current. If R is the resistance of a conductive medium of length L and the area of conductivity A, then its resistivity value is:

$$\rho = \frac{R.A}{L} \quad (2)$$

Since the earth is not homogeneous, the resistivity value obtained represents all the layers which the potential line passes through, not the resistivty value of a specific layer, known as apparent resistivity. Apparent resistivity defined as:

$$\rho_a = k\frac{V}{I} \quad (3)$$

Where k is a geometry factor that differs between every configuration of electrode.

$$k = \frac{2\pi}{\left(\frac{1}{C_1P_1} - \frac{1}{C_2P_1}\right) - \left(\frac{1}{C_1P_2} - \frac{1}{C_2P_2}\right)} \quad (4)$$

DATA AND PROCESSING

The *ERT* and *SP* survey were done in December 2017, conducting twelve 300-m-length survey lines. Four lines located in both proposed location of Cluster A and B, and 4 lines conducted in the proposed Access Road. Thirty electrodes were used on each line, with ten meters space between electrodes.

Wenner, *Schlumberger*, and *Dipole-dipole* configurations were used on each survey line. The raw data obtained from the instrument is further

processed using RES2DINV to obtain resistivity vertical sections.

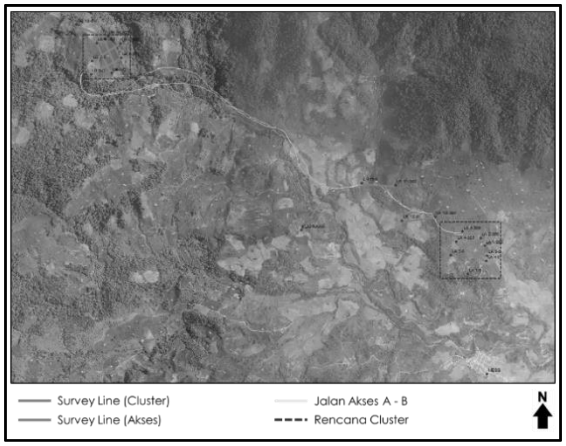


Figure 3. ERT Survey Line in Margabayur

RESULTS AND DISCUSSION

Cross-section Interpretation

The inversion method were used to convert the apparent resistivity value to true resistivity. The inversion result were used to depict the subsurface condition based on the material's resistivity value. Self Potential values were also used to determine the layer's relative saturation. Three survey lines were chosen as the representative subsurface conditions of each proposed locations.

Cluster A

Cross section of Line 1 could be seen in Figure 4. Line 1 extends from Soutwest to Northeast with length of 300 meters. Field survey suggests that top layer of this line is a product of pyroclastic rocks, which match with the inversion results. Tomograph shows that shallow layer consists of dry pyroclastic and saturated layer. Below the pyroclastic we could find a saturated layer, which is either a water-carrier layer or water-saturated layer, followed by pyroclastic layer beneath it. Low resistivity value in this section is interpreted as an alteration product. Based on the SP data, we could interpret an upflow in the middle of the section.

SP survey along Line 1 (SW-NE) shows an erratic potential value in the upper layer. The center part of upper layer was dominated by wet area, while in the southwest and northeast part of the Line tend to be dry. The northeast end of the Line is shown as a wet area, which has been visually confirmed as a swamp. The middle and bottom layers of this Line show similar characteristics with the top layer.

Cluster B

Cross section of Line 8 is shown in Figure 5. On-site observations on this SW-NE line suggests that the top layer is composed by products of pyroclastic rocks. Based on the results of ERT inversion, the top layer of this line is interpretated as dry pyroclastic and saturated layer. Layers beneath the top layer are dominated by pyroclastic rocks.

SP survey along Line 8 from southwest to northeast show erratic values from top to bottom layers. These positive erratic values indicate a water-saturated layer, which was confirmed by field observation.

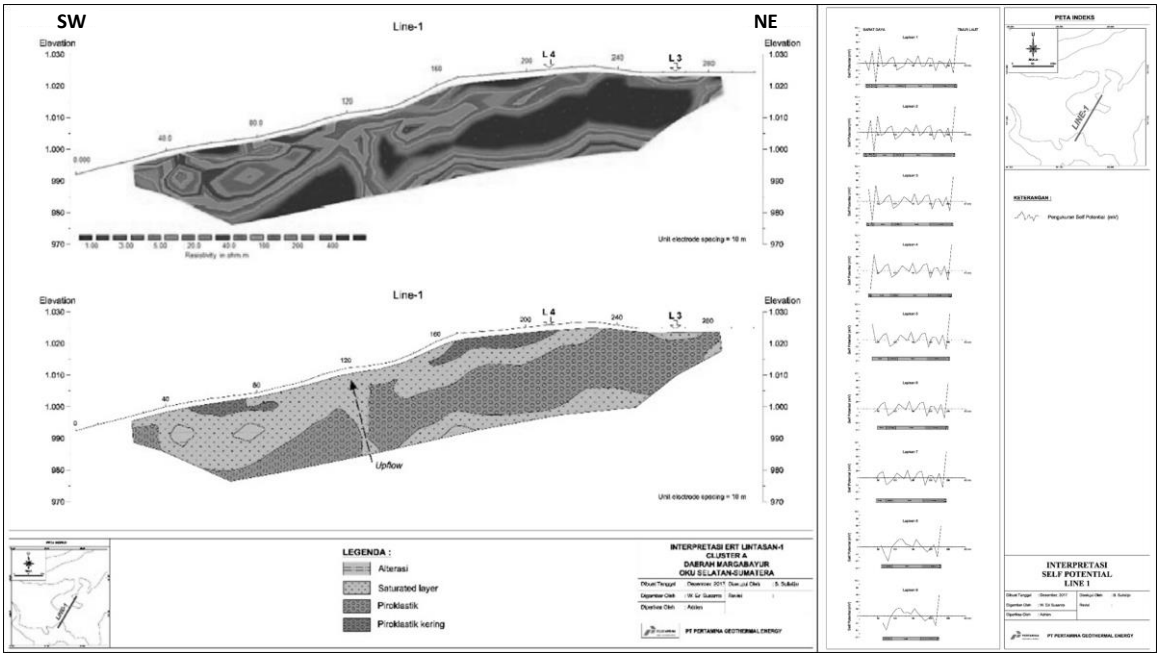


Figure 4. Resistivity Tomograph and SP in Line 1, Cluster A.

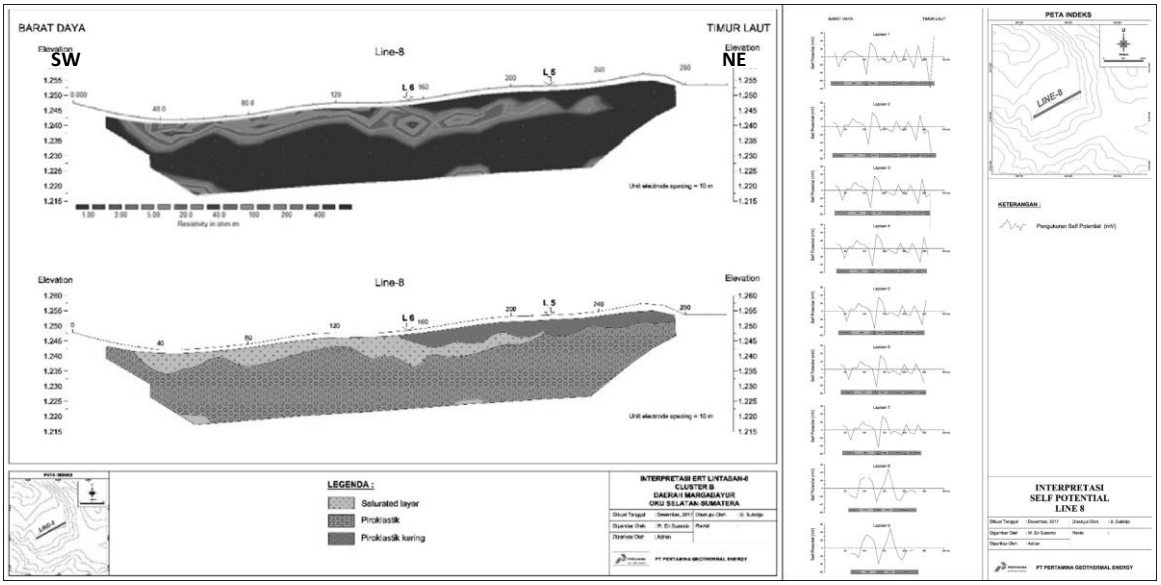


Figure 5. Resistivity Tomograph and SP in Line 8, Cluster B

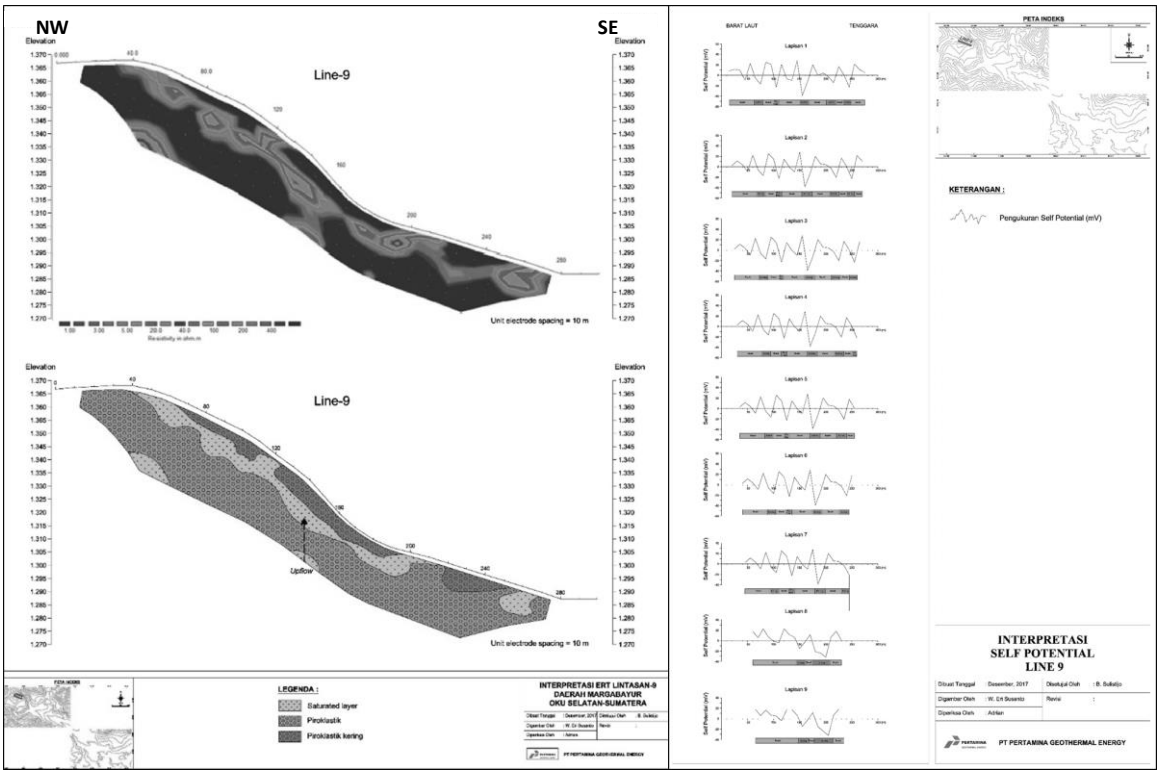


Figure 6. Resistivity Tomograph and SP in Line 9, Access Road

Access Road

Line 9 is located to the northwest of Cluster B, extending from northwest to southeast with a length of 300 meters as can be seen in Figure 6. Visual observation along the line show products of pyroclastic rock as the top layer. From SP we could interpret dry pyroclastics as the top layer, followed by saturated layer. The layers below the saturated layer are dominated by pyroclastic rocks. Based on the ERT inversion, we could interpret an upflow in the center part of the line.

SP survey along Line 9 (NW-SE) shows erratic values for the upper and middle layers. Positive erratic values indicate a wet area which was confirmed by field survey. The deeper layers in northwestern part of the line is dominated by wetlands.

Landslide Potential

Based on the tomograph, we could infer that Access Road (*Figure* 7) and Cluster A (*Figure 8*) has the potential for landslide disaster, whereas Cluster B has a more stable subsurface condition.

The lines located in Cluster A and Access Road shows a problematic condition. This condition is

characterized by the presence of massive rocks with easily detached grains (the pyroclastic rock layers), which furthermore followed by water-saturated layer beneath it that might act as the sliding plane when it is fully saturated.

Under these condition, the proposed location of Access Road has the greatest risk of landslide, not only because it has a potential sliding plane but also a steep slope. The presence of upflow also increases the risk of landslide due to the possibility of water to access the saturated layers. When the saturated layer becomes fully saturated, the pyroclastic rocks above it could fall as a mass flow (*Figure 7*).

On the other hand, geohazard potential in Cluster A is caused by the presence of altered rocks in the water-saturated layer. The alteration which is usually found in similar setting is an argilic type which is dominated by clay. The clay tends to swell and form a slippery surface, thus it became a sliding plane for other rocks positioned above it (*Figure 7*).

Based on these observations, we could prevent and mitigate earlier. We could determine another possible and potential location for Access Road or cellar as a prevention, or we could use disaster mitigation plan such as piling and gabion installation.

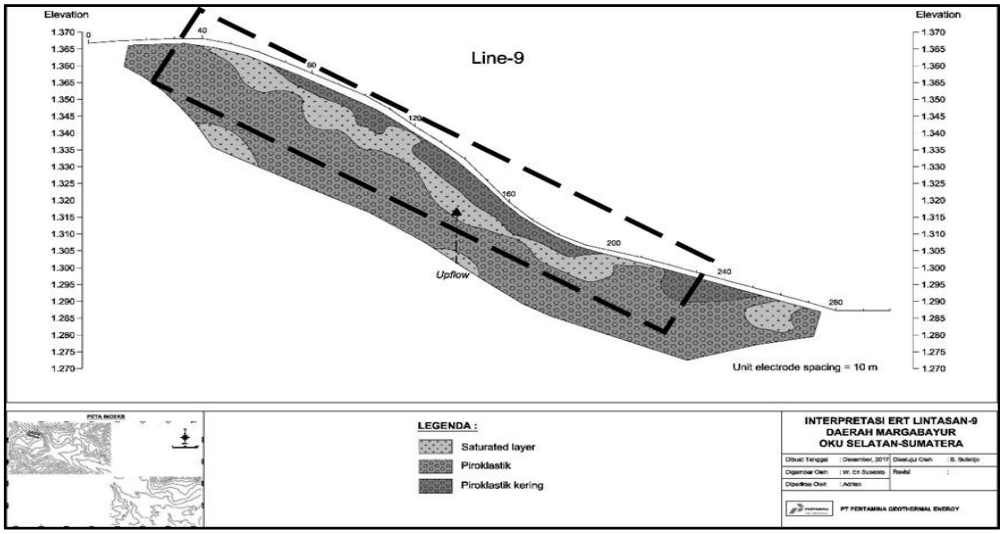


Figure 7. Geohazard Potential in Access Road

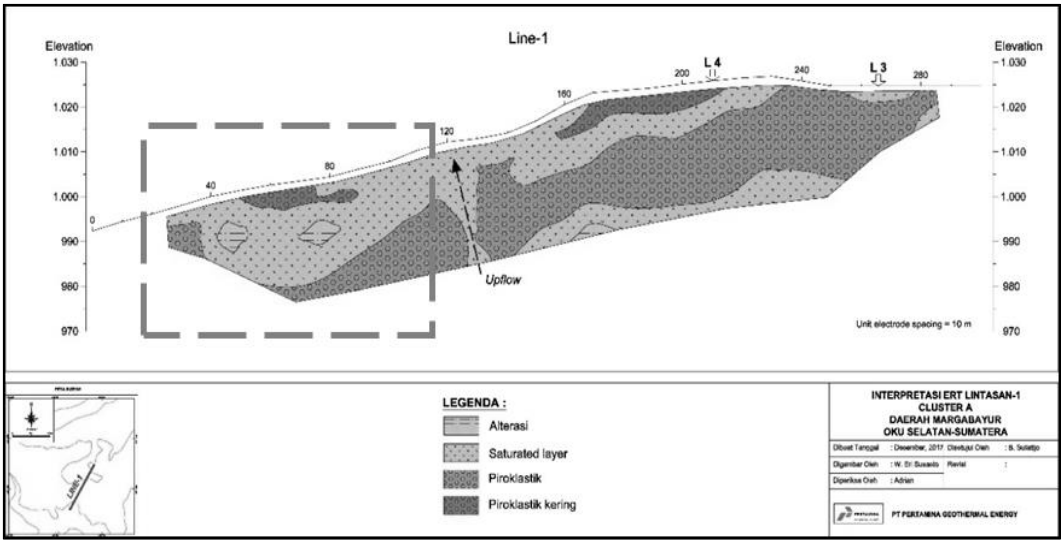


Figure 8. Geohazard Potential in Cluster A

CONCLUSION

1. The results of ERT interpretation shows that the subsurface of proposed location of *Cluster A* and *Access Road* consists of pyroclastic rocks, dry pyroclastics, saturated layer, and altered rocks. On the other hand, *Cluster B* consists of pyroclastic rocks, dry pyroclastics, and saturated layer. The integration between resistivity tomograph and self potential suggest a possibility of upflow in several locations.
2. *Self Potential* surveys were able to show the wet and dry part in each layer qualitatively
3. Proposed location of *Cluster A* and *Access Road* are at risk of landslide disaster due to the possibility of forming a sliding plane caused by water-saturated layers or altered rocks.

REFERENCES

Darman, H. and Sidi, F.H. (2000). "An Outline of The Geology of Indonesia". Ikatan Ahli Geologi Indonesia.

Johnson, W.J. (2003). "Application of The Electrical Resistivity Methode for Detection of Underground Mine Workings." Geophysical Technologies for Detecting Underground Coal Mine Voids. KY: Lexington

LKFT Universitas Gajah Mada. (2011). "Laporan Pengambilan Sampel dan Data Geologi Lapangan Survey Geolodi Daerah Prospek Panasbumi Margabayur Kabupaten Ogan Komering Ulu Selatan Propinsi Sumatra Selatan". Yogyakarta

Pioqinto, W.P.C., and J. A. Caranto. (2005), "Mitigating the Impact of Landslide Hazard in PNOC-EDC Geothermal Field". *World Geothermal Congress.* Antalya: Turkey.

Sulistijo, B., Adriyanto D.K and Danu Baranti. 2018. "Laporan Studi *Electrical Resistivity Tomography* Rencana Cluster A, B, dan Jalan Akses Margabayur". PT Pertamina Geothermal Energy.

PERMEABILITY DISTRIBUTION IN CALDERA SYSTEM OF THE LUMUT BALAI GEOTHERMAL FIELD

Sapto Trianggo Nurseto, R.A. Julia Satriani, and Mochamad Husni Thamrin

PT. Pertamina Geothermal Energy
Skyline Building 19th floor, Jl. MH. Thamrin No.9, Jakarta 10340
Email: sapto.trianggo@pertamina.com; mk.julia.alibazah@pertamina.com

ABSTRACT

Lumut Balai geothermal field is one of the example of geothermal field that occurs in caldera system, which is then referred to as Old Lumut Caldera. Located in Penindaian Village, Muara Enim Regency, South Sumatra Province, Lumut Balai Geothermal Field is one of the fields operated by Pertamina Geothermal Energy. Currently there are twenty nine existing wells which are evenly distributed within the Old Lumut Caldera and outside of the caldera's rim. Data from these wells reflect the permeability distribution in Lumut Balai Geothermal Field.

Permeability is a vital aspect in geothermal system. Generally, permeability in geothermal field is related to geological structures such as major faults and fractured zones. Based on data obtained during exploration, permeable zones in Lumut Balai Geothermal Field, aside from being controlled by structural geology are also controlled by primary formation host and lithology contact. The permeability distribution model in Lumut Balai Geothermal Field shows that the main permeability could be found within the Old Lumut Caldera. Wells that are drilled within the caldera shows total loss circulation zones from around 600 masl to around -1000 masl (total depth of the deepest well in the caldera). Whereas in wells drilled outside of the caldera found no significant total loss circulation zones.

Methods used in acquiring these data are surface data, geophysical measurements, borehole image logging, well testing, and drilling parameters which are then superimposed to deduce the permeability zones in each well. Borehole image could infer the fracture zones in a well and determining its trend and geometry, well testing especially the PLT and PTS measurement could provide information regarding feed zones in a well's fracture zone. Correlation between the wells results in a permeability distribution. After being inputted into 3D modelling software, a comprehensive permeability distribution model could be acquired.

Permeability distribution model in a geothermal area is essential to comprehend because it is an important information in well targeting. Permeability information will assist in planning well trajectory and predicting total loss circulation zones in planned wells as the targeted productive zones.

Keywords: Geothermal, Lumut Balai, Permeability Distribution, 3D Modelling.

INTRODUCTION

Permeability

Permeability is one of the main components of a geothermal system. In volcanic settings, which are one of the most common geological setting in geothermal, permeability is mostly controlled by geological structures such as faults and fracture zones. It could also be controlled by lithological contact and the formation host's characteristics.

Understanding the permeability distribution of a geothermal field is an essential key to the exploration's success. By comprehending the permeability distribution, well targeting process could be more efficient by planning well trajectory and predicting total loss circulation zones more accurately.

Geoscience of Lumut Balai

Lumut Balai is located approximately 292 km southwest of Palembang, around 8 hours of driving from the Palembang airport. Geoscientific research in Lumut Balai has been ongoing since 1993, which includes geological research, geochemical research, and geophysical research. The first exploration well was drilled in 2008 until currently there are 20 production wells, and 9 injection wells in Lumut Balai geothermal field. In 2018 Pertamina Geothermal Energy is planning to carry out CoD with 2x55 MWe capacity.

Surface Geology

Situated in Old Lumut Caldera, which is approximately ±9 km in diameter, Lumut Balai is an

example of geothermal field that occurs within a caldera.

Caldera is highly related to volcanic activity. Volcanic occurences in Sumatera is closely related to Sumatera Fault System (SFS)'s activity. This could be proven by the distribution of Neogen until Quarternary around Sumatra Fault and expanding from southeast to northwest of Sumatera. Old Lumut Caldera is located around 60 km east of the Komering Segment, eastern side of Sumatra fault.

Volcanic eruption center in Lumut Balai (Pandan Hill – Penindaian Hill – Ringgit Hill – Lumut Hill) forms a north-south lineage pattern. This north-south trend is thought to be the product of Pre-Tertiary N-S faults reactivation by the Quarternary-Recent stress system (Sieh and Natawidjaja, 2000).

Geological Structure

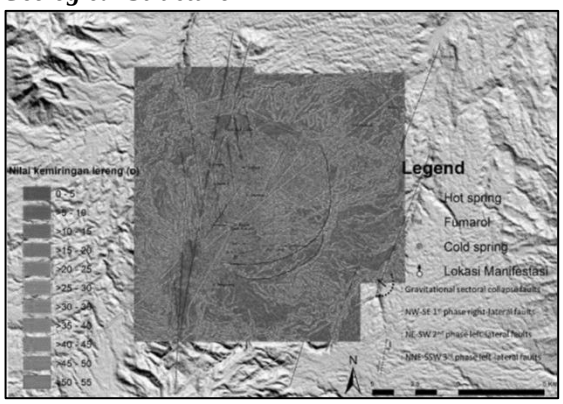


Figure 1: Slope analysis of Lumut Balai topography.

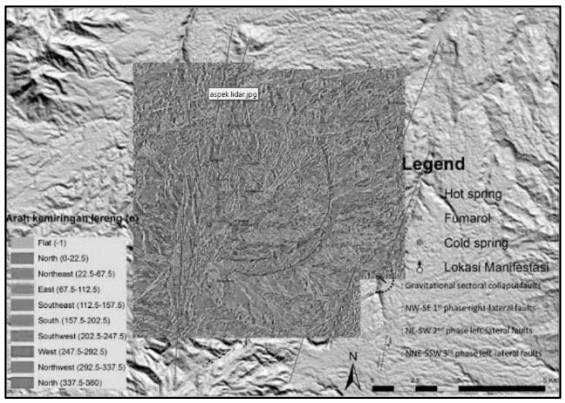


Figure 2: Aspect anlysis of Lumut Balai topography. A circular caldera rim could be identified, it is inferred as Old Lumut Caldera

LiDAR and IFSAR image analysis inferred that the geological structures in Lumut Balai shows an old volcanic complex that has collapsed, forming a giant caldera, which is then referred to as Old Lumut Caldera. This volcanic complex was built by the series of eruption center which are Bt. Pandan, Bt. Ringgit, Bt. Lumut, dan Bt. Balai. On the margin of the caldera's rim, a new eruption center could be seen, on the southeastern flank of the caldera is Bt.Lumut and on the northwestern side is Bt.Balai. All across the western flank of the Old Lumut Caldera, a relatively N-S trending fault could be found, this fault is also considered as the western side of Lumut Balai geothermal prospect's boundary. The two lineament pattern in the center of Old Lumut Caldera could be interpreted as NE-SW and NW-SE faults. Some major faults are associated with the occurrence of geothermal manifestations such as Air Ringkih Fault, Gemuha Besar Fault, Patahan Fault, Udangan Fault, sesar Ogan Kanan Fault, and Tanjung Tiga Fault. Meanwhile on the eastern side, the geothermal prospect boundary is limited by Old Lumut Caldera rim. These geological structures could be further explained as follows:

a. Old Lumut Caldera (KLT)

This caldera's occurrence is seen through the scarp morphologies on the east, north, and southern part with the southwest section buried by the Bt. Lumut Muda eruption products and was cut through by Gemuha Besar Fault.

b. Gemuha Besar Fault (SGB)

This fault has N-S orientation and cross cuts two eruption centre's which are Bt. Asahan and Bt. Lumut. By observing the morphology of steep scarp, valleys, the occurrence of manifestation and field measurement data N300ºE/85º on the northern part of the field, it is inferred that this fault is dipping to the west. The occurrence of geothermal manifestation to the west of the fault concludes that Gemuha Besar Fault is a normal dip-slip fault with its western block as the hanging wall. Minor faults obvious lineaments trending NW-SE and could also be seen near this fault.

c. Air Ringkih Fault (SAR)

This fault is proven by morphology data in the form of steep scarps facing NW with NE-SW trend, also by the occurrence of Air Ringkih and Bunbun geothermal manifestation. Air Ringkih Fault is a normal fault with its NW block as its hanging wall. Several offsets could be found through the Air Ringkih Fault line as it was also crossed by Patahan Fault trending NE-SW.

d. Udangan Fault (SUD)

This fault is inferred by scarp lineament facing west trending NE-SW, and geothermal manifestation occurrences on the eastern side of the scarps. Based on this data, it could be concluded that Udangan Fault is also a normal with its western block as its hanging wall.

e. Fault Patahan (SPT)
Patahan Fault trends NW-SE and crosses over Air Ringkih Fault. Several geothermal manifestations could be found on the surface of Patahan Fault's fault line.
f. Ogan Kanan Fault (SOK)
Ogan Kanan Fault trending NE-SW is proven by scarp lineaments and Ogan Kanan 1 and Ogan Kanan 2 geothermal manifestations. It is concurred that this fault is a normal fault with its NW block as its hanging wall.
f. Tanjung Tiga Fault (STT)
Tanjung Tiga Fault is located outside of Old Lumut Caldera, on the southern part of Lumut Balai geothermal prospect. Its occurrence is marked by NW-SE lineaments and Tanjung Tiga geothermal manifestation with its large dimension.

Based on the trend and type, the faults in Lumut Balai could be divided into two main groups, which are: faults that are not related to the regional stress pattern, faults that are related to the regional stress. The first group is more closely related to the Lumut Balai Caldera's formation and radial faults found on the Old Lumut Volcano's body. The second group is related to the regional stress pattern with faults trending N-S, NE-SW, NW-SE, and W-E.

According to the regional tectonic pattern, faults trending N-S and NE-SW are first faults to develop and is thought to be the main fault lane in Lumut Balai. This fault lane is at the centre of Lumut Balai's Quaternary volcanic activity. These faults have likely been reactivated by younger regional stress, proven by the geothermal manifestation occuring along the faults near Bt. Lumut - Panindayan and Bt. Bunbun-Sepanas Hilir. Fault systems trending NW-SE are the latest to develop, and reactivated by the Sumatran Fault such as Patahan Fault and sesar Tanjung Tiga Fault.

The main fault system trending N-S and NE-SW that crosses over Lumut Balai Caldera rim are the main manifestation control at the surface that are spread concurringly as the faults' trend. In other words, N-S and NE-SW fault controls the permeability of the prospect area, so that the fluids could flow to the surface and forms geothermal manifestations, such as Gemuha Besar Fault (U-S) and Air Ringkih Fault (TL-BD).

Stratigraphy
Based on geological data from PGE (2018), Lumut Balai is at least divided into fourteen rock units. These fourteen units are determined by surface mapping obtained from around Lumut Balai geothermal field, outside of and within the Old Lumut Caldera, with elevation starting from 870 masl to 1880 masl. In addition, morphological characteristics are also obtained from LiDAR images enabling a more accurate rock unit determination.

All of the rock samples obtained from the field are then petrographically analysed, which is then known that the Old Lumut Caldera is dominated by extrusive rocks such as andesite, pyroxene andesite, andesite lava, breccia, tuff, altered tuff, and conglomerate. From surface mapping, there are no intrusive rocks found. Most of the samples found on the surface have been hydrothermally altered and intensively weathered.

From the analyses result and surface data plotting, the lithological distribution pattern could be concluded, which is heavily influenced by the succesion of eruption center. It is then inferred that Lumut Balai has undergone at least two destructive phases (PGE, 2018), this is evident in the lithological distribution related with the morphology and elevation.

Based on the geological data, it is deduced that the oldest lithology in Lumut Balai is the Tertiary Basement, consists of metasediment in the form of meta-shale and meta-sandstone, which could be found in the northeastern part of Lumut Balai around Bunbun Hill. The youngest lithology is the quarternary Pyroxene Andesite which is a part of Young Lumut formation.

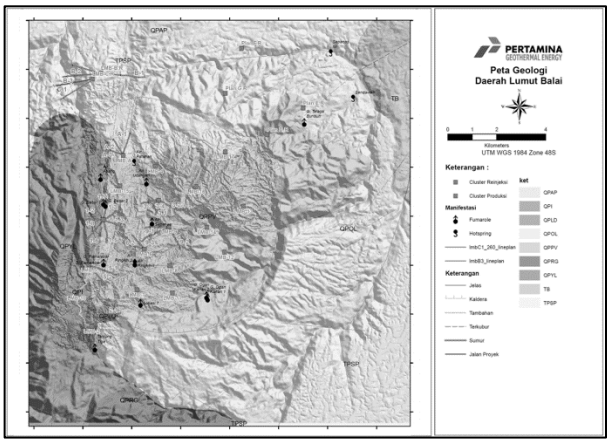


Figure 3: Lumut Balai Geological Map

METHOD

Surface Mapping

The surface data obtained by observing and measuring outcrops in the field is one of the main data used for this research. Outcrops from Cluster

LMB-2, LMB-6, LMB-8, LMB-9, LMB-10, WPS 6 and WPS 7, Sepanas River, Air Patahan River, and outcrops all along the side of the cluster's road has been observed, measured, and analyzed for this paper's purposes.

The data obtained from the observation are lithology, lithological contacts, alteration mineral assemblage, and strike-dip measurements of joints and slicken line. Hand specimens and clay samples were also taken from the outcrop to be further analyzed in the laboratory.

Slicken line and joint strike-dip measurements are then plotted to the geological map to determine the structural geology trend in the area.

Geophysical Data

Geophysical measurements, such as magnetotelluric and gravity measurement has been carried out before Lumut Balai's drilling campain begun. Magnetotelluric measurement is utilized to diferentiate the subsurface resistive and conductive zones. By setting the resistive and conductive zones apart, permeable zones could be inferred by identifying openings in the conductive layers or often interpreted as the clay cap. Openings in the clay cap could indicate the presence of major faults.

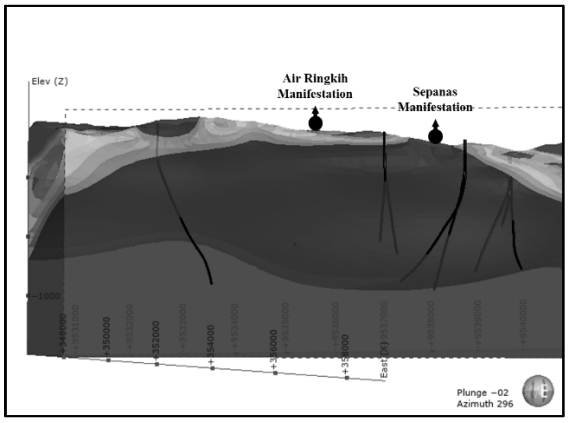


Figure 4: An example of of Lumut Balai MT section. Openings in conductive layers shown in lighter gray indicates the presence of faults or permeable zones, resulting in surface manifestations.

Gravity measurements could give an overview of the density distribution of the subsurface lithologies. The more solid, heavy and, compact the rocks, the denser it is. Less dense areas could mean porous or permeable litologies or the presence of fracture or fault zones.

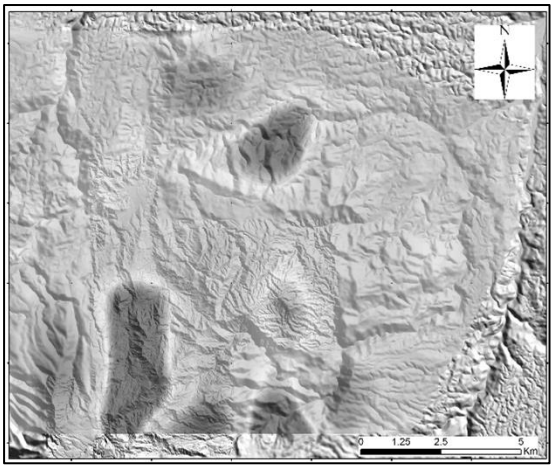


Figure 5: Lumut Balai density map. Areas in red (appeared darker in this figure) are denser than the green and blue areas (appeared lighter in this figure).

During Lumut Balai drilling campaign, borehole image logging was carried out in some of Lumut Balai's wells to determine the subsurface fracture zones and distinguish its major trends.

By picking out the conductive fractures seen through the borehole image log, a rosette diagram which represents the distribution of the fractures' strike and dip could be constructed. Furthermore, by correlating the conductive fracture zones from each wells, a 3D fracture zone model could be constructed.

Drilling Parameter

Certain parameters shown while drilling could also assist in determining permeable zones in the well, such as drill kick, and partial or total loss circulation. In this research, the total loss circulation zones – which often occurs in the reservoir zones, starting from the top of the reservoir to the well's total depth (TD) – are correlated to determine the distribution, and the zone's thickness in each well.

Reservoir Data

Reservoir measurements method used to determine the permeability distribution covers well completion test and PTS logging after the well has reached its total depth. These measurements could differentiate feed zones in a well which indicates good permeability zones. These zones are usually located in the total loss circulation zones.

3D Permeability Modelling

The total loss corculation zone is then also displayed in a 3D modelling software to visualize the zone's geometry in a 3D block model in order to further understand the permeability distribution in Lumut Balai. This is then further refined by geophysical and lithological data and compiled into a 3D Permeability Model.

RESULT

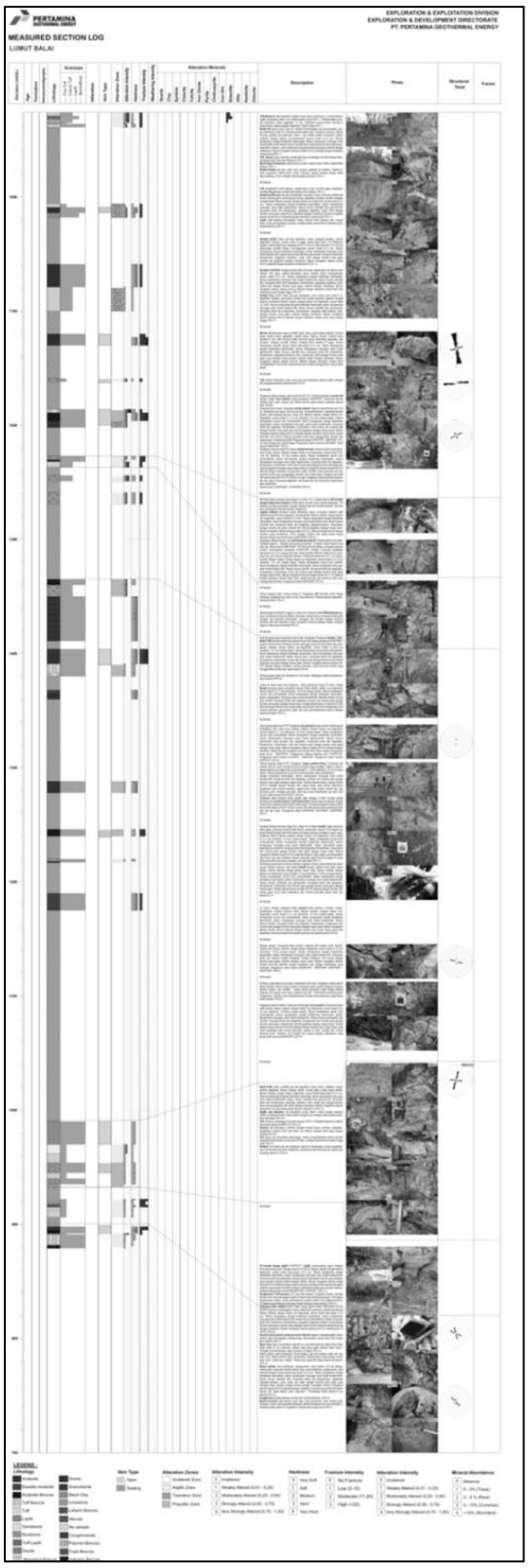


Figure 6: Measured section of Lumut Balai surface mapping. The log gives information regarding the lithology, alteration, and structures found on Lumut Balai's surface, and are correlable to a few of Lumut Balai's wells.

Strike dip measurements of joints and slicken sides during surface mapping results in an updated Lumut Balai fault database (Table 1) and confirms inferred subsurface fault zones and connecting them with the faults found on the surface.

Table 1: Lumut Balai Fault Assesment

Lumut Balai Fault Assessment													
	Geology					Geochemistry		Geophysics		Reservoir		Assessment	
No.	Fault	Field Measurement	Remote sensing Image	Lithological Offset	Drilling Evident	Borehole Image	Tracer Test	Manifestation	MEQ	Gravity	PLT Feedzone	Impact for Reservoir	Level of confidence	Impact for Geothermal System
1	Air Ringkih	Azimuth, Dip ,no measurement found, scarp measureme	Distinct	Not Found	TLC/drilling break	LMB-5	-	Air Ringkih and Bunbun Complex	-	Confirm	Yes	conduit / barrier / compartemen	High	High
2	Air Udangan	Surface Geological Mapping Data (PGE-UGM)	Distinct	Yes	TLC confirm on LMB-A	-	-	Air Patahan and Air Udangan	-	Confirm	Yes	-	High	High
3	Old Lumut Caldera	-	Distinct	Yes	TLC confirm on LMB-19.R	LMB-19.R	-	No	-	Confirm	Yes	Barier	High	High
4	Gemuh a Besar	Surface Geological Mapping Data (PGE-UGM)	Distinct	Yes	LMB-A	Yes		G. Besar and Air Abang	-	Confirm	Yes	-	High	High
5	Bukit Lumut	Surface Geological Mapping Data (PGE-UGM)	Distinct	-	-	-	-	No	-	Confirm	-	-	High	Low
6	Penind aian	Slickenside N 300° E/ 85°, fracture N 220° E, and Surface Geological Mapping Data (PGE-UGM)	Distinct	-	LMB-B	Yes	-	No	-	Confirm	No	Barier	High	Low
7	Ogan Kanan	-	Distinct	-	-	-	-	G.Ogan Kanan 1, 2	-	No	-	-	Low	Low

From the field assessment it could be concluded that the productive faults in Lumut Balai are Air Ringkih, Air Udangan, Old Lumut Caldera, and Air Gemuha Besar, proven by geological, geochemical, and geophysical data. Geologically, Air Ringkih Fault is proven through field observation, drilling activities in the form of drilling break and borehole image logging, while from geochemical aspect Air Ringkih Fault provides a conduit for Air Ringkih and Bunbun manifestations, and is proven in geophysics' gravity measurements. Meanwhile, Air Udangan Fault is proven by field measurements and lithological offsets, gravity measurements, also by drilling parameters in Cluster A wells. Air Udangan Fault is the main permeability path for Air Patahan and Air Udangan manifestations. Old Lumut Caldera is proven by drilling activities in cluster 19.R, gravity data, and lithological offsets found in the field. Lastly, Gemuha Besar Fault is proven by field measurements, lithological offsets, loss circulation zones in Cluster A, gravity data, and by the presence of Gemuha Besar and Air Abang manifestations.

These faults are also proven through borehole images carried out in several wells in Lumut Balai. The borehole image logging can indicate bed boundaries, fractures, faults, and lithofacies. Seen in Figure 7, the dark areas indicates the presence of a fault zone.

The conductive faults and fractures are then summarized in a rosette diagram to understand their strike (azimuth) trend. The trend is then matched with the surface fault trend by overlaying the diagrams on Lumut Balai structure map. There are a significant similarities between the fracture trend from borehole image and the faults found on the Lumut Balai surface.

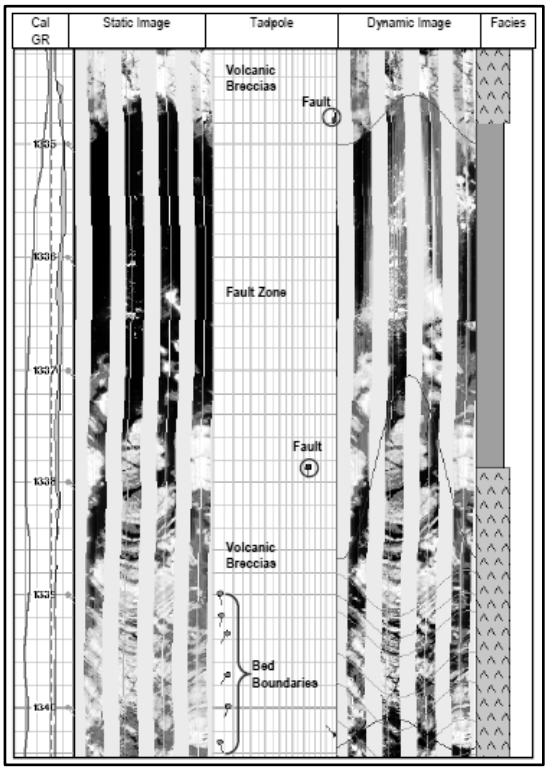


Figure 7: Borehole image data shows fault zone in volcanic breccia lithology in well LMB-5, the fault appeared black meaning the fault is conductive.

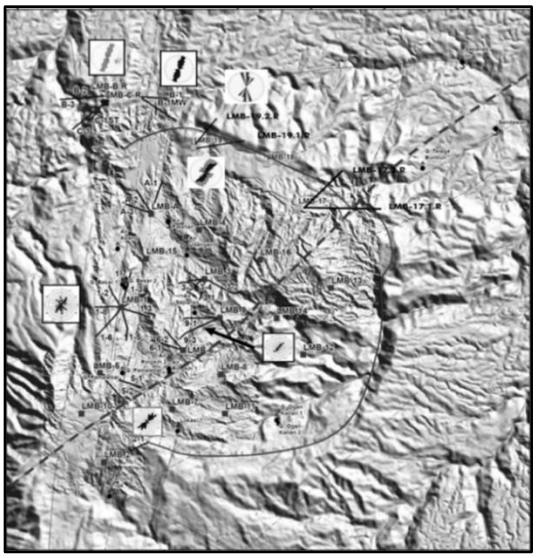


Figure 8: Rosette diagram of fractures inferred through borehole image logging overlain on top of Lumut Balai structure map

A correlation of total loss circulation zones could provide information regarding the elevation distribution of total loss circulation zones. As seen in Figure 9 the shallowest loss circulation zone could be found inside the Old Lumut Caldera in Cluster 3 with elevation around 750 meters above sea level (mASL), while the deepest loss circulation zone are found in wells outside of Old Lumut Caldera, particularly in the injection clusters with elevation approximately -1000 mASL.

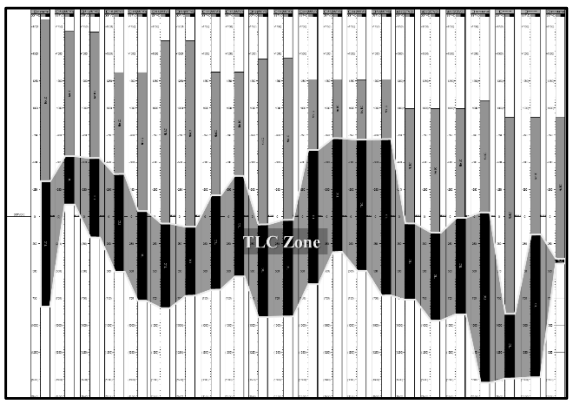


Figure 9: Correlation of total loss circulation zones in Lumut Balai's wells

Some of the injection wells that were drilled outside of Lumut Caldera did not encounter total loss circulation zone, which further proves that in Lumut Balai geothermal field, most of the good permeability could be found inside of the Old Lumut Caldera where the productive faults could be found.

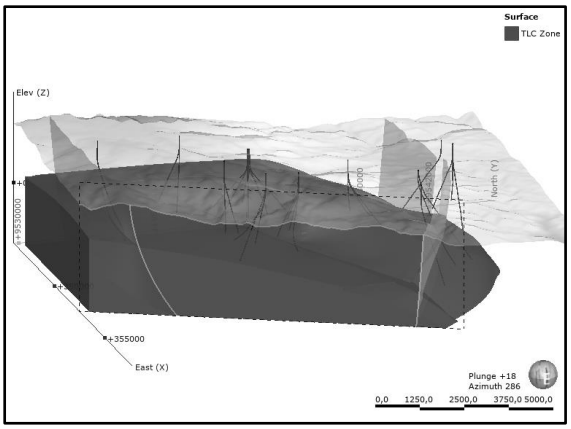


Figure 10: 3D block model of Lumut Balai's permeability distribution. The permeability dissipates to the north of the field, outside of the caldera.

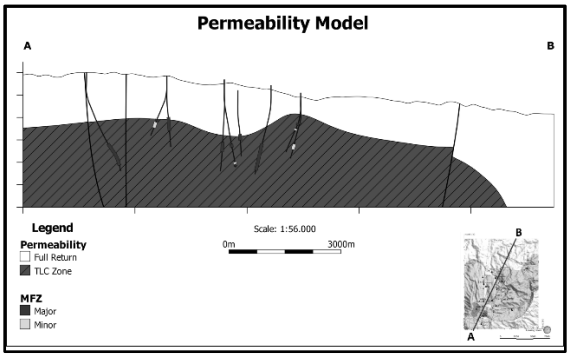


Figure 11: 2D Section from 3D block model of Lumut Balai's permeability distribution correlated with the major and minor feed zones in Lumut Balai.

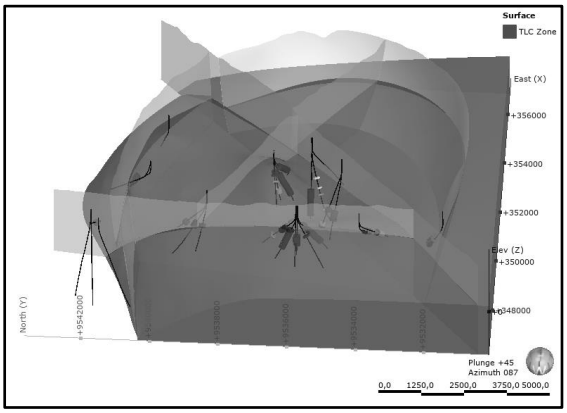


Figure 12: Lumut Balai's permeability distribution model and the major active faults in Lumut Balai

After inputting the data into 3D modelling software, a 3D permeability distrubution block model could be constructed. This 3D model provides information regarding the geometry of the subsurface permeability zones.

As seen in Figure 10, the permeable zone is the thickest inside the caldera, especially near Cluster 3 and Cluster 1. The peak of the permeable zone forms a NE-SW lineament, parallel with the NE-SW fault just to the south of the clusters. To the northwest, out side of the caldera no loss circulation zones have been found, therefore the permeability model looks quite similar to a dome structure where the peak of the dome is in the center of Old Lumut Caldera, and starting to thin out to the perimeter of the caldera's rim.

In correlation with major and minor feed zones in Lumut Balai, all of the feed zones are found within the permeable zone, and are most concentrated – more intensely found and in longer interval – in the center of the caldera.

This model will still continually be refined along with drilling activities in new clusters and future wells, and along with further geophysical and geochemical measurements. So far, this comprehension of Lumut Balai's permeability distribution has served greatly in well targeting purposes, proven by the sucess of Cluster 18 drilling where the actual drilling targets in the well matches precisely with the prognosis' planned target by only a few meters margin of error.

CONCLUSION

Lumut Balai geothermal field is one of the examples of geothermal field located within a caldera. In Lumut Balai's case, the good permeability is found within the caldera with little to no permeability found outside of the Old Lumut's Caldera.

A combination of geological, geophysical, geochemical, drilling, and reservoir data are used to construct a wholesome permeability distribution model.

A good permeability distribution model in geothermal exploration is essential since it could greatly assist in well targeting processes, planning well trajectory, increases the success rate in finding total loss circulation zones or permeable zones in future wells as the targeted productive zones.

REFERENCES

PGE. (2018), *Asesment Struktur Lumut Balai*

PGE. (2018), *Evaluasi Pemboran Sumur Reinjeksi Daerah Lumut Balai*

PGE. (2018), *Final Well Report*

PGE. (2017), *Laporan Survey Geologi Lumut Balai.*

PGE-Pusat Penelitian Panas Bumi FT UGM. (2014), *Laporan Akhir Studi Pola dan Kinematika Struktur Geologi, Hidrogeologi, dan Simulasi Reservoar Lapangan Panas Bumi Lumut Balai, Sumatera Selatan PT Pertamina (PERSERO).*

PGE-Pusat Penelitian Panas Bumi FT UGM. (2012), *Pengadaan Jasa Konsultan Studi Alterasi dan Fasies Volkanik Proyek Geothermal Lumut Balai.*

Sieh, K. and D. Natawidjaja (2000), Neotectonics of the Sumatran fault, Indonesia. *Journal of Geophysical Research*, **105**, pp.28295-28326.

EXPLORATION ACTIVITIES TO REDUCE UNCERTAINTIES OF A BLIND GEOTHERMAL PROSPECT. CASE STUDY: GEOTHERMAL PROSPECT "X" AT INDONESIA

Khalif Rahman, Wisnu Subroto, and Riki Irfan

Medco Cahaya Geothermal
The Energy Building, 50th Floor, SCBD Lot 11A
Email: khalif.rahman@medcoenergi.com

ABSTRACT

The geothermal prospect area "X" is located in Java Island of Indonesia. The prospect was considered as a blind geothermal system due to lack of surface manifestations. PT Medco Cahaya Geothermal (MCG) has accomplished Geological, Geochemical and Geophysical studies. The geology and geophysics data indicate possible of geothermal prospect beneath the study area. While none of thermal manifestations around the area, thus reservoir temperature and the reservoir fluid characteristic are highly uncertain. The deep slim vertical well is targeted based on geology and geophysical data interpretation to reduce reservoir temperature and fluid chemistry uncertainties prior any further exploration standard well drilling that might result to high economic risk. The pressure, temperature and spinner (PTS) survey was conducted to slim well and it found that temperature is more than 280 deg C at the bottom hole. As it is found that temperature and pressure is very high, well was flow tested and was able to collect fluid which confirmed the occurrence of benign fluid. This paper will discuss some exploration activities held on a blind geothermal prospect which has successfully reduce some uncertainties on exploration stages and as well as result to lowering risk before standard exploration well drilling.

Keywords: 3G, exploration activity, blind geothermal prospect.

INTRODUCTION

PT Medco Cahaya Geothermal (MCG) has been awarded by the Ministry of Energy and Mineral Resources (MEMR) of Indonesia to proceed the exploration stage prior to development in the "X" geothermal prospect area. The prospect "X" was considered as a blind geothermal system because of lack surface manifestations as common indications of geothermal system occurrence. The whole concession area covers about 62,620 Ha. The prospect area "X" located in Java Island Indonesia (figure 1).



Figure 1: Geothermal prospect area "X" location at Java Island Indoensia (Google Earth, 2018)

The hidden or "blind" geothermal system is a geothermal system that do not have readily identifiable surface manifestations. Although the frequency of occurrence of these concealed resources is largely a matter of speculation, there exists a need to develop a methodology for identifying promising targets for subsequent confirmation by deep drilling (Garg et.al. 2010).

The "X" geothermal prospect was covered the large half-caldera rim structure at the north and some parasitic cones in the disappeared southern rim of caldera. Several hot springs were distributed at the north of rim caldera indicates that the prospect may has the potential to be developed. In the southern part parasitic cones were also suggest the presence of the continuous volcanic activity in the prospect area and indicate potential heat source. Landsat image of "X" area is shown on Figure 2.

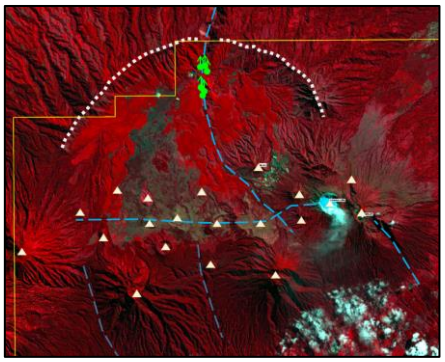


Figure 2: Landsat imagery shows the geological settings in prospect area "X"

Several morphological features are recognizable in situ and are generally associated with fault structures beside to those described associated with recent volcanic activities. The flat area within this caldera

covers an area of about 160 km^2 and limited to the east by an intra-caldera volcanic complex. The prospect area "X" has experienced multiple volcanic eruptions that have emitted breccias, tuffs, lavas and pyroclastic deposits. The presence of small craters and calderas morphology are indications of explosive in the past.

Moreover, based on the results of previous research conducted by PERTAMINA back 1990s has given clue and indication that there is possible prospecting geothermal system, in regard of the temperature gradient hole data. Thus, MCG continue the exploration to able to explore and get more detail information prior further development program.

EXPORATION ACTIVITIES

The national energy policy in Indonesia since decade ago was really supported the renewable energy development including geothermal energy utilization for give additional supply to the national electricity need. Thus, the exploration activities in country in general was increase since that time.

The "X" area, historically has been studied by PERTAMINA back to 1980s up to 1990s. Some geoscience studies and one temperature gradient well (TGW) has been drilled during the time. The old-time geoscientific study indicates possibility of geothermal potency that supported by the P-01 TGW well information resulted on very good indications of inferred temperature gradient of 270 deg C/km. The liquid samples collected from P-01 TGW well at 300 m and 500 m depth show high HCO_3 and SO_4 with very low Cl content indicates no acidic fluid on the well data. Those result lead company to continue the detail exploration at the "X" prospect.

The "X" prospect is part of the government electricity acceleration program named FTP-2 (Fast Track Program Stage-2), whereby the concession owner need to complete and develop geothermal production under agreement with MEMR and PT. PLN Persero. Ever since the concession granted, PT. MCG has conducted 3G exploration survey (Geological, Geochemical and Geophysical) and drill exploratory well.

The geological setting of the "X" area has given strong indication of the potential heat source location for a geothermal system. Following the big caldera collapse, a second phase of volcanism occurred the southern half of the caldera where the other half of circular shape disappears but has replaced by a series of young volcanic cones at southern caldera rim. The Gravity data has shown high gravity anomaly is found in the southwest of "X" area which coincide the young volcanic cones at the southern part of the caldera. Thus, this information supports the geology interpretation (MCG, 2018).

The geophysics data suggest the present of geothermal cap rock as indicated by MT low resistivity anomaly in the study area. The analysis of MT models found a typical up dome shape of low resistivity anomaly covered higher resistivity zone (Irfan, 2018).

The geochemistry data indicate that the northern thermal manifestations were typical bicarbonate water. It leads no information to predict the reservoir temperature based on surface manifestations. Thus, the "X" area defined as a blind geothermal system. The highest subsurface uncertainty is about reservoir temperature, permeability and fluid. Therefore, it is very important to drill deep enough exploration well to confirm the characteristic of geothermal system.

EXPLORATION STRATEGY

The technical resources assessments conducted by company and reviewed by international consultant indicated that a high-temperature geothermal resource may be in the caldera. The fact that lack of thermal manifestations on the prospect location need to be confirmed by the deep exploration drilling.

Geothermal industry at the time has recently been evaluating the options for lower cost drilling using small diameter wells (slim hole), full coring from surface to the target depth such as used in mineral exploration. The option to drill using coring rigs is considered appropriate for this type of situation, thus encouraging PT MCG to be a pioneer to use deep slim hole at the early stage of exploration drilling.

One of the key benefits of this coring rig, it is small size and has ability to be transported using track mounted vehicles, and have a relatively low daily rate, though they drill slower. In terms of infrastructure, the slim hole drilling only requires small well pad, does not need wider access roads, it is required less water than larger rigs and the water can be hauled by water truck.

The deep slim hole up to 2,000 m depth has not been performed for early stage of geothermal exploration in Indonesia. Therefore, PT MCG need to carefully prepare a suitable contracting scheme consider limited number of drilling contractors that experienced in both geothermal and coring rigs operations. MCG was then applied an IPM Contract scheme with full-turnkey basis, using a milestone / depth payment to mitigate the risk of subsurface uncertainty and technology limitation of the coring rig system.

The coring rig used during drilling activity is shown in Figure 3. This rig of capacity 450 HP was able to perform full coring operation up to 2,000 m depth.

Even though the campaign use coring rigs, standard safety drilling equipment and procedures as required

by the geothermal industry like using blow out prevention and other well control measurement was fully applied.



Figure 3: Coring Rigs which used during slim hole drilling activity at "X" prospect area

RESULT AND DISCUSSION

The main purpose of using deep slim hole method is to reduce the subsurface uncertainty during geothermal exploration stage, especially at the "X" area which categorize as a blind geothermal prospect. The slim hole targeted to drill deep enough deeper than the cap rock interpreted from resistivity data to reach a depth of high temperatures zone which greater than 220 deg C. This well is expected to to provide high quality information regarding lithology, alteration, and rock quality designation to be used in further exploration activities. Thus, full coring samples obtained during the drilling activities, beside the Pressure and Temperature surveys.

PT MCG has completed slim hole drilling at "X" prospect area location during 2016. The photo of drilling activity on Pad X-01 is shown in Figure 4. The X-01 well has continuous cored to total depth (TD) of 2,000 m and demonstrate measured temperature of 291 deg C during well completion test.



Figure 4: Deep slim hole drilling activity at X-01 well in "X" prospect area

The result of X-01 well is beyond expectations. As the deepest slim hole well, it has reached a very high temperature at TD. The pH measured from coring samples is also describe that acidic alterations are not observed in the deep reservoir zone as show in Figure 5. The low intensity of alteration in the cores has suggested a low water-rock interaction in the hydrothermal system. The appearance of anhedral-subhedral epidotes near the TD has suggested the prophylitic zone was located. The permeable zone has encountered at this depth has proved by TLC and PLC occurred during drilling, although the cores minerals suggests low permeability at those depth.

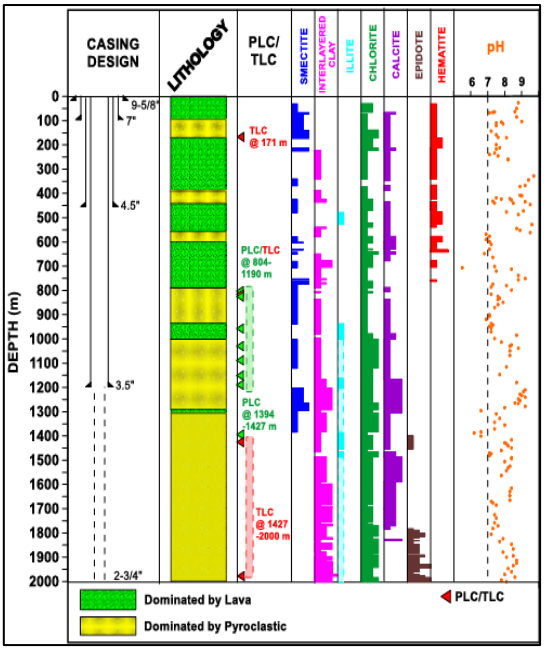


Figure 5: X-01 deep slim hole well drilling result summary

Respecting high temperature and stable wellhead pressure during well shut-in, this given promising indication that the X-01 well has a potential for flowing. Thus, PT MCG decided to conduct a flow testing after consulting with geothermal 3rd party well known consultant on the well testing.

In 2017, the X-01 well flow testing conducted. The well successfully flow and it was confirmed the presence of commercial temperature and benign fluid chemistry in this well site. The photo documentation of X-01 well flow testing is shown on Figure 6.

The high enthalpy fluid (2210 kJ/kg) with very low chloride and very high bicarbonate content suggest that the fluid discharged from X-01 well mostly comes from the boiled shallow aquifer. However, high silica and boron give an indication that some portion of produced fluid might come from deep liquid reservoir.

Based on the wellbore model, the X-01 well has been able to sustain steam production of 2.8 kg/s at 5.8 barg of wellhead pressure in stable condition for 6 days continues flow testing and therefore, fluid samples were successfully collected. Full laboratory analysis of gas and fluid chemistry as well as series of TFT have been conducted (MCG, 2018).



Figure 6: X-01 well flow testing activity

In facts, the results of deep slim hole drilling from X-01 well have provided many important information as expected prior the drilling. Most of the data obtained has been used to renew subsurface interpretation, especially the geophysics models that lead in updating the geothermal conceptual model and delineate the coverage of potential prospect location.

P-01 Temperature gradient well drilled to TD at 620m, while X-01 slim well drilled up to 2,000 m. Both wells were show consistent information about presence of high temperature gradient at "X" geothermal prospect. The P-01 TGW was located South of the prospect has highest temperature gradient which is approximately 270 deg C/km, while the X-01 well located few kilometer north part has lower temperature gradient of about 150 deg C/km. Even though lower compared to P-01, still X-01 well is indicate a gradient of potential geothermal prospect area. The temperature profiles of P-01 and X-01 well is shown on figure 7 and 8 respectively.

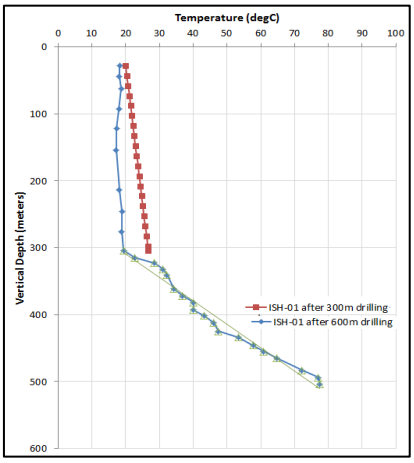


Figure 7: The temperature profile of P-01 temperature gradient well.

This information suggests that the up-flow zone is potentially located on the south of the prospect consistent with the presence of young volcanoes at the southern area and as well as indicates by gravity anomaly from geophysics data (MCG, 2018).

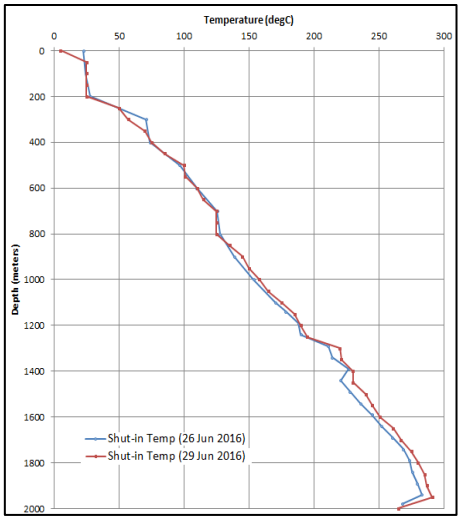


Figure 8: The temperature profile of X-01 deep slim hole well.

CONCLUSION

In summary, the deep slim hole drilling has greatly increased confidence level of possibility of presence of geothermal reservoir beneath on the "X" prospect area. The high temperature, benign geothermal reservoir measured from X-01 deep slim well flow testing has successfully reduced the subsurface uncertainty.

Although, the nature of permeability and character of the potentially productive reservoir is still less clear but overall, the results are sufficiently positive to endorse to move to phase to target next deep full size of exploration and production drilling program.

The deep slim well information has been proven to give important information used for calibrating the resistivity model and at the end able to support on updating the geothermal conceptual model. Thus, the update model expected to be able to predict the geothermal resources potency and as a key factor for basic drilling targeting for further stage reduce the financial risk of the drilling failure or financial risk to the project.

ACKNOWLEDGMENTS

The authors wish to express their gratitude to the Management of PT Medco Cahaya Geothermal for using the data and reports, and their permission to publish this paper.

REFERENCES

Garg, S.K., Pritchett, J.W., Combs, J. (2010) "Exploring for Hidden Geothermal Systems".

Irfan, Riki., Daud Yunus. (2018), "1D, 2D and 3D MT Characteristic on A Blind Geothermal Prospect Area Case Study: Geothermal Prospect Area "BGP" At Indonesia", IIGCE 2018. Jakarta.

MCG, PT. (2017), “unpublished report: Final Report of X-01 Slimhole Drilling”, Subsurface Departement of PT Medco Cahaya Geothermal.

MCG, PT. (2018), “unpublished report: The X Area Pre-Development Plan*”,* Subsurface Departement of PT Medco Cahaya Geothermal. Jakarta.

GEOTHERMOMETER ANALYSIS TO DETERMINE GEOTHERMAL RESERVOIR TEMPERATURE OF PANDAN MOUNTAIN AS POTENTIAL ENERGY OF EAST JAVA

Munif Nur Faizin and Laksono Prabowo

Sekolah Tinggi Teknologi Nasional Yogyakarta
Email: munif.nurfaizin16@gmail.com; laksonoprabowo3@gmail.com

ABSTRACT

Pandan Mountain is located in East Java which is on the border of 3 districts of Bojonegoro district, Ngawi district and Nganjuk district. Physiographically Pandan Mountain is an area of "Over Trust" Zone Kendeng located in the complex area of the structure which is associated with volcanic Kuarter. The presence of hot springs manifestation indicates the existence of geothermal potential in the area of Pandan Mountain. Geochemical analysis of fluids in geothermal areas has important information about reservoir conditions, and fluid chemical analysis is performed to determine geochemical characteristics and natural resource potential.

The method used in this research is descriptive method and analysis of geothermal fluid chemistry. The analysis results were obtained from 4 hot spring samples from 12 manifestations that appeared on the slopes around the study site. For Examples of hot springs taken from Banyu Kuning I, Jari I, Jari II, and Jari III.

Based on the corelation of chemical element and plotting ratio on Trilateral triangle Cl-Li-B diagram (Simmons, 1998) to a geothermal system and analysis of physical properties and geochemical analysis, the samples of Banyu Kuning I, Jari I, Jari II, and Jari III are in the outflow zone. In the plotting of the triangle diagram of Cl-SO_4-HCO_3 (Simmons, 1998) also shows information that Banyu Kuning I hot springs are bicarbonate with Cl content of 615.4 mg / L. While in the Hot Springs Jari I, II and III have properties of chloride with content of Cl 3.747.1 mg / L, 4.913.4 mg / L and 6.848.9 mg / L. The calculation of Na-K geothermometer obtained reservoir temperature at temperature 150-200ºC. Included in medium temperature according to Hochstein and Browne (2000). in its utilization, the manifestation on Pandan Mountain is utilized for hot water bath, and for large scale utilization can be utilized for moderate-temperature geothermal power plant which combined with modern equipment.

Keywords : Fluid Geochemistry, Hot Springs, Chloride, Bicarbonate, Outflow, Na-K Geothermometer

INTRODUCTION

Geothermal exploration has been intensively conducted over the last decade, in which new geothermal manifestations have emerged to give hope for energy availability in the present and future. Several methods are used in the development of geothermal one of them is geochemical method. The geochemical method used in geothermal exploration research is to examine the possibility of developing geothermal resources. The data commonly used in this geochemical method are chemical data of hot water manifestations, isotope data, soil chemical and soil gas data. The data is used to examine the possibility of developing geothermal resources covering various parameters such as resource size, estimate of reservoir temperature and formation permeability (Hutapea, 2010). One way to evaluate the feasibility of geothermal fluid chemistry analysis is to check the equilibrium of ions. This means comparing the molecular concentrations of positively charged species with the number of molecular concentrations of negatively charged species. The content of positively charged ions (cations) such as Ca^{2+}, Mg^{2+}, Na^{+}, K^{+}, Li^{+}, Rb^{+}, Cs^{+}, Mn^{2+}, Fe^{2+}, Al^{3+}, NH^{4+}. The content of negatively charged ions (anions) Cl^{-}, SO_4^{2-}, HCO^{3-}, F^{-}, I^{-}, Br^{-}. As well as the neutral ions of SiO_2, NH_3, B, CO_2, H_2S. Based on the ion content contained in the fluid can be used in a preliminary survey in determining geothermal potential. Can be used to determine geothermal reservoir temperature estimates, geothermal fluid origin, and type of geothermal fluid.

Mount Pandan is located in East Java which is on the border of 3 districts of Bojonegoro, Ngawi and Nganjuk. Physiographically, Mount Pandan is an area of "Over Trust" Kendeng Zone and Anticlinorium Rembang Zone located in the complex area of the structure which is associated with the volcanic quarter. According to local residents, there are many hot springs and hot mud around Pandan Mountain. No one is sure to examine the geothermal potential of Pandan Mountain so it is expected that this Pandan Mountain area has geothermal potential that can be used in the welfare of the community.

Table 1. Result of Analysis Sample Laboratorium use AAS method (Atomic Absorption Spectroscopy)

No	Parameter	Satuan	Hasil uji				Metode uji
			17.390 K	17.391 K	17.392 K	17.393 K	
1	Boron (B)	mg/L	< 0,0120	< 0,0120	< 0,0120	< 0,0120	APHA 2012,Section 3120 - B
2	Natrium (Na)	mg/L	410	7.648	2.224	4.990	APHA 2012,Section 3500 - Na
3	Kalium (K)	mg/L	32	314	133	322	APHA 2012,Section 3500 – K
4	Kalsium(Ca)	mg/L	108,00	52,00	140,00	176,00	SNI 06-6989.12-2004
5	Magnesium(Mg)	mg/L	72,90	51,03	43,74	77,76	SNI 06-6989.12-2004
6	Klorida (Cl)	mg/L	615,4	6.848,9	3.747,1	4.913,4	SNI 6989.19-2009
7	Fluorida (F)	mg/L	0,1558	0,5270	0,5111	0,2792	SNI 06-6989.29-2005
8	Alkalinitas	mg/L	1.049,2	1.964,2	1.805,6	1.390,8	APHA 2012,Section 2310 & 2320 B
9	Sulfat (SO_4)	mg/L	36	336	395	503	SNI 6989.20-2009
10	Lithium (Li)	mg/L	0,72	0,42	0,28	0,53	ALPHA 2012, Section 3500-Li
11	pH	-	7,9	8,4	8,5	7,7	SNI 06-6989.11-2004

METHODOLOGY

The research method used is a combination of field geology data and laboratory data, which then analyzed to use AAS method (Atomic absorption spectroscopy) which aims to know the elements and chemical compounds contained in hot springs and will be compared with the results of eye analysis hot water in the field, the chemical test parameters used against two pools of hot springs are the same ie Boron (B), Sodium (Na), Calcium (Ca), Potassium (K), Magnesium (Mg), Chloride (Cl), Fluoride (F), Bicarbonate (HCO3), Lithium (Li), Sulfate (SO4), ph.

REGIONAL GEOLOGY

The research location entered on the southern part of Bojonegoro Sheet with a scale of 1: 100.000 composed of breakthrough rocks of Andesite Piroksen, Andesite Hornblende entering in units of Intrusion Rock (Qia), Breccia Andesite entering on Breccia Pandan Formation (Qpv) and Calcarenite, tuff carbonate the black clay that is part of the Kalibeng Formation (Tmpk).

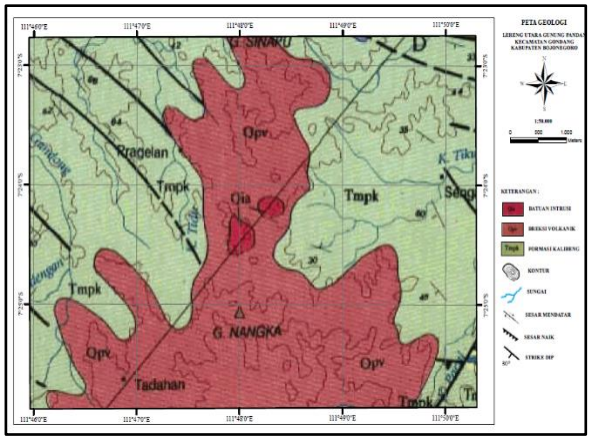


Figure 1. Location Research Map

The geological structure that developed in the research area was a fault of the pavement that was part of the "Over Trust of Kendeng Zone". Geological structure that developed in the area relating west-east trending which is the result of plate compression style that concerns the island of Java.

LITERATURE REVIEW

Geothermal geochemistry is the study of the chemistry of geothermal fluid. Aims to determine the characteristic nature of geothermal reservoirs. Its use in geothermal exploration can be used to identify and assess the potential development of a geothermal resource. Chemical data used are chemical data from manifestations of geothermal (water and gas) and isotope data. The data is used to examine the possibility of developing geothermal resources covering various parameters such as resource size, reservoir temperature estimation, formation permeability (Hutapea, 2010).

GEOCHEMICAL ANALYSIS

The analysis was conducted on 4 samples of hot spring manifestation, namely Banyukuning 1, Jari 1, Jari II and Jari III. Observations were made to see the chemical content in the manifestation which was then analyzed. The analysis uses the Trilinear diagram Cl - SO_4 - HCO_3, Triliniear diagram Na - K - Mg, and Trilinear diagram Cl - Li - B. From the diagram can be detected the characteristics of each manifestation, if related can also determine the character of the reservoir. In addition, the entire value of the fluid geochemistry concentration in the analysis of each concentration value, although not through plotting on the Triliniear Diagram, through the amount of concentration of certain compounds and also the ratio of the elemental ratio value of some particular compounds.

Heat Type Selection

Determination of hot water flow type based on geochemical analysis of hot springs in research area using classification of Trilinear diagram Cl-Li-B (Simmons, 1989), Fluid type analysis using *Cl*, Li and B parameter on the manifestation of hot water of research area obtained.

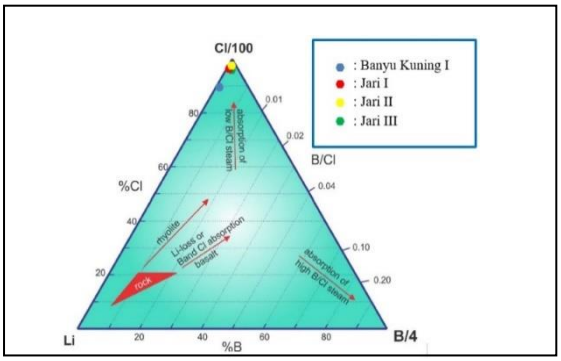


Figure 2. Plotting result Cl, Li and B parameter in the Trilinear diagram Cl-Li-B

Determination of Fluid Type

Determination of hot water type based on geochemical analysis of hot springs in research area using Trilinear diagram HCO_3-SO_4-Cl classification (Simmons, 1998), Fluid type analysis using element and compound from HCO_3, SO_4 and Cl on the manifestation of hot water of research area got result.

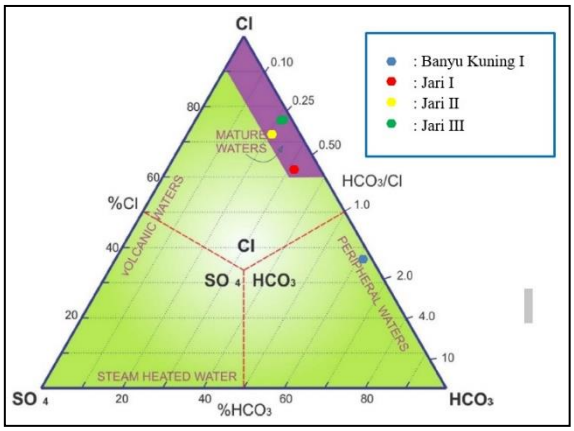


Figure 3. Plotting result HCO_3, SO_4 and Cl parameter in the Trilinear diagram HCO_3-SO_4-Cl

Determination of Under Surface Temperature

Surface temperature calculation of the research area can be done by using Na-K-Mg geothermometer method (Simmons 1998). The analysis of subsurface temperatures using sodium (Na), potassium (K), magnesium (Mg) element parameters and calculation of ion content for springs of research area.

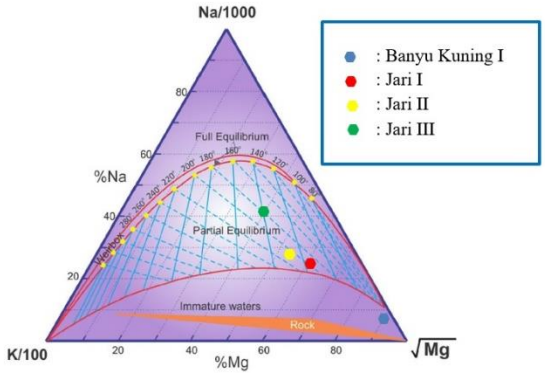


Figure 4. Plotting result Na, K, and Mg parameter in the Trilinear diagram Na-K-Mg

GEOTHERMOMETER ANALYSIS

Geothermal systems associated with volcanic magmatism are generally geothermal systems with high-temperature reservoirs ≥200ºC (Hochstein and browne, 2000). So a good geothermometer used to calculate reservoir fluid temperature at Pandan Mountain is K-Na geothermometer and silica because this geothermometer is valid used to calculate geothermal system having temperature ≥200ºC (Nicholson, 1993). K-Na geothermometer calculation formula as follows:

$t^oC = 1217/ [\log (Na/K) + 1.483] - 273$ (Fournier, 1979 dalam Nicholson, 1993)

$t^oC = 1390/ [\log (Na/K) + 1.750] - 273$ (Giggenbach, 1988 dalam Nicholson, 1993)

The Na-K geothermometer formula usage has limits:

1. Used for water estimated to have a temperature reservoir of ≥180ºC.
2. Used when water contains a low Ca based on the calculation (Log (√Ca / Na) + 2.06)) results in a negative value.

Table 2. The results obtained with Na-K geothermometer

ºC	Jari I	Jari II	Jari III
(Fournier,1979)	176,74	182,29	151,18
(Giggenbach,1988)	194,54	199,78	170,23

CONCLUSIONS AND RECOMMENDATIONS

The geothermal area of Mount Pandan on the northern slope, Gondang Subdistrict, Bojonegoro Regency has karasteristik form of bicarbonate and chloride fluid. Bicarbonate fluid was obtained from Banyu Kuning I sample analysis with higher HCO_3 ratio than Cl and SO_4 as a result of contact with side rock and surface water. Based on the content of Mg-Na-Cl shows the results in line where the state of immature water. While in the sample of Finger I,

Finger II and Finger III have characteristic of fluid in the form of water chloride. This is shown by the small ratio of HCO_3 and SO_4 to Cl. Based on the content of Mg-Na-Cl showing the equilibrium partial point with the temperature of the reservoir is interacted with the Na-K 150º-200ºC geothermometer entering the medium temperature geothermometer. Based on the analysis of Cl-Li-B content, the manifestation appears in the outflow zone which is a more redundant zone than the volcanic morphology.

ACKNOWLEDGEMENTS

The support by lectures of STTNAS Yogyakarta in supporting the writing of this paper is gratefully acknowledged.

REFERENCES

Clements,Benjamin., Robert Hall., et.al. (2009). "Thrusting of a volcanic arc: a new structural model for Java". *Petroleum Geoscience*, Vol. 15 2009, pp. 159–174

Fahrudin., Hengky Priyono Effendi. (2015). "Analysis Of Thrust And Fold Development On Sandbox Modelling With Normal And Compression Behavior, Case Study : Kendeng Zone", *Proceeding, Seminar Nasional Kebumian Ke-8 Academia-Industry Linkage*, Semarang.

Giggenbach and Goguel. (1989). "Chemical Techniques in Geothermal Exploration". Chemistry Division, DSIR, Private Bag**.** New Zealand

Goff, F. Dan Janik, C. J, (2002), "Geothermal Systems", in Sigurdsson, H., dkk., eds. *Encyclopedia of Volcanoes* : Academic Press, New York,p.817-834

Hochstein, M.P dan Browne, P.R.L., (2000), "Surface Manifestation Of Geothermal with Volcanic Heat Source", *In Encyclopedy of Volcanoes*, H. Siguardson, B.F. Houghton, S.R. Mc Nutt, H. Rymerdan J. Stix (eds). Academic Press

Niniek, R.H., Wulandari M. (2010), "Evolution of Cisolok – Cisukarame Geothermal System,West Java – INDONESIA Based on its Surface Manifestation" *Jurnal Geoaplika*, Volume 5, Nomor 1, hal. 049 – 059

Niniek, R.H dan Tri J. (2007), "Hidrologi Air Panasbumi Daerah Cidanau dan Sekitarnya, Anyer, Provinsi Banten Berdasarkan Manifestasi Permukaan", *Jurnal Geoaplika*, vol.2, no.3, hlm.105-119.

Pringgoprawiro, H. (1983), "Biostratigrafi dan Paleogeografi Cekungan Jawa Timur Utara, Suatu Pendekatan Baru", Disertasi Doktor. ITB, Bandung.

Sumayadi, M. (2014), "Geokimia Panas Bumi Gunung Slamet Jawa Tengah", *Seminar Nasional Fakultas Geologi*, Bandung.

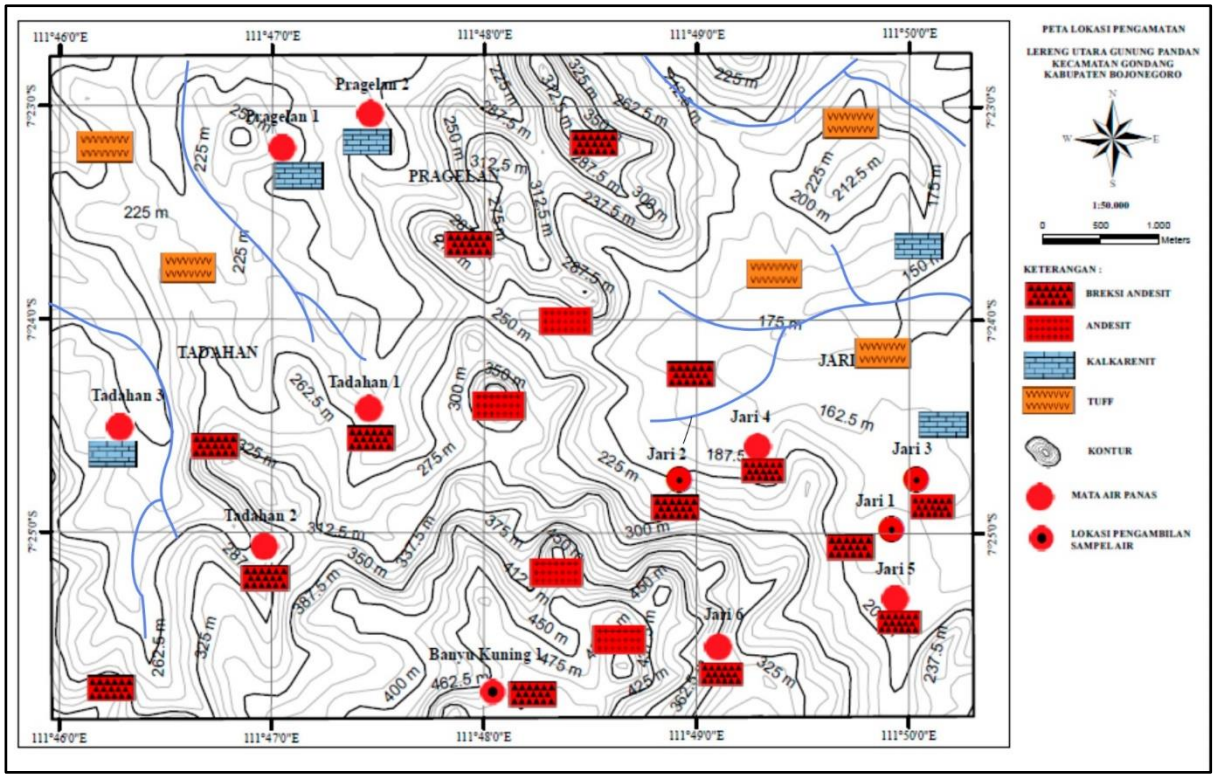


Figure 5. Location Map

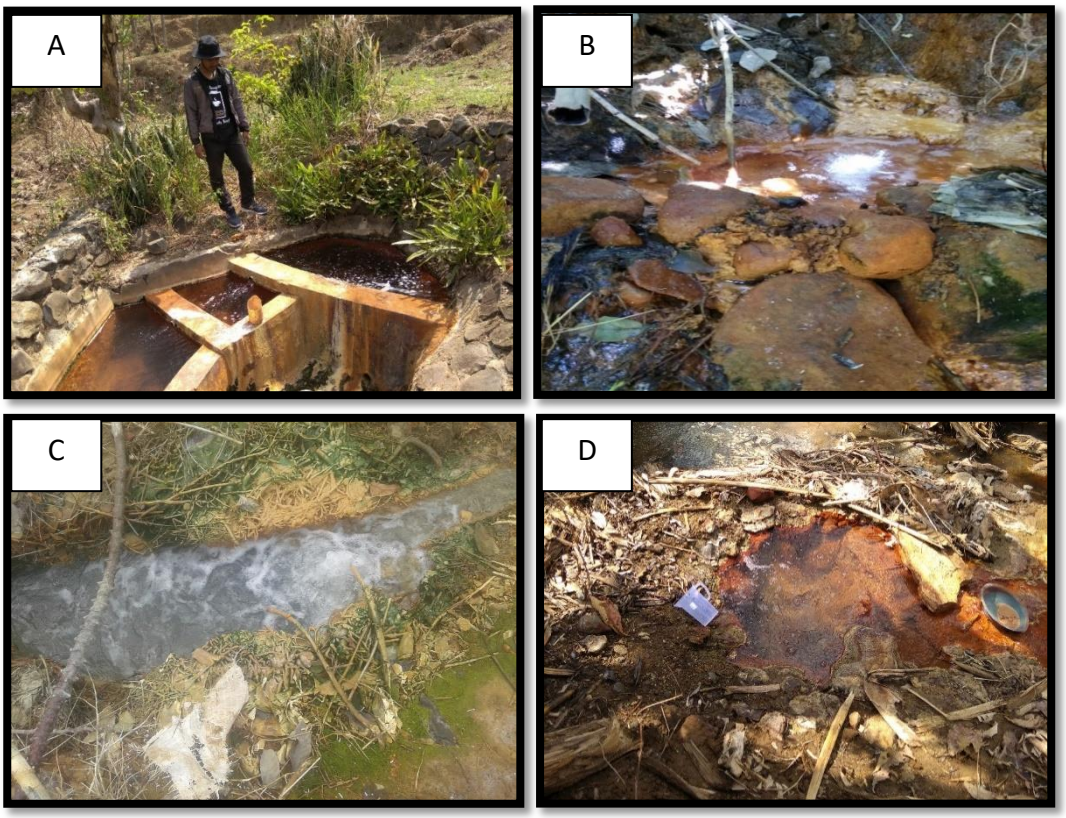


Figure 6. A) The manifestation of hot spring Jari 1 in Jari Village (west-trending photo); B) The appearance of the hot springs of Banyu Kuning 1 in Jomblang Village (northwest trending photo);C) The appearance of the hot jari 3 fingerprint in Jari Village (west direction photo); D) Appearance of jari 2 hot spring springs at Jari Village (south-trending photo)

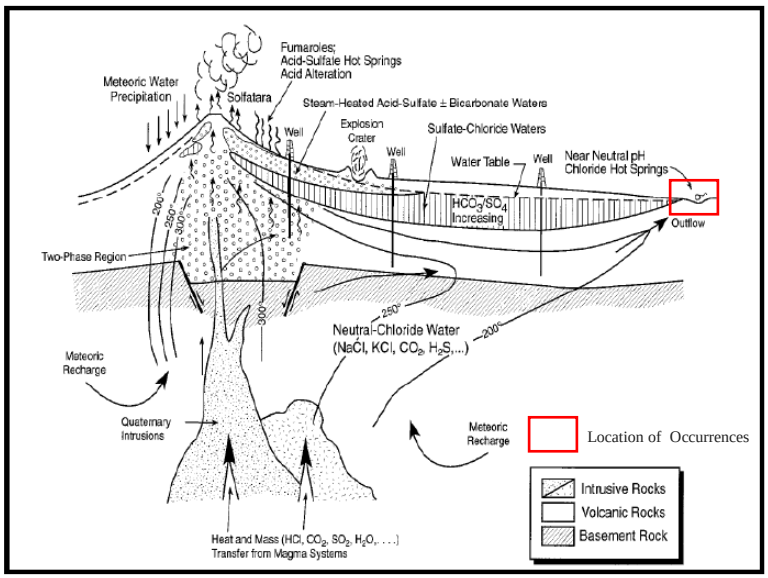


Figure 7. The conceptual model of geothermal stratovolkano andesitic(Hochstein dan Browne,2000)

COMBINATION OF SPECTRAL ANALYSIS AND MOVING AVERAGE METHOD TOWARD RESIDUAL GRAVITY ANOMALY PROFILE TO DETERMINE BASEMENT STRUCTURE

Wahyu Noor Ichwan[1], Agus Sulistyo[1], Fitrianita[1], Fikri Fahmi[1], Wambra Aswo Nuqramadha[1], and Yunus Daud[2]

[1]PT. NewQuest Geotechnology, Pesona Khayangan Estate DC 12, Depok
[2]Master Program in Geothermal Exploration, Graduate Program of Physical Science,
Universitas Indonesia, Jakarta, Indonesia
Email: wahyu.noorichwan@newquest-geotechnology.com

ABSTRACT

Basement structure is one of gravity method's main target. It can be identified from residual gravity anomaly which is superposition of gravity respons from deep anomaly body, shallow anomaly body, and near surface anomaly body. Horizontally, residual gravity anomaly changes with distance and form a wave with certain amplitude and wavelength. Basement structure, which is deep and homogenous, has long wavelength and small amplitude. Its wavelength can be identified by using spectral analysis. Discrete fourier transform was applied toward residual gravity profile data. It produced numbers of spectral amplitude and wavenumber of anomalous bodies from various depth. Spectral amplitude natural logarithmic and wavenumber were plotted and analyzed to determine the basement spectral wavenumber. In general, those data graph formed three trends, which can be interpreted as previous anomalous body. The wavelength of basement structure is calculated from intersection between deep anomalous body and shallow anomalous body trend. Afterwards, the wavenumber was used to calculate number of points which will be used on moving average process toward residual gravity anomaly profile. Smoother residual gravity anomaly curve was produced and the smoothness was proportional to number of points, which were calculated from basement wavelength. Those methods were applied toward sintetic and real data. The application toward sintetic data obtained curve which has similar pattern to the gravity respon of its basement structure. As for real data, resistivity section of MT data was used to confirm the result. Smoothed curve of real data showed similar trend with deep high resistivity body, which is usually interpreted as basement structure.

Keywords: Spectral analysis, moving average method, residual gravity, basement structure.

INTRODUCTION

Basement structure is one of the most important targets in geothermal exploration. It can be identified by using residual gravity data. Because of the depth, basement in general has long wavelength gravity anomaly (Telford, 1989). It can be identified along a residual gravity anomaly data profile, since gravity data amplitude are varying toward distance.

Residual gravity anomaly is superposition of anomalous body response in different depth (Telford, 1989). Unlike basement gravity anomaly, it has shorter wavelength. Long wavelength of basement cannot be observed directly from it. It should be interpreted or generated by using a certain filter.

This paper discusses about method to generate long wavelength from residual anomaly data in order to determine basement gravity anomaly response. Wavelength of those basement gravity anomaly is calculated by using spectral analysis method. The wavelength then used to construct moving average filter.

GRAVITY DATA

Gravity data which are used were residual gravity anomaly along profile from synthetic and real data. The real data is combined with resistivity section. The data can be seen in figure 1, figure 2, and figure 3.

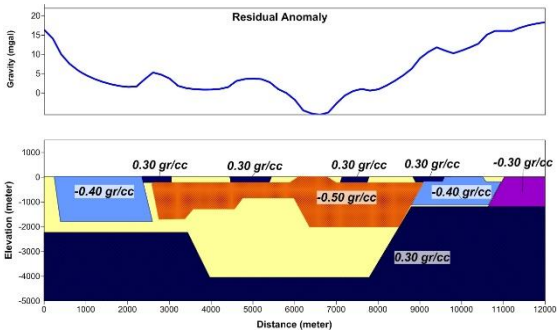


Figure 1: Synthetic model 1, derived from gravity 2D forward modeling

The synthetic data was constructed with the assortment of basement and several anomalous bodies on the top of it. The basement is the deepest body with 0.03 gr/cc density contrast. The first basement model is like a shape of a graben and the second model resemblance a horst followed by graben.

Residual gravity anomaly of real data in figure 3 is often led to misinterpretation since the curve trend

not so similar compared to the high anomaly in resistivity section, which is in general interpreted as basement. For example, in distance 5000 to 8000 m, the high resistivity, which is interpreted as basement, shows descending trend, but the residual gravity data shows upside trend.

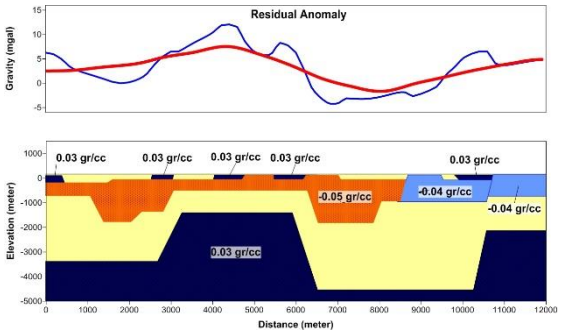


Figure 2: Synthetic model 2, derived from gravity 2D forward modeling

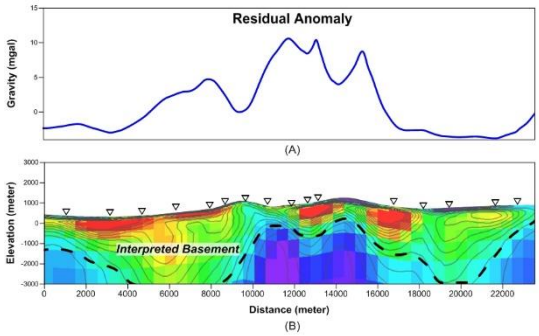


Figure 3: Residual gravity anomaly of real data (top) and resistivity section (bottom)

METHODS

The gravity profile data was processed by using two methods, spectral analysis and moving average.

Spectral Analysis

Spectral analysis has been widely applied to determine depth of anomalous body (Njandjock, 2006). It is done by analyzing a graphic representing power spectral versus wave number provides an estimation of the mean depth around which the sources are distributed (Moral, 2000). In most case, the graph could be distinguished as three segments, which were represented mean depth of anomalous body.

Power spectral and wave number were generated by using Discrete Fourier Transform (DFT) toward gravity data profile. Discrete fourier transform provide spectral amplitudes (Smith, 1999). The spectral amplitudes were converted into power spectral by converting it into its natural logarithmic number (Bansal, 2010).

In spectral analysis of residual gravity anomaly profile, the regional segment is interpreted as power spectral of basement structure, since basement structure is the deepest anomalous body which is contained in residual gravity data. The wave number was then calculated from intersection of regional and residual segment. Furthermore, those wave number was converted to wavelength which would be used to construct moving average filter.

Moving Average Filter

Moving average filter construct output by averaging number of points of input data (Smith, 1999). Since the data were separated by a certain distance, number of points cover total distance which could be called as filter band. The filter band are adjusted so that they covered the wave number of the basement. The basement wavelength, which was obtained from spectral analysis, was divided by data distance to obtain number of points.

RESULTS AND ANALYZIS

Power spectral and wavelength graph from each model are shown at figure 3, figure 4, and figure 5.

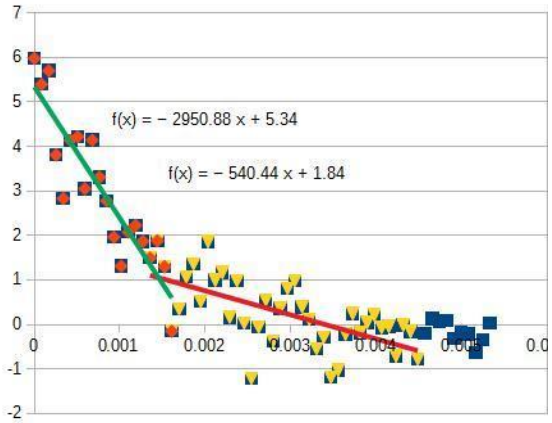


Figure 4: Power spectral vs wavelength of synthetic model 1

Y axis represents power spectral and x axis represents wavenumber. In general, all of the graphs have three segments. The first segment from the left is interpreted as power spectral of basement structure. It has the largest gradient. The second one is interpreted as power spectral of anomalous body above it. Each segment trend line was calculated by using linear least square. Wave number of the basement is wave number value at intersection point of those trend line. The basement wavenumber of synthetic model 1 is 0.00145, synthetic model 2 is 0.0014, and real data is 0.00093.

Moving average result of synthetic model 1 can be seen in figure 2. The wavelength which is calculated from respective wave number is 4333.23 m and covered by 47 number of points. The result of moving average filter using 47 number of points

toward synthetic model 1 is represented as red curve in figure 7 (B). It has long wavelength and have similar pattern with basement anomaly with correlation coefficient 0.967. The short wavelength of the data is reduced. For example, local peak of the data from distance 0 to 2000 meter. Its peak is considerably high, around 15 mgal and 1500 m wide, but it is reduced into around 5 mgal in accordance with regional wavelength.

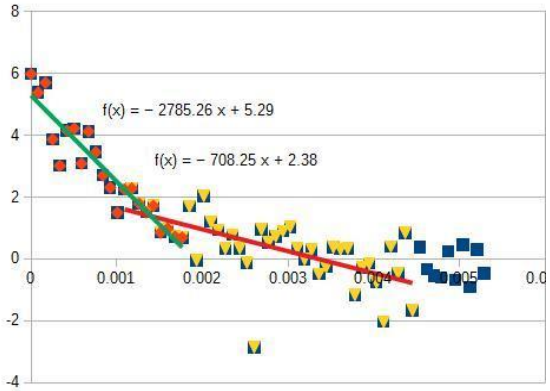


Figure 5: Power spectral vs wavelength of synthetic model 2

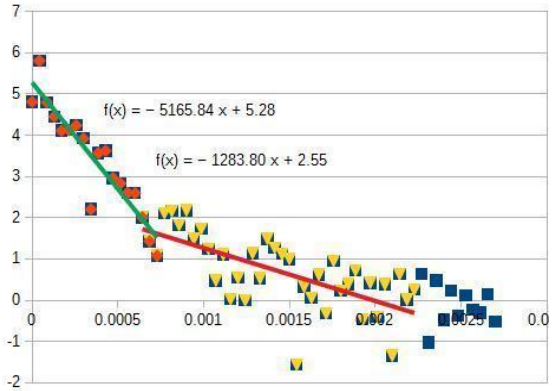


Figure 6: Power spectral vs wavelength of real data

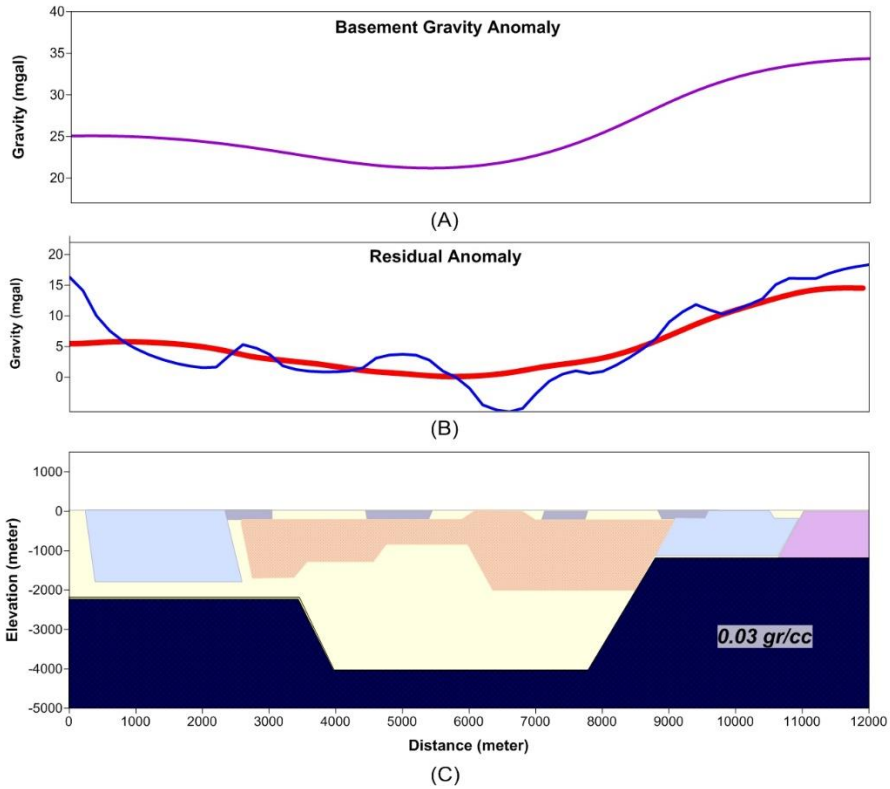


Figure 7: Moving average result of synthetic model 1 using 47 number of points. (A). Gravity anomaly of basement body with 0.03 gr/cc density. (B). Gravity anomaly of synthetic model 1 (blue curve) and moving average result (red curve). (C). Synthetic model 1.

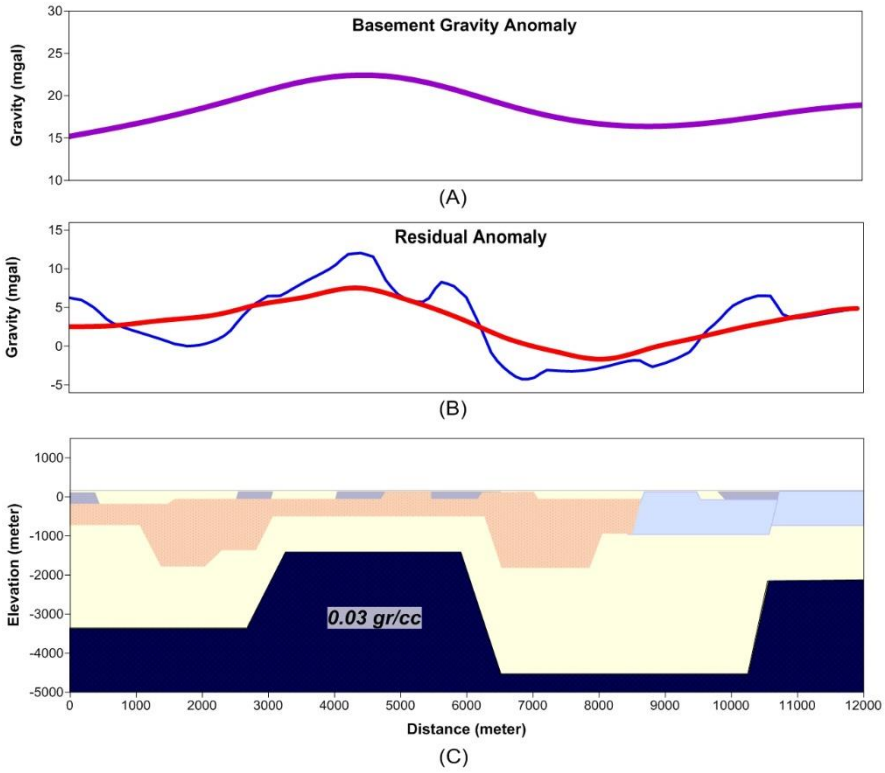


Figure 8: Moving average result of synthetic model 2 using 49 number of points. (A). Gravity anomaly of basement body with 0.03 gr/cc density. (B). Gravity anomaly of synthetic model2 (blue curve) and moving average result (red curve). (C). Synthetic model 2.

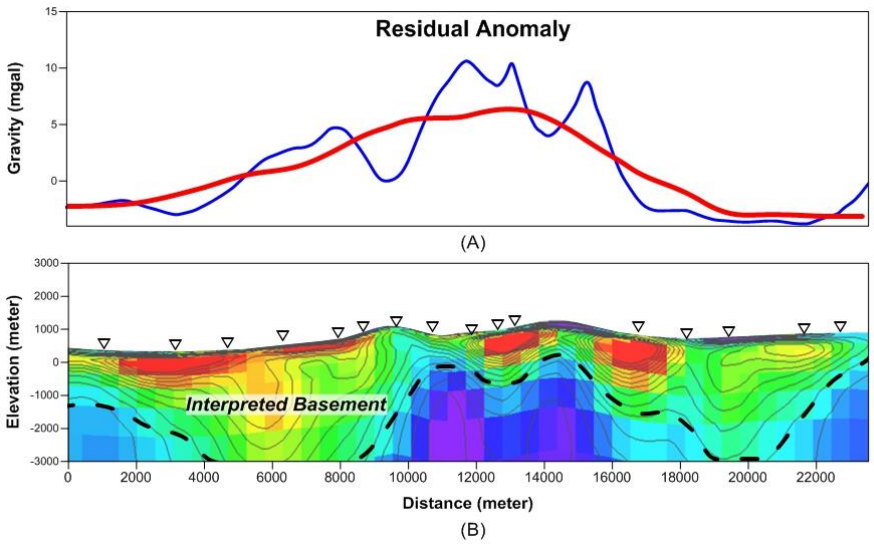


Figure 9: Moving average result of real data residual gravity anomaly using 37number of points compared to resistivity section. (A). Residual gravity anomaly of real data (blue curve) and moving average result (red curve). (B)Resistivity section of real data with interpreted basement (dash line)

.

Moving average result of synthetic model 2 can be seen at figure 8. The model basement wavelength is 4488 mand covered by 49 number of points. The result of moving average filter using 49 number of points is represented as red curve in figure 8 (B). The correlation coefficient between moving average curve and basement anomaly curve is 0.80. Undulations of gravity anomaly data are removed. The filter produces smooth data curve similar to basement gravity anomaly curve. The most notable anomaly change is shown from distance 6000 m to 9000 m. The descending anomaly trend in gravity response is quite low amplitude and have long band, about 3000 m. But it is still reduced by the filter, so the output curve has higher amplitude and smoother anomaly. It is probably the descending trend of basement gravity anomaly descends even more was caused by low density anomalous body above it, so

it was removed. Moving average result of real data can be seen at figure 9. It is compared with resistivity section. Basement is interpreted from resistivity section, the structure with high resistivity. The interpreted basement is represented by dash line.

Basement wavelength value of the data is 6756.11 m and is covered by 37 number of points. The filter produces smooth curve which is represented by red curve in figure 9 (A). Interpreted basement of resistivity data is very undulating compared to moving average curve, since gravity anomaly of the basement should have long wavelength. The resistivity basement form like horst or intrusion structure in the middle of the section. Furthermore, the moving average curve shows similar pattern with the basement. When the basement has ascending trend, the moving average also has the same pattern, unlike the residual gravity anomaly which show some differences in pattern toward basement structure. For example, at the distance of 5000 to 8000 m, the basement shows descending trend but the residual curve shows ascending trend. Moreover, at the distance of 8000 to 1100 m, the basement shows ascending trend but the residual curve shows descending trend. Those condition might cause misinterpretation of the data. All of those unsuitable trends were removed by corresponding filter.

All of the three models show good result, that curve which is produced by moving average filter show similar trend toward basement structure. It is possible that moving average filter pass the curve with equal or longer wavelength. Narrow undulation, even though it has large amplitude, will be reduced to the point where it is suitable toward desired trend.

Although filtered curve shows similar trend, they have different amplitude range. For example, in model 1, basement gravity anomaly has amplitude range from 15 to 25 mgal, while moving average result have amplitude range from 1 to 15 mgal, same as with the residual data amplitude range. This is happened because moving average filter just smooth the curve not restore the superposition component. Residual gravity anomaly is the superposition of basement gravity anomaly which has high amplitude and other anomalous body which has lower amplitude. So, the residual gravity anomaly has obviously lower amplitude range compared to basement.

CONCLUSIONS

Combination of spectral analysis and moving average data can produce curve which is similar to basement trend. It removes local undulation which might cause misinterpretation. Although it produces similar pattern, the moving average curve have different amplitude range compared to basement gravity anomaly curve.

REFERENCES

Telford, M.W., Geldart, L.P., Sheriff, R.E. (1990), "*Applied Geophysics Second Edition"*. New York, Cambridge University Press.7.

Rey Moral, C., Gómez Ortiz, D and Tejero, R. (2000), "*Spectral analysis and Gravity Modelling of the Almazán Basin (Central Spain)", Rev. SOCo Geol. España*, 13 (1): 131-142.

Smith, S.W. (1999), "*The Scientist and Enginer's Guide to Digital Signal Processing"*. California, California Technical Publishing.

Bansal, A. R., Dimri, V. P. (2010), "*Scaling Spectral Analysis of Gravity and Magnetic data"*.

Njandjock, N., P., Dicoum, E., M., Mbarga, T., N., Tabod, C., T. (2006), "*Spectral analysis and gravity modeling in the Yagoua, Cameroon, sedimentary basin". Geofisica Internacional (2006), Vol. 45, Num. 2*, pp. 209-215.

APPLYING AVERAGING METHOD TO SOLVE UNREALISTIC TDEM DATA RESULT STATIC SHIFT CORRECTION IN MT DATA

Agus Sulistyo[1], Fikri Fahmi[1], Diajeng Liati[1], Fitrianita[1], Wambra Aswo N[1], and Yunus Daud[2]

[1]PT NewQuest Geotechnology, Pesona Khayangan Estate, DC12, Depok
[2]Master Program in Geothermal Exploration, Graduate Program of Physical Science, The University of Indonesia
Email: agus.sulistyo@newquest-geotechnology.com

ABSTRACT

Static shift effect is one of the problems that usually occur in Magenetotelluric (MT) data. It is caused by the existence of near surface inhomogeneity, topography and vertical contact. Due to galvanic distortion arising from near surface structures, the measured electric fields for the whole frequency range are affected by a constant shift on a log scale. The effect produces apparent resistivity curves with the correct shape but it is shifted to the upward and downward on the vertical logarithmic axes. In this decade, Time Domain Electromagnetic (TDEM) is commonly used for correcting static shift in MT measurements. It has been shown that magnetic fields are relatively unaffected by near surface structures that cause static shift in MT measurements. Jointly inverting TDEM and MT measurements has been found to be an effective way to deal with the static shift. However, sometimes TDEM curve has different trend with MT curve which causes both curves are not coincided smoothly in the high frequency. Consequently, the resulting MT curve from the static shift correction could give a less rational interpretation result. Therefore, one of the alternatives to conduct static shift correction when MT and TDEM curves has a different trend is using Averaging Method. The averaging method is a geostatistical method that uses the average value from all referenced MT stations to correct the station which affected by the static shift effect. The result from the averaging method represents a subsurface regional condition. Combination of TDEM and averaging method is effective enough for performing static shift correction and can produce realistic subsurface model. Comparison between 3-D MT inversion result and well data confirm that the static shift correction is important and should be conducted properly in MT data.

Keywords: Average method, TDEM, statistic shift correction.

INTRODUCTION

The magnetotelluric method is the most reliable method in geothermal exploration. MT method can be used to delineate reservoir geometry, cap rock and basement layer or plutonic body. The characteristics of geothermal area in Indonesia is located in the complex volcanic structure as well as rugged topography. This condition related to near surface inhomogeneity, topography effect and vertical contact often leads to static shift problem in MT data. The study of static shift effect has been much explained in (Jiracek, 1990; Sulistyo, 2015; Liati, et al., 2018). Static shift effect should be reduced, otherwise, it can influence the processing result and modelling of MT data, which finally affects the interpretation result and drilling recommendation. Therefore, the application of MT technology in geothermal exploration should be done properly.

MT method usually conducted jointly with TDEM method, where the TDEM method is only measured the magnetic fields which relatively unaffected by near surface structure. So, it can be used to correct the MT measurement. However, in several cases, TDEM result can not solve all the static shift problem which causing incompatibility with MT data. Accordingly, new approach is needed to be developed to reduce the static shift effect. A geostatictical method such as cokriging and averaging could become the other solutions to answer this problem. The previous study about cokriging and averaging methods has been done in (Sulistyo, 2015).

Furthermore, this paper focused on the application of TDEM and averaging methods to remove static shift effect of MT data. The averaging method is used when the TDEM data produce unrealistic result. Both methods are then applied in the real data. Moreover, the results are then compared in form of 3-D MT inversion and then confirmed by well.

STATIC SHIFT EFFECT ON MT DATA

Static shifts are defined as vertical displacements of the apparent resistivity sounding curves, between adjacent sites or between two curves at one site, without any other difference in either the shape of the curves or the phase (Xiao, 2004). As already explained previously, static shift effect is usually caused by near surface inhomogeneity, topography effect and vertical contact. Sulistyo, (2015) has perfomed several simulations of static shift effect phenomena in MT data through MT 2D Forward Modeling as shown in Figure 1. The modeling process is conducted by using MT2DFor-X software that is developed by PT. NewQuest Geotechnology.

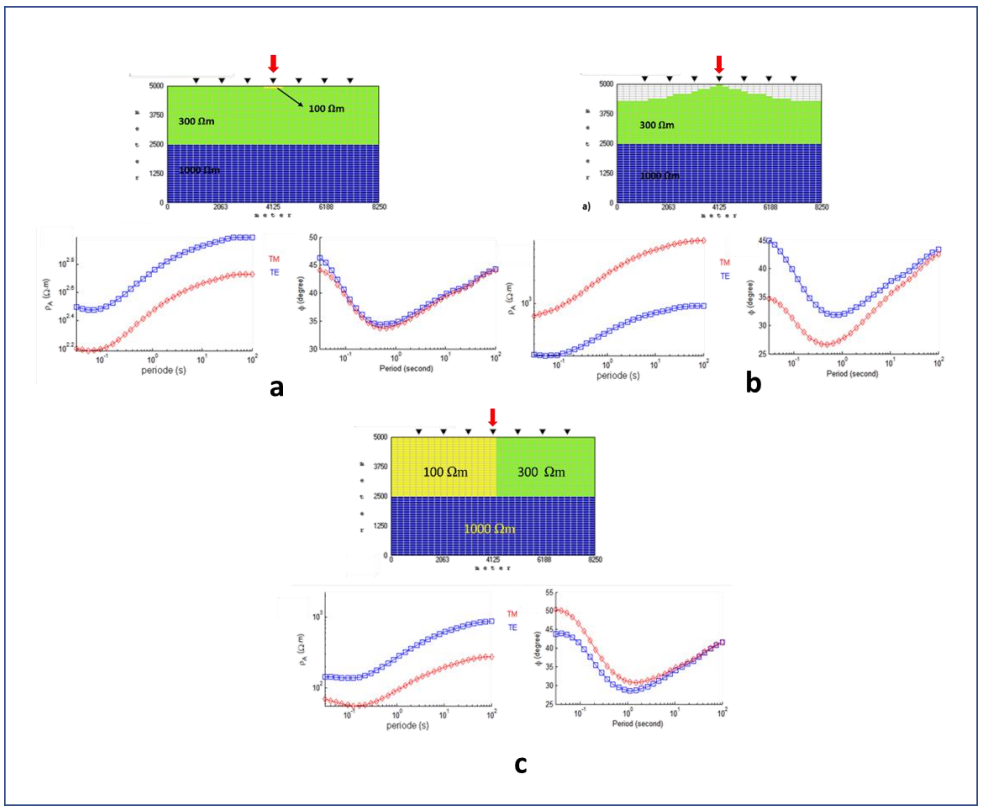


Figure1: Forward modeling of static shift phenomena a) near surface inhomogenity b) topographic effect c) vertical contact (modified after Sulistyo, 2015)

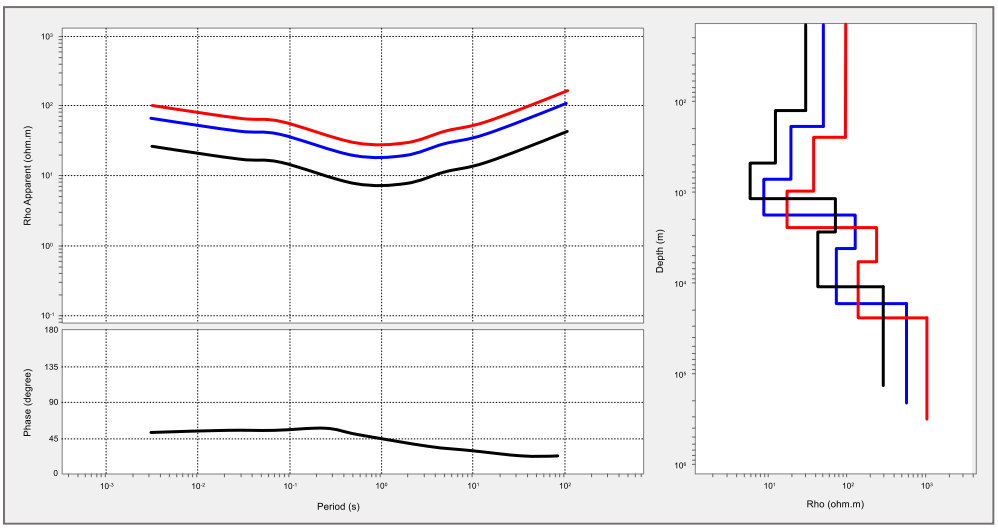


Figure 1. Static shift effect in MT interpretation

The forward modeling shows that the static shifts can severely distort the MT data. The static shift effect causes the MT curve shifted to upwards/downward, so that the curve doesn't describe the real condition of the subsurface. If the static shift effect is not handled properly, it can lead to misinterpretation of resistivity and depth values as shown Figure 1. Furthermore, it will influence the processing and modelling of MT data and guide to a wrong drilling recommendation.

TIME DOMAIN ELECTROMAGNETIC (TDEM)

Time Domain Electromagnetic (TDEM) is an active geophysical method using electromagnetic (EM) induction to determine shallow subsurface structure. It is commonly used for static shift correction.

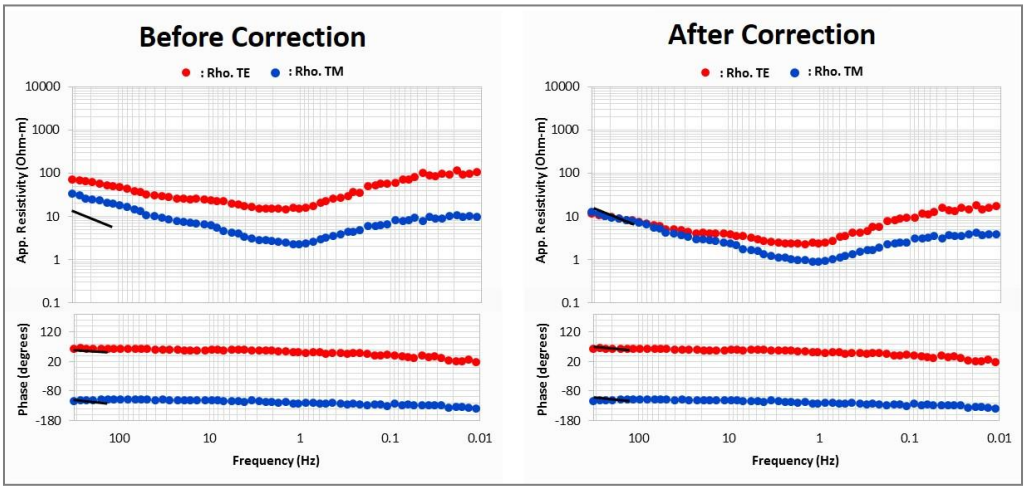


Figure 2. TDEM in MT data Correction

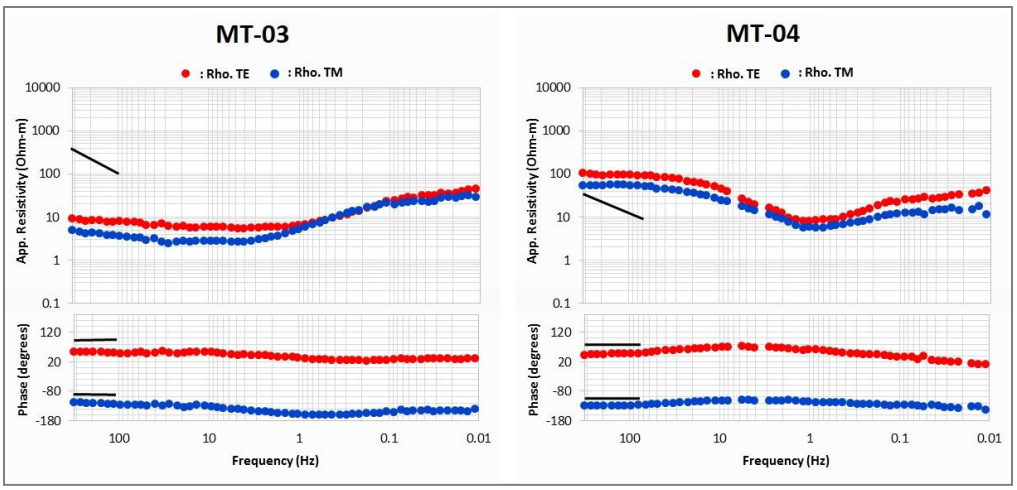


Figure 3. Mismatch between MT and TDEM data

TDEM data that passed field quality control check was processed and modeled to generate 1D inversion model. This data was converted to MT apparent resistivity curve. TDEM resistivity curve will be presented at the high frequency part of the MT curve. It will be used to correct the MT static effect (Irfan, et al., 2010). Static shift correction process in MT data by using TDEM is shown in Figure 2.

However, the used of TDEM for removing static shift effect often encounters a problem such as mismatch between TDEM dan MT data. The example of mismatch which is usually found is different trend curves of both data. Another problem is TDEM generates very different resistivity value with MT data as shown in Figure 4.

AVERAGING METHOD

Averaging method is done by using undisturbed MT data as references for calculating the average resistivity statistically in the high frequency range (associated with shallow depth) as shown in Figure 4. Appplication of averaging method has been clearly demonstrated in the Baikal Region (Berdhichesvsky & Dmitriev, 2008). They are close to the normal curve characterizing the regional background. By using the averaging method, it is assumed that the regional effect representing the subsurface condition will actually emerge after averaging.

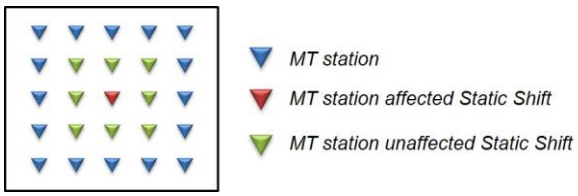


Figure 4. Averaging method in static shift correction

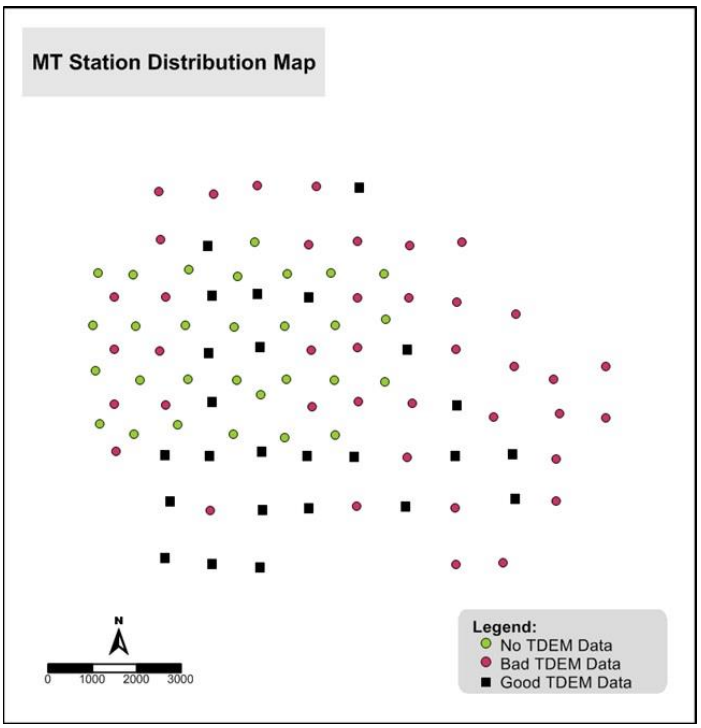


Figure 5. Distribution of MT data

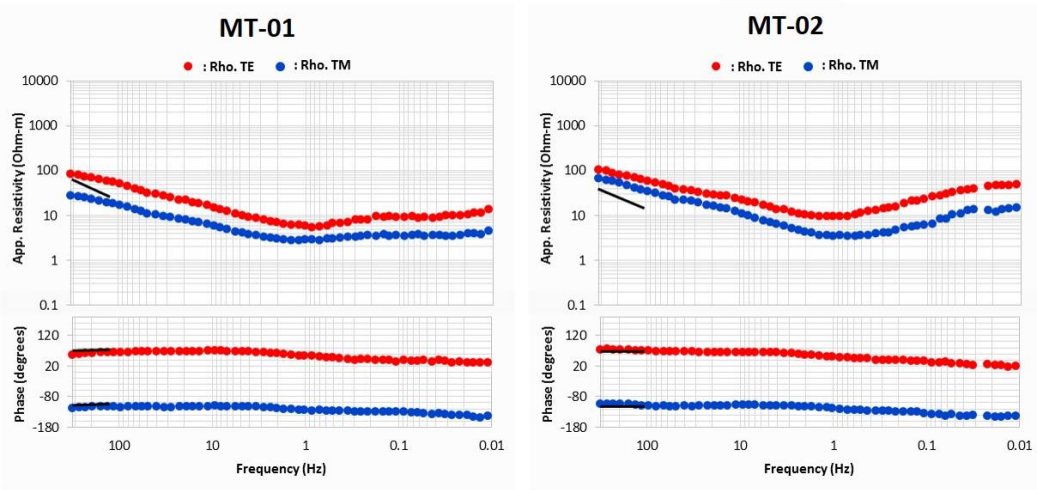


Figure 6. Good correlation between TDEM and MT data

APPLICATION TO REAL DATA

TDEM and averaging methods are applied for correcting MT real data acquired in geothermal area. The total of 94 MT data are distributed as shown in Figure 5. From 94 MT data, 27 data are not provided with TDEM data. The other 67 data consist of 25 good TDEM data and 42 bad TDEM data. Figure 7 shows the example of good correlation between TDEM and MT data. However, 42 bad TDEM data still have to be solved. To accomplish this unrealistic TDEM result, averaging method was applied. Furthermore, to find out the ability of averaging metod in eliminating the static shift effect, the corrected data were than conducted using 3D inversion. The 3-D inversion was carried out by MT3Dinv-X software developed by PT. NewQuest Geotechnology. Then the 3D MT inversion result of corrected data was compared with the other MT data which is not corrected from the static shift effect as shown in Figure 8. Both results show very different image of subsurface condition.

The 3-D inversion of MT data without static shift correction shows shallower and thinner low resistivity zone which is identified from the shallow depth of BOC (Base of Conductor) while 3D inversion result of corrected MT data shows deeper and thicker low resistivity zone.

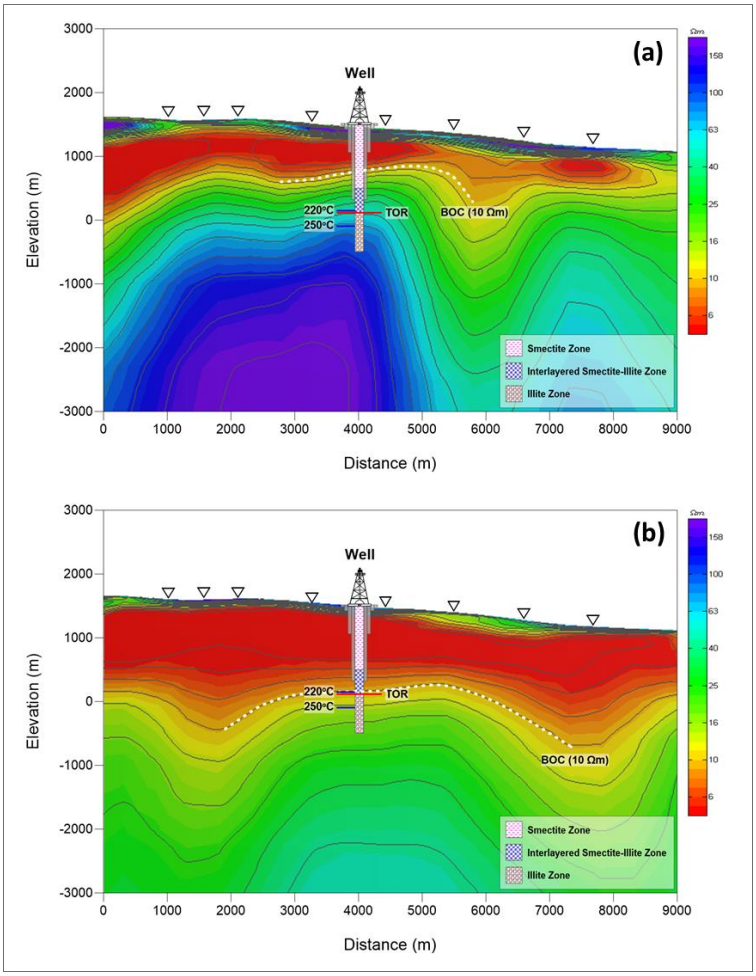


Figure 7. 3-D Inversion results : (a) without static shift correction and (b) with static shift correction.

Besides, 3D uncorrected data inversion result shows that the the posisition of the updome-shape which is interpreted as the heat source is located more to the left of the position of 3D corrected data inversion. Moreover, after confirmed by well, the 3-D inversion results have a good correlation with temperature and lithology of the well. It shows that static shift correction is one of the most important parts of MT data processing that could affect the interpretation result. Incorrect handling in static shift problem can lead to the wrong drilling recommendation as shown in Figure 8 (b).

DISCUSSIONS

Study to remove static shift effect has been attemped using TDEM and averaging method. Both correction has good ability but also has a limitation. Averaging method highly dependent on the MT data distribution of the influenced data by static shift effect and also the present of clean data. If there is no clean MT data which is unaffected by static shift effect, the Averaging method could not be applied since clean MT data is needed as references in correcting the influenced MT data. However, based on the results, Averaging method has been proven in eliminating the effect of static shift and give a good result in imaging the subsurface condition. Averaging method can be one good solution to overcome the absence of TDEM data as well as the unrealistic TDEM curve.

CONCLUSIONS

MT is one of the powerful method in geothermal exploration. Therefore, a proper way in applying this method must be well noticed in order to avoid mislead in delineating subsurface condition. Static shift effect plays important role in MT data processing. If it is not treated properly, it could affect further interpretation and also cause misleading in well targeting.

In delineating subusurface structure through 3-D inversion, there is a big difference between MT data which are corrected from static shift effect (using Averaging method) and uncorrected MT data. The 3D inversion result of uncorrected MT data could not recognize the real condition of geothermal system in this area. It is confirmed by the result which is not in accordance with the location of well. Otherwise, 3D inversion result of MT data which is corrected using Averaging method shows a good agreement with location of well.

ACKNOWLEDGEMENTS

The authors gratefully acknowledge management PT. NewQuest Geotechnology for supporting this research by providing the data, software and also for helpful discussions on this study.

REFERENCES

Berdhichesvsky, M. & Dmitriev, V. (2008), "*Model and method magnetotellturic"*. Berlin: Springer.

Irfan, R., Kamah, Y., Gaffar, E. & Ts.Winarso. (2010), "*Magnetotelluric Static Shift Correction Using Time Domain Electromagnetics Case Study: Indonesian Geothermal Rough Fields"*. Bali, World Geothermal Congress.

Jiracek, G. R. (1990), "Near surface and electromagnetic distortion in electromagnetic induction". Dalam: *Surveys In Geophysics.* Netherland: Kluwer Academic Publisher, pp. 163-203.

Liati, D., Sulistyo, A., Nuqramadha, W. A. & Daud, Y. (2018), "*Study of static shift correction for magnetotelluric (mt) data using averaging and cokriging methods upon 3-dimensional forward model of geothermal field"*. Bandung, IIGW.

Sulistyo, A. (2015), "*Koreksi Pergeseran Statik Data Magnetotellurik (MT) Menggunakan Metode Geostatistik Cokriging dan Averaging dibandingkan dengan data Time Domain Electromagnetic"*. Jakarta, IIGCE.

Xiao, W. (2004), "*Magnetotelluric exploration in the Rocky Mountain foothills, Alberta",* Edmonton: Universitas Alberta.

MATRIX PERMEABILITY CONTRIBUTION IN X-1 EXPLORATION WELL

Hendy Sujarmaitanto, Ricsen Halomoan, and Timbul H. Silitonga

PT. Pertamina Geothermal Energy
Skyline Building 19th Floor Jl. MH. Thamrin no. 9 Jakarta 10340 Indonesia
Email: Hendy.S@pertamina.com

ABSTRACT

Permeability is the main target in every exploration geothermal well. Usually the main target in drilling is secondary permeability that controls the permeability of the reservoir itself and generally it is indicated by structural geology on the surface. In the other hand, the fact that primary permeability also contribute to become a potential pathway of the reservoir fluid can't be ignored. Moreover, in some condition primary permeability takes an important role in reservoir permeability. However, it's kind of difficult to be identified, because it is formed in the same time with the lithology and not visible from the surface. So that required a good knowledge and comprehensive data to get a distribution pattern. Well X-1 evaluation results showed that the primary permeability had more significant contribution than secondary permeability. The result of FMI, DSI, PLT, drilling loss zone and PT test integrated analysis supported with the evidence of epidote presence and silicification along the zone characterizing a good permeability so that hydrothermal fluid can pass through this zone. Expected Permeability zone which contributes as the feedzone can be divided based on spinner response and PT test. In well X-1 the permeability can be categorized in two kind of permeabilities, Secondary and primary permeability. The secondary permeability was associated with structural geology, while the primary permeability was resulted from matrix permeability. Secondary permeability was formed in Andesite with high intensity Continuous Conductive Fracture (CCF) and Discontinuous Conductive Fracture (DCF) with N(North) – S(South) orientation and Minor – Moderate PLT response in 9-7/8 inch hole section. Whereas the primary permeability was formed in Andesite Breccia with low intensity Continuous Conductive Fracture (CCF) and Discontinuous Conductive Fracture (DCF), scatter orientation and Moderate – Major PLT response in 12-1/4 inch hole section. The lateral distribution of this permeability which is potential as a feedzone will be confirmed by PTS Flowing test. As the result, the secondary permeability is not the only reliable permeability in geothermal reservoir however the matrix permeability of the rock can strongly contribute as a permeable zone and also a good option for well targetting.

Keywords: Permeability, feedzone, PTS, well targetting.

INTRODUCTION

Well X-1 was one of the exploration wells in PT. Pertamina Geothermal Energy. The well was located in Sumatra Island. Volcanism activity in Sumatra was generated by a subduction between Eurasian plate and Indo-Australian plate in a shallow depth. Geothermal system generally was controlled by regional fault system called "Great Sumatran Fault". This dextral strike-slip fault zone accomodated a good secondary permeability to the geothermal reservoir.

Beside the secondary permeability, there is also primary permeability. In certain circumstances it also contributes for a good reservoir fluid pathway.

This study based on several data consisting of drilling cutting and core sample, FMI, DSI, Spinner response, drilling loss zone and PT test, correlated in order to describe the subsurface condition especially in permeability which controlled the reservoir fluid pathway.

DATA ANALYSIS

Several methods were used to analyze the drilling cuttings and cores sample including binocular analysis of the drilling cuttings sample at the well, petrographic microscope analysis of thin sections, X-ray diffraction to qualitatively identify individual minerals, especially clays, and fluid inclusion analysis for determination of homogenization temperature of fluids trapped in host mineral in the rock.

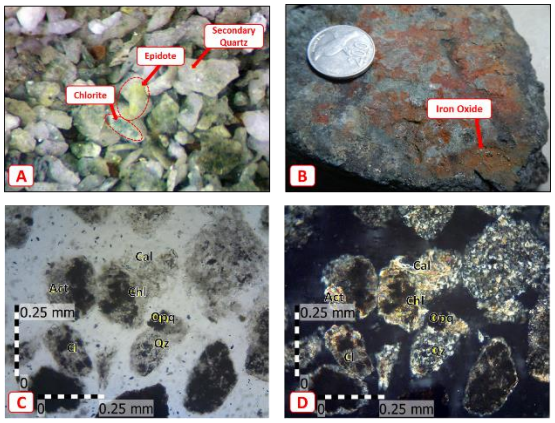


Figure 1: (A) Cutting Sample on Altered Andesite at 2007 mD, (B) Core Sample Iron Oxide on Andesite Breccia at 2663 mD, Thin Section Sample Plane-polarised (C) and cross-polarised (D) showed Highly Silicification on Tuff at 1839 mD, dominated with Quartz and others alteration mineral such as Actinolite, Chlorite, Calcite and Opaque.

RESULTS

Lithology

Drilling cuttings sample and thin section analysis were used for determination of the lithology unit in Well X-1. The analysis were done at the rig site where the samples were analysed using binocular microscope and confirmed later in the laboratory using thin section analysis. The result showed that the lithological of the well dominantly composed of andesite, andesite breccia and tuff .

Hydrothermal Alteration and Mineral Distribution

The distribution of hydrothermal minerals (Figure 2) in well X-1 is described below:

Table 1: Distribution of Hydrothermal Alteration Mineralogy of Well X-1

DEPTH (mD)	LITHOLOGY	THIN SECTION ANALYSIS											XRD ANALYSIS	VEIN	Alteration Degree	NB	ALTERATION ZONE
		SECONDARY MINERAL (%)															
		Cal	Qz	Cl	Chl	Ep	Opq	Ser	Act	Fe-Ox	Zeo	Alu	Bio	Py						
1340	Tuff	7	5	10	5	4	3	3	3	4	-	2	-	16	Chlorite, Quartz, Plagioclase, Pyrite	Cal	Moderate		High Temperature Prophylithic
1440	Andesite Breccia	7	10	15	5	3	3	-	-	4	-	-	-	11	Chlorite, Quartz, Plagioclase, Anhydrite, Pyrite	Qz, Cal	Moderate		High Temperature Prophylithic
1539	Tuff	2	60	5	3	2	2	2	-	2	-	-	-	2	Chlorite, Quartz, Plagioclase, Pyrite	Qz dominated	Very Strong	Silicification	High Temperature Prophylithic
1638	Andesite Breccia	3	40	5	3	2	3	25	2	-	-	-	-	7	Illite, Quartz, Plagioclase, Anhydrite, Pyrite		Very Strong	Silicification	Phyllic
1743	Andesite Breccia	2	50	4	2	-	2	20	3	-	-	-	-	<1	Illite, Quartz, Plagioclase, Anhydrite, Pyrite		Very Strong	Silicification	Phyllic
1839	Andesite Breccia	3	55	4	2	-	2	15	4	2	-	-	-	4	Illite, Quartz, Plagioclase, Pyrite		Very Strong	Silicification	Phyllic
1905	Andesite Breccia	3	45	3	-	-	2	10	4	-	-	15	-	7	Illite, Quartz, Plagioclase, Wairakite, Pyrite		Very Strong	Silicification	Phyllic
2001	Andesite	7	25	2	2	2	5	-	1	-	-	-	-	7	Illite, Chlorite, Quartz, Plagioclase, Pyrite		Moderate	Silicification	High Temperature Prophylithic
2100	Andesite	4	55	5	2	2	5	2	1	2	-	-	-	7	Illite, Chlorite, Smectite, Quartz, Plagioclase, Anhydrite, Pyrite		Very Strong	Silicification	Pottasic
2171	Andesite	2	50	3	5	-	5	-	-	4	-	-	10	-	-	Cal	Very Strong	Silicification	Pottasic
2172	Andesite	2	55	5	3	1	5	-	-	2	-	-	6	-	-	Qz	Very Strong	Silicification	Pottasic
2173	Andesite	16	20	7	8	-	5	10	-	2	-	-	-	-	-		Strong	Silicification	Phyllic
2174	Andesite	2	55	-	3	1	5	2	-	2	3	-	6	-	-	Qz	Very Strong	Silicification	Pottasic
2175	Andesite	3	55	-	3	1	3	2	-	2	-	-	7	-	-	Qz	Very Strong	Silicification	Pottasic
3012	Andesite	25	20	5	-	-	5	20	-	-	-	-	-	-	-	Qz	Very Strong	Silicification	Phyllic
3014	Andesite	40	20	1	-	-	5	30	-	-	-	-	-	-	-		Very Strong	Silicification	Phyllic

Some of high temperature minerals were found in well X-1, such as epidote, sericite and actinolite. Epidote first appears at 1182 mD. The mineral is identified from rock cuttings by its yellow to greenish yellow colours. Epidote tends to form under a rather restricted temperature range, generally above 200^0 C (Reyes, 2000). Sericite first appears at 500 mD and identified from thin section, it is colourless and replacing the fragment and the matrix. The presence of sericite indicates temperature more than 270^0 C (Reyes, 2000). Actinolite is also identified from thin section and first appears at 1149 mD, it is colourless and replacing the matrix. Actinolite tends to form in temperature above >290^0 C (Utami,2005)

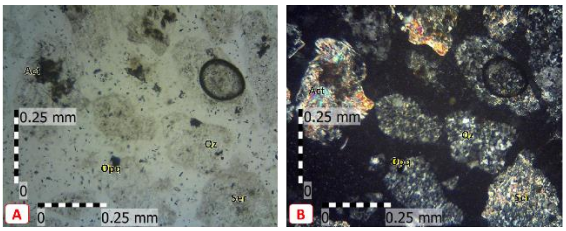


Figure 2: Thin Section Sample Plane-polarised (A) and cross-polarised (B) showed Highly Silicification on Tuff at 1743 mD, dominated with Quartz and high temperature alteration mineral such as Actinolite and Sericite.

Indicator mineral for permeability such as wairakit first present at 1101 mD, analysed using thin section analysis. The presence of calcite, iron oxide and abundance of pyrite also indicate a good permeability zone (Lagat, 2007). At several depth, hydrothermal alteration mineral are observed in the veins. Calcite and quartz vein suggesting the zone is fractured and highly permeable.

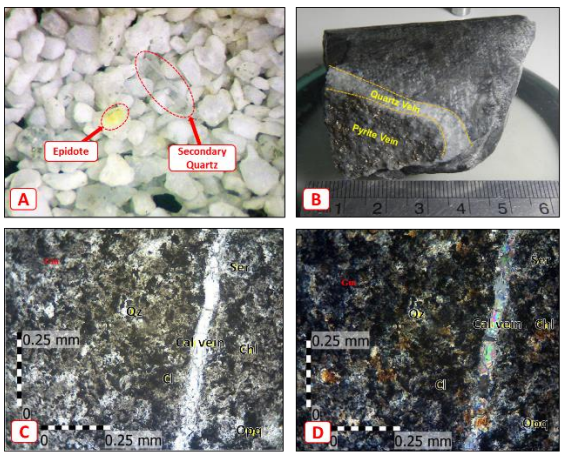


Figure 3: (A) and (B) Core Sample Quartz and Pyrite vein on Altered Andesite at 3012 mD, Thin Section Sample Plane-polarised (C) and cross-polarised (D) showed Calcite Vein on Tuff at 2173 mD.

Alteration degree start from 1539 mD marked by highly intensity of alteration. Silicification process is dominant until the bottom hole.

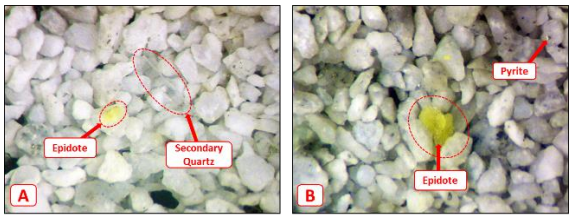


Figure 4: (A) and (B) Cutting Sample: Silicification on Altered Andesite at 1845 mD and 1923 mD

Hydrothermal Alteration Zones

The distribution of the hydrothermal minerals with depth in well X-1 is dependant on temperature, because they are formed at specific temperatures in a geothermal system. In this well the mineralization pattern shows five distinct zones as shown in Table. The top zone is the Argillic zone, dominated with clay minerals-chlorite-calcite-quartz. XRD result showed the clay minerals consist of halloysite and smectite, the zone extends from 54 – 402 mD. This is the lowest grade mineral alteration zone indicating temperature range of >120^0 C. The second zone is the Propylitic Low Temperature Zone, dominated with chlorite-sericite-quartz-calcite. The zone extends from 500 – 1101 mD suggesting the formation temperature range 270 - 310^0 C. The third zone is the Propylitic High Temp Zone, dominated with chlorite-quartz-calcite-epidote-actinolite. The zone extends from 1149 – 1539 mD and it is characterized by abundance of epidote and actinolite suggesting the formation temperature range 300 - 340^0 C. The fourth zone is the Phylic Zone, dominated with sericite-calcite-quartz. The zone extends from 1638 – 1905, 2173 and 3012 – 3014. The zone is marked by the appearance of sericite suggesting the formation temperature above 270^0 C. The fifth zone is the Potassic Zone, dominated with quartz-biotite-actinolite-chlorite. The zone extends from 2171 – 2176. The zone is marked by the presence of biotite suggesting the formation temperature above 310^0 C.

Permeable Zones

The integrated study performed between FMI data, Sonic, PLT, Mineral Indicator for permeability, drilling loss zone and PT survey is used to determine a potential permeable zone.

Structural interpretation includes identifying and determining the orientation of features using the FMI image. Open fractures have a dark appearance on the image due to invasion by conductive drilling mud. Conductive fracture are well developed over the entire interval. Conductive fractures were subdivided into continuous conductive fracture (CCF) and discontinuous conductive fracture (DCF). In 12-1/4 hole section both continuous and discontinuous conductive fracture strongly demonstrate NNE-SSW orientation. In 9-7/8 hole section both continuous and discontinuous conductive fracture strongly demonstrate N-S orientation (see Figure 5).

Table 2: Hydrothermal Alteration Zone of Well X-1

Depth (m)	Alteration	Temp Range (^{0}C)
54 - 402	Clay – Chlorit – Calcite-Quartz (Argillic)	>120^0 C
500 - 1101	Chlorite-Sericite-Quartz-Calcite (Propylitic Low Temp)	270^0 - 310^0 C
1149 - 1539	Chlorite-quartz-Calcite-Epidote-Actinolite (Propylitic High Temp)	300^0 - 340^0 C
1638 – 1905, 2173, 3012-3014	Sericite-Calcite-Quartz (Phyllic)	>270^0 C
2171- 2176	Quartz-Biotite-Actinolite-Chlorite (Potassic)	>310^0 C

PLT response in 12-1/4 hole section shows at interval 1824.8 – 1848.9 mD correspond with moderate injection 13.34% intake. It is possibly associated with matrix porosity of andesite breccia without a continuous conductive fracture (CCF) and discontinuous conductive fracture (DCF) formed in this interval.

PLT response in 12-1/4 hole section shows at interval 1891.4-1995.7 mD correspond with major injection 48.05% intake. It is possibly associated with matrix porosity of andesite breccia with a scatter orientation of continuous conductive fracture (CCF) and discontinuous conductive fracture (DCF) in this interval.

PLT response in 9-7/8 hole section shows at interval 2423-2443.8 mD (1.18% intake), 2485.6 – 2514.1 mD (2.14% intake), Both conductive fracture are well developed. Continuous conductive fracture (CCF) strongly show N-S strike and discontinuous conductive fracture (DCF) dominantly show NNW-SSE strike. Depth interval 2629 – 2632 mD (0.15% intake), correspond with minor injection Continuous conductive fracture (CCF) mainly show NNE-SSW strike and discontinuous conductive fracture (DCF) dominantly show NNE-SSW strike associated in Andesite.

At depth intervals 2745.6 – 2830 mD and 2896.3 – 2957.6 mD Continuous conductive fracture (CCF) and Discontinuous conductive fracture (DCF) strongly demonstrate NNW-SSE strike, associated with andesite and correspond with 12.16% and 16.88% moderate injection of PLT data.

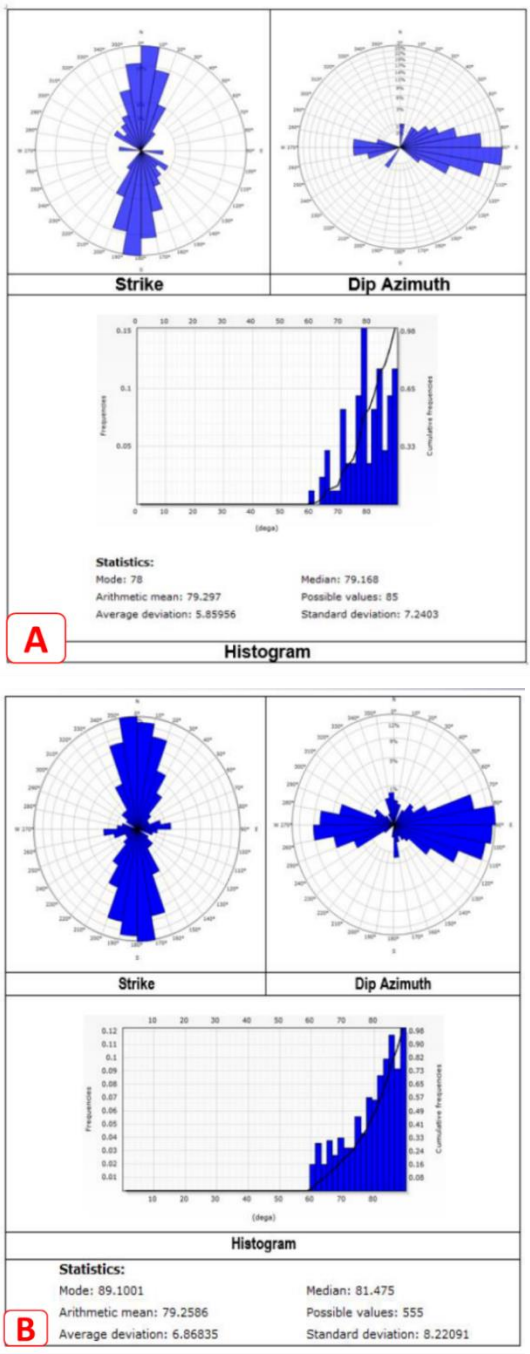


Figure 5: (A) 12-1/4 section hole showed NNE-SSW orientation for CCF & DCF (B) 9-7/8 section hole showed N-S orientation for CCF & DCF

Table 3: CCF & DCF fracture orientation

Depth (m)	Intake (%)	Injection	Fracture Orientation
1824.8 - 1848.9	13.34	Moderate	No CCF & DCF
1891.4 - 1995.7	48.05	Major	CCF show scattered strike
2423 - 2443.8	1.18	Minor	CCF strongly show N-S strike
			DCF dominantly show NNW-SSE strike
2485.6 - 2514.1	2.14	Minor	CCF strongly show N-S strike
			DCF dominantly show NNW-SSE strike
2629 - 2632	0.15	Minor	CCF mainly show NNE-SSW strike
			DCF dominantly show NNE-SSW strike
2745.6 - 2830	12.16	Moderate	CCF and DCF show NNW-SSE strike
2847.1 - 2883.2	6.11	Minor	CCF and DCF show NNW-SSE strike
2896.3 - 2957.6	16.88	Moderate	CCF and DCF show NNW-SSE strike

A potential interval at depth 2847.1 – 2883.2 mD associated with Continuous conductive fracture (CCF) and Discontinuous conductive fracture (DCF) in Andesite. They strongly show NNW-SSE strike and correspond with 6.11% minor injection of PLT data.

Drilling Loss Zone

12-1/4 hole section already entered the reservoir zone, marked by the existence of loss circulation zone, either Partial Loss Circulation (PLC) or Total Loss Circulation (TLC). The first PLC was occure at depth 1491 – 1498 mD, with rate 0.3 – 0.4 BPM. Then the rate tends to enlarge to 6-7 BPM, from 1498 – 1506 mD. The first TLC occurs in depth 1926-1946 mD with rate 19 BPM. Total Loss Circulation condition continues in 9-7/8 hole section with rate >18 BPM until the Total Depth (TD)

Integrated Analysis

As the result, the entire study interval was divided into eight (8) permeable zones as listed below (see Figure 6) :

- Permeable Zone 1 (1824.8 – 1848.9 m)
- Permeable Zone 2 (1891.4 – 1995.7 m)
- Permeable Zone 3 (2423 – 2443.8 m)
- Permeable Zone 4 (2485.6 – 2514.1 m)
- Permeable Zone 5 (2629 - 2632 m)
- Permeable Zone 6 (2745.6 - 2830 m)
- Permeable Zone 7 (2847.1 – 2883.2 m)
- Permeable Zone 8 (2896.3 – 2957.6 m)

PERMEABILITY TYPE

Secondary Permeability

From the Integrated Data Analysis, permeable zones in Well X-1 can be divided into eight (8) permeable zones. Six of eight permeable zones (Permeable zone 3 – 8), was classified as a Secondary Permeability which associated with structural geology. Secondary permeability was formed in Andesite with high intensity Continuous Conductive Fracture (CCF) and Discontinuous Conductive Fracture (DCF) with dominantly N(North) – S(South) orientation correspond with a good sonic response, associated with presence of loss zone and Minor – Moderate PLT response in 9-7/8 inch hole section.

Primary Permeability

Two permeable zones (Permeable Zone 1 & 2) indicates a primary permeability, this zone was a resulted from matrix permeability which is formed on the Andesite Breccia. Minor CCF and DCF correspond with good sonic response associated with presence of loss zone and Moderate – Major PLT response in 12-1/4 inch hole section. Mineral indicator for permeability also can be found in this

zone, such as wairakite associated with silicification. The integrated study performed between FMI data, Sonic, PLT, Mineral Indicator for permeability, drilling loss zone and PT survey is used to determine a potential permeable zone.

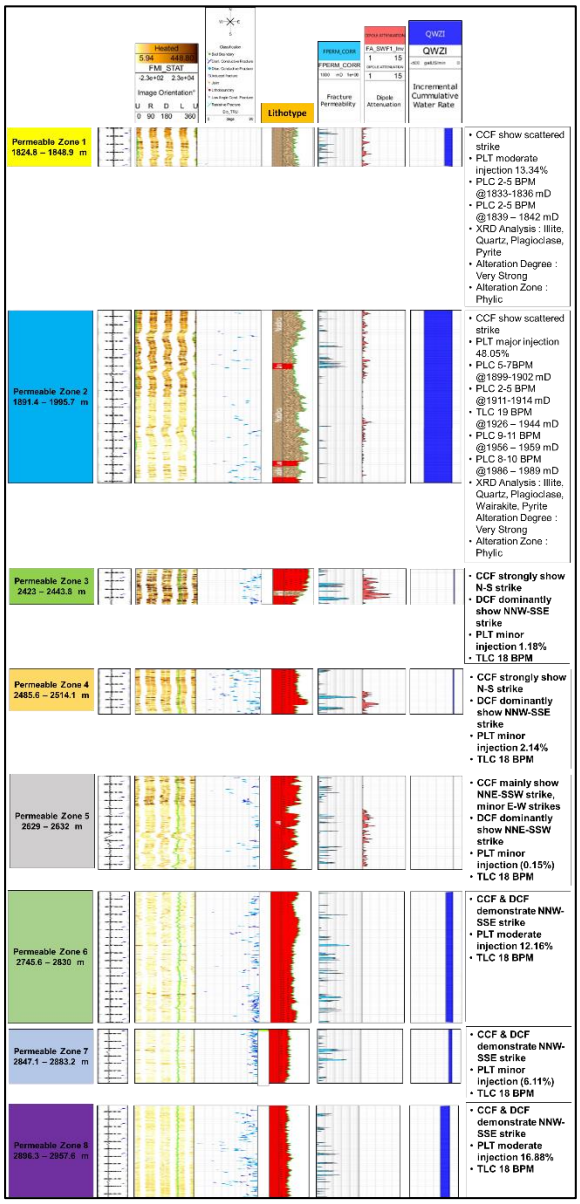


Figure 6: Permeable Zones in Well X-1 from Integrated Data Analysis

DISCUSSION

In well X-1 the permeability can be categorized in two kind of permeabilities, Secondary and primary permeability. The secondary permeability was associated with structural geology, while the primary permeability was resulted from matrix permeability. Secondary permeability was formed in Andesite with high intensity Continuous Conductive Fracture (CCF) and Discontinuous Conductive Fracture (DCF) with N(North) – S(South) orientation and Minor – Moderate PLT response in 9-7/8 inch hole section. Whereas the primary permeability was formed in Andesite Breccia with low intensity Continuous Conductive Fracture (CCF) and Discontinuous Conductive Fracture (DCF), scatter orientation and Moderate – Major PLT response in 12-1/4 inch hole section. The lateral distribution of this permeability which is potential as a feedzone will be confirmed by PTS Flowing test. As the result, the secondary permeability is not the only reliable permeability in geothermal reservoir. However, the matrix permeability of the rock can strongly contribute as a permeable zone and also a good option for well targetting.

CONCLUSION

The lithology of Well X-1 is composed of dominantly Andesite Breccia and Andesite. Hydrothermal alteration and mineral distribution in this well showed that some of high temperature minerals were found in well X-1, such as epidote, sericite and actinolite. Indicator mineral for permeability such as wairakit also present in Well X-1. At several depth, hydrothermal alteration mineral are observed in the veins. Calcite and quartz vein suggesting the zone is fractured and highly permeable. As the final result, Well X-1 can be divided into eight (8) permeable zones, Permeable Zone 1 (1824.8 – 1848.9 m) , Permeable Zone 2 (1891.4 – 1995.7 m) , Permeable Zone 3 (2423 – 2443.8 m) , Permeable Zone 4 (2485.6 – 2514.1 m) , Permeable Zone 5 (2629 - 2632 m), Permeable Zone 6 (2745.6 - 2830 m), Permeable Zone 7 (2847.1 – 2883.2 m), and Permeable Zone 8 (2896.3 – 2957.6 m). Six of eight permeable zones (Permeable zone 3 – 8), was classified as a Secondary Permeability which associated with structural geology and Two permeable zones (Permeable Zone 1 & 2) indicates a primary permeability, this zone was a resulted from matrix permeability.

REFERENCES

Lagat, Jhon. (2007), *"Hydrothermal Alteration Mineralogy in Geothermal Fields with Case Examples From Olkaria Domes Geothermal Field, Kenya"*. Proceedings, Short Course II on Surface Exploration for Geothermal Resources. UNU-GTP and KenGen, Lake Naivasha, Kenya, November 2-17, 2007.

Reyes, G. Agnes. (2000), *"Petrology and Mineral Alteration in Hydrothermal Systems"*. From diagenesis to volcanic catastrophes. UNU-GTP, Orkustofnun, 2000.

MICRO SEISMIC STUDY IN PATUHA GEOTHERMAL FIELD

Akhmad Fanani Akbar[1], Reza Jamil Fajri[1], Chevy Iskandar[1],
Randy Wijaya Atmaja[1], Elfina[1], and Andri Dian Nugraha[2]

[1]PT Geo Dipa Energi Persero, Recapital Building 8th Floor, Jl. Aditiawarman Kav 55, Jakarta
[2]Institut Tekonologi Bandung, Jalan Ganesha 10, Bandung
Email: akhmad@geodipa.co.id

ABSTRACT

Micro seismic monitoring had been conducted from January 1st until later April 4st 2018 in Patuha Geothermal Field using 9 seismometers (3 channels & sampling rate 200 sps) that are placed near well locations and fault distribution. The objective of this study is to identify permeable areas, pattern of reinjection fluid, and production activity. 654 micro seismic events (ts-tp < 3 second) and 640 regionals (ts-tp > 5 second) was identified in this period, but only 491 micro seismic events have clear onset of P and S waves arrival time. The initial location of the hypocenter was determined by using a nonlinear algorithm (NonLinLoc software) based on a velocity model obtained from another geothermal field. All hypocenter location and 1-D velocity model have been simultaneously updated using Velest software. In general, the distribution of micor seismic event locations is scattered around the Patuha geothermal field. Some clusters of micro seismic events are located beneath a fault and production wells, while the other cluster is located beneath injection well. Micro seismic events are distributed at depth of 0 – 500 masl. The Brune model was implemented to calculate the moment magnitude Mw of the micro seismic events in Patuha geothermal field. Many of the micro seismic events were detected with magnitudes ranging from -1<Mw<1.5. The focal mechanism solution is highly heterogeneous while we used 67 selected events with minimum uncertainty.

Keywords: Patuha geothermal field, micro seismic, hypocenter, focal mechanism, velocity, magnitude.

INTRODUCTION

Patuha Geothermal Field is in three districts, Bandung, West Bandung, and Cianjur, West Java Province, Indonesia. Thermal manifestations such as fumaroles, hot springs, warm springs, and mud pools are found throughout this field. Based on the Commercial Operation Date (COD) on September 2014, Patuha was able to produce 55 MW.

Unfortunately, the performance of production well showed that is has been declining for the last 3 years, causing it hard to sustain its production at 55 MW as it was initially commissioned. Injection management should be carried out to help solve this matter. One of the methods to support this is by conducting micro seismic monitoring as it is believed to give an illustration of the fluid movement in the hydrothermal system. Based on previous practices, distributing of seismometers on geothermal field can be used for reservoir monitoring. The main objectives of this study is to contribute in imaging and monitoring the hydrothermal system activities. Focusing especially in production & injection well monitoring, and permeable fault identification.

This is the first time for a micro seismic study to be carried out on Patuha Geothermal Field. As there has been no previous study on earthquake activities specifically around this area, it has been a challenging project for us to do this study. Our strategy to obtain the best recording data is by distributing the location of seismometers in possible area for micro seismic events to occur. 9 seismometers have been deployed on several locations around injection wells, production wells, and fault areas. In hoping to detect micro seismic events from injection & production activities and identifying permeable faults.

DATA & METHODOLOGY

Seismometer Network

Six seismometers have been deployed since January 1st, 2018 in Patuha Geothermal Field (Figure 1, indicated by red squares). As additional seismometer, we deployed 3 seismometers since 4th January 2018 and 2 additional seismometers since 4th February 2018. All seismometer is deployed until 4th April 2018.

All station additional seismometer has similar physical installation design (post hole seismometer), including its instrument box, and GPS antenna, except the last additional seismometers is surface type. Every station consists of a three-component high-resolution borehole seismometer type IESE S31f-2 with natural frequency of 2 Hz. It is equipped with RefTek RT130 data logger with 3 high resolution channels, sampling rate of 1-1000 sps, and storage capacity until 8 GB. The S31f-2 is deployed as a shallow posthole sensor for use in micro seismic detection and analysis. The S31f-2 is designed for installation up to 100 m vertical holes, for this study we installed it at depth of 3-4 m. While the data logger, battery, and GPS were placed inside the metal box (Figure 2). For the two additional stations used surface seismometer with specification

Guralp 6TD integrated seismometer and digitizer and using 12 V accu battery 100ah as power source.

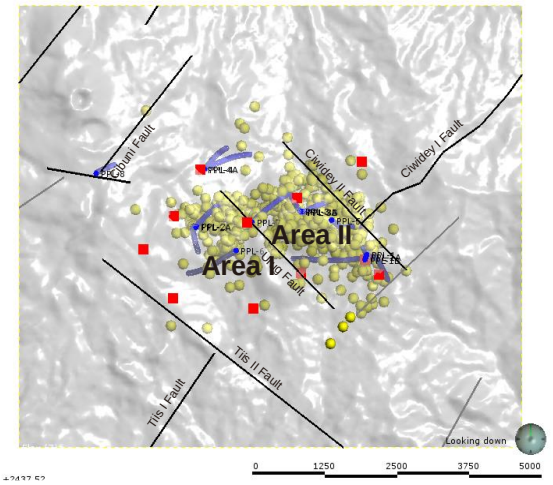


Figure 1: Distribution of 491 micro seismic events (yellow circles) with fault lines (black lines) and fault lines prediction (remote sensing) from previous study (modified after Pradipta, 2016).



Figure 2: Detail set up of seismometer station. Data logger, battery, & GPS placed inside the metal box (top left). Seismometer IESE S31f-2 (top right). surface seismometer and recorder deployed on concrete, (left bottom) cables, gps, and battery as power source (right bottom)

The spacing between stations is around 1 km with network coverage of injection wells, production wells, and faults at Patuha Geothermal Field. It aims to detect micro seismic events and regional earthquakes to delineate structures in Patuha Geothermal Field. In first week of acquisition data, we do analysis signal to noise ratio to evaluate our station network deployment. *Signal*-to-noise ratio (SNR or S/N) is a ratio to measure how much signal has been corrupted by the background noise. SNR can be defined as the *signal power* to *noise power* ratio. The signal radiated by the source is weakened and distorted by geometric spreading and attenuation and due to reflection, diffraction, mode conversion, and interference during their travel through the Earth (Bormann, P. et al, 2012). Based on the signal to noise ratio result we move a seismometer and it also used as reference to deploy two additional seismometers.

Micro Seismic Identification

The P-and S-wave arrival times of events were picked manually to obtain high quality data using Seisgram2K v.60 (Lomax, 2006). In this study, the time difference between the P- and S- waves (ts-tp) that has values less than 3 second of event are classified as micro seismic events. 654 micro seismic events and 670 regional events (Ts-Tp > 3 second) was identified during January 1st, 2018 until April 4th, 2018, but 491 micro seismic events have clear onset of P and S waves arrival time. After we identified the micro seismic events (figure 3), we then determine the P- and S-waves. The onset of P-wave arrival time can be easily determined by observing the data on the vertical component (Z). While determining the S-wave arrival times sometimes require band pass filter and transform it into frequency domain to enhance the accuracy of wave picking. After we picked the onset of P- and S-waves arrival times, the travel time of P- and S-waves are plotted in a Wadati diagram. The best determination of P- and S-waves arrival time is represented by a linear trend line. 5,548 and 5,352 for P and S arrival phases successfully identified to determine hypocenter location.

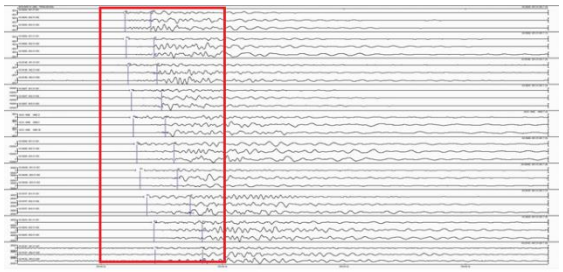


Figure 3: 10 seismographs 3-component records of a micro seismic. Vertical lines indicate arrival times for P and S waves that are manually picked. The red box shows time-window 2 seconds. The seismograms show the three components (one vertical and two horizontal) recorded at 10 stations.

Hypocenter & 1D Velocity Determination

In some micro seismic studies, the hypocenter location is biased to its condition because the

inversion results are trapped in pitfall condition (minimum local) and unknown initial 1D velocity model. To accommodate this condition, we use nonlinear inversion. NonLinLoc is a free software package for nonlinear locating earthquakes (Lomax et al., 2001). It supports a grid search method and two non-linear search methods. The advantage of using NonLinLoc is its ability to map the complete probability density function (PDF) of the earthquake location, detecting multiple minimal in the PDF, 1D and 3D models for location, solution quality assessment through non-linear error estimates, and Gaussian error estimates.

Beside the onset of P- and S- wave arrival time, as input, velocity model is also needed to determine hypocenter location. But since this is the first time of a micro seismic study to be conducted in Patuha Geothermal Field, we do not have an initial velocity model. We used a velocity model obtained from micro seismic study of another geothermal field located nearest from Patuha, Wayang Windu Geothermal Field, (Palgunadi, 2017). This model obtained from 45 seismometers network that is not only around Wayang Windu Geothermal Field, but also around Darajat, Kamojang, and Papandayan area.

After the initial hypocenter location is determined from NonLinLoc results, we then tried to construct a 1-D velocity model of Patuha Geothermal Field. This model was carried out to simplify the subsurface condition. The 1-D velocity model is created to determine the hypocenter location and as an initial velocity model for seismic tomography (Kissling et al., 1994). One of the methods used to determine the 1-D velocity model was the coupled velocity-hypocenter method using the VELEST software program version 3.1 (04/10/95) (Kissling, 1995).

VELEST used joint hypocenter-velocity method to relocate micro seismic events, seismic wave velocity model determination used for subsurface 1-D imaging, and station correction are done simultaneously using Geiger method. The number of model parameters (m) is 5 + N, (x, y, z, t, station corrections, and N is the number of 1-D velocity model layers). As a first step, the parameters are defined with focal m_0 (x, y, z, t_0), and seismic wave velocity model (1-D). The next step conducting ray tracing of earthquakes to obtain Tcal (travel time calculation). Inverse modelling can be used by completing damped matrix least square approach [At A + L] (A = matrix Jacobi, Jacobi matrix At = Transpose; L = damping matrix). Using the value of damping will affect the value of the perturbation parameter model (Δm). The relationship between the magnitude of the damping and the value of Δm is the opposite. Results of inverse modelling are in the vector of improved parameter model (Δm), which consists of the hypocenter and velocity model. In the next step, it is used in forward modelling as input. In the iteration, there is an RMS value between the observation and calculation travel times, so the iterations number can be set up to the expected RMS.

Moment Magnitude

The micro seismic signal is not only signal from ground motion but also it is affected by instrument response. It is very important to separate the instrument correction with ground motion signal before determining micro seismic magnitude.

The Brune model was implemented to calculate the moment magnitude M_w of the micro seismic events. This model is applicable to all types of earthquakes and allows an estimation of the source radius and stress drop. Moment magnitude is defined as:

$$M_w = \frac{2}{3}\log M_0 - 6.07$$

M_0 is the seismic moment in Newton meters. It can be calculated by fitting the frequency spectrum of displacement of a seismic signal to the theoretical source spectrum $S_0(f)$ of the Brune model (Brune, 1970), which is defined as:

$$S_0(f) = \frac{\Omega_0}{\left[1+(f/f_c)^{\gamma n}\right]^{1/\gamma}}$$

where Ω_0 is the long-period amplitude, f_c is the corner frequency, $n = 2$, and $\gamma = 2$ is high-frequency source-spectral roll-off.

The first step is to obtain Ω_0 and f_c for each microseismic event by applying spectral fitting. To begin with, for a single event, the P phase of each recording station was windowed from a seismic trace. The seismic trace was adjusted after instrument correction to obtain ground displacement in meters.

Once each of Ω_0 and f_c is obtained from the spectral fitting, the seismic moment M_0 for each receiver and each phase (P and S) can be calculated:

$$M_0 = \frac{\Omega_0 4\pi\rho V^3 R}{F_R}$$

Focal Mechanism

To determine micro seismic focal mechanism, we need hypocenter location and velocity model from previous calculation. Besides that, the polarity of seismogram first motion is required to determine focal mechanism. The polarity is denoted by “up” represent compression zone or “down” represent dilatation zone.

In this study, we use a focal mechanism inversion program developed by a team from ITB, based on the polarity phase of the seismic wave. It is adapted and modified from non-linear hypocenter determination algorithm developed by Lomax (2000). The possible focal mechanism solutions (strike, dip, and rake) are treated similarly to the 3D coordinates of the hypocenter location. So that the grid-search method can be applied to find the solution of the coordinates focal mechanism.

The random number techniques are used to accelerate the determination of focal mechanism solutions and to determine the solution uncertainties. Because of the limited micro seismic polarity phase data, usually the solution obtained is not unique, but in the form of a cloud of a coordinate strike, slip and rake of the focal mechanism. The uncertainties of the solution are then analyzed from the geometry of the cloud.

RESULTS & DISCUSSION

Hypocenter Location

After onset of P- and S-waves arrival time is determined, the initial location is determined using NonLinLoc. The result from NonLinLoc is used as an initial hypocenter location. The average error RMS of hypocenter location determination (figure 4) is quite low (average 0.05 second). RMS error mean an accurate hypocenter determination. The precision of the computational solution, which is based on various model assumptions probably as real accuracy of the location and origin time because the NonLinLoc used nonlinear algorithm.

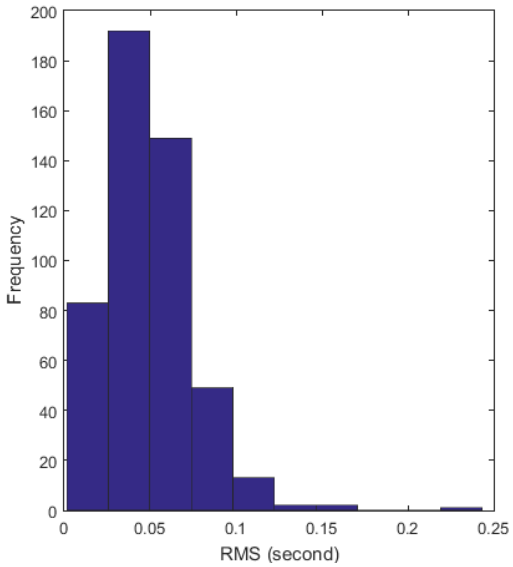


Figure 4: Error RMS of hypocenter location from NonLinLoc calculation results. The average error RMS is around 0.05 second

The hypocenter location of micro seismic events is located beneath around well trajectory (injection and production well) and fault. Two compartment of micro seismic events (Area I and Area II) and its boundaries are interpreted (Figure 1 & 6) with Urug Fault as separator of those compartments. Northern boundary of Area II is Ciwidey II Fault (NE-SW) and southern boundary of Area II is Ciwidey Creater Fault (NW-SE) that is identified from remote sensing analysis in previous study (Pradipta, 2018).

Micro seismic events in Area I is around trajectory of three production wells and in Area II is around injection well and production. Most of the productive well is in Area II. We also compare the existence of micro seismic event with the production and injection data (Figure 6). But after we analyzed it, there is no correlation between well activities (injection and production). The existence of micro seismic events is not corelated with the injection rate like another field because the injection rate in Patuha (average 110 ton/h) is smaller than others. If we compare injection rate in Salak geothermal field is 150-560 ton/h (Tanuwidjaja, 2015) and Darajat geothermal field is 72-504 ton/h (Perdana, 2014), it means the injection rate in Patuha geothermal field is one half until one quarter than another geothermal field.

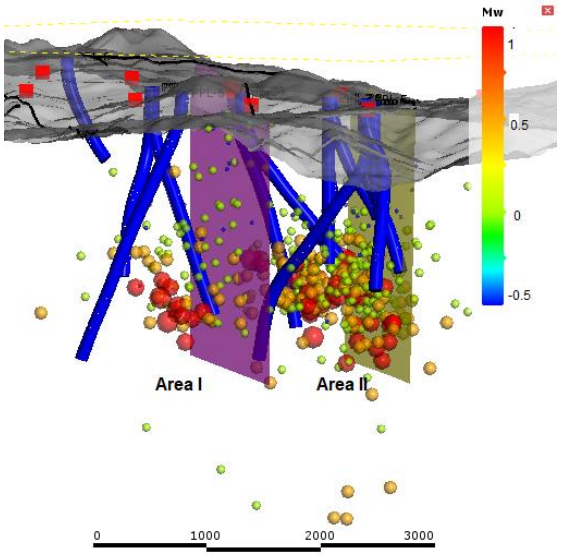


Figure 5: Micro seismic events (circles) distribution clustered in two areas is around well trajectory (blue line) in 3D view. The micro seismic events are separated into two areas (Area I and Area II) by Urug Fault (blue area). Circle size represent Mw values.

Magnitude

Map of magnitudes distribution (Figure 5) shows that micro-earthquakes around Patuha production area generally range between -1 and 1.5 Mw. The results came with high dense number of micro-earthquakes in Patuha concession area. It is possible that because the distribution of network station which is centered at concession of Patuha area. Thus, many stations could record events with small

magnitudes which occurred at concession area. This event may associate to reservoir activities in the reservoir of Patuha.

Velocity Model

The initial velocity model was processed using MATLAB computer program to randomly generate 100 starting velocity models as VELEST input. Then, each model was processed using VELEST software by applying ten different velocity damping parameters (0.01 to 1.0). The VELEST output with smallest RMS was selected as the best final velocity model. This velocity medol results will be used to determine hypocenter location for next study.

Focal Mechanism

Among a total of 491 events used as inputs, 67 events were found to have a good quality. The uncertainty of these selected 67 events is less than 30°. It is worth to note that the solution of focal mechanism inversion consists of two planes, i.e. fault plane and conjugate plane, which have similar surface displacement characteristics. Therefore, we need an additional data to distinguish which one is the fault plane and the conjugate plane. The required data is the in-situ stress information, surface structure observation, and hypocenter alignment. As the surface structure in Patuha is complex and the in-situ stress is unknown, we could only rely on the alignment of the hypocenter. We also performed cross-correlation technique to support the fault plane analysis based on hypocenter alignment.

In general, the focal mechanism solutions are highly heterogeneous. Most of events have mechanism of normal to strike slip, and view in the south have thrusting mechanism. This heterogeneity might be caused by the injection and production activity which perturbed the in-situ stress condition. Therefore, a heterogeneous pattern of focal mechanism patterns is observed. A similar condition of this focal mechanism heterogeneity is also observed in Soultz, France (Sahara et al., 2014; Schoenball et al., 2014), Salak geothermal field (Stimac et al., 2008). But several minor fault with orientation of NE-SW are identified.

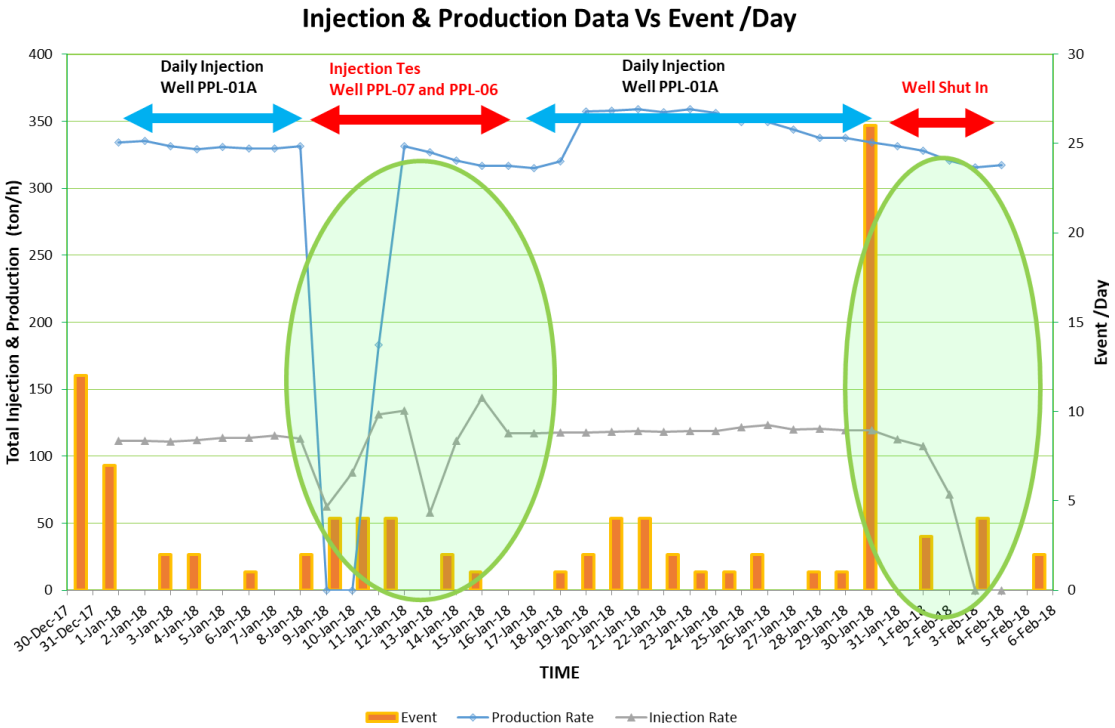


Figure 6: Chart showing no correlation between production and injection rate with amount of micro seismic events per day

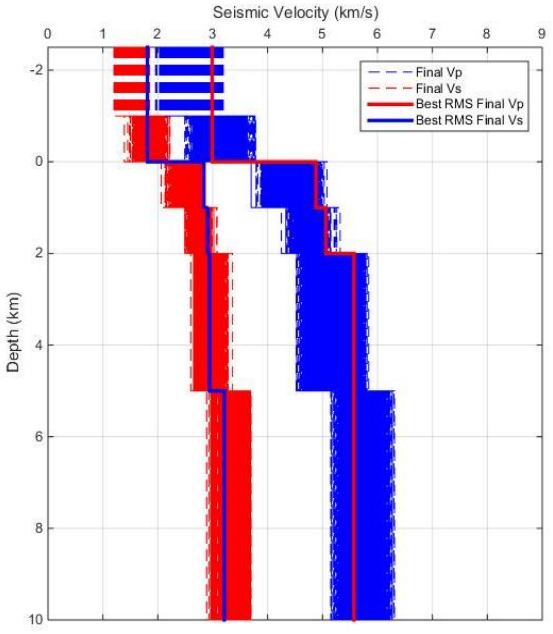


Figure 7: The VELEST output of 1000 initial velocity models

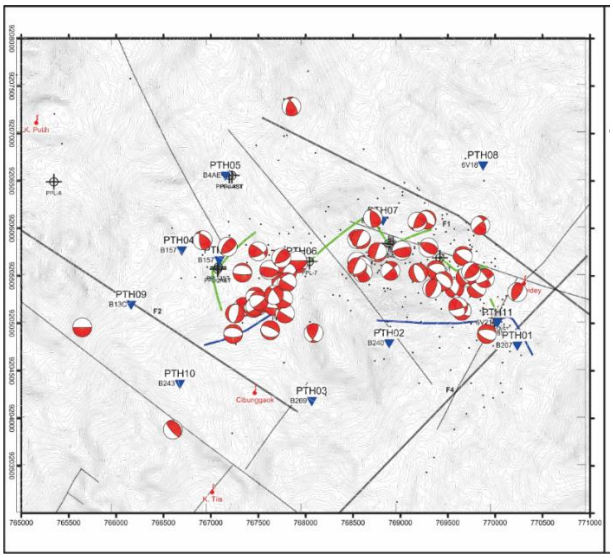


Figure 8: Plot of focal mechanism distribution with solution uncertainty of less than 30º in the Patuha Geothermal field

CONCLUSION

The hypocenter location has been determined using an advanced non-linear inversion technique. In which, 491 micro seismic events have been picked and located from 5,548 and 5,352 for P and S arrival phases. The hypocenter location of micro seismic events is located beneath around well trajectory (injection and production well) and fault. Two compartment of micro seismic events (Area I and Area II) and its boundaries are interpreted with Urug Fault as separator of those compartments. Northern boundary of Area II is Ciwidey II Fault (NE-SW) and southern boundary of Area II is Ciwidey Creater Fault (NW-SE) that is identified from remote sensing analysis in previous study. Micro seismic events in Area I is around trajectory of three production wells and in Area II is around injection well and production. We compare the existence of micro seismic event with the production and injection data, but there is no correlation with micro seismic existence. It is different with micro seismic study in another geothermal field, the micro seismic existence is in line with injection rate because the injection rate in Patuha is smaller than other geothermal field.

Focal mechanism results show the role of each major faults, e.g. sealed or permeable. Three faults are identified as the boundary of the micro-earthquake zone, which might also be the reservoir boundary, and one fault is identified as a sealed fault that form two compartments within the reservoir.

REFERENCES

Brune J.N. (1970), *"Tectonic stress and the spectra of seismic shear waves"*, from earthquakes, *J. geophys. Res.*, 75, 4997–5010.

Bormann, P., Engdahl, B., Kind, R. (2012), *"Seismic Wave Propagation and Earth models"*. In: Bormann, P. (Ed.), New Manual of Seismological Observatory Practice 2 (NMSOP2), Potsdam: Deutsches Geo For schungs Zentrum GFZ.

Lomax, A., J. Virieux, P. Volant, and C. Thierry-Berge. (2000), *"Probabilistic earthquake location in 3D and layered models"*, in Advances in Seismic Event Location, C. H. Thurber and N. Rabinowitz (Editors), Kluwer Academic Publishers, Dordrecht/Boston/London, 101–134.

Lomax, A. and A. Michelini. (2009), Mwpd: "A Duration-Amplitude Procedure for Rapid Determination of Earthquake Magnitude and Tsunamigenic Potential". From P Waveforms, *Geophys. J. Int*., 176, 200-214, doi: 10.1111/j.1365-246X. 2008.03974.x

Kissling, E., Ellsworth W.L., Eberhart-Phillips D., and Kradolfer U. (1994), *J. Geophys. Res*, 99, 19635-19646.

Kissling, E. (1995), *"Program VELEST USER'S GUIDE"*. – Short Introduction, Zurich: ETH Zuerich, 1-31.

Lomax, A., and A. Curtis. (2001), *"Fast, probabilistic earthquake location in 3D models using Oct-Tree Importance sampling"*. Geophys. Res. Abstr., 3.

Palgunadi, K.H., Nugraha, A.D., Sule, M.R., and Meidiana T. (2017), "Steam and Brine Zone Prediction around Geothermal Reservoir Derived from Delay Time Seismic Tomography and Anisotropy Case Study: "PR" Geothermal Field". *Southeast Asian Conference on Geophysics.*

Perdana, M.W., Nelson, C., and Nordquist, G. (2014), "Microseismic Monitoring in Darajat Geothermal Field: Observations in Moving Injection to DRJ-AI Well". *Proceedings Indonesia International Geothermal Convention & Exhibition 2014*

Pradipta, R. A. (2016), *"Penentuan Zona Permeabilitas Menggunakan Citra ALOS Palsar, Pemetaan Geologi, dan Geokimia Tanah dan Udara Tanah (Hg-CO2), Studi Kasus Lapangan Panasbumi Ciwidey, Kabupaten Bandung"*, Tesis Magister, Institut Teknologi Bandung

Sahara, D., Schoeball, M., Kohl, T., Mueller, B.I.R. (2014), *"Impact of fracture networks on borehole breakout heterogeneities in crystalline rock"*. International Journal of Rock Mechanics and Mining Science.

Schoenball, M., Dorbath, L., Gaucher, E., Wellmann, J.F., Kohl, T. (2014), *"Change of stress regime during geothermal reservoir stimulation"*. Geophysical Research Letters 41, 1163–1170. https://doi.org/10.1002/2013GL058514

Stimac, J., Nordquist, G., Suminar, A., Sirad-Azwar, L. (2008), *"An overview of the Awibengkok geothermal system, Indonesia"*. Geothermics, Indonesian geothermal prospects and developments 37, 300–331. https://doi.org/10.1016/j.geothermics.2008.04.004

Tanuwidjaja, R., Nelson, C., and Nordquist, G. (2015), "Injection Induced Seismicity at Western Salak Geothermal Field". *Proceedings Indonesia International Geothermal Convention & Exhibition 2014*

BUILDING A 3D EARTH MODEL OF SILANGKITANG GEOTHERMAL FIELD, NORTH SUMATRA, INDONESIA

Drestanta Yudha Satya[1], Yoshio Soeda[2], Peter Drakos[3], Doddy Astra[1], and Enrique Manuel Lima Lobato[2]

[1]Sarulla Operations Limited, [2]West Japan Engineering Consultant, Inc., [3]Ormat Technologies, Inc.
[1]The Energy Building 51st Floor, SCBD Lot 11A, Jl. Jend. Sudirman Kav. 52-53, Jakarta 12190, Indonesia
[2]Denki-Bldg., Sunselco Annex 8F,1-1,1-Chome, Watanabe-dori, Chuo-ku, Fukuoka, Japan 810-0004
[3]6225 Neil Road, Reno, Nevada 89511, USA 89511-1136
Email: drestanta.yudha@sarulla-geothermal.com; soeda@wjec.co.jp; pdrakos@ormat.com;
doddy.astra@sarulla-geothermal.com; lima@wjec.co.jp

ABSTRACT

The 3D Silangkitang (SIL) earth model has been generated by integrating multidisciplinary (geology, geophysics, geochemistry and reservoir engineering) data and interpretations to produce a more accurate geothermal conceptual model. Ultimately, 3D earth model like this should be utilized as reference to construct a numerical simulation model which will aim to predict reservoir performance and support field management decisions such as injection management and make-up well targeting. The 3D SIL model was designed as an evergreen tool that can be easily updated with data from recent reservoir performance and drilled well data. This model demonstrates key elements in geological framework such as the importance of major structural trends and also the impacts of specific formations within the reservoir. SIL geothermal wells purposely target faults related to the Great Sumatra Fault Zone (GSFZ). The GSFZ is a major right-lateral, strike-slip fault system which traverses the entire length of Sumatra. At SIL, the fault distribution and geometry has been well defined by the integration and interpretation of well geology, tectonic geomorphology and surface geology. The highest permeability of the SIL reservoir is controlled by faults and fractures associated with localized releasing bends and steps within the GSFZ. This paper documents the approach and workflows which were applied to construct a 3D earth model as an instrument for geothermal reservoir evaluation and management.

Keywords: 3D earth model, great sumatera fault zone, permeability, Silangkitang Geothermal Field.

INTRODUCTION

The Silangkitang (SIL) Geothermal Field is located in the Tapanuli Utara District, North Sumatra Province, Indonesia. The field is located approximately 35 kilometers southeast of the town of Tarutung. Silangkitang and is one of several prospects in the Sarulla contract area (Figure 1). Sarulla Operation Limited (SOL), a consortium of Medco Energi Internasional Tbk., Itochu Corporation, Kyushu Electric Power Co. Inc., Ormat Technologies, Inc., and INPEX Corporation, has been granted the rights to utilize the Sarulla geothermal resource for power generation under the framework of a Joint Operating Contract (JOC) with Pertamina. SIL started commercial generation of 110 MW on Mar 18, 2017. Currently SOL has 3 units commercially running at Namora-I-Langit (220 MW) and Silangkitang (110 MW) under a single contract. Currently at SIL there are 4 production wells and 9 injection wells to support full power generation.



Figure 1: Location map of the Silangkitang geothermal field (Google Maps,2018)

The SIL field is situated within the Barisan Mountains, which are both structurally uplifted and covered by young volcanic rocks. There are eleven active volcanoes along the mountain chain, but none of those is positioned in the Sarulla vicinity. However, there are abundant volcanic eruptive centers within and adjacent to the contract area that are less than 1 million years old.

The main surface expression of the SIL hydrothermal system is comprised of a series of boiling springs and fumaroles concentrated along a 2.5-km length of the eastern floor and foothills of the valley (Figures 1 and 2). The springs are located further out in the valley whereas the fumaroles are mostly found along the main Great Sumatra Fault Zone (GSFZ) trace in the foothills. The chemistry of the springs and fumaroles is strongly indicative of a high temperature neutral chloride geothermal system. Geophysical surveys executed in the

prospect show an area of low resistivity related with the clustered thermal manifestations. This local conductive layer coincides with the shallow clay-rich alteration and elevated temperature of a geothermal system. The reservoir boundary shown in Figure 2 is delineated from the distribution of the shallow conductive layer.

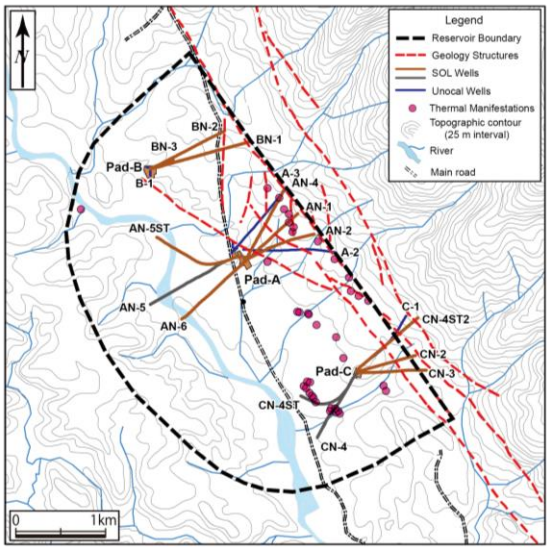


Figure 2: The SIL basemap showing well penetrations, geology structures, and reservoir boundary.

GEOLOGIC FRAMEWORK

Regional Geology

The geology in the Sarulla region of North Sumatra is dominated by two major superimposed tectonic features, a dextral strike-slip fault and an active volcanic arc (Figure 3). The regional basement in the Sarulla district is Paleozoic Meta-sediments which were initially part of Sundaland and have been accreted to the Eurasian boundary during the Triassic (Hickman et al., 2003). Mesozoic granitic rock intruded older facies including Jurassic and Cretaceous sediments, meta-sediments and mafic volcanics that covered Paleozoic basement.

A chain of thermal manifestations including fumaroles and hot springs is situated along the edge of the Sarulla graben, adjacent the district of Silangkitang. The thermal features are concentrated in a 1 x 2.5 km^2 band west of the Tor Sibohi fault and about 1 km north of a rhyolite dome with a K-Ar age of 0.12 ± 0.08 Ma (Gunderson et al., 1995). It seems the Tor Sibohi fault is in critically stressed condition thus the fault zone has enhanced permeability (Townsend and Zoback, 2000). The exploration, production, and re-injection wells drilled at SIL, encountered a geothermal system whose permeability is strongly controlled by the Great Sumatra Fault.

The Great Sumatra Fault (GSF) is likely to have been active as a right-lateral strike-slip fault when seafloor spreading started in the Andaman sea during the Mid-Miocene (Hickman et al., 2003). Pre-Volcanic sediments were deposited in the sea during Mid-Miocene to Pliocene. The Sarulla graben seems to have been constructed by extension nearly perpendicular to northwest GSF through Plio-Pleistocene (Hickman et al., 2003). The basin generally has an asymmetric graben to half-graben profile which is indicated by gravity models across the extent of basin in SIL (Figure 3). SIL lies above a local sub-graben formed between the Tor Sibohi fault and the intersecting Hutajulu fault. Neogene and Quaternary volcanic and volcanoclastic rocks cap Tertiary sediments.

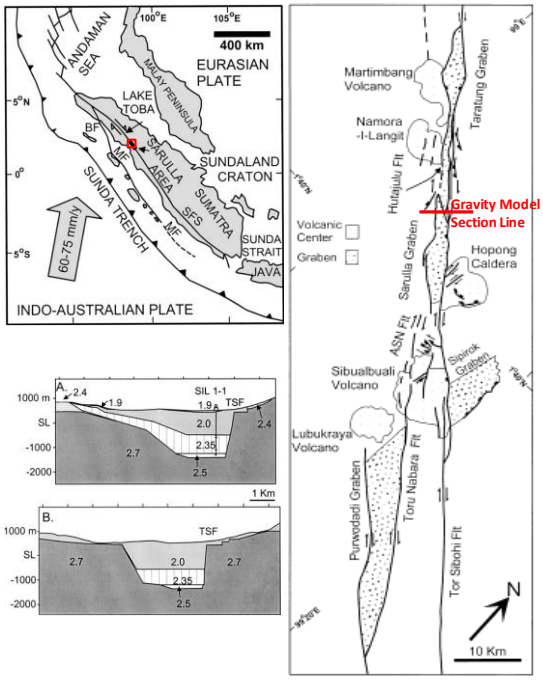


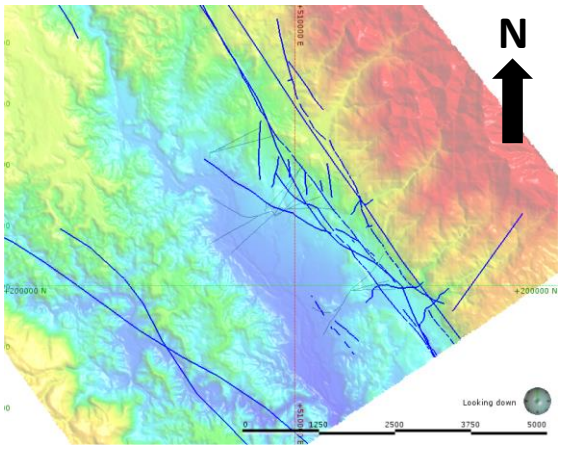
Figure 3: General tectonic setting map of Sumatra. Red square denotes Sarulla location (top left). Regional tectonic map showing Sarulla graben. Red line denotes gravity model section line (right). Gravity model cross sections (bottom left) (Hickman et al., 2003).

Geologic Structures, Stratigraphy, and Hydrothermal Alteration

The team defined faults which have an important role in the subsurface by influencing flow, distribution of permeable entries, offsets in lithologies and other reservoir characteristics (e.g. tracer flow pathways, alignment of geophysical anomaly, pressure or temperature differences in the reservoir, subsurface fluid chemistry, etc.).

The SIL structural map was mainly developed from lineament interpretation by different individuals from both aerial photos and satellite imageries and augmented with surface field mapping (Figure 4).

With the new LiDAR data acquired in 2015, the surface structures were refined by topographic interpretation based upon the tectonic geomorphology using stereoscopic images prepared from LiDAR DTM and later confirmed by field checking.



Figures 4: Topography surface expression at SIL from LiDAR data. Faults, topographic lineaments, gravity lineaments and resistivity discontinuities were interpreted as polylines.

The graben extends in a NW-SE direction, parallel to the GSF. The Paleozoic Meta-sediments are exposed at the surface east of the GSF in the SIL area (SOL Internal Report, 1996). Those rocks are mainly meta-argillites with minor composition of quartzites, marls, and marbles. The Paleozoic interval in one well is massive and rigid and comprises generally open fractures that are filled by secondary minerals based on observation from the recovered conventional core. The top of basement is deep within the graben and is overlain by mainly thick young volcanic rocks (Figure 5).

Tertiary sediments, were encountered by two wells west of the GSFZ. This facies, which is a sequence of fine to coarse-grained sedimentary rocks, is interpreted extending east from the GSFZ as a thin layer underlying the thick ash flow tuff unit. These rocks ranging from shale to conglomerate are described as valley-filling river deposits preceding most of the volcanic activity in the area (SOL Internal Report, 1996).

Overlying the Tertiary Sediments is a thick accumulation of Rhyolite ash flow tuff, namely Sarulla Graben Tuff formation. This formation which consists of primarily rhyolitic tuff and dacitic tuff with thin mudstone interbeds. Most production and re-injection wells found permeable zones in this formation.

Younger facies atop the tuff, include a thick sequence of fine-grained rocks interpreted as lake deposits. The variation in lithology in this formation is thought to represent different source rocks for sediments laid down in the same depositional environment (SOL Internal Report, 1996). The uppermost part is a recent alluvium layer consisting of pebble conglomerate and poorly consolidated sandstone.

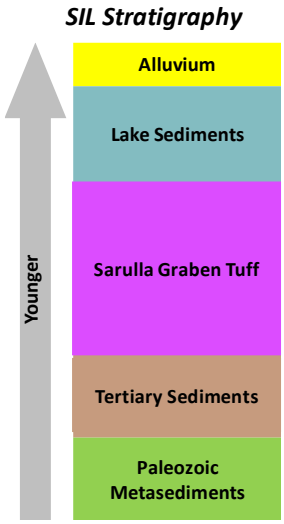


Figure 5: Stratigraphy column for SIL area.

In general, the hydrothermal alteration minerals are consistent with current thermal conditions (SOL Internal Report, 1996). Moving deeper into the reservoir, the clays grade from pure smectite near the surface, through mixed-layer illite-smectite, to pure illite. Epidote and chloride which are ferromagnesian minerals are less abundant than in a typical andesite-hosted system while illite mineral which represents the silisic character is more common. In the deep section, SIL wells encountered high temperature minerals which consist of quartz, calcite, illite, chlorite, pyrite, hematite, magnetite, anhydrite, leucoxene, and epidote.

RESERVOIR CHARACTERISTIC AND CONCEPTUAL MODEL

The Silangkitang geothermal system consists of two major elements: a high permeability upflow region within the Great Sumatra Fault Zone, and a main sub-lateral aquifer of lower permeability that spreads to west from the fault (SOL Internal Report, 1996). The analysis of regional and local geological and geophysical data, chemistry of fluid, trends of initial temperatures and pressures, well interference and pattern of tracer returns are integrated to interpret geothermal fluid-flow patterns in SIL. The Great Sumatra Fault system is the main structure controlling permeability for the SIL geothermal system. It allows the high temperature source to heat the system and geothermal fluid to move from high to low pressure regions beneath the low resistivity layer.

Heat Source and Upflow

The commercial Silangkitang reservoir is a high temperature (535 – 590ºF) geothermal resource. The highest temperatures may correspond to a magmatic body or cooling intrusion at depth beneath the SIL geothermal system. This feature represents a relatively shallow, high-grade heat source for the system. Geological studies do not clearly designate an exact location for such a heat source. The measured temperature specifies that upflow of hot geothermal fluid at SIL into the reservoir occurs at or near to the subsurface location of the NW-bearing Pad-A (Figure 2). The upflow was hypothesized along the main, eastern strand of the GSF. This interpretation is supported by recent geochemistry analysis using newly drilled well data. Simatupang (2017) mentioned, that according to Na-K-Mg Giggenbach Ternary diagram, liquids are in full equilibrium with observed high temperatures in wells AN-1, AN-2 and AN-4 (Figure 6). Bottom-hole locations for AN-wells are to the NE of Pad-A.

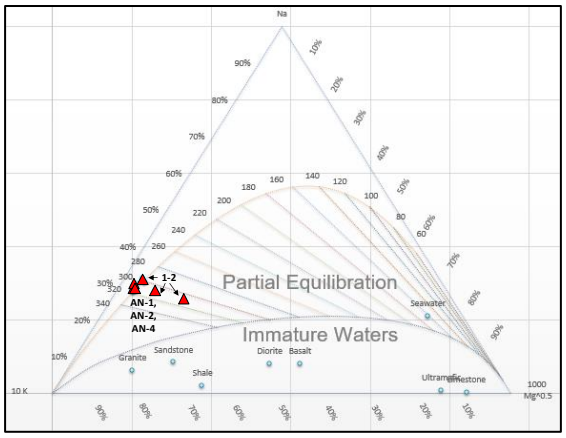


Figure 6: The Na-K-Mg Giggenbach Ternary of wells at Pad-A (Simatupang, 2017).

Reservoir Permeability

Both production and injection wells that penetrated the GSFZ obtained good permeability while other wells drilled to the west encountered lower permeability. The wells at Pad-A and Pad-B have better permeability as compared with the wells at Pad-C. Detailed mapping along the surface trace of the GSFZ identified releasing bends and fault steps which indicate zones of dilation and correlate with the main upflow zone in the area to the NE & E of Pad-A. It is interpreted that a locally developed extensional stress field related with strike-slip faulting of the GSFZ contributes to the creation of high permeability at SIL. Similarly, the permeable zone east of Pad-B is confirmed along subsidiary N-S striking faults of the GSF and at the intersection of these subsidiary faults and main strand of the GSF. This group of N-S faults enhance permeability at the Pad-A and Pad-B areas. This observation indicates that the main permeable zone at SIL is likely controlled by faults and fractures associated with releasing bends and steps within the GSFZ.

Geophysical Characteristics

Resistivity and gravity measurements have been executed in the SIL area. Anomalies indicated by both surveys help define the SIL geothermal system in the Sarulla graben.

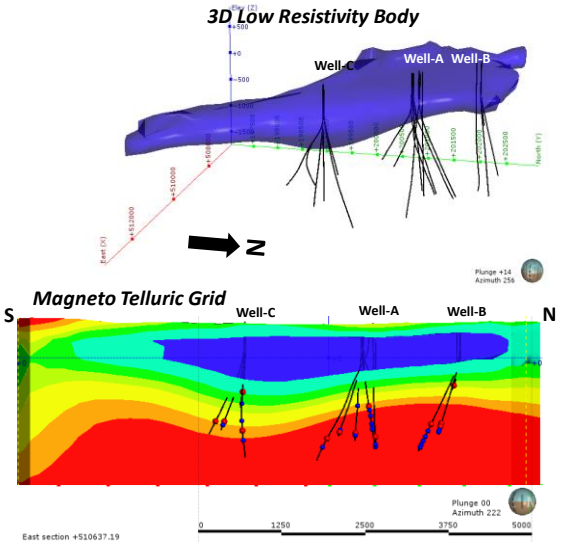


Figure 7: The 3D snapshot showing conductive layer at SIL (above). The NW-SE cross section showing most of the permeable entries at SIL were encountered below interpreted clay cap based on resistivity value of 5 ohm-meter (bottom). Red circles denote major feedzones while minor entries are indicated by blue circles.

Resistivity Interpretation

The correlation of low resistivity with smectite and smectite-illite mixed layer clay alteration at SIL is comparable to signatures observed over similar high-temperature volcanic-hosted geothermal systems. At SIL, the shallow sediments are clay rich, which generates a shallow high-conductive layer throughout the valley. This low resistivity region is believed to represent an amalgamation of enhanced clay content of argillically altered rocks and elevated formation temperatures above the deep SIL geothermal system (SOL Internal Report, 1996). Based on rock description, the enhanced clay layer correlates with the conductive layer of 5 ohm-meter and was considered a clay cap or caprock (Figure 7). An interpolant model is created and iso-surfaces representing selected resistivity values are processed and displayed. Since resistivity data point input which is the 3D inversion result is very dense, no anisotropy was introduced. Resistivity volume intervals are also outputs of the interpolant model. Largely, the shallow low resistivity body extends above the graben filling rock, capping the reservoir section where most of production and re-injection wells tap permeability.

Gravity Interpretation

The Paleozoic rocks are interpreted to have high density as compared with sedimentary and volcanic fill of the graben. The model of gravity and drilling result indicated that the GSF has very steep dip. A gravity low correlates with the Silangkitang geothermal system that associated with extensional tectonics. This low bouguer anomaly is identified at the topographically low land, which is bounded its northeastern side by GSFZ. Along geologically recognized GSFZ, a gravity lineament is also recognized (Figure 3). The top of high density body from gravity model was interpreted as bottom of reservoir.

Geothermal Fluid Movement

In natural conditions, hot geothermal fluid moves upward along high permeable GSFZ and enters into the horizontal aquifer which is the principal outflow for the SIL system. The hot fluid seems to come in the geothermal reservoir from a deep level at a location close to the Pad-A. Based on measured downhole temperatures, ascending fluids flow to at least as far as the Pad-B and Pad-C pad which are located NW and SE of the SIL core area, respectively. Fluid within the main reservoir migrates under the low-permeability clay-rich layer, according to the relatively high temperatures observed there (Figure 8). Some fluids move further up the fault and feed the many thermal features (fumaroles and springs) at the surface.

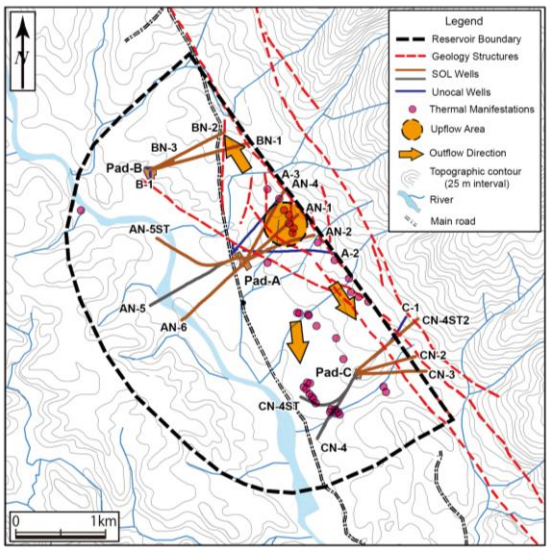


Figure 8: Map showing geothermal fluid movement in SIL reservoir.

BUILDING A 3D EARTH MODEL

Representing a geological model in three-dimensions (3D) compared with the flat, two-dimensional maps and cross-sections that were prevalent earlier could better portray the conceptual model of a geothermal system. Building the earth model or geological environment is frequently the foremost stage in constructing integrated geothermal models. An iterative multidisciplinary approach using geology, geophysics, geochemistry, and reservoir engineering data in reconciling and integrating such a diverse set of inputs benefits by building common understanding and alignment within the work team. The team decided to create an earth model as an evergreen tool that can be updated periodically with new reservoir performance interpretation and well data. At its most basic, a geological model is a volume that covers the area of interest constrained at surface by the topography. This forms the foundation from which the model is then successively refined by adding structures and stratigraphy. With the ability to look in detail by rotating the 3D model, it has become an essential tool to better understand the subsurface geology, including designing wells. Lastly, it is the framework when starting to build the numerical model.

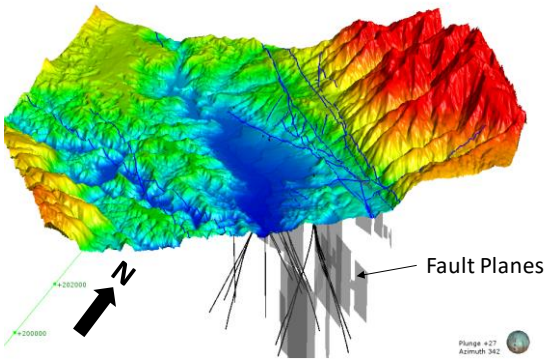


Figure 9: Creating fault meshes based on interpreted polylines.

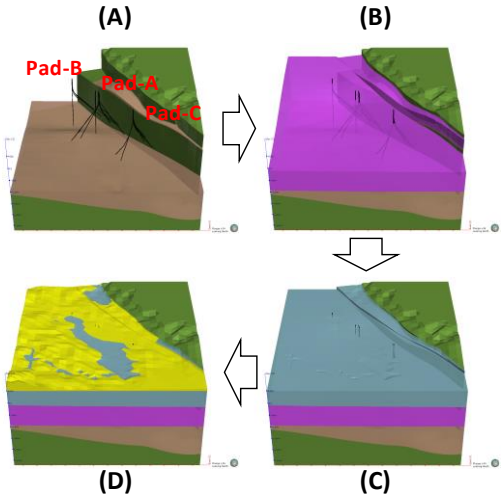


Figure 10: Series of stratigraphy blocks showing the order of facies deposition at SIL. (A) Tertiary Sediments, (B) Sarulla Graben Tuff, (C) Lake Sediments, and (D) Alluvium.

In the model, initially the structures were delineated as polylines then those lines were converted to

meshes with specific dip angle (Figure 9). Major structures that play an important role to SIL subsurface geology conditions include, two NW-SE orientated faults within the GSFZ and several N-S striking faults near the Pad-B location. These major faults within the GSFZ were incorporated into the geology model to constrain offset stratigraphy layers. Including, shallow basement rock along the eastern portion of the GSFZ as compared with the one in the western side and these two faults have nearly vertical dip angle (Figures 10 and 11). One of the SIL wells penetrated completely through the GSFZ and encountered Paleozoic meta-argillite basement at depth on the eastern side of GSFZ. Other wells may be reached the basement, but it is not confirmed yet due to no cutting samples (blind drilling interval). The N-S striking faults correlate with a good permeability zones that were intersected by some wells from Pad-A and Pad-B.

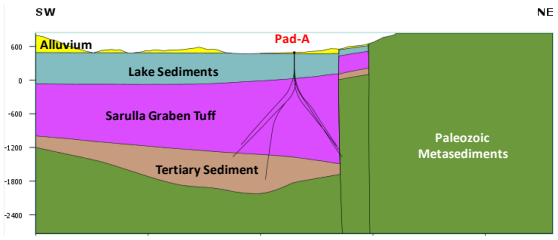


Figure 11: The NW-SE Cross section displaying stratigraphy strata at SIL (below).

Since there is no well which intersects the Paleozoic Meta-sediments west of the GSFZ, the gravity interpretations were integrated as a constraint to better represent the basement rock in the model. The modeled surface interpreted from gravity data is used as an indicator of the basement depth, at regional scale, and affords useful guidelines where there is no surface or downhole data.

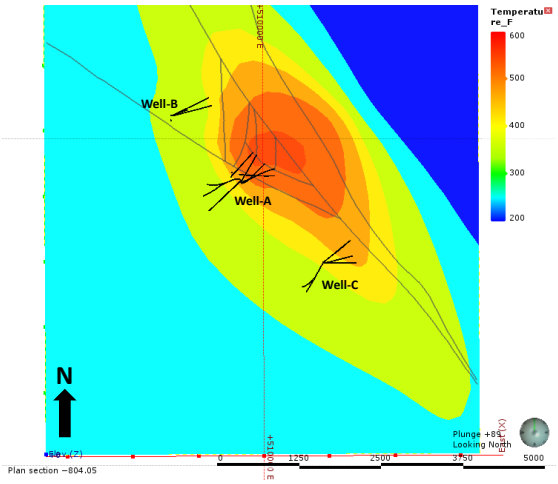


Figure 12: Horizontal slices at -804.05 m elev. showing temperature zoning. Principal geological faults and wells trajectory location (from surface to -804.5 m elev.) are plotted in the section.

Again, in facies modeling the gravity model was used as a reference to distribute Tertiary Sediment facies where there is no well data. Gravity data shows basement highs at both west and east boundaries of the graben, so the Tertiary Sediment formation is interpreted thinning at these graben boundaries (Figure 11). In the model, younger formations were created using lithology information from drilling (Figure 10).

Downhole temperature profiles representing inferred stable reservoir conditions are integrated into a geothermal model. The core objective in constructing 3D visualization of temperature is to support interpretation of commercial reservoir volume and conceptual model of the geothermal system. At SIL, temperatures are highest within fault zones, specifically near Pad-A location. The high temperatures were interpreted to propagate east of the GSFZ rather than to the west where several wells showed limited permeability. Temperature declines as fluid outflows laterally away from the GSF (Figure 12). Within the fault zone, temperature decreases to the southeast (Pad-C) and northwest (Pad-B) from Pad-A. To better represent the conceptual understanding about SIL temperature, especially in the vicinity where there is no well data, an interpolant was applied in the model using the trend of the GSF strike direction.

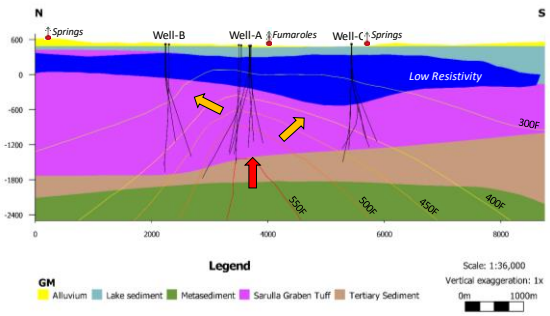


Figure 13: The N-S 2D cross section through the 3D SIL earth model with geological facies, distribution of temperatures and smectite-rich alteration based on well data and low electrical resistivity interpretation. Red arrow denotes location of inferred upflow area from heat source located at vicinity of Pad-A. Two orange arrows showing both NW and SE directions of outflowing fluid.

The conceptual model of the SIL geothermal system is well represented by the 3D earth model. In areas where there is no well data the conceptual model was primarily adopted to distribute the reservoir properties. Figure 13 shows the N-S cross section of the SIL geothermal system. As shown in the figure, the highest temperature area in the system is located near Pad-A. The geothermal fluid flows outward to lower pressure regime to the NW and SE along the

GSFZ. Most production and re-injection zones are associated with the Sarulla Graben tuff formation.

An earth model is the framework to support a realistic numerical model grid. Therefore, it is important to collect and interpret field data accurately. An Earth model can provide general value of several reservoir properties according to distribution of lithology or rock facies and hydrothermal alteration. Distribution of caprock from resistivity anomaly was used as a reference for determining the area of interest for the numerical grid. Figure 14 shows the grid design for the reservoir numerical model and simulation study that was produced using Leapfrog. After the conceptual model was developed and agreed upon by the geoscientists, a numerical grid model was constructed. The reservoir parameters that were set are adjusted during the calibration process to well data in steady and dynamic states.

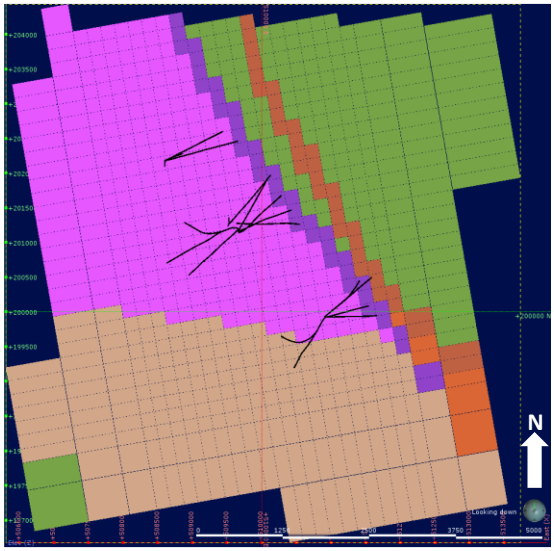


Figure 14: A depth slice of SIL numerical model grid that adopts lithology distribution from earth or static model. Some reservoir properties were distributed following the facies model. Different color represents different formation and fractures. Main faults are represented in dark purple, orange, and dark brown color.

The handover process from earth model to numerical model is not only a single stage. There would be back and forth process to fit numerical model and conceptual or geological model. The 3D earth model is a good tool to facilitate further discussion between scientist and engineer to have concession about which kind of numerical parameters should be used to accommodate conceptual understanding about geothermal systems since earth model has better visualization in 3D and could be spatially edited according to new interpretation and data. This aids in reducing the iteration process and create a more aligned numerical model to conceptual model.

ADVANTAGES OF A 3D INTEGRATED APPROACH

Well planning

In the development stage, to make sure production supply and injection capacity always support full power generation there may be a need to drill additional production and injection wells. This is common when the reservoir pressure declines overtime and/or there is problem with an existing injection well. An Earth scientist needs to prepare preliminary designs for future make up well targets. The 3D earth model could help the scientist to better visualize interpreted geological structures and stratigraphic layer target. Adjusting angle and direction of the well plan could be done in one single interface with the geological model. The implication to have 3D earth model is not only a better visualization tool but also to improve the interpretation and to significantly reduce working time on well targeting.

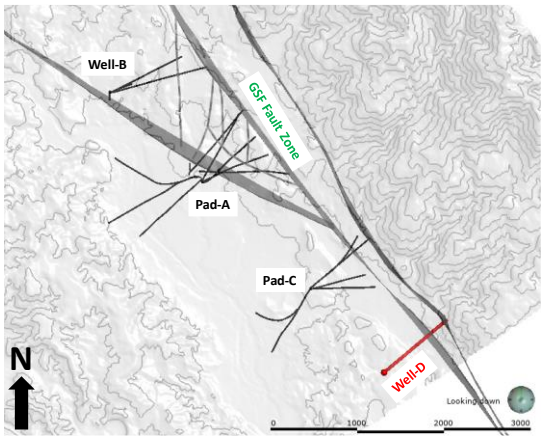
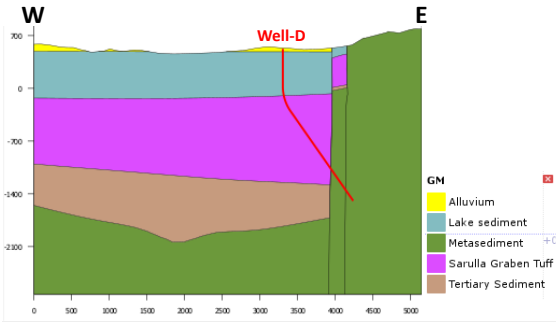


Figure 15: Contour map showing location of Well-D plan. The well is located south of existing Pad-C that target the same NW-SE geology structure.

As shown in the example, Well-D was planned as an injector to target the GSF fault. To maximize encountering the target, the well aims to hit the target at azimuth 45 degree with inclination of 35 degree (Figure 15 and 16). The modeling software allows a scientist to generate several well alternatives in terms of target depth, inclination, and direction then decide the best option to fulfil the well objective and target the desired geological features in the 3D earth model. Various subsurface information for the well plan could be simply obtained from the model.

Prognosis on lithology or formation, temperature, and resistivity are necessary information for the drilling team to finalize the drilling program, including optimizing drilling fluid and selecting appropriate tool for logging (Figure 16 and 17). By

doing all of these, the team could reduce uncertainty of subsurface condition and prepare mitigation plans to reduce drilling risk.



Measured From	Measured To	Vertical From	Vertical To	GM
0	37.737	0	37.737	Alluvium
37.737	500	37.737	500	Lake sediment
500	638.24	500	636.903	Lake sediment
638.24	850	636.903	828.635	Sarulla Graben Tuff
850	1837.13	828.635	1637.25	Sarulla Graben Tuff
1837.13	2235.31	1637.25	1963.42	Metasediment
2235.31	2300	1963.42	2016.41	Metasediment

Figure 16: Top cross section showing Well-D trajectory to NE to penetrated two faults. Different color denotes different geology facies. Bottom table summarizes possible lithologies which would be encountered by Well-D plan.

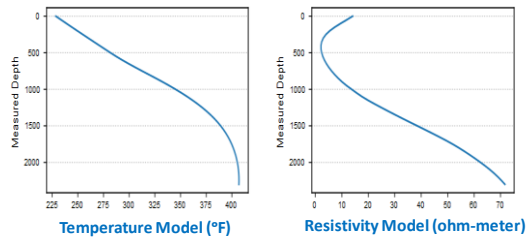


Figure 17: Graphics showing temperature (left) and resistivity (right) prognosis with depth for Well-D plan.

CONCLUSION

The 3D earth model presented in this paper is of a fault-controlled geothermal system of the SIL geothermal field using Leapfrog Geothermal version 3.5 modelling software. Detailed analysis on GSFZ distribution at SIL was performed since GSFZ has a primary control for stratigraphy interpretation and permeability distribution in this field. The distribution of meta-sediment basement rock was delineated by interpretation of well data, regional gravity and by integrating LiDAR data interpretation.

The modeling software allows the scientist to have integrated interpretation on some subsurface data to define a conceptual model for the SIL geothermal system. According to measured temperature and pressure data, the present-day upflow is structurally controlled with the heat source located right below the upflow zone where some fumaroles were observed. Geothermal fluid is inferred to be outflowing to the Northwest and Southeast via the GSFZ and below a developed clay cap. This fluid pattern is also consistent with interpretation of surface and subsurface fluid geochemistry analysis. The reservoir at depth is fault or fracture controlled that can be targeted in rocks at intermediate depth within Sarulla Graben Tuff facies. The integration of these datasets and use of powerful visualization tools allowed us to better understand the system.

Use of the 3D earth or static model provided a better representation of drilling targets such as fractures and specific formations. It was also very useful in viewing real time trajectories as wells were being drilled, avoiding potential collisions and production interference with nearby wells. The ultimate goal of having an earth model is to convert it into a numerical model grid. The SIL earth model honors faults and fractures associated with the GSFZ as the main permeability source for the geothermal system. This key feature is well-adopted into the numerical model where the highest permeability is assigned in this particular fault zone. The current earth model is generated using existing available data and considered as not final yet. The model was designed as evergreen model that can be updated easily with new well data and interpretation.

ACKNOWLEDGEMENT

I thank Sarulla Operations Limited (SOL) and Pertamina Geothermal Energy (PGE) for supporting this project and granting permission to publish this paper. Also, this project could not have been undertaken without the support and encouragement of West JEC and Ormat.

REFERENCES

https://maps.google.com/

Gunderson, R. P., Dobson, P.F., Sharp, W.D., Pudjianto, R., Hasibuan, A. (1995), *"Geology and thermal features of the Sarulla contract block, North Sumatra, Indonesia"*. Proceeding of the World Geothermal Congress 2, 1183-1188.

Hickman, R.G., Dobson, P.F., van Gerven, M., Sagala, B.D., Gunderson, R.P. (2004), *"Tectonic and Stratigraphic Evolution of the Sarulla Graben Geothermal Area, North Sumatra, Indonesia"*, Journal of Earth Sciences 23, 435-448.

Silangkitang Project Resource Feasibility Study. SOL Internal Report, 1996.

Simatupang, C.H. (2017), *"Silangkitang Conceptual Model with Newly Drilled Well Based on Geochemistry Interpretation"*, SOL Internal Presentation Material.

Townsend, J., Zoback, M.D. (2000), *"How Faulting Keep the Crust Strong"*. Geology 28, 399-402.

FLUID CHEMISTRY CHARACTERISTIC OF NAMORA I LANGIT, A GEOTHERMAL SYSTEM WITHIN THE GREAT SUMATERA FAULT

Christovik Simatupang[1], Koji Matsuda[2], Elisabeth Easley[3], and Doddy Astra[1]

[1]Sarulla Operations Limited, The Energy Building, 51st Floor, SCBD Lot 11A, Jl. J. Sudirman, Jakarta 12910, Indonesia
[2]West Japan Engineering Consultants, Inc., Denki Bldg. Annex, Watanabe-dori 2-1-82, Chuo-ku, Fukuoka 810-0004, Japan
[3]Thermochem, Inc., 3414 Regional Parkway, Suite A, Santa Rosa, California, United States
Email: christovik.simatupang@sarulla-geothermal.com; mazda@wjec.co.jp; elisabeth@thermochem.com; doddy.astra@sarulla-geothermal.com

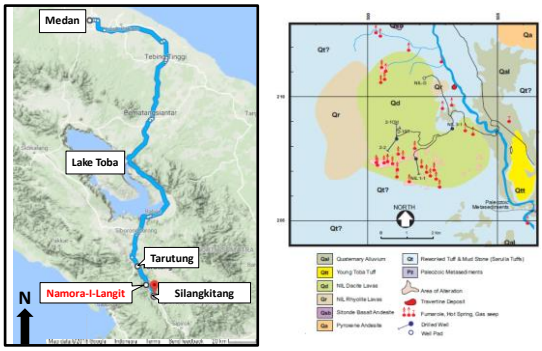
ABSTRACT

The Namora I Langit (NIL) geothermal resource is currently producing 232 gross MW. The NIL geothermal field is observed as a distributed permeability system and identified as liquid-dominated system with high temperature (>250°C) and high gas (> 1 wt.% in the reservoir fluid and ~7 wt.% at wellhead). The NIL geothermal field has been operated since October 2017 for Unit 1 and May 2018 for Unit 2 with the support of 11 production wells and 10 injection wells. Most of the production wells are drilled away from the Great Sumatera Fault (GSF) while the injection wells are mostly perpendicular to the GSF. The production wells are drilled towards the hypothetical upflow zone in the central of the prospect while most of the injection wells are drilled in the outflow zone which located in the eastern area of the prospect. The produced Non-Condensable Gas (NCG) at the wellhead is within 6.0 – 9.0 wt.% with the highest one is shown by the most eastern and the northern wells meanwhile relatively lower gas is demonstrated by the western and southwestern wells. The South and SW wells show relatively higher H_2S content. All the production well shows Na, K, Cl and SiO_2 concentrations below 1100 ppm in total fluid with pH ranging from acidic to alkaline. The southern wells drilled towards the hypothetical upflow exhibit low pH with elevated SO_4 and Mg, while wells drilled towards east and north show neutral pH with lower SO_4 and Mg. The Na-K-Mg Giggenbach plot demonstrates a partial equilibrium state of reservoir fluid at the NIL geothermal field. The helium isotope R/Ra values, $\delta\ ^{18}O$, and $\delta\ ^{2}H$ indicate a contribution of fluids from a shallow origin, and high positive $\delta\ ^{34}S$ isotope values are similar between acid and neutral wells. Down Hole Sampling (DHS) was conducted for several wells and results exhibit lower pH at the deeper feedzones. Two geochemical models are proposed to explain the fluid origin and flow at NIL, namely dissolution of magmatic gases and condensation of steam and H2S oxidation and dissolution in shallow oxygenated groundwater. Ongoing efforts are underway to collect more data collected during exploitation to narrow the uncertainty and further constrain the reservoir fluid origin and evolution.
Keywords: Namora I Langit, fluid chemistry, great sumatera fault, geothermal system.

INTRODUCTION

The NIL geothermal field is located about 300 kilometers Southeast of Medan in North Sumatera at an elevation of 800 – 900 meters above sea level.

NIL is situated on the eastern flanks of two coalescent Quaternary dacitic volcanic centers located at the northern end of the Sarulla graben. The NIL dacitic complex is located around 7 km apart from the strands of the GSF defining the graben and thus overlies graben-filling rocks. The geothermal system in this area is associated with numerous surface thermal features with temperatures range from near boiling to superheated steam (77-117 °C). The elevation of these thermal feature ranges from 1000 m asl to 1100 m asl in the northern zone of the NIL complex. The location of the NIL reservoir area is 1-3 km away from the GSF and the orientation of major fault structures suggests that the GSF zone influences the local structural regime, however evidence from reservoir engineering models suggests that the NIL reservoir is a distributed permeability system.



(a) *(b)*

Figure 1. (a) Map of Sarulla geothermal field which shows the location of the contract area from Medan (taken from Google Map) and (b) a geological map of NIL.

RESULTS

The NIL geothermal field has been operated by Sarulla Operations Limited (SOL) since October 2017 for Unit 1 and May 2018 for Unit 2 with the support of 11 production wells and 10 injection wells. Most of the production wells are drilled away

from the GSF while the injection wells are mostly perpendicular to the GSF.

Geochemistry data is important to understand and monitor a geothermal reservoir from development drilling through commercial exploitation. Ongoing surveillance activity is most useful if the baseline chemistry is collected and an initial state model is defined before commercial exploitation begins. Chemical data from all production wells, surface thermal manifestations, and surface facilities should be monitored to interpret the changes in reservoir processes as the response to the development strategy, i.e. the impact of injection, marginal recharge influx, and acid fluid invasion.

The components of a geochemical conceptual model, such as upflow, outflow, recharge and areas associated with reservoir process like, boiling, condensation, high gas, steam cap development, etc. can be determined. Incorporation of the geochemical model with other geoscience data must be completed to create an integrated conceptual model. In this paper, the liquid chemistry, gas chemistry, helium isotopes, sulfur isotopes, and oxygen-18 and deuterium isotopes were utilized to develop interpretations to define geochemical conceptual models for the NIL geothermal field. Some limitations exist in understanding the geochemistry characteristics in the injection area near the eastern margin of the field because fluid chemistry and isotope samples were not initially collected from the injection wells. Additionally, the static pressure and temperature downhole data collected for most wells during initial production flow tests did not exhibit stable temperature profiles.

Fluid chemistry of the production wells during long term flow test was the basis in establishing the initial chemical state of the field. The parameter that is used to define the reservoir such as pH, SO_4, Mg, Cl, R/Ra, $\delta^{34}S(SO_4)$, $\delta^{18}O$, and $\delta^{2}H$, H_2S/SO_4 ratio, and NCG. The wells that utilized in the interpretation are 18 wells that drilled during appraisal and development stage of the asset, except the injection wells.

pH

The initial pH, measured at 25 °C from separated brine samples, for wells drilled toward and beneath the main fumarole complex demonstrate low pH < 5 meanwhile the wells drilled away showed pH > 5 (Figure 2). Wells with a blue well track trajectory were drilled and tested during the initial Unocal exploration drilling campaign in the late 1980's and wells with a red well track were drilled and tested from 2015 to 2018 during the development drilling campaign by SOL. This pH data indicates the presence of acid fluid in NIL. The lateral distribution shows a possible acid source in southern and/or western part of the field. However, there are two wells that demonstrate anomalous pH values (<3) as compared with the surrounding wells. These wells are drilled from the southernmost wellpad towards the northwest and penetrate both shallow and deep feedzones.

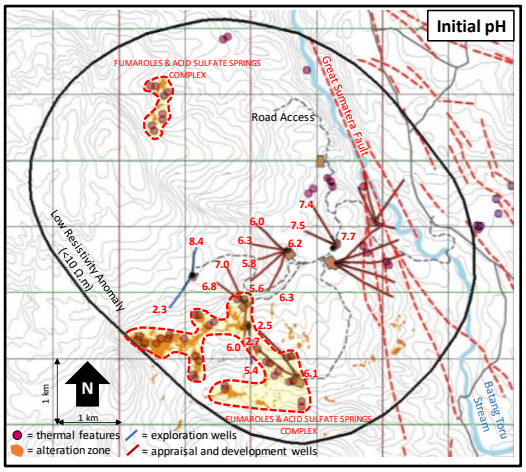


Figure 2. Map of NIL geothermal field initial pH distribution from the production well data. Numbers in red font are pH values measured from separated brine at ambient temperature.

SO_4

The initial SO_4 distribution (Figure 3) from production well data may be correlated with the initial pH distribution. The trend in low pH is correlated with high SO_4 concentration and vice versa.

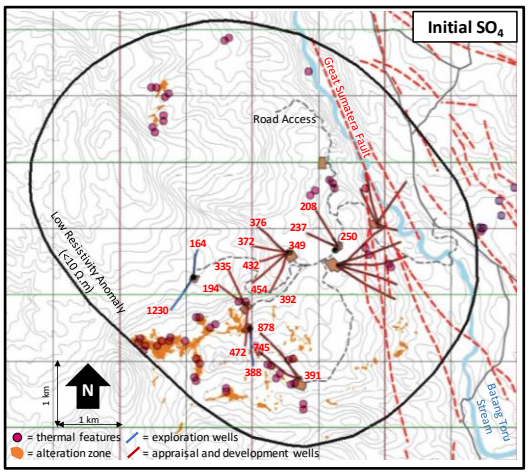


Figure 3. Map of NIL geothermal field initial SO_4 distribution from the production well data. Numbers in red font are reservoir SO_4 concentration in ppm.

This consistent trend between pH and SO_4 gives an indication of the acid source fluid type and the process of how the acid is formed. The anomalous concentration that is encountered by one of the SW wells (1230 ppm) may indicate where the source is located, however this sample was collected during the initial exploration drilling campaign in 1998 and

the well is currently non-operational, hence the data cannot be further validated. The SO_4 concentration from the Unocal well drilled toward south (388 ppm) and the SOL wells that drilled within the southern area (745 and 878 ppm) possibly indicate another potential acid source with lower SO_4 concentration as compared with the SW well (1230 ppm).

Mg

The distribution of the Mg concentration from the production wells shows correlation with pH and SO_4. The highest Mg is shown by the same well that shows the lowest pH and SO_4. This phenomenon can be explained by either rock dissolution due to acid fluid or signature of shallow water. The latter hypothesis is supported by the fact of high Mg wells associate with surface thermal feature distribution.

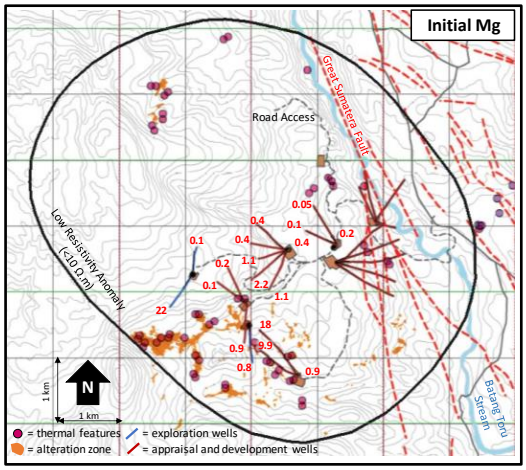


Figure 4. Map of NIL geothermal field initial Mg distribution from the production wells data. Numbers in red font are reservoir Mg concentration in ppm.

Cl

The near-neutral pH production wells drilled towards the northwest, west and southwest exhibit Cl within the range of 750 – 1137 ppm while the neutral-pH wells in the central area show lower range within 620 – 760 ppm. The acid pH wells in the south and southwest produced chloride ranging from 860 to 1092 ppm. The chloride concentration in NIL is relatively low as compared with the other liquid dominated system on the island of Java. The possibility of the contribution of HCl fluid is indicated by the anomalous value observed at the SW well which shows concentration of 1092 ppm. This is considerably higher than the surrounding wells and the well also exhibits the lowest pH and the highest SO_4 concentration in NIL.

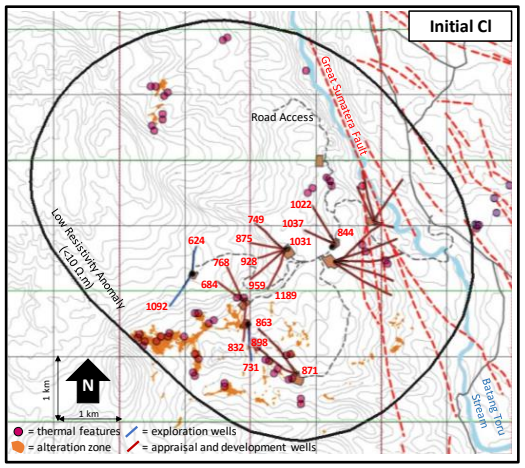


Figure 5. Map of NIL geothermal field initial Cl distribution from the production well data. Numbers in red font are reservoir Cl concentration in ppm.

$\delta^{18}O$

The presence of relatively heavier $\delta^{18}O$ is explained by the exchange of $\delta^{18}O$ with the rock or mixing between recharge/shallow (lighter $\delta^{18}O$) and andesitic/magmatic (heavier $\delta^{18}O$) waters. The heavier isotope is observed at wells that is located at the northern, southern and southwestern of NIL, meanwhile the wells that located within the central area show lighter $\delta^{18}O$. The northern wells that exhibit $\delta^{18}O$ at 4.9 are identified as the heaviest $\delta^{18}O$ amongst all the production wells. This fact indicates that the produced liquid at these wells is identical with a geothermal fluid type that has an intense water-rock interaction or less mixing with the lighter isotope liquid.

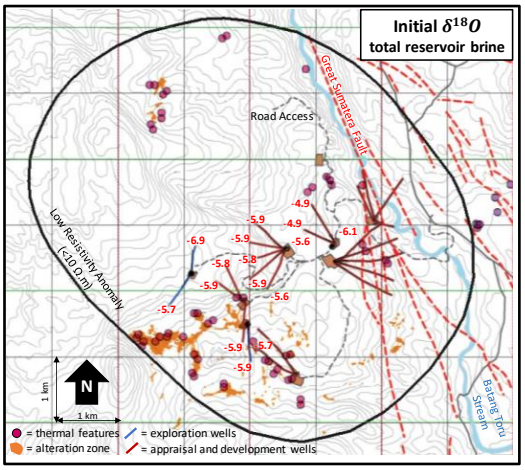
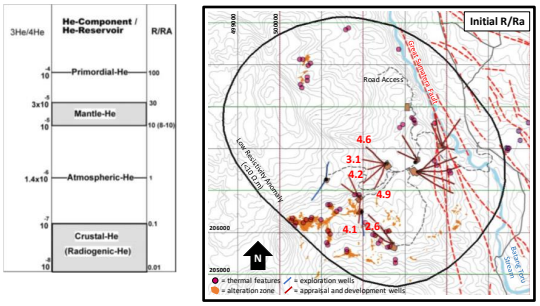


Figure 6. Map of NIL geothermal field initial $\delta^{18}O$ liquid distribution from the production wells data. Numbers in red font are $\delta^{18}O$ in ‰ for the total reservoir brine.

Helium

The sampling result from some of the wells at NIL shows the ratio of R/Ra within the range of 2.6 – 4.9. The lowest value is recorded at the Southern well

while the remaining wells exhibit ratio greater than 3.1 and lower than 5.0. The range of helium isotope samples at NIL plot on the low end of the range for volcanic arc environments and have some mantle helium, however not the elevated helium (i.e, R/Ra >7) that is expected from deep magmatic fluid (Kennedy et al., 2000). The low helium R/Ra values indicate that all wells sampled are enriched with atmospheric-He in the reservoir liquid at NIL, likely due to meteoric water inputs. The lowest R/Ra ratio in the southern well indicates the strongest contribution of meteoric water, potentially influenced by shallow groundwater.



(a) *(b)*

Figure 7. (a) Major He-components and He-reservoirs (R = $(^3He/^4He)_{sample}$, Ra = $(^3He/^4He)_{atmosphere}$) (Güleç, 2013). (b) Map of NIL geothermal field which shows the initial R/Ra distribution from the production wells data. Numbers in red font are ratio R/Ra.

NCG

The NCG samples and total fluid enthalpy measured during production flow tests suggest that the system is liquid dominated and the produced steam at the wellhead is generated from a brine flashing in the wellbore and not from excess steam. The NCG distribution between the exploration and the development wells exhibit the same N-S trend. The higher NCG is shown by wells drilled within the central and southern part of the field meanwhile the lower NCG is shown by the western and eastern wells. Two wells in the northern part of the field exhibit the highest NCG (1.55 to 1.73 wt% total discharge), which may indicate that the reservoir liquid feeding these wells is the most enriched with NCG. The N-S distribution of the moderate range (1.22 to 1.38 wt % total discharge) of NCG is suspected to be controlled by structures.

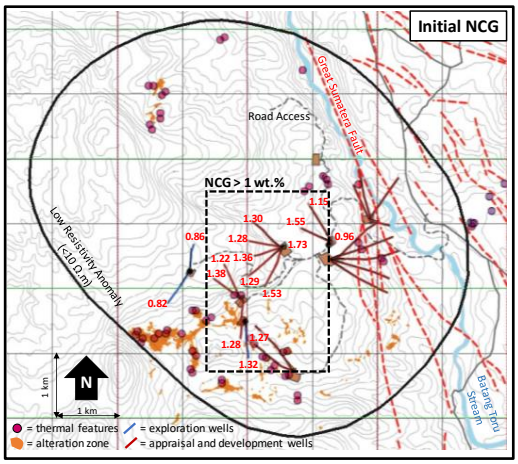


Figure 8. Map of NIL geothermal field which shows the initial distribution of NCG at wellhead from the production wells data. Numbers in red font are NCG total discharge in wt.%.

$\delta^{34}S(SO_4)$

The $\delta^{34}S(SO_4)$ value of all wells at NIL shows the same value. Moreover, both wells with low pH and alkaline pH exhibits high $\delta^{34}S(SO_4)$ value (> 30 ‰).

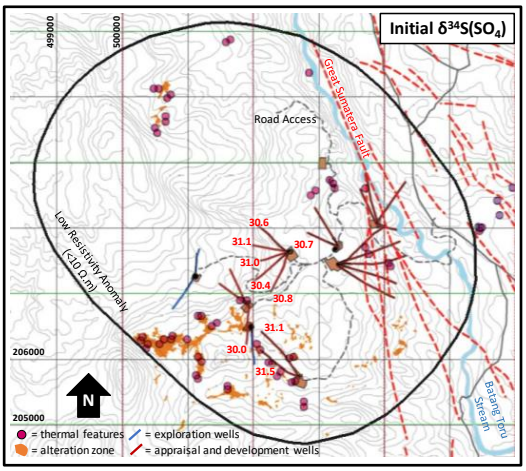
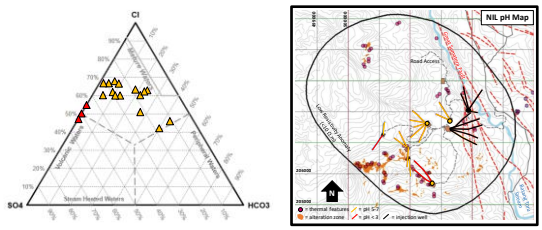


Figure 9. Map of NIL geothermal field which shows the initial $\delta^{34}S(SO_4)$ liquid distribution from the production wells data. Numbers in red font are $\delta^{34}S(SO_4)$ in ‰.

INTERPRETATION

Cl-SO_4-HCO_3

The ternary plot of Cl-SO4-HCO3 (Figure 10a) is aimed to identify the maturity of a Cl-bearing water and determine if it is associated with a mature (neutral) chloride geothermal system by the proportion of the major anions present in geothermal water (Powell, 2010).



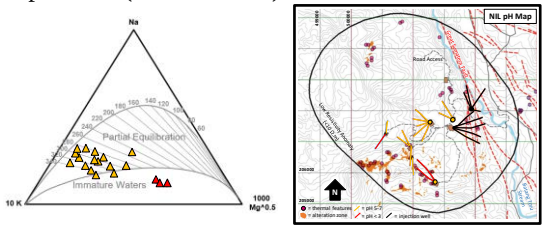
(a) *(b)*

Figure 10. (a) Cl-SO_4-HCO_3 ternary plot; orange triangles are wells with pH > 5 while the red triangles are wells with pH < 3. (b) Map of NIL geothermal field which shows the pH distribution of the production wells; colors are identical with the ternary plot.

The low pH (<3) wells plot as volcanic waters, while the other production wells shows chloride-sulfate waters with varying levels of bicarbonate. Several wells are located close to the low pH wells and demonstrate a mixing trajectory between the acid fluids and a chloride end-member. It is important to note that none of the fluids produced from the NIL geothermal reservoir are mature, equilibrated, chloride waters. This is consistent with the Cl concentration shown in Figure 5.

Na-K-Mg

A "geoindicator" that illustrates both the evidence that supports the interpretation of equilibrated water at high temperature and the influence of shallow processes and possible equilibration at lower temperature (Powell, 2010).



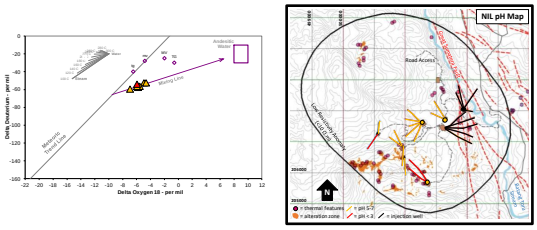
(a) *(b)*

Figure 11. (a) Na-K-Mg ternary plot; orange triangles are wells with pH > 5 while the red triangles are wells with pH < 3. (b) Map of NIL geothermal field which shows the pH distribution of the production wells; colors are identical with the ternary plot.

The fact that most of the wells that associated with low pH plot in the immature water in Figure 2 indicates that the low pH has strong relation with high magnesium liquid. Meanwhile the other wells located within the central area are partially equilibrated with the reservoir rock. This plot also reveals another interesting fact where the most NE wells are the closest production wells to the full equilibrium line.

$\delta^{18}O$ and $\delta^{2}H$

The ^{18}O shifts depend also on the initial isotope composition of the liquid and solid phases involved in the exchange process as well as on the water/rock ratio, or on system dynamics.



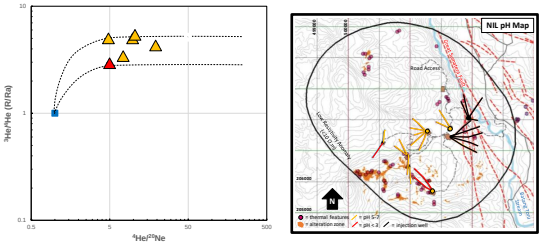
(a) *(b)*

Figure 12. (a) Stable isotope of $\delta^{2}H$ and $\delta^{18}O$ liquid diagram from all production wells and analogues from Miravalles and Tongonan using Geochemical Plotting Spreadsheet (Powell, 2010). (b) Map of NIL geothermal field which shows the pH distribution of the production wells; colours are identical with the plot of (a).

The second process affecting the $\delta^{2}H$ and $\delta^{18}O$ values of geothermal liquids is mixing between local meteoric waters and waters of different origin, namely, magmatic, marine, connate, and other high-salinity waters (Giggenbach, 1991). The NIL production wells surprisingly demonstrate almost the same value in $\delta^{2}H$ and $\delta^{18}O$ despite a wide range in pH. Additionally, the most isotopically enriched samples in $\delta^{18}O$ are observed for the most northeast wells, which is consistent with the Na-K-Mg ternary plot (Figure 11) where the same wells plot close to the full equilibrium line.

He Isotope

Helium (He) has two stable isotopes, ^{3}He and ^{4}He. The production rate of ^{3}He is very low compared to ^{4}He.



(a) *(b)*

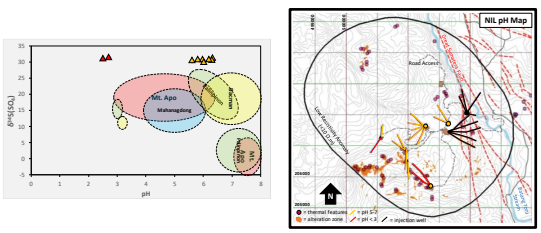
Figure 13. (a) R/Ra vs $^{4}He/^{20}Ne$ liquid cross plot from all production wells. Blue square is Air/ASW R/Ra of 1. (b) Map of NIL geothermal field which shows the pH distribution of the production wells; colors are identical with the plot of (a).

Crustal/Radiogenic-He has an R/RA range of 0.01-0.1 (Andrews, 1985; Welhan et al., 1988)

meanwhile Mantle-He has $^3He/^4He$ ratio of around R/RA ≈ 8-30, reflecting the dilution of Primordial-He with that produced by radiogenic processes in the mantle (Mamyrin and Tolstikhin, 1984; Farley and Neroda, 1998). The presence of high $^3He/^4He$ ratios (i.e., > 7) in volcanic regions may be indicative of a young volcanic heat source. The fact that none of the wells that show R/Ra ratios > 5 indicate mixing with atmospheric helium as compared with the primordial-He. This is consistent with the low Cl concentration and partial equilibration with reservoir rock (Figure 5, 10 & 11).

$\delta^{34}S(SO_4)$

The isotopic composition of sulfur species in geothermal discharges may similarly be used to obtain information on the fluid origin. The fact that the sulfur isotopes cease to equilibrate within the geothermal environment (except in hot acid waters) because of unfavorable conditions for isotope exchange, and thus retain the signature of the last equilibrium temperature. The "heavy" (>15 ‰) dissolved sulfates are thought to be directly derived from SO_2 disproportionation at greater depth while the close to 0 ‰, "light" sulfates are typically found in thermal areas, draw sulfate from H_2S oxidation at or near the surface. There is no isotope exchange at all in this shallow environment, thus the sulfate adopts the ratio of the sulfide source. Those sulfates with ratios in between (i.e., 0‰ > X > 15‰), are most likely produced by mixing of the deep, $\delta^{34}S(SO_4)$-enriched fluid and the shallow, $\delta^{34}S(SO_4)$-depleted water, such as in thermal features and steam condensates (Bayon & Ferrer, 2005). The same $\delta^{34}S$ values observed in all the sampled wells indicates NIL reservoir fluid comes from the same source. The high $\delta^{34}S$ ratio suggests that the reservoir fluid may associate with an environment where SO_2 disproportion at greater depth is possible. The comparison of NIL with the other acid geothermal systems supports the hypothesis of the same sulfate liquid source that supply the NIL system.

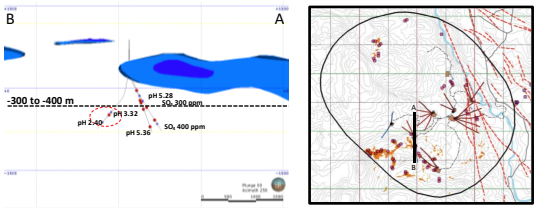


(a) *(b)*

Figure 14. (a) $\delta^{34}S(SO_4)$ vs pH cross plot from all production wells. (b) Map of NIL geothermal field which shows the pH distribution of the production wells; colors are identical with the cross plot.

DHS

The DHS was conducted on some production wells that located within the S, SW and central in flowing condition. The result shows lower pH at wells that drilled away to the area where the less intensity of low resistivity anomaly. The pH is trending lower and sulfate is trending higher over depth.



(a) *(b)*

Figure 15. (a) The pH and SO_4 vertical distribution. (b) Map of NIL geothermal field which shows the well distribution.

DISCUSSION

The characteristic of NIL geothermal fluid is low to moderate pH, high sulfate, low chloride, partially equilibrated and high gas. The fluid within the current exploited area is interpreted to come from the same source as evidenced by sulfur isotope. The contribution of liquid from shallow depth seems to contribute as shown by helium isotope while the contribution from the deep liquid is shown by the high value of sulfur isotope. The reservoir liquid shows a typical of geothermal fluid from its $\delta^{18}O$ and $\delta^{2}H$ but the liquid has not achieved full equilibrium with the reservoir rock or mixed with the other type of liquid and re-equilibrated.

CONCLUSION

Currently there are multiple models that developed by SOL, WJEC, and Thermochem and work is currently being carried out to gather more data to further constrain the models. The first priority is to measure stable PT data from all the wells.

ACKNOWLEDGEMENT

We would like to thank Sarulla Operations Limited and Pertamina Geothermal Energy (PGE) for granting permission to publish this study, especially to William Lajousky III and Shinichi Aburaya for supporting us in making this paper.

REFERENCES

Andrews, J. N. (1985), "The Isotopic Composition of Radiogenic He and its Use to Study Groundwater Movement in Confined Aquifer", *Chemical Geology*, 49, pp 339-351.

Bayon, F.E.B., Ferrer, H. (2005), "Sulphur Isotope Ratios in Philippine Geothermal Systems", *Use of Isotope Techniques to Trace the Origin of Acidic Fluids in Geothermal Systems*, IAEA.

Farley, K. A. and Neroda, E. (1998), "Noble Gases in the Earth's Mantle", *Annual Review of Earth and Planetary Sciences*, 26, pp 189–218.

Giggenbach W.F. (1991), "Chemical Techniques in Geothermal Exploration", *In Application of Geochemistry in Geothermal Reservoir Development.* (F. D'Amore, co-ordinator), UNITAR, pp 119-144.

Güleç N. (2013), "Isotope and Gas Geochemistry of Geothermal Systems", *IGA Academy Report 0112*.

Kennedy, B.M., Fischer, T.P., Shuster, D.L. (2000), "Heat and Helium in Geothermal Systems", *Proceedings, 25th Workshop on Geothermal Reservoir Engineering, Stanford University*.

Mamyrin, B. A. and Tolstikhin, I. N. (1984), "Helium Isotopes in Nature". *Elsevier, Amsterdam*.

Powell, T. (2010), "Spreadsheets for Geothermal Water and Gas Geochemistry". *Proceedings, 35th Workshop on Geothermal Reservoir Engineering, Stanford University*, CA, SGP-TR-188.

Welhan, J.A., Poreda, R.J., Rison, W., and Craig, H. (1988), "Helium Isotopes in Geothermal and Volcanic Gases of the Western United States", *I. Regional Variability and Magmatic Origin. Journal of Volcanology and Geothermal Research*, 34, pp 185-199.

ASSESSING THE IMPACT OF FAULTS AND FRACTURES ON PERMEABILITY BASED ON BOREHOLE DATA IN ULUBELU GEOTHERMAL FIELD, LAMPUNG, INDONESIA

Muhammad Tajul Arifin, Imam Muhammad Prasetyo, Graniko Reza Pratama,
Mochamad Husni Thamrin, and Hary Koestono

PT. Pertamina Geothermal Energy
Menara Cakrawala 19th floor, Jl. M.H. Thamrin No.9, DKI Jakarta, 10430
Email: muhammad.tajul@pertamina.com

ABSTRACT

Aside from volcanic activity, the geological structure in Ulubelu Geothermal Field strongly depicts the consequence of dextral movement at the southern tip of Sumatran Fault Zone. It produces northwest – southeast (NW-SE) alignments that can be clearly observed on the morphology. Although the NW-SE structures is obvious on the surface but there have been no publications about the influence of faults and fractures on permeability in Ulubelu Geothermal Field. The study is conducted by integrating borehole data from six wells to assess the impact of these structures to the permeability of the wells. The study reveals permeability of the wells is clearly controlled by the intensity of the geological structures. Northwest – southeast structures including faults and conductive fractures are the main factors that can be divided further to rank the intensity of fracturing. It is evidenced that wells intersected by fault zone give the highest permeability. When the fault is absent, the permeability deteriorates and leaving the intensity of continuous conductive fractures contribute to some degree.

Keywords: Ulubelu Geothermal Field, permeability, fault and fracture.

INTRODUCTION

A geothermal system could be found in an area around the dextral strike-slip fault movement forming pull-apart basin and the volcanic cluster (Muraoka, et al., 2010). The condition found in Ulubelu geothermal field is one of its example. The field is located at the southern tip of Sumatra Island near the termination of Sumatra Fault Zone (Figure 1). Therefore, its geological structure is influenced by both tectonic and volcanic activities. There are numerous faults and circular features as the result of tectono-volcanic activity.

The Ulubelu Geothermal Field (UGF) occupies 2-3 km wide depression with dominant NW-SE structures (Figure 2). These structures are parallel – sub parallel with the greater Semangko Fault (southern segment of SFZ). The occurrence of manifestation around the field is mainly associated with these NW-SE structures that provide permeability for ascending hydrothermal fluid to the surface. Evidence from UBL-03 and UBL-26 in Trianggo, et al., 2015 shows that the NW-SE fault and their associated fractures are the productive structures in the subsurface of Ulubelu.

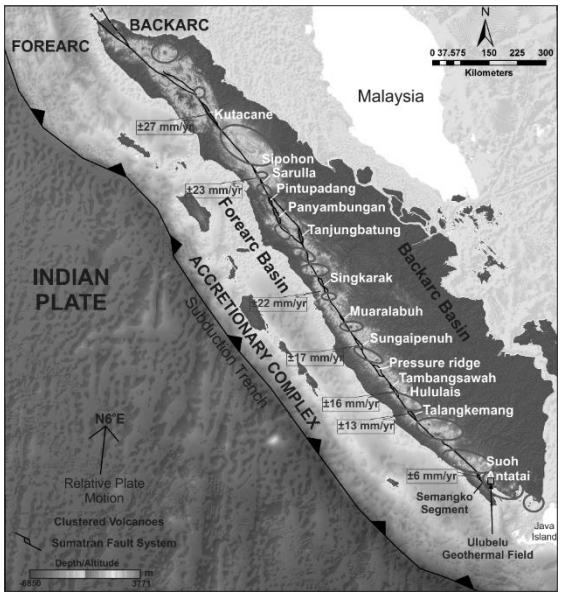


Figure 1: Tectonic map of Sumatra showing the relative location of Ulubelu Geothermal Field (UGF) at the southern tip of Sumatra Fault Zone (SFZ) (modified from Muraoka, et al., 2010, Barber, et al., 2005, Darman & Sidi, 2000, Sieh & Natawidjaja, 2000).

Based on evidence from both surface and subsurface as explained above, we know faults and its associated fractures enhance the permeability of the existing rocks. Secondary permeability allows greater hydrothermal fluid to flow from subsurface to the surface. However, it is difficult to exactly quantify both sructures contributing to the fluid flow in geothermal. Study regarding this matter has never been made before. The following chapters discuss the integration of borehole geology and reservoir data in UGF to reveal the effect of faults and fractures on permeability (Figure 2).

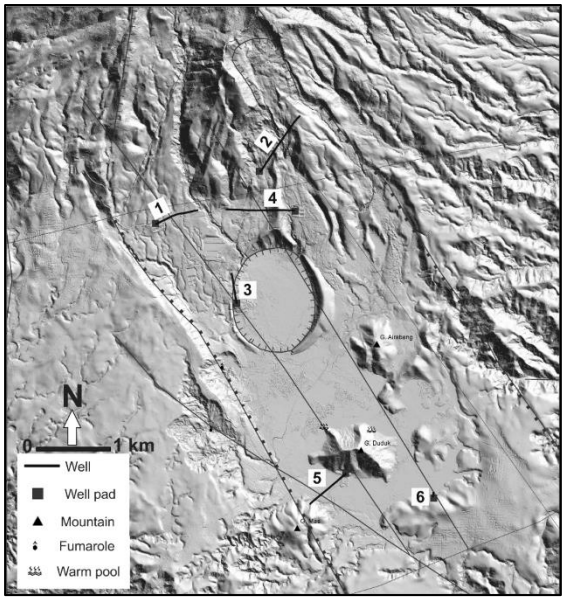


Figure 2: Geological structure of Ulubelu Geothermal Field dominated by NW-SE faults and some circular features. The trajectory of six wells that were used in this study (wells 1-6).

METHODOLOGY

Borehole image data and production logging tools (PLT) survey with heating up temperature profiles and drilling circulation from six wells were used for this study to assess the influence of faults and fractures to reservoir rocks permeability.

There are five types of sinusoidal feature that has been identified as fractures and fault on the borehole image data (Figure 3); (1) Continuous conductive fracture (CCF) is characterized by dark, brownish, blackish sinusoid that cuts across the borehole. (2) Discontinuous conductive fracture (DCF) is similar to CCF but it only partially cuts the borehole. (3) Low angle conductive fracture (LACF) is characterized by either continuous or discontinuous sinusoid with dark, brownish, blackish colour and has dip magnitude of <30º. (4) Resistive fracture (RF) has bright or whitish sinusoid colour. (5) Fault (FA) is identified based on the washed out borehole due to intense fracturing that caused distorted image. Then the identified fractures were plotted based on depth and fracture strike to see the distribution on each well.

Conductive fracture exhibit darker colour on the image due to its low resistivity value. Several reasons could make that situation such as filled by conductive drilling mud if it is an open fracture, mineralized by pyrite or clay minerals. Meanwhile, the resistive fractures have brighter colour due to its higher resistivity value. Higher resistivity value occurs as the fracture filled by resistive minerals such as calcite, quartz or others.

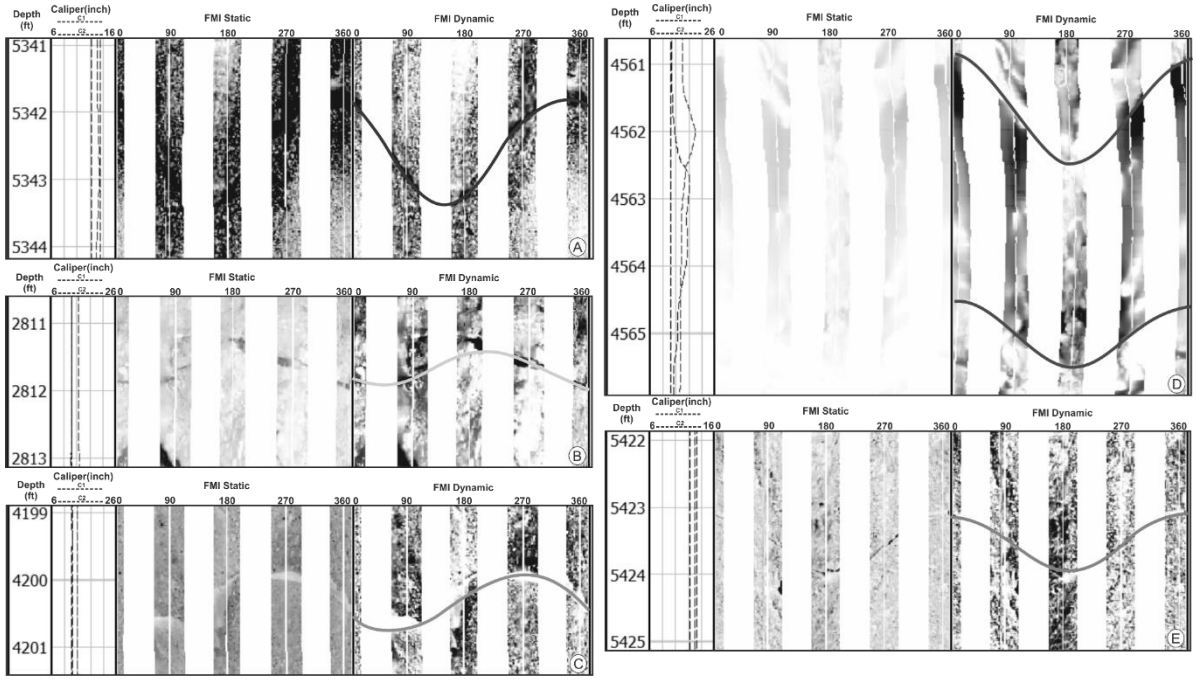


Figure 3: Five type of planar features on the borehole image data. (A) Continuous conductive fracture (CCF); (B) Low angle continuous conductive fracture (LACF); (C) Resistive fracture (RF); (D) Fault (FA); Discontinuous conductive fracture (DCF)

Production logging tools (PLT) survey data is utilized to locate the depth of feedzones and flow contibutions from each entry. Minus percentage in the flow contribution reflects the flow from borehole into formation, while the positive percentage suggests that the flow runs from formation into the borehole. Fracture density (fracture/m) for four fractures type (CCF, DCF, LACF, RF) then were calculated by using the depth interval of each feed zone. Fault is excluded from the calculation of fracture density as it is rarely found and for practical reason in the plotting against contribution to separate fault with the other fractures. Feed zones with contribution <5% are also excluded from fracture density calculation. Moreover, fracture density and flow contribution were plotted to reveal the impact of fracture and fault to the permeability.

RESULTS & DISCUSSIONS

Thorough analysis have been made from the wells data. It shows the NW-SE fracrures trend is predominate with dip direction either to the SW or SE. All the data is represented on elevation in meters above sea level (masl). Each well is reviewed below:

Well 1

It could be seen on the chart below (Figure 4) this well is dominated by NW-SE fractures with SW dip azimuth. Feed zones with > 5% contribution were calculated its fracture density. The temperature profile does not give us insight about the location of feed zones as it was directly measured 128 days after the well completion.

From top to bottom borehole, resistive fractures took place from elevation 0 to -850 masl and covers two major feed zone. The occurrence of resistive fractures is often interpreted as sealed fractures due to deposition of resistive mineral (eg quartz, calcite). Although dominated by resistive fracture, on the interval of two major feed zone at elevation -146 to -262 masl and -574 to -853 masl, there are faults and some continuous conductive fracture that are responsible to the flow contribution (see the fracture density chart). The fault on elevation around -207 masl is also responsible to the total loss circulation.

Well 2

From the chart below (Figure 5), we can infer that the well is also influenced by NW-SE fractures. These fractures are dominated by SW dip azimuth from elevation -350 to -650 masl, while the SE dip azimuth intensity starts from elevation -650 masl downward. Around elevation -600 to -650 masl a deflected temperature profile is observed. It is indicated that the main feed zones with numerous conductive fractures around that elevation are responsible for it. It is noticeable that from elevation -800 to -900 masl around 40% flow contribution is concentrated there due to intensive fracturing. Meanwhile, the rest flow contribution (60%) is distributed on the upper part with 500 m thick.

Well 3

This well is similar to ohers, dominated by NW-SE fractures from top to bottom of the logged interval, with NE-SW as the subordinate (Figure 6). The increasing intensity of conductive fractures is correlated with the progression of mud circulation losses from intermittent to fully total at around -400 to -500 masl and sharp temperature deflection (-500 to -600 masl). The deflected temperature profile is controlled by the main feed zone (80% contribution) on elevation -540 to -600 masl where it contains a lot of conductive fractures (CCF, DCF, LACF) with very minor resistive fracture. Besides that, there are numerous wide open fracture (20 – 25 cm) found in this interval (Figure 7). Resistivity fractures intensity increases just after the main feed zone. The second and smaller feed zone is contributed from less intense conductive fractures, accumulating 20% contribution.

Well 4

The logged borehole image data could only be obtained up to elevation -1000 masl while the feed zones are located deeply starts from elevation -900 masl downward. So we are limited to discuss only at the covered zone which covers half of the first feed zone (Figure 8). The fractures itself dominate the well with NW-SE strike and NW dip azimuth that contains discontinuous conductive fractures, resistive fractures with less conductive continuous fractures and the low angle conductive fractures. When the resistive fractures decreases at elevation -900 masl, while at the same time entering the first feed zone, temperature profile increases and turns to convective profile at elevation -1030 masl. In the half of first feed zone, the fractures are dominated by discontinuous conductive fracture with 0,65 fracture/m. Within this first feed zone, we found a break in circulation while drilling that caused TLC for a while and then became total loss around elevation -1000 masl.

Well 5

In general, the well is dominated by NW-SE fractures consisting of discontinuous conductive fracture with minor continuous conductive fractures (Figure 9). At the top of the logged interval, the minor feed zone at elevation -160 masl caused total loss circulation for several minutes. Later on the drilling circulation became intermittent along with two feed zones containing some continuous conductive fractures.

Total loss circulation occurred from elevation -440 masl downward. At the same elevation, the temperature profile shows convective profile which indicates good permeability down there. Within the TLC interval, the fracture intensity increases sharply

and there is a major feed zones with 70% contribution at elevation -560 masl due to fault (Figure 3D). The fractures become more intense with NW-SE strike and NE or SW dip azimuth. Around 80% flow contribution is located within this TLC interval.

Well 6

The well is a vertical well as we can see on Figure 2. It is dominated by NW-SE fractures with either dipping to NE or SW with NE-SW as the subordinate fractures (Figure 10). Intense fractures distribution occurs at depth between -650 to -1200 masl. In this interval there are several minor feed zones that counts up to 20% flow contribution within this 550 m thick interval. There were two occasions when the drilling intersected total circulation loss zone and both are within above interval.

Around elevation -1200 masl downward, total loss circulation occurred and there is a deflected profile temperature. Within this TLC interval, nearly 80% flow contribution comes from 4 (four) feed zones. The largest one is at the elevation -1230 masl. Near this depth, the borehole image data failed to record the image for 5 m length due to washed out borehole. It is possibly caused by intensive fracturing or faulting occurred at the washed out interval.

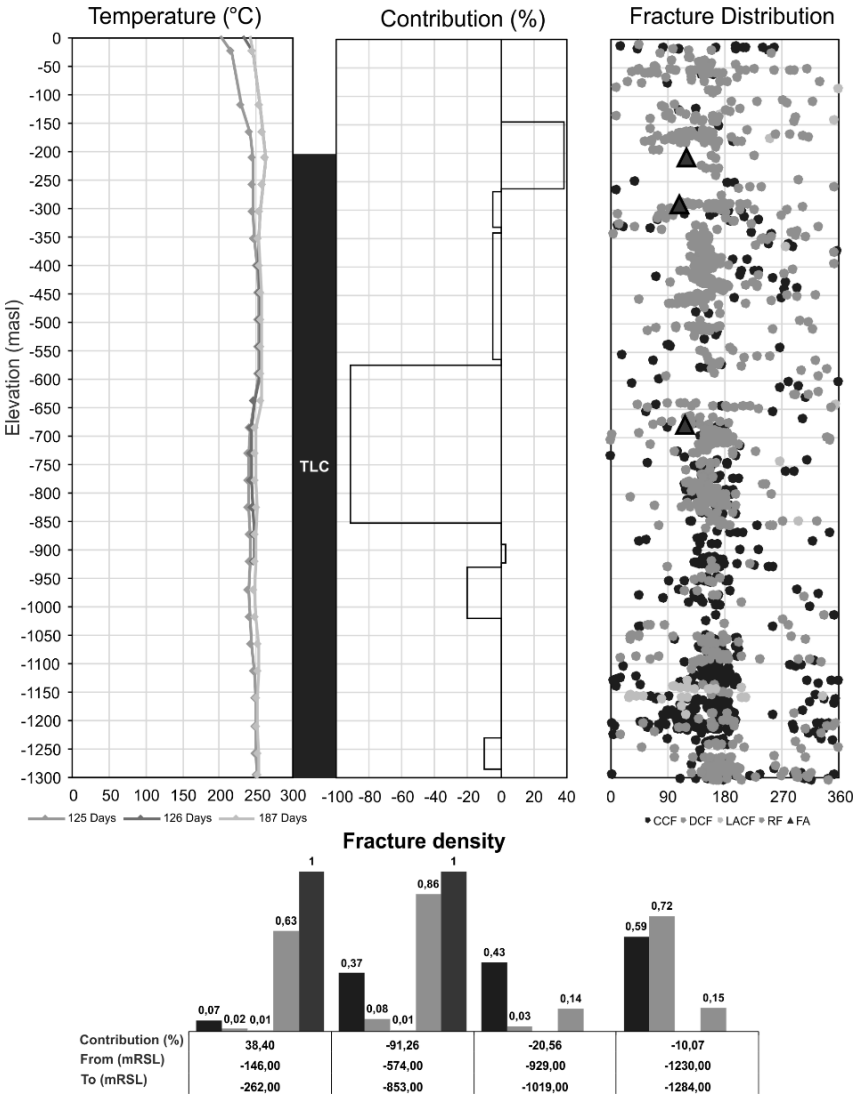


Figure 4: Temperature, drilling circulation, flow contribution, fracture distribution and fracture density of Well 1. Notice that the start of TLC coincides with the fault.

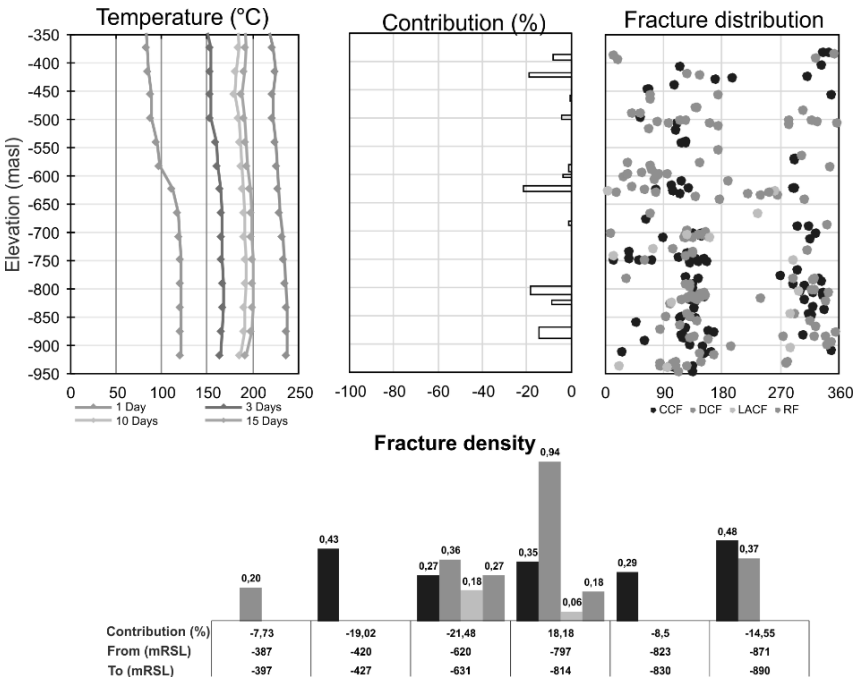


Figure 5: Temperature, flow contribution, fracture distribution and fracture density of Well 2. No loss circulation found, only partial. Feed zones from -800 to -900 masl contribute to 40% flow.

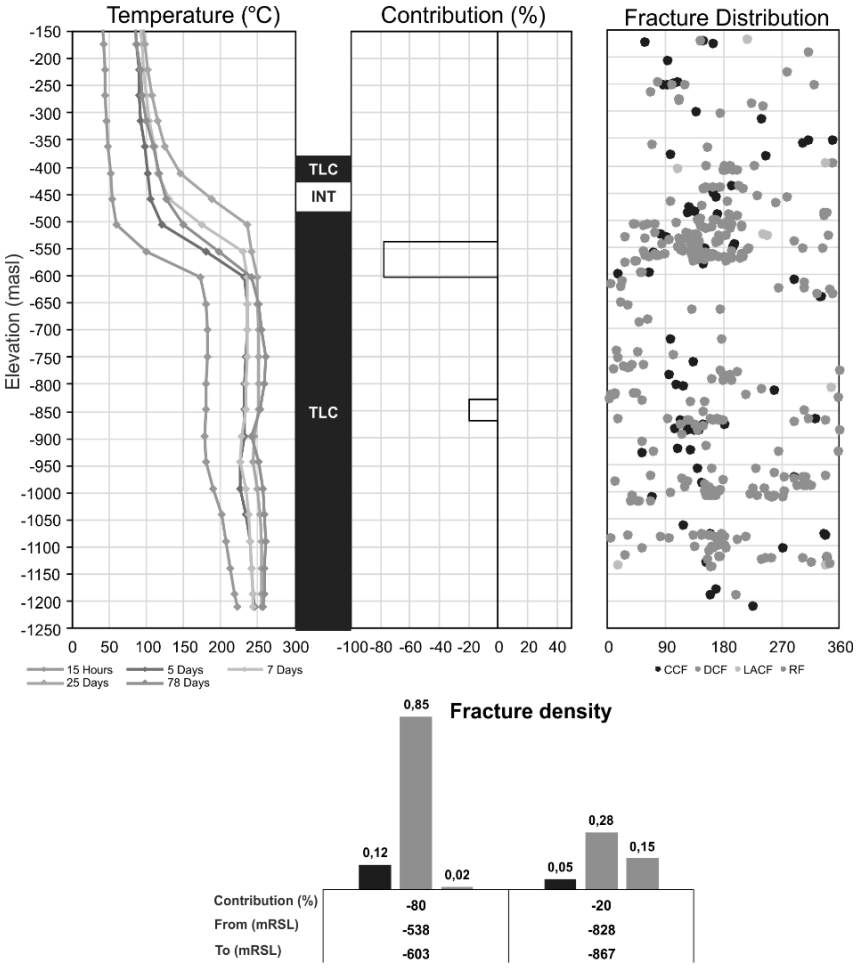


Figure 6: Temperature, drilling circulation, flow contribution, fracture distribution and fracture density of Well 3. Sharp deflection on temperature correlates with the first feed zone around -540 to -600 masl.

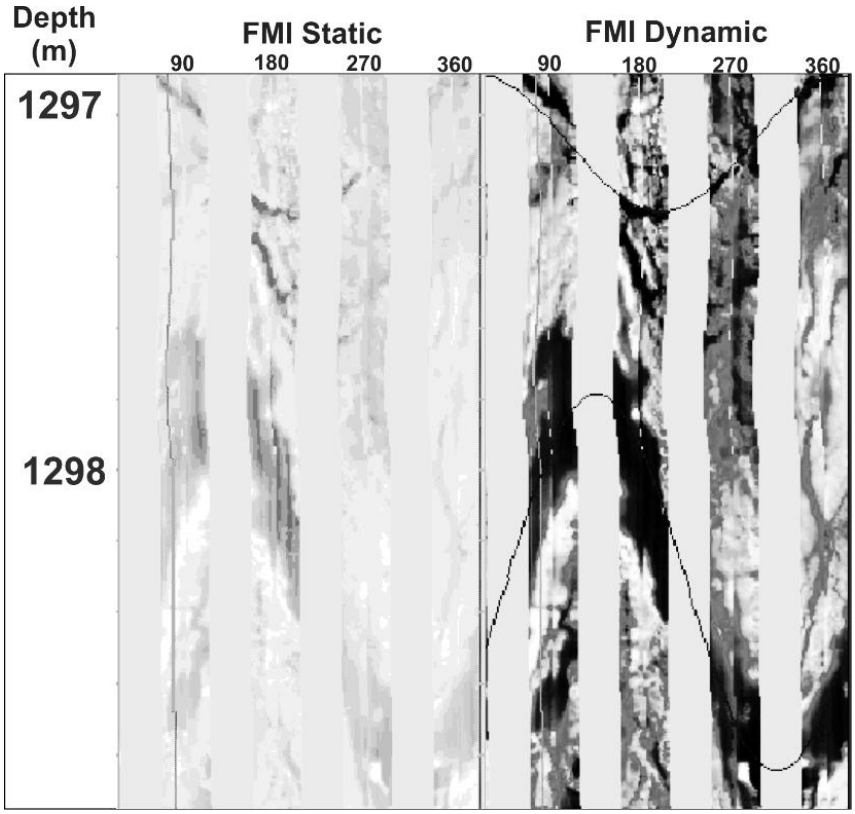


Figure 7: Widely open continuous conductive fracture in Well 3 that contributes as the major feed zone.

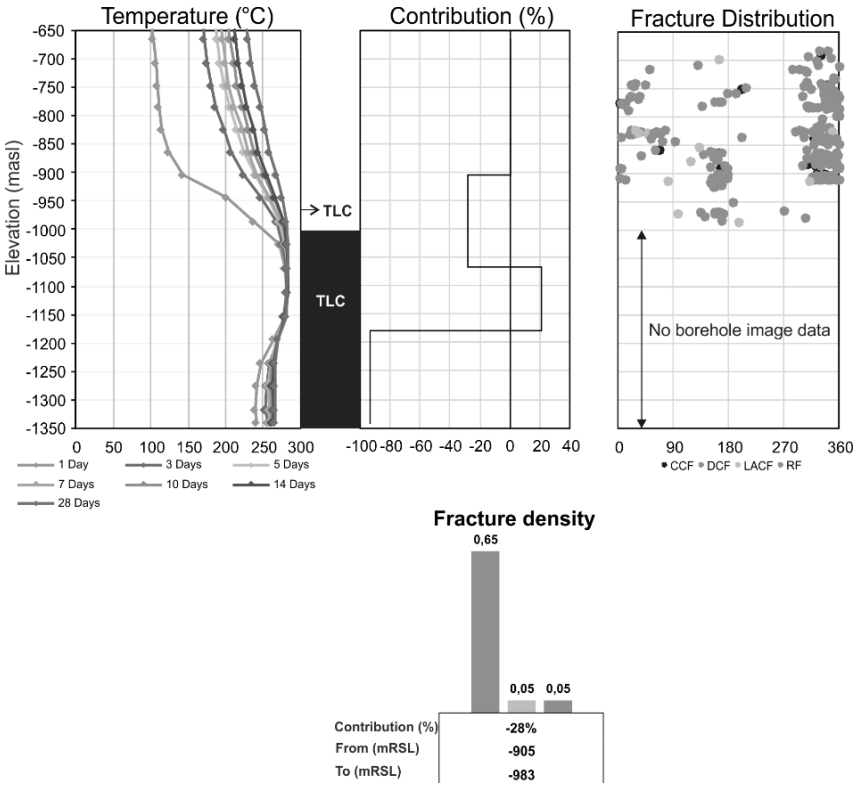


Figure 8: Temperature, drilling circulation, flow contribution, fracture distribution and fracture density of Well 4. The TLC zone coincides with convective temperature profile with major flow contribution that indicates good permeable structure although there is no borehole image data.

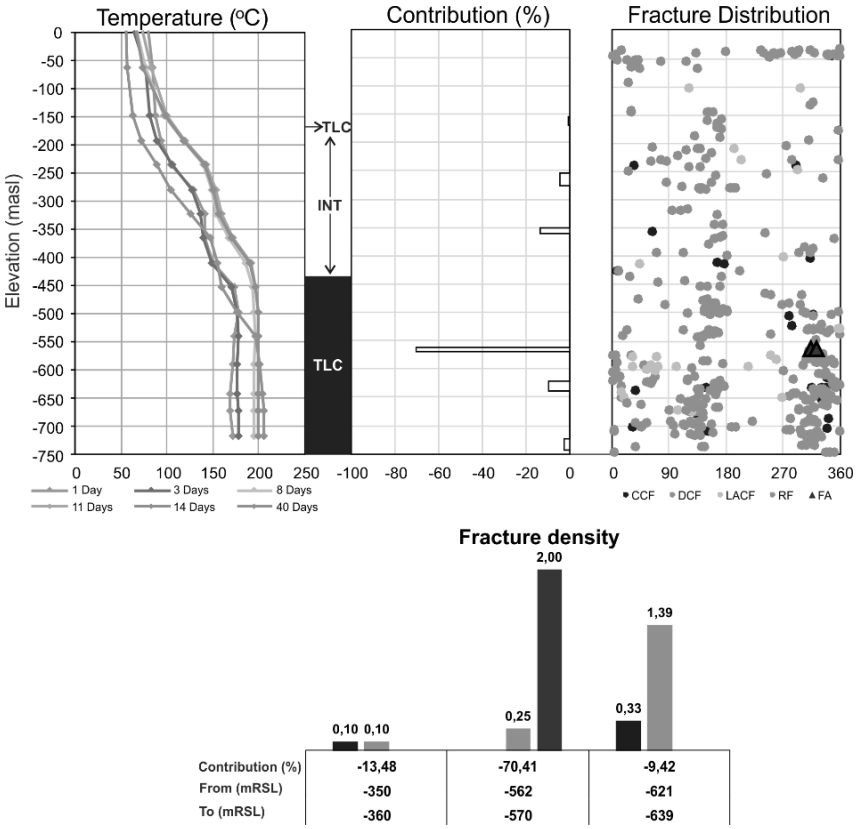


Figure 9: Temperature, drilling circulation, flow contribution, fracture distribution and fracture density of Well 5. Fault on elevation -560 masl contributes to the 70% flow. The TLC zone coincides with the convective temperature profile.

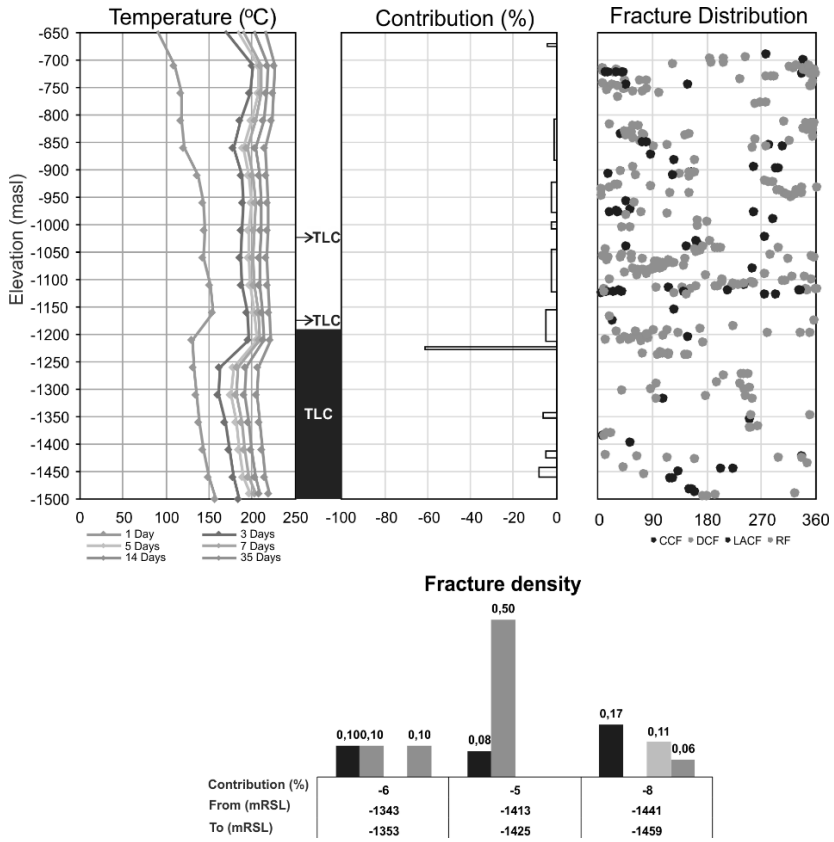


Figure 10: Temperature, drilling circulation, flow contribution, fracture distribution and fracture density of Well 5. It is interpreted that major feed zone in elevation -1230 masl is contributed by fault.

Fracture density vs flow contribution

The study above reveals that the more intense or dense the conductive fractures (including CCF, DCF, LACF and fault) in a well, the greater the flow contribution. The resistive fracture is excluded from this assumption as it is interpreted that the open fractures are deposited by resistive minerals such as calcite, quartz, etc.

Plotting the fracture density against the flow contribution from each feed zones gave insight about how much the influence of fault and conductive fractures to the flow contribution (Figure 11). In this calculation, faults are excluded from the calculation and count as 1.

It is observed that there are 4 (four) ranks of feed zone based on the fault and conductive fracture density. The first one is when the feed zone has <0,6 conductive fractures/m, the flow contribution only counts as maximum as 20%. Second, when the density is > 0,6 conductive fractures/m, the flow contribution is as minimum as 10%. Third, at the 1st feed zone in Well 2, 80% flow contribution is due to the occurrence of widely open conductive fractures as seen on Figure 7. Fourth, flow contribution increases significantly if the fault intersect the wells such as in Well 1, Well 4 and Well 6.

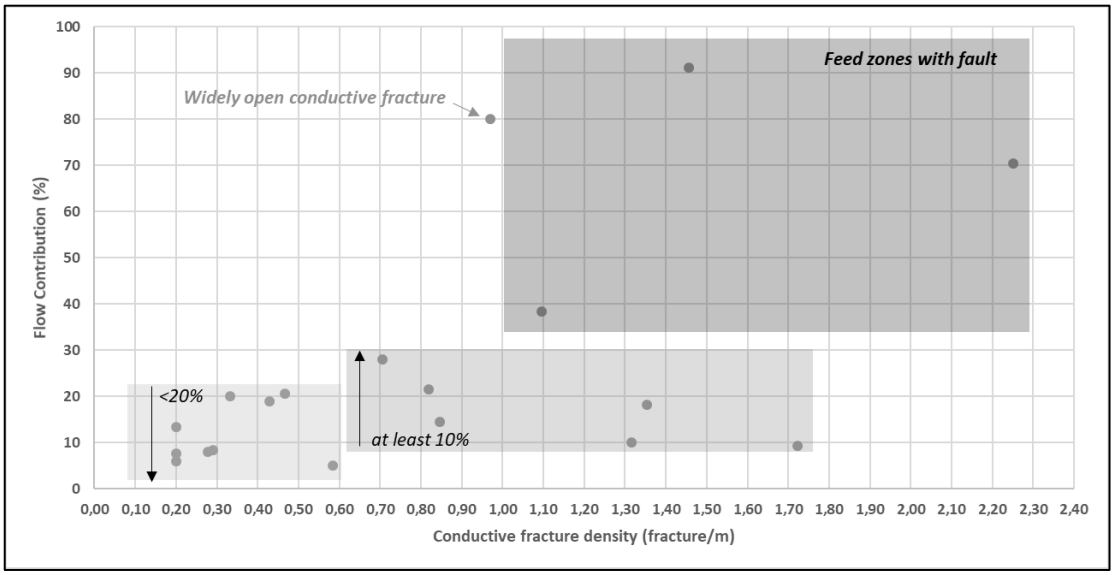


Figure 11: Conductive fracture density including CCF, DCF, and LACF and fault which is count as 1 plotted against flow contribution. Four feed zones rank are made; (1) Feed zones with <0,6 conductive fracture density (translucent green box); (2) Feed zones with >0,6 conductive fractures density without fault (translucent blue box); (3) Feed zones with widely open conductive fractures (orange text); (4) feed zones with fault (translucent red box).

Feed zone characterization and its application to the field development

By plotting the feed zone with its flow contribution and elevation in a bubble chart (Figure 12), it is observed that feed zones from the wells on the western part and the eastern part behave differently. Wells in the western part have major feed zone starting from elevation -150 to around -550 masl. Meanwhile, the eastern part of the field, major feed zone is found starting from elevation around -1150 to -1250 masl.

Although Well 1 succeeded to penetrate to elevation of -1200 masl, the flow contribution in this depth is quite small (only 10% contribution). Furthermore, well 3 also reached to elevation around -1250 masl and found no feed zone at this depth. On the eastern part, due to hole problem Well 2 could not reach the elevation deeper than -1000 masl.

In order to plan a make-up well for the field, we know that if we put the well on the western part and target the same structure, we could limit the well penetration up to elevation less than -1000 masl. Meanwhile, if the well is planned on the eastern part and target the same structure, we have to drill up to elevation -1200 to -1300 masl in order to maximize the flow contribution.

The variety depth of feed zones in this field requires more analysis that will be discussed comprehensively later in another paper. It is related with the distribution of clay cap and subsurface structure based on magnetotelluric (MT) model and subsurface geology evidences.

CONCLUSION

Based on the surface data, the UGF is dominated by NW-SE structures. The trend is also consistent with the subsurface data as shown on the fractures

distribution from this study. The NW-SE structures, comprised of conductive fractures (CCF, DCF, LACF) and faults, intersected by the wells are mainly responsible to the geothermal fluid flow contribution. The more intense distribution of conductive fractures in the feed zone, the greater the flow contribution. Identification of feed zones controling factor and relatively quantifying the contribution of faults and fractures will greatly assists the future field development and plan the effective make-up wells.

REFERENCES

Barber, A.J., Crow, M.J., and Milsom, J.S. (2005), *"Sumatra: Geology, Resources and Tectonic Evolution"*. Geological Society, London, Memoirs, 31 (2005), 290 pp.

Darman, H., and Sidi, F.H. (2000), *"An Outline of the Geology of Indonesia"*, Indonesian Association of Geologists, Jakarta, 192pp.

Muraoka, H., Takahashi, M., Sundhoro, H., Dwipa, S., Soeda, Y., Momita, M., and Shimada, K. (2010*), "Geothermal Systems Constrained by The Sumatran Fault and Its Pull-Apart Basins in Sumatra, Western Indonesia"*, Proceedings World Geothermal Congress, Bali, Indonesia, 25-29 April.

Sieh, K. And Natawidjaja, D. (2000), *"Neotectonics of the Sumatran fault, Indonesia"*. Journal of Geophysical Research.

Trianggo, S., Sardiyanto, Koestono, H., Thamrin, M.H., Kamah, M.Y. (2015), *"Evaluation of The Productive Geological Structure in Ulubelu Geothermal System"*, Proceedings World Geothermal Congress, Melbourne, Australia, 19-25 April.

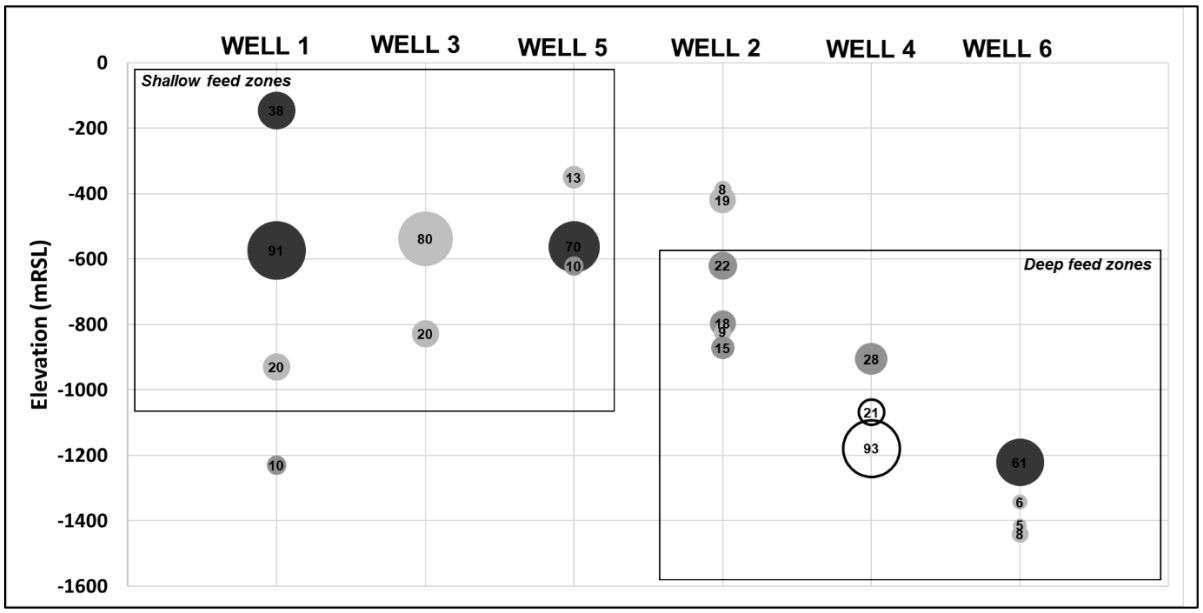


Figure 12: Feed zone distribution across the wells and its rank based on the fault and conductive fracture density. Note that the western part of the field is shallower than the feed zones in the eastern part (see map on Figure 2 to see the location of the wells). The bubble is coloured based on the rank on Figure 11. Bubble size reflects the flow contribution. The numbers within the bubble is the percentage of the flow.

UPDATED LITHOLOGICAL AND TEMPERATURE MODEL IN SORIK MARAPI GEOTHERMAL FIELD, INDONESIA

S. Mulyani[1], Z.F. Sarmiento[3], A.C. Licup, Jr.[2], V.R. Chandra[2], R. Hendry[2], S. Nasution[2], R. Hidayat[2], P.P. Sari[1], Jhonny [1], and D. Juandi[1]

[1]Schlumberger
[2]PT Sorik Marapi Geothermal Power
[3]KS Orka Renewables PT Ltd
Email: smulyani@slb.com; zammy.sarmiento@ksorka.com; armando.licup@ksorka.com; vicky.chandra@ksorka.com; ridha.hendry@ksorka.com; syukri.nasution@ksorka.com; ryan.hidayat@ksorka.com; psari2@slb.com; jjhonny@slb.com; djuandi@slb.com

ABSTRACT

Sorik Marapi is one of geothermal field in Indonesia that has been drilled, with results indicating the existence of a high temperature-neutral resource. To achieve the target 240 MW installed capacity, understanding reservoir condition of this field at exploration stage is the key. In this case, lithology and temperature values in geothermal can be used as parameters for reservoir characterization and creating dynamic reservoir model. Initial modeling works in the field has been completed and discussed in previous study to create 3D conceptual subsurface model, including structural, lithology, resistivity and temperature distribution. This paper deals with the 3D modeling studies conducted in the same field, based on available data from surface exploration (3G-geological, geochemical & geophysical) surveys, and additional data from deep drilling in several wells path.

The objective of this new paper is to build updated geological and temperature models with additional 10 wells data and give explanation about reservoir characterization in Sorik Marapi geothermal field, including new reservoir delineation based on the new model. The 3D subsurface modeling uses Petrel® software from Schlumberger which allows multidiscipline data integration. The 3D model containing structural, lithology, resistivity and temperature model from the 14 wells in the area. The workflow in the models starts with data loading and quality control, prepare structural model and 3D grid for reservoir property modeling, create 3D model of lithology, resistivity and temperature. The result of this study will be the 3D subsurface static model defining the vertical and lateral resource boundaries as well as the prime resource areas which would be the basis of designing next well targets. This model can be expanded to build updated numerical model, as parameter for reservoir simulation of geothermal field in the next stage.

Keywords: Updated model, updated wells, lithology model and temperature model, Petrel, Sorik Marapi, Indonesia

INTRODUCTION

This project reference field is Sorik Marapi that located in North Sumatra, Indonesia (Hochstein and Sudarman,1993). Sorik Marapi geothermal power plant unit 1 has ready for their production stage in March 2018, with capacity 20 MW (www.industri. bisnis.com). Meanwhile, the production of Sorik Marapi power plant unit 2 has been targeted at September 2018. The total capacity that will be produced by this field is 240 MW by 2022 (Filtech Energy Drilling, 2017).

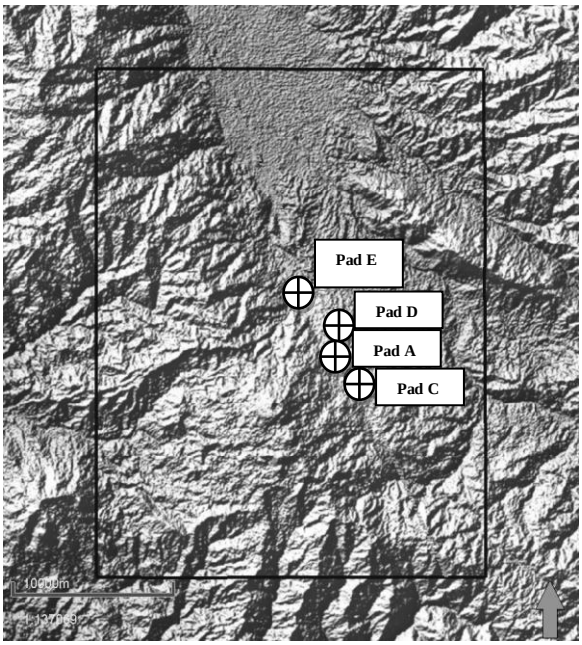


Figure 1: Project boundary (black square) of study area, with well pads from North are E, D, A and C.

The model boundary used in this project same with the previous study, as shown in Figure 1. The study area is 7.37 km^2 that cover 23.9 km x 31 km in length. Coordinate position of that area is 11069749-11093602 for x-axis and 65186-96200 for y-axis.

A conceptual 3D subsurface model built in the previous study based on 2 well pads data (A and E) (Sagala et al., 2018). The model was built sequentially from structural model, lithology model, resistivity model and temperature model. Since they are built in the same 3D grid, all of results should be compatible with each other (Licup, A.C., et. all, 2017). Now on its exploration drilling and production stage, Sorik Marapi Geothermal Power get additional wells data from pad C and pad D that used to calibrate and update the previous model. The updated model includes lithology and temperature models which built by using Petrel® software.

EXISTING 3D SUBSURFACE MODEL

The Existing 3D model was built based on surface data such as topography points, faults lineament and formation boundaries (Akar et al., 2011). The vertical range of 3D model is -3000 to 2000m from sea level datum. The lateral dimension of cell grid which construct entire 3D model is 25 x 25m, with cell thickness 45m. Based on the information provided by the model, it consists of structural, lithology, resistivity and temperature distribution.

Structural Model

The structural model of previous study (Hamilton, 1979; HelpSieh & Natawidjaja, 2000; Cattin et al., 2009; Muraoka et al., 2010; Weller et al., 2011; Blanco et al., 2015), gave information about the faults plane position in the subsurface. Several faults plane with major direction Southwest – Northeast (SW-NE) shown by Figure 2. The trace of those faults influenced the topography at the surface with some clear lineament.

Lithology Model

The existing lithology model built based on the conceptual delineation from available well data (pad A and E). There are four main unit formation of lithology in Sorik Marapi field, they are: dacitic dike, sibanggor volcanic, roburan volcanic, and sorik volcanic. The stratigraphic relationship between three volcanic formations showing conformable contact, with intrusion by dacitic dike (Figure 3).

This model used as reference for updated lithological model, based on additional information of lithology from well pad A, C and D.

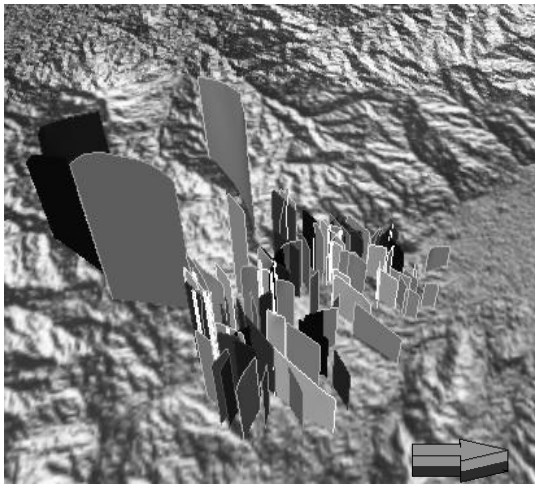


Figure 2: Faults plane at structural model with major direction SW-NE (Licup, A.C., et al., 2017)

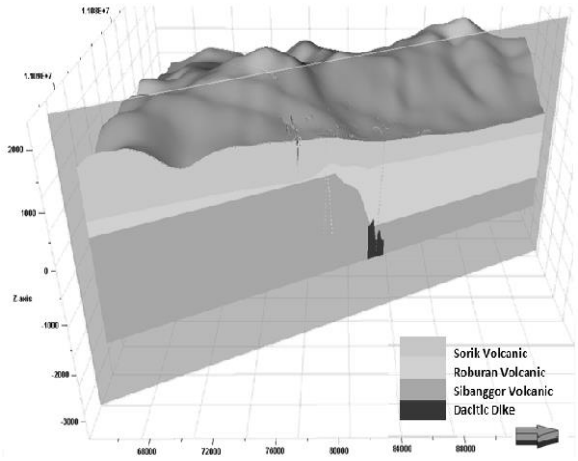


Figure 3: Lithological distribution of Sorik marapi field with conformable contact between sibanggor, roburan and sorik volcanics, and intrusion contact by dacitic dike.

Resistivity Model

The resistivity model was built based on resistivity point values which derived from magneto telluric data. The interpolation method used kriging algorithm, that good for dense data modeling. Basically, this algorithm will assign all cells without resistivity value, based on the interpolation of values from neighboring cells. This algorithm and its modification mainly used for creating updated model.

Result of resistivity modeling gave information about the resistivity value distribution for entire area. Based on the existing data, the range value of resistivity is 0-500 ohm.m (Figure 4). As product of geophysical method (magneto telluric) done in the surface, there is no update for this model. Even though, this soft

data will be used in the further analysis while doing update temperature modeling.

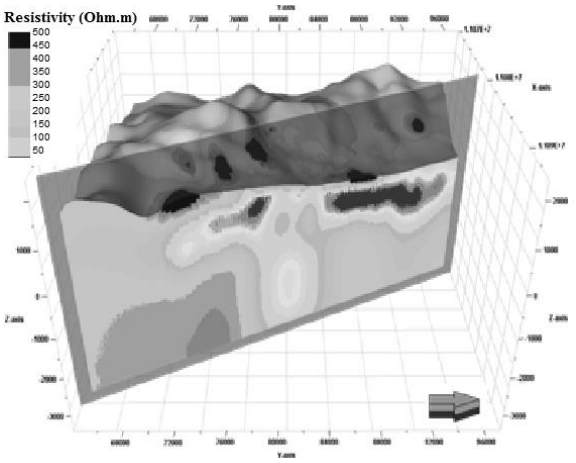


Figure 4: Resistivity model based on points with resistivity attribute which derived from magnetotelluric data in Sorik marapi field (Licup, A.C., et al., 2017)

Temperature Model

One of the main objectives of this entire study is updating temperature model. Existing model built based on the correlation function between resistivity values and temperature well point data. With limited available data which came from Pad A and Pad E, the result shown distribution of temperature value with high deviation at certain well path (well E201).

Figure 5 show the temperature distribution from previous study, with range values 25-270ºC. By having additional well temperature data, the Existing model can be calibrated and updated to get better understanding of subsurface temperature.

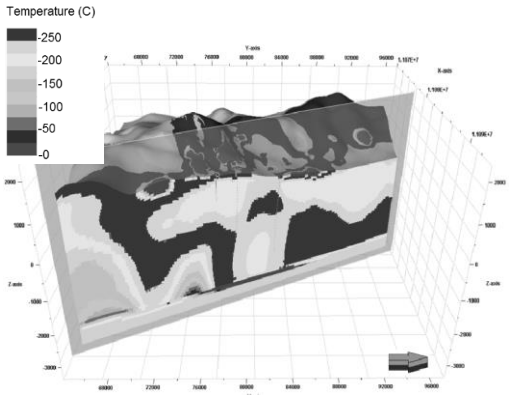


Figure 5: Existing temperature model based on resistivity & temperature function, with range values 25-270ºC.

DATA AND METHODOLOGY

To update the existing model, additional well data that consisted of lithology and temperature were given. The summaries of additional well data shown at table 1 below. By including four Existing well path data, there are total 17 wells path from 4 pads that used for this project.

Table 1: Summaries of Existing and additional wells data with the available information to be used in this project

Data	Wells	Lithology	Temp. Points	Temp. Log
Existing	SM E-201	-	Yes	-
	SM E-202	-	-	-
Additional	SM A-101	Yes	-	Yes
	SM A-102	Yes	Yes	-
	SM A-103	Yes	Yes	Yes
	SM A-104	Yes	Yes	Yes
	SM A-105	Yes	-	-
	SM A-106	Yes	-	Yes
	SM A-107	Yes	-	Yes
	SM C-109	Yes	-	Yes
	SM C-111	Yes	-	Yes
	SM C-113	Yes	-	Yes
	SM C-114	Yes	-	Yes
	SM C-115	Yes	-	-
	SM D-108	Yes	-	-
	SM D-110	Yes	-	-
	SM D-112	Yes	-	-

Lithology data of several well path provided as stratigraphic marker (well tops). They gave information about the position of formation's contact along well path. Identification and classification of lithology formations done by using well data, based on characterization of each formation lithology units. Temperature data available for nine well path as continues log data. With small increment, this data gave more detail information of temperature, rather than temperature point well data that has been used in the previous study.

Methodology done in this project is 3D modeling by using Petrel® software. Workflow for this study consist of four main steps: model preparation, data analysis, updating model, and results validation. The flow chart for this workflow shown in Figure 6.

Data preparation is the first step done in this project by having Existing model of structural, lithology, resistivity and temperature data from previous study. This step includes loading additional well data into existing project. Data importing process started from well head information that have the coordinate location of wells, followed by well path, well log temperature, and lithology as well tops. Quality

control of those data applied by displaying them at 3D window and checking for their values.

Data Analysis is the second step which done by comparing the result of existing lithology and temperature model with the lithology and temperature data from additional wells. If the existing model is match, there is no need to rebuild the model. Those result will become calibrated model based on the update data. If the existing model is not match, rebuilding is needed. The modeling process could be similar with the previous study, with more information from additional well data.

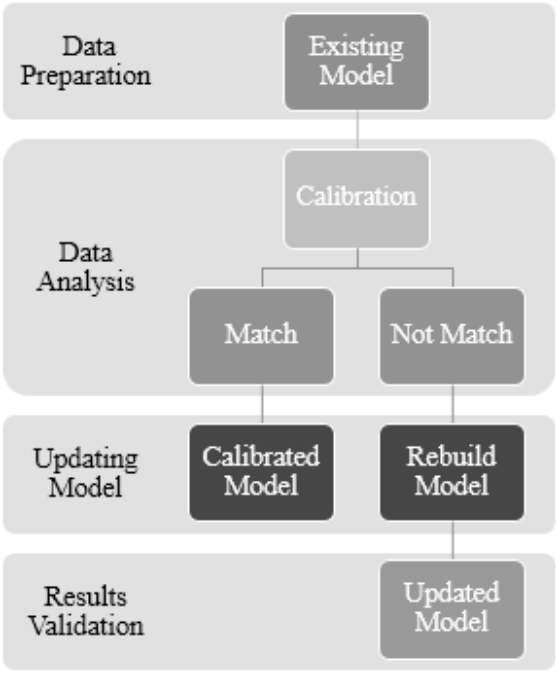


Figure 6: Workflow for calibrating and updating the Existing 3D Subsurface Model by using Petrel® software.

Results validation is the last step that needed to check the compatibility of updated model. This process can be done qualitatively based on the models' values at histogram or statistic information. To validate the last results, some blind well test which excluded during modeling process was used to do cross check with results value at their location. Similar values are a proof that the updated model is accurate, and vice versa.

RESULTS MODEL

There are two updated models that will be discussed in this project, they are lithology and temperature model. Each result used different approach to calibrate and rebuild the model. Both results analyzed at the same 3D grid structural model that consist of faults plane and properties information.

Lithology Model

Based on the workaround for this project, first step to be implemented is data calibration. The comparison between existing lithology model and additional lithology data done by displaying them at well section window.

The existing lithology model can be extracted along well path as discrete log. New lithology data displayed as marker (well top) that show the position of formation's contact and correlation for all wells.

Based on those contact, zone logs created by having formation's information at certain thickness. Figure 7 displaying several wells with discrete log from existing lithology model at the second column, and zone log from additional data at the third column. The connected lines are the contact position from three formations, they are sorik, roburan, and sibanggor volcanic. There is no information for dacitic dike formation from additional wells.

Based on those comparison, it clearly shows the deviation between existing lithology model with the well marker from additional data. For the example at well SM C-109, SM C-111, and SM A-103, the contact position between roburan and sibanggor are approximately 100m higher than the contact position based on existing lithology model. At well SM A-102, those contact position is 100m lower, and the roburan volcanic thickness is thinner compared with the existing model. Since there are many un-match results, rebuilding the lithology model is needed.

To rebuild the new lithology model, the surfaces contact used as input for 3D grid were updated based on the correct position of well tops data. The surface editing done for sorik, roburan and sibanggor formations. Figure 8 show the difference surfaces of sibanggor before (above) and after (below) editing.

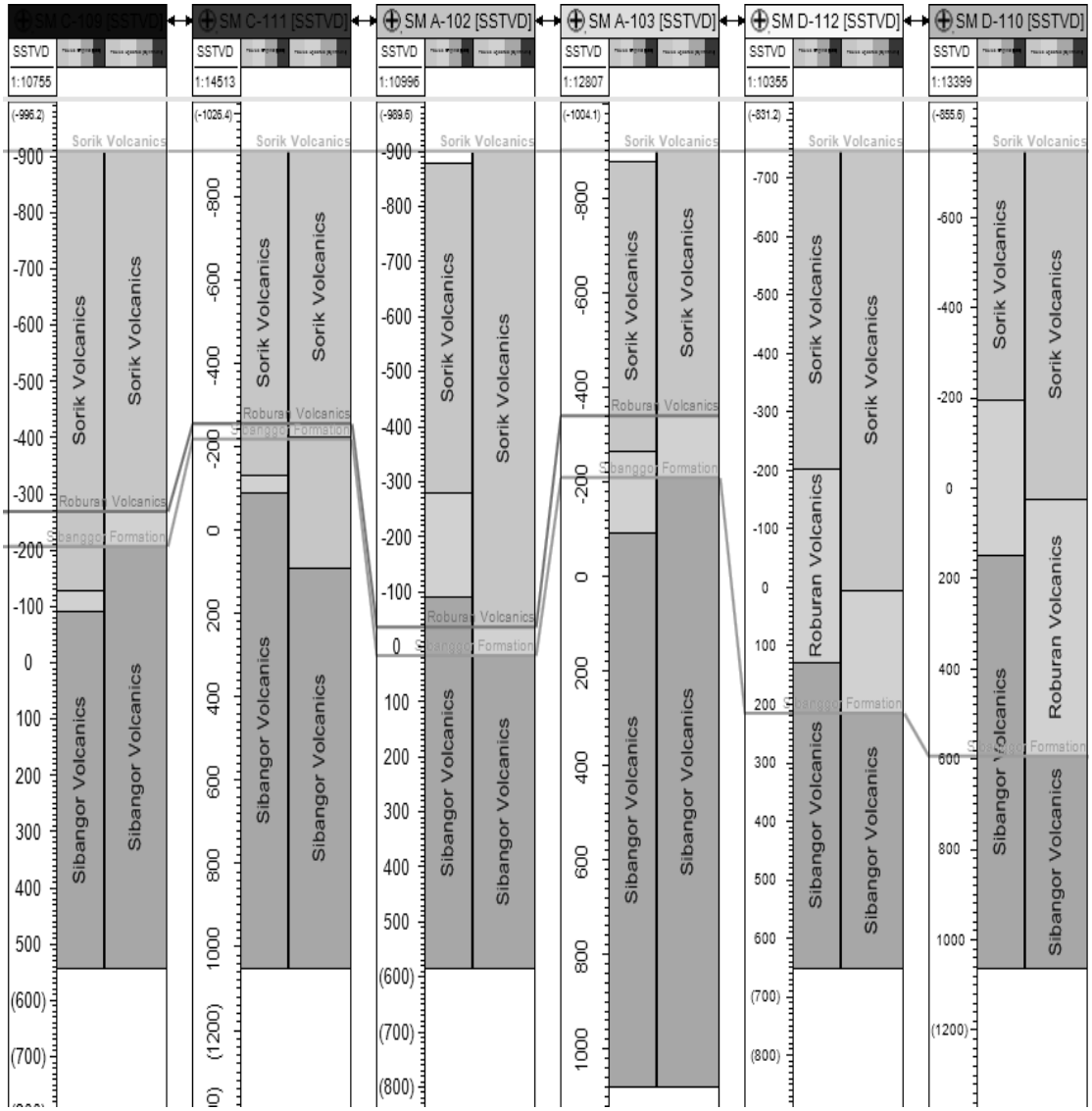


Figure 7: The comparison between discrete log from existing lithology model and zone log from additional data.

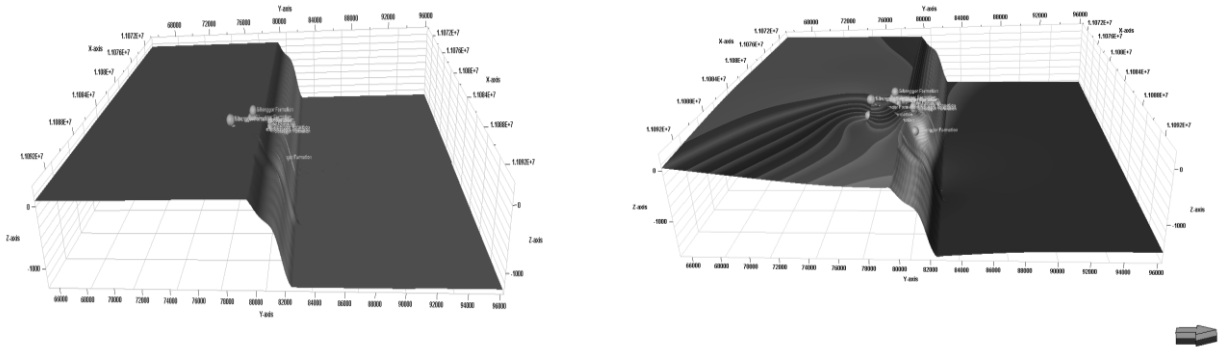


Figure 8: Sibanggor surface used for rebuilding 3D grid lithology (right) and the original surface used for creating existing lithology model (left).

By using updated surfaces, the new 3D grid was built to get new lithology model (Figure 9). The distribution of formation's information done by using geometrical modelling with method assign value between surfaces and polygon.

Updated lithology model can be validated based on histogram results (Figure 10). The formation distribution shows largest proportion for sibanggor volcanic (51.8%), followed by roburan volcanic (36.2%), sorik volcanic (11.9%) and the smallest proportion is dacitic dike (0.2%).

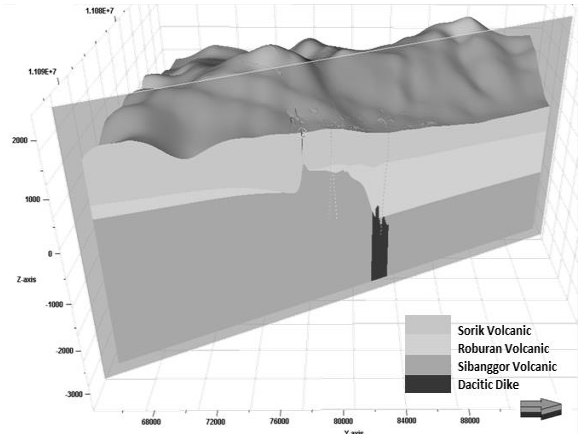


Figure 9: Updated lithology model in Sorik marapi field.

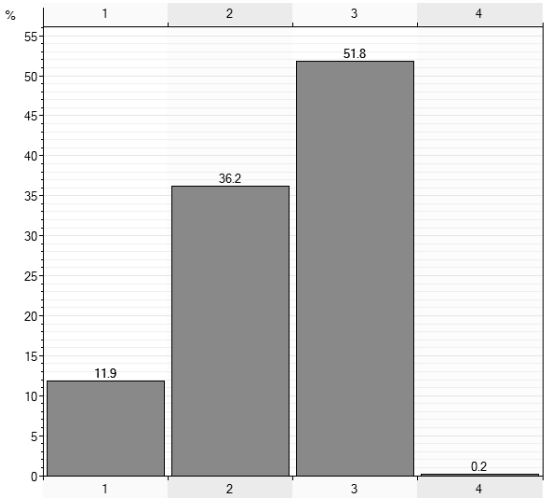


Figure 10: Histogram chart of lithological properties from updated model with information of formation's proportion for sorik volcanic (1), roburan volcanic (2), sibanggor volcanic (3) and dacitic dike (4).

Interpretation for lithology results done based on updated model. Overall there is no specific change in formation's classification. However, this new lithology model shows different thickness for each formation (excluded dacitic dike which kept as original). This model also gave new information related with the stratigraphic contact between three volcanic formations. In the existing model from previous study, those contacts are conformable for each of them. The additional data showing direct contact between sorik and sibanggor volcanic as shown in well SM C-111 (Figure 7) and intersection at Figure 9 where we found at depression morphology.

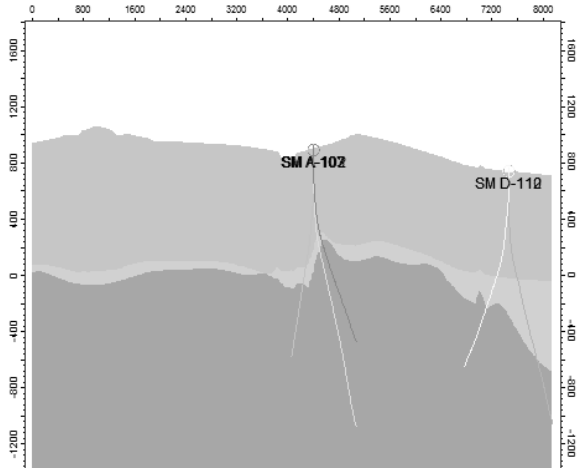


Figure 11: Intersection between pad A and pad D with lithology distribution that show small direct contact between sorik (1st zone) and sibanggor (2nd zone) volcanic, where there is possibility of erosional contact of sorik and roburan (3rd zone) volcanic.

There are some possibilities for that contact, whether the roburan volcanic was not deposited at entire area due to topography level so the young sorik volcanic was deposited directly above sibanggor volcanic, or the young sorik volcanic have erosional contact with roburan volcanic. The contact morphology of sorik and roburan volcanic found at some location at certain intersection. Figure 11 taken from cross section between well pad A and pad D. The lithology distribution near one of well path from pad A showing the direct contact between sorik volcanic (highest zone) and sibanggor volcanic (lowest zone) even though they are at relatively flat topography. It shows an evidence that the possibility of erosional contact below sorik volcanic is bigger. This new information can update the geological model in sorik marapi geothermal field.

Temperature Model

As the updating process for lithological model, data comparison for temperature was done to calibrate the

existing model. The temperature data was imported as log ASCII and displayed as continues well log. The existing temperature model from previous study was extracted along well path the displayed as discrete log based on cell thickness of the grid. Figure 12 below shows some well path at well section window with temperature continues log fromnew well data in the second column, and temperature discrete log from existing model in the third column.

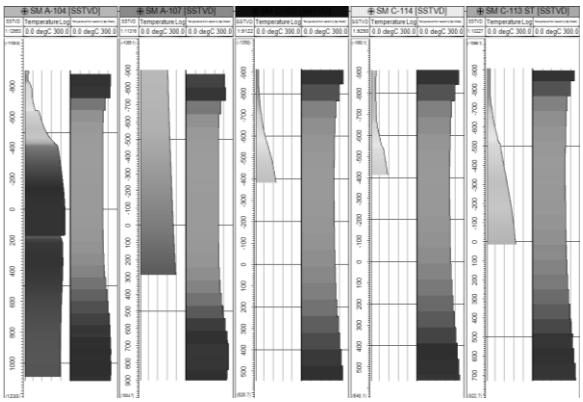


Figure 12: The comparison between temperature log from new wells data (second column) and temperature from existing model (third column).

The data comparison gave visualization of how difference the existing temperature model compared with new additional data. One of good example for the comparison results is temperature model along well SM A-107 which has relatively similar range with temperature value from additional data. However, most of existing temperature model from previous study couldn't captured low resistivity at shallow area. Since the existing model is not match with the new data, so it needs to be updated.

To rebuild the update temperature data, the first process is upscaling the temperature continues logs for all of wells data. This process implemented to get the temperature value for cells penetrated by wells path, based on available temperature logs data. Algorithm to be used while upscaling the log data into cells is arithmetic calculation. The result of upscaled log shown at Figure 13 as below.

Available upscaled temperature log then used as main input for petrophysical modeling to interpolate them for entire cube. Due to limited data of wells, additional data can be used as secondary variable while modeling the temperature. In this case we tried to use available resistivity model. To see correlation between resistivity values from existing model, the resistivity model has been extracted into well log then used to create cross plot with temperature logs, as shown at Figure 14.

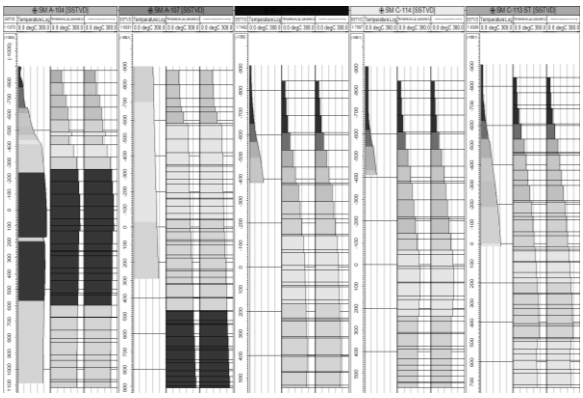


Figure 13: The temperature log data from additional wells (second column) and upscaled temperature data from 3D grid (third column) at well section window.

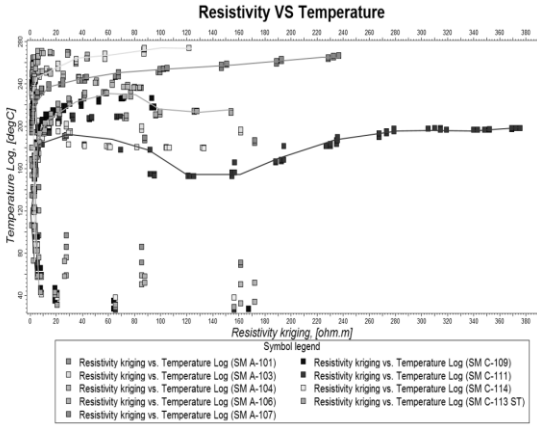


Figure 14: The cross plot between resistivity and temperature log from additional wells data, each point represents specific value at certain wells.

The cross-plot result show general trend which is at low resistivity, the temperature value can have very big range. While at medium to high resistivity, each well have relatively stable temperature (small range values) with certain trends as shown by connected lines. The correlation function created based on all available data as shown at Figure 15.

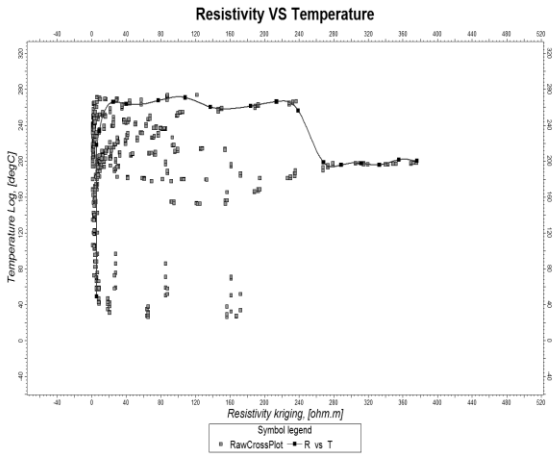


Figure 15: Nonlinear function graph based on the relationship between resistivity and all available temperature logs data.

The function formula derived based on those graphic is:

$$y = 196.249 + 0.1238x - 0.002x^2 + 4.9\ 10^6\ x^3$$

Those function is used for secondary variable while modeling temperature model. This model built by using upscaled temperature log as main input, and kriging algorithm as the method. The updated temperature model result is shown at Figure 16.

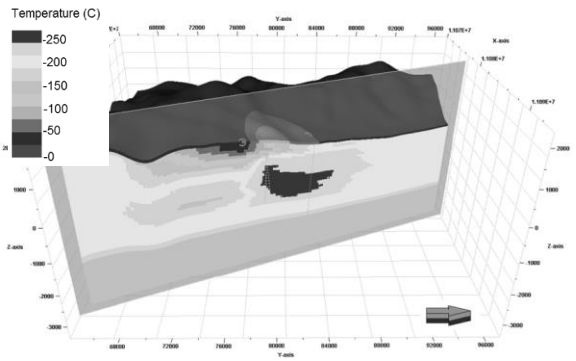


Figure 16: The updated temperature model based new additional data and nonlinear function.

Values range of temperature result is 27-274ºC, with average temperature value in the surface around 25ºC. High temperature zone can be found under well pad A, B and D. To validate this result, quality control can be done by displaying all values at histogram window and see their comparison. The information consists of the proportion of temperature values from original well logs, upscaled cells, and the model results (Figure 17).

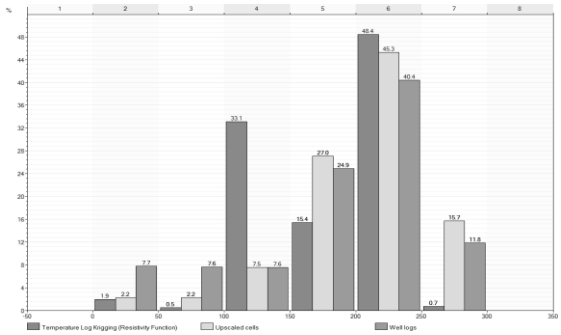


Figure 17: Histogram window to see the comparison of temperature values from well logs, upscaled and model.

Based on the updated temperature results, the model couldn't capture very high and very low temperature values, while medium temperature values proportion was being overestimated. The reason of this results could be caused by large volume and very thick grid cell. To increase the quality of this process, temperature model should be created by using finer 3D grid with small grid cell.

Another method to validate the result is by using blind well test which is excluded during modeling process. The wells used are well SM E-201 and SM A-102 that don't have temperature logs data. The validation done by displaying those wells with temperature well point value and updated temperature model extracted along well path. Based on the comparison, the updated temperature model at well SM E-201 has big deviation, while the values at well SM A-102 relatively match with the temperature well point data (Figure 18).

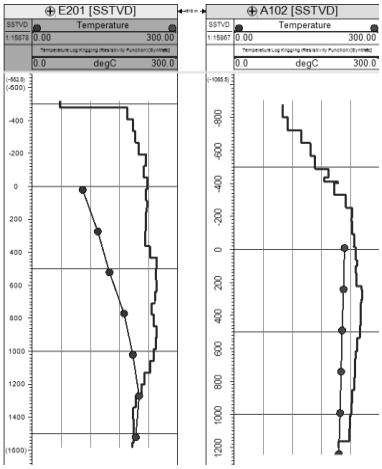


Figure 18: The comparison between extracted value of updated temperature model (line) with temperature point well data (dots) at well SM E-201 and SM A-102.

Wells position could be the reason of different results between both wells. Since well SM A-102 located near other well path at pad A, the accuracy is higher rather than well SM E-201 that located very far from other wells used for modeling. The temperature results and well position could be seen at Figure 19.

The hottest zone in sorik marapi geothermal field can be filtered for certain values (245-275ºC) to see their distribution a shown at Figure 20. The first hottest zone with shallower position is representative of volcanic area near Sorik Marapi Volcanoes. Deeper hottest zone with many wells could be identified as reservoir area.

Distribution of reservoir zone is located in the east of Sorik volcanoes. That zone has nearly ball shape with some lateral boundaries that separate the zone from cooler area. Figure 21 show the location of hottest zone and lower temperature zone at the same elevation. Based on the structural data in the sorik marapi field, there are two faults called Tobelirang and Sibanggor Besar which located at east boundary. Both faults may act as seal of hot temperature zone in the east part. So, the area in the east of those faults has lower temperature (130-190ºC) which shown by green color area. For the west boundary of high temperature zone is more controlled by the distribution of Sibanggor volcanic, which is the formation where the reservoir zone located.

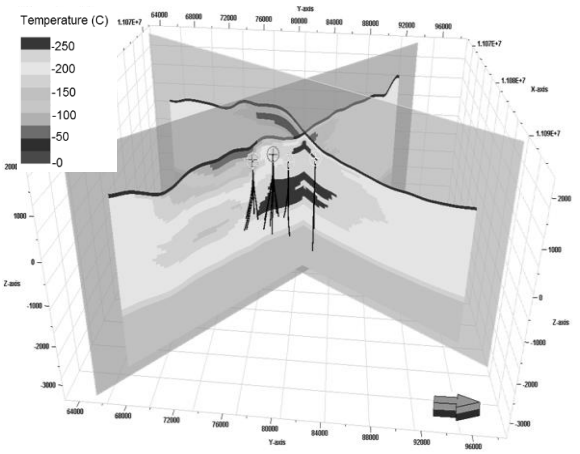


Figure 19: Updated temperature model and the wells position, from North (arrow direction) the well orders are pad E, D, A and C.

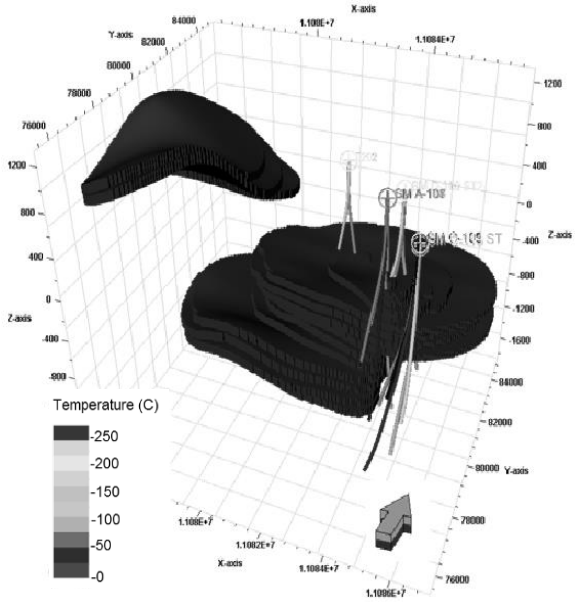


Figure 20: Hottest (245-275ºC) zone delineation based on updated temperature model that demonstrates the location or reservoir area.

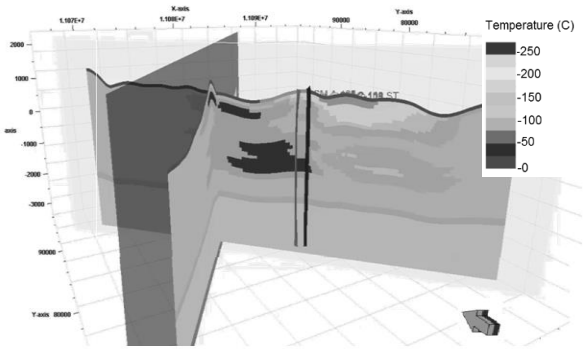


Figure 21: Tolbelirang fault (bold vertical line) and Sibanggor Besar fault (light vertical line) that separate high temperature (red zone) and lower temperature (green zone) in the same elevation and formation.

DISCUSSION

Updated model based on additional well data in Sorik marapi field can be used to get new information about reservoir boundary and condition. To get better result for this model, any additional well data of lithology and temperature can be very helpful. Other parameters that have certain trend with temperature values could be added as secondary parameter for modeling those values.

CONCLUSIONS

1. The challenges to update the existing model is the limited data as some area.
2. Most of results at existing model from previous study need to be updated because they show noncompliance with additional new data.
3. Rebuilding process done for lithology and temperature model by using kriging method from lithological zone log and upscaled value.
4. The updated lithology model shows the same formations distribution, with additional information for the stratigraphic relationship and those area.
5. The updated temperature model shows delineation of hottest zone, with faults and formation distribution as boundaries. This information can be used for reservoir characterization, parameter in simulation model and drilling strategy.

ACKNOWLEDGEMENTS

The authors would like to thank you for the managements of KS Orka, PT SMGP and Schlumberger who allowing us to use the data and software in the preparation of this manuscript.

REFERENCES

Akar, S., Atalay, O., Kuyumcul, C., Solarog'lul, U.Z.D., Colpan, B., Arzuman, S. (2011), 3D Subsurface Modeling of Gümüs¸köy Geothermal Area, Aydın, Turkey. *GRC Transactions*,Vol. 35.

Blanco, D.F., Philippon, M., Hagke, C.V. (2015), Structure and Kinematics of the Sumatran Fault System in North Sumatra (Indonesia). *Tectonophysics*. pp 1-12.

Cattin, R., Chamot-Rooke, N., Pubellier, M., Rabaute, A., Delescluse, M., Vigny, C., Fleitout, L., Dubernet, P. (2009), Stress change and effective friction coefficient along the Sumatra-Andaman-Sagaing fault system after 26 December 2004 (Mw = 9.2) and the 28 March 2005 (Mw = 8.7) earthquakes. *Geochemistry, Geophysics, Geosystems* Vol. 10, Q03011.

Filtech Energy Drilling Company. (2017), *Sorik Marapi Geothermal Power Plant ("PLTP Sorik Marapi") 240 MW, Notice of Resources Confirmation*, Unpublished Technical Report.

Hamilton, W. (1979), Tectonics of Indonesia Region. *US Geological Survey Professional Paper* 1078. pp. 18-38

Hochstein, M.P., Sudarman, S. (1993), Geothermal resources of Sumatra. *Geothermics Vol. 22*, pp 181–200.

Licup, A.C. Jr., Sarmiento, Z.F., Omac, X.L., Maneja, F.C., Chandra, V.R., M.B. Esberto, M.J.Z., Villareal, Baltasar, A.S.J., Mulyani, S., Sari, P.S., Jhonny, P.P., Juandi, D. (2017), Geothermal 3D Subsurface Modeling – A Case Study from Sorik Marapi Field, Indonesia. PROCEEDINGS, The 5th Indonesia International Geothermal Convention & Exhibition 2017.

Muraoka, H., Takashi, M., Sundhoro, H., Dwipa, S., Soeda, Y., Momita, M., Shimada, K. (2010), Geothermal systems constrained by the Sumatra Fault and its pull-apart basins in Sumatra, Western Indonesia. In: *Proceedings World Geothermal Congress* – Bali, Indonesia, pp. 1–9.

Petrel*. (2010), Schlumberger Information Solution, Petrel Software Online.

HelpSieh, K., Natawidjaja D. (2000), Neotectonics of Sumatra fault, Indonesia. *Journal of Geophysical Research* Vol. 105, pp. 1-30.

Sagala, B.D., Chandra, V.R., Purba, D.P. (2018), Conceptual Model of Sorik Marapi Geothermal System Based On 3-G Data Interpretation, Researchgate.

Weller, O., Lange D., Tilmann F., Natawidjaja D., Rietbrock A., Collings R., and Gregory L. (2011), The Structure of the Sumatran Fault revealed by local seismicity. *Geophysical Research Letters*, Vol. 39, pp. 1-7

www.industri.bisnis.com/read/20180225/44/742878/ pltp-sorik-marapi-siap-beroperasi-maret-2018

COMPARISON BETWEEN AUTOMATIC LINEAMENTS EXTRACTION AND MANUAL LINEAMENTS EXTRACTION METHODS FOR GENERATING FAULT AND FRACTURE DENSITY MAP: A CASE STUDY FROM CANDI UMBUL TELOMOYO GEOTHERMAL FIELD, MAGELANG, CENTRAL JAVA

Albertus Ivan[1] and Jason[2]

[1]Geothermal Engineering Department, Bandung Institute of Technology, Bandung, Indonesia
[2]Geological Engineering Department, Trisakti University, Jakarta, Indonesia
Email: albertusivanw@gmail.com; jasonkartasasmita@yahoo.com

ABSTRACT

Fault and Fracture Density (FFD) method is one of the method that can be utilized to delineate geothermal prospective area by extracting and analysing lineaments from various data sources, such as DEM or satellite image. This method is used to aid and simplify early geothermal exploration stage because it is relatively cheap and less time consuming. Lineaments extraction is a crucial part to generate the FFD map. Manual lineaments extraction is the common method that is usually used, but it is a tedious process and the quality of the extracted lineaments depends on the skills and the objectivity of the interpreter. This paper aims to extract lineaments automatically by using panchromatic band (8) satellite image from Landsat-8 on the study area of Candi Umbul Telomoyo geothermal field, Magelang, Central Java and compare it with the result generated from manual lineaments extraction. Four (4) applications were used in this study: ENVI 5.1, PCI-Geomatica 2015, ArcGis 10.3, and RockWorks 16. Before starting the extraction processes, the satellite image was processed with several methods, such as layer stacking and forward PC rotation to obtain a better image quality. Automatic lineaments extraction can be done by adjusting the algorithm parameter of 'Line: Lineament Extraction" module on PCI-Geomatica 2015. The result from the automatic lineaments extraction method, which is the length of the lineaments, the FFD map, and the rose diagram, shows more or less similar result as compared to the manual lineaments extraction that had been done by the team from Pusat Sumber Daya Geologi (PSDG) Bandung on 2011.

Keywords: Automatic Lineament Extraction, Candi Umbul Telomoyo, FFD, Landsat-8, Rose Diagram.

INTRODUCTION

In the geothermal exploration process, one of the method that is used to deliniate the prospect zones is lineament analysis from satellite image. From this analysis, the highest geological structures density zones can be detected. These geological structures are potentially permeable zone that can act as paths for thermal fluid to flow from the reservoir at depth to the shallower level (Suryantini and Wibowo, 2010). At some geothermal exploitation activity, it has been proven that these permeable zones are significant drilling targets to place production wells (Soengkono, 1999a and 1999b).

The lineament analysis method have been used many times for geothermal exploration. However, the method that is used until today is manual lineament extraction. Meanwhile, there is another method, which is automatic lineament extraction method by using several software that is faster and shows more or less similar result as compared to the manual lineament extraction. Therefore, this paper aims to show that automatic lineament extraction can be used and more efficient compared to the manual lineament extraction.

This case study was held at Candi Umbul Telomoyo geothermal field, which covers Temanggung Regency, Magelang Regency, Boyolali Regency, Semarang Regency, and Salatiga City, Central Java Province, Indonesia (Figure 1).



Figure 1: Location of the study area.

GEOLOGICAL SETTING

Tectonic Setting

Java Island is located at the active margin plates between Eurasia continental plate and Indian oceanic plate which has been colliding since Late Cretaceous. The major tetonic elements as an effect of Eurasian and Indian plate interaction are subduction zone, magmatic-volcanic belt, accretionary crust, back-arc basin, and fore-arc basin (Figure 2). As the result, Java Island is composed by the combination between Eurasia continental crust (mostly West Java and northern part of Central Java), accretionary crust between two

plate (southern part of West and Central Java and mostly East Java), magmatic and volcanic igneous rock of Java volcanoes belt, and all the sedimentary rock derived from it. In this case, Central Java position becomes unique because this area is a transition zone between continental crust and accretionary crust (Satyana and Purwaningsih, 2002).

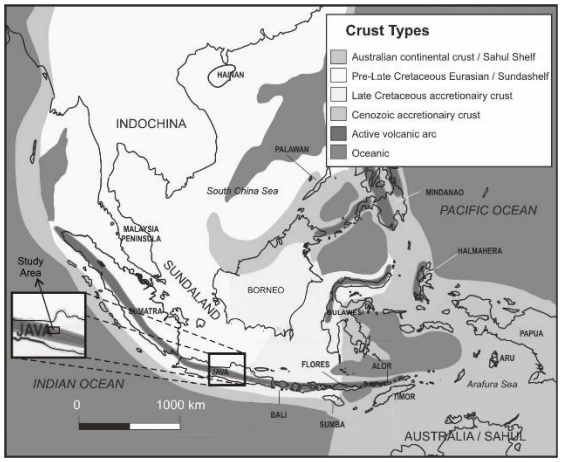


Figure 2: Map of Southeast Asia showing the different crustal type in the region (Doust and Lijmbach, 1997).

Physiography

Physiographically, Candi Umbul Telomoyo geothermal field is located in the North Serayu mountain range zone (Figure 3). In these zone, a volcanic complex were formed in NW-SE trend, which is Mount Ungaran-Telomoyo-Merbabu-Merapi ranges that is located at quarternary volcanic environment. The products of the volcano are pyroclastic rocks and lava with andesit-basaltic composition (Hermawan and Rezky, 2011).

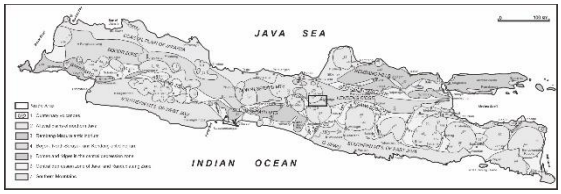


Figure 3: Physiographic sketchmap of Java and Madura island (Van Bemmelen, 1970).

Stratigraphy

Stratigraphy of the study area was arranged based on the relative connection between each lithology unit. The naming of it is based on the eruption center, mechanism, and the genesis of the lithology. Based on the field research (Hermawan and Kholid, 2010), the lithology of the study area can be separated into 18 units, which consists of one sedimentary rock, 16 volcanic rocks, and one surface deposit (Figure 4).

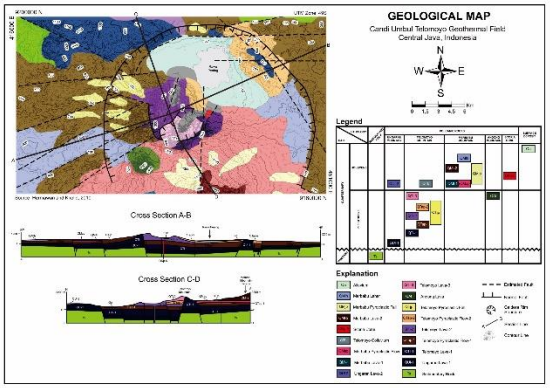


Figure 4: Geological map of Candi Umbul Telomoyo geothermal field (Hermawan and Kholid, 2010).

Structure

There are two types of geological structures that develops at the study area, the volcanic structures and tectonic structures. This volcanic structures were formed because of the Telomoyo Mountain volcanic activity, so it created caldera rim structure and the normal faults with NW-SE trend (Figure 4). These structures also provides the presence of Candi Umbul and Pakis Dadu geothermal manifestations (Hermawan and Kholid, 2010).

DATA

The data used in this study is Landsat 8 OLI/TIRS image (Path 120 Row 65). There are 11 spectral bands. Band 1 until 9 are Operational Land Imager (OLI) spectral bands and band 10 and 11 are Thermal InfraRed Sensor (TIRS) spectral bands (Table 1) (Loyd, 2013). Band 8 was chosen for this study because band 8 is a panochromatic band with 15 meters resolution so it is useful in the extraction of geological formations and rock features (El-Sawy et al. 2016) (Figure 5).

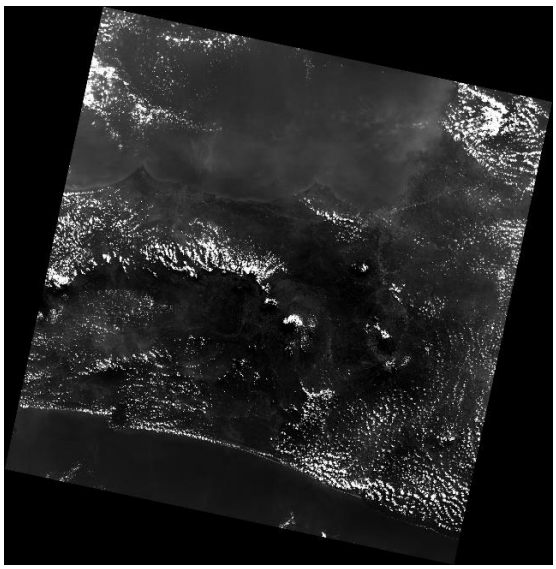


Figure 5: Satellite image of band 8 from Path 120 Row 65, acquisition date on June 6, 2018 (EarthExplorer, 2018).

Table 1: Landsat 8 OLI/TIRS bands (Loyd, 2013)

Band Number	Length (µm)	Resolution
1	0.433 – 0.453	30 m
2	0.450 – 0.515	30 m
3	0.525 – 0.600	30 m
4	0.630 – 0.680	30 m
5	0.845 – 0.885	30 m
6	1.560 – 1.660	30 m
7	2.100 – 2.300	30 m
8	0.500 – 0.680	15 m
9	1.360 – 1.390	30 m
10	10.6 – 11.2	100 m
11	11.5 – 12.5	100 m

METHODOLOGY

The aim of this paper is to compare automatic lineament extraction method and manual lineament extraction to show that the automatic method is more effective than the manual method because it takes less time to generate. There are four applications that are used in this study, which is ENVI 5.1, PCI-Geomatica 2015, ArcGis 10.3, and RockWorks 16. The flowchart of the automatic lineament extraction are shown in (Figure 6).

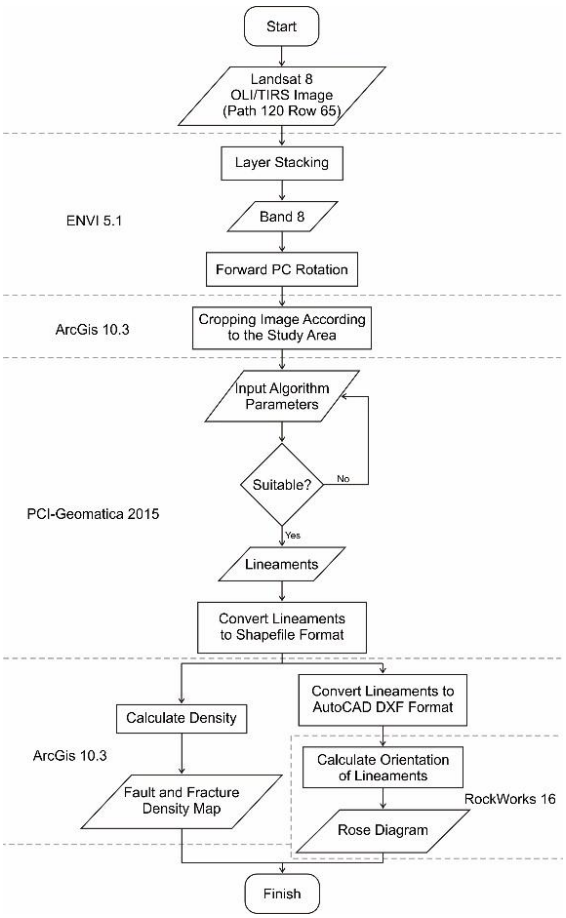


Figure 6: Flowchart for automatic lineament extraction.

The first step is layer stacking. This process aims to combine all the bands into one single file. Second, apply the forward PC rotation process to band 8. This process was done to remove the noises from the satellite image (Figure 7). After the noises are removed, the image is cropped according to the study area (Figure 8).

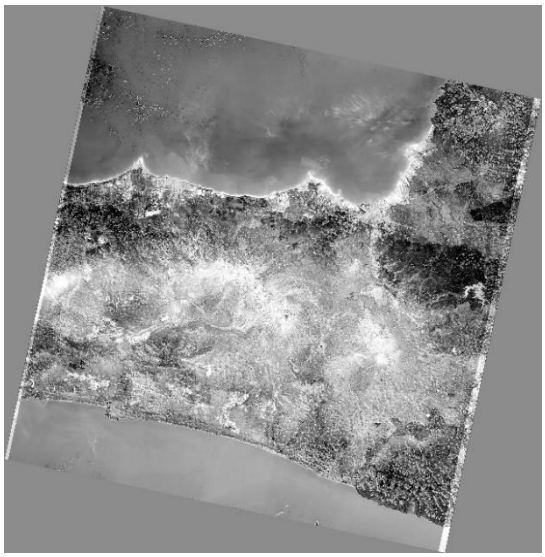


Figure 7: Satellite image of band 8 after applied by forward PC rotation.

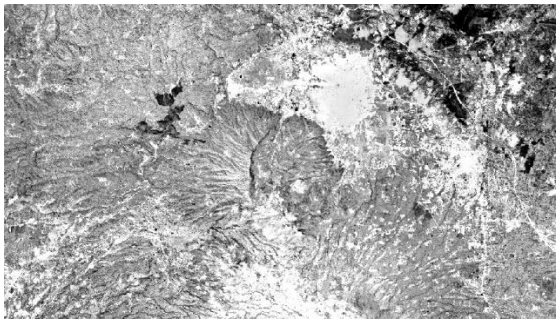


Figure 8: Satellite image of band 8 after applied by forward PC rotation and cropped according to the study area.

The next step is extracting the lineament using algorithm parameters. These parameters are explained briefly according to the Sarp (2005). There are six parameters used in the algorithm:

RADI (Filter radius): This parameter specifies the radius of the edge detection filter (in pixels). It roughly determines the smallest-detail level in the input image to be detected. The data range for this parameter is between 0 and 8192.

GTHR (Gradient threshold): This parameter specifies the threshold for the minimum gradient level for an edge pixel to obtain a binary image. The data range for this parameter is between 0 and 255.

LTHR (Length threshold): This parameter specifies the minimum length of curve (in pixels) to be considered as lineament or for further consideration (e.g., linking with other curves). The data range for this parameter is between 0 and 8192.

FTHR (Line fitting error threshold): This parameter specifies the maximum error (in

pixels) allowed in fitting a polyline to a pixel curve. Low FTHR values give better fitting but also shorter segments in polyline. The data range for this parameter is between 0 and 8192.

ATHR (Angular difference threshold): This parameter specifies the maximum angle (in degrees) between segments of a polyline. Otherwise, it is segmented into two or more vectors. It is also the maximum angle between two vectors for them to be linked. The data range for this parameter is between 0 and 90.

DTHR (Linking distance threshold): This parameter specifies the minimum distance (in pixels) between the end points of two vectors for them to be linked. The data range for this parameter is between 0 and 8192.

To acquire the best result for the lineaments, it is necessary to do several experiments by changing the number of the six controlling parameters above. There are some researchers who gave recommendation for the algorithm such as Kocal (2004), Sarp (2005), Abdullah et al. (2010), Ibrahim and Mutua (2014), and El-Sawy et al. (2016). After that, the lineaments were converted into shapefile format (.shp) to generate the fault and fracture density (FFD) map. The lineaments was also converted into autocad dxf format (.dxf) for the purpose of generating the rose diagram. After all the steps above were done, the result were compared with the manual lineament extraction report (Hermawan and Rezky, 2011).

RESULTS

Lineaments

The lineaments were generated using a module from PCI-Geomatica 2015 software called Line: Lineament Extraction. The extraction process was done by changing the six parameters several times. Several lineament maps were generated using different parameters values until it got the most suitable values (Table 2) these lineaments are considered as fault lines according to the satellite image view (Figure 8).

Table 2: Suggested parameters values

Parameters	Value
RADI	5
GTHR	5
LTHR	15
FTHR	3
ATHR	15
DTHR	10

The result from automatic lineament extraction (Figure 9) shows that the extracted lines are shorter than the manual lineament extraction (Figure 10), it goes to show that the automatic method is more specific The distribution of the lines are more or less similar.

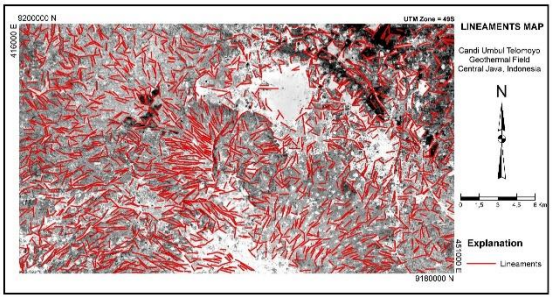


Figure 9: Lineaments map generated from automatic lineament extraction method.

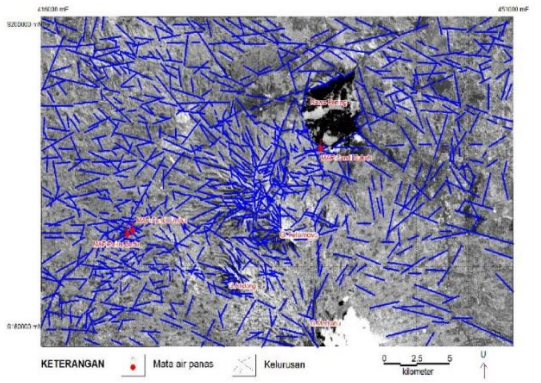


Figure 10: Lineaments map generated from manual lineament extraction method (Hermawan and Rezky, 2011).

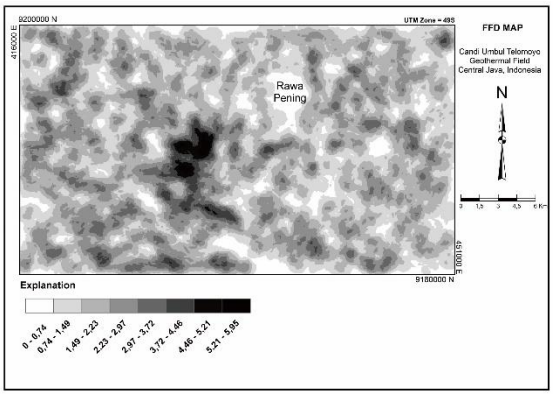


Figure 11: FFD map generated from automatic lineament extraction method.

Fault and Fracture Density (FFD) Map

The FFD map was generated using ArcGis 10.3 software. This map shows the density anomaly of the lineaments that is assumed as the recharge area, which have the highest permeability. The result from automatic method shows that the highest density area is located around southwest Rawa Pening (darkest area) (Figure 11). Meanwhile, the manual method show that the highest density area is larger than the automatic method but still at the same area, which is also at the southwest Rawa Pening (Figure 12). Compared to the manual method, the automatic method generates the density value that is a little bit lower, but more or less similar with the

manual method. The automatic method generates between 0 – 5.95 Km/Km^2 and the manual method generates between 0 – 7 Km/Km^2.

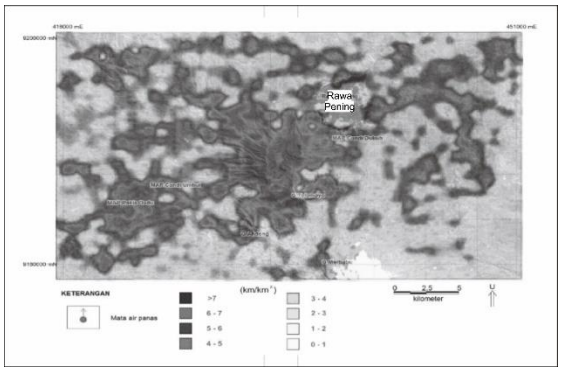


Figure 12: FFD map generated from manual lineament extraction method (Hermawan and Rezky, 2011).

Rose Diagram

The rose diagram was generated using RockWorks 16 software. The result from the diagram shows that there are four main structural trends generated from the automatic method (Figure 13). Compared with the manual method (Figure 14), the main trends shows the almost similar trends with about 10º to 40º difference but still a the same trends (Table 3).

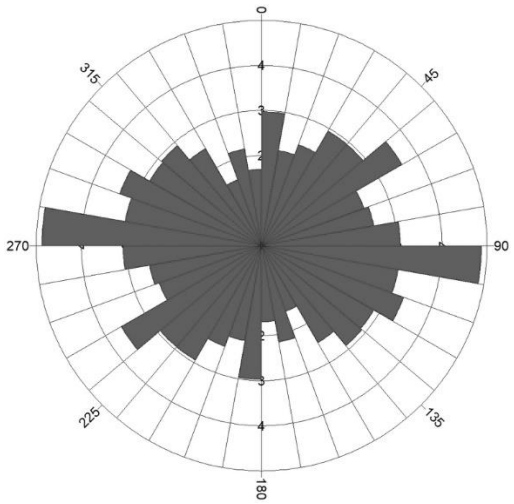


Figure 13: Rose diagram generated from automatic lineament extraction method.

CONCLUSIONS

This study has shown that the result from the automatic method is more or less similar with the manual method. The lineaments are shorter but it have the same distribution area. The FFD map has a lower density value, but shows the same prospect area, althougth the manual method shows the larger density area and the automatic method shows the more specific area. The rose diagram shows almost similar main structural trends with about 10º to 40º difference. In conclusion, the automatic method is more efficient compared to the manual method because it takes less time to generate and the results are accountable.

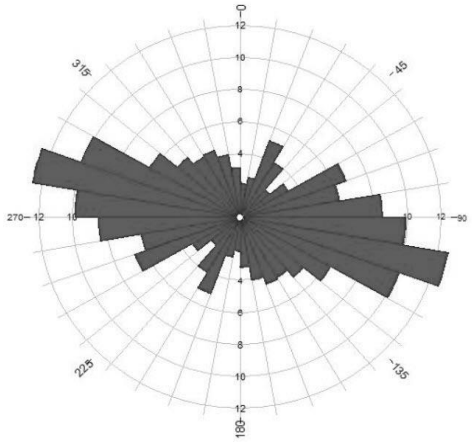


Figure 14: Rose diagram generated from manual lineament extraction method (Hermawan and Rezky, 2011).

Table 3: Result of rose diagram from automatic method and manual method showing the main structural trends

Trends	Automatic	Manual
N-S	N0º–10ºE or N170º–180ºW	N20º–30ºE or N150º–160ºW
NE-SW	N50º–60ºE or N120º–130ºW	N60º–70ºE or N110º–120ºW
E-W	N90º–100ºE or N80º–90ºW	N100º–110ºE or N70º–80ºW
NW-SE	N110º–120ºE or N60º–70ºW	N150º–160ºE or N20º–30ºW

REFERENCES

Abdullah, A., Akhir, J. M., and Abdullah, I. (2010), "Automatic Mapping of Lineaments Using Shaded Relief Images Derived from Digital Elevation Model (DEMs) in the Maran – Sungai Lembing Area, Malaysia", *Electronic Journal of Geotechnical Engineering*, **15**, 949-957.

Doust, H. and Lijmbach, G. (1997), "Charge Constraints of the Hydrocarbon Habitat and Development of Hydrocarbon Systems in Southeast Asia Tertiary Basins", *Proceedings of an International Conference on Petroleum Systems of SE Asia and Australasia*.

EarthExplorer. (2018), "Path 120 Row 65 [Satellite Image]", Retrieved June 6, 2018 From https://earthexplorer.usgs.gov/.

El-Sawy, K., Atef, M. I., El-Bastawesy, M.A., and El-Saud, W.A. (2016), "Automated, Manual Lineaments Extraction and Geospatial Analysis for Cairo-Suez District (Northeastern Cairo-Egypt), Using Remote Sensing and GIS", *International Journal of Innovative Science, Engineering & Technology*, **3**, 491-500.

Hermawan, D. and Kholid, M. (2010), "Penyelidikan Terpadu Daerah Panas Bumi Candi Umbul-Telomoyo, Provinsi Jawa

Tengah", *Prosiding Hasil Kegiatan Pusat Sumber Daya Geologi*.

Hermawan, D. and Rezky, Y. (2011), "Delineasi Daerah Prospek Panas Bumi Berdasarkan Analisis Kelurusan Citra Landsat di Candi Umbul – Telomoyo, Provinsi Jawa Tengah" *Buletin Sumber Daya Geologi*, **6**, 1-10.

Ibrahim, U. and Mutua, F. (2014), "Lineament Extraction Using Landsat 8 (OLI) in Gedo, Somalia", *International Journal of Science and Research*, **3,** 291-296

Kocal, A. (2004), "*A Methodology for Detection and Evaluation of Lineaments from Satellite Imagery*", Master's Thesis: Middle Easth Technical University.

Loyd, C. (2013), "Landsat 8 Bands", Retrieved July 7, 2018 From https://landsat.gsfc.nasa.gov/.

Sarp, G. (2005), "*Lineament Analysis from Satellite Images, North-West Ankara*", Master's Thesis: Middle East Technical University.

Satyana, A.H. and Purwaningsih, M.E.M. (2002), "Lekukan Struktur Jawa Tengah: Suatu Segmentasi Sesar Mendatar", *Proceedings Indonesian Association of Geologist (IAGI)*, Yogyakarta – Central Java Section.

Soengkono, S. (1999a), "Te Kopia Geothermal System (New Zealand) – The Relationship Between Its Structure and Extent", *Geothermics*, **28**, 767-784.

Soengkono, S. (1999b), "Analysis of Digital Topographic Data for Exploration and Assessment of Geothermal System", *Proceedings 21st New Zealand Geothermal Workshop*.

Suryantini and Wibowo, H.H. (2010), "Application of Fault and Fracture Density (FFD) Method for Geothermal Exploration in Non-Volcanic Geothermal Systems; A Case Study in Sulawesi-Indonesia", *Proceedings World Geothermal Congress*, Bali, Indonesia.

Van Bemmelen, R. W. (1970), "*The Geology of Indonesia, 1A: General Geology of Indonesia and Adjacent Archipelagoes*", 2nd ed.: The Hague.

HYDROTHERMAL ALTERATION CHARACTERISTIC OF CEMENT CONSTRUCTION CHANGES: A CASE STUDY OF BUKIT KASIH GEOTOURISM AREA

Listiana Alifia Nurlaely, I Wayan Warmada, and Ilham Dharmawan Putra

Geological Engineering Department, Faculty of Engineering, Universitas Gadjah Mada
Grafika St.2 Bulaksumur, Sinduadi, Mlati, Sinduadi, Sleman, D.I. Yogyakarta 55284
Email: listiana.alifia.n@mail.ugm.ac.id

ABSTRACT

Bukit Kasih geotourism area is one of essential elements of geothermal education in Minahasa District, North Sulawesi. Bukit Kasih is a place that include various aspects, such as geothermal, aesthetical, and cultural as the supporting values of society education for locals and tourists. In the first decade of 2000 until now, the damaged cement constructions and geothermal manifestations are parts of many issues that can be seen in Bukit Kasih, as it held important role to serve an enjoyable and safety geotourism activities. This research is conducted as preliminary approach by knowing the hydrothermal alteration characteristics present in cement construction at Bukit Kasih geotourism area to support other advance future research in order to build a better cement construction for geotourism activities. Several samples from cement constructions and rocks are analyzed thorough petrography and X-ray diffraction (XRD) as the methods in this research. The results show that several neutral pH and low temperature hydrothermal alteration suite mineral such as smectite, chlorite, calcite, sericite, anhydrite, and secondary silica minerals are identified, as well as the presence of acid pH and low temperature hydrothermal alteration minerals such as kaolinite and alunite are also identified. The hydrothermal alteration minerals in this study are mainly found present as replacement minerals of primary constituents and depositional minerals from geothermal fluids. The weakening of cement constructions is believed happen due to the replacement of primary constituent by secondary hydrothermal alteration minerals. This study also suggest further research to find the mixed cementing materials for construction as well as the geotechnical aspects experiment in order to creates education, so that geothermal energy can be accepted by locals and tourist.

Keywords: Bukit Kasih, cement construction, geothermal manifestation, hydrothermal alteration, weakening

INTRODUCTIONS

Backgrounds

Bukit kasih is one of geotourism sites in Tompaso Geothermal Field, Minahasa District, North Sulawesi. This area is composed by several geothermal manifestation such as fumaroles, steaming grounds, hot and boiling springs, solfataras, and altered rocks. Survey in this area shows that the presence of steaming grounds in Bukit Kasih are disseminated widely in the slope and peak of the hills, meanwhile the presence of hot springs in mainly found in lower parts of the slope. Altered rock are present due to hydrothermal fluid activity, i.e. in the surface where hot water and steam from steaming and fumarole activity can be seen affecting the formation of altered rocks. Bukit Kasih geotourism area not clearly free from problems. The damaged cement constructions are one of the problems appear in this area, as can be seen that stairs and building in this area are damaged because of the reactions between hydrothermal fluids came from geothermal manifestation with cement materials. Based on those backgrounds, the research about the characteristics of damaged cement construction are need to be done. This research plays important role as preliminary method in findings the solutions for the damaged cement problems, which can support further research in the future. In the end, this research can be counted as one of effort in creating safe an enjoyable geothermal geotourism education in Bukit Kasih area.

Goals

Based on point of backgrounds above, the goals of this research is aimed to:

1. Understand the characteristics of hydrothermal alteration happened in cement materials from infrastructure at Bukit Kasih geotourism area
2. Identify the presence of secondary hydrothermal alteration minerals in the cement constructions at Bukit Kasih geotourism area.

REGIONAL GEOLOGY

Physiography

Based on literature study, study area location is abutting with the remnants of collapsing volcanic edifices of Mt Rindengan. Geomorphological condition of the study area mainly composed by cone-shaped mountainous terrain with average elevation of 970 masl. This area is consist of several geothermal manifestation, appear as past processes of volcanism in this area (Savitri, 2016).

Physiography

The study area can be divided into two (2) main stratigraphic groups, the tertiary pre-caldera group and quaternary post-caldera group. Tertiary-aged units are consist of basement rock (Tb), and Tondano Tuff (Tf). Quaternary-aged unit (oldest-youngest) are consist of lengkoan volcanic rock (Qlk), Rindengan volcanic 1 (Qrd 1), Rindengan volcanic 2 (Qrd 2), Rindengan volcanic 3 (Qrd 3), Sempu volcanic 1 (Qsp 1), Sempu volcanic 2 (Qsp 2), Soputan volcanic (Qst), and Tondano lake sedimentary deposit (Qal). Bukit kasih is composed by Rindengan volcanic 3 unit, which consist of andesitic lavas, bomb, lapilli, and tuff.

Physiography

Bukit kasih area is passed by Soputan sinistral fault with orientation of East/ Northeast to West/ Southwest. Soputan fault are located in the center of Tompaso geothermal field and extends from east flank of Rindengan to Mt. Luuk - Umeh in about 17 kilometers length. Sardiyanto and Nurseto (2013) in Sardiyanto et al. (2015) stated that Soputan fault is main controlling structure in Tompaso geothermal field, together with other minor structure relatively directed northeast to southwest. This faults later controls the flow of hydrothermal fluid and the distribution of geothermal manifestation in the study area.

Geothermal Manifestation of Bukit Kasih

Geothermal manifestations present in Bukit Kasih consist of fumaroles, solfatara, hot and boiling water springs, steaming grounds, and altered rocks. Fumaroles presence indicate that this area act as upflow zone. Hot and boiling springs are showing the temperature of 50^{O} C with pH about 6, meanwhile boiling springs show temperature of 94^{O} to 97^{O} C. Steaming ground are found with the temperature ranged from 52 to 97^{O} C. Altered rock in Bukit Kasih can be divided into three characteristics, the reddish brown colour that present due to ferric ion oxidation, the yellow colour due to its H2S content, and white colour rock which contain clay minerals (PT PGE, 2013 in Siahaan, 2017).

METHODS

Sample collected from the field (cement and rocks) are analyzed using megascopic, petrography, and XRD methods. Samples of cement are taken in 7 location points, and rock are taken in 1 location point (see figure 1). In this study, petrographic observation and XRD analysis will be done by using standard guide, such as Barker (2014) for petrographic observation and Chen (1977) for XRD analysis.

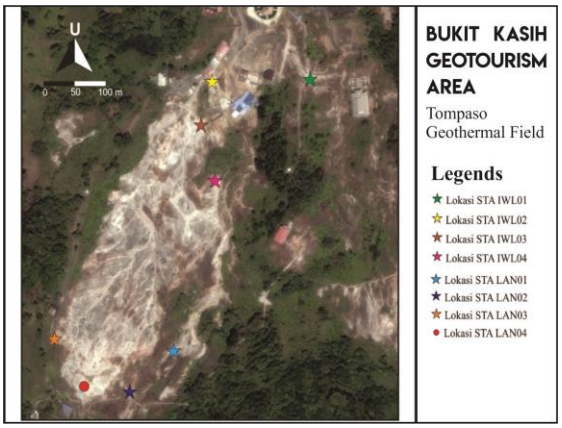


Figure 1: Point of sampling locations in Bukit Kasih geotourism area

RESULTS AND DISCUSSIONS

Megascopic and Petrographic Observation

Three representative samples are taken to be discussed in this study, they are LAN01, LAN02, and LAND 03. The megascopic observation results are discussed as:

- Megascopic observation of LAN01 shows brownish white color, this sample is mainly consist of sulfur and clay minerals (figure 2). This sample is heavily damaged, that made primary minerals are hard to be observed.
- Megascopic observation of LAN02 sample shows whitish red color, this sample consist of carbonate, sulfur, iron oxides, and clay minerals (figure 2). This sample also show characteristic of heavily damaged by the process of hydrothermal alteration, make it hard to observe the primary minerals.
- Megascopic observation of LAN03 sample shows that carbonate minerals, sulfur, and clay minerals are present composed the sample. This sample is also has been damaged, makes it hard to be observed only thorough megascopic observation (see figure 2)



Figure 2: LAN01 (a), LAN02 (b), and LAN03 (c) that showing different charateristics in hand specimen.

The petrographic observation results are discussed as:

- Petrographic observation of LAN01 sample show brownish white color at plane polarized light (PPL) and grayish black at cross polarized (XPL). The mineral present in this cement as mixed materials are plagioclase and pyroxene, which has been partly/ fully replaced by clay minerals (figure 3). The observation of intensity of alteration shows that LAN01 sample has experienced moderate to high intensity of alteration, with the style of alteration is dominantly selective replacement. The presence of clay minerals and quartz are expected as the product of plagioclase and pyroxene replacement, meanwhile, the presence of carbonate minerals, i.e. calcite, also present, expected as the product of dissolution and precipitation processes of cementing materials (see figure 3)
- Petrographic observation of LAN02 sample shows whitish brown/ whitish red color in PPL, and grayish black in XPL. Cement materials shows change in texture because of alteration, along with the presence of plagioclase and pyroxene as mixed materials that has been replaced by hydrothermal alteration process into iron oxide, quartz and clay minerals (see figure 3)
- Petrographic observation of LAN03 sample shows brownish white color of sample in PPL, and brownish black color in XPL. The texture of cement materials are totally altered, along with the presence of secondary hydrothermal alteration minerals, such as clay minerals and quartz as the replacement product of plagioclase and pyroxene. Observation of intensity of alteration also show high intensity of alteration, with pervasive style of alteration (see figure 3).

X-Ray Diffraction Analysis

XRD method is used to identify the presence of secondary hydrothermal alteration minerals, especially from clay minerals group. In this study, 4 samples of altered rock (IWL01 – IWL04) are analyzed thorough bulk and clay (multiple treatment), and other 4 sample of altered rock (LAN00-LAN03) also have been analyzed, but only to identify the presence of clay minerals, due to intensive alteration. Several hydrothermal alteration minerals are identified (see table 1), such as quartz, plagioclase, pyrite, alunite, calcite, gypsum, hematite, sericite, and cristobalite (bulk), and kaolinite, smectite, and chlorite (clay analysis). Several representative XRD samples can be seen in figure 4, 5, and 6.

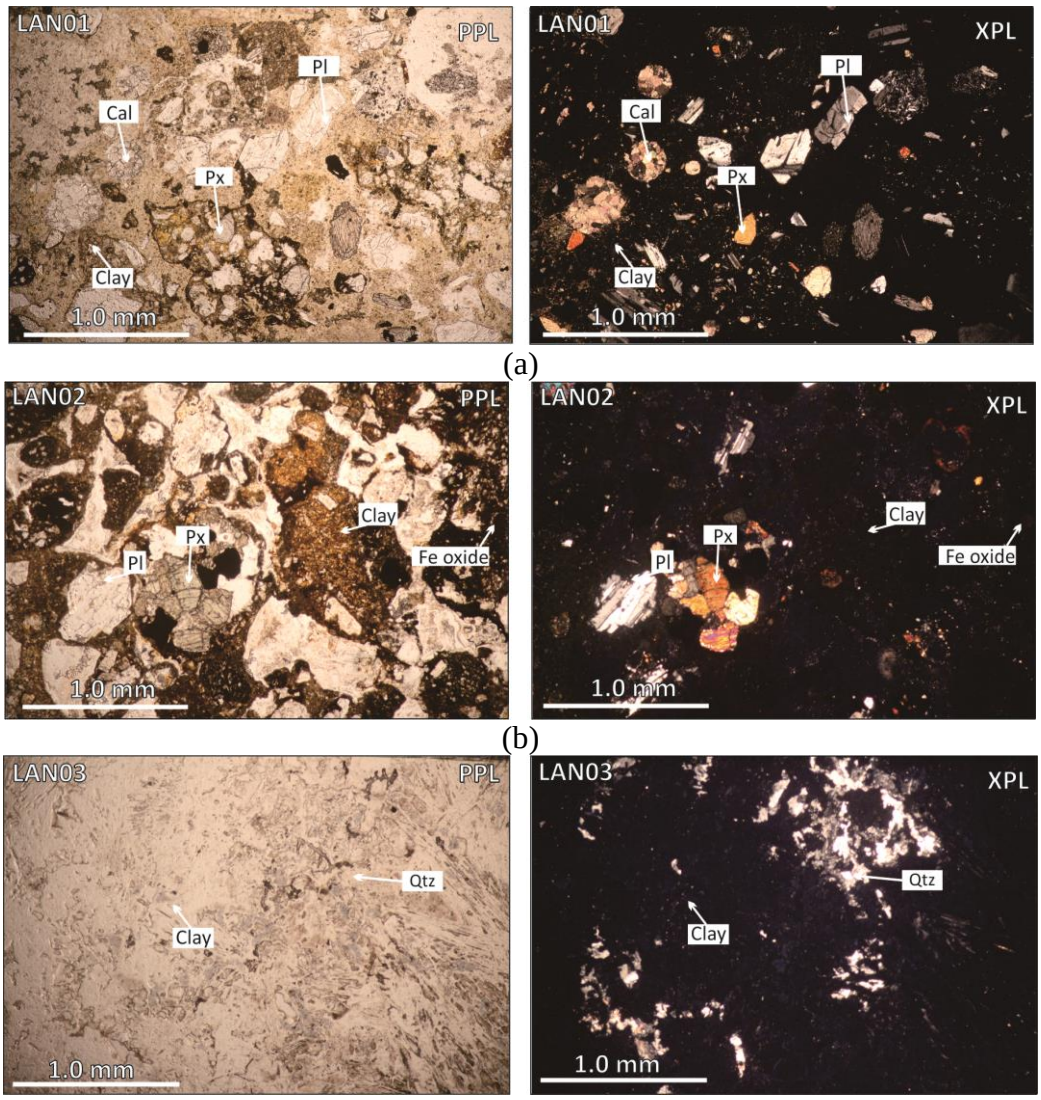


Figure 3: LAN01 (a), LAN02 (b), and LAN03 (c) samples in thin section

Table 1: Summary of XRD analysis conducted for 8 sample of altered rock from Bukit Kasih

No	Sample ID	Bulk*	Clay*
1	IWL 01	Gp, sec. qz, chl, and cal	Sme and chl
2	IWL 02	Gp, ser, chl, cal, crs, and hem	Kao and chl
3	IWL 03	Gp, alu, chl, sec. qz, and hem	Kao and chl
4	IWL 04	Gp, sec. qz, chl, and cal	Sme and chl
5	LAN 01	-	Kao and chl
6	LAN 02	-	Sme and chl
7	LAN 03	-	Chl
8	LAN 00	-	Chl

*Abbreviation of mineral name based on Whitney and Evan (2010)

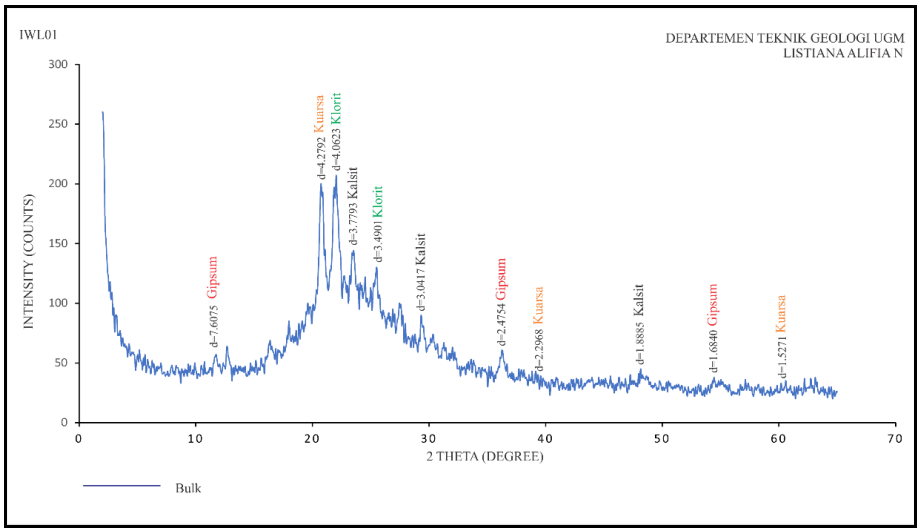


Figure 4: Bulk analysis from IWL01

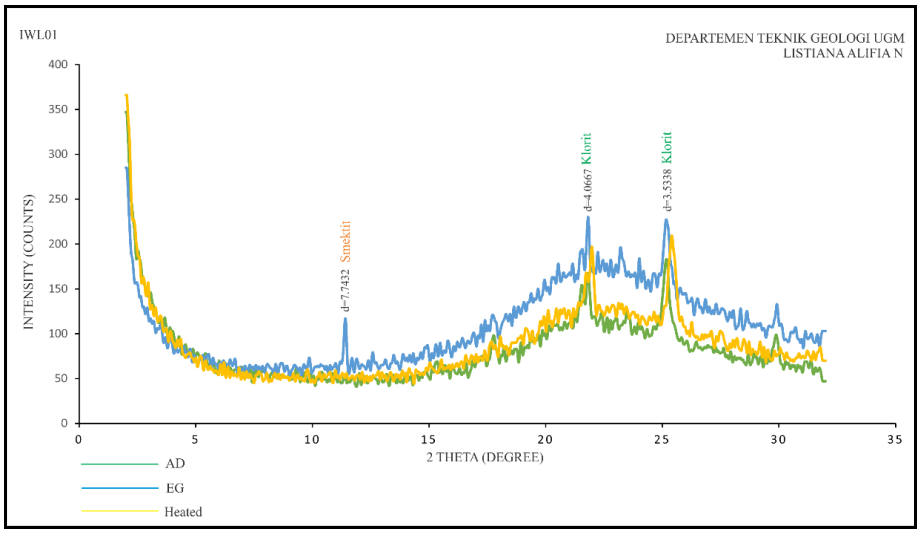


Figure 5: Clay analysis from IWL01

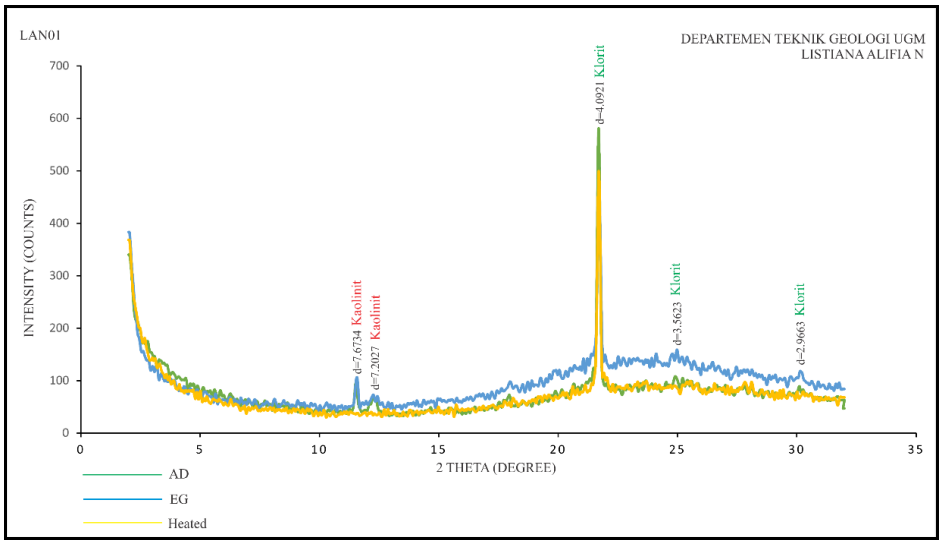


Figure 6:. Clay analysis from LAN01

Based on observation and analysis above, can be seen that the changes in cement construction are happened due to hydrothermal activity of geothermal manifestations. The changes occur in cement material consist of replacement (selective and pervasive), and dissolution process, that increasing the porosity of the cement materials. The minerals found in this research are mainly formed at low temperature (<200^{O} C), or have long temperature range, such as smectite, kaolinite, chlorite, sericite, and secondary quartz. The presence of kaolinite and alunite in several sample also indicate acid pH (Reyes, 2000).

The weakening of cement materials are expected happen because of the presence of the clay minerals that replaced cement materials, Winarti et al (2016) mentioned that clay minerals have swelling properties, especially smectite. On the other hand, the presence of high intensity of hydrothermal alteration also indicate that the changes in rocks are intensively happened. Further/ advanced treatments are need to be conducted in Bukit Kasih, i.e. using new

CONCLUSIONS

1. Hydrothermal alteration characteristics of cement construction in Bukit Kasih geotourism area are consist of high degree/ intensity of alteration, selective style of alteration, and characterized by the presence of alunite group minerals and sulphate minerals, dominantly composed by sulfur.
2. Hydrothermal alteration minerals identified from megascopic, petrography, and XRD method in this study are kaolinite, chlorite, smectite, calcite, gypsum, sericite, alunite, pyrite, cristobalite, and secondary silica minerals, which are mainly formed at low temperature (<200^{O} C), in neutral to acid (low pH) environtment.

REFERENCES

A. G. Reyes, (2000), Petrology and mineral alteration in hydrothermal systems: From diagenesis to volcanic catastrophes, *UNU GTP Lecture notes.*

Barker, A. J., (2014), *A Key for Identification of Rock-forming Minerals in Thin-Section, United Kingdom, CRC Press, 181p*

Chen, P. Y., (1977), *Table of key lines in X-ray powder diffraction patterns of minerals in clays and associated rocks.*

Sardiyanto, Nurseto, S.T., Prasetyo, I. M., Thamrin, M. H., Kamah, M. Y., (2015). Permeability Control on Tompaso Geothermal Field and Its Relationship to Regional Tectonic Setting. *Proceedings World Geothermal Congress 2015. Melbourne.*

Savitri, K.P., (2016), Geology and Geothermal Setting of Tompaso Geothermal Sistem, Indonesia, with Comparisons of Andesite Alteration Patterns with Wairakei, New Zealand, *M.Sc. Thesis.* Victoria University of Wellington. Australia.

Whitney, D. L. and Evans, B. W., (2010), Abbreviations for names of rock-forming minerals, *journal of American mineralogist, **95,** pp 185- 187.*

Winarti, D., Karnawati, D., Hardiyatmo H.C., and, Srijono, (2016), Mineralogical and Geochemical Control of Altered Andesitic Tuff upon Debris Slide Occurences at Pelangan Area, Southern Mountain of Lombok Island, Indonesia, *Journal of Applied Geology*, **1,** 19 – 28

Yeftamikha, (2017), Aplikasi Studi Alterasi Hidrotermal dalam Pengembangan Lapangan Panas Bumi "YMS", Kabupaten Minahasa, Sulawesi Utara. *Skripsi.* Universitas Gadjah Mada. Yogyakarta

SIMULATING GROUND THERMAL ANOMALY UNDER CONDITIONS OF DENSE VEGETATION BASED ON LAB AND FIELD MEASUREMENTS TO SUPPORT THERMAL INFRARED REMOTE SENSING TECHNIQUES

Asep Saepuloh[1], Suryantini[1], Christoph Hecker[2], and Robert Hewson[2]

[1]Faculty of Earth Sciences and Technology, Institut Teknologi Bandung, Bandung, Indonesia
[2]Faculty of ITC, University of Twente, Twente, The Netherlands
Email: saepuloh@gl.itb.ac.id

ABSTRACT

The ground temperature and emissivity anomalies could be used as an indicator for the existence of geothermal surface manifestations such as hot springs, fumaroles, or altered surfaces with remaining thermal at a crater rim. The ground temperature could be measured directly at the field using ground thermometer. However, field measurements are inefficient for large investigated areas and extracting Land Surface Temperature (LST) based on satellite thermal infrared sensor is also complicated due to several unknown parameters such as noise from the environment and object emissivity. Moreover, field studies under the conditions of dense vegetation makes the problem worse due to the shallower layer penetration of the response at wavelengths of thermal infrared compared to microwave energies. Overcoming the problem, we tried to estimate the kinetic temperature from the simulated steam spot using thermal infrared camera FLIR C2 with an accuracy of 2°C. The lab simulations were performed proportionally to ground variables such as the vegetation cover, height of the sensor, and diurnal effects. According to the simulations, the steam spot from boiling water 98°C recorded by the sensor at heights more than 1.2 m equivalent to spatial resolution 0.2 cm is constant about 37.2°C. We also observed that the vegetation cover reduced the measured temperature with thermal efficiency 33%. For diurnal effect, the detected temperature is constant regardless time observations. The background temperature influenced the vegetation covering steam spot with efficiencies 30% and 50% for day and night observations, respectively. These simulation results were used for further study into thermal infrared remote sensing techniques for thermal features identification. Field investigations were also performed to clarify the applicability of the thermal infrared camera to the measured ground temperature.

Keywords: Land Surface Temperature, Geothermal, FLIR C2, kinetic temperature, vegetation

INTRODUCTIONS

The temperature and emissivity anomalies extracted from thermal infrared (TIR) remote sensing could be used as an indicator for the existence of geothermal surface manifestations such as hot springs, fumaroles, mud pools, and steaming ground (Hodder, 1970). The ground temperature could be measured directly at the field using contact system such as ground thermometer. However, field measurements are inefficient for large investigated areas (Saepuloh et al., 2013). The laboratory and field experiments presented in this paper are aimed to support thermal infrared remote sensing for geothermal features detection (Kuenzer and Dech, 2013).

Extracting kinetic temperature of ground target based on satellite thermal infrared is complicated due to several unknown parameters such as emissivity and noise from environment (Kahle and Alley, 1992). Therefore, brightness temperature is the most optimal applicable parameter to assess the ground thermal anomaly in assumption that the atmospheric effect is not significant (Jiménez-Muñoz and Sobrino, 2003). Moreover, investigated field study under conditions of dense vegetation makes the problem worse due to the shallower layer penetration of the response at wavelengths of thermal infrared compared to microwave energies (Saepuloh et al., 2012).

In this study we simulated the "steam spots" as detected by the thermal infrared camera using a boiling water to obtain the effect of sensor height and variation of vegetation cover as well as diurnal temperature to the measured steam spot. We also calculated the effect of resolution to the measured temperature and efficiency of vegetation covers reducing temperature of targets. In addition to the lab measurement, we also measured ground temperature at mud pool, steaming ground (altered surface), and hot spring using the same thermal infrared camera.

EQUIPMENT AND METHOD

Detecting kinetic temperature of the objects at ground surface level is the aim of the thermal infrared remote sensing. Straight forward to the problem, we applied a simulation to estimate the kinetic temperature from a steam spot using thermal infrared camera FLIR C2. The FLIR C2 is a pocket-sized thermal camera and designed for a wide range of applications to find heat patterns that point out hotspots. The camera was utilized by

visible (VIS) and infrared (IR) sensors with spectral range 7.5 - 14 µm and resolution 640×480 pixels for VIS and 80×60 pixels for IR sensor (FLIR, 2014). The object temperature range -10°C to 150°C with accuracy ±2°C makes this camera is plausible for measurement at geothermal field.

Measuring the target temperature, a static 200 cm vertical road was used as center of the height adjustable camera positions. Then, the steam spot was simulated using boiling water which is maintained temperature at 98°C by a heater pot and located at the bottom part of the vertical road (Figure 1). The lab simulations were performed proportional to ground variables including height of the sensor, vegetation cover, and diurnal effect. To obtain the elevation and the resolution impact to the measured temperature, the steam spot was measured every 5 cm height. The minimum and maximum heights are located at the pot cover (=0 cm) and top of the road (=200 cm), respectively. According to this method, the camera produced 40 measurements from different height. For analyzing vegetation cover to the measured temperature, we used leaves cover 0, 25, 50, 75, and 100% of total upper pot surface area. Cover 0 and 100% mean that the upper pot are opened and closed totally by vegetation, respectively. This experiment will support the evidence of temperature relationship for partial canopy cover conditions (Kustas and Anderson, 2009). To obtain the air temperature variation over time to the measured temperature, we measured the steam spot every hour in open area for 24 hours. The measurements were performed using fixed height 200 cm and vegetation cover 0 and 25%.

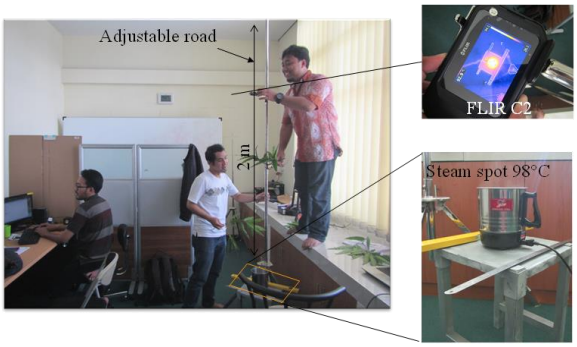


Figure 1: Experimental design using FLIR C2 at lab scale to measure a simulated steam spot using boiling water.

Confirming the applicability of the thermal infrared camera and lab measurement results, we also performed a field scale measurement using the same thermal infrared camera. The field measurements were designed following 1 m grid scanning for each surface thermal feature illustrated by dark green zone in Figure 2. The height of camera was fixed 200 cm to keep a constant spatial resolution. There were three measured locations of surface thermal features consisting mud pool, steaming ground, and hot spring at Wayang Windu Geothermal Field. The number of grid at each location was selected according to terrain and safety conditions.

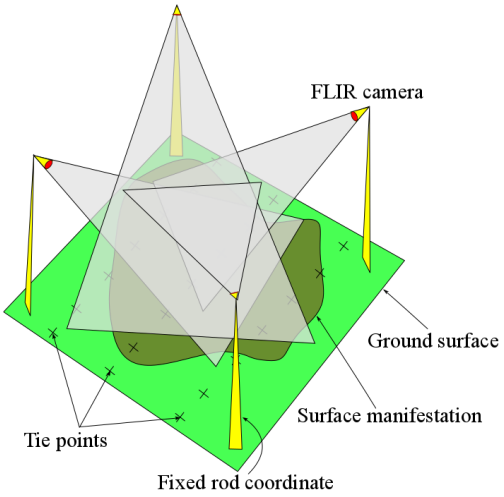


Figure 2: Surface temperature measurement design at field using FLIR C2 camera.

LAB SCALE EXPERIMENTAL RESULTS

The first experiment is aimed to obtain the sensor elevation sensitivity to the measured temperature. The steam spot measurements were performed indoor with room temperature 25.5°C at 13.40 AM. The thermal infrared camera was aimed to the target vertically and the boiling water inside the pot was opened to the free air. The measured temperatures with height variation were depicted in Figure 3A. There is no clear correlation due to large different temperature variation within height. However, the general trend is a decreasing temperature along with increasing sensor height. The large variation of measured temperature presented by medium correlation determination (R2) about 0.5 was predicted by contact of the water vapor to the sensor. An opened water pot caused a contact between the water vapor and the lens of the sensor. Therefore, the measured temperature is higher and lower than the steam spot itself.

Omitting the contact with water vapor, we used a closed water pot so that the measured target is the heated cap of the water pot. A relatively persistent decreasing curve was obtained by this method as presented by Figure 3B. The decreasing curve pattern was consistent up to sensor height 120 cm. The higher sensor position than 120 cm showed that the measured temperature is constant about 37.2°C. The lower variation of measured temperature presented by higher R^2 about 0.8 than opened pot was achieved.

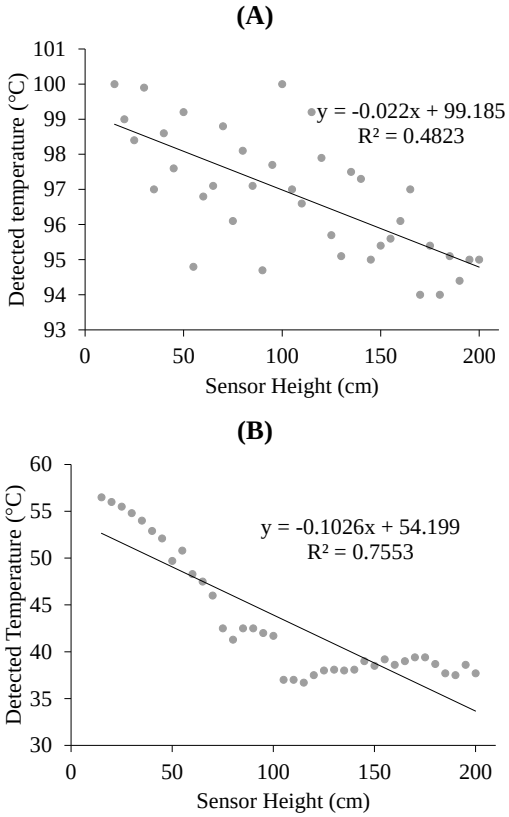


Figure 3: Large variation of detected temperature at different sensor height due to water favor effect (A) and small variation from isolated steam spot with constant temperature achieved at height more than 120 cm (B).

The second experiment was a vegetation cover effect to the measured temperatures by the sensor. The result showed that the decreasing temperatures agreed with the increase of vegetation covers (Figure 4A). The high R2 about 0.98 indicated that vegetation cover affected the measured temperature persistently. According to the measurement, a small thermal signature could be detected at 100% vegetation cover with thermal efficiency 0.33 (=31°C/94.48°C). This condition encourages the usability of thermal infrared sensor even though under dense vegetation cover.

For the third condition, the experiment is aimed to obtain the background temperature from the diurnal effect. The fixed sensor height at 200 cm was used under two conditions of vegetation cover: 0 and 25%. The measurement results are depicted by Figure 4B. The air temperatures which were measured every hour showed almost constant about 27°C. For vegetation cover 0%, the measured steam spot temperatures are also almost constant regardless time observation about 98°C. On the contrary, the large variation of measured temperatures was obtained under vegetation covers 25%. According to the 2nd experiment, the measured temperatures should be constant about 80°C. The large temperature variation under vegetation 25% infers that the vegetation covers affected strongly by diurnal temperature, but not for the steam spot.

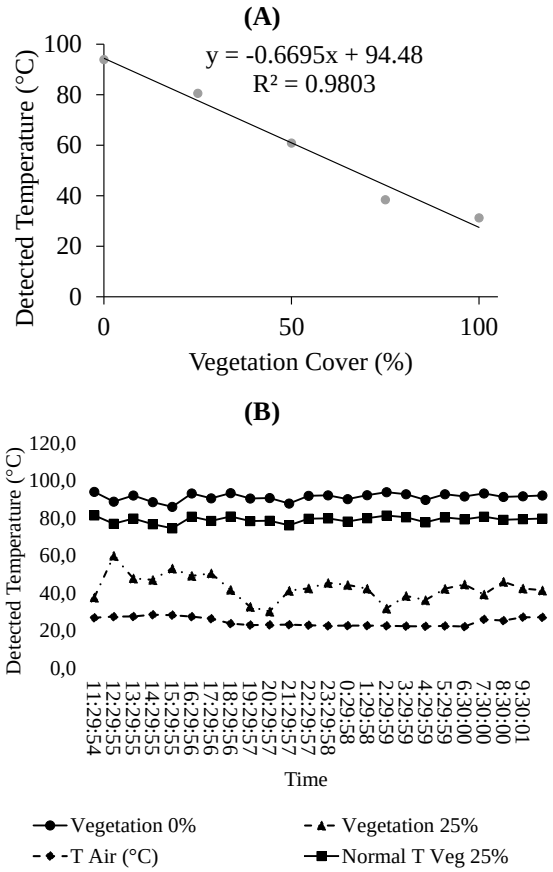


Figure 4: Vegetation reduces detected temperature gradually, but small signature still observed at 100% covers with thermal efficiency 0.33 (A) and the steam spot temperature is constant over time and independently to diurnal temperature (B).

FIELD SCALE EXPERIMENTAL RESULTS

Obtaining the applicability of the thermal camera for field measurement, we measured three locations of surface thermal features. The first feature was located at mud pool presented by Figure 5A. The ground surface at this location is covered by thick vegetation presented by green portions in the aerial photographs.

There were about 80% ground surface covered by grasses and trees. Therefore, the satellite thermal infrared sensor will detect only small amount of the remaining surface temperature. According to the 2nd lab measurement, the thermal efficiency for 80% vegetation cover is 0.43. Therefore, the ground temperature about 72ºC might be detected by the thermal infrared sensor about 29.5ºC.

On the contrary, there are no vegetation covers at steaming ground presented by Figure 5B. The

ground surfaces are composed chiefly by alteration clays and fumaroles. Some spots contained ground thermal presented by high temperature more than 60ºC on the bright spots of the aerial photographs. For the hot spring, the maximum detected temperature is about 53ºC at the hot water surfaces. Some spots at the ground surfaces covered by grass were also detected higher than surrounding temperatures. The green pale of the grass in the aerial photographs was predicted as stressed vegetation due to soil contact with hydrothermal fluid.

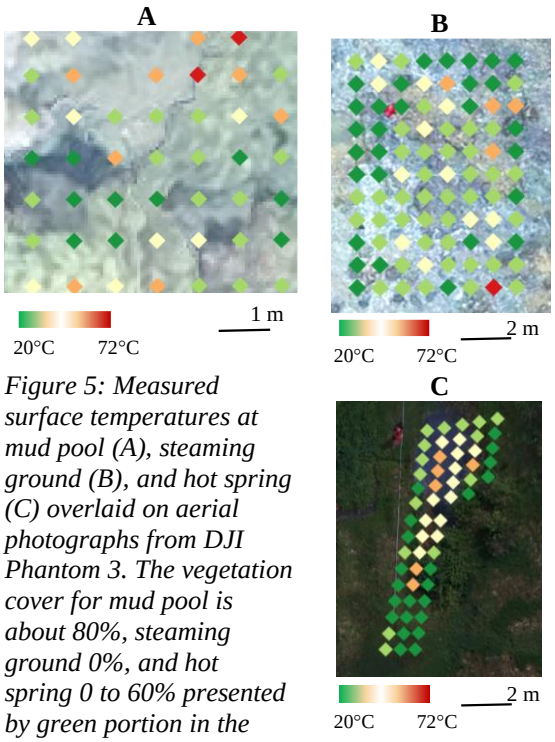


Figure 5: Measured surface temperatures at mud pool (A), steaming ground (B), and hot spring (C) overlaid on aerial photographs from DJI Phantom 3. The vegetation cover for mud pool is about 80%, steaming ground 0%, and hot spring 0 to 60% presented by green portion in the background visible images.

CONCLUSION

The height of sensor reduced the detected temperature, but constant measurement was achieved at height more than 120 cm. Decreasing detected temperature is concordance with sensor resolution, but constant at low image resolution less than 0.2 cm. Vegetation also reduces he detected temperature constantly, but small signature still observed at 100% cover with thermal efficiency 0.33.

The target temperature is constant over time and independently to the background temperature. The vegetation reduced temperature about 30% in the day and 50% in the night observations. The presented experimental results will be used for correcting ground temperature derived by TIR remote sensing.

REFERENCES

FLIR, 2014. User's manual FLIR Cx series.

Hodder, D.T., 1970. Application of remote sensing to geothermal prospecting. Geothermics 2, 368IN1369-380.

Jiménez-Muñoz, J.C., Sobrino, J.A., 2003. A generalized single-channel method for retrieving land surface temperature from remote sensing data. J. Geophys. Res. Atmospheres 108.

Kahle, A.B., Alley, R.E., 1992. Separation of temperature and emittance in remotely sensed radiance measurements. Remote Sens. Environ. 42, 107–111.

Kuenzer, C., Dech, S., 2013. Thermal infrared remote sensing. Sens. Methods Appl. Remote Sens. Digit. Image Process. 17.

Kustas, W., Anderson, M., 2009. Advances in thermal infrared remote sensing for land surface modeling. Agric. For. Meteorol. 149, 2071–2081.

Saepuloh, A., Koike, K., Omura, M., 2012. Applying Bayesian Decision Classification to Pi-SAR polarimetric data for detailed extraction of the geomorphologic and structural features of an active volcano. IEEE Geosci. Remote Sens. Lett. 9, 554–558.

Saepuloh, A., Urai, M., Aisyah, N., Sunarta, Widiwijayanti, C., Subandriyo, Jousset, P., 2013. Interpretation of ground surface changes prior to the 2010 large eruption of Merapi volcano using ALOS/PALSAR, ASTER TIR and gas emission data. J. Volcanol. Geotherm. Res., Merapi eruption 261, 130–143.

MULTI-SOURCE REMOTE SENSING DATA ANALYSIS FOR GEOTHERMAL TARGETING ON FLORES ISLAND

Christoph Hecker[1], Robert Hewson[1], Agung Setianto[2], Asep Saepuloh[3], and Freek D. van der Meer[1]

[1]University of Twente, Faculty ITC, The Netherlands
[2]Universitas Gadja Madah, Yogyakarta, Indonesia
[3]Institut Teknologi Bandung, Bandung, Indonesia
Email: c.a.hecker@utwente.nl; r.d.hewson@utwente.nl;
agung.setianto@gmail.com; saepuloh@gl.itb.ac.id;

ABSTRACT

Flores Island of Indonesia (Nusa Tenggara Timur) has potential for geothermal energy that is still, for the most part, in its development and exploration phase. There is considerable interest to determine the optimal geothermal exploration techniques and the key area(s) for further investigations on Flores Island. This study summarizes past studies on Flores Island, and the methodology and results of this study's' multi-spectral satellite remote sensing and geospatial techniques used to map geothermal terrain including its fumaroles. In particular, Advanced Spaceborne Thermal Emission and Reflection Radiometer (ASTER) day and night time imagery and Shuttle Radar Topography Mission (SRTM) products were examined to test their suitability for geothermal exploration. However spatial resolution issues as well as vegetation and cloud cover limited the results from day time ASTER image interpretation. The night-time ASTER thermal showed it's potential to identify thermal anomalies associated with volcanic activity on Flores Island however its coarse image pixel size of 90 meters again limited its application. It was found that the SRTM Digital Elevation Model (DEM) as various processed and filtered products, provided a useful geospatial data set to interpret for lineaments that potentially related to the structural features, in part associated with geothermal activity. These preliminary interpreted structural lineament-related structure results were used to recommend areas within the central region of Flores Island to undertake more detailed geothermal investigations at higher spatial resolution using airborne thermal imaging and LiDAR-based DEM techniques.

Keywords: Flores Island, remote sensing, satellite data, ASTER, SRTM, thermal infrared, lineament-related structure, geothermal

INTRODUCTIONS

The volcanic terrain of Flores Island within the Lesser Sunda Islands of eastern Indonesia is an area highly prospective for geothermal energy. It is located approximately 1500 km east of Jakarta. Interest in its potential has been raised during the collaborative Dutch – Indonesian GEOCAP Project and highlighted during workshop case studies demonstrating remote sensing and geophysical exploration techniques. There are several active geothermal energy fields within its 14250 km2 area however its development is at an earlier stage than other geothermal energy prospects elsewhere in Indonesia such as within Java. Consequently, there is a need to determine the optimal geothermal exploration techniques and key area(s) of interest on Flores Island. This study aims to test optical and thermal multi-spectral remote sensing, and topographic modelling techniques to assist the exploration of geothermal activity on Flores Island. In particular, this study summarises the remote sensing and geospatial interpretation of the imagery derived from the Advanced Spaceborne Thermal Emission and Reflection Radiometer (ASTER) multi-spectral satellite and Shuttle Radar Topography Mission (SRTM). As part of this study, it is also an objective to recommend areas within Flores Island for more detailed geothermal investigations.

The geothermal prospectivity of Flores Island can be divided into three main areas: the Western, the Central (or Bajawa) and the Eastern zones (Figure 1a). These are affected by the various structural tectonic and volcanic features of these regions. Muraoka et al. (2002) describes the large scale subducting and colliding forces from the Australian-Indian, Eurasian and New Guinea plates generating these structural features of Flores Island. In particular, these forces influence the faulting and folding of the Central or Bajawa Zone which in turn also affects the presence of its geothermal fields (Muraoka et al., 2002). Muraoka et al. (2002) highlights and maps these N-S fault lines and the NE-SW to E-W fold axes apparent within the Bajawa Zone (Plate 1, Muraoka et al., 2002). Such faulting and folding also influences the topography, including the volcanic landforms apparent in the Digital Elevation Model (DEM) information derived from the SRTM (Figure 1b) (https://reverb.echo.nasa.gov/). In addition, geothermal and hydrothermal activity can alter the mineralogy of the surrounding host rocks in which the vents or fumaroles release hot chemically enriched fluids. This activity can produce the accumulation of alteration minerals such as various clay, sulphate, opaline-silica and carbonate rich

minerals. Characterisation of hydrothermal alteration minerals using shortwave infrared (SWIR) spectroscopy on well drill cores from central Flores Island has previously shown the presence of argillic alteration minerals such as kaolinite, dickite, and halloysite (Aswin and Nanlohy, 2002). This study investigated the feasibility of mapping such alteration indicator minerals using day time ASTER SWIR and thermal infrared (TIR) imagery on Flores Island. Subtle thermal anomalies have also been previously identified using night time ASTER by Urai et al., (2002) in the central Flores Ngada District. Night time ASTER thermal data was examined in this study for signs of temperature anomalies above the surrounding background, suggestive of such surface fumaroles.

Elevation data from the SRTM was also used in this study and interpreted for lineaments and fault lines that could be possibly associated with geothermal fumaroles. It was suggested by Muraoka et al. (2002) that geothermal activity is produced by buried north-south dyke-like magmatic bodies heating fluids that are vented along N-S fractures or faults. Various image processed products from the Digital Elevation Model SRTM data were generated in this study to assist the interpretation of lineaments, including artificially illuminated / shaded relief and slope aspect imagery. Processing and filtering of the Flores Island SRTM DEM by Fourier Filter Transformation (FFT) was also undertaken to assist this interpretation.

The results in this study are presented to show the potential argillic geothermal mineral signatures available in the limited areas exposed to ASTER remote sensing. More significantly, the topographic modelled and filtered DEM products were interpreted for lineaments within the three geothermal Flores Island zones, (Figure 1a) and incorporated into recommendations for future detailed investigations

METHODOLOGY

Discriminating geothermal indicator minerals using spectroscopy

The results of fundamental research into mineral spectroscopy (Lyon & Burns, 1963; Adams & Filice, 1967; Hunt & Ashley, 1979; Vincent & Thomson, 1972; Vincent et al., 1975) laid the basis for later geological remote sensing and prompted the launch of such multi-spectral satellite sensors as NASA's Landsat TM in the late 1980s' and ASTER in 1999 by Japan's METI and NASA. The relationship of the spectral bands of Landsat TM, ASTER, HyMap and the more recent WV-3 sensors to common material spectral signatures is shown in Figure 2. The freely available ASTER imagery has the advantage of additional thermal bands, while the new DigitalGlobe commercial WV-3 sensor has higher spatial VNIR-SWIR resolution. ASTER measures six bands within the SWIR wavelength region including the clay / AlOH absorption feature centred at 2.2 um (Figure 3). ASTER bands 5, 6 and 7 have potential to qualitatively reveal changes in the AlOH/clay composition from changes in the absorption feature wavelength shift (Figure 3). Abundance and compositional indices for minerals and/or mineral groups with absorption features such as AlOH in Figure 3, can be devised as shown using such band ratios and relative band depth arithmetic (Crowley et al., 1989).

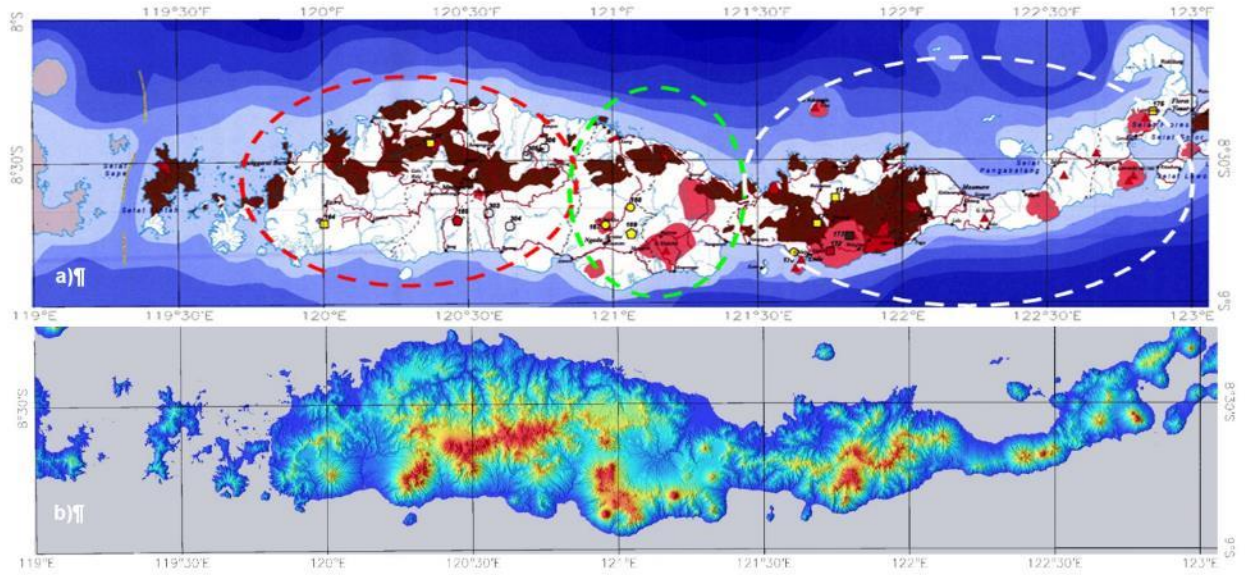


Figure 1:a) Geothermal Prospectivity Map and three significant areas, Western zone(red dashed line), Central (Bajawa) zone (green dashed line) and Eastern zone (white dashed line), supplied by the Indonesian Geological Agency, Bandung; b) SRTM 30m DEM with topography

Table 1 summarises some of the key geothermal minerals described by Brady et al. (2006) and Littlefield & Calvin (2014). Each potential indicator mineral is listed with potentially diagnostic band ratio / relative band depth algorithms, as calculated from spectral data from the described wavelength regions (Table 1).

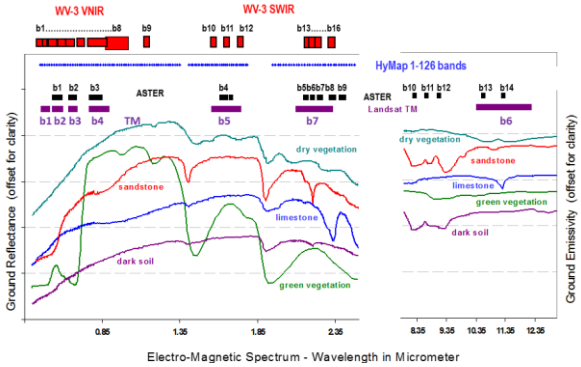


Figure 2: Reflectance spectrum of common surface materials and various remote sensing sensors measuring at these wavelengths

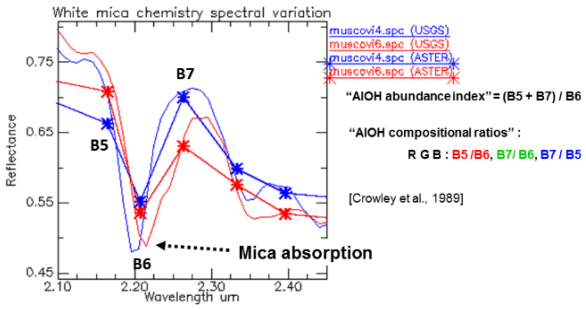


Figure 3: Spectra of AlOH clay/white mica and their ASTER resampled equivalent. Example band parameters as listed, estimate AlOH clay content and composition

Table 1: Key geothermal minerals and their representation with ASTER band parameters derived from the listed wavelength regions

Indicator Geothermal minerals	Potential diagnostic wavelength region	ASTER band parameter
Quartz ; Opaline silica	TIR ; SWIR	B13 / B10 ; (B5 + B8) / (B6 + B7)
Alunite	SWIR	B7 / B5
Kaolinite	SWIR	B7 / B5
Montmorillonite	SWIR	(B5 + B7) / B6
Chlorite	SWIR	(B6 + B9) / (B7 + B8) (or (B6 + B9) / B8) (Masked by higher values B5 / B4 Ferrous)
Calcite	SWIR, TIR	(B6 + B9) / (B7 + B8) (or (B6 + B9) / B8) ; B13 / B14
Gypsum	TIR	(B10 + B12) / B11

Example spectral signatures of these indicator minerals from the USGS VNIR-SWIR spectral library (Baldridge et al. 2009) as laboratory and at equivalent ASTER band resolution are shown in Figures 4. Similarly TIR signatures for some geothermal indicator minerals are shown using the Johns Hopkins University spectral library (Baldridge et al. 2009) and for their equivalent ASTER band resolution in Figure 5.

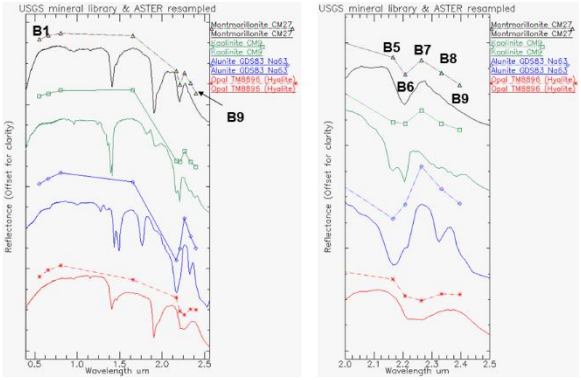


Figure 4: a) Spectra of montmorillonite, kaolinite, alunite and opaline silica and their ASTER resampled equivalent 0.5 to 2.5 um; b) Close up of spectra 2.0 to 2.5 um

Extracting lineaments from topographic modelled and filtered DEMs

DEMs derived from SRTM is available at 30 metre pixel resolution from the NASA/USGS REVERB data portal (https://reverb.echo.nasa.gov/). Several versions of the SRTM DEM data are available including the 90 metre and the recently released 30 metre resolution versions (https://lta.cr.usgs.gov/SRTM1Arc). This study accessed and utilised the SRTM 1 Arc-Second Global data at 30 m resolution in GeoTIFF format and mosaicked the downloaded 1 degree tiles encompassing the Flores Island.

Topographic modelling of the SRTM DEM imagery was undertaken using ENVI version 5.3 software (http://www.harrisgeospatial.com/ProductsandSolutions/GeospatialProducts/ENVI.aspx) to generate shaded relief and aspect image products. Shaded relief was simulated at different illuminated azimuth (0 and 270 degrees) and elevation angles (50-60 degrees) to enhance the N-S and ENE-WSW to E-W fault lines and fold axes described by Muraoka et al. (2002). The aspect slope imagery was classified into 4 classes, NNE (45-90º), SSE (135-180º), WSW (225-270º) and NNW (315-360º).

FFT filtering of the Flores island DEM imagery was undertaken using techniques described by Florinsky (2012) and using the ENVI version 5.3 software (http://www.harrisgeospatial.com/ProductsandSolutions/GeospatialProducts/ENVI.aspx). Two FFT filtered versions of the SRTM data were generated to enhance the higher spatial frequency DEM information. User defined elliptical high pass cut off filters were applied, with a border margin of 50 pixels to reduce high frequency artefacts at the filter margins, before an inverse FFT was applied to generate the filtered DEMs (Figure 6 a, b & c).

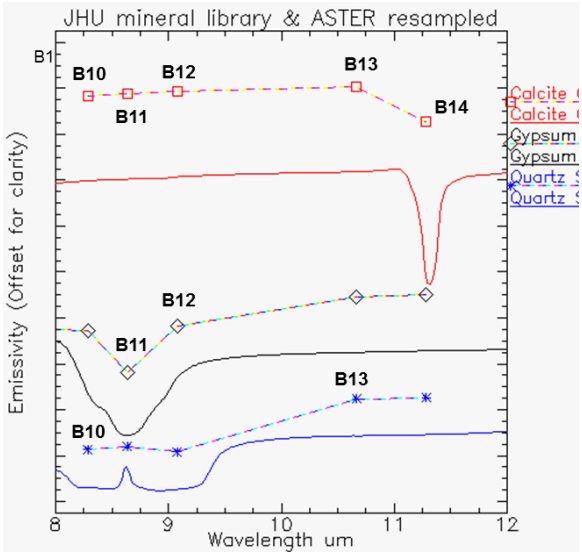


Figure 5: Spectra of calcite, gypsum and quartz within the thermal wavelengths 8 to 12 um

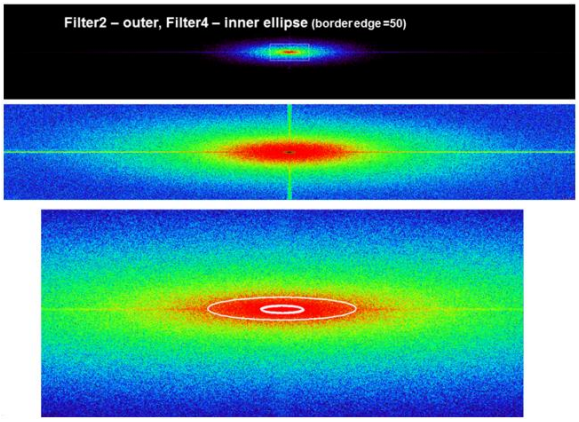


Figure 6: Images representing 2 D FFT spectrum of SRTM 30 m DEM a) complete 2D spectrum; b) close up of a); c) close of b) showing the cutoff filters applied and shown in Figure 13 e.g. Filter 2 = outer ellipse, Filter 4 = inner ellipse

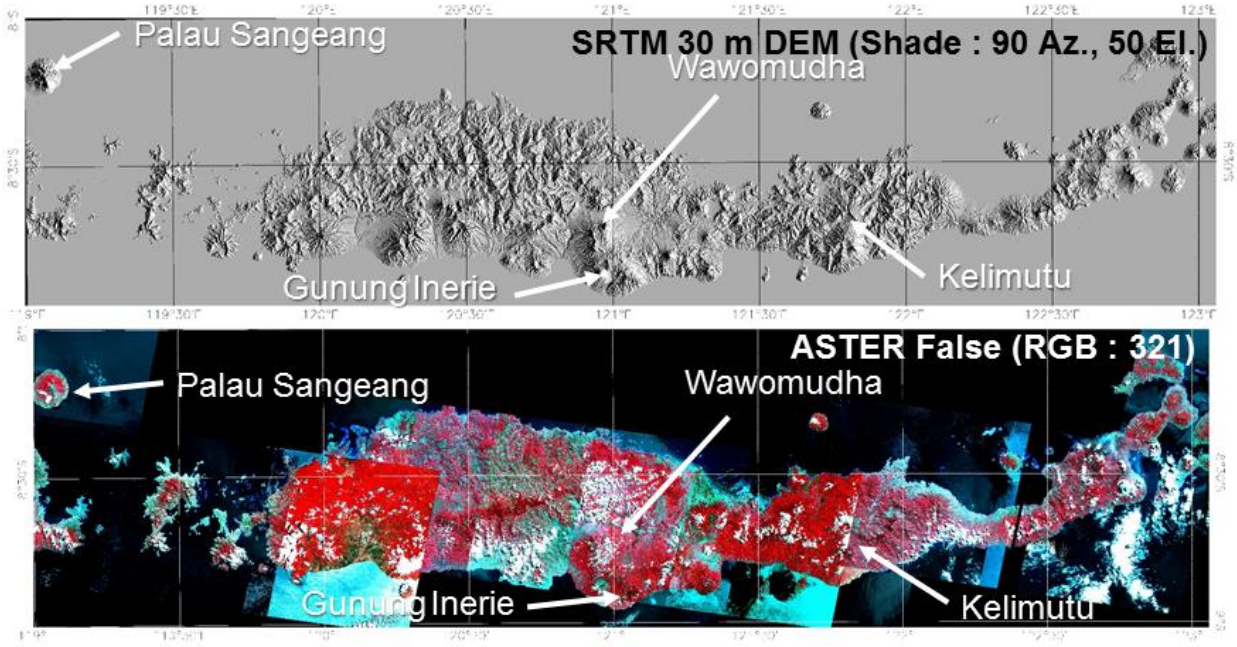


Figure 7: a) SRTM 30m DEM with topographic shading from easterly illumination; b) ASTER false colour (RGB : Bands 3,2,1). Sites of major volcanos with bare exposures are listed

These FFT filtered products were generated in an attempt to separate large scale volcanic topography (e.g. cones) from the more subtle and higher spatial frequency ridges and land forms, potentially related to fracture lineaments. ERDAS ERMapper software (http://www.hexagongeospatial.com/products) was also used for the final display and lineament interpretation of the above DEM products for each of Western, Central and Eastern Flores Island geothermal zones (1a).

RESULTS

ASTER map products and spectral signatures in exposed Flores Island sites

The densely vegetated and often cloud covered mountainous terrain in Flores Island proved a challenging area to use ASTER imagery (Figure 7a and b). The False colour RGB composite of ASTER bands 3, 2 and 1 highlights the chlorophyll vegetation in areas of bright red in this multiple ASTER scene mosaic that covers Flores Island (Figure 7b). Several sites (Figure 7a and b) were examined in this preliminary study as part of the

Advanced Geothermal Exploration Workshop, Bandung, 2016.

Mt Inerie in Central Flores is a prominent volcanic landform with some large exposed bare rock surfaces on its slopes. The ASTER VNIR False colour and Normalised Difference Vegetation Index (NDVI) imagery showed no or reduced green vegetation on Mt Ineries' slopes, particularly on its northern and northeastern flanks (Figure 8a and b). Kaolinite and AlOH clay is detected by the ASTER band products in its northern slopes (Figure 8c). The south eastern flanks are affected by thick cloud cover. However, problems with cloud artefacts are apparent in the southern slopes (Figure 8c). A preliminary examination of the ASTER VNIR-SWIR surface reflectance spectra within Ineries' exposed slopes reveal argillic / clay and possibly MgOH/carbonate signatures.

The Wawamudha volcano, also in central Flores, contained another limited exposed area of bare rock ground to apply ASTER's remote sensing. This area also revealed possibly argillic altered clay spectral signatures (alunite?) although further validation ground/field truthing is required.

Mapping thermal anomalies using ASTER surface kinetic temperature products

The volcanic activity at Palau Sangeang (Figures 7 a & b, 9), just offshore the north western coast of Flores Island, offers the opportunity to test the mineral mapping and thermal anomaly mapping capabilities of ASTER imagery. The issue of cloud and vegetation cover also proved a difficulty here but two scene acquisitions (2004-11-04 and 2006-09-07) were merged to reduce at least the effects of the clouds (Figure 9). The two options of image merging were interpreted for AlOH / clay content with mixed results. The ASTER scene acquired on 2006-09-07, and to a lesser extent the 2004-11-04 acquisition, revealed clay anomalies particularly in the central part of the island (Figure 10). The surface kinetic temperature products generated from these two day-time ASTER acquisitions revealed variable temperature anomalies, with a noticeable anomaly of 53o C at the summit of the volcanic dome for the 2006-09-07 scene (Figure 11).

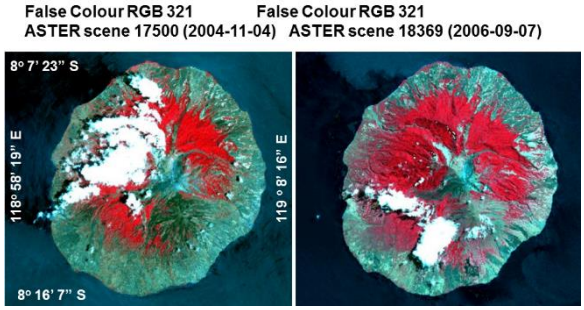


Figure 9: False colour imagery of Palau Sangeang

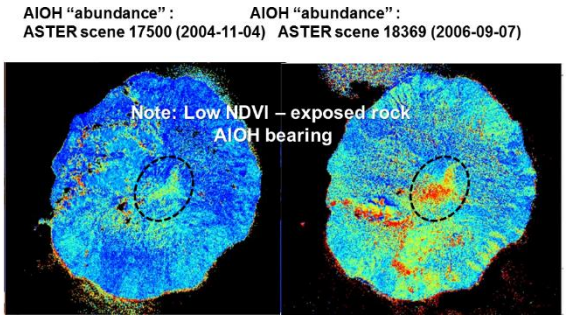


Figure 10: ASTER AlOH content interpretation of Palau Sangeang. Black dashed circle area highlights exposed potential clay altered areas (green to red). Note cloud shadow artefacts producing false anomalies south west of ASTER scene 18369 (right).

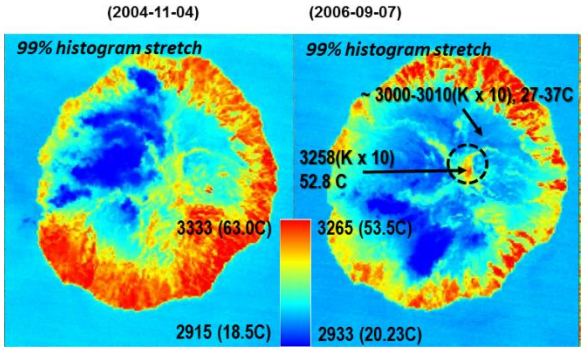


Figure 11: Day time ASTER surface kinetic temperature product of Palau Sangeang. Black dashed circle area highlights bare exposed area described in Figure 16

Surface kinetic temperature products from night time ASTER acquisitions over Palau Sangeang were accessed from seven dates between 2003-05-12 to 2014-08-21 and shown as an overlay to shaded DEM relief in Figure 12. These generally highlighted the cooling effect of the elevated volcanic summit at night however anomalously higher temperatures were observed from 2014-06-02 to 2014-08-21. In particular a river of hot lava appears apparent running down its flanks on the 2014-07-20 and 2014-08-21. However night time ASTER thermal imagery accessed and examined over the rest of Flores Island failed to identify isolated anomalies, potentially associated with geothermal fumaroles. There were less night time than the day time acquisitions available which may handicap their recognition, depending on the geothermal activity duration. However the night time ASTER temperature data over the Mt Inerie area did reveal a similar subtle thermal anomaly, as described by Urai et al., (2002) (Urai et al.,'s Figure 8). Urai et al., (2002) found a rise in the ASTER brightness temperature anomaly approximately 6 km east of Mt Inerie, in the Nage geothermal area. As with Urai et al. (2002)'s study, a subtle anomaly of only a few degrees above

background temperature was observed. It should be noted that any thermal anomaly would be an averaged estimate over the measured 90 metre ASTER TIR pixels.

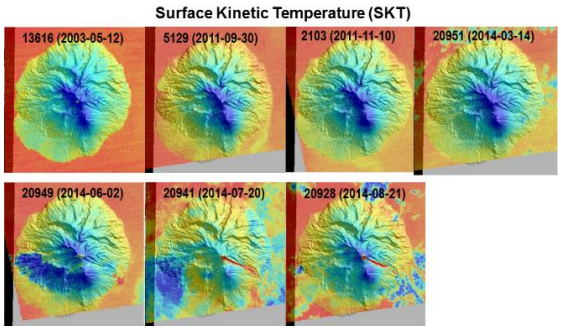


Figure 12: Chronological sequence of night time ASTER surface kinetic temperature imagery of Palau Sangeang draped over SRTM 30m DEM. Blue : low temperature; red high. Note high temperatures associated with lava flows from 2014-06-02 to 2014-08-21.

Lineament interpretation from SRTM DEM products

Examples of the products generated from the SRTM DEM for structural interpretation are shown in Figure 13 for an area in the Central Zone. The high quality SRTM DEM at 30 metre pixel resolution is apparent from the elevation display and shaded relief product in the central geothermal zone (Figures 13 a & b). The FFT filtered DEM products derived from the high pass cutoff filters 4 (moderate frequency pass filter) and 2 (high pass frequency filter) shown in Figure 6, are indicated for this same area in Figures 13 c and d, respectively. The north – south topographic features are generally more apparent in the moderate high pass frequency product (Figure 13 c) with only the more subtle finer features shown in the higher pass filtered product (Figure 13 d). Figures 14 a to d show an example from the Flores Bajawa area, include the locations of the established geothermal fields, lineament interpretation from the area. The lineaments shown are a compilation of the interpretation from the various DEM map products described in Section 2.2 and 3.2.

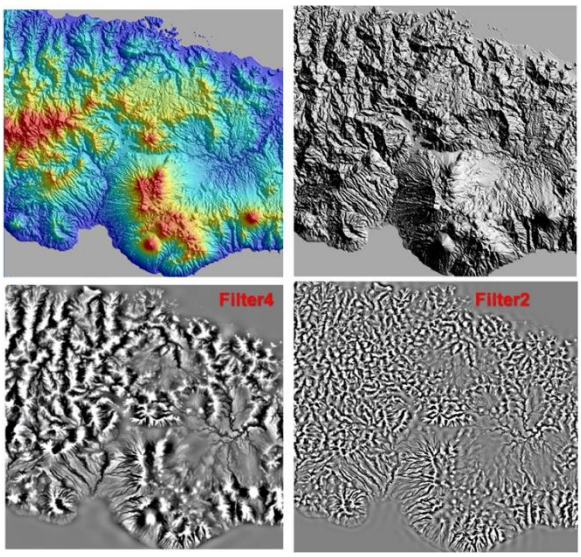


Figure 13: Example imagery of Central Flores SRTM 30 m imagery. a) Pseudo coloured DEM draped over sun shaded imagery; b) Sun shaded imagery (azimuth : 90 degrees, elevation 55 degrees; c) FFT 2-D filtered at moderate pass spatial frequency (Filter4); d) FFT 2-D

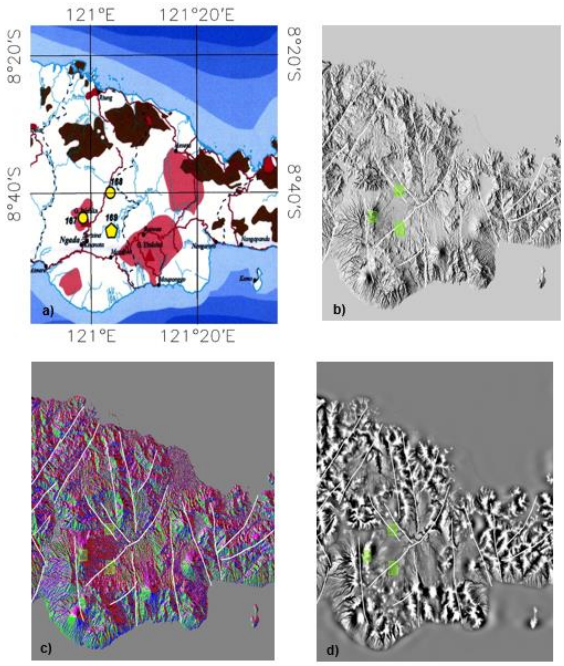


Figure 14: a) Central zone of Flores Island, supplied by the Indonesian Geological Agency, Bandung; b) Shaded DEM with lineament interpretations; c) Aspect modelled from DEM with lineament interpretations; d) FFT 2-D filtered at moderate high pass spatial frequency (Filter4) with lineament interpretations. Geothermal fields shown as green squares

CONCLUSION AND RECOMMENDATION

Vegetation and cloud cover on Flores Island together with ASTER's coarse 30 metre SWIR pixel resolution combine to limit the application of day time ASTER VNIR-SWIR remote sensing for the mapping geothermal indicator minerals. Spectral signatures from small exposures within volcanic terrain do suggest the presence of argillic minerals however ground truthing and spectroscopy of field samples is required. If future field sampling and spectrometer measurements prove successful in identifying geochemical indicator minerals then field or laboratory proximal sensing could be useful as a routine and efficient technique for ground based geological and geothermal prospect mapping.

The application of ASTER night-time thermal imagery also provided limited results for geothermal anomalies mainly because of the coarse spatial resolution of the ASTER TIR instrument (e.g. 90 metre pixels). Averaging temperature anomalies from geothermal fumaroles of a few metres in dimension, from a 90 x 90 metre pixel sampling area will limit the chances of their discovery. It is anticipated however that a higher spatial resolution thermal sensor or camera, capable of measuring radiance or surface temperature of within smaller pixel dimensions could prove more successful at detecting active geothermal fumaroles.

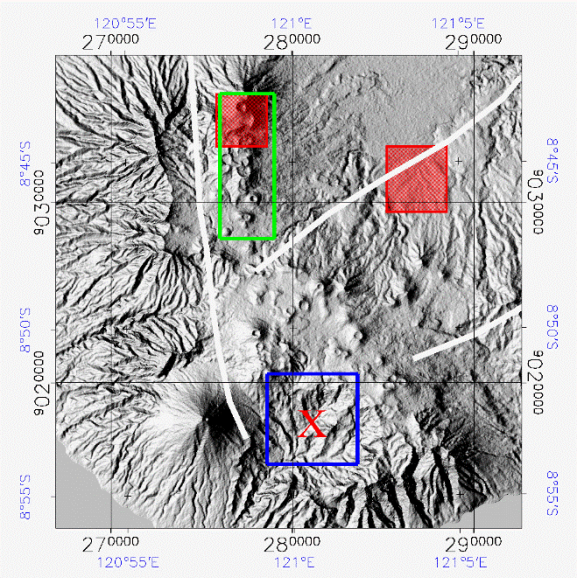


Figure 15: Shaded SRTM DEM within the Central Bajawa Zone of Flores Island, showing recommended detailed study areas A (blue box) and B (green box) for further high spatial resolution Lidar DEM and thermal imaging. Red X : Nage geothermal area (Urai et al., 2002)

The lineament interpretation from the SRTM DEM products are likely to include geomorphological features that may or may not be related to fault lines or fractures associated with geothermal activity. The trends of these lineaments however appear generally consistent with the NNW and NE trends of fault structures and fold axes described by Muraoka et al. (2002). The lineaments interpreted for the Central or Bajawa Zone (Figure 14 b, c & d) show a relatively high density and pass through the currently recognized geothermal fields as marked. This area is also in the vicinity of the Nage geothermal area east of Mt Inerie, previously identified by thermal imagery (Urai et al., 2002). This suggests that this is an area worthy of further investigations for more detailed structural studies and thermal observations. The shaded relief DEM product also reveals the presence of minor cones in a north-south alignment north of Mt Inerie, as shown in Figure 14 b, and at a finer scale in Figure 15. Two areas are recommended to undertake more detailed LiDAR DEM and thermal camera observations, areas A (25 km2) and B (24 km2) as marked in Figure 15. Higher resolution LiDAR deployed in a ground return mode, should facilitate more detailed structural features such as fractures and fault lines. Also airborne thermal camera with a higher spatial resolution also offers the potential to detect the hydrothermal emissions from fumaroles of limited dimensions.

ACKNOWLEDGEMENTS

This study was financially supported by the Geothermal Capacity Development Programme Indonesia-Netherlands (GEOCAP). The ASTER L2 data products were retrieved from the online Data Pool, courtesy of the NASA Land Processes Distributed Active Archive Center (LP DAAC), USGS/Earth Resources Observation and Science (EROS) Center, Sioux Falls, South Dakota, https://lpdaac.usgs.gov/data_access/data_pool. The authors would also like to thank the Indonesian Geological Agency, Bandung for supplying a hardcopy map of the geothermal potential areas of Nusa Tenggara Timur.

REFERENCES

Adams J.B. and Filice, A.L., (1967). "Spectral reflectance 0.4 to 2.0 microns of silicate rock powders", Journal of Geophysical Research, 72, pp. 5705–5715.

Aswin, D and Nanlohy, (2002), "Characteristic of hydrothermal alteration minerals on MT-1 and MT-2 wells, Mataloko, central Flores, East Nusatenggara, Indonesia by using short-wave infrared reflectance spectroscopy", Bulletin of Geol. Surv. Japan, vol. 53, pp. 323-328.

Baldridge, A. M., S.J. Hook, C.I. Grove and G. Rivera, 2009. "The ASTER Spectral Library Version 2.0," Remote Sensing of Environment, vol 113, pp. 711-715.

Crowley, J.K., Brickley, D.W. and Rowan, L.C. (1989), "Airborne imaging spectrometer data of the Ruby Mountains, Montana: mineral discrimination using relative absorption band-depth images", Remote Sensing of Environment, 29, pp. 121–134.

Florinsky, I.V. (2012), "Digital Terrain Analysis in soil science and geology", Elservier, Amsterdam, First Ed., 2012, ISBN 978-0-12-385036-2

Hunt, G.R. and Ashley, R.P. (1979), "Spectra of altered rocks in the visible and near infrared", Economic Geology, v. 74, pp. 1613–1629.

Kratt, C., Calvin, W., and Coolbaugh, M., (2006), "Geothermal exploration with Hymap hyperspectral data at Brady–Desert Peak, Nevada", Remote Sensing Environ., Vol. 104, pp. 313-324.

Littlefield, E.F. and Calvin, W.M., (2014), "Geothermal exploration using imaging spectrometer data over Fish Lake Valley, Nevada", Remote Sensing Environ., Vol. 140, pp. 509-518.

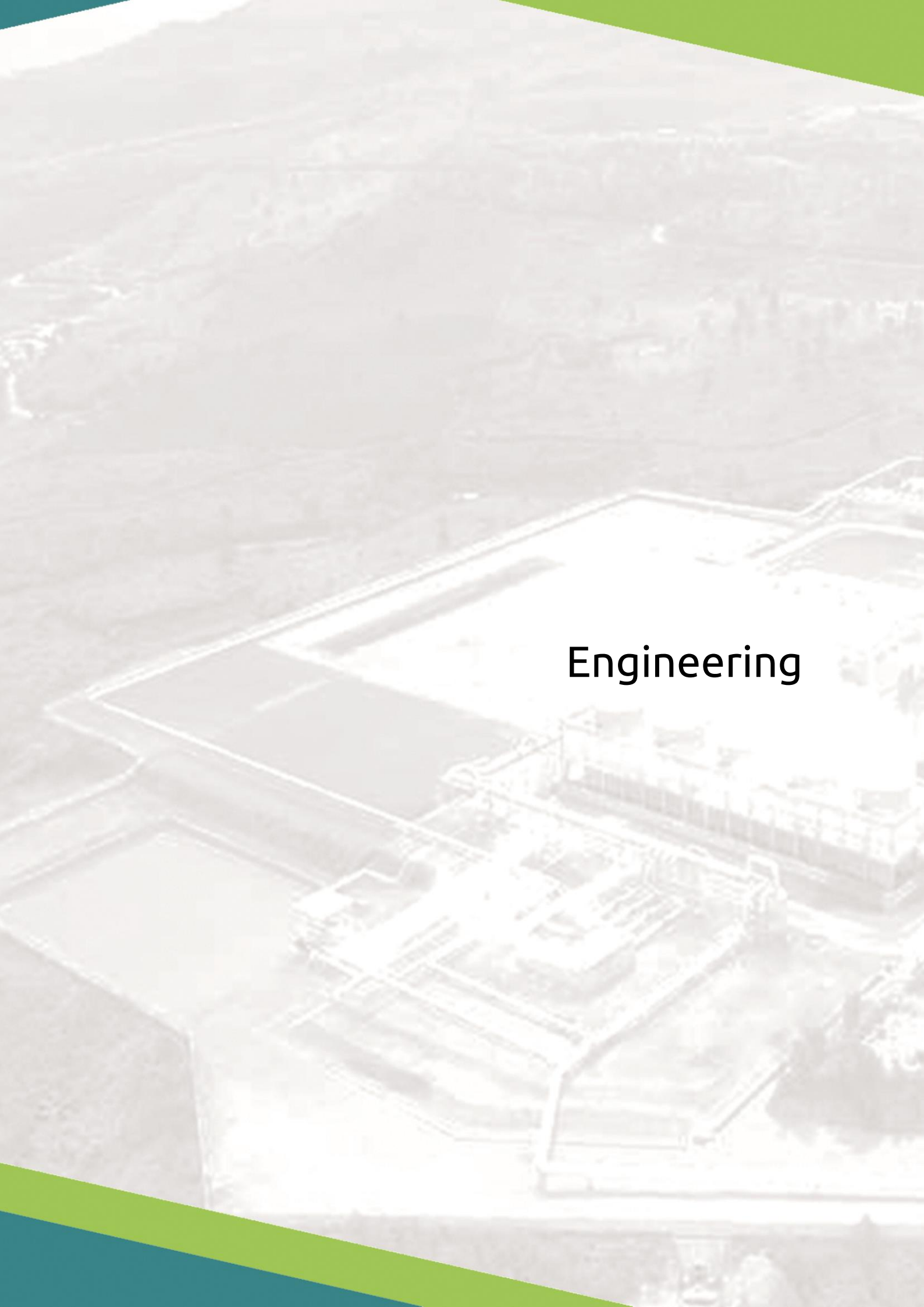
Lyon, R.J.P., and Burns, E.A. (1963), "Analysis of rocks and minerals by reflected infrared radiation", Economic Geology, 58, pp274–284.

Muraoka, H., Nasution, A., Urai, M., Takahashi, M., Takashima, I., Simanjuntak, J., Sundhoro, H., Aswin, D., Nanlohy, F, Sitorus, K., Takahashi, H., and Koseki, T., (2002), "Tectonic, volcanic and stratigraphic geology of the Bajawa geothermal field, central Flores, Indonesia," Bulletin of Geol. Surv. Japan, vol. 53, pp.109-138.

Urai, M., Muraoka, H., and Nasution, A., (2002), "Satellite remote sensing data and their interpretations for geothermal application: A case study on the Ngada District, central Flores, Indonesia.", Bulletin of Geol. Surv. Japan, vol. 53, pp. 99-108.

Vincent, R.K. and Thomson, F. (1972), "Spectral compositional imaging of silicate rocks," Journal of Geophysical Research, 77, 14, pp2465–2472.

Vincent, R.K, Rowan, L.C., Gillespie, R.E. and Knapp, C., (1975), "Thermal-infrared spectra and chemical analyses of twenty-six igneous rock samples", Remote Sensing of Environment, 4: 199-209. International Geoscience and Remote Sensing Symposium (IGARSS), 9–13 July. 3p.



Engineering



HYBRID DRILL BIT IMPROVES DRILLING EFFICIENCY IN GEOTHERMAL APPLICATION IN LUMUT BALAI FIELD, INDONESIA

Fakhri Ade Andika[1], Mada Amatori Sutan[2], and Widoyo Krisnanto[1]

[1]Pertamina Geothermal Energy
[2]NOV ReedHycalog
Email: mk.fakhri.ade@pertamina.com; mada.sutan@nov.com; widoyo.krisnanto@pertamina.com

ABSTRACT

Geothermal market were dominated primarily by roller cone bits from big hole to smallest hole section. It is well known that because of the very hard nature of the volcanic formations in geothermal wells, the polycrystalline diamond compact (PDC) cutters cannot efficiently drill geothermal wells. However, PDC technology advancement nowadays brings the bit type to be able to overcome the challenges. Some benefits that PDC bit may offer to the drilling operation: eliminate the risk of losing cones in the hole, eliminate the bearing life limitation, which is a time-consuming problem that consequently increases the overall well cost. There are a lot of reason that drill bit companies have been continuously working to improve the quality of PDC cutters and improve the PDC cutter drill-ability where it can penetrate better in the application to improve drilling efficiency while reducing trips to save total drilling cost. A thorough analysis has been performed to have the solution in Geothermal drilling, such as the PDC bit blade count requirement and cutter size to use, and the most suitable cutter type(s) to drill the volcanic rock. The evolution of Poly-crystalline Diamond Compact (PDC) cutter technology and hybrid drill bit design, which combined PDC and diamond impregnated bit, extends bit durability and expands the application range of drilling in highly compressive strength and abrasive lithologies. By having dual cutting structure of shearing with PDC cutter and grinding with impregnated diamond as rock failure mechanism, such design maximizes drilling efficiency in these harsh environments. The first PDC hybrid drill bit run in Lumut Balai field was performed by 9.875" FT716 (a 7-bladed, 16mm cutters with hybrid impregnated-diamond layer) with successful one run to TD from shoe to shoe broke the field record in the 9.875" hole section with 1,021 m interval drilled and high ROP performance at 13.6 m/hr ~ 4.4 min/m. The dull condition was excellent with IADC dull grade of 1-1-WT-S-X-1-CT-TD. In this application, the use of hybrid drill bit technology improves ROP performance and reduces overall drilling cost. Previously, it would typically require several roller cone bits to reach target depth. The paper explains on the bit unique design and the benefits which can be used as reference to drill the well with similar characteristics, and moreover similar challenges.

Keywords: PDC, hybrid drill bit, geothermal drilling, Lumut Balai.

INTRODUCTION

The concept of hybrid drill bit technology has been developed considerably by drill bit manufacturers for some time. As the demand in drilling in hard and abrasive environment increased over the past decade, drill bit manufacturers are developing new technologies and strategies to capture this potential market (Garcia et al, 2013; Nicholl et al, 2013). At the same time, the need to maximize drilling efficiency is critical to operators in order to reduce drilling time and save cost (Putra et al, 2015).

Advancements of PDC cutter technology, impregnated diamond material mix, drill bit design, and manufacturing capabilities allow a more durable and reliable fusion design. This hybrid drill bit has been designed to maximize interval drilled with dual cutting mechanism, coupled with right selection of thermostable PDC cutters for extended durability in hard and abrasive formations.

APPLICATION

Lumut Balai geothermal field on the island of Sumatera in Indonesia is part of the PT Pertamina Geothermal Energy working area. The project is located on Sumatera Island, South Sumatra Province, Penindaian village, sub-district of Semende Darat Laut, Muara Enim regency, about 292 km southwest of Palembang (Figure 1). Drilling activity in Lumut Balai geothermal field started in mid-2008, with well LMB 1-1 being the first well drilled (Sulistyardi, 2010). It is an exploration well and its profile is a straight-standard hole, but successive wells will be directional big holes.

LMB-19.2.R is selected to be the subject well for the PDC trial run in 9.875" hole section. The justification is looking at numerous roller-cone bit runs were required to drill the section in previous wells. Some of the runs were pulled due to bit hours which open an opportunity for PDC bit to overcome the challenge.

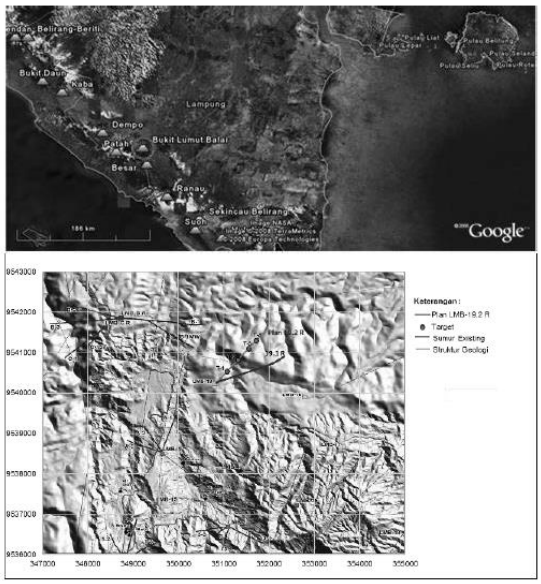


Figure 1: LMB-19.2.R location in Lumut Balai field

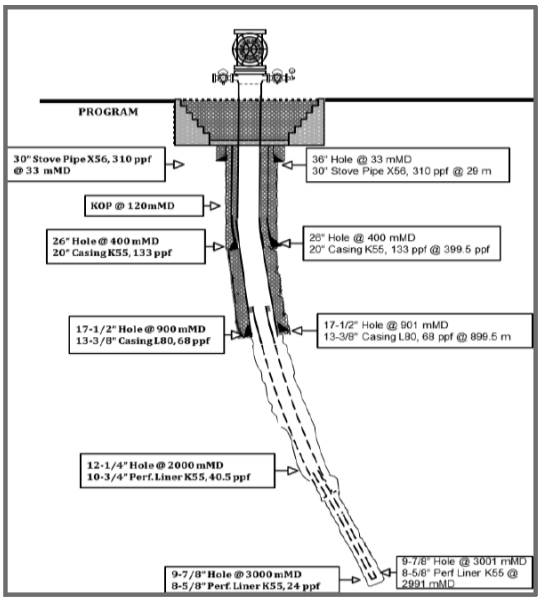


Figure 2: LMB-19.2.R well design with 3,000m TD in 9.875" hole section.

The offset wells include LMB-A1, LMB-A2, LMB-C1.R and LMB-19.1. Rock strength analysis was performed to study the application feasibility and resulted in value ranging from 10-45 kpsi with rock lithology of metamorphic breccia andesite (see Figure 3).

The hybrid drill bit technology is targeted to reduce drilling costs and time in application where the bit durability is limited especially while drilling in harsh rock environments. In harder rock or difficult lithologies that are not drillable with a PDC bit, a Roller Cone (RC) bit is generally used to drill the section. However, in a RC bit there is limitation on its durability as the bearing will start to fail depending on Weight on Bit (WOB), hours, and RPM. Therefore, the need to trip out to change the bit has been considered as a contributing factor in Non-Productive Time (NPT).

The hybrid drill bit has dual cutting structure of shearing with PDC and grinding with impregnated diamond. This fusion of technology helps to prolong bit durability in harsh application, while at the same time optimizes ROP.

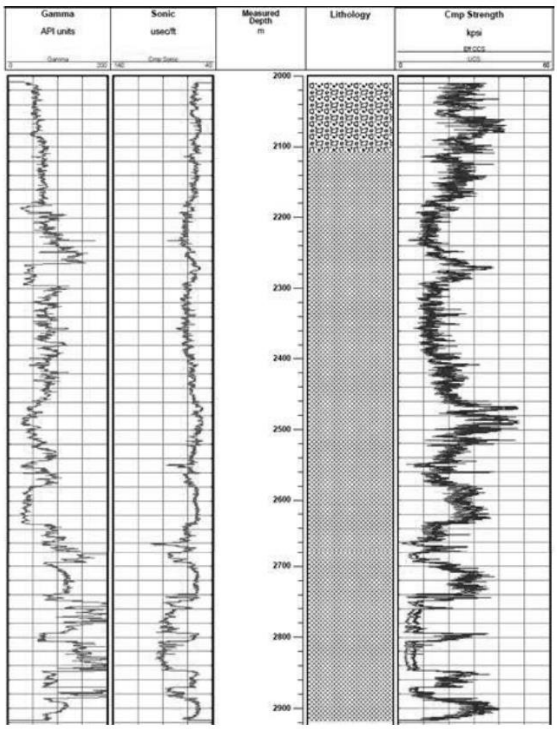


Figure 3: Rock strength analysis in LMB-C1 well resulted in 10-45 kpsi rock.

HYBRID DRILL BIT – DESIGN CONCEPT



Figure 4: NOV ReedHycalog FuseTek™ Hybrid Drill Bit (Garcia et al, 2013)

Bit body

At first glance, there is no difference in appearance between conventional PDC and hybrid drill bit bodies. Upon detail examinations, it can be seen that most of the blade material is composed of impregnated diamond and tungsten carbide matrix specifically designed to maximize durability and abrasion resistance.

The impregnated diamond mix applied in the hybrid drill bit blade has been optimized to wear at specific rate, which allow diamond cutting surface to self-sharpen once the primary cutting structure has worn. Therefore, in cases where the primary cutting structure has been worn, the diamond impregnated material in the blade area will help to grind and penetrate the hard lithologies.

Cutting structure

The hybrid drill bit has two different cutting structures: PDC cutter and impregnated diamond mix material. The primary cutting structure is the PDC cutters which are located in the first row on the blade while the secondary cutting structure is composed of diamond impregnated mix materials with the shape of PDC cutter tracking behind the primary cutting structure on the blade.



Figure 5: Dual cutting structure as rock-failure mechanism in hybrid drill bit: shearing and grinding.

Latest premium shaped cutter technology also been selected to be used in the bit design. This technology consists of a high-performance range of PDC cutters fine-tuned to the specific application to overcome critical failure modes. The latest premium cutter technology uses refined diamond feeds, increased sintering pressures to provide denser diamond with high toughness, and high-abrasion resistance that maintains thermal stability using deep leach technology. The shaped cutter technology provides efficient point loading to the formation while maintaining durability to complete the section. By creating subsurface cracks that propagate to the rock surface, shape cutters allow for thin and uncondensed cuttings, making an efficient use of energy. The technology also incorporates a polished mirror finish that reduces friction on the cutting face of the cutter, improves ROP and reduces the cutter temperature to avoid thermal degradation.



Figure 6: Shaped premium cutter technology with mirror finish.

THE RESULT

The first 9.875" hybrid drill bit used in LMB-19.2.R well drilled through 1,021m of formation interval to section Target Depth (TD), which consist of hard and abrasive metamorphic breccia andesite. The bit drilled from 1,980 m to 3,001 m in 75.21 hours with average on-bottom ROP of 13.6 m/hr or 4.4 min/m in a motor BHA. At surface, the bit was dull graded 1-1-WT-S-X-I-CT-TD.

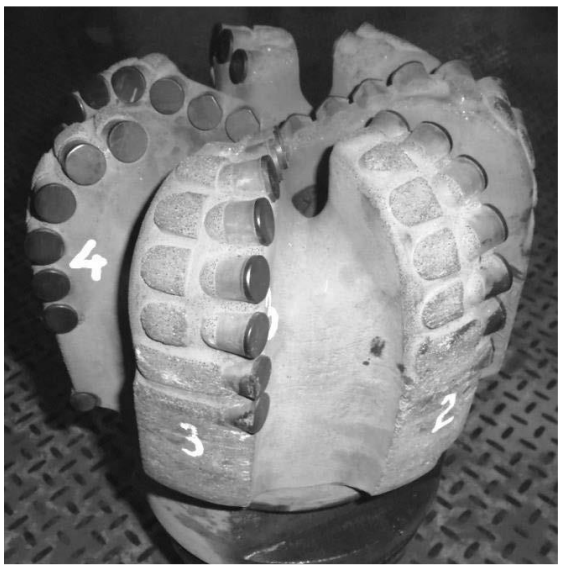


Figure 7: The 9-7/8in ReedHycalog FT716 dull bit with shaped cutter technology after drilled 1,021m interval completing shoe-to-shoe interval in a single run. Graded: 1-1-WT-S-X-I-CT-TD.

The drilling parameter log shows that when the WOB was increased there was some substantial increase in ROP ranging between 6 –36 m/hr.

however it is also reported that the parameter was controlled at 12-15 m/hr or 4-5 min/meter for hole cleaning and steering purpose. The low level of Mechanical Specific Energy on the entire run suggests that all the energy that was applied in the drill string was used effectively to drill the formation although total lost circulation was encountered. No steering issue was reported while achieving good directional performance at 48deg inclination and resulted in 9.92m center to center plan. The 9.875" hybrid FuseTek™ FT716 drilled the section faster at least by 7 rig days over the drilling plan. Overall, this was a promising first run and offered confidence in the next wells that there is a significant improvement in term of ROP.

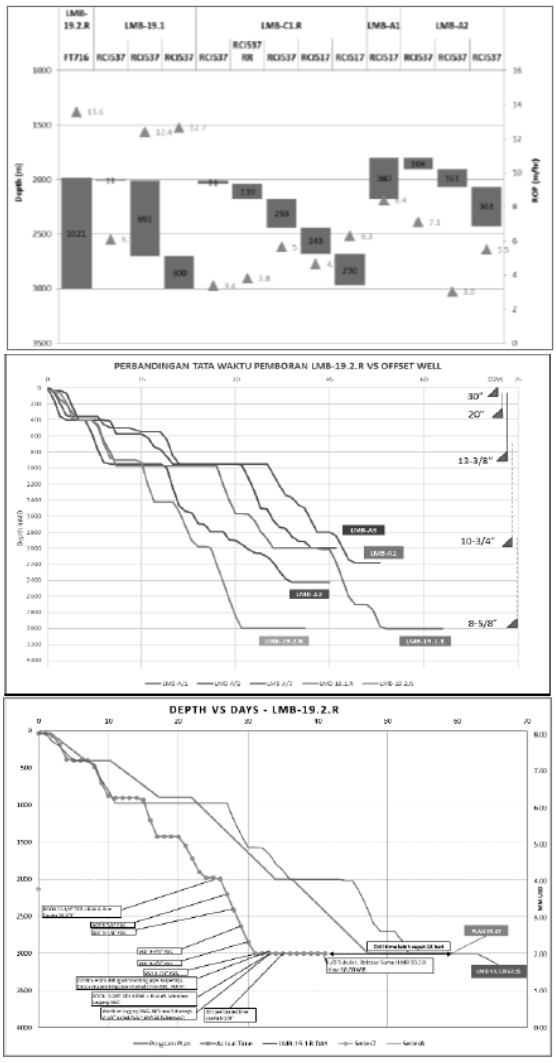


Figure 8: Hybrid drill-bit performance plot against offset wells. The subject bit successfully drilled the section a single run while replacing 2-4 roller cone bit runs while delivering higher ROP performance saved 7 rig days compared to plan.

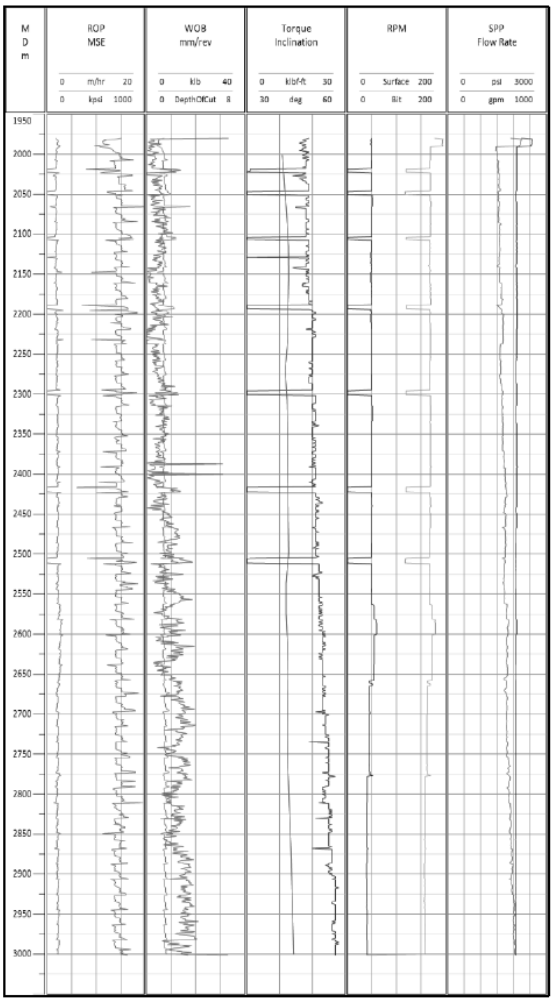


Figure 9: Drilling parameter plot shows low MSE through-out the run indicating high drilling efficiency.

Drill bit economic analysis

Cost per interval analysis is a good measurement to evaluate the performance and cost efficiency of a drill bit run. This calculation is based on the relationship of on-bottom drilling time, trip time, interval drilled, rig cost, and bit cost as shown in below equation:

$$C = B + R(D+T) / I \quad \ldots\ldots(1)$$

Where:

C = Cost per interval ($/m)
B = Bit cost ($)
R = Rig rate per hour ($/h)
D = On-bottom drilling time (h)
T = Trip time (h)
I = Interval drilled (m)

Figure 10 summarize the cost per interval comparison between 9 7/8" section offset wells and the subject wells. The hybrid drill bit reduce cost per interval significantly as much as 39-87 % more economics than offset wells.

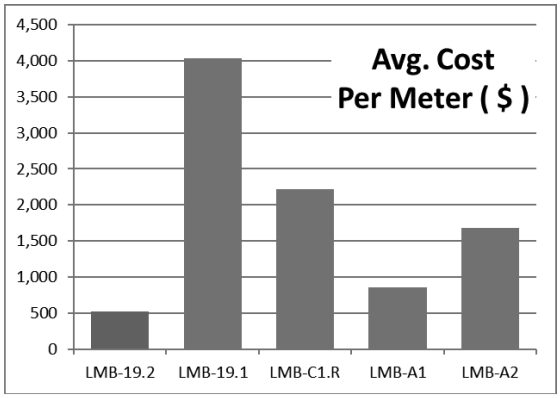


Figure 10: Hybrid drillbit performance has successfully reduced cost per meter by 39-87% over offset well performance.

CONCLUSIONS

1. The hybrid drill bit with dual cutting structure is suitable with hard and abrasive application in Lumut Balai field.
2. New record of the longest interval drilled in 9.875" hole section, Lumut Balai field by drilling the whole section interval – shoe to shoe in a single bit run. This achievement saved 7 rig days while reducing cost per meter by 32-65% over offset well performance.
3. Recorded highest avg ROP of 9.875" hole section in Lumut Balai field by significantly improve drilling efficiency and set the new benchmark at 13.6 m/hr or 4.4 min/m.
4. Excellent dull condition of 1-1-WT-S-X-I-CT-TD shows that the bit design is well suited to the application.

REFERENCES

Garcia, A., Barocio, H., John, D. S., and Avila, E. A. P. (2013), "Hybrid Bit Technology Expands Application Range in Harsh Rock Environments": *Paper Society of Petroleum Engineers (SPE)* 166766 presented at the SPE/IADC Middle East Drilling Technology Conference and Exhibition, Dubai, UAE.

Garcia, A., Barocio, H., Nicholl, D., Belhenniche, S., Quijada, R., Veloz, C., and Cevallos, M. (2013), "Novel Drill Bit Materials Technology Fusion Delivers Performance Step Change in Hard and Difficult Formations": *Paper Society of Petroleum Engineers (SPE)* 163458 MS presented at the SPE/IADC Drilling Conference and Exhibition, Amsterdam, The Netherlands.

Nicholl, D., Garcia, A., Barocio, H., Sha, D., and Jian, Z (2013), "New Hybrid Bit Exceeds Expectation in Challenging Application in Tarim Field, China": *Paper IPTC* 16622 presented at the 2013 International Petroleum Technology Conference, Beijing, China.

Putra, N. R. B., Leonanto, R., Darmawan, K., Waragai, T., Tokuda, N. (2015), "Hybrid Drill Bit Improves Drilling Efficiency in Abadi Field, Indonesia" *Indonesian Petroleum Association Thirty-Ninth Annual Convention & Exhibition* – IPA15-E-120.

Sulistyardi, H. B. (2010), "Basic Design of Lumut Balai 2x55 MW Geothermal Power Plant, Indonesia". *GEOTHERMAL TRAINING PROGRAMME*, Reykjavik, Iceland. Number 29.

GEOTHERMAL DRILLING CORROSION PROBLEM ROOTS RELATED WITH DRILLING FLUIDS

Ariya Dwinanto[1], Ashadi[1], Yudi Hartono[1], Haris Siagian[1], Gilang Kharisma[2], and Joni Sofian[2]

[1]PT Sokoria Geothermal Indonesia – A project of KS Orka Renewables Pte Ltd
[2]PT Halliburton Indonesia
Email: ariya.priyono@ksorka.com ; ashadi@ksorka.com ; yudi.hartono@ksorka.com ; haris.siagian@ksorka.com ; gilang.kharisma@halliburton.com; joni.sofian@halliburton.com

ABSTRACT

Sokoria geothermal prospect is located at Flores Island in East Nusa Tenggara Province, Indonesia, more detail is on the southwest side of Kelimutu volcano. KS-Orka carried out a drilling campaign on the propose to get better understanding of the Sokoria geothermal system and to provide some production fluid for the electricity generator turbines. Related to the geothermal environments, corrosion is a part that has to be minimized and mitigated. Corrosion may be defined as the destruction of metal through electrochemical and mechanical action between the metal and its environment. Drilling on geothermal field can be challenging if geothermal fluid chemistry provides metal corrosion of the drilling equipment's material. This fluid chemistry is normally unknown until deep production wells are drilled and tested. This paper will discuss about the corrosion problem related with the surface and subsurface conditions problem roots. Problem roots of the corrosion may be the effect of these two related group: surface condition and subsurface conditions. Surface conditions are related with the water supply, air drilling usage and oxidation by air. Subsurface conditions are related with the formation and subsurface fluids. Specifically on subsurface conditions, major contributors of chemical corrosion are: pH, dissolved oxygen (O_2), dissolved carbon dioxide (CO_2), dissolved hydrogen sulphide (H_2S), ammonia (NH_3), sulphate (SO_4), chloride (Cl) and suspended solid material and its deposit. Both conditions may lead to the metallic materials being corroded and becoming unusable. One definite problem encountered on drilling operation will associate with the bottom hole tools used and many surface equipments which are used to deliver the dedicated water supply. Bottom hole tools such as drill pipes, wireline tools and bottom hole assembly are few to mention on the list of equipment to be exposed on corrosion problem. Surface equipments such as water pumps, valve, steel pipes often has direct conjunction effects related to corrosion problem. Problem from minor to major will cause non performing time which directly will hurt the drilling cost overall. Knowing the environment and equipment specification with some proper monitoring may serve the alternative solution on mitigating problems and avoiding non performing time on drilling operations. Corrosion monitoring will guide to have a better mitigation on reducing the corrosion rate.

Keywords: Corrosion, Drilling, mitigation

INTRODUCTION

Corrosion is a major concern when drilling in a geothermal environment (Prasetia et al, 2010). Corrosion may be defined as the destruction of metal through electrochemical and mechanical action between the metal and its environment. Corrosion can results in high costs associated with maintenance, materials and loss in production (Karlsdottir et al, 2015).

The General Process

There should be 3 components to corrosion occurs (Zarrouk, 2012). With simple explanations the components are:

1. Anode : the part of substance that gives the electrode.
2. Cathode : the part of substance that takes the electrode.
3. Electrolyte : Conductive substance that is usually fluid which will enhance the electrode to jump from anode to cathode.

On Drilling operations steel metals functions as anode. Where under a chemical reaction, the Fe or iron element will give $2e^-$ (dissolves) and transfer it to the cathode. On the other side, gas inside the drilling fluids will functions as cathode, predominantly oxygen, hydrogen and carbondioxide. The third part Electrolyte, has been given by the drilling fluids (figure 1). Here are the common anode and cathode reactions within the corrosion process within the steel inside the drilling operations:

Anode reaction:
$Fe^0 \rightarrow Fe^{2+} + 2e^-$
(iron dissolves)

$Fe^{2+} + 2(OH)^- \rightarrow Fe(OH)_2$
(dissolved iron forms iron hydroxide)

1st Cathode reaction:
$2H^+ + 2e^- \rightarrow H_2$ (hydrogen gas)

2nd Cathode reaction:
$O_2 + 2H_2O + 4e^- \rightarrow 4\ OH^-$
(source: (1990 - 2007))

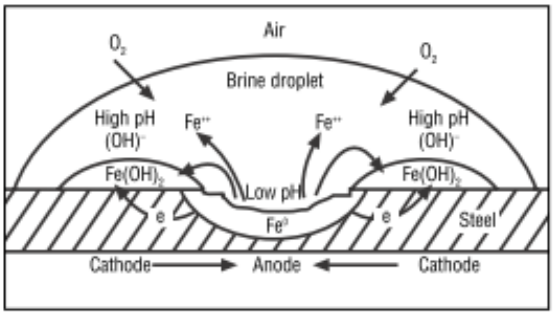


Figure 1: Anode and Cathode reaction on the corrosion process illustration. (source: (1990 - 2007))

Thus by simple logics, corrosion can be disrupted by the help of insulations of drill pipe thus it cannot contact with the cathode or gases and electrolyte or drilling fluids. Or corrosion can be disrupted by changing material for drill pipe thus it is more reluctant to the corrosive environment. Both which in conclusion will hamper the electrode to jump between anode and cathode (Abbott et al, 1997).

Corrosion Factors

Different environment will differ the rates of corrosion. Some case it will induce the corrosion rate or on the other hand, will hamper the corrosion activity. Here are those factors:

pH: corrosion will be accelerated on acidic environment (pH<7) and will de-accelerate on alkaline (pH>7) environment (figure 2). On special H_2S occurences alkaline (pH>7) environment will lower down this electrolyte thus reduces the corrosion rate (figure 3).

Dissolved salts: corrosion will increase then decrease in a specific manner when the dissolved salts reach into certain concentration. Corrosion deaccelerate because increasing salt will depress the oxygen concentration (figure 4).

Pressure: corrosion will increase with adding pressure (figure 5).

Temperature: corrosion will increase by adding temperature. Increasing temperature will decrease the oxygen level but will accelerate the chemical reaction (figure 6).

Mineral scale: Mineral scale will corrode only a certain parts of steel underneath the scale. As example precipitation of usually $CaCO_3$ will affect certain parts of steel underneath the scale.

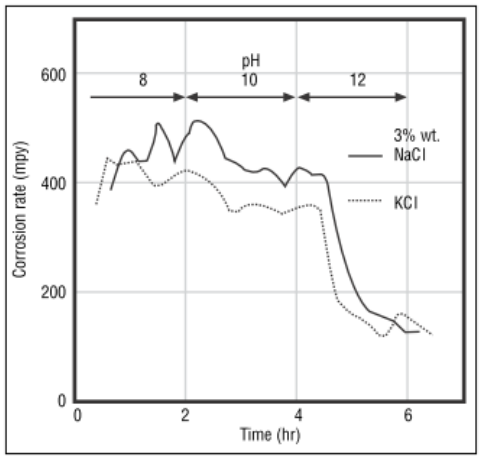


Figure 2: Corrosion reaction rate decrease in alkaline environment. (source: (1990 - 2007)).

pH	% S^{2-} as H_2S
5.0	98.000
6.0	90.000
6.5	70.000
7.0	50.000
7.5	25.000
8.0	10.000
9.0	1.000
10.0	0.100
11.0	0.010
12.0	0.001

Figure 3: Corrosion reaction rate decrease in alkaline environment by hampering the S^{2-} thus $2H^+$ cathode concentration. (source: (1990 - 2007)).

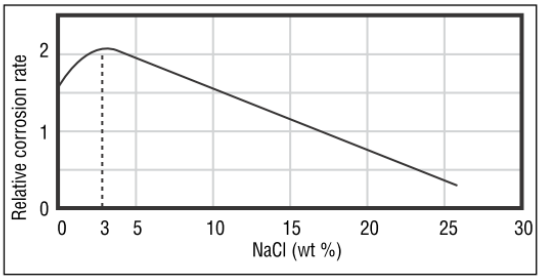


Figure 4: Corrosion reaction rate increase and decrease in a specific dissolved salt concentration. (source: (1990 - 2007)).

Dissolved gasses: Oxygen, Carbon-dioxide and Hydrogen Sulfide will be a good cathode for the corrosion process, thus increasing of gasses will accelerate the corrosion effect.

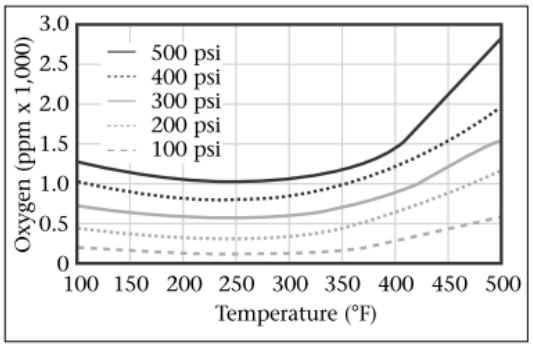


Figure 5: Corrosion reaction rate increase by adding pressure. (source: (1990 - 2007)).

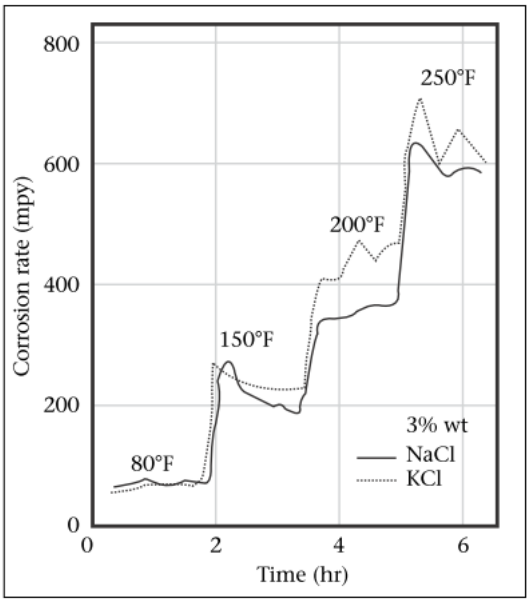


Figure 6: Corrosion reaction rate increase by adding Temperature. (source: (1990 - 2007)).

GEOTHERMAL DRILLING

Drilling Fluid Perspective

A general understanding with one specific strategy on drilling geothermal in a drilling fluid perspective may include two big parts:

Drilling with full return (full circulation) : Drilling with full circulation, drilling fluid will be maintain to preserve a good hole cleaning operations thus adding viscosifier, potassium chloride (KCl or salt) and polymers to add the rheology may enhance the hole cleaning with certain goals.

On drilling with full return, we can focus on applying best corrosion inhibitors inside the mud system. Or scavengers thus can prevent gases to be a good cathode inside the electrolyte.

Drilling with total loss circulation (TLC) or partial loss circulation (PLC): Drilling with loss circulation has been entitled the most common phase when approaching the production zone. Drilling fluids may be switch from mud to water based fluid or even aerated fluid to prevent valuable pricey mud vanishing to the formations.

On drilling with loss circulation, we can focus on applying best corrosion inhibitors inside the hi-vis mud and injecting corrosion inhibitors suitable for the air drilling operation (should air is introduce to the drilling operation).

By means on both situations looking for a proper initial water supply generation may decrease the drilling budget significantly. Most of the concern may include by searching the normal pH=7.

Mitigation on the corrosion activity

To mitigate the corrosion activities, we may want to do in subsequent order monitor, analyze and react. One common method corrosion monitoring is by using the friendly drill pipe corrosion coupons. In similar to the drill pipe inner dimensions, it will be inserted in the last drill pipe box before the heavy weight drill pipes. And will be exposed to minimum 40-100 hours to the drilling operations. Drill pipe corrosion coupons will then be analyzed for its weight (comparing the initial before submerging it thru the drilling operation with the final weight) and then be analyzed for its certain type of the corrosion cause. When the type of corrosion cause and rate has been compiled then a reaction will have a way to decrease the corrosion rate.

These types of corrosion from which dissolve gases may be detected by analyzing the scale deposits and pits. Scale deposits type and causes:

Table 1: Type of corrosion cause related with the cathode factors (source: (1990 - 2007)).

Type of scale deposits or byproduct	Cause
Iron oxide	dissolve oxygen
Magnitite	dissolve oxygen
Iron sulfide	dissolve hyrogen sulfide
Iron carbonate or siderite	dissolve carbondioxide
Calcium / magnesium carbonate	dissolve carbondioxide

Unfortunately dissolve hydrogen gass cause cannot accurately be detected using the drill pipe corrosion coupons scale deposits or byproduct. This specific cause should be analyzed by looking on the possible H_2S concentration and its effect within a specific environment. The Garrett Gas Train is used to monitor sulfide concentrations. The gas train separates the gas from the liquid, thereby preventing contamination of the gas by the liquid phase. A Draeger Tube is the preferred H_2S detector for quantitative sulfide analysis. A lead acetate paper disk can be used in the Garrett Gas Train for determining the presence of H_2S.

Below are the common equation to look at on,

Corrosion rate (lb/ft^2/yr) =

$$\frac{K\ x\ [initial\ wt\ (g) - final\ wt\ (g)]}{total\ exposure\ time\ (hr)}$$

Corrosion rate, mills/yr =
Corrosion rate (lb/ft^2/yr) x 24.6
(source: (1990 - 2007))

After knowing what cause which corrosion occurs, then start with the remedies to reduce the rates. Table which will discuss some remedies related with the causes will be listed on the attachments (Table 5).

STUDY CASE

On Sokoria drilling campaign we indeed discover corrosion rate activity. We manage to mitigate the problem by including the process which are: monitor, analyze and react.

Monitor

We did monitor the corrosion rate by implementing the corrosion ring inside the 5" drill pipe. It has been inserted in the last drill pipe box before the heavy weight drill pipes. Excluding on the 26"section on MTB A-01 and MTB A-02 which we did not obey the best drilling practice and instead put it on the HWDP, which results on bias because of the mechanical damage (not related with the corrosion activity).

Besides both mechanical damage corrosion rings, others are recovered with various results. One may want to agree is the corrosion rate grouping. Which we use on the standard as below:

Corrosion Evaluation (Lb/ft^2/yr)

0 - 2	Low
2 - 4	Moderate
4 - 6	High
6+	Severe



Figure 7: Corrosion ring damage because of mechanical non corrosion reactions.

The results for the corrosion rate of each corrosion ring discovered are:

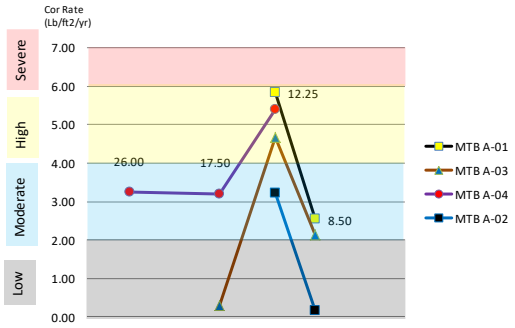


Figure 8: Corrosion ring recap per section

Below are one example which we recovered from MTB A-02 on 12-1/4" drilling section and with the result of moderate corrosion rate or 3.23 Lb/ft^2/yr.



Figure 9: Corrosion condition on one of the corrosion ring coupons.

Analyze

Corrosion ring treatment after recovered are examed. The main purpose on the event is to know about the cause, and what factors do corresponds with the corrosion rate activities.

MTB A-01 is the initial exam process. And resulted with a relative bigger number on the corrosion rate.

Main cause of the corrosion ring should be recognized related with the dissolve gass. One simple method to know the identification of CO_2 is to recognize a bubble present by adding HCl 15%.

Factor which resulted with the expected results are KCL content and air drilling operations. When reaching 17-1/2" and 12-1/4", the KCL content are assumed to be accumulated and will give higher corrosion rate activity (Table 2).

It agrees too on the air drilling operations. As for an example when drilling is introduced with air drilling it will give higher corrosion rate. Which happens at MTB A-04 section 12-1/4" (Table 3).

Table 2: KCl percentage data

	KCl (%)			
	MTB A-01	MTB A-02	MTB A-03	MTB A-04
Section 26"	0	3	5	5
Section 17-1/2"	3	3	5	6
Section 12-1/4"	3	3	6	water
Section 8-1/2"	water	water	water	-

Table 3: Air Drilling Corrosion Inhibitor injections

	Air Drilling Corrision Inhibitors (gph)			
	MTB A-01	MTB A-02	MTB A-03	MTB A-04
Section 26"	0	N/A	0	0
Section 17-1/2"	0	N/A	0	0
Section 12-1/4"	0	N/A	0	0
Section 8-1/2"	6-8	0*	4-7	7-9**

Notes

* 4 gph when releasing stuck pipe

** 4 gph when releasing stuck pipe

The other supporting factors that we may found as an additional factors are: sand content and flow rate. Flow rate react as a blasting effect related with the salt content and sand content. Bigger the flow rate then, tendency of the higher corrosion rate may occur. Table below describes the best within the flow rate usage. MTB A-04 remains the biggest flow rate, considering MTB A-01 thru MTB A-03 are standard hole and MTB A-04 is a big hole alone.

The summary of the causes are:

1. Main factor of the cause is because dissolve oxygen and carbondioxide.
2. Factors that support the higher rate or lower rate are: dissolve salt which is KCl content and Air drilling operations.
3. Factor that may support which we found is part of the mechanical blasting activity are: sand content and flow rate.
4. Factors that may not give some additional info are: Temperature and Pressure. As temperature will remain similar at every sections on Standard hole (Avg section 17-1/2" (27^{o}C), Avg section 12-1/4" (37^{o}C), Avg section 8-1/2" (47^{o}C). Likewise with pressure which will give the particularly similar bottom hole pressure.

Table 4: Flow rate average on every sections

	Avg. Flow Rate (gpm)			
	MTB A-01	MTB A-02	MTB A-03	MTB A-04
Section 26"	530	580	615	1000
Section 17-1/2"	900	890	990	1000
Section 12-1/4"	920	890	960	940
Section 8-1/2"	850	630	780	860

React

After knowing the causes which we have decided that it is because of the dissolve oxygen and dissolve carbondioxide. Then as on table recommendation. We react with improvements on particularly MTB A-03 and MTB A-04. Things that we improve are:

1. Add corrosion inhibitor on the mud and add corrosion inhibitor on the Hi-Vis whenever TLC or PLC occurs.
2. Add lime / gypsum to participate the carbonate.
3. Use degasser.
4. Maintain pH as possible at 10.
5. Add corrosion inhibitors on the text steam air drilling pump system whenever air drilling is used.

Results has been a little of improvement on MTB A-03. With relatively poor improvement on MTB A-04. One may now discuss about what corrosion inhibitor rate may approve the best results on Big Hole and Standard Hole. A tweak of some additional of corrosion inhibitor may result a better corrosion rate. Which at the short term, will increase the drilling budget. But at long term may serve as best solutions as severe corrosion rate will give possible failures on many drilling equipments.

CONCLUSIONS

1. Geothermal is somehow challenging in the corrosion perspective. It contains many possibilities to hamper down the drilling operation and thus increasing the drilling budget.
2. Geothermal drilling environment on with its own characteristics will include 3 main factors of corrosion: cathode (gases), anode (steel metals) and electrolyte (drilling fluids).
3. In dealing with the corrosion hazards, one may want to analyze the water source first, thus knowing factors which will induce the corrosion rate, as example: pH and gases contents.
4. On drilling process maintaining an acceptable corrosion rate is the primary object. With the simple corrosion drill pipe ring one may do the mitigation process: by monitoring, analyze and react.

REFERENCES

(1990 - 2007). Various best drilling procedures from Mud Service Company and Air Service Company.

Abbott, S., Augsburger, J., Bilka, D., Branam, N., Carlson, T., Coles, B., Cornay, F., Dalton,

F., Donaldson, A., Ellice, M., Estes, B., Ferreira, C., Guillory, J., Guillot, W., Haag, J., Hemphill, T., King, B., Laing, C., Leggett, L., Lindow, K., Marks, R., Mody, F., Morales, L., Moreno, H., Paiuk, B., Pérez, J., Pless, M., Seims, D., Shumate, T., Strickland, D., Valenziano, R., Vesely, D., and Vice, P. (1997), "Baroid Fluids Handbook". *Baroid Drilling Fluids, Inc.* Houston, Texas.

Karlsdottir, S. N., Ragnarsdottir, K. R., Thorbjornsson, I. O., and Einarsson, A. (2015). "Corrosion Testing in Superheated Geothermal Steam in Iceland". *Geothermics*, 53 (2015) 281 – 290.

Prasetia, A. E., Salazar, A. T. N., and Toralde, J. S. S. (2010), "Corrosion Control in Geothermal Aerated Fluids Drilling Projects in Asia Pacific". *Proceedings World Geothermal Congress 2010*.

Zarrouk, S. J. (2012), Scaling and Corrosion in Geothermal Wells. New Zealand.

Table 5: Remedies related with the type of corrosion cause (cathode related). (source: (1990 - 2007))

Fluids	Cause	Possible source	Remedies
Water-base drilling fluids	dissolve oxygen	gass disolves on surface equipments : shakers, hopper and other agitation process.	(1) Use degasser (2) Condition mud to shear or maximize breakout (3) add corrosion inhibitors (4) add oxygen scavenger
Water-base drilling fluids	dissolve Carbondioxide	gass disolves from formation fluids	(1) Use degasser (2) Condition mud to shear or maximize breakout (3) Raise pH to 10 (4) add corrosion inhibitors (5) add (lime/gypsum) to precipitate the carbonate (6) add scale inhibitors
Water-base drilling fluids	dissolve Hydro Sulfide	bacterial action (old un-maintained mud) and gas influx	(1) Use degasser with flare (2) Condition mud to shear or maximize breakout (3) Raise pH to > 11.5 (4) add corrosion inhibitors (5) add zinc oxide as a scavenger (6) add oxygen scavenger (7) add scale inhibitors (8) inhibit bacterial growth (9) use high lime mud (10) use non-sulfonate base additives on pipe dope lubricants
aerated introduction to drilling fluids	dissolve oxygen, Carbondioxide and Hydro Sulfide	From compressors and boosters of aeration generation	(1) Raise pH to > 11.5 (2) add corrosion inhibitors

UTILISING TOUGH2 SIMULATOR TO MANAGE THE LIMITATION OF CURRENT ANALYTICAL METHOD IN GEOTHERMAL PRESSURE TRANSIENT ANALYSIS

Daniel W. Adityatama, Nadira O. Wisesa, Dorman P. Purba, and Eylem Kaya

University of Auckland
Department of Engineering Science, The University of Auckland, Private Bag 90210, Auckland, New Zealand
Email: dadi977@aucklanduni.ac.nz, daniel.adityatama@outlook.com

ABSTRACT

Characterization of reservoir is essential in geothermal exploration or development. An accurate and reliable information regarding geothermal reservoir is very useful to make strategy on how to best exploit the geothermal resource in the most economical way. One of the most common reservoir characterization is pressure transient analysis (PTA). However, the analytical model for PTA is mainly developed for petroleum application, thus there are many basic assumptions that does not fit into real geothermal reservoir condition.

Several studies have concluded that numerical approach to PTA is required to overcome the limitation of current analytical model. This paper reviews the limitation of current analytical model in geothermal PTA and explore the possibility of using TOUGH2 simulator for geothermal PTA. Various well models and reservoir parameters were simulated in TOUGH2 and the result was analysed with commercial PTA software. The results were then compared with the actual values assigned to the numerical models to see the discrepancy between numerical and analytical model. Several factors and variables that might mislead the interpretation of PTA data were identified, and the result is expected to lay groundwork to future numerical PTA studies in geothermal.

Keywords: TOUGH2, PTA, reservoir simulation

INTRODUCTION

Reservoir characterization is an essential part in geothermal exploration or development. An accurate and reliable information regarding geothermal reservoir. A reliable characteristic may be obtained by combining and analysing large amount of data from multiple discipline such as 3G (geology, geochemistry, and geophysics) and drilling data into a complete conceptual model. In this manner, the well testing on a geothermal reservoir is a crucial step in obtaining the data required, as it might provide reservoir engineers with important properties such as reservoir permeability and storativity.

One of the important well test analysis commonly used is pressure transient analysis (PTA), obtained by observing the transient condition for a relatively short time after pressure perturbation has been created in the reservoir. However, the analytical model for PTA is mainly developed with petroleum or groundwater application, so there are many assumptions that violates the actual condition of geothermal reservoir (McLean & Zarrouk, 2015).

The purpose of this study is to review the limitation and potential pitfall for current existing analytical PTA methods, and also investigates the effect of various reservoir parameters on the PTA results and the characteristic appearance of the derivative plot shapes. A series of numerical models were constructed to incorporate complex production / injection record into a geothermal reservoir and the corresponding pressure response. The pressure response of the numerical model was analysed by SAPHIR, a commercial PTA software by KAPPA to generate the pressure derivative plot, estimate the reservoir properties, and evaluate the accuracy of the interpretations. The parameters used were subjected to manual sensitivity analysis to identify their effect on characteristic appearance of the derivative plot shapes for realistic interpretations of the reservoir properties.

BACKGROUND

Previous Studies On Numerical PTA in Geothermal

The analytical model for PTA is mainly developed for petroleum application where the condition is mainly at lower temperature and simpler reservoir structure. The geothermal reservoirs are non-isothermal, thus have different (non-uniform) fluid properties across the reservoir, and the fluid properties are dependent on thermodynamic conditions; e.g. composition, pressure, temperature, and saturation (O'Sullivan, Croucher, Anderson, Kikuchi, & Nakagome, 2005). The high temperature of geothermal reservoir also creates a condition where boiling or condensation might occur, complicating the calculation due to the presence of two-phase fluid. Therefore, there is a need to replace the linear diffusivity equation with non-linear form which require numerical models to solve (Earlougher, 1977; McLean & Zarrouk, 2015; O'Sullivan et al., 2005), and previous studies has been done to address the limitation of PTA in geothermal application.

O'Sullivan (1987) used MULKOM simulator to study the effect of fractured media compared to uniform porous media in pressure drawdown/buildup and injection test. In 2005,

O'Sullivan et al., developed Automated Well Test Analysis System (AWTAS) that use numerical method to calculate the model response. McLean & Zarrouk (2015) studied the application of pressure derivative method in geothermal and its common issues that might be encountered, such as downflow, slow valve closing, and two-stage pump shutdown. McLean & Zarrouk (2017) further developed a practical framework for numerical simulation of PTA dataset using TOUGH2 simulator and PyTOUGH scripting language. This framework was used to investigate the effect of cold water injection and a case study for field data from before and after deflagration.

Numerical and Analytical Model Software Used

TOUGH2 simulator was used in this study to calculate non-isothermal flows of multicomponent, multiphase fluids in porous media (Pruess, Oldenburg, & Moridis, 2012). The version used is AUTOUGH2, which has specialized features for geothermal application that was developed by The University of Auckland (Yeh, Croucher, & O'Sullivan, 2012).

The Python-based PyTOUGH scripting library was used for the setup and simulation automation of TOUGH2 (Croucher, 2011). The TOUGH2 graphical tool and interface, TIM, was utilised for assisting in visualising TOUGH2 simulation (Yeh, Croucher, & O'Sullivan, 2013).

The analytical PTA software used was SAPHIR, a commercial well test analysis software by KAPPA Engineering. SAPHIR can generate a pressure derivative plot from pressure history data and match it with KAPPA's database to estimate the reservoir's characteristic and properties (Houze, Viturat, & Fjaere, 2008).

TOUGH2 Simulator Software Setup Step

The step-by-step methods used to set the numerical model in this study are as follow:

- Set up the model grid structure and reservoir parameters by using PyTOUGH or TIM.
- Set up the testing parameter used (primary variables, production/injection time and rate, time stepping, etc.). Modelling pressure transient test requires closely-spaced time steps after pressure shut-in to correctly capture the pressure response (McLean & Zarrouk, 2017). However, very close time steps can result in a very large dataset and greatly increase the running time. To solve this, the simulation was divided into two stages: first stage was for everything before the pressure shut-in, and the second stage was from the start of the transient period until the end of the test. The closely-spaced time steps are assigned on the early period of the second stage.
- Running the simulation and combining the pressure history data for both stages of the test. The data obtained were then processed to generate a pressure derivative plot.

NUMERICAL MODEL SETUP

Model Geometry

The 1-D radial geometry was used due to the reason that normal square grid typically used for reservoir modelling in TOUGH2 cannot reproduce the pressure response behaviour seem in a geothermal well test (McLean & Zarrouk, 2015).

The geometry grid setup used is a single-layer radial model with three components (Figure 1):

- Well block
- Skin zone blocks
- Reservoir zone blocks

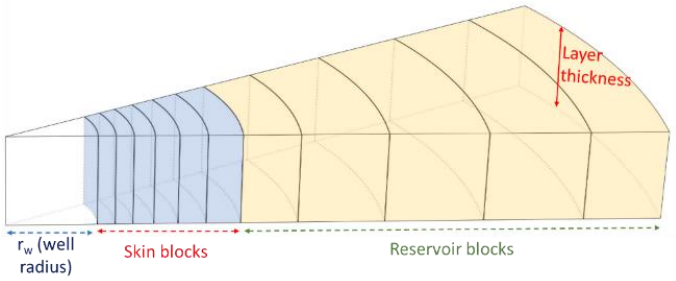


Figure 1: 1-D radial geometry schematic.

The requirement to have a very fine grid structure in the region that is very close to the well block is achieved by using logarithmic radial block spacing. The total number of blocks is 100 blocks, with 1 well block, 14 skin blocks, and 85 reservoir blocks. To simulate the infinite-acting flow, the reservoir size was made very large, with the reservoir radius of 132 km. McLean & Zarrouk found out that the pressure response is insensitive to the number of skin zone and reservoir zone block number.

Model Parameter Setup

Pressure transient analysis in geothermal reservoirs involves a complex process of heat transfer and flow of multicomponent fluid mixtures in the reservoir, including boiling, condensation and dissolution. Conventional analytical well test analysis methods do not account for some of these phenomena. TOUGH2 geothermal reservoir simulator can model these physical processes including the phase transitions from a single-phase (vapour or liquid) into a two-phase mixture. Therefore, to obtain realistic predictions for practical PTA problems that involve multicomponent, multidimensional flow effects over a broad range of space and time scales, numerical models were set up and the various aspects of model design and reservoir parameters

were investigated. The model parameters used are summarized in Table 1.

Table 1:. Model parameters

Well block properties	
Radius (r_w)	0.1 m
Porosity value	0.9
Permeability value	10000 mD
Compressibility	6E-8 Pa^{-1}
Skin blocks properties	
Block number	14 blocks
Skin zone span (r_{skin})	3.875 m
Porosity value	0.1
Permeability value	2 mD
Skin factor value	14.63
Reservoir zone properties	
Radius	132 km
Block number	85 blocks
Porosity value	0.1
Permeability value	10 mD
Layer thickness	600 m

The linear model of relative permeability value was used for this study, with the S_l = 0.3 and S_v = 0.05 (Figure 2)

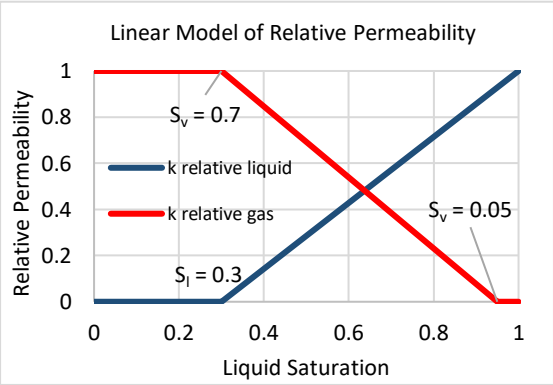


Figure 2: Linear relative permeability curve.

This study modelled single-phase reservoir model, using *water, water with tracer Equation of State* (EOS1) is used. The primary variables for EOS 1 used are as follow:

- $T_{reservoir}$ = 250°C
- $P_{reservoir}$ = 80 bar. This high reservoir pressure was used to accommodate the drawdown test without causing the reservoir to flash. Previous attempts to run the simulation with lower pressure showed that even for drawdown rate as low as 8 kg/s will cause the water to flash.

INJECTION/FALLOFF TEST

Test Setup

The models were subjected to injection/falloff test with single injection rate (25 kg/s) for 24 hours, and the falloff period of 96 hours. A reference model is used to simplify the process of comparing the result of sensitivity analysis. The pressure history results of the numerical model were inputted to SAPHIR to generate a pressure derivative plot and obtain the reservoir properties estimated by analytical model. Manual sensitivity analysis was conducted for each of the parameters given in Table 2.

Table 2: Reference model parameters and the value range tested.

Parameter	Reference Parameter	Value Range
Layer thickness (m)	600	250, 500, 600
Well radius (m)	0.1	0.1, 0.2, 0.3
Well block presence	With well block	With well block, no well block
Well block compressibility (1/Pa)	6E-8	1E-4, 1E-20 (extreme) 3E-8, 6E-8, 9E-8
Skin zone permeability(mD)	2	1, 2, 22, 100, No skin block
Injectate temperature	134°C	50°C, 134°C, 250°C

The SAPHIR's analytical model can only specify one fluid properties, and several previous studies concluded that it is best to use properties of water at reservoir temperature, even though in real condition the water temperature varies with time (Grant, 2011; McLean & Zarrouk, 2017).

Layer Thickness

The layer thickness represents the feed zone of the geothermal reservoir. In the real geothermal well, not all of the open hole parts of the well are the feed zone, but as the most of the time the information of the feed zone location on the well is not available, the layer thickness can only be estimated by a reservoir engineer. The pressure derivative plot is shown on Figure 3. Increasing the layer thickness will shift the pressure derivative plot down, but still retains its shape.

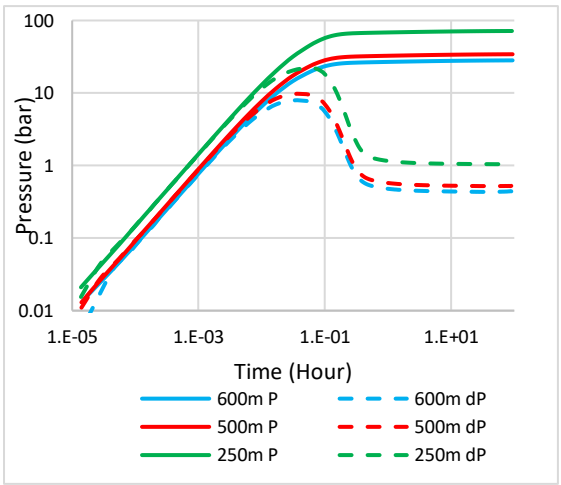


Figure 3: Pressure derivative plot: changing layer thickness.

The analytical model give close estimation on the reservoir properties, particularly the permeability value, but the skin factor value is overestimated by 62% to 79% (Table 3Table).

Table 3: SAPHIR's analytical model result: changing layer thickness.

Thickness (m)	k (mD)	Δk (mD)	Skin	Δskin
600	10	0	23.6	8.97
500	10.5	0.5	25.5	10.87
250	10.2	0.2	26.2	11.57

Well Radius

Changing the well radius with a smaller value will shift the pressure derivative plot to the right, while still retaining the overall shape (Figure 4).

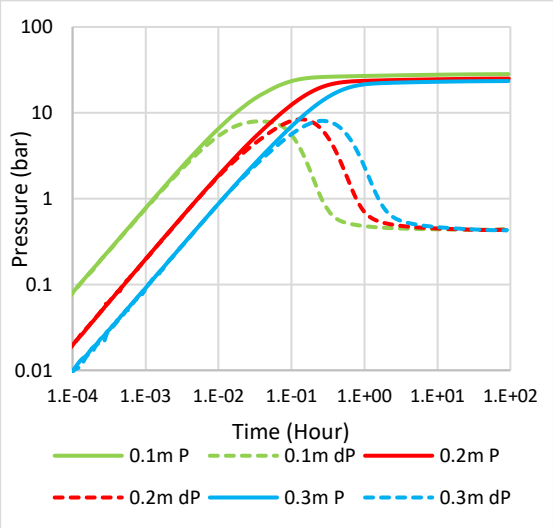


Figure 4: Pressure derivative plot: changing well radius.

The reservoir properties calculated by analytical model do not differ much between the three models, however the skin factor value is overestimated as in the layer thickness experiment case (Table 4).

Table 4: SAPHIR's analytical model result: changing well radius.

Radius (m)	k (mD)	Δk (mD)	Skin	Δskin
0.1	10	0	23.6	8.97
0.2	10	0	21	6.64
0.3	10.5	0.5	20.7	6.49

Well Block Compressibility Value

To closely simulate the open hole section of the well on TOUGH2, it is important to assign large enough compressibility value on the well block. The first experiment for sensitivity analysis considers the effect of changing the well compressibility value. An experiment was set to see the sensitivity of the model to well block compressibility value used. Assigning smaller well block compressibility value shifts the pressure derivative plot to the left, similar to the effect of using different well block radius (Figure 5). However, using very small well block compressibility value will greatly shift the plot to the left, while almost removing the unit slope line of wellbore storage. Using extremely large value (C = 1E-04 Pa^{-1}) caused incorrect pressure response, potentially due to the numerical instability in TOUGH2.

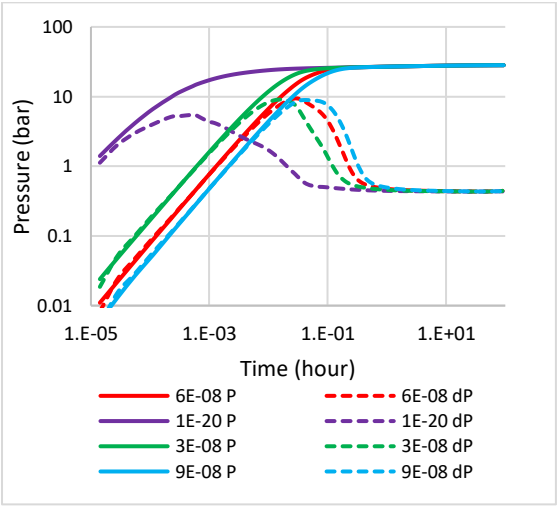


Figure 5: Pressure derivative plot: changing well block compressibility.

The effect of different well block compressibility is minor to the analytical model result, as the reservoir permeability and skin factor values between the models are quite similar.

Table 5: SAPHIR's analytical model result: changing well block compressibility.

Compressibility (1/Pa)	k (mD)	Δk (mD)	Skin	Δskin
3E-08	9.96	0.04	23.4	8.77
6E-08	10	0	23.6	8.97
9E-08	10.4	0.4	24.8	10.17

Skin Factor Value

The effect of changing skin zone conditions are simulated by changing the permeability value of the skin blocks. The skin factor value tested are varied as summarized in table 6.

Table 6: Model skin block parameters.

k_{skin} (mD)	$k_{reservoir}$ (mD)	Skin factor
No skin block	10	0
1	10	32.91
2 (reference)	10	0
22	10	-2.00
100	10	-3.29

Changing the skin block permeability, which in turn changing the skin factor value, will affect the hump after the wellbore storage period on the pressure derivative plot (Figure 6). The higher the skin factor value (positive skin value, the bigger the hump). The

overall unit slope of wellbore storage period and flat line of infinite-acting flow is relatively unaffected.

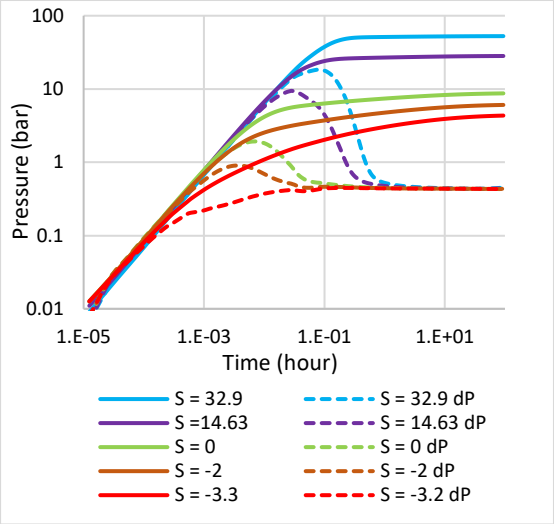


Figure 6: Pressure derivative plot: changing skin block permeability.

Analytical model gives close result for reservoir permeability, but the skin factor value is overestimated for all of the positive skin models (Table 7). The model without skin blocks (skin factor = 0) and the models with negative skin value (enhanced permeability at the skin zone) however, only shows slightly over exaggerated skin factor value. This overestimation of skin factor value is possibly caused by the effect of injecting the reservoir with the colder water. This will be explored in the later section of this paper.

Effect of Injectate Temperature

One of the main uncertainties when analyzing injection/falloff test is the impact of the injectate temperature. Different water temperature would gave different chemistry of the injection brine. The higher the temperature difference between injectate and reservoir fluid in the operational phase could increase the permeability due to physical effect of stimulation (Table 8). However, the changes in the rock properties due to chemical reactions or mechanical deformation was not considered in these numerical experiments.

Table 7: SAPHIR's analytical model result: changing skin block permeability.

Actual skin factor value	Analytical model result			
	k result (mD)	Δk (mD)	Skin factor	Δskin
32.9	9.95	0.05	50.7	17.8
14.63	10	0	23.6	8.97
0	10.5	0.5	2.14	2.14
-2.00	10.4	0.4	-1.05	0.95
-3.29	10.4	0.4	-3.09	0.21

Table 8: SAPHIR's analytical model result: effect of different injectate temperature.

Injectate temperature	k result (mD)	Δk (mD)	Skin factor	Δskin
50°C	10.4	0.4	58.8	44.17
134°C	9.96	0.06	25.8	11.17
250°C	9.95	0.05	17.5	2.87

The analytical model does not account for the difference between the reservoir temperature and injectate fluid temperature. This is problematic in injection/falloff test as much cooler water is injected into hot reservoir. Several studies in the past concluded that it is best to use water properties at reservoir temperature, even though in real condition the water temperature varies with time (McLean, Zarrouk, & Wilson, 2016). The numerical model is able to include the properties of both the hot reservoir and cold injection fluid. The pressure derivative plot result is shown on Figure 7.

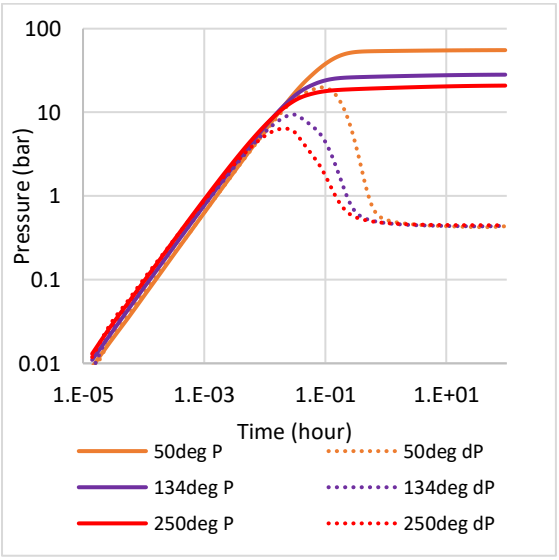


Figure 7: Pressure derivative plot: effect of different injectate temperature.

Injecting hot reservoir with cold water resulted in a bigger hump after the wellbore storage period that could be misinterpreted as higher skin factor value. As expected, the analytical model result confirms this, as the higher the temperature difference between reservoir and injectate, the higher the skin factor value estimation, exceeding the actual values assigned to the models. This explains the reasons why all of the previous models in injection/falloff scenarios always have overestimated skin factor value.

Water Compressibility, Viscosity, and Density Value Used in SAPHIR Input

The analytical model can only specify one fluid temperature for the analysis and has proven may mislead the interpretation, especially in the injection/falloff case. A series of experiments was carried out by running SAPHIR's analytical model

with different input of fluid compressibility and viscosity values based on the reservoir temperature (250°C) and the injectate temperature (134°C). The compressibility value used are derived from the correlation from Suárez-Arriaga & Samaniego (2014) that are applicable for fluid pressure from 20 bar to 300 bar and temperature of 120°C to 370°C. The correlation used are as follow:

$$C_{liq}(P,T) = \frac{a_0 + a_1 T + a_2 T^2 + a_3 P + a_4 PT + a_5 P^2}{b_0 + b_1 T + b_2 P} + C_0$$

Where the constant coefficients are:

$a_0 = 93.1663311586$
$a_1 = -0.1968009864$
$a_2 = -0.1189515785 \times 10^{-3}$
$a_3 = -0.4047179477$
$a_4 = -0.00214683589$
$a_5 = -0.1049847203 \times 10^{-3}$
$b_0 = -1.2926119842 \times 10^{6}$
$b_1 = -4139.4544963629$
$b_2 = 1157.3957523284$
$c_0 = 0$, if the **T ≤ 260 °C**
$c_0 = 6.1870252 \times 10^{-8}$, if the **T > 260 °C**

The analytical model generates the similar result for different total compressibility value used, both for the reservoir permeability and skin factor value (Table 9). However, significant difference was observed on the calculation using different viscosity value. Using fluid viscosity value based on the injectate temperature overestimates the permeability value by 95 % (Table 10).

Table 9: SAPHIR's analytical model result for different fluid compressibility input.

C (MPa^{-1})	k (mD)	Δk (mD)	Skin	Δskin
1.320E-3 [1]	10	0	23.6	8.97
6.476E-4 [2]	10	0	23.2	8.57

Table 10: SAPHIR's analytical model result for different viscosity value inputted.

Viscosity (μPa.s)	k (mD)	Δk (mD)	Skin	Δskin
106.1 [3]	10	0	23.6	8.97
206 [4]	19.5	9.5	23.6	8.97

Another complication is that TOUGH2 input for injection/production rate is on mass flow rate (kg/s) for this study), while SAPHIR input for injection/production rate is in volume flow rate (m^3/s in this study). Therefore, the mass flow rate from TOUGH2 must be converted into volume flow rate by dividing it with fluid density value that will gives a close match of reservoir properties. An experiment was conducted by comparing the analytical model result using density of water at injectate temperature and analytical model result using density of water at reservoir temperature. The analytical model give similar skin factor value for both of the density value used, but slight difference was found on the reservoir permeability result (Table 11). Using the density value of water at reservoir temperature (250°C) will give a closer match with actual value assigned in numerical model when compared to using density of water at injectate temperature.

Table 11: SAPHIR's analytical model result for different water density value used.

Density (kg/s)	k (mD)	Δk (mD)	Skin	Δskin
798.89 [5]	9.96	0.04	23.4	8.77
931.40 [6]	8.54	1.46	23.4	8.77

DRAWDOWN/BUILDUP TEST

The models were subjected to drawdown/buildup tests with a single drawdown rate for 48 hours, and a buildup period of 192 hours. The vapour saturation value during drawdown stage was monitored to ensure that the set of parameters used will not cause boiling. The manual sensitivity analysis was conducted for the parameters shown in Table 12.

Table 12: Reference model parameters.

Parameter	Reference Parameter	Value Range
Layer thickness (m)	600	250, 500, 600
Well radius (m)	0.1	0.1, 0.2, 0.3
Skin zone permeability(mD)	2	1, 2, 22, 100, No skin block

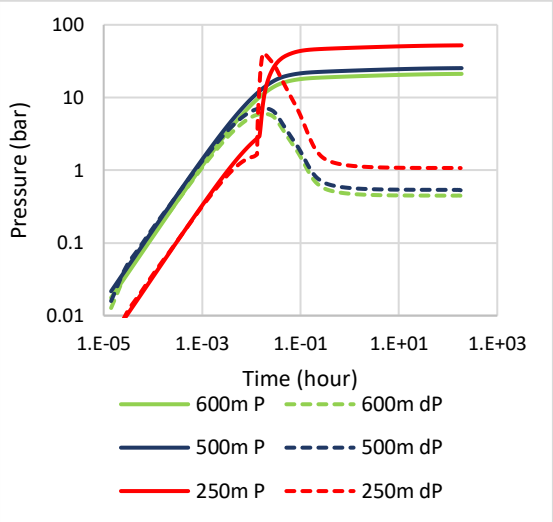


Figure 8: Pressure derivative plot: changing layer thickness.

[1] Compressibility value for water at 250°C
[2] Compressibility value for water at 134°C
[3] Viscosity value for water at 250°C
[4] Viscosity value for water at 134°C
[5] Density for water at 250°C
[6] Density for water at 134°C

Layer Thickness

The experiment was carried out in the similar manner with the injection/falloff experiment on layer thickness. Since the models with small layer thickness has smaller volume, they gave more rapid pressure drop during drawdown, thus making them more susceptible to flashing. TOUGH2 simulation results demonstrate this fact, as can be seen in Figure 8, the model with smallest thickness (250 m) flashed during drawdown, resulting in a different and unrecognized pressure response profile when compared to reference and 500 m model (Figure 8).

The SAPHIR's analytical model result shows very close match to the parameter input to TOUGH2 when compared to the injection/falloff test result that always overestimate the skin factor value. This is due to there is no significant temperature change during drawdown/buildup test, unlike the injection case where much cooler water is injected to the hot reservoir.

Table 13: SAPHIR's analytical model result.

Thickness (m)	k (mD)	Δk (mD)	Skin	Δskin
600	10.1	0.1	15.5	0.87
500	10.1	0.1	15.4	0.77
250	Flashed	Flashed	Flashed	Flashed

Well Radius

The effect of varying the well radius in drawdown / buildup test is similar with the injection/falloff case, as changing the well radius will shift the pressure derivative plot to the left or right (Figure 9). However, the skin factor value is not overestimated due to the absence of different fluid temperature (Table 14).

Table 14: SAPHIR's analytical model result for different well radius.

Radius (m)	k (mD)	Δk (mD)	Skin	Δskin
0.1	10	0	23.6	8.97
0.2	10	0	21	6.64
0.3	10.5	0.5	20.7	6.49

Skin Factor Value

The effect of changing skin zone conditions are simulated by changing the permeability value of the skin blocks, similar to the injection/falloff case. The skin blocks permeability used was also similar as shown in Table 6.

The higher the skin block permeability value used, the bigger the hump after wellbore storage period (Figure 10). There was no fluid flashing observed during drawdown for all of the 5 skin block permeability value used, thus the pressure derivative plot can still be recognized by SAPHIR.

As the drawdown/buildup models does not involve flashing and significant temperature difference during the pressure transient test, the skin factor value estimated by SAPHIR is close to the original value assigned in the numerical model setup (Table 15).

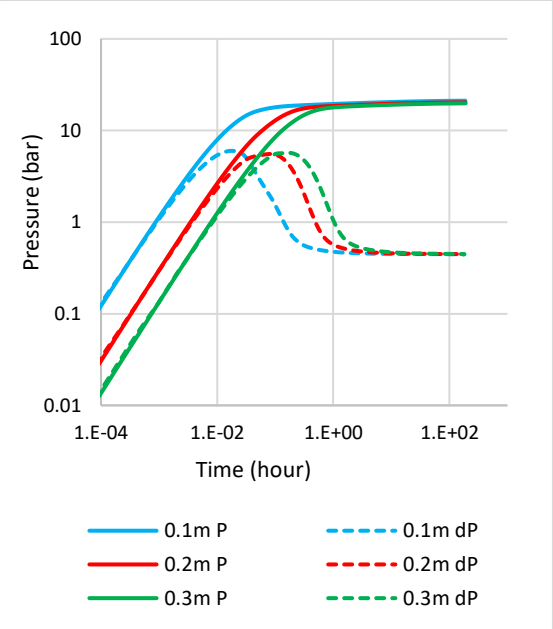


Figure 9: Pressure derivative plot: changing well radius.

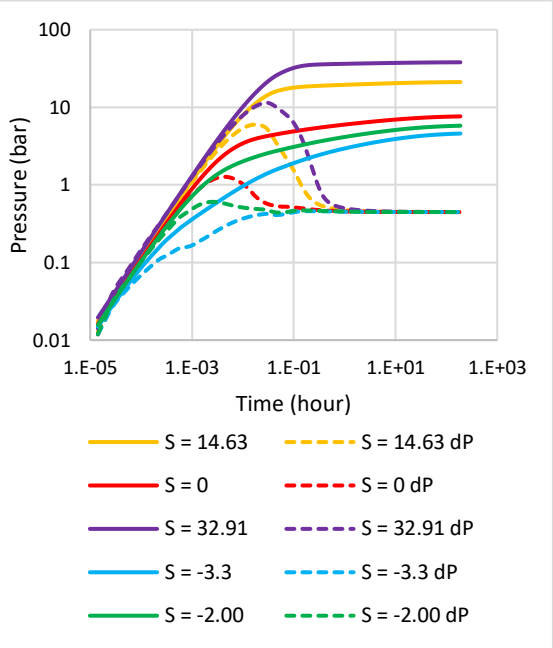


Figure 10: Pressure derivative plot: changing skin zone condition.

Table 15: SAPHIR's analytical model result: changing skin zone conditions.

Actual skin factor value	Analytical model result			
	k (mD)	Δk (mD)	Skin factor	Δskin
32.9	10.1	0.1	34.6	1.7
14.63	10.1	0.1	15.4	0.77
0	9.95	0.05	0	0
-2.00	9.95	0.05	-1.99	0.01
-3.29	9.95	0.05	0	0

FINDINGS AND DISCUSSION

The purpose of this study is to review the limitation and potential pitfall for current existing analytical PTA methods, and also investigates the effect of various reservoir parameters on the PTA results and the characteristic appearance of the derivative plot shapes. The following findings were found:

Layer thickness
The pressure derivative is sensitive to the change of layer thickness as the change in layer thickness will shift the pressure derivative curve up and down. There is no significant difference in reservoir properties estimated by SAPHIR's analytical result between models tested, however, model with smaller layer thickness is susceptible to flashing during drawdown. The flashing would give different pressure response that will not be recognised by SAPHIR.

Well radius
All of the well radius value used give close match between TOUGH2 input parameter and SAPHIR analytical model result. However, in real geothermal well, the well radius of 0.2m and 0.3m is not realistic, as most of the open hole section of geothermal well is drilled with 8" diameter bit (~ 20 cm). The 0.2m and 0.3m radius are tested in this chapter to see the effect of changing well radius on the wellbore storage region of pressure derivative plot.

Skin factor
The results of the experiments for the effect of different skin block permeability value used, the higher skin factor will create bigger hump after the unit slope, while negative skin value (higher permeability value in skin zone blocks) show smaller hump, and even for the skin factor of -3.19 the pressure derivative plot shows no hump at all, resembles a fractured reservoir pressure derivative plot. The skin factor of 14.62 was used to represent the damaged zone inside the reservoir due to drilling using mud or due to mineral deposition, while the skin factor of -2 was used to represent the negative skin case, which is the most common in geothermal wells since they are usually produce from fractured volcanic rocks that show stimulated behaviour. (Arkan, Akin, Parklaktuna, 2002)

Well block compressibility value
The model is sensitive to the well block compressibility value assigned, as changing the well block compressibility value will shift the pressure derivative plot to the right of left in a similar manner with changing the well radius. The reservoir permeability value estimated by analytical method for the three models do not differ much, but the smaller well block compressibility value assigned will results in slightly higher skin factor value. However, extremely changing the well block compressibility value to a very small value will significantly alter the pressure derivative plot as is shifts the plot to the left and almost make the unit slope region (wellbore storage effect) not observable. Changing the well block compressibility to a very high value on the other hand will result in strange result possibly due to numerical instability in TOUGH2.

Injectate temperature
The result for injection/falloff test seems to always overestimate the skin factor value. This is due to the temperature difference between relatively cool injectate and the hotter reservoir. The higher the temperature difference, the bigger the hump on the pressure derivative. An analytical model that does not take this temperature difference will interpret the result as very high skin value. The injectate temperature of 134°C is used as the reference model parameter, as it is the typical temperature of the separated geothermal water.

Water compressibility and viscosity value (input to SAPHIR)
For injection/falloff test, both of the compressibility value of injectate water (134 °C) and reservoir (250 °C) give close results to each other, however, for the viscosity value the different result is obtained. If the analytical model uses viscosity value for cooler injectate temperature, the reservoir permeability value (k) will be overestimated. Therefore, for analysis with conventional analytical model it is best to use the properties of the reservoir instead of the injectate water.

Water density value
The SAPHIR's analytical model shows that using the density of water at reservoir temperature gives closer reservoir permeability value to actual value inputted to TOUGH2 when compared to using density of water at injectate temperature. Therefore, the density of water at reservoir temperature should be used to convert the mass flow rate input in TOUGH2 into a volume flow rate in SAPHIR.

SUMMARY

The analytical model for PTA in geothermal has recognised limitations due to the high temperature and complex reservoir conditions in geothermal. Various studies in the past have emphasized the requirement for robust numerical approach to overcome the limitation of analytical method in geothermal PTA. This study shows that flow in porous media simulator such as TOUGH2 can be utilised as a tool for numerical PTA in geothermal to address the limitation of the analytical model.

The experiments conducted in this study shows that the conventional analytical model can be used to analyse the geothermal PTA dataset to some extent, but as the geothermal reservoir becoming more complex (transition to two-phase, high temperature difference between injectate fluid and reservoir, high gas content), the interpretation should be done with caution, as the result might be misleading.

FURTHER WORKS

This study is an attempt to identify the potential pitfall of analytical model application in geothermal PTA dataset on the simplest model of pressure transient in geothermal, which is a single-phase fluid in an infinite homogeneous porous reservoir. Further study should be carried out to study the effect of following reservoir conditions during geothermal well test:

- Geothermal reservoir containing CO2.
- Geothermal reservoir with initially two-phase condition.
- Multiple feed zone conditions.
- Fractured reservoir conditions. Geothermal wells often shows the effect of fractures, therefore numerical model should be able to represent that condition, for example by using MINC (Multiple Interacting Continua) formulation.

ACKNOWLEDGEMENT

Authors would like to acknowledge New Zealand Ministry of Foreign Affairs and Trade (MFAT) for the financial support to study in Geothermal Institute, The University of Auckland, under New Zealand ASEAN Scholarship scheme.

REFERENCES

Croucher, A. (2011), PyTOUGH: A python scripting library for automating TOUGH2 simulations. Paper presented at the *Proceedings of the New Zealand Geothermal Workshop, , 21* 1-6.

Earlougher, R. C. (1977), *Advances in well test analysis*. Henry L. Doherty Memorial Fund of AIME New York, NY, USA.

Grant, M. A. (2011), In Bixley P. F. (Ed.), *Geothermal reservoir engineering* (2nd ed. / Malcolm A. Grant, Paul F. Bixley.. ed.). Burlington, MA: Burlington, MA : Academic Press 2011.

Houze, O., Viturat, D., & Fjaere, O. S. (2008), Dynamic data analysis. *Paris: Kappa Engineering, 694*

Mclean, K., & Zarrouk, S. J. (2015), Geothermal well test analysis using the pressure derivative: Some common issues and solutions. *Geothermics, 55*, 108-125. 10.1016/j.geothermics.2015.01.010

McLean, K., & Zarrouk, S. J. (2017), Pressure transient analysis of geothermal wells: A framework for numerical modelling. *Renewable Energy, 101*, 737-746.

McLean, K., Zarrouk, S. J., & Wilson, D. (2016), Application of numerical methods for geothermal pressure transient analysis: A deflagration case study from New Zealand. Paper presented at the *Proceedings 41st Workshop on Geothermal Reservoir Engineering, Stanford University, Stanford, California,*

O'Sullivan, M. J. (1987), Aspects of geothermal well test analysis in fractured reservoirs. *Transport in Porous Media, 2*(5)10.1007/BF00211105

O'Sullivan, M. J., Croucher, A. E., Anderson, E. B., Kikuchi, T., & Nakagome, O. (2005), An automated well-test analysis system (AWTAS). *Geothermics, 34*(1), 3-25.

Pruess, K., Oldenburg, C., & Moridis, G. (2012), *TOUGH2 user's guide, version 2*. Berkeley, California: Earth Science Division, Lawrence Berkeley National Laboratory, University of California.

Suárez-Arriaga, M., & Samaniego, F. (2014), A set of new correlations for the compressibility of two-phase water and for the steam Z factor in a wide thermodynamic range.

Yeh, A., Croucher, A. E., & O'Sullivan, M. J. (2013), TIM–Yet another graphical tool for TOUGH2. Paper presented at the *Proc. 35th New Zealand Geothermal Workshop,*

Yeh, A., Croucher, A. E., & O'Sullivan, M. J. (2012), Recent developments in the AUTOUGH2 simulator. Paper presented at the *Proc. TOUGH Symposium 2012*, 17-19.

GEOTHERMAL WELL TESTING USING A NEW ATMOSPHERIC SEPARATOR AND METERING SYSTEM IN SARULLA, NORTH SUMATERA, INDONESIA

Elisabeth Easley, Nurlianto Sadji, and Winahyu Setyo Utami

PT Thermochem Indonesia
Email: elisabeth@thermochem.com, nurlianto@thermochem.com, winahyu@thermochem.com

ABSTRACT

Geothermal production well flow testing has been traditionally conducted using atmospheric flash cyclone separators equipped with a James-tube at the two-phase inlet and weir box at the brine drain outlet. Although this equipment is robust and versatile, it often suffers from substantial errors in mass flow rate and enthalpy measurement, especially at high enthalpy. These errors can be traced to low accuracy in brine rate measurement by the weir technique, and brine carry-over from the top of the separator due to poor separation efficiency. Thermochem has developed a Low-Emissions Compact Muffler (LECM), which is a new type of atmospheric separator that includes a James-tube at the separator inlet and high-accuracy electromagnetic brine flow meters (MagMeters) on the separator outlet. The total discharge enthalpy derived from an LECM system produces results that are in close agreement with surface Tracer Flow Test (TFT®) measurements, quartz geothermometer temperatures, and flowing downhole pressure-temperature (PT) surveys. The LECM system was initially used for geothermal well testing in Chile, Bolivia and Japan, and was recently introduced to Indonesia during ongoing well testing over the last 3 years on 15 new production wells at the Sarulla geothermal project in North Sumatra.

Keywords: Well testing, LECM, TFT, Sarulla Goethermal Project

INTRODUCTION

The Sarulla geothermal area was commercially developed by Sarulla Operations Limited (SOL) and is located within the Great Sumatra Fault Zone in Northern Sumatra. Exploration of the Sarulla field began in 1993 under the direction of UNOCAL North Sumatra Geothermal Ltd. (UNSG) under a Joint Operation Contract (JOC) with Pertamina (Wolf and Gabbay, 2015). Explorations program included 3G surveys was conducted from mid-1993 through early 1998 which were used to target 13 deep wells (Gunderson et al, 2000). The resource areas currently under commercial operation include Namora-I-Langit (NIL) and Silangkitan (SIL), as shown in Figure 1. During development drilling at NIL and SIL, an LECM was used for 28 day long-term production flow tests for 15 newly drilled production wells to supply the NIL Unit 1, NIL Unit 2, and SIL Unit 1 combined-cycle power generation facilities with a total generation capacity of 330 MWe (Ganefianto et al, 2015).

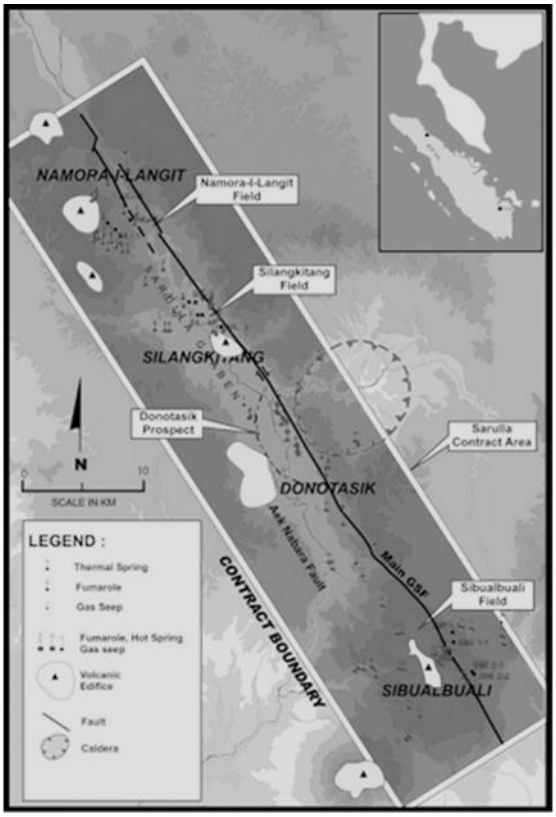


Figure 1: Geothermal prospects within the Sarulla contract area. Courtesy of UNOCAL (from Ganefianto et al, 2015).

PT Thermochem Indonesia was contracted by Halliburton Logging to perform short-term rig tests and long-term production flow tests during development drilling operations and successfully completed all production tests to date using the LECM technology, with confirmation of LECM enthalpy temperature and flow measurements using Tracer Flow Tests (TFT®), quartz geothermometry, and flowing PT survey data as a quality control measure. A complete discussion of the well test activities and methodology, LECM design, results from flow tests for the NIL (NIL 2n, NIL 1n, NIL 3) and SIL (SIL 1n-1, SIL 1n-2, SIL 1n-4), wells, and discussion of LECM data comparisons to quality control measurements are included in the following.

METHODOLOGY

The 28 day long-term production flow tests for SIL and SIL wells were initiated after well completion, completion of short-term tests including injectivity tests, pressure falloff tests, and gross permeability tests, and 15 days of heating. A summary of work activity conducted by PT Thermochem during the Sarulla development drilling campaign is included in Table 1.

A schematic of the general well test facility design is shown in Figure 2, which includes the two-phase line from the wellhead, injection and sampling ports for TFT®, James tube, diffuser, LECM, LECM brine outlet manifold, brine bypass, and MagMeters. For each wellpad tested, the LECM remained in the same location and the two-phase flow lines were changed between each production test.

The Thermochem LECM, as detailed in Figure 3, is fabricated with the same outside dimensions as ISO shipping containers, which allows the pre-fabricated mufflers to be transported by standard trucking and ocean freight shipping lines worldwide, and to remote areas such as Sarulla. The internal structures are heavily fortified with steel bracing, lined with steel plates and seal-welded to hold a water level in a leak-tight lower basin. CFD-designed baffle plates help separate brine from steam in the lower container. The upper steam stack is designed to enable droplet settling given the low steam velocity through the large cross-sectional area (< 4.5 m/s). Stainless steel mist elimination pads remove fine droplets and aerosols, resulting in very low brine carry-over up to high flow rates. The inlet to the muffler is fitted with a James Tube for continuous total mass flow estimation, a diffuser expansion tube to reduce flow velocity and noise as two-phase fluids enter the LECM, and the brine outlet pipe manifold is fitted with magnetic flowmeters (MagMeters), providing much higher accuracy than weirs typically used with conventional atmospheric separators. Low brine carry-over eliminates the errors typically associated with cyclone separators used on high mass flow or high-enthalpy wells, where the brine flow is biased low and enthalpy high due to loss of brine through the top of the separator stack.

The James Tube and brine flowmeter combination allows continuous measurement of steam flow, brine flow and total enthalpy. A two-phase orifice plate serves to provide throttling and back-pressure on the well, reducing wear on the two-phase flow control valve. The muffler design with the mist pads and low inlet velocity minimizes noise emissions during well testing. The two-phase flow line includes injection and sampling ports used to conduct TFT® and geochemistry sampling for quality control measurements during flow testing operations.

The LECM, two-phase piping and brine metering manifold was equipped with instrumentation including a wellhead pressure transmitter, line temperature transmitter, line pressure transmitter, orifice plate differential pressure (DP) transmitter, James Tube lip pressure transmitter, LECM water level transmitter, LECM body pressure transmitter, and 3 brine manifold magnetic flowmeters for a wide turn-down range (50 to > 600 ton/hr brine). All instrumentation was interfaced to a solar-powered data logging system reading data on 5 second intervals and recording 1-minute averages. The instrument ranges are listed in Table 2.

Due to the wellpad configuration and simultaneous drilling operations, the two-phase flow lines were designed within the pad space limitations and were not always suitable lengths for TFT® on the two-phase flow lines. In these instances, single-phase brine TFT® was conducted on the LECM brine outlet for comparison to MagMeter brine flow measurements. During production flow tests, TFT® measurements and geochemistry samples were collected at least once for each target WHP and flowing PTS surveys were conducted at the end of each test, however some survey profiles indicated that stable downhole temperatures had not been reached.

Table 1: Summary of well testing activities conducted by PT Thermochem for the Sarulla geothermal area (includes NIL and SIL).

Job Description	Quantity
Down Hole Sample	6
Flowing TPS Survey	17
Caustic Soda Injection	3
Injection Survey	2
Install Pressure Transmitter & Data Logger	8
Install Wellhead Test and Pressure Test	19
Line Instalation	9
Long Term Flow TEST	17
Maintanance Well Testing Facilities	44
LECM Mobilization	5
Short Term Injection TEST	54
Static PT Survey	35
Tracer Analysis	17
WPM Job	5

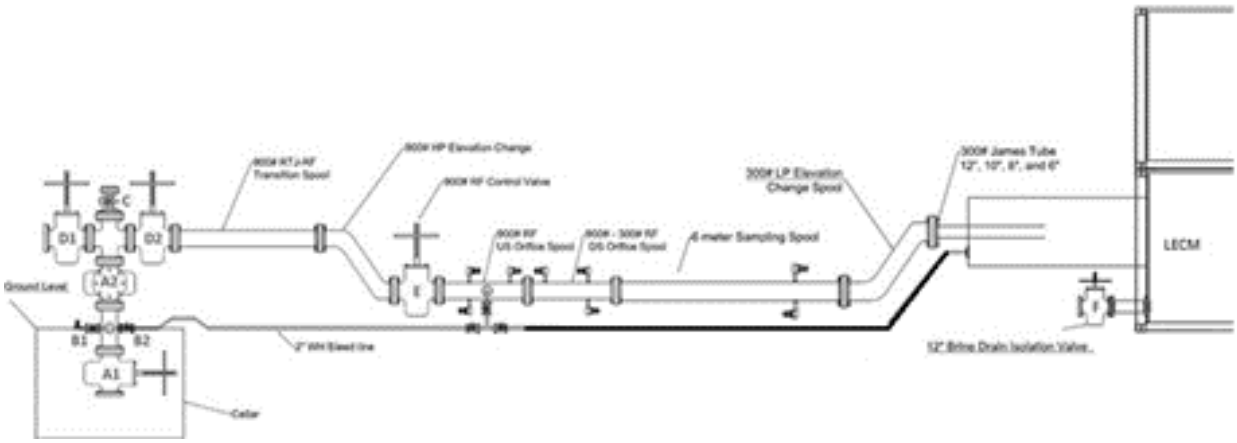


Figure 2: General design of the well test facility including two-phase flow line, James tube, diffuser, LECM, and LECM brine outlet. Layout of each well test facility varied depending on wellpad design and ongoing simultaneous operations.

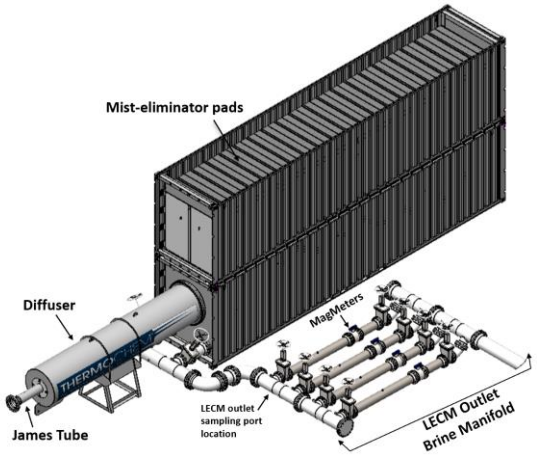


Figure 3: Schematic of the LECM components, including James tube, diffuser, mist eliminator pads, LECM outlet brine manifold, location of LECM brine outlet sampling port, and MagMeters.

Table 2: LECM flow line and instrument range specifications.

LECM and Flow Line Instrumentation Specification		
Process Location	**Measurement Range**	**Calibrated Range**
Wellhead Pressure	0-4000 psia	0-1000 psia
Two-Phase Orifice Pressure	0-2000 psia	0-400 psia
Two-Phase Line Pressure	0-800 psia	0-500 psia
Two-Phase Line Temperature	-50-400 C	0-250 C
James Lip Pressure	-300-300 psi	0-200 psig
LECM Water Level	-250-250 in H2O	0-36 in H2O
LECM Pressure	-250-250 in H2O	0-10 in H2O
Brine Manifold Leg	53-530 m3/hr	200-460 m3/hr

RESULTS

Two LECM units were used to test 15 wells at NIL and SIL with test flow rates up to 750 T/hr total mass flow and production capacity up to 31 MW_e. The maximum flow rates at the LECM, enthalpy, and calculated MW output for each well is shown in Table 3. Only data from NIL 2n, NIL 1n, NIL 3, and SIL 1n are discussed. The LECM was used for a long-term test on well WJP 1-3, however the WJP pad test data is not included in this discussion.



Figure 4: LECM operating at 650 ton/h mass flow, 75% of design capacity (brine bypass to mud pit).

The LECM design equipped with MagMeters on the brine manifold outlet has allowed for an improvement in traditional brine flowrate measurements by V-notch weirs used with cyclone separators or other atmospheric separators. The MagMeters are configured in a manifold tee on the LECM outlet that may be adjusted to accommodate for low or high flow rates depending on the well output condition. TFT® is a geothermal industry standard for measuring steam and brine flow rates and total fluid enthalpy (Hirtz et al, 2001 and Grant and Bixley, 2001), and thus, the TFT® method was selected as a quality control parameter to assess the accuracy of MagMeter and enthalpy measurements during long term flow tests. A comparison of TFT® measured brine flow rates on the single-phase LECM brine outlet to the brine flow rates measured by MagMeters is shown in Figure 5. A linear regression was calculated and the coefficient of determination (R-squared value) suggests that the MagMeter data variability is within 99.6% of the linear regression line.

Table 3: Maximum total mass flow rate, enthalpy temperature, and generation capacity of NIL and SIL wells tested with the LECM.

Well	WHP bara	Total Flow ton/hr	Enthalpy Temp °C	MWe
NIL 2N-1	21.5	653	256	17.6
NIL 2N-2	34.1	704	269	22.4
NIL 2N-3	14.3	424	267	13.3
NIL 2N-4	35.4	596	272	19.7
NIL 2N-6	18.2	501	267	15.6
NIL 2N-7	29.0	748	265	22.7
NIL 1N-5	32.0	552	270	21.0
NIL 1N-7	28.0	683	270	22.1
NIL 1N-8	32.7	583	276	18.7
NIL 3-2	27.0	560	270	17.9
NIL 3-3	29.0	315	260	10.1
SIL 1N-1	58.4	656	306	31.1
SIL 1N-2	60.5	646	306	30.4
SIL 1N-4	49.0	516	302	23.5

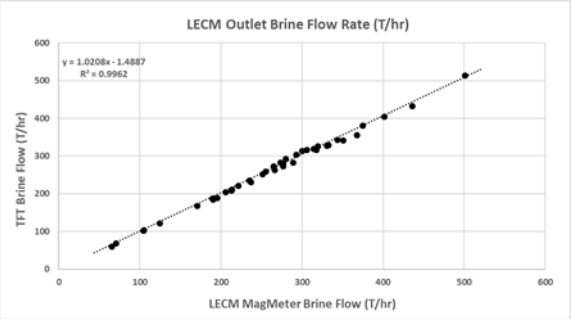


Figure 5: Comparison of brine flow rates (T/hr) at the LECM outlet by TFT® and MagMeters for flow tests conducted on NIL 2n, NIL 1n, NIL 3, and SIL 1n wells.

To understand if the linear regression model is an appropriate fit and if any bias exists in the data, the relative percent difference was observed for a range of test flow rates, as shown in Figure 6. The relative percent difference in the TFT® and MagMeter flow rates show that the data falls within ± 5%. Interestingly, between approximately 275 to 305 T/hr flow rates, the relative percent difference between TFT® and MagMeter data increases. This may be related to opening of an additional brine flow leg as the well flow rate increased. Additionally, the TFT® measured flow rate is biased high compared to the MagMeter brine flow, however for the range of data shown in Figures 5 and 6 the average relative percent difference between TFT® and MagMeter measurements is only 1.32% which is an acceptable agreement between the two measurement methods.

The LECM enthalpy temperature was also compared to TFT® enthalpy temperature measurements from tests conducted on the two-phase flow lines upstream of the LECM. Due to limitations in space which restricted the length allowed for two-phase flow lines, some wells did not produce acceptable TFT® data on the two-phase lines due to incomplete mixing of tracers over short mixing distances. In these cases, the LECM outlet TFT® data was still used to validate the MagMeter flow rates as discussed for Figures 4 and 5, since the longer flow line distance through the LECM allowed for further tracer mixing. Figure 7 illustrates a comparison of TFT® enthalpy temperatures from the two-phase line and LECM enthalpy temperatures from the time of the TFT® survey (in °C). A linear regression was calculated for data from both the NIL and SIL areas and the coefficient of determination of 94.5% suggests that the variance of the data provides a reasonable fit to the regression, however this could have been improved if longer two-phase flow lines were available to conduct the TFT®.

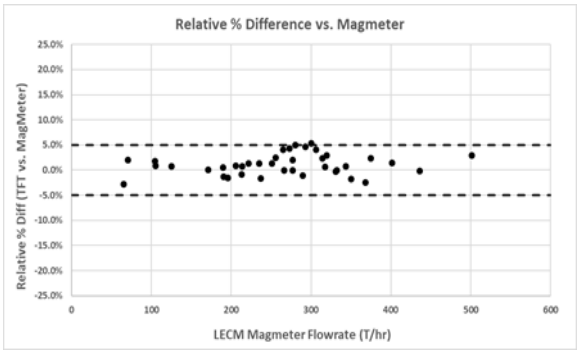


Figure 6: Relative percent difference of TFT® and MagMeter brine flow rate data for a range of LECM MagMeter flow rates for wells on NIL 2n, NIL 1n, NIL 3, and SIL 1n well pads.

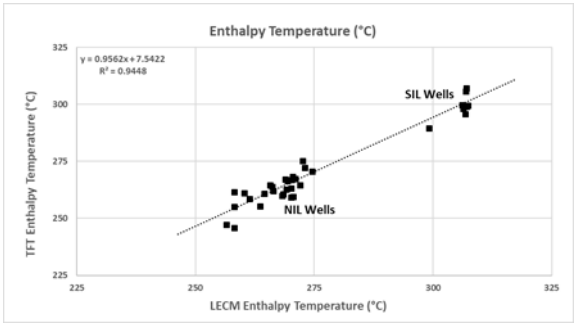


Figure 7: TFT® enthalpy temperatures compared to LECM enthalpy temperatures (°C) for flow tests conducted on NIL 2n, NIL 1n, NIL 3, and SIL 1n wells.

A comparison of the relative percent difference between TFT enthalpy temperature and LECM enthalpy temperature, as detailed in Figure 8, indicates that the TFT® measurement generally under-predicts the enthalpy temperature compared to the LECM enthalpy temperature. After a thorough review of TFT® quality control data and additional tracer mixing experiments, it was determined that the consistent low bias in TFT® enthalpy temperatures is likely due to errors in TFT® steam flow measurements from incomplete mixing of tracers in flow lines that were shorter than the

minimum distances recommended for complete tracer mixing (generally >15 meters) due to limited space on the wellpad. This highlights an advantage of using the LECM system during production flow tests, since the length and configuration of the two-phase flow line will not have an effect on enthalpy measurements on well pads with limited space availability for two-phase flow lines. Even with the known limitations in steam flow measurements due to flow line mixing distances, the relative percent difference for the TFT® enthalpy temperature compared to the LECM enthalpy temperature is still within ± 5%.

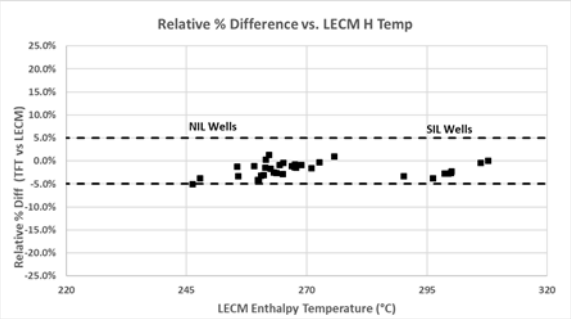


Figure 8: Relative percent difference for TFT® and LECM enthalpy temperatures for a range of LECM enthalpy temperature values from wells on the NIL 2n, NIL 1n, NIL 3, and SIL 1n wellpads.

As an additional measure of quality control, the LECM enthalpy temperatures were also compared to calculated quartz geothermometer temperatures from samples collected during the long-term flow test, as well as flowing PT surveys conducted at the end of the long-term test. The linear regression and coefficient of determination for quartz geothermometer temperatures compared to LECM enthalpy temperatures in Figure 9 suggests that 95.8% of the variance provides a reasonable fit to a linear regression. The relative percent difference for quartz temperatures compared to LECM enthalpy temperatures (Figure 10) indicates that the LECM temperatures are biased low compared to the quartz geothermometer, however the test comparisons were within ± 5%.

The maximum temperature recoding during flowing PT surveys conducted at the end of the long-term tests were compared to the average LECM enthalpy temperature for each well, as shown in Figure 11. A review of the PT profiles for each well suggests that some profiles were not stable. This may explain why the linear regression coefficient of determination is lower compared to the other methods used to assess quality control on the LECM. Despite some of the flowing temperature profiles not being stable, the relative percent difference comparison (Figure 12) indicates that the overall agreement between flowing PT and LECM enthalpy temperatures is within ± 5%.

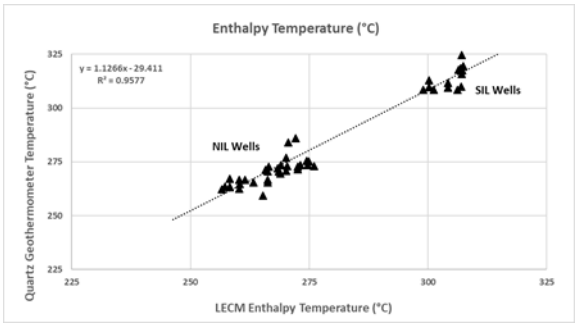


Figure 9: Quartz geothermometer temperatures compared to LECM enthalpy temperatures (°C) for flow tests conducted on the NIL 2n, NIL 1n, NIL 3, and SIL 1n wells.

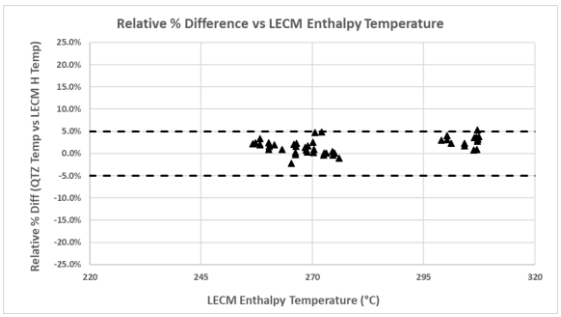


Figure 10: Relative percent difference for quartz geothermometer temperatures compared to LECM enthalpy temperature values from wells on the NIL 2n, NIL 1n, NIL 3, and SIL 1n wellpads.

Current operations are being conducted by SOL to re-survey all the wells for flowing PT data. Once these surveys have been completed, an additional assessment can be made to the LECM enthalpy temperature with stable PT data.

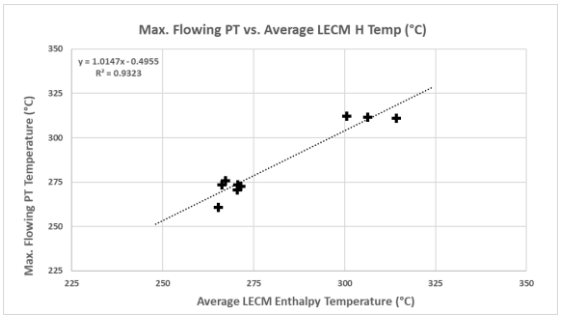


Figure 11: Maximum flowing PT temperatures compared to average LECM enthalpy temperatures (°C) for flow tests conducted on the NIL 2n, NIL 1n, NIL 3, and SIL 1n wells.

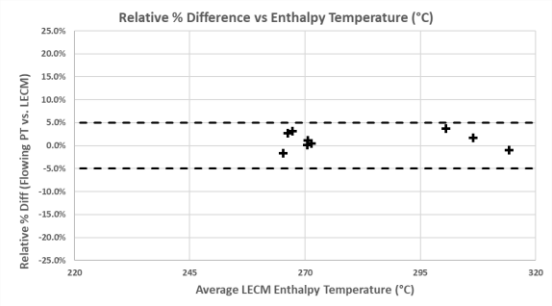


Figure 12: Relative percent difference for flowing downhole temperatures from PT surveys compared to LECM enthalpy temperature values from wells on the NIL 2n, NIL 1n, NIL 3, and SIL 1n wellpads.

DISCUSSION

The results presented herein for the LECM system from the NIL and SIL production tests is the first large-scale assessment of the quality and reproducibility of test data from the LECM units when used extensively over multiple years for long-term flow testing on high-capacity geothermal wells in harsh terrain and extreme environmental conditions. The two units that were used for the operations were able to sustain flow testing for flow rates up to 750 T/hour total mass flow and output capacity of 31 MW_e.

The comparison of brine flow rates from TFT® measurements on the LECM brine outlet to the LECM brine manifold MagMeter show excellent agreement and suggest that the MagMeters are an improvement to traditional weir measurements conventionally used for geothermal production testing. Additionally, the enthalpy temperature values calculated from the LECM measurements show excellent agreement with two-phase TFT® measurements, quartz geothermometer temperatures, and flowing PT survey data. The LECM unit provides an advantage for flow testing production wells on well pads with limited space, since TFT® flow rate and enthalpy measurements require a mixing distance of at least 15 meters for optimal results. Real-time data logging provides continuous data that can be verified at any time during production testing using quality control parameters including TFT®, geothermometry temperatures calculated from separated brine samples, or flowing PT surveys.

CONCLUSION

The LECM well testing unit developed by Thermochem has proven to be a robust system that provides high-accuracy flow rate and enthalpy measurements for geothermal production well flow tests. The LECM units have been verified as an improvement to traditional cyclone separators equipped with weir box measurements with high accuracy in brine flow measurements from MagMeters on the outlet of the LECM, as well as the internal LECM unit design with baffles and mist eliminator pads on the upper stack to improve separation efficiency and reduce brine carryover out of the top of the unit. These improvements to the traditional design of well testing equipment allow for more reliable real-time enthalpy and flow rate test results for a wide range of well outputs. The LECM units are easily transported to remote locations and able to sustain extensive long-term flow testing on high-capacity wells in harsh terrain and extreme environmental conditions.

REFERENCES

Ganefianto, N., Hirtz, P V., and Easley, E. (2015), "A brief history of the Sarulla geothermal field development.". *GRC Bulletin*, March/April 2015.

Grant, M. A., and Bixley, P. F. (2001), "Geothermal Reservoir Engineering". 2nd edition book, *Academic Press, Elsevier*.

Gunderson, R., Ganefianto, N., Riedel, K., Sirad-Azwar, L., and Suleiman, S. (2000), "Exploration Results in The Sarulla Block, North Sumatra, Indonesia". *Proceedings World Geothermal Congress 2000*.

Hirtz, P. N., Kunzman, R. J., Broaddus, M. L., and Barbitta, J. A. (2001), "Developments in Tracer Flow Testing for Geothermal Production Engineering". *Geothermics*, vol. 30, pp. 727–745.

Wolf, N., and Gabbay, A. (2015), "Sarulla 330 MW Geothermal Project Key Success Factors in Development". *Proceedings World Geothermal Congress 2015*.

NEW TECHNIQUES FOR ACID BRINE CORROSION CONTROL IN GEOTHERMAL WELLS

Paul von Hirtz, Elisabeth Easley, Russell Kunzman, and Darrell Gallup

Thermochem, Inc.
Email: paul@thermochem.com, elisabeth@thermochem.com
russ@thermochem.com, darrell@thermochem.com

ABSTRACT

Extensive pilot testing of corrosion mitigation technologies has been performed on geothermal wells producing acid-sulfate brine in Indonesia. This work involved two-phase sampling in the wellbores to determine acid feed zone depths and vertical profiles of brine composition for chemical modeling and corrosion and scaling by chemical mass balance. A full-scale pilot test facility was designed and built to measure corrosion and scaling rates as a function of sodium hydroxide and corrosion inhibitor injection rates downhole and on the surface. A mitigation strategy for severely corrosive acid-sulfate wells has been developed to minimize corrosion and scaling on the surface and subsurface through a balanced application of treatment chemicals.

Keywords: Pilot Testing, acid brine corrosion, geothermal well.

INTRODUCTION

Geothermal power is an established renewable energy resource that provides reliable baseload generation worldwide. In conventional hydrothermal vapor-dominated systems, long-term production (over decades) can yield superheated, corrosive steam (due to hydrogen chloride, HCl). Liquid-dominated systems may suffer from acidic fluids due to a variety of sources and mechanisms over the lifetime of these projects. Geothermal resource exploitation near active volcanic systems and from high-temperature deep-seated resources, including enhanced geothermal systems (EGS), may produce both corrosive steam and brine. Such highly corrosive conditions might limit the future development of these deep, high-temperature resources, as well as many conventional resources that encounter acid-fluid influence.

In North Sumatra, Indonesia, acid brine production has been a known development risk at the Sarulla Namora Langit (NIL) geothermal resource since initial drilling and well testing in 1998 by Unocal (Ganefianto et al, 2015). Sarulla Operations Limited (SOL), a consortium of Medco-Itochu-Kyushu-Ormat, was granted the rights in 2006 to utilize the Sarulla geothermal resource for power generation under a Joint Operating Contract (JOC) with the national oil and geothermal company, Pertamina. The first well drilled by SOL was found to have acid-sulfate brine character (although still neutral), based on results from a long-term flow test in 2015. In late 2016, another newly drilled well produced strongly acidic fluids on initial discharge. The brine pH ranged from 2.5 - 3.0 (at 25 °C). The brine chemistry was elevated in sulfate, magnesium, iron and manganese compared to other neutral NIL wells. The sulfate was most likely derived from a magmatic source, the magnesium was dissolved from reservoir minerals, while the iron and manganese were primarily from liner and casing corrosion. A two-phase downhole sampling (DHS) program was conducted by Thermochem, Inc. (TCI) on this well. The wellbore chemistry and calculated feedzone compositions indicated all zones were acidic. But the acidity of the entries, expressed as milliequivalents acid per kg brine (meq/kg), varied by up to a factor of 20. Another well on the same pad produced acidic fluid during flow tests in early 2017 with similar chemistry. Shortly after the Commercial Operation Date (COD) of the NIL Unit 1 plant, two previously neutral wells began producing acid brine. In early 2018, a third well on another pad began producing acidic brine, and a few months later 2 more wells became acidic. Currently a total of 5 wells connected to the NIL power plants and 3 others not connected are acidic (not including first Unocal well).

The acid fluid at Sarulla is characterized by elevated sulfate levels and classified as acid-sulfate brine. Figure 1 shows the acid character trends for the NIL area wells as a function of bicarbonate and sulfate concentrations over several months as acid fluid intruded. Bicarbonate is an important parameter to monitor since it is steadily depleted in neutral brine by acid influx, until it reaches zero and the brine pH becomes < 4. Sulfate is also an indication of acid character, but sulfate levels are already elevated in neutral brines at Sarulla, so acid influence is more difficult to detect by sulfate alone. The brine pH will remain near neutral until all the bicarbonate is depleted, then turn sharply acidic, so pH cannot reliably predict the on-set of acid fluids.

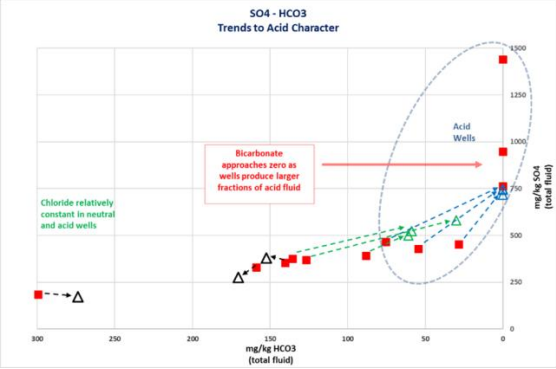


Figure 1: Acid character trends for the NIL area wells.

Occurrence of Acidic Fluids in Geothermal Systems

There are many geochemical processes that result in acidity of geothermal fluids. Hydrogen chloride (HCl) is the most prevalent in terms of the number of wells in service producing acidic fluids worldwide. But HCl is typically found in vapor-dominated systems, resulting from dry-out and superheat of the reservoir and/or influx of magmatic gases. Sulfuric acid is a common form of acidity associated with andesitic to dacitic-hosted liquid-dominated geothermal systems in the Philippines, Japan, Taiwan, Indonesia, Costa Rica, and Mexico (Reyes, 1991). Acid-sulfate brine may form after the influx of volcanic gases, such as sulfur dioxide (SO_2) and sulfur trioxide (SO_3), and can infiltrate a benign geothermal fluid system, causing the liquid to become highly acidic. Other inputs of magmatic gas may include H_2S, HF, and HCl. Additionally, immature geothermal systems may contain acidic fluids of magmatic origin that are not yet completely neutralized by the rock. These systems have been avoided in most commercial developments.

Acidic brine may also be caused by the influx of shallow acid-sulfate fluids that percolate to depth along faults into a deeper, benign geothermal reservoir. In this process acid-sulfate fluid is formed by the reaction of oxygenated meteoric water in the vadose zone with hydrogen sulfide (H_2S) from geothermal steam (Reyes, 1991). In this case the corrosion of geothermal wells often manifests as external casing corrosion when the well is exposed to the shallow acidic fluids. These shallow fluids may or may not directly affect the produced fluids, depending on the well completion design, casing integrity, and proximity of acid fluids to permeable faults that allow percolation to depth.

Acidic brine may also form through contact of neutral waters with buried solfataras and acidic minerals (from relic solfataras, advanced argillic mineralization in veins from an older system, near-surface pyrite oxidation). This process is typically limited to isolated areas within a reservoir and the acid may become depleted over time (Reyes, 2000). This requires fresh mineral surfaces for fluid rock interaction with continual fracturing and opening of fresh surfaces, therefore acid production is mass-limited and the acid may become depleted over time. This mechanism would produce localized and less pervasive acid fluids which is not consistent with the observed field-wide chemistry.

Acidic brine can be created by the influx and heating of seawater to temperatures of 300 °C or more. At high temperatures, magnesium in seawater precipitates as magnesium hydroxide ($Mg(OH)_2$), chlorite (ClO_2^-), and/or magnesium hydroxide sulfate hydrate ($2MgSO_4.Mg(OH)_2.H_2O$), causing the pH to drop dramatically.

In the Sarulla NIL reservoir, a probable model for acid-brine formation is the dissolution of magmatic gases into neutral chloride brine (Figure 2). This process can produce large quantities of acid fluid, which is consistent with the NIL wells that have continuously produced acid through commercial operations. This model requires relatively high inputs of magmatic gas over a large area and assumes magmatic gas injection from deep in the system, requiring permeable faults. These features are consistent with the relatively uniform reservoir chemistry and relatively homogeneous vertical chemistry profiles from DHS surveys.

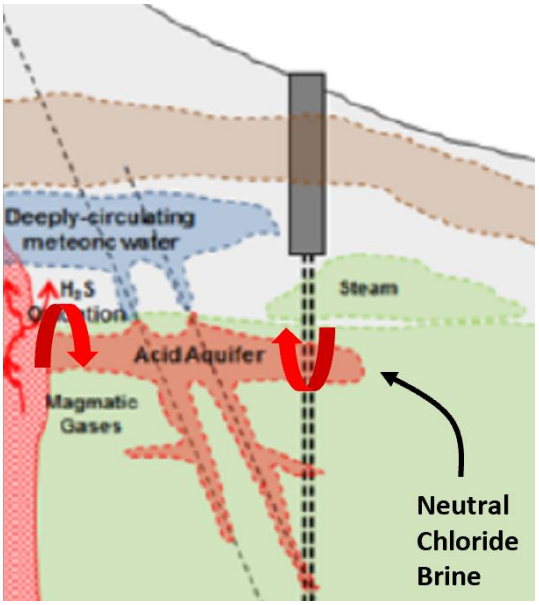


Figure 2: Possible acid-brine model for NIL (modified from Sugiaman et al, 2004).

Acid Fluid Impacts to Wells and Piping

Acid-sulfate brine and HCl in steam can cause severe corrosion damage to well casing and surface piping. The rate of corrosion is strongly affected by temperature and pH for acid-sulfate brine and by steam superheat (or saturation) for HCl. After 16 days of flowing the first new acid well at NIL, inspection of the wellhead piping and master valves indicated no significant damage. But there was

substantial corrosion downstream of the flow control valve (FCV) which was exposed to lower temperatures and higher velocities than the wellhead and casing, as shown in Figure 3.



Figure 3: Upstream / downstream of FCV after 16 days.

Unique Aspects of Downhole Corrosion and Mitigation Chemistry

The pH of acid-sulfate brine changes significantly with temperature. For the NIL brine chemistry, which is high in sulfate (600 – 1200 mg/kg), pH can increase by 2 units between 20 and 200 °C. This is due to the weak dissociation of bisulfate ion at high temperatures (2nd dissociation of H_2SO_4), as shown by the equations below and depicted in Figure 4.

1. $H_2SO_4 \rightarrow H+ + HSO_4^-$
   First dissociation of sulfuric acid
2. $HSO_4^- \rightarrow H+ + SO_4^-$
   Second dissociation of sulfuric acid

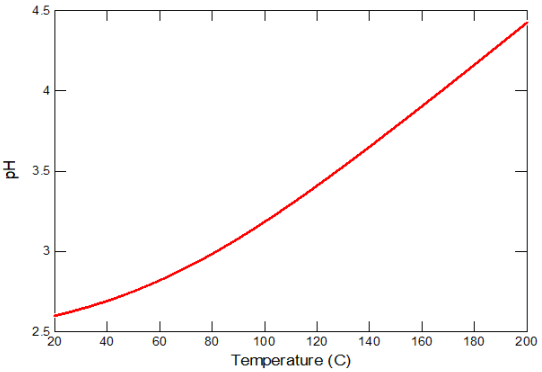


Figure 4: The pH of NIL acid-sulfate brine as a function of temperature.

Corrosion mitigation by downhole caustic injection has been proven commercially effective in several geothermal fields around the world. This was first done at The Geysers by Thermochem in 1990 (Hirtz et al, 1991), in the Aidlin and Northwest Geysers fields (Hirtz et al, 1990) where some wells produced over 100 ppm HCl in steam. Downhole caustic injection was needed in the wells with HCl that were saturated or low in superheat to prevent severe casing corrosion. Wells with HCl and high superheat only needed to be treated at the surface. In 1998, downhole caustic injection was used in acid-sulfate wells in the Tiwi geothermal field in the Philippines by Unocal.

Beginning in 2000, downhole caustic injection was used successfully in the Miravalles field in Costa Rica, and continues to be operated today, including utilization of these fluids in a binary bottoming cycle (Hernández, 2015).

There have been some complications with wellbore scaling reported from Miravalles, related to neutralization of the brine. Figure 5 is a photo of downhole injection tubing at Miravalles after scale formed around the tubing in the wellbore (Moya et al, 2005). The scale was identified as anhydrite and "complex amorphous silica". It is important to note that pure amorphous silica scale (Opal A) is undersaturated and cannot form in the wellbores or production piping systems at Miravalles or Sarulla. These "complex silica" scales are amorphous magnesium-, calcium-, iron-silicates (typically classified as clay minerals) (Gallup, 1993). These scales form under very different conditions than pure amorphous silica scale, and aluminum- and iron-rich amorphous silica scale, which are the primary scales of concern for the power plants and reinjection systems. The main difference is that these scales have retrograde solubility and deposit at high temperatures, not low temperatures, and their solubility is very sensitive to pH.

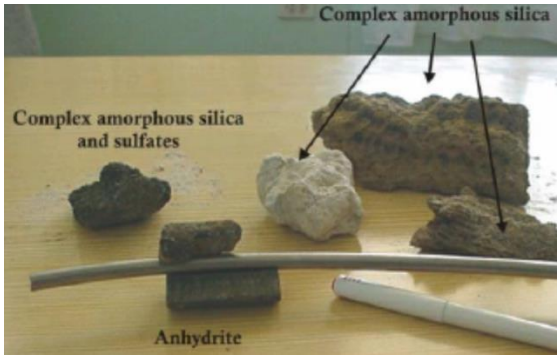


Figure 5. Wellbore scale from Miravalles, Costa Rica (Moya, 2005).

There are some unique aspects of the NIL brine chemistry that present opportunities to minimize chemical costs, corrosion and scaling throughout the neutralization process from wellbore to the power plant binary bottoming units. The main points that can be exploited are summarized below.

1) The brine pH is significantly higher at high temperatures, in wellbore and at wellhead.
   a) The highest corrosion rates are in surface equipment where they are more easily managed.
   b) Lower caustic dosing rates downhole are possible than needed for full neutralization.

c) This may allow corrosion inhibitor use at lower costs than full neutralization by caustic.

d) It may also be possible to manage surface corrosion by appropriate material selection.

2) The minerals that have potential to deposit from the brine have retrograde solubility.

a) The highest scaling rates will be in the wellbore, not on the surface.

b) Mg-silicate scaling can be managed downhole by pH control. Excessive caustic dosing will result in scaling. Therefore, management of scaling is consistent with the strategy to manage corrosion as described in part 1) before.

c) Fe-based scaling can be further managed by minimizing corrosion.

d) Anhydrite is undersaturated for NIL brines, due to a lower calcium concentration (than Miravalles).

e) Cooling the brine reduces the acid-sulfate related scaling potential of these fluids. With corrosion properly managed, no scaling impacts are expected at the binary bottoming units.

3) The same acid (H_2SO_4) must be *added back* at the NIL plants for pH-modification.

a) If caustic dosing can be minimized downhole and corrosion managed as described in part 1) and 2), the residual acid in the brine has a substantial *value* in terms of chemical costs for pH-mod. This can help off-set the costs of caustic used for partial neutralization.

b) Even if acid wells are fully neutralized to pH 5, their production off-sets the production of alkaline wells and reduces the chemical costs for NIL plant pH-modification.

Downhole Sampling and PTS Surveys

A flowing PTS log was conducted on the pilot test well before DHS collection to confirm the entry depths for DHS targeting and their relative contributions for mass balance and modeling purposes. To effectively mitigate both corrosion and scaling downhole, it is necessary to have high-resolution chemistry profiles with depth. The Thermochem combination DHS-PTS high-temperature two-phase sampling tool was deployed to obtain flowing pressure and temperature of the production well and to collect samples of brine for analysis. This tool has a titanium fluid path and is ideally configured for acid-brine sampling under two-phase conditions, including the collection of heavy metals critical to performing chemical mass balance on corrosion and scaling processes. Example DHS data from one acid well is given in Figure 6 and Table 1. Corrections were made in the free acidity values from each survey to account for the acidity lost due to corrosion of steel, according to the oxidation reaction $M + 2\ H^+ = M^{+2} + H_2$.

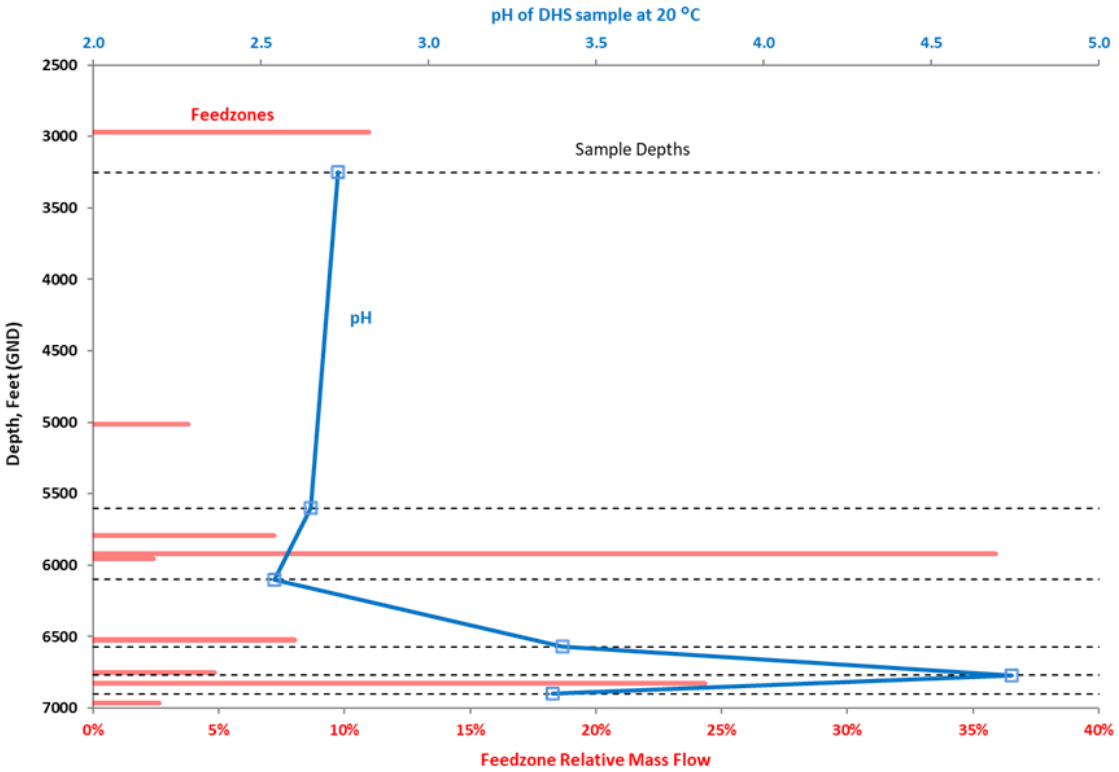


Figure 6: Flowing Downhole pH, Feedzones and Sample Depths.

Table 1: Flowing downhole sample chemistry, including calculated composition of entries by mass balance.

Lab Number:	21070-3	*Calculated*	21074 - 1	21074 - 2	*Calculated*	21074 - 3	*Calculated*	21078 - 3	*Calculated*	21078 - 1	*Calculated*	21078 - 2
Sample Date:	13-Dec-16		13-Dec-16	14-Dec-16		15-Dec-16		16-Dec-16		16-Dec-16		16-Dec-16
Sample Depth, ft. gnd:	Surface		3250	5600		6100		6570		6770		6900
Entries, ft. gnd:	2968 - 6965	2968	5011 - 6965	5794 - 6965	5794 - 5953	6525 - 6965	6525	6752 - 6965	6752	6826 - 6965	6826	6965
Temperature at Depth, C:	NA		254	259		257		257		257		258
Casing / Liner Size, in.:	NA	13 3/8 casing	10 3/4 blank	10 3/4 perf.	10 3/4 perf.	7 perf.	7 perf.	7 perf.	7 perf.	7 perf.	7 perf.	7 perf.
Phase Condition[1]:	2-phase	2-phase	Bubble-point	1-phase	1-phase	1-phase	1-phase	1-phase	1-phase	1-phase	1-phase	1-phase
Mass Flow of Entries, t/h:	159.8	17.6	142.2	136.2	72.6	63.5	12.8	50.8	7.7	43.1	38.9	4.2
Analyte	*Total Fluid Concentrations, mg/kg*											
Sodium	759	725	763	831	849	810	870	795	817	791	787	828
Potassium	189	107	199	218	222	213	221	211	312	193	190	225
Calcium	4.26	<5	5.78	6.72	6.84	6.58	4.51	7.10	<5	9.68	10	7.9
Magnesium	9.91	9.79	9.93	11.7	8.73	15.1	<5	24.1	42.6	20.8	20.3	25.4
Lithium	4.67	3.28	4.84	5.52	6.05	4.91	5.31	4.81	4.98	4.78	4.76	4.94
Strontium	0.080	0.198	0.065	0.223	0.251	0.191	0.525	0.107	<0.5	0.151	0.159	0.077
Iron	19.1	--	14.7	10.3	--	4.62	--	92.3	--	66.4	--	142
Boron	28.2	24.0	28.7	32.4	34.1	30.4	38.8	28.3	28.9	28.2	28.3	27.3
Silica	547	436	561	588	611	562	502	577	661	562	561	573
Manganese	6.64	--	5.30	7.43	--	8.17	--	36.4	--	33.6	--	41.5
Chloride	960	848	974	1050	1076	1020	1203	974	1136	945	939	1000
Fluoride	4.25	<5	5.06	5.72	6.01	5.39	9.61	4.33	8.36	3.61	3.48	4.77
Sulfate	767	649	782	865	751	995	1063	978	1649	858	830	1120
Total Acidity (meq/Kg)[2]	**2.83**	**2.97**	**2.81**	**2.84**	**0.81**	**5.15**	**4.73**	**5.26**	**14.0**	**3.70**	**3.31**	**7.32**
TDS	3302	2915	3350	3640	3614	3670	3431	3730	5184	3470	3413	4000
Calculated pH (25 C)[3]	2.74	2.70	2.74	2.75	3.19	2.51	2.56	2.50	2.12	2.64	2.68	2.37
Calculated pH (255 C)[3]	4.73	4.60	4.72	4.78	5.08	4.51	4.62	4.48	3.92	4.63	4.67	4.30

1. All concentrations reported directly or corrected as needed to single-phase, total fluid basis
2. Total acidity includes correction for Fe and Mn oxidation: $M + 2\,H^+ = M^{+2} + H_2$
3. Calculated pH based on total acidity and includes gas in total fluid

Neutralization Pilot Test and Laboratory Analysis Results

During the pilot test, field chemistry measurements were made in addition to sample collection for laboratory analysis. The primary sample collection points were upstream of the FCV, upstream of the James Tube and the Low-Emissions Compact Muffler (LECM) brine header, as shown in Figure 7. A photo of the full-scale pilot test facility in service is given in Figure 8. The bine pH was checked manually on-site against an on-line automatic pH meter. Dissolved iron analyses were performed routinely on-site to assess downhole and surface corrosion rates by chemical mass balance. Likewise, calcium and magnesium were measured on-site to assess downhole and surface scale deposition rates (anhydrite, Mg-silicates and clays) by chemical mass balance. Complete brine analysis was conducted at Thermochem Laboratories on samples collected during the test.

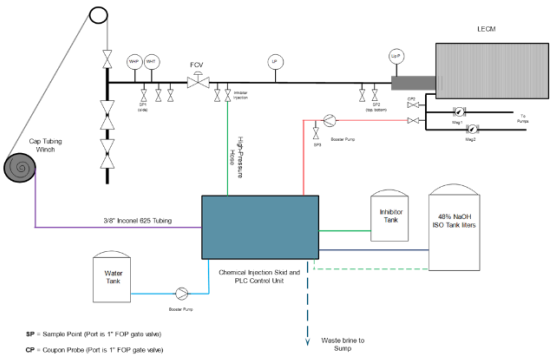


Figure 7: Pilot Test Facility P&ID.



Figure 8: Pilot Test Facility.

Corrosion Measurements and Results

The primary objective of the pilot test was to measure corrosion rates in the wellbore and on the surface as a function of pH and inhibitor concentration. Three methods were employed to measure corrosion in the well casing and liner:

1) Acoustic Borehole Image (ABI) logs run before and after the pilot test.
2) Corrosion coupons installed at the wellhead.
3) Chemical mass balance based on dissolved iron in brine, mass flow rate and surface area.

Two methods were employed to measure corrosion in the two-phase surface piping:

1) Corrosion coupons installed in the flowline.
2) Chemical mass balance based on dissolved iron in brine, mass flow rate and surface area.

The ABI logs did not detect any significant corrosion damage to the casing or liner and was determined to be in good condition after the 30-day test period, plus an additional 5 short flow intervals (24 – 48 hours) with the brine unabated at pH 2.5.

Corrosion coupons were installed upstream of the FCV near the wellhead which is at full wellhead pressure. This location experiences a lower pressure than deeper in the well, and therefore represents a worst-case condition for casing corrosion. Higher pressure, higher temperature and lower fluid velocities in the wellbore result in lower corrosion.

The concentration of dissolved iron measured in samples collected upstream of the FCV was used to assess corrosion in the wellbore by mass balance, assuming the iron comes from the corrosion of casing and liner. The neutral wells at NIL have very low levels of iron in the brine (< 0.1 ppm). The mass flow rate of iron is divided by the density of the steel and the total surface area of the casing/liner to calculate an average metal loss rate in mm/year.

Corrosion coupons were installed downstream of the FCV and upstream of the James Tube at the end of the two-phase flowline. All coupons were installed in side-stream flow tees attached directly to the pipeline and operated at pipeline pressure and temperature, using retractable coupon holder probes. The probes could not be inserted directly into the two-phase flow given the high velocity which would break the coupons off the holders. The concentration of dissolved iron measured in samples collected downstream of the FCV and upstream of the James Tube were used to assess corrosion in the two-phase flow line by mass balance, after correction for iron already dissolved at the wellhead from casing corrosion.

As shown in Table 2, the corrosion rate at the wellhead based on coupons was very low (0.25 mm/yr) even at pH 3.0 – 3.3. After the FCV, the temperature drops from about 225 °C (25 bara) to between 170 and 195 °C (8 - 14 bara). At these lower temperatures the corrosion rate increased by a magnitude, to 2.4 mm/yr. Close to the same value was confirmed at the other end of the two-phase pipeline (before James Tube). In the LECM brine header, the corrosion rate increased further by about 100% to 5 mm/yr at 96 °C.

In Table 3, the corrosion rates based on coupons are shown at full neutralization to pH 5.0. The corrosion rate at the wellhead was not much lower than at pH 3 (0.19 mm/yr), due to general corrosion reactions with the brine in the near neutral range. Again, as shown in Figure 1, the pH increases dramatically with temperature, and pH 3.0 brine at 25 °C has a pH of 4.9 at 225 °C.

After the FCV, at temperatures of 170 and 195 °C, the corrosion rate of the neutralized brine (pH 5 at 25 °C) was barely measurable at 0.1 mm/yr. This low rate is confirmed at the other end of the two-phase pipeline (before James Tube). In the LECM brine header, there was no corrosion measured due to a slight amount of scale formation. This is expected because silica is supersaturated.

Table 2: *Coupon Corrosion Rates, pH ~ 3.*

Location	Weight Change	Exposure Time	Corrosion Rate	Corrosion Rate	Comments
Wellhead	-0.0417 g	8 days	-9.9 mils/yr	-0.25 mm/yr	smooth, gray, no pits
After FCV	-0.4008 g	8 days	-95 mils/yr	-2.4 mm/yr	smooth, gray, no pits, red, rusty, rough around bolt holes
Before James Tube	-0.3223 g	8 days	-76 mils/yr	-1.9 mm/yr	smooth, gray, no pits, red, rusty, rough around bolt holes
LECM Header	-0.6189 g	6 days	-195 mils/yr	-5.0 mm/yr	red, rusty, rough edges

Table 3: Coupon Corrosion Rates, pH 5.

Location	Weight Change	Exposure Time	Corrosion Rate	Corrosion Rate	Comments
Wellhead	-0.0315 g	8 days	-7.4 mils/yr	-0.19 mm/yr	smooth, gray, some pits
After FCV	-0.0137 g	8 days	-3.2 mils/yr	-0.08 mm/yr	smooth, gray, no pits
Before James Tube	-0.0164 g	8 days	-3.9 mils/yr	-0.10 mm/yr	smooth, gray, no pits
LECM Header	0.0128 g	8 days	--	--	smooth gray scale

Figure 9 shows the dissolved iron concentrations in samples collected from the surface piping upstream of the James Tube at a pressure of approximately 8 bara (170 °C). The average iron concentration at pH 3.33 was about 2 ppm, and the concentration doubled to 4 ppm at pH 3.03. The corrosion rates under these conditions at the surface were very high. At pH 3.03 the corrosion rate in the two-phase piping based on chemical mass balance was 13 mm/yr and at pH 3.33 the corrosion rate 7.3 mm/yr.

Figure 10 shows the dissolved iron concentrations in samples collected from the surface piping upstream of the James Tube at pressures of 8 bara (170 °C) and 14 bara (195 °C) at an average pH of 5.08. The average corrosion rate at pH 5 over this entire interval was 0.66 mm/yr, while the rate was 1.1 mm/yr at 8 bara (170 °C) and 0.29 mm/yr at 14 bara (195 °C). Since the NIL two-phase pipeline pressures are around 13 bara, the corrosion rate between the FCV and separators is expected to be close to 0.3 mm/yr for brine fully neutralized to pH 5. This is a relatively low corrosion rate and typical for most geothermal production gathering systems. This data emphasizes the sensitivity of the acid-sulfate brine corrosiveness with temperature.

Figure 11 shows the dissolved iron concentration at the wellhead at approximately pH 3 and a pressure of about 25 bara (225 °C). The average iron concentration more than doubled from pH 3.03 to pH 3.33. However, the corrosion rates under these conditions at the wellhead and in the wellbore were very low. At pH 3.03 the corrosion rate in the casing based on chemical mass balance was 0.21 mm/yr and at pH 3.33 the corrosion rate was only 0.08 mm/yr. This demonstrates the sensitivity of the corrosion rate to temperature. The fluid velocity is also lower at the higher pressures which will be expected to reduce corrosion rates as well.

At pH 5, dissolved iron at the wellhead was reduced even further as shown in Figure 12. The average corrosion rate calculated by chemical mass balance at pH was 0.03 mm/yr in the wellbore.

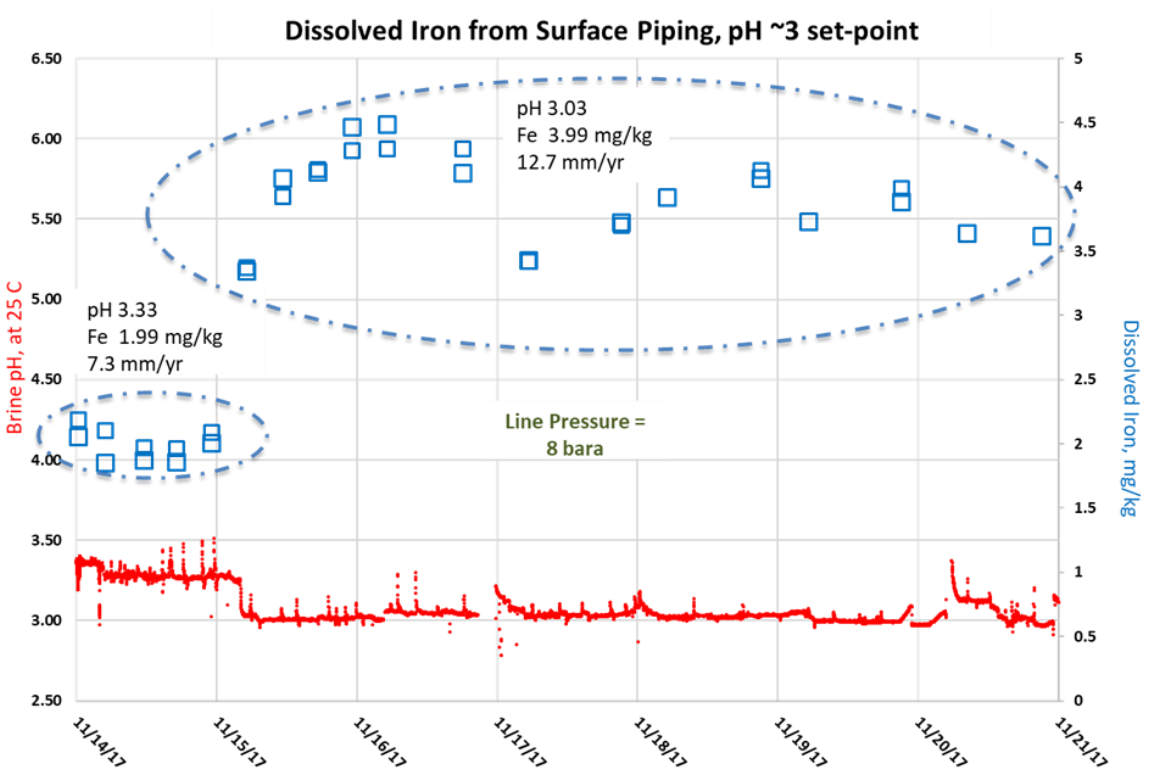


Figure 9: Mass Balance Corrosion Rates on Surface, pH ~3.

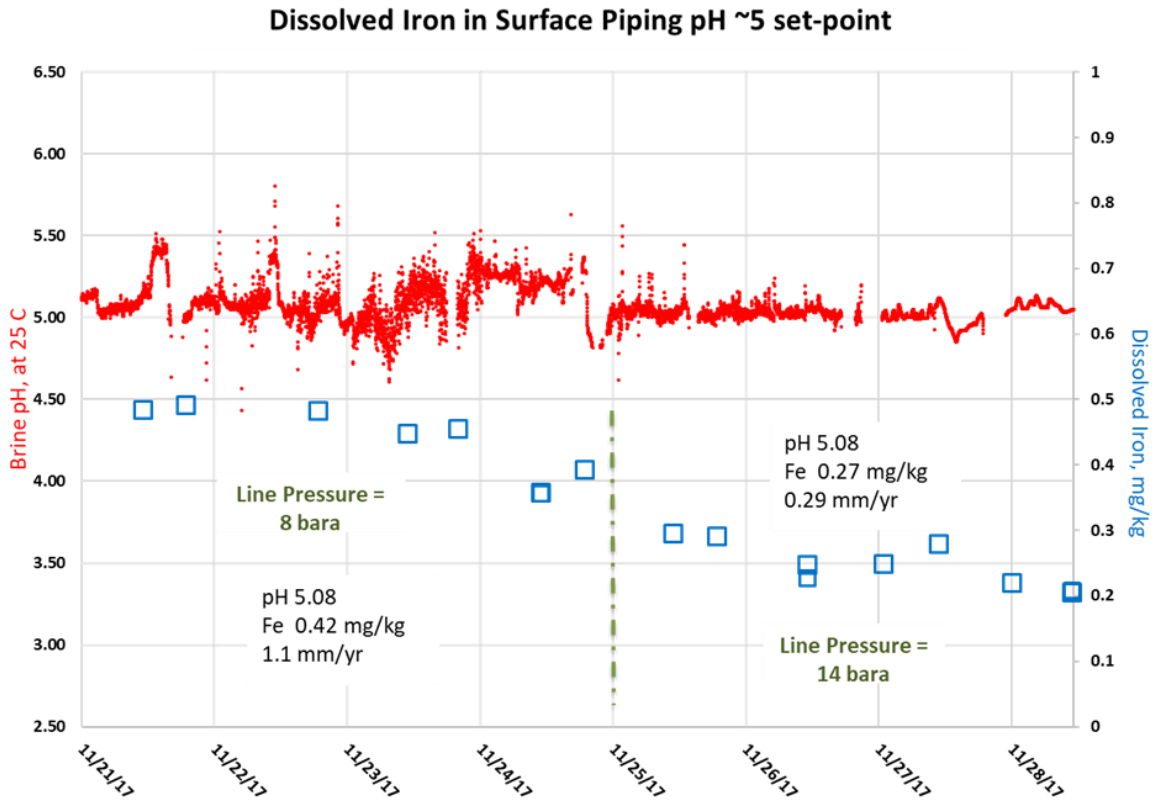


Figure 10: Mass Balance Corrosion Rates on Surface, pH 5.

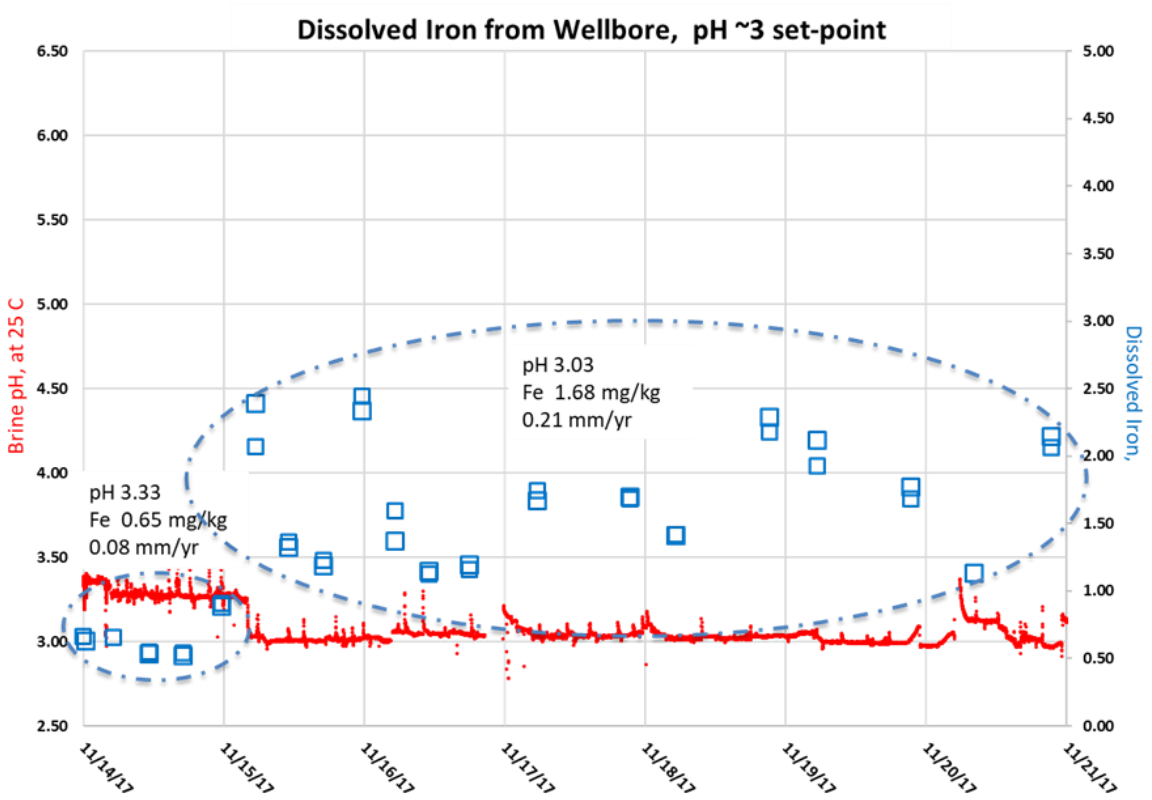


Figure 11: Mass Balance Corrosion Rates in Wellbore, pH ~3.

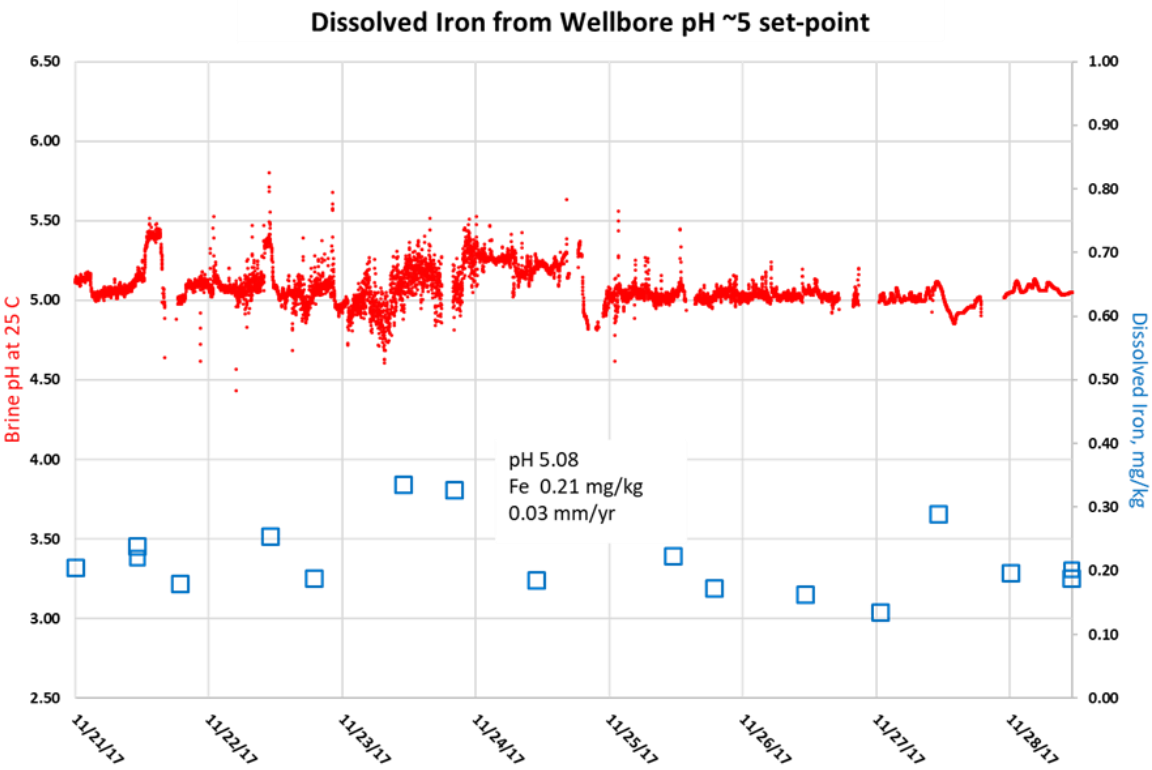


Figure 12: Mass Balance Corrosion Rates in Wellbore, pH 5.

Inhibitor Chemical Evaluation

A major focus of the pilot test was to evaluate chemical inhibitors for use in acid-sulfate brine corrosion mitigation applications (Crossland et al, 2011; Cassidy et al, 2007). Although these specialty chemicals can have a relatively high cost and it is challenging to inhibit corrosion in pH 2.5 brine, we hoped to develop a process where the brine is partially neutralized with caustic to about pH 3.0 – 3.3 in the wellbore, and an inhibitor is injected at the wellhead to control surface corrosion. Even if the total chemical cost were about the same as for full neutralization, this combined process with partial neutralization would result in substantial cost savings at the power plants by reducing the amount of acid needed for pH-modification. The Sarulla power plants are combined cycle, with back-pressure steam turbines and binary heat exchangers for separated brine, resulting in a high amorphous silica scaling potential.

For example, the average acidity of two of the first acid wells is about 4 meq/kg total fluid. At 1200 t/h combined production from these wells, the amount of acid produced is 130 % of the total acid needed for pH-mod at one NIL unit. Now that most wells in the NIL area are acidic, there is the potential to eliminate the need to purchase sulfuric acid for pH-modification. The acid cost was expected to be almost US$2,000,000/year based on the initial neutral reservoir chemistry.

TCI requested proposals from several vendors to supply corrosion inhibitors for testing in this application, including some that claimed to have experience in geothermal acid-brine corrosion mitigation. Nalco proposed to use a blend of quaternary ammonium salts with a substituted imidazoline. The thermal stability was reported to be up to 270 °C based on lab tests. The product is basically a filming amine and was essentially the same product proposed by the other vendors.

As recommended by Nalco, the inhibitor was injected at a rate resulting in a concentration in brine of about 60 ppm initially for 24 hours as a passivation step, then reducing the rate to 5 ppm continuously for maintenance of the protective film. This practice is common in the oilfield to form a film barrier to prevent acids from contacting steel. Inhibitor was injected through a quill immediately downstream of the FCV. The corrosion rates calculated by chemical mass balance in the two-phase surface piping at pH 3.0 was 15 mm/yr at an inhibitor concentration of 11 ppm, double the recommended value. The inhibitor rate was doubled again to 21 ppm, but the corrosion rate was essentially the same at 16 mm/yr. The inhibitor was shut-off completely and the corrosion rate remained at 16 mm/yr. There was obviously no benefit from injecting the inhibitor on the surface for partially-neutralized brine at pH 3.0. Near the end of the test another inhibitor trial was attempted with downhole injection. Caustic injection was suspended and inhibitor was injected through the downhole tubing to a concentration of 150 ppm in the brine for 24 hours. The wellbore corrosion rate based on chemical mass balance dropped from 1.3 to 1.1 mm/yr. This is probably not a statistically significant difference.

An attempt was then made to co-inject inhibitor with caustic for partial neutralization downhole, but the injection tubing plugged soon after the mixture had passed through the entire length of tubing and the test was terminated. The manufacturer was consulted prior to this final test and did not think the mixture should result in any problems. TCI conducted a bench test with the mixture and only found a hydrocarbon phase separation.

The inhibitor tested is a film-former type that requires the polar headgroup of the imidazoline moiety to adsorb on the steel surface and the hydrophobic tailgroup to form a barrier with oil from the produced fluid. Some possible explanations for failure of the inhibitor include: (1) the inability of the head group to adsorb to steel, (2) the inability to form an oily tail barrier to the flowing brine, and (3) velocity and shear effects detrimental to adsorption of the headgroup on the steel.

TCI is investigating alternative corrosion inhibitors and has a laboratory screening program in progress. A review of inhibitor chemistry is discussed below to help provide explanations for the failure of organic inhibitors to control acid-sulfate brine corrosion and to guide the selection of alternative inhibitors for this application.

Weak sulfuric acid in geothermal brine at 20 to 180 °C is extremely corrosive toward mild steel and most corrosion-resistant alloys (Jayaperumal et al, 1997; Feng et al, 1991). Sulfuric acid reacts with iron in piping to form ferrous sulfate, a non-protective corrosion product:

$$H_2SO_4 + Fe \rightarrow FeSO_4 + H_2$$

There are several ways of mitigating acid-sulfate geothermal brine corrosion; the primary method of course being pH neutralization with NaOH. Corrosion inhibitors have been used to control corrosion from dilute acids in many industrial applications, and they can be categorized as: passivating (anodic), cathodic, vapor-phase/volatile, and film-forming.

Passivating corrosion inhibitors are not normally used in the geothermal industry. They consist of phosphate and polyphosphates, tungstate and silicate and require the presence of oxygen.

Passivating inhibitors that do not require the presence of oxygen include chromate, nitrite, molybdate and vanadates. Cathodic inhibitors are not used in oil and gas or geothermal production operations. An example of a cathodic inhibitor is zinc(II) ions in zinc oxide, which retards the corrosion by inhibiting the reduction of water to hydrogen gas.

Vapor-phase corrosion inhibitors are organic compounds that have sufficient vapor pressure to essentially travel to the surface of the metal by gas diffusion and physically adsorbing onto the surface. Examples are: dicyclohexylamine nitrite or carbonate, dimethylamine phosphate, small volatile amines, and benzotriazole. These inhibitors are mostly applied in corrosion caused by gases such as CO_2 and H_2S.

Film-forming corrosion inhibitors (FFCIs) are the most common used in oil and gas and geothermal operations. They are used in well stimulations and in surface applications. The effectiveness of a FFCI is partly determined by the strength of its adsorption to the metal surface forming a protective layer that physically prevents corrosive chemicals from penetrating to the metal surface. FFCIs can be small molecules or polymers. However, many FFCIs are organic surfactants with a polar head group and a hydrophobic tail. The headgroups are designed to interact with iron atoms on the surface and the hydrophobic tails attract liquid hydrocarbons (in oil and gas applications). An oily film is formed which further prevents the corrosive aqueous phase from penetrating to the metal surface. It has been shown that under some multiphase flow conditions (such as surging), parts of the pipe wall are left unprotected by surfactant FFCIs, giving the possibility of localized corrosion.

Regarding the structure of FFCIs, most contain heteroatoms in one of more head groups, which bind via lone pairs of electrons to iron atoms on the metal surface. Typically, N, P, S and O atoms are found in the headgroup. The most common categories of FFCIs are: phosphate esters, various nitrogenous compounds and sulfur compounds often with other heteroatoms such as N. The most common nitrogenous compounds include amine salts of carboxylic acids, quaternary ammonium salts and betaines, amidoamines and imidazolines, polyhydroxy and ethoxylated amines/amidoamines, and amides (Kelland, 2009).

The product we tested consists of imidazoline salts, thiogylcolic acid and a quaternary ammonium salt, and is therefore a classic FFCI. There are several potential reasons why the FFCIs examined to date have failed to exhibit corrosion inhibition at NIL:

Headgroup non-adherence

If the polar headgroup gets protonated by hydrogen ion at low pH, then the filmer will not be attracted to the metal surface containing iron or iron corrosion product.

Tailgroup non-barrier

Imidazoline and amide in FFCIs rely on oil to form the protective hydrophobic barrier against produced fluid in the tail group. The absence of oil in the geothermal brine precludes the barrier at relatively low dosages. It may require several hundred ppm of FFCI to achieve the needed hydrophobicity of the tailgroup.

Flow Conditions

It has been shown that the corrosion behavior and the effectiveness of FFCIs are highly dependent on flow conditions. Multiphase flow conditions, slugging or surging can adversely affect the headgroup of imidazoline, amides, and quaternary ammonium compounds from adsorbing onto the metal surface.

While the FFCI had been injected into both two-phase flow on the surface and single-phase brine downhole, surging and varying velocity of flow after boiling in the wellbore and variation in velocities may be responsible for the FFCI not adhering to the steel metal surfaces (Wang et al, 2002).

Sheer stress greater than 300 Pa reduces the boundary layer thickness required for a FFCI to perform acceptably. Any real fluids moving along the solid boundary will incur a shear stress on that boundary. A no-slip condition dictates that the speed of the fluid at the boundary (relative to the boundary) is zero, but at some height from the boundary the flow speed must equal that of the bulk fluid. The region between these two points is aptly named the boundary layer. For all fluids in laminar flow, the shear stress is proportional to the strain rate in the fluid where the viscosity is the constant of proportionality. The shear stress is imparted onto the boundary as a result of the gain or loss of velocity. Therefore, when the thickness of the FFCI is too low, corrosion inhibition can suffer.

Imidazoline-based inhibitors have failed to control corrosion at NIL apparently due to either the polar headgroup not adhering to the piping or the tailgroup not providing the hydrophobic barrier in the absence of oil. Much higher dosages of imidazoline-based inhibitors may be required to provide the hydrophobic barrier (boundary layer thickness due to shear stress). The inability of the polar headgroup to adhere to the steel surface could be due to brine velocity effects (sheer stress) or protonation by the sulfuric acid. We conclude that non-imidazoline

FFCIs and other inhibitors (polymeric) should be evaluated and this effort is on-going now.

Scale Deposition and Geochemical Modeling

Mineral deposition in wellbores has been known to occur in wells being treated with caustic downhole for acid brine neutralization. As mentioned previously, anhydrite ($CaSO_4$) was found to form upon neutralization at Miravalles. This is due to an increase in $SO4^{=}$ ion activity with increasing pH by shifting equilibria from the bisulfate (HSO_4^-) ion to sulfate. Calcium levels are much lower at Sarulla so this scale will not form. The following minerals were identified by geochemical modeling as having the potential to deposit from NIL acid brine upon full neutralization (pH 5 – 6) at wellbore temperatures:

1. Minnesotaite $(Fe^{2+}, Mg)_3Si_4O_{10}(OH)_2$.
2. Greenalite $(Fe^{2+}, Fe^{3+})_{2\text{-}3}(Si_2O_5OH)_4$.
3. Talc $H_2Mg_3(SiO_3)_4$ or $Mg_3Si_4O_{10}(OH)_2$.
4. Sepiolite $Mg_4Si_6O_{15}(OH)$.
5. Dolomite $CaMg(CO_3)_2$.
6. Brucite $Mg(OH)_2$.
7. Magnesite $MgCO_3$.

Although predicted by modeling to become supersaturated at elevated pH and temperature, the first four minerals above may not actually form under geothermal conditions (they are typically metamorphic or sedimentary minerals). Some of these minerals above have probably formed at Miravalles, although sufficiently detailed scale deposit analyses have not been reported in the literature to confirm this. Most of these minerals contain magnesium, which is elevated in acid brines. These minerals have retrograde solubility, becoming more soluble at lower temperatures. The greatest risk for deposition is in the wellbores at high temperature and high pH. These minerals can be managed with proper pH control at a given temperature.

The methods used to detect scaling in the well included the ABI logs to visualize any scale deposits and estimate thickness, inspection of the downhole chemical injection head assembly and tubing, chemical mass balance of the mass-limited species involved in these scales.

The pre- and post-neutralization test ABI logs did not detect any wellbore scale. The bottom hole assembly and the tubing were completely free of any deposits when retrieved at the end of the test. Calcium and magnesium concentrations were monitored throughout the entire test in wellhead and surface piping brine samples. A short test was conducted to deliberately induce scaling in an effort to find the pH where scaling by these minerals in the wellbore would clearly occur.
Figure 13 shows the magnesium and calcium concentrations in wellhead brine as a function of pH throughout the test. No difference in calcium concentration was observed at any pH. A short test conducted at pH 6.2 resulted in a significant drop in magnesium to 5.3 ppm. This represents a very high scaling rate of 3.4 kg/h as a magnesium silicate deposit, or about a 40 mm/yr scaling rate localized over the 7" liner section in the well.

A very small difference in magnesium was detected between the pH 3 and pH 5 test intervals, with a drop of about 0.6 ppm magnesium. This represents about 0.38 kg/h as a magnesium silicate deposit, or a 4.5 mm/yr scaling rate localized over the 7" liner section. During the one-week test interval at pH 5, this equates to a scale thickness of less than 0.1 mm, which may not have been detectable by the ABI log. Scaling rates calculated above are roughly estimated because factors such as the exact mineral deposited, the mineral density and the area of deposition are not precisely known. We can conclude that some scaling will occur by this process at pH 5, but it should be manageable. Some scale is desirable since it will likely protect the liner and casing from corrosion.

Given the retrograde solubility of the minerals that have greatest potential to deposit from the neutralized acid-brine, scaling problems are not expected on the surface. The risk of magnesium silicate scaling will further diminish through the binary heat exchangers at the power plants due to cooling, and both iron and magnesium silicates are controlled in the same manner as pure amorphous silica, using pH-modification.

Commercial Application

Soon after the pilot testing was completed, several additional production wells in the NIL power plant area became acidic. At that time, it became urgent to finalize and implement the neutralization process on a commercial scale. The caustic injection skid (CIS) from the pilot test was transferred to one of these wells (the pilot test well was not connected to the plant yet). Thermochem then designed and built 3 new CIS units for the additional acidic wells, and another 2 shortly after that.

The CIS units are designed to precisely meter concentrated NaOH (48%) and measure and control the brine pH after the NaOH injection. The CIS provides a continuous pH signal to the power plant distributed control system (DCS) and allows for remote pump output adjustment and emergency shut-off remotely from the control room. The CIS units are equipped with 2 independently controlled high-pressure metering pumps for NaOH. These units can be operated with both pumps in service so that one pump feeds NaOH downhole while the other pump injects at the wellhead. This configuration is necessary where there are deep, low-flow acidic entries that need to be treated. When injecting the full amount of NaOH required for

neutralization of the entire well flow, overdosing will occur in the deep zones causing scale formation (primarily Mg-silicates). The final process design provides for the minimum NaOH injection downhole to mitigate corrosion in the wellbore with the balance injected at the wellhead. The nature of the acid brine chemistry allows for partial neutralization at high-temperatures, making this 2-stage injection process feasible.

The CIS obtains a brine sample from the two-phase pipeline downstream of the wellhead caustic injection point through a sampling separator that is continuously on-line. The sample stream is cooled, the flowrate measured by a magnetic flowmeter and flowrate controlled to a set-point using an electronic flow control valve. The sample stream is then passed to an on-line pH analyzer for pH measurement. The pH-analyzer is automated for calibration and cleaning cycles, which are controlled through a local programmable logic controller (PLC). This is the same automatic pH-monitor design that TCI builds for pH-modification systems at power plants.

The CIS is fully controlled by the local PLC. The processed pH signal is sent to the plant DCS, but the pH-control logic loop is performed by the local PLC, adjusting the NaOH metering pump to dose the brine at the required rate to maintain the pH set-point. A designated primary pump for downhole injection is set to direct proportional flow control based on a well production flow-related signal from the DCS (2-phase orifice flow or FCV position). The proportional factor is automatically updated at pre-programmed intervals by a proportional–integral (PI) pH-control logic routine. The pump designated as secondary for surface injection is controlled through a continuous PI pH-control logic loop based on the measured surface pH.

Routine monitoring is performed for Fe, Mn, Mg and Ca in the produced brine to calculate corrosion and scaling rates downhole and on the surface. The Inconel 625 tubing and chemical injection head assembly have proven very reliable so far and we have not had the need to monitor Fe continuously at the surface as done at Miravalles to detect downhole tubing failures (Moya and Mora, 2010). The commercial CIS unit is shown in Figures 14 and 15, and the chemical injection head in Figure 16.

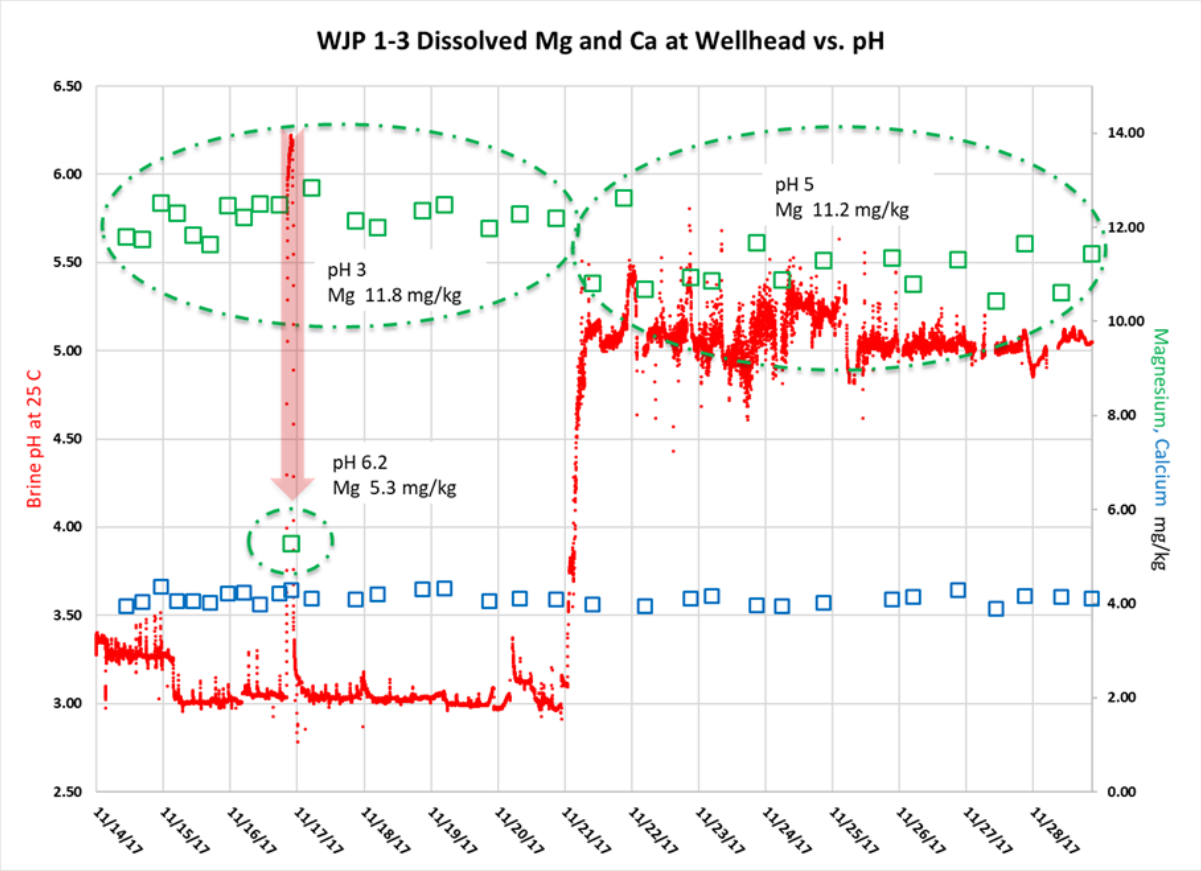


Figure 13: Mg and Ca concentrations at wellhead vs. Inhibitor and pH.

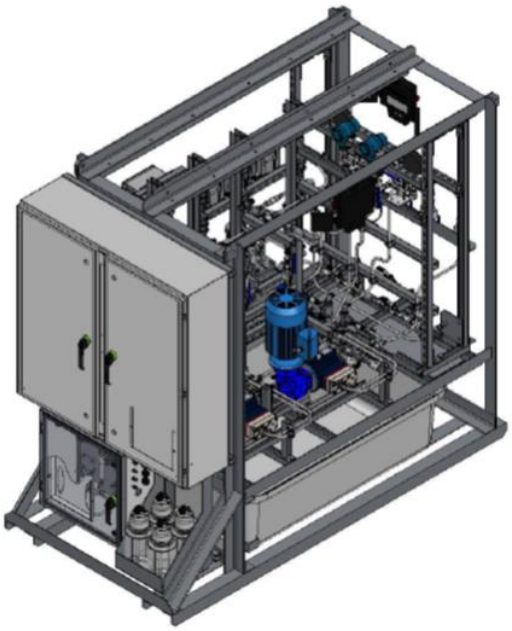


Figure 14: Commercial CIS Unit.



Figure 15: Commercial CIS Unit.

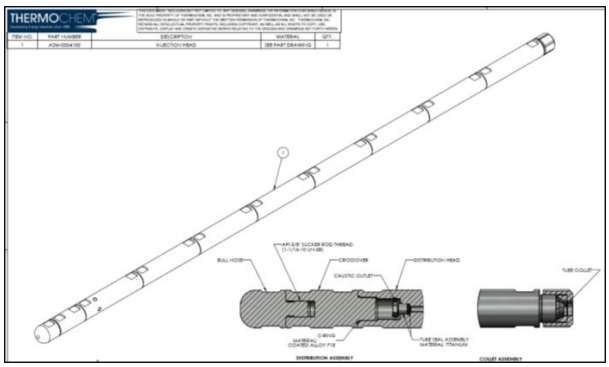


Figure 16: Chemical Injection Head and Weight Assembly.

CONCLUSIONS

The neutralization pilot test successfully demonstrated that acid-sulfate brine produced from NIL wells can be treated effectively. Acidic wells are now being produced to the 220 MW NIL power plants at Sarulla with 2-stage downhole and surface caustic injection.

Corrosion rates of the well liner and casing were acceptable with partial neutralization to pH 3.0 and pH 3.3 (25 °C), at 0.2 and 0.08 mm/yr, respectively. Due to lower temperatures and higher velocities, corrosion in the two-phase surface piping was much higher. At pH 3.0 (25 °C) the corrosion rate was 13 mm/yr and at pH 3.3 (25 °C) the corrosion rate was 7 mm/yr. At pH 5 (25 °C) the corrosion rate was reduced to about 0.3 mm/yr.

The filming amine corrosion inhibitor tested was not effective in mitigating corrosion with partial neutralization to pH 3 (25 °C), apparently due to either the polar headgroup not adhering to the piping or the tailgroup not providing the hydrophobic barrier in the absence of oil. There is a significant potential commercial advantage in partial neutralization if surface corrosion can be controlled. The natural acid produced from these wells can off-set the acid cost for pH-modification scale control at the power plants. Evaluations of other potential inhibitors are on-going.

Several magnesium silicate minerals can deposit from neutralized acid brine at NIL based on geochemical modeling. Scaling could be severe if caustic is substantially over-dosed to pH ≥ 6. A 2-stage neutralization process has been developed to minimize both scaling and corrosion.

Commercial CIS units were designed and built by Thermochem for automatic on-line 2-stage acid brine neutralization downhole and on the surface. Currently there are 7 CIS units at Sarulla.

REFERENCES

Cassidy, J. M., McNeil, R. I., and Kiser, C. E. (2007), "Understanding formic acid decomposition as a corrosion inhibitor intensifier in strong acid environments". SPE 106185.

Crossland, A., Woollam, R., Vera, J., Palmer, J., John, G., and Turgoose, S. (2011), "Corrosion inhibitor efficiency limits and key factors". NACE 11062.

Feng, Y., Siow, K. S., Teo, W. K., and Hsieh, A. K. (1991), "The synergistic effects of propargyl alcohol and potassium iodide on the inhibition of mild steel in 0.5 M sulfuric acid solution." Corrosion Science, 41, 829-852.

Gallup, D. L. (1993), "The use of reducing agents for control of ferric silicate scale deposition". Geothermics, 22, 39-48.

Ganefianto, N., von Hirtz, P., and Easley, E. (2015), "A Brief History of the Sarulla Geothermal

Field Development". Geothermal Resource Council Bulletin.

Hernández, J., Mora, Y. and Rivera, E. (2015), "Commercial Production Wells Acid 15 Successful Years of Activity, Miravalles Geothermal Field, Costa Rica". *Proceedings World Geothermal Congress 2015,* Melbourne, Australia.

Hirtz, P., Miller, J., and Prabu, E. (1990), "Operational Results of a Dry-Steam Resource Chloride Corrosion Mitigation System". *Geothermal Resources Council TRANSACTIONS, Vol. 14, Part II,* pp. 1667 – 1675.

Hirtz, P., Buck, C, and Kunzman, R. (1991), "Current Techniques in Acid-Chloride Corrosion Control and Monitoring at The Geysers". *Proceedings, Sixteenth Workshop on Geothermal Reservoir Engineering*, Stanford Geothermal Program, Stanford University, pp. 83-95.

Jayaperumal, D., Muralidharan, S., Subramanian, P., and Venkatachari, G. (1997), "Propargyl alcohol as hydrochloric acid inhibitor for mild steel – temperature dependence of critical concentration". Anti-Corrosion Methods & Materials, 44, 265-268.

Kelland, M. A. (2009), "Production Chemicals for the Oil and Gas Industry". CRC Press, Boca Raton, FL. Chapter 8.

Moya, P., Nietzen, F., and Sánchez, E. (2005), "Development of the Neutralization System for Production Wells at the Miravalles". *Geothermal Field Proceedings World Geothermal Congress 2005,* Antalya, Turkey.

Moya, P., Mora, Y. (2010), "Iron Meters for Production Wells at the Miravalles Geothermal Field". *Proceedings World Geothermal Congress 2010,* Bali, Indonesia.

Reyes, A. (1991), "Mineralogy, distribution, and origin of acid alteration in Philippine geothermal systems." Geological Survey of Japan Report, No. 277.

Reyes, A. (2000), "Petrology and mineral alteration in hydrothermal systems: From diagenesis to volcanic catastrophes." Geothermal Training Programme, Reykjavik, Iceland. Published in April.

Sugiaman, F., Sunio, E., Molling, P. and Stimac, J. (2004), "Geochemical Response to Production of the Tiwi Geothermal Field, Philippines", *Geothermics*, 33, pp 57-86.

Wang, H., Wang, H., Shi, H., Kang, C., and Jepson, P. W. (2002), "Why corrosion inhibitors do not perform well in some multiphase conditions: a mechanistic study". NACE 2276.

FIELD EXPERIMENTS OF DRILLING GEOTHERMAL WELLS USING PDC BITS IN JAPAN

Hiroyuki Imaizumi[1], Tetsuji Ohno[1], Hirokazu Karasawa[1], Kuniyuki Miyazaki[1], Eko Akhmadi[2], Masahiro Yano[2], Yosuke Miyashita[2], Naoto Yamada[3], Tetsuomi Miyamoto[3], Masatoshi Tsuzuki[4], Satoshi Kubo[4], and Yasuyuki Hishi[4]

[1]National Institute of Advanced Industrial Science and Technology (AIST),
[2]Mitsubishi Materials Corporation Central Research Institute,
[3]K. Maikai Co., Ltd. Chiba Factory,
[4]Japan Oil, Gas and Metals National Corporation
Email: hiroyuki.imaizumi@aist.go.jp, t-ohno@aist.go.jp, karasawa.h@aist.go.jp, miyazaki-kuniyuki@aist.go.jp, eko@mmc.co.jp, msyano@mmc.co.jp, miya@mmc.co.jp, naoto.yamada@kmaikai.co.jp, tetsuomi.miyamoto@kmaikai.co.jp, tsuzuki-masatoshi@jogmec.go.jp, kubo-satoshi@jogmec.go.jp, hishi-yasuyuki@jogmec.go.jp

ABSTRACT

Geothermal energy is one of renewable energies and the CO_2 emission from geothermal power generation is smaller than that from fossil power generation. Japan has the world's third largest reserve of geothermal resources (23,470 MW), however has only 530 MW (2.2%) of generation. To promote the geothermal power generation, it is important to shorten the lead time for the energy production and to reduce the drilling cost by using a high-performance drilling bit. In Japan, research and development regarding PDC bits targeting the drilling of geothermal wells is currently conducted. A PDC bit is one of fixed cutter bits and has lower potential of mechanical failure as compared with conventional roller-cone bits, while it is generally pointed out that a PDC bit has a problem with its durability, particularly when used in drilling hard rocks. We have developed and fabricated PDC cutters and matrix bodies of 8-1/2 inches PDC bits. Two PDC bits were used in two different sites of geothermal development in Japan and the drilling performance of the bits were observed. One bit has shown high drilling speed of 120 m per day in average (instantaneous maximum speed of 15 m per hour) and its life of 161 m against the rock layer composed mainly of tuff with approx. 120 MPa of uniaxial compressive strength (UCS). The other one has also shown the drilling speed of 48 m per day in average and its life of 109 m against the extremely hard and abrasive andesite layer with 150-200 MPa of UCS. No more than 1/32 inches gage loss was observed on the both bits after the field drilling tests. The differences in drilling speed and bit life between the two bits can be caused by the hardness or abrasiveness of the drilled rocks and/or their bit design, especially the back-rake angle of PDC cutters. The angle of the PDC cutters on the former bit was steeper than that on the latter.

Keywords: PDC bits, geothermal well drilling, Japan

INTRODUCTION

Geothermal energy is one of the principal renewable energies. Geothermal power generation discharges less CO_2 than fossil power generation and can stably supply electricity as compared with solar power and wind power generation. According to the report by METI, Japan (Ministry of Economy, Trade and Industry, 2017), total amount of geothermal resource in Japan is approximately estimated as 23,470 MW and is the third place of the world, following the United States and Indonesia. However, the actual geothermal power generation in Japan is only 530 MW.

It is pointed out that less development and/or less utilization of the geothermal energy in Japan is related to the construction cost and duration of geothermal power plant. Therefore, to activate the development and/or utilization of geothermal energy and to increase the electrical power plant capacity, reduction of drilling cost of geothermal wells is one of important factors. Development of drilling technique can directly reduce the cost and duration of the construction. Specifically, it is an urgent issue to develop drilling bit with higher drilling efficiency and durability.

Recently, use of PDC (Polycrystalline Diamond Compact) bits rapidly has been spread in the drilling wells for oil and gas, replacing conventional roller-cone bits. It is reported in 2010 that PDC bits (including diamond bits) account for an astounding 65% of footage drilled in oil and gas applications and still do not appear to have peaked in their development (Bellin et al., 2010). This is probably because that the PDC bits have replaced the roller-cone bits to drill the stratum mostly composed of soft to medium-hard rocks in the oil and gas development. However, the stratum in geothermal developing sites tends in general to be not only hard abrasive rocks such as granites but also heterogeneous with geological fractures. Consequently, this geological condition causes larger load for the drilling bits. Some trials using

commercially buyable PDC bits have been carried out at the geothermal developing sites in Japan. It can be summarized that research and development of the PDC bit as well as the PDC cutters for drilling geothermal wells is necessary to achieve the drilling with higher efficiency at lower cost compared to the drilling using conventional roller-cone bits.

In the present study, we developed several kinds of PDC cutters and manufactured two PDC bits with diameters of 8 and 1/2 inches, targeting application to the geothermal well drilling. We also conducted field experiments using the two PDC bits at two geothermal developing sites and acquired drilling performance of the PDC bits. We set the present goals of the drilling performance as follows:
- Drilling efficiency: 120 m per a day,
- Drilling length (Durability): 750 m for a PDC bit in drilling stratum (rocks) of uniaxial compressive strength (UCS) with about 100 MPa, and
- Gage loss of bit in drilling: less than 1/16 inches.

DEVELOPMENT OF PDC CUTTER

Since the early 1970s, PDC has become established as a high-performance and cost-effective alternative to conventional tools in the most demanding industrial applications, such as high-temperature drawing of wire (Anonymous, 1991), machining of metal matrix composites (Cook, 1998), fiber reinforced plastics, high Al-Si alloys (Clark and Sen, 1998), and abrasive wood composites (Clark, 1993), drilling in various rock formations (Feenstra, 1988), etc.

The process of manufacturing polycrystalline diamond compact cutters has been accomplished by sintering diamond powder on a cemented carbide substrate with Cobalt as a binder by applying high pressure and high temperature (HPHT) to the components (Field, 1992). The common actual region of the PDC sintering condition is shown in Fig. 1.

Referring to Fig. 2, a schematic view of an assembly of the sintering materials is illustrated in which a mass of a plurality of diamond particles are placed adjacent to a substrate. In this paper, the average diamond grains size used to form the polycrystalline diamond ranges from about 2 to 30 μm.

The combination of the high pressure and the heat allows the catalytic material (usually Cobalt) to flow from the substrate to the diamond enabling the diamond-to-diamond sintering process and the substrate to diamond bonding (Bertagnolli and Vale, 2000). An HPHT apparatus is utilized to exert the pressure and conduct an electric current to a cell assembly. The cell assembly is the combination of many components responsible for transferring the pressure, heating, and containing the samples to be sintered.

In particular, the temperature of the HPHT process was at least about 1,300 °C to about 1,800 °C, and the pressure of the HPHT process was at least about 5.0 GPa to about 8.0 GPa for a time sufficient for adjacent diamond particles to bond to one another, thereby forming an integral PDC compact having the polycrystalline diamond body and the substrate that are bonded to one another (Hall, 1975; Gledhill, Scott and Bird, 2017).

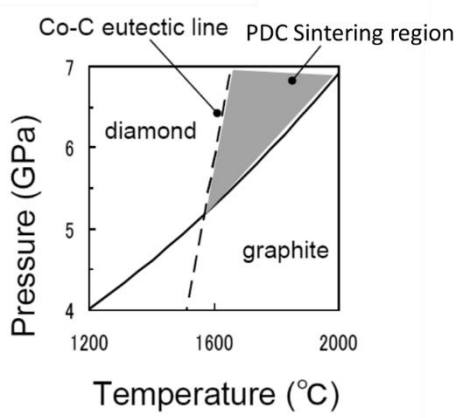


Figure 1: High pressure and high temperature sintering condition of polycrystalline diamond compact.

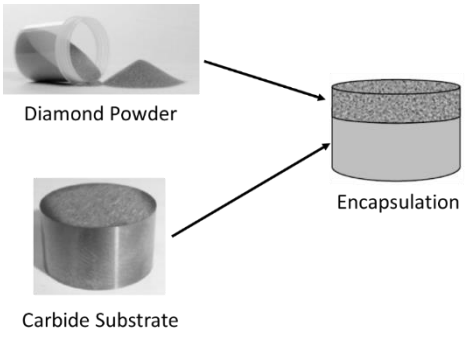


Figure 2: Schematic view of the encapsulation of the PDC starting materials.

Following formation of the integral PDC compact, the sintered body was processed through a variety of finishing operations to remove excess material and configure the sintered compact for use by an end user. Such finishing operations include grinding and polishing the outside diameter of the compact, cutting, grinding, lapping, and polishing the faces of the PDC, and grinding and lapping at least one chamfer into the sintered compact between the working surface and the outer diameter of the sintered compact.

As a final product, the PDC cutter as shown in Fig. 3 with a dimension of 13.44 mm in diameter and 8 mm in total thickness having a thick diamond layer of about 1.7 mm was made. The SEM observations confirmed that the microstructure of the PDCs showed uniform diamond grain distribution and sintered well. Fig. 4 (a) and (b) show the microscopy

photographs of PDCs with relatively fine and coarse grain sizes, respectively. The dark parts are diamond grains and the white areas are cobalt binders. It was clear that diamond grains are bonded to each other with some cobalt residual existing at the grain boundaries.

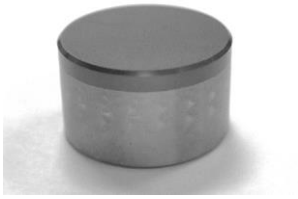


Figure 3: PDC cutter with 13.44 mm in diameter and 8 mm in thickness.

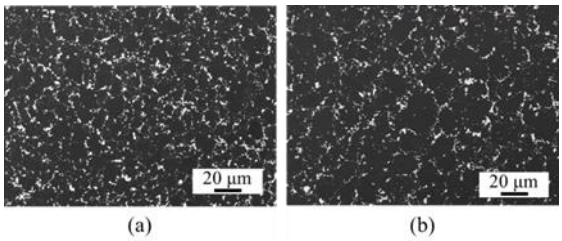


Figure 4: Microstructure of the PDC cutters. (a) high wear resistance type, (b) high toughness type.

The aim in using the fine and coarse diamond grains as a starting material was an attempt to make the high wear resistance PDC and high toughness PDC, respectively. In general, a negative correlation is observed between the abrasion resistance of PDCs and the grain size of the diamond grits (Deng, Nilen and Ozbayraktar, 1997). As the wear resistance is inversely proportional to the fracture toughness, which is directly a result of the inverse relationship between the hardness and the fracture toughness, high impact toughness PDC cutters with coarse diamond grains for tough and uneven drilling conditions and high abrasion resistance PDC cutters with fine diamond grains for drilling conditions where high wear is common, were successfully manufactured.

The wear resistance and the toughness of the above mentioned PDC cutters were evaluated at laboratory using turning lathe on granite log for the wear test and the industry de facto standard of drop-tower impact testing for the toughness evaluation before actual use in geothermal drilling field. The results of the wear and impact test are summarized in Fig. 5 (i) and (ii). From these graphs, it is confirmed that the PDC with fine diamond grains is high wear resistance type (a) and the PDC with coarse diamond grains is high impact type (b).

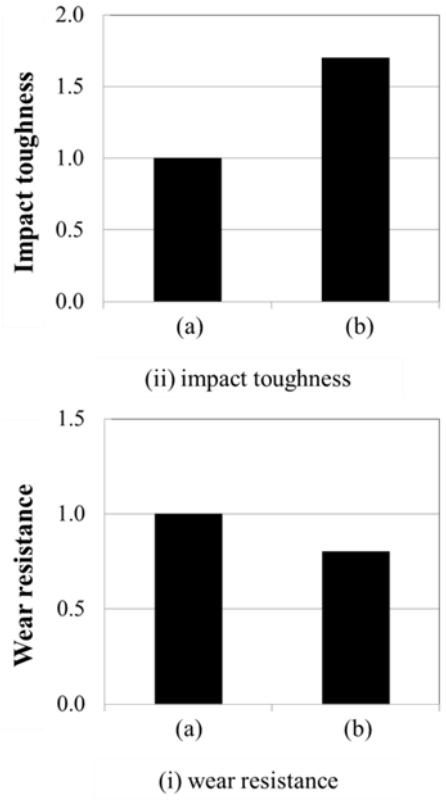


Figure 5: Characteristics of two types of PDC cutters. (i) wear resistance, (ii) impact toughness

MANUFACTURING TECHNIQUES OF PDC BITS

Conceptual design evaluation methods for two types of 8-1/2" PDC bits

To develop PDC bits applicable to the drilling of geothermal wells in Japan, two types of 8-1/2" PDC bits were designed targeting higher penetration rate and durability compared with that of conventional roller-cone bits. Both bits have eight blades so as to place many PDC cutters on the bit face to reduce the load (reaction force) worked on an individual PDC cutter. The two bits are hereafter referred to as "Bit A" and "Bit B". In the designing stage of the bits, structure analysis of the bits was carried out. Fig. 6 shows the 3D CAD model of Bit A designed using 3D CAD software (Autodesk Inventor Simulation 2016). Bit A has 50 PDC cutters with 13.44 mm in diameter arranged on its bit face. To equalize the reaction forces worked on the PDC cutters that are involved mainly in rock drilling, the structure analysis has been repeated iteratively to find better arrangement with less force of the PDC cutters under the general drilling conditions for the relevant bit size: the weight on bit (WOB) is 70 kN and the torque on bit (TOB) is 5 kN·m. As shown in Fig. 7, it was confirmed that the reaction forces were ever-increasing outward from the bit center, but those on the adjacent cutters were almost equal. Fig. 8 shows the result of the structure analysis performed under the same conditions of WOB and TOB on Bit B, which had additional 25 PDC cutters (backup

cutters) arranged behind the 25 cutters (primary cutters) in the nose and the shoulder of Bit A. The upper/lower dotted line shows the envelop of the reaction forces on the primary/backup cutters. The reaction forces of the primary cutters of Bit B were obviously smaller than those of the cutters of Bit A, as compared with the cutters at the same distance from the bit center.

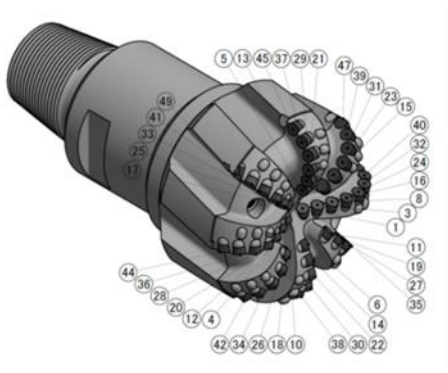


Figure 6: 3D CAD modeling for 8-1/2" PDC bit (Bit A).

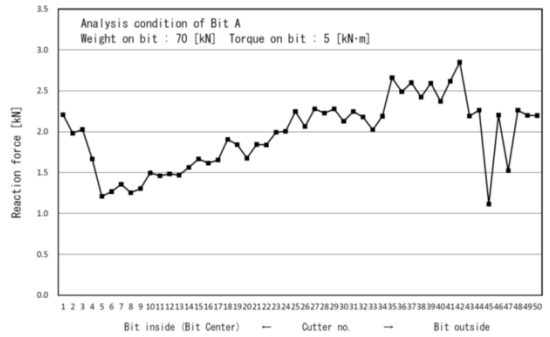


Figure 7: Distribution of reaction forces of PDC cutters on Bit A.

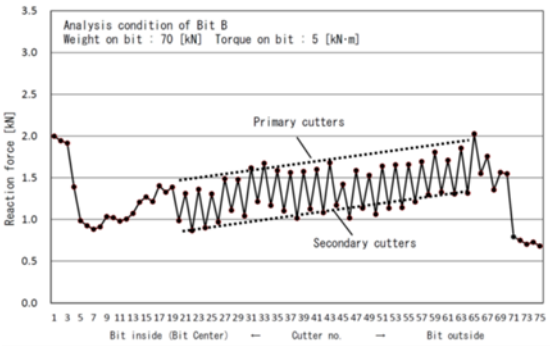
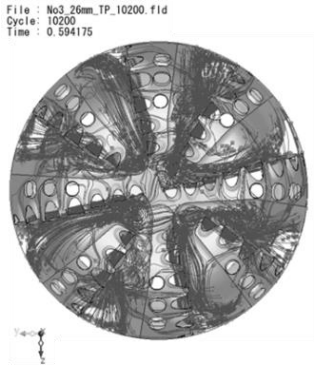
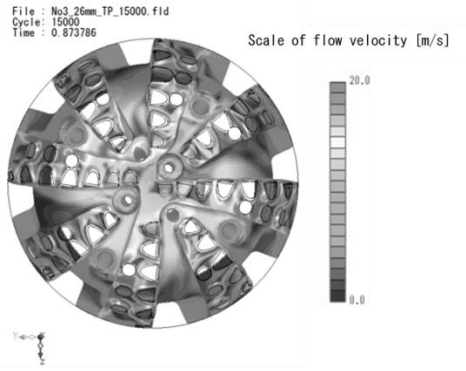


Figure 8: Distribution of reaction forces of PDC cutters on Bit B.

In addition to the arrangement of PDC cutters, the efficiency of the removal of cuttings is one of the important factors influencing the drilling performance of the bit. The visualization of drilling fluid flows was carried out by using the fluid analysis software SCRYU / Tetra V12 to verify the drilling fluid flow discharged from the nozzles and holes of Bit A. Autodesk Inventor Simulation 2016 was used for the 3D space modeling. The bit rotation speed was set to 200 rpm on the assumption that a top drive on the ground device and a downhole motor in the drilling hole were used in combination during drilling geothermal wells. Flow rate of the drilling fluid and its specific gravity were set to 1,800 L/min and 1.1, respectively, which are general drilling conditions for the relevant bit size. The particle tracking method was applied for the visualization of the trajectory of virtual particles in the flow. The trajectory of particles was thought to depend on the clearance between the surfaces of the bit blade and the hole bottom. In the fluid analysis, the clearance was set to "in-between space," which is intermediate between the "maximum space" and "minimum space." The former is in the case that the edges of cutters are just in contact with the surface of the hole bottom and the latter is that the surfaces of the bit blade, where the cutters are worn out, are in close contact to the hole bottom.



(a)



(b)

Figure 9: Flow simulation of drilling fluid (water) on the bit face of Bit A. Figures (a) and (b) show path lines of particles and flow velocity distribution, respectively. Bit rotation and flow rate are 200 rpm and 1,800 L/min, respectively.

Path lines of the particles arbitrarily selected are shown in Fig. 9 (a). Flow passages around the faces of PDC cutters on each blade appear to be sufficient although the clearance was restricted, and thus both the removal of cuttings and cooling of the PDC cutters are thought to be well performed. Fig. 9 (b) shows the flow velocity distribution, and it became clear that the flow velocity in the vicinity of two

water holes around the bit center was larger and that four nozzles placed outside the bit cone area contributed to increase of the flow rate around the secondary blades.

Fabrication of 8-1/2" PDC bit

By reference to the research reports (Agawani et al., 2016; Radhakrishnan et al., 2016; Schilling et al., 2016) which indicated that vibrations and impact shocks worked on the bit greatly affect bit damage and wear of the cutters during drilling, and under the geological condition that there are frequently hard formations with high abrasivity and heterogeneous strata in the geothermal development in Japan, the two 8-1/2" PDC bits corresponding to IADC code M433 were fabricated. For Bit A, the PDC cutters with "impact resistance" were used, and for Bit B, those with "wear resistance" were used. All of the PDC cutters were 13.44 mm in diameter. Specifications of both bits are summarized in Table 1. Bits A and Bit B have 8 blades and their bit face designs are basically common. For Bit A, relatively steeper back rake angle was adopted and aims at larger rate of penetration (ROP). Arresters (impact suppression chips) were attached on Bit A behind the PDC cutters in the shoulder and nose portions to protect the PDC cutters from excess vibrations and impacts. For Bit B, gentler back rake angle compared to Bit A was adopted with the aim of making the bit life longer. Moreover, the 25 backup cutters were placed behind the primary cutters in the shoulder and nose portions, where the load worked on the cutters became larger during drilling, and thus the PDC cutters were arranged in two rows on each blade.

FIELD EXPERIMENTS

The field experiment, in which the Bit A was used have been reported in detail as the technical report (Imaizumi et al., 2017).

Drilling performance of Bits A and B before field experiments

Prior to the field experiments, drilling test was conducted in a laboratory using Bit A and Bit B to obtain their initial drilling performance, which is hereafter referred to as "pretest." Fig. 10 shows a complete view of the drilling apparatus used in the pretest. Thrust and rotation forces are driven by a hydraulic unit and a direct-current motor, respectively. Drilling depth (the displacement of thrust yoke), WOB, TOB and rotary speed were measured using a displacement transducer, two load cells, a torque transducer and an electromagnetic tachometer, respectively. ROP was calculated by time derivative of the drilling depth. In the pretest, Emochi andesite (UCS = 79-98 MPa, average: 86 MPa) was used as drilled rock samples. During drilling, rotary speed was kept constant at 100 rpm and a drilling fluid (water) was circulated at a flow rate of 190 L/min to remove cuttings out of a bore.

Table 1: Specifications of 8-1/2" PDC bits newly developed for drilling geothermal wells in field experiments.

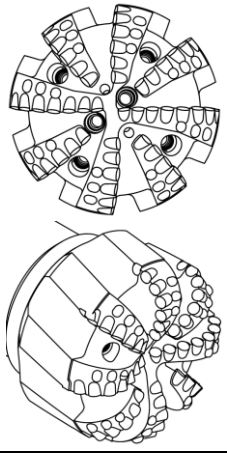
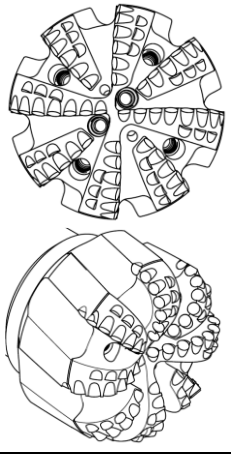
Developed 8-1/2" PDC Bit		Bit A	Bit B
Number of blade		8	8
IADC code		M433	M433
PDC cutter	Size	ϕ13.44 mm	ϕ13.44 mm
	Number of Primary cutter	50	50
	Number of Backup cutter	-	25
	Number of Gage cutter	8	8
	Total cutters	58	83
	Chamfer	exist	exist
Arrester		exist	none
Nozzle	Number of nozzle hole (Nozzle OD)	6 (ϕ20.4 mm)	6 (ϕ20.4 mm)
	Number of water hole (Hole ID)	2 (ϕ10 mm)	2 (ϕ10 mm)
Bit face			



Figure 10: Drilling apparatus.

Fig. 11 shows ROP-WOB relationship measured in the pretest. ROP increased linearly with WOB for both bits. ROP of Bit A reached as high as 50 cm/min (30 m/hr) when WOB is 25 kN. At equal WOB, ROP of Bit B was approximately 30 cm/min (18 m/hr). The main factor for the lower ROP of Bit B compared with that of Bit A is considered to be the difference in the back-rake angle of PDC cutters; the back-rake angle (< 0) of PDC cutters equipped with Bit B (−20°) is gentler than that with Bit A (−15°).

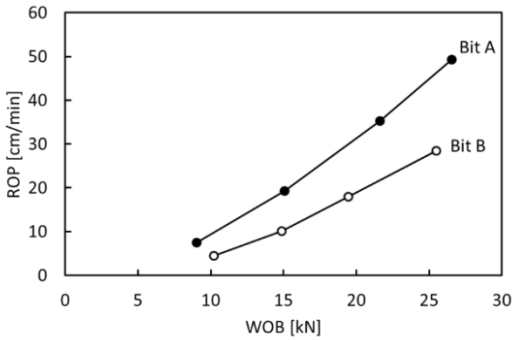


Figure 11: ROP-WOB relationship measured in the pretest using Bit A and Bit B.

Site specifications

Both of Bit A and Bit B were installed in two different sites of geothermal development in Japan: Bandai site (in Fukushima prefecture) and Kijiyama site (in Akita prefecture). Specification of the sites are summarized in Table 2. In each site, the drilling performance test was made as a part of drilling a structural boring well. The bits were used in the hold section (tangent section) of directional wells. The geological formation of the target well section in Bandai site consists of dacite tuff breccia and lapilli tuff with breccia. In the site, some rock cores were sampled from the well section just above the well section where Bit A was used. Its uniaxial compressive strength (UCS) obtained from the laboratory strength test was 122 MPa on average.

Table 2: Summary of site specifications, test conditions and results.

Site specifications		
Site	Bandai site	Kijiyama site
Well	Structural boring well (directional well)	Structural boring well (directional well)
Depth of target section (8-1/2" hole diameter)	1,600-2,000 m (hold section)	1,200-1,800 m (hold section)
Geological formation	Late Miocene dacite tuff breccia and lapilli tuff (mostly welded) with breccia	Neogene andesite lava and hornblende dacite pyroclastic rock (with basalt intrusive rock)
Uniaxial compressive strength (UCS)	122 MPa	150-200 MPa (estimated)
Test conditions		
Bit	Bit A	Bit B
Rotary speed	206 rpm (combination of downhole motor and top drive)	100-150 rpm (combination of downhole motor and kelly drive)
ABH angle	−	0.93°
Test results		
Drilled length (Measured depth)	161 m (1,756-1,917 m)	109 m (1st use: 1,210-1,249 m and 2nd use: 1,414-1,484 m)
Drilling time (bit-run time)	31 hrs	56 hrs
Average drilling speed (1 day = 24 hrs)	125 m/day	48 m/day
IADC dull grade (in/out)	3/3	1/3
Gage loss	< 1/32 in.	< 1/32 in.

Andesite lava and hornblende dacite pyroclastic rock were mainly drilled by Bit B in Kijiyama site. The UCS of the formation was estimated to be 150-200 MPa from the laboratory strength test conducted on the rock samples recovered from a different well in the neighborhood of Kijiyama site. Adjustable bent housing (ABH) system was employed in the drilling performance test in Kijiyama site. The bend angle was set to 0.93°.

RESULTS

Fig. 12 shows the changes in ROP and WOB with the drilled length in the field experiment for Bit A in Bandai site. The WOB was raised to 70 kN during the first 5 hrs of the test. The ROP reached about 16 m/hr with increase of WOB and continued to be kept until the drilled length of about 40 m. After that, the ROP slightly dropped to 11 m/hr and continued decreasing to 1.5 m/hr, while the WOB was almost constant at 70 kN. Then, the bit reached its life at the drilling time of 31 hrs. The drilled length was 161 m and thus the average drilling speed of Bit A was 125 m/day.

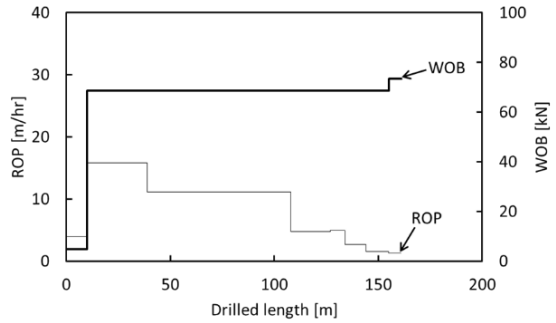


Figure 12: Changes in ROP and WOB in the field experiment for Bit A in Bandai site.

Fig. 13 shows the changes in ROP and WOB with the drilled length in the field experiment for Bit B in Kijiyama site. The WOB was gradually raised up to 30 kN. The ROP reached a maximum of 8 m/hr at the drilled length of 18 m, before the test was halted due to the unexplained decline of ROP at the drilled length of 39 m. Since the wear of the PDC cutters equipped with Bit B was very little, we decided to reuse Bit B in the same well after drilling subsequent formation with another bit. In the 2nd use, the ROP ranged from 2 m/hr to 5 m/hr while the WOB was maintained under 50 kN before the ROP decreased rapidly at the total drilled length of 82 m. At the drilled length, Bit B was considered to encounter with hard intrusive basalt from observation results of the cuttings. Bit B was continuously used with the WOB over 50 kN until the ROP decreased to 1 m/hr or lower. From the total drilled length (109 m) and drilling time (56 hr), the average drilling speed of Bit B was calculated to be 48 m/day.

Wear observation

Fig. 14 shows top-view images generated by 3D scanning of Bit A and Bit B after the field experiments. Dark grey area on each PDC cutter means the wear of the cutter. The large wear is observed on the PDC cutters on nose, taper and shoulder of both bits. IADC dull grades for inner/outer rows of Bit A and Bit B evaluated as 3/3 and 1/3, respectively. There were not chipped or lost cutters on Bit A. Although the wears on the primary PDC cutters of Bit B was smaller than that of Bit A, many primary cutters on the shoulder of Bit B appeared to be delaminated. One possible reason for this delamination is that the cutters on the shoulder of Bit B were exposed to large impact due to the employment of ABH system, by which Bit B is strongly made contacts to the rock strata. Gage losses for both bits were less than 1/32 in.

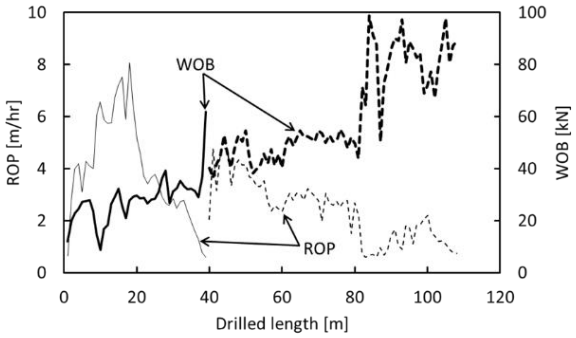


Figure 13: Changes in ROP and WOB in the field experiment for Bit B in Kijiyama site. Solid/Broken lines indicate the 1st/2nd use of Bit B.

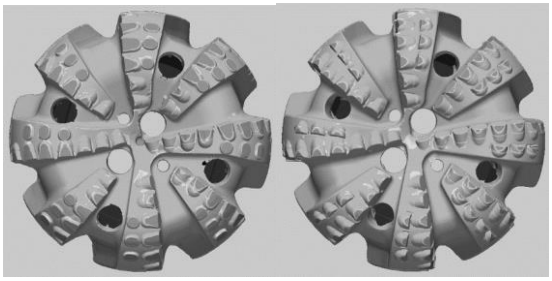


Figure 14: Top-view images of Bit A (left) and Bit B (right) after the field test.

Drilling performance of Bit A and Bit B after field experiments

To measure the decrease in drilling performance of Bit A and Bit B through the field use, they were subjected to the laboratory test again after the field test, which is hereafter referred to as "posttest." The posttest was conducted under the equal conditions with the pretest. The ROP-WOB relationship obtained in the posttest is shown in Fig. 15 by single logarithmic plot to display the results of the pretest concurrently. The ROP of both bits clearly declined due to the progress of wear of the cutters. Note that the ROP of Bit B was higher than that of Bit A after field experiment; the magnitude relation of ROP of

Bit A and Bit B was reversed through the field experiment, which is thought to occur because of the larger wear on the cutters of Bit A compared with that of Bit B as described above. As seen in Fig. 15, Bit B may still keep the potential to drill softer rock such as Emochi Andesite (UCS = 86 MPa) at the ROP of 1 cm/min (0.6 m/hr) with the WOB of 64 kN.

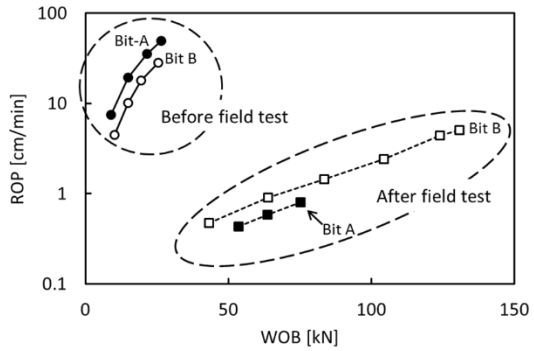


Figure 15: ROP-WOB relationship measured in the posttest using Bits A and B.

CONCLUSION

To develop the PDC cutters aiming at geothermal well drilling, we have established the manufacturing process by means of sintering diamond powder on a cemented carbide substrate with cobalt as a binder under HPHT. Appropriate combination of the high pressure and the heat allowed cobalt to flow from the substrate to the diamond enabling the diamond-to-diamond sintering process and the substrate to diamond bonding, and the control of the HPHT and the material grain size determined physical characteristics of the PDC cutters made in the process. Consequently, we successfully made the two types of PDC cutters having high wear resistance and high impact toughness by using the fine and coarse diamond grains as starting materials, respectively.

To achieve higher drilling speed and durability of the PDC bits, we have chosen a bit design with 8 blades on which larger number of PDC cutters can be installed and therefore the load worked on individual PDC cutter must be smaller. Specifically, arrangement of the PDC cutters has been determined through iterative structure analyses to make the difference in reaction forces between the adjacent cutters as small as possible. We developed two types of the PDC bits. One has a row of the PDC cutters (primary cutters) on each bit blade and the other two rows (primary and backup cutters). The former has relatively steeper back rake angle of the cutters with impact toughness which aims at higher drilling speed with the arresters just behind the primary cutters to decrease excess vibration and/or impact, and the latter relatively gentler angle of the cutters with wear resistance which aims at high durability of the bit.

Drilling performance of the two PDC bits was investigated at two different geothermal energy development sites. The drilled length and drilling time of Bit A/Bit B were 161 m/109 m and 31 hours/56 hours, respectively. Large wear of the cutters located from nose to shoulder of the both bits was observed. Especially some of the primary cutters on the shoulder of Bit B have been extremely worn and the diamond layers of the PDC cutters have been delaminated. Moreover, the gage loss of the both bits have been less than 1/32 inches. As compared to the present goals described in INTRODUCTION, target values concerning drilling efficiency and gage loss have been achieved, while the targeted drilling length (durability) remains unachieved. Note that the rock stratum encountered in our field experiments seemed to have higher UCS than expected. Therefore, research and development have to be continued in order to improve the characteristics of PDC cutter and the bit design.

ACKNOWLEDGEMENT

This study has been carried out as a research and development project of the Japan Oil, Gas and Metals National Corporation (JOGMEC). We would like to greatly appreciate to Tohoku Electric Power Co., Inc. as the developer and TEISEKI DRILLING CO., LTD. as the drilling contractor of Kijiyama site for understanding and cooperation to the research and development project.

REFERENCES

Agawani, W. et al. (2016), "Application Focused Drill Bit Engineering Delivers Consistent Improvement in Efficient Drilling Performance," *ADC/SPE-180673-MS*.

Anonymous. (1991), "Syndie & Monodie -The Largest Die Blank Range in the World," *Industrial Diamond Review*, **51(4)**, 168-172.

Bellin, F. et al. (2010), "The current state of PDC bit technology," *World Oil*, **September**, 41-46.

Bertagnolli, K. E. and Vale, R. (2000), "Understanding and Controlling Residual Stress in Thick Polycrystalline Diamond Cutters for Enhanced Durability," *Finer Points*, USA.

Cook, M. W. (1998), "Diamond Machining of MMC Engineering Components," *Industrial Diamond Review*, **58(1)**, 15-18.

Clark, I. E. and Sen, E. K. (1998), "Advances in the Development of Ultrahard Cutting Tool Materials," Industrial Diamond Review, 58(2), 40-44.

Clark, I. E. (1993), "PCD Wood Tools -a New Design Concept," Industrial Diamond Review, 53(2), 73-76.

Deng, L., Nilen, R. and Ozbayraktar, S. (1997), "The Effect of Diamond Grit Characteristics on the Microstructure and Abrasion Resistance of PCDs Sintered by HPHT," Proceedings of the 41st International Conference on Advanced Ceramics and Composites, 38 (3).

Feenstra, R. (1988), "Status of Polycrystalline Diamond Compact Bits: Part 1 -Development," Journal of Petroleum Technology, 40(6), 675-684.

Field, J. E. (1992), "The Properties of Natural and Synthetic Diamond," Academic Press, London, UK.

Gledhill, A., Scott, D. E. and Bird, M. W. (2017), "Polycrystalline diamond compacts having interstitial diamond grains and methods of making the same," US Patent Application No: 20170234077.

Hall, H. T. (1975), "Polycrystalline diamond composites," US Patent No: 3913280.

Imaizumi, H. et al. (2017), "Development of PDC bit for drilling geothermal wells," J. Geotherm. Res. Soc. Japan, 39(4), 217-227 (in Japanese).

Ministry of Economy, Trade and Industry. (2017), http://meti.go.jp/committee/sougouenergy/shigen_nenryo/pdf/022_04_00.pdf.

Radhakrishnan, V. et al. (2016), "Conical Diamond Element Technology Delivers Step Change in Directional Drilling Performance," IADC/SPE-180515-MS.

Schilling, J. et al. (2016), "Innovative Conical Diamond Element Bit Significantly Reduces Drilling Cost of Laterals," IADC/SPE-180499-MS.

BEST PRACTICE FOR MASTER VALVE CHANGE 2017 CAMPAIGN IN GEOTHERMAL INDUSTRIES

Ramadhan Primantara Harmanto, Paulus Panggabean, and Sigit Winarno

Star Energy Geothermal (Darajat & Salak) Ltd.
Email: uezg@starnergy.co.id; ppyu@starenergy.co.id; Sigit.winarno@starenergy.co.id

ABSTRACT

Master Valve Change program is a project opportunity captured in Well Intervention Opportunity (WIO), as one of end products of Geothermal Subsurface Reliability & Optimization (GSRO) process. These process is conducted through 4 steps, i.e. Well Surveillance, Analysis & Optimization, Well Intervention Program, Lookback & Lessons Learned. Through Well Surveillance, well integrity condition is monitored and updated in database. Included in well integrity monitoring parameters are casing integrity (monitored thru caliper log result and annual casing head thickness measurement) & valve condition (including existing master valve, side valves and top valve condition). Should any damage or malfunction is observed, the well should be included in Well Intervention Opportunity Register as candidate for Master Valve Change program that will be a part of Drilling & Completion team to lead the execution.

Keywords: Geothermal campaign, master valve, WIO, GSRO.

OBJECTIVES

This paper explains the success story of changing existing master valve and side valves with integrity issues (e.g. leaking, stuck open/stuck close, hard to operate). This procedure should be a common strategy of changing a malfunction valves utilized in geothermal industry since its exposure to high temperature - other than failure in maintenance - could also be a contributing factor to the valve's lifetime reduction in geothermal industry.

INTRODUCTION

The Darajat and Salak Geothermal Field are located near Garut City (for Darajat Field) and Sukabumi City (for Salak Field), West Java Province, Indonesia. It is a hot water and vapor-dominated geothermal resource operated by Star Energy Geothermal (SEG) with a total installed capacity over than 600 MW (Figure 1). Darajat Field initial development began operations in late 1994 with 55 MWe unit I, owned and operated by PLN (Rejeki et al, 2010) and Salak Field started its operations in February 1994 with the first two units totaling 110 MW, operated by the Indonesian utility company or PLN (Pasikki et al, 2015).

The Master Valve Change program of Darajat and Salak 2017 aimed to complete execution on selected wells in Darajat and Salak (from list of top critical wells) to maintain wellbore integrity. Successful execution should fully restore master valve and side valves function to isolate wellbore pressure and temperature. It will reset well flag from red to yellow or green in Well Analysis Summary flagging (depending on Well Integrity rating & Production Assurance rating) and also reduce well criticality rating, both as part of Formal Asset Review.

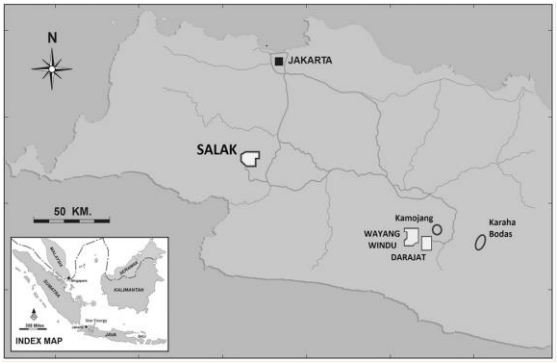


Figure 1: Map showing the location of the geothermal fields operated by Star Energy Geothermal, namely, Salak, Wayang Windu and Darajat. Also shown are the other geothermal fields in this geothermal province in West Java, Indonesia.

To be able to identify which valves to be changed, a monitoring program is in place as part of routine surveillance program. Through this monitoring program, valve condition on each well is updated. Valve damage or malfunction is mostly observed during logging program. In mechanical caliper survey, well production elbow is removed, hence existing master valve condition is obviously observed. Side valve condition is observed during well online. Should a steam is observed at rock muffler during well online then side valve connected to bleed line is leaking or malfunctioned. In the other hand, leak or malfunction of the side valve connected to instrumentation can be observed during maintenance of instruments (pressure gauge, transmitter). The current condition is then updated in valve database.

Master Valve Change was conducted to replace existing valves (master valve and side valves) installed at wellhead to ensure good isolation of wellbore pressure and temperature, to maintain wellbore integrity. By utilizing a lubricator and packer that was designed specifically for geothermal

well, the program was executed smoothly without any incident report started from the preparation and demobilization.

In lookback & lesson learned, these campaign was run successfully in previous 2017 based on agreed well objectives thru a comprehensive project package method conducted in timely manner.

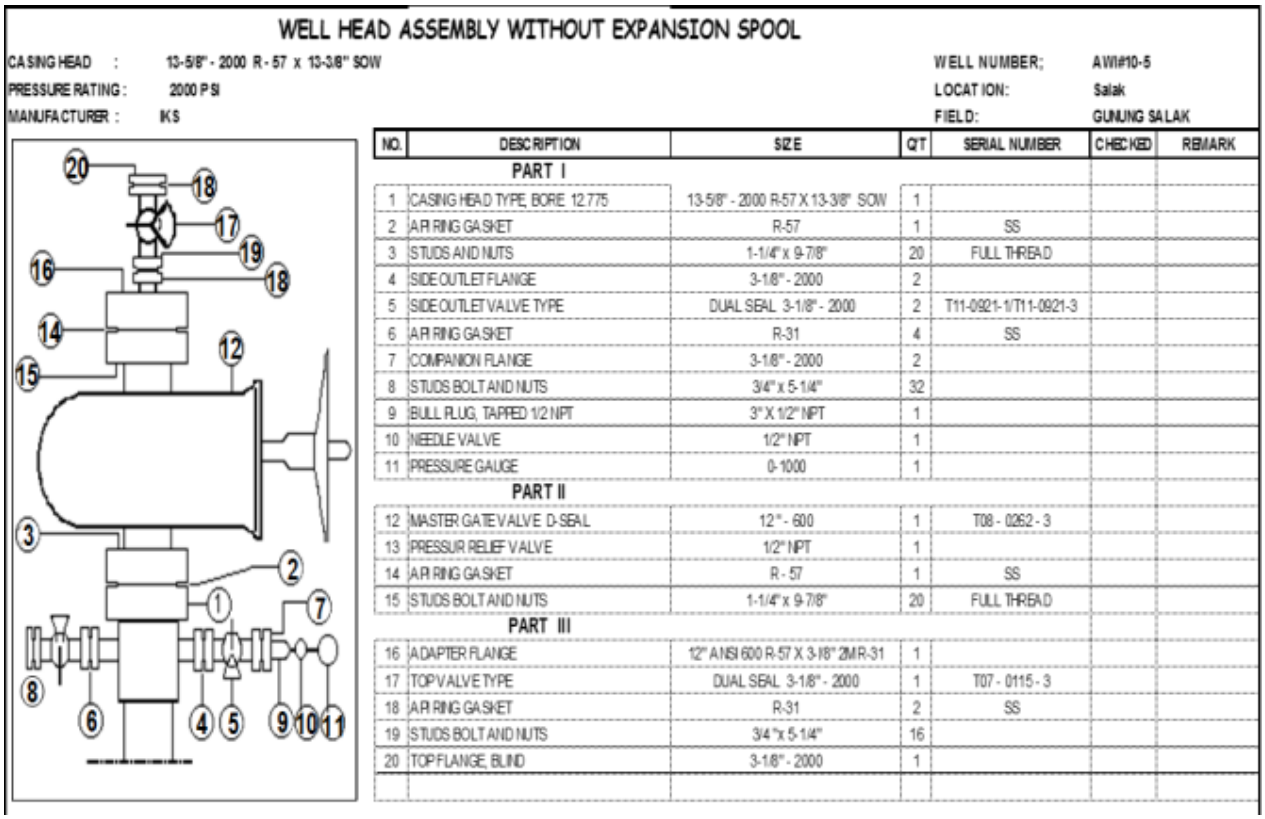
WELL SURVEILLANCE

Master Valve Change is a routine program conducted to replace existing valves (master valve and side valves) installed at wellhead to ensure good isolation of wellbore pressure and temperature, to maintain wellbore integrity. To be able to identify which valves to be changed, a monitoring program is in place as part of routine surveillance program.

Through this monitoring program, valve condition on each well is updated. Valve damage or malfunction is mostly observed during logging program. In mechanical caliper survey, well production elbow is removed, hence existing master valve condition is obviously observed. Side valve condition is observed during well online. Should a steam be observed at rock muffler during well online then side valve connected to bleed line is leaking or malfunctioned. In the other hand, leak or malfunction of the side valve connected to instrumentation can be observed during maintenance of instruments (pressure gauge, transmitter). The current condition is then updated in valve database.



Figure 2: Salak & Darajat Field Wellhead Schematic.



WELL HEAD ASSEMBLY WITHOUT EXPANSION SPOOL

CASING HEAD : 13-5/8" - 2000 R - 57 x 13-3/8" SOW
PRESSURE RATING : 2000 PSI
MANUFACTURER : IKS

WELL NUMBER: AWI#10-5
LOCATION: Salak
FIELD: GUNUNG SALAK

NO.	DESCRIPTION	SIZE	QT	SERIAL NUMBER	CHECKED	REMARK
	PART I					
1	CASING HEAD TYPE, BORE 12.775	13-5/8" - 2000 R-57 X 13-3/8" SOW	1			
2	A.R RING GASKET	R-57	1	SS		
3	STUDS AND NUTS	1-1/4" x 9-7/8"	20	FULL THREAD		
4	SIDE OUTLET FLANGE	3-1/8" - 2000	2			
5	SIDE OUTLET VALVE TYPE	DUAL SEAL 3-1/8" - 2000	2	T11-0921-1/T11-0921-3		
6	A.R RING GASKET	R-31	4	SS		
7	COMPANION FLANGE	3-1/8" - 2000	2			
8	STUDS BOLT AND NUTS	3/4" x 5-1/4"	32			
9	BULL PLUG, TAPPED 1/2 NPT	3" X 1/2" NPT	1			
10	NEEDLE VALVE	1/2" NPT	1			
11	PRESSURE GAUGE	0-1000	1			
	PART II					
12	MASTER GATE VALVE D-SEAL	12" - 600	1	T08 - 0262 - 3		
13	PRESSUR RELIEF VALVE	1/2" NPT	1			
14	A.R RING GASKET	R - 57	1	SS		
15	STUDS BOLT AND NUTS	1-1/4" x 9-7/8"	20	FULL THREAD		
	PART III					
16	ADAPTER FLANGE	12" ANSI 600 R-57 X 3-1/8" 2M R-31	1			
17	TOP VALVE TYPE	DUAL SEAL 3-1/8" - 2000	1	T07 - 0115 - 3		
18	A.R RING GASKET	R-31	2	SS		
19	STUDS BOLT AND NUTS	3/4 "x 5-1/4"	16			
20	TOP FLANGE, BLIND	3-1/8" - 2000	1			

Figure 3: Salak & Darajat Wellhead Schematic

Updated valve database is one of several inputs during well criticality update process. A well with damaged or malfunctioned valves will have higher criticality on wellhead integrity. Same data is also used in well analysis summary. In the end, it will result on a list of well candidates for Master Valve Change program.

WELL WORK OPPORTUNITY MANAGEMENT

The master valve change project was started with analysis phase. The analysis phase is divided into project risk analysis, well criticality analysis, and SWOT analysis. Those analyses delivered the comprehensive result in selecting the well candidate that will be executed for changing the master valve.

Project Risk Analysis

Technical project analysis was conducted by listing out all potential risks and each mitigation plan for executing the project. Project risks such as: insufficient steam buffer, lack of man power, lack of caliper data, and motor vehicle crash. Those project risks should be mitigated soon to avoid any project deviation.

Insufficient of steam buffer is the highest priority to be mitigated due to the urgency of master valve changing when steam buffer is still available. Lack of man power from other related department, such as Mechanic Support is the other project risk and it shall be mitigated by doing the project before or after other big scale other department project. Each project planner shall share and communicate early with other department in providing additional manpower as necessary.

Lack of caliper data on some candidate wells will be a driver for project team in estimating the packer setting depth inside the wellbore. These caliper data shall be provided by conducting the update of caliper logging job and ensuring the casing tally is right or correlating the location of casing connection.

From table 1, after taking into account valve condition, business impact, wellwork candidate for well clean out/acid, impact on surveillance program, steam supply buffer, caliper data availability and requirement to change casing head, candidates with highest round score for Darajat are DRJ-16 and DRJ-12.

Table 1: Darajat Well Candidate Assessment

No.	Well	MV Condition: *1. Hard to operate *2. Minor passing *3. Hard to operate, severe leak	Business Impact: *1. < 5 kg/s *2. 5 - 10 kg/s *3. > 10 kg/s	Wellwork Candidate: *1. Not planned *2. Planned within 5 years *3. Planned for next year	Impact on Surveillance	Steam Supply Buffer: *1. Unit-3 (no buffer) *2. Unit-2 (10 - 20 kg/s buffer) *3. Unit-1 (> 20 kg/s buffer)	Round Score	Caliper Data Availability	Require Casing Head Change?
1	DRJ-16	3	3	1	3	1	11	NO	NO
2	DRJ-12	3	1	2	2	3	11	YES	YES
3	DRJ-18	3	2	1	2	2	10	YES	NO
4	DRJ-7	2	2	1	2	3	10	YES	NO
5	DRJ-5A	2	2	1	2	3	10	YES	NO
6	DRJ-21	2	3	1	2	1	9	YES	NO

Table 2: Salak Well Candidate Assessment

No	Well Name	Type	Well Production (kph)	Well Status	MV Size	MV Condition
1	Awi 9-9	Producer	369.57	ON	12" #600	Good (upgrade Spec)
2	Awi 10-5	Producer	180	ON	12" #600	Passing
3	Awi 10-4	Producer	147.8	OFF	12" #600	Passing

				SCORING				
No	Well Name	MV Size	MV Condition	Risk Assessment Result	Business Impact	Status	Total Score	Caliper Data (< 2 yrs)
1	Awi 9-9	12" #600	Good (upgrade Spec)	7	1	0	8	3-Jan-17
2	Awi 10-4	12" #600	Passing	7	3	0	10	n/a
3	Awi 10-5	12" #600	Passing	7	2	1	10	n/a

Nonetheless, DRJ-16 has no caliper data and its acquisition will require well kill first since the master valve is stuck open (cannot be fully closed). Not to mention that it also has wire fish inside wellbore. While DRJ-12 has problem with its casing head where changing casing head will involve more risk and more cost. Hence, the top following candidates for Darajat 2017 Master Valve Change are DRJ-18 and DRJ-7 (Star Energy, 2017).

From table 2 above, after taking into account valve condition, business impact, well status, risk assessment and caliper data availability candidates with lowest score for Salak are AWI 9-9, AWI 10-5 and AWI 21-2. Nonetheless, AWI 10-5 has no caliper data and it plan to get caliper data once fishing job is completed.

All well candidates should be included on well criticality assessment that was relied on HES risk table 6x6. Other analysis that was utilized, project team generated the SWOT analysis as shown in table 4.

Table 3: Well Criticality Table

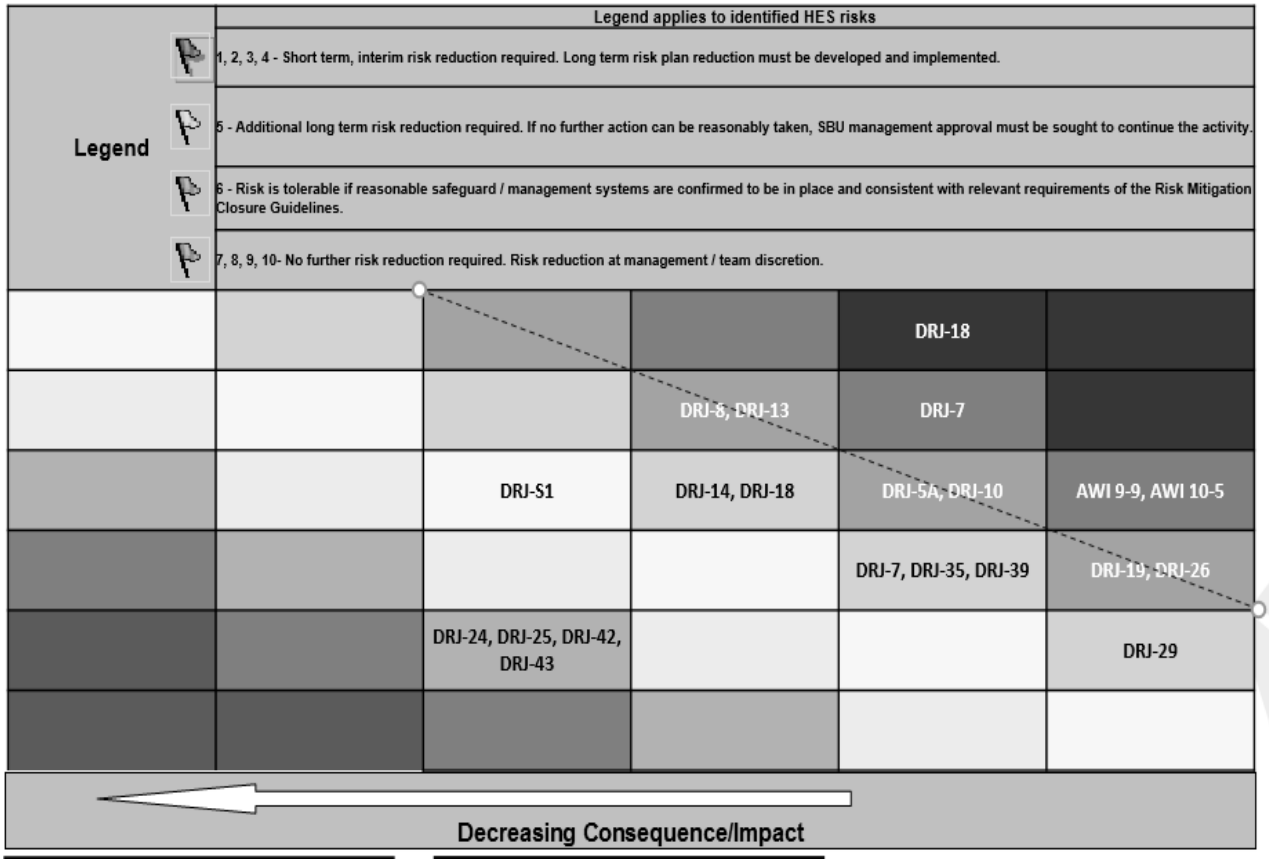


Table 4: Project SWOT Analysis for MV Change Campaign

Strengths (internal to SE or project)	- Support from Salak & Darajat Asset Management (e.g. works required from O&M will be communicated thru Work Order(s)) - Experienced multidisciplinary team member from previous 2016 MV Change program (Chevron Geothermal Company, 2016) - Existing TNG contract - Available master valve, side valve stock (brand new and ex-used) for well candidates at Salak & Darajat - Commitment from management to conduct Darajat & Salak Master Valve Change
Weaknesses (internal to SE or project)	- Current TNG contract will be expired by the end of year. - Double block procedure is currently not available - Limited steam supply buffer for Darajat
Opportunities	- Showcase Star Energy for compliance to Safety, health, and Environment - Eliminate potential losses (financial & reputation) from possible well control problem
Threats	- Community issue during program preparation/execution - Mobilization issue - Force majeure

The SWOT analysis is one of analysis tools for project team in filtering the urgency executing the project by comparing the strengthen, the weaknesses, the opportunities and threats that will impact to project campaign.

After analysis phase, then continued with operation preparation phase that was defined by the cost estimation, VBWO, RACI chart, and risk assessment. The cost estimation for master valve change project was depended by the field location and valve material utilized.

VBWO (Value Based Well Objective) is the minimum measurement from one well job that must be aligned together within all department in assessing the well project successes. For these project, VBWO covered IFO (incident Free Operation), well control handling, and AFE project that must be 10 % variances. By utilizing SMART goal in setting the goal, it delivered a good result.

RACI (Responsible, Accountable, Consulted, Informed) Chart will help the project team in pointing the right party to be communicated for any project handling. In these master valve change project, the parties were Drilling and Completion, Operation and Maintenance, HES (Health, Environment, and Safety), Production, and each function of leadership management. RACI chart should be agreed by all parties to get awareness of each job procedures on-site.

Risk Assessment for these project was divided into 5 sections, started from the early mobilization and demobilization, scrapping of scale inside the wellbore in first 50 feet, well isolation using TNG packer, master valve and wing valve installation, and production time (TNG, 2016). Risk assessment created to address the existing safeguards already in place, scoring of existing safeguards, and additional safeguards that may help to increase the scoring of risk mitigation.

In the field operation phase, there were defined into 4 stages: Pre-Mobilization stage, Mobilization stage, Installation stage, and Packer releasing stage. Each stages will generate the individual procedure on field that should be elaborated among department.

Pre-Mobilization Stage

Pre-mobilization stage included PT. TNG, Asset Department, HSE, and Operation and Maintenance department. These stage was the beginning of on-site execution phase. There was some action conducted to align all parties, such as: Obtain all necessary Work permits, conduct pre-installation pressure test to all the replacement valves following the API Specs 6A or API Specs 6D standards. Record the pressure test using Barton Chart. Test the 12" Class 600 master valves, 3" Class 600 wing valves, and 3-1/8" API 2M wing valves. All of records shall be well-documented and stored as main Company asset.

Conduct wellhead and site inspection with Asset Group and business partners. These wellhead and site inspection to obtain the update of actual field condition in arranging the well lay-out and transportation strategy. Site inspection shall be conducted 3 weeks prior equipment mobilized to field. Figure 7 shows the on-site arrangement of PT. TNG equipment.

Beside the main equipment from PT. TNG, all supporting heavy equipment and light vehicle should be installed DIMS. Prepare JMP & load matrix for mobilization inter well.

Asset O&M Group to shut-in the well one-two days prior to valve change. Install scaffolding around the wellhead. Remove the production line and fence as per site survey conducted as per shown in Figure 8 (if necessary). Executing the shut-in well shall need the well pressure built-up historical data, if the well has a fast build-up, then project team shall provide the killing pump to mitigate the well built-up risk.

Table 5: VBWO Salak AWI 10-5 Well

SALAK Wells VBWO
AWI 10-5
Master Valve Change Campaign 2017

Item	Priority	Project Objectives	Measure	S	M	A	R	T
1	High	Incident and accident free	Zero incident (DAFW, TRI, MVC)	✓	✓	✓	✓	✓
2	High	Maintain well control at all times	Zero uncontrolled flow	✓	✓	✓	✓	✓
3	Medium	Total project cost	Actual cost is ±10% from approved AFE budget (Salak AFE)	✓	✓	✓	✓	✓

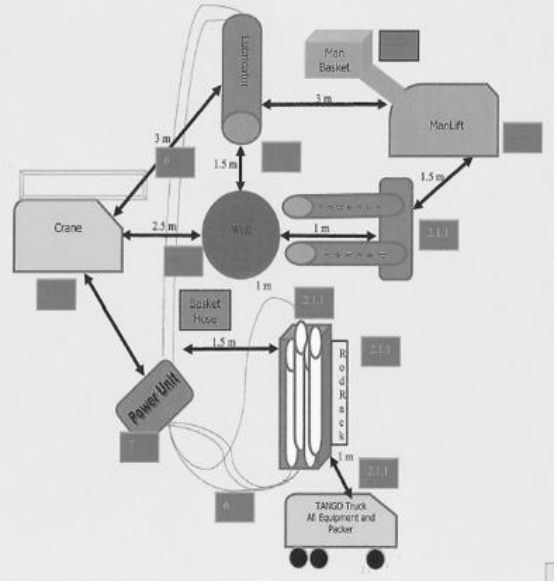


Figure 7: Pad Lay-Out for Geothermal Packer Installation.

These back-up killing pump shall be ready on-site with baker tank, and water delivery system. Digital pressure gauge and flow meter at the backside (wing valve) are installed and enough baker tanks are available. Proper temporary piping restraint system was utilized, the flow meter at back side pumping line was installed, all lines were pressure and flow tested. Flush all manifold to ensure no debris or solid trap, prepared additional quenching line to be able pump in to well thru both wing valves if required, ensured delivered flow rate to the pad is higher than minimum flow rate required for killing operation (MQR projection + safety factor).



Figure 8: Scaffolding installed on master valve without pipeline.

Mobilization Stage

Mobilization stage covered the field preparation when all equipment was on-site. List of activities in this stage were:

1. Secure work permit from Operations Group. Check the temperature of the wellhead.
2. Conduct pre-job safety meeting and hazard hunt. Discuss valve change procedure and JSA.
3. Mobilize 50-ton crane, man lift, boom truck, and TNG equipment to location. Conduct pre-use inspection and prepare JMP for all vehicles.
4. Implement H2S management plan. Install H2S monitor, bug blower, and wind sock. Assign 2 muster points. Use H2S monitor to check wellhead and cellar area to determine any potential presence of H2S. Prepare SCBA and form a rescue group. Conduct H2S orientation and SCBA training. Conduct H2S drill prior to start of each valve change operation. O&M to provide tanks filled with water for bleeding NCG.
5. Unload and rig-up the TNG equipment as per Figure 7. Redress the packer. Install barricade around the high pressure lines and the TNG working area.
   a. DSM to verify the certification of the O-ring and packing element is suitable for geothermal use.
   b. Install proper restrain on the high pressure lines.
6. Valve mechanics to bleed-off the trapped gas between service valve and adapter flange. Keep the service valve close. Open the master valve and inject packing to its pack-off assembly. Prepare well for installation of the TNG lubricator.
7. Install calibrated pressure gauge on one of the wing valve for wellhead pressure monitoring. Prepare Barton Chart to record pressure during inflow test, which will be installed on the bleed valve of the lubricator.
8. Pressure test TNG lubricator equipment.
   a. TNG will provide the written safety procedure for all pressure tests.
   b. Connect Hydraulic Hose.
   c. Check and take picture of Stripper Rubber condition. Replaced as necessary.
   d. Perform a lubricator stump test and record the pressure test chart. If there is a leak, do not proceed until leak is repaired. Release pressure after finish.
   e. Re-correlate TNG depth to Original KB depth refer to well candidate

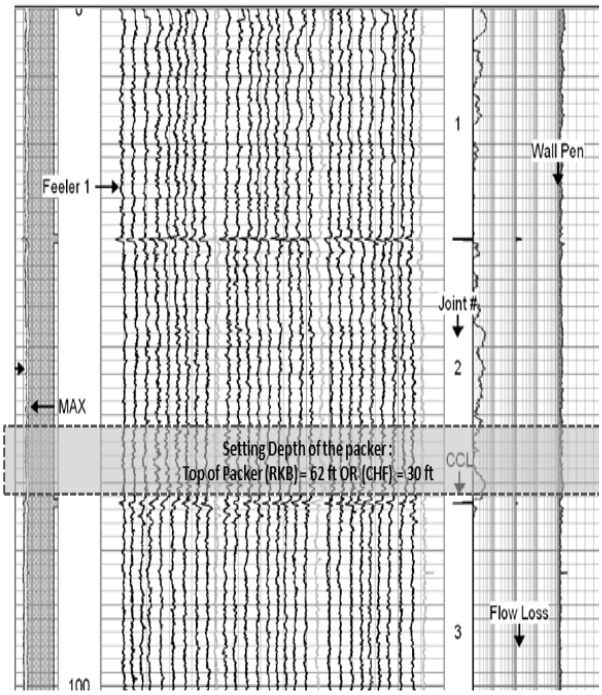


Figure 9: Caliper Survey with a depth of Top of Packer at 62 ft or 30 ft below casing head flange.

A setting depth should be located not in casing collar depth and free-scale wellbore. If packer was located in wrong depth, packer would set hardly or should be resettled.

Installation Stage

Installation stage was started with make up 13-3/8" mill and casing scraper inside the lubricator. N/U lubricator on top of 12" Class 600 service valve. Pressure test the flange connection between service valve and TNG lubricator using wellbore pressure. Monitor pressure for 10 minutes. The pressure should be equal to the shut-in pressure of the well and remain constant. Check the flange connection for potential leaks. These step should be confirmed properly to avoid any unexpected incident when packer installed inside wellbore.

Run-In-Hole 13-3/8" mill and casing scraper to clean out 13-3/8" tieback casing in early 50-65 ft-MD (equivalent to 38 ft below CHF). Pulled out of hole mill and casing scraper inside the lubricator and close service valve. Bleed-off pressure. Nipple down lubricator and laid down mill and casing scraper. Inspected mill and scraper for any sign of casing problems, such as casing parted.

Make up 13-3/8" TNG geothermal packer inside the lubricator and nipple up lubricator back to the top of service valve. Opened the 12" Class 600 service valve slowly. Pressure test the flange connection between service valve and TNG lubricator. Monitor pressure for 10 minutes. The pressure should be equal to the shut-in pressure of the well and remain constant. Check the flange connection for potential leaks.

Run-in-hole geothermal packer and set the top of the packer at around 50-65 ft-MD. Each well has a different setting depth, and prepared 5 ft upper/lower estimation if packer does not seal). Confirm if the packer slips were properly set by conducting push test to 30,000 lbs and pull test to 77,000 lbs, and confirm if the rubber element is energized by inflow test. Push and pull test should be passed to achieve the inflow test.

Conducted an inflow test the TNG geothermal packer. Bleed trapped pressure inside the lubricator slowly. Monitor pressure build-up inside the lubricator for 30 minutes. Open the bleed valve and check for flow. Any build-up shall not exceed 10% of the initial shut-in pressure over the 30 minutes, these to accommodate potential temperature effects.

Disconnected the running rod from the set TNG geothermal packer. Pulled of hole running rod. Nipple down the lubricator, service valve, and old master valve. Conducted dye penetrant test on casing head top flange (by O&M Team). Check flange for ring groove for any cracks.

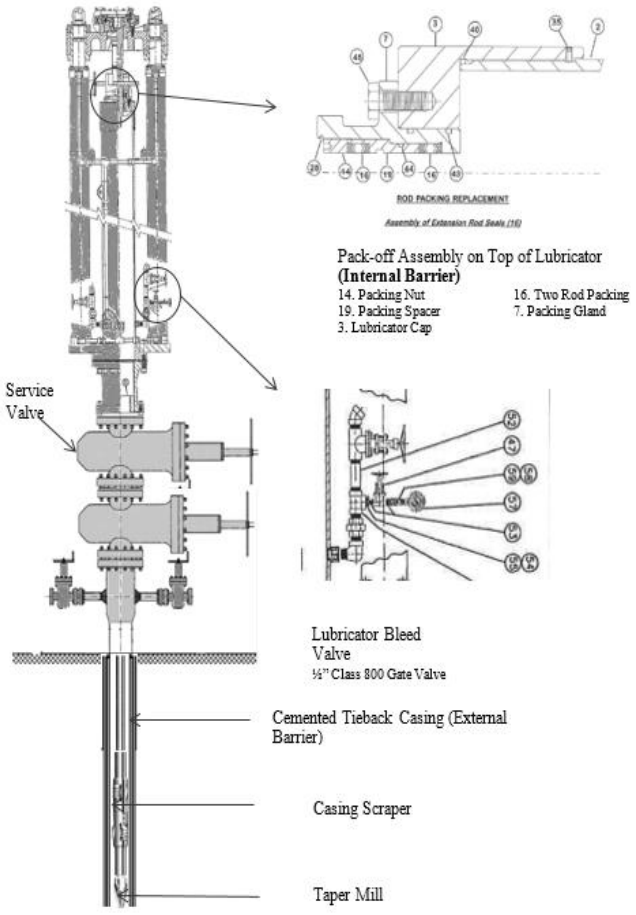


Figure 10: Barrier Configuration while running and TOH the packer.

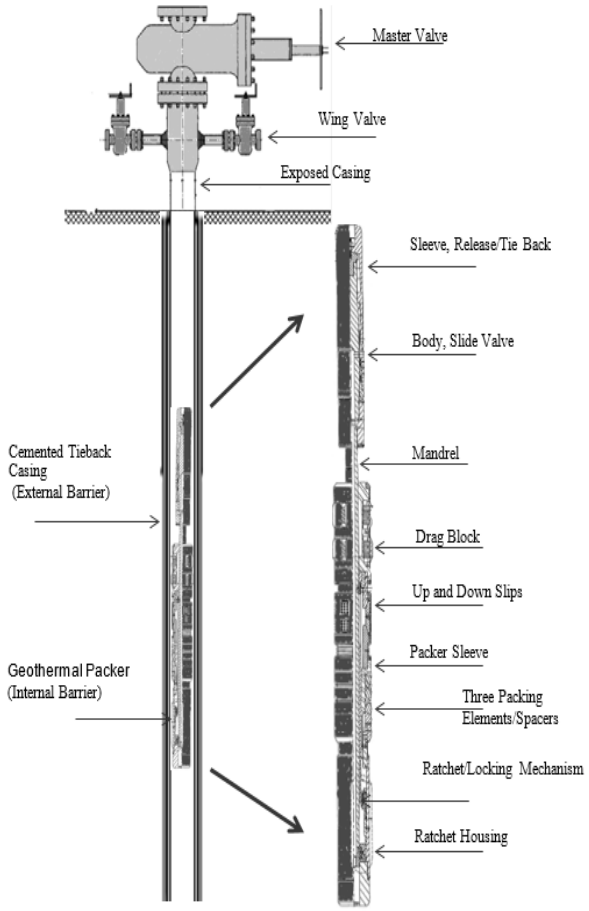


Figure 11: Barrier Configuration during wellhead valve installation.

Installed the new master valve. These master valve should be available and properly tested prior installation. Some wells might be installed with additional adapter if different class size (class 600 and class 900). Utilized new RX-57 ring gaskets with API monogram and xylan platted bolts/nuts. Torque-up 1-1/4" X 9-7/8" bolts properly. Followed bolting pattern when making-up flange connection. Mention the serial number of the master valve (old & new) in the daily report.

Nipple up lubricator on top of the new master valve with a closed bleed valve. Open the new master valve. RIH running rod and connect to the packer. Replaced the wing valves and utilized new RX-31 ring gaskets with API monogram and xylan platted bolts/nuts. Torque-up ¾" X 5-3/4" bolts properly. Followed bolting pattern when making-up flange connection. Mention the serial number of the wing valves (old & new) in the daily report. While doing a wing valve replacement, one of wing valve should be connected with kill line as a contingency plan if well pressure existed.

Opened the equalizing valve to allow well bore pressure to equalize in the lubricator. Observed for leak at the same time testing the wing valve & flange connection for 10 minutes. The pressure should be equal to the shut-in pressure of the well and remain constant. Check the flange connection for potential leaks. In case of leak, closed the equalizing valve. Conducted push and pull test and inflow test to confirm that packer is still holding. Bleed off pressure inside the lubricator before conducting any repair.

Retrieved geothermal packer inside the lubricator as per TNG Procedure (TNG, 2016). Closed the master valve. Bleed trapped pressure. Nipple down lubricator and Laid down the packer. Well should be secured after that and handed over to Asset Team.

PROJECT PERFORMANCE

Master valve change 2017 project delivered a good result that was exceeded than the plan for some wells. This achievement drove the efficiency of project cost until 25%.

Mobilization time and operation time summary for master valve change project previous year was shown on Figure 13 and Figure 14.

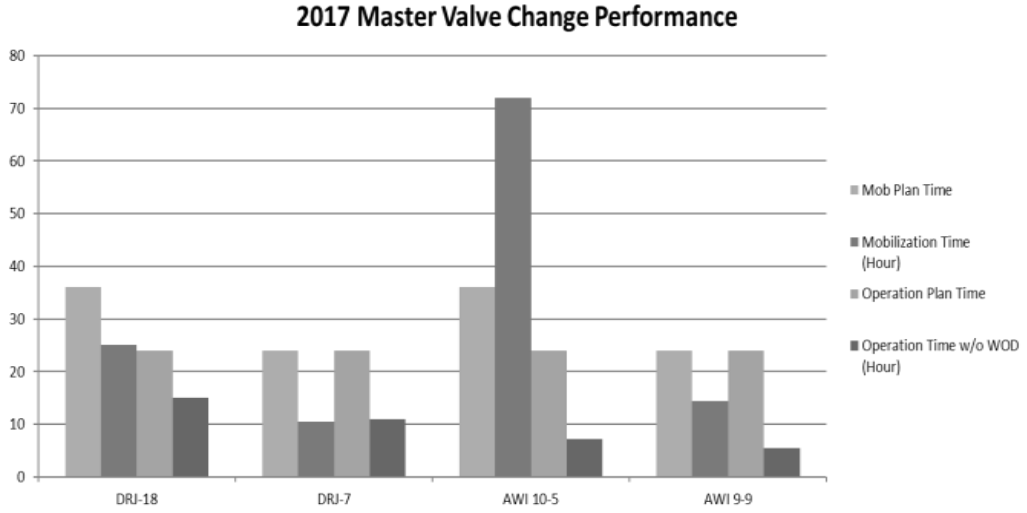


Figure 12: 2017 Master Valve Change Performance Result Chart.

Mobilization time summary in Figure 13 presented two wells has lesser hours than others, due to short distance inter well, while others needed inter field movement.

Operation time in Figure 14 below here displayed the consecutive reducing operation time from the beginning of project, and achieved best-in-class for 5.5 hours for one well execution.

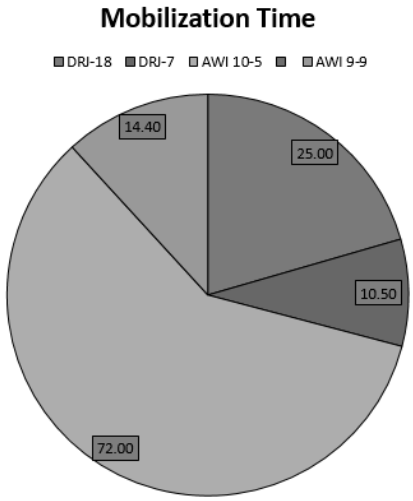


Figure 13: 2017 Master Valve Change Performance Result for Mobilization Time.

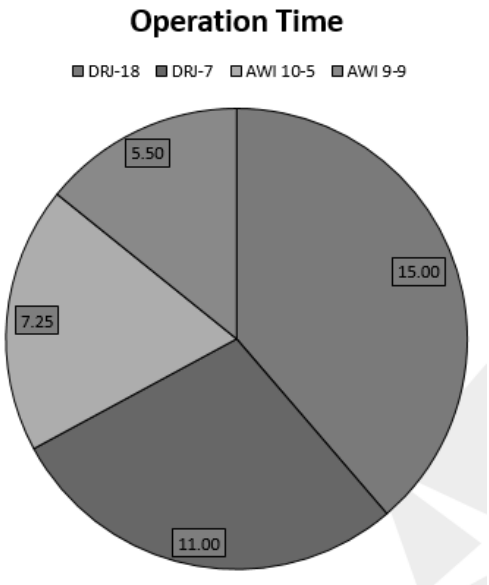


Figure 14: 2017 Master Valve Change Performance Result for Operation Time.

LESSON LEARNED

Some lesson learned in previous 2017 Master Valve Change campaign acquired during the preparation, execution, and post-execution phases (Star Energy, 2017). In preparation phase, project team should conduct a longer review on pipeline modification design to compensate the substitution of valve series, and coordinate with other company business entity in arranging a similar project, so moving schedule can be well-optimized.

In execution phase, some lesson learned were attained, such as preparing the back-up killing pump to kill the well prior execution, reducing the flange connection testing time from 30 minutes to 10 minutes, and changing the master valve first, then continued with wing valve for the final installation. These changing schedule will let executor team has a specific line to kill the well as contingency plan.

In post-execution phase, contractor invoice restatement was a good lesson learned in encouraging each contractor to confirm the field cost estimation before company representative approval.

CONCLUSION

Wellhead packer equipment has been successfully applied in the geothermal setting in various wells and project in Star Energy Geothermal (Salak & Darajat). A review of the projects on how the technology has been used effectively around the geothermal company in proceeding the changing of passing master valve set.

Master valve project is a regular project that is planned in Star Energy Geothermal (Salak & Darajat) in regards to maintain the wellhead integrity of the well. Project team always penetrate the best lesson learned to achieve the safer, the better, and the faster project execution.

ACKNOWLEDGMENT

We thank to Star Energy Geothermal Company (Salak & Darajat), PT. TNG (Mr. Nurman Sitanggang and team) and other business partner company who were elaborated in this project.

REFERENCES

Chevron Geothermal Company. (2016), "Master Valve Change Campaign record".

Pasikki, R. G., Maria, R. S., Abdurachman, F., and Peters, C. (2015), "Potential Utilization of Idle Wells in Salak Geothermal Field, Indonesia". *Proceedings World Geothermal Congress 2015.*

Rejeki, S., Rohrs, D., Nordquist, G., and Fitriyanto, A. (2010), "Geologic Conceptual Model Update of the Darajat Geothermal Filed, Indonesia". *Proceedings World Geothermal Congress 2010.*

Star Energy. (2017), "Master Valve Change Programs for 2017 Campaign in Darajat and Salak".

TNG. (2016), "Standard of Procedure Packer – WI No. 03 revision No.1".

SUCCESSFUL OPERATION OF CLEAN OUT WELL WITH HWU AT WAYANG WINDU

Ridha Budi Nugraha, Redha Bhawika Putra, and Mulyadi

Star Energy Geothermal
Jl. Asia Afrika No 8 Jakarta
Email: ridha.nugraha@starenergy.co.id

ABSTRACT

MBA-C well is a geothermal well on-shore Wayang Windu drilled in 2007 completed with 10-3/4" perforated liner set at 1599 mMD. This well has scaling problem, mainly from silica which is common for a geothermal well. Initial production rate after drilling on this well was 46 kg/s. Production rate keep declining afterward down to 20 kg/s prior project execution. There were several initiatives to clean out this well to regain the performance to avoid short steam supply on the past such as well broaching, well washing, and CTU, but the result was not satisfied. Several alternatives of work over unit are evaluated to execute this project. Lessons learned from previous project in Wayang Windu indicated that Hydraulic Workover Unit (HWU) may perform higher success ratio to clean out and acidize the well. Technically, this is due to higher push capability and its rotary capability compare to CTU. It also has less equipment loads and smaller wellpad space requirement compare to workover rig. Proper plan is conducted by engineering team to define operational steps to clean out this well with minimum risk and optimum time. Operational risks and mitigations are discussed, include well control issue. Two bit runs were successfully executed on this operation to clean out scale inside 13-3/8" casing and 10-3/4" perforated liner prior to pumping acid. Steam gain after clean out well was very satisfied and exceeding steam gain target. Therefore, clean out operation for geothermal well with HWU is a doable option.

Keywords: Wayang Windu, HWU, well clean out.

INTRODUCTION

The Wayang Windu Geothermal Field is located 40 km south of Bandung City in West Java Province, Indonesia. Wayang Windu field is associated with andesitic stratovolcanos of the Sunda Volcanic Arc (Mulyadi and Ashat, 2011), and for development area is heading to the north which located on Malabar Mountain (Malik and Abidin, 2012). It is a steam-dominated geothermal resource operated by Star Energy Geothermal (SEG) with total installed capacity of 227 MW (Figure 1).

Well MBA-C has total depth of 1599 mMD finished with 10-3/4" perforated liner as production liner (Figure 2).

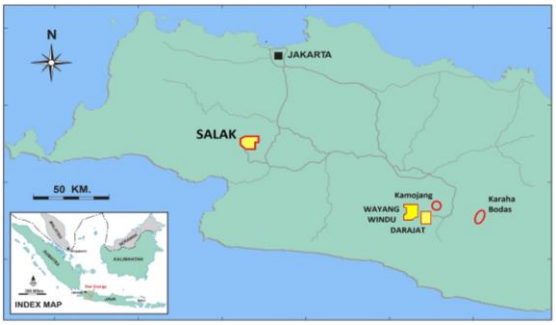


Figure 1: Map showed Star Energy Geothermal operation area. One of them is Wayang Windu field.

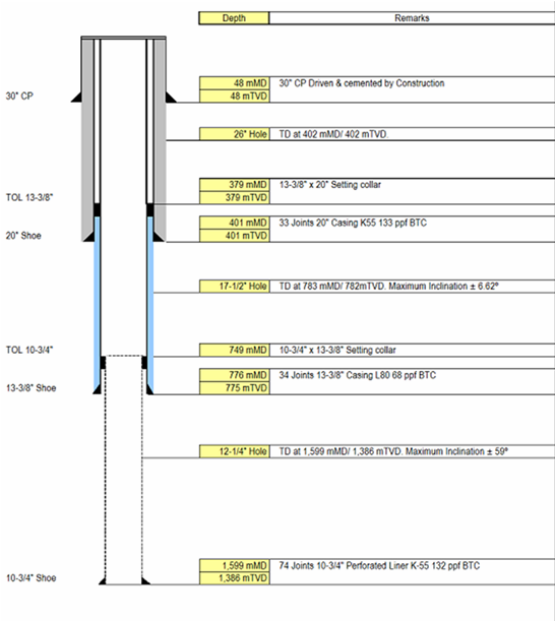


Figure 2: Well schematic diagram well MBA-C

Initial production capacity of this well was 47 kg/s steam and enthalpy of 2785 kJ/kg. MBA-C contributed 6% from total production in Wayang Windu field (Wayang Windu Sub Surface, 2017). Since the beginning of production, one of well problem is wellbore scaling caused by silica. Silica scaling is triggered by superheated condition when re-flashing of fluid occured in the wellbore therefore deposited solid material (Wayang Windu Sub Surface, 2017). Silica was observed starting from depth 725 - 791 mMD on this well. It also found at depth 810 mMD, 1360, and 1526 mMD with scale catcher (Wayang Windu Sub Surface, 2017).

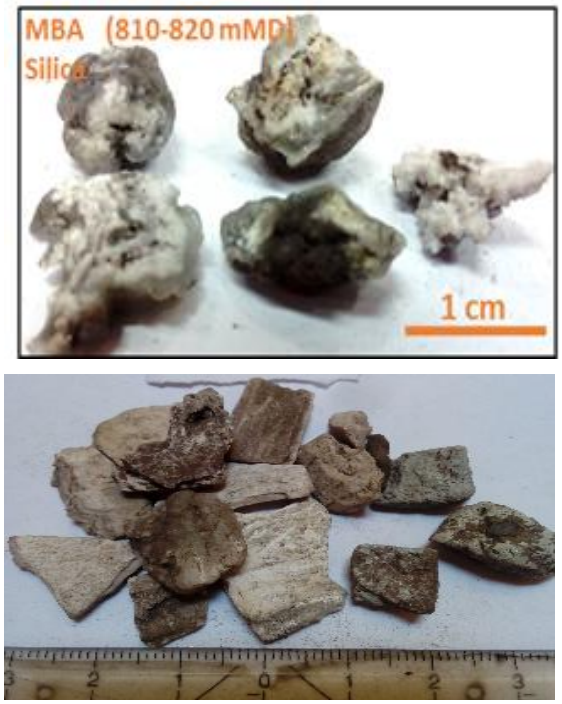


Figure 3: Silica scale found at depth 810, 1360, and 1526 mMD well MBA-C.

With this condition, current production decline rate can up to 31.3%/year as seen on figure 3.

Well intervention program was initiated several time to regain well production rate. On 2012 clean out and acidizing was held. It could recover up to 8 kg/s steam. Well washing was held in 2015 and 2016 could recover 7 kg/s and 0.7 kg/s steam respectively. Therefore, plan to clean out the scale and acidize the well was initiated in 2017 since from the last well intervention program, it was the most successful method to get high steam gain.

Several option was selected as method to deliver clean out and acidizing program. There were 3 methods selected on the planning phase of this project, they were CTU, Hydraulic Workover Unit, Workover Rig. The comparison plus pro and cons of them showed on Table 1.

Several criteria was made to choose the method, there are:

1. Low operational cost.
2. High possibility of removing wellbore scale.
3. Less dilution during acid process to increase success ratio of acidizing job.
4. Capable to handle high pressure and high rate acid displacement.
5. Less site preparation and less site space.
6. requirement during execution.
7. No required to shut in nearby well to avoid loss steam generation during execution.

Based on the above criteria, HWU was choosen as method to deliver the clean out and aciziding program.

Hydraulic workover unit (HWU) is basically a well servicing system that is capable to run and retrieve jointed pipes and perform well repairs or workovers (Ohia et al, 2014). A 460K workover hydraulic unit was used for this operation. Reconstruction work had to be done to put the unit so that it could be suitable for rotating the drill string. Such reconstruction work included fabricating a substructure below the lower work basket where the hydraulic workover unit "sit down" on it. With this configuration, the entire weight of unit will not be rested on the wellhead. A class III BOP was installed on top master valve below substructure. In all, this unit after reconstruction has two work basket; one at the stationary slip window and one at the topmost situated above the jack (four hydraulic cylinder). This baskets/platforms provide a work area large enough to allow personnel to safely carry out activities associated with workover operations.

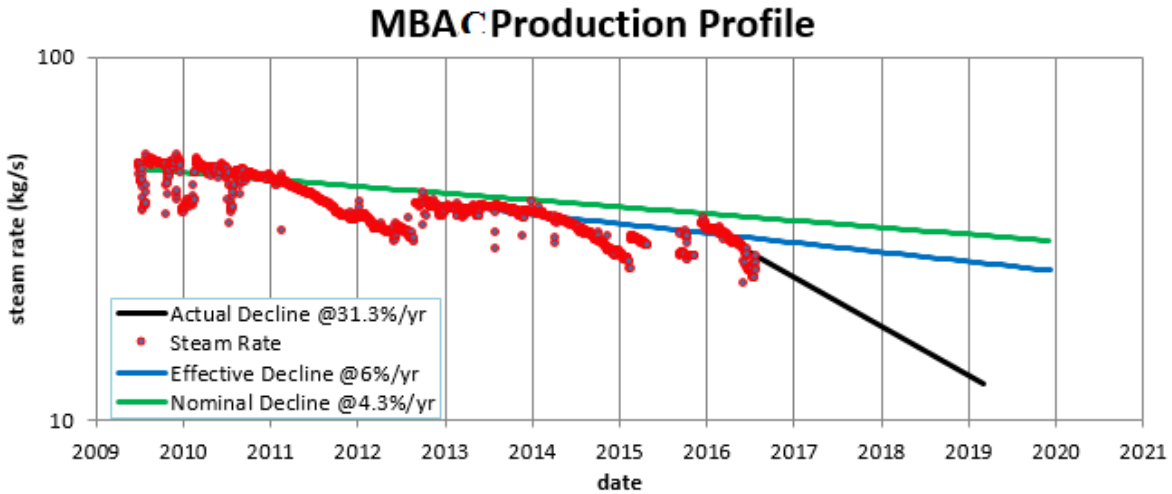


Figure 4: MBA-C Production Profile

Table 1: Comparison between CTU, HWU, and Workover Rig.

Parameter	CTU - 2-3/8"	HWU (snubbing unit)	Rig WO 550 HP
Daily cost ($)	~ 35,000	~ 17,500	~ 26,500
	Equipment, personnel,	Equipment, personnel, Rent 3-1/2" DP	Equipment, personnel, Rent 3-1/2" DP, Top drive, Rent fishing tool
Parameter	CTU - 2-3/8"	HWU 450K (snubbing unit)	Rig WO 550 HP
Drill Pipe Size	2-3/8"	3-1/2" - 5"	3-1/2" - 5"
Pumping Rate	8 BPM	16 - 24 BPM	16 - 24 BPM
Stand Pipe Pressure	3000 psi	3000 psi	3000 - 5000 psi
Pull-out Capacity	40 klbs	450 klbs	300 klbs
Maximum Bit Size	Max 8"	Max 14"	Max 20"
BHA configuration	Motor + Bit	Rotary table + DC / HWDP + Bit DC / HWDP + mud motor + Bit	Rotary table + DC / HWDP + Bit DC / HWDP + mud motor + Bit Top drive + DC / HWDP + Bit
Contractor	BHGE, SLB.	Lekom Maras, Elnusa, Sapta Well	Many
Number of Personnel in Site (including contractor)	6 - 10 person	10 - 14 person	10 - 14 person
Well Intervention Activity	Clean-out - (1 - 2 days) Acidizing and Clean Out - (3 - 4 days)	Clean-out - (4 - 5 days) Acidizing - (6 - 9 days)	Clean-out - (6 - 7 days) Acidizing - (8 - 9 days)
Pro	- Minimum site preparation - Faster R/U, R/D, Operation, Mob-demob	- Need less site preparation - Possible not shut-in the nearby well (less steam loss) - Moderate overpull capacity, pumping rate	- Higher overpull capacity, torque, pumping rate - Higher success ratio of clean-out process
Cons	- Have limited capacity (pull-out, torque, pumping rate) - Lower success ratio of milling the scale - Possibility wear the casing during milling process - High dilution effect (acid process)	- Longer R/U, R/D, Operation, Mob-demob - Lowest torque (only using rotary table)	- Need site preparation cost - Need wider area (consequence jeopardize MV) - Have to shut-in the nearby well (steam loss) - Longer R/U, R/D, Operation, Mob-demob

The 460K Hydraulic Workover Unit used in this project has two power pack units that provide the rig with hydraulic power. It also utilize 3 mud pump that work simultaneously during operation. Two mud pumps use for quenching well thru wing valve and one mud pump use for pumping water thru string. Two water tanks with capacity 500 bbls each were used and always keep on full condition throughout the process to make sure that water is sufficient to quench the well.

CLEAN OUT WELL

Quenching The Well

Prior to spud in, the well was quenched by pumping condensate water thru both of wing valves on wellhead on shut in condition and blind ram BOP closed. Intial well head pressure (WHP) was observed 380 psi. Quenching process was started with low pump rate and gradually increase (table 2). This is required as the cooling induces high tensional stresses in the casing steel, the pumping should be done at a slow rate (Thorhallsson, 2003).

Table 2: Pumping schedule during well quenching

Pump rate (BPM)	WHP (Psi)	Duration (hr)
1	380	2
1.5	249	1
2	255	2
3	109	2
4	17	2
6	6	2
8	-2	2

After well on vaccum condition, a minimum quenching rate (MQR) was observed. This is a minimum pumping rate to keep well on vaccum condition during operation. Master valve slowly opened while observing well head pressure followed by opening blind ram on BOP. After master valve and blind rame were opened, an increase in WHP was observed, therefore pump rate need to be increased to keep well on vaccum condition. Well back to vaccum condition after pump rate increase to 16.5 BPM. Continue to pump with this pump rate during clean out operation.

Clean Out 13-3/8" Casing

BHA #1 with 10-5/8" bit was made up and run in the hole to clean out scale inside 13-3/8" casing down to top of 10-3/4" liner. BHA #1 configuration showed in table 2.

A hydraulic jar installed in the BHA to prevent if any stuck occured during operation we can still jarring down or up to release the string. Three joints of drill collar were installed below Bowen oil jar to maximize jar efficiency and jar effectivenes. The rest of drill collar installed above the jar to give additional weight to the string.

The 10-5/8" bit successfully run in hole from surface to top of 10-3/4" liner at depth 749 mMD. Several obstruction was observed during run in hole bit.

Obstruction was cleaned out by putting the HWU on "drilling" mode; rotate the bit while pumping thru the string with 9 BPM. Circulate on bottom in 10-3/4" top of liner was established to make sure that any scale accumulated on top of liner was cleaned. The BHA was pulled out of hole after circulation and prepare to run BHA #2 with 8-1/2" bit. For the whole clean out process, pumping through wellhead wing valve was kept on going to keep well under vaccum condition.

Table 3: BHA #1 configuration

Item	Size (in)	Quantity
Bit Varel DT1GJMRS, 117	10-5/8	1
Bit sub 6-5/8" reg box X 4-1/2" IF box	8	1
Cross over sub 4-1/2" IF pin X 3-1/2" IF box	6-5/8	1
Cross over sub 3-1/2" IF pin X 4-1/2" reg pin	5-3/4	1
Bit sub 4-1/2" reg box X 3-1/2" IF box with float	5-3/4	1
Spiral Drill Collar	4-3/4	3
Bowen oil jar	4-3/4	1
Spiral Drill Collar	4-3/4	5
Drill Pipe	3-1/2	70

Table 4: BHA #1 Reaming Parameter

Parameter	Value
Weight on Bit	3 klbs
RPM	20 – 30
Drilling Torque	1100 – 1200 ft.lb
Pump rate	9 BPM
Pump pressure	50 psi
ROP	7 m/hr

At depth 762 mMD, observed torque increase erratically to 1800 – 2000 ft.lb after WOB increased to 5 klbs. String was reciprocated several times prior to continue operation. This shows that one of HWU limitation for reaming operation is torque and high WOB.

Clean Out 10-3/4" Perforated Liner

BHA #2 was run to clean out scale inside 10-3/4" liner (table 4) with 8-3/4" bit on the bottom of it. It was run to depth 1399 mMD. Several obstruction was observed during run in hole bit. Same as previous hole section, obstruction was cleaned out by reaming down the hole until all obstruction clear. Circulation on bottom at depth 1399 mMD was established prior to pull the bit to surface.

Table 5: BHA #2 Configuration

Item	Size (in)	Quantity
Bit Varel DT3GJP, 137	8-3/4	1
Bit sub with float	5-3/4	1
Spiral Drill Collar	4-3/4	3
Bowen oil jar	4-3/4	1
Spiral Drill Collar	4-3/4	5
Drill Pipe	3-1/2	134

After well was confirmed clean from any obstruction, BHA #2 was pulled out from the hole.

Table 6: BHA #2 Reaming Parameter

Parameter	Value
Weight on Bit	3 klbs
RPM	40
Drilling Torque	1000 – 1100 ft.lb
Pump rate	9 BPM
Pump pressure	100 psi
ROP	4.3 m/hr

Scale inside 10-3/4" liner was harder than scale inside 13-3/8" casing. This can be observed from slow ROP gained with quite same reaming parameter. Same as reaming on previouse hole section, an increase in WOB caused drilling torque increase erratically. Therefore, we kept drilling with quite same parameter as previouse hole section.

Aciziding the Well

MBA-C has two main feedzone at its production section as showed on table 7 below.

Table 7: Feedzone depth in Well MBA-C

Target location (m-GL)	Well		
	Width (meter)	MBA-C	
		Contribution (%)	Remarks
800	15	15	Feedzone
1120	35	85	Feedzone

The acidizing treatment will be performed at treatment interval based on above feedzone depth. The treatment interval are 800 - 815 mMD and 1120 - 1155 mMD in sequence pumping from bottom to top. The objective of the acidizing treatment is to

remove remaining silica scale inside the well bore and as well as near wellbore of the feeding zone the above mentioned interval.

A 3-1/2" diffuser was run with 3-1/2" DP to treatment interval (Table 8).

Table 8: BHA #3 Acidizing Diffuser

Item	Size (in)	Quantity
Diffuser	3-1/2	1
Cross over	5-1/2	1
Bit sub with float	5-3/4	3
Drill pipe	3-1/2	110

After diffuser run and set on the treatment interval, annular BOP was closed prior to start acidizing process. First step was to pump preflush water at 17-20 bpm for estimated volume 200 bbls. Quenching well through wing valve was stopped after pumping preflush. A 20%HCl preflush followed by 9%HCl - 9%HF main acid was pumped into the well through DP at 17-20 bpm. Positif wellhead pressure will be observed during this process and the number can be almost the same as initial shut in wellhead pressure. Displacement of acid was made by pumping 1000 bbls condensate water through DP at 17-20 bpm. Pumping rate was decreased step by step when pump volume approach 1000 bbls and condensate water slowly pumped thru wing valve to establish quenching well. After pumping displacement finish, wellhead pressure was monitored and after well back to vaccum condition annular BOP can be opened.

Table 9: Acid volume pumped on treatment interval

Treatment Zone	Top MD (m)	Bottom MD (m)	Interval Length (m)	Acid System	Acid Coverage (gal/ft)	Total Volume (bbl)
#1 Zone	1120	1155	35	20% HCl	70	192
				9% HCl - 9% HF	140	383
#2 Zone	800	815	15	20% HCl	70	83
				9% HCl - 9% HF	140	165
					Total	823

OPERATIONAL TIME AND NON PRODUCTIVE TIME (NPT)

MBA-C well was safely cleaned out and acidized in 6.38 days; 1.62 days faster than the plan which was 8 days. This can be achieved due to not to many obstruction found on the well and higher reaming ROP than plan.

During well execution there was 0,5 hour well NPT due to well control event. At depth 1308 mMD while reaming to depth 1310 mMD, observed wellhead pressure (WHP) increase to positive and well got flowing. WHP started increasing after one of mud pump broken down that impact on reduce in water pumping into the well. The well was shut in as soon as well flowing therefore prevent to uncontrolled flow. Well was killed by increase pump rate into the well while repair the broken mud pump. After 0,5 hour, well back on vaccum condition and operation was continued.

Another NPT during operation was power pack failure during pull out of hole BHA #1 due to overheat. Contractor need to switch power pack to the back up one and it spent 1,25 hours before the operation was continued.

Table 10: NPT generated during operation

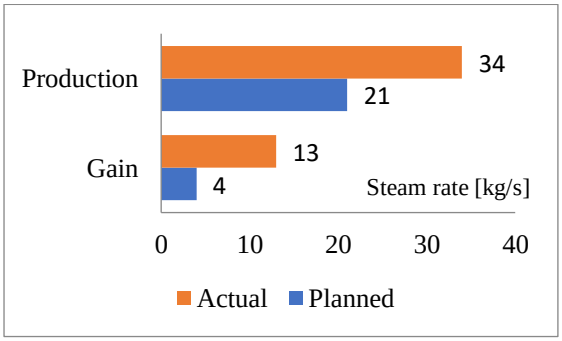
No	NPT Type	Duration
1.	Well control event	0,5 hour
2.	Power pack failure	1,25 hours
Total		1,75 hours

This total NPT was only 1% from total operation days.

CLEAN OUT RESULT

Well MBA-C was put back on operation in 24 hour after rig release. The process was started by flashing the steam to rock mufler until steam clean from any contaminant. After that steam entered the system and steam flow rate was measured. Post well clean out indicates that significant steam was gained.

Figure 5: Well MBA-C Clean Out Result



This result made the highest steam gain after well intervention program conducted in well MBA-C during its well life.

CONCLUSION

Star Energy Geothermal has successfully cleaned out and acidized well MBA-C with the highest steam gain in well intervention history; 13 kg/s steam gain. Appliying defensive drilling technique during reaming obstruction has effectively cleaned obstruction inside casing without any stuck pipe event. Moreover, stringent risk management has avoid any uncontrolled well flow spilled to environment.

Some of outcomes during this well intervention program are as follow:

1. Clean out and aciziding well in Geothermal with Hydraulic Workover Unit (HWU) is a doable option by giving capability to ream hard scale

obstruction and capability to pump acid with high pump rate.

2. Clean out and acidizing well using Hydraulic Workover Unit (HWU) has the cheapest cost structure among CTU and Rig Workover unit.
3. Some of lesson learned captured in this project can be followed up for the next well intervention program utilizing HWU.

REFERENCES

Ohia, N., Anayadiegwu, C., and Igwilo, K. (2014), "A Review of Hydraulic Workover Unit (HWU) Application for Well Repairs in Nigeria", *Petroleum & Coal* 56(4) xxx-331, ISSN 1337-7027, Nigeria, July 2014.

Malik, D., and Abidin, Z. (2012), "Geochemistry Monitoring During Drilling in Wayang Windu Field, Indonesia". *Proceedings New Zealand Geothermal Workshop,* Auckland, New Zealand.

Mulyadi., and Ashat, A. (2011), "Reservoir Modeling of The Northern Vapor-Dominated Two-Phase Zone of The Wayang Windu Geothermal Field, Java, Indonesia". *Proceedings Thirty-Sixth Workshop Geothermal Reservoir Engineering* Stanford, California.

Thorhallsson, S. (2003), "Geothermal well operation and maintenance", *GEOTHERMAL TRAINING PROGRAMME* IGC2003 - Short Course, Reykjavik, September 2003.

Wayang Windu Sub Surface. (2017), "Wayang Windu Well Intervention Project 2017-2018". *Star Energy Geothermal* in-house report.

UPDATING CONCEPTUAL MODEL USING NUMERICAL MODELLING FOR GEOTHERMAL GREEN FIELD PROSPECT AREA IN ATADEI, EAST NUSA TENGGARA, INDONESIA

Marchel Christian Supijo, Akbar Dwi Wahyono, and Ade Lesmana,
Abdul Hadi Harahap, Sutopo, Heru Berian, Welly Prabata

Geothermal Master Program, ITB
Email: marchelbinsus@gmail.com

ABSTRACT

Atadei geothermal prospect area is situated in Lembata Regency, East Nusa Tenggara, Indonesia. Ammonia geothermometer estimation indicated reservoir temperature of about 221°C, with the upflow zone discharging thermal manifestation of steaming ground, fumaroles and acid sulfate springs in three separated locations namely Watuwawer, Lewo Kebingin, and Lewokeba. Such temperature value is a typical of the geothermal system in which liquid phase dominated the reservoir. During its earlier exploration stage, which very limited subsurface data, nevertheless, an interpretation of subsurface condition and lateral extent of the geothermal area have been developed by predecessor researchers. This includes interpretation of reservoir geometry, the fluid contains (i.e steam caps formation), fluids flow pattern and some structural geology that may form permeability and reservoir depth. Such interpretation will most likely encounter some difficulties due to the limited initial data and directly impact the accuracy of the interpreted model features, particularly the conceptual model of Atadei. Therefore, we have proposed updating the conceptual model of Atadei by using TOUGH2.0-Numerical Modelling, in purpose to adding significant information regarding the reservoir characterization to avoid. inaccurate interpretation during the early exploration stage. Based on the parameters obtained from the reservoir numerical modeling, a more robust model is successfully representing the heat and mass flow within the system. Eventually, the updated geothermal system, the play types and the reservoir characterization of Atadei can be better and confidently suggested as flat terrain geothermal system influenced by an active or recent magmatic play type with intrusive magma chamber and a liquid dominated reservoir with underlying steam caps. The last but not least, based on comprehensive study of integrated geoscience and reservoir numerical modelling, some insightful recommendations for further exploration campaign until early development stage of Atadei geothermal prospect area have been well proposed in this study.

Keywords: Numerical modelling, conceptual model updating, Atedai Green Field.

INTRODUCTION

To meet Indonesian geothermal target by 2025 which is 7242 MW stated by ESDM (2017), the Indonesian government has committed conducting development in geothermal prospect including the prospected areas in East Indonesia. One of the prospect areas in East Indonesia which currently under development is Atadei geothermal prospect area. Atadei is situated in Lembata Regency, East Nusa Tenggara, Indonesia. The location of Atadei geothermal field is shown in Figure 1 and the prospect area is considered as located in remote area. To reach Atadei from Jakarta would take around two consecutive days and this is counted as one of the challenges found in developing this field.



Figure 1. Atadei Location (Google Maps, 2018)

PT. PLN (a state-owned company), since April 2017 has been the concession owner of this field based on SK-permits No. 1894 K/30/MEM/2017. Initially, the geological, geochemical, and geophysical surveys of the study area was conducted as preliminary surveys, followed by drilling the temperature gradient wells along with explorations well to delineate the potential extension of this geothermal prospect area. The location of surface features distribution from Atadei geothermal project is shown in Figure 2.

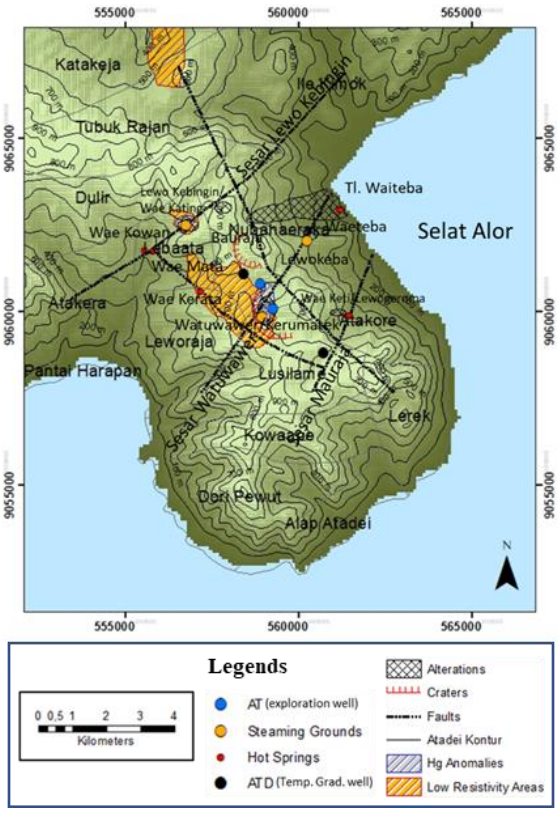


Figure 2. Surface feature distributions of Atadei geothermal field (after PSDMBP, 2017)

In this study, the integrated geoscience studies of Atadei geothermal field conducted by the predecessor authors is presented and reviewed as input data available for numerical modelling. Subsequently, the natural heat and mass flow model will serve as a significant additional information to propose an updated conceptual model of Atadei geothermal green-field area. The updating conceptual model is necessarily proposed because the model presented by Nanlohy et. al (2003) has not defined the geothermal system and the thermal fluids flow pattern with a better and detail illustration.

CONCEPTUAL MODEL REVIEW

Geoscience Reviews

Geology review

During May 2000, the explorations that covered around 100 km^2 in the vicinity of Atadei geothermal field produced a geological map that represents the study area as shown in Figure 3.

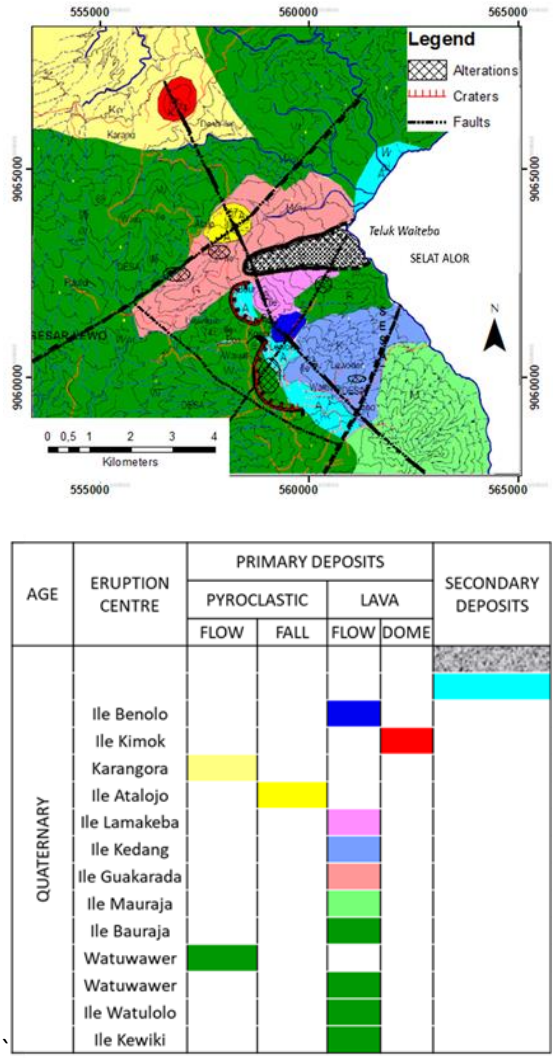


Figure 3. Geological Map of Atadei (after PSDMBP, 2017)

Based on volcano-stratigraphy, in general, the volcanic products and deposits in Atadei area are divided into two groups. The old volcanic crops out in northern and southwest part of the study area The young volcanic product is found in the eastern part of the study area. Aswin, *et al.* (2001), mentioned the cones of young volcanic were formed along with the main lineament which direction is almost N-S.

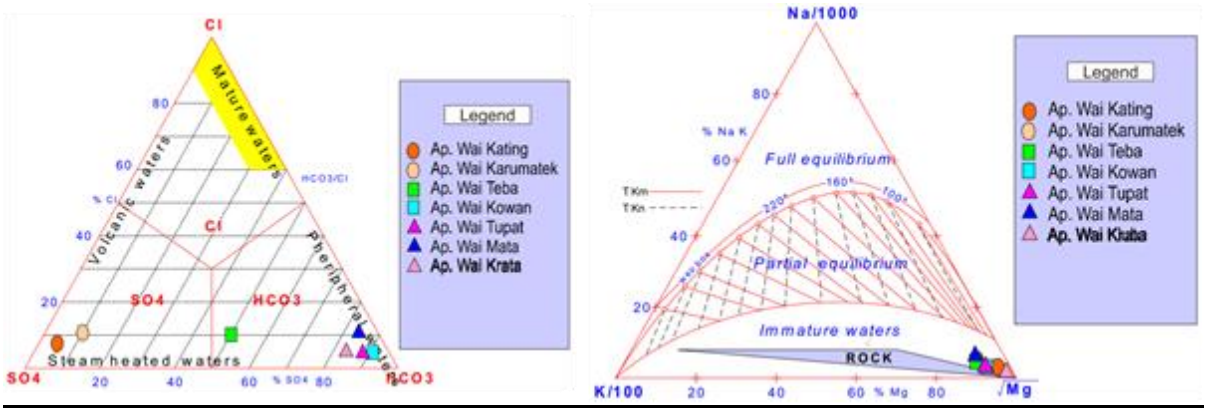


Figure 4. The ternary plot of water types "Cl-SO4-HCO3" and ternary plot of ion alkali geothermometer "Na-K-Mg" proposed by Giggenbach (1988), after (Nanlohy at. al, 2003)

The cones consist mostly of andesite pyroxene lava and pyroclastic (flow and fall) with two NE-SW (Lewo Kebingin and Mauraja) faults control the geothermal surface manifestation in this study area.

Geochemistry review

According to the previous study of geochemistry survey and analysis conducted by Nanlohy et. al (2003), most of surface thermal features are found at the vicinity of the three SW-NE main faults in Atadei geothermal prospect. Those main faults are Watuwawer Fault which controls the typical upflow features such as fumaroles and acid hot springs in Watuwawer and Lewokeba; Lewo Kebingin Fault which rules the typical mixture manifestation where fumaroles, acid sulfate and bicarbonate springs were found in just close proximities to the Lewo Kebingin, Wae Mata, and Wae Kowan; Mauraja Fault solely controlling the outflow type of manifestation (bicarbonate waters or dilute chloride-bicarbonate water) in Wai Keti and Wai Tupat. The figure of the ternary plot of water types "Cl-SO_4-HCO3" and ternary plot of ion alkali geothermometer "Na-K-Mg" proposed by Giggenbach (1988) is shown in figure 4.

Since there are no springs were classified as partial equilibrium which made the geothermometer "Na-K-Mg" is not applicable. Thus, the reservoir temperature is estimated using geothermal-gases. Based on ammonia geothermometer calculation, the reservoir temperature is 221°C.

The calculated reservoir temperature, then, to be used to estimate the depth of top reservoir (TOR) during the early stage of geothermal exploration by using the method proposed by Saputra et,.al (2016). The procedure for estimating the depth of top reservoir is illustrated in figure 5. Assuming that the temperature in the interval is conductive and is dominated by a clay cap, thus, the gradient is considered linear.

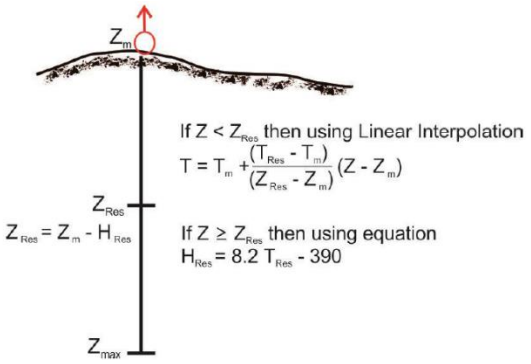


Figure 5. Illustration on the determination of subsurface temperature using temperature from surface manifestation (Saputra et al., 2016).

The result of the early estimated top reservoir in depth is illustrated in figure 6. It states that the calculated temperature reservoir of 220°C present in the depth of -800 masl, later it is estimated as the top of the reservoir.

Meanwhile, the type of fluids which dominated the reservoir can be predicted earlier in exploration stage by using analysis in water and gas chemistry. This approach is derived from the theory proposed by Nicholson, K (1993) and further elaborated by Glover, R.B (1991).

As the fluid migrates to the surface, a reduction in the confining pressure within the geothermal system will cause the steam and gases- phase to separate from the liquid phase (i.e the fluid boils and creates steam formation). After boiling, the residual liquid is therefore depleted in gas relative to the original fluid composition, although portions of all gases (especially the more-soluble species CO_2, H_2S, NH_3) will be retained in the liquid phase. Since, at given temperature, the gas ratios in the steam will differ from those in original fluid (Nicholson, K, 1993).

According to Glover, R.B (1991), relatively to early-formed steam, later-formed steam has the following

characteristics: “the gas concentrations in steam will fall as more steam is formed and the (less-soluble gas/ more soluble gas) ratio will similarly decrease as the proportion of the more-soluble gas increases relative to the least soluble gas”. For the common geothermal gases, the solubility order is (least soluble) $N_2 < O_2 < H_2 < CH_4 < CO_2 < H_2S < NH_3$ (most soluble).

In the case of Atadei, AT-1 and AT-2 exploration well monitoring programs were carried out in 4 stage, the 1st stage was in Juni 2005, 2nd stage in Juli 2005, 3rd stage in October 2005 and the 4th stage in December 2005. The method used in this program comprised the water and gas chemistry analysis in the wells and manifestation surrounding the wells. The result of gas chemistry analysis in AT-1 and AT-2 shown that composition of geothermal gases can be described in figure 7.

From the analysis of gas chemistry conducted by Asyadipura. S, et. al (2005) show that the proportion of the more-soluble gas (CO_2) in the wells are higher relative to the least soluble gas (N_2). Meanwhile the laboratory analysis result of gas chemistry of Karun/Watuwawer manifestation near the AT-1 and AT-2 show that H_2O dominates the gas distributions (more than 99% mole) among the other gases, such as CO_2, H_2S dan N_2 (with total concentration less than 0.8 mole). It is further can be suggested from the Glover, R.B (1991) theory explained above that in the area around the exploration wells AT-1 and AT-2 some steam caps have been further formed.

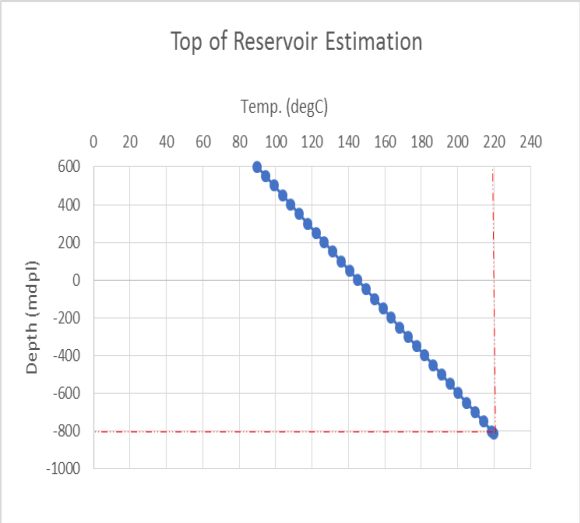
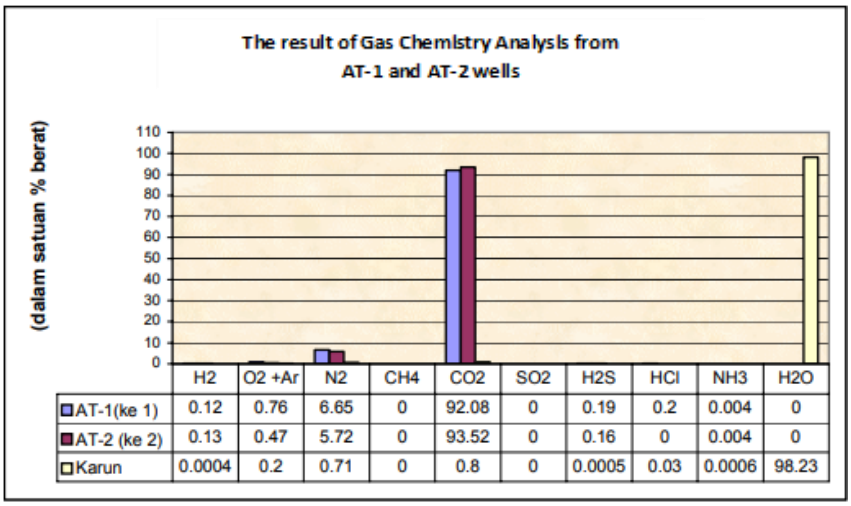


Figure 6. The result of the early estimated top of the reservoir using the method proposed by Saputra et,.al (2016).



	H2	O2 +Ar	N2	CH4	CO2	SO2	H2S	HCl	NH3	H2O
AT-1(ke 1)	0.12	0.76	6.65	0	92.08	0	0.19	0.2	0.004	0
AT-2 (ke 2)	0.13	0.47	5.72	0	93.52	0	0.16	0	0.004	0
Karun	0.0004	0.2	0.71	0	0.8	0	0.0005	0.03	0.0006	98.23

Figure 7. Graph of gas chemistry analysis from AT-1 and AT-2 wells (Arsyadipura. S, et. al, 2005)

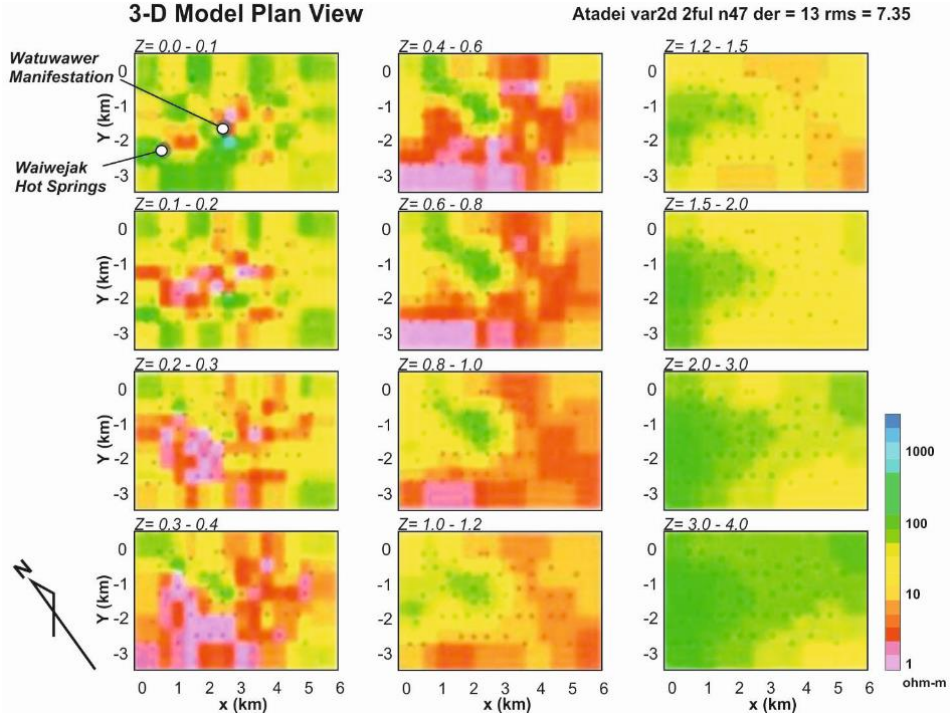


Figure 8. 3D MT Inversion in Atadei Geothermal Prospect Area sliced in several depths (PSDMBP, 2017)

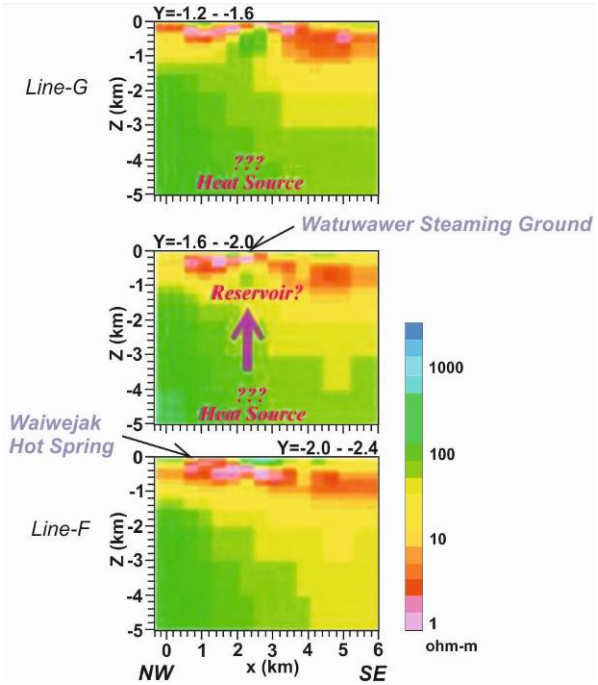


Figure 9. NW-SE cross-section of 3D MT Inversion of Atadei Geothermal Prospect Area

Geophysics review

The magnetotelluric survey has been notably indicated the low resistivity layers beneath the Watuwawer manifestation at the near surface of about 200 meters, it extends at the greater depth around 400 meters to the East and the West of Atadei geothermal prospect area. At below 1400 m depth or -800 masl, the contrast of higher resistivity occurred and thickened which is later suggested as reservoir rock. The exception applied for Watuwawer doming which is attained the contrast resistivity at relatively shallower depth around 1200 m depth or around -700 masl. It is necessarily agreed with the estimated depth of top reservoir using method proposed by Saputra et,.al (2016) in the earlier exploration stage. Therefore, the authors have adequate confidence in determining the depth of top reservoir at 1400 m depth and 1200 m depth only for doming/ upflow area to be assigned in the numerical model. The result of 3D MT inversion by PSDMBP (2017) is shown in Figure 8, followed by Figure 9 which illustrate the NW-SE cross-section of Atadei.

The result of MT survey also shows some consistencies to the *Direct Current Resistivity* survey conducted earlier with varied space configurations AB/2 = 250, 500, 750, 1000 and 2000 meter.

The resistivity data showed that the low resistivity zone beneath the Watu-wawer caldera relatively occurred at the shallower depth than in any others locations. Being consistent with the presence of fumaroles in the Watuwawer caldera, it strongly suggests that small steam cap has developed naturally in that particular area.

The sounding resistivity also indicated another small dooming of suggested steam caps present at Lewo Kebingin and Lewokeba.

Well Data

Two gradient temperature wells namely ATD-1 and ATD-2 were drilled to reach a depth of 250 meters, these wells were drilled with the aim to get a better understanding of temperature gradient especially in upflow zone and to delineate the extent of the reservoir at the boundary of the Atadei geothermal field. ATD-1 is situated in the Watuwawer caldera representing temperature gradient in upflow area, meanwhile, ATD-2 is situated in Mauraja nearly intersected with Mauraja Fault in which representing the temperature distribution in the boundary or outflow area (Soetoyo,2008).

Two years later in 2004, two exploration wells were drilled around the prospect areas of Watuwawer caldera and Bauraja crater, namely AT-1 and AT-2. It is aimed to get a better understanding of temperature distribution, particularly in upflow zone. AT-1 was drilled to the depth of 830.5 m and AT-2 was drilled to the depth of 750 m.

The result of well testing shows AT-1 had well head pressure at 7 kscg and AT-2 had well head pressure at 0 kscg. However, the temperature of both wells at the wellhead is relatively similar to the environment temperature, thus the pressure measured at AT-1 wellhead is principally not come from the geothermal fluid. Logging temperature is applied to AT-1 until to the depth of 450 m and found the temperature was at 96.5°C (Sitorus et. al, 2005). The temperature profile from AT-1 well is shown in figure 10.

The SE-NW oriented cross-section of this study area is demonstrated in Figure 11, followed by the initial conceptual model which is illustrated in Figure 12. At the initial conceptual model proposed by Nanlohy et. al (2003) it appears that hot geothermal fluid is upwelling from the deep part of the Watuwawer caldera. The deep leakage of fracture permeability from Watuwawer Fault and fissures from Watuwawer-caldera rims serve as pathways in which the hot thermal fluids ascend through these given vertical permeability. Meanwhile, the depth of top reservoir at around -400 masl was obtained through *Direct Current Resistivity method*.

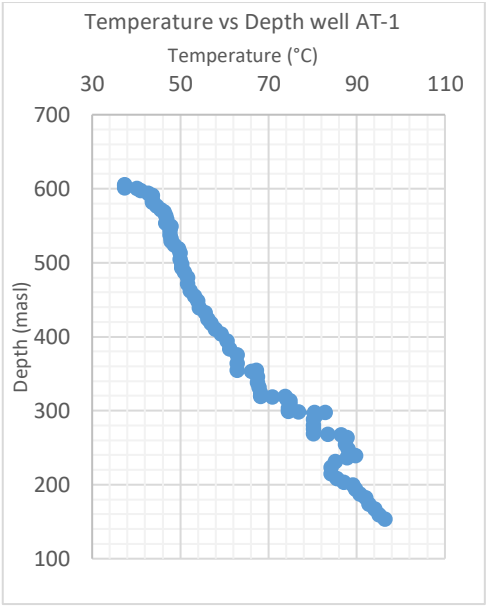


Figure 10. The temperature profile of well AT-1 (Sitorus et. al, 2005)

However, the initial conceptual model has not comprised the fluid flow pattern and isothermal gradient because of lacking information in wells data especially at the greater depth which might lead to the author's inadequate confidence in interpreting of such deterministic model. It is hoped that the result of reservoir numerical modeling would give significant input to better detail the conceptual model, especially through deterministic approach.

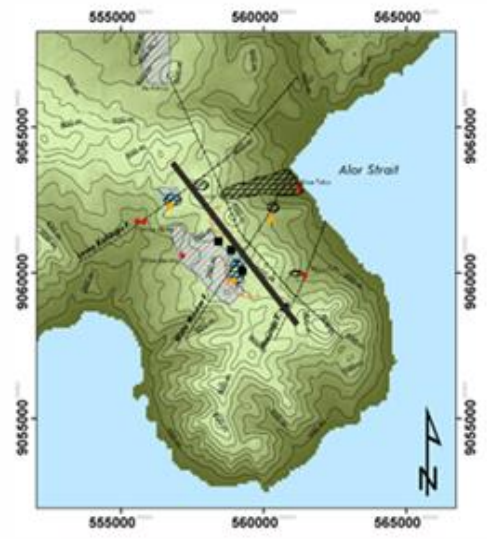


Figure 11. NE-SW cross-sectional area of Atadei Geothermal Prospect Area

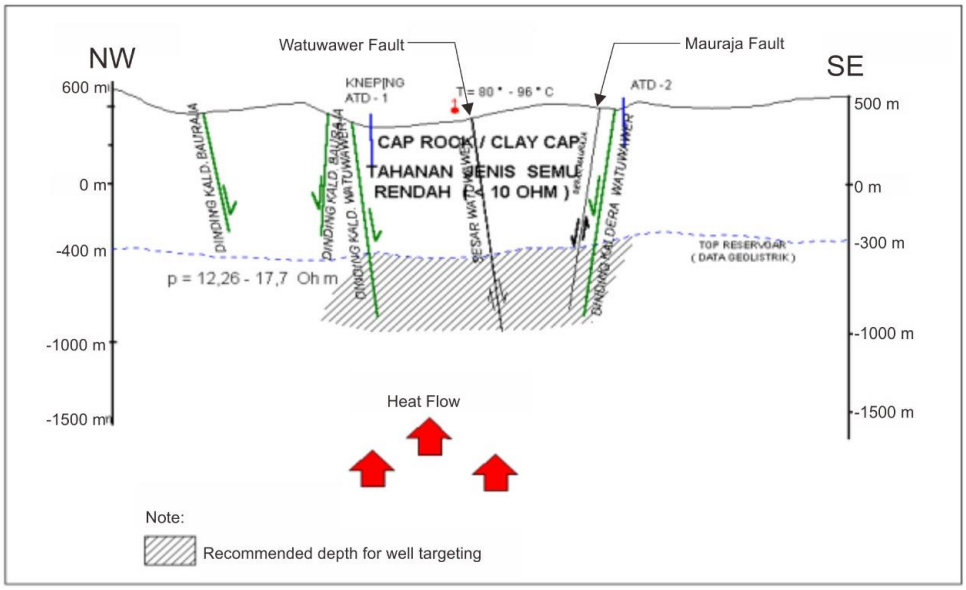


Figure 12. Conceptual Model of Atadei Geothermal Prospect Area proposed by Nanlohy et. al (2003)

NUMERICAL MODEL

Model Description

Gridding and layering

The grid of the model is rotated at 127° to the East to accommodate the material assignment to be necessary in arrangement with the alignment of conceptual model. It is covering a total area of 6.4 km x 5 km or equal to 32 km^2 and a total thickness of 3.45 km (i.e. from 950 masl to -2500 masl)-which is demonstrated in Figure 13. The horizontal dimension of grid blocks varies from the smallest 200 m x 200 m to the biggest 500 m x 500 m, the smallest grid blocks are used near the reservoir area, wells, and faults to increase the modeling accuracy on that area. The model is divided into 13 layers with some of the top layers follow the real topographical condition. The total number of grid blocks is 4862 by using rectangular grid type. This model used EOS1 for water and water for tracer because of data limitation and to simplify the modeling process.

Initial and boundary condition

The initial condition is needed to input the initial temperature and pressure for each grid-block on the model to fasten the process in running the model. At the initial condition, the normal gradient is used for both temperature and pressure. Meanwhile, the top layer is set to constant at the atmospheric conditions with the pressure is set at 1E-05 Pa and the temperature is at 25^O C.

Inside the boundary, it is assumed that there are no flows of fluid. Hot water with constant enthalpy and the mass rate are injected into the Watu-wawer base reservoir to represent the deep heat flux to the system. The amount of the deep up-flow discharge obtained from the initial state calibration with the rate of 26 kg/s and the enthalpy of 1500 kJ/kg. The lateral boundaries are assigned to be impermeable.

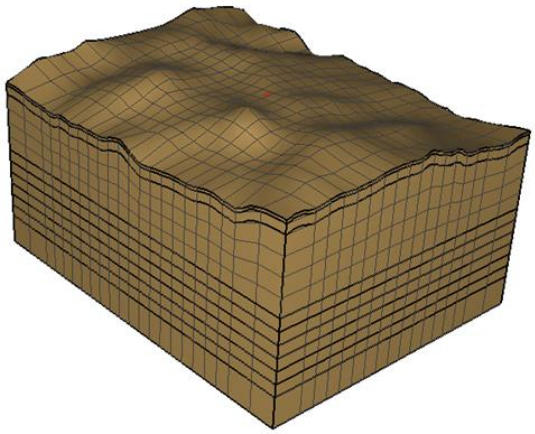


Figure 13. 3D View of Atadei gridding model

Rock properties (assign material)

During the numerical modelling, determining permeability structure is the most essential step to be iteratively adjusted until the natural state condition was achieved. The iterative process is done by several trial and errors. The permeability structure used in the final modelling is shown in table 1 and its distribution to the grid model also shown in figure 14.

Table 1. Material properties

Material	K_{xy} (mD)	K_z (mD)	Color
ATM	10	10	
GW	0.002	0.002	
CAPR	0.00001	0.00001	
BOUND	0.00005	0.00001	
HEAT	100	100	
RES1	60	30	
RES2	40	30	
RES3	15	15	
RES4	10	10	
RES5	100	200	
RESMT	60	30	
FAULT	50	50	
BASE	3	1	
FAUL1	30	20	
TRNS	90	50	

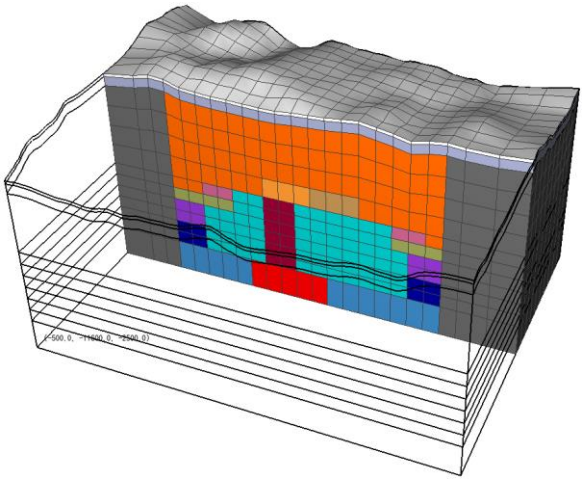


Figure 14. Material assignment to the gridding model

Numerical Modelling Result

Initial state calibration

During the initial state calibration, also called natural state modeling, the computer model was run until natural steady state conditions were reached. The results were then compared against actual wells temperatures and reservoir temperature estimation obtain from geothermometer. To obtain a good fit between model results and field observation data, the permeability structures was adjusted in an iterative process.

There is only one observation well available to match the model, it is obtained from AT-1. The dummy wells in Atadei area were also used to match the reservoir temperature by comparing with the temperature estimation obtained from the ammonia geothermometer, considering well AT-1 was not reached the depth of reservoir.

The modeling process was carried out by using a pre- and post-processor of TOUGH2. Figure 15 indicates the temperature matching of AT-01. It shows a very good match between the actual and the modeled temperature. The temperature distribution in top of reservoir is also shown in figure 16, it is necessarily agreed with the temperature estimation from geothermometer.

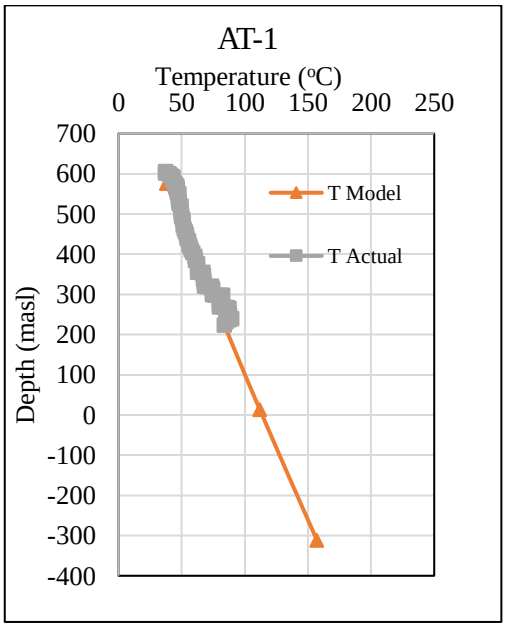


Figure 15. AT-1 temperature matching

Reservoir characterization

The dummy wells AGP-1 which have been applied to the model is in close proximity with the AT-1 which its temperature and pressure response is shown in figure 17. The temperature and pressure profile indicates steam cap is formed in between 1200 – 1400 m depth.

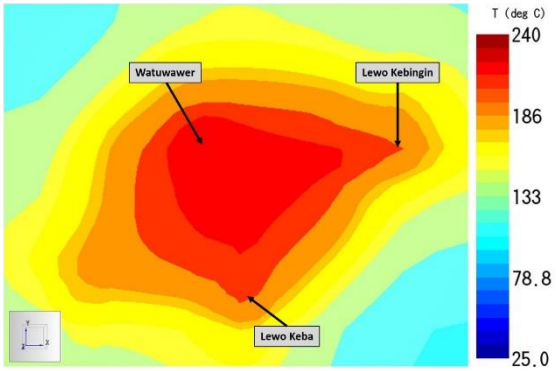


Figure 16. Temperature distribution of the model in the top reservoir

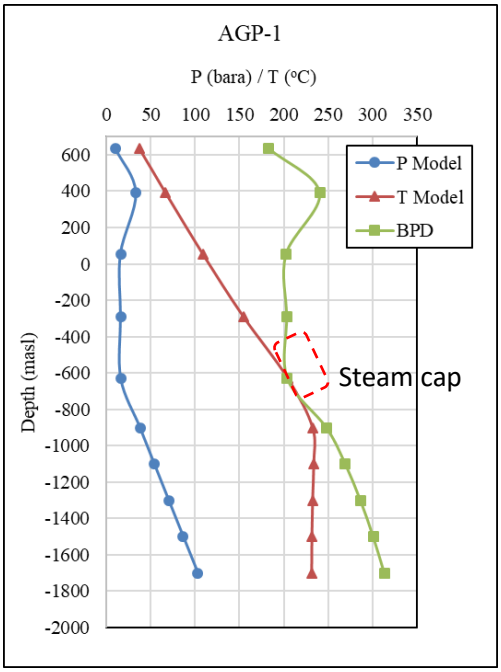


Figure 17. AGP-1 temperature and pressure profile

As suggested earlier during the integrated geoscience study, especially from data MT- *DC Resistivity* and fluid chemistry show that there are 3 small doming of suggested steam caps present at Watuwawer, Lewo Kebingin and Lewokeba. In figure 18 shows temperature and pressure profile of dummy well AGP-2 in which representing Lewokeba steam cap doming and figure 19 shows profile of dummy well AGP-3 representing Lewo Kebingin formed steam cap.

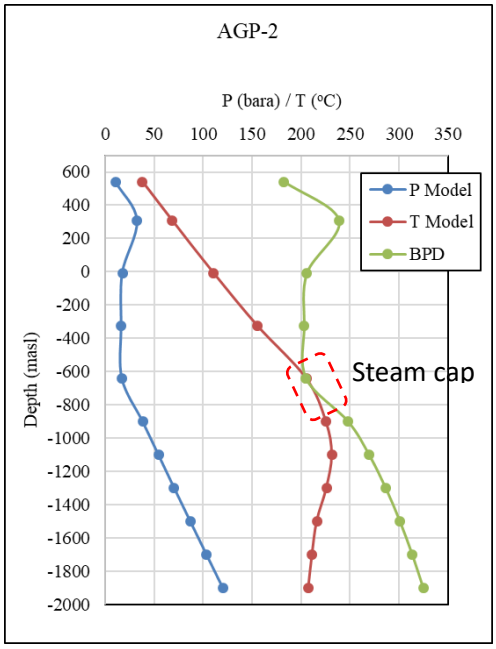


Figure 18. AGP-2 temperature and pressure profile

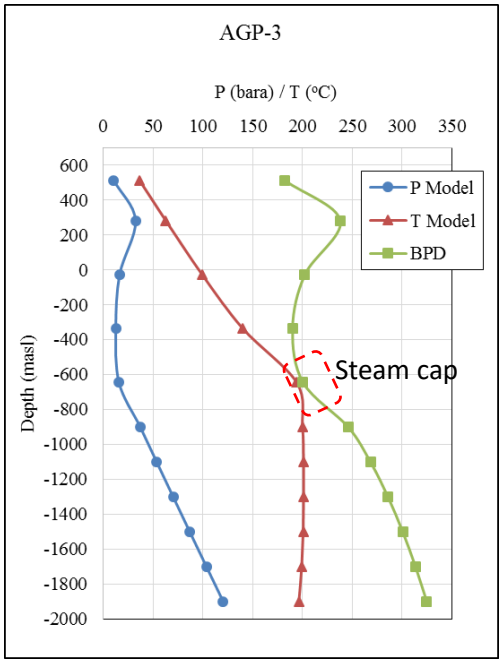


Figure 19. AGP-3 temperature and pressure profile

Meanwhile, the distribution of gas saturation in the reservoir which indicated as steam caps is found relatively further steam formation in Watuwawer and most likely thin steam cap present in Lewo Kebingin and Lewo Keba as illustrated in figure 20.

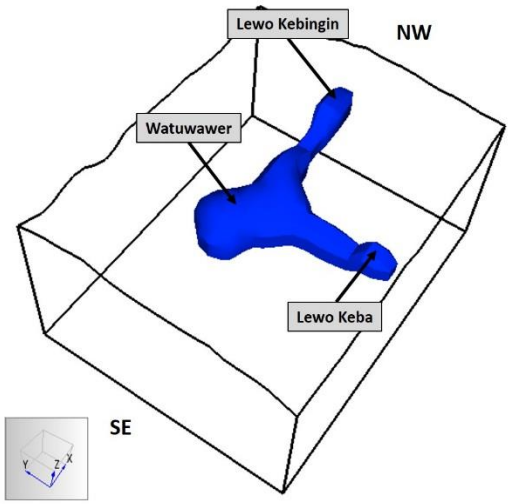


Figure 20. Steam cap distribution of numerical model

One of key driver outcomes of the reservoir numerical modelling is simulation of heat and mass flow within the system, as illustrated in figure 21. It concludes the whole fluid flow process from the upwelling geothermal heat flow beneath the Watuwawer caldera in which the hot fluids ascends directly through the given vertical fracture permeability later emerge as upflow manifestation in Watuwawer, Lewo Keba and Lewo Kebingin. The residual fluids circulate within permeable zones as the hot fluid with lighter in density ascends until it reach the impermeable layers where heat losses

occurs resulting some cooling fluids descending back to the reservoir and some other flow laterally until it emerge as outflow manifestation in the surface in Mauraja and Lewo Kebingin.

This result serves as significant information for isothermal map beneficial in updating conceptual model of Atadei geothermal system.

The updated conceptual model shown in figure 22 is designed based on comprehensive geoscience reviews and numerical model approach. It appears that hot geothermal fluid is upwelling from the deep part of the Watu-wawer caldera. The deep leakage of fracture permeability from Watu-Wawer Fault and Lewo-Kebingin Fault control the flows of hot fluids-in which it ascends through the given vertical permeability-with some fluids flow laterally to the Southeast until rising to the surface through Mauraja Fault as outflow. In contrary to the initial model, there is a change in determining the depth of top reservoir as the updated model has followed the interpretation of Magnetotelluric data rather than DC-Resistivity in which Nanlohy et. al (2003) had followed. It stated that in general top of reservoir of Atadei geothermal area is situated around the depth of -800 masl, the only exception applied for Watuwawer area in which the reservoir reached the depth of -700 masl.

Updated conceptual model

CONCLUSION

Play type in the Atadei prospect area based on integrated geoscience study conform with heat and mass flow of numerical model can be categorized as an active or recent magmatic play type with intrusive magma chamber (play type classification by IGA in Geothermal Exploration Best Practice, 2014). It is influenced by active faulting which allowing the deep rooted magmas to intrude beneath flat terrain with no volcanism. As a typical characteristic of this play type, the upflow and outflow zones occur in the close proximity - provided by the topography of volcano to support this -in which found in the vicinity of Lewo Kebingin Fault.

A liquid dominated reservoir with most likely underlying thin steam caps present in three area namely Watuwawer, Lewo Kebingin and Lewo Keba is attained in the depth of -800 masl, the exception applies to the Watuwawer doming area where it reaches the depth around -700 masl.

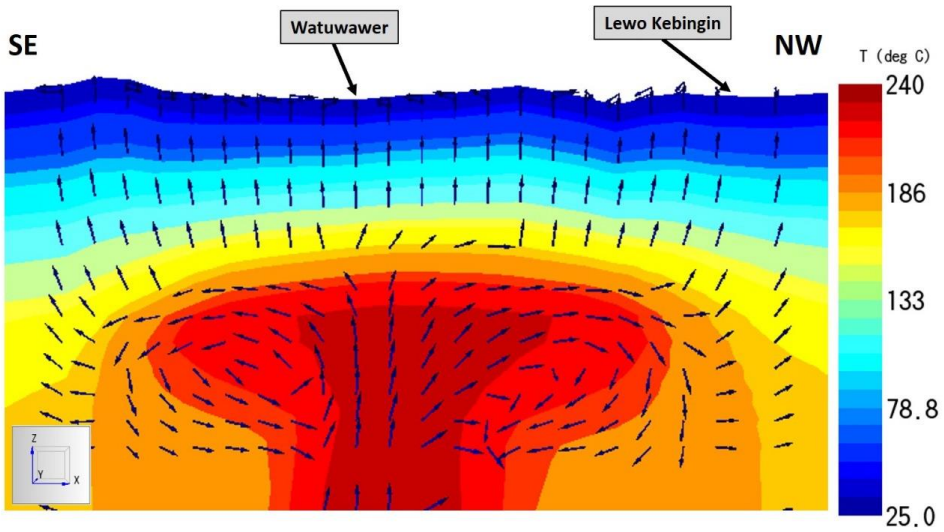


Figure 21. Vertical slice of numerical model

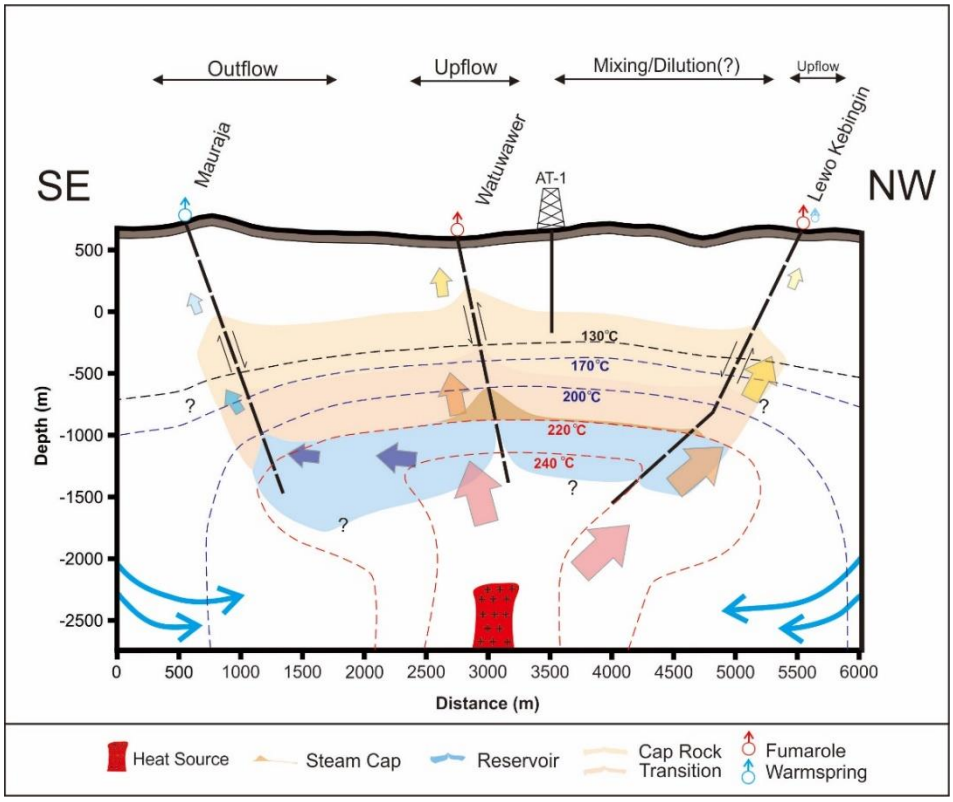


Figure 22. Updated Conceptual Model

RECOMMENDATIONS

Based on the integrated geoscience reviews collected from several published scientific papers and field reports together with the numerical model attained in this study, the authors would like to give recommendation for the exploration stages in Atadei Geothermal Prospect Area. It is aimed to decrease the uncertainty and to increase the confidence in reservoir characterization, particularly regarding the reservoir geometry and its temperature. The recommendation is summarized as follow:

1. Targeting new exploration wells at least 3 wells which reach the reservoir depth in three upflow area namely Watuwawer, Lewo Kebingin and Lewo Keba to obtain temperature profile in upflow zone and to confirm the suggested thin layer of steam cap in that area.
2. Prioritizing in well targeting for early development stage around the Watuwawer area as it is identified as a center of upwelling of deep hot thermal water below the surface. Less confidence in suggesting of well targeting in the other two upflow zones as main production area, given the result of numerical modelling.
3. More detail Magnetotelluric survey with the survey design covering from Watuwawer to Lewo Kebingin area in order to indicate the connection and the continuity of low resistivity layer between Watuwawer and Lewo Kebingin upflow zone.
4. Conducting additional geophysical surveys to accomplish the accuracy in identifying geological structure which controlling the geothermal system including estimation of heat source location in Atadei. The most recommended survey methods is gravity survey combine with geomagnetic survey covering all prospect area.
5. More data sampling and analysis of water and gas geochemistry particularly fluids inside the wells, to assess the quality of fluids in the reservoir. It is subsequently increasing confidence in determining the stage of steam formation within the reservoir which later be beneficial for scenario of production optimization.

ACKNOWLEDGEMENT

The authors would like to thank to the people in geothermal laboratory of ITB who helping the authors in finishing this paper and geothermal master program lecturers, especially Nenny Miryani Saptadji, Suryantini, M. Ali Ashat, Dimas Taha Maulana and Angga Bakti Pratama for reviewing this paper.

REFERENCES

Arsyadipura, S., Sulaeman, B., and Dahlan. (2005), "Pengujian Uap/Monitoring Sumur Panas Bumi AT-1 danAT-2 Atadei, Kabupaten Lembata, Nusa Tenggara Timur Tahun 2005", Pemaparan Hasil Kegiatan Lapangan Subdit Panas Bumi, 2005.

Aswin, D., Sundhoro, H., Munandar, A., Suparman and Sulaeman, B. (2001), "The Potential of Atadei Geothermal Field Based on Geological, Geochemical and Geophysical Studies, Lomblen Island-East Nusatenggara", Proceeding of the 5th INAGA ANNUAL SCIENTIFIC CONFERENCE.

Giggenbach, W.F. (1988), "Geothermal Solute Equilibria – Derivation of Na-K-Mg-Ca geoindicators", Geochim, Cosmochim, Acta, 52, 2749-2765.

IGA. (2014), "Geothermal Exploration Best Practice", Bochum University of Applied Sciences (Hochschule Bochum) Lennershofstr. 140, D-44801 Bochum, Germany

Nanlohy, F., Kusnadi, D., Sundhoro H. (2003), "Program Pengembangan Lapangan Panas Bumi Atadei Kabupaten Lembata – Nusa Tenggara Timur," Kolokium Hasil Kegiatan Inventarisasi Sumber Daya Mineral – DIM, TA. 2003.

Nicholson, K. (1993), "Geothermal Fluids-Chemistry and Exploration Techniques", Germany: Springer-Verlag Berlin Heidelberg.

Saputra, M.P., et al. (2016), "Geological, Isothermal, and Isobaric 3D Model Construction in Early Stage of Geothermal Exploration", IOP Conf. Series: Earth Environ. Sci. 42 012009

Soetoyo. (2008), "Kondisi Lingkungan Pasca Pemngeboran Sumur Eksplorasi AT-1 dan AT-2 di Lapangan Panas Bumi Atadei, Lembata, Nusa Tenggara Timur," Pusat Sumber Daya Geologi.

Sitorus, K., Munandar, M. (2005), "Karakteristik Geotermal Sumur Eksplorasi AT-1, Lapangan Panas Bumi Atadei, Kabupaten Lembata-NTT," Kolokium Hasil Lapangan DIM 2005.

AERATED DRILLING OPTIMIZATION FOR 12-1/4" HOLE SECTION

Tunjung Wicaksana Ranukusuma

UPN "V" Yogyakarta
Jl. SWK 104, Condongcatur, Yogyakarta
Email: tunjungwicakcana@gmail.com

ABSTRACT

In geothermal drilling, the process of a cleaning cutting and dry hole in drilling operations is very important. Because it greatly affects the rate of penetration of the drill bit into the borehole and reducing the time of drilling. Usually, the geothermal reservoir has a less pressure than the hydrostatic pressure. When the drilling at the reservoir interval there will be a partial loss or total loss condition. The solution of any problem is drilled by aerated drilling that has been known as a powerful method to increase the chance of return, decrease torque and increase of the drilling penetration rate (ROP). Proper composition of water and liquid is required to have optimum results on both objectives. Aerated Drilling is one of using the addition of compressed air to the drilling fluid to reduce the differential pressure between hydrostatic pressure and the pore pressure. The method that we used is an analysis of pore pressure to gain the ECD (equivalent circulating density) for the 12-1 / 4 "hole of the sample well are evaluated. The sample of the well represents the wells drilled in Geothermal Field. The ECD (equivalent circulating density) determined by ratio influences the composition of the liquid and the air phase. After determine the composition of aerated fluid, it will influence the velocity of aerated fluid in the drill string and annulus. From the total flowrate of aerated fluid, it can be calculated the annular velocity and determine the flow pattern, the cutting of concentration in the annulus, the cutting transport ratio, and the particles bed particles index. Purpose of this paper is obtained from the best ECD for 12-1 / 4 "hole section from the sample well.

Keywords: Aerated drilling, ROP, ECD, geothermal drilling.

INTRODUCTION

Aerated drilling is a method of injecting compressed air into the liquid circulation. Aerated Drilling is used to reduce loss circulation and increases the rate of penetration (ROP). This evaluation Aerated Drilling in the field of geothermal conducted using Air Laws that annular velocity (Vann) of aeration fluid should be greater than 100 ft / min (Ashadi and Dumrongthai, 2015; Putra, 2008; Subiatmono et al, 2001) and greater than the sum of the critical velocity (Vc) and the terminal velocity (Vt), so we can get a better hole cleaning.

The density of aerated drilling fluid can be changed at a certain depth which is influenced by temperature and annular pressure. Aerated drilling fluid consists of two phases, namely the liquid phase as the bottom liquid (bentonite liquid, KCL brine, or water) and air, which is injected into the liquid circulation to reduce the hydrostatic pressure in the annulus (nitrogen, oxygen, argon, neon, etc.).

BASIC THEORY

Aerated drilling theory already widely published in books, journals and papers. The author writes some basic theories of aerated drilling:

Advantages of Aerated Drilling

Aerated drilling provides many advantages compared to conventional drilling. Several advantages can be described as follows:

Increases rate of penetration

In Aerated Drilling, chip hold-down force of rock eroded reduced so cutting that would have the effect of explosion due to the formation pressure greater than the pressure of the liquid in the annulus. Viscosity rise will increase the friction loss, adding to the pressure drop, and reducing the speed obtained, therefore, when the viscosity increases, the chip clearance time will be increased resulting in lower ROP. Aerated Drilling in the viscosity of aeration fluid will be decreased due to the addition of air so that the ROP will increase.

Prevent stuck pipe

To prevent this stuck pipe then using drilling fluid that has a lower density to provide a lower hydrostatic pressure, lower water loss, and a thin liquid cake (Nugroho et al, 2017). This can be done by applying Aerated drilling Drilling on the formation which if done would have overbalanced drilling pipe stuck.

Components of Aerated Fluid

Aerated drilling fluid consists of two phases, namely the liquid phase as a base liquid (KCL brine, or water) and air, which is injected into the circulation liquid to reduce the hydrostatic pressure in the annulus (Nas and Toralde, 2010; Hole, 2006; Lyons, 1996).

Liquid phase

Normally a lightweight aerated drilling fluid is used as a liquid phase in which the main components are

water (water base liquid). If possible, fresh water is often used for basic liquid because it is easily obtained with the addition of KCL, polymers and other additives.

Air phase

In geothermal Aerated Drilling , air phase used is free air or nitrogen can also because it is easily obtained and inexpensive (Dwinanto and Sudjati, 2014). Free air is composed of 78% nitrogen, 21% oxygen, and the remainder other aires such as argon, neon and more. Use of outdoor air is also non-toxic so once used as a mixture of sludge aeration can be dumped directly into without damaging the environment. As for the use of nitrogen itself needed a special tool called nitrogen processing / membrane unit (NPU / NMU) in which the nitrogen concentration of free air be 90% -95%.

Aerated Drilling Injection Technique

There are two basic techniques of air injection into the liquid circulation. First is mix the liquid and air before entering into the drillstring. Second is mix the liquid and water in the annulus.

Injection of air through the drill pipe

In Aerated Drilling geothermal, air phase to the air phase mixing of bottom liquid phase performed on the surface before entering the drillstring. Not required subsurface equipment that does not increase costs. During the process of connecting and tripping can not be injecting air so that the bottom hole pressure control is not good. The volume of air required for injection is less than another injection technique. In drillstring fluid flow is two-phase and in the annulus there was three-phase that are air, water and cutting.

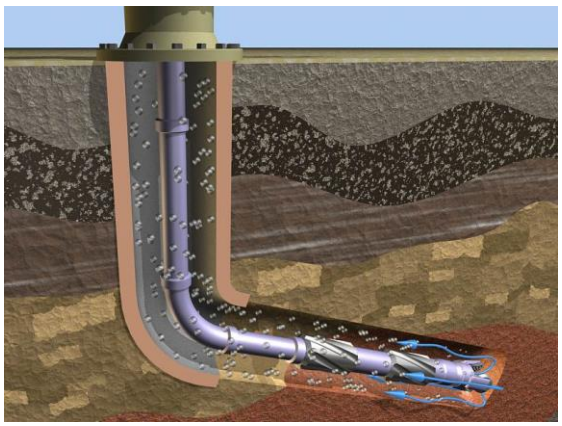


Figure 1: Illustration of Annular Injection

Injection of air through the drill pipe

Air reinjection is done in the annulus to lighten the bottom liquid phase. Flow at drilstring is one phase that is only the start of liquid. In this reinjection techniques required additional equipment so the cost and volume of air that it takes more. The air can be injected into the annulus during the splicing process and tripping but subsurface control is not good enough.

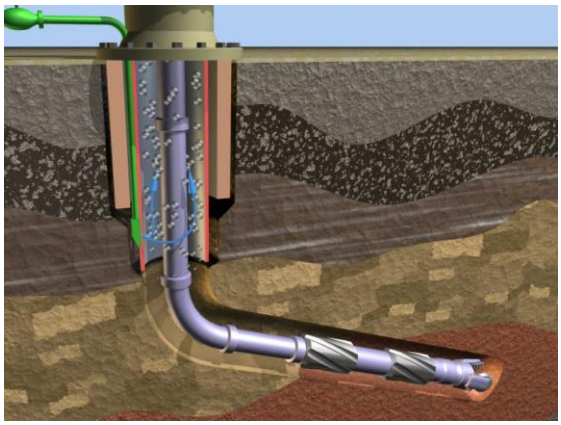


Figure 2: Illustration of Parasite String Injection

Aerated Drilling Equipment

In general, the equipment's used in the aerated drilling are:

1. Compressor
   The compressor is used to supply air to send the compressed air up to 1150 cfm at pressures of 150-350 psi.
2. Rotating Blow Out Preventer
   (RBOP) mounted above Blow out Preventer (BOP). RBOP serves to regulate the flow through the wellbore (Adams et al, 1985).
3. Booster
   Booster will continue output of the compressor and provide additional pressure to 2500 psi.
4. Separator
   Separator used must be able to separate the air with bottom liquid.
5. Float Valve
   Float valve which is mounted on the bit groove serves to hold back from the annulus to the drillstring and also serves to hold the air flow to the drillstring when tripping operations.

In figure 3, there is a schematic circulation of aerated drilling process, in which liquid circulation of air from the booster pumps and meet the standpipe. So aerated drilling technique in this scheme is the air injection technique through the drill pipe.

METHODOLOGY

In planning of the application of aerated drilling method, it is necessary to consider three aspects for the success of drilling, such as:

1. The hydrostatic pressure from aerated fluid.
2. The capacity to drain aeration slurry on liquid motors, boosters and liquid pumps.

3. Annulus velocity differential with a minimum velocity of aerated to circulate cutting.

In aerated drilling, it is expected that the difference of hydrostatic pressure and pore pressure is smaller. in order to avoid loss of circulation that caused by the entry of drilling fluid into the pores and fractures during drilling, the key is to gain the optimize ECD for aerated drilling that can dry cutting from the bottom hole to the loss zone (total loss). In the field, to determine the amount of formation pressure obtained from the historical study of data when the pore pressure obtained from Pressure & Temperature Survey during shut-ins (Figure 4).

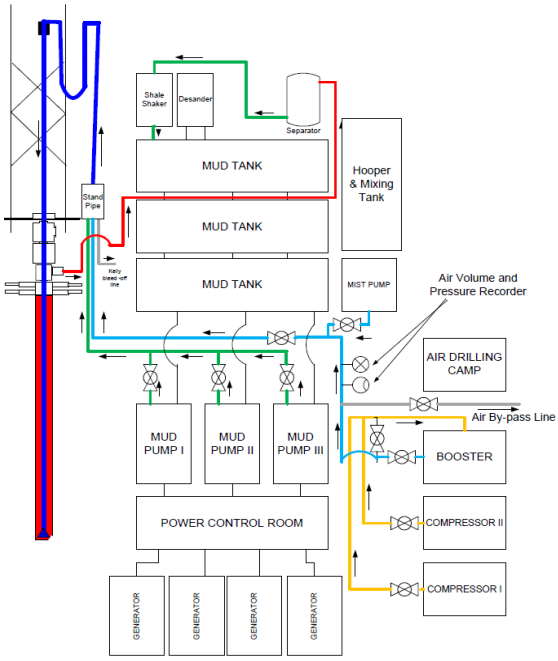


Figure 3: Illustration of Aerated Circulation Drilling System Layout

Calculation BHP

Air is a compressible fluid so that the volume will respond to changes in pressure and temperature. If 1 scf of air injected at the surface, at a depth with pressure and temperature of the air volume will be:

$$VGP = Vgs \left(\frac{T_2 \cdot P_1}{T_2 \cdot P_2}\right) \text{..... (1)}$$

Where:

VGP = Volume of air at a depth (D), cuft
Vgs = Volume of air on the surface condition (s), scf
T1 = Surface temperature (s), R°
T2 = Average temperature at a depth (d), Ro
= {(D / 2) x ΔT} + T_1
P1 = Surface pressure, psia
P2 = Average pressure at a depth, psi
= {(D x ΔP) + P_1} / 2

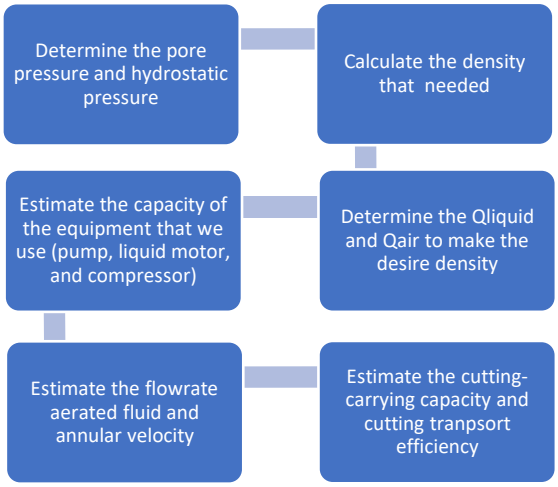


Figure 4: Workflow for the gain optimize ECD for the application of aerated drilling.

ΔT = The temperature gradient, °F / 100 ft
ΔP = The pressure gradient, psi / ft

Air density will also change to the conditions of pressure and temperature at certain depths. If the air gravity (S) = 1, then the air density (ρgs) on the surface condition are:

$$\rho gs = \frac{2730 \; x \; S \; x \; P_1}{T_1} \text{ ..... (2)}$$

Hence the level of air density (ρgp) at a certain depth is:

$$\rho gp = \rho gs \left(\frac{T_1 \cdot P_2}{T_2 \cdot P_1}\right) \text{..... (3)}$$

Where:

ρgs = Density of the air at surface conditions, scf
ρgp = Density of the air in the condition of a depth, pcf
S = *gravity* air
T1 = Surface temperature (s), R°
T2 = Average temperature at a depth, R°
P1 = Surface pressure, psia
P2 = Average pressure at a depth, psi
= {(D x ΔP) + P_1} / 2

Thus the air flow rate to the desired depth can be calculated by:

$$Qgp = QGS \left(\frac{T_2 \cdot P_1}{T_1 \cdot P_2}\right) \text{..... (4)}$$

Where:

QGS = Volumetric rate of air injection at the surface, scfm
T1 = Surface temperature (s), R°
T2 = Average temperature - average at a depth, R°
P1 = Surface pressure, psi
P2 = Average stress - average at a depth, psi
= {(D x ΔP) + P_1} / 2
Qgp = Volumetric rate of air injection at depth, gpm

Having obtained the volumetric rate at a depth of air injection, the next is to determine the volumetric rate of air injection at the surface with the following equation:

$$QGS = Qgp \left(\frac{T_1 \cdot P_2}{T_2 \cdot P_1}\right) \text{..... (5)}$$

Where:

QGS = Volumetric rate of air injection at the surface, scfm
T1 = Surface temperature (s), Ro
T2 = Average temperature at a depth, Ro
P1 = Surface pressure, psia
P2 = Average pressure at a depth, psi = {(D x ΔP) + P_1} / 2
Qgp = Volumetric rate of air injection at depth conditions, gpm

By knowing the liquid flow rate and the air at depths then aerated fluid density can be calculated by the following equation:

$$\rho A.\ QA = \rho_1, Q1 + \rho gp.\ Qgp$$
$$\rho A.\ (Q1 + Qgp) = \rho_1, Q1 + \rho gp.\ Qgp$$

$$\rho A = \frac{(\rho_m \cdot Q_m) - (\rho_{gp} \cdot Q_{gp})}{(Q_m - Q_{gp})} \text{ ..... (6)}$$

Where:

ρA = Density of the fluid aeration, ppg
QA = Volumetric air injection rate, gpm
ρm = Density of the liquid, ppg
qm = Total flow rate, gpm
ρgp = Density at a depth conditions, ppg
Qgp = Volumetric rate of air injection at depth, gpm

By knowing the density of the fluid aeration, it can be calculated much pressure aerated fluid hydrostatic with the following equation:

$$Ph = 0.052 \times \rho_A \times h \text{ ..... (7)}$$

Where:

Ph = Hydrostatic pressure, psi
ρA = Density of the fluid aeration, ppg
h = Depth, ft

The liquid fraction in aerated drilling liquid

Based on the above equation, the volume fraction of air in the drillstring will be reduced with the increasing depth.

$$Fls = \frac{V_{ls}}{V_{gs} + V_{ls}} \text{..... (8)}$$

$$Phi = \frac{F_{lo}}{\left\{F_{lo} + \frac{(1 - F_{lo})}{\left(\frac{P}{P_o}\right)}\right\}} \text{..... (9)}$$

$$FGS = \frac{V_{gs}}{V_{gs} + V_{ls}} \text{..... (10)}$$

$$FGP = \frac{F_{go}}{\left\{F_{go} + \frac{(1 - F_{go})}{\left(\frac{P}{P_o}\right)}\right\}} \text{..... (11)}$$

Where:

Flo = Liquid fraction at surface,%
Fgo = Fraction of air on the surface,%
Phi = Fraction of the liquid at depth,%
FGP = Fraction of air at a depth,%
VGO = Volume of air on the surface,%
VGP = Volume of air at a depth conditions, cfm
Vt = Total volume, cfm
P = Pressure at a certain depth, psi
Po = Atmospheric pressure, psi

Aerated slurry viscosity

Determine the magnitude of the two-phase fluid viscosity at any depth which have different pressure and temperature, can be found using the following equation:

uA = (FGP. μgp) + (1 - FGP). mL ... (12)

Where:

uA = Aerated slurry viscosity, cp
μgp = Air viscosity, cp
mL = Viscosity of liquid, cp
FGP = Fraction of air at a depth, %

Velocity and pattern of aeration fluid flow

Aerated slurry velocity can be determined using the following equation:

In the annulus (Vann):

$$Vann = \frac{Q_A}{\left(\frac{\pi}{4}\right) \cdot (D_h{}^2 - D_{op}{}^2)}, \text{ Fpm ... (13)}$$

Where:

Vp = Aeration velocity in the drillstring, fpm
QA = Aeration flow rate, cfm
Dh = Diameter of the drillpipe, inch
dh = Drill hole diameter, inch
Dop = Outer diameter drillpipe, inch

By knowing the velocity of the aerated fluid. Aeration fluid flow pattern can be estimated using the Reynolds number:

To flow in the annulus:

$$NRE = \frac{15.47 \cdot D_{ep} \cdot \rho_A \cdot V_{ann}}{\mu_A} \text{ ..... (14)}$$

Where:

NRE = number *Reynold*
dip = Diameter of the drillpipe, inch
Dep = Hydraulics annulus diameter, inch
ρA = Density of the aeration fluid, ppg
Vp = Aeration velocity in the drillstring, fpm
uA = Aerated fluid viscosity, cp
Vann = Velocity aerated fluid in the annulus, fpm

Theoretically, will flow: laminar if NRE <2000 transition if 2000 <NRE <4000 and turbulent if NRE> 4000

cleaning cutting

It takes a critical velocity (Vc) to clean the cutting of the drill hole so that the concentration of cutting inside the annulus does not exceed the critical concentration (Cc) which is not more than 5%.

$$vc = \frac{ROP}{60 \cdot C_c}, \text{ Fpm} \quad \text{..... (15)}$$

Where:

vc = Critical velocity, fpm
ROP = *Rate of Penetration*, Ft/hr
cc = Critical concentration ((0.01778 x ROP) + 0505)

Cutting have a tendency to move in opposite directions with the drilling fluid or cutting so-called terminal velocity (Vt). Drill dust terminal velocity for laminar flow pattern, transition, and turbulent through drill powder.

In laminar flow:

$$Vt = 4980.dc\left(\frac{\rho_c - \rho_A}{\mu_A}\right) \quad \text{..... (16)}$$

In a stream of transition:

$$Vt = 175.dc.\left[\frac{(\rho_C - \rho_A)^{\frac{2}{3}}}{(\rho_A \cdot \mu_A)^{\frac{1}{3}}}\right] \quad \text{..... (17)}$$

In turbulent flow:

$$Vt = 92.6\sqrt{dc\ \left(\frac{\rho_C - \rho_A}{\rho_A}\right)} \quad \text{..... (18)}$$

The equation for the minimum velocity of the liquid in the annulus to clean cutting from holes contained in the directional path.

For $\theta \leq 45$ °:

$$Vt\ corr = Vt\left[1 + \frac{\theta \cdot (600 - RPM) \cdot (3 + \rho_A)}{202500}\right], \text{ fpm ...(19)}$$

For $\theta \geq 45$ °:

$$Vt\ corr = Vt\left[1 + \frac{(600 - RPM) \cdot (3 + \rho_A)}{4500}\right], \text{ fpm ..... (20)}$$

Where:

Vmin = Minimum velocity, fpm
vc = Critical velocity, fpm
Vt = Terminal velocity, fpm
ρA = Density of the liquid, ppg
ROP = *Rate of Penetration*, Ft / hr

Reynold Numbers for cutting:

$$NREC = \frac{15{,}47 \cdot \rho_A \cdot V_{t\,koreksi} \cdot dc}{\mu_A} \quad \text{..... (21)}$$

Theoretically, laminar flow through if NREC <1, the flow transitions if 1 <NREC <2000, the flow will be turbulent if NREC >2000.

Thus cleaning the drill holes will be good enough if the aeration fluid velocity in the annulus (Vann) cumulatively bigger the critical velocity (Vc) and terminal velocity (Vt) cutting.

$$Vann > Vc + Vt \quad \text{..... (22)}$$

Where:

Vann = velocity aerated fluid in the annulus, fpm
Vc = critical velocity, fpm
Vt = terminal velocity, FTM

By using these equations can be known whether the removal of the drill dust from the annulus is good or not:

1. Appointment pretty good, if:
   Vann> Vmin
2. Appointment of powder is not good, if:
   Vann <Vmin

The amount of transport efficiency *cutting*s determined by:

$$VT = V_{ann} - Vt \quad \text{..... (23)}$$

$$Ft = \frac{V_T}{V_{ann}} \text{ x } 100\% \quad \text{..... (24)}$$

For optimization *Rotating Blow Out Preventer* determined having regard to the concentration of cutting, the maximum concentration of the well is 5% (Rabia, 2001; Bourgoyne, 1986).

$$ca = \frac{ROP\ x\ {D_h}^2}{14{,}71\ x\ F_t\ x\ Q} \quad \text{..... (25)}$$

Where:

ROP = *Rate of penetration*, Ft / hr
VT = *cutting transport*, Ft / min
et = efficiency *cutting transport*,%
ca = concentration *cutting* in the drilling fluid in the annulus
dh = Drill hole diameter, inch
Q = Aeration flow rate, gpm

CASE STUDY

In this case study, drilling was carried out using aerated drilling method on a 12 1/4 "section at a depth of 940 MMD - 1600 MMD. On a 12-1 / 4" section occurs total loss, so that aerated fluid does not return to surface that we call the blind drilling. Due to the total loss of the cutting is also not circulated come to the surface, so that the cutting will be entered into the zone of loss. from the reservoir of data, authors can plot the gradient pore pressure and gradient fracture (Figure 5).

Once we know the gradient pore pressure and fracture gradient, if we do with conventional drilling, there will be a large difference pressure between the pressure of the hydrostatic column and pore pressure. In the first experiment the author did a simulation with the usual liquid with density at 9 ppg which can be seen in figure 6.

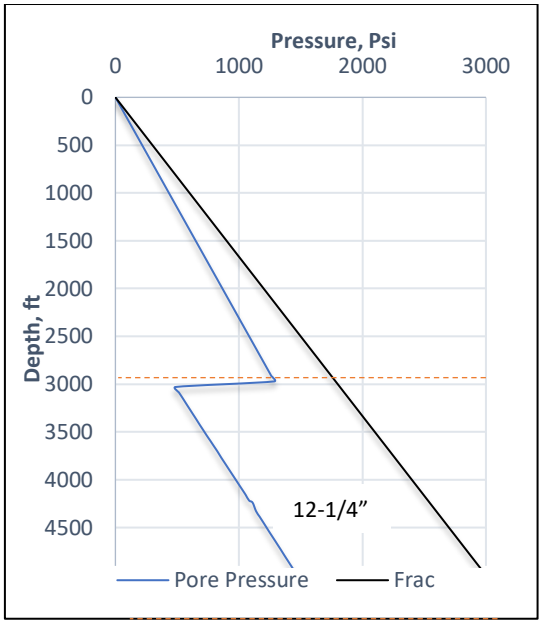


Figure 5: Gradient Pore Pressure and Pressure Gradient fraction.

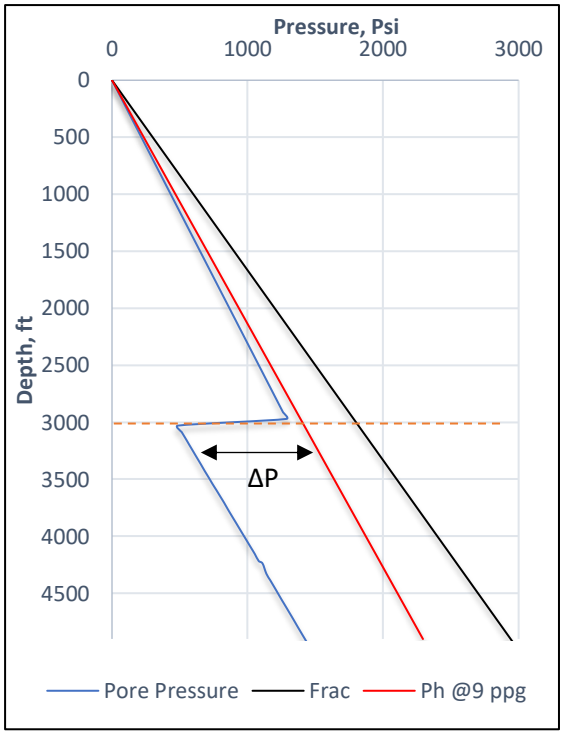


Figure 6: Illustration of Hydrostatic pressure of 9 ppg on Gradient Pore Pressure and Pressure Gradient Fracture

From figure 6 it can be seen that the delta pressure between the pore pressure of hydrostatic pressure so is far, then for decrease the differential pressure between hydrostatic pressure and pore pressure is needed aerated drilling to gain lower density. Author determines the aerated fluid pressure hydrostatic we simulated trial and error using gas law equation that restricted the ability of equipment. In this paper the capacity of the equipment used in the implementation of aerated drilling can be seen in Table 1.

Table 1: Specification of Equipment for aerated drilling.

equipment	unit	total Capacity	
Liquid Pump	2	Horse Power, HP	3136
		Flowrate, gpm	1438
		Pressure, psi	3737
compressor	1	Flowrate of 250 psi, scfm	1150
booster	2	Flowrate @ 2500 psi, scfm	4000
Liquid Motor	1	Range flowrate, gpm	600 - 1200

By using the gas law calculations are used to determine a combination of liquid and a flowrate of water so as to calculate the total flowrate while the liquid motor, that aerated fluid flowrate does not exceed the capacity of the motor liquid. Then the author did three scenarios, with each ECD increment 1 ppg.

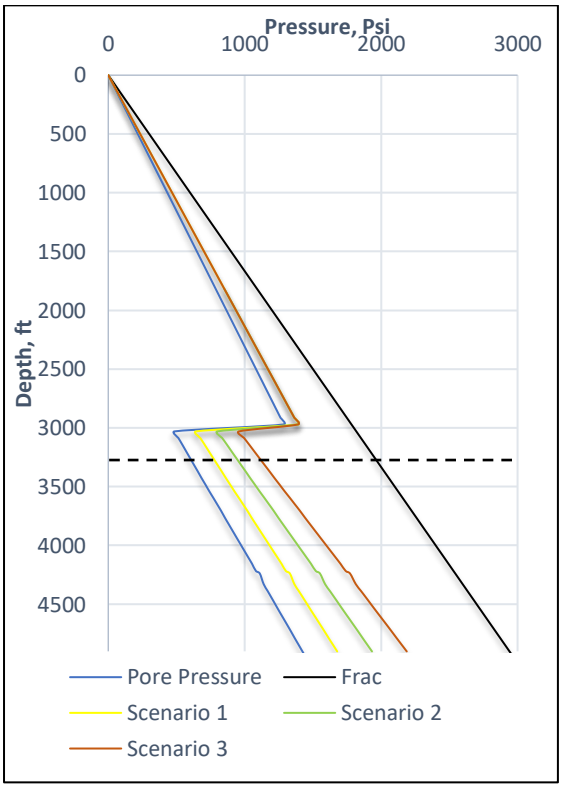


Figure 7: Illustration of Pressure Window for 3 scenarios

Author uses one depth to calculated in order to compare its performance, which is at a depth of 3256 ft TVD. With constant liquid flowrate is equal to 700 gpm. So that in this scenario price obtained 3 air injection surface.

Table 2: Comparison between 3 scenarios @ 3256 ft TVD

	scenario 1	scenario 2	scenario 3
ECD, ppg	4.5	5.5	6.5
Ph, psi	768	937	1106
Water Injection, scfm	5078	3164	1885
ratio	54.27	33.82	20:15

From table 2 the density of each scenario is 4.5 ppg, 5.5 ppg and 6.5 ppg, where each scenario its aerated ECD difference of 1 ppg. From the density of aerated fluid, obtained the hydrostatic pressure column where the greater the density, the greater the hydrostatic pressure. For the determination of air injection at the surface is determined by the ECD of the liquid, liquid flowrate and the desired ECD. In this paper flowrate and the ECD of the liquid it becomes variable fixed at 700 gpm and 9 ppg. So each of the required water injection scenario are 5078 scfm, 3164 scfm, and 1885 scfm and each ratio of air and liquid are 54.27, 33.82 and 20:15.

From the results if associated with equipment used for scenario 1 the capacity of the equipment used is not sufficient, so that the necessary upgrade equipment for the booster. But for scenario 2 and 3 can be done with the available equipment.

Having obtained the required air injection are used to determine the total flowrate occurring in the BHA mud motor and the annular velocity calculation so that it can be seen cleaning the cutting at the base of the drill hole. If aerated fluid cannot clean cutting at the bottom of the borehole, there will be the problem of stuck pipe.

At a depth of 3256 ft TVD total flowrate in mud motors, annular velocity and cleaning cutting at the base of the drill hole for the third scenario can be seen in Table 3. It shows a comparison of each scenario, for a total flow rate in scenario 1 exceeds the capability of 1200 gpm mud motors, so that when it is done it will cause a liquid motor burned out. In scenarios 2 and 3 on the capacity of the liquid motor can be used, but the scenario 2 flow rate produced greater than scenario 3.

Each flow rate in each scenario, annular velocity is proportional to the flow rate that scenario 1 is greater than scenarios 2 and 3, and scenario 2 greater than scenario 3.

The greater velocity makes the greater the Reynold number, where the Reynolds number of each scenario is greater than 4000. Thus, in the third scenario in the form of turbulent flow. Turbulent flow is expected to circulate the liquid so that the cutting can be carried away by the aerated fluid.

Table 3: Comparison between 3 scenarios @ 3256 ft TVD

	scenario 1	scenario 2	scenario 3
Tot flow rate, gpm	1481	1186	990
Annular Velocity DC, fpm	421	337	281
DP annular velocity, fpm	290	232	193
NRE DC	38104	37 314	36 787
NRE DP	26221	25 678	25 315
Ft DC,%	88.6	87.55	86.7
Ft DP,%	83.49	81.9	80.68
Vmin, fpm	249.8	200.7	167.9
Ca DC,%	0.5	0.64	0.77
Ca DP,%	0.78	0.99	1.2

The result of cutting transport (Ft) in the drill collar and drill pipe in each scenario is greater than 80%, so that transport cutting is good. And the minimum velocity (Vmin) to bring cutting under the annular velocity so that aerated fluid can clean cutting from the bottom of the drill hole. the Cutting Concentration (Ca) is less than 5% so cutting concentration is small enough so as to avoid the problem of stuck pipe.

From the results of the three scenarios, the analysis results for scenario one needs a upgrade booster and liquid motors (if available), if there is no equipment capable then the scenario 1 is not recommended even if the end result is most flattering. For scenario 2 all the equipment is still in its capacity so that there is no hindrance in the implementation and the results are better than scenario 3.

CONCLUSION

Aerated drilling geothermal wells used in the hole 12-1 / 4 "for their loss zone, the effect of total loss makes pore pressure smaller than usually. So aerated drilling is suitable to use in this condition.

Each scenario, annular velocity is equal to the flowrate that scenario 1 is better than scenarios 2 and 3, then scenario 2 is better than scenario 3.

In scenario 1 results of the simulation indicate that the equipment such as booster, compressors and mud motors had to do the replacement.

From the scenarios 2 and 3 can be seen that the results of the scenario 2 shows the total flowrate is higher than scenario 3. So the scenario 2 is the most optimum for aeration drilling in 12-1 / 4 " Section.

REFERENCES

Adams, N. J., Charrier, T., and Research Associate. (1985), "Drilling Engineering: A Complete Well Planning Approach", Penn Well Pub. Company., c1985, Tulsa, Oklahoma. Chapter 18. Page: 678-730.

Ashadi, and Dumrongthai, P. (2015), “Successful Implementation of Aerated Drilling in Improving Geothermal Drilling Performance”. Proceedings from World Geothermal Congress 2015.

Bourgoyne, A. T. (1986), "Applied Drilling Engineering", First Printing, Society of Petroleum Engineering, Richardson, Texas. Chapter 2. Page: 42 -52 and chapter 4 page 113-280.

Dwinanto, A., and Rachmat, Sudjati. (2014), "Aerated Underbalance Drilling Screening Assessment at "X" Geothermal Field in Indonesia". Proceedings from Thirty-Ninth Workshop on Geothermal Reservoir Engineering Stanford University, California. SGP-TR-202.

Hole, H. (2006), "Aerated Fluids for Drilling of Geothermal Wells", United Nations University Geothermal Training Progamme, Okustofnun – National Energy Authority, Iceland.

Lyons, W. C., and Plisga, Garry J. (1996), "Standard Handbook of Petroleum and Natural Air Engineering", Air Research Institute, Chicago, Illinois. Chapter 9 page: 213 - 244. Chapter 12 Page: 283-309

Nas, S., and Toralde, S. S. (2010), "Aerated Fluids Geothermal Drilling Operation in Asia Pacific". Proceedings from World Geothermal Congress 2010.

Nugroho, A. W., Hermawan, S., and Lazuardi, B. H. (2017), “Problem Mitigation in Geothermal Drilling, Case Studies of Stuck Pipe and Lost Circulation”. Proceedings from 42nd Workshop on Geothermal Reservoir Engineering Standford University, California, SGP-TR-212.

Putra, I. M. B. K. A. (2008), " Drilling Practice with Aerated Drilling Fluid: Indonesian and Icelandic Geothermal Fields", Pertamina Geothermal Energy, Kamojang. GEOTHERMAL TRAINING PROGRAMME, Number 11, IS-108 Reykjavik, Iceland.

Rabia, H. (1985), "Oil Well Drilling Engineering, Principles and Practice", Universty of Newcastle Upon Tyne, Graham and Trotman Ltd, London. Chapter 7. Page: 198-199 and 218 - 225. Chapter 8 page 233-268.

Subiatmono, P., Yulianto, I., and Kennedy. (2001), “*Penerapan Teknologi Pemboran Underbalanced pada Sumur Lapangan Jatibarang Pertamina DO Hulu Cirebon*”. Proceeding from Simposium Nasional IATMI, Yogyakarta.

ENHANCING PERMEABILITY OF NO-TOTAL-LOSS-CIRCULATION WELL BY POWER WASH: CASE STUDY ON TULEHU GEOTHERMAL FIELD

Tony Widiatmoro, Miman Afiff, Hendra Y. T. Tondang, and Yudistian Yunis

PT PLN (Persero)
Jalan Trunojoyo Blok M1-135, Kebayoran Baru, Jakarta 12160, Indonesia
Email: tony.widiatmoro@pln.co.id

ABSTRACT

Power wash was performed in the TLU-B02 well before the Completion Test by taking advantage of the high pumping capability of drilling rig pumps. Power wash was decided to be implemented due to the notion that the well has low permeability but possibly high temperature as indicated by the temperature reading of measurement-while-drilling (MWD) tool reached 160^{0}C and having no Total Loss Circulation (TLC), just a few Partial Loss Circulation (PLC). The cumulative PLC occurred is 1850 bbls, which is 384 bbls higher than the cumulative PLC occurred in TLU-C01 well. The result of Power Wash is relatively promising. Even though no drastic breakdown was visible during the program, the improvement of permeability is obvious. This is indicated by the increasing of injection rate capability by 50 m3/h at the same Wellhead Pressure (WHP), as well as further result of the long-term production test. The TLU-B02 was capable to discharge two-phase fluid throughout the 20-days test period, with the brine and steam rate 60-80 t/h and 10-20 t/h, respectively. Comparing to the TLU-C01 well, in which it was failed to sustainably discharge fluid, the Power Wash program in TLU-B02 is proven to be effective in enhancing the well permeability and productivity.

Keywords: Powe wash, PLC, ehancing permeability, Tulehu Geothermal Field.

INTRODUCTION

Tulehu geothermal field is located in Ambon Island, Maluku Province. After several geo-scientific surface surveys and total six thermal gradient holes (40 – 150 m deep) had been drilled in 2008 and 2009, the first exploratory well TLU-A1 was drilled in December 2010 to July 2011 (930 m drilled depth). Following this exploratory drilling, another drilling campaign was conducted in between June 2017 to April 2018, in which four wells were successfully drilled to 1800 – 1900 m depth and two of which were tested.

Power wash was performed in the TLU-C1 and TLUB-2 wells before the Completion Test by taking advantage of the high pumping capability of drilling rig pumps. Power wash was decided to be implemented since the wells have no Total Loss Circulation (TLC), just a few Partial Loss Circulation (PLC) but possibly high temperature as indicated by the temperature reading of measurement while-drilling (MWD) tool reached 160 ^{0}C. The cumulative PLC occurred in TLU-B2 is 1850 bbls, which is 322 bbls higher than the cumulative PLC occurred in TLU-C1 well.

SUMMARY OF LOSS CIRCULATION ON TLU-C01 AND TLU-B02

It should be noted that estimated partial losses are based on active pit volume changes, while mud pump strokes are used for total losses. In many cases the amount of fluid loss during partial lost circulation is underestimated because new fluid is being added to the pits on a continuous basis.

TLU-C01

Approximately only 1528 bbls of fluid was lost in TLU-C1 during drilling. In 17 ½" and 12 ¼" hole section, no losses encountered. The 8 ½" hole section was drilled with full mud return until 1388 m where 1.6 bpm PLC first occurred, then after pump Loss Circulation Material (LCM) pills, it backs to full mud return until PLC again in 1426 to 1448 m with 3.50 bpm, following with several PLC up to 1491 m depth, then starting from 1491 until 1900 mMD (total depth), full mud return was undergone (PT PLN, 2018. Well Drilling Report of TLU-C1). The figures below summarize loss circulation on TLU-C1.

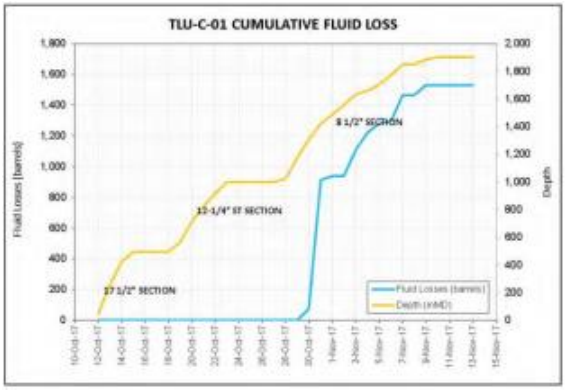


Figure 1. Fluid Losses in TLU-C1

TLU-B02

Approximately only 1850 bbls of fluid was lost in TLU-B2 during drilling, which is 322 bbls higher than fluid loss in TLU-C1. No losses were occurred

during drilling hole 17-1/2" and 12-1/4" holes. The 8-1/2" hole section was drilled with partial loss circulation occurred in several depth (see Figure 2 below). Introduction of aerated drilling at depth intervals: (1) 1,362 to 1508 mMD, (2) 1513 to 1666 mMD, and (3) 1712 to 1734 mMD, disguised the PLC and ceased the partial losses at the respective intervals. Only during the system changed back to mud system, PLCs were then rediscovered (PT PLN, 2018. Well Drilling Report of TLU-B2).

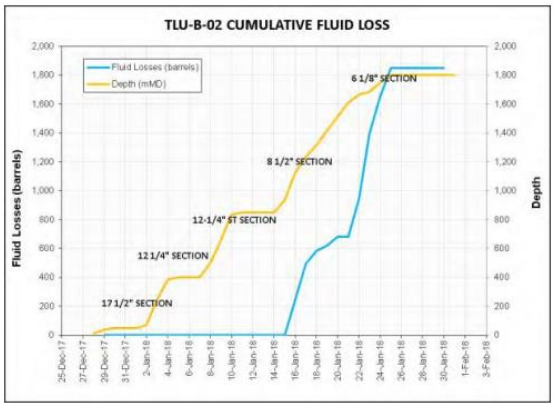


Figure 2. Fluid Losses in TLU-B2

HYDRAULIC FRACTURING AND POWER WASH

Hydraulic Fracturing is a technique commonly used in oil and gas field to enhance permeability of inherently tight well. The technique involves high pumping pressure and high volume of viscous fluid to create a conductive fracture in the rock formation extending from the wellbore connecting into the reservoir. It might need proppant material which are mixed at the surface with the viscous fluid then flowing and distributing the proppant, depositing it in the created fracture to hold the fracture open. Otherwise, it would close when the fluid stops flowing.

Power Wash is slightly different than hydraulic fracturing in terms of proppant material use and fracture creating. The concept of power wash is to inject the water into the fracture/crack zone (PLC zone) around the well with some additional pressure so that the small crack, which might have been plugged by mineral deposits over time, is cleaned and opened more, thus create good connection to the reservoir. Power wash does not use proppant material and does not create fracture, instead just cleaning and opening the existing fracture.

As in the geothermal environment the rock type is not sedimentary but compact volcanic rock, it is difficult to create fractures due to a high fracture pressure gradient, high Young's modulus and compressive strength (Jia et al., 2013). It is also observed that a significant increase of permeability by fracturing in volcanic rock shall require pore pressure in the order of 3.5 MPa or equal to roughly 350 bar (Eggertsson, et al., 2018). Meanwhile, the "weak point" of the well is exactly around the existing fracture zone which induced PLCs at the deeper levels. Power Wash possibly contributes to improve the permeability at the observed fracture zone (PLC zone), and as the rock formation is compact, the requirement for proppant material no longer exists. In addition, even proppant material is used, it is hard to control the distribution of proppant material in volcanic rock formation due to the heterogeneity of fracture along both horizontal and vertical direction (Cheng et al., 2016). Table 1 below shows the difference between Hydraulic Fracturing and Power Wash.

POWER WASH IN TLU-C01 AND TLU-B02

Power wash in TLU-C1 and TLU-B2 were performed for 26 and 20 hours, respectively. The pressure of the power wash which has been carried out in other geothermal fields often exceeds 50 barg. Considering the maximum working pressure of the wellhead equipment (10"ANSI900 valve) is about 150 barg, the pressure of 50 barg is only 33% of the maximum pressure (safety factor = 3). Therefore, it is recommended to carry out power wash with wellhead pressure of 50 barg (or more, maximum 75 barg at safety factor of 2, depending on the site condition). The power wash is carried out after running the perforated liner. The general sequence is shown in Figure 3.

Table 1. Comparison of Hydraulic Fracturing and Power Wash

Hydraulic Fracturing	Power Wash
Proppant material used	Not using Proppant
Viscous fluid pumped	Fresh water pumped
Creating fracture	Clean and open existing fracture
Usually used in Sedimentrary rock	Usually used in Volcanic rock



Figure 3. General Sequence of Power Wash

The example of the power wash program implemented in Tulehu is as follows.

1) Install pressure gauge at well head with range 0 to 3000 Psig and close Master Valve.
2) Start water injection into the well through 3 1/8" wing valve at small flow rate and monitor the wellhead pressure.
3) Increase flow rate step by step. Keep monitoring the wellhead pressure.
4) Increase flow rate step by step. Keep monitoring the wellhead pressure.

5) If there is pressure drop at wellhead (indication of permeability increase), increase injection rate and keep wellhead pressure at predetermined value again.

6) If there is no drop of wellhead pressure after one day pumping (depending on the site condition), terminate power wash work.

TLU-C01

Power wash commenced on 11 November 2017 at 5.46 pm and finished on 12 November 2017 at 8.00 pm. Once the power wash started, the well accepted about 23.62 m3/h of water, with the increasing wellhead pressure to the stable pressure of 29.78 barg. The injection rate then was increased up to 40.88 m3/h and wellhead pressure increased to about 36.4 barg at the maximum (PT PLN, 2017. Power Wash Program of TLU-C1).

There was an indication of the permeability improvement, although it was not significant. The indication was clearly seen by comparing the WHP and the injection rate between hours 10 and hours 25, in which at the almost similar WHP (± 36 barg), the well could have accepted around 4.5 m3/h more water at the end of the program (see Figure 4).

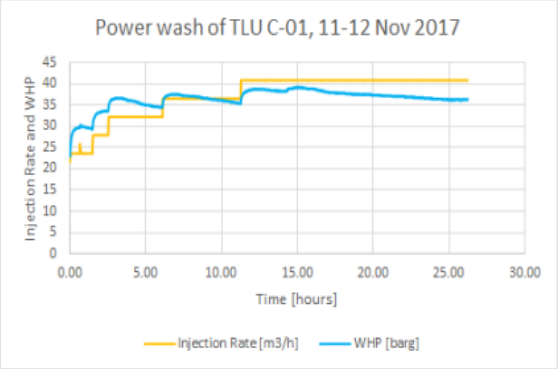


Figure 4. Injection Rate and Wellhead Pressure during Power Wash Program in TLU-C1

TLU-B02

Power wash commenced on 27 January 2018 at 3.00 pm and finished on 28 January 2018 at 11.00 am. Once the power wash started, the well accepted about 45.2 m3/h of water, with the increasing wellhead pressure to the pressure of 3.3 barg (see Figure 5). The injection rate was increased up to 320 m3/h and wellhead pressure increased to about 38.13 barg at the maximum (PT PLN, 2018. Power Wash Program of TLU-B2).

There was no drastic breakdown during the program, yet the improvement of permeability is obvious. The indication was clearly seen by comparing the WHP and the injection rate between hours 8 and hours 18, in which at the almost similar WHP (± 33 barg), the well could have accepted around 48 m3/h more water at the end of the program. Nevertheless, the WHP recorded at hours 18 should be carefully noticed since this pressure was not stabilized yet. This is part of the main challenge encountered during power wash, which is related to the availability of water. It was often to switch off the pump due to the insufficient amount of available water. This led to the shorter available time to obtain stable pressure at certain injection rate.

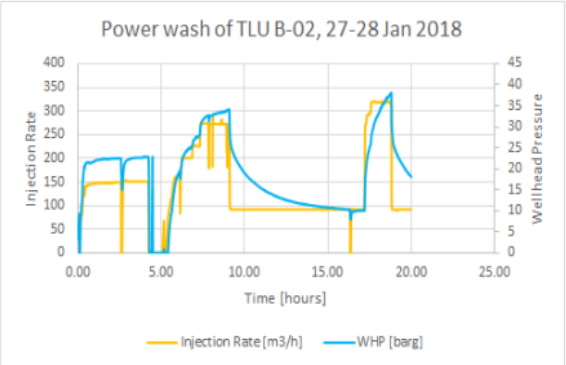


Figure 5. Injection Rate and Wellhead Pressure during Power Wash Program in TLU-B2

DISCUSSION

Injectivity Increase on TLU-C01 and TLU-B02 during Power Wash

As the wellhead pressure and injection rate were monitored, injectivity of the well could be easily obtained. This injectivity value was obviously not comparable to the injectivity obtained by Multi-rate Injection Test, as the wellhead pressure was used, instead of downhole pressure. Yet, at least, it could be used as a success indicator of the program.

As shown in Figure 6 and 7, both TLU-C01 and TLUB02 indicate injectivity increase at the end of the program, with the higher increasing of injectivity on TLU-B02 than on TLU-C01. Around 8.93 m3/h/bar of injectivity was observed on TLU-B02, achieving 2.34 m3/h / bar of injectivity increment. On the other hand, the raise of injectivity on TLU-C01 was not satisfying as the injectivity finally observed was only 1.12 m3/h / bar, not much different than the initial (0.8 m3/h / bar), suggesting almost no improvement of permeability on TLU-C01.

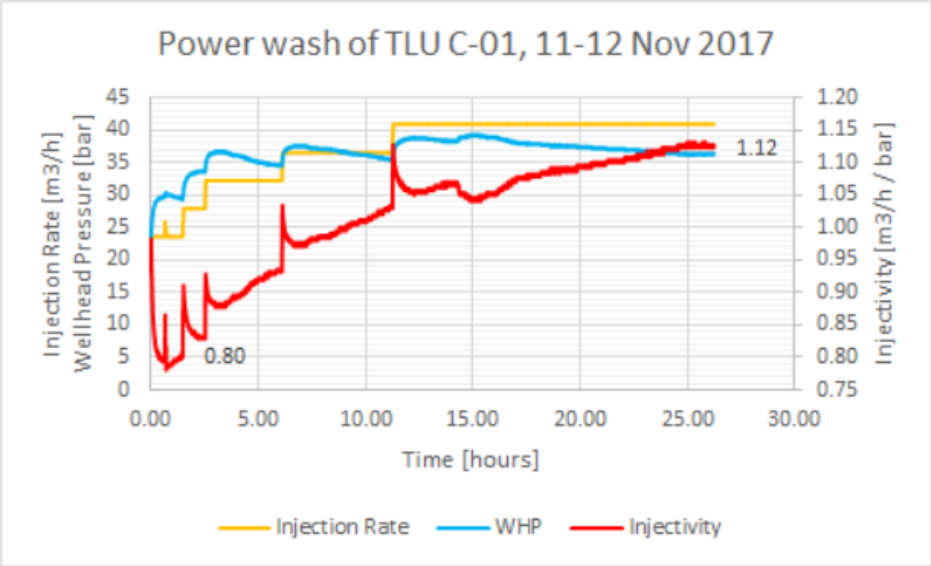


Figure 6. Injectivity Observation during Power Wash on TLU-C01

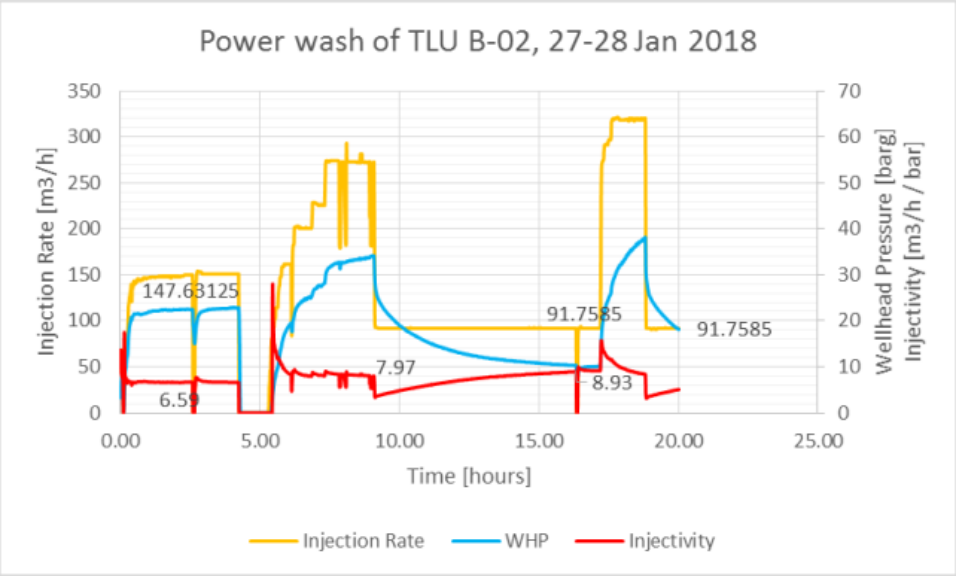


Figure 7. Injectivity Observation during Power Wash on TLU-B02

The injectivity increase on TLU-B02 was clearly seen when comparing the observed injectivity during first four hours with the observed wellhead pressure which was gradually decreasing from hours 9 and relatively stabilized at hours 16, as the injection rate was previously decreased and kept constant at approximately 91.75 m3/h (see Figure 7). The initial injectivity is around 6.59 m3/h when the injection rate was kept constant at around 147.63 m3/h, suggesting the improvement of permeability on TLU-B02.

Result Difference on TLU-C01 and TLU-B02

As discussed in the previous section, despite amount of fluid losses on the well TLU-B2 is relatively similar to TLU-C1, power wash in TLU-B2 successfully enhanced permeability of the well. Though, the utilization of aerated drilling in TLU-B2 should be duly noted, since it underestimates the fluid losses.

By assuming that most fluid loss went directly to the corresponding drilled depth, more than 1100 bbls (±60%) of fluid had lost in the depth interval of 1600 to 1800 mMD in TLU-B2 (see Figure 8), whereas in TLU-C1 most fluid (800 bbls; 52%) lost in the shallower depth interval (1300 – 1400 mMD) (see Figure 9).

Since the power wash relies on the created hydrostatic pressure, the success of power wash in TLU-B2 might be supported by the deeper PLC zone encountered. Therefore, at this deeper existing fracture zone, pressure gained by hydrostatic is higher and more beneficial to clean and open the fracture.

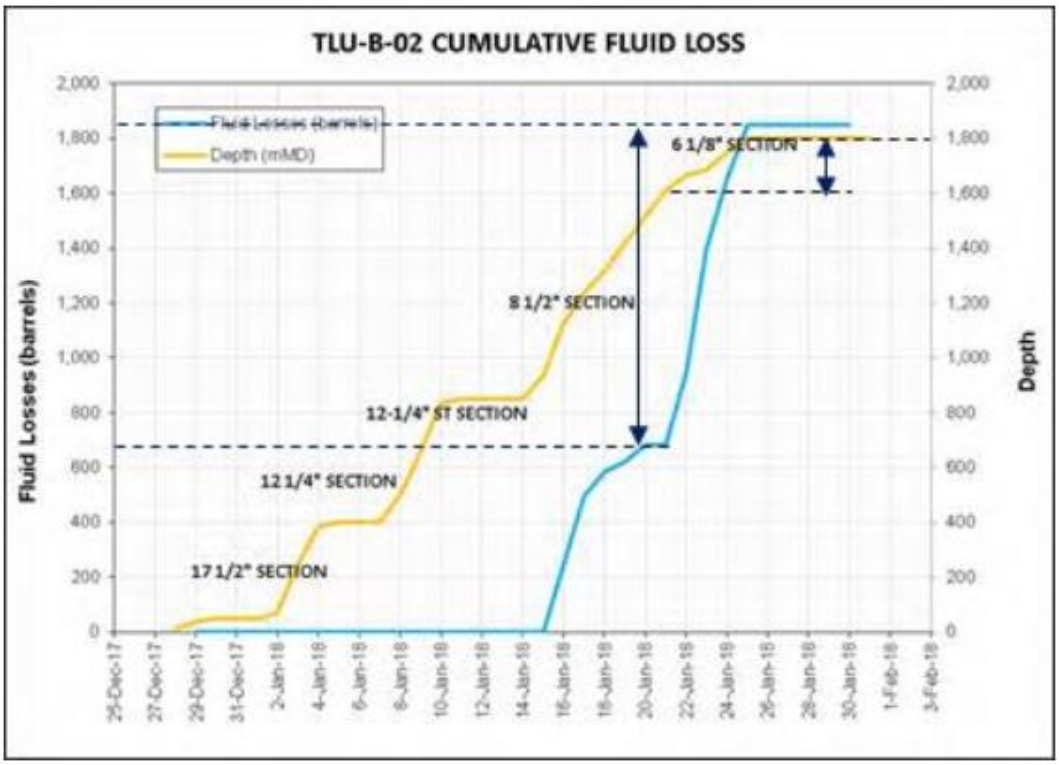


Figure 8. Cumulative Fluid Losses in TLU-B2 showing dominant PLC Zone at 1600 – 1800 mMD interval

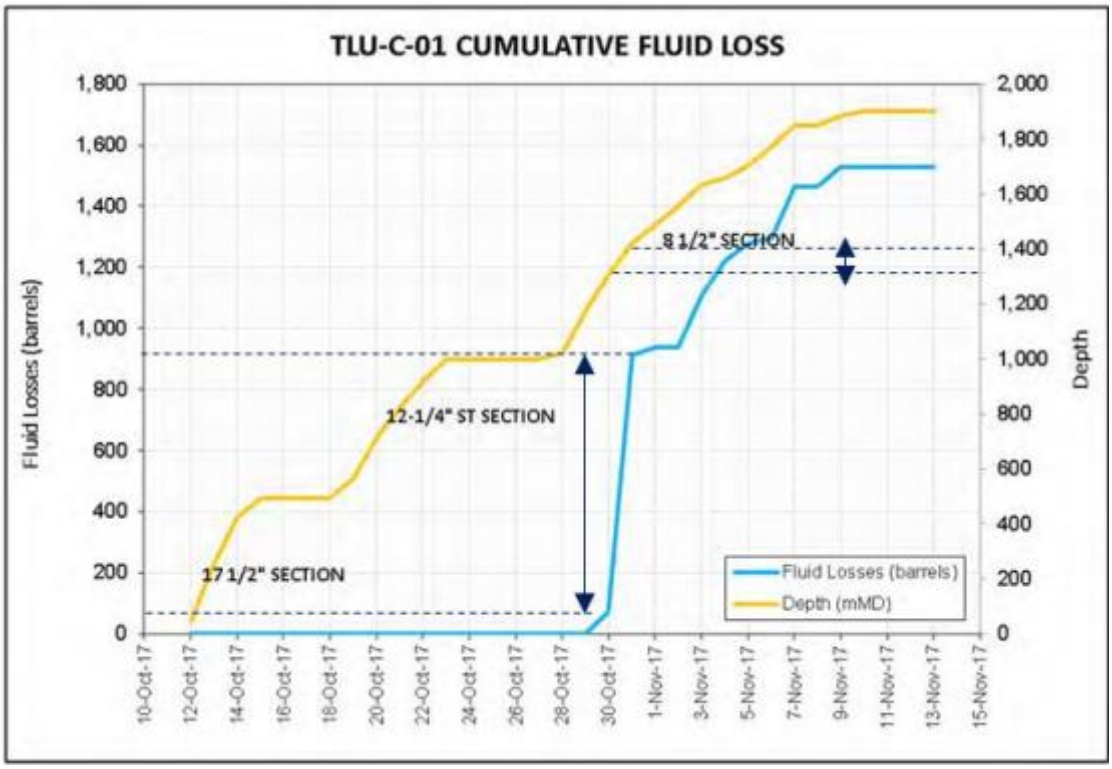


Figure 9. Cumulative Fluid Losses in TLU-C1 showing dominant PLC Zone at 1300 – 1400 mMD interval

The unsatisfied result of power wash program on TLU-C01 might be also due to the very low permeability of the well, as even trying to increase the amount of injection rate in order to obtain more hydraulic advantage, the wellhead pressure will rise excessively led to the emerging safety issue (see Figure 10). TLU-B02, on the other hand, still has slightly higher permeability than TLU-C01, thus the attempt of increasing injection rate would be

relatively less prone to the emerging safety issue due to the high pressure.

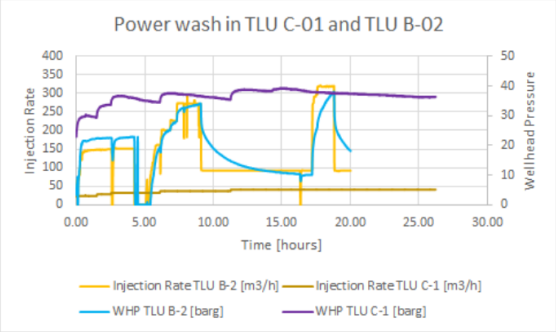


Figure 10. Injection Rate and Wellhead Pressure during Power Wash Program in TLU-C1 and TLU-B2

As the permeability of TLU-C1 is very low even after power wash program, which was indicated by low absorption capability of water, it was decided to skip all the Completion Test program, including Water Loss Test, Injectivity Test, and Pressure Fall-Off Test, except the heat-up survey. The maximum recorded temperature was 185.1 ^{0}C at the maximum depth, 1880 m. Following the heat-up survey, TLU-C1 was tried to be discharged but it was unsuccessful.

On the other hand, as the permeability of TLU-B2 is relatively higher than TLU-C1, the Completion Test was performed. The injectivity and the permeability thickness in the order of 6.21 t/h / bar and 1.6 darcym, respectively, were observed. Once air-cap stimulation in TLU-B2 was finished and the pressure released, it was successfully discharge geothermal fluid continuously and the production test lasted for 20 days (PT PLN, 2018. Production Test Report of TLU-B2). The TLU-B2 was capable to discharge two phase fluid, with the brine and steam rate around 60- 80 t/h and 10-20 t/h, respectively. The well is estimated to be able to supply steam for 1.5-2.0 MWe Single Flash plant (see Figure 11).

CONCLUSION

The result of Power Wash in TLU-B2 is relatively promising. Even though no drastic breakdown was visible during the program, the improvement of permeability is obvious. This is indicated by the increasing of injection rate capability by 50 m3/h at the same Well-head Pressure (WHP), as well as further result of the long-term production test. The TLU-B2 was capable to discharge two-phase fluid throughout the 20-days test period, with the brine and steam rate 60-80 t/h and 10-20 t/h, respectively. Comparing to the TLU-C1 well, in which it was failed to sustainably discharge fluid, the Power Wash program in TLU-B2 is proven to be effective in enhancing the well permeability and productivity.

The deeper of dominant PLC zone encountered during drilling, the higher possibility of permeability enhancement by power wash. This was well represented by the comparison of dominant PLC zone, cumulative fluid losses and the result of power wash in TLU-C1 and TLU-B2.

ACKNOWLEDGEMENT

This program has been supported by JV West Japan Engineering Consultants, Inc and PT Connusa Energindo as the Consultant in the development of Tulehu geothermal field. Most of the figures in this work are cited from the Consultant report.

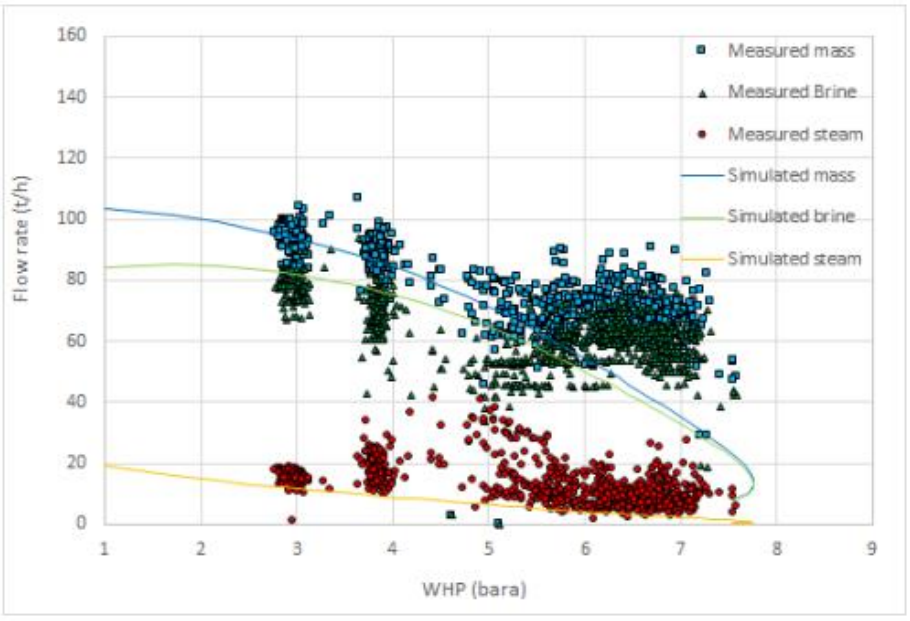


Figure 11. TLU-B02 Deliverability Curve and Matching Analysis

REFERENCES

Adele, M. A., 2009. *Evaluation of Maintenance Management Through Benchmarking in Geothermal Power Plant,* Iceland: United Nations University.

Eggertsson, G., Lavallée, Y., Kendrick, J., & Markússon, S. (2018). Improving fluid flow in geothermal reservoirs by thermal and mechanical stimulation: The case of Krafla volcano, Iceland. *Journal of Volcanology and Geothermal Research*. doi:10.1016 /j.jvolgeores.2018.04.008

Cheng, H., Huang, Bo., Han, S., & Fu, Y. (2016). Optimal design of hydraulic fracturing for deep volcanic reservoir in Zhungeer Basin. *Material Sciences, Engineering and Chemistry Web of Conferences*.doi:10.1051/matecconf/2017.10 020 02

Jia, L., Chen, M., Sun, L., Sun, Z., Zhang, W., Zhu, Q., & Jin, Y. (2013). Experimental study on propagation of hydraulic fracture in volcanic rocks using industrial CT technology. *Petroleum Exploration and Development, 2013, 40(3),* 405 - 408.

PT PLN (Persero). (2017). *Power Wash Program of TLU-C1*. West Japan Engineering Consultants, Inc.

PT PLN (Persero). (2018). *Power Wash Program of TLU-B2*. West Japan Engineering Consultants, Inc.

PT PLN (Persero). (2018). *Well Drilling Report of TLU-C1*. West Japan Engineering Consultants, Inc.

PT PLN (Persero). (2018). *Well Drilling Report of TLU-B2*. West Japan Engineering Consultants, Inc.

PT PLN (Persero). (2018). *Production Test Report of TLU-B2*. West Japan Engineering Consultants, Inc.

SILICA SCALE CONTROL IN GEOTHERMAL BOTTOMING CYCLE PLANTS BY pH-MODIFICATION AND THERMAL QUENCHING

Paul von Hirtz and Darrell Gallup

Thermochem, Inc.
3414 Regional Pkwy, Santa Rosa, CA, USA
Email: paul@thermochem.com

ABSTRACT

Flash, Organic Rankine Cycle (ORC) and combined-cycle geothermal power plants processing fluids from moderate to high-temperature (250 – 350 °C) reservoirs are prone to amorphous silica and silicate scaling in surface equipment and injection wells. Scaling can reduce plant generation capacity factors and cause loss in well injectivity. Advances in production chemistry and power plant engineering in the geothermal industry has led to the capability to control these scale deposits at very high levels of supersaturation. This allows much greater utilization of geothermal resources compared to older plants designed conservatively to maintain temperatures above silica saturation limits. Optimization of the pH-modification process and introduction of new combined-cycle geothermal power plants provides opportunities for highly efficient geothermal power generation. Many single-stage flash plants worldwide can achieve an increase of 30% or more in power generation from the same resource by adding an ORC bottoming plant to the existing facility, in conjunction with pH-modification for silica scale control.

Keywords: Silica scale control, pH modification, geothermal power plant.

INTRODUCTION

Worldwide output from geothermal sources has increased over 50% in the past 10 years. The worldwide installed generation capacity is currently over 14 GW and expected to rise to almost 17 GW by 2021 (Geothermal Energy Association, 2015). These geothermal power projects convert the energy contained in hot rock to electricity by using water to adsorb heat from the rock and transport it to the earth's surface, where it is converted to electrical energy through turbine-generators. It is estimated that more than 97% of current geothermal reservoir production is from magmatically driven reservoirs. Geothermal reservoirs may also develop outside regions of volcanic activity, where deeply penetrating faults allow groundwater to circulate to depths of several kilometers and become heated by the geothermal gradient (Bertani, 2015).

More than 90% of exploited fields are "liquid-dominated" under pre-exploitation conditions with reservoir liquid in equilibrium the crystalline silica minerals, typically quartz. "Vapor-dominated" systems, such as The Geysers in California and Larderello in Italy, produce dry steam without liquid and therefore the geothermal fluid does not carry high-concentrations of silica. The steam is passed directly through a steam turbine with minimal cleaning upstream. Typically, moderate to high-temperature water from (>220°C) "Liquid-dominated" reservoirs is partially flashed to steam in one or more stages. Heat is converted to mechanical energy by passing the flashed and separated steam through a steam turbine. About 15% of geothermal generation worldwide is generated by ORC technology where a heat exchanger extracts heat from pumped, unflashed hot water and a secondary working fluid drives a turbine. A small percentage of total generation is by combined-cycle technology, which includes a steam turbine and ORC cycle technology in one plant.

The flash, ORC and combined cycle plants processing fluids from liquid-dominated fields often have to manage scaling in the separated liquid. Technology development and execution have made it possible to exploit geothermal resources that might not have otherwise been accomplished. A major focus of production chemistry and engineering in the geothermal energy industry has been to control scale deposits from the geothermal fluids. The most ubiquitous and troublesome mineral scale encountered in geothermal power generation and injection facilities is amorphous silica or poorly-crystalline silicates. This paper discusses the occurrence and mitigation of silica scale in geothermal energy production.

THE GEOCHEMISTRY OF SILICA

The concentration of silica (SiO_2) in geothermal brine[1] is usually controlled by the dissolution of quartz and occasionally chalcedony from the geological strata of the reservoirs:

$$SiO_{2(qtz)} + 2H_2O = H_4SiO_4^0{}_{(aq)} \qquad (1)$$

The predominant form of dissolved silica is monosilicic acid, $Si(OH)_4$. Silica solubility at reservoir temperatures (above about 185°C) is usually controlled by the polymorph quartz; solubility at temperatures less than about 185°C is often controlled by the polymorph chalcedony, which is more soluble than quartz. For example, at 185 °C the solubility of quartz is 213 ppm as SiO_2,

while the solubility of chalcedony is 274 ppm as SiO_2. Therefore, chalcedony can substantially increase the amount of dissolved silica present in lower-temperature produced geothermal fluids above that expected from quartz equilibrium.

The solubility of silica deposited within geothermal surface facilities is controlled by amorphous silica and/or metal silicates phases. Quartz is virtually never found in surface production facilities and rarely deposited in or near production wellbores. The deposition of silica or silicate as a scale is primarily controlled by its polymerization and precipitation as amorphous silica or poorly-crystalline silicates, which are more soluble than quartz. The solubilities of quartz and amorphous silica as a function of temperature in pure water are illustrated in Figure 1. Equations to calculate the solubility of quartz and amorphous silica in pure water are available from various sources (Weres, 1982; Fournier, 1985 and Arnórsson, 2000).

Quartz deposition is negligible under most geothermal production conditions due to its slow precipitation kinetics compared to amorphous silica or poorly-crystalline silicates. Precipitation of amorphous silica may occur immediately after cooling or be delayed, depending on the pH and supersaturation ratio.

By convention in geothermal literature, produced geothermal waters are termed "brine", even though not technically the correct geochemical definition for the lower salinity fluids.

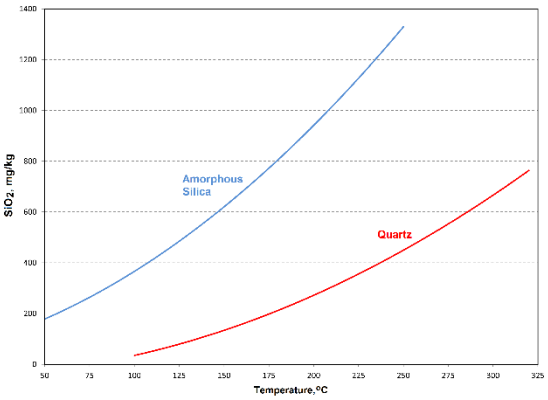


Figure 1. Solubility of quartz and amorphous silica as a function of temperature in pure water

THE THERMODYNAMICS OF SILICA

Although quartz is thermodynamically more stable than amorphous silica, extreme conditions of temperature, pressure, and/or alkalinity are required for the growth of quartz at measurable rates in aqueous solutions. The greater solubility of amorphous silica relative to quartz is a distinct advantage for geothermal resource production facilities because it limits the precipitation of silica from produced waters. The solubility curves of amorphous silica and quartz both increase with temperature to ~300°C and then decrease due to the decreasing density and solvent power of water. The decrease becomes rapid as the critical point of water (374°C) is exceeded.

Dissolved salts and pH also affect the solubility of silica in aqueous solutions. Fournier and Marshall (1983) have developed equations to calculate the solubility of amorphous silica at circum-neutral pH from 25 - 300°C using the concept of effective density of water and "salting out" effects of mixed electrolytes. Cations exhibiting elevated "hydration numbers," such as the alkaline-earths, depress the solubility of amorphous silica more than cations exhibiting low "hydration numbers" due to "free" water available for solvation. The effect of salinity and temperature on amorphous silica solubility is shown in Figure 2.

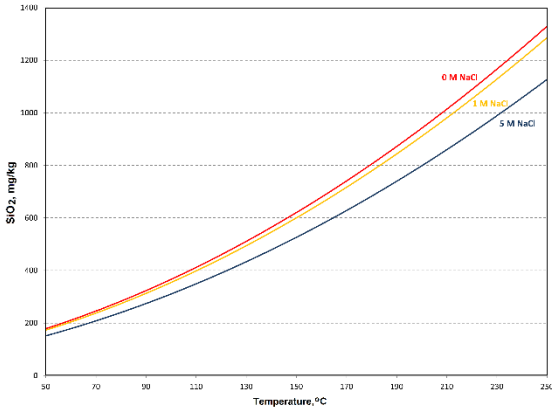


Figure 2. Solubility of amorphous silica as a function of temperature in NaCl solutions

The solubility of silica is substantially independent of pH until the pH increases into the alkaline range. Goto (1955) examined the effect of pH on the solubility of amorphous silica from 0 - 200°C and from pH 5.5 to 10.0. As expected, the solubility of amorphous silica increased with increasing temperature, while solubilities remained relatively constant over the pH range of about 5.5 – 8.5. Above pH 8.5, the solubility increased significantly according to the reactions:

$$H_4SiO_4 = H_3SiO_4^- + H^+ \text{ or,}$$
$$H_4SiO_4 + OH^- = H_3SiO_4^- + H_2O \qquad (2)$$

An expression for the relationship between pH and the solubility of monomeric silica is given by the following equation (Wahl, 1977):

$$\log \frac{w_s - w_m}{w_m} = pH + \log K_1 \qquad (3)$$

where w_s = total solubility of monomeric silica
w_m = mass fraction of molecular silicic acid

The first ionization constant for molecular silicic acid, K_1, controls the extent of the reaction:

$$H_4SiO_4 = H_3SiO_4^- + H^+ \quad (4)$$

where $K_1 = 10^{-9.7}$ at 25°C

The ionization constant can be calculated at higher temperatures using the following equation:

$$1n\ K_1 = -16.76 - \frac{1661}{T} \quad (5)$$

where T = temperature, K

The effect of pH on the equilibrium solubility of monomeric silica does not generally have practical significance until the flashed geothermal brine pH is significantly above pH 7, where monosilicic acid begins to dissociate according to equation 4 above. This increases the thermodynamic solubility of silica because the silicate ion has a very high solubility. At a fixed concentration of total dissolved silica, the silica saturation ratio or silica saturation index (SSI, the ratio of silica concentration to solubility under the given conditions) decreases with increasing pH. At high pH silica precipitation can be thermodynamically inhibited.

Non-alkali and alkaline-earth cations present in geothermal fluids may react directly with silicic acid to form metal silicates. These silicates are usually poorly-crystalline; their X-ray diffraction patterns exhibit broad humps that are shifted from the normal opal-A hump centered near the diffraction angle of 23° 2θ, where 2θ is the angle between the X-ray incident beam and the detector (Manceau, 1995; Gallup, 1997b and Manceau, 2005). X-ray absorption spectroscopic studies show that the silicates exhibit Si-O-M bonding and are not simply mixtures of silica and metal oxides/hydroxides.

Some examples of iron silicate scales and their formation reactions are:

$$Fe(OH)2 + Si(OH)4 = FeSiO3(s) + 3\ H2O \quad (6)$$

$$Fe(OH)3 + Si(OH)4 + Mg2+ = Fe(OH)3{\cdot}SiO2{\cdot}MgO(s) + H2O + H2(g) \quad (7)$$

$$Fe2+ + Si(OH)4 + H2O = Fe(OH)3{\cdot}SiO2(s) + H2(g) + 2\ H+ \quad (8)$$

Depending on the geothermal brine source, silica scaling may be exacerbated by the presence of calcium, magnesium, iron, aluminum, and manganese. Aluminum-rich and iron-rich amorphous silicates are the most common and exhibit significantly lower solubilities than pure amorphous silica. Aluminum can begin to affect amorphous silica solubility at low levels, on the order of only 1 ppm in the brine. Aluminum-rich amorphous silica scale deposits at temperatures that are 25°C or more below that of pure amorphous silica (Björke, 2012), so they can have a profound impact on power cycle and silica scale treatment process design. Increasing a first- or second-stage flash temperature by 25°C (a 4 bar increase from 150°C to 175°C flash) could make a geothermal power project economically nonviable.

SILICA PRECIPITATION KINETICS

While chemical thermodynamics determine the absolute solubility of silica, various factors affect the kinetic rate at which silica polymerizes and precipitates as colloids or by molecular deposition. The kinetics of silica polymerization and molecular deposition are influenced by the degree of supersaturation, temperature, by catalysts (fluoride), and nucleation site availability.

The maximum rate of silica precipitation typically occurs at a temperature approximately 25- 50°C below the silica saturation temperature as geothermal brine cools by flashing steam or from conductive heat loss. As the supersaturation ratio approaches 2, silica polymerization and precipitation proceeds rapidly at approximately neutral to moderately alkaline pH (pH 6.6-8.5). Weres et. al (1982), postulated that the silica precipitation process consists of the following steps:

1. Formation of silica polymers of less than nucleus size.
2. Nucleation of an amorphous silica phase in the form of colloidal particles.
3. Growth of supercritical amorphous silica particles by further chemical deposition of silicic acid on their surfaces.
4. Coagulation or flocculation of colloidal particles to give either a precipitate or a semi-solid material.
5. Cementation of the particles in the deposit by chemical bonding and further molecular deposition of silica.
6. Growth of a secondary phase in the interstices between the amorphous silica particles (occurs rarely).

A solid surface in contact with a supersaturated solution of amorphous silica may have a layer of amorphous silica on it, with continued deposition proceeding by Step 3 alone. If colloidal amorphous silica particles form in the supersaturated solution, these may adhere to the surface (Steps 4 and 5), and Step 6 may follow. The formation of amorphous silica colloidal particles from a supersaturated solution is often referred to as homogeneous nucleation, which is the dominant process at the high initial supersaturation ratios required for rapid polymerization of amorphous silica. Heterogeneous nucleation applies to the deposition of amorphous silica on pre-existing colloidal amorphous silica particles, but it is not actually a nucleation process.

This relatively slow process resembles homogeneous nucleation and replaces it at low supersaturation. Nucleation by other scale particles can also occur to provide surfaces for amorphous silica deposition (Kindle, 1984). The formation of amorphous silica on Fe^{+2} is most likely, followed by silicates of aluminum, magnesium, and calcium.

The nucleation process frequently includes an induction (delay) time during which the concentration of molecular silicic acid remains constant. After some time, the concentration of molecular silicic acid begins to decrease, which indicates that polymerization is occurring. This induction time may be interpreted as the approximate time required for sub-critical clusters of amorphous silica to grow to critical nucleus size. The induction time is longer at lower saturation ratios because the critical nucleus size is larger at these ratios.

Another interpretation of induction time is simply the length of time required for enough particles to nucleate and grow to a point where the concentration of molecular silicic acid measurably decreases. Rapid attainment of steady-state nucleation is implicit in this interpretation. Therefore, an initially slower nucleation rate may be ignored for practical purposes. This interpretation applies to induction times observed for both homogeneous and heterogeneous nucleation. Furthermore, a threshold value for amorphous silica supersaturation may be necessary to achieve nucleation. Similar to dissolution of both quartz and amorphous silica, temperature, degree of supersaturation, pH, dissolved salt concentration, and fluoride ions can affect the rate of silica nucleation (Iler, 1982). Both Iler (1982) and Weres et. al (1982) report that the rate of silica deposition is proportional to the sodium ion concentration, i.e., dissolved NaCl or other electrolytes may promote faster solubility equilibrium. They also report a ten-fold increase in deposition rates upon increasing the water pH from 5 to 6, and that fluoride catalyzes the silica polymerization reaction. Conversely, the kinetics of silica deposition slows dramatically as the pH is lowered into the acidic range.

Experimental studies have been conducted at the Lawrence Berkeley National Laboratory (LBNL) to determine heterogeneous and homogeneous amorphous silica nucleation rates under specific conditions. Using batch and continuous flow experimental results, Weres, et al (1982) developed an empirical equation to calculate the rate of molecular deposition of amorphous silica over a broad range of temperature and molybdate active silica concentrations. A theoretical approach to the formation of colloidal silica particles by homogeneous nucleation was also developed at LBNL, and was incorporated into the computer code SILNUC. The molecular deposition model developed at LBNL has been calibrated and modified by von Hirtz and Gallup (2000) through numerous field trials measuring actual scale deposition rates in pilot test plants. The new computer modeling code called DEPOSITION also accounts for the effect of aluminum when the process involves precipitation of aluminum-rich silica scale.

The polymerization of monosilicic acid is depicted in Figure 3. At high rates of deposition, the dissolved silica first polymerizes to colloidal silica particles that nucleate in the brine. The rate of homogeneous nucleation depends very strongly upon the SSI. Roughly, polymerization is relatively slow when the SSI is below 2, and very fast when the SSI is above 3.

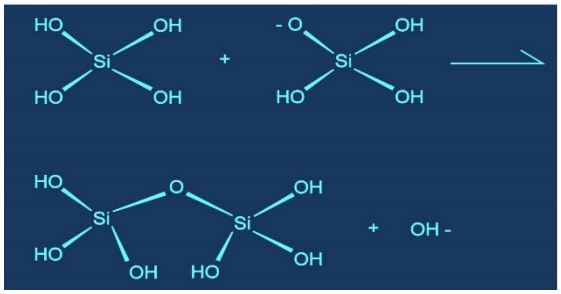


Figure 3. Polymerization process of monosilicic acid.

The condensation (polymerization) reaction of silicic acid and the reaction of silicic acid with silicate anions are, respectively:

$$2H4SiO4 = (OH)3Si{\cdot}O{\cdot}Si(OH)3 + H2O \qquad (9)$$

$$H4SiO4 + H3SiO4- = (OH)3Si{\cdot}O{\cdot}Si(OH)3 + OH- \qquad (10)$$

When the SSI is too small for rapid homogeneous nucleation to occur, heterogeneous nucleation and molecular deposition on solid surfaces dominate. Vitreous silica scale formed by molecular deposition alone is sometimes observed at high temperatures. It should be noted that colloidal silica particles also grow by molecular deposition, so in either case molecular deposition is a significant factor in silica scaling processes.

Colloidal silica particles may be coagulated by cations in the brine; calcium and iron are particularly effective in this regard. The same electrostatic forces cause colloidal silica particles to adhere to solid surfaces. Corrosion accelerates the deposition of silica scale on steel because it releases iron ions.

Once attached to a solid surface, colloidal silica is converted to solid scale by molecular deposition of dissolved silica between the particles (Step 6 above). Solid deposits may form at a high rate (centimeters per year) where both colloidal silica and substantially supersaturated dissolved silica are present.

At low pH, molecular deposition and nucleation are catalyzed by traces of hydrogen fluoride. Above pH 4, the rate of molecular deposition is proportional to the negative surface charge on amorphous silica. The rates of nucleation and coagulation also increase with surface charge. Increasing salinity increases surface charge, and accelerates all three processes.

SILICA SCALING EXPERIENCE IN GEOTHERMAL POWER PRODUCTION

The historical experience with geothermal fluid injection (disposal of produced brine, sometimes referred to as "reinjection") suggests that silica scaling in injection wells is the greatest concern, more so than thermal breakthrough to production wells. This concern has severely limited the efficiency of early geothermal flash plants due to conservative designs intended to maintain injection fluids at or below the SSI limit. Figure 4 shows the first-stage flash pressure and temperature required to maintain injection fluids at an SSI of 1 (at silica saturation limit), as a function of the reservoir temperature which controls the amount of silica produced based on quartz solubility. At a reservoir temperature of 300°C, the flash temperature is limited to about 200°C to prevent silica supersaturation. Over the full range of reservoir temperatures shown, the flash temperature can only be roughly 108°C less than the reservoir temperature to keep the SSI at 1 or less. Many flash plants have been built worldwide that are under-utilizing the resource by maintaining high flash pressures and injecting hot brine that could generate more power if silica scaling were controlled.

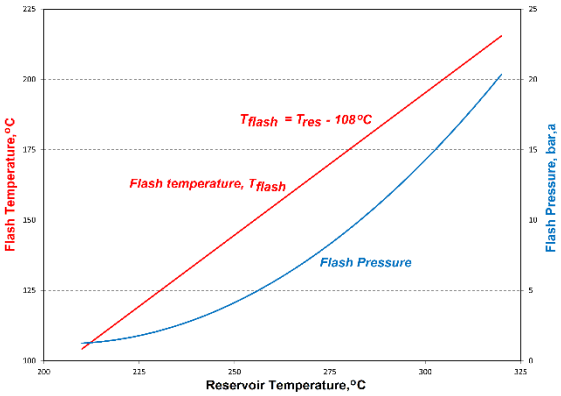


Figure 4. First-stage flash pressure and temperature required to maintain an SSI of 1 as a function of the reservoir temperature.

The potential injection well impacts are a legitimate concern. Injecting brine that contains colloidal silica or supersaturated dissolved silica risks formation damage; coagulated colloidal silica will accumulate in pores and fractures in the formation. If the brine is hot and contains enough dissolved silica for rapid molecular deposition to occur (>1 mm/y), molecular deposition alone may seal pores and fine fractures in the receiving formation, thereby reducing injectivity. The loss of sufficient injection well capacity may require curtailment of power generation. For most projects the bine from a geothermal power plant must be injected.

At high levels of supersaturation (>2) and near-neutral pH, massive silica scale deposition may occur in the low-pressure (LP) separators of dual-flash plants, and downstream in the injection lines and wells (Figure 5). Typically, amorphous silica scaling does not occur in production well bores. However, silicate scaling has been common in production wellbores tapping high-temperature, high-salinity fluids rich in heavy metals. Current and past examples are the Salton Sea (California), Puna (Hawaii) and Milos (Greece).



Figure 5. Massive silica precipitation in a pipeline due to polymerization after a second flash.

The metal silicates behave similarly to monomeric deposition forming quickly as hard, glassy solids. Their deposition rate and adherence depends on the metal surface material. For example, it was found that a manganese silicate scale adhered tightly to a variety of steels and corrosion-resistant alloys, an iron silicate scale adhered tightly to carbon steel, but not corrosion resistant alloys, and a rather pure amorphous silica scale adhered less tightly to carbon steel and not at all to alloys (Gallup, 2004).

In the case of the metal silicates, several reactions may be responsible for deposition, such as:

$$Fe(OH)_2 + Si(OH)_4 = FeSiO_3(s) + 3H_2O \quad (11)$$

$$Fe(OH)_3 + Si(OH)_4 + Mg^{2+} = Fe(OH)_3{\cdot}SiO_2{\cdot}MgO(s) + H_2O + H_2(g) \quad (12)$$

$$Fe_2+ + Si(OH)_4 + H_2O = Fe(OH)_3{\cdot}SiO_2(s) + H_2(g) + 2H+ \quad (13)$$

$$2Al(OH)_{30} + Si(OH)_{40} = Al_2O_3{\cdot}SiO_2(s) + 5H_2O \quad (14)$$

$$2Al(OH)_4^- + Si(OH)_{40} = Al2O_3{\cdot}SiO_2(s) + 5H_2O + 2OH^- \quad (15)$$

ORC and combined-cycle geothermal power plants

that subcool the brine below silica and silicate saturation temperatures may suffer from both amorphous silica and silicate scaling in heat exchangers, dramatically lowering the heat transfer, increasing the pressure drop, and reducing power generation.

HISTORICAL TECHNIQUES FOR SILICA/SILICATE SCALE INHIBITION

Silica deposition occurs to some extent in all high enthalpy, liquid-dominated geothermal operations. Silica scale inhibition/control methods employed in geothermal fields have generally been specific to brine chemistry, process conditions, and brine-handling/disposal regimes. The most common methods employed for mitigating silica scale deposits in geothermal brine-handling systems include, but are not limited to: (a) hot brine reinjection at or below amorphous silica saturation conditions, (b) adjustment of brine pH (acid to retard silica polymerization kinetics or base to convert $Si(OH)_4$ to $H_3SiO_4^-$, (c) aging, evaporation or pond retention to precipitate silica, (d) crystallization-clarification to purposely precipitate silica/silicates, (e) removal of silica from brine by controlled precipitation with metal cations, (f) dilution with fresh water or condensate, (g) reducing agent treatment to control ferric silicate scales, and (h) treatment with "organic" scale inhibitors/dispersants, such as phosphino-carboxylates.

A few geothermal fields dispose of the spent brine at the surface. Some fields located near coastlines or rivers have discharged spent fluids into the ocean or other waterways (Sugiaman, 2004). This practice has obvious potential environmental impacts due to the presence of salinity, heavy metals, and other toxic species such as boron and ammonia. At least partly because of environmental restrictions, injection of brine, cooling tower water and steam condensate is now the industry standard. The principal advantage of injection is that the net withdrawal of mass from a geothermal system is greatly reduced. Reservoir pressure is supported so that production well outputs can be maintained for a longer time (Gallup, 2007). The principal disadvantages of injection are scaling and thermal breakthrough where cool brine may flow directly to production wells before it has been in contact with hot rock long enough to reheat, causing a reduction in output from the production wells. This is a common challenge for geothermal energy production. The fractured nature of the rocks in geothermal systems often allows an unpredictable path from injector to producer. This problem is mitigated by increasing the distance between injection and production wells and managed by careful monitoring and inter-well chemical tracer testing.

Some geothermal fields utilize dilution of the silica-supersaturated geothermal brine with fresh water to reduce the silica concentration to below the saturation point. Hot steam condensate or fresh heated water is typically used in these applications. Cold dilution water does not have a significant net effect on silica saturation due to the opposing effects of cooling and dilution. Table 1 lists the silica saturation as a function of cold condensate (60ºC) dilution of hot brine (200ºC) for a combined-cycle geothermal project. A 50% dilution of the brine with condensate results in only a minor decrease in silica supersaturation.

Table 1. Amorphous silica saturation after cold condensate dilution of hot brine (Gallup, 2010)

Condensate fraction[1]	Mixture temp. °C	SiO_2 conc. ppm	Mixture SSI
0.0	207	1130	1.13
0.1	193	1017	1.13
0.2	179	904	1.13
0.3	164	791	1.12
0.4	150	678	1.09
0.5	135	565	1.05

[1]Condensate temperature = 60°C.

In some cases, the pH of the flashed brine is high enough (>9), that the solubility of silica is enhanced to the point where amorphous silica deposition is suppressed. The silica becomes thermodynamically inhibited due to the dissociation of silicic acid to soluble silicate ions (eq. 4). This is more common for very dilute geothermal fluids that are high in alkalinity (Dixie Valley and Beowawe, Nevada, USA, are examples) However, often such high-pH brines deposit aluminum, calcium and magnesium silicates.

Holding spent brine at near-neutral pH in ponds with net residence time of hours or days can convert dissolved monomeric silica to colloidal silica, reducing supersaturation. This prevents the cementation of weakly adherent deposits and their conversion to solid scale. Deposits from the aged brine tend to be soft and easy to remove. Candelaria (1996) postulated that neither adherent gel nor solid scale will form if the silica is in colloidal form. The hypothesis relies on the requirement of monomeric silica to cement silica colloids together. Application of this procedure at the Botong field (Philippines) showed that the colloidal silica (30 nm size range) formed a gelatinous, fluffy precipitate that did not settle in the ponds and was transported into the injection wells. After three years the precipitate had not caused a serious decline in injection capacity. Clearing the settling ponds of deposited silica and allowing passage of the solids to wells resulted in a substantial decline in injection capacity within a week, likely caused by plugging of the reservoir

formation. This result demonstrates that the effects of deposition and plugging of colloidal suspensions are related to particle size.

Maintaining a low geothermal brine pH (<6) retards the nucleation, growth, and coagulation of colloidal silica particles and the scaling rate from supersaturated solutions by molecular deposition. The pH of produced brine can be maintained close to the original reservoir pH by simply not flashing the brine, as in an ORC cycle with downhole pumped brine production. Flashing of geothermal brine always results in an increase in pH due to outgassing of CO_2 and disproportionation of bicarbonate. The resulting increase in carbonate consumes hydrogen ions:

$$2\ HCO_3^-(aq) \rightarrow CO_3^=(aq) + CO_2(g) + H_2O$$

$$H^+ + CO_3^=(aq) \rightarrow HCO_3^-(aq) \qquad (16)$$

The pH of geothermal brine in the reservoir is largely controlled by carbonic acid/bicarbonate equilibria. Carbonic acid is a weak acid at reservoir temperatures (>200°C) but becomes a stronger acid at temperatures below 100°C.

$$H_2CO_3 = H^+ + HCO_3^-(aq) \qquad (17)$$

Therefore, cooling brine without flashing results in a lower pH at the surface than in the reservoir. An ORC geothermal power plant at Blue Mountain (Nevada, USA) is operating without significant silica scale deposition and without treatment even though the SSI is 1.75 at an outlet temperature of about 70°C. Because of relatively high dissolved CO2 in the brine and the low heat exchanger outlet temperature, the pH of the brine drops from 6.25 to 5.72 units naturally through this cooling process due to the increased acidity of carbonic acid.

pH-MODIFICATION

When acid is added to brine for silica scale control, the process is termed pH-modification (or pH-Mod). This technique has been utilized at several fields to slow the polymerization and molecular deposition kinetics of silicic acid. The acids that may be used in this application include HCl, H_2SO_4, H_2SO_3, HF, organic acids, and acid precursors such as urea·acid adducts or chlorinated hydrocarbons. The selection of the acid must be compatible with the brine to avoid forming by-product scales (Gallup, 1996).

Gallup studied the silica inhibition properties of H_2SO_3 and sulfite salts up to 200°C. H_2SO_3 inhibits silica scaling by slowing silica polymerization and forming soluble sulfite-silicate complexes, which results in increased amorphous silica solubility. In a comparative test with HCl and H_2SO_3, sulfurous acid (H_2SO_3) maintained the highest silica concentration in solution. The use of H_2SO_4 in brine acidification is undesirable in some cases due to secondary precipitation of alkaline-earth sulfates. The hypersaline brines produced at the Salton Sea require HCl for pH-modification for this reason. The solubility of alkaline-earth sulfites increases with decreasing pH and the primary product of calcium/bisulfite interactions below pH 5.5 is soluble calcium bisulfate. Consequently, H_2SO_3 can be used to treat most geothermal brines without the formation of by-product scales. Even though H_2SO_3 is more expensive than HCl or H_2SO_4, the costs can be mitigated by manufacturing H_2SO_3 onsite by incinerating H_2S or elemental sulfur from H_2S abatement systems. Enough H_2S is typically available at most facilities to meet all acid requirements (Gallup, 1997a).

It was suggested by Lovelock that acetic acid could be used for pH-modification (Lovelock, 2017). Although technically possible, this method is not practical nor economically feasible in most applications. Concentrated acetic acid is more dangerous to handle than concentrated sulfuric acid, it is semi-volatile and flammable. But the main problem is that acetic acid is prohibitively expensive compared to H_2SO_4, as shown in Table 2 below for a bottoming cycle application in Indonesia. With adequate design of the pH-modification process as discussed later in this paper, there is no need to use expensive weak acids or buffers for this purpose.

Table 2. pH-Mod Costs - Sulfuric vs. Acetic Acid

Target pH	Brine Flow	Alkalinity, as HCO3	Acid Type	Acid Rate	Annual Cost[1]
at 20 C	Ton/hr	mg/kg	wt. %	kg/hr	USD
5.0	1179	30	98% H2SO4	29	$ 73,463
5.0	1179	30	100% CH3COOH	36	$ 488,680

1. Based on Sulfuric Acid price per ton: $ 288
2. Based on Acetic Acid price per ton: $ 1,530

Hirowatari and Yamauchi (1990) reported on the injection of exhausted gases into the brine to decrease the brine pH. The exhausted gases were 70% CO_2 and 2% H_2S. Brine pH decreased with increasing liquid-to-gas ratios as expected, and the gas injection lowered the pH from 7.0 to 5.2, resulting in a 97% reduction in scale deposition.

Gas injection was practiced at the Coso geothermal field in California (USA) for both H_2S emissions and silica scale control for over 12 years and is still utilized at the Puna field in Hawaii (USA). At the start of the 270 MW Coso project, 100% of the noncondensable gas (NCG) from surface condensers in dual-flash plants was injected at rates of 35,000 to 45,000 kg/hr field-wide. The brine pH was lowered from about pH 8 to 5, effectively controlling silica scaling. Ultimately complications with gas injection such as corrosion due to residual oxygen and gas breakthrough to some production wells led to the installation of conventional H2S

abatement units and pH-modification systems that injected sulfuric acid to the brine. Condensing turbine plants, even when equipped with surface condensers, have significant levels of oxygen in the off-gas due to in-leakage, resulting in severe corrosion if injected with brine and condensate.

The geothermal energy industry has little direct experience using NCG injection for purposes of pH-modification in silica scale mitigation. Gas injection has historically been performed for H2S and CO2 emissions control. NCG injection for pH-control alone typically requires much lower injection rates than for emissions control. Given the low gas injection rates usually needed for pH-modification, gas breakthrough to production wells and "vapor lock" at the injection wells may not be issues.

Gas injection has been utilized at the Puna plant in Hawaii since start-up, for both emissions control and scale control. The relatively low gas levels at Puna have allowed 100% gas injection without any gas breakthrough to production wells for the life of the project (>20 years). Gas injection at Puna results in an injectate (combined brine/condensate) pH of about 4.5 units, and has been very effective in mitigating silica scale at an SSI of over 2.0. The main reason gas injection has not been widely implemented by the industry for pH-control and silica scale mitigation is that only ORC combined-cycle plants with back-pressure vaporizers for steam condensation can provide a suitable source of oxygen-free NCG for injection.

Gas injection for pH-modification has been demonstrated successfully at the Sarulla project in Indonesia through a series of pilot tests. It was shown that the target pH in a range of 4.8 to 5.2 pH units (at 20 °C) could be easily achieved by injecting NCG from back-pressure ORC units used to condense turbine steam. The amount needed varied from 9 to 18% of the total available NCG, depending on the plant. The gas injection process would displace about US$2,000,000 per year in sulfuric acid cost, but it requires a plant retrofit for gas compressor installation. This process is much more efficient if included in the original plant design.

SCALE INHIBITORS

Threshold-type scale inhibitors have not been effective in preventing amorphous silica scale because these inhibitors are designed to disrupt crystal formation and growth (i.e., calcite scale) and have no efficacy on the formation of amorphous solids. Threshold scale inhibitors may be effective on crystalline silicate scales and there are many commercial inhibitors for this type of scale in cooling water treatment. Amorphous silica scale and silicate scales often get confused in discussions of scale inhibitor treatment for geothermal brine by chemical treatment vendors.

Organic additives were investigated by Gallup (2002) and Gallup and Barcelon (2008). They tested over 50 organic additives, whose ingredients included phosphonic acids, phosphonates, phosphinocarboxylic acids, acrylate polymers, polyacrylamides, oxyethylenes, poly-maleates, sulfonates, carboxylic acids, polyethyleneimines, caustic soda, and quaternary ammonium compounds. They concluded that organic additives will likely continue to see limited use in the geothermal industry. Organic additives may make silica deposits softer and easier to remove, but do not prevent polymerization or increase solubility. This means that the silica exists in solution as suspended solids, which have the potential to cause damage in injection wells. It was found that overdosing of the additives in many cases led to flocculation rather than dispersion. Organic scale inhibitors may just move the scaling problem downhole where it can cause greater damage to an overall geothermal power project. Injection well clean-out and re-drilling is much more expensive than cleaning surface equipment and pipelines.



Figure 6. Pilot test heat exchanger after exposure to brine for 30 days with "silica scale inhibitor".



Figure 7. Pilot test heat axchanger after exposure to brine for 30 days with pH-modification

Despite laboratory tests that have not shown efficacy of scale inhibitors, some have been tested in pilot plants and even on full scale geothermal power plants. As shown in Figures 6 and 7, silica scaling was greatly enhanced by use of a silica scale inhibitor on an ORC brine heat exchanger in Hawaii compared to pH-mod in concurrent tests.

A full-scale test conducted at the Blundell geothermal plant in Utah, USA, also resulted in massive scaling of heat exchanger tubes. Figures 8 and 9 show the ORC preheaters after exposure to brine for one year with Nalco "GEO 982" compared to pH-modification for one year, respectively. This plant has now returned to the pH-modification process after one year using this inhibitor.



Figure 8. ORC preheater after exposure to brine for 1 year with Nalco GEO 982 "silica scale inhibitor".



Figure 9. The same ORC preheater after exposure to brine for 1 year with pH-mod

CURRENT SCALE CONTROL TECHNIQUES AT HIGH SUPERSATURATION

A major advancement in the exploitation of liquid-dominated geothermal fields has been the application of "bottoming cycle" heat recovery systems to maximize the heat extraction and power generation from a given resource. An ORC or a second-stage flash added to a single-flash plant is considered a bottoming cycle. In the case of an ORC plant, the heat from single-phase brine is transferred to an organic working fluid. This secondary working fluid is vaporized, passed through a turbine to generate electricity, condensed and recycled. Many ORC plants are used as the sole source of electricity production (i.e., stand-alone plants), in which case the hot brine, using submersible production well pumps, is maintained under pressure through the entire process from production to injection. This process has the advantage of not concentrating silica due to flashing and maintaining the brine pH low by not releasing dissolved CO_2.

In contrast to most stand-alone ORC plants, ORC bottoming plants can result in very high levels of amorphous silica supersaturation, where the SSI may be 2 or greater. Successful processing of high silica fluids through ORC heat exchangers can be attained with pH-modification and the rapid reduction of temperature through the heat exchangers which reduces the kinetics of silica deposition. Thermodynamic stability prevents any possibility of scale deposition, while kinetic stability results in an extended time before deposition will occur. It is the kinetic stability that allows the successful operation of an ORC bottoming plant by taking advantage of the kinetic effects of both thermal quenching (inherent with an ORC) and low-pH (normally augmented by acid injection).

As discussed previously, the non-release of the acid-gases (CO_2 and H_2S) in the ORC process maintains the brine pH at a lower level. Upon cooling in an ORC heat exchanger, the brine pH will drop further due to the increased acidity of carbonic acid at the lower temperature. This often provides an advantage in silica scale control for ORC plants since the pH is lower than in a dual-flash process and silica scale is kinetically inhibited to some extent. A comparison of these two processes is depicted in Figure 10.

Whether a dual- or triple-flash system or an ORC system is used as a bottoming cycle, amorphous silica usually becomes highly supersaturated at the outlet temperature of the process. Generally, only single-flash plants are operated at or below the silica saturation limit. Historically single-flash geothermal plants were built for this reason, to prevent the possibility of silica scale, but at the expense of maximum resource utilization.

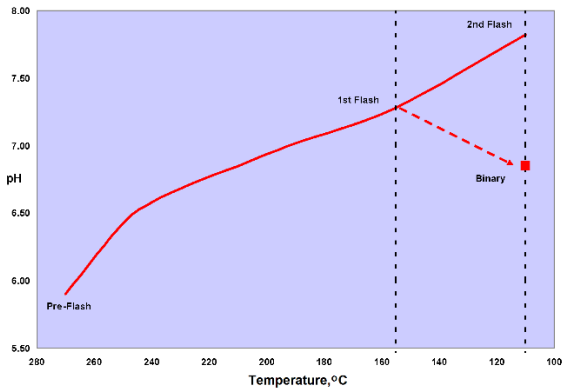


Figure 10. Example of brine pH changes as a function of flash and subcooling (binary) (Gallup,2010)

The solubility of quartz and amorphous silica as a function of temperature is shown in Figure 11 below. Also plotted (heavy red line) is the concentration path for brine flashed from single-

phase reservoir conditions in equilibrium with quartz at 300°C to a typical single-flash power plant condition of 160°C, then to a second-stage flash to 110°C. The dashed blue line shows the path from first flash to subcooling in an ORC plant as an alternative bottoming process to the second flash. The ORC plant does not further concentrate the silica but usually cools the brine to a lower temperature than the second flash. Note that the concentration of silica in the brine begins to exceed the amorphous silica solubility at less than 200°C.

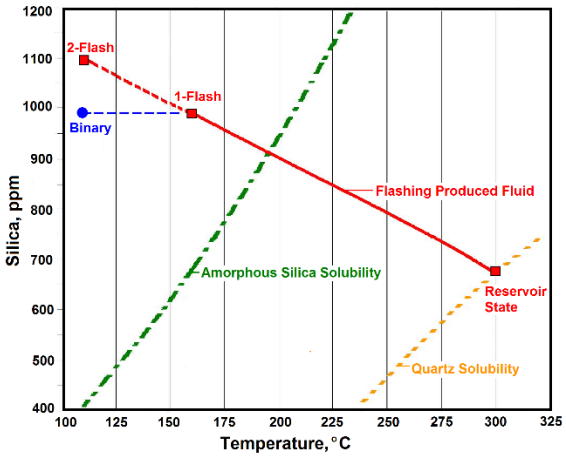


Figure 11. Solubility of quartz and amorphous silica as a function of temperature and flash vs. subcooling (binary) processes.

In the multiple flash processes, steam is generated in stages while brine concentrates and the fluid temperature drops in each stage. As described above, the ORC plant does not concentrate the brine but usually extracts more heat resulting in a lower outlet temperature. If amorphous silica saturation is exceeded, scaling is thermodynamically possible. Depending on the fluid temperature, pH and salinity, scale may deposit immediately or be kinetically delayed for a significant amount of time.

As an example of thermal-quenching, the Nesjavellir geothermal plant in Iceland cools geothermal brine in a heat exchanger bottoming cycle to 55°C to heat potable water for the city of Reykjavik. In the process, silica in the geothermal fluid becomes supersaturated to an SSI of 4. Due primarily to the rapid cooling and the low outlet temperature of the geothermal brine, scaling is minimal, and the heat exchanger tubes are only cleaned once per year (Figure 12). Since the brine is not pH-modified, silica polymerization does occur upon aging. The brine is held in ponds and diluted with steam condensate prior to injection (Gestur, 2001).

A combined-cycle Puna plant in Hawaii relies on both thermal quenching and pH-modification to control silica at extremely high levels of supersaturation. The plant flashes 300°C reservoir brine to 200°C where it is slightly undersaturated in silica, then passes that brine through an ORC bottoming cycle where it becomes highly supersaturated (SSI 3.5) at 80°C. The natural brine pH is 6.0 and reduced to 5.5 after condensate addition. The pH is further reduced to 4.5 with acid injection to control scale through the ORC heat exchangers which are operating at very high SSI.

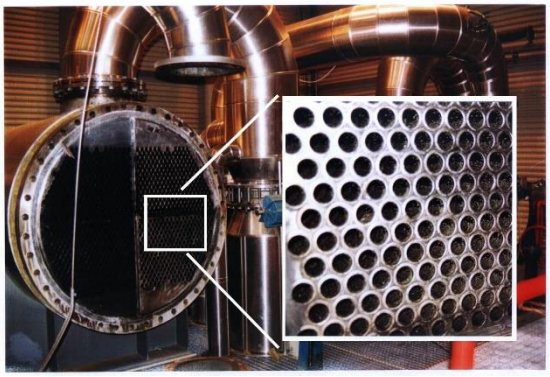


Figure 12. Nesjavellir geothermal plant heat exchanger after one year at SSI of 4 (55°C) (Gallup, 2010).

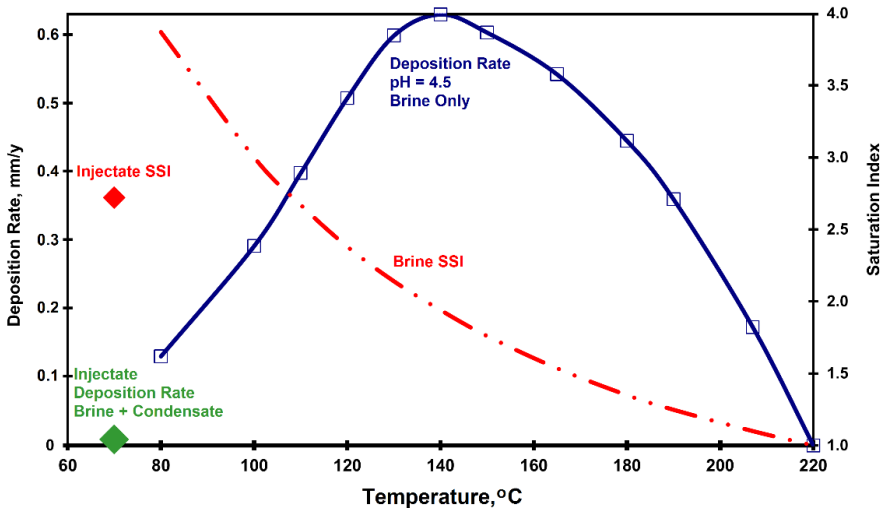


Figure 13. The silica saturation index (SSI) and predicted silica scaling rate (mm/y) for combined-cycle bottoming plant with pH-Mod in Hawaii

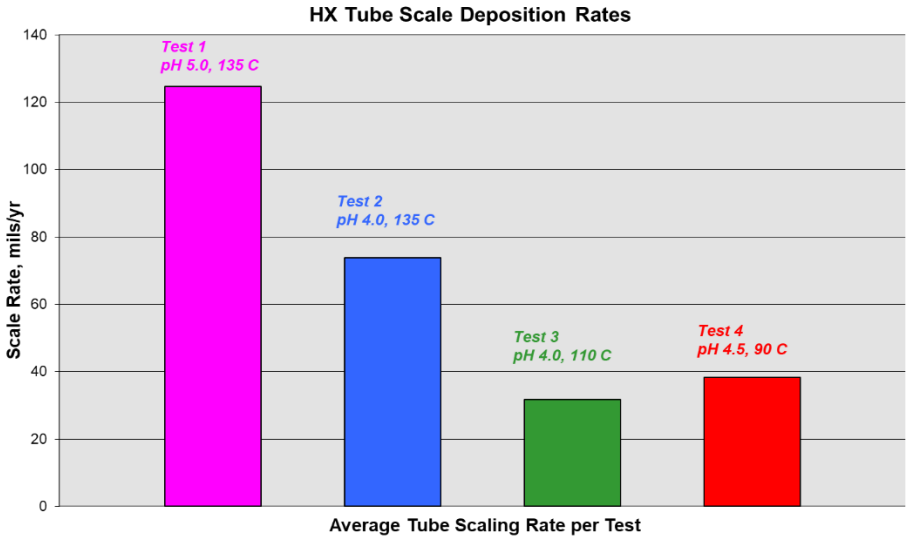


Figure 14. Initial Heat Exchanger Pilot Test Scaling rates (mil/y) for a combined-cycle bottoming plant with pH-Mod in Hawaii.

Figure 13 shows the SSI and predicted scaling rate from DEPOSITION model (von Hirtz and Gallup, 2010) for the fluids in this plant as a function of temperature. The molecular deposition rate of silica is reduced 80% from a temperature of 140°C to 80°C, simply by cooling the brine, due to thermal quenching and kinetic inhibition. The thermal quenching process is only possible with the pH carefully controlled within the target range to prevent any polymerization. This is currently the most extreme example of high-SSI brine being successfully processed with maximum resource utilization.

Figure 14 displays the results of the initial pilot testing for this plant. Note that the heat exchanger tube scaling rate actually dropped over 50% when the brine temperature was reduced from 135 to 110 °C at the same pH of 4 units.

GUIDELINES FOR OPTIMUM pH-MOD SYSTEM DESIGN

The only proven technology for the control of amorphous silica scale in both ORC and multi-flash power cycles at high levels of supersaturation (>1.5) is pH-modification. The other proven option specifically for flash plants is the CRC process which is used exclusively at the Salton Sea, CA, USA, and outside the scope of this paper. Although pH-modification is very effective in controlling silica scale in surface equipment and downhole, it can be difficult to control the pH without proper control instrumentation since the target value is typically at the inflection point of the acid titration curve for the brine (pH 4.5-5.0), where bicarbonate is the dominant alkaline species being neutralized in the process. Poor pH control (± 0.5 units or worse) can result in corrosion of carbon steel pipelines and inadequate scale inhibition.

Dissolved CO_2 in the brine (>200 ppm CO2) smooths out the pH response curve to acid, resulting in more precise and stable pH control. Dissolved CO_2 in brine diminishes rapidly with flash pressure, and even more so with multistage flashing.

Figure 15 show typical pH-modification dosing curves with acid treatment into HP brine after first flash and into LP brine after a 2nd flash. An ORC bottoming cycle process would normally be applied to the HP brine after first flash. The HP curve (red line) is relatively flat near the target pH region, where an ~25% change in the total acid dosing rate results in a pH change of only 1 unit.

The pH-modification curve for LP brine (blue line) shows that a change of only 4% in the acid dosing rate results in a pH change of 1 unit. This is a very difficult process to control and is not possible without stable brine flow. The control is more difficult when acid is injected upstream of the second flash vessel which results in greater CO2 loss from the brine than occurs with injection into the single-phase brine after second flash. In many cases acid must be injected upstream of the second flash to prevent the on-set of rapid silica polymerization.

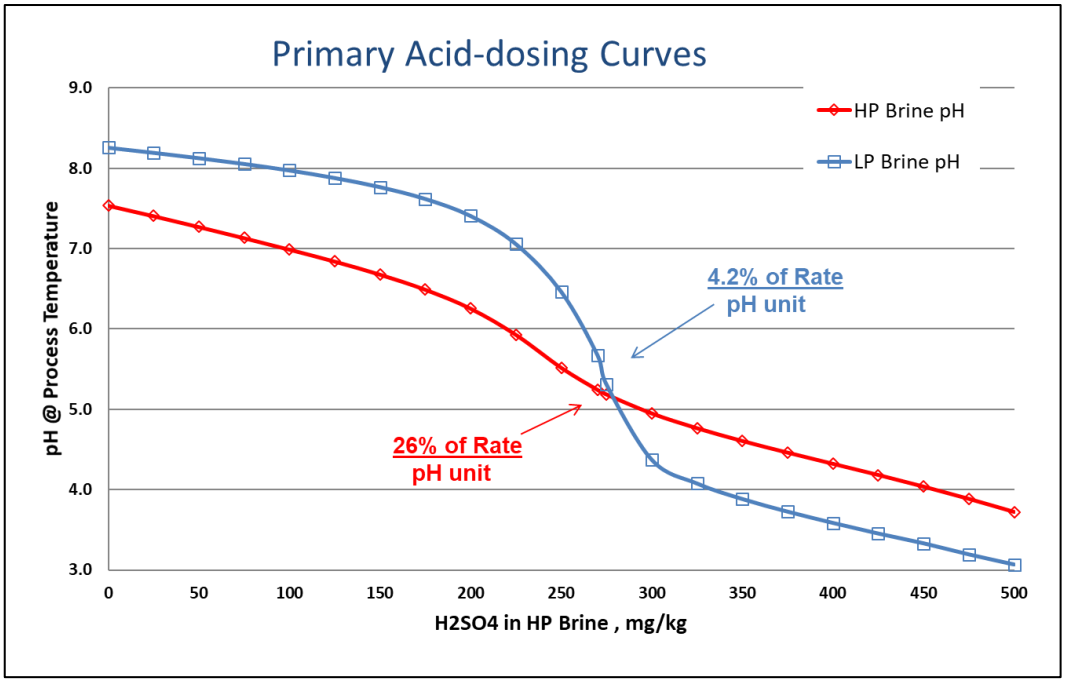


Figure 15. Typical pH-modification curves for HP and LP brine treatment

A properly-design pH-modification system must include careful consideration of the following:

1. Brine flow control – *Flow Stability*
2. Acid delivery system – *Dosing Response*
3. Control system – *Dosing Response*
4. Brine flow measurement – *Dosing Control*
5. pH measurement – *Dosing Control*
6. Acid mixing and corrosion resistant materials – *Corrosion Control*

Brine flow measurement and control

The pH-modification process is much easier to control if the incoming brine flow is stable. The primary control variable for acid-dosing is the brine flow signal. The brine flow measurement does not need to be accurate, but must be linear and reproducible. The absolute accuracy in brine flow is not important since the acid-dosing is a proportional response. But brine flow surging and signal noise can result in a substantial increase in the variability of the pH. **Figure 16** shows data for brine flow at the outlet of the high-pressure (HP) separator at the Kawerau dual-flash plant. The high variability in the brine flow rate measured by an orifice meter was confirmed to be a real phenomenon by using on-line TFT® measurements (also plotted in Figure 16). The that the on-line TFT® measurement is labeled as "TFT CBM" (continuous brine monitor).

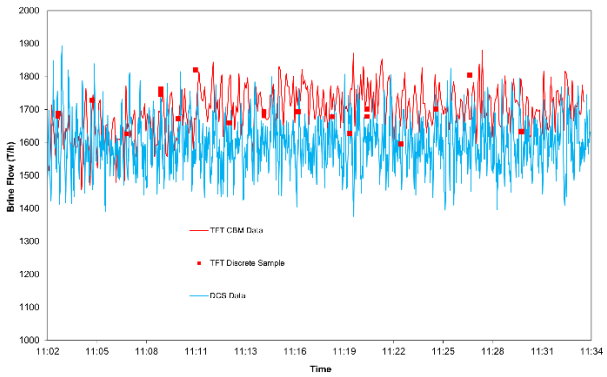


Figure 16. Highly variable brine flow at outlet of a HP separator at dual-flash Kawerau plant.

The pH control system logic is shown in Figure 17. The acid-dosing pump is proportioned directly to the brine flow signal, and the factor used in that proportional control is updated periodically in a separate control loop that measures the pH of the treated brine downstream. The acid pump control cannot rely on the measured pH alone, as the response time would be far too long. The acid-to-brine ratio needed to reach a given target pH is relatively constant, but may change as the brine chemistry varies due to shifts in alkalinity content. The actual dosing ratio also changes due to process variables such as drift in the output of the acid pump at a given set-point, acid viscosity due to temperature, drift in the brine flowmeter response, etc. All of these errors are compensated for by the secondary pH loop control.

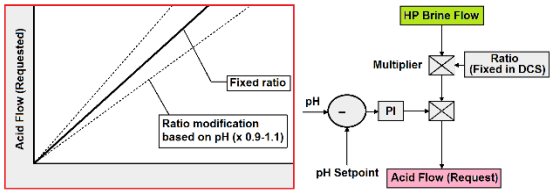


Figure 17. Control system logic for pH-modification process.

The highly variable brine flow shown in Figure 16 results in highly variable pH values and an unacceptable pH range (Figure 18). The target pH in the example shown is 4.80 units (measured at 20°C), but the actual pH drops to 3 units and has an overall range of 2 pH units. The pH was computer-modeled (plotted in red) based on the brine chemistry, acid-dosing rate and brine flow rate data to demonstrate this was real variability and not pH measurement noise. The wide range in pH caused severe corrosion in the LP two-phase piping and LP separator, requiring a major investigation, redesign and retrofit of the Kawerau plant beginning about a year after it was commissioned (Addison, 2015).

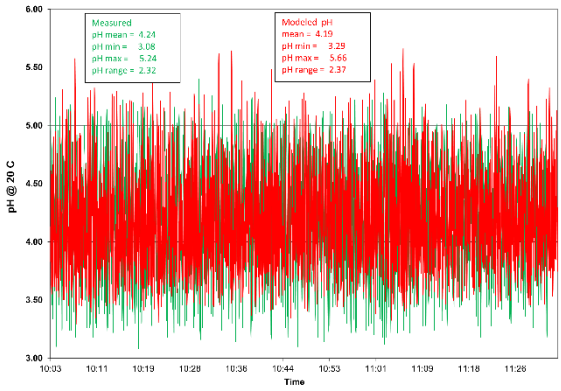


Figure 18. pH of highly variable HP brine resulting from unstable brine flow and slow dosing response: set-point = pH 4.8 at 20°C.

Control system and acid delivery response time

An acid-dosing system can require several seconds to respond to changes in brine flow. Some of this time is consumed by the distributed control system (DCS) to command adjustments in the acid pump rate based on brine flow variations. There is an additional electromechanical and/or hydraulic response delay in the acid pump between the DCS command to increase rate and another second or more may be consumed in delivering the acid from the pre-mixing piping to the main brine line. Figure 19 shows an example of a substantial response time off-set between surges in brine flow and the delivery of acid to meet those surges, again for the case where brine flow was highly variable. Efforts must be made in the overall design of a pH-modification system to reduce the acid delivery response time as much as possible, especially in cases where the inlet brine flow is not stable.

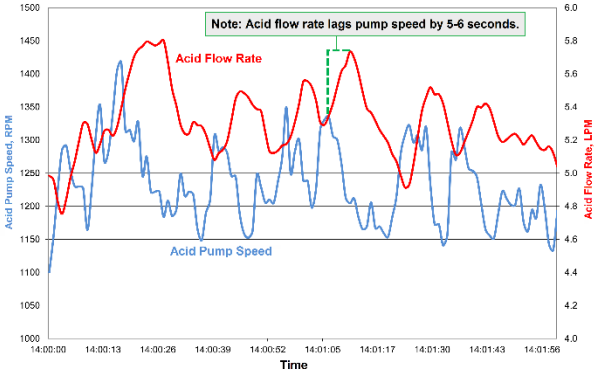


Figure 19. Response time off-set between surges in brine flow and the delivery of acid.

Work has been performed at some plants using a "feed-forward" parameter to predict surges in the inlet brine flow, so that acid dosing could be under a cascade control scheme that includes advance warning of brine flow variations, allowing time for the acid pump to respond appropriately. High correlations (r^2 = 0.9) have been identified between the first derivative of the HP separator level and the HP brine flow at the dual-flash plant in New Zealand (Addison, 2015). The limitation with any feed-forward parameter is that the lead vs. lag time will not remain absolutely constant and will require on-line statistical analysis of the relationship to maintain synchronization. In this case, fixed time off-sets for separator level maintain high correlations only over 10 to 15 minutes, and then need to be updated for drift. Any feed-forward approach for a complex two-phase flow system will be difficult and may not produce the required results for acid-dosing synchronization and pH stability.

pH measurement

An on-line pH monitoring system is required for pH-modification, with automatic calibration and pH probe cleaning capability, and sample stream flow measurement and control. Accurate pH measurement is critical for both scale and corrosion control to maintain the pH within an acceptable range for materials exposed to pH-modified brine, and to provide alarms through the DCS in case of pH excursions outside an acceptable range. A modern on-line automatic pH-monitor is shown in Figure 20.

The pH is measured from a small side-stream of cooled brine within about 10 m downstream of the acid-dosing point. The pH at process temperature will be shifted from the measurement temperature, and this must be considered in the system design and setting of the target pH. Geochemical, process chemistry and corrosion modeling is always conducted at the actual temperature of the fluid being modeled. Thus, when the target pH for the brine to be treated is first estimated from chemical modeling, the appropriate correction (off-set) must be applied to the on-line measurement.

The pH of geothermal brine in the pH modification process is buffered within the range of 4-5 pH units by second dissociation of sulfuric acid, bisulfate ion:

1st: $H_2SO4 \rightarrow H^+ + HSO_4^-$

2nd: $HSO_4- \rightarrow H^+ + SO_4^=$ (18)

Bisulfate is a weaker acid at high temperature. At 20°C, only 10% of the total available H^+ ions are associated in the bisulfate ion ($HSO4^-$), making bisulfate a strong acid at low temperatures. At 120°C, bisulfate is a much weaker acid, with 75% of the total available H^+ ions still associated. Figure 21 displays the correction curves for high-alkalinity brine that is pH-modified, over a range of pH values as a function of temperature. At pH values near 4, the pH is over 1 full unit lower at measurement temperature than at the HP flash process temperature. At pH 5, it is about 0.5 units lower at measurement temperature than at the process temperature.



Figure 20. On-line automatic pH-monitor at Sarulla

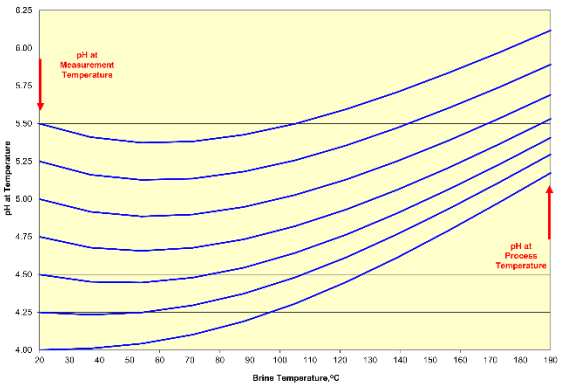


Figure 21. Correction curves for HP brine pH as a function of temperature.

Acid mixing and corrosion-resistant materials

In the pH-modification process, the concentrated acid is typically sulfuric and must be diluted immediately prior to injection. Concentrated acid cannot be injected into a hot brine pipeline due to localized "hot-spot" corrosion that may occur, even if high alloys are used. It is not safe or practical to pre-dilute the concentrated sulfuric acid and store it in separate tanks, so it is always diluted on-line using a side-stream of brine or condensate. Hotwell condensate from direct contact condensers cannot be used for acid dilution as it contains dissolved oxygen on the order of 100 ppb or more, which will greatly accelerate corrosion downstream. The acid is diluted to a concentration of about 1%, and then injected into a static mixer in the main brine pipeline to be treated. The dilution water flowrate needed would typically fall in the range of 2-10 kg/s.

Cold, concentrated sulfuric acid (98%) is not corrosive to carbon steel, but it is typically handled in stainless steel and/or plastic piping and tanks (polypropylene or polyethylene with oxidation-resistant liner). Hot, dilute sulfuric acid (1% range) is extremely corrosive to steels. Below 120°C, dilute sulfuric acid can be handled in Hastelloy C-276 alloy piping and fittings, but above 120°C Hastelloy C-276 alloy will be destroyed quickly. Above 120°C and below 200°C PTFE Teflon-lined pipe and fittings can be used. Above 200°C the only suitable material for hot, dilute sulfuric acid is tantalum.

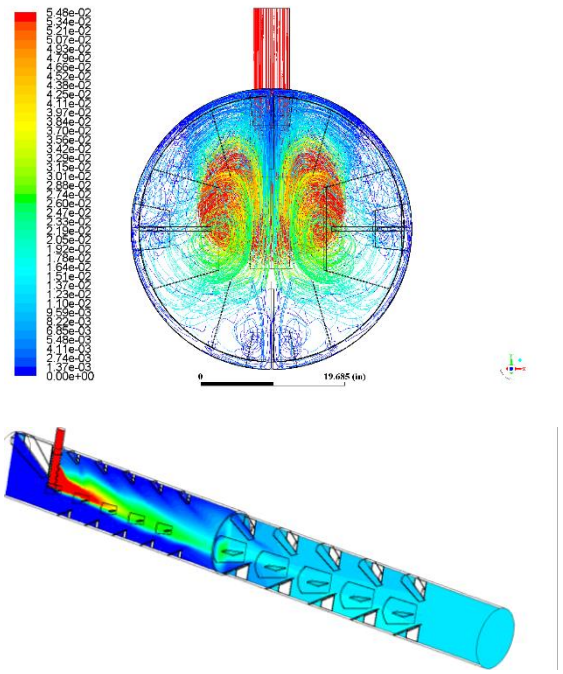


Figure 22. Graphical CFD analysis output for a 24-inch HP brine static mixer and tantalum quill.

The diluted acid is injected into a full-line size static mixing spool constructed of Hastelloy C-276 alloy (regardless of brine temperature). A Teflon-lined and jacketed injection quill, a Hastelloy-shrouded

solid PTFE quill, or a solid tantalum injection quill is used to deliver the dilute acid to the center of the static mixer inlet. It is important that computational fluid dynamic analysis (CFD) is performed on the piping system with static mixer over the range of brine flow expected, to ensure mixing will be sufficient under actual plant conditions. An example CFD graphical output is shown in Figure 22.

After the static mixing spool, the brine piping system may return to carbon steel in cases where the brine flow is stable and pH reasonably well controlled (4.5-5.0 ± 0.2 pH units). In the case of the Kawerau dual-flash plant discussed above, the carbon steel piping between the HP separator and the inlet to the LP separators had to be replaced with super-duplex 2507 alloy piping (Addison, 2015). This was necessary given the high corrosion rates that had been experienced in the two-phase piping (Addison, 2015) as the result of highly variable pH.

Finally, it is important to ensure there are no possible sources of oxygen intrusion to the pH-modified brine. There may be sources of aerated Hot-well condensate passing to the brine through pump seal water flush streams. If non-condensable gas is injected, there should be less than 1 ppm in the gas. Air leaks are prevalent in any vacuum extraction system for NCG and the gas from such systems should never be injected into the acidified brine. Even compressors that take gas from a positive-pressure ORC steam condenser may contain oxygen due to air intrusion on the suction side of the compressors. In the complete absence of oxygen, corrosion rates of carbon steel piping and injection well casing exposed to pH-modified brine (4.5-5.0 ± 0.2 pH units) are typically negligible.

SUMMARY

There continues to be a huge potential for geothermal energy development worldwide. Renewable geothermal energy is currently used to generate electric power in over 25 countries, for a total of more than 14 GWe electric power generation. Geothermal energy has the potential to be the world's primary source of baseload renewable power (GEA, 2015; Bertani, 2015).

Since geothermal energy utilization involves direct heat transfer between water and rock in a reservoir, the silica content of geothermal brine is usually near saturation with respect to crystalline silica minerals (typically quartz or chalcedony). But the kinetics of crystalline silica dissolution/precipitation is slow, so in the time it takes to extract the energy on the surface and re-inject the fluids, quartz or chalcedony precipitation does not occur. However, amorphous silica deposition is possible and does occur once the fluid is supersaturated due to cooling. Fortunately, the kinetics of amorphous silica deposition is relatively slow, but scaling still can easily occur within the time-frame of fluid processing and handling.

In early geothermal development silica scaling was a significant limiting factor in the amount of energy that was extracted from a resource. Recent production engineering and chemistry advances have greatly reduced these barriers by implementing technology to control silica/silicate scaling from geothermal produced fluids. Proven engineering strategies such as combined-cycle plants and pH-modification are currently the primary means to mitigate silica scale. Many single-flash plants worldwide can achieve an increase of 30% or more in power generation from the same resource by adding an ORC bottoming plant to the existing facility (Mulazzani, 2015), in conjunction with pH-modification for silica scale control.

The pH-modification technology described in this paper has been known for over 10 years, but the same mistakes have been made repeatedly in the pH-modification process design and implementation at most new geothermal plants attempting to utilize this technology. These include the recent large-scale dual-flash and combined cycle geothermal power projects at Kawerau, New Zealand (100 MW, Fuji), Nga Awa Purua (130 MW, Fuji) and Sarulla (330 MW, Toshiba/Hyundai). These plants required complete retrofits and replacement of the originally-installed pH-modification equipment after problems ranging from pipeline corrosion failures to scaling of injection wells occurred, resulting in over US$30MM in damage in the case of Kawerau (Addison, 2015).

With careful implementation of the pH-modification process and appropriate brine outlet temperature selection, silica scaling can be controlled to acceptable levels in both surface equipment and injection systems at most geothermal resource sites worldwide, even where silica concentration in the brine is 1000 ppm or more. Typically brine outlet temperatures from these plants can be 80 °C or less.

REFERENCES

Addison, S., von Hirtz, P., Gallup, D. (2015), Brine Silica Management at Mighty River Power, New Zealand, *Proceedings, World Geothermal Congress* (2015).

Arnórsson, S. (2000), The quartz and Na/K geothermometers. 1. New thermodynamic calibration. *Proceedings World Geothermal Congress 2015*, 929-934.

Bertani, R. (2015), Geothermal Power Generation in the World 2010-2014 Update Report *Proceedings World Geothermal Congress* (2015).

Candelaria, M. N. R. (1996), Methods of coping with silica deposition – the PNOC experience.

Geothermal Resources Council, Transactions, 20, 661-672.

Featherstone, J. L., Van note, R. H., Pawlowski, B. (1979), S. A cost effective treatment system for the stabilization of spent geothermal brines. *Geothermal Resources Council, Transactions*, 3, 201-204.

Featherstone, J., Butler, S. and Bonham, E. (1995), Comparison of crystallizer reactor clarifier and pH mod process technologies used at the Salton Sea geothermal field. *Proceedings World Geothermal Congress*, 2391-2396.

Featherstone, J., Gallup, D., von Hirtz, P. (2015), Compatibility Testing of Salton Sea Geothermal Brines. *Proceedings, World Geothermal Congress* (2015).

Fournier, R. O. and Marshall, W. L. (1983), Calculation of amorphous silica solubilities at 25° to 300°C and apparent cation hydration numbers in aqueous salt solutions using the concept of effective density of water. *Geochimica et Cosmochimica Acta*, 47, 587-596.

Fournier, R. O. (1985), The behavior of silica in hydrothermal solutions. In *Reviews in economic geology, 2,* ed. B. R. Berger and P. M. Bethke, 45-61. Society of Economic Geologists.

Gallup, D. L. (1996), Brine pH modification scale control technology. *Geothermal Resources Council, Transactions*, 20, 749-752.

Gallup, D. L. (1997a), The interaction of silicic acid with sulfurous acid scale inhibitor. *Geothermal Resources Council, Transactions*, 21, 49-53.

Gallup, D. L. (1997b), Aluminum silicate scale formation and inhibition. *Geothermics*, 26, 483-499.

Gallup, D. L. (2002), Investigations of organic inhibitors for silica scale control from geothermal brines. *Geothermics*, 31, 415-430.

Gallup, D. L. (2004), Unusual adherence of manganese silicate scale to metal substrates. *Geothermal Resources Council, Transactions*, 28, 529-532.

Gallup, D. L. (2007), Advances in geothermal production engineering in recent decades. *Geothermal Resources Council Trans.*, 31**,** 11-15.

Gallup, D. L. and Barcelon, E. (2005), Investigations of organic inhibitors for silica scale control from geothermal brines. II *Geothermics*, 34, 756-771.

Gallup, D. L. and Kitz, K. (1997), Low cost silica, calcite and metal sulfide scale control through on-site production of sulfurous acid from H_2S or elemental sulfur. *Geothermal Resources Council, Transactions*, 21, 399-403.

Gallup, D., Sugiaman, F., Capuano, V., and Manceau, A. (2003), Laboratory investigation of silica removal from geothermal brines to control silica scaling and produce usable silicates. *Applied Geochemistry*, 18, 1597-1612.

Gallup, D., von Hirtz, P. (2010), Control of Silica Scaling in Geothermal Systems Using Silica Inhibitors, Chemical Treatment and Process Engineering, Chapter 9, *The Science and Technology of Industrial Water Treatment*, CRC Press.

Geothermal Energy Association (GEA). (2015), Annual U.S. & Global Geothermal Power Production Report.

Gestur G. (2001), Reykjavik Energy, personal communication.

Goto, K. (1955), Research on the state of silicic acid in water (Part 2): Solubility of amorphous silicic acid. *Journal of the Chemical Society of Japan, Pure Chemistry Section*, 76, 1364-1366.

Hirowatari, K. and Yamauchi, M. (1990), Experimental study on a scale prevention method using exhausted gases from geothermal power stations. *Geothermal Resources Council, Transactions*, 14, 1599-1602.

Hirtz, P. (2004), Thermochem, Inc. internal report to Ormat.

Iler, R. K. (1979), The chemistry of silica. New York: John Wiley & Sons.

J. Björke, B. Mountain, T. Seward. (2012), The Solubility of Amorphous Aluminous Silica: Implications for Scaling in Geothermal Power Stations, New Zealand Geothermal Workshop 2012 Proceedings, 19 - 21 November.

Kindle, C. H., Mercer, B. W., Elmore, R. P., Blair, S. C. and Myers, D. A. (1984), Geothermal injection treatment: Process chemistry, field experiences and design options. PNL-4767, UC-66d.

Lovelock, B., Guidos, J. (2017), Acetic Acid Dosing to Manage Silica Scaling, Proceedings The 5th Indonesia International Geothermal Convention & Exhibition (IIGCE), Indonesia

Manceau, A. and Gallup, D. L. (2005), Nanometer-sized divalent manganese-hydrous silicate domains in geothermal brine precipitates. American Mineralogist, 90, 371-381.

Manceau, A., Ildefonse, Ph., Hazemann, J. L., Flank, A. M., Gallup, D. L. (1995), Crystal chemistry of hydrous iron silicate scale deposits at the Salton Sea geothermal field. Clays & Clay Minerals, 43, 304-317.

Mulazzani, D. (2015), Case Study to Upgrade and Optimize an Existing Geothermal Power Plant, Proceedings, Indonesia International Geothermal Conference and Exhibition.

Sugiaman, F., Sunio, E., Molling, P. and Stimac, J. (2004), Geochemical response to production of the Tiwi geothermal field, Philippines. Geothermics, 33, 57-86.

von Hirtz. P., and Gallup, D. (2000), DEPOSITION model, Thermochem internal software documentation.

Wahl, E. F. (1977), eothermal energy utilization. New York: John Wiley & Sons.

Weres, O., Yee, A., Tsao, L. (1982), Equations and type curves for predicting the polymerization of amorphous silica in geothermal brines. Society of Petroleum Engineers Journal, February 9–16.

3D NATURAL STATE MODEL OF SILERI GEOTHERMAL SYSTEM, DIENG GEOTHERMAL FIELD, INDONESIA

Rheza Akbar Dewantara[1], Khasani[1], and Ruly Husnie Ridwan[2]

[1]Department of Mechanical and Industrial Engineering, Faculty of Engineering
Universitas Gadjah Mada,Yogyakarta, Indonesia
[2]PT Geo Dipa Energi (Persero), Jl. Aditiawarman Kav. 55 Jakarta Selatan 12160 Indonesia
Email: dewantara.akbar@gmail.com; khasani@ugm.ac.id; ruly@geodipa.co.id

ABSTRACT

A three-dimensional numerical reservoir modeling of Sileri area at Dieng geothermal field was developed for natural-state condition as a basis of production stage simulation and future scenarios for development. Before development, the Sileri geothermal reservoir was a liquid-dominated system with a base temperature of about 325°C indicated by chemistry and physical measurements. Surface exploration surveys and the findings derived from drilling, logging and well testing of geothermal wells were used to build a 3D numerical model of the geothermal system natural state by means of the TOUGH2 reservoir simulator, supported by Petrasim graphical interface. The numerical model was intended to check the consistency of the conceptual model, to give a better picture of the reservoir thermodynamic conditions, and constraints the mass and heat flows through the system. The output of the natural state model was validated by six wells from the actual measurement and verified by pressure and temperature. Running time is set at 1m.a. relatively satisfactory good match was obtained between temperature and pressure profiles of six wells with the model for natural state simulation and can represent the actual model.

Keywords: Reservoir modeling, Sileri, natural state, TOUGH2

INTRODUCTION

Indonesia is blessed with abundant of geothermal energy potential and can be an alternative energy to be developed in the future, especially for electricity generation, replacing the dependence on the use of hydrocarbon energy sources that decreases in the amount of its reserves. Indonesia's geothermal resources are among the largest in the world, with around 40 percent of the total geothermal resources worldwide, with speculative and hypothetical reserves of 30,000 MW. To-date the Government of Indonesia (GOI) has identified 325 geothermal prospects (Wahjosoedibjo and Hasan, 2018). Since 2002, PT Geo Dipa Energi started to operate commercially Dieng Unit 1 with an installed capacity of 60 MW for Java – Madura – Bali in interconnection system. According to the Statistic PLN 2013, the electricity needs in Java at the end of December 2013 amount to about 26,768 MW (78.3% of total needs in Indonesia). The concession area includes 3 geothermal active sectors named Sileri, Sikidang and Pakuwaja (Sirait et al, 2015). Sileri area is characterized by steam production with high temperature at a relatively deep location. The reservoir temperature ranges from 300°C -335°C. The area of Sikidang is relatively shallow and the temperature is lower than that of Sileri. The reservoir temperature ranges from 240-300°C, with zone of production in most wells encountered at a depth of - 1400 to 1500 m (Layman et al., 2002). The aim of this research is to develop the reservoir model of Dieng geothermal field, especially at Sileri area and to study the fluid dynamic system through the analysis of properties such as pressures and temperatures in natural state condition that can be used as a basis for production and forecast.

CONCEPTUAL MODEL

The stratigraphy of Dieng geothermal field consists of quartz volcanic rock deposits consisting of andesite and pyroclastic lavas. The oldest Dieng Volcanic deposited sample had been from dating measured by Boedihardi et al (1991) which put the age at 3.6 Ma (Nurpratama et al, 2015). The geological map of Dieng field is shown in Figure 1. The conceptual model of Dieng field is presented in Figure. 2. In this study, the numerical simulation is focused on the Sileri Area, since most of the wells are located within this area. There are some vital components for a conceptual model of a potential geothermal area, namely: heat source, reservoir structure (e.g., good permeability, lithologically or structurally determined), recharge fluids, and discharge zones/thermal signatures (Utami, 2015). The resistivity values in the Sileri area and the variation of the distribution of distribution in Dieng geothermal field are typically shown in Figure 4. Based on the drawings at 1250 m to 0 m the value of resistivity increases where the low resistivity layer (<8 ohm-m) is detailed in red which indicates that the area can be interpreted as an upwelling thermal fluid area at shallow depth (Bogie and Kusumah, 2008) resulting in alteration of rocks that eventually develop into caprock of the geothermal system. The hot springs in Dieng are divided into several types determined by comparing the concentrations of Cl, SO4, and HCO3 in the triangle diagram of Cl-SO4-

HCO3 (Giggenbach, 1988). Based on the concentration of the three elements / coumpounds, hot springs are divided into three zones. Sileri Crater is in the deep zone of Cl waters. Bicarbonate water derived from condensation moisture by a heat sourceunder it. The intensive entry of water chloride makes the type of water bicarbonate into water chloride (Nicholson, 1993).

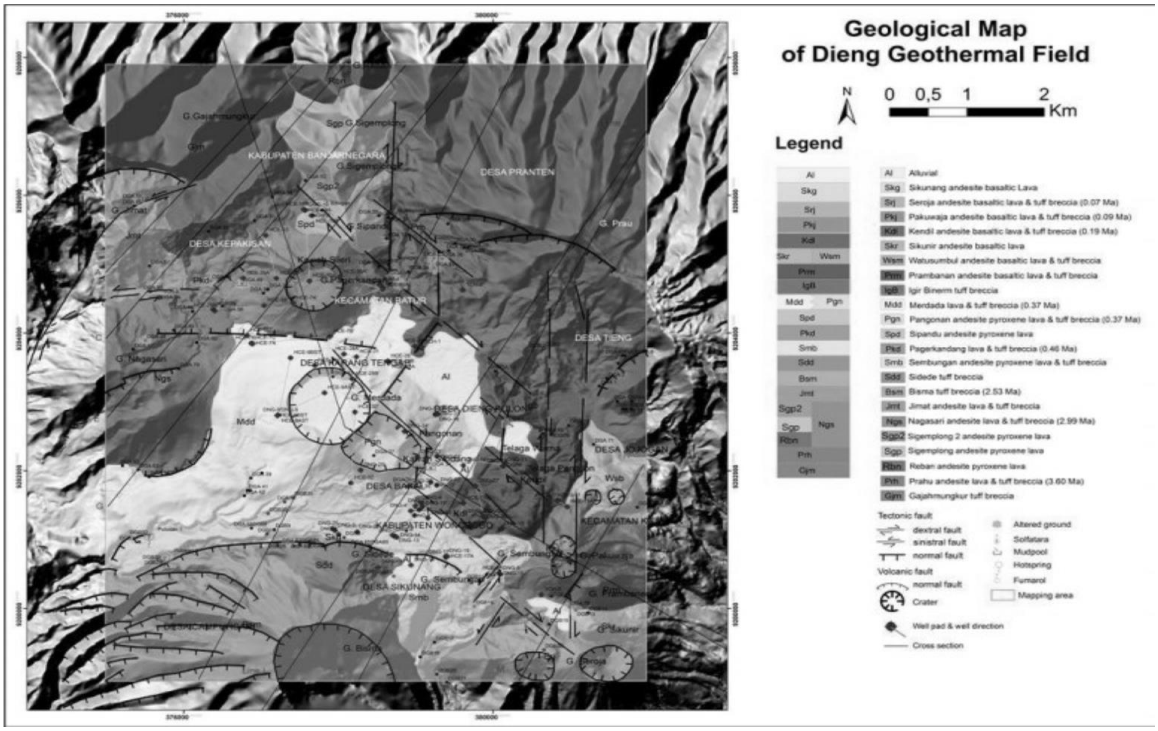


Figure 1: Geological map (Nurpratama, 2015)

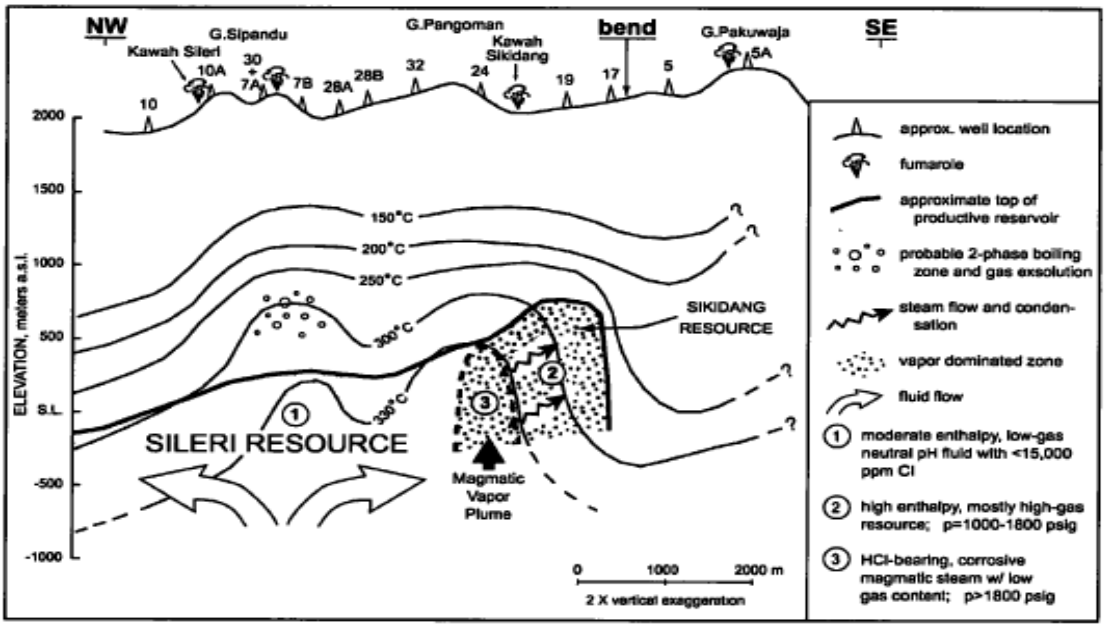


Figure 2: Conceptual Model (Layman, et.al, 2002)

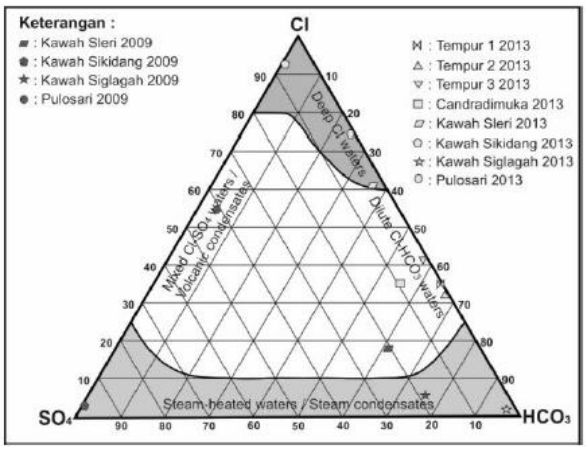


Figure 3: Terniary diagram of Cl-SO4-HCO3

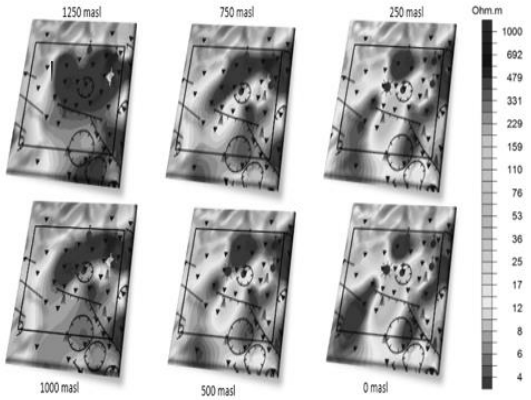


Figure 4: Resistivity from MT data

RESERVOIR MODELLING

Grid

The layer and surface of the model follow the MT and surface topographics contour and EOS 3 for the State in the model. The modeling is carried out by dividing the reservoir system into a number of blocks or grids that are interconnected each other in accordance with structure of geosciences data. The grid or sub-volume modeling can be either diagonal or parallel depending on the boundary and shape of the reservoir. The size and number of grids are adjusted to the extent and size of the volume of the reservoir by the size of each grid representing the reservoir zone extent.

The smaller size of the grid used, the more detailed the simulation results will be obtained. The model is 3.0 km x 2.5 km and -2.0 km to 2.50 km above sea level. Figure 4 shows a resistivity from magnetotelluric data with an interval of 250 m depth. The model is further divided into 20 vertical grid layers with 6 types of rocks adapted to geological data in the layers based on the layer structure and data from the rock. The reservoir properties consist of rock and fluid properties in the geothermal system.

Rock properties include porosity, permeability, heat conductivity and specific heat. The property of the rock that gives great effects on the fluid flow is the permeability. We used EOS 3 which assumed that the fluid is water and steam flowing in the model. There are 6 types of rocks to describe the reservoir and are assumed as isotropic heterogeneous conditions. The block are made by considering several factors such as the location of wells, reservoir boundaries, rock structure patterns, rock properties, and the location of the manifestations on the surface. This model is limited by some boundary conditions such as from the boundary model taken from the boundary of the Sileri region and the restriction of the faulty regional model. Surface boundary condition is done by entering the specified temperature at 25°C and 325°C of heat source. The location of the heat source is on the north side of the model and its made by matching the heat source coordinates with model structure and filling the parameters corresponding to the heat source conditions. Heterogenity of rock porosities, saturation of water and steam in reservoirs and fluid characteristics, either laterally or vertically can be taken into model.

VALIDATION

Calibration for some parameters which are normally temperature and pressure in the wells is done to obtain the appropriate conditions between the simulated conditions and the actual state so that the model can be used as a reference for the field development scenarios, mainly the prediction of production from the field. The property change for the model is only carried out on permeability and porosity because that parameters are most influential to changes in temperature distribution.

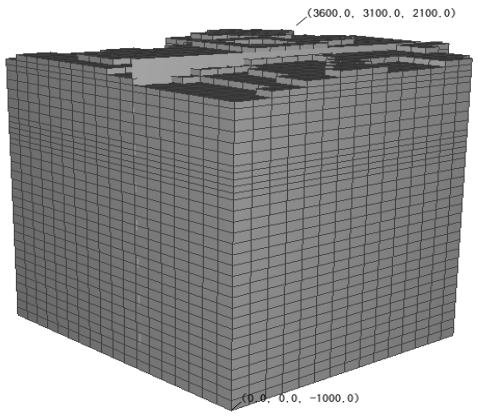


Figure 5: Mesh and Grid.

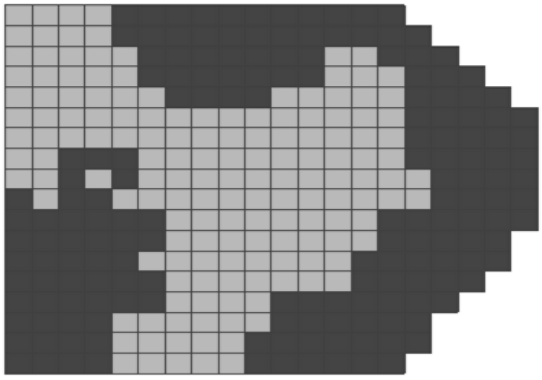
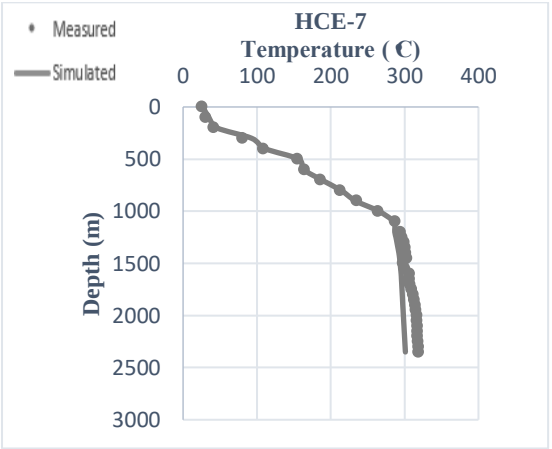
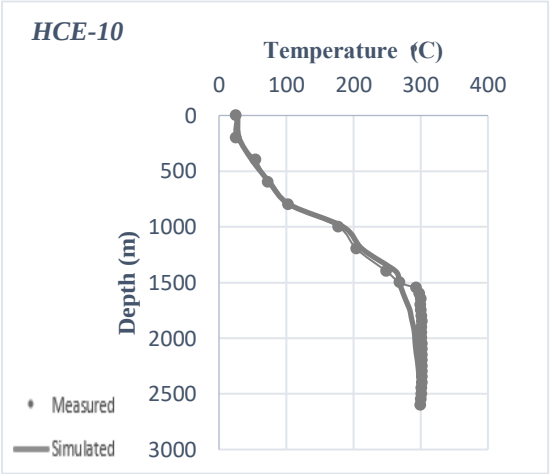
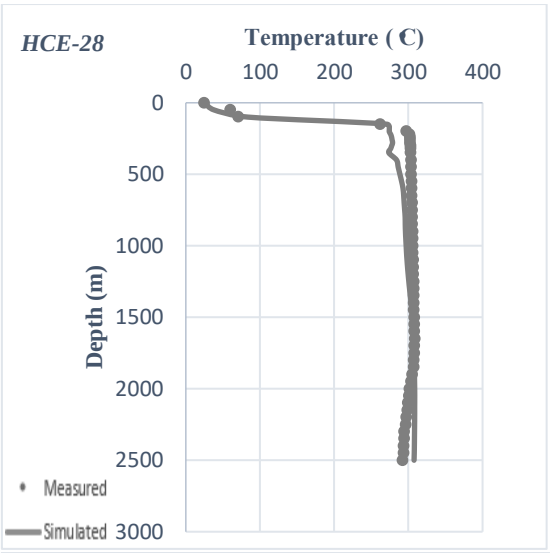


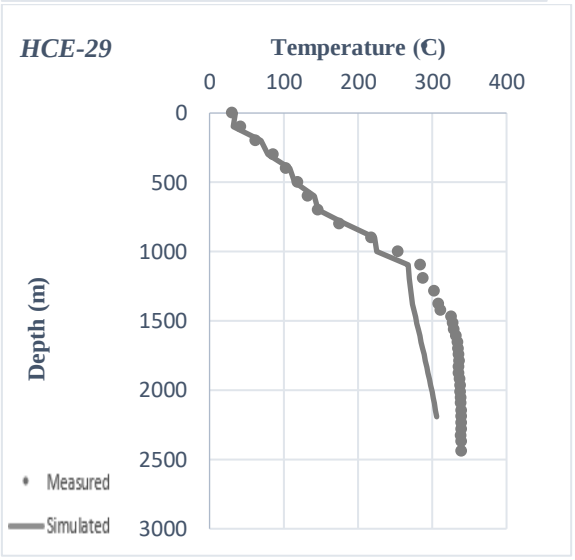
Figure 6: The rock types at -250 masl.

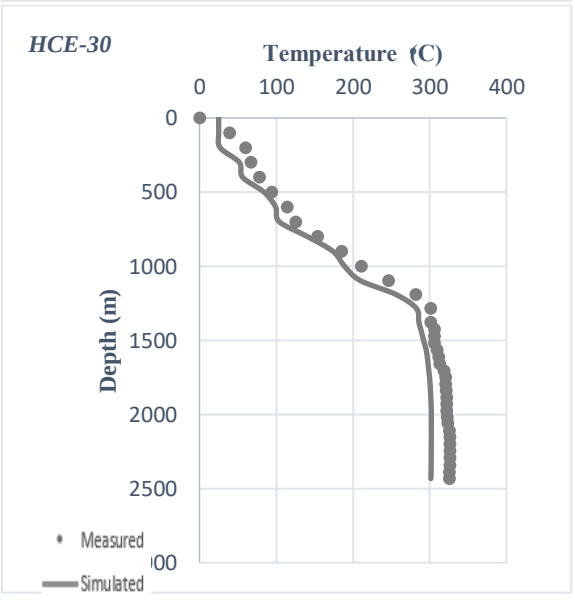
Other property values in rocks such as density, thermal conductivity dont change too much because it will be relatively same unchanged in alteration conditions and will not affect too much on the temperature distribution. This model assumes with corey permeability, the wetting and non-wetting phase-relative permeabilities to be independent of the saturations of the other phases. The results are plot of curves between depth versus temperature and pressure as shown in Figures 7 and 8.











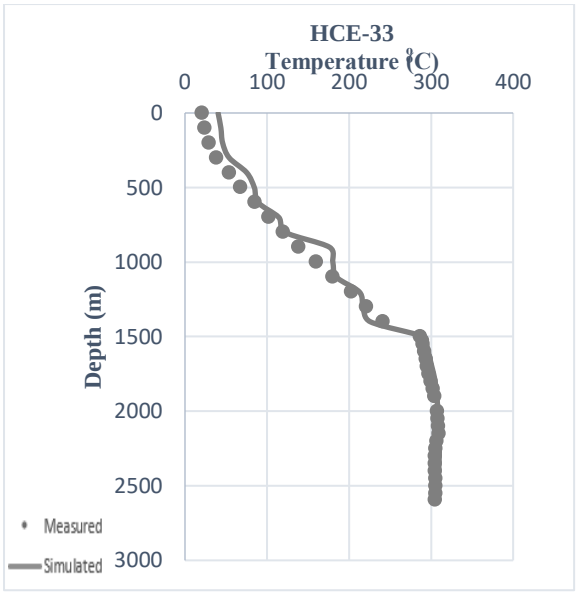
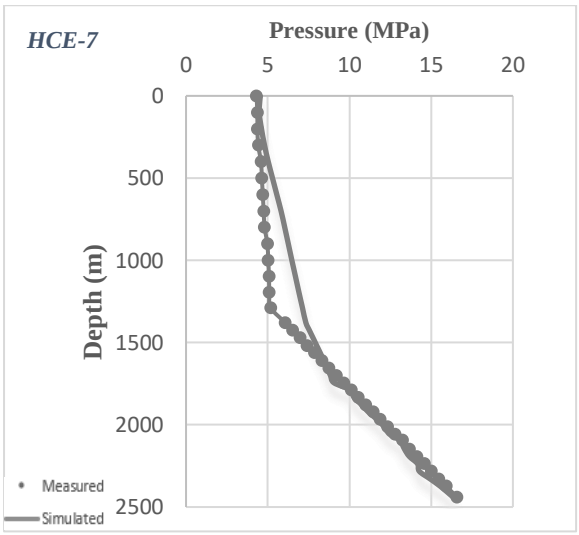
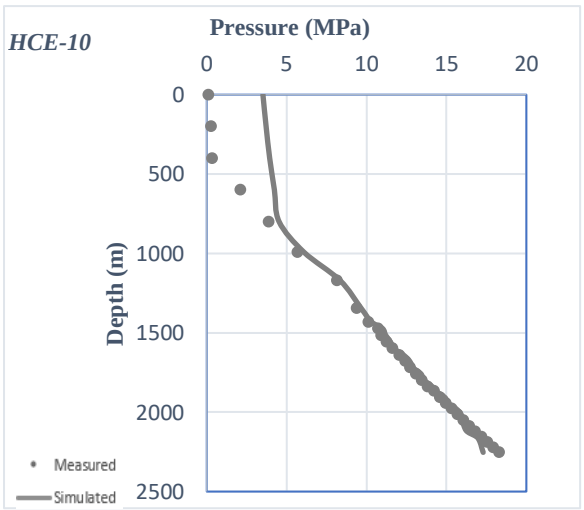
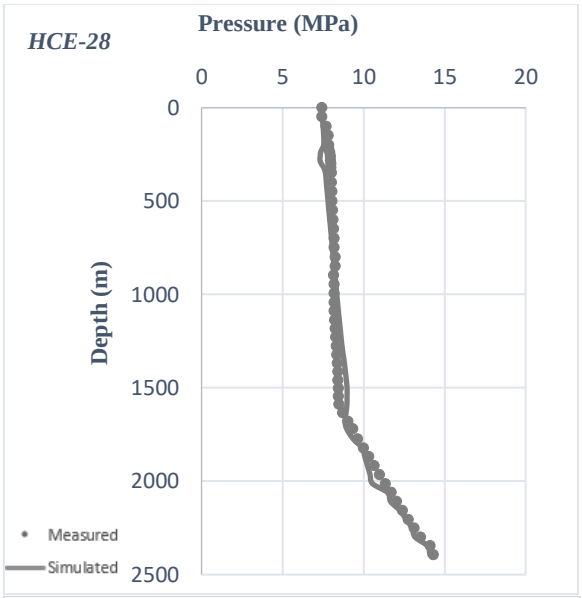
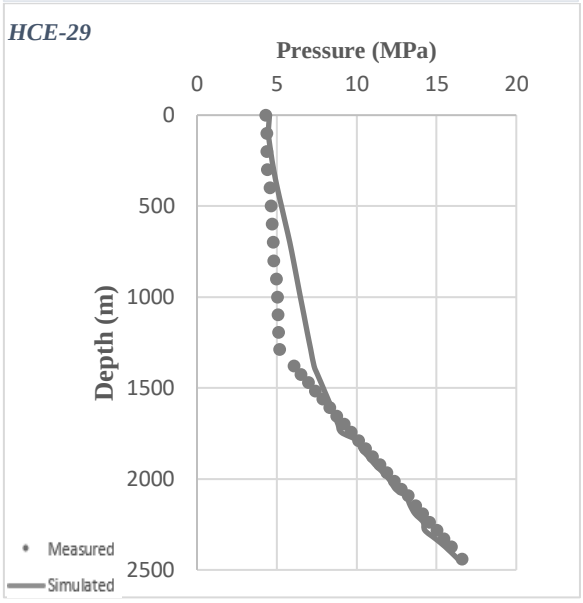


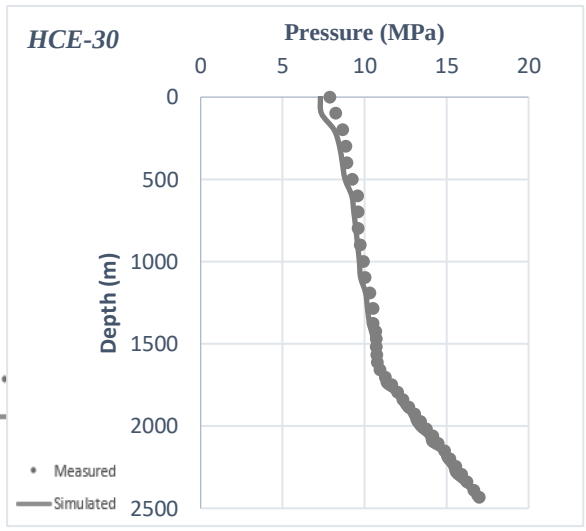
Figure 7: Measured and simulated temperature profiles of 6 wells.











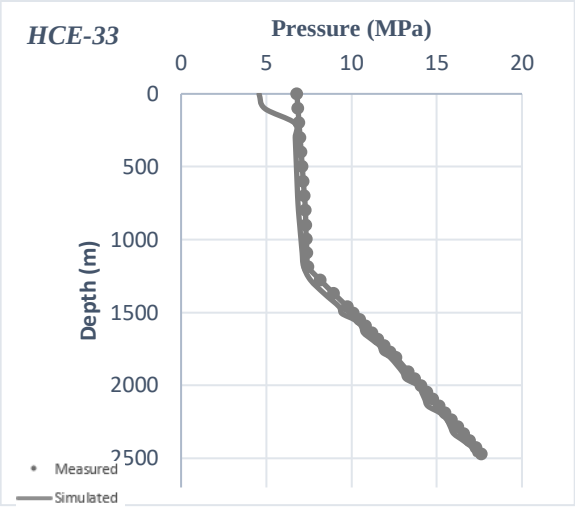


Figure 8: Measured and simulated Pressure profiles of 6 wells.

It can be seen that relatively good matchings have been achieved between measured and simulated pressure and temperature profiles in some wellbores, except for pressure profile in Well HCE10 did not show a good result and quite difference between measured and simulated pressure in the upper most level in the wellbore. This suggests that it should be checked on the history of measurement activity. The graph under measured conditions is unchanged and close to 0 MPa at a depth up to 500 m.

RESULTS AND DISCUSSION

Dieng geothermal field consists of several areas including Sileri, Sikidang, and Pakuwaja and have enough geothermal energy potential to be utilized for power generation but not of all areas can be developed due to resource problems, mainly scaling and high content of non-condensable gas. The area that has been developed is Sileri, as liquid dominated reservoir system. The geological and geoscience data are widely used in determining the boundary of the area in the analysis or conceptual model. From geological data, it will be obtained geological and stratigraphic maps which are then used for the reconstruction of the layer model of Dieng geothermal field. The conceptual model is a useful tool for predicting the behavior and as a development basis of geothermal field. The model illustrates concepts and ideas based on existing data by predicting the location of physical features and how they affect system behavior. For example, the location of outflows and upflow zones are very important and controlled by the most important parameters such as temperature distribution and permeability. Accuracy of simulation model is tested using the alignment data between temperature and pressure of simulation results with measured (P & T surveys) called the validity test of the simulation model as shown in Figures 7 and 8. The plot between the two coincides the model can be considered to represent the actual conditions and can be used as an initial model for development and the advanced scenarios of the field. When plot between two types of temperature profiles is poor, re-alignment will be done between the simulation and field conditions such as the amount of heat in the fluid below the surface, the sub-surface heat flux and the permeability of the rock will be re-simulated with the iteration process until it reaches the harmonic result. From temperature profiles of some wells, it can be interpreted that the heat flowing from 0 to 1500m depth is conduction. This is indicated by a linear graph of gradient temperature that increases to depth. It can also be interpreted that the ripple medium is impermeable. In such layers the rocks are andesite with the thermal conductivity is 1.8 W (m / K). The rock absorbs heat and used to raise the temperature so that the heat flowing to the upper part becomes reduced. In this zone it can be observed that andesite rock acting as a caprock. The depth below 1500m is a commonly coarse-grained microdiorite. In rocks with coarse grains will make the layers porous and have higher porosity and permeability. The graph shows the trend is relatively straight and the pressure changes are not too large. Under these conditions the possibility of fluid convection may occur which has a relatively constant temperature and at 1500 m there is a fracture caused from the drilling process which means the fluid.

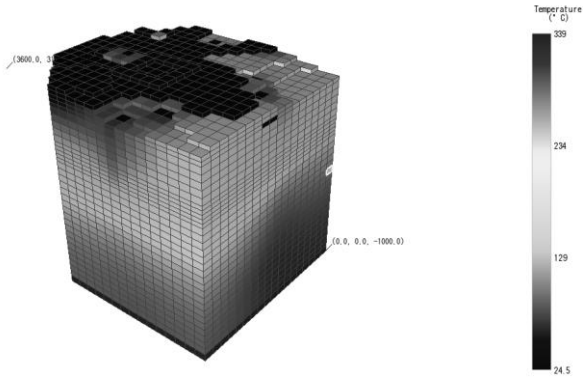


Figure 9: Temperature Model.

Flows in a low permeability region to high permeability region. So, heat is lost when the fluid flows upwards and to raise the rock temperature. Grid model and after meshing, we will get 3D results from the rock layers with the desired various parameters (temperature, pressure, rock density, porosity etc.).

Temperature distribution from model shows good in Figure 9. The temperature contrast at the values of about 200ºC, 250ºC and 300ºC. This temperature distribution also indicates that there is an upflow zone below the Sileri area. Figure 10 shows the fluid flow moves horizontally at a depth of -1500m, it is caused by high porosity and high permeability

reservoir rocks will lead convection fluid flow in all directions. Above -1500m the direction of flow is only vertical flow. Vertical direction permeability (ky) will cause the fluid flow distribute through heat convection in the rock passed over it in a compact rock zone.

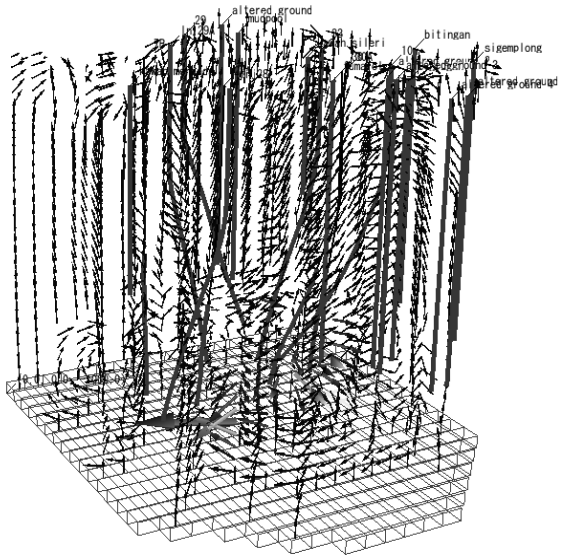


Figure 10: Upflow and Lateral flow model.

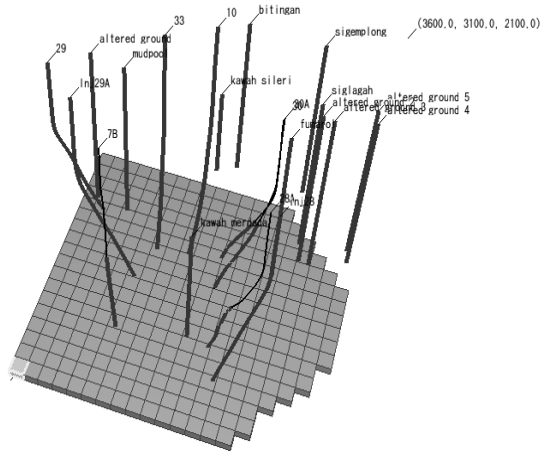


Figure 11: Wells in the model.

Kx and kz usually has greater permeability more than kz direction. Some rocks permeability such as andesite pyroxene z- permeability (kz) has a bigger value than kxy. It caused by cracks along kz as an effect of overburden pressure or drilling process and forming a perpendicular fracture. Running time is less than rock age because at condition 1m.a. we assume that condition is already steady and conditions up to the rock age will be the same.

CONCLUSION

A numerical model of the Sileri, Dieng geothermal field has been developed using TOUGH2 (Pruess et al, 1999) and focused on the Sileri area, because it is very productive and still can be developed to increase production capacity. The results are summarized as follows:

1. The model is derived from multiple data integration. These interconnections and data constraints are used for construct a conceptual model.
2. The reservoir is identified at the location below 1500 m with microdiorite rock. The natural state simulation is performed and reaches steady condition for 1 m.a year.

ACKNOWLEDGEMENT

The authors wish to thanks to Geocap (Geothermal Capacity Building) Program for the supports so that this research can be finished. The appreciation is due to PT. Geo Dipa Energi for using and publishing the data.

REFERENCES

Boedihardi, M., Suranto, and Sudarman S. (1991), "Evaluation of Dieng Geothermal Field. Review of Development Strategy," *Proceedings Indonesian Petroleum Association,* Proceedings 20th Annual Convention, Indonesia, p. 347-361.

Bogie, I., and Kusumah, Y, I. (2008), "Formation Imaging at the Wayang Windu Geothermal Field, West Java, Indonesia," *Western Pacific Regional Branch.*

Giggenbach, W, F. (1988), "Chemical Techniques in Geothermal Exploration," *New Zealand: Chemistry Division, DSIR, Private Bag.*

Layman, E, B., Agus, I. and Samsudin, W. (2002), "The Dieng Geothermal Resource, Central Java," *Indonesia Geothermal Resources Council Transactions*, Vol. 26, 22-25.

Nicholson, K. (1993), "Geothermal Fluids, Chemistry & Exploration Techniques," *Berlin, Germany: Springer Verlag, Inc.*

Nurpratama, M. I., Atmaja, R. W., Elfina., Wibowo Y. T., Harijoko, A., Husein, S., Sudarno, I., Setianto, A., and Utami, P. (2015), "Detailed Surface Structural Mapping of the Dieng Geothermal Field in Indonesia," *Proceedings World Geothermal Congress 2015 Melbourne, Australia.*

Pruess, K., Moridis, G., and Oldenburg C. (1999), "TOUGH2 User's Guide, Version 2.0," *Earth Science Division lawrence Berkeley National Laboratory University of California.*

Sirait, P., Ridwan, R. H., and Battistelli, A. (2015), "Reservoir Modeling for Development Capacity of Dieng Geothermal Field, Indonesia," *PROCEEDINGS, Fourtieth*

]Workshop on Geothermal Reservoir Engineering Stanford University, Stanford, California, January 26-28.

Utami, P. (2015), "*Geothermal Geology"*. Unpublished lectures note, University of Auckland, New Zealand.

Wahjosoedibjo, A., and Hasan, M. (2018), "Indonesia's Geothermal Development: Where is it Going?" *PROCEEDINGS, 43rd Workshop on Geothermal Reservoir Engineering, Stanford University, Stanford, California.*

DRILLING RISK IN GEOTHERMAL WELL

Jul Rafli, Birean Sagala, Haris Siagian, and Dhani Sanjaya

Geoscience Department, PT Sokoria Geothermal Indonesia – A project of KS Orka Renewables Pte Ltd
Recapital Building 5th Floor, Jl Adityawarman Kav 55, Jakarta Selatan 12160
Email: haris.siagian@ksorka.com

ABSTRACT

Drilling technology in geothermal fields is adopted from oil and gas drilling technology. Although geothermal reservoir and oil/gas reservoir are similar, but the facts show that there are several differences that affect modifications in geothermal drilling. Therefore, it is needed to define the main differences between geothermal fields and oil/gas fields, and then consider those to make better geothermal drilling design. The main challenges associated with drilling geothermal wells are related mostly to hardness of igneous and volcanic rocks being drilled. The high temperature of formation is also a consideration in the drilling process at geothermal wells. See the difference between oil / gas and geothermal wells, then drilling practice on geothermal well is also different. Some of the problems that occur during the drilling process are among others caused by condition of drilled formation (high clay mineral and loss zone), equipment and materials used during drilling, acidic water used as drilling fluid as a case in Sokoria project, and experience man power in geothermal drilling environment. From several causes it makes the drilling process becomes constrained and takes longer so that the impact on the high cost of drilling operations and even worse will impact on the loss of wells that have been drilled. This paper presents drilling risk in geothermal well based on formation rocks, hole condition and Acidic water supply for drilling fluids as a case in Sokoria drilling campaign. Several ways to overcome and anticipate problems in the drilling of geothermal wells can be done in order to reduce drilling risk.

Keywords: Drilling technology, drilling risk, geothermal well.

INTRODUCTION

Drilling is an important activity in geothermal utilization for accessing geothermal reservoirs with hot water and steam (Makuk, 2013). The main challenge in the drilling of geothermal wells is related to hard formations and high temperature reservoirs that are different from the drilling of oil and gas wells. The formation rocks encountered in the drilling of geothermal wells are frozen and volcanic rocks, where the compressive strength of these rocks is greater than that of sedimentary rocks (sandstone and carbonate rocks) in oil and gas drilling (Augustine et al, 2006). The geothermal well temperature gradient ranges from 12-13 F / 100 ft or more, higher than the temperature gradient of oil and gas wells in the range of only 5F / 100 ft) and in general the geothermal reservoir of the pressure gradient is lower than the normal water pressure gradient. Some of the problems that occur during the drilling process are among others caused by:

1. Condition of drilled formation (high clay mineral and loss zone).
2. Equipment and materials used during drilling.
3. Acidic water used as drilling fluid as a case in Sokoria project.
4. Experience man power in geothermal drilling environment.

Some of the challenges and risks encountered during geothermal drilling determine the performance of geothermal wells and geothermal fields including non-productive time (NPT), productive time, the quality of well-making processes, costs, and production achievements

DRILLING GEOTHERMAL WELL

Geothermal reservoirs, known as hydrothermal reservoirs, are distinguished from oil or gas reservoirs. In most of formations, the reservoir pressure is lower than hydrostatic pressure of water column. This condition is also associated with high temperature which affects the phase of reservoir fluid. To drill the well in geothermal area, the different conditions have to be considered are:

1. Reservoir Temperature In geothermal system, temperature is relatively high, varied from 125°C to above 225°C. Based on classification by Hochstein (1990), Indonesia is included into medium to high enthalpy reservoir which is dominated by vapor or superheated steam.
2. Lithology Formations found are hard silicified volcanic, such as andesite, basalt, dacite, and rhyolite. These formations have compressive strength around 240+ MPa. They are also basically abrasive with quartz content above 50%. This feature will lower rate of penetration (ROP) in drilling.
3. Potentially Lost Circulation Zones Fractured zones with high permeability existed in reservoir can cause partial or total lost circulation. Solid or material suspended in the mud also can plug the formation into that permeable zones.

4. Non-condensable Gas and Corrosion Hole condition is highly corrosive with pH range of 3 to 5 because of existence of non-condensable gases, such as carbon dioxide (CO2) and hydrogen sulfide (H2S). Corrosion problem limit the materials applied for drilling equipment and lower the casing strength. It also leads to casing failure caused by sulfide stress cracking. Substantially, H 2 S is one of avoided hazard during the drilling operation.



Figure 1: The drill pipe and drill collars corrosion coming out from wellbore.

HIGH CLAY MINERAL

Persistent formation related drilling problems have been attributing to the presence of an unstable lithology and swelling. From thin section and SEM analysis, these samples consist of very fine-grained glass. brown colored matrix which is semi opaque. Contained within in the matrix are minor opaque grains and irregularly shaped clay rich area interpreted to have originally been vitric clasts to plagioclase crystal clasts. This matrix is considered to be a mixture of originally vitric material which has weathered to clay and iron oxides. Mineralogy determined from XRD analysis show dominantly interlayered illite-calcium smectite (15% illite). Clay from tuffaceous siltstone (Smectite, illite and calcium smectite) indicated it can swell and reactive with water.

Problem Drilling

Upon being drilled the high clay minerals or tuffaceous siltstone come into contact with the drilling fluid. This cools the tuffaceous siltstone, allowing water to move into the smectite layers, resulting in increasing volume. As the tuffaceous siltstone consist of greater than 80%smectite, even though the smectite Is a calcium and occurring in interlayers, this is a significant volume increase. This combined with the low mechanical strength of the rock forces the tuffaceous siltstone into the hole.



Figure 2: High Clay Minerals from coring will swelling when reaction with water.

Based on Kingston-Morrison study (1997), as the smectite are initially occur in at lower temperature than in a geothermal field they are not totally dehydrated to begin with, so there is little volume increase by hydration if they are converted to calcium smectite. In addition, since potassium is a smaller ion it can shrink the clay and bind their layer together. However, in this instance the calcium smectite are at a temperature of over 100C in the reservoir and are dehydrated and there is significant volume increase upon cooling and hydration. Where formation smectite are converted to potassium smectite, which require greater than 5 wt% potassium in solution, the interlayer gap is reduced and the clays can shrink.

The initial grace period to collapse of tuffaceous siltstone is around 48 hours. When sudden massive losses of circulation have been encountered severe collapse of shallower overlying tuffaceous siltstone bed can occur within an hour or two, perhaps as a result of reduction of confinement pressure.



Figure 3: High Clay Minerals from drilling cutting will swelling when reaction with water.

LOSS OF CIRCULATION

The instability of the wellbore and the loss of circulation is one of the main problems causing unproductive time during drilling. The problem of wellbore instability causes many other problems, ranging from stuck pipes, collapse of formation, narrowing of wells, and other problems. Stuck pipe can occur due to drill hole stricture, inefficiency of wellbore well cleaning and drilling fluid pressure too high. Pipe incidents are stuck in the drilling process of geothermal wells resulting in significant increase in time and drilling costs. The stuck pipe occurs in several mechanisms that depend on the indication and causal factors.

Some characteristics of geothermal reservoirs are located at high temperatures and even extreme temperatures (hot gradients (12-13F / 100 ft or more), hard rocks (igneous rocks such as granite, breccia and others) and formation fluids in the form of water and steam. The geothermal systems in Indonesia are generally hydrothermal systems that have high temperatures (> 225C) and only a few have medium temperatures (150-225C).

The types of rocks in the geothermal reservoir generally consist of rocks such as andesite, granite, granodiorite, quartzite, greywacke, basalt, rhyolite and volcanic tuff. rocks in the geothermal reservoir are generally harder, abrasives (quartz content above 50%) and multiple fractures (fracture width up to 5 cm). Unlike the oil and gas reservoir, the geothermal reservoir fluid is water and steam. The pressure of the geothermal formation is lower than the normal water pressure gradient (0.433 psi / ft), so there is often a problem of circulatory loss.

In addition to high temperatures, another characteristic of the geothermal reservoir is the presence of fractures that will affect the fluid flow of the reservoir. However, the presence of fractures can lead to a loss of circulation that inhibits drilling and coupled with formation pressure which is usually lower than normal water pressure (0.433 psi / ft).

The instability of the wellbore will bring some impacts on the drilling of geothermal wells.

1. The well hole will become unstable as there is a fracture in the formation rock and the invasion of the drilling fluid into the formation. If there is a shale formation, then the water content in the drilling fluid will be absorbed and swelling occurs. This will cause the diameter of the borehole to be smaller and the risk of stuck pipe higher.
2. The unconsolidated formation may cause problems with the removal of the drilling cutting and are at risk of collapse. Drill holes (wash out) can occur in this formation and cause problems in the drilling shaft removal process because the anular velocity will decrease and problems with the cementing process as the amount of cement needed will increase.
3. In the sloping hole, the risk of instability of the wellbore will be higher. These problems will cause difficulties at the time of well hole cleaning and cementing operations.

One of the most costly problems in the drilling of geothermal wells is the loss of circulation, ie the loss of drilling fluid as it enters into the pores or fractures of the formation. Here are some of the disadvantages of circulatory loss during drilling:

1. If the drilling fluid can not clear the wellbore and remove the drilling cutting, the drilling cutting will fall back into the well around the drill pipe circuit and cause the pipe to be stuck.
2. The cost of drilling fluid is quite expensive, especially in high temperature conditions. Therefore loss of drilling fluid due to loss of circulation will increase the drilling cost.
3. In geothermal wells, production zones or reservoir zones are typically zones of circulatory loss, so it is sometimes difficult to restore productivity as before drilling in the event of circulatory loss.
4. Loss of circulation can decrease the height of the fluid column in the well, so the hydrostatic pressure of the drilling fluid can be smaller than the formation pressure. This will cause the kick, ie the inclusion of formation fluid (gas, hot water, and hot steam) to the wellbore. This incident can occur in both productive and non-productive zones.
5. At no-produced zone intervals, the circulation loss zone should be sealed to make the wellbore cased and cemented. Loss of circulation during the cementing process will lead to increased drilling costs and cause instability of the wellbore. Casings that are not tied to the

formation as well as the incidence of fractures on the cement will cause leakage during production and the casing will be more quickly damaged. This will increase the cost of the well and the repair process is quite complicated.

6. The placement of lost circulation material (LCM) is difficult to do because the upper and lower zones of the circulatory loss zone are often not well known. LCM is used to close loose circulation zones that may have connections with other loss zones.

EQUIPMENT AND MATERIALS USED DURING DRILLING.

Usually thermal formations contain corrosive fluids (H2S and CO2) and high solids (eg TDS / Total Dissolve Solid above 250,000 ppm). This condition causes the rate of drill penetration and bit age is usually low and corrosion occurs. In addition, there is a risk of danger from both gases during drilling operations. Therefore, equipment and materials used in geothermal drilling are different from those used in oil and gas drilling such as drilling pipes, pumps and supporting facilities for water delivery system during drilling.

The equipment and materials used should have sufficient reserves during drilling. Transport materials should be well programmed. The role of materials man and drilling engineer becomes an important part of the availability of equipment and materials during drilling so that drilling performance can be better.

Analysis of variables for determining the performance of wells and geothermal fields includes non-productive time (NPT), productive time, the quality of well-making processes, costs, and production achievements. Based on the analysis, to predict and optimize a drilling operation in an effort to increase production. The drilling of geothermal wells becomes more expensive due to 3 main reasons:

1. Technical challenges are associated with high temperatures, hard rocks and corrosive fluids. This is coupled with potential problems of wellbore instability (pinched pipe) and loss of circulation.
2. Requires large diameter production holes, since the production rate of the geothermal fluid required to generate electrical energy is also high. In some drilling of geothermal wells, it takes more number of casing to reach a certain target at the same depth when compared to oil and gas wells.
3. Unique things because most geothermal wells, even in the same field, have different characteristics than oil and gas wells in the same field, so that previous well experiences cannot be used as a reference.

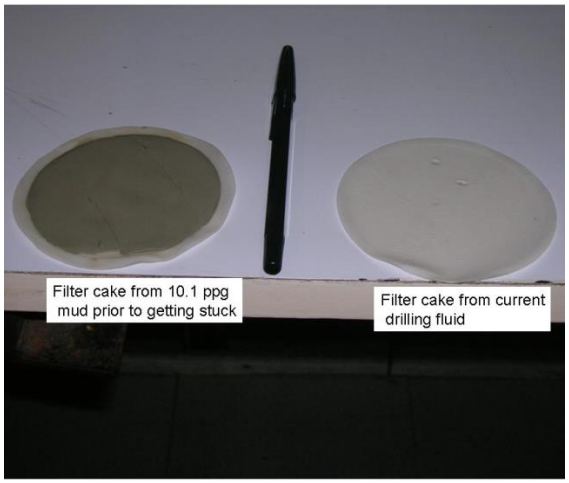


Figure 4: Mudcake produce from mud used drilling in geothermal well.

ACIDIC WATER USED AS DRILLING FLUID AS A CASE IN SOKORIA PROJECT

Generally, geothermal drilling uses a water supply for well circulation from existing rivers around the drilling site and the source of the water source has a neutral PH 7. However, it is different with the geothermal field in okoria, where the water source used for drilling needs has a PH low ranging from 3-4 (acid PH) this is caused by a water source that can be used only from streams with low PH water. A considerable distance of 12-14 km from wellpad becomes a challenge to optimize during the drilling process.

With the above conditions, it is necessary to specially design the good for the water pump and the pipe used for the water supply is made of corrosive resistant material. Suitable spare parts should always be available so that the water supply during drilling is not constrained.

EXPERIENCE MAN POWER IN GEOTHERMAL DRILLING ENVIRONMENT

All of the personnel involved in the geothermal drilling play a role in optimizing and successful drilling. Although Drilling technology in geothermal fields is adopted from oil and gas drilling technology but the facts that there are some differences that affect modification in geothermal drilling. Therefore, it is needed to define the main differences between geothermal fields and oil fields, and then consider those to make better geothermal drilling design. Good cooperation and peer-to-peer communication in their respective fields is essential and an understanding of the planned drilling program is the target of drilling success. Thus, experience man power in their respective fields is required. Most of the problems that occur in drilling

are caused by human error in understanding and running the drilling program that has been created.



Figure 5: Water with low PH around 3-4 for supply drilling circulate storage in water pond at wellpad.

In planning for the drilling of geothermal wells, an integrated analysis of all fields including reservoir, geology, drilling and production is needed so that the barriers and risks of drilling can be prevented (Marbun and Zulkhifly, 2011). In preparing the drilling plan of geothermal wells, it is necessary to do the following stages. For that, the required data as follows:

1. Targeting of each well.
2. Preparation of the operating program used.
3. Determination of parameters on mud, equipment, and others.
4. Estimated cost of mud, equipment and others.
5. Preparation of basic chart example: cost vs. depth and Days vs. Depth.
6. Monitor parameters during drilling operations.
7. Identification and validation of NPT.
8. Evaluate the ability to clean the wellbore.
9. Monitor wellbore cleaning capability.

NPT and Cost

Most wellbore problems are caused by the instability of the wellbore resulting in pinched, reaming, multiple check trips, holding up, difficulty logging, mud losses that can affect cementing, fishing, sidetrack, or well closing processes. Statistics show that 65% of stuck incidents in pipelines are the result of errors in planning, while 68% of incidents occur due to worker turnover.

4 levels in the NPT associated with sludge problems, among others:

1. Problems related to mud.
2. Loss of circulation – Formation.
3. Loss of circulation – Self-induced.
4. Wellbore related problems.

NPTs associated with drilling operations except for the loss of mud circulation:

1. Problem sticky clay (swelling clay).
2. Casing is not installed perfectly due to Tuffaceous Siltstone or unstable formation.
3. Piped pipes / fishing job / sidetracking due to lifting cutting capacity during drilling.
4. Differential sticking.

Therefore, it is needed to define the main differences between geothermal fields and oil/gas fields, and then consider those to make better geothermal drilling design.

CONCLUSIONS

1. Although Drilling technology in geothermal fields is adopted from oil and gas drilling technology but the facts show that there are several differences that affect modifications in geothermal drilling.
2. The main challenge in the drilling of geothermal wells is related to hard formations and high temperature reservoirs that are different from the drilling of oil and gas wells.
3. Generally, geothermal drilling will break through formations with high clay mineral content and tuffaceous siltstone formations are swelling and cause drilling problems.
4. The instability of the wellbore and the loss of circulation is one of the main problems causing unproductive time during drilling. The problem of wellbore instability causes many other problems, ranging from pinched pipes, collapse of formation, narrowing of wells, and other problems.
5. The availability of adequate equipment and materials required during drilling will optimize the performance of the drilling.
6. Well-planned drilling programs and good teamwork as well as experienced crew will also improve drilling success and reduce drilling problems.

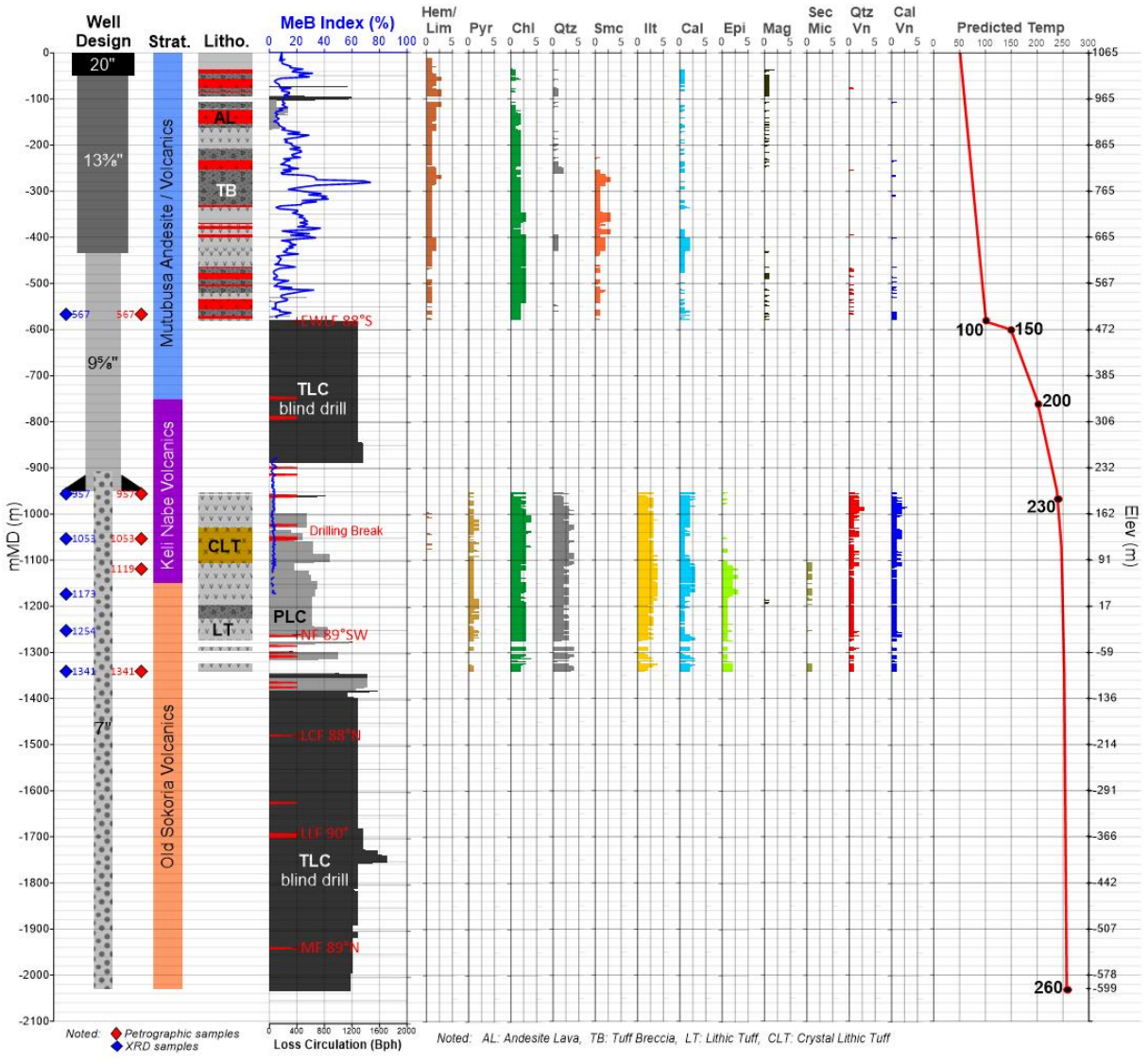


Figure 6: Composite log of Well XYZ showing lithology, loss circulation, MeB graph and alteration minera l

REFERENCES

Augustine, C., Tester, J. W., and Anderson, B. (2006), "A Comparison of Geothermal with Oil and Gas Well Drilling Costs". *PROCEEDINGS, Thirty-First Workshop on Geothermal Reservoir Engineering*, Standford, California..

Hochstein, M. P. (1990), "Classification and Assessment of Geothermal Resources". *Geothermal Institute, University of Auckland, New Zealand.*

Kingston-Morrison. (1997), Report on Tuffaceous Siltstone; from Wayang Windu Geothermal project, West Java, Indonesia: Kingston Morrison (unpublished).

Makuk, I. K. (2013), "Reducing Geothermal Drilling Problems to Improve Performance in Menengai". *GETOHERMAL TRAINING PROGRAMME*, Reykjavik, Iceland.

Marbun, B., and Zulkhifly, S. (2011), "Geothermal Well Integrity", *Proceedings 11th Annual Meeting and Conference Indonesia Geothermal Association 2011.*

THE EFFECTS OF FRACTURE INTENSITY IN DRILLING BIT PERFORMANCE THROUGHOUT DEVELOPMENT PHASE OF HULULAIS GEOTHERMAL FIELD

Fatah Gunawan, Graniko Reza Pratama, Freddy Haryo Armanto, and Widoyo Krisnanto

Pertamina Geothermal Energy, Jakarta Pusat 10340
Email: fatah.gunawan@pertamina.com, graniko.pratama@pertamina.com,
freddy.armanto@pertamina.com, widoyo.krisnanto@pertamina.com

ABSTRACT

The expansion of electricity generation throughout Bengkulu Province is supported by the development of Hululais geothermal field. The initial plan was to develop 2 x 55 MW geothermal power plant which is owned and operated by PT Pertamina Geothermal Energy. After a series of drilling development wells, it can be found that bit selection are playing a significant role to obtain a good drilling performance levels. The bit selection requires a conclusive understanding of the rock formation characteristics and geological model that control the rocks strength around the field. A typical challenges are the hard and abrasive rock formation, combine with the intensity of fractured and faulted zones. Moreover, the borehole temperature as the nature of geothermal reservoir field above 225°C exposed directly to the bit and influenced the bit performance along the way. The performance analysis has been carried out through the history data from several wells that are using a double row (hybrid) PDC bit. The results shows that a magnitude of high temperature wells does not really affected the performance of PDC bits since there are no bearing needs to have a seal structure. However, the result also represents that a bit performance are also governed by the degree of fracture intensity which is formed naturally in the rock formation. Facing a similar range of rocks strength based on the rock type and the value of unconfined compressive strength (UCS) sometimes doesn't work properly in selecting the bits. By having a clear description of the fracture intensity, the bit optimization could be further developed and improved the drilling performance itself.

Keywords: Fracture intensity, drilling bit performance, Hululais Geothermal Field

INTRODUCTION

The Hululais geothermal field, owned by P.T. Pertamina Geothermal Energy (PGE), plan to develop 110 MW for two power generation units using 12 (twelve) production wells and 3 (three) injection wells (Kamah et al, 2015). Based on the analysis of drilling operation in Hululais field between 2011 – 2018, the type of rock formation (Nusantara et al, 2017) at prospect zone or the outer zone that has been penetrated are governed the performance of the drilling bits. Since the first drilling well until 2017, the roller cone bit especially Tungsten Carbide Insert (TCI) type are fully utilized in all section of the drilling wells. However, even though this type of bit is very durable in drilling the hard formation, this type of bit has a limitation because of the bearing inside the cone has a maximum number of revolution the bit could achieve before it fails. By relying on the reliability chart, most of the drilling operation put a certain safety number of the maximum revolution number (e.g 80%-90%) to minimize the risk of having cone parted inside hole (Gunawan et al, 2018).

The problem identification was started when the actual number of bits required to drill section 12.25-in and 9.875-in rarely meet the target on the drilling program. Insert bit with IADC 537 are constantly used to drill in 12.25-in and 9.875-in section in Hululais field. This 12.25-in bits can achieved 200-400 m footage averagely before pulled out due to penetration problem or bearing limitation. The ROP are ranging between 11 – 13 min/m. While in 9.875-in bits, the average footage are 150-300 m with 13-15 min/m penetration rate. To drill a typical interval length of each section between 1000 – 1200 m, it needs 3-5 bits or even more depends on the type of formation. Figure 1 and 2 shows a performance comparison of 12.25-in and 9.875-in TCI bits in Hululais field.

Within the boundary prospect area, most of the rock type formation are consist of andesite rocks. Moreover, in some production clusters, granite or granodiorite type of rocks suspected as the heat source or the basement rocks for geothermal system in this area. This type of rocks are commonly known as hard and abrasive formation which directly impact in consuming more number of bits than the any other type of formation (Noviasta et al, 2017). The low footage results in more trips, thus increase the daily drilling cost. Not only the loss causing by the low performance of the TCI effect the drilling cost, but the hard rock formation also causing the poor trajectory control. It raise the degree of torque and drag along the way to the bottom and push the drill string into the limits.

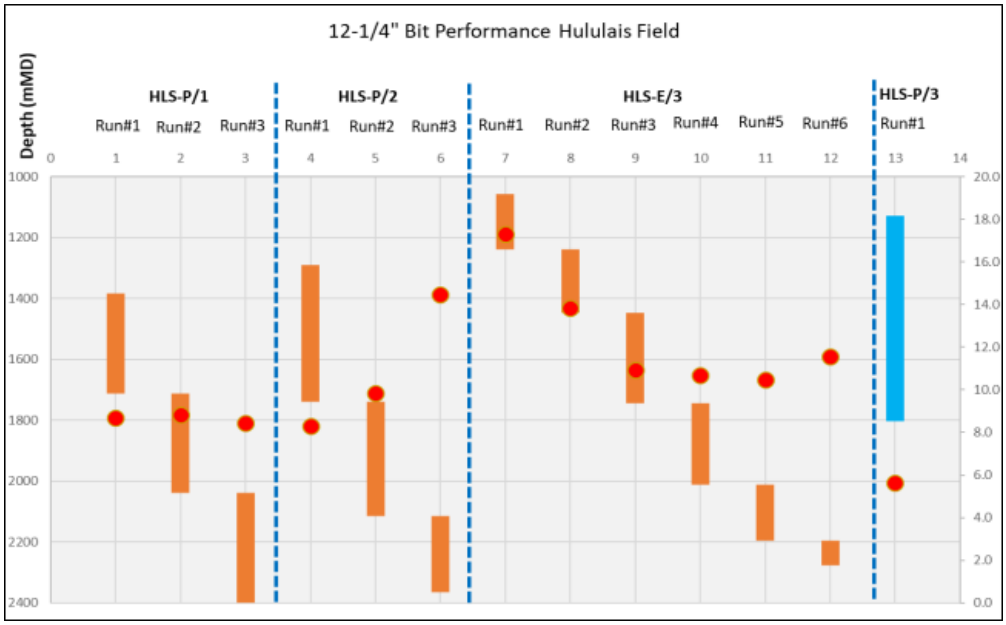


Figure 1: 12.25" Bit Performance Hululais Field

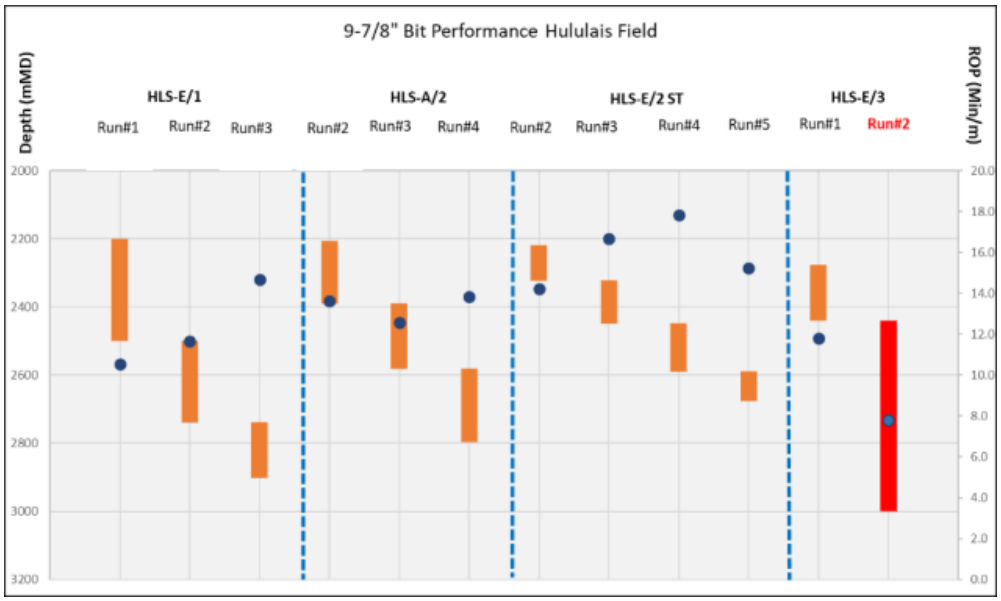


Figure 2: 9.875" Bit Performance Hululais Field

The entire identification problems above proved that the bits selection and improvement are urgently needs. Since 2017, the new type of bit that has no similar weakness are utilized. By the helps of drill bit engineering and manufacturer, PGE started to use a hybrid PDC drill bit technology. As the demand in drilling in hard and abrasive rocks environment increased over the past decade, most of the drill bit manufacturers are developing new technologies and strategies. Based on the need to maximize drilling efficiency, it is critical for the operators to reduce drilling time and save cost (Andika et al, 2018). With the dual cutting structure, and significant improvement of wear and impact resistance from the right selection of PDC cutters, implementing a hybrid drill bit technology could increase the bit durability and penetration rate. Therefore, eliminating the tripping time and having a good trajectory control.

Prior to the run of the hybrid bits, there were several phase included such as rock strength analysis, offset dull grading analysis, FEA modelling and simulation to design the bit and generated roadmap drilling parameter. The rocks strength analysis are based on the sonic log data, calculated into a certain numbers of unconfined compressive strength (UCS) in kpsi. Usually, the close range of the UCS value with the assumption of similar rock formation results in the same bit design. However, in Hululais field, some cases shows that it is not always a proper bit design to be implemented.

This paper will emphasize on the performance comparison between two bits in 9.875-in section that has been run in different clusters but penetrating the same type of rock formations (e.g. granodiorite) with the similar range of rock compressive strength. The main difference between these wells are the fracture intensity that naturally developed in the reservoir rocks formation. The basic idea of this paper is to persuade the bit engineer and designer to start consider this matter (degree of fracture intensity or heterogeneous of rocks formations) within their bits models and simulation, thus giving the operators company the most fit and deliverable bit design.

BITS APPLICATION

The first hybrid drill bits has been implemented in well HE-3, using 9.875-in hole section as the trial run. According to previous two wells at the same clusters, 3-5 TCI bits required to drill around 800 m. most of the bits are pulled out the hole with under gauged condition due to formation abrasiveness. Rock strength analysis was performed using the data from the offset wells. It resulted in value ranging from 18-27 kpsi (spike up to 30 kpsi) with lithology type of andesite breccia and diorite intrusion. The abrasion high to very high (Figure 3).

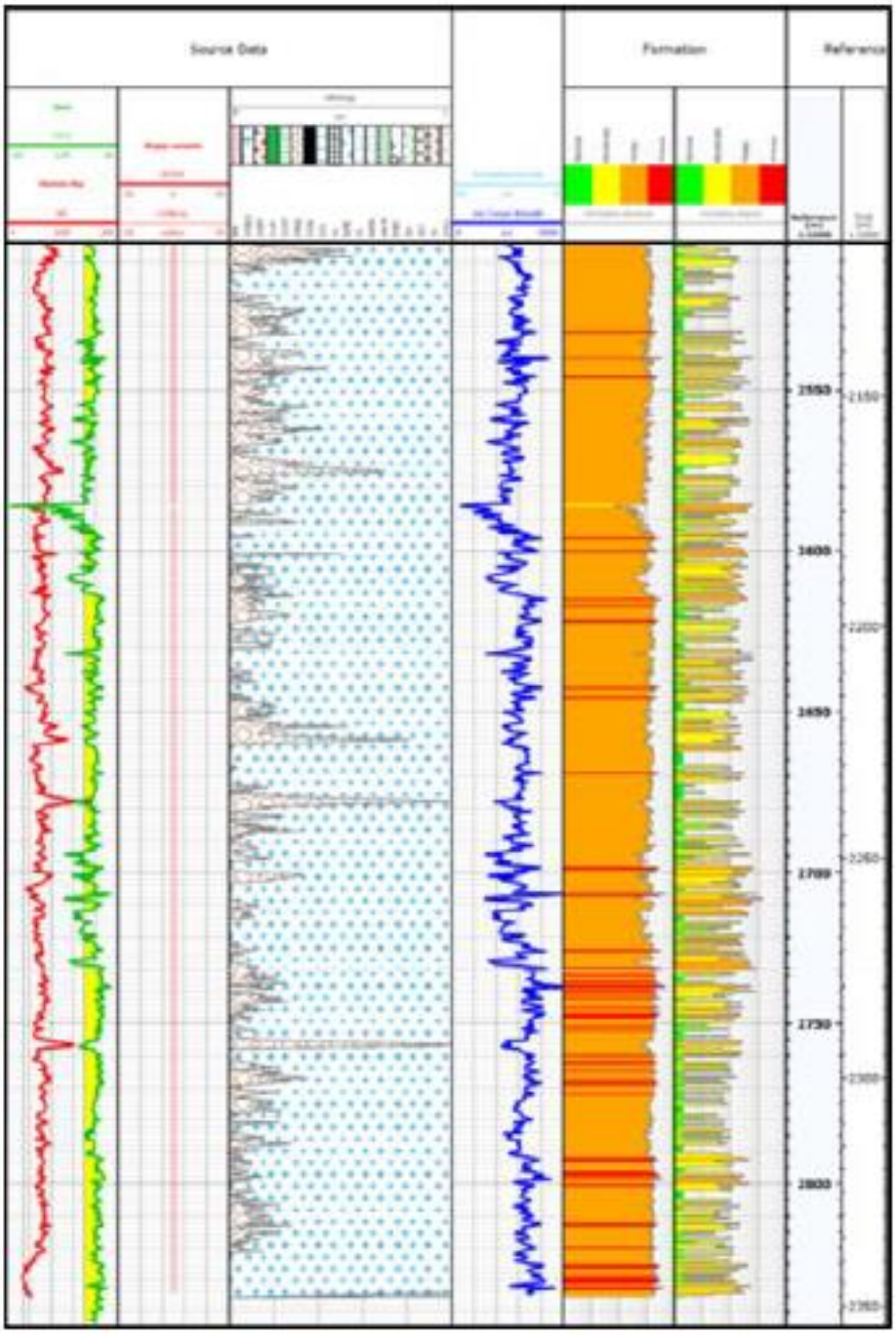


Figure 3: Rock strength analysis in HE-2 well resulted in 18-27 kpsi.

The first trail run of this new bit is reasonably meet the target required, since it drills through 700 m interval length section. However, it was pulled out not because of the bit performance, but because it has reached the Total Depth (TD). The bit was pulled out of the hole with good dull grading (2-1-WT-A-X-I-CT-TD) means that this bit still eligible to be re-run for the next well. Compared to the offset wells, hybrid bit also produced higher ROP with similar parameters applied. By using around 18.6 klbs of WOB and 200 RPM, the ROP of this bit increased around 60% compared to average TCI ROP. Based on MSE and CPF analysis, lower mechanical specific energy needed to drill with higher penetration rate with lowest CPF value shows higher efficiency (Figure 4). Good trajectory control was reported according to DLS value and distance to directional plan.

Meanwhile, after the success of the first trial run, the same type of the hybrid bit were run in well HH-2. The rock strength analysis using the offset wells data (well HH-1) projected the similar range number of UCS with the data from Cluster E. It is resulted in 18-27 kpsi sometimes up to 30 kpsi, with lithology of granodiorite all the way to bottom section (Figure 5). The key target was to drill 800 m interval section until Total Depth (TD). Two new bits has been prepared to anticipate whether it meets the target or failed. The first bit was drilled through 125 m and pulled out due to drilling tools problem. The average ROP is 18 min/m, with the average WOB of 25 klbs, 200 TRPM and 825 gpm flowrate. The bit was pulled out with dull grade 2-1-BT-N-X-I-WT-DTF. Due to unpromising ROP, the next bit was utilizing several TCI bits until using the hybrid bits again at the 5th run. The performance of the second hybrid bit was similar and not deliver the performance required. Even though the ROP increase into 12 min/m, but after drill through 168 m, the ROP was significantly decrease. Then, it was decided to pull out the bit with dull grade at surface 4-2-WT-C-X-I-RO-PP. A various drilling parameters were applied to increase the performance of the bits, although it still not really lifted the bit performance.

These two findings between well HE-3 and well HH-1 shows that the extensive pre-job planning doesn't always work properly even comes with the similar prognosis data. Some variables are need to be reconsider. At first glance, the difference between these two wells was found according to the borehole imaging data analysis. The log data shows that the fracture intensity are subsequently different between these two wells. At the first well (HE-3), the fractures are fully developed along the interval section, while in the second well (HH-1), the lithology distribution is quite fresh with no intense fracture mechanism spotted.

FRACTURE INTENSITY

The possible factor that is affecting the performance of the PDC bit in the Hululais field is fracture intensity. This is evidenced by two drilling data at well HE-3 and HH-1 on 9.875-in section, with the same lithology formation, granodiorite, but comes up with different fracture intensity. PDC bit usage is more effective on well which the fractures are more developed. This number are derived from the logged interval, resampled for every 50 m. The numbers on the X-axis shows a sum of fractures includes Continous Conductive Fractures (CCF), Discontinues (DCF), Low Angle (LACF), Resistive Fracture (RF) and Possible Fault (PF).

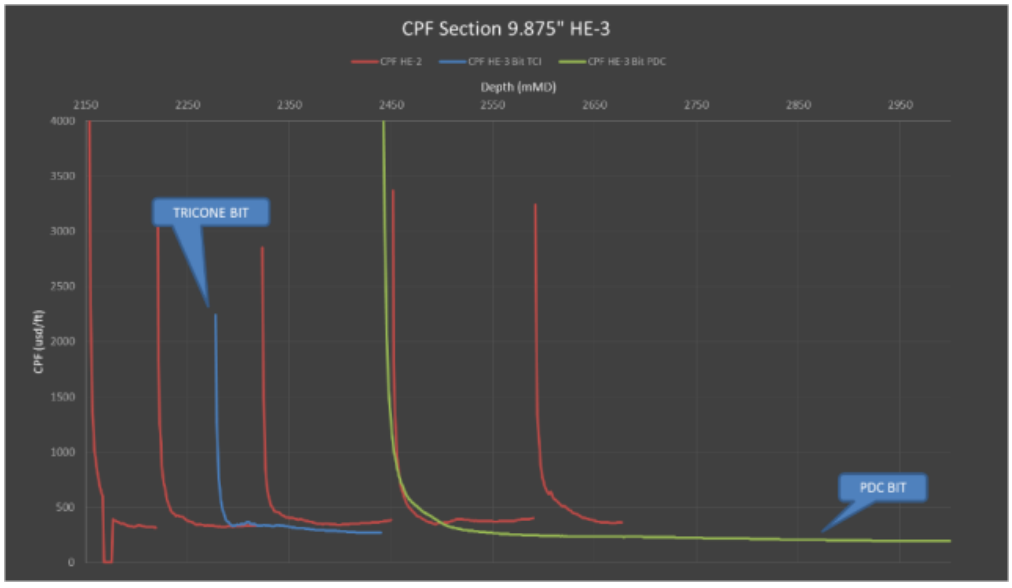


Figure 4: CPF analysis of bit size 9.875-in Cluster E Hululais

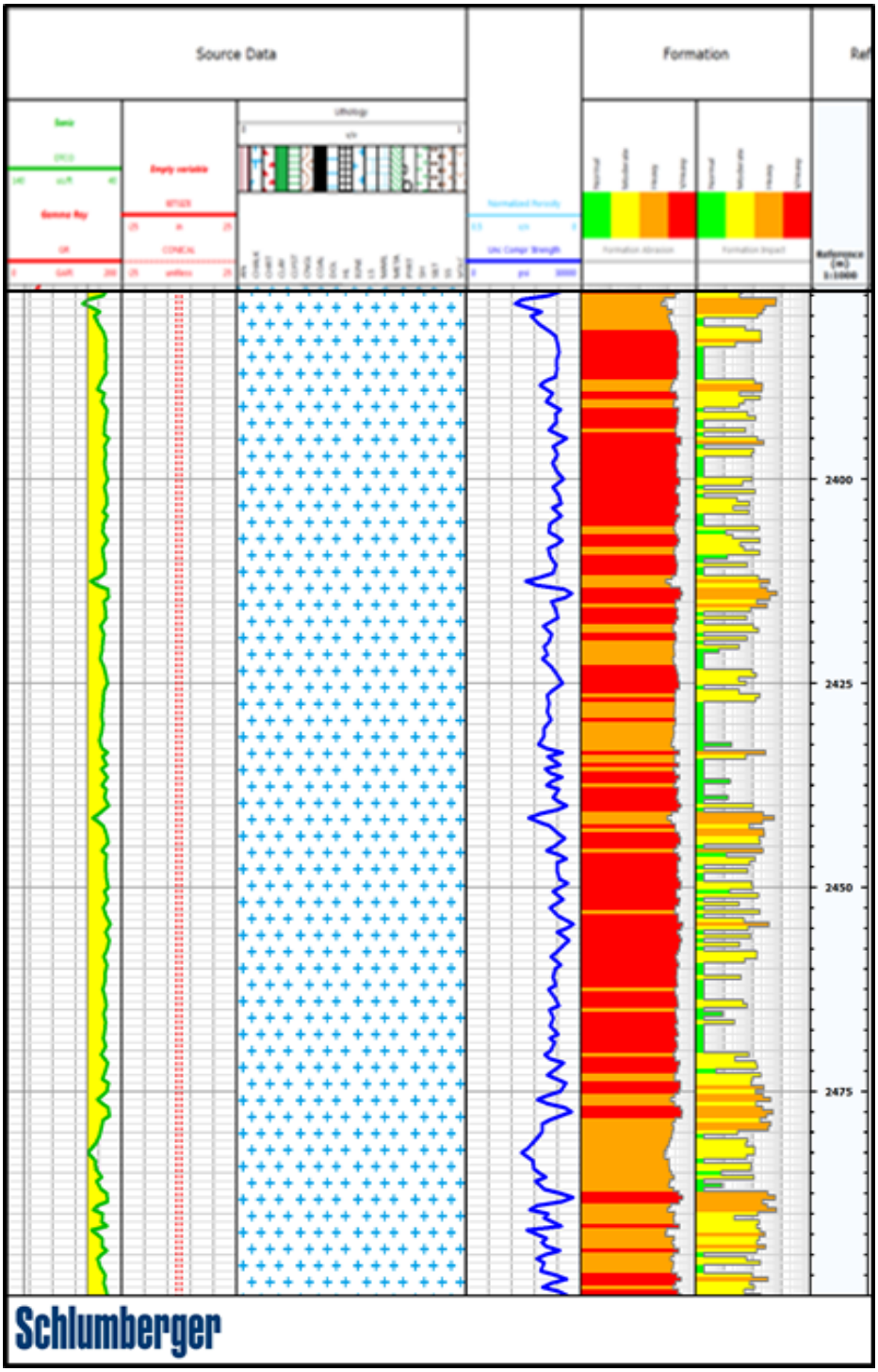


Figure 5: Rock strength analysis in HH-1 well resulted in 20-28 kpsi.

Figure 6 shows the fracture intensity at the well HE-3 that obtained from the borehole image logging. It can be seen that the development of the fracture in the 9.875”-in section at a depth of 2250 - 2850 mMD is quite intensive, especially at interval 2650 – 2750 mMD where the continuous fracture are most developed as it also shown form the appearance of of borehole Image at Figure 7 (in mTVD). Most of the fractures at that interval creates some major feeds to the wellbore as it spotted by the images.

Figure 8 shows the intensity of the fracture in the well HH-1 is not really developed. The Discontinous Fracture are spotted at the early section, but the fracture intensity decreases all the way until 3150 mMD where the formation becomes more massive (Figure 9). It is in line with the increasing of UCS number at the interval where the appearance of the borehole images shows no fracture developed. Fracture is dominated by RF and joints.

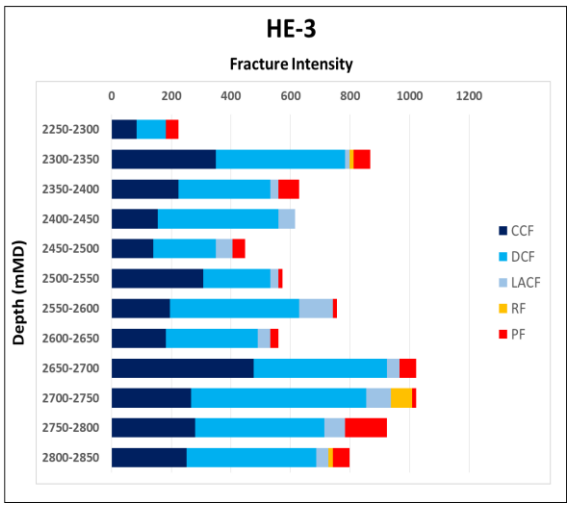


Figure 6: Fracture intensity in Well HE-3 from borehole image analysis.

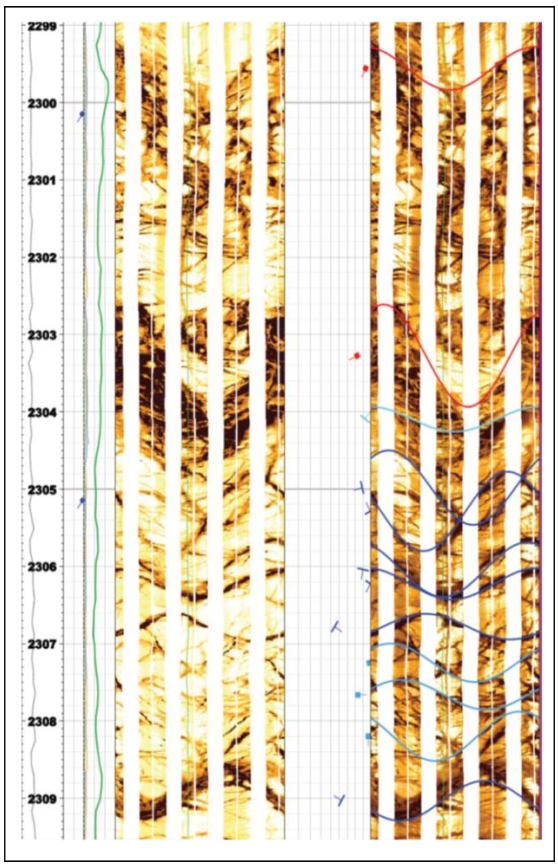


Figure 7: Appearance of fracture on borehole image at well HE-3.

CONCLUSIONS

1. Although the hybrid drill bit with dual cutting mechanism is suitable with hard and abrasive formation in Hululais field, there are two cases where the performance of the bit are also driven by the fracture intensity aspects.

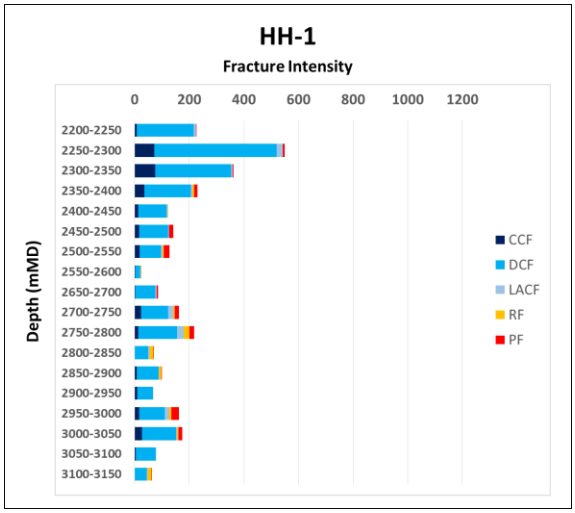


Figure 8: Fracture intensity in Well HH-1 from borehole image analysis.

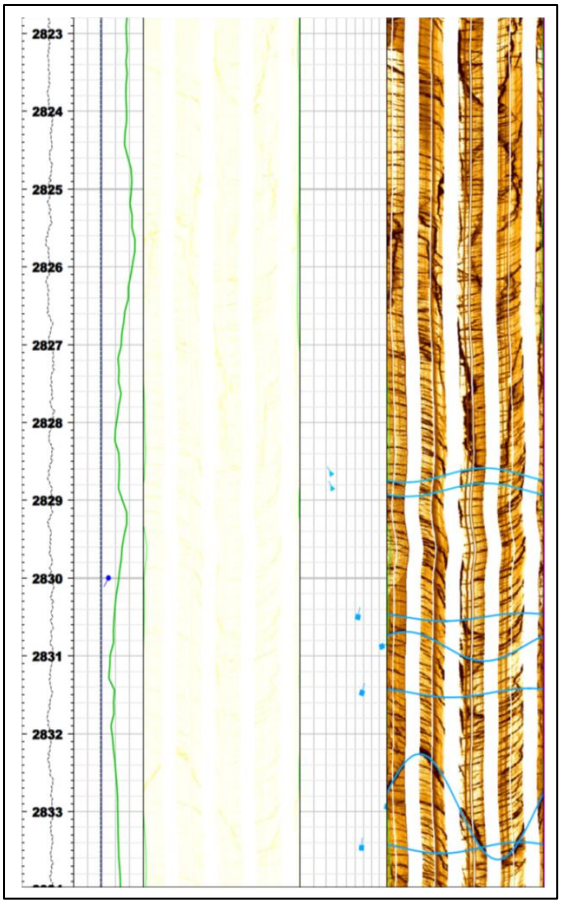


Figure 9: Appearance of fracture on borehole image at well HH-1.

2. From the comparison of two wells in Hululais field, where HE-3 has more fracture intensity than HH-1 and according to drilling operation data, it was found that the performance of hybrid PDC bit is more effective on HE-3 it can be concluded that the fracture intensity affects the performance of PDC bit.

3. It is important for the process of bit engineering design to take the degree of fracture intensity or into account, hence it will lead to the proper bit design that is compatible with the specific type of formation.

REFERENCES

Andika, F.A., Sutan, M.A., and Krisnanto, W. (2018), "Hybrid Drill Bit Improves Drilling Efficiency in Geothermal Application in Lumut Balai Field, Indonesia": 6th Indonesia International Geothermal Convention and Exhibition, Jakarta, Indonesia.

Gunawan, F., Krisnanto, W., Mardiana, M. R. Y., Noviasta, B., and Febriarto, H.B. (2018), "Conical Diamond Element PDC Bit as a Breakthrough to Drill Hard Geothermal Formation in Indonesia": *Paper Society of Petroleum Engineers (SPE)* no. SPE-191100-MS, IADC/SPE Asia Pacific Drilling Technology Conference, Bangkok, Thailand.

Kamah M. Y., Palmelay, A. C., Rahardjo, I. B., Thamrin, M. H., Hartanto, D. B., Silaban, M. S., and Sasradipoera, S. D. (2015), "Successful Exploration Campaign and to be Developed in Hululais Geothermal Field, Bengkulu Indonesia". *Proceedings World Geothermal Congress 2015.*

Nusantara, V. D. M., Prasetyo, I. M., Thamrin, M. H., and Siahaan, E. (2017), "3D Geological Modelling: An Advanced Method to Build Geological Baseline Model in Hululais Geothermal Prospect, Bengkulu, Indonesia". *New Zealand Geothermal Workshop Programme*, New Zealand.

Noviasta, B., Napitupulu, G., Scagliarini, S., Centeno, M., Ardianto, D., Mardiana, M. R. Y., Kurnia, A. Z., and Bao, J. F. (2017), "Drilling Optimization in Hard and Abrasive Geothermal Volcanic Rock Using Innovative Conical Diamond Element Bit". *New Zealand Geothermal Workshop Programme*, New Zealand.

PRODUCTION IMPROVEMENT THROUGH SCALE REMOVAL BY JETWASH KAMOJANG GEOTHERMAL FIELD

Sabda Indrakusuma Nugroho, Sendy Hendriana,
Fernando Pasaribu, and Marihot SP. Silaban

Pertamina Geothermal Energy
Jakarta Pusat 10340

ABSTRACT

Kamojang Geothermal Field is a vapor-dominated system with a total installed capacity of 235 MW, Kamojang currently has five power plants (i.e., Units I, II, III, IV, V). The unit I generate 55 MW, Unit II and III generate 55 MW respectively, Unit III generate 60 MW and unit V generate 35 MW. During the generation for more than 30 years, Kamojang wells have experienced decline in production. It directly affects steam supply to the power plant. The most important program to resolve steam availability is to drilling makeup well. Limited access and unsuccessful drilling makeup well as expected in the last 10 years becomes a problem in order to maintain longterm production. Generally, the decline of production in Kamojang field is affected either by hole problem or reservoir damage. There are seven well that were indicated having hole problem due to scaling such as KMJ-A, KMJ-B, KMJ-C, KMJ-D, KMJ-E, KMJ-F, KMJ-G, KMJ-H, and KMJ-I. In this case, Hole cleaning aims to dissolve scaling that cause decline of production. Jetwash using 4, 90 degree is used for hole cleaning and it is expected to clean the scale in the liner and production casing. As result total of seven wells experienced increase in production after hole cleaning. It gains approximately 8 MW. In addition, the advantages of this jetwash are reduction in cost and time as well compared.

Keywords: Jetwash, scale removal, production improvement, Kamojang Geothermal Field.

INTRODUCTION

The primary problem that occurs in Kamojang field is how to maintain steam supply to the power plant. It is indicated with production decline steadily.

Currently, decline production in Kamojang field reaches 7% /year. The strategy to solve production decline is through drill makeup well (Saptadji, 2001) but it has a problem due to limited land access, the success ratio of drilling makeup well within 10 years under the target and reservoir condition have been depleted. Another option to maintain steam supply by hole cleaning. Hole cleaning is a process to remove as much as possible the material produced by the bit when it is drilling the formation and taken to the surface (Ferreira, 2012).

Scaling has formed due to a dynamic production process in a wellbore, it resulted in decline production well and obstacle while logging tool survey (Grant and Bixley, 2011). The aim of hole cleaning is to clean the wellbore from scaling with the result that increases steam supply and clears the obstruction in the wellbore.

DATA AND METHOD

The technical evaluation within well selection process for hole cleaning program is performed by monitoring several reservoir and wellbore parameters:

Analysis of production variants well

Analysis variants is a systematic process to identify variants or deviations of well production data projected between natural declines and actual production data. The more variants or deviation that occurs, the more potential for possible hole problems in the wellbore or formation. The production deviation is closely related to the change in values of the two main production parameters i.e CWB (kg/s-bar) and PI' Prime (m3).

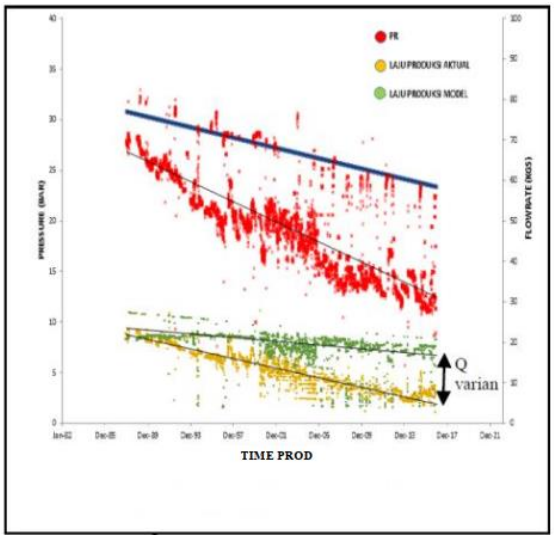


Figure 1: Variants Production KMJ A

CWB is a value that describes the condition of the wellbore, if CWB shrinks during production then it may indicate a change in the diameter of the wellbore, whether due to scaling or casing problem. PI value describes the changing condition in the feed zone. By monitoring trend of PI and CWB values, a

well can be identified as damaged in wellbore or feed zone through its production variants.

The empirical approach used to identify changes in the value of CWB (kg / s-bar) and PI Prime (m3) refers to the formula developed by Acuna (Acuna and Pasaribu, 2010):

$$\left(Psi - \frac{W\ vs}{PI}\right)^2 - WHP^2 = CWB\ W^2 \qquad (1)$$

Where :

Psi	: Shut-in Pressure (bar)
WHP	: Wellhead Pressure (bar)
W	: mass rate (kg/s)
Vs	: Viskositas kinetic steam (bar-s-m3)/kg
PI	: Produktivity index (m3)
CWB	: Wellbore storage(kg/s-bar)

From CWB and PI, to calculate natural production rate model used formulas which are the development of formulas (1) defined by Eq:

$$W = C_{WB}^2 \left(\left(\frac{P_{rg}^2}{A} - \frac{P_f^2}{C_{wb}^2}\right)^{0.5} - \frac{v_{rg}}{PI} P_{rg}\right) \qquad (2)$$

$$A = \frac{1}{\left(\frac{1}{C_{WB}}\right)^2 + \left(\frac{v_{rg}}{PI}\right)^2} \qquad (3)$$

This model is optimized to identification fluid flow in wellbore and feed zone so it's possible to explain characteristics well deliverability curve in terms of productivity index (m3) and wellbore storage (kg/s bar) (Acuna, 2008). This application method is used in every Kamojang Geothermal well, for example, the case is seen in the well of KMJ A. By looking at the trend of CWB parameters decline continuously, then there is an indication that the well has reduction inside diameter of the wellbore either because of scaling or mechanical problem.

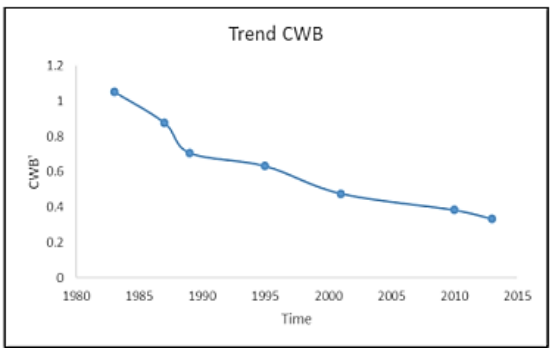


Figure 2: *Trend CWB KMJ A*

By applying a production variance method to wells in Kamojang field, 65% of production wells are indicated by damage to the wellbore or feed zone.

Well intergrity logging

The next evaluation is wellbore checking with well integrity logging:

Go devil

Go devil is a tool used to observe the diameter condition of the casing. Go devil size used in accordance with the size of production casing and well-perforated liner, this is intended to determine a depth of obstruction caused by scaling.

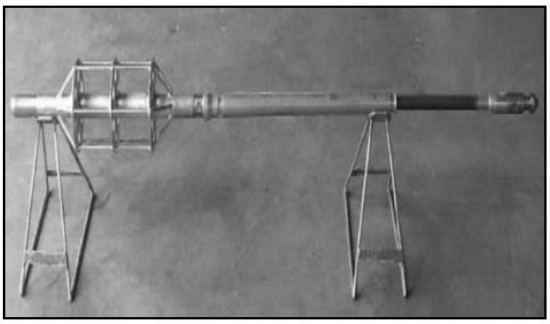


Figure 3: Go devil

Table 1: ID Casing & Go devil

No	Casing Size	Godevil Size
	inch	inch
1	13 3/8	10, 8.5, 5.5 & 3.5
2	10 3/4	8.5, 5.5 & 3.5
3	9 5/8	8.5, 5.5 & 3.5
4	7	5.5 & 3.5

Impression Block (IB)

Impression block is a tool used to check the profile of obstruction in the wellbore. The size of the impression block used is adjusted to the size of the casing to be measured.



Figure 4: Impression Block tool profile

Scale catcher

Scale catcher is a tool used to take out scale in a wellbore. Scale identification depth based on Go devil and Impression block.

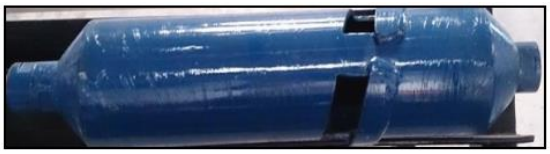


Figure 5: Scale Catcher

Several examples of scales are found in almost all wells indicated by constriction of the wellbore, here is an example of the scale obtained:



Figure 6a: Scale in Production Well

As a result of the presence of scaling causes decline of production significantly.

PTS Flowing

PTS flowing logging aims to measure the contribution of each feed zone in the well before hole cleaning or acidizing job. it can be used also to provide visualization of the casing diameter change due to scaling in wells by looking at the change of velocity response on spinner response.

Well Production Test

Well production test is done by a Modified Isochronal Test (MIT) with minimum operational WHP (Wellhead Pressure) setting at 4 WHP setting. MIT is proven effective save the operational time of production test. Data obtained is a baseline of productivity well before Hole Cleaning job.

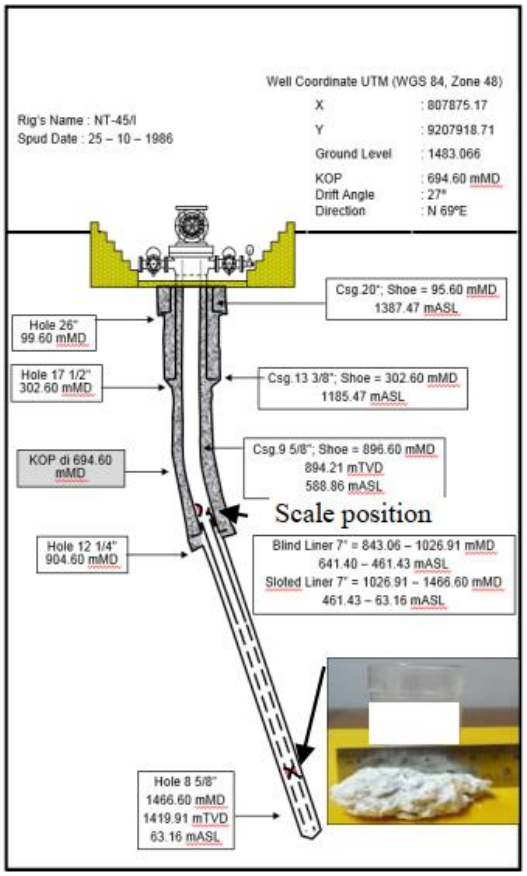


Figure 6b: Scale in Production Well

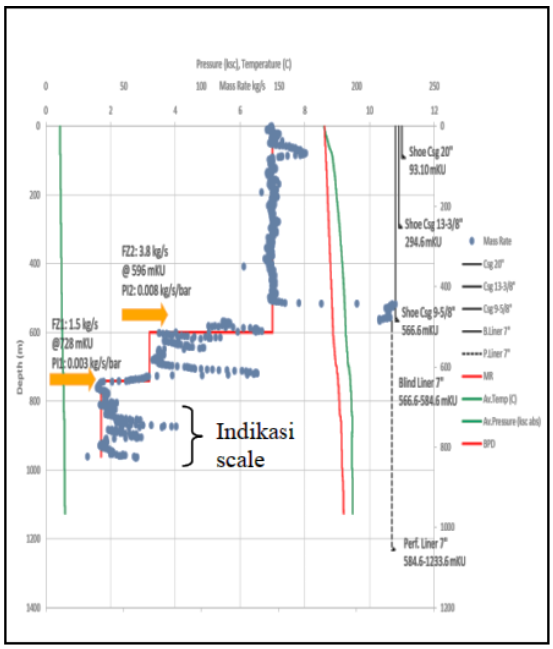


Figure 7: PTS flowing Profile

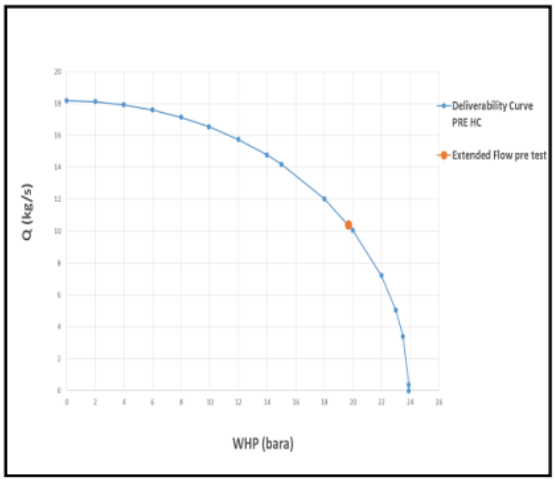


Figure 8: IPR MIT

Single Economics Calculation

Based on technical evaluation obtained well a candidate for Hole Cleaning which has potential to increase steam gain, further evaluation is done by single economics, with single economics can be known a feasible or not. An indicator of a program is feasible to do by looking at the parameter of DPI (Discounted Profitable Index) minimum 1.3.

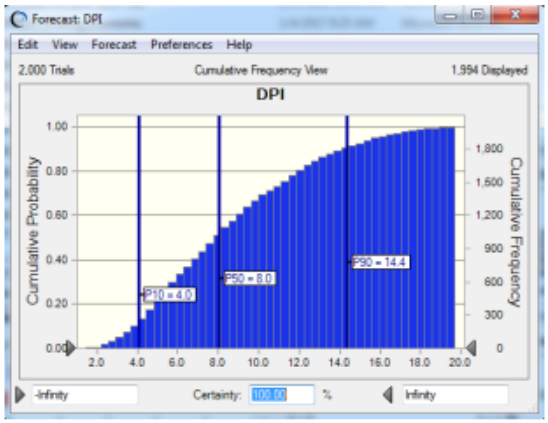


Figure 9: Single Economics Calculation

Candidate Well

Based on the technical and economic evaluation result, we get the candidate Hole Cleaning wells in 2017, as in Table 2.

Operating Hole Cleaning

Hole cleaning is done by mechanical reaming and jet washing, it aims to clean the wellbore of the scaling formed inside a casing and perforated liner, hole cleaning program is as follows:

1. Mechanical reaming using taper mill and flat mill with size 5.5 inch.
2. Jet Washing using 2 type of nozzle:
    1) Angle 45-degree nozzle is used forn cleaning scaling in the target of the obstacle depth in the wellbore.
    2) Angle 90-degree nozzle is used to clean scaling in perforated liner or feed zone depth target.

Table 2: List of Hole Cleaning Candidates

NO	WELL NAME	PRODUCTION VARIANT		DECLINE	GO DEVIL			SC	GAIN	ECONOMICS
		ΔQ TON/HR	MW MW	%/YEAR	8" (mKU)	5.5" (mKU)	3.5" (mKU)	SCALE	MW	DPI (≥)
1	A	40.5	5.06	18%	519	621	882	silica amorf	2.7	1.3
2	B	29.74	3.72	18%	852	852	1006		2	1.3
3	C	27.36	3.42	6%	350	350	951	silica amorf	1.8	1.3
4	D	24.48	3.06	4%	797	1200	1200		1.6	1.3
5	E	20.74	2.59	11%	843	852	-	-	1.36	1.3
6	F	13.03	1.63	11%	802	1316	-	silica amorf	0.9	1.3
7	G	9	1.125	11%	843	995	995		0.6	1.3
8	H	7.74	0.97	15%	712	1474	-		0.5	1.3
9	I	0	0	4%	661	667	1175	Silica amorf	0	0

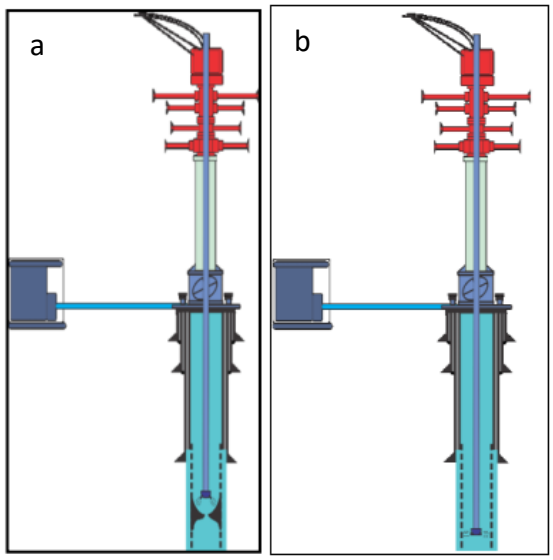


Figure 10. (a) Angle 45^o (b) Angle 90^o

Operation jet wash is done by Reciprocating procedure especially in feed zone depth as much as 3 times repetition.

RESULT AND DISCUSSION

Hole Cleaning job has been successfully done in 7 candidate wells i.e KMJ A, KMJ B, KMJ C, KMJ D, KMJ E, KMJ F & KMJ I. To evaluate post hole cleaning job performed Well integrity and production test to know well condition after the hole cleaning. An example result from KMJ F is:

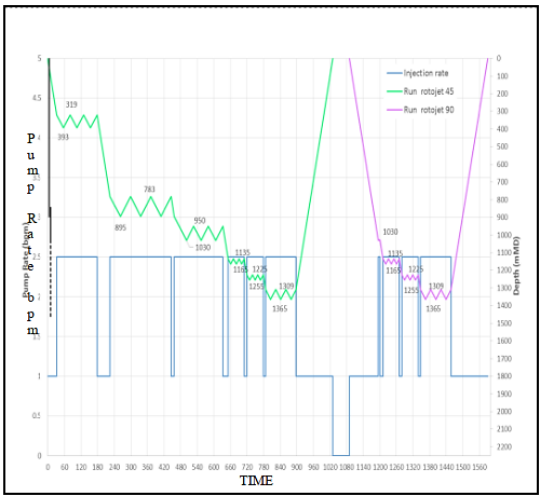


Figure 11: Jet Wash recipocate graph

Well integrity

Checking well integrity is done by run logging go-devil. Post Hole Cleaning logging results indicate that the scaling formed along the borehole has been successfully removed, with the following data:

Table 3: Data comparison Maximum Clear depth well pre & post Hole cleaning

Go devil	MCD (Pre HC)	MCD (Post HC)
8.5 "	802 m	843 m
5 1/2"	1263 m	1442 M
3 1/2 "	1316 m	1442 m
1 1/4" x Nose 2 "	1348 m	1442 m

PTS Flowing

PTS flowing is done to measure the change of Productivity Index (kg-s/bar) at the feed zone after Hole Cleaning. Comparison data of PTS flowing at KMJ F is shown in Table 4.

Comparison of PTS flowing data between pre-HC and post-HC showed an increase of the productivity index (kgs- / bar) at 1355 mD (Major Feedzone). Based on spinner reading is known productivity well increasingly. Data indicate that before Hole Cleaning well KMJ F can produce 5.5 kg/s with operational WHP 11 bar, but after done Hole Cleaning wells able to produce 9.1 kg/s with operational WHP 23.34 bar.

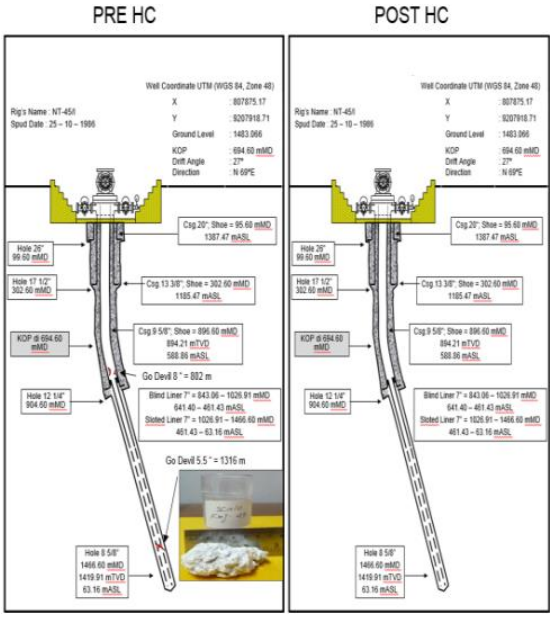


Figure 12: Comparison of hole condition profile the pre & post Hole cleaning well

Table 4: Comparison of PTS data flowing Pre & Post Hole Cleaning

Parameter	Pre HC	Post HC
TKS	11 bar	23.34 bar
Flow di surface	5.5 kg/s	9.1 kg/s
Impeller	10 P	10 P
PI (kg/s/bar)	Pre HC	Post HC
FZ @1355 mKU	0.013	0.030

Production Test

Post-HC production test at well KMJ F is done by Modified Isochronal Test (MIT) in same WHP setting (Figure 13).

Post-HC production test shows a significant increase in productivity of wells of 6.9 kg/-s at an operational WHP of 11 bar.

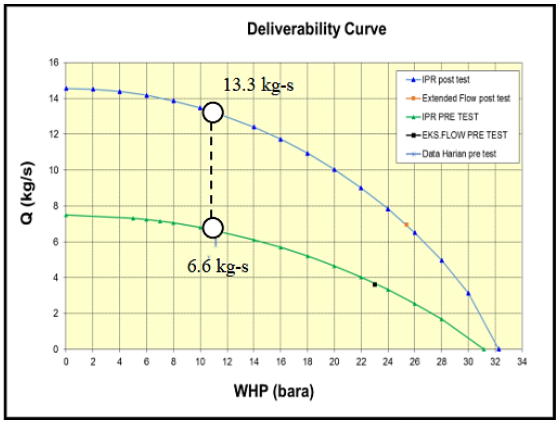


Figure 13: Comparison of MIT Pre & Post Hole Cleaning Test results

Overall, based on pre-HC and post-HC well test results, Hole Cleaning effectively improves hole conditions and well productivity, the following are Total Cumulative Steam Gain Production Post-HC for wells that have been done Hole Cleaning:

Table 5: Total Cumulative Steam Gain Production Post – HC

WELL	WHP	STEAM GAIN CALCULATION		
	OPERATION	Pre HC	Post HC	Gain
	bar	MWe	MWe	MWe
KMJ E	12	7	8	1
KMJ A	8.7	3.3	3.3	0
KMJ C	8.5	4.03	4.9	0.8
KMJ D	14	3.06	5.0	1.9
KMJ F	11	3	5.97	2.97
KMJ B	13	3.5	4.7	1.2
KMJ I	14	6.6	6.6	0
TOTAL				7.9

In total, Hole cleaning activities conducted in 7 Kamojang field wells were able to provide additional steam availability of 7.9 MWe and can effectively clean the scaling formed in the production casing and slotted liner. In addition of steam availability from Hole Cleaning positively impacts to makeup well plan.

CONCLUSIONS

1. Hole cleaning is effectively able to clean the scaling formed in the production casing and slotted liner holes.
2. Hole cleaning effectively increase the productivity of wells, which in total can provide additional vapor availability of 7.9 Mwe.
3. Hole Cleaning efficiently has a positive impact on reducing the costs and needs of makeup wells as part of a steam availability field availability strategy.

ACKNOWLEDGEMENTS

The author would like to thank the management of PT. Pertamina Geothermal Energy for the permission to publish this paper. The discussions with the reservoir team member are very much appreciated.

REFERENCES

Acuna, J. A. (2008), "A New Understanding of Deliverability of Dry Steam Wells", *Proceedings Geothermal Resources Council Conference, Reno, NV.*

Acuna, J. A., and Pasaribu F. (2010), "Improved Method for Decline Analysis of Dry Steam Wells", *Proceedings World Geothermal Congress 2010, Bali, Indonesia*.

Ferreira, E. J. S. (2012), "Hole Cleaning Performance Monitoring During The Drilling of Directional of Directional Wells". *Licenciado em Engenharia Geológica, Faculdade de Ciências e Technologia, Universidade Nova de Lisboa, Portugal*.

Grant, M. A., And Bixley, P. F. (2011), "Geothermal Reservoir Engineering Second Edition". *Academic Press, Elsevier, Auckland*.

Saptadji, N. M. (2001), "Teknik Panas Bumi". *Institut Teknologi Bandung: Bandung*.

WELL TRAJECTORY PLANNING ISSUES IN GEOTHERMAL DEVELOPMENT FIELD

Tommy Souvanir, Redha Bhawika Putra, Edyson Purba, and Ajie Soeryo Koesherbowo

Star Energy Geothemal
Sentral Senayan - II Office Tower, Jl. Asia Afrika No. 08
Email: tommy.souvanir@starenergy.co.id; redhaputra@starenergy.co.id;
edyson.purba@starenergy.id; ajie.koesherbowo@starenergy.id

ABSTRACT

Geothermal fields are mostly located in forestry area. This condition limits the geothermal operation to have a spacious drilling pad. In the development phase, in order to maintain the production rate, drilling new wells are required. However, additional wells in limited space of drilling pad have led to well trajectory planning issues. Other aspects on how well trajectory planning issues became more complicated are proper of drilling pad layout, cellar arrangement and cellar selection for new well, well direction and poor directional survey quality of existing well. In general, well trajectory issues can be grouped into 1) Collision; 2) Well interference during drilling; and 3) Production interference. At shallow depth (prior entering reservoir), collision issue may occur with adjacent well in the same pad. At deeper section of the reservoir, collision issue can happen with nearby well in the same pad or with other well from different drilling pad. Well interference during drilling usually occurred in deeper section (inside the reservoir) where the losses have been occurred. Drilling fluids can penetrate a nearby well due to the existence of any fractures or fault that acts as channeling and also because of the differential pressure between drilling wellbore and nearby wellbore. Production interference is occurred and able to be identified after a new well is produced. If it is happened, the reservoir system can be affected which may lead to a massive damage to production in long-term. This paper will share several cases, best practices, and lessons learned of well trajectory planning issues that occurred in Salak, Darajat and Wayang Windu geothermal fields. They are mature fields and already in development phase for quite a long time.

Keywords: Well drilling, trajectory planning, goethermal development field.

INTRODUCTION

In 2003 Star Energy was established as a private energy company whose operation bases are mainly in Indonesia. In geothermal sector, the company acquired 100% share in the operation of Star Energy Geothermal (Wayang Windu) Ltd Power Plant in Pangalengan, West Java in November 2004 in which two units of geothermal power plant supplies a total of 227 MW of electricity to PLN. From Wayang Windu field, Star Energy has 12,960 hectares of concession area (Slutz, 2011). In the future, Wayang Windu may expand its power generation capacity by striving to obtain steam for a potential development of Unit 3 (Star Energy, 2018). In early 2018, Star Energy Consorsium have acquired Salak and Darajat Geothermal Power Plants which generate 413 MW geothermal electricity and supply 275 MW of steam, includes geothermal assets in Philippines of Tiwi-Makban Geothermal Power Plants which currently is producing approximately 326 MW of steam (Diningrat et al, 2018). This is a major step for Star Energy Group to become one of the biggest geothermal operator in the world and to achieve its vision of becoming the geothermal operator of 1200 MW in 2028.

WELL TRAJECTORY PLANNING ISSUES

In development phase of geothermal fields, additional of a new makeup well leads to several trajectory planning issues which are 1) Wellbore collision; 2) Well interference during drilling; and 3) Production interference.

Wellbore Collision

Along with increasing new makeup well, risk of collision between new makeup well with adjacent wells start to occur. At shallow depth (prior entering reservoir), collision issue may occur with adjacent well in the same pad. At deeper section of the reservoir, collision issue can happen with nearby well in the same pad or with other well from different drilling pad.

Collision issues can be caused by the following:

a) **Inaccurate surface coordinate**, usually caused by these factors: inconsistence of Datum reference, Datum reference conversion error and Surface coordinate survey error.

b) **Poor quality survey of adjacent well,** due to losses condition –most of the time the directional tool has signal loss or distortion- that was led decision to drill with standard rotary BHA and blind drilling. In this condition, available options for directional survey are single shot survey or projection to TD from the last point survey.

c) **Adjacent well trajectory design tends to create shallow collision issue** such as well trajectory directed to underneath existing cellar and the trajectory nudging or kick off at shallow depth.

d) Improper pad layout, cellar arrangement and cellar selection for new well practice such as additional new cellar on top of adjacent well trajectory or too close with adjacent well trajectory and well trajectory crossing at shallow depth due to improper plan in early phase of pad development.

Several collision issues in planning phases in Star Energy Geothermal fields are:

a) Shallow collision due to adjacent well was directed to underneath of new well cellar. One of the example cases is AWI 10-4 collision issue. It is reported that it collided with adjacent wells (AWI 10-3 ST1 and AWI 10-1) at shallow depth. It is because AWI 10-3 was directed to underneath of AWI 10-4 cellar as shown in Figure 1. Figure 2 shows separation factor of AWI 10-4 with AWI 10-3 ST1 and AWI 10-1 are below 1.5 SF. Figure 3 explains the center to center separation of AWI 10-4 with AWI 10-3 ST1 and AWI 10-1 is less than 60 feet distance at 1,500 feet depth (Souvanir, 2012).

b) Well location in the map and the software shifted and deviated from actual location. Figure 4 represents the deviated cellar point after plotted in a compass. The yellow dot shows original cellar point while the green dot shows re-survey cellar point. Based on root cause analysis, the shift caused by inconsistence of Datum reference and surface coordinate error from previous surveys.

c) Huge ellipse uncertainty of adjacent well due to projection to TD and single shot survey. Figure 5 and 6 show huge ellipse uncertainty plot and collision report of MBA-7. This huge ellipse uncertainty was caused by MBD-3 poor quality survey with single shot starts from 1,100 feet depth.

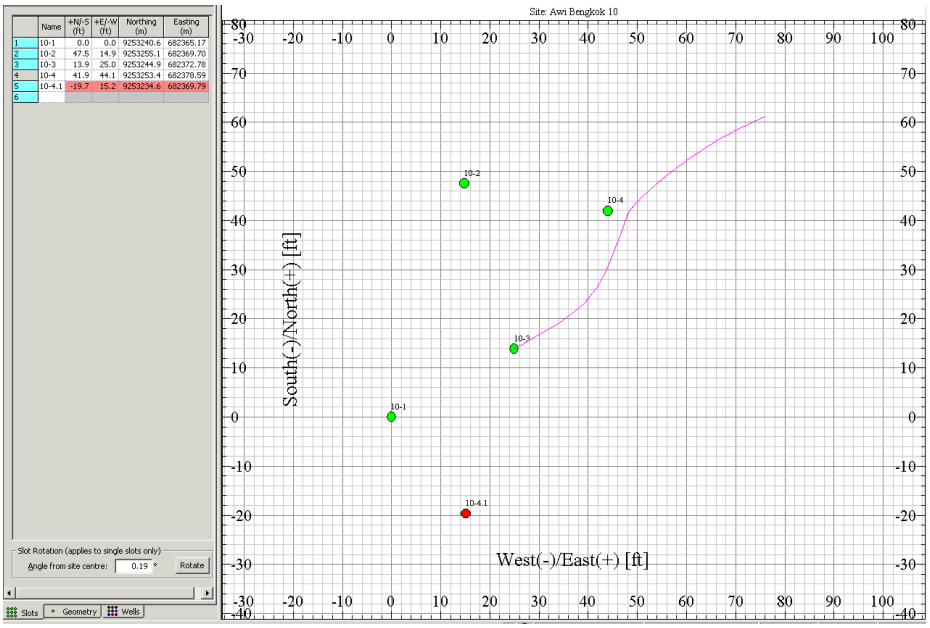


Figure 1: AWI 10-4 Spider Plot.

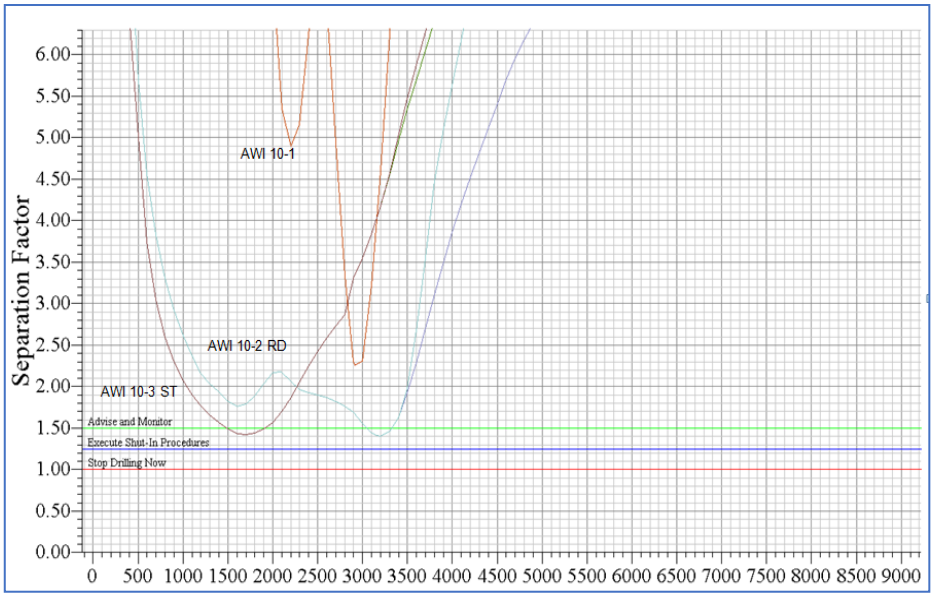


Figure 2: AWI 10-4 Separation Plot.

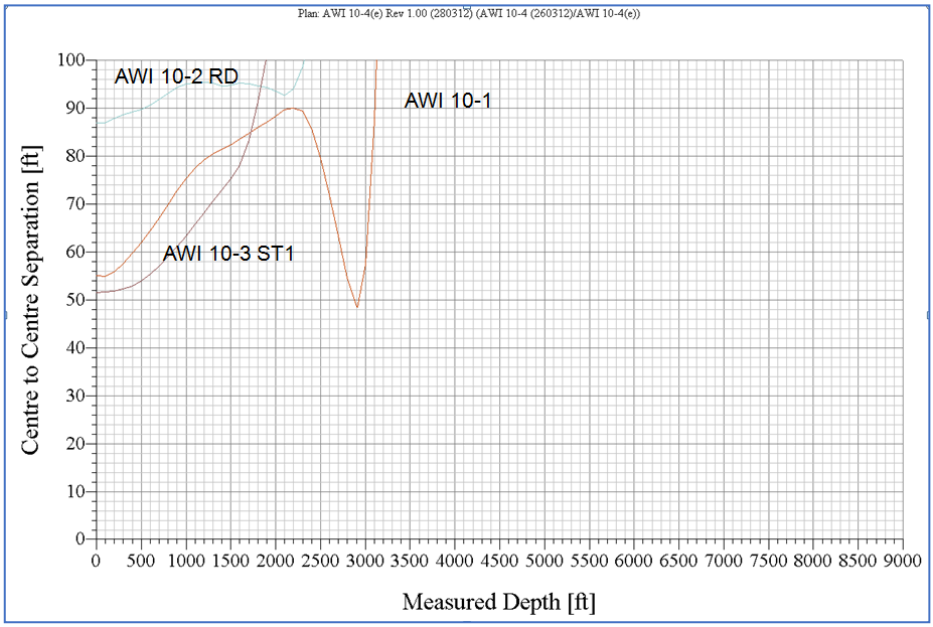


Figure 3: AWI 10-4 Center to center separation.

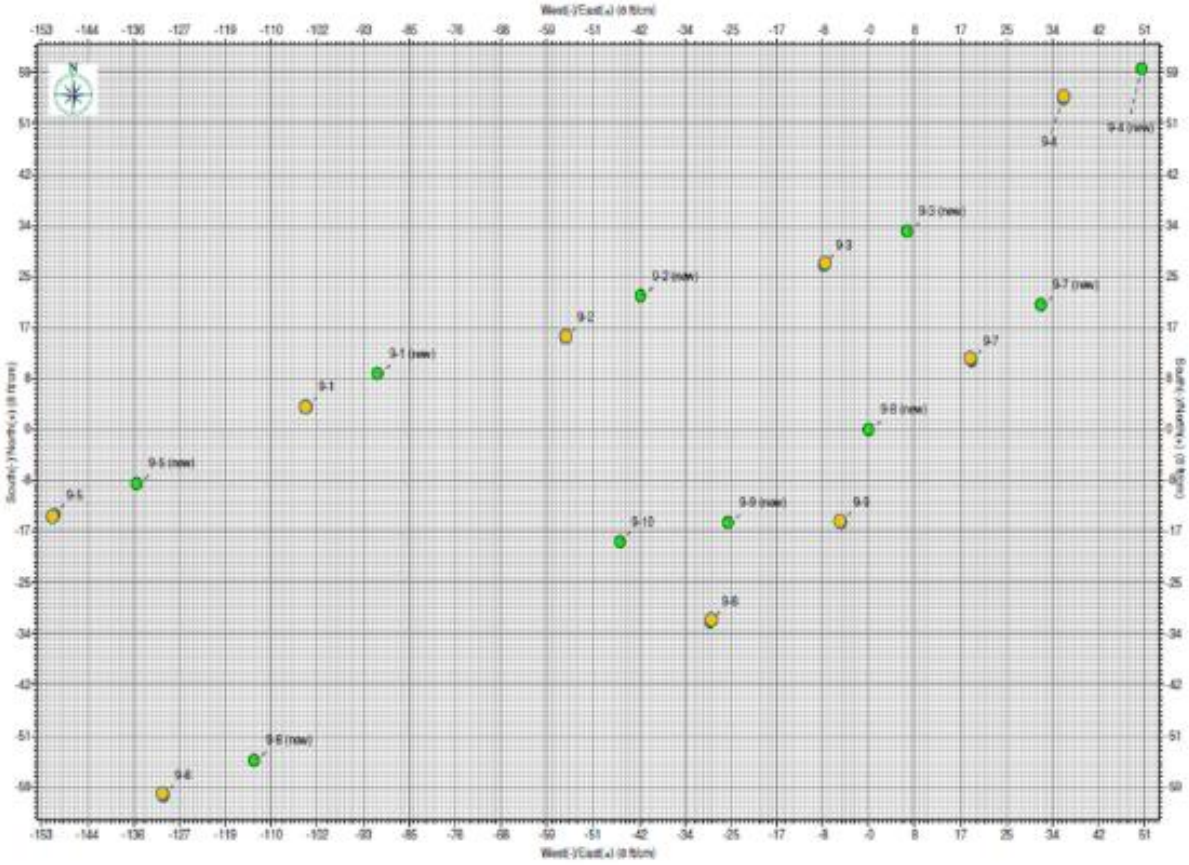


Figure 4: AWI 9 pad cellar plot.

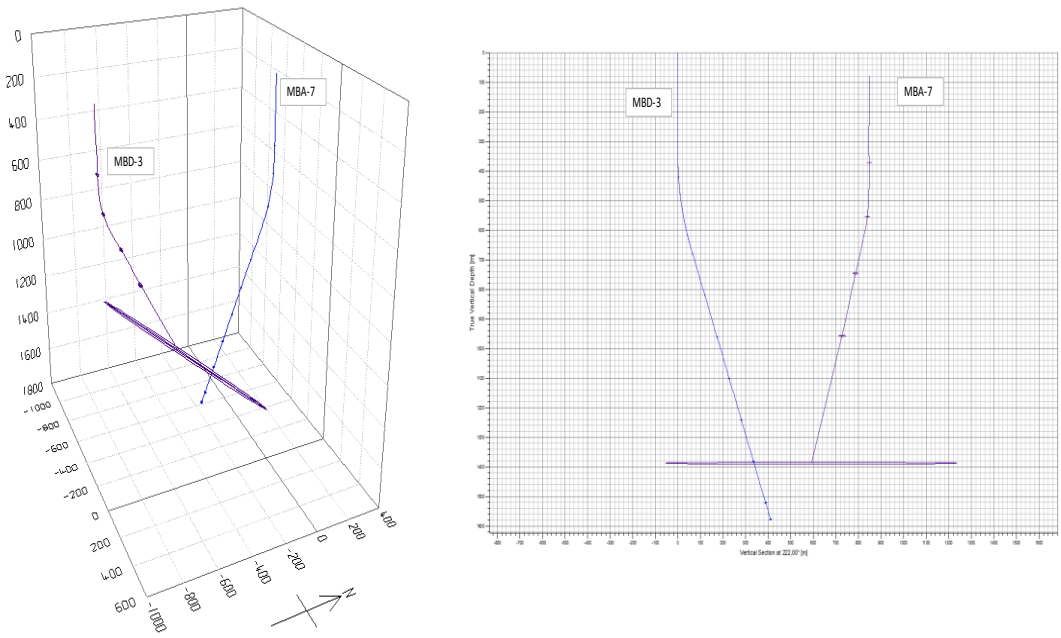


Figure 5: 3D and Plan view plot of MBA-7 Huge Ellipse Uncertainty.

Offset Design — MBD - MBD-03 - MBD-03 - MBD-03 Definitive Survey

Survey Program: 29-INC, 257-MWD, 517-CB-MAG-SS, 1126-INC

Offset Site Error: 0,00 m

Offset Well Error: 0,00 m

Reference Measured Depth (m)	Reference Vertical Depth (m)	Offset Measured Depth (m)	Offset Vertical Depth (m)	Semi Major Axis Reference (m)	Semi Major Axis Offset (m)	Highside Toolface (°)	Offset Wellbore Centre +N/-S (m)	Offset Wellbore Centre +E/-W (m)	Distance Between Centres (m)	Distance Between Ellipses (m)	Minimum Separation (m)	Separation Factor	Warning
1.097,28	1.061,56	1.259,26	1.128,38	4,27	350,38	-2,35	-491,09	-422,59	469,97	169,81	290,15	1,585	
1.127,76	1.090,02	1.279,99	1.145,56	4,46	386,71	-0,72	-480,20	-426,56	440,69	115,16	325,52	1,354	Advise and Monitor
1.158,24	1.118,47	1.300,71	1.162,74	4,66	423,03	1,02	-469,31	-430,52	421,71	59,50	362,21	1,164	Execute Shut-In Procedure
1.188,72	1.146,93	1.321,43	1.179,92	4,85	459,36	2,88	-458,42	-434,48	403,08	2,81	400,27	1,007	Execute Shut-In Procedure
1.219,20	1.175,38	1.342,16	1.197,10	5,05	495,68	4,87	-447,53	-438,45	384,84	-54,90	439,74	0,875	Stop Drilling Now
1.249,68	1.203,84	1.362,88	1.214,28	5,24	532,01	7,00	-436,64	-442,41	367,06	-113,57	480,63	0,764	Stop Drilling Now
1.280,16	1.232,30	1.383,60	1.231,46	5,44	568,33	9,27	-425,75	-446,37	349,81	-173,10	522,91	0,669	Stop Drilling Now
1.310,64	1.260,75	1.404,32	1.248,64	5,64	604,65	11,70	-414,86	-450,34	333,16	-233,27	566,44	0,588	Stop Drilling Now
1.341,12	1.289,21	1.425,05	1.265,82	5,83	640,98	14,28	-403,97	-454,30	317,22	-293,77	610,99	0,519	Stop Drilling Now
1.371,60	1.317,66	1.445,77	1.283,01	6,03	677,30	17,03	-393,08	-458,26	302,08	-354,09	656,17	0,460	Stop Drilling Now
1.402,08	1.346,12	1.466,49	1.300,19	6,23	713,63	19,94	-382,19	-462,23	287,89	-413,50	701,40	0,410	Stop Drilling Now
1.432,56	1.374,57	1.487,22	1.317,37	6,42	749,95	23,02	-371,31	-466,19	274,79	-471,02	745,81	0,368	Stop Drilling Now
1.463,04	1.403,03	1.507,94	1.334,55	6,62	786,28	26,26	-360,42	-470,15	262,94	-525,33	788,26	0,334	Stop Drilling Now, ES, SF
1.493,52	1.431,48	1.476,00	1.308,07	6,82	730,29	21,33	-377,20	-464,05	257,94	-461,39	719,33	0,359	Stop Drilling Now
1.524,00	1.459,94	1.476,00	1.308,07	7,02	730,29	21,33	-377,20	-464,05	254,50	-446,97	701,47	0,363	Stop Drilling Now
1.537,69	1.472,72	1.476,00	1.308,07	7,10	730,29	21,33	-377,20	-464,05	254,13	-435,95	690,08	0,368	Stop Drilling Now, CC

Figure 6: MBA-7 Collision Report

Wellbore Interference during Drilling

Geothermal well drill to permeable reservoir system which consist of fault and natural fracture. Reservoir fluid is steam for single phase system and brine (hot water) for dual phase system.

Less compressible reservoir fluid combined with permeable reservoir lead to low pressure reservoir system if compare to oil and gas reservoir system.

When drilling into reservoir section, the wellbore has a level of drilling fluid which resulting wellbore hydrostatic pressure higher than reservoir fracture pressure. This creates total loss condition.

In an adjacent well where the wellbore pressure equal or event lower than reservoir pressure, during drilling when total losses condition occurs, there is a risk of drilling fluid enter adjacent wellbore that stop the production or in worst condition, drilling mud will damage the formation that terminate the production.

Example case of this wellbore interference during drilling is Darajat-20 steam production declining. Figure 7 shows that originally Darajat 20 has a good production and suddenly drop when Darajat 30 is drilled (Hadi et al, 2008).

This phenomenon is identified caused by DRJ-30 drilling mud breakthrough because drilling mud observed at surface while performing flow test in April 2008.

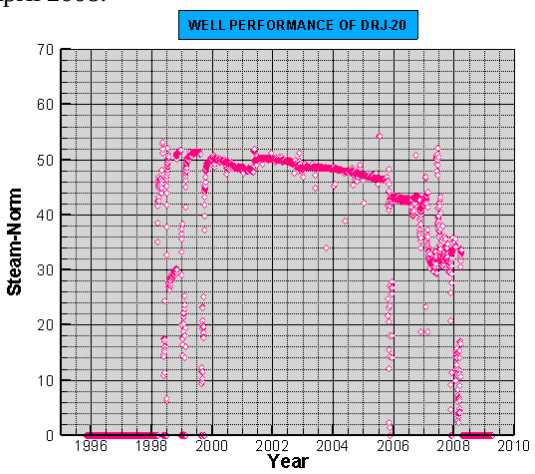


Figure 7: DRJ Steam Production Decline

Production Interference

In development phase where new makeup well keeps adding and targeting to the same reservoir in order to maintain steam production, it will lead to the risk of production interference between adjacent well that extract the same resource.

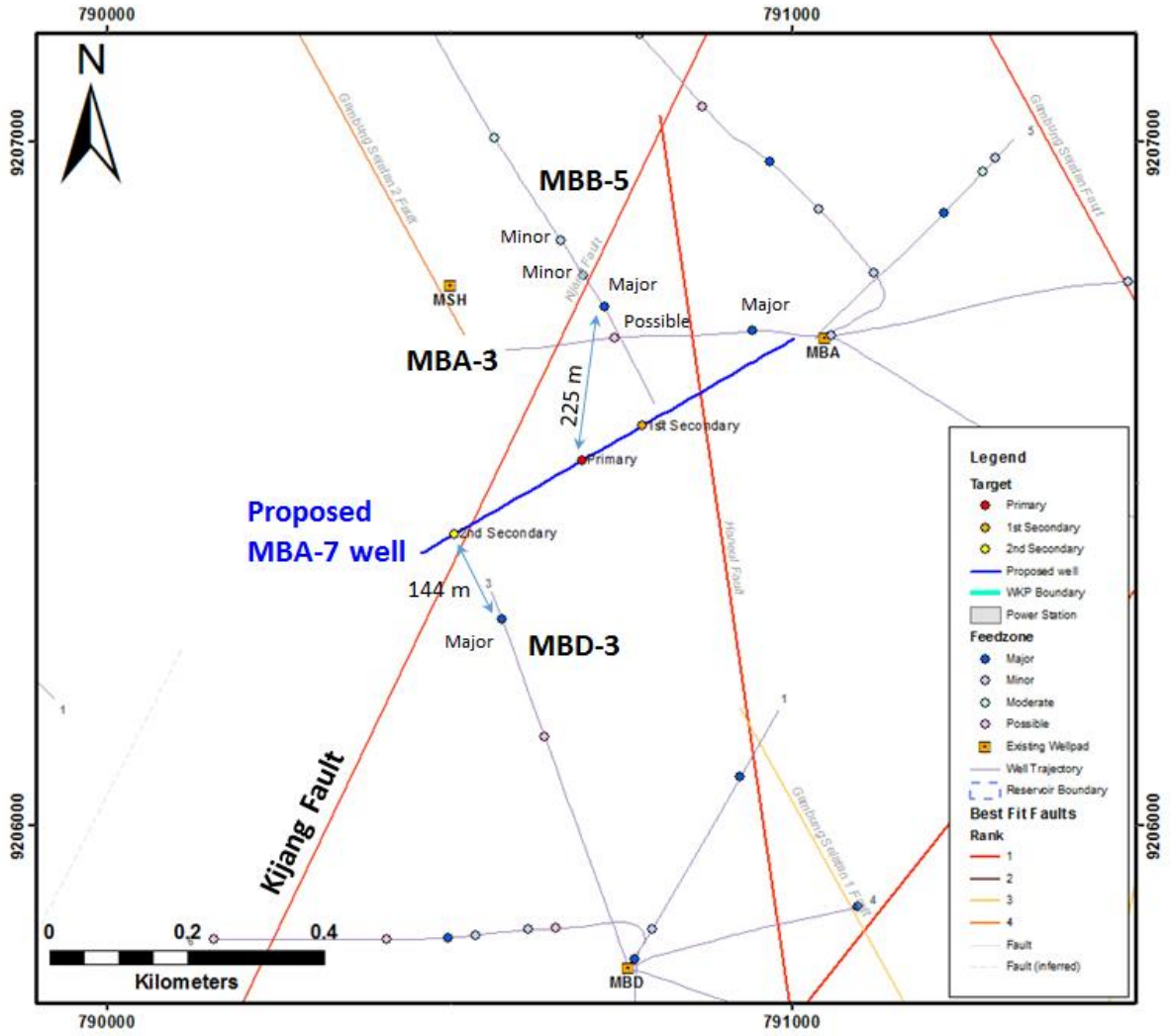


Figure 8: MBA-7 feed zone spacing with adjacent well.

This production interference cannot be identified during drilling process; it can only be identified after new well is produced where it affected to the reservoir system that can lead to massively damage for field production in long-term run.

Although the production interference is only able to confirm after the well is drilled and completion test is completed, however in well planning phase, the risk of production interference can be mitigated through ensuring adequate well spacing with adjacent well. Best practice in Star energy fields (Salak, Darajat dan Wayang Windu) to mitigate production interference through maintain feed zone spacing radius at minimum 300 meter (1000 ft).

Figure 8 shows MBA-7 feed zone spacing plot with nearby well feed zone in the reservoir section. MBA-7 deep feed zone target has spacing 144 meter with MBD-3 and MBA-7 mid feed zone target depth has spacing with MBB-5. In order to mitigate risk of interference with adjacent well, several MBA-7 well trajectory alternatives are assessed during planning phase such as 3D well, 2D well with depth kick off, and well target azimuth shifting to ensure MBA-7 has 300 meters feed zone spacing radius with MBD-3 and MBB-5.

CONCLUSION

In development phase of geothermal fields, additional of a new makeup well leads to several trajectory planning issues which are 1) Wellbore collision; 2) Well interference during drilling; and 3) Production interference.

In order to mitigate wellbore collision issue, the assessment must be conducted through spider plot to check surface coordinate survey quality, collision report to check the separation factor and center to center separation and drilling pad cellar plot to check surface coordinate shifted and deviated from actual location.

To assess the risk of wellbore interference during drilling and production interference, adequate well spacing with adjacent well must be asses through measure feed zone spacing radius with adjacent

REFERENCES

Diningrat, W., Sugiono, S. R. A., and Wicaksono, R. A. (2018) "MBA-7 well prognosis," Well Decision Team Phase 2/3 Decision Support Package, Well Decision Team Star Energy Internal Report.

Hadi, K, H., Choiri, M. and Pazziugan, D. (2008) "Memorandum production engineering work-over proposal for DRJ-20," Drilling and Completion Star Energy Internal Report.

Slutz, J. (2011), "Star Energy – Geothermal Development in Indonesia". USC Center for Geothermal Energy. Retrieved from https://cpb-us-e1.wpmucdn.com/sites.usc.edu/dist/c/116/files/2017/03/77357-1aaq752.pdf

Souvanir, T. (2012) "AWI 10-4 Collision Assessment Report," AWI 10-4 Phase 2/3 Decision Support Package, Drilling and Completion Star Energy Internal Report.

Star Energy. (2018), "Star Energy Geothermal (Wayang Windu) Green Bond Framework". *Star energy*, Indonesia. Retrieved from https://www.starenergy.co.id/StarEnergy/files/e0/e08b417c-99f3-4e37-95b2-75072f871d60.pdf.

WASTE HEAT RECOVERY USING THERMOELECTRIC GENERATOR FOR POWER GENERATION

Hendra Ardi Kurniawan, Hafid Suharyadi, and A. Djumarma Wirakusumah

Polytechnic of Energy and Mineral Akamigas
Jalan Gajah Mada No.38, Cepu, Central Java, Indonesia 58315
Email: kurardi@gmail.com

ABSTRACT

Efficiency is one of the essential aspects of the power generation. A way to improve energy efficiency is done by utilizing the heat waste. This paper presents a study of power generation using a thermoelectric generator. The Thermoelectric generator is a device to convert heat into electricity without moving components. Thermoelectric components have a high electrical conductivity and low thermal conductivity. Furthermore, it is acceptable to change the insulators materials with the thermoelectric generator, because the material principal of thermoelectric is same as the insulator materials which are formed by low conductivity materials. The heat loss caused by the temperature differences from inside and outside of the pipeline. By calculating the heat loss, the waste heat value can be known. As a result, this study will present a potential power generation based on the waste heat recovery in the pipeline.

Keywords: waste heat recovery, power generation, thermoelectric generator

INTRODUCTION

The increasing of energy demand forces industry players especially in the field of power generation to continue improving their efficiency. In general, only one-third of the total energy was utilized while the remaining is rejected as a waste heat (Remeli et al, 2015). One way to improve the efficiency is by utilizing the waste heat. Thermoelectric power generation offers a promising technology in the direct conversion of waste-heat energy, into electrical power (Ismail and Ahmed, 2009). A thermoelectric generator (TEG) can be used in order to absorb the waste heat. The TEG is a solid state device without any moving parts that is capable to convert the thermal energy into electrical energy directly and reversibly.

In the geothermal energy, the heat from earth is transferred through pipes into the steam turbine. The temperature difference between inside and outside of the pipes make the heat continually loss to the environment as where the temperature differences happen. Today's technologies use insulator made of calcium calcite to reduce the heat loss which is still proven effective. The low thermal conductivity of the insulator makes the heat flow through the medium becomes slowly and consequently reduces the heat loss. Changing the insulator with the TEGs is technically acceptable because the work principal of the insulator and TEG require the same materials. The work principal needs a substance with a low thermal conductivity to make the heat flows slowly. The smaller thermal conductivity creates more heat loss that will be reduced and increased the TEG performance (Zhang and Zhao, 2015).

The TEGs will change the function of the insulator as the heat loss reducer and also become the power generation sourced by waste heat. The heat loss from the inside of the pipe will flow through the pipes and continue to transfer to the TEGs and then release to the environment. The power generated can be used as a power for telemetry sensors or electronic devices in the remote area. Nowadays, TEG is to be found in the market easily.

THERMOELECTRIC GENERATOR (TEG) OVERVIEW

A thermoelectric generator module is made up by many elements of n- and p- type semiconducting materials which connected in series and parallel as electrical and thermally, respectively. TEG is a very effective device with no pollutants and power input requirements, small size, high reliability, and feasibility in a wide range of temperature makes the TEG as an environtmental friendly energy conversion technology (Zhang and Zhao, 2015). Although the efficiency of the thermoelectric generator is only about 5% (Orr et al, 2016) but may provide a useful electrical power in certain applications. The efficiency is limited by the Carnot efficiency where the higher temperature difference will create a higher efficiency.

$$ZT = \frac{S^2 \sigma T}{K} \quad \text{..... (1)}$$

The performance of TEG is defined by a dimensionless figure of merit (ZT) which depends on the thermoelectric material properties seebeck coefficient (S), electrical conductivity (σ), and thermal conductivity (K). Conceptually, to obtain a higher ZT, both seebeck coefficients and electrical conductivity should be larger, while thermal conductivity must be smaller (LeBlanc, 2014). The TEG is illustrated in Figure 1.

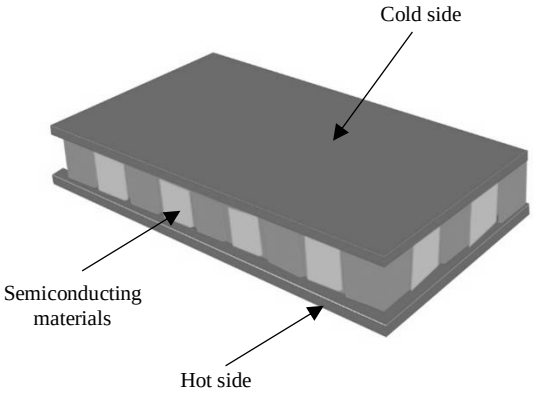


Figure 1: The schematic of TEG

The TEG has two sides that have different functions respectively; to absorb the heat and release the heat (furthermore, it is called as cold side). The TEG is made of semiconductor materials that surrounded by electrons. When the heat comes to the hot side, the electrons on the hot side will have more energy than the electron in the cold side. Therefore, the electrons migrate from the hot side to the cold side, and vice versa. The phenomenon where the temperature differences can generate a voltage is known as a thermoelectric effect.

THE HEAT RECOVERY SYSTEM MODEL

Description of the System Design

The concept of a power generation system to connect hot pipes and TEG has been developing before, and has been applied in some industrial sectors. In this paper, the development of TEG is expanded in the geothermal industry where the system consists of TEG sandwiched between the hot pipe and the heat sink. The one side of TEG will be placed in the hot pipe side then the heat will flow from inside of pipes into TEG, while the other side will be plugged with a heat sink to absorb fresh air (cool). Due to the heat transfer from the higher temperature into the lower temperature, the temperature difference between TEG will present a power generation.

The Figure 2 explains the heat comes from the geothermal fluid flows out to the environment through the pipe, TEG, and heat sink. Sometimes, the geothermal fluid consists of steam, brine, or both of them. In geothermal, the pipe is a metallic pipe that is commonly constructed from a carbon steel. The pipe has a very high thermal conductivity, therefore, they are easy to transfer heat from the inside of the pipe with passively. The TEG receives the heat from the pipe at the one side, and then it is defined as the hot side. The heat flows through n- and p- type semiconducting materials and cause migration of electron than a voltage will be generated. The heat continuously release to the environment. The heat sink has functioned as a heat releaser and cold catcher, it helps the TEG module to release heat and make the TEG cold side becomes cooler.

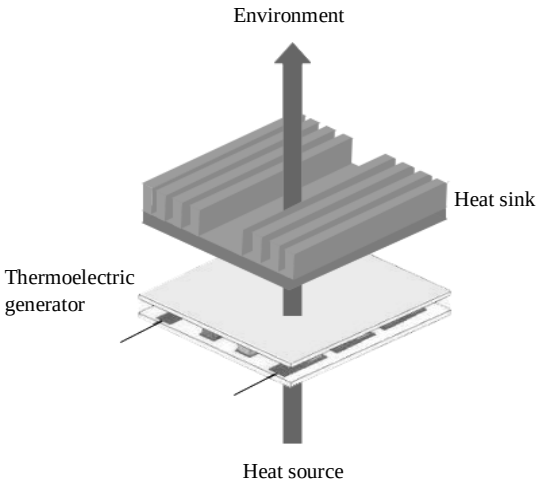


Figure 2: Waste heat recovery system

Figure 3 explains the TEG installed in the geothermal pipe. The insulator before changed with TEG, has a function to reduce heat loss to the environment. As mentioned before, the insulator and the TEG have the same principle work where both of them consist of the lower thermal conductivity, the higher efficiency will be. The most popular TEG formed by Bismuth-Telluride (LeBlanc, 2014), while the insulator is made by calcium silicate. The thermal conductivity is different for each material where insulator in this case calcium silicate has the lower thermal conductivity rather than Bismuth Telluride. It is technically present that to reduce 1 watt of heat loss using insulator materials will be more effective than using TEG materials.

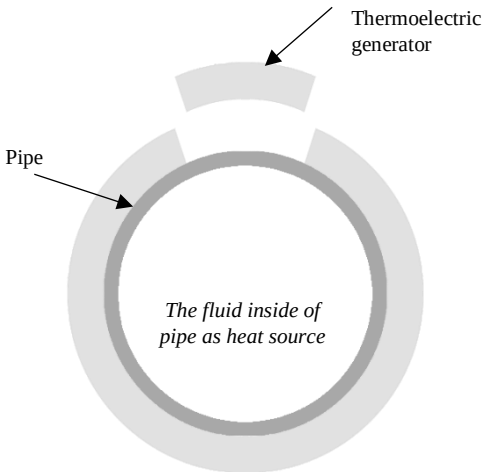


Figure 3: The design of installed TEG on pipe

Calculation of the System Design

The heat transfer from the geothermal fluid

The operation pressure at the geothermal industry has a big contribution to the fluid conditions. The temperature of the fluid follows the thermodynamic law and the rise of pressure will make an increase in the temperature. In this system design, the pressure and temperature are assumed constant and spread radially in the pipe.

The heat transfer in the pipe

The thermal conductivity of materials that are used in the geothermal industry has to well understand, especially in the pipe. The pipe has a great number of thermal conductivity which makes heat easily flows through the pipe, therefore, the heat value transferred from the inside to outside of the pipe is measly change.

The heat transfer in the TEG module

The technology of TEG has been increasing fast since last decade as TEG are widely used and have a massive production. The TEG materials are improved at a high temperature. Therefore, the larger temperature difference is created and the more power to generate and will be resulted in higher efficiency.

System Design Application & Calculation Example

Table 1 is the detail specifications of TEG used in this system design.

Table 1: Detail specifications of TEG used in this system design.

Dimensions (mm)	40 x 40
Operating pressure	-50°C ~ 200°C
Thermal conductivity	In the table 2

The heat transfer depends on the material properties. The actual module test data was used to derive the material properties. However, there are a number of material properties TEG that can be defined by a mathematical model: effective Seebeck coefficient (SM), electrical resistance (RM) and thermal conductable (KM). These material properties at a certain temperature difference can easily find in the Tabel 2.

Electrical power generated calculation

A geothermal field with a steam dominated reservoir has the operating pressure is 9.1 bar gauge at the pipeline. The pipe is constructed by carbon steel 24" schedule 40. In the pipe will be installed a telemetry sensor at a remote area with the requirement for 12-volt, 1.5 ampere. The waste heat recovery system is installed as the power generator to the telemetry sensor. The environment temperature is assumed constant at 20°C, and it has been determined that an efficient air-cooled heat sink of TEG up to 30°C.

Tabel 2: Average Modules Material Properties at various Parameters (Sources: ftp://ftp.dii.unisi.it)

Temperature		SM	RM	KM
–C	–K	V/K	ohms	w/K
-100	173.2	0.0352	1.3089	0.5742
-90	183.2	0.0368	1.3435	0.5697
-80	193.2	0.03843	1.3908	0.5616
-70	203.2	0.04005	1.45	0.5512
-60	213.2	0.04166	1.52	0.5396
-50	223.2	0.04325	1.6	0.5278
-40	233.2	0.0448	1.6888	0.5168
-30	243.2	0.0463	1.7856	0.5073
-20	253.2	0.04773	1.8894	0.5002
-10	263.2	0.04908	1.9993	0.4961
0	273.2	0.05034	2.1142	0.4956
10	283.2	0.0515	2.2332	0.4992
20	293.2	0.05253	2.3553	0.5074
30	303.2	0.05343	2.4796	0.5204
40	313.2	0.05418	2.605	0.5384
50	323.2	0.05477	2.7307	0.5617
60	333.2	0.05519	2.8556	0.5903
70	343.2	0.05542	2.9789	0.6242
80	353.2	0.05544	3.0994	0.6632
90	363.2	0.05525	3.2163	0.7072
100	373.2	0.05483	3.3285	0.7559
110	383.2	0.05417	3.4352	0.8088
120	393.2	0.05325	3.5354	0.8656
130	403.2	0.05206	3.628	0.9257
140	413.2	0.05059	3.7121	0.9884
150	423.2	0.04882	3.7867	1.0531

Based on the case 1, the system parameter can be summarized as below.

Operation pressure : 11.5 bar gauge
Operation temperature : 185°C
ID pipe 24" : 0.5922 meter
OD pipe 24" : 0.6096 meter
Temperature hot (T_h) : 185°C (458.15°K)
Temperature cold (T_c) : 30°C (303.15°K)
Output voltage (V_0) : 12 Volts
Output current (I) : 1.5 Amperes

The preliminary calculation can be done using the following equation:

1. Temperature average (T_{av})

$$T_{av} = \frac{T_h + T_c}{2} \quad \text{.....(2)}$$

$$T_{av} = \frac{458.15 + 303.15}{2} = 380.65°K$$

2. Load resistance (R_L)

$$R_L = \frac{V_0}{I} \quad \text{..... (3)}$$

$R_L = \frac{12}{1.5} = 8.0\ ohms$

3. Output power (P_0)

$P_0 = V_0 \times I$ .....(4)

$P_0 = 12 \times 1.5 = 18\ watts$

4. Differential temperature (DT)

$DT = T_h - T_c$ .....(5)

$DT = 458.15 - 303.15 = 155°K$

In order to minimize the TEG damage, it is necessary to select relatively the higher TEG specification. For this case, the selection for TEG is based on the maximum operating temperature, the TEG with 127-couple and 6-ampere module to be used in this system design. The number of SM, RM, and KM at the T_{av} = 380.65 for this TEG can be found in Table 2, and the result is summarized below:

S_m : 0.0543 volt/°K
R_m : 3.4080 ohms
K_m : 0.7953 watts/°K

Based on the case study, the required load has been calculated as 18 watts. Then, the maximum output power (P_{max}) of one TEG module can be calculated using following equation:

$P_{max} = \frac{(S_m \times DT)^2}{4 \times R_m}$ .....(6)

$P_{max} = \frac{(0.0543 \times 155)^2}{4 \times 3.4080} = 5.203\ watts$

Calculate the minimum TEG module needed to generate 18 watts.

NoTEG = P_0 / P_{max}.....(7)

NoTEG = 18 / 5.203 = 3.45 ≈ 4 modules

The requirement are of TEG to generate 18 watts is about 64 cm^2.

The thickness of TEG calculation

The TEG, the heat loss reducer as a function of the isolator, has to have a capability to reduce the heat loss as same as the insulator function. The thickness is the important one, at the insulator where the more thickness of insulator will be more effective to reduce heat loss. This principle also can be applied in the TEG. Based on the previous preliminary calculation, the thermal conductivity of TEG has been known. It is just a simple step to calculate how much is the thickness needed to reduce the heat loss as same as the insulator function.

In normal condition where the pipe is insulated with insulator, in this case with insulator thickness of 0.065 meter and thermal conductivity of insulator 0.064 W/m°K at $T_{average}$ = 380°K shows heat transfer about 654.54 W/m. So the thickness of TEG needed to achieve heat transfer as the insulator is done by following calculation:

Heat loss equation (W/m °K):

$Q/_L = \frac{2\pi k(T_i - T_o)}{ln\left(\frac{R_O}{R_i}\right)}$

$654.87 = \frac{2 \times 3.14 \times 0.82(185-20)}{ln\left(\frac{R_O}{0.6069}\right)}$

And the result is 1.62 meter.

SYSTEM DESIGN RESULT

The result of a mathematic model of the waste heat recovery system is presented in Figure 4. The thermodynamic law controls the temperature fluid depends on the operating pressure. The power output as described in the Equation 6 shows that differential temperature has a great impact of the value of power output. The higher pressure will create a higher differential temperature that causing an increase of power output.

Maximizing the applied of TEG is needed in order to gain the maximum power output of each TEG module. The number of TEG module that needed is figured in Figure 6. A small number of the module is needed when the operating pressure is high and the cold temperature is small.

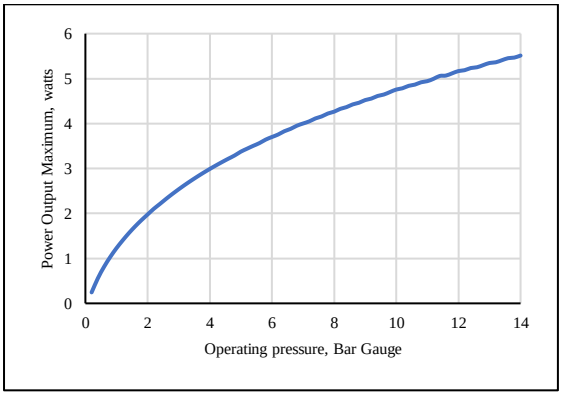


Figure 4: The number of power output at certain operating pressure.

As described before that the system model works as the insulator, the thickness of TEG is needed to be determined. The result at Figure 6 presents that to reduce the number of heat loss as same as the insulator work, the thicker TEG will reduce the number of the heat loss that caused by the increasing of operating pressure.

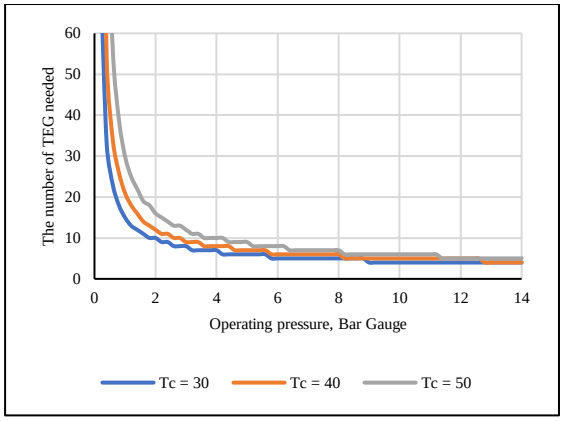


Figure 5: The number of TEG needed to generate 12-volt, 1.5 ampere at certain operating pressure.

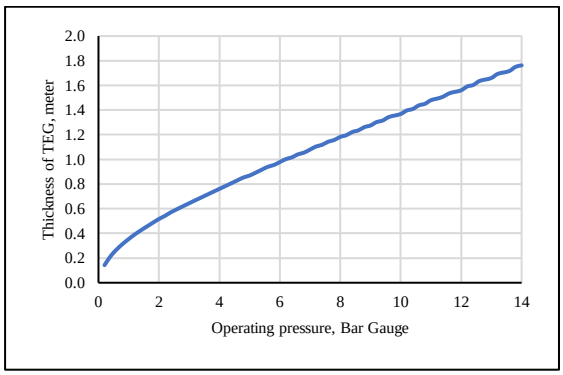


Figure 6: Thickness of TEG to reduce 654.86 W/m heat loss at certain operating pressure.

CONCLUSION

A mathematic waste heat recovery system design has been developed as a replacement of the insulator in the geothermal pipe. In the system models, the heat source comes from the fluids while the cooler is the temperature of the environment. The system model shows:

1. It is necessary to change the insulator with TEG to get added value of waste heat.
2. The increase of operating pressure creates the increasing differential pressure that causing a higher output power generation.
3. The number of TEG modules is needed depending on the differential temperature. The decreasing of differential temperature cause the increasing number of TEG needed.
4. The more thickness of TEG will reduce more heat loss and generate more power output.
5. The thickness of TEG needed in this system design is mathematically acceptable, but it need more comprehensive technically study.

SUGGESTION

The real experiment and continuous study are needed to prove the mathematics system model. Although it necessary to change the insulator with TEG, the efficiency and the technical construction of TEG in this system are still the main problems.

REFERENCES

Ismail, B. I., and Ahmed, W. H. (2009), "Thermoelectric Power Generation Using Waste-Heat Energy as an Alternative Green Technology". *Recent Patents on Electrical Engineering*, 2, 27-39.

LeBlanc, S. (2014), "Thermoelectric Generators: Linking Material Properties and Systems Engineering for Waste Heat Recovery Applications", *Sustainable Materials and Technologies*, 1-2, 26-35.

NN, "Average Modules Material Properties at various Parameters", *ftp://ftp.dii.unisi.it*.

Orr, B., Akbarzadeh, A., Mochizuki, M. and Singh, R. (2016), "A Review of Car Waste Heat Recovery Systems utilizing Thermoelectric Generators and Heat Pipes", *Applied Thermal Engineering*, 101, 490-495.

Remeli, M.F., Kiatbodin, L., Singh, B., Verojporn, K., Date, A., and Akbarzadeh, A. (2015), "Power Generation from Waste Heat using Heat Pipe and Thermoelectric Generator", *Energy Procedia*, 75, 645-650.

Zhang, X. and Zhao, L. (2015), "Thermoelectric Materials: Energy Conversion between Heat and Electricity", *Journal of Materiomics*, 1, 92-105.

RESOLVING THE SHIFTING OF PRESSURE, TEMPERATURE AND SPINNER DATASET USING GEOSTATISTICAL PREDICTION DATA METHODS : IN CASE OF SINGLE ERROR DATA RECORDED TOOLS

Erwandi Yanto, Fadiel Evan Marastio, Benedict Amandus Hananto, and Ristio Efendi

PT. Pertamina Geothermal Energy
Skyline Building, 19th Floor, Jakarta Pusat, Daerah Khusus Ibukota Jakarta 10340
Email: erwandi.yanto@pertamina.com

ABSTRACT

The package of data recorded from routinely well measurement are Pressure, Temperature, and Spinner Measurement either Injection, Production or even Monitoring Wells. Somehow, the measurements operation faces several obstacles which affect the quality of recorded data. In this case, Pressure, Temperature and Spinner measurements in Well "K" during the operation was going well, but after downloading the Log Down and Log Up dataset with speed 20, and 30 ft/min, there was a difference pattern between Log Up and Log Down Data in speed 30 ft/min, through comparing all the data, it can find that the Log Up of speed 30 ft/min is an anomaly among the other data where the data was shifted lower than others. This paper will propose several geostatistical methods such as regression and Monte Carlo. Finally, the best methods to predict and repositioned the data is regression methods with the regression coefficient 0.9. This method could be assigned for any kind of shifting dataset with the constraint of another normal pattern of dataset.

Keywords: Geostatistical prediction, shifting PTS, error data record.

INTRODUCTION

Pressure-temperature-spinner (PTS) surveys are a valuable surveillance tool for determining and monitoring of subsurface conditions in geothermal wells and evaluating changes in reservoir conditions (Axelsson, 2013; Acuña and Arcedera, 2005; Drenick, 1986).

A spinner is an impeller that is used to measure fluid velocity and attached in the bottom of pressure temperature downhole tools (Buscato, 2012). The impeller will rotate due to fluid flow in the blade of spinner, with the frequency being proportional to the relative velocity between the tool and fluid:

$$f = \frac{V_{tool} - V_{fluid}}{C}$$

Or

$$V_{fluid} = V_{tool} - C \times f$$

C is the pitch of the impeller in meters/cycle. V is velocity. f is frequency/ rotate per second.

Almost all downhole tools today are using electronic instruments including for pressure and temperature measurement. Although electronic instruments provide greater accuracy and frequency of measurement, electronic instruments also can still be subjected to errors associated with data recording and processing.

According to Grant and Bixley (2011) there are some possibilities for data to become offset or shifted with respect to depth, such as:

1. For electronic instrument that can record and processing data with some time interval, the pressure-temperature-spinner profiles are recorded while tool is moving (speed 15 m/min 45 m/min). This shifted depth due to moving tools doesn't happened in mechanical downhole instrument, because the tools are recording while it is held stationary at fixed station in the wellbore (Peter and Acuña, 2010).
2. Thermal expansion of the wireline and liner. Due to measurement are held while the well is flowing, there are possibilities that make the wireline expanded because of the heat. The expression of the expansion is given by:

$$\Delta L = \alpha L \, (T_{avg} - T_o)$$

Where:

α = coefficient of expansion
Tavg = average downhole temperature
To = surface temperature

To reduce the shifting depth and referenced to a certain depth casing collar locator are included in PTS logging tools, so the log can be referenced to casing or liner connection (Steingrímsson, 2013).

Time lag between measurement and recording (downhole data and depth measurements are merged) depending on whether logging is real time or memory mode. The shifted depth can be checked by comparing data from Log Up and Log Down in the same interval.

MATERIALS AND METHODS

Several Critical materials are:

1. PTS Memory Tools.
2. Toolbox.

3. Fuel.
4. Tissue.
5. Lubricator.
6. Personal Protective Equipment.
7. Slickline Unit.
8. Boom Truck / Crane.

Tool Components:

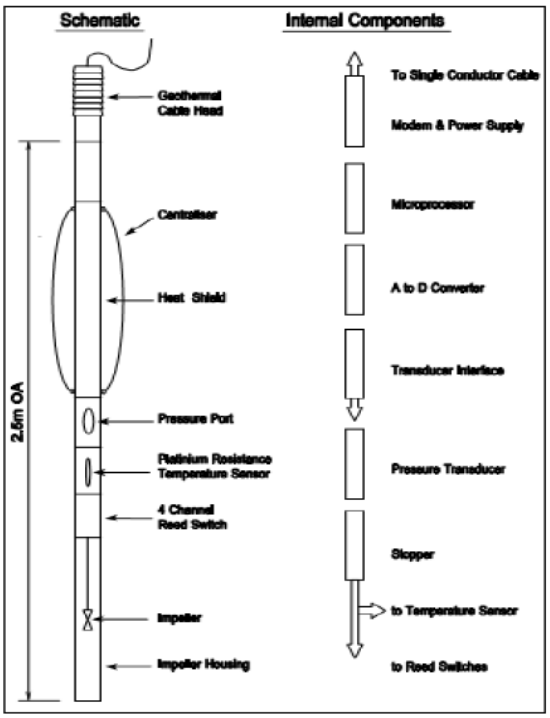


Figure 1: PTS Tool (Stevens, 2000)



Figure 2: Operation Procedures.

Methods:

Operation Procedures:

1. Preparation and Measurement of Pressure, Temperature, Spinner, including rig up equipment, run in hole through log up and log down with speed:
   a. 20 ft/min
   b. 30 ft/min
2. The interval survey from 753 – 2659 mMD

Download recorded data from PTS:

1. Analyze the dataset: average the value of cable speed, spinner rotation, categorize the depth, temperature and pressure.
2. Apply statistical analysis to predict the shifted using regression, especially linear regression.

RESULTS

The statistical methods could be applied in terms of single error data such as single error data logging down with cable speed of 30 m/min while the other data as the guidance to predict and re-positioning the error data into the proper position.

Due to the error was just found in certain depth exactly at 650 – 732 mMD, then it can resolve with comparing the suitable data value at the same depth in another cable speed data which is Log Up data with cable speed 30 m/min, Log Down 20 m/min and Log Up 20 m/min.

As the first parameter to be considered in the recorded data is cable speed data, so we need to adjust the similar and proper speed into 30 m/min as it must. The crossplot between depth of 735 – 1365 mMD applied to acquire the regression equation. Linear regression shows an equation: y = 336.29x – 9000, with y refers to depth, and x is the cable speed.

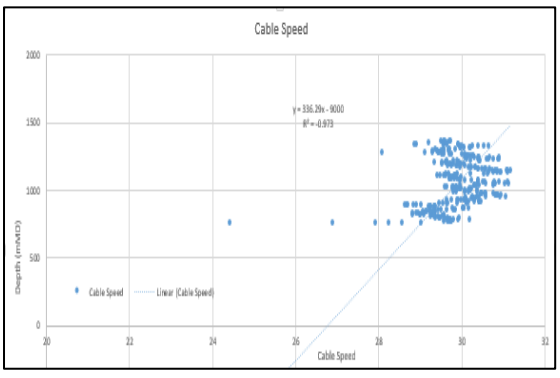


Figure 3: Crossplot Cable Speed Data.

Depth: 753 – 1365 mMD
Linear Regression methods applied to predict the values of shifted dataset.
y = 336.29x - 9000
R^2 = -0.973

Secondly, the spinner rotation should also be adjusted with linear regression as well as the cable speed at the depth interval 735 – 1365 mMD, and the equation: y = -4.5733x – 1900 will be applied to those interval.

The crossplot between depth and rotation shows as follow :

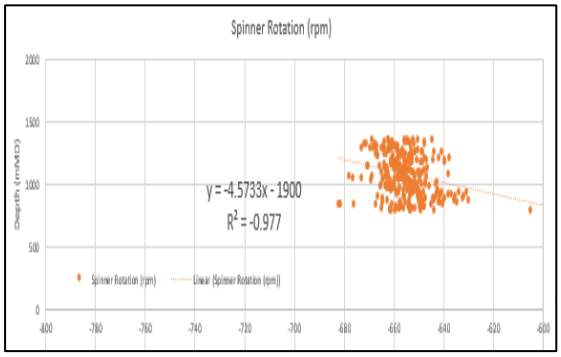


Figure 4: Crossplot Between Depth and Rotation.

Depth: 753 – 1365 mMD
y = -4.5733x - 1900
R^2 = -0.977

Then, we need to assure that all the parameters to calculate mass rate at the end of PTS data analysis was matched each other especially for all the cable speed during measurement operation. Here is the slope calculated with the formula:

Slope = Spinner Rotation/Cable Speed

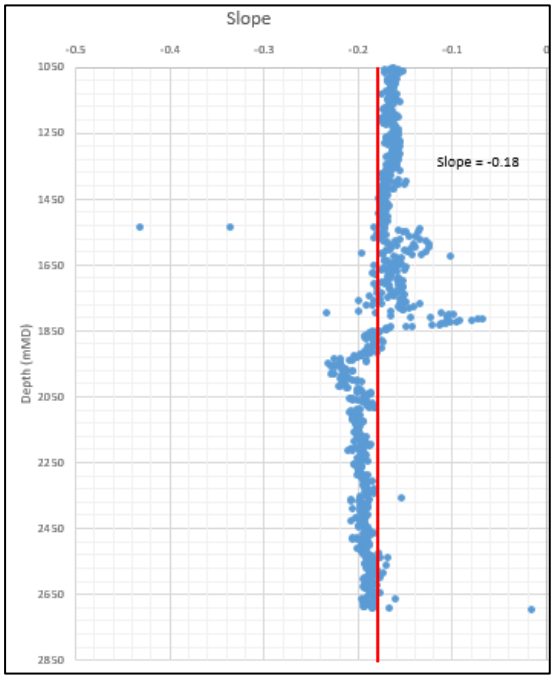


Figure 5: Representative Slope = -0.18

Critical parameters such as cable speed, spinner rotation and supported with slope value will be used to calculate fluid velocity. Actually, it was not necessary to use linear regression as well as speed and rotation previously, but in this case, otherwise it was calculated and there's also linear regression equation to validate and confirm the fluid velocity value of certain interval which is especially for 735 – 1365 mMD.

The regression trendline and equation of Well "K":

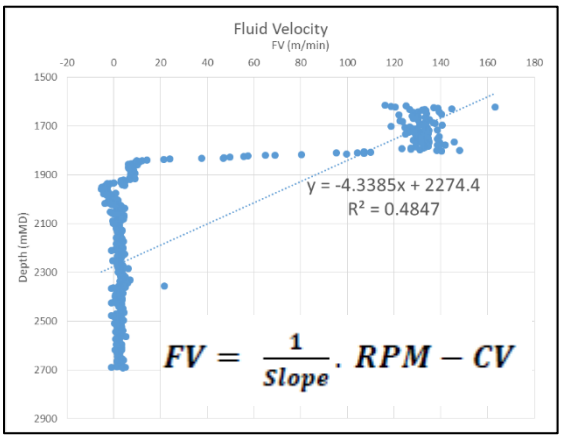


Figure 6: Well "K" Regression Trendline.

Depth: 753 – 1365 mMD
y = -4.3385x – 2274.4
R^2 = -0.4847

As the final purpose of this method is to resolve the error and shifted on PTS data, so there should be a comparison between unresolved and after resolving the error data refers to the figures as follows:

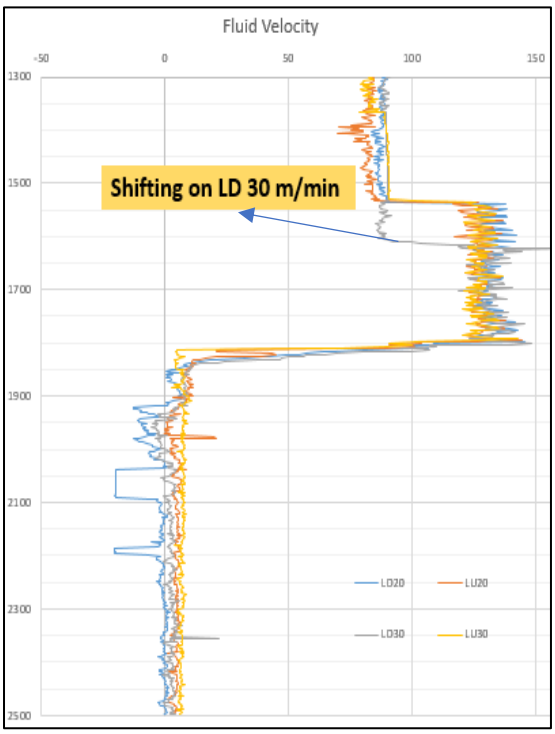


Figure 7: Shifting Data of Log Down with Speed 30 m/min.

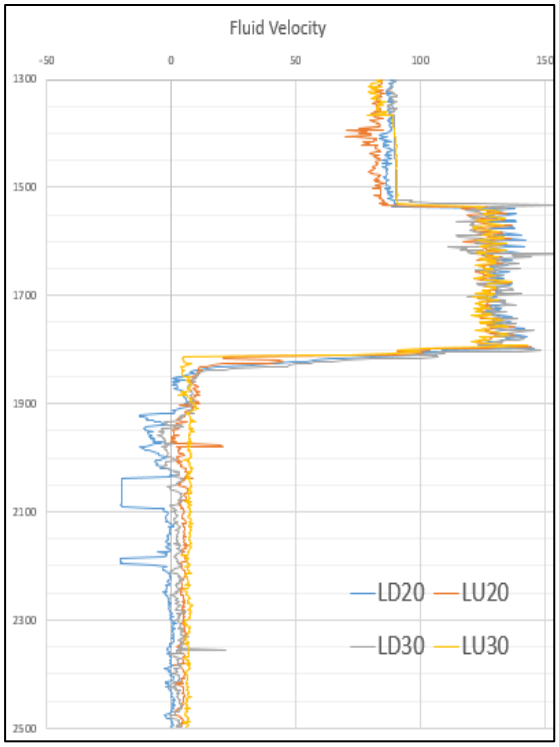


Figure 8: Resolved Data of Log Down with Speed 30 m/min.

Production test data shows that a surface flow of 56.88 Kg / S (100% Opening). WHP at PTS 4.4 Kscg / Throttling 50%. Pressure Max 151.51 Kscg @ 2700 mMD. Temperature Max 295.87^{0}C @ 2700 mMD. Indication of Major Feed Zone at 1850 mMD. Sinker Bar 2" can only enter up to 2981 mMD. PTS Tools can only enter up to 2700 mMD.

CONCLUSION AND RECOMMENDATION

There are some possibilities for data to become offset or shifted with respect to depth, such as:

1. For electronic instrument that can record and processing data with some time interval.
2. Thermal expansion of the wireline and liner.
3. Time lag between measurement and recording (downhole data and depth measurements are merged). Statistics method which used to resolve the shifted data.

REFERENCES

Acuña, J A., and Arcedera, B. A. (2005), "Two-Phase Flow Behavior and Spinner Data Analysis in Geothermal Wells". PROCEEDINGS from Thirtieth Workshop on Geothermal Reservoir Engineering Stanford University, California. SGP-TR-176.

Axelsson, G. (2013), "Geothermal Well Testing". Short Course V on Conceptual Modelling of Geothermal Systems, El Savador.

Buscato, N. M. (2012), "Quantifying Feed Zone Contributions from Pressure-Temperature-Spinner Data and Pressure Transient Analysis Using Well Tester". GEOTHERMAL TRAINING PROGRAMME, Reykjavik, Iceland. Reports 2012 Number 7.

Drenick, A. (1986), "Pressure Temperature Spinner Survey in a Well at The Geyser". Eleventh Workshop on Geothermal Reservoir Engineering Stanford University, California. SGP-TR-93.

Grant, M. A., and Bixley, P. F. (2011), "Geothermal Reservoir Engineering Second Edition". Academic Press, Oxford.

Peter, P., and Acuña J. A. (2010), "Implementing Mechanistic Pressure Drop Correlations in Geothermal Wellbore Simulators". Proceeding from World Geothermal Congress 2010.

Steingrímsson, B. (2013), "Geothermal Well Logging: Temperature and Pressure Logs". Short Course V on Conceptual Modelling of Geothermal Systems, El Salvador.

Stevens, L. (2000), "Pressure, Temperature and Flow Logging in Geothermal Wells". Proceedings from World Geothermal Congress 2000.

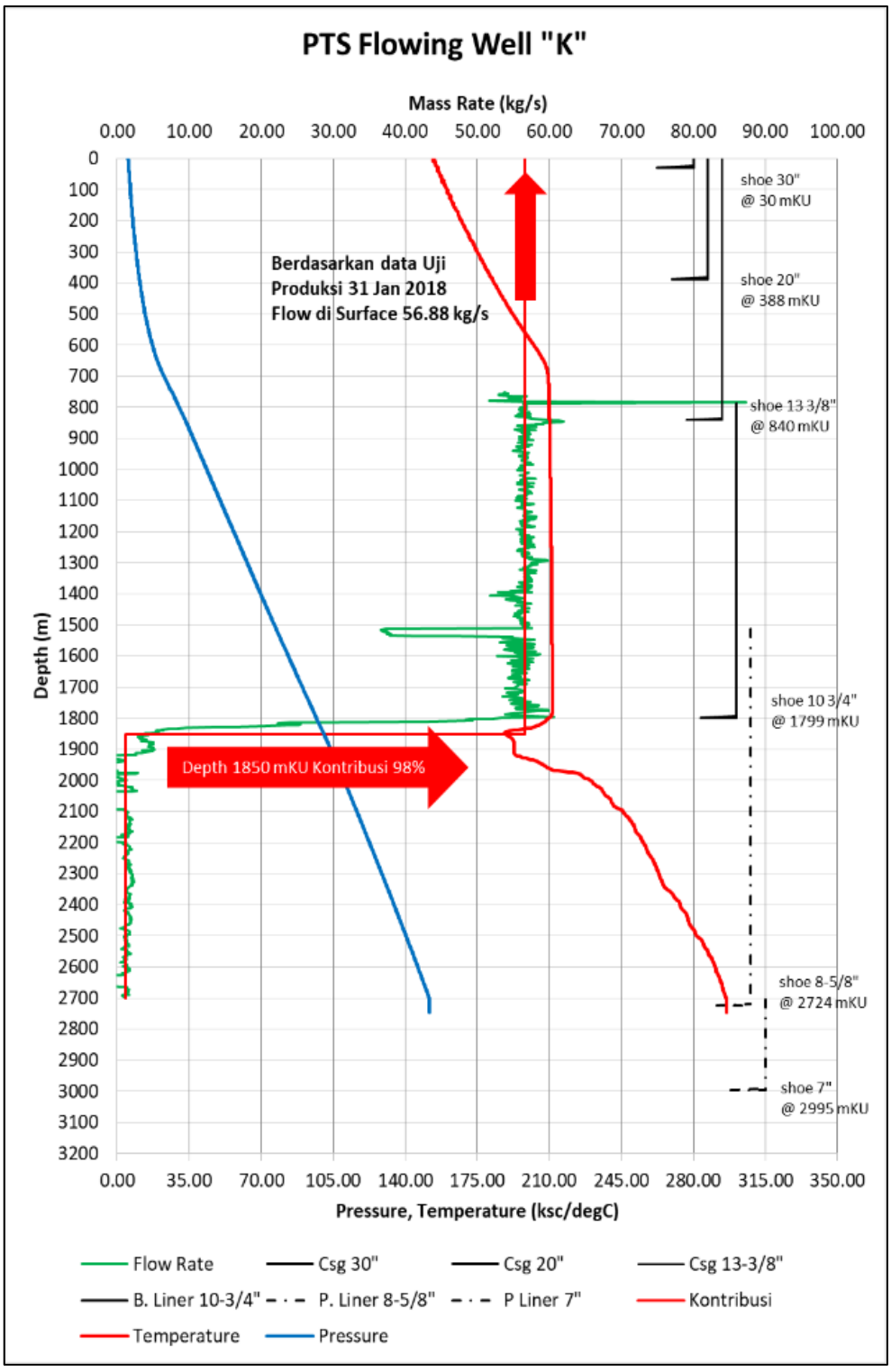


Figure 9: PTS Flowing Well "K".

NUMERICAL INVESTIGATION FOR ESTIMATION OF ROCK TEMPERATURE IN ENHANCED GEOTHERMAL SYSTEM

Muhammad Qarinur, Hideaki Yasuhara, and Naoki Kinoshita

Department of Civil and Environmental Engineering, Ehime University
Matsuyama 790-8577, Japan
Email: mqarinur@gmail.com

ABSTRACT

Numerical modeling was used to estimate rock temperature in the geothermal reservoir. It is important to develop a new geothermal resource and improve production performance probably by Enhanced Geothermal System (EGS). In this research, we have used COMSOL Multiphysics (COMSOL 5.3a, 2017) to simulate the coupled thermal and hydraulic (TH) processes in the geothermal reservoir by using the local thermal non-equilibrium theory. The reservoir is treated as a fractured porous medium by adopting discrete fractured model (DFM). A geothermal field in Lahendong, Indonesia is simulated to study the characteristics of fluid flow and heat transfer. Based on the results, the rock temperature in the production well LHD-5 will decrease faster because of close to the injection wells. The rock temperature in the production well LHD-23 shows almost no change and the system can maintain a stable running condition. It is found that the distance between injection wells and production wells is crucial to the performance and service life of the geothermal reservoir.

Keywords: Numerical modeling, rock temperature, EGS, Lahendong.

INTRODUCTION

Geothermal energy is the one of renewable energy for reducing dependence on gas and other fossil fuels. Based on the origins and conditions of production, geothermal resource are divided into hot dry rock (HDR) and hydrothermal (Qu et al., 2017). The temperature-depth relationship (i.e., geothermal gradient), permeability, porosity and the amount of fluid saturation in the geothermal reservoir are important in assessing geothermal resources potential (Massachusetts Institute of Technology, 2006). High average thermal gradients, high rock permeability and porosity, sufficient fluids in place, and an adequate reservoir recharge of fluids are the characteristics of the hydrothermal reservoir. Compared to the hydrothermal resources, HDR resources may have higher temperature potential, but may not produce energy sufficiently because of deeply buried, low permeability, low porosity, insufficient reservoir volume, and the absence of naturally contained fluids. Therefore, Enhanced Geothermal System (EGS) can be used to stimulate fractures in the rock to create a connected path through which fluids can be induced to flow and extract heat (Xu et al., 2015).

Currently, several useful models have been developed for modeling flow and temperature of EGS. Jiang et al. (2014) simulated long-term heat extraction using three-dimensional transient model for EGS subsurface thermo-hydraulic processes. Xu et al. (2015) studied coupled hydro-thermal model for EGS by using equivalent pipe network (EPN). Yao et al. (2018) used thermal-hydraulic-mechanical (THM) coupling to simulate and analyze the heat extraction in EGS based on discrete fracture model. The modeling method and procedure aforementioned may be provided for the current study.

In this study, a mathematical model incorporating thermal and hydraulic coupling is adopted to estimate the rock temperature in the geothermal reservoir by using the local thermal non-equilibrium theory. Adopting discrete fracture model (DFM), the geothermal reservoir is treated as a fractured porous medium that consists of the rock matrix and discrete fractures. Finally, the 3D numerical model of the Lahendong geothermal field is created in COMSOL Multiphysics 5.3a to predict the evolution of rock temperature in the geothermal reservoir.

METHODOLOGY

Model Overview

Thermal and hydraulic coupling method in this study based on discrete fracture model (DFM) consists of two parts (i.e., the rock matrix and discrete fractures) (Figure 1). The discrete fracture model (DFM) uses grid nodes to represent flow relationship between fracture to fracture, fracture to matrix, and matrix to matrix (Liang *et al.*, 2016).

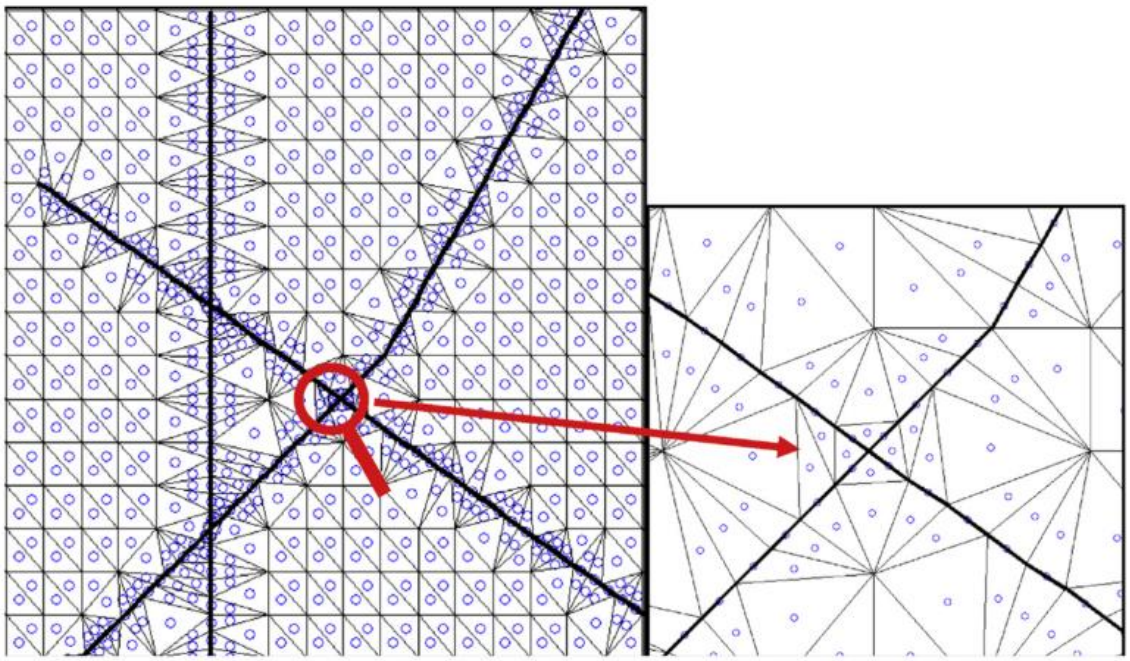


Figure 1: The unstructured grid and the node of DFM (Liang *et al.*, 2016).

Governing Equations

The governing equations of thermal and hydraulic coupling model are described as follows:

Rock mass flow

The rock matrix permeability is less than that of the discrete fractures. Because of that, flow in the rock matrix is calculated by Darcy's law and that in the discrete fractures is done by the modified Darcy's law. The equations for the rock matrix and discrete fracture flow are expressed by (Liang *et al.*, 2016; Yao *et al.*, 2018).

$$S\frac{\partial p}{\partial t} + \nabla\left(-\frac{\kappa}{\eta}(\nabla p + \rho_w g \nabla z)\right) = -\frac{\partial e}{\partial t} + Q \qquad (1)$$

$$d_f S_f \frac{\partial p}{\partial t} + \nabla_\tau\left(-d_f \frac{\kappa_f}{\eta}(\nabla_\tau p + \rho_w g \nabla_\tau z)\right) = -d_f \frac{\partial e_f}{\partial t} + Q_f \qquad (2)$$

where S is the rock matrix storage coefficient [1/Pa], p is the hydrostatic pressure [Pa], t is the time [s], κ is the rock matrix permeability [m^2], η is the dynamic fluid viscosity [Pa·s], ρ_w is the fluid density [kg/m^3], g is the gravitation [m/s^2], e is the volumetric strain of rock matrix [-], Q is the source-sink term of the seepage process [s^{-1}], d_f is the discrete fracture thickness [m], S_f is the discrete fracture storage coefficient [1/Pa], ∇_τ is the gradient operator restricted to the fracture's tangential plane, κ_f is the discrete fracture permeability [m^2], e_f is the volumetric strain of discrete fracture [-], Q_f is the flow exchange between rock matrix and discrete fracture [s^{-1}].

Rock mass temperature

Energy conservation in rock matrix is described as (Saeid et al., 2013):

$$\rho C_s \frac{\partial T_s}{\partial t} + \nabla \cdot (-\lambda \nabla T_s) = 0 \qquad (3)$$

where ρ is the rock density [kg/m^3], *Cs* is the specific heat capacity of rock matrix [J/kg/K], *Ts* is the rock temperature [°C], λ is the thermal conductivity of rock [W/m/K].

Energy conservation in the discrete fracture is defined as (Chen et al., 2013; Yao et al., 2018):

$$d_f \rho_w C_w \frac{\partial T_f}{\partial t} + d_f \rho_w C_w \cdot u_f \nabla_\tau T_f = \nabla_\tau \cdot \left(d_f \lambda_f \nabla_\tau T_f\right) + h(T_s - T_f) \qquad (4)$$

where C_w is the specific heat capacity of fluid [J/kg/K], T_f is the water temperature in the discrete fracture [°C], u_f is the fluid flow velocity in the discrete fracture, λ_f is the thermal conductivity of fluid [W/m/K], h is the convection efficiency [W/m^2/K].

Coupling effects

TH coupling effect

One of the most important factors that affect the coupling is the properties of the work fluid in the reservoir. The density of water is no longer a constant value due to the influence of high pressure and high temperature in the reservoir. The effects can be expressed in the function of pressure and temperature as follows (Zhao *et al.*, 2015):

$$\frac{1}{\rho_w} = 3.086 - 0.899017(4014.15 - T)^{0.147166} - 0.39(658.15 - T)^{-1.6}(p - 225.5) + \delta_w \quad (5)$$

where T is the water temperature [K], p is the absolute water pressure [Pa], and δ is a function of "p" and "T"; in general, the value of δ does not exceed 6% of $1/\rho_w$.

Dynamic viscosity (η) is also affected by the temperature of water, $\eta = v\rho_w$ in which v is the kinematic viscosity of water. A commonly used empirical formula for the kinematic viscosity can be expressed as follows:

$$v = \frac{0.01775}{1+0.033T_f+0.000221T_f^2} \quad (6)$$

The density and the viscosity of water are greatly affected by the temperature. Therefore, they are important in the process of seepage and heat transfer in the geothermal reservoir.

RESEARCH AREA

The Lahendong geothermal field is located in Tomohon, North Sulawesi, Indonesia. Currently, the Lahendong geothermal field has six units with a total production capacity of 120 MW (Pambudi, 2018). In this study, five wells in Cluster-5, Lahendong Unit III Geothermal Power Plant, comprising three injection wells (LHD-19, LHD-20, LHD-21) and two production wells (LHD-5, LHD-23) are simulated to evaluate geothermal reservoir temperature. The research area and the well locations are shown in Figure 2.

Computational Model

Based on the actual conditions (Koestono, 2010), the locations of injection and production wells are shown in Figure 2. The 3D computational model in the current study is also shown in Figure 3. It is assumed that the reservoir is located at 2,450 m below the ground surface with a domain of 1500m x 1500m x 1200 m (Figure 3 and Figure 4). The reservoir rock is assumed to be homogenous and the fault zone is assumed as the fracture area.

According to the drilling well design in the well LHD-23, the length of each slotted liner pipe in the injection and production wells in Cluster-5 is assumed to be 300 m with diameter 7 inch. The finite element mesh used in the calculation is shown in Figure 5.

Initial and boundary conditions

In the simulations using the present model, the total heat extraction period is 100 years with each time step of 1 year. The influence of temperature gradient is not considered in the domain. Therefore, the temperature variation along the depth is ignored. A thermal insulated boundary is selected for the external conditions. The initial temperature of the reservoir is 230 °C with the hydrostatic pressure of 12 MPa. In the injection wells, 83.3 kg/s of cold water at the temperature of 40 °C is injected, and 31.7 kg/s production rate in the production well has been determined (Prabowo *et al.*, 2015). For the other external conditions, an impermeable boundary is selected, and it is assumed that reservoir pressure has reached a steady state before water injection.

Model parameters

The accuracy of obtaining results that match the actual conditions in numerical simulations depends on the selection of computational parameters. Due to lack of several data to perform numerical simulations, several parameters are selected by assumptions and references of the existing numerical simulations. The parameters used in the numerical model are listed in Table 1 (Khasani *et al.*, 2001; Utami, 2011; Brehme *et al.*, 2016; Yao *et al.*, 2018).

Table 1: Model parameters in reservoir

Parameter	Value	Unit
$\boldsymbol{\rho_w}$	1,000	[kg/m^3]
$\boldsymbol{\eta}$	9.54 x 10^{-5}	[Pa·s]
C_w	4,200	[J/kg/K]
C_s	1000	[J/kg/K]
λ_f	1.8	[W/m/K]
λ_s	2.5	[W/m/K]
h	3000	[W/m^2/K]
ρ_s	2740	[kg/m^3]
κ	2.3 x 10^{-14}	[m^2]
κ_f	1.3 x 10^{-11}	[m^2]
S	1.0 x 10^{-8}	[1/Pa]
S_f	1.0 x 10^{-9}	[1/Pa]
α_T	2.0 x 10^{-6}	[1/K]
ϕ_s	0.105	[-]
ϕ_f	0.3	[-]
d_f	0.001	[m]
g	9.81	[m/s^2]

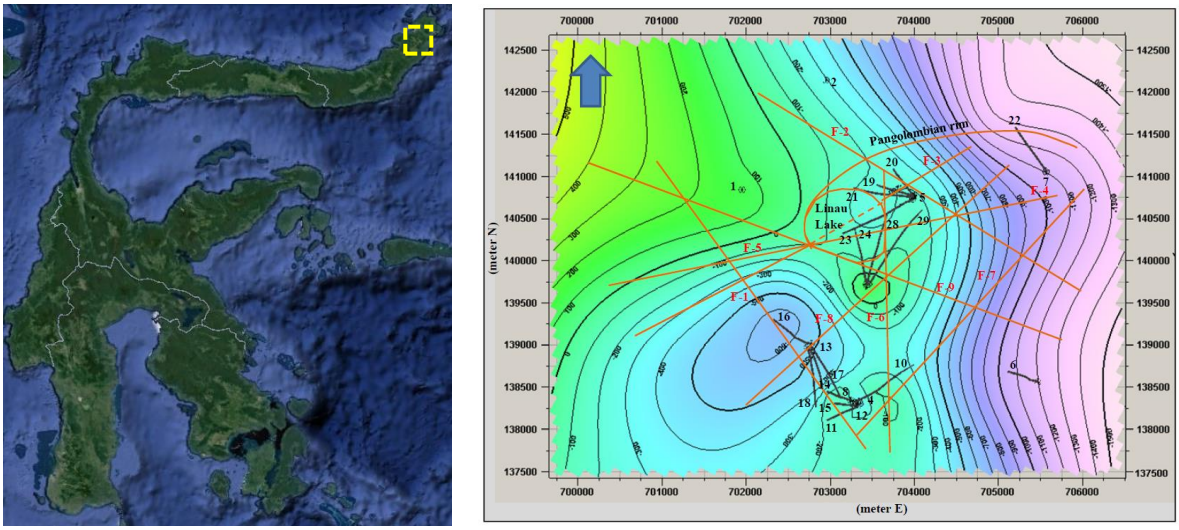


Figure 2: Location of the research area and wells at Lahendong geothermal field (Koestono, 2010).

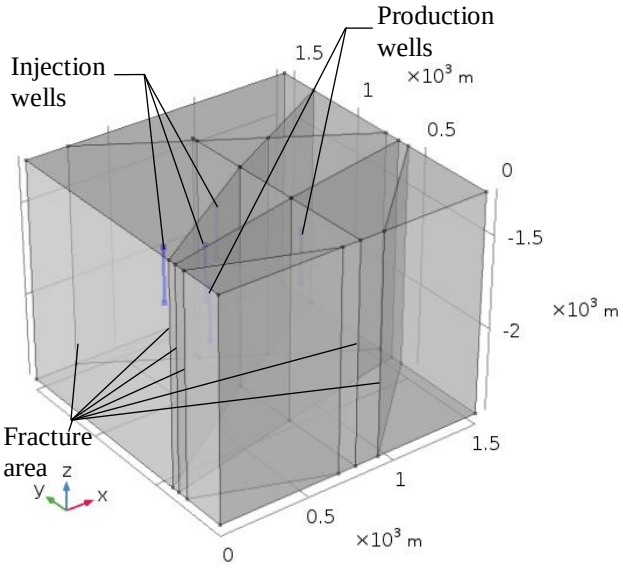


Figure 3: The 3D model geometry of Lahendong geothermal field.

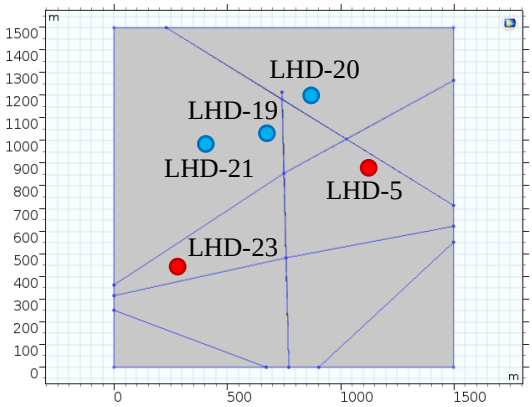


Figure 4: A cut plane at Z = 1750 m.

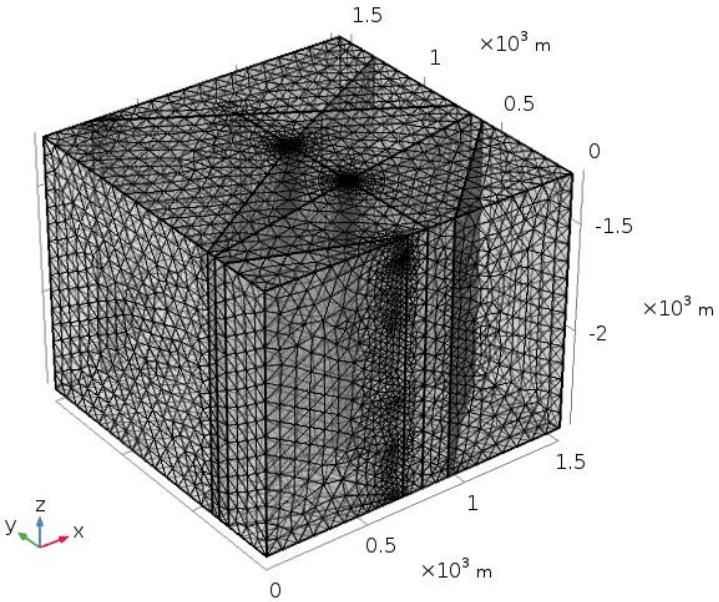


Figure 5: Mesh system of Lahendong geothermal field (tetrahedra elements 182597).

RESULTS

Fluid Production Temperature

The evolution of the fluid production temperature is shown in Figure 6. The average outlet temperature remains constant at 230 °C for about 20 years. After 20 years, the temperature of the production well especially in LHD-5 began to decline. The outlet temperature decreases from 230 °C to 216 °C for about 100 years. In the production well LHD-23 the temperature little changes because the system can maintain a stable running condition for about 100 years. This is because the production well LHD-23 position is farther from the injection well than the production well LHD-5, so the time required in the process of decreasing the reservoir temperature is longer.

From these results, it can be concluded that the determination of the distance of the injection wells with the production well becomes important in determining the service life of the geothermal reservoir.

Injection Pressure

The evolution of the injection well pressure is shown in Figure 7. In the beginning, the injection well pressure in the injection well LHD-19, LHD-20, and LHD-21 increases quickly from 12 MPa to 13.7 MPa, 13 MPa, and 12.8 MPa respectively. The pressure in the injection well LHD-19 is higher than the others because the position is between LHD-20 and LHD-21 and the injections from the two wells should affect the injection pressure of LHD-19. On the other hand, the pressure on the injection well LHD-21 is lower than the others because it is relatively further than the other injection wells.

After one-year production time, the injection pressure increases more gently. In the 100-year production time, the pressures in the injection well LHD-19, LHD-20, and LHD-21 increase to 21.5 MPa, 20.8 MPa, and 20.5 MPa respectively. It can be concluded that the injection pressure should maintain a high level, to achieve the requirement of constant injection and production rates of 83.3 kg/s and 31.7 kg/s, respectively.

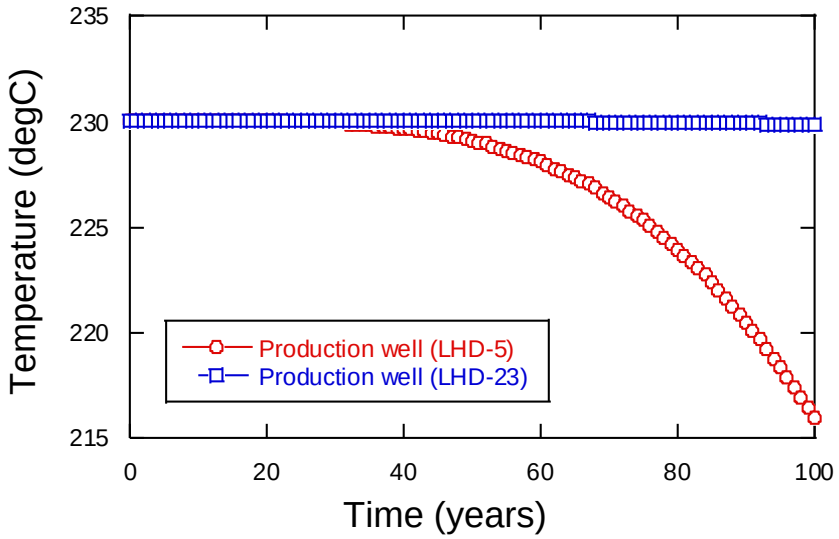


Figure 6: Evolution of rock temperature in production wells.

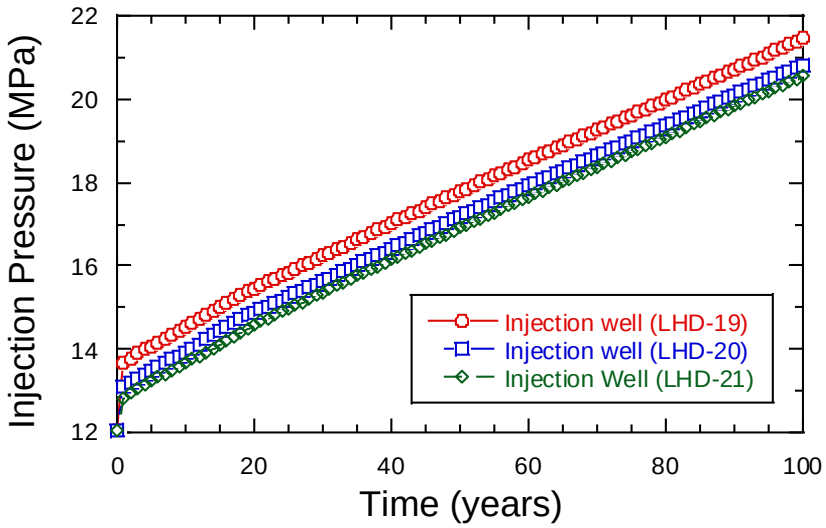


Figure 7: Evolution of the injection well pressure.

Distribution of Rock Temperature

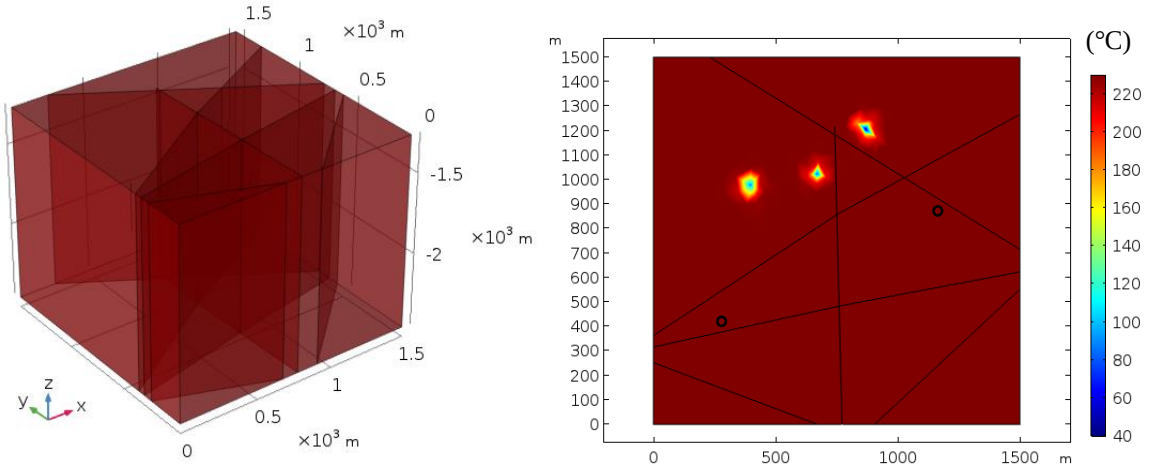
The rock temperature distribution in the reservoir with time is shown in Figure 8. In the initial stage (Figure 8(a)) with the injection of 40 °C water temperature, the rock temperature exchange occurs in the rock matrix. The temperature in the rock matrix decreases gradually by forming the low-temperature zone. However, the rock temperature close to the production wells almost has no change, and the system can maintain the sustained and stable output of heat production.

As shown in Figure 8, the production wells begin to undergo a temperature change gradually. It is indicated that the steady and continuous heat output is beginning to decline. Finally, the low-temperature zone in the reservoir will expand and reach the production well (Figure 8(c) and (d)). Because of that, the water temperature in the production wells gradually decrease with time.

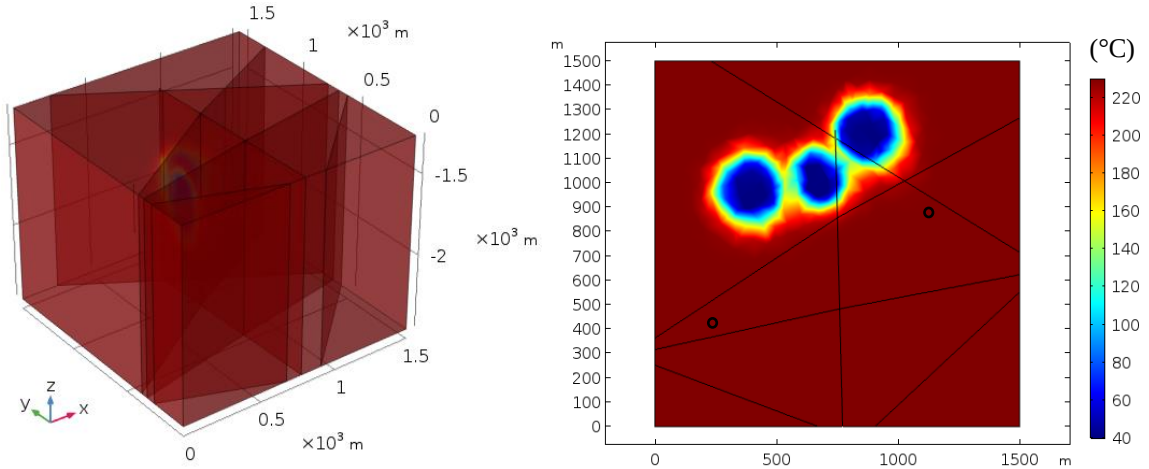
CONCLUSIONS

Thermal and hydraulic (TH) coupling by adopting discrete fracture model was established to estimate the rock temperature of the Lahendong geothermal reservoir. The rock temperature in the production well LHD-5 decreases faster than that in the production well LHD-23. It is because the location of LHD-5 is closer to the injection wells. The rock temperature in the production well LHD-23 little change for 100 years, and the system can maintain a stable running condition throughout the simulation period.

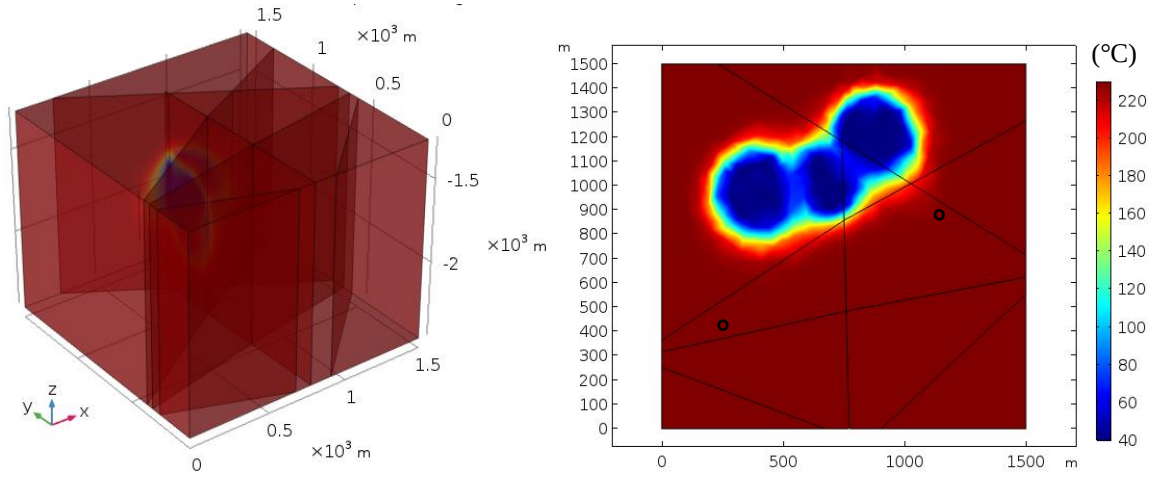
However, due to lack of in-situ data and specific research in this reservoir area, the results shown in the current work cannot be well validated yet, and the validation must be accomplished by actual measurements and/or experiments under in-situ conditions. Furthermore, the effects of mechanical and chemical processes are not considered in this work, and should be considered in the future work to obtain more plausible estimation of the energy production.



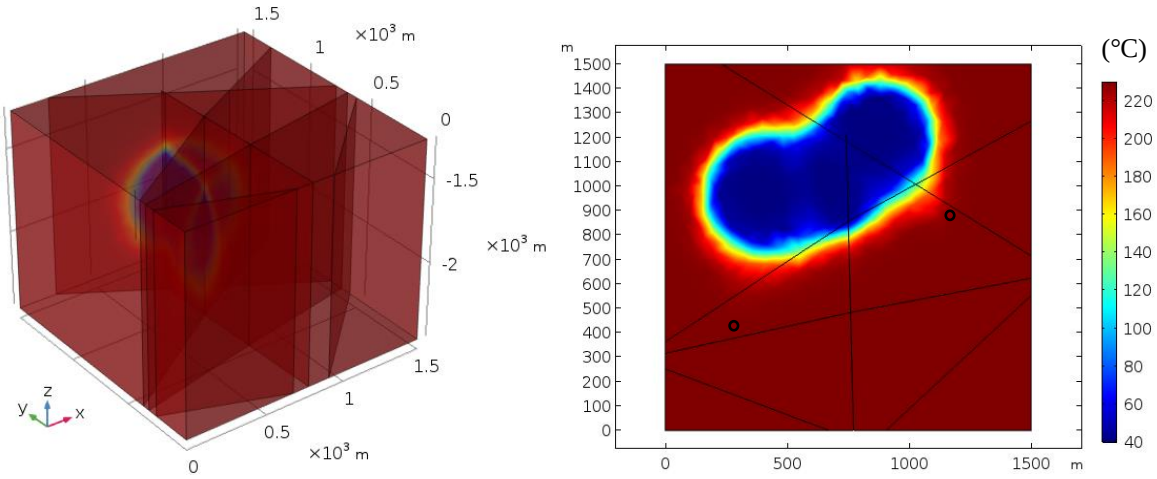
(a) lifespan 1 year



(b) lifespan 25 years



(c) lifespan 50 years



(d) lifespan 100 years

Figure 8: Temperature evolution in the fracture and a cut plane at z = 1750 m.

REFERENCES

Brehme, M. *et al.* (2016), 'Permeability distribution in the Lahendong geothermal field: A blind fault captured by thermal–hydraulic simulation', *Environmental Earth Sciences*, 75(14).

COMSOL 5.3a. (2017), 'COMSOL Multiphysics Reference Manual', p. 1150. Available at: www.comsol.com.

Jiang, F. *et al.* (2014), 'A three-dimensional transient model for EGS subsurface thermo-hydraulic process', *Energy*. Elsevier Ltd, 72, pp. 300–310.

Khasani *et al.* (2001), 'Interpretation of Well Logging Data', in *Proceeding of the 5th INAGA Annual Scientific Conference & Exhibitions*. Yogyakarta.

Koestono, H. (2010), *Lahendong Geothermal Field , Indonesia : Geothermal model based on wells LHD-23 and LHD-28*. United Nations University.

Liang, B. *et al.* (2016), 'A systematic study of fracture parameters effect on fracture network permeability based on discrete-fracture model employing Finite Element Analyses', *Journal of Natural Gas Science and Engineering*, 28, pp. 711–722.

Massachusetts Institute of Technology. (2006), "*The Future of Geothermal Energy, Impact of Enhanced Geothermal Systems (EGS) on the United States in the 21st Century", Idaho National Laboratory*. Available at: http://www.eere.energy.gov/geothermal/pdfs/structure_outcome.pdf.

Pambudi, N. A. (2018), 'Geothermal power generation in Indonesia , a country within the ring of fire : Current status, future development and policy', *Renewable and Sustainable Energy Reviews*, 81(July 2017), pp. 2893–2901.

Prabowo, T. *et al.* (2015), 'Tracer Test Implementation and Analysis in Order to Evaluate Reinjection Effects in Lahendong Field', *World Geothermal Congress 2015*, (April), pp. 1–6.

Qu, Z. Qing, Zhang, W. and Guo, T. Kui. (2017), 'Influence of different fracture morphology on heat mining performance of enhanced geothermal systems based on COMSOL', *International Journal of Hydrogen Energy*. Elsevier Ltd, 42(29), pp. 18263–18278.

Saeid, S., Al-Khoury, R. and Barends, F. (2013), 'An efficient computational model for deep low-enthalpy geothermal systems', *Computers & Geosciences*, 51, pp. 400–409.

Utami, P. (2011), "*Hydrothermal Alteration and The Evolution of The Lahendong Geothermal System, North Sulawesi, Indonesia"*. University of Auckland.

Xu, C., Dowd, P. A. and Tian, Z. F. (2015), 'A simplified coupled hydro-thermal model for enhanced geothermal systems', *Applied Energy*, 140, pp. 135–145.

Yao, J. *et al.* (2018), 'Numerical simulation of the heat extraction in 3D-EGS with thermal-hydraulic-mechanical coupling method based on discrete fractures model', *Geothermics*, 74(September 2017), pp. 19–34.

Zhao, Y. *et al.* (2015), 'THM (Thermo-hydro-mechanical) coupled mathematical model of fractured media and numerical simulation of a 3D enhanced geothermal system at 573 K and buried depth 6000–7000 M', *Energy*, 82, pp. 193–205.



General



LAND ACQUISITION PROCESS AND CHALLENGES IN GEOTHERMAL EXPLORATION PROJECT IN INDONESIA

Dorman P. Purba[1], Daniel W. Adityatama[1], Satria P. Hasymi[2], and Vicky R. Chandra

[1]The University of Auckland, New Zealand
[2]Indonesia Geothermal Lawyer Association (IGLA)
Email: dpur769@aucklanduni.ac.nz

ABSTRACT

Indonesia is believed to have the biggest geothermal energy potential in the world, 29 GWe, spread over the archipelago. However, the development rate is considered slow where in the last 34 years, from 1981 to 2017, Indonesia only managed to utilize 6% of its total geothermal potential. Furthermore, a target has been set by Government of Indonesia to reach 7,200 MWe installed capacity from geothermal energy in 2025 which requires installation rate of 620 megawatt per year. This target could only be achieved with significant collaborated-effort from all stakeholders. One of the identified challenges in achieving this goal are issues related to land acquisition process, especially in the early exploration phase where the local community is not familiar yet with a geothermal project. What makes land acquisition process in geothermal project is unique compared with other projects is that most of geothermal prospect area are located on the forestry and volcanic area, which usually state-owned, but most of the times there are local people that already claim ownership or make a living on the land (food gathering, farming, wood gathering, etc.), further complicate the problem. Many times, these issues become more intricate due to the lack of understanding from the geothermal developer side on the land regulation in Indonesia and on the local community custom. In the long run, failure to manage land acquisition issues properly may lead to project delay and potentially bring a significant economic impact to the project. Literatures review are conducted to summarize several aspects of land acquisition process such as type of land, land requirement for exploration project, land survey and mapping, law, regulation and standards, land and crop appraisal, negotiation and payment method, land registration and creating land database. In additional, several case studies related to land acquisition in Indonesia will be discussed to provide a better context of this research. Finally, this study aims to develop a general guide in acquiring land for geothermal exploration project in Indonesia based on land regulation in Indonesia and IFC standards.

Keywords: Land accusation, regulation, IFC standards.

INTRODUCTION

Challenges in Developing Geothermal Energy in Indonesia

Indonesia is believed to have enormous geothermal energy potential, approximately 29 GWe (Bertani, 2016; MEMR, 2017; Darma et al., 2010; Fauzi et al., 2005; Suryantoro et al., 2005; Ibrahim et al., 2005). Utilization of geothermal energy in Indonesia has been started since 1981 through Kamojang unit I Geothermal Power Plant in West Java with 30 MWe installed capacity (Darma et al., 2010; Hochstein and Sudarman, 2008). Until 2018, Indonesia has successfully developed 1924.5 MWe of geothermal energy and rank second of geothermal energy producing countries in the world, under the United States (ThinkGeoEnergy, 2018). However, this achievement is still only equivalent to ± 6% of its total potential and still far from the Indonesian government's target of 7,200 MWe installed capacity in 2025.

To achieve this predetermined target, the Government of Indonesia need to achieve additional installed capacity by approximately 620 MWe annually from 2018 to 2025. Some of the challenges identified in developing Indonesia's geothermal energy are:

1. Single buyer - Condition on single power generation government agency for the purpose to serve the public creates additional challenge to set appropriate regulation (Poernomo et al., 2015; Setiawan, 2014).

2. Overlap with conservation/protected forest land - Around 41.6% of the geothermal potential is in the area of protected forests or conservation areas (Setiawan, 2014).

3. Lack of awareness among consumers and society about renewable (green) energy development – Often creates minimum support from the local community (Setiawan, 2014).

In Indonesia, stakeholders involved in a geothermal energy development project include central government, Developer Company, local government, local community, and academic institution. The quality of communication and cooperation between all stakeholders is believed to

be very influential in determining the success of Indonesia to reach its geothermal target.

This study focuses on the challenge of geothermal development projects related to land acquisition. The existence of land in an energy development project, both oil and gas and geothermal is very important because of the following:

1. Land is required as the footprint or base to build any infrastructures to support the project.
2. Land is one of the main assets that will be included in the list of company assets when the project assessment is carried out.
3. Land is an asset that will survive during a natural disaster or other force majeure where other assets such as buildings, equipment, and other physical goods may be lost during a natural disaster (flood, landslide, earthquake, etc.).

Failure to manage the land acquisition process can result in rejection by the local community and lead to project delays that can adversely affect the economic project.

Research Objectives

The objectives of this research are:

1. To develop a list of land usage in a geothermal development project in Indonesia, with focus on the exploration phase.
2. To recap several case studies in Indonesia related to land acquisition.
3. To review the law in Indonesia that regulate land acquisition.
4. To summarize land acquisition process for geothermal exploration project in Indonesia.
5. To create a list of potential challenges that might be encountered in the land acquisition process.

METHODS

This study uses the literature review method combined with the experience of the authors in managing land acquisition activities in several geothermal projects in Indonesia.

LAND ACQUISITION OBJECTIVES IN GEOTHERMAL EXPLORATION PROJECT

The purpose of land acquisition in a geothermal exploration project is for the construction of supporting infrastructures, which are discussed below.

Access road

Access road is one of the most important components in any energy development project. Land acquisition at the beginning of the project is generally focused on opening road access from existing road, usually built by the government, to the area of interest where drilling will be conducted (wellpad location).

In general, the width of land required for access roads in geothermal projects ranges from 8 to 15 meters, depending on the needs of the project. The minimum width of 8 meters is based on 6 meters for the road body and 2 meters for drainage construction on both sides of the road. If taking into account the need for future steam pipe construction then the cleared land may reach a width of 15 meters.

Land acquisition for access road needs not only to open new road but also to improve or expand existing road. This is to facilitate the mobilization of drilling rig equipment. Land acquisition for an existing road is usually required to widen the road body and modify the bend to allow drilling rig equipment to maneuver.

In planning and land acquisition for access road, geothermal developers in Indonesia will coordinate with the local public works office especially if there are modifications to the existing road that owned by the local government.

Wellpad

Wellpad or drilling site is a component that is also important since it facilitate the wells as the main asset in geothermal development projects. The area of land needed for the wellpad depends on the type of well to be constructed. Total depth and well diameter will affect the type of drilling rig used, and ultimately affect the required wellpad area.

In general, at the exploration stage of two well types that are often chosen by geothermal developers in Indonesia are standard hole and slimhole well types (Figure 1). While the comparison between the size and layout of the typical wellpad of both types of exploration wells is shown in Figure 2.

Basecamp, warehouse and site office

In the early stages of a geothermal project, these three facilities should be integrated in one location to facilitate monitoring and communication among personnel. Basecamp is an area for living facilities consisting of containers equipped with beds and bathrooms for site personnel from outside the region.

Warehouse is used for storage of all drilling materials such as casing, liner, wellhead, cementing material, drilling fluid material. While site office is the working space established near the project site.

The area of land required for basecamp, warehouse and site office depends mainly on:

1. The number of drilling rigs operated - the addition of rig numbers will increase the number of personnel to be facilitated so that the area of the basecamp will also increase.
2. Stock of drilling materials, especially casing to avoid downtime due to wait-on-material. The higher number of casing stock stored in the warehouse, the wider basecamp required.

Staging area

This facility is used as temporary storage of various materials used for well construction or drilling operation. Usually the location of the staging area is selected in the flat area between the wellpad and the basecamp closer to the wellpad than the basecamp. Some of the expected benefits of a staging area are:

1. Minimize wellpad area - wide wellpad can be optimized for drilling equipment and materials to be used within 1-2 days ahead only. Other materials that will not be used in 2 days can be stored in the staging area.
2. Reduce the risk of downtime or non-productive time (NPT) due to wait-on-material. Often basecamps, warehouses and site office are located close to the city center or sea port.

The area of land needed for the staging area is usually much smaller than the basecamp and wellpad area, which ranges between 1,000-5,000 m^2.

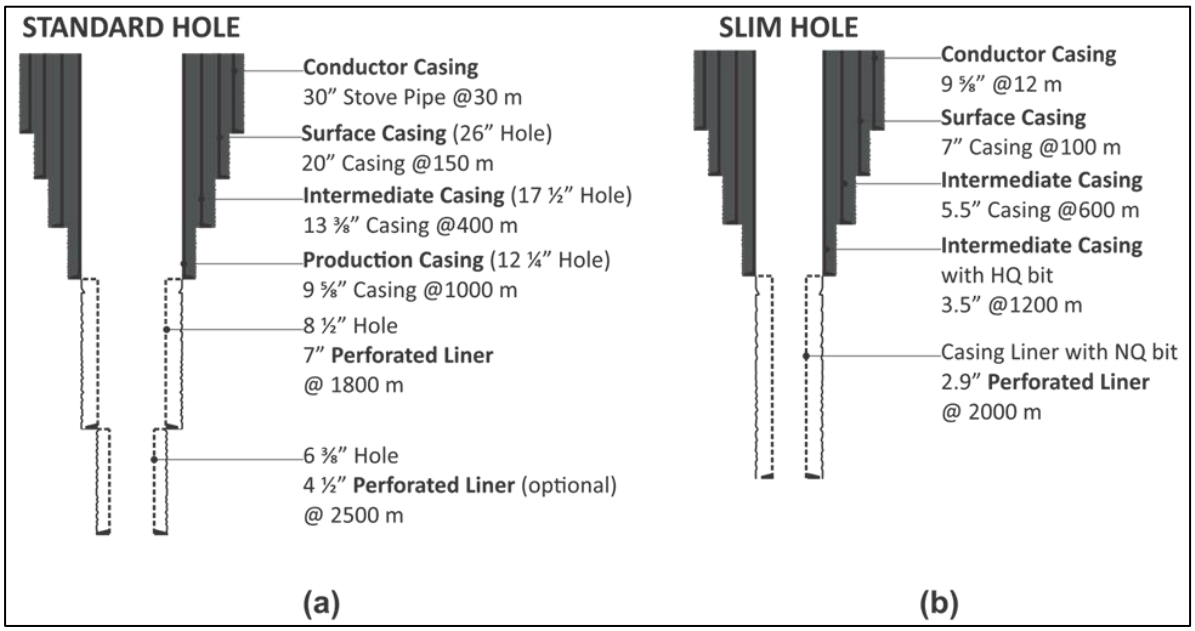


Figure 1: Comparison between two well types commonly utilized in geothermal exploration in Indonesia (a) Standard hole (b) Slim hole

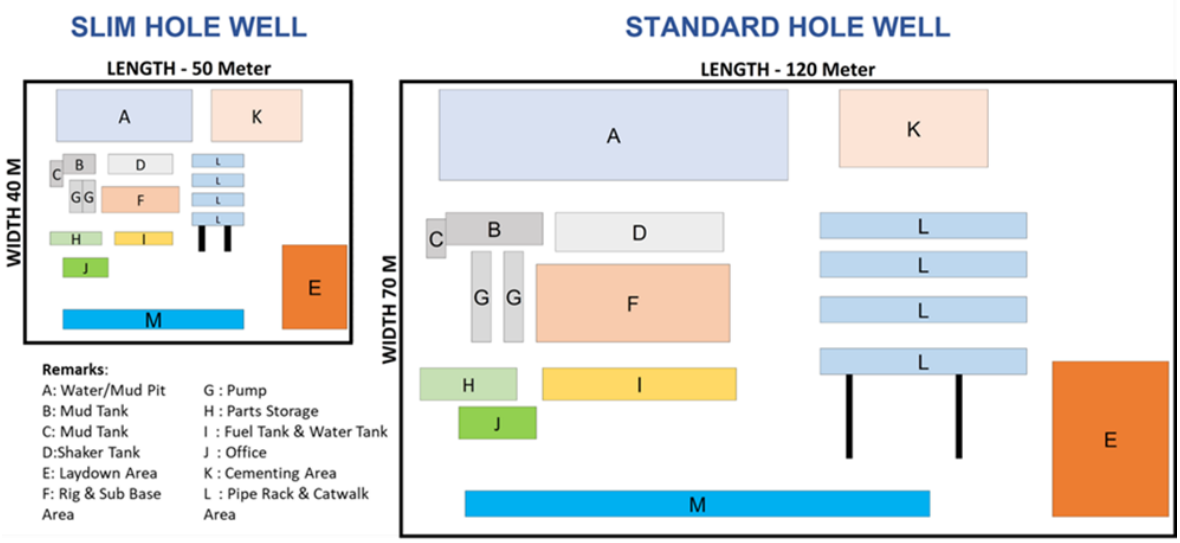


Figure 2: Comparison between wellpad size and layout of standard hole and slim hole

Soil disposal site

Indonesia geothermal systems are located in high-relief terrain and are associated with volcanic activities. This condition often makes earthwork on a site more difficult to achieve a cut-to-fill balance. It is likely that more soil or dirt will be unused and require a facility or site to dump the excess dirt.

REGULATION RELATED TO LAND ACQUISITION IN INDONESIA

Some of the law and regulation applicable in Indonesia related to land acquisition are as follows:

Forestry area

1. Law No. 5 of 1960, regarding Agrarian Principles.
2. Law No. 41 of 1999 as amended by Law No. 19 of 2004, regarding Forestry.
3. Government Regulation No. 44 of 2004, regarding Plan on Forestry.
4. Government Regulation No. 45 of 2004, regarding Forestry Protection.
5. Government Regulation No. 6 of 2007 as amended by Government Regulation No. 60 of 2009, regarding Forest Management and Forest Management Planning.
6. Government Regulation No. 76 of 2008, concerning Rehabilitation and Reclamation of Forestry.
7. Forestry Minister Regulation No. P.50 of 2016 regarding using and borrowing forest area guidance.
8. Memorandum of Understanding between Ministry of Forestry No. NK.16/Menhut-II/2011 and Ministry of Energy and Mineral Resources No. 7662/05/MEM.s/2011 concerning Acceleration on Geothermal Activity Exploration Permits Within Production Forest, Protected Forest, and Conservation Forest Area.
9. Internal Affair Ministry Regulation No. 5 of 1974 regarding rules of land provision and handover for company's interest.
10. Bupati or Local Government Decree in each district regarding agricultural and growing plants quality pricing;

Non-forestry area

1. Law No. 5 of 1960, regarding Agrarian Principles.
2. Law No 30 of 2004 as amended by Law 2 of 2014 regarding Law of Notary.
3. Law No. 11 of 1974, regarding Water Resources.
4. Law No. 26 of 2007, regarding Spatial Arrangement.
5. Presidential Decree No.34 of 2003, regarding Policies on Land.
6. Presidential Regulation No.10 of 2006 regarding National Land Body.
7. Ministry of Land/Head of National Land Agency Regulation No.5 of 2015 as amended by Ministry of Land/Head of National Land Agency Regulation No. 19 of 2017 regarding the procedure to obtain location permit.
8. Bupati or Local Government Decree in each district regarding agricultural and growing plants quantity pricing.

IFC Performance Standards

Other than these listed regulations, there is also IFC (International Finance Corporation) performance standards, which are sets of performance standards and guidance notes on land acquisition, created based on the Wold Bank's Equator principle. In the land acquisition activities, the geothermal developer or local government could opt to comply with the standards set out by the PS5 of IFC, in order to satisfy the requirements of World Bank for financing matter.

The basic principles of the IFC Performance Standards can be summarized as follow:

1. Livelihood restoration of displacement (physical and/or economical) as a direct impact of the project.
2. Prior and informed consent to affected parties.
3. Willing buyer-willing seller principle.
4. Compensation of land and others asset to be calculated at market value plus the transaction costs.

Utilization by local community

The flat areas are already utilized by the local community for farming or housing. The process of compensating for the livelihood of a family in rural areas in Indonesia is often not easy, especially if the land is the only asset they possessed. It is common in volcanic area in Indonesia; the local people use flat areas of land for plantations or rice paddy.

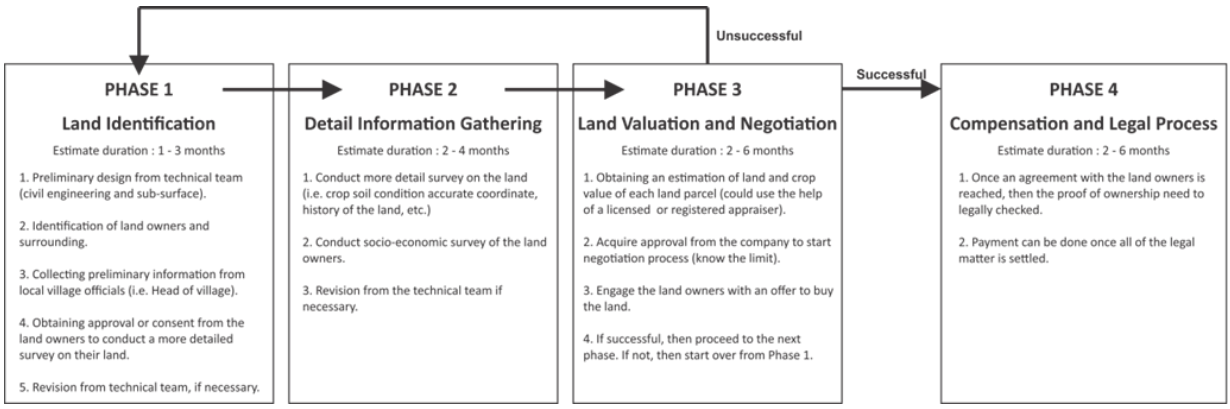


Figure 3: One option of land acquisition process that may be implemented in geothermal exploration project in Indonesia

LAND ACQUISITION PROCESS

Based on the literature review, there is not yet any written detail guideline from the Indonesian government related to land acquisition process specifically for geothermal project in Indonesia. Therefore, any geothermal developer in Indonesia may develop their respective procedures while still referring to the applicable regulations listed earlier.

Authors of this study propose a general process of land acquisition in a geothermal exploration project as illustrated in Figure 3.

POTENTIAL CHALLENGES IN LAND ACQUISITION IN INDONESIA

Some of the challenges that may be encountered in the land acquisition process in Indonesia are discussed below.

Difficulties in finding flat area

As has been discussed earlier, Indonesia geothermal systems are mostly located in the high-relief terrain which makes it difficult to find a relatively flat area to build any supporting infrastructure.

The mitigation option for this risk is to purchase a larger area of land to allow the engineering team to perform earthwork and construction on the sloped soil by considering safety (i.e space to build slope or staging level and construct proper drainage system).

The mitigation option for this is to allow sufficient time for the land owner to pass through the transition period from one source of livelihood to another. The negotiation process will usually be difficult if the land buyer (geothermal developer or local government) imposes a tight schedule for the landowner to move immediately from the land they have worked on for years.

Located inside National Park area

Setiawan (2014) mentioned that the overlap with conservation/protected forest land is still around 41.6% of the geothermal potential is in the area of protected forests or conservation areas. Whereas in the existing rule, geothermal development is not possible to be done in that area since geothermal is still regarded as the mining industry according to Geothermal Law, and based on the rules in the field of forestry, mining cannot be done in the protected forest or conservation areas.

Mitigation options for this situation are by skewing slopes from nearby locations outside the National Park boundary. If skewed drilling is not possible because it is too far, it should be discussed with the central government in this regard.

PATH FORWARD

This study is still in preliminary and still stages will be continued by collecting best practices from various land acquisition cases in Indonesia within the geothermal project. The ultimate goal of this study is the creation of a proposed land acquisition handbook that can be implemented in geothermal energy development projects in Indonesia.

REFERENCES

Bertani, R. (2016), "Geothermal power generation in the world 2010–2014 update report", *Geothermics*, 60, 31-43.

Darma, S., Poernomo, A., Pramono, A., Brahmantio, E. A., Kamah, Y., and Suhermanto, G. (2010), "The role of Pertamina geothermal energy (PGE) in completing geothermal power Plants–Achieving 10,000 MW in Indonesia". Paper presented at the *Proceedings World Geothermal Congress 2010.*

Fauzi, A., Darma, S., and Siahaan, E. E. (2005), "The role of Pertamina in geothermal development in Indonesia", Paper presented at the *Proceeding World Geothermal Congress, 2005.*

Hochstein, M. P., and Sudarman, S. (2008), "History of geothermal exploration in Indonesia from 1970 to 2000", *Geothermics*, 37, 220-266.

Ibrahim, R. F., Fauzi, A., and Suryadarma. (2005), "The progress of geothermal energy resources activities in Indonesia". Paper presented at the *Proceeding World Geothermal Congress*, 1-7.

MEMR (2017), "Pemerintah optimis capai target kapasitas terpasang panas bumi pada tahun 2017 [Press Release: The government is optimistic to achieve geothermal installed capacity target in 2017]", Ministry of Energy and Mineral Resource. Retrieved from http://ebtke.esdm.go.id/post/2017/10/09/1771/pemerintah.optimis.capai.target.kapasitas.terpasang.panas.bumi.pada.tahun.2017.

Poernomo, A., Satar, S., Effendi, P., Kusuma, A., Azimudin, T., and Sudarwo, S. (2015), "An Overview of Indonesia Geothermal Development – Current Status and Its Challenges". Proceedings World Geothermal Congress 2015.

Suryantoro, S., Dwipa, S., Ariati, R., and Darma, S. (2005), "Geothermal deregulation and energy policy in Indonesia", Paper presented at the *Proceedings World Geothermal Congress 2005*.

Setiawan, H. (2014), "Geothermal Energy Development in Indonesia: Progress, Challenges and Prospect". International Journal on Advanced Science Engineering Information Technology Vol. 4 (2014) No. 4 ISSN: 2088-5334.

ThinkGeoEnergy. (2018), "Top 10 geothermal countries based on installed capacity – year end 2017", Retrieved from http://www.thinkgeoenergy.com/top-10-geothermal-countries-based-on-installed-capacity-year-end-2017/.

DRILLING MANPOWER AND EQUIPMENT TRANSFER FROM PETROLEUM TO GEOTHERMAL INDUSTRY: A PRELIMINARY STUDY ON SKILL ASSESSMENT

Mukhamad F. Umam[1,2], Dorman P. Purba[2], Daniel W. Adityatama[2], and Bart Van Campen[2]

[1]PPSDM-Migas Kementerian ESDM, Cepu, Indonesia
[2]The University of Auckland, Auckland, New Zealand
Email: mukhamad.umam@esdm.go.id

ABSTRACT

Indonesia has vast geothermal energy potential, estimated at around 27,000 MWe or about 40% of world geothermal reserves (IEA, 2008). However, up to 2017, Indonesia's geothermal power plant installed capacity was only 1,805 MWe or 6% of this estimated potential. To keep up with high growth of electricity demand while trying to reduce the use of fossil fuel power plant, the Government of Indonesia (GoI) aims to have 7,241.5 MWe geothermal power plants installed capacity by 2025, or around 5,433 MWe increase in 7 years. In line with such an almost four-fold increase in installed capacity, the availability of human resource in geothermal industry is becoming more crucial both quantitatively and qualitatively. This includes drilling experts and crew as well as geoscientists and power plant operators. In order to provide such an increase in manpower in a limited timeframe, many geothermal developers in Indonesia choose to recruit experienced manpower from similar industries such as the oil and gas due to a degree of similarity between these industries, especially in drilling. However, this paper will argue that such an approach might lead to safety and operational issues as these workforces often use the same common practice in their previous industry without realizing that there are several fundamental differences between drilling in geothermal and petroleum. The first part of this paper will map the current Indonesia geothermal drilling human resource condition and the existing skill gap, including a quantity estimate of human resources required. Subsequently, this study will highlight the fundamental differences in drilling on those industries to give better understanding on manpower requirement in geothermal. Several studies or publications and Indonesia competency standards will be discussed and compared to identify the current condition in Indonesia. Several approaches related to human resource capacity building are discussed in this paper to help fulfil the existing gap in geothermal industry and support the Government of Indonesia target in 2025.

Keywords: Skill assessment, safety and operational issues, drilling manpower.

INDONESIA'S GEOTHERMAL RESOURCE POTENTIAL AND CURRENT ENERGY MIX

Most sources agree that Indonesia has one of the highest geothermal energy potential in the world. This enormous potential is, however, not fully utilised with only 6% of its maximum estimated potential are currently installed. The target from the GoI is to have 7,241.5 MWe geothermal installed capacity in 2025. Figure illustrates the progress of geothermal power installed capacity from 1983 and the projected installed capacity in 2025. To achieve this target, the GoI issued a number of geothermal regulations to improve and accelerate geothermal power development such as the National Energy Policy (KEN). KEN is described in Government Regulation No. 79 of 2014 on national energy policy. The government targets energy independence and national energy security that is achieved by realizing the development of technological capabilities, energy industry, and domestic energy services in order to be independent and increase the capacity of human resources to create jobs.

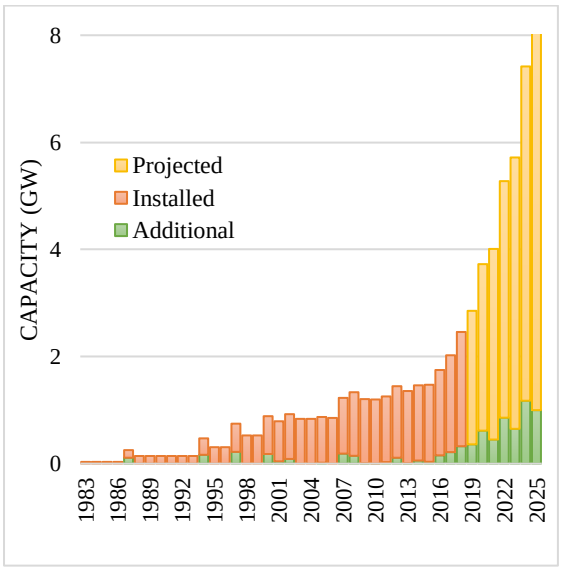


Figure 1: Installed, additional (some are planned) and projected capacity of Indonesian geothermal power plant from 1983 to 2025 (Adapted from Darma et al., 2010; Darma et al., 2015; RUEN, 2017; MEMR, 2017)

One of the national energy policy targets for the fulfilment of energy supply and energy use is the

achievement of optimal primary energy mix in 2025, with the intended share of new energy and renewable energy of at least 23%, a share of petroleum of less than 25%, with coal at 30%, and natural gas at 22%. Furthermore, by 2050, the share of new energy and renewable energy is targeted at least 31%, as long as its economy is met; with petroleum at less than 20%, coal at least 25% and the role of natural gas is at least 24%.

The government is also encouraging and strengthening the development of the energy industry in order to accelerate the achievement of energy supply and energy utilization targets, strengthening the national economy and the absorption of employment, including by increasing domestic capability to support geothermal exploration and electricity supporting industries. One plan is to strengthen the field of research, development, and implementation of energy through the preparation and upgrading of human resources capability and application of technology and safety in the field of energy and improvement of the mastery of domestic energy technology through the research, development and application of energy efficient technology.

Indonesia's national energy policy is mentioned above and further described in the Presidential Regulation of the Republic of Indonesia Number 22 Year 2017 About the General Plan of National Energy (RUEN). The National Energy Board (DEN) as the drafting body of RUEN performs a series of modelling exercises as a reference in energy development in Indonesia until 2050. The result of modelling of primary energy supply shows that geothermal contribution to New and Renewable Energy (EBT) supply is 21.8 MTOE or 23.6% in 2025 and 58.8 MTOE or 18.6% by 2050. While the modelling results of the development of EBT power plants show geothermal generating 7,241.5 MW in 2025 and 17,546 MW in 2050 or 59% of the geothermal potential of 29.5 GW. However, this RUEN does not specify much about the development of human resources as a step to achieve the target of geothermal power plant development (PLTP). Strategic steps for the development of PLTP according to RUEN include improving the quality and quantity of potential resources and geothermal resource surveys, preliminary survey and exploration assignments by government agencies or business entities and assignments of State-Owned Enterprises (BUMN) or Public Service Bodies (BLU) to develop PLTP.

INDONESIA'S GEOTHERMAL AND OIL AND GAS MANPOWER

Estimated Numbers – Current and Future

The number of personnel requirement for geothermal development are logically aligned with the installed capacity. Jennejohn (2010) estimated that each MW capacity will create 4.25 full-time positions and 16 person*years for direct, indirect, and induced employment. Hence, the 5,433 MW requirement until 2025 will create approximately 23,000 jobs with 87,000 person-year employment. These staff include geologists, geophysicists, geochemists, drillers, engineers, hydrologists and other skilled personnel for operations and maintenance to be prepared before embarking on a geothermal field development project (Smillie et al., 2015).

On the other hand, SKK Migas (2016) projected that oil production will drop 6% annually from 786 thousand barrels in 2015 to less than 520 thousand barrels per day in 2020 and beyond. This decline in production will obviously affect to the number of workers in the oil industry. For example, during the recent drop of oil price in 2014 to 2017, about six thousand people or 5 % of worforce lost their jobs in upstream oil and gas industry as shown in Figure 2 (SKK Migas, 2017).

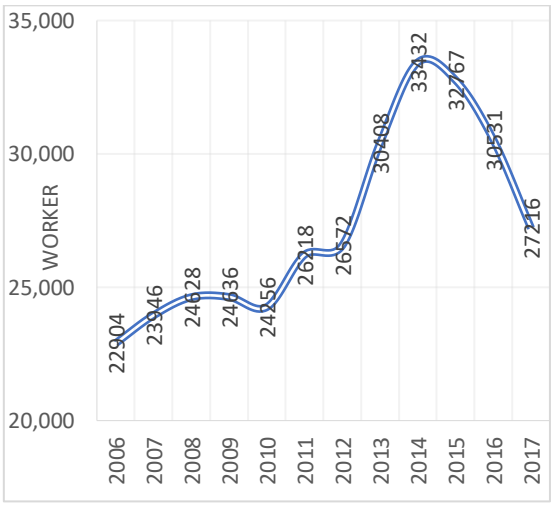


Figure 2: Workforces in upstream oil and gas industry from 2006 to 2017 (adapted from SKK Migas, 2017)

How to Fill This Needs: Current Strategy and Proposal

The conventional way to fill the geothermal personnel needs is by training and development of newcomers into qualified professionals. This can be done by formal education in vocational schools, polytechnics, and universities to introduce scientific aspects of the use of geothermal energy in the school curriculum. This can also be accomplished by training and certification in an accredited and standardized training center. However, this method has some drawbacks, especially the length of time it takes to train a skilled workforce that is ready to work. Another shortcoming is the limited geothermal training programs available in Indonesia for young staff to become experienced.

A study on human resource development and program strategy for geothermal energy in Indonesia was conducted by East Harbour Energy (EHE) in 2015. One of their proposal is to recruit and retain existing human resources from similar industries such as oil and gas. This paper proposes to implement this method to fill the staff needed to support rapid geothermal development in Indonesia.

DIFFERENCES OF OIL & GAS DRILLING WITH GEOTHERMAL DRILLING

Drilling is one of the most important and costly phases in the development of both petroleum and geothermal fields. Anderson et al. (2011) estimates that drilling for exploration and production accounts for more than 42% of total geothermal development costs. Petroleum drilling technology was developed since more than 150 years ago, while the first geothermal well was drilled in the early 20th century. Hence, geothermal drilling adopts many technologies from petroleum drilling. The ability of the drilling engineer to identify the various challenges in drilling is a key factor in the success of this operation.

However, petroleum and geothermal drilling is not exactly the same in all respects. Indeed, Tilley et al. (2015) found that geothermal drilling commonly takes longer and spends more money for the same depth due to harder rock and a bigger hole. The main difference between the two is the location and type of resources where geothermal fluid – often occurs in fractures and cracked hard volcanic formations – while petroleum is in the pore space of sedimentary formation (Capuano, 2016). Until recently, most geothermal drilling used equipment and an experienced workforce from oil and gas drilling. Several significant differences between drilling condition in oil and gas industry with geothermal are described below.

Drilling Conditions

Rock Formation

Oil and gas drilling targets porous sediment formations consisting mostly of sandstone and mudstone, so that drilling is relatively uncomplicated and fast in terms of penetration. These sediments are formed by erosions such as clay or sand and weathering of rocks by biochemical activity such as calcareous rocks or may also be formed from the evaporation of salts and gypsum from old lagoons buried beneath rock layers. This is formed respectively due to the compression, heating and packing of natural rocks, which from time to time makes the initially loose sediment into solid rock. Furthermore, tectonic-related geological processes produce folds that can lead to the formation of mountain ranges and major sea trenches leading to the formation of anticlines, synclines and fractures where oil and gas can be trapped (Rouzaut et al., 2011).

On the other hand, geothermal liquids usually form in pathways such as fractures and faults in igneous and hard metamorphic rocks due to the establishment of volcanic formations. In geothermal drilling, Watson (2013) explains that various types of rocks that are expected to be encountered include strong fragile rocks in compression but weak in tension, and rocks with cracks arising from stress concentrations due to imperfections in the microstructure of stones such as rhyolite, andesite, diorite and greywacke. Moreover, another concurring structure that can be used as a geothermal drilling path is secondary mineralization rock, which has changed due to geothermal fluid flow, so that the rock becomes plastic and easily defective.

Geothermal regions are formed due to tectonic pressures that produce faults and fractures within a wide range. The presence of faults and fractures indicates a large permeability, but often leads to loss of circulation, which is a major problem in geothermal drilling. Another obstacle is that existing fractures may extend naturally and may also form during drilling as a result of pressure on the hole and may occur throughout the wellbore. Thus, the main distinctions of geothermal drilling and petroleum drilling are geological complexities in geothermal reservoir environments and poor geological map capabilities that make exploration drilling for geothermal development wells relatively blind (Tilley et al., 2015). Moreover, poor interconnection of geothermal rocks and hard volcanic igneous rocks that may exist from the surface to the total depth will affect the selection of the bit and rate of penetration (ROP). As a result, drilling equipment for oil and gas exploration will not provide the same results in geothermal exploration (Capuano, 2016).

Reservoir Pressure

Reservoir pressure in oil and gas drilling can be very high due to compaction effects, diagenetic effects, differential density effects and fluid migration effects (Bourgoyne et al., 1985). Devold (2013) explains that the pressure from the oil and gas reservoirs can reach 90 MPa, but the specific crude oil weight of 790 to 970 kg per cubic meter will reduce the pressure on the wellhead to one MPa per 100 meters depth of the well. As a result, the wellhead's static pressure is much lower and will decrease further due to production.

In geothermal drilling, however, reservoir pressure is usually inferior or might be lower than hydrostatic pressure compared to a hydrocarbon reservoir, because the stored fluid is still liquid. The pressure will be formed when the liquid phase turns into a gas. Tilley et al. (2015) asserted that the very low

occurrence of this low pressure added with the fault could cause other problems such as lost circulation of drilling fluid during drilling and cementing operations with a probability of 33-50%.

In summary, the use of mud as a drilling fluid in geothermal drilling may not be feasible due to sub-hydrostatic pressure in the reservoir. In addition, the mud may cause irreversible formation damage by reducing or destroying permeability if the mud gel is lost to productive fractures. Thus, it is recommended to use pressurized air, aerated water or mixed mud as drilling fluids for geothermal drilling (Capuano, 2016).

Reservoir Temperature

In contrast to reservoir pressure, typical temperatures in petroleum reservoirs are usually lower than geothermal wells. Although oil and gas drilling tools have temperature limitations, this is commonly not used as a constraint parameter due to the flexibility of drilling fluid selection. Oil and gas usually form at depths of 3000-4000 meters, but the depth of the oil wells can be over 6,000 meters, while the temperature in the reservoir increases with increasing depths of up to more than 200ºC (Devold, 2013).

On the other hand, the geothermal reservoir formation at the same depth is hotter than the sediment formation of most oil and gas reservoirs with temperatures from 160°C to above 300°C. Finger & Blankenship (2010) explain that common types of rocks in geothermal reservoirs are hot, hard, abrasive, heavily cracked and under pressure. The rocks are mainly granite, granodiorite, quartzite, greywacke, basalt, rhyolite and volcanic tuffs. This condition indicates that geothermal drilling is more challenging due to a low penetration rate, fast bit rate and fast corrosion rate.

The high temperature factor in the geothermal environment poses a challenge in drilling and other geothermal operations, as it may present a risk of blowout and boiling that should be included in geothermal development designs (Tilley et al., 2015). The high temperatures of the geothermal reservoir could also cause a rise in the drilling fluid temperature as it comes back to the surface. Hence, the quality and durability of cementing, casing, drilling tools, materials and equipment must be able to withstand these temperatures.

These aforementioned dissimilarities in drilling conditions infers that there are also differences in drilling methods and tools and equipment involved. These differences, if not fully understood by the drilling personnel, could lead to potential problems in the drilling operations. Table summarizes the differences in geothermal drilling and petroleum drilling.

Due to the aforesaid distinctions, the drilling methods and challenges might not be exactly comparable. The distinct drilling operations also raise particular risks or hazards in geothermal drilling. Therefore, workers who want to move from oil and gas to geothermal drilling must be sure to have sufficient competency to avoid risks that can lead to accidents, and financial and time losses of developments on a wider scope.

Table 1: Summary of drilling in petroleum and geothermal.

Parameters	Petroleum	Geothermal
Rock formation	Mostly sandstone/ mudstone, sedimentation layer	Igneous & hard metamorphic rock (e.g. rhyolite, andesite, diorite, etc.)
Reservoir pressure	High (might reach 90 MPa).	Relatively low, might be lower than hydrostatic pressure.
Reservoir temperature	Up to 200°C, relatively low	High temperatures (160°C to above 300°C)
Drilling fluid	Bentonite blends	Aerated mud or water with air or nitrogen mixture
Drilling bits	Typically, Polycrystalline Cutter (PDC)	Roller cone or drag bits, impregnated diamond bits
Drilling orientation	Vertical, deviated, horizontal	Typically, vertical or J-shaped, horizontal drilling is unlikely
Casing	perforated production casing	Slotted liner, large diameter casing
Cementing	protecting casing from hydrocarbon corrosion	Limit casing transformation / deformation due to high temperature, prevent thermal fatigue
Completion	perforating and swabbing with NaCl salt water	Slotted liner installation and swabbing with brine

Potential Problems in Geothermal and Petroleum Drilling

Loss of Circulation

Geothermal drilling is notorious with lost circulation or significant mud loss because a geothermal production zone is one with high permeability that allows unlimited flow of water or steam. A highly permeable, cracked and faulted formation is a feature of a geothermal reservoir so that a convective geothermal hydrothermal system can form. However, the loss of circulation often occurs in the formation above the reservoir, as most of the geothermal systems are in areas with high cracks resulting in partial or complete loss of drilling fluid

circulation in geothermal drilling (Finger and Blankenship, 2010). This drilling with no return is called blind drilling.

Protection of effective loss zones from damage becomes an important aspect in drilling and completion of geothermal wells. Lost circulation is an expensive and common problem encountered in geothermal drilling. Common loss circulation prevention is to maintain proper mud weight, maintain hole cleanliness and install casing to protect weak formations. Other possible solutions are by adding a small mixture of bentonite and LCM (Loss Circulating Material) to drilling mud or sealing an unproductive loss zone with cement (Tuttle, 2005).

If the prevention fails, then drilling is usually continued by blind drilling with water, or by using more sophisticated techniques of air drilling or aerated fluid drilling. In addition to minimizing formation damage, water drilling also reduces the cost of expensive mud losses into formation and improves drilling rates despite the casing in the lost circulation zone needing to be strengthened. Habtemariam (2012) cautioned that circulatory loss could lead to some risks in drilling such as a stuck drilling pipe due to non-returning cutting back to the bottom hole assembly and a blowout caused by decreasing fluid levels in the wells to form liquids, gases and vapours.

Stuck Pipe Mechanism

Pipe sticking is the most common challenge in both oil and geothermal drilling where drill strings cannot be lowered or rotated due to various causes. This chapter will explain some of the causes of sticking including mechanical, pressure differences, caving, key seats, unconsolidated formations, bailing and other issues that make hole cleaning, cementing, casing or liner jobs extremely difficult.

Mechanical pack-off

Mechanical sticking is the attachment caused by cuttings and pieces collected above the drilling unit. The cause is cutting that fails to be lifted by drilling fluid due to lost circulation, an unstable borehole or degradation of the well bore by drilling fluid. The accumulation of cuttings may also occur in wells with non-solid and easily collapsing drill holes such as directed or horizontal wells. This is a common issue in geothermal drilling whenever the hole deviates from straight downwards. In a weak formation, there will be a tendency of gravel debris formation, especially limestone with variations in size from gravel to large stones. The indication of sticking can be seen from the increased pressure of the circulating pump, an increase of torque, drag in pulling out the drill string and stagnant ROP.

The solution to mechanical sticking is to keep the drill hole clean during operation by means of liquids or mixtures with appropriate density, rate, viscosity, and high rotation speeds on deviated drilling. Habtemariam (2012) adds minimizing surge pressure and using low-pressure circulation to clear the hole. However, if the sticking cause is a fault or crack formation then the solution is to work up and down the drill string to break the formation debris.

Caving

Caving, otherwise called caving sloughing is the collapse of the borehole when drilling penetrates unstable formations that easily collapse. The sloughing or unconsolidated formation can collapse around the drill pipe to make it stick, complicates the cleaning of the hole, and can make a hole with a very large diameter like a cave, so fluid velocity decreases (Finger & Blankenship, 2010). In drilling of oil and gas wells, this is more common, especially when meeting shale. Shale formations can flow plastic materials inward or downward causing mechanical stickiness. This plastic behaviour may also have found at salt formation. Each formation can collapse if the weight of the mud is not high enough to control it. Indications of this problem are increased pump pressure, increased drill powder or cutting, drag and bridges, increased torque, bit balling and increased mud viscosity (Habtemariam, 2012).

To minimize the occurrence of caving, the use of mud must be properly designed both in density and viscosity to hold the wall of the borehole so as not to collapse. Habtemariam (2012) added that all clay rocks tend to peel so caving should be prevented and eliminated. He suggested that prevention could be done by reducing filter losses from drilling mud, using calcium chloride drilling mud to increase formation strength, speeding up drilling processes in sensitive formations and isolating sensitive formations.

Key seats

Key seats commonly occur on deviated holes because of the friction of the drill string series with the top of the borehole thus forming the shape of a keyhole if the drill hole is viewed from above. The key seat usually occurs when the BHA is pulled out the hole along the drilling path (Mitchell, 2006). When the key seat occurs, the drill string should work and rotate gradually with minimum stress. Habtemariam (2012) explains that sometimes a tool called a key-seat reamer is installed in the BHA to open enough holes when pulled out of the hole, so that the drill collar can be passed if it encounters a blockage like a key seat.

Key seat prevention could be done by avoiding sharp or dogleg bends with suggested turns. The tighter use of BHA tends to minimize severe dogleg

events, keeps the holes aligned properly, rotates and recycles drill threads whenever possible, increases pumping rates, and minimizes pipe rotation. Designing the BHA carefully minimizes the length of the rat hole under the casing (Habtemariam, 2012). Another solution according to Mitchell (2006) is to pull back the drill pipe from under the key seat and back into the opening so as to drill the key seat that has made the jam.

Different pressure

Drill strings can stick to the wall of the wellbore due to the difference between the drilling fluid pressure and wellbore pressure. In geothermal drilling, it is common to encounter soil layers with less pressure than the cooling water column at the same depth or under pressure, which can cause the pipe to stick to the wall of the wellbore (Finger & Blankenship, 2010). An indication of this occurrence is increased torque, drag, drilling strings failing to rise or fall even though the drill liquid circulation is not disturbed. In oil and gas drilling, the occurrence of stickiness is due to this pressure difference when the drilling meets porous and permeable formation, when the mud is too heavy, so the hydrostatic pressure of the sludge exceeds the formation pressure, and when the mud is less stable due to high water loss or a thick mud cake. This type of sticking can occur on both deviated wells and upright boreholes without any symptoms prior to pinching.

The sticking is due to differential pressure which can be reduced by oil lubrication around the trapped part to reduce fluid loss and help equalize the pressure around the drill pipe, thus reducing the weight of the sludge with filtration or aerated fluid water (Finger & Blankenship 2010; Mitchell, 2006). Another approach is by installing a stabilizer and spiral grooved drill collar on the drill circuit and to keep the horizontal stress value to a minimum to prevent instability of the wellbore (Vollmar et al, 2013). Another solution is to free the drill string immediately by moving the drill string as much as possible, rotating the drill string on the connection, moving the pipe downward, using the grooved or spiral drill collar, thus minimizing the length of the drill collar and BHA (Habtemariam, 2012).

Other Problems

In addition to some of the above-mentioned causes, there are still many causes of pipeline jamming such as string scrapings by foreign objects in drill holes like sledgehammers, farm bars or the use of non-functioning devices. Inefficient balling or flushing on drilling clay formations caused by drilling mud does not carry all cuttings to the surface with some of them remaining united, which could also cause congestion. Furthermore, swelling or blackening of clays may also cause clogged pipes or pushing of ongoing strings. Another cause is the collar or stabilizer that can cause the release of large cement ruptures and falls into the drill holes can make the drill strings to stick because the distance between the casing and collar is not large enough, so that a small piece can make the drill thread to jam.

Drillers should anticipate these problems before commencing drilling operations so that they are ready with solutions. According to Habtemariam (2012), the rubbish problem can be solved by ensuring the bottom hole is in good condition, checking downhole equipment regularly, being careful when working on the rotary table and leaving the hole closed when the drill string comes out of the hole. Other precautions are drill-level controls to ensure the holes are cleaned, circulating the bottom to the net shaker and maintaining proper drilling fluid properties. The driller should also recognize any increased pulling force, always reciprocating and rotating the pipe during circulation, increasing the mud weight for constriction of the hole due to plastic flakes, fresh water circulation for saline hole strikes (Mitchell, 2006), enlarging drill diameters to prevent sticky casing from clay swelling and to control annular velocity. On suspicion of clashing, the driller should direct the drill string up and down to try to release the blockage gradually until the free drill string is freed.

Directional Drilling

Directional drilling has long been applied in geothermal, oil, and gas drilling. However, in the oil and gas industry, deviated drilling can reach more than 80 degrees – commonly called horizontal drilling. The horizontal drilling purpose is to maximize the production of hydrocarbons. Tilley et al. (2015) asserted that exploration and geothermal development in the future can clearly utilize horizontal drilling to cut off sub-vertical fractures better with the support of directed drilling tools and high temperature resistant electronic systems.

According to Nguyen (1996), horizontal wells are drilled when the following three conditions are found in drilling for oil and gas. First, when vertical fractures are dispersed and rarely found in cracked reservoirs. Second, when there are thin beds with a thickness of less than 15 to 20 meters, especially if there is a gas cap or underlying aquifer. Third, in having tight formations when the plane fracture can only be opened by hydraulic fracture work. Horizontal well drilling is often required to reach the subsurface, while laterally away from the point at which the bit enters, and also to reach different parts of the structure and achieve higher production (Devold, 2013).

For geothermal wells, it is important for the wellbore to cut as much as possible from the fault formation. However, because of topography, for example, the drill rig cannot be precisely above the geological target. Hence, several wells can be drilled from one

prepared location and then directed to the intended fault. In practice, the deviation of the drill string will increase the torque and drag resulting in a limited depth of the well (Finger & Blankenship, 2010). A well-shaped S or J-shaped well is widely used in the geothermal industry, but only by selecting the right material that can withstand high temperatures and the angle of well deviation (Capuano, 2016).

Well Control

Well control is the prevention of formation fluid entering into the borehole due to the hydrostatic pressure of the drilling mud being less than the pore pressure and releasing it safely if it enters the wellbore. Well control is crucial for successful drilling operations, so it should be well planned with proper casing design, precise action when drilling begins and prompt and precise reactions to unexpected events that may harm the well. Formation fluid will flow into the wellbore as the pore pressure is higher or over pressure because the high and shallow temperature of the static head of the drilling fluid in the cracked or permeable layer is called a kick. If this kick is not properly controlled it can lead to catastrophic and costly blow out disasters and can even result in loss of life, equipment, and drill rigs, as well as damage to the environment (Finger & Blankenship, 2010).

Oil and gas wells have high pressure so must be controlled by a weighted drilling fluid, but most geothermal fields have a lower pore pressure characteristic and less liquid pressure in a fully drilled well, so the drilling fluid into a well is called a drill loss circulation.
The key to controlling the kick is to have an appropriate chassis arrangement depth to allow closure of the well in the event of a kick at an early stage. This is especially important for preventing deadly toxic gases such as H2S that they may carry. In most oil and gas drilling, gas zones are formed over reservoirs but in geothermal drilling, gas zones may form on fractures along drilling, both shallow and deep, so many of these possibilities are undetectable. Killing drilled wells is done by inserting cold drilling mud into the hot fracture zone to prevent hot steam or lethal gas from penetrating to the surface. Each kick should be treated as a gas kick, since it is not usually known whether it is gas or hot liquid until it is confirmed otherwise (Vollmar et al., 2013).

The main indicator for detecting kicks by Finger & Blankenship (2010) is by comparing measurements of inrush and drill outflows. The kick occurs when the outflow reading is greater than the inrush. Conversely, there is lost circulation when the inrush readings are larger than the outflow. Another method is to anticipate the flow coming from the well, whether it is mixed with gas, or if the temperature rises quickly or the rate of penetration of drilling becomes faster. The cause of unexpected steam or gas flows may be due to the temperature and formation pressure in the drilling plan being too low.

To avoid damage to formation and clogging of geothermal reservoirs with a dry vapour source, drilling generally uses air where drilling returns are air plus steam from the reservoir. Vollmar et al. (2013) assert that because the vapour runs out of the atmosphere, the temperature only reaches a boiling point for vapour in the atmosphere that is 100ºC or does not exceed the normal BOP rubber work limit of 121ºC.

Location Accessibility

Indonesia's geothermal systems are mostly located in areas with high reliefs and volcanoes with surface manifestations that drain fluid at active boiling temperatures along the volcanic arc (Hochstein & Sudarman, 2015). This is of course a challenge for the development of geothermal fields. The volcanic area produces high slope soils, a variety of hard volcanic rocks such as pyroclastic, lahars, and hydrothermal alteration areas that have potential H2S gas hazards and hydrothermal eruptions. Another challenge is that potential drilling sites are sometimes located in protected forests that are a great distance from access to major roads, thus making it difficult to mobilize drilling equipment. Although located on slopes with crumbly and unconsolidated pyroclastic rock layers, transport traffic will become densely packed where heavy equipment is transported, before, during and after drilling, so the roads require good strength and adequate load capacity.

Unlike petroleum drilling, which is usually located in the lowlands or near the sea, the development of a geothermal drilling platform with a slope of up to 25% is necessary, not to mention the safety aspects associated with soil and hydrothermal changes. Investments in geothermal drilling have become larger in civil works to give higher stability to the platform before starting drilling. To build a drier pad on a slope is usually used by a cut and fill technique where half of the pad is built with filler material to compensate for the excavated area and to build a flat surface.

DRILLING COMPETENCY STANDARD IN INDONESIA

The differences and the specific typical problems in geothermal drilling discussed previously highlight that it is crucial for drilling personnel in geothermal to be fully aware of these factors. One of the paramount tools to ensure and assess the understanding and capability of the drilling workforce is by applying comprehensive competency standards. Hence the existing drilling competency standard in Indonesia must be assessed.

The Indonesian Qualifications Framework (IQF) established by Presidential Decree No. 8 of 2012 is a reference that equates to learning outcomes resulting from formal or non-formal education, as well as learning outcomes gained through work experience. This is the base of the development of a national skills training system and the application of competency standards in the skills training sector as described by the Minister of Manpower and Transmigration (MoMT) decree no. 227 year 2003. As a result, the national skills training system is implemented based on three pillars of a competency-based training system, namely user-defined competency standards, competency-based skills training programs, and competency certification.

Drilling competency standards have been applied in Indonesia since 2007. The application of this standard is not limited to oil and gas drilling. Indeed, the scope is covered for both geothermal and hydrocarbons. Drilling competencies mapping is defined in the decree of the MoMT (2008) and revised by the decree of Minister of Manpower (MoM) (2015). There are five levels or qualifications of personnel that can be gained. The later regulation also divides competencies into three competency types, namely general competencies which consist of seven units, core competencies that consist of 40 units, and the special competencies that consist of three units.

This competency standard is formally deemed applicable for both drilling sectors, namely oil and gas drilling and geothermal drilling. The share of competencies for both areas can facilitate the transfer of labor from one sector to another. On the other hand, since the competency units in this standard are developed from the oil and gas sector, the holders of the qualification, in practice cannot be directly employed in the geothermal sector, despite having the qualification. E.g. oil and gas staff might misinterpret problems such as a stuck pipe and loss of circulation mechanisms inappropriately without proper training on geothermal drilling. Thus, this could lead to lengthy drilling time or drilling failure in severe cases.

This paper suggests some additional learning program of geothermal drilling to be developed and delivered at universities and training centers. Moreover, separated geothermal drilling standard should also be designed based on its distinction from oil and gas drilling.

CONCLUSION AND RECOMMENDATIONS

There are fundamental differences between geothermal and oil and gas drilling which make the drilling methods and challenges might not be exactly comparable. The geothermal reservoir often occurs in fractures and cracked, hard volcanic formations, whereas the hydrocarbon reservoir generally takes place in the porous space of sedimentary formation. However, these distinctions have not been acknowledged by the drilling competency standards in Indonesia, as there are none that are specific to geothermal drilling.

Generally, there are three types of companies that are involved in drilling operations: drilling contractors, operating companies and service companies. In Indonesia, the drilling contractor and service company both usually work in the oil and gas, and geothermal field. Thus, the shift in environment from oil and gas to geothermal and vice versa is unavoidable. The migration of such workforce is nothing new in drilling industries in Indonesia, despite very little additional conversion training, which can lead to wrong approaches. This migration can therefore also help to provide significant numbers of staff into the geothermal sector.

This paper suggests that learning programs are needed for migration with different durations and materials for each level. The training program would need to include a general geothermal-vs-oil-gas drilling introductory course to understand geothermal characteristics and challenges such as steam kick, waste management, and geo hazards. Furthermore, on-the-job training, supervised work and mentoring are also needed to fill the competencies gap.

In a wider study still to be published, several existing facilities and infrastructures have been identified in Indonesia that could support the conversion program (Umam, 2018). These include government and private training centers, universities with petroleum or geothermal departments, and geothermal companies operating in Indonesia. The mentioned study proposes that PPSDM Migas, as a government training institution, to be utilized to implement the conversion program. PPSDM Migas has the facilities to commence geothermal drilling training and indeed has a mandate from MEMR to promote geothermal training under MEMR-BPSDM's new strategic plan. Currently, PPSDM Migas offers several trainings and certifications for oil and gas drilling qualifications. This center already has some experience in delivering geothermal drilling training for oil and gas workers through a recent course, although this was offered for an engineer's level. Therefore, PPSDM Migas is a suitable organization to facilitate the conversion of drilling technicians and operators from oil and gas to geothermal sectors.

Furthermore, geothermal companies might provide their future employees with on-the-job training and mentoring programs, while universities and training centers could assist the companies by delivering short courses, workshops, and trainings in geothermal drilling. In this way, unemployment

from the oil and gas sector can be reduced while supporting the government's targets in 2025. Thus, the geothermal HRD needs of Indonesia can be met effectively and efficiently.

ACKNOWLEDGEMENT

Authors would like to acknowledge drilling experts from Indonesia and New Zealand for their advices and especially for New Zealand Ministry of Foreign Affairs and Trade (MFAT) for the financial support to study in Geothermal Institute, The University of Auckland, under New Zealand ASEAN Scholarship scheme.

REFERENCES

Anderson, A., Prencipe, L., Todaro, R. M., Cuyler, D., and Eide, E. (2011), *"Federal Interagency Geothermal Activities"*. Office of Energy Efficiency and Renewable Energy (EERE), Washington, DC (United States). Retrieved from https://www1.eere.energy.gov /geothermal/pdfs/ngap.pdf.

Bourgoyne, A.T., Millheim, K. K., Chenevert, M. E., ProQuest (Firm). (1985), *"Applied Drilling Engineering, Society of Petroleum Engineers"*. ProQuest Ebook Central. Retrieved from http://ebookcentral.proquest .com/lib/auckland/detail.action?docID=3405 014.

Capuano, L. E. Jr. (2016), *"Geothermal well drilling. In Geothermal Power Generation (pp.107–139)"*.Elsevier. https://doi.org/10.10 16/b978-0-08-100337-4.00005-x.

Darma S., Harsoprayitno S., Setiawan B., Hadyanto, Sukhyar R., Soedibjo A. W., Ganefianto N., Stimac J. (2010), *"Geothermal Energy Update: Geothermal Energy Development and Utilization in Indonesia"*. Proceedings World Geothermal Congress 2010. Bali, Indonesia. Retrieved from https://www.geothermal-energy.org/pdf /IGAstandard/WGC/2010/0128.pdf.

Darma S., Tisnaldi, Gunawan R. (2015), *"Country Update: Geothermal Energy Use and Development in Indonesia"*. Proceedings World Geothermal Congress 2015. Melbourne, Australia. Retrieved from https://pangea.stanford.edu/ERE/db/WGC/pa pers/WGC/2015/01038.pdf.

Devold, H. (2013), *"Oil and gas production handbook: an introduction to oil and gas production"*. Lulu.com. Retrieved from https://library.e.abb.com/public/34d5b70e18 f7d6c8c1257be500438ac3/Oil%20and%20g as%20production%20handbook%20ed3x0_ web.pdf.

East Harbour Energy [EHE]. (2015), *"Indonesia, Geothermal Energy Human Resource Development Programme – Strategy"*. A report for Government of Indonesia through the New Zealand Ministry of Foreign Affairs and Trade (MFAT).

Finger, J., and Blankenship, D. (2010), *"Handbook of best practices for geothermal drilling"*. Sandia National Laboratories, Albuquerque. Retrieved from https://www1.eere.energy. gov/geothermal/pdfs/drillinghandbook.pdf.

Habtemariam, W. B. (2012*), "Main technical issues regarding problems when drilling geothermal wells"*. United Nations University, Geothermal Training Programme. Retrieved from http://www.orkustofnun.is/go gn/unu-gtp-report/UNU-GTP-2012-36.pdf.

Hochstein, M. P., and Sudarman, S. (2015), *"Indonesian volcanic geothermal systems"*. In Proceedings World Geothermal Congress, Melbourne, Australia (pp. 19-25). Retrieved from https://pangea.stanford.edu/ERE/db/ WGC/papers/WGC/2015/16006.pdf.

IEA. (2008), *"Energy Policy Review of Indonesia"*. International Energy Agency, Head of Communication and Information Office, France. Retrieved from http://www.iea.org /publications/freepublications/publication/ind onesia2008.pdf.

Jennejohn, D. (2010), *"Green Jobs through Geothermal Energy"*. Geothermal Energy Association. Pennsylvania, Washington, D.C. Retrieved from http://www.geo-energy.org/ pdf/reports/GreenJobs_Through_Geothermal _Energy_Final_Oct2010.pdf.

MEMR. (2017), "Pemerintah optimis capai target kapasitas terpasang panas bumi pada tahun 2017 [Press Release: The government is optimistic to achieve geothermal installed capacity target in 2017]". Ministry of Energy and Mineral Resource. Retrieved from http://ebtke.esdm.go.id/post/2017/10/09/1771 /pemerintah.optimis.capai.target.kapasitas.ter pasang.panas.bumi.pada.tahun.2017.

Ministry of Manpower and Transmigration Decree, Indonesia [MoMT Decree]. (2008), Standar Kompetensi Kerja Nasional Indonesia Sektor Industri Minyak Dan Gas Bumi Serta Panas Bumi Sub Sektor Industri Minyak Dan Gas Bumi Hulu Bidang Pengeboran Sub Bidang Fluida Pengeboran, Komplesi Dan Kerja

Ulang Sumur [MoMT Decree no 245/2008, Indonesian National Competency Standards for Drilling Fluid, Completion and Well Workover]. https://jdih.kemnaker.go.id/data_puu/SKKNI%202008-245.pdf.

Ministry of Manpower Decree, Indonesia [MoM Decree]. (2015), Standar Kompetensi Kerja Nasional Indonesia Kategori Pertambangan Dan Penggalian Golongan Pokok Pertambangan Minyak Bumi Dan Gas Alam Dan Panas Bumi Bidang Pengeboran Darat [MoM Decree No. 133/2015, Indonesian National Competency Standards for Onshore Drilling]. https://jdih.kemnaker.go.id/data_puu/SKKNI%202015-133.pdf.

Mitchell, R. F. (2006), *"Petroleum Engineering Handbook: Drilling Engineering"*. Society of Petroleum Engineers. ProQuest Ebook Central. Retrieved from http://ebookcentral.proquest.com/lib/auckland/detail.action?docID=3405012.

Nguyen, J.P. (1996), *"Oil and Gas Field Development Techniques: Drilling"*. Editions 25 Rue Ginoux, Technip 75015 Paris, France. Retrieved from https://app.knovel.com/hotlink/toc/id:kpDOGFDT05/drilling-oil-gas-field/drilling-oil-gas-field.

Rouzaut B., Nadine, Favennec, Jean-Pierre. (2011), Oil and Gas Exploration and Production - Reserves, Costs, Contracts (3rd Edition Revised and Updated). Editions Technip. Online version available at: https://app.knovel.com/hotlink/toc/id:kpOGEPRCC2/oil-gas-exploration-production/oil-gas-exploration-production.

RUEN. (2017), Rencana Umum Energi Nasional, An attachment of Presidential Decree Number 22/2017. Retrieved from http://sipuu.setkab.go.id/PUUdoc/175146/Lampiran%20I%20Perpres%20Nomor%2022%20Tahun%202017.pdf.

SKK Migas. (2016), Laporan Tahunan 2016. Satuan Kerja Khusus Minyak dan Gas Bumi, Kementerian Energi dan Sumber Daya Mineral [The Special Taskforce for Upstream Oil and Gas Business Activities, Ministry of Energy and Mineral Resources, 2016 Annual Report]. Retrieved from https://skkmigas.go.id/images/upload/file/AR_SKK_MIGAS_INDO_2016.pdf.

SKK Migas. (2017), Laporan Tahunan 2017. Satuan Kerja Khusus Minyak dan Gas Bumi, Kementerian Energi dan Sumber Daya Mineral [The Special Taskforce for Upstream Oil and Gas Business Activities, Ministry of Energy and Mineral Resources, 2017 Annual Report]. Retrieved from https://skkmigas.go.id/images/upload/file/2018/05/AR_SKK_MIGAS_INDO.pdf.

Smillie A., Satar S., Saptadji N., Aminzadeh F., Setianingsih R. (2015), *"Capacity Building in the Geothermal Sector in Indonesia, a Unique Collaboration"*. Indonesian Geothermal Association. Retrieved from http://cgs.usc.edu/assets/002/94801.pdf.

Tilley, M., Eustes, A., Visser, C., Baker, W., Bolton, D., Bell, J. Nagandran, U., and Quick, R. (2015), Optimizing Geothermal Drilling: Oil and Gas Technology Transfer (No. NREL/CP-6A10-66399). NREL (National Renewable Energy Laboratory (NREL), Golden, CO (United States)). Retrieved from https://pangea.stanford.edu/ERE/db/GeoConf/papers/SGW/2015/Eustes.pdf

Tuttle, J. D. (2005), Drilling Fluids for the Geothermal Industry—Recent Innovations. Geothermal Resources Council Transactions, 29.

Umam, M. F. (2018), Geothermal Human Resource Development in Indonesia: Utilizing the Advances of the Oil and Gas Industry. Master Thesis. University of Auckland. Auckland.

Vollmar, D., Wittig, V., and Bracke, R. (2013), Geothermal Drilling Best Practices: The Geothermal translation of conventional drilling recommendations-main potential challenges. International Geothermal Association: Home. Retrieved from http://www.geothermie-zentrum.de/fileadmin/media/geothermiezentrum/GeothermieCampus_Bochum/Departments/Advanced_Drilling_Technologies/Forschung_und_Projekte/Geothermal_Drilling_Best_Practices_DV_VW_10-2013.pdf.

Watson, A. (2013), *"Geothermal engineering"*. Springer-Verlag New York. Retrieved from https://link.springer.com/content/pdf/10.1007/978-1-4614-8569-8.pdf.

GEOTHERMAL DRILLING IN INDONESIA: A REVIEW OF DRILLING OPERATION, EVALUATION OF WELL COST AND WELL CAPACITY

Eko Hari Purwanto, Eko Suwarno, R. Fitrah Lukman, and Budi Herdiyanto

Directorate of Geothermal, Ministry of Energy and Mineral Resource, Indonesia
Email: eko.hari@esdm.go.id

ABSTRACT

The composition of geothermal electricity price is strongly influenced by the main components of the exploration, development and installation of steam field facilities and power plants. Studies show that well costs account for almost up to 60% investment of geothermal projects, therefore effectiveness of geothermal drilling is essential in order to achieve desired projects economics. This paper presents a short history of geothermal drilling operation in Indonesia and review of geothermal drilling operation and offers statistical study of geothermal well costs and well capacity of geothermal fields in Indonesia. Review of drilling operation covers types of wells, casing design, common acquired depths, commercial/ contract schemes and operational difficulties in order to achieved desired drilling targets. This paper also evaluates drilling problems and Non-Productive Time in several wells in Indonesia. This study performs well cost comparison with reference to drilling conducted from 2011 to 2018 using statistical charts in order to illustrate the trend of drilling costs in Indonesia. Evaluation of the geothermal wells is conducted to understand depth ranges, average well output and drilling success rate.

Keywords: Indonesia geothermal drilling, well cost, well capacity

INTRODUCTION

Geothermal energy originates from the heat energy contained in underneath the earth crust and is generally associated with the presence of volcanoes. Indonesia is tectonically located in the area of plate tectonic collision that resulted in hundreds of volcanoes that are spread in Indonesia volcanic belt from Sumatera to Eastern Indonesia. Until 2017, the Geological Agency of Indonesia has identified 342 geothermal prospect locations with a total of 28,508 MW of resources. However, until now the utilization of geothermal power generation up to June-2018 is around 1948.5 MW which only accounted for 6.8% of the total resources (MEMR, 2018).

Geothermal developers believe that one of the main factors that inhibit geothermal development is the high risk of upstream. Sanyal et al (2014) identifies that upstream risk is substantially affected by resource availability, well costs and well productivity. According to Hochstein & Sudarman (2008), the risks on the upstream are smaller with the addition of development stages. At the exploration stage, drilling the first well will reduce the risk to 40% and drilling the second well will lower the risk to 30%. Furthermore, drilling a third to fifth well will reduce the risk further of development to only 20%.

Several studies show that geothermal drilling is responsible for up to 60% of project cost for geothermal projects worldwide (Lukawski et al, 2004; Finger & Blankeship, 2010). Gehringer and Loksha (2012) explains that in Iceland, exploration and development drilling accounts for up to 34% for geothermal power development while a study case of 50 MW geothermal projects estimate that 45% of investment costs are contributed by drilling.

In Indonesia, case studies of cost distributions for geothermal projects in Indonesia shows that drilling accounts for 46 and 58% of geothermal projects using a 5 and 55 MW projects respectively (ARUP, 2017). Other study which presented by Quinlivan (2017) show that total of exploratory, appraisal and development drilling accounts up to 36% of geothermal power generation project.

Historically in Indonesia, geothermal well costs are rarely been published due to confidentiality and proprietary nature of data therefore it is difficult and insufficient to evaluate well cost to a reasonable statistical confidence. However, there is demand from geothermal industry and research in Indonesia to provide evaluation of well costs and well productivity to support desired geothermal projects economics with aims to accelerate geothermal power development in Indonesia.

EXPLORATION DRILLING HISTORY

The exploration of geothermal resources in Indonesia began in 1920s through geochemical prospecting in Kamojang area by the Volcanological Survey of Indonesia, which is followed by exploration drilling to a depth of 128 m (Hochstein & Sudarman, 2008). However, the exploration only began to experience a significant increase since 1974, marked by drilling in several field, such as Kamojang, Dieng and Darajat. In Kamojang, drilling activities continued progressively with a development well drilling at KMJ-6 (611 m deep) in 1974.

In Dieng, geoscientific survey and shallow drilling were conducted from early 1960s by UNESCO, United States Geological Survey and French contractor BEICIP which then followed by extensive production drilling in 1977-1994 by PERTAMINA which covered Sikidang and Sileri prospects. In Darajat, first exploration drilling DRJ-1 conducted in 1976 to 760 m (Hochstein & Sudarman, 2008; Layman et al, 2002).

Geothermal drilling activity in Indonesia has grown progressively from 1980 as shown in Figure.

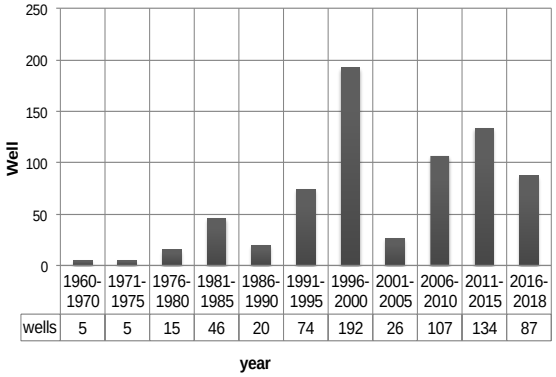


Figure 1: Geothermal drilling activity in Indonesia from 1970s to June 2018

Geothermal Drilling increased from 1990-1995 which may be caused by assignment by the Government to PERTAMINA on almost of Indonesia geothermal working area (GWA) and implementation of Joint Operating Contract (JOC) following Presidential Decree 22 of 1981 and 49 of 1991 which enable private companies to participate in geothermal enterprising, in which at least 7 Energy Sales Contract (ESC) were signed between JOC and PT PLN. Positive trend peaked at late 1990s to 2000 where Government enacted Presidential Decree 39 of 1998 due to fiscal and monetary reason, which halted several projects. The second period of is peaked in 2011-2015 where at least 10 ESC were signed with PT PLN.

During the period of 1995-2000, several exploratory drilling in Indonesia is carried out by employed temperature gradient core hole drilling (TCH). TCH well is drilled mainly using a small sized-casing to a depth of less than 1100 m to 1300 m. The purpose of TCH is to gather information of temperature gradient and other subsurface geological information before proceeded to drill further large sized well in the prospect area. This scheme is carried out mainly by JOC operator in Karaha, Dieng, Patuha, and Bedugul. As examples, 18 TCH well is drilled in Karaha whereas 17 TCH well is drilled in Patuha.

However, from 2005 to date, the number of exploration drilling which is carried out by geothermal developer ranges reduced to minimum 1 to 3 wells, with an average of 5 exploration wells. This is done by taking into account exploration strategy which is used by the geothermal developers are commonly targeted to reach a depth of reservoir to confirm geothermal resources existence and conceptual model obtained from geoscientific surveys. Therefore, if the exploration well is successful, it can also be used as production well. Until June 2018, Indonesia has at least 711 geothermal wells that were drilled by State owned enterprise (SOE), JOC contractors and other private companies. Well data containing number of wells, maximum drilling depth, maximum temperature, reservoir depths and field well output are presented in appendix A. This numbers does not include temperature gradient wells which were conducted by Geological Agency of Indonesia.

WELL DESIGN

Well targeting is prepared in order to confirm geoscientific model then exploratory well is designed to achieve certain depths as required by geoscientists. Planning in drilling activities is very important because it requires experience and engineering in its implementation with the aim of achieving the expected reservoir target by keeping in mind the safety aspect and at the cost of being economical as possible.

Well sitting in geothermal wells require some of major consideration such as topography and civil aspects, environmental impact, target feed zone, geological hazard and cost influence.

The Indonesian government has determined the definition, size and objectives of geothermal wells through the Indonesian National Standard (SNI) 7985 of 2015. In the case of well design, well criteria can be divided based on the size of the production casing. There are three types of well design in Indonesia which have been used by geothermal industry namely large wells (big hole), standard hole and slim hole. Slim hole and standard hole commonly used for exploration purposes, whereas big hole design is mainly used for development and production purposes.

To compare well design for different well which are used in Indonesia, 60 well designs from 11 fields in Sumatera, Java and Sulawesi are gathered as references in order to obtain common well design and depths information. **Error! Reference source not found.** shows the typical size of the well along with depth interval of the design casing of geothermal wells in Indonesia. For large diameter wells (big hole) installation of casing 30 is generally done using auging/ crane. The next sections are drilled by a drilling rig with a 26" bit with a depth interval of 170-650 mMD for 20" casing installation. The next section is drilled using a 17-1/2" bit with 400-1400 mMD depth interval to install 13-3/8" casing. The next sections are drilled using 12-1/4”

bit at 1050-2400 mMD intervals for the installation of 10-3/4 " production liners. Last section is carried out by drilling using a 9-7/8" bit with an interval of 1550-3000 mMD which is cased by 8-5/8" production casing and 7" slotted production liner.

For standard hole (regular diameter), the depth sections are similar but diameters of casing are 18-5/8" for surface casing, 13-3/8" for anchor casing. For standard hole cases, the examples are taken from 3 exploration wells in Sorik Marapi and 2 exploration wells in Baturaden, the installation of casing 30" covers 30-40 mMD depths and are further covered by 18-5/8 casing which are installed in interval 150-165 mMD. The next sections are covered by 9-5/8" production casing in interval 750-900 mMD which are followed by installation of 7" production liner at depth 950-3500 mMD (Isa et all, 2017; Sasongko, 2017).

Several deep slim hole has already been drillied in the early 1990s. The latest slim hole drilling is implemented in 2 exploration wells in Blawan Ijen. The operation is carried out using core drilling rig to achieve 2000 mMD depth (Rahman and Subroto, 2017).

Slim hole drilling is suitable for high risk geothermal prospect exploration with following condition: high resources uncertainty, difficult access and small capital budget. However deep slim hole drilling may need longer drilling time due to technical issues occurred during drilling which are mainly resulted by lack of specific deep slim hole drilling knowledge and inadequate drilling design.

DRILLING COMMERCIAL SCHEMES

Geothermal enterprising involves high capital which resulted in uprising risk, therefore high expenses should be mitigated. In exploration side, specifically in drilling it is important to keep cost as low as possible. In Indonesia at least four drilling schemes/ contracts to handle drilling operations for exploration and development namely:

1. Discrete contract.
2. Semi-integrated project Managemen contract (IPM).
3. IPM contract.
4. Bundled contract.

Every contract has advantage and disadvantages (Isa et al, 2017; Kelley, 2017; Zuhro & Arif 2015) explains as follows:

1. Discrete contract is generally used by geothermal company that has complete organisational, techical capability and experienced personel to plan and execute drilling operation and have continuous drilling program. Normally this type of contract has 24-30 contracts to be managed by companies.
2. Bundled services is a modification of discrete contract and semi-IPM contract which simplify contract to less than 13-20 contracts. This type of contract enable geothermal company to only communicate with contactor project manager and enhance communication process.

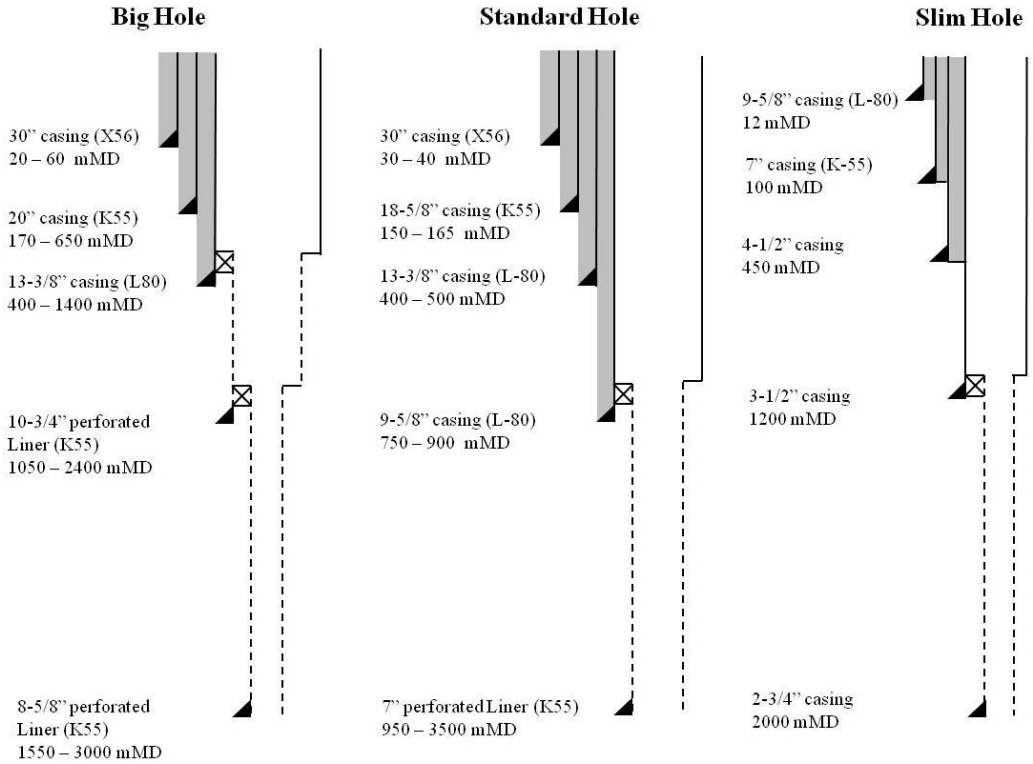


Figure 2: General well design and interval depth of geothermal wells in Indonesia.

3. Semi-IPM contract enables geothermal companies to simplify contracting process. This scheme is generally selected by geothermal companies that have wide-ranging exploration areas to keep costs as minimum as possible while maintaining control of the drilling quality. This type of scheme reduce contract up to 8 contract.
4. Full IPM contract is generally used when geothermal company has limited organizational capability in preparing and execute drilling operation. This type of contract only use 1 contract but rely heavily on IPM contractor and is hard to change out one service nevertheless is suitable with exploration area that only assign less drilling.

Drilling contracts types of the last eight years were gathered from 22 active field and the result can be seen in Figure 3.

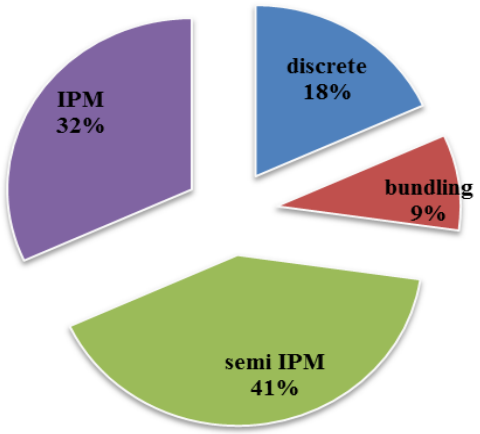


Figure 3: Distribution of geothermal drilling contract from 2010 to 2018

OPERATIONAL CHALLENGES

During drilling campaign, geothermal developers normally encounter obstruction and challenges that derived by both equipment problem and subsurface technical problem. Finger and Blankenship (2010) and Vollmar et al (2013) divide potential subsurface problems in geothermal drilling as follows:

1. High temperature
   Problems which caused by temperature mostly tools temperature limitation, extreme thermal stress on the tubular. Corrosion rate increases and degraded drilling fluid.
2. Lost circulation
   Around 10% of total cost of geothermal project is due to loss circulation combating. Loss circulation may cause several effects such as:
   a. Cost increase since drilling fluid is expensive.
   b. Hydrostatic head reduction that may lead to wellbore influx.
   c. Stuck pipe due to poor cutting removal.
3. Wellbore instability
   This problem is usually cause by mechanically unstable formation, swelling/ shrinking clays and differential stress that may lead to drilling obstruction.
4. Cementation and casing
   Lost circulation during cementing often lead to poor cementing which can cause trapping water that can cause casing collapse.

Pertamina Geothermal Energy (PGE) had issues with rig equipment where drilling operation had to be postponed for three months because of waiting for rig spare part. PGE initiated usage of Tie Back System to replace dual-stage cementing collar (DSCC) in order to avoid production casing collapse Zuhro and Arif (2015). Combating loss circulation and unexpected well formation may also cause drilling delay.

Problems encountered during drilling can cause non-productive time (NPT), which can result in cost overruns. NPT in geothermal drilling in Indonesia that assessed from 22 drilling in 2016 is presented in figure 4.

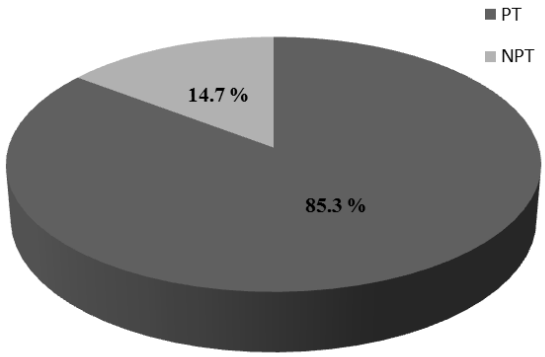


Figure 4: PT vs NPT in of drilling in 2016

Activities that lead to NPT of drilling activity in 2016 is largely dominated by loss combating, cement plug, stuck pipe handling, side tracking and fishing.

WELL DEPTH AND COSTS

Costs required for geothermal well generally include drilling costs, well completion, well pad construction costs, permitting and other supporting costs. Well costs analyzed in this study are limited to the costs required to complete the drilling of the wells starting from the provision of drilling material to completion of drilling.

Studies on drilling costs in Indonesia have been largely undertaken by geothermal developers but the results are rarely published. Previous research was conducted by Lukawski (2014) to determine the ratio of geothermal and oil and gas drilling costs in the world. For geothermal field in Indonesia, Sanyal

et al (2014) have studied geothermal drilling cost and correlation with well productivity.

Depth is main determinant of the drilling cost of a geothermal well, which typically drilling cost in any country increases exponentially with depth (Sanyal et al, 2014). Figure 5 shows histogram of depth of 609 wells which indicating that geothermal wells in Indonesia ranges from about 800-3500 mMD with mean value of drilling depth of 1960 mMD.

We examine 121 geothermal wells from 213 wells drilled in 2011 to 2018. Drilling costs were normalized using the US Department of Labor Bureau's Producer Price Index (PPI) to escalate the well cost (US Departement of Labor, 2018). Figure 6 describes the well cost-depth data obtained from 121 well which we analyzed.

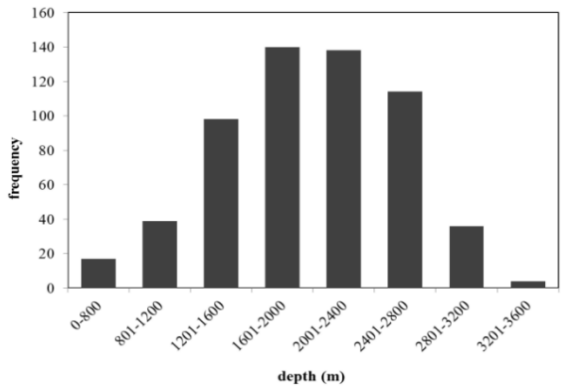


Figure 5: Histogram of geothermal well depth in Indonesia

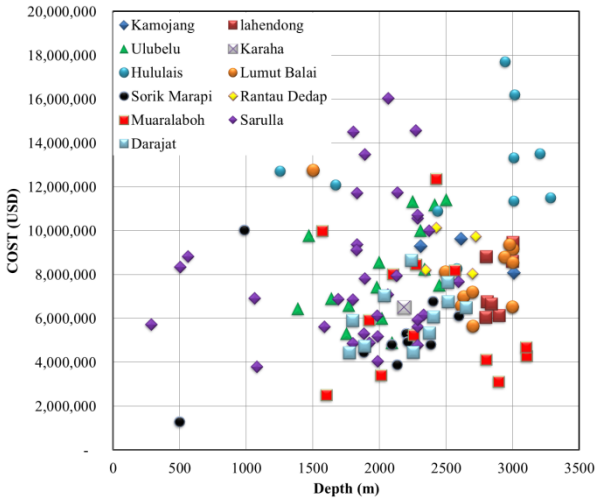


Figure 6: geothermal well cost as a function of measured well depth

Figure 6 explains that drilling costs in Indonesia are typically around US$ 4 million to US$ 9 million with an estimated drilling depth ranges generally from 1,500-3,000 mMD. The diagram ignores the fact that drilling is using either standard hole or big hole. Studies explain that large hole well costs 120% of normal standard hole, whereas slim hole costs only 25-35% of standard hole.

Zuhro & Arif (2015) explains that one way to measure drilling performance is geothermal drilling unit cost/ GDUC (US$/m). Figure 7 describes geothermal unit cost as a function of depth. The result show that GDUC in geothermal area in Indonesia varies from 1000 up to more than 5,000 US$/m, however statistical analysis suggests that mean GDUC in Indonesia from 2011 to 2018 is about 3,960 US$/m as a baseline.

Furthermore, we conducted analysis based on drilling contracts of geothermal drilling in Sumatera. The results of the analysis explain that geothermal companies which using discrete and bundling drilling contracts have the least unit cost cost compared to those using contracts semi-IPM and full-IPM which compared in table 1.

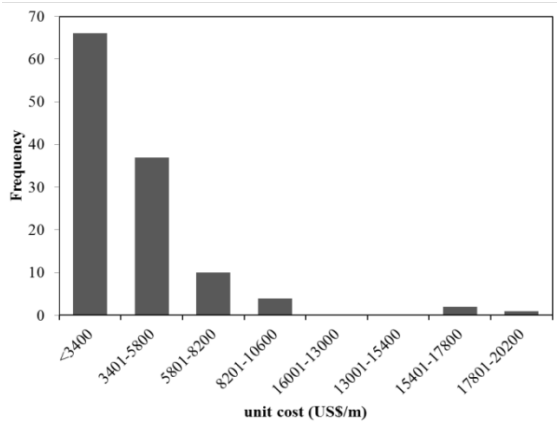


Figure 7: frequency distribution of GDUC

Table 1: Comparison of GDUC in geothermal field in Sumatera

Type of drilling contract	Number of well analyzed	Average GDUC (US$/m)
Discrete	19	2,930
Bundled	18	3,027
Semi IPM	46	3,963
IPM	33	5,411

WELL OUTPUT AND SUCCESS RATIO

Sanyal et al (2014) divides well commerciality based on its capacity, which defines that commercial wells in Indonesia ranges from 3 MW to 40 MW. Well capacity of less than 2 MW and sometimes 3 MW is considered non-commercial well and can be functioned as injection well. This study uses the same assumptions of commercial well have well output larger than 2 MW, however in some cases well with output less than 2 MW can be connected into production system. Figure 8 describes well output distribution in commercial well in Indonesia.

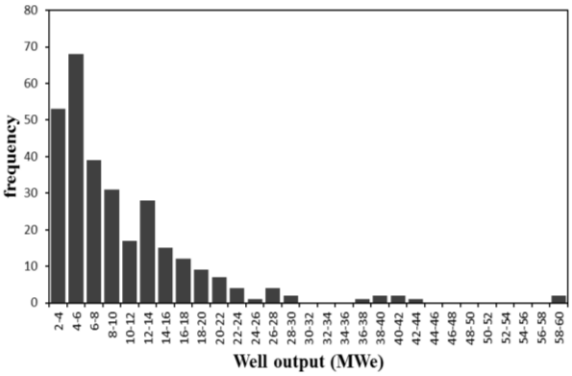


Figure 8: distribution of commercial well output in Indonesia

We calculate drilling success ratio based on commercial well divided by total well in every geothermal field. The result, based on our evaluation, shows drilling success ratio ranges from 33% to 87%.

CONCLUSION

1. Number of well in Indonesia are up to 711 wells.
2. Geothermal area in Indonesia varies from 1000 up to more than 5,000 US$/m with GDUC in Indonesia from 2011 to 2018 is about 3,960 US$/m as a baseline.
3. Based on our evaluation, shows drilling success ratio ranges from 33% to 87%.

ACKNOWLEDGEMENT

We would like to appreciate Directorate of Geothermal who supports this publication.

REFERENCES

ARUP. (2017), "Geothermal Resources in Indonesia – Recommendations for Geothermal Tariff System". *Ministry of Energy and Mineral Resources and The United Kingdom's Foreign and Commonwealth office* (unpublished).

Finger, J., and Blankenship, D. (2010), "Handbook of best practices for geothermal drilling". *Sandia National Laboratories, Albuquerque*.

Gehringer, M., and Loksha, V. (2012), "Geothermal handbook: planning and financing power generation". Energy Sector Management Assistance Program (ESMAP). *The International Bank for Reconstruction and Development, The World Bank Group, Washington DC, United States, Energy Sector Management Assistance Program Technical Report, 2* (12), 164.

Hochstein, M. P., & Sudarman, S. (2008), "History of geothermal exploration in Indonesia from 1970 to 2000". *Geothermics, 37*(3), 220-266.

Isa, B., Hartono, Y., Jayanto, C., Putra, W.M. (2017), "A non IPM Contract for Exploration Drilling in PT Sorik Marapi Geothermal Power". IIGCE 2017.

Kelley, M. (2017), "Geothermal Drilling Contracting and Haliburton Integrated Project Management". (unpublished).

Layman, E.B., Agus, I., Warsa, S. (2002), "The Dieng Geothermal Resource, Central Java, Indonesia". *Geothermal Resources Council Transaction, Vol. 26.*

Lukawski, M. Z., Anderson, B. J., Augustine, C., Capuano Jr, L. E., Beckers, K. F., Livesay, B., and Tester, J. W. (2014), "Cost analysis of oil, gas, and geothermal well drilling". *Journal of Petroleum Science and Engineering*, *118*, 1-14.

MEMR. (2018), "Doing Bussiness in Geothermal". (unpublished).

Quinlivan, P. (2017), "Geothermal Project Management". (unpublished).

Rahman, K., and Subroto, W. (2017), "Challenge in Green Field Geothermal Exploration". (unpublished).

Sanyal, S. K., Morrow, J. W., Jayawardena, M. S., Berrah, N., and Li, S. F. (2014), "Geothermal Resource Risk in Indonesia–A Statistical Inquiry". In *International Conference on Renewable Energy and Energy Efficiency, World Renewable Energy Congress–Indonesia*.

Sasongko, B.P. (2017), "Exploration Project PT Sejahtera Alam Energy". (unpublished).

US Departemen of Labor. (2018), "PPI industry data for Oil and gas". Retrieved from https://www.bls.gov/ppi/.

Vollmar, D., Wittig, V., and Bracke, R. (2013), Geothermal Drilling Best Practices: The Geothermal translation of conventional drilling recommendations-main potential challenges. International Geothermal Association: Home. Retrieved from http://www.geothermie-zentrum.de/fileadmin/media/geothermiezentrum/GeothermieCampus_Bochum/Departments/Advanced_Drilling_Technologies/Forschung_und_Projekte/Geothermal_Drilling_Best_Practices_DV_VW_10-2013.pdf.

Zuhro, A.A., and Arif, G.R. (2015), "Pertamina Geothermal Energy Drilling Campaign". World Geothermal Congress 2015.

Appendix A: Geothermal well and subsurface information

GWA/ Field	Total number of wells	shallow well (<1000 mMD)	deep well (>1000 mMD)	unsuccessfull well (< 2 MWe)	successfull well (> 2 MWe)	Success ratio (successful well/ total well)	Maximum drilled depth (mMD)	Maximum drilled depth (mTVD)	Reservoir zone depths (mTVD)	Maximum reservoir temperature (° C)	Maximum well output (MWe)	total well output (MWe)	average well output (MWe)
Kamojang	92	14	78	43	49	53%	3009	2582	680-2000	245	11.0	271	5.5
Lahendong	51	0	51	31	20	39%	3003	2683	920-2500	358	22.0	152	7.6
Ulubelu	50	1	49	27	22	45%	2537	2394	1000-2275	282	16.0	225	10.2
Sibayak	10	0	10	3	7	70%	2302	2116	1575-2100	284	4.0	21.6	3.1
Karaha	32	18	14	6	8	57%	3076	N/A	1400-2000	296	8.7	40.5	5.1
Lumut Balai	27	0	27	4	23	85%	3003	2639	800-2850	251	13.9	127	5.5
Hululais & Bukit Daun	18	1	17	3	6	67%	3280	N/A	1600-2900	300	14.0	69	11.5
Sungai Penuh/ Kerinci	5	0	5	1	1	50%	3300	2798	1800-2400	281	3.8	4	2.0
Kotamobagu	5	3	2	2	0	0%	2510	N/A	-	160	0.0	0	0.0
Salak	110	5	105	11	72	87%	3200	3200	950-1700	327	36.4	512	7.1
Darajat	49	2	47	9	34	79%	2890	2474	650-1200	248	38.0	281	8.3
Wayang Windu	55	1	54	12	32	73%	2496	2314	900-1600	270	39.0	231	7.2
Sarulla	48	0	48	14	14	50%	2590	N/A	1200-2000	311	55.0	471	33.6
Bedugul	9	6	3	1	2	67%	2979	2678	500-1200	326	4.0	7	3.5
Dieng	52	5	47	18	20	53%	3214	2980	1400-2300	369	22.0	269	13.5
Patuha	31	19	12	3	9	75%	2701	2273	670-850	239	9.5	57	6.3
Ulumbu	3	2	1	2	1	33%	1890	N/A	600-800	263	15.0	15	5.0
Mataloko	7	7	0	1	6	86%	756	756	>700	205	1.4	N/A	N/A
Tulehu	5	0	5	1	4	20%	1900	1719	N/A	205	4.0	4	1.0
Cibuni	3	1	2	2	1	33%	1550	1550	700-1500	243	4.4	4	1.0

GWA/ Field	Total number of wells	shallow well (<1000 mMD)	deep well (>1000 mMD)	unsuccessfull well (< 2 MWe)	successfull well (> 2 MWe)	Success ratio (successful well/ total well)	Maximum drilled depth (mMD)	Maximum drilled depth (mTVD)	Reservoir zone depths (mTVD)	Maximum reservoir temperature (° C)	Maximum well output (MWe)	total well output (MWe)	average well output (MWe)
Muaralaboh	16	1	15	3	8	73%	3103	2860	1100-2500	310	31.5	151	18.6
Rantau Dedap	6	0	6	1	5	83%	2723	2180	1400-2110	288	20.1	39.4	7.9
Sorik Marapi	16	0	16	5	6	55%	2593	2382	800-1700	280	15.7	62	10.3
Sokoria	4	0	4	N/A	N/A	under testing	2072	2062	N/A	255	0.0	0	0.0
Jaboi	2	0	2	1	1	50%	1300	1300	1100-1300	260	4.8	4.8	4.8
Baturaden	2	0	2	2	0	0%	3447	3447	N/A	238	1.6	1.6	1.6
Blawan Ijen	2	1	1	2	0	0%	2000	2000	>1970	291	0.0	0	0.0
Tangkuban Perahu	1	1	0	1	0	0%	612	N/A	N/A	0	0.0	0	0.0

EVALUATION OF TAX ALLOWANCE INCENTIVE IMPACT TO THE GEOTHERMAL PROJECT IN INDONESIA

Pratama, A.R. and Hendra, R.

Directorate General of New, Renewable Energy and Energy Conservation
Ministry of Energy and Mineral Resources
Email: aulia.pratama@esdm.go.id, roy.hendra@esdm.go.id

ABSTRACT

Despite its abundant potency, geothermal development in Indonesia requires high capital investment and poses high exploration risk in its early stage, and this calls for funding and other necessary resources from investors. One of Indonesian government's breakthroughs to attract investors to develop geothermal industry is by implementing tax allowance incentives. As stipulated in the Government Regulation (PP) No.1/2007, all domestic corporate taxpayers involved in geothermal exploration, geothermal drilling, and electricity generation from geothermal can apply for and be granted tax allowance incentives. At a more general level, the incentives were originally intended to expand the national industry, increase the national export commodity, develop the infrastructure, and provide more job vacancies in Indonesia. Particularly in geothermal industry, this incentive is expected to lower geothermal project cost so that investors will be interested in developing geothermal and to simultaneously ensure affordable electricity to all people. In response to the above motives, this study examines how the tax allowance incentives impact geothermal project cost and assesses whether this incentive can be effective to turn geothermal projects economically feasible in the current tariff regime.

Keywords: Tax allowance, geovernment regulation, geothermal project.

INTRODUCTION

The tax allowance incentives have been implemented since 2007. Since then, the Government Regulation (PP) No.1/2007 has been amended several times to give more easiness for investors and to broaden the scope of the industry so that more investors can apply for this facility. Even with these in mind, however, there are not many geothermal developers applying for and utilizing this government's facility.

A study by Coordinating Ministry for Economic Affairs (2015) reported two issues affecting why the tax allowance incentives have not been optimally utilized. First, the socialization of this facility has not been conducted effectively. Since the first regulation was issued, there have been many alterations to it, which was to make this facility more attractive and accessible to various kinds of industry. However, in spite of the positive changes in the regulation, which were thought to bring benefits for investors, it is still the management of the companies which has the final say, and the fact that not many companies have applied for the incentive may be related to the second issue. The next concern is felt by several companies which make use of this facility but raise an objection about the financial audit the Ministry of Finance which is deemed very detailed and strict. Hence, many investors do not feel at ease in using this facility.

TAX ALLOWANCE INCENTIVES FACILITY

In tune with the original propose, the main criteria to be granted this facility applies to industries which have high investment value, create lots of domestic job vacancies, and employ a high number or amount of local content (human, natural, and other resources). The investment value should be at least 30 billion Rupiahs, and the domestic manpower should be at least 100 people (Directorate General of Taxation, 2017).

According to the Regulation of The Ministry of Finance No. 89/PMK.10/2015, the tax allowance incentive will be available in the form of:

1. Income tax reduction for six years from the commencement of operation. The income tax reduction is deducted from taxable income value. Within the first 6 years of production, the taxable income will be reduced by 30% of their total capital investment or 5% reduction per year.
2. Accelerated depreciation and amortization. The depreciation and amortization are calculated since the date of tax allowance's decree. The useful life, the depreciation method, and amortization method can be seen in Table 1. The category of asset is regulated in Ministry of Finance Decree No. 138/KMK.03/2002 about Category of Asset for Depreciation. In this study, all of geothermal assets will be assumed as Category 3 since the geothermal activity is somehow similar to a mining activity. The illustration of income tax calculation and depreciation calculation can be seen in Attachment 1.

Table 1: Depreciation method for tangible asset (Regulation of The Ministry of Finance No. 89/PMK.10/2015)

Tangible asset category	The useful life	Depreciation methods	
		Straight-line method	Balance-decrease method
Non-buildings asset			
Category 1	2 years	50%	100%
Category 2	4 years	25%	50%
Category 3	8 years	12,5%	25%
Category 4	10 years	10%	20%
Building assets			
Permanent	10 years	10%	
Non-permanent	5 years	20%	

3. Eligibility for income tax rate of 10% dividends paid to foreign taxpayers, or at a lower rate if there is a tax treaty between Indonesia and the taxpayer's country.
4. Compensation for fiscal losses for 5 years, which can be increased to a maximum of 10 years. The additional period can be achieved with the following condition:
    a. Additional 1 year, if the applicant conducts the activity in the allocated industrial areas.
    b. Additional 1 or 2 years, if the applicant hires more than 500 or 1000 Indonesian workers for more than 5 years.
    c. Additional 1 year, if the applicant invests more than 10 billion Rupiahs for infrastructures which can possibly improve the surrounding economic and social condition.
    d. Additional 2 years, if the applicant spends 5% of total investment in developing production efficiency in 5 years.
    e. Additional 1 year, if the applicant uses at least 70% of local content since year-4.
    f. Additional 2 years, if the applicant expands their business to specific sectors funded by their earnings after tax; and/or
    g. Additional 2 years, if the applicant exports at least 30% of the total sales for the specific business sectors.

During the incentive period, the applicant is not allowed to transfer the fixed asset, except for the purpose of Tax Allowance Incentive, until the incentive period is done. The detailed procedure of applying the tax allowance can be seen in Attachment 2.

GEOTHERMAL FINANCIAL MODEL

To answer the research question of how the tax allowance incentives impact geothermal project cost, a simple geothermal financial model of 55 MW geothermal project was developed to calculate how much a project's internal rate of return (IRR) based on the electricity selling price. The financial model compares the IRR of the project with and without tax allowance incentives. The project's numerical figures use several assumptions taken from WestJEC's study (2016) on geothermal generation cost, and its characteristics can be seen in Attachment 3.

Next, a sensitivity analysis was carried out to evaluate each component in the tax allowance incentives. The income tax rate of 10% dividends paid to foreign taxpayers is case-specific and very difficult to be analyzed. Hence, there are 5 different scenarios:

1. Without Tax Allowance Scenario. In this case, the depreciation period is assumed two times longer which is 16 years.
2. Accelerated Depreciation Scenario. The depreciation period is assumed to be 8 years, but there is no income tax reduction and compensation for fiscal losses.
3. Fiscal Loss Compensation Scenario. The depreciation period is assumed to be 8 years, and there is fiscal loss compensation facility. The fiscal loss compensation period is assumed to be 5 years.
4. Income Tax Reduction Scenario. The depreciation period is assumed to be 8 years, and there is income tax reduction facility for 6 years.
5. Tax Allowance Scenario. The combination of 3 incentives facility.

The impact of each scenario on the project's IRR was then evaluated.

As a note, in the current tariff regime, geothermal electricity price should follow annual Average Generation Costs (known in Indonesian as *Biaya Pokok Penyediaan* or BPP) for each electrical island/(sub) grid (Campen et al, 2017). However, if the relevant local BPP is lower than the national BPP, the tariff can be negotiated between the geothermal developer and PLN. The BPP regulation was designed to keep electricity affordable to all-people. The BPP will be updated annually by PLN and issued by MEMR. The current national BPP value is 7.66 UScent/kWh, and this is used as a baseline for the financial model used in this study.

The detailed BPP values can be seen in Attachment 4 according to Minister of Energy and Mineral Decision No. 1772 K/20/MEM/2018.

RESULT

The impact of the tax allowance incentives on the project's IRR in a certain range of electricity price in Table 2.

Table 2: Result of sensitivity analysis of without tax allowance and tax allowance scenarios

Electricity Price (US cent/kWh)	Project IRR		Project IRR Difference
	Without Tax Allowance	With Tax Allowance	
7	5.06%	5.08%	0.02%
7.66	5.83%	5.97%	0.14%
8	6.20%	6.39%	0.17%
9	7.23%	7.40%	0.17%
10	8.16%	8.40%	0.24%
12	9.81%	10.27%	0.46%
14	11.25%	11.86%	0.60%
16	12.56%	13.16%	0.60%
18	13.75%	14.35%	0.60%
20	14.85%	15.45%	0.60%

The table above applies the first (Without Tax Allowance) and fifth (Tax Allowance) scenarios, and the result shows one general trend. In both cases where in one case the tax allowance is implemented and in the other it is excluded, the higher the electricity price is, the higher the project's IRR is. However, the two scenarios reveal an interesting finding if attention is paid closer to the project's IRR difference. If the tariff is higher, the impact of incentive will be higher. In short, the tax allowance incentives have less impact if the electricity tariff is smaller. Thus, the tax allowance incentives do not give a significant impact and help to reduce BPP.

A further sensitivity analysis to evaluate the impact of other tax allowance components was conducted, especially in the second, third, and fourth scenarios, and the results were presented in the Figure 1 below.

In the Accelerated Depreciation Scenario, the result shows that accelerated depreciation in small tariff may give negative impact to the project. The cash flow in the beginning of production will be negative if depreciation is accelerated. On the other hand, when the tariff is higher, the accelerated depreciation will give positive impact to IRR because it helps reduce the income tax.

As to the third (Fiscal Loss Compensation) and fourth (Income Tax Reduction Incentive) scenarios, the bar graph displays contrasting findings. Compared to the without tax allowance scenario, the fiscal loss compensation will give a more visible impact when the tariff is smaller, but it has no impact when the tariff is big. In contrast, the income tax reduction incentive will give an impact when the tariff is bigger, and it has no impact when the tariff is smaller.

To explain the fourth scenario, when the tariff is small, the cash flow during the early period of production might be very small or even negative. Hence, the income tax reduction facility will not give any impact since the taxable income is already small (or even negative). On the other hand, the fiscal loss compensation plays an important role when the cash flow is negative. It is, however, important to note that this compensation is given not in the form of money or subsidy to the project but, rather, tax reduction.

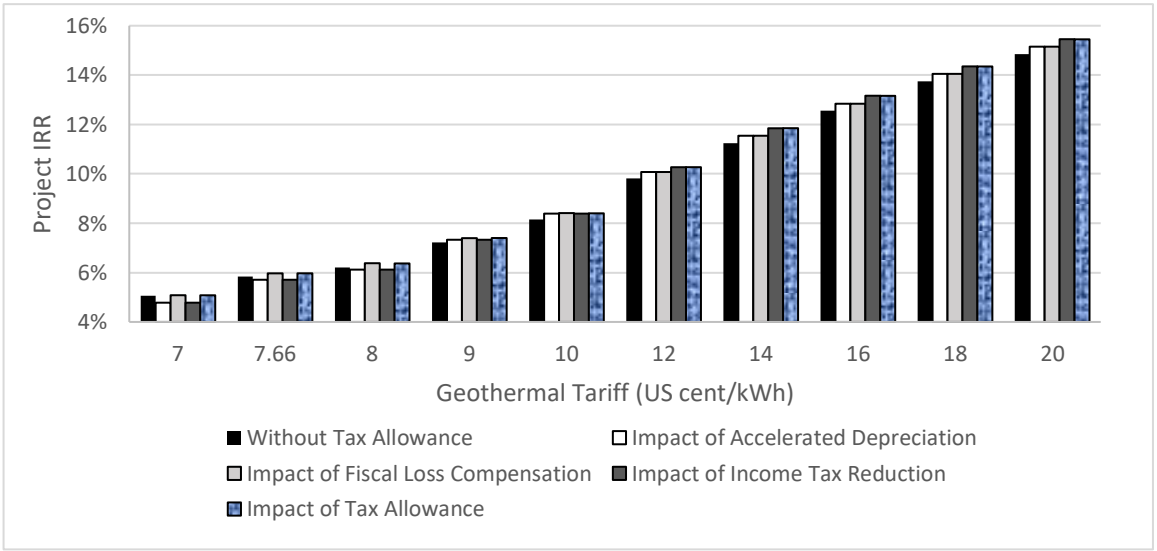


Figure 1: Comparison of results (Project IRR) of all scenarios

SUMMARY AND RECOMENDATION

This study investigated how the tax allowance incentives impact a geothermal project's cost. Calculations using a geothermal financial model show several findings, as follows:

1. The impact of the tax allowance incentives will vary greatly for the geothermal project. In general, the impact is smaller when the project has small tariff or small electricity sales.
2. The income tax reduction incentive will be calculated since the first commencement of production. The taxable income in the commencement of first unit production may be negative. Hence, staging-development scenario will get less impact from this incentive.
3. The income tax reduction incentive also may not give any impact if the electricity tariff is low.
4. On the contrary, the compensation for fiscal losses will not give any impact if the electricity tariff is high.

Some recommendations from this study include:

1. In order to increase the impact of tax allowance, the income tax reduction incentive should start from when the taxable income has positive value.
2. Socialization about possible incentive facility to prospective geothermal developers should be more massive and done more often.
3. The bureaucracy process ought to be simplified to give more easiness to potential investors.
4. Further research and evaluation about current geothermal projects which have applied for this incentive should be conducted to obtain empirical data from the field.
5. Further research on other possible policy options to help the acceleration of geothermal development in Indonesia should be carried out.

ACKNOWLEDGEMENTS

Our sincere thanks to go to Directorate of Geothermal, Ministry of Energy and Mineral Resources and Fiscal Policy Agency, Ministry of Finance who provided an opportunity to finish this study.

REFERENCES

Campen, B. V., Pratama, A.R., Lawless, J., Randle, J., and Archer, R. (2017), "*Analysis of New Indonesian Geothermal Tariff System and Impact of Feasibility of Geothermal Power Plants in Eastern Indonesia in the Next Decade"*. Paper presented at the 39th New Zealand Geothermal Workshop, Rotorua, New Zealand. Retrieved from https://www.researchgate.net/publication/320619618_Analysis_of_New_Indonesian_Geothermal_Tariff_System_and_impact_of_Feasibility_of_Geothermal_Plants_in_Eastern_Indonesia_in_the_Next_Decade/download.

Coordinating Ministry for Economic Affairs. (2015), "*Kajian Efektivitas Fasilitas Pajak Penghasilan untuk Penanaman Modal di Bidang-Bidang Usaha Tertentu dan/atau di Daerah-daerah Tertentu (Tax Allowance)"*. Jakarta: *Kedeputian Bidang Koordinasi Ekonomi dan Makro Keasdepan Fiskal*.

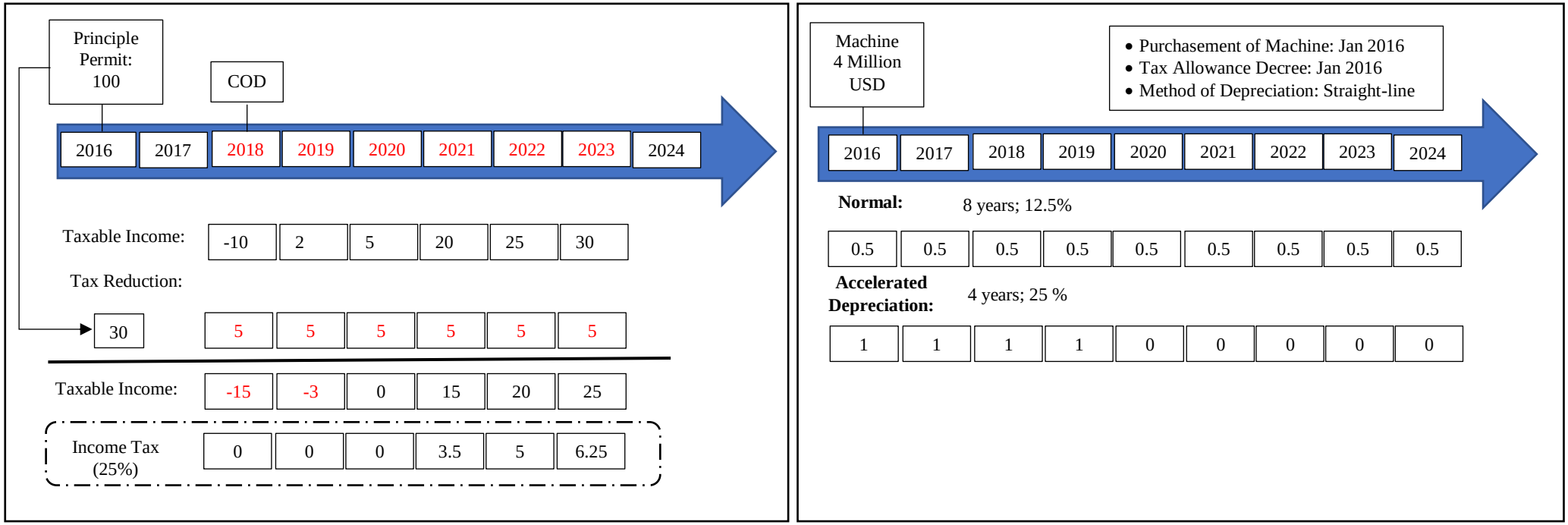
Directorate General of Taxation. (2017), *"Fasilitas/Insentif Pajak Penghasilan"*. *Yogyakarta: Ministry of Finance*.

Minister of Energy and Mineral Decision No. 1772 K/20/MEM/2018. (2018), "Amount of Basic Cost of Provision of Generation for PT Perusahaan Listrik Negara (PERSERO) for 2017". Jakarta: Ministry of Energy and Mineral Resources.

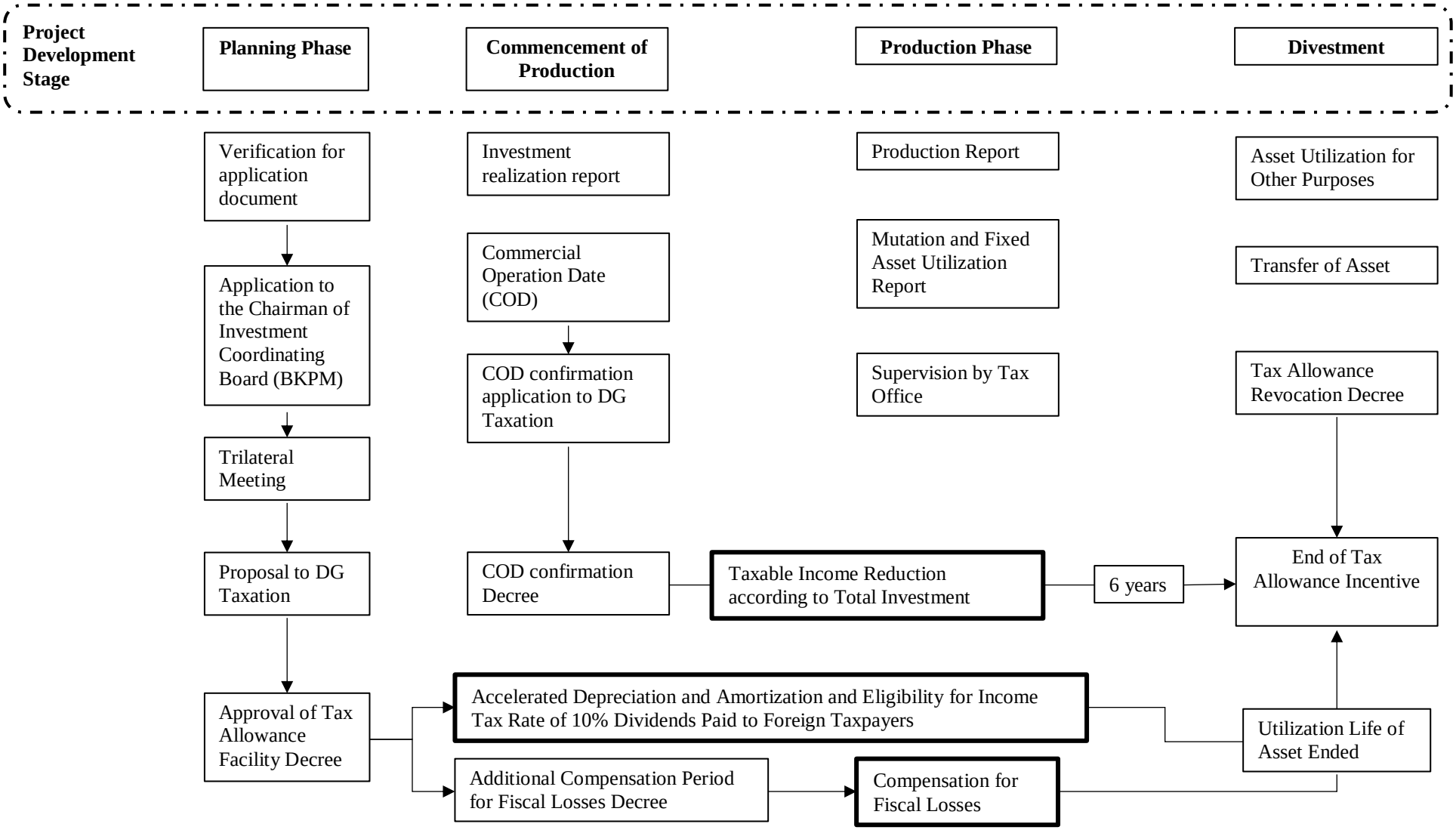
Regulation of The Ministry of Finance No. 89/PMK.10/2015. (2015), "Procedures For The Granting of Income Tax Facilities For Investment in Certain Business Fields and/or in Certain Regions and Transfer of Assets and Sanctions on Domestic Taxpayers Given Income Tax Facilites". Article 2 part (2).

West Japan Engineering Consultants, Inc/WestJEC. (2016), "*Review Report on Benefit of Geothermal Energy: Avoided Cost by Geothermal Energy"*. Jakarta, Indonesia: Author.

Attachment 1: Illustration of income tax calculation (left) and depreciation calculation (right). (Directorate General of Taxation, 2017)



Attachment 2: Utilization of tax Allowance Incentive in project development stage (Directorate General of Taxation, 2017)



Attachment 3: Geothermal project cost assumptions (Modified from WestJEC, 2016)

No.	Steam Field Assumption	Value
1	Project capacity	55 MW
2	Capacity factor of power plant	90%
3	Sales of electricity per year	433,62 GWh
4	Inflation	2.50%
5	Corporate income tax	25.00%
6	Royalty	2.50%
7	Duration of exploration and construction stage	7 years
8	Number of production well	10
9	Success rate of production drilling	70.00%
10	Production drilling cost	6 million USD
11	Number of reinjection well	10
12	Success rate of reinjection drilling	90.00%
13	Reinjection well drilling cost	4.5 million USD
14	Operation years	30
15	Royalty	2.50%
16	Production Bonus	0.50%
17	Geothermal Working Area	
	a. Confirmation area	100,000 ha
	b. Construction area	5,000 ha
18	G&G Study Cost	4.75 million USD
19	Engineering & Feasibility Cost	7 million USD
20	Land acquisition and Preparation Work Cost	15 million USD
21	Administration Cost	20 million USD
22	Conventional power plant cost	1500 USD/kW
23	Total Capital Expenditure	282.2 million USD
	Tax Allowance Incentives	
24	Investment tax credit	5% of total investment for 6 years
25	Depreciation period	8 years
26	Depreciation method	Straight-line
27	Compensation period of fiscal losses	5 years

Attachment 4: Geothermal Average Generation Cost (BPP) values for each Region / Subsystem in 2017 (Minister of Energy and Mineral Decision No. 1772 K/20/MEM/2018)

No	Region / Subsystem	BPP / Geothermal Ceiling Tariff (US cent/kWh)
1	**Aceh**	**11.14**
	Weh Island	13.58
	Simeuleu Island	11.97
2	**North Sumatera**	**9.77**
	Nias	20.00
3	**West Sumatera**	**7.25**
	Mentawai Archipelago	19.30
4	**Riau**	**10.98**
5	**Riau Archipelago**	
	Bintan	15.34
	Tanjung Balai Karimun	12.57
	Natuna	15.39
	Anambas	20.00
6	**South Sumatera, Jambi, Bengkulu (S2JB)**	**7.18**
	Enggano Island	20.00
7	**Lampung**	**6.99**
8	**Bangka**	**16.79**
9	**DKI Jakarta**	6.81
	Kep. Seribu	20.00
10	**Banten**	**6.81**
	Panjang Island	20.00
11	**West Java**	**6.81**
12	**Central Java**	**6.81**
	Karimun Jawa	20.00
13	**East Java**	**6.83**
	Madura (isolated)	20.00
	Bawean	12.69
	Gili Ketapang	20.00
14	**Bali**	**6.81**
	Tiga Nusa	18.12
15	**West Borneo**	**12.64**
16	**South Borneo & Central Borneo**	**8.58**
17	**North Borneo & East Borneo**	**11.07**
18	**North Sulawesi** (Manado, Gorontalo, Kotamobagu)	**13.00**
	Toli -Toli	16.62
	Tahuna	19.15
	Palu	8.44
	Luwuk	15.69
19	**South Sulawesi**	**7.28**
	Kendari	14.38
	Bau - Bau	16.21

No	Region / Subsystem	BPP / Geothermal Ceiling Tariff (US cent/kWh)
	Selayar	15.26
20	**West Nusa Tenggara**	
	Tambora (Bima & Sumbawa)	16.73
	Lombok	13.90
21	**East Nusa Tenggara**	
	Sumba	17.00
	Timor	18.09
	West part of Flores Island	17.72
	East part of Flores Island	16.49
22	**Moluccas**	
	Ambon	20.00
	Seram	20.00
	Saparua	16.59
	Buru	16.48
	Ternate - Tidore	20.00
	Sanana	13.98
	Bacan	14.08
	Halmahera (Tobelo, Malifut, Jailolo, Sofifi, Maba)	20.00
	Daruba	20.00
	Tual	20.00
	Dobo	20.00
	Saumlaki	16.73
23	**Papua**	
	Jayapura	13.78
	Sarmi	13.98
	Biak	15.99
	Serui	14.77
	Nabire	13.81
	Wamena	20.00
	Timika	16.51
	Merauke	15.39
	Tanah Merah	14.31
	Manokwari	14.78
	Sorong	13.100
	Teminabuan	13.96
	Fak Fak	20.00
	Kaimana	20.00
	Bintuni	20.00
	Raja Ampat	20.00
24	**Other Small Subsystem**	**20.00**
NATIONAL BPP		**7.66**

INSTITUTIONALIZED PUBLIC-PRIVATE PARTNERSHIP FOR GEOTHERMAL DEVELOPMENT IN INDONESIA: PRELIMINARY APPROACH OF PLN INITIATIVE

Yodha Yudhistra N., Suardi Nur, Hendra Y. T. Tondang, and Yudistian Yunis

PT PLN (Persero) – DIVEBT, Jl. Trunojoyo Blok M-I No.135, Jakarta, Kebayoran Baru, 12160, Indonesia
PT PLN Gas Geothermal, Jl. Aditiawarman No.55, Jakarta, Kebayoran Baru, 12160, Indonesia
The University of Dundee, Centre for Energy, Petroleum and Mineral Law and Policy
Nethergate, Dundee, DD14HN, Scotland UK
Email: yodha.yudhistra@pln.co.id

ABSTRACT

Current portfolio of energy production, mostly based on fossil fuels, and the growing of energy consumption go on opposite direction of the government's goal for climate change mitigation. Indonesian government is targeting to achieve 23% share of renewables and clean energy sources in national energy mix in 2025 where geothermal power as one of the largest contributor. As single off taker, PLN expects to develop geothermal power in close collaboration with the private sector, not only limited in a contractor-supplier relation but also in deep partnerships where both PLN and the private sector undertakes a considerable responsibility in running and managing the business. These models are recognized as institutionalized public–private partnerships (iPPP) / joint ventures. This work will look at framework of how the risk is allocated, transferred and managed in PLN Geothermal iPPP Initiative to develop its Geothermal Working Areas (up to 800 MW). Portfolio construction is simulated to assess risk reduction benefit and its impact on project feasibility by implementing this scheme.

Keywords: Geothermal Indonesia, iPPP, geothermal working area.

INTRODUCTION

In COP 21, it is set that in 2027 the target for emission for Indonesia is 1,200 Mt. CO_2 equivalent. To achieve this objective and to provide cushion to support system economics if fossil energy prices increases, geothermal energy need to be developed in Indonesia. In 2027, the total generation capacity will be 500 TWh where 20% will be supplied by renewables including 10% by geothermal energy. Nevertheless, in order to accomplish this energy mix target, especially in geothermal sector, technical and pricing policy challenges need to be addressed.

Technical challenges includes insufficient data in bidding stage, lack of competency and less equity fund of developer.

According to Castlerock (2009), the pricing policy includes four areas for attention, namely:

1. Exploration (upfront) risk.
2. Segmented pricing framework.
3. Fund to incremental cost gap.
4. New Geothermal Working Area tender process.

Nonetheless, to accelerate the development of geothermal energy is slightly of an enormous task due to the aforementioned obstacles.

This paper will present preliminary approach of PLN initiative to address first and second pricing policy issues by promoting institutionalized public-private partnership (iPPP) / joint-venture. First, the paper will clarify the concept and rationale of iPPPs. Their benefits, pointing out the risks allocation. The economics behind geothermal power plants is also addressed, identifying the key success factors and making a deeper investigation on the risk sharing scheme adopted for the development of geothermal power plants. A general overview of the geothermal electricity sector will be presented, dividing the value-chain into its main components and identifying the key stakeholders in each sub-system, as well as the respective industrial organization model. A public selection procedure for a package of 360 MW geothermal capacity is discussed next, focusing on the process of selection of the private partner, on the risk sharing scheme adopted and on the portfolio construction.

THE INDONESIAN GEOTHERMAL ENERGY SECTOR

The country's total potential geothermal resources and reserves are estimated at 28,994 MWe (megawatts-electrical) with an installed capacity of 1948.5 MWe (approximately 6.7 percent of the total resources and reserves). One of the key risks in geothermal energy development is associated with the electricity market. Until recently, Indonesia's geothermal resources have been underutilized partly due to pricing disagreements between the PLN, the state-owned electricity company as off-taker, and the government. Even when geothermal licenses were granted, developers delayed exploration; waiting for power-purchasing agreements with the PLN, which were in turn on hold in anticipation of the government's pricing approval.

IPPP ARRANGEMENTS IN THE GEOTHERMAL ENERGY SECTOR

iPPP definition

The importance of the geothermal sector for climate protection and electricity price cushion is driving PLN as public utility to seek innovative approaches to harnessing private sector upstream management skills and investment capabilities, i.e. institutionalized Public-Private Partnership (iPPP).

An iPPP operates like a share corporation in terms of governance and autonomy. In an iPPP, the public partner (i.e. PLN) will create a new company and can retain the majority share while a private operator with the capacity to optimize the processes and improve efficiency, or multiple private investors joined with the operator, hold the minority share – and vice versa. In addition, the private partner enters into a management contract with the public partner for day-to-day operations. A joint-venture (JV) in the geothermal sector has specific features that complicate the provision and management of services. These include a monopoly market with location-based pricing, the high cost of entry, and exploration risk. The iPPP model can help mitigate major risks by drawing on the strengths of both the public and private partners.

Benefit of using iPPP model

Public party prefer to take a substantial stake in a project company or maintain a substantial stake in a utility involved in an iPPP. However, as the public and private sectors work in very different manners and have different processes and priorities, in practice this can cause challenges. Benefit of this model are (World Bank, 2013):

1. Access to different sources of finance.
2. Public party can exercise some degree of control over day to day operations or at least key decisions (at board and shareholder level).
3. Transparency (accounts and finances presented to board).
4. Public perception – this is not privatization or private provision of a service.
5. Sustainability – continuity of partners – even if private partner changes.
6. Share of profits.

However, as share ownership alone does not necessarily guarantee these advantages, attention needs to be given to the shareholder agreement. Indeed, a private party can achieve a number of these advantages with 49% shareholding if the structure is properly designed which will be described later in case study analysis.

This model is mainly intended to address the fact that renewable energy still has a higher cost than traditional sources, and financing mechanisms need to be found to overcome this gap, and foster the development of these technologies (Yue et al., 2001).

Comparison between iPPPs and traditional models

iPPP arrangements, as a development model, should be compared with the traditional development methods to ensure that value for money is delivered. This means comparing the cost of developing the project under an iPPP scheme, with the hypothetical risk-adjusted cost of the project if developed solely by the public sector (Devapriya, 2006). It is then necessary to estimate the cost of construction and maintaining the installation (investment and O&M expenses) along with the risk entirely assumed by the public sector, contrasting to iPPP projects where risks are allocated to the private sector. If the value for money delivered by the iPPP solution is higher, then this development model should be adopted. In the case of geothermal power generation this question does exist because energy production is now carried out mostly by contractual PPP (cPPP) with independent private companies. The third alternative to geothermal energy project delivery is under a traditional model of public works, where can be extended to the development and management of the steam-field is private, but the power-plant is public (PLN).

THE ECONOMICS BEHIND A GEOTHERMAL POWER PLANT

Pricing model and policy

Tariff should meet system economics, if not governmental support will be required to compensate power production cost (BPP) increase. Trade-off between system and project economics. Factors that affect tariff can be categorized into two main components:

1. Controllable, such as infrastructure, study & investigation, drilling success ratio & cost, well capacity, FCRS & power-plant, project financing.
2. Uncontrollable, such as regulation, social, etc.

Power-system economics, i.e. local BPP is regulated in Ministry of Energy and Mineral Resources (MEMR) Decree No. 50/2017. The local BPP values are stated in MEMR Act No. 1404 K/20/MEM/2017.

Investment

Geothermal investment cost includes 3G (geological, geophysical, and geochemistry) studies, infrastructures, exploration drilling (20%), production and injection drilling (30%), fluid collection system, and power plant (50%). The value per MW installed varies depending on resources quality and economy of scale. In general, economy

of scale allows both unit capital cost (in US dollars per kW installed) and unit O&M cost (in cUSD/kWh) to decline with increasing installed capacity. The values ranging between 3,000 – 10,000 USD/kW.

Operation and Maintenance Cost

According to GeothermEx, operation and maintenance cost of geothermal power plants approximately ranges from 2.0 cUSD/kWh for a 5 MW plant to 1.4 cUSD/kWh for a 150 MW plant (Sanyal, 2005). Geothermal wells generally undergo "harmonic" decline in well productivity with time (Sanyal, et al, 1989), thus make-up well cost should be taken into account as OPEX. Drilling cost per well usually varies between 4 – 8 mil. USD, depending on well depth and location.

This numbers relate to resource risk which has most influenced merit measures of potential resource base, drilling success ratio, levelized power cost (cUSD/kWh), discounted profit-to-investment ratio, and internal rate of return.

GEOTHERMAL PARTNERSHIP SCHEME

Introduction

As aforementioned described, iPPP model enables access to different sources of finance. The public partner can provide the political influence to help access low-cost, public financing for the joint venture that would otherwise not be accessible to a private operator. Contrarily, the private partner may be able to help access market finance that the public partner's credit rating would otherwise not allow (at least not on favorable terms), and help to win the confidence of International Financial Institutions (IFIs) (Castro and Janssens, 2011). This correlates to the fact that in order to meet power-system economics (local BPP), low-rate loan is required by the developer.

Therefore, the iPPP initiative is expected to answer the above requirement. As Currently, PLN has been assigned 11 Geothermal Working Areas (GWAs) with total capacity of 360 MW, which is listed in Table 1.

Ulumbu 1, 2, 3, 4 are now online with total capacity of 10 MW supplied by one well ULB-2. Power plant with capacity of 2.5 MW has been installed in Mataloko. However, due to technical problem, the plant is dismantled.

The future PLN field expansion of will be accomplished by using partnership scheme as depicted in Figure 1 below.

Table 1: Geothermal Working Areas of PLN assignment.

System	GWA	COD	Capacity
Java	Tangkuban Parahu	2024/25	60
	Ungaran	2024	55
Sumatera	Kepahiang	2024	110
	Danau Ranau	2030	20
Non - Java Sumatera	Tulehu	2020	20
	Ulumbu 5/6	2021/23	40
	Mataloko 2	2023	20
	Atadei	2023	10
	Songa Wayaua	2023	10
	Oka Ile Ange	2030	10
	Gc. Sirung	2028	5

During the exploration stage, after private partner is selected, partner and PLN will sign a Head of Agreement (HoA). In this HoA, at least but not limited, the following substance will be covered:

1. Terms of agreement and exploration period.
2. Successful exploration criteria.
3. Work Program and Budget for exploration.
4. Rights and obligations.
5. Termination and default.
6. Asset and land.

Share Holder Agreement (SHA) and Geothermal Power Production Agreement (GPPA) models will be also be provided upfront.

Selecting the private partner

For the evaluation of selections to phase A, the following technical 5 criteria were used: (A) Resource study; (B) Drilling; (C) Reservoir management; (D) EPC and (E) O&M. To each criteria was attributed a weight of 40%, 35%, 25%, 5% and 5%, respectively. Table 3 systematizes the criteria and weights in the selection evaluation model of this case-study. Given the criteria weights for this public selection, the economic and financial factors were valued 60%, while the technical had a relative weight of 40%. This means that PLN strongly preferred the creation of an upstream capability (a weight of 90% given to the upstream experiences). In financial criteria, at least a working capital of 20% of total project cost must be provided to attract equity investment to the project.

Risk sharing

Risk in iPPP projects is a critical matter for the success of this model, and its correct allocation is essential to ensure a better value for money than traditional scheme, i.e. public work, upstream - downstream, cPPP (IPP) models

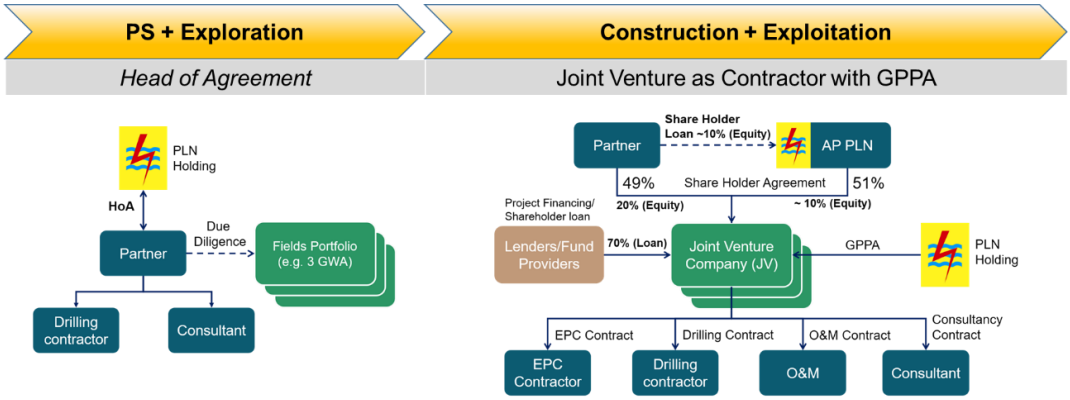


Figure 1: iPPP geothermal scheme: from exploration to exploitation structure.

Table 2: Main risks at PLN geothermal iPP Partnership.

Risk type	Risk description	Risk allocation		Probability	Impact level
		PLN	Private		
Financial	• Risk of insolvency of lenders • Uncertainty about rising inflation • Evolution of the financial burden • Amendment of conditions of tariff by the regulatory authorities	x	x	Medium	High
Legal	• Likelihood of new legislation with an impact on the structure cost • Stricter regulations	x		Low	High
Price	• Electricity production cost volatility (opportunity cost)	x		High	High
Demand and competition	• Location and displacement of enterprises • Threat about the coming of new competitors into the business	x		Low	High
Performance	• Uncertainty about the quality of service for drilling and power-plant maintenance • Increasing demand in service quality	To Be Determined*		Medium	Medium
Environmental	• Obtaining the environmental impact study • Location of geothermal power plant on protected forest area	x	x	Low	Medium
Accessibility	• Risk of damage of current roads • Risk of occupation of private property	x	x	Medium	Medium
Grid failure	• Risk of a failure in the distribution grid, affecting energy usage	x		Low	High
Grid connection	• Risk of non-generation of power pre-agreed • Loss of entitlement to power not available	x		Low	High
Security	• Accidents during the exploration, construction and operation stages	x	x	Medium	Medium
Licenses	• Acceptance of expropriation • Obtaining licenses for construction and operation	x	x	Low	Medium
Planning and design	• Definition of projects outputs • Adequacy of construction projects as defined in specific design	x	x	Low	Medium

Exploration	• Risk of failure of geothermal resource • Uncertainty about geological and environmental conditions	PT SMI – SOE Drilling *	x	Medium	High
Construction	• Delays in the commissioning of the geothermal power plant • Equipment damages during operation or during the installation • Difficulty in providing material	x	x	Low	Medium
Operation and maintenance	• Uncertainty of the availability of steam/brine (losses caused by well damage, failures of income) • Facilities state • System reliability • Availability of equipment • Uncertainty about the quality of maintenance services • Risk of availability of infrastructures	x	x	Medium	High
Force majeure	• Natural disasters, vandalism, war, epidemics	x		Low	High

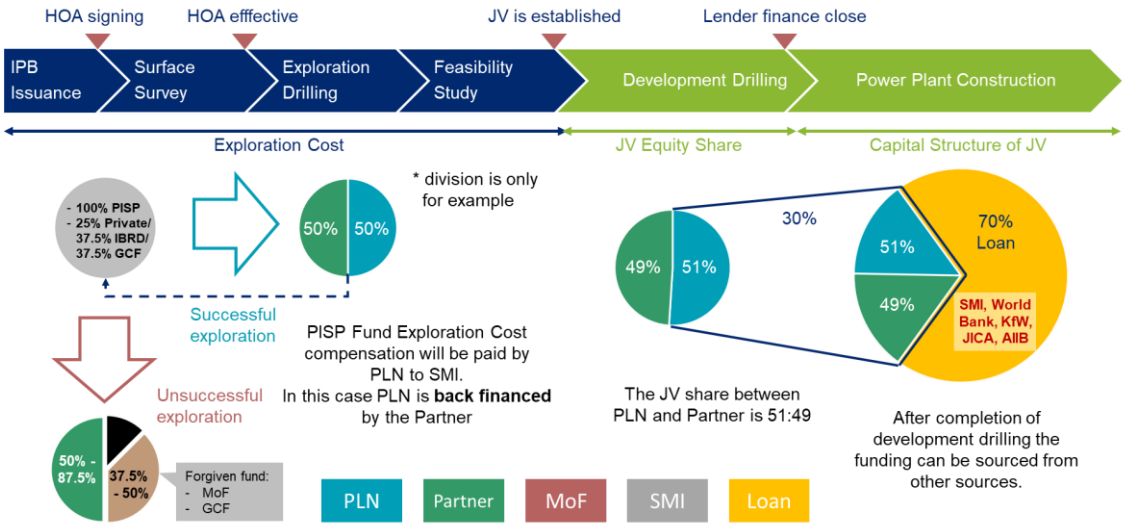


Figure 2: How exploration fund turn into paid-in capital in PLN geothermal iPPP.

The joint-venture (JV) is entrusted with the responsibility of construction, financing and managing the power plant, but this does not mean, however, that it bears all the associated risks. With this type of development the aim is that each partner does what it is best fitted and prepared to, ensuring that services and infrastructure are provided as efficiently as possible. Although complex, a generally accepted principle for risk sharing is that each agent should bear the risk that is best capable of dealing with the risks associated with geothermal. The geothermal contract does not have a risk matrix or a study discriminating all the risks involved in a geothermal project. But this is the best methodology to identify, evaluate and allocate them, as mentioned in Table 2. As one might expect, in a iPPP contract the risks are mainly shared between the public and the private sectors, except for the risk of legal, price, force majeure, demand and competition risks. The risks most likely to occur are those related to the safety issue of workers, the accessibility to geothermal sites, operation and maintenance, the party performance, and after all those risks, the ones associated to the financial aspect. The sequence of project development will be first IPB issuance, followed by partner selection. By default, equity for exploration should be provided by private partner. Nevertheless, Ministry of Finance, PT SMI are now preparing so called geothermal fund. There are two exploration fund windows that can be employed in this partnership scheme (i) PISP fund and (ii) private. Forgiveness scenario will be applied in this financing scheme, e.g. up to 50% of exploration fund will be forgiven in case of unfeasible project. After exploration is successful, exploration fund will be recognized as 50:50 PLN-Partner equity shares, and further JV shares. After completion of development drilling the funding can be sourced from other sources, such as World Bank, SMI, JICA, KfW, AIIB, AFD, etc.

CASE STUDY ANALYSIS

It is clear that currently the political priority given to geothermal power development to PLN as single off-taker. In fact, the investments in this field are being used by the government as a representation of the country's ability to transform and deal with future challenges of renewable energy provision.

This leads to the discussion on the risk-sharing assumptions of the contract. The risk-sharing matrix shows a large majority of risks being entirely (or mostly) assumed by the joint venture. This is a desirable principle for a successful iPPP, but, unfortunately, may not always achieved. Nevertheless, the demand risk is not completely removed from the public sector (PLN), since in case of a grid failure the energy produced would be paid but not sold.

With regard to approach local BPP, one of the main benefit of iPPP is that the public partner can provide access to low-cost, public financing for the joint venture that would otherwise not be available to a private operator. The advantage is quantified and presented in Figure 3. Main assumptions used in the simulation are:

- Reservoir temperature of 240 °C.
- Steam water ratio of 5.4 (dryness of 84%).
- Wellhead, incremental, single-flash condensing generation units.
- Investment cost of 4,400 $/kW (55 MW).
- Debt to Equity ratio of 70:30.
- Tenor between 20 years for G to G loan; 15 years for SOE soft loan; and 10 years for commercial loan.

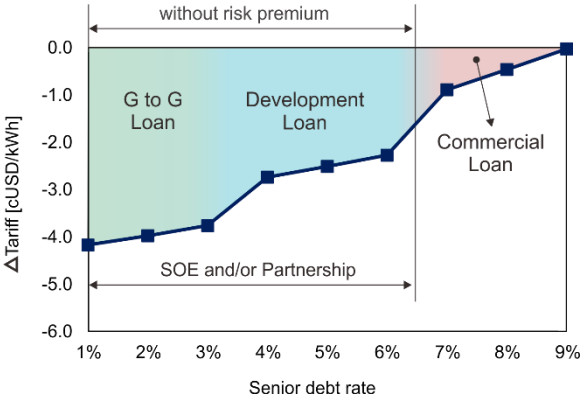


Figure 3: Tariff reduction sensitivity to senior debt rate.

From Figure 3, it can be shown that development and G to G loan lowering the tariff by 2.2 – 4.1 cUSD/kWh corresponds to senior debt rate of 6.5% to 1%. Nevertheless, time-lagging due to long processing time of low-cost financing is not included yet in the simulation.

PLN as single off-taker will recognize the fields as one or several packages. Thus, portfolio construction can be applied which helps to reducing revenue risk, which provided a framework for seeking to maximize returns at a given level of uncertainty, especially, in Indonesia, due to local power production cost (BPP). There are adjustable parameters that increase the flexibility of this scheme which are listed in Table 3.

Table 3: Description of the financial model adjustable parameters.

Parameter	Range value
Target ROE	10 – 17 %
Sr. debt rate	0 – 6 %
BOOT time	8 – 25 years
PLN dividend until BOOT	5 – 51%
Sr. debt rate portion	70 – 90 %

SHL portion	0 – 15 %
Mezzanine portion	0 – 15 %
SMI exploration fund	0 – 30 mil. USD

Figure 4 illustrates the risk characteristics of three different fields in different location, as they compare to each other and to their typical category benchmark, local BPP. Simulation results one of three fields is not feasible due to fact that the economical tariff higher than local BPP (119% BPP). While Field B & C tariff are 75% and 71% local BPP, respectively.

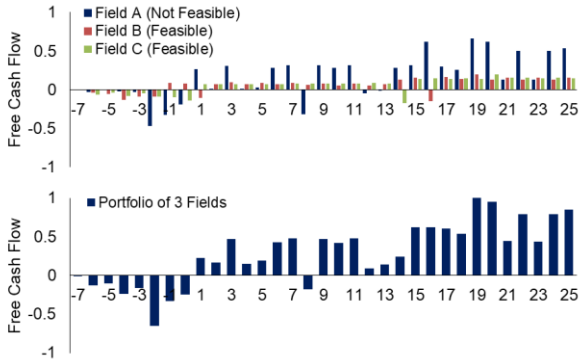


Figure 4: Portfolio construction: free cash flow of three fields in multiple locations.

It is interesting to observe that by implementing portfolio construction, two fields (Field B & C) cash flow will result ca. 1.8 million USD cost saving per year, combined with Field A. This example, thus, show a positive impact of portfolio construction to increase probability of project feasibility.

CONCLUSION

Overall, iPPP appears to be positive attempt to accelerate geothermal development in Indonesia. While not conclusive, there are opportunity that iPPPs have ability to improve operational efficiency in regulatory regimes and contractual specificities. A strong public partner like PLN (as off-taker with enormous financial profile) can lead to a power balance between partners in a public-private joint venture. Appealing in iPPP arrangements, PLN attempts to pursue an opportunity of developing large, massive investments with minium public expenditure, bringing the expertise and profit-oriented approach of the private sector, to geothermal projects of public service delivery.

This paper presents a preliminary approach of an institutionalized PPP applied to geothermal power plants, in Indonesia. This was the first iPPP attempted to be carried out in this sector, and it is clear the political commitment in promoting the development of this sector in Indonesia using private leverage to induce growth. Confirmation can be found in the evaluation factors under the partner selection procedure that 90% of technical weight given to the upstream skills and partner should provide 20% of total project cost, which is commonly recognized as exploration cost portion. There are still some barriers regarding the development of this sector related to the cost per unit of power. In fact, from an economic perspective, there is an extra cost (risk) related with this energy type, when compared to more conventional energy sources. This work focuses into two main objectives: the first comprised in the analysis of an iPPP arrangement for geothermal energy projects, focusing on understanding the factors of access and competition aspects related to a business of this nature, and the second considered the analysis of the risks related with this sector, including portfolio construction to mitigate the risk.

Based on the analysis presented in this work, PLN geothermal iPPP is designed to catalyze fast track process to GPPA (payback), compliance to Government regulation for tariff determination (MEMR Decree 50/2017), achievement of geothermal capacity target, COD acceleration, and development of marginal geothermal fields.

Private partners are particularly sensitive to revenue risk, since they are mostly interested in the financial viability of the project. Mechanisms for sharing the risk between the public and private sectors as a way to overcome the revenue risks are of great importance. Value can be created by incorporating flexibility in different stages of a project life cycle. Government support, which can be interpreted as a form of call/put option, may play important roles in iPPP–BOOT project success and, when necessary, should be carefully designed and formulated. Further work is to conduct a study into how real option analysis can be applied in modeling the contractual/managerial flexibilities to mitigate and manage the revenue risk in iPPP projects.

REFERENCES

Castlerock. (2009), "Geothermal Pricing & Incentive Policy Study". Work Report to Ministry of Energy and Mineral Resources.

Castro, V., and Janssens, J. G. (2011), "Mixed Private-Public Ownership Companies "Empresa Mixta" ". Work Report to World Bank.

Devapriya, K. A. K. (2006), "Governance issues in financing of public-private partnership organizations in network infrastructure industries". International Journal of Project Management 24, 557–565.

Sanyal, S. K., A. J. Menzies, P. J. Brown, K. L. Enedy and S. Enedy (1989). "A Systematic Approach to Decline Curve Analysis for The Geysers Steam Field, California." Trans.

Geothermal Resources Council, Santa Rosa, California, p. 415.

Sanyal, S. (2005), "Cost of Geothermal Power and Factors that Affect It", Proceedings World Geothermal Congress 2005. Antalya, Turkey.

World Bank. (2013), "Joint Ventures/Government Shareholding in Project Company". Retrieved from https://ppp.worldbank.org/public-private-partner ship/agreements/joint-ventures-empresas-mixtas.

Yue, C., Liu, C. Liou, E. M. L. (2001), "A transition toward a sustainable energy future: feasibility assessment and development strategies of wind power in Taiwan", Energy Policy 29, 951–963.

A DECADE OF THE WORLD BANK ENGAGEMENT IN INDONESIA GEOTHERMAL SECTOR

Muchsin Chasani Abdul Qadir

The World Bank, Jakarta - Indonesia
Email: mqadir@worldbank.org

ABSTRACT

The useful roles of geothermal energy to provide cleaner power generation and reduce the greenhouse gas emissions has made the World Bank emphasizes it as one of key priorities for the energy engagement strategy in several countries. Geothermal is also one of the valuable indigenous clean energy resource in Indonesia in which the national grid is dominated by fossil-fueled generation. In Indonesia, the World Bank has been more than a decade having engagement in the geothermal sector, which including carbon finance transaction, investment projects, and advisory services & analytics. The support to Indonesia has been increasing during the years and involving more various stakeholders, including with Ministry of Energy & Mineral Resources, Ministry of Finance, Ministry of Environment & Forestry, PT. PLN, PT. Pertamina Geothermal Energy, and PT. Sarana Multi Infrastruktur. The latest geothermal project is supporting Government of Indonesia to conduct exploration drilling prior to concession tender. A total of $369 million in loans and grants has been committed to support geothermal development in Indonesia. This paper will describe the World Bank geothermal journey in Indonesia during the past ten years, including a brief information of global geothermal support provided by the World Bank.

Keywords: World Bank, geothermal support, clean energy

INTRODUCTION

Renewable energy is one of main priorities along with universal access and energy efficiency as have been outlined in the Directions for the World Bank Group's Energy Sector to achieve a sustainable energy future for all (The World Bank, 2013). As a form of renewable energy, geothermal is an indigenous and relatively low-cost source to produce power in baseload operation. The geothermal development, which can replace the fossil-fueled generation, may address the issue on local and global environmental impacts such greenhouse gas emissions. During a high and volatile fossil fuel prices, geothermal could mitigate risks due to price volatility. Accelerating geothermal and other renewables complemented with sustainable development of hydropower and the gas sector is also emphasized as the strategy for renewable energy and low carbon development under the latest International Bank for Reconstruction & Development (IBRD)/ International Finance Corporation (IFC)/ Multilateral Investment Guarantee Agency (MIGA)'s Country Partnership Framework for Indonesia (The World Bank, 2015). In doing the support on geothermal, the WBG provides it in environmentally, financially, fiscally, and socially sustainable way of energy development.

This paper describes the World Bank's support on the geothermal development in the last ten years with a focus on geothermal sector in Indonesia. Current global support for geothermal in various countries is also presented in this paper.

GLOBAL GEOTHERMAL SUPPORT

A total of more than $900 millions of loans and grants/Technical Assistance is provided by the World Bank (IBRD/IDA) currently to support geothermal development globally. The client includes countries from Asia and Pacific, Africa, and Latin America (see Figure 1). There are several supports that are provided on those countries such as power plant and steam gathering system development (Indonesia), exploration drilling (Armenia, Djibouti, Indonesia, Turkey), resource assessment (El Salvador, Fiji, Kazakhstan, Mexico), and enabling policy development (Mexico, Chile, Kenya).

The WBG engagement in global geothermal sector is also provided through IFC and Energy Sector Management Assistance Program (ESMAP). IFC, an institution under the WBG providing financial services to private sector, has recently agreed to provide a $90 million of equity loan to Energy Development Corporation (EDC) of the Philippines. The loan will support EDC's capital requirements and other general corporate purposes for existing geothermal operations (IFC, 2018). ESMAP is a partnership between the WBG and 18 donor partners to provide analytical and advisory services in the sustainable energy sector to low and middle-income countries. Among other supports from ESMAP, Global Geothermal Development Plan (GGDP) is a key initiative of ESMAP and other multilateral/bilateral development to address the primary obstacle of geothermal development: cost and risk of exploration drilling. The key pillars of the GGDP are focus on upstream support, global knowledge works, and Technical Assistance (TA) on preparation of geothermal investment project, strengthening of enabling environment in client countries, strengthening capacity of implementing

agencies, and assessment of geothermal resources (ESMAP, 2018).

On the area of geothermal knowledge activities, many reports and publication have been produced by different institutions under the WBG. ESMAP is leading in number of publications which includes "Scaling-Up Renewable Geothermal Energy in Indonesia", "Geothermal Resource Risk in Indonesia: A Statistical Inquiry", "Geothermal Handbook | Planning and Financing Power Generation", "Comparative Analysis of Approaches to Geothermal Resource Risk Mitigation: A Global Survey", and "Greenhouse Gases from Geothermal Power Production". IFC also published geothermal reports on exploration and drilling such as "Geothermal Exploration Best Practices: A Guide to Resource Data Collection, Analysis, and Presentations for Geothermal Projects", " Success of Geothermal Wells: A Global Study", and "Best Practices Guide for Geothermal Exploration". A joint technical assistance between the World Bank and Asian Development Bank (ADB) produced a report "Unlocking Indonesia's Geothermal Potential" (ADB and The World Bank, 2014).

THE WORLD BANK GEOTHERMAL SUPPORT IN INDONESIA

A total of $369 million geothermal support has been provided and/or committed by the World Bank to Indonesia, since early engagement back in 2007 until now. Loans (IBRD and CTF) has been the major share of the supports accounting 81.3% from the total number and the grants (CTF, GEF, Profor, Netherland, and New Zealand) as the remaining amount. The total number does not include any Advisory Services and Analytics which were provided as part of policy dialog with Government of Indonesia. The different supports to Indonesia geothermal sector by the World Bank is presented in Figure 2 below.

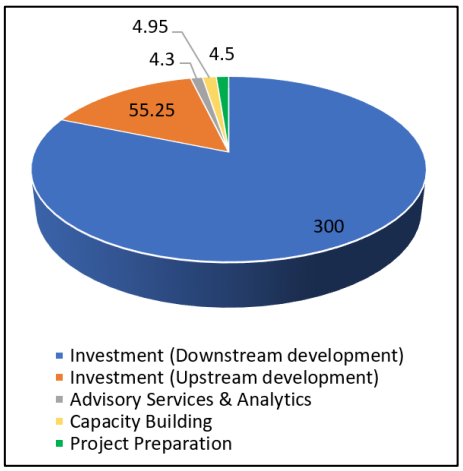


Figure 2: Geothermal Support by the World Bank to Indonesia.

The following section describes the geothermal journey of the World Bank engagement in Indonesia for the last decade.

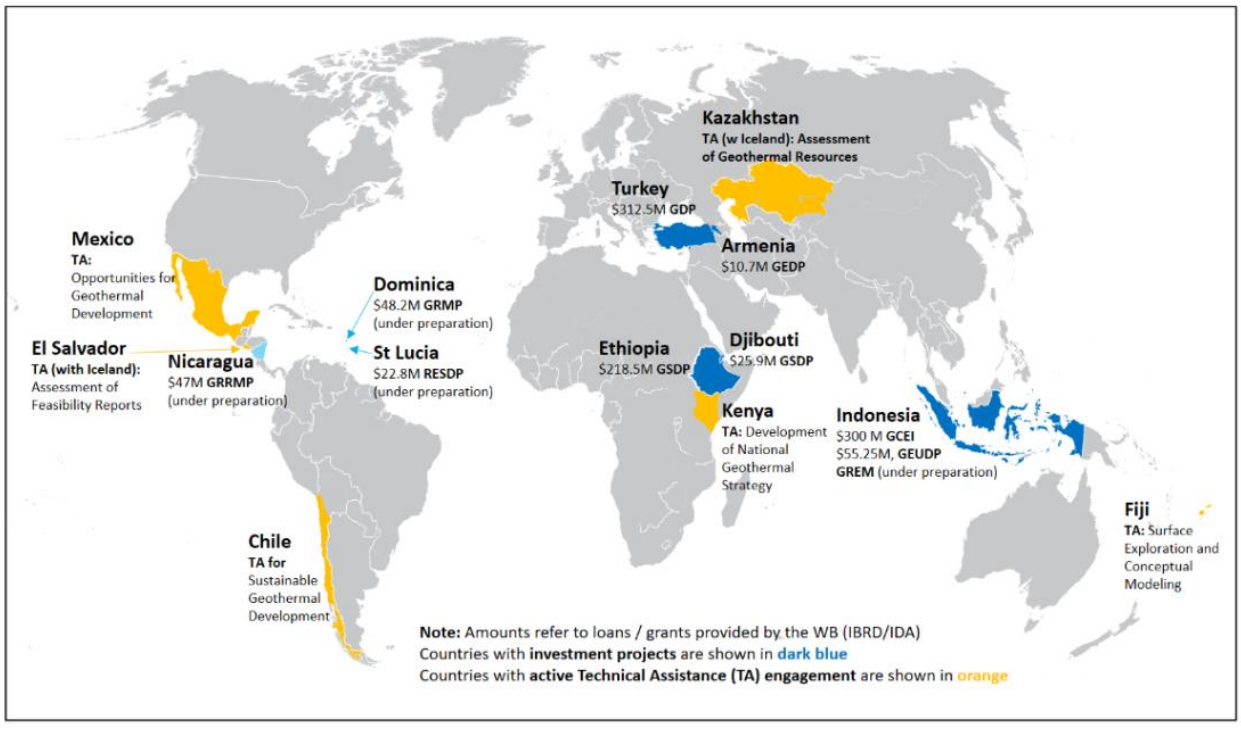


Figure 1: Worldwide Geothermal Support by the World Bank.

Carbon Finance Transaction

Purchasing of CO_2 emissions avoided by PT. PLN's Lahendong II geothermal power plant (20 MW) under the Clean Development Mechanism (CDM) at 2007 was the first World Bank geothermal activity in Indonesia (The World Bank, 2013). As the trustee of the Netherland Clean Development Mechanism Facility, the World Bank was expected to purchase the Certified Emission Reduction (CER) induced by the power plant from 2008 to 2012. Until its completion at 2012, the total recorded emission reductions (ERs) was 215,778 tCO_2 or 63.5% of scheduled ERs in the purchase agreement. It was a first experience for PT. PLN to have carbon finance transaction from geothermal power plant with many lessons learnt were built, however, the project did not have any chances for replication to other geothermal project following the collapse of carbon trading market due to very low CER price.

Advisory Services and Analytics

A Global Environment Facility (GEF) grant-financed was implemented at 2008 by Ministry of Energy and Mineral Resource (MEMR). The project, namely Geothermal Energy Power Development, provided $4 million of GEF grant to support MEMR in preparing and implement geothermal sector reform and assisting the transaction of geothermal power investment (The World Bank, 2008). This support was timely needed after the issuance of the first Geothermal Law at 2003. The expected outputs of this project were the development of pricing mechanism, upstream risk mitigation measure, and implementing regulation of the Geothermal Law. The project was also intended to develop procedure and provide support on the transaction of geothermal concession tender. A number of studies were produced by the project and, directly or indirectly, has influenced the development process of geothermal tariff setting, tender regulation, and other geothermal implementing regulations. In parallel with the project, the development of geothermal resource risk mitigation was led by Ministry of Finance (MoF) through establishment of Geothermal Fund Facility at 2011.

Following stalled of 2012 geothermal Fit-in-Tariff regulation due to conflicting with another regulation at higher level, a joint support from the World Bank and ADB was provided to MEMR at 2014 for the development of a new tariff approach (ADB and The World Bank, 2014). The study recommended a new ceiling tariff based on avoided cost in three different areas (Sumatera/Java/large coal power plant dominated, East Indonesia/small coal power plant dominated, and small islands/off grid with diesel dominated). The new ceiling tariff approached was not based on production cost of geothermal energy, but mainly from the avoided thermal generation cost and added with externalities such as avoided greenhouse gas emissions, volatility of oil/coal price, and local employment. MEMR adopted the recommended ceiling tariff and issued a new geothermal tariff regulation at 2014.

In collaboration with Ministry of Environment & Forestry (MoEF) and MEMR, a TA on Sustainable Geothermal Power Development in Forest Areas was commenced in 2017. Most of prospective geothermal resource in Indonesia are in the forest areas and even many of them are located inside the conservation forest. The forestry status and its land acquisition process have been identified as one of key issue for geothermal development. The TA assessed the potential environmental and social impacts for 327 geothermal sites in Indonesia and summarized it in the report "Rapid Environmental and Social Assessment of Geothermal Power Development in Conservation Forest Areas".

Investment Projects

There are two geothermal investment projects which are supported by the World Bank at this moment.

Geothermal Clean Energy Investment Project

The project was designed to support PT. Pertamina Geothermal Energy (PT. PGE) in developing Ulubelu Units 3-4 and Lahendong Units 5-6 geothermal power plants and its steam gathering facilities with total capacity of 150 MW (The World Bank, 2011). The project financing scheme includes $175 million of IBRD loan and $125 million concessional Clean Technology Fund (CTF) loan. The financing support was complemented with the grants from Netherland ($2.5 million) and New Zealand ($6.95 million) to support the project preparation and capacity building program with the client. The concessional CTF loan helped the project to increase its commercial viability, specifically for Lahendong 5-6. The construction of both power plants has been completed in 2016-2017 and now in operation commercially generating electricity to PT. PLN's grid.

Geothermal Energy Upstream Development Project

The initiative of government sponsored exploration drilling to address high resource risk and upfront capital cost is facilitated under the Geothermal Energy Upstream Development Project (The World Bank, 2017). The project utilizes $49 million CTF grant, $6.25 million GEF grant, and $49 million Infrastructure Financing for Geothermal Sector (Pembiayaan Infrastruktur Sektor Panas Bumi or PISP, formerly Geothermal Fund Facility). The implementing agency is PT. Sarana Multi Infrastruktur (PT. SMI) which also the manager of PISP fund for geothermal development. The first drilling at Waesano Flores is scheduled at early 2019. By the end of the project, it is expected that

exploration drilling for four sites will be carried out and will enable at least of 65 MW geothermal power development.

FUTURE INITIATIVE

Building on a long engagement around geothermal energy in Indonesia, the World Bank is currently preparing a facility for geothermal resource risk mitigation support. The facility will provide financing support for geothermal drilling exploration with an element of partial loan forgiveness for unsuccessful exploration drilling. Both State Owned Enterprise and private geothermal developers will be able to access the facility which will be launched in 2019. This initiative will unlock geothermal investments through risk mitigation for exploration drilling and is expected to attract commercial finance and leverage several billion dollars in private sector funding (The World Bank, 2017).

Table 1: Geothermal Engagement in Indonesia by Other Multilateral/Bilateral Institutions.

Projects	Supports
Sarulla Geothermal Project	ADB supports private sector project finance
Rantau Dedap Geothermal Project	ADB supports private sector project finance
Muara Laboh Geothermal Project	ADB supports private sector project finance
Lumut Balai Geothermal Project	JICA supports PT. PGE on downstream development finance
Tulehu Geothermal Project	JICA supports PT. PLN on exploration drilling finance
Hululais Geothermal Project	JICA supports PT. PLN on the engineering services of power plant construction
Geothermal Development Policy	JICA supports MEMR/MOF/Geological Agency/PT. SMI
Kamojang Geothermal Project	KfW supports PT. PLN on the rehabilitation of existing power plant
INZ – Geo (Partnership Cooperation)	New Zealand supports JICA supports MEMR/Geological Agency/PT. SMI on capacity building related activities
Fixed Tariff Study and Development of Flores Geothermal Island Roadmap	UK (Prosperity Fund) supports MEMR

CONCLUSIONS

During the last ten years, the World Bank engagement in Indonesia geothermal sector has been covering various areas and helping the sector to address main issues that could hinder the development. In recent years, the World Bank sees that high resource risk and huge capital upfront for exploration are the main and urgent issues to be addressed. Government sponsored exploration drilling at implementation stage and resource risk mitigation facility at preparation stage are efforts that the World Bank offers to address those geothermal sector issues.

REFERENCES

Energy Sector Management Assistance Program/ESMAP. (2018), "Global Geothermal Development Plan (GGDP)". Retrieved from https://www.esmap.org/GGDP.

International Finance Corporation/IFC. (2018), "IFC Project Information Portal". Retrieved from https://disclosures.ifc.org/#/projectDetail/SII/39842.

The World Bank. (2008), "Project Appraisal Document on a Proposed Global Environment Facility (GEF) Grant of US$4 Million to the Republic of Indonesia for a Geothermal Power Generation Development Project". *Document of The World Bank*, for official use only.

The World Bank. (2011), "Project Appraisal Document on a Proposed Loan in the Amount of US$175 Million and a Proposed Loan from the Clean Technology Fund in the Amount of US$125 Million to the Republic of Indonesia for a Geothermal Clean Energy Investment Project (Total Project Development in Ulubelu Units 3 & 4 and Lahendong Units 5 & 6". *Document of The World Bank*, for official use only.

The World Bank. (2013), "Implementation Completion and Results Report for Lahendong II Geothermal Power Project".

The World Bank. (2013), "World Bank Group Sets Direction for Energy Sector Investments". Retrieved from http://www.worldbank.org/en/news/feature/2013/07/16/world-bank-group-direction-for-energy-sector.

The World Bank. (2015), "Country Partnership Framework for The Republic of Indonesia for the Period FY16 – FY20". *Document of The World Bank*, for official use only.

The World Bank. (2017), "Project Appraisal Document on a Proposed Clean Technology Fund (CTF) Contingent Recovery Grant in the Amount of US$49 Million and a Global Environment Facility (GEF) Grant in the Amount of US$6.25 Million to the PT Sarana Multi Infrastruktur (PERSERO), Indonesia for the Geothermal Energy Upstream Development Project". *Document of The World Bank*, for official use only.

The World Bank. (2017), "Geothermal". Retrieved from https://www.worldbank.org/en/results/2017/12/01/geothermal.

The Asian Development Bank/ADB and the World Bank. (2014), "Indonesia Geothermal Tariff Reform: Tariff Methodology Report".

The Asian Development Bank/ADB and The World Bank. (2014), "Unlocking Indonesia's Geothermal Potential".

AN EXAMINATION OF THE POTENTIAL OF PUBLIC PRIVATE PARTNERSHIPS (PPPS) TO STIMULATE THE DEVELOPMENT OF GEOTHERMAL ENERGY IN INDONESIA: CONCEPT AND ANALYSIS METHODS

Suardi Nur[1], Dr. Ariel Bergmann[1], and Prof. Bruce Burton[2]

[1]Centre for Energy, Petroleum, Mineral Law and Policy (CEPMLP), University of Dundee
[2]School of Business, University of Dundee
Nethergate, Dundee DD1 4HN, United Kingdom
Email: nnur@dundee.ac.uk

ABSTRACT

The development of Indonesian geothermal energy has progressed slowly. The government will most likely fail to achieve the target as stated in its geothermal development road map. Many barriers to geothermal energy investment have been identified, such as an insufficient selling price, and excessively high risks, particularly in resource development and exploration. According to Nugraha et al. (2017) Government provision of tax incentives have less impact on reducing resource risk compared to financial incentives in form of interest rate incentive and government support for exploration drilling. Furthermore, there is no clear risk sharing mechanism, resulting in developers bearing a disproportionate risk compared to other potential investments (Castlerock, 2010). This paper proposes a conceptual framework model of Public-Private Partnerships (PPPs) in risk allocation and financing that addresses the critical barriers to investing. The conceptual design identifies approaches to reduce risks borne by private companies (geothermal project developers). It focuses on 3 key features of PPP frameworks: 1) risk analysis, 2) identifying optimal risk allocation between public and private sectors, and 3) exploring effective government financial support options, with objective to establish a balanced and functional PPP contractual agreement.

Keywords: Geothermal development, PPPs framework, finance, risk allocation project management.

INTRODUCTION

Private sectors have been participating in financing infrastructure services across the world in multi forms of partnerships (Broadbent and Laughlin, 2003). Initial purpose of adopting a PPPs model is to reduce government financial burden and enhance the efficiency of infrastructure project construction (Kang, et al, 2012). In United Kingdom, the partnerships model between public and private sector in delivering the public services is known as Private Finance Initiative (PFI) that has been introduced in 1992 (Spackman, 2002). In the United States of America and Canada such partnerships are often termed as Public-Private Partnerships (PPP or P3) (Vining et al, 2005).

There are different perspectives on PPPs definition amongst scholars. Some scholars view PPPs as a new governance tool that will replace the traditional method of project procurement through more competitive tendering. Others see PPPs as only a "language game" of public management by including the established procedure of engaging the private sector in realizing the public services (Hodge & Greve, 2007).

Although there is no consensus on definition of PPPs, all available definitions are emphasized on "long term contract", "risk and profit sharing" and "jointly to produce a product or service". This shows that PPPs is a long term collaboration, risk and profit sharing of public and private sectors to produce a product or service (Hodge & Greve, 2007).

Project financing has been used to as one of financing model to finance PPPs project (Daube et al, 2008). The successful to finance The Channel Tunnel project between Britain and France in 1987 and Dartford Bridge project have influenced the application of project financing techniques for BOT concession projects (Yescombe, 2007).

Geothermal energy project in Indonesia has used project financing as financing model to finance the project. However, there are many projects cannot be completed as the project fail to achieve financial close. The issues in geothermal project financing is high risk coupled with high upfront cost as reported by JICA (2009) *"The barriers which hinder smooth development of geothermal energy are the development risks of underground resources and the burden of enormous up-front investment"*

The implementation of PPPs scheme for geothermal project is expected to solve this investment barriers through the optimal risk allocation framework between government and developer to reduce the risks to be borne by private sector. According to Dailami and Klein (1997) in PPPs project government can reduce the risk to be borne private sector by providing financial supports in form of subsidies, guarantee, and capital contribution.

THEORETICAL FRAMEWORK

The objective of a PPPs project is to established synergetic effect through risk transfer, combination of specific expertise and economic competence of private and public sector that are developed through optimal risk allocation that reflect the partners capacity (Girmscheid, 2013). The purpose of optimal risk allocation is to minimize total project cost. Girmscheid (2013) cited Girmschied (2006) postulates three dimension of risk allocation:

1. Risk allocation to influence the probability of occurrence.
2. Minimizing of impact; and
3. Risk coverage capacity of risk taker.

The goal of risk allocation in the case of geothermal project in Indonesia is to minimize project cost of private partner. The interest of Government as public partner to participate in PPPs contractual agreement is for the purpose of economic development and improving social welfare while the interest of private firms are profit maximization, and expense reduction through provided incentives, which can lead to cost-cutting of private firms (Shrestha, 2015).

This relationship is explained by neoclassical theory of the firm that later is enhanced with Principal Agent (PA) theory. Profit maximization in this case refers to maximization of expected net present value of future profit. Principal Agent (PA) theory explains the relationship between public and private partners which has difference of interest for the project.

In this project, Government are the principal and Private Sector firms are the agents. All parties are assumed to focus on their own interests. The interest of government to involved in PPPs contractual arrangement is for provision of power. Meanwhile the firms have interest to maximize shareholder wealth.

According to (Stiglitz, 1989), therefore principal will try to align the agent to act according to his interest by designing an incentive scheme. However even under an optimal incentive scheme, agents still have their own interest or objectives therefore conflict of interests can remain.

According to Oudot (2005), another issue in PPPs contractual arrangement is the relation between an informed person (the Agent) and an uninformed one (the Principal), this information asymmetry can cause two issues which called adverse selection and moral hazard that can lead to higher risk in the realisation of the project.

Thus, according to De Palma et al (2012) PPPs contractual arrangement of the principal-agent model must be built with optimal risk sharing contract based on assumptions:

1. Information is asymmetric between the parties.
2. The agent may act at its own interests that may be contrary to those of the principal interest.

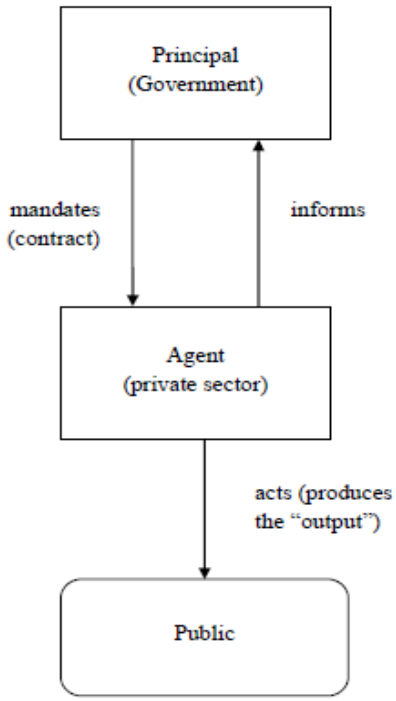


Figure 1: Principal agent framework (De Palma et al, 2012)

RISK MANAGEMENT IN PPP PROJECT

European Commission (2003) in the EU Guidelines for Successful Public and Private Partnerships defined risk as: *"Any factor, event or influence that threatens the successful completion of a project in terms of time, cost or quality".*

Risk management is important in dealing with risk impact by identifying potential risk factors and assessing the consequences of identified risks on the project. Risk management process can be applied to evaluate the risks associated with the project (Tummala & Burchett, 1999).

Risk management approaches have been developed diversely among the authors. Ward & Chapman (2003) outlines a generic risk management framework for projects referred as to SHAMPU (Shape, Harness, and Manage Project Uncertainty) process.

A more simplified process is presented by Project Management Body of Knowledge (PMBOK® Guide) book, the sequences of risk management process consist of risk management planning, risk identification, risk analysis (qualitative and

quantitative), risk response planning and risk monitoring and control (Project Management Institute Inc, 2000).

In PPPs project risk management process is crucial for successful of the project as the identified risks have to be allocated to the party that is best able to manage (i.e. influence and control) the risk at the least cost (Ke et al, 2010).

RISKS IN GEOTHERMAL PROJECT

Located between the Mediterranean Volcanic Belt and the Circum-Pacific Volcanic Belt, Indonesia has all classifications of geothermal resources. It has been identified there are 312 geothermal sites spread around Indonesia with total potential power production of 28,910 MWe (DGNREEC, 2015). However, these abundant resources are not optimally utilized to generate electricity. In geothermal sector, only approximately 6% or 1,698.5 MW of Indonesia's geothermal resources has been utilized (DGNREEC, 2017).

Risk in geothermal are reduced progressively through increasing investment in exploration and development (Castlerock, 2010). The indicative correlation of cost and risk reduction in green-field geothermal project is illustrated by Quinlivan et al (2015) in figure 1. Assessment conducted by Assessment conducted by (GeothermEx Inc, 2010) drilling success rate in Indonesia is about 62% , however the ratio is derived from database which includes the drilling of exploration wells, confirmation wells, development wells and make-up wells. Therefore, the exploration drilling success rate should be lower than this success rate.

Deloitte Development LLC (2008) estimates at least 6-8% or US$ 9 to 15 million of total project expenditure that allocated for exploration stage is at risk (see Figure 2).

More detail cost breakdown and typical risk allocation model in geothermal project development is provided by GeothermEx Inc. (2010) in table 1. They estimate 7-15% of risky cost has to be borne by private developer during exploration stage. Therefore, at this stage geothermal project is definitely not bankable until further development stage i.e after feasibility study that confirms its economic viability.

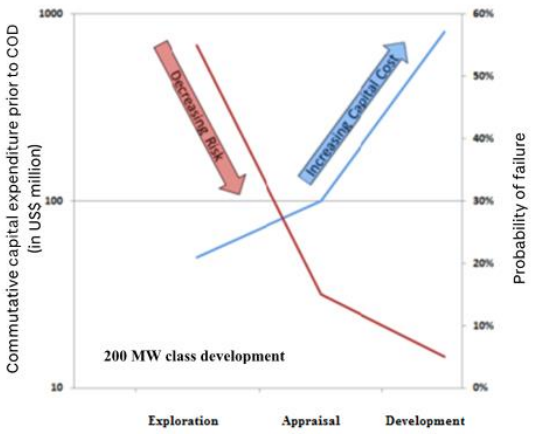


Figure 2: Indicative capital cost versus risk reduction in green-field geothermal project (Quinlivan et al,2015)

Table 1: Typical Risk Allocation in Geothermal Project

Stage	Cost (Thousand US$)	Total Cost (%)	Risk allocation
Regional reconnaissance studies to select prospect for exploration	250 - 500	~ 1	Typically borne by government; may be borne in part by private developer
Detail surface exploration: geology, geochemistry, and geophysics	1,000-1,500	2 -6	Often borne by government; usually augmented or borne by private developer
Temperature gradient Drilling: 3 to 5 holes @ 100-500 m depth	300 – 2,000	~ 1	Occasionally borne by government; usually borne by private developer
Deep exploratory holes drilling: 1 to 3 holes @ 1.5 to 2.8 km depth	7,000 – 23,000	3-7	Occasionally borne by government; usually borne by private developer
Long term flow testing and numerical simulation of reserves ('Bankable document)	500 – 1,000	> 1	Very rarely borne by government; almost always borne by private developer

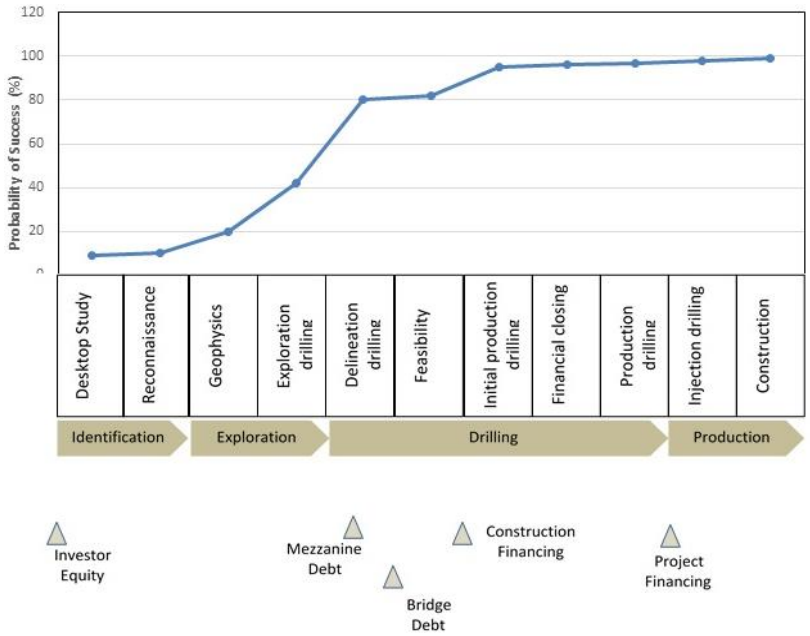


Figure 3: Development stages of geothermal project and their typical financing sources (Deloitte Development LLC,2008).

Considering this nature, at this stage it is often the concession winning bidder fails to achieve financing close for the project as the developers have to rely on their equity to finance exploration stage (Gehringer and Loksha, 2012).

Normally, loans financing is available after exploration drilling where the probability of success is reaching 40% (see figure 3).

Resource/Exploration risk

Geothermal resource risk can be divided into three categories: 1) drilling and well completion, 2) initial well characteristics and 3) resource degradation overtime (Robertson-Tait et al, 2008).
United Nations Environment Programme (2004) defines exploration risk as the risk of not successful in achieving (economically acceptable) minimum levels in thermal water production (minimum flow rate) and reservoir temperature.

The mitigation strategy to reduce resource risks starts with an understanding geological setting and an accurate assessment of resources by employing sufficient geological, geochemical and geophysical surveys to acquire accurate data of surface manifestations and sub-surface geological setting such as permeability and fluid flow (Matek, 2014).

Operation risk

Operation risks in geothermal include all the risks occurred during operation stage. The risks can be inform of resource degradation and operation risks caused by geothermal fluid chemistry to power plant installation such as pipe line and turbine that caused by chemical composition of geothermal fluid (Schulz et al, 2007).

Poor injection strategy can lead to greater decline of reservoir pressure or temperature than anticipated natural rate of resource degradation that potential to reduce power plant performance (Matek, 2014). The strategy to manage this risk is by conducting proper reservoir modelling based on accurate geological, geochemical and geophysical data. The change in reservoir condition can have an impact on power plant operation and efficiency, sometimes the power plant system needs to be modified to match new resource condition as happened in Geyser geothermal field.

The most significant risks in geothermal power plant operation that is originated from geothermal fluid chemistry are scaling and corrosion of injection system and injection wells. These risks are occurred due to presence of Silica (Si), Calcium Carbonate ($CaCO_3$), or Iron (Fe) in geothermal brine. It requires appropriate geochemical assessment and a chemical injection treatment (Matek, 2014).

Credit risk

In project finance, credit risk is relatively high at the inception of project and tend to diminish over the life of project (Sorge, 2004). Project finance usually is characterized by large capital intensive and require substantive investment upfront. These characteristics coupled with high leverage and non-recourse debt, have implication on the term structure of credit risk. Long maturity project finance loans are not necessarily perceived by lender riskier than short-term credit. However, long-term commitment of lenders might make them exposed to the risk of political interference by host government. In this case the lenders will require the guarantees from multilateral development bank or export credit guarantee to commit for longer maturity loan,

particularly in emerging countries.

Credit enhancement, with additional collateral or third party guarantee, is widely believed as one of the most effective uses of public fund made available to support financing renewable energy projects (Marsh, n.d.). One of credit enhancement facility that has attracted interest from the World Bank is Guarantee Facility for Sub-Saharan Africa or GuarantCo. Credit enhancement provided by the Multilateral Financial Institutions (MFIs) has also been proven as an effective tool to mitigate perceived and actual credit risk.

THE APPROACH

Optimal risk allocation between parties is crucial success factor in PPPs project (Girmscheid, 2013). Therefore, the focus of in this paper is to propose a concept to identify a framework for the optimal allocation of risk between public and private parties in PPP arrangement so as to improve the viability of geothermal project in Indonesia.

This study is conducted with a view to providing theoretical and practical contribution in the area of risk allocation in PPPs project within the context of geothermal energy project. Thus, the proposed approach is expected to contribute to theoretical and practical insights. The approach of this study is using multi methods, therefore the triangulation results of empirical study of risk allocation and quantitative risk analysis using Monte-Carlo simulation of a case study could provide a more comprehensive understanding of risk allocation and its impact on value maximization (i.e. NPV) of geothermal PPPs; this will in turn contribute to deductive theoretical development within the neo-classical and principal-agent framework.

ANALYSIS METHODS

This study is using multi method research framework by combining the quantitative modelling approach with case study and empirical studies by using Delphi questionnaire survey.

To perform quantitative risk analysis, a case study is selected. The probability and impact of risks are analyzed by using probabilistic risk analysis of NPV model simulated with Monte Carlo simulation by using @RISK software. This analysis is conducted to figure out the probability and impact of risky variables on project financial viability. The results are expected to indicate whether the project is viable in absent of optimal risk allocation and government supports. The form of government financial support can be in form of capital contribution such as government drilling, interest rate subsidy or guarantee.

Optimal risk allocation is empirically studied by using Delphi questionnaire survey. Based on this study, the optimal risk allocation framework is developed. Delphi survey has been used frequently for empirical data collection construction in management research (Hallowell & Gambatese, 2009). It widely used for complex areas where consensus or convergence of opinion of experts is required on specific subject by using series of questionnaire surveys.

Table 2: Risk Allocation model framework for PPPs geothermal project in Indonesia.

Risk type	Risk factor	Risk probability	Risk impact	Risk allocation model (%)	
				Private	Public

Delphi panelist is selected carefully, because the results produced are directly related to the competency of panelist. The criteria used to guide the selection of Delphi subjects are having related background and experience concerning the geothermal project development. Considering the time, the size of panel is around 8 to 10 members. Delphi questionnaire survey is conducted in number of round until the consensus is obtained. However, considering the time 2 round surveys is preferred for this study. Mean score and standard error for each risk factor is used to determine the criticality of identified risks. Kendall's *W* is used to measure the degree of consensus and Cronbach's alpha is used to assess the reliability, or internal consistency, of the test items. Based on this optimal risk allocation framework, Monte Carlo simulation will be performed again to see the impact of optimal risk allocation on project NPV.

PRELIMINARY RESULT OF RISK ANALYSIS

Risk analysis has been conducted to a 55 MW rated power plant. The total investment cost of the project is estimated US$ 198 million. The project is assumed to obtain financial support from government inform of capital grant for exploration stage US$ 9 million and government provide loan guarantee to lender (junior loan) for a loan amounted that makes the developer able to get lower interest compare to commercial loan from third party (senior loan). This loan is available after feasibility study which will be used to finance development stage and Engineering, Procurement and Construction (EPC).

Table 3: The loan amount used in the model

Loan	Amount (US$ million)	Interest rate (%)	Repayment (yrs)
Senior loan	72	6.5	10
Junior loan	97	4.5	10

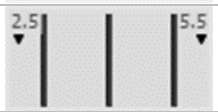
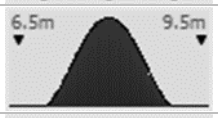
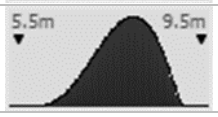
In this project, public partners and developers decided to use 10% IRR as financial viability indicator. Others assumption used in the @RISK model are:

1. Discount rate: 10%
2. Corporate income tax: 34%
3. Royalty rate: 2.5%
4. Production bonus: 0.5%
5. Power plant capacity factor: 95%

Uncertain variables:

1. Base price/MWh (Min. US$ 100, Max 115).
2. Number of exploration wells (Min. 3, Max. 5).
3. Number of production wells (Min. 6, Max 8).
4. Exploration drilling cost (Min. US$ 7 million, Most Likely US$ 8 m, Max. US$ 9 m).
5. Production drilling cost (Min. 6 m, Most Likely US$ 7, and Max. US$ 8 m).

Table 4: Distribution function used in the model

Name	Graph
Base price ($/MWh)	
Number of exploration wells	
Number of Production wells	
Exploration Drilling cost/well	
Production Drilling cost/well	

These uncertainty will be simulated in the model by using @RISK software in 10,000 iteration to assess the impact of these uncertainty on the project NPV and IRR.

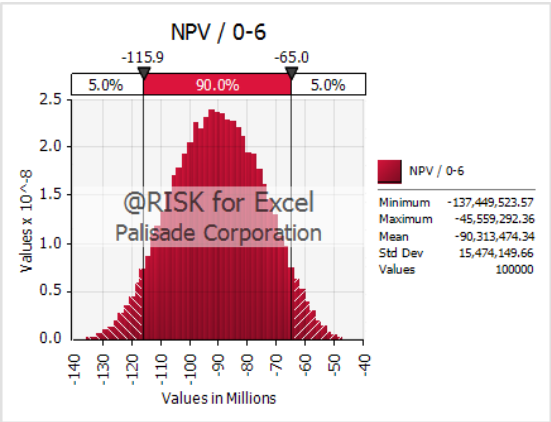


Figure 4: Project NPV with existing risk allocation contractual agreement

The simulation results show with existing financial supports in the project contractual arrangement, the project is still not financially viable which are indicated by NPV minus US$ 90 million and mean IRR 6%, which is far below the target of 10%.

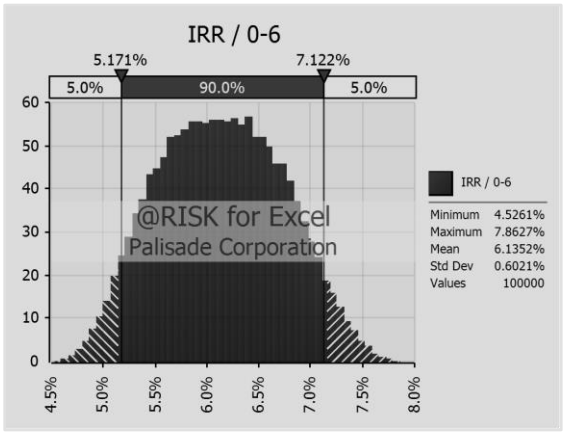


Figure 5: Project IRR with existing risk allocation contractual agreement.

Assuming developers are not eligible for tax holiday, this incentives scheme is not able to improve the viability of project. In this case, the developer has to negotiate the price above US$ 115/MWh. The simulation shows with the base price US$ 140 – 160/MWh the probability of the project to have positive NPV is 91% with IRR 12%.

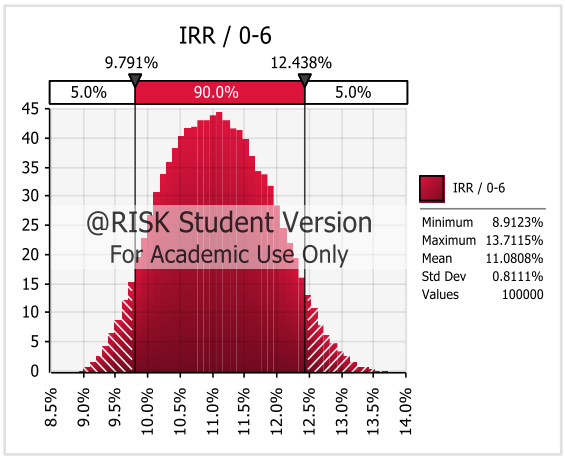


Figure 6: Project IRR simulated with base price US$ 140-160/MWh.

CONCLUSION

The preliminary result of case study shows that with existing risk allocation between government and developer, the project is still not financially attractive for developer. The possibility to bring project financially viable is by increasing the electricity tariff between US$ 140 to 160 per MWh. Practically PLN as single buyer will negotiate the price based on MEMR regulation No. 12/2017.

PPPs framework can be alternative solution to reduce the selling price with incentives schemes.

Therefore, in further this study will develop an optimal risk allocation framework that can be used as a guide during risk negotiation between public and private sector to form a balanced and functional PPPs contractual agreement for geothermal project.

REFERENCES

Broadbent, J., and Laughlin, R. (2003), "Public Private Partnerships: An Introduction". Accounting, Auditing & Accountability Journal, Vol 16, Issue: 3, pp.332-341. Retrieved from https://doi.org/10.1108/09513570310482282.

Castlerock. (2010), "Phase 1 Report: Review & Analysis of Prevailing Geothermal Policies, Regulations and Costs". Jakarta: Ministry of Energy and Mineral Resources.

Dailami, M., and Klein, M. (1997), "Government Support to Private Infrastructure Projects in Emerging Markets", Policy Research Working Paper, No. 1688. Washington: World Bank.

Daube, D., Vollrath, S., and Alfen, H. W. (2008), "A comparison of Project Finance and the Forfeiting Model as financing forms for PPP projects in Germany". International Journal of Project Management, 26(4), 376–387.

De Palma, A., Leruth, L. E., and Prunier, G. (2012), "Towards a Principal-Agent Based Typology of Risks in Public-Private Partnerships". Reflets et Perspectives de La Vie Économique, Tome LI (2), 57. Retrieved from https://doi.org/10.3917/rpve.512.0057.

Deloitte Development LLC. (2008), "Geothermal Risk Mitigation Strategies Report". Departement of Energy - Office of Energy Efficiency and Renewable Energy Geothermal Program. Retrieved from https://www1.eere.energy.gov/geothermal/pdfs/geothermal_risk_mitigation.pdf.

Directorate General for New and Renewable Energy and Energy Conservation /DGNREEC. (2015), "Statistik EBTKE 2015". Retrieved from http://ebtke.esdm.go.id/post/2016/02/02/1105/statistik.ebtke.2015.

Directorate General for New and Renewable Energy and Energy Conservation /DGNREEC. (2017), "Doing Business in Geothermal". Jakarta, Indonesia.

European Commission. (2003), "Guidelines for Successful Public - Private Partnerships". Directorate General Regional Policy, Bruxelles, Belgium. Retrieved from http://ec.europa.eu/regional_policy/sources/docgener/guides/ppp_en.pdf.

Gehringer, M., and Loksha, V. (2012), "Geothermal Handbook: Planning and Financing Power Generation". Energy Sector Management Assistance Program (ESMAP) Technical Report 002/12. Washington DC, USA. Retrieved from https://www.esmap.org/sites/esmap.org/files/DocumentLibrary/FINAL_GeothermalHandbook_TR002-12_Reduced.pdf.

GeothermEx Inc. (2010), "An Assessment of Geothermal Resource Risk in Indonesia". The World Bank, California, USA. Retrieved from https://repit.files.wordpress.com/2013/11/an-assessment-of-indonesia-geothermal-resource-risks-2010.pdf.

Girmscheid, G. (2013), "Risk Allocation Model (RA Model)". In The Routledge Companion to Public-Private Partnerships (p. 216). Oxon: Routledge.

Hallowell, M. R., and Gambatese, J. A. (2009), "Activity-Based Safety Risk Quantification for Concrete Formwork Construction". Journal of Construction Engineering and Management, 135 (10), 990–998. Retrieved from https://doi.org/10.1061/(ASCE)CO.1943-7862.0000071.

Hodge, G. A., and Greve, C. (2007), "Public-private partnerships: An international performance review". Public Administration Review, 67(3), 545–558. Retrieved from https://doi.org/10.1111/j.1540-6210.2007.00736.x.

Japan International Cooperation Agency/JICA. (2009), "Study on Fiscal and Non-Fiscal Incentives to Accelerate Private Sector Geothermal Energy Development in The Republic of Indonesia, Final Report (Summary)". West Japan Engineering Consultants, Inc.

Kang, C., Feng, C., and Kuo, C. (2012), "Comparison of royalty methods for build–operate–transfer projects from a negotiation perspective". Transportation Research Part E: Logistics and Transportation Review, 48 (4), 830–842. Retrieved from https://doi.org/10.1016/j.tre.2011.10.002.

Ke, Y., Wang, S., Chan, A. P. C., and Lam, P. T. I. (2010), "Preferred risk allocation in China's public-private partnership (PPP) projects". International Journal of Project Management, 28(5), 482–492. Retrieved from https://doi.org/10.1016/j.ijproman.2009.08.007.

Marsh. (n.d.), "Scoping Study on Financial Risk Management Instruments for Renewable Energy Projects". Marsh & McLennan Companies. Retrieved from http://www.globalclearinghouse.org/Infradev/assets%5C10/documents/UNEP%20-%20Scoping%20Study%20on%20Financial%20Risk%20Management%20Instruments%20for%20Renewable%

20Energy%20Projects%20%20%28n%20a%29.pdf.

Matek, B. (2014), "The Manageable Risks of Conventional Hydrothermal Geothermal Power Systems". Geothermal Energy Association. Retrieved from http://geo-energy.org/reports/Geothermal%20Risks_Publication_2_4_2014.pdf.

Nugraha, H. S., Saefulhak, Y., and Pangaribuan, B. (2017), "A Study on the Impacts of Incentives to the Geothermal Energy Electricity Price in Indonesia using Production-based Cost Approach". Proceedings The 5th Indonesia International Geothermal Convention & Exhibition (IIGCE) 2017.

Oudot, J. (2005), "Risk-allocation : theoretical and empirical evidences. Application to Public-Private Partnerships in the defence sector". The 9th Annual Conference of the Institutions of Market, 1–20.

Project Management Institute Inc. (2000), "A guide to the project management body of knowledge (PMBOK® guide)". Book. Pennsylvania. Retrieved from https://doi.org/10.5860/CHOICE.34-1636.

Quinlivan, P., Batten, A., Wibowo, M., Hinchliffe, S., Rahayu, D., Doria, I., Yahmadi, A., and Tondang, H. Y. T. (2015), "Assessing Geothermal Tariffs in the Face of Uncertainty, a Probabilistic Approach". Proceedings World Geothermal Congress 2015.

Robertson-Tait, A., Hennerberger, R., and Sanyal, S. (2008), "Managing Geothermal Resource Risk - Experience from United States". Workshop on Geological Risk Insurance, World Bank Geothermal Energy Development Program (GEOFUND), Karlsruhe, Germany. Retrieved from https://pangea.stanford.edu/ERE/pdf/IGAstandard/GeoFund/Germany2008/Robertson-Tait.pdf.

Schulz, R., Jung, R., Pester, S., and Schellschmidt, R. (2007), "Quantification of Exploration Risks for Hydrogeothermal Wells". Proceedings European geothermal Congress 2007 (pp. 1–6).

Shrestha, A. (2015), "Risk allocation in public private partnerships: a principal agent approach". The University of Melbourne. Retrieved from https://minerva-access.unimelb.edu.au/handle/11343/58552.

Sorge, M. (2004), "The nature of credit risk in project finance". BIS Quarterly Review (Vol. December). Retrieved from http://www.bis.org/publ/qtrpdf/r_qt0412h.pdf.

Spackman, M. (2002), "Public-private partnership: Lessons from the British approach". Economic Systems, 26(3), 283–301. Retrieved from https://doi.org/10.1016/ S0939-3625(02)00048-1.

Stiglitz, J. E. (1989), "Principal and Agent". Allocation, Information and Markets In J. Eatwell (Ed.), pp 241-253. Palgrave Macmillan.

Tummala, V. M. R., and Burchett, J. F. (1999), "Applying a Risk Management Process (RMP) to manage cost risk for an EHV transmission line project". International Journal of Project Management, 17(4), 223–235. Retrieved from https://doi.org/10. 1016/S0263-7863(98)00038-6.

United Nations Environment Programme. (2004), "Financial Risk Management Instruments for Renewable Energy Projects (First edition)". United Nation Publication, Oxford, UK.

Vining, A. R., Boardman, A. E., and Poschmann, F. (2005), "Public–private partnerships in the US and Canada: “There are no free lunches”. Journal of Comparative Policy Analysis: Research and Practice, 7(3), 199–220. Retrieved from https://doi.org/10.1080/13876980500209363.

Ward, S., and Chapman, C. (2003), "Transforming project risk management into project uncertainty management". International Journal of Project Management, 21(2), 58. Retrieved from https://doi.org/10.1016/S 0263-7863(01)00080-1.

Yescombe, E. R. (2007), "Chapter 1 – What are Public–private Partnerships?", Public-Private Partnerships Principles of Policy and Finance, 1-14. Retrieved from . https://doi.org/10.1016/B978-075068054-7.50025-3.

ENERGY CONSULTING AND USAGE OF SUSTAINABLE ENERGY IN HARZ

Syouma Hikmahtiar

Technische Universität Clausthal
Institute of Petroleum Engineering, Clausthal University of Technology,
Clausthal-Zellerfeld, Lower Saxony, 38678, Germany
Email: syoumahikmahtiar@yahoo.co.id

ABSTRACT

After decades of extensive usage of fossil energy resources, a politically-steered campaign promoting the usage of renewable energies was implemented in Germany. Although the different forms of sustainable energies are known to the public, the realization of some forms of them suffer due to the misconceptions and misplaced fears. In particular, geothermal technology recently has been subject to concerns due to accidents that occurred in pilot projects. Taking into account the technical advances in geothermal engineering, this technology is no longer in a premature state but a well-engineered and stable technology. The introduction and enlightenment of the public about geothermal technologies is of a paramount value, to support the spreading and development of this environmentally friendly sector of the renewable energies. Based on an academic recognition as an energy consultant, the energy consulting for the residential row house was carried out as a free of charge sample study. The process of the energy efficiency evaluation and energy consulting was realized in the energy consulting software ENVISYS EVEBI 8.3. For the evaluation of the current energy efficiency, the inhabited areas of the building were evaluated in terms of the used area and volume. A thermal frame was created. Within this thermal frame, all structures and components of the house were taken into consideration to obtain the total thermal emission of the house, as the thermal frame represents the border of the heated living space. For the structure of the exterior wall, no blueprint could be provided by the house owners. Since the exterior walls of a building are the largest area for thermal emission, their structure is of great importance for evaluation of the energy efficiency. However, the detailed structure of the exterior wall can only be obtained by destructive testing. To choose the heat pump, the current market of heat pump was considered. In this research, heat pumps from the company Viessman were taken into account. As illustrated in one of this result, based on the total thermal power demanded, Vitocal 300-G heat-pump type 10 was chosen. This heat pump provides 10.36 kW total thermal power which covers the demand for the house. In order to check the results from the calculation based on VDI guideline, the geothermal system was simulated using simulation program FEFLOW. For the simulation default values of FEFLOW and default values for double U-shape borehole heat exchangers were used. From the rate budget of FEFLOW, this system provides around 9.2 kW thermal energy for the heat-pump evaporator, which is more than demanded value of 8.43 kW.

Keywords: Sustainable energy, geothermal technology, FEFLOW, Harz, Germany.

DEFINITION OF SUSTAINABILITY AND GEOTHERMAL SYSTEMS

Geothermal energy is known as an environmentally friendly, clean, flexible, and renewable energy (Rybach and Mongillo, 2006). Environtmental friendly that means geothermal energy as a source of electricity and heat that have balance emissions of CO_2. Renewable energy refers to characteristics of resource to keep producing the best quality of energy and be ready to use with same condition. However, sustainability means ability of producing energy in long periods with all kind of treatment of production. Long term productivity means how great the geothermal energy economic for users is.

Table 1: Situation, consequences and recommendations for a policy on the sustainable thermal usage of shallow geothermal energy (Bonte et al, 2011).

Situation	Consequences	Policy
Current Status • Introduce geothermal energy • Add installation for shallow geothermal	*Environmental* Primary: • Influence on groundwater quality Secondary: • Global warming potential • CO_2 balance	*Environmental Assessment* • Groundwater quality
Effect • Temperature Anomalies	Social • Worries	*Monitoring*

In this research an essential geothermal energy reintroduce to the citizens that this resource totally outstanding. If the installation for shallow geothermal works properly, production cycles and lifetime will be under control. Steady production over long period with low maintenance should be economic. Conditions of temperature anomalies can be monitored during the systems perform by considering consequences. In Osterode, gypsum and karst are dominated (Herrmann, 1957). Chemical contents in groundwater directly use for cooling and heating process make the temperature change because equilibrium condition of mineral controls the mobilization of organic sediments (Arning et al, 2006). Pro and cons reach the peak

when citizens are entangled in systems, the Fukushima nuclear disaster still makes people scared and worried about the branding name of "renewable energy".

Consequence that influence on groundwater quality caused by groundwater organisms and ecosystems (Hancock et al, 2009). There are no big significant influence of temperature above freezing point, so that is why shallow geothermal energy has no influence on kind or amount of microorganisms (Schippers and Reichling, 2006).

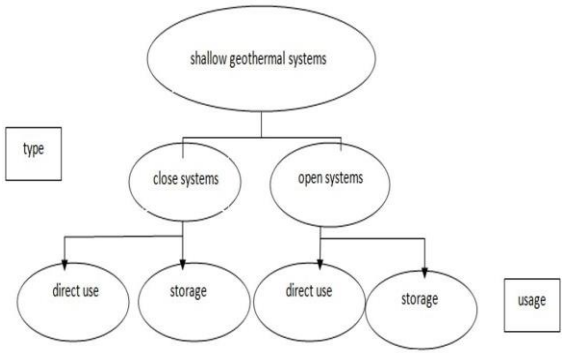


Diagram 1: Workflow of shallow geothermal systems (Blum et al, 2011) with modification.

The approval process for shallow geothermal exploitation have different stages. First, basic information such as groundwater temperature forecasting. Usually each region has a prediction of forecast on that area, so the minimum requirements already complete. Second, from design area obtained all data about wells/heat exchangers, temperature condition, pumping rates, heat power demand, thermal efficiency and estimation of time exploitation. Third, the final process is exploitation license means all possibilities for exploitation is compatible with requested criteria.

RESIDENTIAL HOUSE FOR THE SAMPLE STUDY AND ENERGY CONSULTING

Representative object for the energy consulting

To show up the opportunities for energy efficiency improvements in combination with energy generation from geothermal sources in the Harz region, a residential building was chosen as a representative object to carry out a sample study. As criteria for the selection process of the building, some frame parameters were set. As a first criterion, the residential building has to be located in the Harz area. Second, the type of building should be representative for a common type of residential building within the surrounding area. Furthermore, regarding the applicability of measures for energy efficiency improvements, the surveyed building should have potentials for these measures in terms of both applicability and feasibility. As a last criterion, the building should have the potential to install a shallow geothermal heat pump. In particular this means that an adequate area of the property should be available for the shallow geothermal system. Circumstances of the house owners, such as age, gender and social background were not taken into consideration for the selection of the building.

On-site visit at residential row house in Osterode am Harz

In consideration of the criteria for the selection process of the residential building as mentioned before, a residential row house in the city of Osterode am Harz was chosen for the energy efficiency survey and the design of a shallow geothermal heat pump system. Figure 1 shows the front view of the row house, the red border indicates one of the three parts of the multi-party row house and therefore the surveyed part of the house.



Figure 1: Front view of the residential row house in Osterode am Harz (own recording from on-site visit)

The row house is located in northwest of the Osterode city center in the Hohensteiner street. Figure 2 is a map extraction and shows the location of the row house and the vicinity of the house.



Figure 2: Location of the row house and surrounding area (Google Earth, 2018)

From the on-site surveys in Osterode am Harz it could be inferred that a considerable number of the residential buildings, especially north of the city center of Osterode am Harz, were built as multi-party row houses. Therefore, this house is considered to be a representative building within the Osterode am Harz county. During the on-site

visit of the row house, a comprehensive survey of the building could be done and necessary data for the energy consulting could be acquired, including blueprints and pictures of the building. Table 1 shows an overview of the basic building data.

Table 1: Basic building data from the residential row house in Osterode am Harz (on-site visit).

Year of completion	1965
Living area	92,49 m²
Inhabitants	2
Heat supply	Natural Gas
Installed heat capacity	19 kW

Through an informal meeting with the house owners more details of the house could be acquired. The house owners bought the house in spring 2015, after it got partially refurbished by the former owners. The former owners have invested in new windows in 2005 and in a new natural gas heating system in 2009. However, the exterior walls have not been insulated yet. After moving in, the house owners started to refurbish the interior construction, which is still in progress. For the situation of the adjacent parties of the row house, the first party on the left of the house is not inhabited and therefore not supplied with heat. The third party in the right part of the row house is inhabited and therefore permanently supplied with heat. These conditions play a significant role for the evaluation of the energy efficiency.

Evaluation of energy efficiency and energy consulting

Based on the preceding input from the on-site visit, the next task was to carry out a comprehensive evaluation of the energy efficiency of the building, followed by suggestions to improve the energy efficiency of the building in form of an energy efficiency consulting.

The professional title of an energy consultant for residential buildings is not subject to legal protection and can therefore be used by anyone. However, the state support mechanisms for energy efficiency improvements within the scope of on-site consulting can only be accessed by a formal recognition as an energy consultant at the Federal Office of Economics and Export Control of Germany. (BAFA, 2014) Based on an academic recognition as an energy consultant, the energy consulting for the residential row house was carried out as a free of charge sample study. The process of the energy efficiency evaluation and energy consulting was realized in the energy consulting software ENVISYS EVEBI 8.3.
For the evaluation of the current energy efficiency, the inhabited areas of the building were evaluated in terms of the used area and volume. A thermal frame was created, as it can be seen in figure 3. Within this thermal frame, all structures and components of the house were taken into consideration to obtain the total thermal emission of the house, as the thermal frame represents the border of the heated living space.

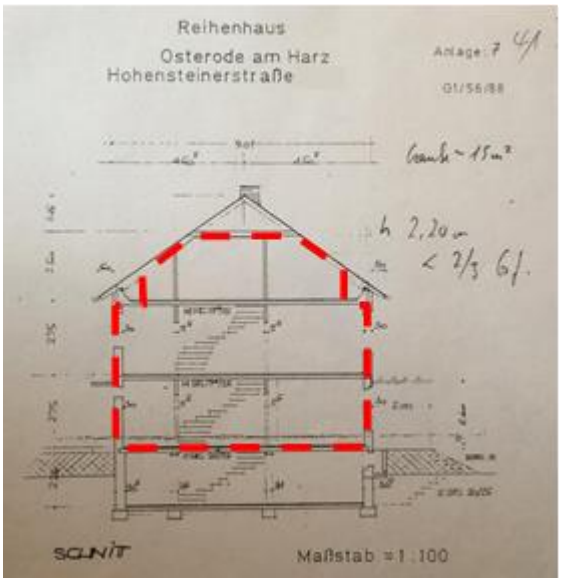


Figure 3: Cutting pattern with internal structure of the residential row house in Osterode am Harz (own recording from on-site visit).

For the structure of the exterior wall, no blueprint could be provided by the house owners. Since the exterior walls of a building are the largest area for thermal emission, their structure is of great importance for evaluation of the energy efficiency. However, the detailed structure of the exterior wall can only be obtained by destructive testing. Therefore, the setup of a commonly used exterior wall from 1965 has been used, as shown in the upper part of figure 4.

After the model of the current state of the building has been created, the efficiency properties of the building could be inferred. The resulting specific heat demand of the building equals to 195kWh/m^{2}a. According to this value, the building is classified as efficiency class "F". The efficiency of the building appears to be relatively low, especially considering the recent refurbishment of the windows. The most inefficient component of the system is the exterior wall. The assumed parameters for the exterior wall coincide with both the dimension of the current natural gas heating system and the records of the natural gas consumption over the last years.

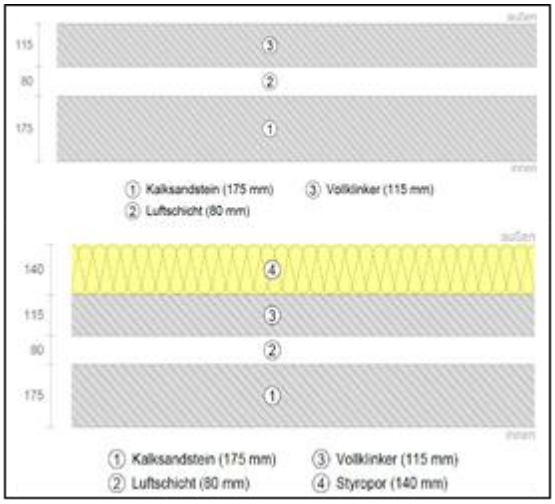


Figure 4: Assumed initial exterior wall structure (upper part) and suggested wall structure with insulation (lower part).

Consequently, for the energy consulting approach the exterior walls were the object with the highest priority. The lower part of figure 4 shows the design of polystyrene insulation layer on the outer walls. With this optimization, the specific transmission heat loss improved in terms of figures from 1.55w/m^{2}K to 0.241w/m^{2}K. With this optimization of the exterior wall, the specific heat demand of the building results in 118. According to this new heat demand, the building would be classified as efficiency class "D". As this energy consulting is on a theoretical basis and the probability for the suggested measures to be realized in the near future is relatively low, no profitability analysis of the suggested measures was carried out. A further option for an energy efficiency measure would be the installation of a shallow geothermal heat pump system, to replace the natural gas heating system. Figure 5 shows the garden area of the residential row house, which is potentially available for the installation of the geothermal system.



Figure 5: Garden area of the residential row house (own recording from on-site visit).

DESIGN OF THE GEOTHERMAL HEAT PUMP

Input data

The test house is located in Osterode am Harz, roughly 10 kilometers in south west direction of Institute of Petroleum Engineering of Clausthal University of Technology. The positioning of the house and garden can be seen in figure 6, the red border indicates the surveyed part of the house and the garden area.



Figure 6: Test house positioning and close-up image of the garden area (Google Earth,2018).

The living area of the house is 92.49 m² and the area of the garden is around 50 m² which is separated from the neighboring houses. Input information for the climate and soil condition of the house were extracted from the Thermomap, an EU co-funded project which determines the potential for shallow geothermal energy in Europe. A summary of the information is shown in the table 2.

Table 2: Summary of exported climate and soil data (Themomap, n.d.)

Mean annual air temperature	8.17 °C
Minimum annual air temperature	-3 °C
The maximum monthly Precipitation	90 mm only in June
The thermal heat conductivity	1.09 W/mk
The heat capacity of soil	2.05 MJ/m^{3}K
The soil bulk density	1.3 g/cm^3

In general a heating system needs to provide thermal energy for heating of the house and hot water for sanitary applications. Usage time for the heating system annually is 2100 hours and heat demand for the thermal heating is 195kWh/m^{2}a. With the known of living area, the total amount of energy usage per year equals 18,035kWh/m^{2}a. Based on the total amount of energy per year, the optimal thermal power for heating the house is P_T=8.59kW. This is in clear contrast to the installed heating system with a thermal power of 19 kW, indicating an oversizing of the current natural gas

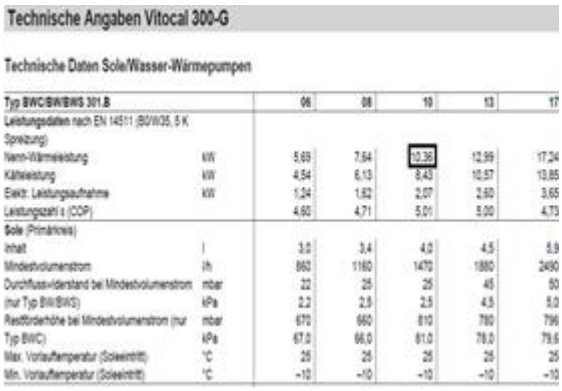
heating system. In addition, extra heat for hot water needs to be taken into account. Assumptions mentioned in table 3 are considered to calculate the thermal power for hot water P_{Hw}. According to the assumptions, the thermal power for hot water for each person is 0.2 kW. Taking into account the 2 inhabitants of the house and adding a 10 % backup for simultaneous usage, the total thermal power demanded is 9.89 kW.

Table 3: Assumptions to calculate the thermal power for hot water.

Water usage per person	70 liter per day
Number of inhabitants	2 people
Initial water temperature	5°C
Heated water temperature	65°C
Thermal power for hot water	

Selection and design of the heat pump system

To choose the heat pump, the current market of heat pump was considered. In this study heat pumps from the company Viessman were taken into account. As illustrated in figure 7, based on the total thermal power demanded, Vitocal 300-G heat-pump type 10 was chosen. This heat pump provides 10.36 kW total thermal power which covers the demand for the house.



Technische Angaben Vitocal 300-G

Technische Daten Sole/Wasser-Wärmepumpen

Typ BWC/BW/BWS 301.B		06	08	10	13	17
Leistungsdaten nach EN 14511 (B0/W35, 5 K Spreizung):						
Nenn-Wärmeleistung	kW	5,69	7,64	10,36	12,99	17,24
Kälteleistung	kW	4,54	6,13	8,43	10,57	13,85
Elektr. Leistungsaufnahme	kW	1,24	1,62	2,07	2,60	3,65
Leistungszahl ε (COP)		4,60	4,71	5,01	5,00	4,73
Sole (Primärkreis)						
Inhalt	l	3,0	3,4	4,0	4,5	5,9
Mindestvolumenstrom	l/h	860	1160	1470	1860	2490
Durchfluss-widerstand bei Mindestvolumenstrom	mbar	22	25	25	45	50
(nur Typ BW/BWS)	kPa	2,2	2,5	2,5	4,5	5,0
Restförderhöhe bei Mindestvolumenstrom (nur	mbar	670	660	810	780	796
Typ BWC)	kPa	67,0	66,0	81,0	78,0	79,6
Max. Vorlauftemperatur (Soleeintritt)	°C	25	25	25	25	25
Min. Vorlauftemperatur (Soleeintritt)	°C	-10	-10	-10	-10	-10

Figure 7: Viessmann ground source heat pump data sheet (Viessmann, n.d.).

According to VDI (Association of German Engineers) code 4640 part two (VDI, n.d.), considering the thermal heat conductivity of the soil in the test house (1.09 W/mk), for normal hard rock and water-saturated sediment, specific heat extraction rate is 50 W/m. As shown in figure 7 evaporation capacity of the chosen heat-pump is 8.43 kW. Shallow geothermal ground heat exchanger systems has three main categories, open-loop, closed loop and other systems, for example water in the abandoned mines. In this study a closed loop ground heat exchanger is preferred. Closed loop shallow geothermal heat exchangers can be generally categorized as horizontal and vertical heat exchangers as shown in figure 8.

FEFLOW simulation of the selected heat pump system

In order to check the results from the calculation based on VDI guideline, the geothermal system was simulated using simulation program FEFLOW. For the simulation default values of FEFLOW and default values for double U-shape borehole heat exchangers were used. The profile sketch of the double U-shape heat exchanger can be seen in figure 9.

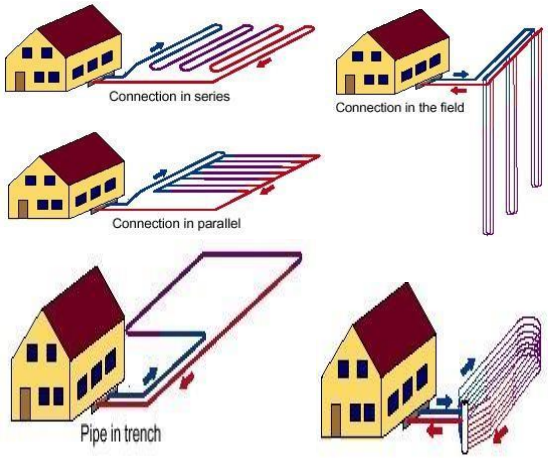


Figure 8: Different types of closed loop ground heat exchangers (Sanner, 2001)

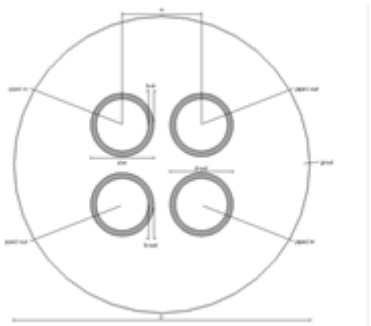


Figure 9: Profile sketch of the double U-shape borehole heat exchanger (FEFLOW)

As it is calculated above the length necessary for the ground heat exchanger tubing is 168.6m. To cover this length 3 borehole heat exchangers with a distance of 3m to each other and depth of 15m were positioned in the garden area. This process has been illustrated in figure 10.

The depth of the reservoir was set to 20m to cover the borehole heat exchangers. Temperature of 8 °C was assumed for the initial temperature of the reservoir based on the average annual temperature of the region. Value of the water rate for the borehole heat exchanger was set to cover the demanded value by selected heat pump (1470 l/h). The model was simulated for the period of 1 day. From the rate budget of FEFLOW, this system provides around 9.2 kW thermal energy for the heat-pump evaporator, which is more than

demanded value of 8.43 kW. The chart for heat rate budget can be seen in figure 11.



Figure 10: Supermesh view of the model in FEFLOW (FEFLOW).

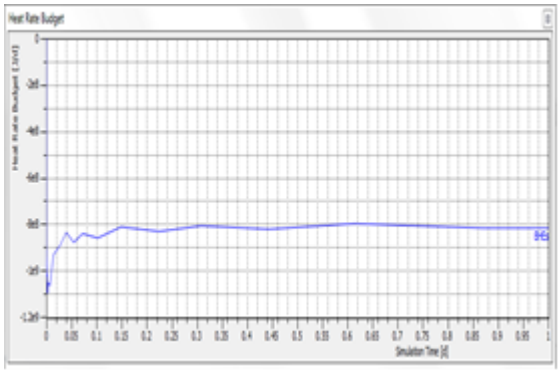


Figure 11: Heat rate budget (FEFLOW)

Figure 11 shows a more or less stable heat rate throughout the day. It is assumed that the energy extracted from the ground will be recharged simultaneously to the extraction of the heat. The effect of the borehole heat exchangers on the temperature of their surrounding soil is illustrated in figure 12.

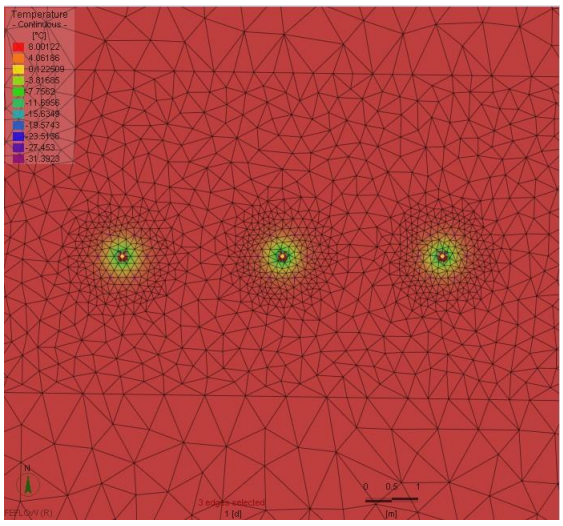


Figure 12: Temperature distribution of the geothermal system after 1 day.

DEMOGRAPHIC ANALYSIS OF OSTERODE AND ANALYSIS OF STAKEHOLDERS

Starting position of the district Osterode

The district Osterode am Harz with 74,367 inhabitants and is located in the south-east of Lower Saxony in the Harz region. It covers an area of 63,602nd The county particularly marked by craft enterprises. 2013 there were 609 craft shops and 99 craft similar establishments. 5152 workers were employed in 2013 in the craft. Industrial companies are also represented in the district of Osterode. 2013 there were 64 industrial enterprises with 7241 employees. The unemployment rate in 2013 is 8.7%.

The largest town of the district, the city of Osterode, has 22,317 inhabitants. Since the 1970s, the county experienced a decline in population. Many young people emigrate from Osterode. In 1975 the population of the district was still at 94 807 inhabitants. 2013 there were only 74 367 inhabitants. In particular, the joint communities have had significant losses in population in recent years. The county has a total of 44 298 households Osterode (as at 30 June 2012). 19,317 households are households with one person, two people with 16,623, 4,427 with three people, with 2,811 people and 1,120 four with five or more persons. From the statistics of migration flows is to recognize that in particular people aged 18 to 25 years but also to emigrate from the county between 25 and 50 years. By contrast, however it attracts especially the group of 50 to 65 years old man within the vicinity and district of Osterode am Harz.

Stakeholder analysis

To analyze the different actors of the district Osterode individual actors are examined in more detail, that are relevant to the project. This will be done using the so-called stakeholder analysis, which is the first step for questioning the stakeholder analysis is an instrument that is originally emerged from the Business Administration. In the stakeholder analysis, the goals and interests of the various actors are identified and shown, which are connected with the project. For this stakeholder analysis, only the stakeholders to analyze who explicitly to do with the project. The actors are analyzed on the basis of various factors, and this as much as possible quantified. Such influencing factors for this project are the influence and the power of the actor to the project's success. Another influencing factor is the attitude towards the project. This factor is influenced by the moral ideas of the actor. These moral ideas are influenced by the general political attitude of the actor. Here the knowledge and fears about the geothermal energy play a major role.

The most important actor is the homeowners who have a garden on their property. This actor is essential for the success of the project, because without their permission no questioning of their group can be carried out. Since this group of actors is also the largest group in the whole project and without their consent fails the project, these stakeholders must be examined most precisely. This scrutiny is carried out at a later stage using a survey of homeowners. The first analysis initially first hypotheses about the group of homeowners are set up with its own garden, which will be verified or disproved later by using the questionnaire. First hypotheses about the homeowner would be that the homeowners have a financial interest in a geothermal plant among others. Through the construction of a geothermal plant investment costs and arise later in regular maintenance costs, but in the longer term will decrease the cost of energy for the home. After a few years, what needs to be checked individually depending on the building, the geothermal pump profitable. The calculation of the costs and the long- term costs and cost savings carried out by a break-even analysis, and a simple cost accounting, which must be performed individually for each house.

Another important player in the project is the financial services locally. This actor is relevant to the project, since the private installation of a geothermal plant costs a lot of money and can be performed by private homeowners. For the private establishment of a geothermal system a credit is generally required. To what extent this factor will be relevant for the project, will be analyzed in more detail as in the survey of homeowners, because amongst other things, the financial situation of the homeowner is asked. The financial service providers, which are mainly in Osterode banks, have to give an interest loans to customers and to post their interest rates to as profit. Accordingly, banks have an interest in ensuring that liquidity is assured and there will be no loan defaults.

CONCLUSION

This cooperation project between Clausthal University of Technology and Göttingen University was a great opportunity to work in an interdisciplinary group environment with the interaction of people from different backgrounds. Finding out the challenges and figuring out solutions for these, was a unique experience with people from disciplines like Mechanical and Power Engineering, Geology, Social Science, Political Science. All together, these participants broaden the horizon of the project, without focusing on one field only. Regarding the technical side of this project work, clear results could be obtained.

First, the energy consulting for the building delivered the desired results. For the sample study, measures for the improvement of the energy efficiency could be shown. Taking a look at a larger scale, the Osterode county has a large potential for energy efficiency measures in the residential building sector. Both, the age of the buildings and their properties are fitting for energy efficiency measures, also in combination with sustainable energy from shallow geothermal systems. On the other side, for a comprehensive energy consulting process the essential amount of data, especially regarding the structure and thermal properties of the exterior walls, needs to be acquired even by destructive testing. Within this sample study, measures like this are not to be realized.

Second, the design of a shallow geothermal heat pump system for the sample study could also deliver reasonable results. Although the available garden area is relatively small, the Feflow simulation showed that the necessary thermal output can be provided. It is suggested, that a more comprehensive comparison of different heat pump system should be carried out, to obtain an optimal system. Another weakness of the survey is the limited availability of soil data from online databases. For the calculation of the tubing, the worst-case parameters from the VDI 4640 guideline part 2 were taken into consideration.

All in all for the technical side of the project, feasibility factors were not taken into account. No profitability analyses for the surveyed systems have been carried out. Further studies should take into account the profitability as a major factor, regarding the probability of realization of these projects. Regarding the social side of the project, the importance of the different stakeholders, involved in this kind of projects, has been pointed out. To achieve a successful realization of measures towards energy efficiency and usage of sustainable energy sources, stakeholders need to be identified, approached and involved in the whole process of the project. Based on this interaction between the technical and the social side, a campaign or program to promote energy efficiency and sustainable energy measures could be implemented in the Osterode county.

REFERENCES

Arning, E., Kölling, M., Schulz, H. D. Panteleit, B., and Reichling, J, (2006), “Einfluss oberflächennaher Wärmegewinnung auf geochemische Prozesse im Grundwasserleiter (Effect of nearsurface thermal extraction on geochemical processes in aquifer)”. *Grundwasser* 11, 27– 39.

Blum, P., Campillo, G., and Kölbel, T. (2011), "Techno-economic and spatial analysis of vertical ground source heat pump systems in Germany". *Energy* 36, 3002–3011.

Bonte, M., Stuyfzand, P. J., Hulsmann, A., and Beelen, P. V. (2011), "Underground thermal energy storage: environmental risks and policy developments in the Netherlands and European Union". *Ecology and Society* 16, 22.

Hancock, P. J., Hunt, R. J., and Boulton, A. J. (2009), "Preface: hydrogeoecology, the interdisciplinary study of groundwater dependent ecosystems". *Hydrogeology Journal* 17, 1–3.

Herrmann. (1957), Zechstein formations. groundwater investigation area in the South Harz.

Rybach, L., and Mongillo, M. (2006), "Geothermal Sustainability—a review with identified research needs". *Geothermal Resources Council (GRC) Transactions* 30, 1083–1090.

Sanner, B. (2001). "Shallow Geothermal Energy", *Proceedings of the European Summer School on Geothermal Energy Applications*, University of Oradea, Romania, pp. 191- 212.

Schaetzle, W. J. (1980), Thermal energy storage in aquifers: design and applications. Elsevier Science & Technology Books, 593 pp 177. Editor:Pergamon, Oxford, UK.

Schippers, A., and Reichling, J. (2006), "Laboruntersuchungen zum Einfluss von Temperaturveränderungen auf die Mikrobiologie des Untergrundes". *Grundwasser* 11, 40–45.

Internet Source

Bundesamt für Wirtschaft und Ausfuhrkontrolle/BAFA, (2014). http://www.bafa.de/bafa/de/energie/energiesparberatung/vorschriften/vob_richtlinie_2014.pdf. (12/09/2015).

Google Earth, (2018). https://www.google.com/earth/ (27/05/2018).

Thermomap, (n.d.). http://www.thermomap-project.eu (28/09/2015).

VDI, (n.d.), https://www.vdi.de/richtlinie/vdi_4640_blatt_2-thermische_nutzung_des_untergrundes_erdgekoppelte_waermepumpenanlagen/. (24/09/2015).

Viessmann, (n.d.), http://www.viessmann.de/content/dam/vi-brands/DE/Produkte/Waermepumpen/Vitocal-300-G/DB-5368800_Vitocal_300-G_46-kW.pdf/_jcr_content/renditions/original.media_file.download_attachment.file/DB-5368800_Vitocal_300-G_46-kW.pdf.

GEOTHERMAL MENTORING PROGRAM – EMPOWERING WOMEN IN THE INDUSTRY

Jane Brotheridge[1], Jane Bydder[1], Andy Blair[2], and Riki Ibrahim[3]

[1]Jacobs NZ Limited, Upflow Ltd (NZ),
[2]PT Geo Dipa Energi
Email:Jane.Brotheridge@jacobs.com

ABSTRACT

To celebrate International Women's Day (8 March) this year and in conjunction with 60 years of friendship and collaboration between Indonesia and New Zealand, an event was hosted by New Zealand's Ministry of Foreign Affairs and Trade (MFAT) to highlight and celebrate the contribution women make to the geothermal sector in Indonesia. The key message throughout the event was the vital need to increase the participation of women in the industry where numbers currently stand at 10-15% at graduate levels and even lower at middle and senior management levels. Mentoring young woman through their careers was noted as a key facilitator in encouraging them to remain in the industry and to push for managerial roles and responsibilities. This event provided the perfect opportunity to launch a mentoring program specifically for women in the Indonesian geothermal industry. Those who volunteered to be mentors could either be men or women. It is recognised in other mentoring programs around the world the importance of having male representation in this initiative, as it is men in senior positions who will be able to advocate and encourage women to advance. The program has now been running for four months and feedback from both mentors and mentees has been positive. Mentors considered the experience of joining a formal mentoring program as a personal development opportunity to develop their own coaching and communication skills. For the mentee the program provides the opportunity to seek professional advice from someone outside of their immediate working environment, including feedback and support. The geothermal sector in Indonesia needs to be actively involved in supporting and encouraging women in the industry, to have open and candid discussions on structural, organisational and societal barriers that hinder gender equity and to give women the tools and a voice to reach for the top.

Keywords: Gender equity, mentoring, women in geothermal

BACKGROUND

Part of the *2030 Agenda for Sustainable Development* is Sustainable Development Goal 5: Achieve gender equality and empower all women and girls. However, the United Nations Economic and Social Council (2017) notes that achieving gender equality will require further "vigorous efforts, including legal frameworks, to counter deeply rooted gender-based discrimination that often results from patriarchal attitudes and related social norms."

Progress has been made in some areas - women have closed much of the gender gap in health and education outcomes, however inequality persists in economic participation and political empowerment. Just 22% of individuals holding senior managerial positions are women (World Economic Forum, 2017).

Gender parity is fundamental to the performance of societies and economies. Female talent is an under-utilised resource, and this is particularly true in science, technology, engineering and mathematics (STEM) fields where women tend to be underrepresented at graduate level, in addition to dropping out in large numbers over time. Hewlett et al (2008) states that 52% of women in STEM fields quit their jobs, with the majority doing so in their mid-to-late 30s.

Harvard Business Review (HBR) provides reasons for this extraordinary figure as:

1. Hostility of the workplace culture;
2. A sense of isolation when a woman is the only female on her team or at her rank;
3. A disconnect between women's preferred work rhythms and risky behaviour which is recognized and rewarded in male-dominated fields;
4. Jobs with long work-weeks and significant travel are particularly prevalent in science, engineering, and technology companies; and
5. The mystery around career advancement, with a lack of sponsors to discern the pathway upward.

It is career guidance and sponsorship, as well as support to endure the hostility and isolation of the working environment, that the mentoring program outlined in this paper seeks to address.

Mentoring is especially important for females in settings where there are few women, because they often have difficulty building social capital at work (Chrisler and McCreary, 2010).

We first consider women in STEM fields in general, and the geothermal industry in particular. We then look at the role that mentoring can play in empowering women, and discuss effective methods for delivery of mentoring. We then present findings from the geothermal industry mentoring program.

WOMEN IN STEM

There is a shortage of talent in the labour force around the globe, particularly in STEM fields - of the top ten most difficult jobs to fill, six are STEM-related (Feldhaus and Bentrem, 2015). Even in scientific fields where women are present, they are underrepresented in policy-making and programming (UNESCO, 2015).

As an example, women represent just 3% of PT Indonesia Power's operations, maintenance and engineering workforce; while they account for 36% of its human resources, finance and administrative staff (Orlando et al, 2018).

Yet as outlined above, women are leaving STEM fields in significant numbers. Dawson et al (2015) note that this is due "not to a deficit in academic preparation, ability, or talent but rather to a drop in confidence that is triggered by a range of experiences along the STEM pathway." This includes the reasons listed above, as well as an environment that includes "few role models and mentors, a dearth of female peers, intimidation, and implicit or overt bias against women". They note that six out of seven women identified a lack of guidance and support as a reason for their decision to leave science.

The low rate of participation of women in STEM is an issue for society as a whole. Women in areas with inequitable participation rates have lower salaries, more limited career and professional development opportunities, and less say in the development of their personal lives and their society (Allmendinger 2002). Societies in which women are underrepresented in STEM also pay a collective economic price in the form of shortages of skilled labour.

WOMEN IN GEOTHERMAL

Developing a geothermal power project is a complex problem which is inherently risky due to the unknown nature of the resource and its long-term behaviour. It necessitates a multi-disciplinary approach with collaboration and understanding between scientists, engineers, operators, financial and legal specialists and others. Knowledge sharing is a crucial part of a successful development team.

Women's direct employment by energy infrastructure projects is constrained by traditional gender roles and social norms, and a lack of technical and professional skills. Whilst nearly 50% of the global workforce is comprised of women, just 15% work in Industry (ILO, 2018), and that proportion has been decreasing over time.

As noted by Janik et al, (2018), geothermal projects employ mainly men for both skilled and unskilled jobs, and the technical jobs consist mainly of engineers, geologists, geochemists and geophysicists: "Therefore, women are far underrepresented in positions of influence, decision-making, or team-leading in the industry." The reasons for this include those outlined above as well as "the inertia from more than a century of power sector labour segregation".

Given the nature of geothermal energy, the lack of a safe and suitable work environment deters many women from the sector, for example a lack of sanitary facilities and separate quarters on site, or discrimination on the basis of physical strength.

Yet we know that gender balanced teams can increase company performance. Ernst and Young (2016) found that among power utilities, those with the most female executive and governance representation outperformed those companies with the least. In 2011 Reykjavik Energy (OR) were determined to eliminate the gender pay-gap (which at that time was 7% in favour of men). By 2017 they had closed this gap and increased the number of women on their board. What OR found is that the gender make-up of the energy sector can be changed quickly if there is the resolve of management to do so. and they now receive a higher number and higher quality job applications from both genders (Bjarnason, 2017).

Getting women into the geothermal industry, retaining them and moving them into positions of decision-making and policy design is imperative. The Geo-INZ program (MFAT-sponsored support to the Indonesian geothermal industry) includes a work stream on Gender Equity and Women's Empowerment (GEWE), with a framework as shown in Figure 1.

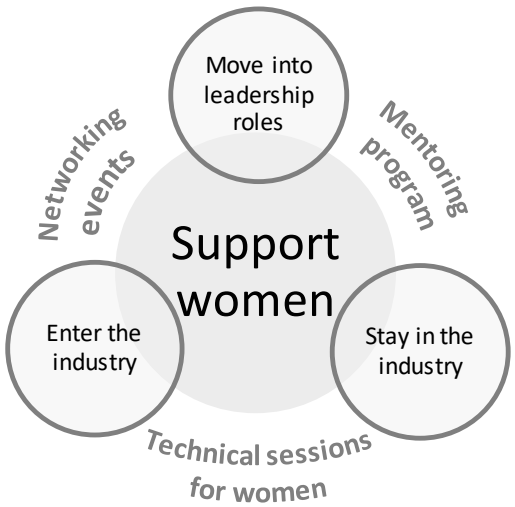


Figure 1: Geo-INZ GEWE Framework

The International Women's Day event was the initiation of this framework. Figure 2 shows attendees from government, universities, developers, NGO's and consultants.

Women who attended the event had experienced the following obstacles to their career progression:

1. Lack of awareness of opportunities;
2. Lack of sponsorship;
3. Lack of support from senior leaders;
4. Unfair evaluation or promotion criteria; and
5. Lack of support from supervisor.

34% of women felt they had been discriminated against at their workplace. 100% of the women wanted more flexible working arrangements such as flexi-time, longer maternity leave and less time in the field.



Figure 2: Attendees at the International Women's Day Event.

Key issues for women in the industry included:

1. The need (but sometimes lack) for support from family, friends, community, leaders;
2. The requirement to spend time in the field (particularly for mothers);
3. The lack of opportunity to move up;
4. Lack of training on what constitutes harassment and discrimination, and the lack of protection for victims;
5. The traditional nature of the education system; and
6. The perception that women cannot commit 100% to their career because of their other commitments (such as family).

Some opportunities were identified, such as networking. Women were encouraged to join groups, get to know their leaders, become more "visible" and improve their communication and interpersonal skills through networking, as well as networks being able to provide support through strength in numbers.

However, many of the women felt at a loss on how to improve things in the industry and move forward. The authors believe a key part of moving forward is to introduce mid-career women to a network of female peers and role models through an effective mentoring program.

MENTORING

Research into mentoring ahead of initiating the program showed that mentored individuals are not only more satisfied with their careers, more likely to expect career success, and more satisfied with their jobs, but also have more favourable salary, bonuses, and total compensation (Kao et al, 2014). Furthermore, mentees prove to be more resilient, which is valuable in terms of coping successfully in challenging roles, tasks, and situations.

Dawson et al (2015) found that "women's persistence in the sciences and engineering is directly linked to the availability of a strong mentor." They further note that not only does mentoring increase the professional skills of the mentee, but "equally importantly, mentoring can provide the psychosocial support needed to counter the elevated stress and discouragement and the falling confidence that some women in STEM experience."

The core elements of effective mentoring programs include communication and support. Stoeger et al (2013) further note the need for effective role models, frequent interaction between mentors and mentees and setting concrete mentoring goals.

GEO-INZ MENTORING PROGRAM

The Geo-INZ mentoring program kicked off in April 2018, with fourteen pairs of mentors and mentees. The program runs through until November 2018. It is anticipated that the program will run again in subsequent years, and grow as this year's mentees become next year's mentors. The main purposes of the program included:

1. Development and support of junior staff;
2. Enhancement of leadership, coaching and communication skills of senior staff;
3. Transfer of knowledge and experience to build capacity within the industry;
4. Gain an understanding of the obstacles women in the industry face and how to overcome them; and
5. Extend the networks of both mentors and mentees.

In terms of the gender of mentors, the research is conflicting: Kao et al (2014) find that cross-gender mentoring is beneficial, while Stoeger et al (2013) cites studies which show that same-gender role models are more effective, and that female mentors "also help their mentees by counselling, advising, instructing, and sharing knowledge with them."

Given the very small pool of potential mentors, and the fact that the authors believe that men must be included and encouraged to help address the gender gap, males as well as females were invited to be mentors.

Participants were asked to meet at least four times, either in person or online as a number of mentors are based in New Zealand. They were also asked to set goals for the program at the first meeting.

LESSONS LEARNED

To date there have been some successes, with one mentee stating that: "The mentoring program has benefited me in building up my professional portfolio as well as enhancing the overview of further career and study path in different perspectives. It is highly

recommended to everyone, esp. women leaders in geothermal industry to take part in the program". However, there have been some failings, mainly around a lack of responses of mentees to their prospective mentors.

Mid-way (August 2018) through the Geo-INZ mentoring program the key learnings are as follows:

Significant resources are required. It takes significant time and resources to administer a successful program, and to fully participate in one. Interaction and engagement takes hard work from both parties in order to reap the benefits of mentoring.

Female mentors are rare gems. Women have trouble finding other women to mentor, especially in a male dominated industry. Due to the lack of diversity there is a shortage of senior level women and those that exist are less visible than their male counterparts. Female mentees need to be open to having male mentors.

Finding time to connect is tricky. It was common for mentees to only contact their mentors on their own time i.e. lunch breaks, after work, weekends. Therefore, is was not always convenient with mentors to arrange a mutually suitable time. One suggestion to help resolve these issues is for the organisation which the mentees work for allocates time during work hours that employees can meet or call their mentors without using their personal time. This is relevant at the start of mentoring relationship as it takes time for the benefits of the interaction to be realised. Therefore, mentees aren't seeing benefits straight away which makes it difficult to prioritise this time over other more immediate priorities and demands.

Training is helpful. Studies have shown that success rates increase when both the mentor and mentee receive training on how to manage their mentoring relationship, in which case one can expect a 90% success rate. Through training ambiguity is removed as to what it means to mentor by better defining the "what" and "how" of mentoring (Neal et al, 2018). However, training wasn't possible with participants in different geographical locations and the mentoring program was virtual in many instances.

Individuals have differing needs. Some mentees and mentors will appreciate access to online tools and resources whilst they are beginning their mentoring relationship and others will feel overly pressured if pushed to use them.

Relationships are difficult. Relationships are personal and not easily to create intentionally i.e. formal as opposed to informal mentoring relationships. Forced connections can be awkward, especially in a corporate environment, and some relationships will not work with no fault of either participant. Matching mentees and mentors who can build trust and rapport is crucial for a successful engagement. Mentees need to understand that a mentorship is not a friendship; the purpose of the relationship is to achieve a clearly defined goal. It is essential to clarify and articular the goal of the relationship in order to ensure expectations are aligned.

Engagement is everything. Engagement is possibly the hardest part of the program to manage. Whilst it is important for mentees to feel pressure to engage and use the program effectively it is also counterproductive to force them through the relationship. Whilst success is often determined by talent and aptitude, mentoring requires real commitment and willingness to be open, vulnerable, and ready to hear the messages and lessons provided by the mentor. Internal conflict exists when the mentees are not open because they fear looking stupid or weak to a mentor, often someone they admire from the community in which they work.

Both parties can win. Meaningful experiences and strong relationships can develop from mentoring, where both mentees and mentors symbiotically grow from the experience.

Mentoring is a challenging program to successfully implement, however the potential outcomes, both tangible and intangible, are worthy of the necessary investment in efforts and resources.

CONCLUSION

Developing geothermal power is complex and necessitates a holistic approach with collaboration and understanding between those involved. Knowledge sharing is a crucial part of a successful development team; however, women often feel isolated in such male-dominated environments.

Mentoring builds social capital, provides an avenue to share wisdom, practical experience and network, and helps women advance in their careers thus supporting the push for more diversified workplaces.

The Geo-INZ mentoring program provides the opportunity to mould a successful program by implementing ongoing learnings and gaining support of government and industry.

The authors plan to hold a networking event for the participating mentors and mentees later this year, to gain feedback and assist in planning for next year's program. At this time the planned improvements for the program for next year (2019) include:

1. Developing and implementing training for mentors.
2. Creating mentor support groups for mentors to discuss challenges with other mentors.
3. Provide group activities where all mentees and mentors can connect and interact, and
4. Working with organisations to support mentees through the allocation of work time for mentoring.

REFERENCES

Bjarnason, B. (2017), "Gender Inequality in the Energy Sector". *Reykjavík Energy*.

Chrisler, J. C. and McCreary, D. R. (2010), "Handbook of Gender Research in Psychology Volume 2". *Gender Research in Social and Applied Psychology, Springer.*

Dawson, A. E., Bernstein, B. L., and Bekki, J. M. (2015), "Providing the Psychosocial Benefits of Mentoring to Women in STEM: Career WISE as an Online Solution". *New Directions For Higher Education*, no. 171, 2015.

Ernst & Young. (2016), "Women in Power and Utilities Index 2016". *EYGM Limited.*

Feldhaus, C., and Bentrem, K. (2015), "STEM mentoring and the use of the principles of Adult Mentoring Inventory". *International Journal of Mentoring and Coaching in Education*, Vol. 4 Issue 3, pp.213-235.

Hewlett, S. S., Luce, C. B., and Servon, L. J. (2008), "Stopping the Exodus of Women in Science". *Harvard Business Review.* Retrieved from https://hbr.org/2008/06/stopping-the-exodus-of-women-in-science.

International Labour Organisation/ILO. (2018), "World Employment and Social Outlook: Data Finder". Retrieved from http://www.ilo.org/weso data.

Janik, V. L., Fridriksson, T., Morris, E., Greene, J., Newson, J., and Matinga, M. N. (2018), "Gender and Geothermal: Guidance Note". *Global Geothermal Development Plan Iceland Geothermal Conference*, Reykjavik, Iceland.

Kao, K., Rogers, A., Spitzmueller, C., Lin, M. and Lin C. (2014), "Who should serve as my mentor? The effects of mentor's gender and supervisory status on resilience in mentoring relationships". *Journal of Vocational Behavior*, 85 (2014) 191–203.

Kim, H. (2017), "Investigating the effects of work-family spillovers, gender, and formal mentoring on career goal of managers". *International Journal of Manpower*, Vol. 38 Issue: 8, pp.1065-1085.

Neal, S., Boatman, J., and Miller, L. (2018), "Women as Mentors: Does She or Doesn't She? A Global Study of Businesswomen and Mentoring". *Development Dimensions International*. Retrieved from https://www.ddiworld.com/DDI/media/trend-research/womenasmentors_rr_ddi.pdf?ext=.pdf.

Orlando, Beatriz, M., Janik, V. L., Vaidya, P., Angelou, N., Zumbyte I., and Adams N. (2018), "Getting to Gender Equality in Energy Infrastructure: Lessons from Electricity Generation, Transmission, and Distribution Projects". *Energy Sector Management Assistance Program (ESMAP)*, Technical Report 012/18, Washington, DC: World Bank.

Stoeger, H., Duan, X., Schirner, S., Greindl, S. and Ziegler, A. (2013), "The effectiveness of a one-year online mentoring program for girls in STEM". *Computers & Education*, 69 (2013) 408–418.

United Nations Economic and Social Council. (2017), "Progress towards the Sustainable Development Goals: Report of the Secretary-General".

United Nations Educational, Scientific and Cultural Organization/UNESCO. (2015), "UNESCO Science Report: Towards 2030". Retrieved from https://en.unesco.org/unesco_science_report.

World Economic Forum. (2017). "The Global Gender Gap Report 2017". *Insight Report World Econommic Forum 2017.* Switzerland.

MOBILE EVAPORATOR FOR WATER BASED MUD GEOTHERMAL DRILLING

Lely Fitriyani

PT. Prasadha Pamunah Limbah Industri
Desa Nambo Cileungsi Bogor
Email: lely.fitriyani@ppli.co.id

ABSTRACT

Geothermal energy is a resource that intensively developed to be new favorable alternative compare to the conventional energy resources. Exploration of geothermal energy shall involve water base mud drilling that may produce WBM cuttings and WBM mud that required to be treated appropriately prior being discharged to the environment. PT. Prasadha Pamunah Limbah Industri (PPLI) as an integrated and experienced waste management facilities respond to the challenges by introducing new technology. This technology proved that waste management can be improved significantly so that the product would be able to be discharged safely to the environment with reasonable energy consumption. Mobile Evaporator (ME) is current innovation that offers an opportunity to reduce high cost of waste transportation and recycles liquid waste more eco-friendly unlike conventional liquid waste treatment. Mobile evaporator removes most dissolved ions from liquid waste and produces pure distilled water that meet environmental threshold limit value (TLV). Mobile Evaporator is designed to promote onsite water recycling, reduce the volume of waste water, and also reduce fresh water consumption at the project site. So far, there are not so many mobile units that able to treat highly polluted waste water from industrial activities in remote areas. Mobile Evaporator unit is capable of treating industrial waste which contain high Total Dissolved Solids (TDS) and Chemical Oxygen Demand (COD) with very high efficiency. Mobile evaporator (ME) unit is a unit that works base on the principle of onsite distillation process. Separation conducted base on the difference of boiling point. Waste water that contain high Total Dissolved Solids up to 20 000 ppm and 8000 ppm Chemical Oxygen Demand would be heated by using recycling heat system unit to be evaporated and condensed as distilled water. While, the remaining concentrate that unable to be evaporated would be collected in separate containment for further treatment into disposal facility. The process capacity of mobile evaporator is 40-55 m^3. It is surely much higher compare to some other separation equipment. In the other hand, it is also require less replacement of spare parts or media that normally used by filtration or membrane separation process. Once the efficiency expected reduced, the chemical cleaning would be conducted to retain the process efficiency. The process itself is segregated to four main processes: Pre-heating process of service water or fresh water, circulating of pre-heated water into the tube in the vacuum concentrator as part of heat recycle unit system, contacting the wastewater into the heated tube that allows the evaporation process and remain the concentrator that unable to be evaporated, condensing the evaporated mist into liquid form that would be discharged. This current innovation shall be considered as an alternative waste water treatment for water base mud geothermal drilling.

Keywords: TDS, COD, Liquid Waste, Brine Treatment, Evaporator, Distillation, Wastewater Treatment, water base mud, geothermal, drilling.

INTRODUCTION

Geothermal drilling produces significant amounts of solid waste; therefore, suitable disposal methods are needed (Chemwotei, 2011). General challenge in geothermal drilling is about liquid waste that produced in liquid waste treatment and disposal costs were hypothesized to be dependent on several variables, including the volume of liquid to be treated per unit time, the brine chemistry, the efficiency of the treatment processes, the characteristics of the resource and site, and the standards for liquid effluent treatment and disposal (Wells et al, 1981).

Total Dissolved Solids (TDS) content, and the stringency of effluent regulations were hypothesized to increase treatment costs when all other factors seemed to be constant. Both the capital and operating costs of wastewater-treatment systems were found to be expressed only as functions of liquid flow rates and treatment process TDS removal efficiency. Additional industry experience with hydrothermal brines may provide information on the impact of brine chemistry on treatment costs. The cost functions developed in this report are primarily sensitive to the liquid flow rate and the TDS removal efficiency (ibid).

High TDS wastewater has been studied by several researches that previously mentioned Super concentrators such as spray dryers, crystallizes and evaporators then volume reduce the waste liquid by removing the remaining water resulting in a product suitable for disposal by landfill (Dalan, 2000; Dixon, 2004; Wilf et al, 2007).

Mobile evaporator is a super concentrator that applying treatment process unit which is designed to

be able to reduce high TDS and high COD content of liquid wastewater that is also faced by geothermal industry. The distillation process principle may able to evaporate pure water release out of the inorganic matters that would stay as concenctrate of the treatment process. Distillation process inside close circulation system of mobile evaporator by using heat pump. The circulation is conducted several times to release as much as pure water from heated liquid wastewater.

Having the experience of implementing mobile evaporator at conventional gas drilling that produce liquid wastewater from its water base mud operation procedure, we would also see an interest to apply the unit to geothermal water base mud drilling. Seeing the typical waste have almost same challenges to be solved regarding TDS and COD, the following implementation result from conventional drilling shall be considered to make possibility of mobile evaporator implementation at geothermal water base mud drilling.

IMPLEMENTATION IN WATER BASE MUD DRILLING

Application of mobile evaporator at one of water base mud drilling in Indonesia was occured on September 2017 up to March 2018 at a remote area in the the nothern part of Indonesia. Clarified water that has been treated by using physical and chemical unit process. The physical and chemical unit process is called dewatering unit and use coagulation, inline flocculation, and separation process by using centrifugation unit. As experienced, water base mud clarified water has low turbidity and meet almost all liquid wastewater's discharge parameter, except Total Dissolved Solids (TDS) and Chemical Oxygen Demand (COD). Clarified Water Base Mud Wastewater would have varied TDS aroud 11000 ppm up to 48000 ppm depend on percentace of chemical concentration that has been used during the formulation of water base mud. COD would be in range up to 8000 ppm. The following table and figure will show typical of water base mud clarified water.

Table 1. show an average of waste charactheristics during drilling activities at conventionala drilling. The wastewater will enter the pre-treatment of mobile evaporator by using dewatering system. Dewatering system is a unit that implementing coagulation, flocculation, and centrifugation system as a method to reduce suspended solids include some other pollutants that might be precipitated during the separation process. The following figure will show the typical wastewater fluctuated.

Clarified wastewater shall be collected in certain containment, such as storage tanks and or in some pits. During the waiting process prior the enhancement treatment for reducing TDS and COD sometimes ammonia content shall be increased. Therefore a continous process is a recommendation to avoid the ammonification that shall be occured during the waiting process.

Table 1: typical of clarified water from water base mud drilling.

	Source Propeties
COD (mg/L)	4340
pH (mg/L)	8.55
TDS (mg/L)	36200
Temp (°C)	29.7
Oil & Grease (mg/L)	9.2
Sulfide H2S (mg/L)	10.40
Phenol (mg/L)	0.350
Ammonia (mg/L)	11.60

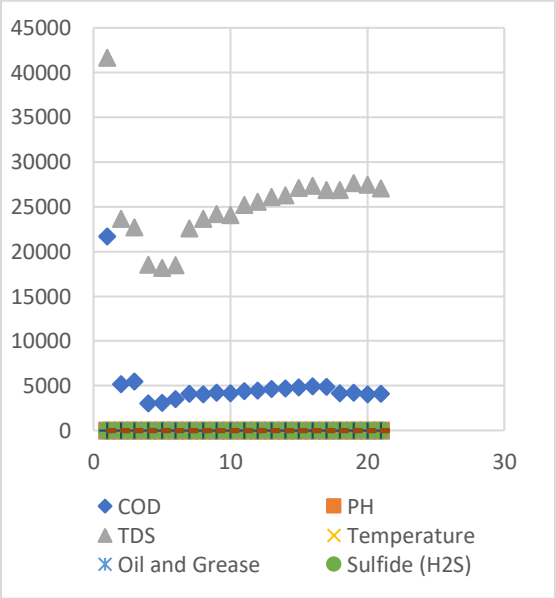


Figure 1: Fluctuation of wastewater charactheristics in water base mud drilling.

In case of low oil and grease content at the containment of clarified waste water, the treatment by using mobile evaporator can be conducted directly. A feed pump with strainer shall be immersed at the feeding containment/pit then would be treated by using ditillation mechanism with a heat recyclying system under vacuum condition.The following figure would show the average of treatment capacity at the mobile evaporator. The average of treatment capacity in hour basis is 2500 l. This shall make the unit has capacity 50 m^3 per day.

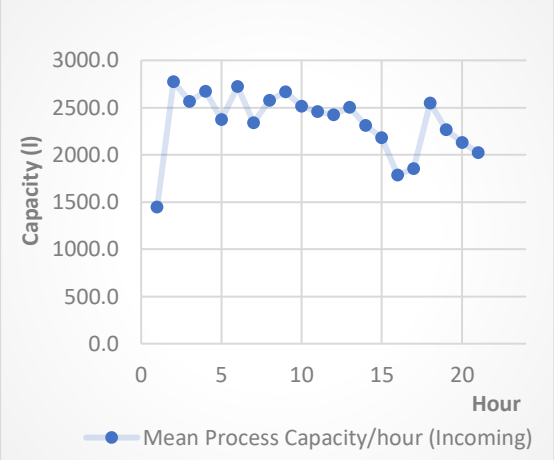


Figure 2: Treatment Capacity at Hourly Basis

Distillate

Produced distilled water would be seen has very high clarity and seem to be a potable water. If the analysis was conducted further base on the table below it was understood that the mobile evaporator process could reduce the TDS and COD content so that all liquid wastewater's discharge parameter has been fulfilled. It may cause the wastewater shall be able to be discharged directly to the environment if the permit has been obtained.

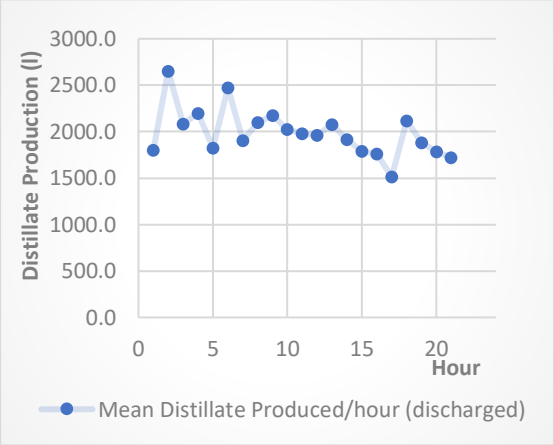


Figure 3: Distillate Production

Looking some treated parameters deeper we would see there is a relationship between the concentration of TDS at the feed containment to the efficiency of mobile evaporator. The following figure would show the higher TDS content at the feeding, the lower efficiency of mobile evaporator would be obtanined. This may be a result of the higher TDS would require more energy to produce mists and the faster scale production would be develop. This two phennomenon would surely reduce the efficiency process of mobile evaporator.

Table 2 will show typical result of distillate water that has been pre-treated by using dewatering unit (DWT-unit) and treated by using mobile evaporator. Dewatering unit was able to reduce around 10% of pollutants, while mobile evaporator was able to reduce all parameters until significantly lower than Threshold Limit Value (TLV).

Table 2: Result of Pre-treatment and Treatment

Fluids Waste Properties				
	Raw	Result DWT	Result EVP	Permen LH No. 19/2010
COD	5210	4020	11	200 mg/l
PH	7.52	6.4	7.17	6-9
TDS	41800	37900	85	4000 mg/l
Temperature	28.2	28.5	26.4	40 °C
Oil and Grease	22	10.6	< 1	25 mg/l
Sulfide (H2S)	31	0.15	0.46	0.5 mg/l
Phenol	1.28	0.92	0.094	2 mg/l
Ammonia	12.1	10.2	1.7	5 mg/l

In figure 4 below it was shown that fluctuation concentration of feed source also give influence to the mobile evaporator unit since. The higher TDS and COD feeded, the lower process capacity and distillate water has been produced.

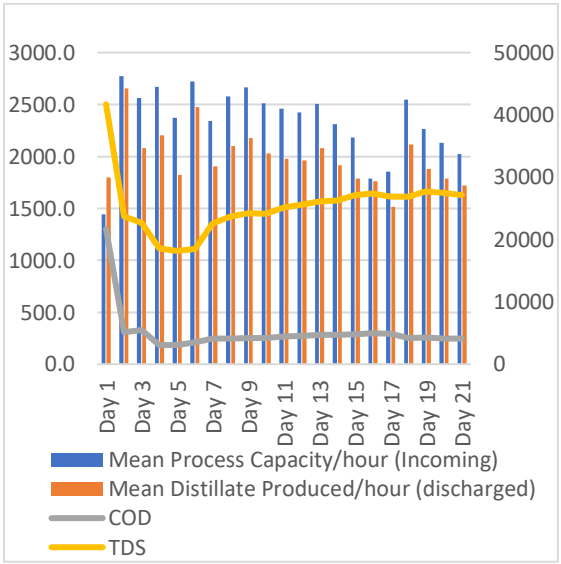


Figure 4: Mobile Evaporator Performance and Waste Characteristics.

Fluctuation TDS concentration as feed source of mobile evaporator during implementation at site observed gave opposite relation to the efficiency of mobile evaporator. A shown in figure 5 the higher TDS made lower efficiency of mobile evaporator.

Some challenges might be occured if the feed waste shall have high oil and grease content. This type of waste shall not be treated directly to the mobile evaporator. Inspite of doing the direct treatment, in-direct treatment shalll be implemented by using oil separator as a pre-treatment for the mobile evaporator. After reaching discharge parameter,

liquid wastewater can be treated by mobile evaporator.

Mobile evaporator was not designed to treat heavy oil content liquid waste, it is designed to give solution for high TDS and COD content to be treated in effective and efficient manners.

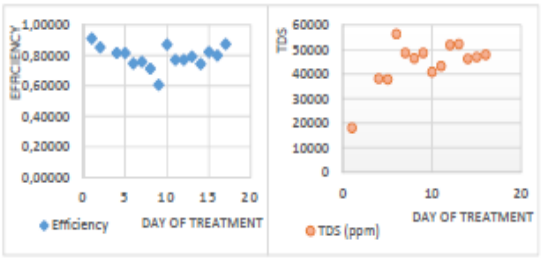


Figure 5: TDS and Efficiency of Mobile Evaporator

Concentrate

By product would be a serious concern for any waste tretment process. Mobile evaporator also produce concentrate as a by product of its treatment activity. The unit is designed to have between 9-19% of concentrate from feeded liquid waste. The implementation of the unit at the water base mud drilling clarified wastewater show the rage of produce concentrate are in between of its design criteria. In average during the implementation at typical wastewater with mentioned at table 1. The average concentrate produced is around 12%.

Energy Consumption

As energy consumption would always became a factor that would be highly considerated for the operating cost, the implementation of mobile evaporator also calculated consumption of fuel that has been used during the treatment at drilling area. The following figure will show the fuel consuption rate that *has been utilized by mobile Evaporator*.

Table 3: Fuel Consumption

Day	Fuel Consumption(l)
1	92
2	438
3	0
4	156
5	670
6	660
7	640
8	640
9	644
10	640
11	640
12	485

Volume of fuel that has been utilized is typical consuption of fuel that consumed by regular 350 KVA generator. It is in average valued in around 610-640 liters per day for 24 hours operation.

DISCHARGING DISTILLATE

As the distillate has passed all liquid waste water discharge parameter, the discharge of distillate to the environment would not have lots of difficulties. The discharge permit or known as Izin Pembuangan Limbah Cair (IPLC) was obtained after some audiencies to the the local envrironmental protection agency.



Figure 6: Distillate Water Discharge

IMPLEMENTATION IN GEOTHERMAL DRILLING

Geothermal sector shall be a sector that would need this equipment due its typical waste characteristics that has similarity with Water Base Mud Drilling at the conventional gas exploration activities. Geothermal exploration activities with their drilling and production activity would produce huge amount of liquid wastewater that contain high TDS and COD.

Besides wastewater characteristics, geothermal drilling and production shall be a filed that would require a unit that has capability to be mobilized easily at the remote area. Mobile evaporator has the capability to mobile quickly to the location due to its containerized shape.

Table 4 below would show the typcal of wastewater at the geothermal location. Having some comparison with the Water Base Mud Drilling Clarified water the gap is not so much could be seen.

Analyzing typical wastewater that typically geothermal drilling has, it seems that it is very prospective that mobile evaporator to be implemented on treating high TDS and high COD waste water that produced by geothermal drilling activities.

Table 4: Typical wastewater of geothermal drilling

Parameter	Result
pH	6,76
Temperature (^{0}C)	28,5
Conductivity (uS/cm)	13140
Total Dissolved Solid (ppm)	8150
COD (ppm))	3800
Turbidity (NTU)	254



Figure 8: Mobile Evaporator Site Set up

CONCLUSION AND RECOMMENDATION

High TDS and high COD wastewater that produced in conventional drilling activities has been treated successfully by using set of mobile evaporator unit so that all parameters of liquid wastewater been able to meet threshold limit value for on-shore drilling operation. The implementation managed to make the discharged fluid from mobile evaporator be recycled for rig usage prior the discharges to the environment. Implementation of the same type of treatment to geothermal drilling does seem as a good opportunity due to the typical characteristics of wastewater are similiar or even lighter compare to the conventional gas. The implementation of mobile evaporator in geothermal sector is a promising method to prevent environmental damage from high TDS and COD wastewater.

REFERENCES

Chemwotei, S. C. (2011), "Geothermal Drilling Fluids", *GEOTHERMAL TRAINING PROGRAMME*, Reykjavik, Iceland.

Dalan, J. A. (2000), *"*9 things to know about zero liquid discharge*"*. *Chemical Engineering Progress*, 96(11), 71-76.

Dixon, G. N. (2004*),* *"*Distillation Process Can Yield Zero Liquid Discharge System*"*. *Industrial Water World*. Retrieved from https://www.waterworld.com/municipal/technologies/article/16210504/distillation-process-can-yield-zero-liquid-discharge-system.

Wells, K. D., Currie, J. W., Price, B. A., and Rogers, E. A. (1981), *"*The Cost of Meeting Geothermal Liquid Effluent Disposal Regulations*"*. *The US Department of Energy, Battelle Memorial Institute*.

Wilf, M., Awerbuch, L., Bartels, C., Mickley, M., Pearce, G., and Voutchkov, N. (2007), "The Guidebook to Membrane Desalination Technology". *Balaban Desalination Publications.*

ANALYSIS OF RISK MITIGATION STRATEGIES

Ari Ingimundarson and Thorsteinn Sigmarsson

Mannvit hf.
Urdarhvarf 6, 203 Kopavogur, Iceland
Email: arii@mannvit.is

ABSTRACT

Geothermal risk mitigation usually involves reducing the risk of the developer in the exploratory drilling phase when the first wells are drilled. In this study, probability distributions regarding drilling success are used to simulate outcomes of exploration campaigns and using the outcomes, characteristics of distinct risk mitigation mechanisms are analyzed. Two drilling campaign scenarios are evaluated. Firstly, the influence of resource risk on a drilling campaign to reach 50 MW electrical output. The second scenario is a drilling campaign to reach 10 MW electrical output. This second scenario emulates an exploration drilling campaign in a green field. The main results of the article are the following. Contingent financial aid that is dependent on the outcome of the drilling provides higher impact per dollar spent and conversely, unconditional financial aid provides poor impact comparatively. Contingent financial aid depending on the success of a group of wells provides much higher impact per dollar spent than considering the wells one by one. It is argued that average risk mitigation cost of providing a guarantee on MUSD/MW is not as high as expected.

Keywords: Risk analysis, drilling campaign, mitigation

INTRODUCTION

Geothermal resource risk is widely known as a fundamental barrier to development of geothermal resources around the world. To address this problem, risk mitigation funds (RMF) are now operating in many of the main geographical areas with recognized geothermal potential. In (Sanyal et al, 2014) a comparative analysis of risk mitigation approaches is presented. Four main categories are discussed.

1. Government takes on the full resource and other project risks by acting as total project developer.
2. Cost-shared drilling for mobilizing private development. Part of the risk of drilling is therefore moved to the private sector.
3. Geothermal resource risk insurance.
4. Early-stage fiscal incentives (exemption from duties, tax credits etc.) that lower the financial expositor developer would face during exploration drilling.

It is mentioned that geothermal resource risk insurance has not been implemented in great scale around the world. Two reasons are given for this. Firstly, the geothermal sector is small and hardly justifying involvement of larger insurance companies. Secondly, due to the high uncertainty, premiums would have to be quite high and hardly affordable for developers.

This paper analyzes the influence of resource risk on key financial variables in a typical geothermal project. It then analyses the impact distinct resource risk mechanisms have on these financial parameters. Risk mitigation has been treated in several papers over the years. Risk in geothermal development is treated among other places in (Ngugi, 2014). Risk mitigation strategies are also discussed in (Deloitte, 2008). Key criteria for judging risk mitigation strategies are:

1. Low risk to the government or public body implementing the strategy.
2. Least cost to the taxpayer that pays for the implementation of the strategy.
3. Greatest impact on the industry.

A summary of existing risk mitigation facilities that specifically deal with resource risk is given in (Robertson-Tait et al, 2017). Attractive features of risk mitigation facilities are summarized there.

METHODOLOGY

In this section the methodology behind the analysis presented in this paper is explained.

Probability of drilling success

The analysis presented in this paper is based on Monte Carlo Simulations using statistics collected on success rate of drilling. A key publication regarding drilling success is (IFC, 2013). There, statistic on drilling success is published for geothermal wells all around the world.

Using the data from this publication, statistical estimates on drilling success can be created. Figure 1 shows the cumulative frequency curve of commercial and failed wells with MW designation and verified status in (IFC, 2013).

The curve can be considered to have two parts. The first part to the left is flat at zero and represents the probability of a failed well. The other part then gives

the probability distribution of certain power output given that the well is not a failure. The probability distribution is "tail-heavy", meaning that high output wells are quite likely and contribute significantly to the averages of output.

Note that success probability is different if the wells are the first wells being drilled in a field or if several wells have already been drilled as there is a learning curve when more wells are drilled in a field. The learning curve effect can be taken into account in simulation by increasing the flat part of the curve giving 0 MW. A successful well is defined in most cases as a well with over 3 MW electricity production. Success rate has also been shown to vary from field to field. The differences in success rate mentioned above are not considered in this article.

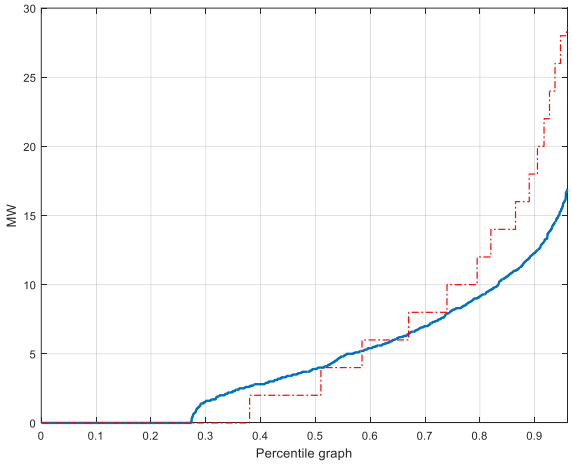


Figure 1: Percentile graph of MW electricity produced created from (IFC, 2013) and the case of Indonesia (dashed-dot) (Sanyal et al, 2011).

In Sanyal et al, 2011, similar information for Indonesia was presented. The percentile graph for MW electricity in Indonesia is also shown in Figure 1. As can be seen, the probability of unsuccessful wells is higher or 38% but the probability of obtaining wells with higher output is also higher.

The distribution from Indonesia is similar to the curve based on (IFC, 2013). On the other hand, as the (IFC, 2013) dataset is more complete and contains much more wells, it is used in the subsequent analysis.

The data presented in the above figure can be used to simulate the results of drilling campaigns by using Monte Carlo Simulation. By using random number generation, a MW output according to the cumulative frequency presented above is calculated. This is repeated until a threshold MW value for the drilling campaign is reached.

Cost of wells

An estimate of the cost of wells is a necessary component to calculate the cost of reaching a threshold MW value in a drilling campaign. The following price model was used for the calculations. The average price was assumed to be US$ 6.5 millions. Variation around the average was assumed to be US$ ±2.5 millions. No consideration was given to different depths of wells.

The cost of a drilling campaign was therefore found by random number generation and finding the corresponding number on the above mentioned cost interval.

Scenarios analyzed

Two distinct case studies or scenarios were simulated representing typical drilling campaigns. These are described in continuation.

Scenario 1. The first scenario simulated was supposed to be representative of drilling for a 50MW power plant. A series of well outputs were simulated by calculating the outputs from the distribution in Figure 1, and adding them until the accumulated output was above 50 MW. For this scenario and the associated financial analysis presented in the next section, key parameters were obtained from (Gehringer and Loksha, 2012). There a somewhat detailed financial model of a 50 MW power plant is published which was used to serve as a base case in the financial analysis presented in this article.

Scenario 2. The second scenario simulated was drilling for an accumulated 10 MW of power. The aim with this scenario was to emulate an initial drilling campaign in a greenfield. Power outputs were generated with a random number generator and using the probability distribution shown in Figure 1. This was done repeatedly, and the power outputs added until the accumulated power of the "drilling campaign" was above 10 MW.

Financial parameters analyzed

The financial parameters analyzed were on one hand total cost of drilling by adding together the total cost of wells in a drilling campaign. On the other hand, in scenario 1, in the case of the 50 MW plant, project internal rate of revenue (IRR) and equity internal rate of revenue were calculated.

The IRR as a function of cost of drilling was calculated by using information in (Gehringer and Loksha, 2012). There, the free project cash flow was given for a typical 50 MW power plant. The total drilling cost is there assumed to be US$ 70 million. It was assumed that this was distributed in the following way over the project timeline.

Table 1 : Total Drilling Cost for a Typical 50 MW Power Plant.

Year	0	1	2	3	4	6
Drilling cost US$ millions	0	0	10	10	25	25

By substituting proportionally, the 70 million with the drilling cost for each simulated drilling campaign, a new free project cash flow could be calculated as well as the project IRR. Note that this approach assumed no change in debt structure irrespective of how the drilling campaign has proceeded. A similar approach was used for IRR of equity. The free cash flow to equity was modified according to the results of each simulated drilling campaign and IRR of equity calculated by using the modified free cash flow to equity. Note that it was assumed that an increase in drilling cost from the above mentioned 70 million would be financed by equity.

Distribution of financial parameters

Decisions on investments from probability distributions of financial parameters typically do not only consider average numbers but rather consider pessimistic estimates such as the 90th percentile, denoted as P90. The understanding is that for the financial parameter in question, 9 out of 10 cases if the investment could be repeated with the same distribution of outcome, the result should be better or the same as the P90 value.

In the following analysis of risk mitigation strategies, the change obtained in P90 is considered a measure of effectiveness of the strategy. The effectiveness should also be compared to the cost of the strategy.

RESOURCE RISK INFLUENCE ON FINANCIAL PARAMETERS

Given the distribution of MW output of geothermal wells shown in Figure 1 and the distribution of cost discussed earlier, the distribution of drilling cost for scenarios 1 and 2 discussed earlier were calculated by using Monte Carlo Simulation. Figure 2 shows the drilling cost distribution for scenario 1. The P90 is around US$ 85 while the P50 is around US$ 65.

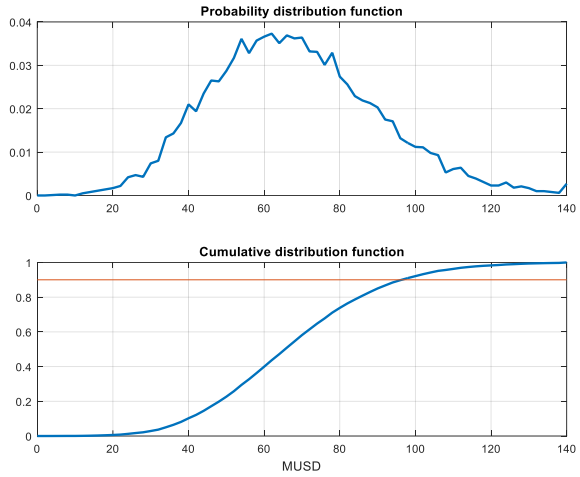


Figure 2: Distribution of cost of drilling for scenario 1. 50 MW case.

In Figure 3 and Figure 4, project IRR and IRR calculated from equity are shown respectively. The P90 of project IRR is 11.5% while P50 is 13.4%. The corresponding numbers of equity IRR is 18% and 25%. The reduction in equity IRR is therefore substantially higher. This is expected as the equity IRR can be more sensitive to changes in the earlier years of the financial horizon than project IRR. Note that equity IRR was not calculated for drilling cost lower than US$ 50 million. This is because in the 50 MW example, total equity in the project is around 62 million in the base case. A reduction of cost of more than 20 million would not necessarily reduce the equity need correspondingly in the project. This cutoff point is on the other hand selected quite arbitrarily. In what follows, only project IRR will be considered for further analysis. The behavior of project and equity IRR is similar for the cases considered in this article.

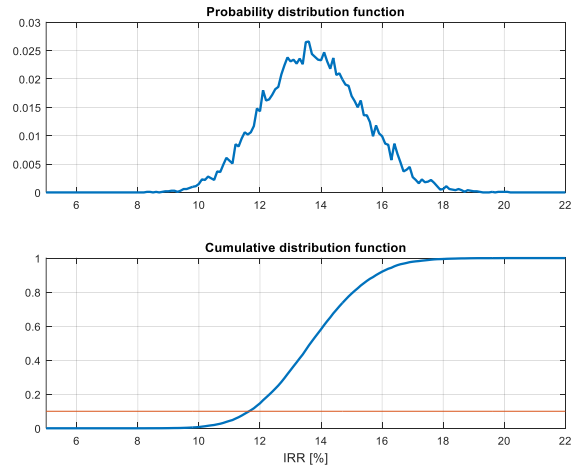


Figure 3: Project IRR distribution for scenario 1. 50 MW case.

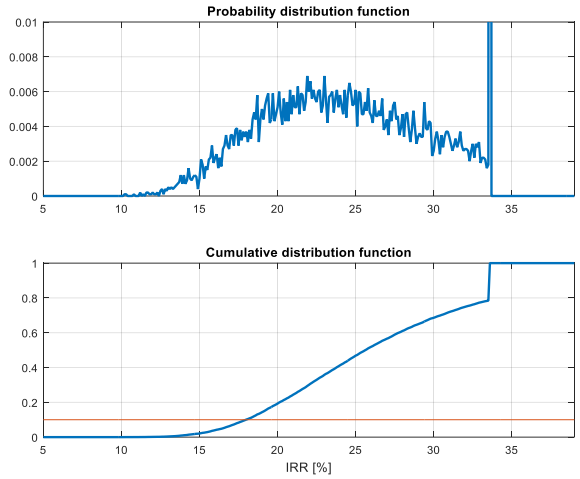


Figure 4: Equity IRR distribution for scenario 1. 50 MW case.

Figure 5 shows the probability distribution for scenario 2. The step seen between 4-9 MW represents the cases where one well is sufficient to generate 10 MW. Also shown is the cumulative distribution function. This shows that the P90 of drilling cost is US$ 33 million compared to a P50 of US$ 17. The proportional difference between P90 and P50 is much larger in scenario 2 than in scenario 1. This is expected as in a drilling campaign with more wells, the variance should be smaller.

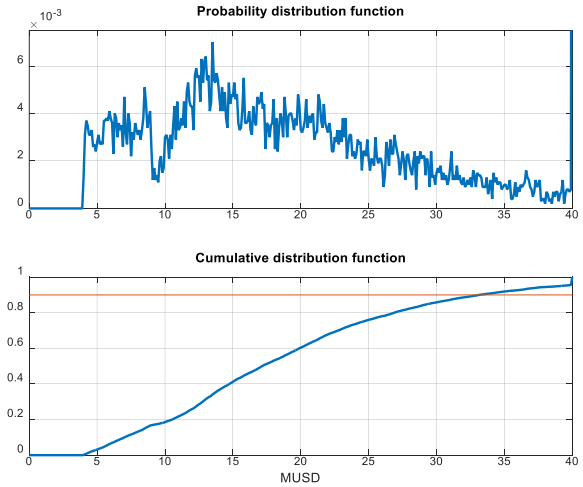


Figure 5: Distribution of drilling cost for scenario 2 (10 MW drilling campaign).

ANALYSIS OF RISK MITIGATION STRATEGIES

The analysis of several risk mitigation strategies is presented in what follows. Both existing risk mitigation strategies and hypothetical ones are considered for increased contrast in the analysis. The discussion begins with scenario 1. The reason being that some of the risk mitigation strategies considered do not influence drilling cost.

Feed-In Tariff

Feed-in tariffs (FIT) are basically policy mechanisms designed to increase the attractiveness of certain investments. In the geothermal case, long term contracts with attractive prices are offered to power producers.

In Figure 6, the IRR for an increase in FIT is shown. The FIT has been increased by 20% from the base case. This causes an improvement of the project IRR for the whole distribution as expected. The IRR distribution for the case of increased FIT is basically the same as for the base case but the curve is translated towards higher IRR.

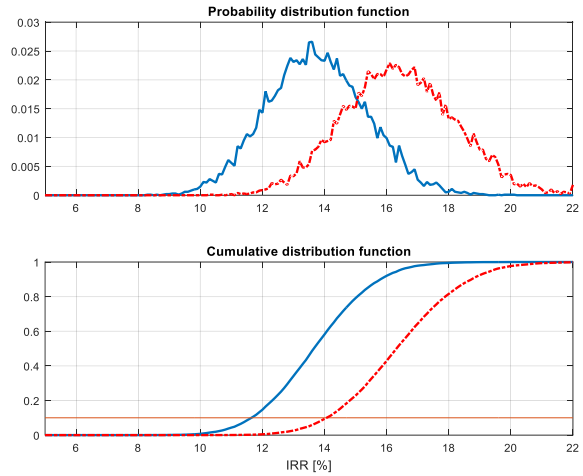


Figure 6: Influence of Feed-In Tariffs on project IRR. The dashed-dotted line corresponds to the Feed-In Tariff case. The solid line curves are the same as in Figure 4.

Cost sharing case - GRMF

The Geothermal Risk Mitigation (GRMF) facility for Eastern Africa was launched in 2012. It provides grants for up to 40% of approved cost of drilling the first 3 wells. The grants are given unconditionally without any need to pay them back.

Figure 7 shows the influence of the GRMF scheme on project IRR. As in the case of FIT, as the GRMF is an unconditional grant, independent of drilling success. The curve is therefore translated towards the higher IRR.

Cost sharing case – GDF

The Geothermal Development Facility (GDF) for Latin America was announced in 2016. It provides contingent grants for up to 40% of approved cost of drilling the first 3 wells. If wells are successful, the developer must pay back 80% of the received grant.

Figure 8 shows the influence of the GDF scheme on project IRR. The GDF is a conditional grant, that depends on drilling success. The curve is translated

towards the higher IRR but even though not noticeable on the figure, the variance is smaller for the CAF case than for the GRMF case.

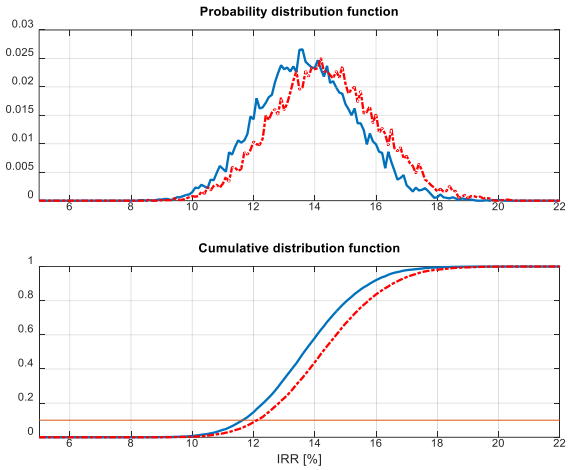


Figure 7: Influence on project IRR under a cost sharing risk mitigation scheme such as the GRMF.

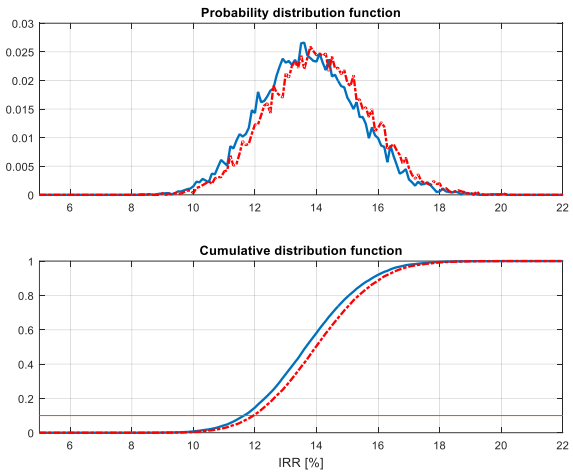


Figure 8: Influence on project IRR under a cost sharing risk mitigation scheme such as the GDF.

Full risk mitigation

A hypothetical case is presented where the developer does not have to pay for failed wells. Drilling cost is under this risk mitigation scheme substantially lower than in the base case.

The figure shows that in addition to a translation of the distributions, the distribution of the full risk mitigation case is narrower than the base case distribution. The slope of the cumulative distribution function is higher than in the base case. This follows a more narrower probability distribution function. Note that this has a bigger impact on the P90 than if the curve is only translated.

Full risk mitigation with premium

A second hypothetical case is presented where the developer does not have to pay for failed wells but pays a premium to enter the risk mitigation scheme. The premium equals the average cost of failed wells when drilling for 50 MW. This would mean that any public entity implementing this scheme would not bear any cost other than administrative cost to implement the cost.

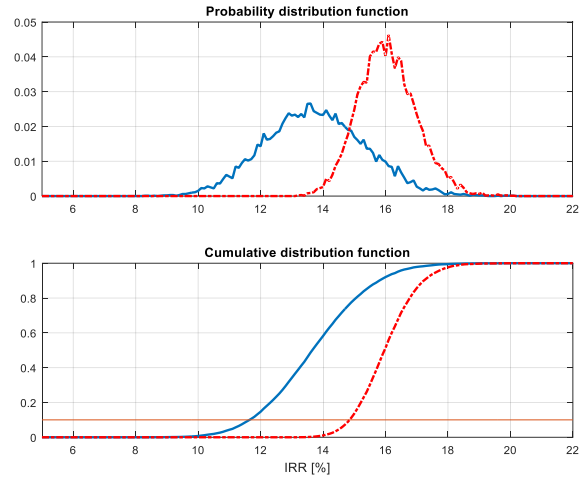


Figure 9: Influence of full risk mitigation on project IRR.

Figure 10 shows the project IRR for full risk mitigation with premium. The figure shows that in this case a substantial reduction in variance is achieved while the average IRR of the distribution does not change from the base case (around 13.5%).

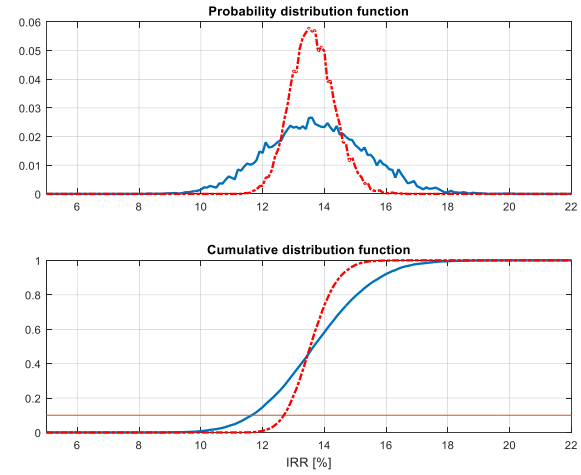


Figure 10: Influence of full risk mitigation with premium on project IRR.

Guarantee of max cost of MW – Group insurance

Another hypothetical case is presented where the developer is guaranteed to pay a maximum value per MW. The value is US$ 1.4 million per MW. This corresponds to US$ 70 million for 50 MW.

In this case, failed wells are “equalized” by good wells in the drilling campaign and therefore the risk mitigation functionality is for the outcome of the total group of wells in the drilling campaign. It can be noticed that a substantial reduction is achieved in the P90. Project IRR P90 and P50 values are similar or around 13.5%

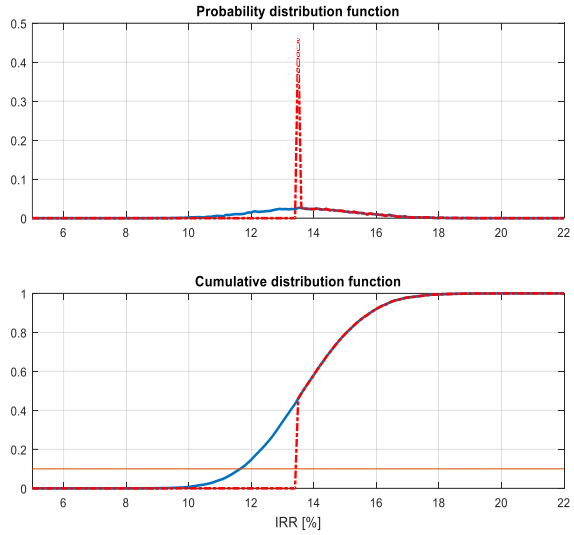


Figure 11: Influence on project IRR if max cost per MW is guaranteed by risk mitigation facility.

Probability distributions for scenario 2

The figures that have been presented for scenario 1 are now presented for scenario 2, see figures 12 to 16. The figures are discussed at a later stage.

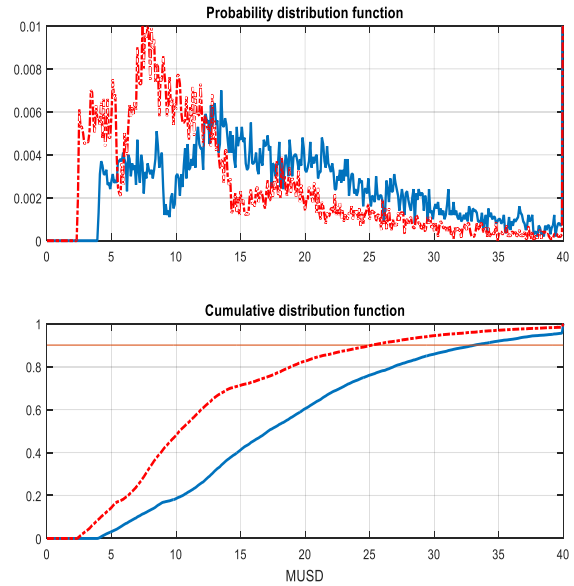


Figure 12: Influence of a cost sharing sharing risk mitigation scheme such as the GRMF on drilling cost for scenario 2 (10MW).

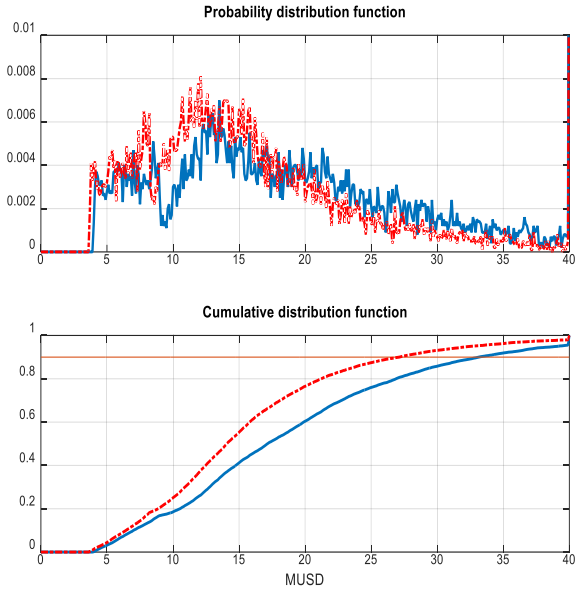


Figure 13: Influence of a cost sharing sharing risk mitigation scheme such as the GDF for scenario 2 (10MW).

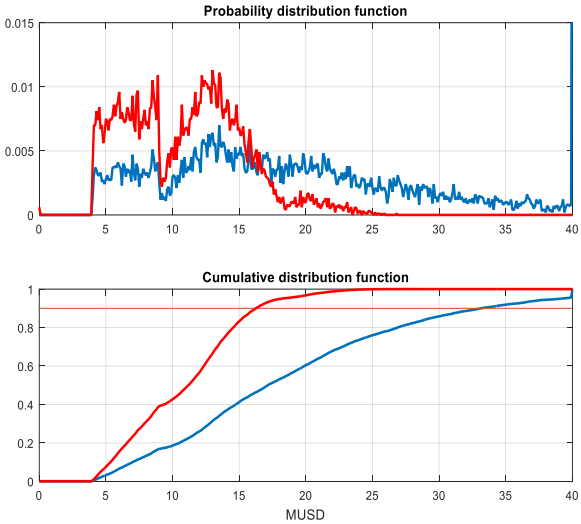


Figure 14: Influence of the full risk mitigation scheme on drilling cost for scenario 2 (10MW).

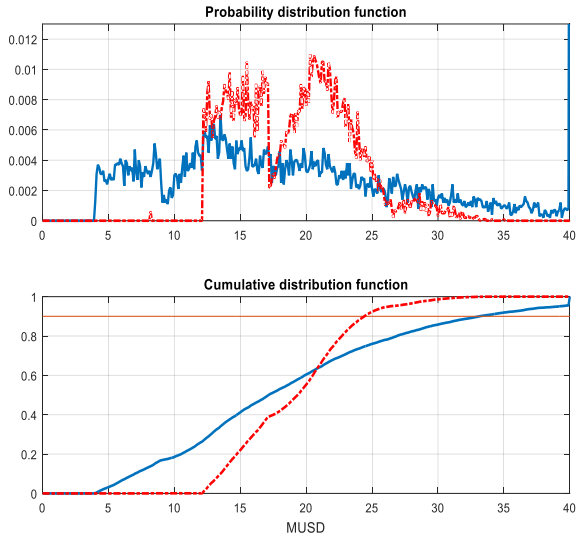


Figure 15: Influence of the full risk mitigation with premium scheme on drilling cost for scenario 2 (10MW).

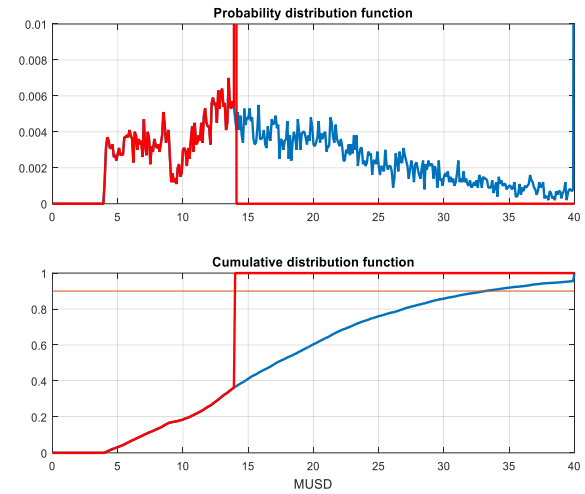


Figure 16: Influence of guaranteeing max cost per MW (US$ 1.4 million) on drilling cost for scenario 2 (10MW).

IMPACT AND COST OF RISK MITIGATION STRATEGIES

The change in the project IRR P90 achieved for each risk mitigation scheme is demonstrated in Figure 17 for scenario 1. Also shown is the mean risk mitigation cost for each drilling campaign. This is the cost the risk mitigation facility would have on the average.

Figure 18 shows similar numbers for scenario 2. On the left the reduction of the drilling cost P90 is shown for all risk mitigation strategies. On the right side the average cost of implementation of the risk mitigation scheme is shown. From the figures it can be seen that a great difference between cost and impact on P90 between the strategies.

The FIT approach to risk mitigation has by far the highest cost while achieving a substantial change in P90. Note that the FIT cost was calculated as the Net Present Value using the WACC of the base case as interest. The impact of the GRMF risk mitigation per dollar spent is on the other hand higher than the FIT approach. However, even though not apparent on the figure, the GDF approach has a higher impact on P90 per dollar spent than the GRMF. This can be explained by the fact that the grant is conditioned on drilling success and does therefore not pay as much for successful wells as the GRMF which does not distinguish between successful and unsuccessful wells.

The hypothetical risk mitigation schemes are of interest as well. If possible to implement, the full risk mitigation with premium has high impact with low cost. On the other hand it can be said that this is actually approach 3 presented in Sanyal et al, 2014, or "Geothermal resource risk insurance". The difference is that in the risk insurance case the premium is higher as it would be set to compensate for failed wells as well as provide the insurance company with profits.

It is interesting to consider the last risk mitigation strategy, namely the guarantee of max cost per MW. This approach provides excellent reduction in P90 while costing a similar amount as existing risk mitigation funds such as the GRMF.

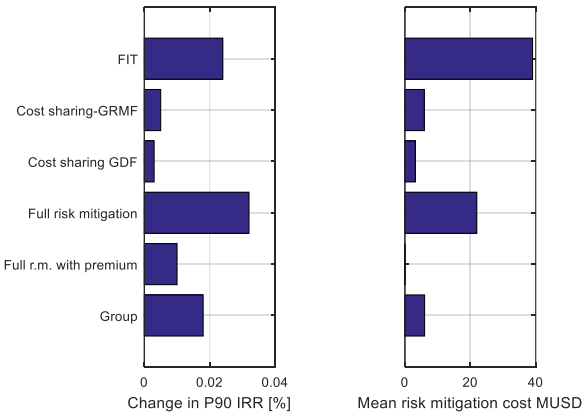


Figure 17: Change in project IRR P90 for each risk mitigation strategy and mean risk mitigation cost per drilling campaign.

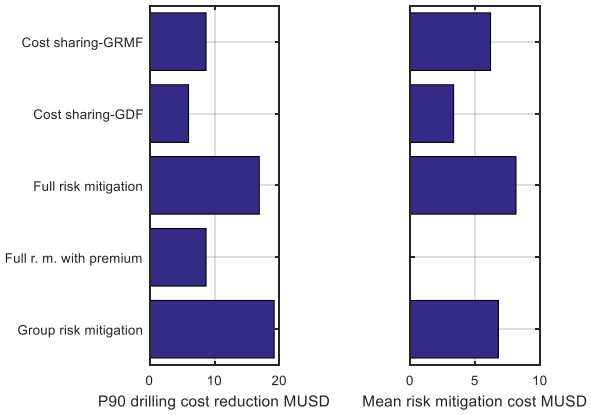


Figure 18: Change in drilling cost P90 for each risk mitigation strategy and mean risk mitigation cost per drilling campaign for scenario 1.

DISCUSSION

The following observations are made on basis of the presented data.

1. Risk mitigation strategies that provide unconditional financial aid provide poorer impact per dollar spent than those that condition the financial aid to drilling success. If the aid is not dependent on drilling success, public funding is spent on projects that have had excellent drilling results and might not need the funding. Risk mitigation strategies that provide aid dependent on the success of the drilling have higher impact in terms of improvement of P90, per dollar spent.
2. Risk mitigation strategies that mitigate the risk of a group of wells providing a max cost of each MW provide the highest impact in terms reduction of P90 per dollar spent.

In summary, for higher impact per dollar spent the risk mitigation strategy should link financial aid to the successful drilling of a group of wells. It is of interest to notice that when the risk of failure of a group of wells is mitigated, the cost is similar to existing risk mitigation facilities. The risk reduction is on the other hand drastically different. Guaranteeing a max cost per MW effectively removes the risk of failure for the developer.

It is on the other hand clear that a risk mitigation facility that gives aid dependent on success is more complex to implement. Overhead of such a facility is increased as success of drilling has to me measured. Note that success of wells is not only dependent on MW output. Other issues can render a well unusable such as the chemical content of the geothermal fluid.

CONCLUSIONS

The main results are the following. Contingent financial aid that is dependent on the outcome of the drilling provides higher impact per dollar spent and conversely, unconditional financial aid provides poor impact comparatively. Contingent financial aid depending on the success of a group of wells provides much higher impact per dollar spent than considering the wells one by one. It is argued that average risk mitigation cost of providing a guarantee on MUSD/MW is not as high as expected.

REFERENCES

Deloitte. (2008), *"Geothermal Risk Mitigation Strategies Report"*. Swiss: Departement of Energy - Office of Energy Efficiency and Renewable Energy Geothermal Program.

Gehringer, M., and Loksha, V. (2012), *"Geothermal handbook: planning and financing power generation"*. Energy Sector Management Assistance Program, The World Bank, Washington, DC.

IFC. (2013), *"Success of Geothermal Wells: A Global Study"*. International Finance Corporation.

Robertson-Tait, A., Richardson, J., Palmateer, A., Nayak, S., Falconer Thomas, A., Roque-Rivera, R. (2017), *"The GeoFutures Facility: A Proposed Geothermal Risk Mitigation Instrument for East Africa"*. GRC Trans. 41.

Sanyal, S.K., Morrow, J.W., Jayawardena, M.S., Berrah, N., Li, S.F. (2011), *"Geothermal Resource Risk in Indonesia"*. A Statistical Inquiry, in: International Conference on Renewable Energy and Energy Efficiency, World Renewable Energy Congress–Indonesia.

Sanyal, S.K., Robertson-Tait, A., Jayawardena, M.S., Huttrer, G., Berman, L. (2014), *"Comparative Analysis of Approaches to Geothermal Resource Risk Mitigation: A Global Survey"*. Energy Sector Management Assistance Program, The World Bank.

IDENTIFICATION OF GEOTHERMAL ENERGY POTENTIAL USING 4G METHOD (GEOGRAPHY, GEOLOGY, GEOPHYSICS, GEOCHEMISTRY) IN TELOMOYO MOUNTAIN COMPLEX, CENTRAL JAVA

Alfath Zain[1], Aulia Umami[1], Desi Kiswiranti[1], and Fadhil[2]

[1]Geological Engineering, Faculty of Mineral Technology,
Institut Sains & Teknologi AKPRIND Yogyakarta, Indonesia
Jl. Kalisahak No. 28, Kompleks Balapan, Yogyakarta, DIY 55222
[2]Geophysical Engineering, Faculty of Mineral Technology,
Universitas Pembangunan Nasional "VETERAN" Yogyakarta, Indonesia
Jl. SWK 104 (Ringroad Utara), Condong Catur, Depok, Sleman, DIY 55283
Email: alfathzain@gmail.com

ABSTRACT

Geographical position of Indonesia lies within ring of fire which has renewable energy potential, it is geothermal. One of which is in the area of Telomoyo Mountain that is created in a volcano quarter complex. Telomoyo Mountain complex is a volcano complex in Semarang, Central Java Province. The presence of hot springs and mineral alteration indicates that Telomoyo Mountain complex has geothermal energy potential. To identify geothermal energy potential optimally, we must analyze with geographical method (Remote Sensing), Geology, Geophysics (Geoelectric) and Geochemistry (Geothermometer). Hot springs manifestation of Candi Dukuh is located in the intensive density lineament structure according to the fault fracture density analysis (FFD), so that the rocks in that area have discontinuity which fuctioned as the exit point for energy and hot fluid. Geological conditions in Telomoyo mountain complex consists of alluvial deposits, scoria cone, Telomoyo volcano rocks, Kendil volcano rocks, and Gilipetung volcano rocks. The results of geoelectric measurement shows that the three highest layers with value (19,8 - 58,1 Ωm) is a layer that has good permeability. This geoelectric measurement location can be interpreted as recharge area. According to the analysis of geochemistry, it shows that the fluid type in the area of Telomoyo geothermal is bicarbonate water type and the characteristic is located in the immature water condition. The genesis of the geothermal formation came from peripheral water that is formed in the area close to the surface and mixed a lot with surface water. There is also manifestation based on the analysis that has been done also shows that there is geothermal energy potential in the research area.

Keywords: remote sensing, geophysics, geothermal, geothermometer, telomoyo

INTRODUCTION

Indonesia is one of a country that has the biggest geothermal potential in the world. Its geographical position that is located on the path of the volcano is also a ring of fire area, which has geothermal potential. Geothermal systems generally related with magmatism activities that formed in certain areas. Geothermal also means a naturally generated heat energy under the ground and its systems formed as a result of heat displacement from heat source that happened in conduction and convection. Geothermal is also an alternative energy sources that can be substitute for fossil energy sources, such as crude oil and coal, when producing electricity.

Each geothermal fields have their own geothermal systems characteristics. For example Mount Telomoyo geothermal area formed in a volcano quarter complex marked by the appearance of manifestation that is hot springs (Candi Dukuh) and mineral alteration. To optimize its geothermal potential, we need a further study of geothermal availability identification.

Geothermal studies in this area is necessary for the next development, reviewed from the role of geo science such as geography, geology, geophysics, and geochemistry as a method to identify the availability of a prospect area and geothermal energy potential optimally.

DATA AND METHOD

Geography

The method used is fault fracture density (FFD) method, in which done by analysing the lineament of Telomoyo volcanics complex with Digital Elevation Model (DEM). Structures lineament analysis is done to determine which location has high anomaly of geological density lineament structure that formed due to the fault and the fractures or what is called fault fracture density (FFD). The lineaments which predicted as geological structures are difference both in contrast hue or relief on image (Figure 1). Furthermore, the density lineament anomaly analysis done by

gridding on every 1 km area. This is according to the density lineament analysis by Soengkono (1999) where the lineament analysis of one geothermal field is 1 km and the units obtained is km/km^2. It is done to know which area has the most intensive structure. This structure is potentially as permeable zone which functioned as the exit point for hot fluid to come up to the surface. The result of density lineament analysis then interpreted as area that potentially has geothermal prospects.

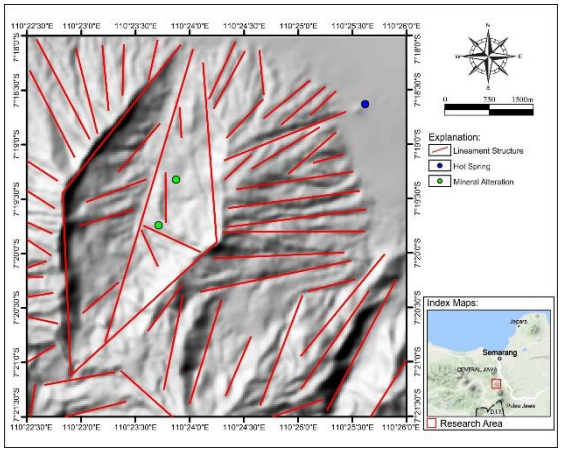


Figure 1: Lineament Structure Map

Geology

Geological condition analysis in the research area is done directly in the field while some is based on literature review. The observation done to know the type of lithology, distributions of geothermal manifestations, geological structure, and geological history in Telomoyo volcanic complex.

Geophysics

The measurement of rock formation resistivity on 3 geoelectric point is done by using Schlumberger sounding method in Telomoyo volcanic complex with the stretch of AB electrode up to 400 m (Figure 2). The principles of geoelectric resistivity method is streaming electric current into earth by contacts of different electrode current, then we measure the potential distribution produced. Subsurface rocks resistivity can be calculated by knowing the currents radiated through those electrode and also the potential value produced. The resistivity value of a medium can be mathematically formulated as following [1]:

[1]

$$\rho = k.V/I$$

Where :

ρ = resistivity
k = geometrical factor
v = potential difference
I = current intensity

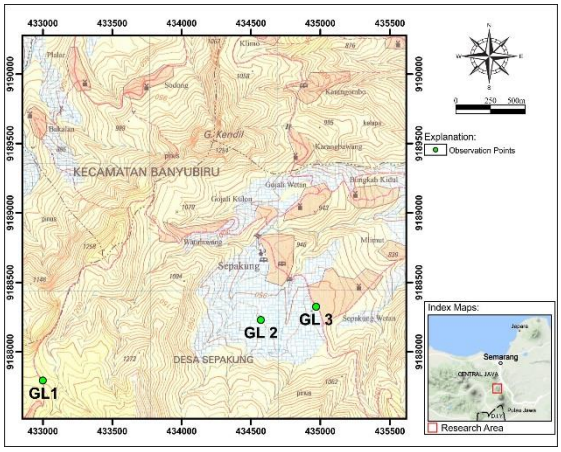


Figure 2: Observation Points Map

The benefit of Schlumberger is because of its ability to detect any non-homogenetic rock layers on the surface, which can be done by comparing the uncertain value of resistivity when the distance of electrode MN/2 changed.

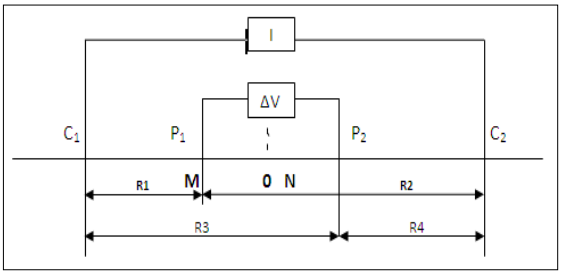


Figure 3: Schlumberger Configuration Compositions

Figure 3 shows the Schlumberger configuration structure. The parameters to be measured are: distance between station with electrodes (AB/2 and MN/2), currents (I), and potential difference (ΔV). The parameters to be calculated are: resistivity (R) and geometrical factor (k). The geometrical factor can be found with formula as following [2]:

[2]

$$K = \frac{2\pi}{\frac{1}{C_1P_1} - \frac{1}{C_2P_1} - \frac{1}{C_1P_2} - \frac{1}{C_2P_2}}$$

$$K = \frac{2\pi}{\frac{1}{b-\frac{a}{2}} - \frac{1}{b+\frac{a}{2}} - \frac{1}{b+\frac{a}{2}} - \frac{1}{b-\frac{a}{2}}}$$

$$K = n\left[\frac{2b}{a} - \frac{a}{4}\right]$$

$$pa = K.R$$

Geometrical factor for Schlumberger configuration can be generally defined as following [3]:

[3]

$$K = \pi \frac{AB^2 - MN^2}{4MN}$$

Geochemistry

This method consist of chemical analysis on thermal manifestation on the earth's surface which is hot springs. Geochemical method used for this research is Solute Geothermometer Na-K-Mg and Ternary Plot Cl-SO_4-HCO_3 to know the fluid type, genesis and equilibrium of geothermal fluid in the area of Candi Dukuh's hot springs in Telomoyo volcanic complex.

RESULT AND DISCUSSION

Geography

Fault fracture density map shows the high fault and fracture density, so that the rocks in area have discontinuity that can be a potential medium for fluid or heat energy to come up to the surface. On geothermal system, the geothermal fluid will flow upwards through the permeable zone which generally came from geological structure. Therefore, the greater the structure density level, the greater its permeability level is. Density anomaly of fault and fracture with value above 3,5 km/km^2 is located from the north side of young Telomoyo volcano to the area of Candi Dukuh (Figure 4).

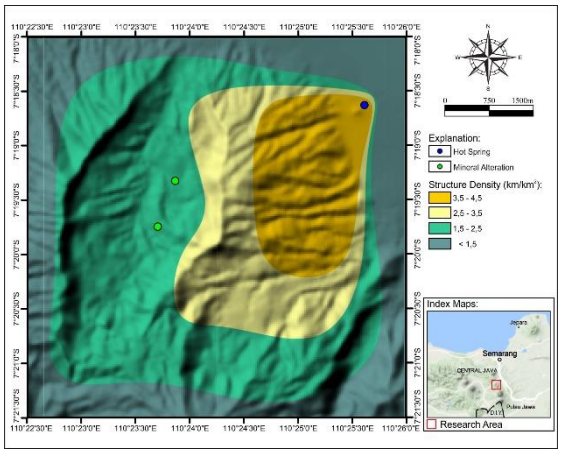


Figure 4: Fault Fracture Density Map

Geology

The research location is in the volcanic cone morphology units, caldera walls ridge, volcanic slopes, volcanic eruption crater, and fluvial landforms such as a swamp. The stratigraphic order on the research area is grouped into several rocks unit from young to old, that is alluvial deposits (Qa) that can be found around Rawa Pening formed as a soil resulted by andesit lava weathering, deposits of cinder cones (Qcc) consists of andesite scoria rocks, Telomoyo Volcanics (Qte) consists of andesite lava, Kendil Volcanics (Qak) consists of andesite breccia, and Gilipetung Volcanics (Qg) consists of andesite lava (Thaden, et al, 1996) (Figure 5). On the research area, the lithology dominant is a volcanic rocks that have thermal conductivity of rocks. The rocks conductivity is one of the nature of the rocks, related to the heat transfer that is happened inside. This transfer happened because of the contact between rocks and geothermal resources.

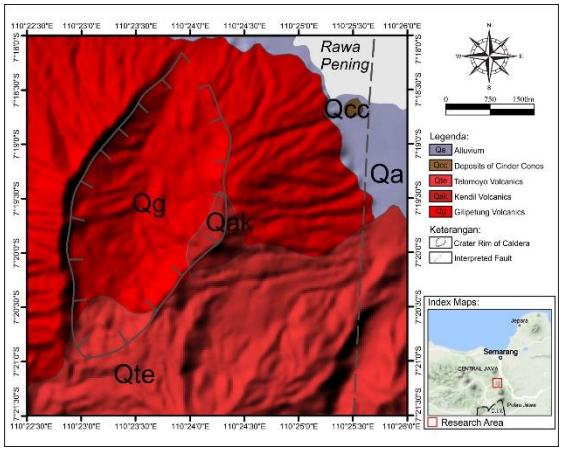


Figure 5: Geological Map

Geothermal manifestation on the research area consist of Candi Dukuh hot springs with the temperature between 35-36°C, this hot springs located in the outflow zone that is affected by the presence of regional structure in the North-South. In addition to the manifestation of hot springs, we can also find mineral alteration argillic type in research area characterised by the presence of kaolin minerals in the former crater of Soropati. This crater formed because of the massive eruption of Telomoyo causing gap inside the earth's inner core. It also causing a collapse due to the gravity and caldera structure collapse that is featured by the structure of the depressive caldera rim. Argillic alteration zone is an upflow zone that is located on the boiling zone from a reservoir and is impermeable, so it has a role as a cap rock. Volcanic rocks that have changed is an evidence of geothermal fluid interaction with the rocks that passed through fracture paths. It shows that the presence of hot springs manifestation and alterated mineral is closely relative with the existence of intensive fracture structure in research area.

Geophysics

Geophysics data used for this research is obtained from study done by Elida Septiana Putriutami, et al, whose data we processed further to be presented in this research. From the modeling results in the Figure 6 obtained from matching curve approach is using software IP2win, then we create subsurface profile by using Corel Draw. According to the resistivity value and geological map analysis in research area can be interpreted into some layers, there are alluvial layer as the top layer with resistivity value around 19,8 - 22,3 ohm.m and depth about 1 - 6,2 meter. Second layer is the breccia layer with the resistivity value around 253 - 473 ohm.m and depth about 6,64 - 18,7 meter. Third layer is sandstone-tuff layer with resistivity value around 38 - 58,1 ohm.m and depth about 18,2 - 49 meter. The last layer is lava layer with resistivity value around 721 - 783 ohm.m and depth approximately more than 130 meter (Figure 6).

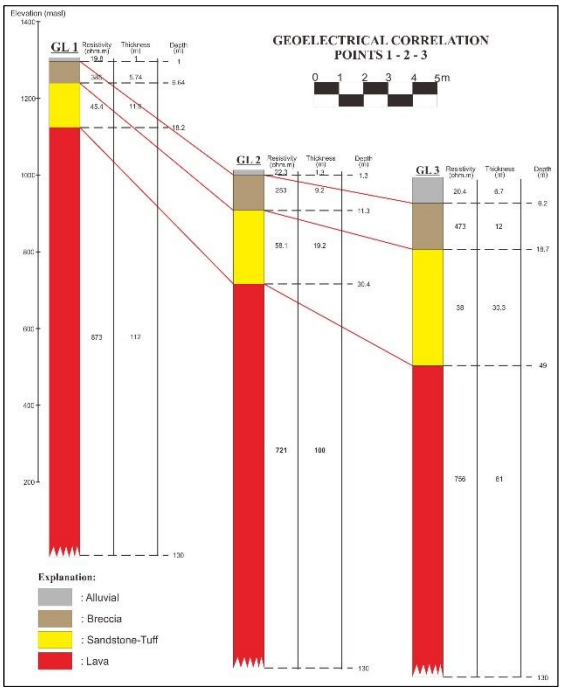


Figure 6: Geoelectrical Correlation Points

Geochemistry

Chemical fluid analysis done on the water sample in hot springs manifestation of Candi Dukuh. The following is the results of laboratorium test from hot springs sample (Table 1):

Table 1. Chemical analysis results

Chemistry Parameter	Test results
Sodium (Na)	243 mg/L
Potassium (K)	16 mg/L
Silicate (SiO_2)	11,954 mg/L
Calcium (Ca)	68,050 mg/L
Magnesium (Mg)	33,71 mg/L
Temperature	36°C
Ph	6,6
HCO_3	392,6 mg/L
Chloride (Cl)	176,9 mg/L
Sulphate (SO_4)	6 mg/L

Chemical data needed to decide the type of reservoir fluid is a relative composition from chloride (Cl), bicarbonate (HCO_3), and sulphate (SO_4), it's done by calculating the percentage from the elements Cl, HCO_3, and SO_4. From the results of calculation, we got that the fluid type of Candi Dukuh hot springs is bicarbonate, it is proven by the percentage of element HCO_3 that is higher than other elements. Next is plotting the percentage value of elements Cl-HCO_3-SO_4 in ternary diagram to know the genesis of the geothermal fluid creation (Figure 7). According to the analysis using ternary diagram, the genesis of geothermal fluid is created from the peripheral water zone that formed in the area close to the surface and also have a lot mixing with meteoric water.

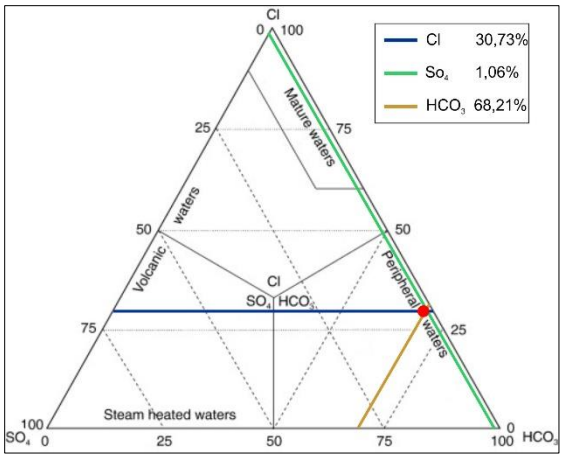


Figure 7. Ternary Diagram Cl-SO_4-HCO_3

The next analysis is using solute geothermometer method by using the composition percentage of Na, K, and Mg, on the geothermal fluid. The results of this analysis used to know the equilibrium of geothermal fluid. The composition calculation results is relative on Na/1000-K/100-√Mg. Furthermore, it is plotting the percentage value of elements in diagram Na-K-Mg (Figure 8). According to the diagram Na-K-Mg, Candi Dukuh hot springs is in immature water situation. This condition shows that the hot springs temperature that come up to the surface is more likely to be low and affected by the mixing between hydrothermal fluid and more shallow water with low silica concentration.

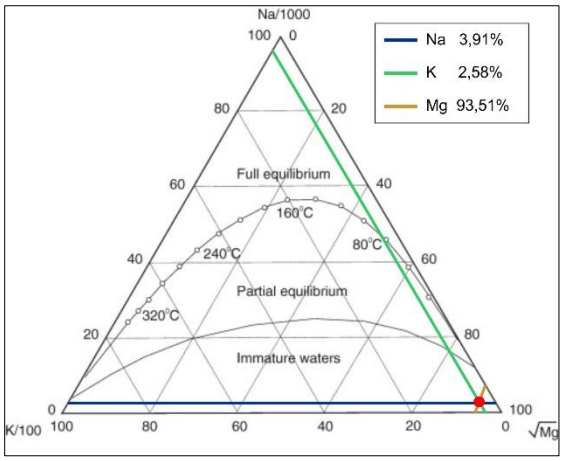


Figure 8. Geothermometer Diagram Na-K-Mg

CONCLUSIONS

Based on the analysis results done with the geothermal manifestation that appeared in area with fault and high fracture density. That things caused by the relation between structure density and permeability, because the highest the structure density level, the highest the permeability level is. Rocks permeability in those area have roles as a discontinuity that can be a potential medium for fluid or heat energy that come up to the surface.

Geothermal manifestation in research area is including alteration mineral and Candi Dukuh hot springs. This hot springs has temperature between 35-36°C and is located in the outflow zone. While the argillic alteration zone is an upflow zone that is located above the boiling zone of a reservoir and characterised as impermeable, so it also acts as cap rock. Volcanic rocks that has changed is an evidence of the interaction between geothermal fluid with rocks that it goes through the fracture tracks.

The subsurface layer in research area is consisting by 4 layers identified to the depth of 130 m to undetected. The top 3 layers which is alluvial deposit, breccia and sandstone-tuff are layers with pore so they can let water through easily. This geoelectric measurement location can be interpreted as recharge area on the geothermal system in Telomoyo volcanic complex.

The fluid type of Candi Dukuh hot springs is bicarbonate and its characteristic of water type is located in immature water condition. The genesis of geothermal fluid creation is formed from the peripheral water zone that is created in area close to the surface and it has a lot of mixing with meteoric water.

ACKNOWLEDGEMENTS

Within this research completion, authors are giving much gratitude for Elida Septiana Putriutami, Udi Harmoko, Sugeng Widada, who have given us the data and help us to get the geophysics data in the research field. Also, we give big thank you for Mrs. Desi Kiswiranti, S.Si., M.Sc., who has guide us and give us valuable instructions thus this research can be done well.

REFERENCES

Azhari, A. P., Maryanto, S., Rachmansyah, A. (2016), Identifikasi Struktur Geologi dan Pengaruhnya Terhadap Suhu Permukaan Tanah Berdasarkan Data Landsat 8 di Lapangan Panas Bumi Blawan. Jurnal Penginderaan Jauh. Volume 13, Nomor 1.

Bemmelen, R. W. Van. (1949), *The Geology of Indonesia*. Vol IA. Goverment Printing Office. Netherland.

Giggenbach, W. F. (1988), Chemical Techniques in Geothermal Exploration Chemistry Division, DSIR, Private Bag.

Hermawan, D., Rezky, Y. (2011), Delineasi Daerah Prospek Panas Bumi Berdasarkan Analisis Kelurusan Citra Landsat di Candi Umbul - Telomoyo, Provinsi Jawa Tengah. Pusat Sumber Daya Geologi. Buletin Sumber Daya Geologi. Volume 6, Nomor 1-2011. Hal 1-10.

Nicholson, K. (1993), Geothermal Fluids; Chemistry and Exploration Techniques, Springer Verlag.

Pambudi, D. Y. W. S., Sakur, M., Ismail, K., Dwiyono, I. F., Setijadji, L. D. (2014), Delineasi Daerah Prospek Panas Bumi Berdasarkan Kelurusan Citra Landsat dan *Digital Elevation Model* (DEM) Daerah Gunung Lawu, Provinsi Jawa Tengah dan Jawa Timur. Prosiding Seminar Nasional Kebumian Ke-7. Jurusan Teknik Geologi, Fakultas Teknik, Universitas Gadjah Mada.

Putriutami, E. S., Harmoko, U., Widada, S. (2014), Interpretasi Lapisan Bawah Permukaan di Area Panas Bumi Gunung Telomoyo, Kabupaten Semarang Menggunakan Metode Geolistrik Resistivity Konfigurasi Schlumberger. Youngster Physics Journal. Volume 3, Nomor 2, April 2014, Hal 97-106.

Thanden, R. E., Sumadirdja, H., Richards, P. W., Sutisna, K., Amin, T. C. (1996), Geologi Lembar Magelang dan Semarang. Pusat Penelitian dan Pengembangan Geologi.

Soetoto. (2015), Penginderaan Jauh Untuk Geologi, Yogyakarta: Penerbit Ombak.

Sumintadireja, P. (2005), Vulkanologi dan Geotermal. Bandung. Departemen Teknik Geologi FTM Institut Teknologi Bandung.

Soengkono. (1999), Analysis of Digital Topographic Data for Exploration and Assesment of Geothermal Systems. *Procceding 21st New Zealand Geothermal Workshop.*

Zendi, A., Rachwibowo, P., Aribowo, Y. (2014), Analisis Litologi dan Struktur Geologi Berdasarkan Citra Landsat Pada Area Prospek Panas Bumi Gunung Telomoyo Dan Sekitarnya, Kabupaten Magelang, Provinsi Jawa Tengah. Jurnal Teknik Geologi Undip. Volume 6, Nomor 1-2014.

THE APPLICATION OF GREEN ENERGY CONCEPT IN BUKIT DAUN GREENFIELD IN BENGKULU PROVINCE TO PROVIDE ELECTRICITY NEEDED IN THE AREA

Syayidu Guntur Ma'arif, Revanza Adirama Anwar, Jeffri Sembiring Meliala, and Timbul H Silitonga

PT. Pertamina Geothermal Energy
Jl. M.Thamrin No. 9, Cakrawala Building 19fl, Jakarta 10340, Indonesia
Email: syayidu.ma'arif@pertamina.com; revanza.anwar@pertamina.com; jeffri.sm@pertamina.com; thsilitonga@pertamina.com

ABSTRACT

Geothermal energy is also known as green energy and renewable energy. But in some geothermal field especially the exploration field, the electricity needs is fulfilled by using diesel generator that produce air and sound pollution. Bukit Daun is one of the exploration fields of PT Pertamina Geothermal Energy located in Bengkulu Province. In this location, there is no electricity grid provided by the national electric company (PLN) and the electricity is fulfilled by using diesel fuel generator (genset). This becomes a problem because it produces air pollution and sound pollution, need great number of diesel fuel and besides that, it just provides electricity in a small area (only in log yard and office). The total diesel fuel which was used to generate the electricity during exploration phase in the area is 27,730L. To resolve this electricity problem, PT Pertamina Geothermal Energy make a concept of the green energy. The green energy concept is the concept that using renewable energy to provide the electricity in the area and with the purpose to decrease the usage of diesel fuel. Bukit Daun location has a hilly topography and have some small river that be used as a water reservoir for the area. Bukit Daun area already has 3 exploration wells and one of them in the state of bleeding. Based on the condition of the area, the renewable energies that can be used are micro and pico hydro, small geothermal generator and solar panel. The estimated power capacity that can be produced from these alternatives electricity grid is around 11kW. As the result of the planning of green energy concept application, PT Pertamina Geothermal Energy target to reduce the diesel fuel usage by about 17% until the end of the exploration phase.

Keyword: Green energy, micro-hydro, pico hydro, geothermal generator, solar panel

INTRODUCTION

Bukit Daun geothermal field is one of the exploration fields of PT Pertamina Geothermal Energy. This field is located in Rejang Lebong, Lebong, and North Bengkulu Regency, Bengkulu Province. This field is within 100 km in the northeast of Bengkulu City. The extent of this field reaches 20 x 30 square km. Bukit Daun field located in the mountain far from the community. The nearest village is 2.6 kilometers from the security post.

The exploration activities in Bukit Daun geothermal field had been started since 1993 by geoscience survey. The exploration drilling is started in 2016, and until now there have been 3 exploration wells which take place in three different clusters. There is some others facility in Bukit Daun field, such as log yard, office, and porta camp which are located in the middle part of the field. The distance from the office to the clusters varies from 2 until 5 kilometers. Log yard and office area are one of the busy points in Bukit Daun field, which the most activities hold in here.

To date, there is no electrical grid from National Company (PLN) in the Bukit Daun geothermal field. The reason why the electrical grid from PLN have not reached this field is that the distance from the nearest community is quite far and the condition of the location is hard to reach because of the hilly morphology. Because of that, the fulfillment of electricity needs in Bukit Daun field for daily activities is using diesel generator with the fossil fuel. The total of diesel fuel usage for the generator until June 2018 from the first time of drilling exploration steps is around 27,730L.

PROBLEMS IDENTIFICATION

As exploration field, Bukit Daun geothermal field still has a lot of things to be fulfilled, one of them is electricity needs. Electricity in exploration field is generally needed for daily activities such as lightning in office and porta camp, drilling activities, and production test activities. Electricity needs in Bukit Daun field are far from sufficient. Electricity access is only in porta camp, log yard, and office, there is no electricity grid in the three clusters and in the street.

Besides the electricity grid that has not been gotten around in the main point in Bukit Daun field, the other problems are the fulfillments of electricity needs is coming from diesel generator as the main source for the porta camp and office. Generally, the diesel generator is the easiest alternative for the fulfillment, and the power capacity from the diesel generator is quite high. However, if we break down deeper, the use of a diesel generator is actually not the best choice.

The use of diesel generator has negative effects on human and the environment. Based on Cackette and

Lloyd (2001), diesel generator produces some of the dangerous gasses in the process of combustion, the dangerous gasses are such as:

1. Carbon Dioxide (CO_2).
2. Carbon Monoxide (CO).
3. Methane (CH_4).
4. Nitrous Oxides (NO_x).
5. Particulate Matter (PPT).
6. Sulfur Oxides (SO_x).
7. Volatile Organic Compounds (VOCs).
8. Heavy Metals (HM).

The gasses which are released from the combustion process can be causing some illness both cancer and non-cancer for human and others living things. The gasses also cause degradation effect for soil, water, and atmosphere.

Hydro One (2009) stated that a spill of diesel fuel from diesel generator can be the main caused of environmental damage in the rural area. The rural area can be meant as the area which far from the community, however, there are still activity from others part such as geothermal exploration field. The spill of diesel fuel can cause soil and water pollution. When a spill occurs action must be taken. This includes removing the contaminated soil or implementing mitigation methods to prevent future accidents (Hydro One, 2009). In 2008 environmental expenses associated with the clean-up, investigation, and monitoring of a large fuel spill at the Kingfisher station cost $263,000 (Indian and Northern Affairs Canada, 2010).

Besides the impact for the environment that is big, the use of a diesel generator is actually not homely. It needs a routine maintenance. Diesel generator can't be over used, there are some limitations on the maximum power generation and the usage time. Based on ISO 8528 (ISO, 2005), there is a classification for diesel generator based on its limitation, among others are:

1. Continous Operating Power/COP: constant load and unlimited usage time.
2. Prime Running Power/PRP: the maximum load varies, but generally the maximum load is 70%, unlimited usage time.
3. Limited Time Running Power/LTP: the maximum load varies but constant, maximum usage time is 500 hours per year.
4. Emergency Standby Power/ESP: the maximum load is 70%, maximum usage time is 200 hours per year.

Based on the classification, the diesel generator that is owned by Bukit Daun field is included in ESP class. Because of that, there is a time limitation every day for the use of the generator which is 8 hours straight. The diesel generator also needs to be maintained to prevent the breakdown. If we calculate the maximum time for one diesel generator is 8 hours, it means Bukit Daun field need at least 3 diesel generators to fulfill the electricity needs every day. With the three diesel generators, it increses the cost of maintenance. Based on Matt et al, 2005, the maintenance cost of a diesel generator which is used on maximum power under 100 kW is around 2-5 US$/kW (Figure 1).

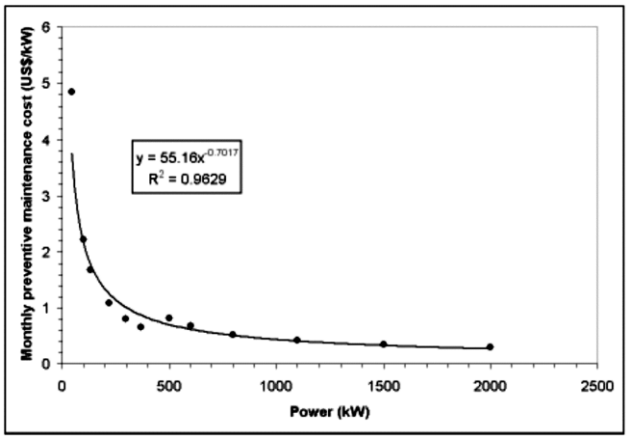


Figure 1: Monthly preventive maintenance cost of diesel generator as a function of their maximum power (Matt et al, 2005).

DISCUSSION

In an attempt to solve the problem of electricity needs in Bukit Daun field, PT Pertamina Geothermal Energy has been done a study about alternative natural resources that can be used to fulfill the electricity needs. The study is about morphological aspect, rainfall, and another potency.

The result of the morphological study, Bukit Daun field is located in the mountain morphology with the elevation is higher than 1,000 masl. As the result of the high elevation, the Bukit Daun field has some surface water flow sources. Total of the river in the area of Bukit Daun field is 3. The first river located near the Water Pump System 1, the second is located in the south of log yard, and the third is located in the north of log yard and constantly toward Water Pump System 2. From this three river, only the third river that has a constant water flow, the others have an intermittent water flow.

The result of rainfall study of Rejang Lebong and Lebong Regency in 2014, Bukit Daun field has intermediate rainfall level with rainfall level of 198.08 – 243.33 mm per year (Badan Pusat Statistik, 2014). If we make it more detailed, generally rainfall level in the Bukit Daun field is higher than 110 mm, the only months that lower than 110 mm are June and October (Badan Pusat Statistik, 2014).. Rainfall in the Bukit Daun location is generally stable and can supply the third river in the north of log yard.

The other potency that Bukit Daun field has is the steam that is an output from bleeding activity in one of the exploration well in the exploration cluster. The steam exits steadily and is only released to the air. This steam has a lot of potentials to be used because this steam has a high temperature and pressure as measured in production test.

As the result of morphological, rainfall, and another potency study, it can be deduced Bukit Daun field have some alternative source to help it fulfill its electricity needs. The resources that can be used are surface water and steam from bleeding activity. Besides that, if we see the general condition, the solar energy can also be used in this location.

Utilization of Solar Power

Sun is one of the natural resources that are everywhere. The sun can be utilized as power plants. There are several things that can affect the effectiveness of solar cell utilization (Asy'ari et al, 2014; Jatmiko et al, 2011; Ferry and Monoian, 2012), such as:

a. Ambient air temperature and wind velocity.
The solar cell can be maximum utilize if the ambient air temperature does not exceed 25ºC. There will be a decreased effectiveness of 0.4% if the temperature is higher than 25ºC or it can be decreased to 20% every 10ºC temperature rise. The wind velocity helps the ambient air temperature to be around 25ºC.

b. Sun radiation level and atmosphere condition.
The condition of Bukit Daun field that still has a lot of high trees will affect the effectiveness of solar cell. The higher the radiation level, the higher it's effectiveness. The atmosphere condition such as climate, rainfall, cloud thickness and air pollution also affect the radiation level.

c. Orientation and position of the panel toward the sun.
The angle between sun light source and panel surface can affect the effectiveness. The optimal angle to produce the highest energy output is 90º. The different location of the solar panel in the earth also have different effectiveness. To increase the effectiveness, there should be a change of the angular position of the panel based on the location's latitude position.

d. The material of the solar panel.
Based on Ferry and Monoian (2012), there are some type of material to build solar panel and its effectiveness, such as: Solar Thermal (the efficiency is 10-75%), Thermal Concentrated / CSP (the efficiency is 20-31%), Photovoltaics / PV (the efficiency is 3-50%), Photoelectrochemical / PEC (the efficiency is 10%), Thermophotovoltaics / TPV (the efficiency is 50-75%), Luminescent Solar Concentrator / LSC (the efficiency is 7%), Thermoelectric (the efficiency is 6-10%), and Solar Chemical (the maximum efficiency is 60%).

Judging from the condition of Bukit Daun field, the application of a solar panel can't be applied maximally because the rainfall level is quite high and some part of the location is still covered by the tree, this affect the radiation level. In addition, a large area of land is required to install solar panel, whereas as we know that the location of Bukit Daun field is very limited and can't be expanded because the surrounding area is a protected forest. It needs a permit to open the protected forest to be solar panel power plants. However, solar panels can be utilized to support electricity needs other than log yard locations, such as on roads and clusters as lighting because it does not require a large power. The utilization of solar panel as lighting in the road and log yard have been implemented in Bukit Daun field.

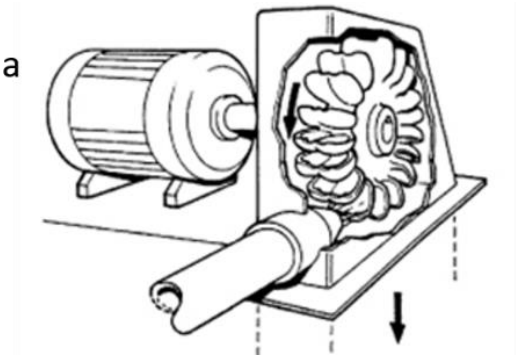
Utilization of Water Energy

As mentioned earlier, the location of the Bukit Daun field has 3 main surface water flows. Of these three flow paths only one has a steady flow throughout the year and is not intermittent. After a further study on this surface water flow path, obtained some results such as discharge and the possibility of different height or head.

Discharge and head will affect the determination of the type of turbine to be used. In general, the type of turbine used in hydroelectric power is divided into 3 based on the difference in its basic mechanism (Nasir, 2014; Yaakob et al, 2014), ie:

1. Impulse turbines is a turbine that is operated by the water pressure which is converted into kinetic energy before entering the turbine runner. The kinetic energy is in the form of high-speed jet that strikes the buckets, mounted on the periphery of the runner. Impulse turbines can be divided into Pelton Turbine or Turgo Turbine and Cross-flow Turbine (Figure 2).

a



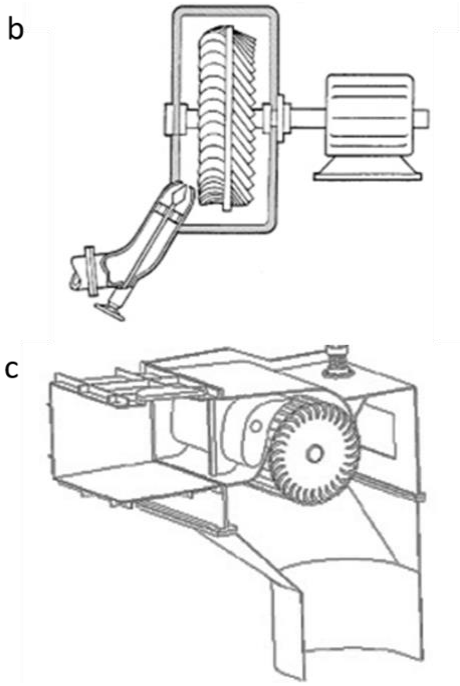
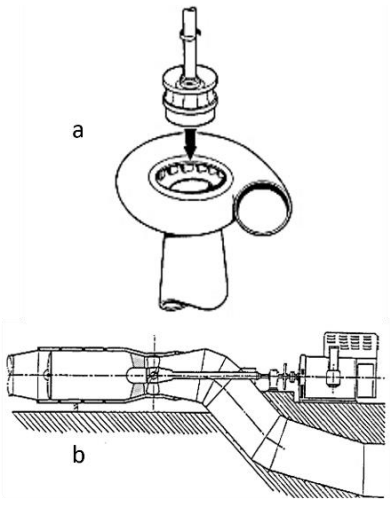


Figure 2: Different type of impulse turbine (a. Pelton turbine, b.Turgo turbine, c.Cross-flow turbine)

2. Reaction Turbine is a turbine that is operated by the water pressure that applies a force on the face of the runner blades, which decreases as it proceeds through the turbine (Nasir, 2014). The turbine casing, with the runner fully immersed in water, must be strong enough to withstand the operating pressure. To reduce the kinetic energy still remaining in water leaving the runner, a draft tube or diffuser stands between the turbine and the tailrace. The function of the draft tube is to reconvert the kinetic energy into flow energy by a gradual expansion of the flow cross section. There is some example of reaction turbines, such as Francis Turbine, Propeller and Kaplan Turbine, Pump as Turbine, Baker's Mill Turbine, and Pipe Turbine (Figure 3).



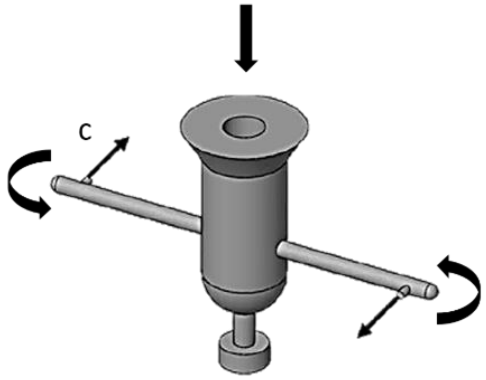


Figure 3: Different type of reaction turbine (a. Francis turbine, b.Propeller turbine, c.Baker's Mill turbine)

3. Gravity Turbine is turbine that driven simply by the weight of water entering the top of the turbine and falling to the bottom, where it is released – for example, an overshot waterwheel (Yaakob et al, 2014). These are inherently slow-running machines. One of the example of gravity turbine is Screw Turbine (Archimedes Screw Turbine). This turbine turns the principle of pumping around, maintaining the advantages and generating energy using the falling water to drive the screw as shown in (Figure 4).

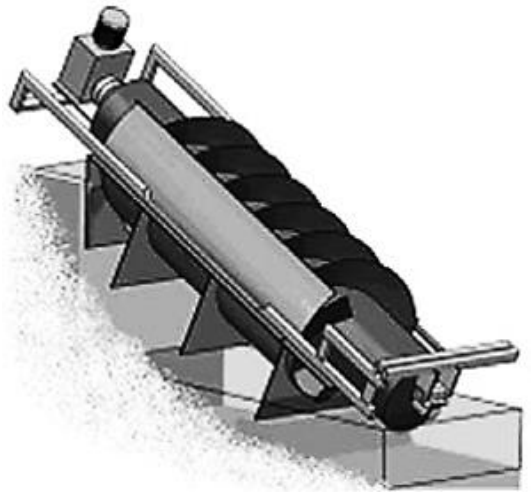


Figure 4: Archimedes Screw Turbine as one of examples of Gravity turbine (Stergiopoulou et al, 2013).

As a result of data retrieval in the river on the north of the log yard, obtained river flow discharge reached 561.3 GPM or equivalent to 0.03543 m3/s. The measurement of flow discharge is done at a point that has a high difference or head reaches 22 meters. Based on these two data, the most suitable type of turbine used as hydroelectric (micro hydro) from this river flow is the Propeller type turbine (Figure 5).

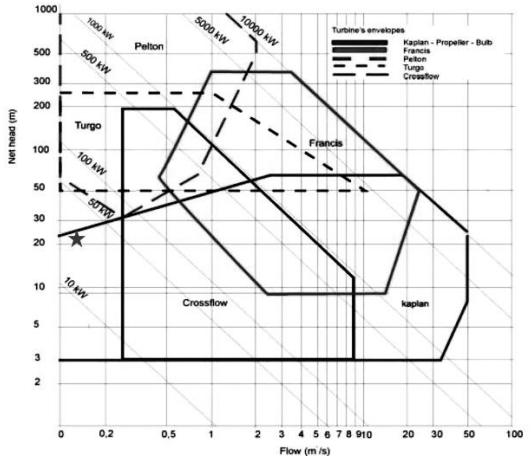


Figure 5: Diagram – comparison of the efficiency of different types of the turbine (Bobrowicz, 2006), the star is the plotting result of data in Bukit Daun field.

The utilization of electricity from this micro hydro can be focused to reduce the burden of diesel generator usage, especially for the light needs in a long-term such as the outdoor lighting of porta camp, log yard, and office. It can't be the main source of electricity because the power output from this micro hydro plan is not enough to fulfill the main needs in log yard area such as water heater, room heater, etc. The shortcoming from the application of micro-hydro is there should be additional infrastructure such as a dam to hold the water flow to make water input into turbine be more stable and not affected by weather and season change. The implementation of the micro-hydro have been started in Bukit Daun field, and to date, the progress has reached the installation of the turbines.

Utilization of Bleeding Steam

One of the exploration wells in Bukit Daun field has been able to drain steam. Until this time, the well is on a bleeding process. Bleeding itself is the process of draining the steam from the wellhead to the mini flash tank to keep the non-artesian wells flowing steam. The steam generated from the bleeding process at the well at the Bukit Daun field is very constant and exits continuously. Until now the steam generated from bleeding activities is still not utilized and only released into the free air due to the status of projects that are still exploration and no power plant facilities.

The location of the cluster is one of the vital locations in the Bukit Daun field. There are many valuable items such as iron pipes, tarpaulins, and so on. There is a need for lighting at this cluster location. In addition, in the location of this cluster is still routinely conducted production testing activities that require a power source to run the measurement tool. Therefore, it is necessary to make use of this bleeding vapor to become one of the alternative power sources in this cluster location. The basic principle of bleeding vapor utilization is similar to geothermal power generation in general, but the difference is on the generation scale.

In the plan, the development of small-scale geothermal power plant will use a turbine with a radial inflow system with blade axial type. The pressure required by this turbine is 4-6 bar with 99% steam composition and temperature reaching 155^{o}C. The voltage output of this small-scale PLTP plan is 10kW. For long-term plans, the electricity generated from PLTP small-scale in this cluster will be streamed into the log yard area, so it can reduce the use of the generator and can be used interchangeably.

SUMMARY

The Bukit Daun field still does not have access to the electricity grid from PLN. Until now, electricity needs in Bukit Daun field still use a diesel generator. The use of this generator is actually not the best choice because it has some disadvantages and negative impact. The negative impact of the use of a diesel generator is it produces some of the dangerous gasses in the process of combustion and diesel generator is not homely and it needs a routine maintenance which is costly.

To address this problem, the Bukit Daun Project design a green energy concept to reduce the use of diesel generators. Based on the on-site study, there are several alternatives to reduce the use of generators, such as utilizing surface water flow, sunlight, and bleeding vapor. The utilization of sunlight will be used for lighting at cluster locations and roads that have the highest radiation levels. Utilization of surface water flow will be used to build a micro hydro power plant with propeller turbine type. This turbine will be installed in a river located on the north side of the log yard. The utilization of bleeding steam will be done in one of the clusters that have an exploration well which can flow a steam. The concept of steam utilization is the same as geothermal power plants in general but on a small scale. In the short term it will be utilized for production test activities, and in the long run, will be withdrawing the electricity grid to log yard to reduce diesel generator usage.

The generating capacity of the three alternatives based on the on-site potential is around 11kW. This makes the use of diesel generators is still needed to be done because the three alternatives are not enough to meet the needs of electricity at the site. In addition, the concept of green energy will only reduce the usage of diesel generator so the usage is not big as it was be.

REFERENCES

Asy'ari, H., Rozaq, A., Putra, F.S. (2014), "Pemanfaatan Solar Cell dengan PLN Sebagai Sumber Energi Listrik Rumah Tinggal*". Jurnal Emitor Teknik Elektro Jurusan Teknik Elektro Fakultas Teknik Universitas Muhammadiyah Surakarta*, Vol 14 No.01, 33-39.

Badan Pusat Statistik. (2014), "Jumlah Curah Hujan Menurut Pos Hujan Terpilih di Kabupaten Rejang Lebong, 2014". Retrieved from Badan Pusat Statistik: *https://rejanglebongkab.bps.go.id/statictable/2015/09/23/15/jumlah-curah-hujan-menurut-pos-hujan-terpilih-di-kabupaten-rejang-lebong-2014-mm-.html*

Badan Pusat Statistik. (2014), "Rata-rata Curah Hujan dan Hari Hujan Menurut Bulan di Kabupaten Lebong, 2014". Retrieved from Badan Pusat Statistik: *https://lebongkab.bps.go.id/statictable/2015/12/16/9/rata-rata-curah-hujan-dan-hari-hujan-menurut-bulan-di-kabupaten-lebong-2014.html*

Bobrowicz, W. (2006), "Power Quality and Utilisation Guide – Small Hydro Power – Investor Guide". Retrieve from Leonardo Energy: *http://www.sier.ro/Small_Hydro_Power.pdf*

Cackette, T. A., and Lloyd, C. A. (2001), "Diesel Engines: Environmental Impact and Control". *Air and Waste Management Association*, 51, 809-847.

Ferry, R., and Monoian, E. (2012), "A Field Guide to Renewable Energy Technologies". *The Land Art Generator Initiative*, 67 page.

Hydro One. (2009), "Remote communities information session 2009". Retrieved from Hydro One Remotes: *http://www.hydroone.com/RegulatoryAffairs/Documents/EB-2008-0232/Stakeholder%20Conference/2009_DX_Rate_App_Stakeholder_Presentation_Rate_Consultation.pdf*

Indian and Northern Affairs Canada. (2010), "Aboriginal and Northern Off-grid Communities". Retrieved from Indian and Northern Affairs Canada: *http://www.aincinac.gc.ca/enr/clc/cen/ogc-eng.asp*

ISO. (2005), "ISO 8528-1". *Reciprocating Internal Combustion Engine Driven Alternating Current Generating Sets.*

Jatmiko, Asy'ari, H., Purnama, M. (2011), "Pemanfaatan Sel Surya dan Lampu LED untuk Perumahan". *Seminar Nasional Teknologi Informasi dan Komunikasi Terapan*, ISBN 979-26-0255-0

Matt, C.F., Vieira, L.S.R., Soares, G.F.W., de Faria, L.P.T. (2005), "Optimization of the Operation of Isolated Industrial Diesel Stations". *6th World Congress on Structural and Multidisciplinary Optimization.*

Nasir, B.A. (2014), "Suitable Selection of Components for the Micro-Hydro-Electric Power Plant". *Advance in Energy and Power 2(1)*, DOI: 10.13189/aep.2014.020102, 7-12.

Stergiopoulou, A., Stergiopoulous, V., Kalkani, E. (2013), "Back to the Future: Rediscovering the Archimedean Screws as Modern Turbines for Harnessing Greek Small Hydropower Potential". *Fresenius Environmental Bulletin*, Vol 22(No 7a), 2053-2058.

Yaakob, O.B., Ahmed, Y.M., Elbatran, A.H., Shabara, H.M. (2014), "A Review on Micro Hydro Gravitational Vortex Power and Turbine Systems". *Jurnal Teknologi*, 69-7, 1-7.

THE ROLE OF PRELIMINARY DATA QUALITY ASSURANCE IN REDUCING GEOTHERMAL EXPLORATION RISK IN INDONESIA

Hevy Julia Umbara, Herry Gunawan, and Triyono Hadi

Patra Nusa Data,
South Tangerang 15314, Indonesia
Email: hjumbara@patranusa.com

ABSTRACT

Geothermal exploration always begins with data collection to understand the characteristic of the field. At a minimum, this preliminary data should contain information regarding the field's geological conditions which also complemented with geochemistry and geophysics study. In most circumstances, these data are provided by the government in which the geothermal field is located. Some countries like the US and Australia are providing online access that allows data users to view live data through online platform. The quality of preliminary data is related to the success of geothermal field exploration. When preliminary data shows ambiguity and inconsistency because of lack data quality assurance throughout the data life-cycle, then the operator will bear a big risk during the exploration drilling stage. As many cases found in Indonesia where several green fields are estimated to be highly productive during the tender, apparently not able to meet production targets so that companies could not get the benefit from the initial power purchase agreement. In order to reduce the risk of operator's failure in geothermal utilization mainly due to the inaccurate preliminary data, a set of data quality assurance procedure has to be performed since field data acquisition stage until those data are presented in a report and used as the source of analysis and interpretation. This paper discusses the standard of what parameters should be checked and assured during the preparation of preliminary data in order to provide quality information of any geothermal field's characteristic. Several parameters including; data types, field staff qualification, tools and equipment, data acquisition methodology, data processing procedure, data completeness check, reporting & presentation as well as data storage and dissemination procedure by the government were explained to illustrate the fact that a good assessment from quality assured preliminary data could deliver necessary references in defining the success of any geothermal field development campaign.

Keywords: Exploration risk, quality data, preliminary.

INTRODUCTION

Geothermal energy is a form of heat that can be extracted from the earth's interior to be used for several kinds of purpose including power generation. For the current situation, most geothermal power is utilized from a system which provides a convective cycle of hot water or steam (in high enthalpy) that continuously transporting the energy from certain heat source underneath into the earth's surface, this type of geothermal system is widely known as a hydrothermal system.

Geothermal exploration in general perspective is an effort to assess the amount of heat that can be extracted from any geothermal system to be used as the source of energy by utilizing various kinds of exploration methodology. In a typical geothermal development project, exploration takes part in the initial stage of the whole processes. This development process can be divided into several main stages namely: Preliminary Survey, Exploration, Test Drilling, Project Review and Planning, Field Development and Production Drilling, Plant Construction, Start-up and Commissioning (Gehringer and Loksha, 2012).

At each stage of the development, various types of data are continuously collected from the geothermal field. This data plays an important role in determining the success of each stage undertaken and supporting decision-making to progress to a further stage (Umbara et al, 2016). This paper will discuss the importance of maintaining data quality to ensure the success of the overall development process and avoid the risk of failure in geothermal energy utilization.

This paper is focused preliminary study data and exploration stage, hereinafter referred to as "preliminary data". This is because the early stages of pre-exploration drilling are the points where the risk of geothermal development is relatively high (see Figure 1). There is no other way to cope with this risk than preparing credible preliminary data at the very beginning of the project, so the understanding of the geothermal system becomes more obvious and the development strategy can be better planned.

Placing first exploratory drill hole in geothermal is tough. Unlike oil and gas industry where surface surveys can describe subsurface conditions quite clearly, geothermal are usually more complicated geologically and surface investigation methods may not adequately described the subsurface conditions in enough detail. Geothermal system is not identical from one place to another so the comparative study could not always be done.

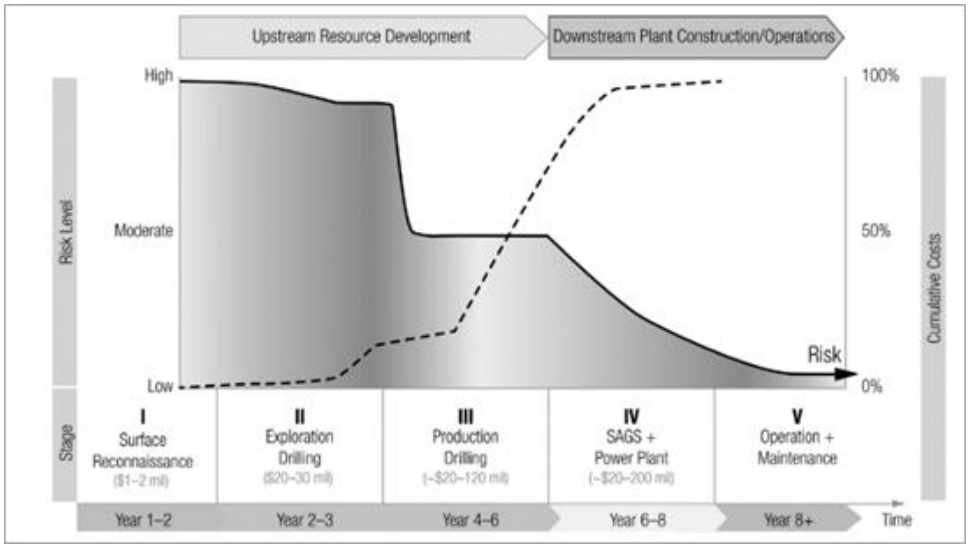


Figure 1: Illustration of risk and cost at different stages of geothermal development. Adapted from Gehringer and Loksha (2012) as cited in Sanyal et al (2016).

Despite limited information that can be obtained from surface surveys, this is the best way that can be done today to investigate the existence and characteristics of any geothermal systems. A good surface investigation will provide a baseline overview and recommendations for conducting the test drilling. To produce a comprehensive picture, supporting data needs to be collected from surface investigation methods such as geological survey, multiple geophysics survey, geochemistry survey, thermal gradient survey, etc.

The stakeholders who do these initial data acquisitions varies from place to place, usually referring to the rules and schemes of geothermal resources ownership applicable in each state/country. In Indonesia, where both surface and subsurface resources belong to the state, this data is mainly provided by the government which already conduct preliminary survey prior the concession area tender (in this case Ministry of Energy and Mineral Resources). Investors can review the potential of specific geothermal concession area from the preliminary data offered by the government through Directorate of General for New and Renewable Energy and Energy Conservation/DGNREEC (EBTKE) when the government opens the concession area tender. However, recently the DGNREEC also open the PSPE (Preliminary Survey Assignment + Exploration) mechanism where the potential developer can apply for an independent investigation + exploration drilling in the field to be acquired, of course with costs and risks borne alone (MEMR No. 36/2017). Mostly, the earlier scheme will certainly be more attractive to investors as it requires a lower up-front cost.

DATA AS THE PIVOTAL ELEMENTS OF GEOTHERMAL DEVELOPMENT

According to ESMAP's Geothermal Handbook on Planning and Financing Power Generation (Gehringer and Loksha, 2012), to implement sustainable geothermal development in a country with geothermal resources potential, the following elements are required to support the effort:

1. Availability of adequate information.
2. Good geothermal institutions.
3. Effective regulations, and
4. Adequate financial support.

Ensuring the availability and quality of geothermal resources data and information is one of the necessary elements on the upstream side of the development process. The availability of good initial data is especially needed when the investor/developer wants to acquire a concession area, whether from a tender or by other mechanisms.

Geothermal preliminary data available in Indonesia

Indonesia has a very comprehensive geothermal map released by EBTKE. This map tells the total potentials of 28,597 MW, which is divided into 11,073 MW of potential and 17,506 MW of reserves, while current geothermal electricity generation capacity is 1924.5 MW (DGNREEC Media Center, 2018). The map also shows that more than 40% of geothermal fields in Indonesia has potency above or equal to 50 MW. This is a good thing because most investors will be interested to develop the plant only if a field has a potential of at least 50 MW (mid-large sized). However, since the geothermal concession area acquisition was opened through a tender mechanism in 2003 (Setiawan,

2014), only a few geothermal investors/developers are interested in acquiring the field. Some tender even failed to be executed due to no participant is registering for the tender.

When a prospective developer wants to acquire a geothermal field in Indonesia, the first thing they are looking for is information about the geothermal field. Indonesia through the state geological agency has conducted surveys in more than 330 fields, in which 123 fields have been registered as concession area and the rest is categorized as "green field". Several neighboring fields are combined into one concession as the final number of the concession area recently is 71 (see Table 1). The preliminary information of this geothermal field and the concession area is currently managed by the government through EBTKE.

Table 1: The 71 geothermal concession areas in Indonesia. Several geothermal concession areas covering more than one geothermal fields.

Concession Area Name	**Field Name**	**Developer**
Sibayak-Sinabung	Beras Tepu, Lau Debuk-debuk, Marike	PT. PGE
Cibeureum-Prabakti	Kawah Ratu, Kiaraberes, Awibengkok	Star Energy
Pengalengan	Gunung Patuha, Kawah Ciwidey, Wayang Windu	Star Energy-Geodipa
Kamojang-Darajat	Gunung Papandayan, Gunung Masigit Guntur, Kamojang, Darajat	PT. PGE- Star Energy
Lahendong-Tompaso	Lahendong, Tompaso	PT. PGE
Sibual-Buali	Sarulla, Sibual-buali, Namora I Langit	Sarulla Operation, Ltd.
Way Panas	Ulubelu	PT. PGE
Kotamobagu	Gunung Ambang, Kotamobagu	PT. PGE
Lumut Balai-Margabayur	Lumut Balai, Ulu Danau, Margabayur	PT. PGE
Karaha-Cakrabuana	Gunung Talagabodas, Gunung Galunggung, Gunung Karaha, Gunung Sawal, Cipanas-Ciawi	PT. PGE
Hululais	Tambang Sawah, Bukit Gedong-Hululais, Lebong Simpang	PT. PGE
Sungai Penuh	Semurup, Lempur	PT. PGE
Iyang-Argopuro	Iyang Argopuro	PT. PGE
Tabanan	Batukao, Penebel, Buyan Bratan	PT. PGE
Tulehu	Tulehu	PT. PLN
Tangkuban Perahu	Maribaya, Tangkuban Parahu, Sagalaherang	PT. PLN
Ulumbu	Ulumbu	PT. PLN
Cibuni	Kawah Cibuni	PT. Kop Jasa K. Teknosa
Dataran Tinggi Dieng	Mangunan-Wanayasa, Candradimuka, Dieng	Geodipa
Ciater	Ciater	PT. PLN
Gunung Tampomas	Gunung Tampomas	PT. WIKA Jabar Power
Rantau Dedap	Rantau Dedap Segamit	PT. Supreme Energy
Gunung Rajabasa	Kalianda, Permata Belirang	PT. Supreme Energy
Liki Pinangwan-Muaralaboh	Liki Pinangwan, Muaralaboh	PT. Supreme Energy
Jailolo	Jailolo	Star Energy
Guci	Guci	PT. Spring Energi Sentosa
Kaldera Danau Banten	Rawa Dano, Gunung Karang, Gunung Pulosari	PT. Sintesa Banten Geothermal
Baturaden	Baturaden	PT. Sejahtera Alam Energy
Jaboi	Iboih, Lho Pria Laot, Jaboi	PT. Sabang Geothermal Energi
Atadei	Atadei	PT. PLN
Songa Wayaua	Songa Wayaua	PT. PLN
Mataloko	Mataloko	PT. PLN
Seulawah Agam	Le Seum-Krueng Raya, Seulawah Agam	PT. PGE
Gunung Ciremai	Sangkanhurip	PT. PGE
Gunung Lawu	Gunung Lawu	PT. PGE
Way Ratai	Natar, Lempasing, Way Ratai	PT. Optima Nusantara Energi & Enel Green Power
Blawan-Ijen	Blawan-Ijen	PT. Medco Cahaya Geothermal
Cisolok Cisukarame	Cisolok, Cisukarame	PT. Jabar Rekind Geothermal
Gunung Talang - Bukit Kili	Gunung Talang, Bukit Kili	PT. Hitay Daya Energy & PT. Dyfco Energy
Gunung Ungaran	Gunung Ungaran	PT. PLN
Umbul Telomoyo	Umbul Telomoyo	Geodipa
Gunung Arjuno-Welirang	Gunung Arjuno-Welirang	Geodipa
Telaga Ngebel	Telaga Ngebel	PT. Bakrie Darmakarya Energi
Sorik Marapi-Roburan-Sampuraga	Sorik Marapi, Roburan, Sampuraga	KS ORKA Renewable.
Sokoria	Sokoria	KS ORKA Renewable.
Hu'u Daha	Hu'u Daha	-
Sipoholon Ria-Ria	Helatoba, Sipoholon Ria-Ria	-
Marana	Marana	-
Suwawa	Suwawa	-
Bonjol	Bonjol	-
Danau Ranau	Danau Ranau	PT. PLN
Gunung Endut	Gunung Endut	-
Simbolon-Samosir	Pusuk Bukit, Simbolon-Samosir, Pagaran	-
Bora-Pulu	Bora, Pulu	-
Sembalun	Sembalun	-
Oka Ille Ange	Oka Ille Ange	PT. PLN
Kepahiang	Kepahiang	-
Graho Nyabu	Air Dikit, Graho Nyabu	-
Gunung Pandan	Gunung Pandan	-

Gunung Hamiding	Gunung Hamiding	-
Gunung Gede Pangrango	Gunung Gede Pangrango	-
Telaga Ranu	Telaga Ranu	-
Songgoriti	Songgoriti	-
Gunung Wilis	Gunung Wilis	-
Gunung Galunggung	Gunung Galunggung, Cigunung	-
Gunung Geureudong	Rimba Raya, Gunung Geureudong, Simpang Balik	-
Lainea	Lainea	-
Tanjung Sakti	Tanjung Sakti	-
Sekincau	Purunan, Gunung Sekincau, Bacingot, Suoh Antatai	-
Gunung Sirung	Gunung Sirung	PT. PLN
Wapsalit	Wapsalit	-

EBTKE will release the information of specific concession area when the tender is open (Table 2).

Table 2: An example of information released during the tender of concession area Graho Nyabu in the Province of Jambi (DGNREEC, 2016).

Concession area name	Graho Nyabu
Concession area location	Kabupaten Merangin and Kabupaten Kerinci, Provinsi Jambi
Area acreage	109.000 Ha
Possible reserve	200 MW
Estimated reservoir temperature	236 ºC
Development capacity plan	110 MW
Project type	Total Project
Ceiling tariff for electricity price	15.9 sen US$/kWh (MEMR No. 17/2014)
COD target	2025

Furthermore, prospective developers can review more data and information related to the offered concession through the book; "Indonesia's Geothermal Potential" released by Directorate of Geothermal - DGNREEC (2017). In this book, reviewers can view a set of information including (see Table 3).

Concession area general information

This general data contains information regarding the concession area registration act., its administrative location as well as recent development status.

Estimated resources/reserves

A single concession area could include one or more geothermal fields, the list of the fields within the concession and its geothermal potential are explained in this section. Although, the background study of how the Mega Watt electricity numbers come up is not explained further in this table.

Development plan capacity

Following the area prospect, the plan of electricity generation capacity is also explained as an insight to the investor of how big the power plant capacity would be and what year it should be online.

Land status (land use)

The land use information that is explained in this datasets is the distribution of forest status within or surround the concession. It is very useful as most of the high-enthalpy geothermal resources in Indonesia is located within the protected forest, and understanding such information becomes significantly important for the developer to address an exploration and development license. Unfortunately, other information such as area topography, natural hazard potential, road access, and important cultural site are not detailly explained. The lack of that information is currently responsible for several issues happened to geothermal resources development in Indonesia.

Table 3: Graho Nyabu geothermal concession area information available in Indonesia's Geothermal Potential book (Directorate of Geothermal, 2017).

Area General Information		
Concession Act.	2781 K/30/MEM/2014	
Area Code	1502225140009	
Acreage	109.000 Ha	
City	Merangin, Kerinci	
Province	Jambi	
Status	Tender Preparation	
Geothermal Field Potential		
Field Name	**Air Dikit**	**G. Nyabu**
Spec. Resources	225 MW	-
Hypothetic Resources	-	-
Possible Reserves	-	200 MW
Probable Reserves	-	-
Proven Reserves	-	-
Development Plan Capacity		
Power Gen. Unit	1 (55MW) & 2 (55 MW)	
COD Target	2025	
Land Status (Forest)		
Conservation Forest	69.759 Ha	
Protected Forest	-	
Production Forest	15.170 Ha	
Reserves Forest	-	
Other Area	24.070 Ha	

Concession area map

This map illustrates the boundaries of the concession areas with geothermal potential (see Figure 2A). In addition to the concession boundary information, this part also describes direction or route instructions to the location of the geothermal prospect.

Geological summary

In the geological summary section, the information presented includes; distribution of rock types within the concession areas (see Figure 2B), geological structure conditions and the inferred permeable zones, regional volcanic history, and interpretation of geothermal system components from the geological model.

Geochemistry summary

The geochemistry summary section shows ternary plot diagrams that represent the chemical characteristics of geothermal fluids taken from the manifestations in the geothermal field. There is also an analysis of temperature estimation (geothermometer) which shows the estimated temperature of the geothermal reservoir (see Figure 2C). Not all of these geochemical illustrations are accompanied by explanations and interpretations; some fields just showing the diagrams only without any further explanations.

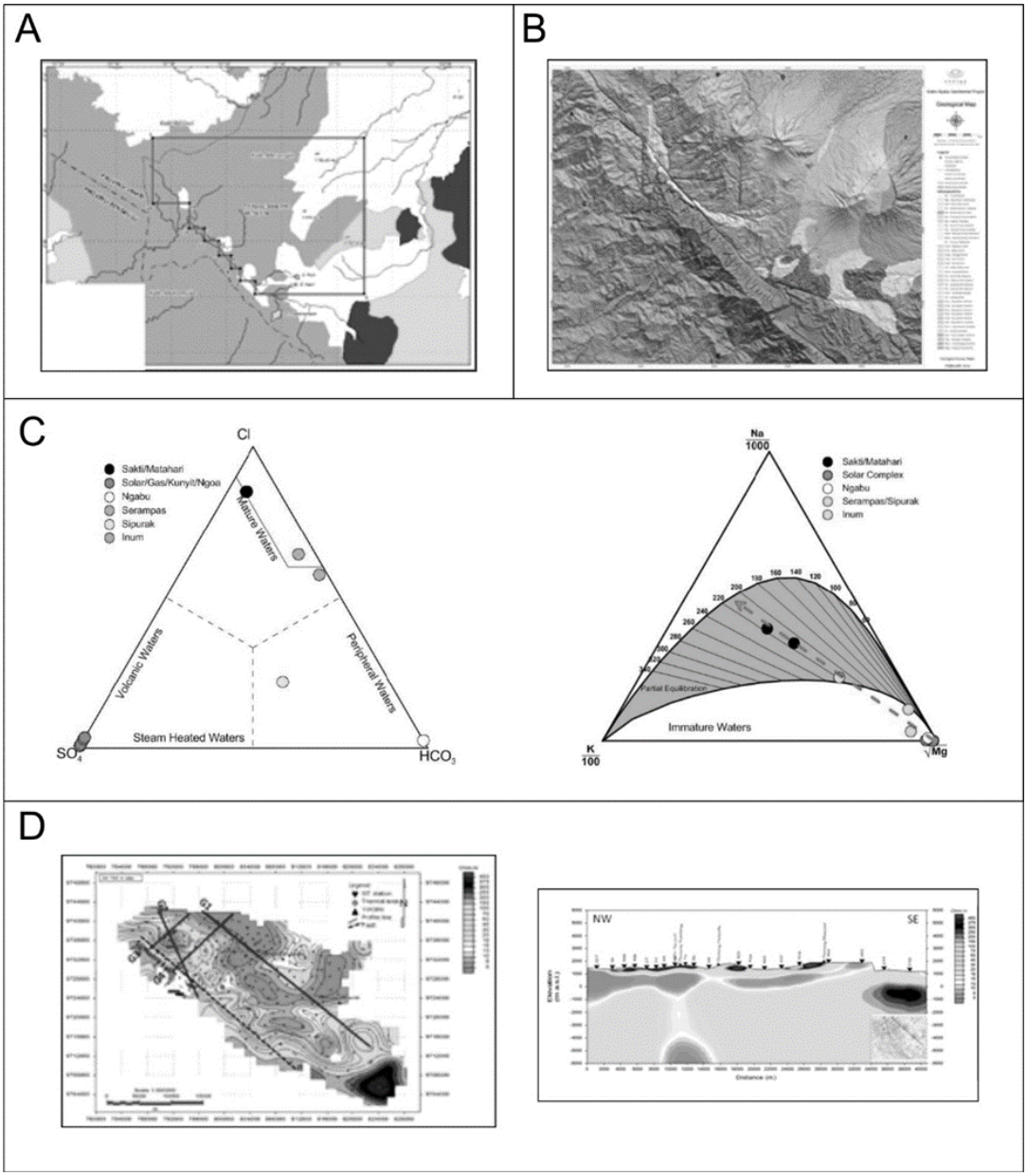


Figure 2: A set of geothermal resources information is displayed in Indonesia's Geothermal Potential books by Directorate of Geothermal-DGNREEC (2017); (A) Maps showing the boundary of the concession area, (B) maps showing the lithology types distribution and other geological features within the concession area, (C) two ternary diagrams representing the fluid chemistry characteristic of the geothermal field and the estimated reservoir temperature, (D) figures showing the resistivity anomaly maps and NW-SE resistivity anomaly sections obtained from the magnetotelluric survey in the geothermal field.

Geophysics summary

There is considerable geophysical data that has been acquired from geothermal fields throughout Indonesia. Most of the data are from Magnetotelluric survey, Gravity survey and Magnetic survey. Some fields have complete data covering all the methods, while others have no geophysical data at all. Only MT data that is available in the Graho Nyabu area within this book as showcased in Figure 2D.

Data source

This point is necessary because the source of the information presented is clearly written in this chapter, the following sections describe some of the sources from which these preliminary data originate.

The source of Indonesia's geothermal preliminary data

This preliminary data provided by the government is the basis for determining the geothermal potential of any concession area. The main sources of these preliminary data can be grouped into three majors, namely:

1. *Geological Agency Geothermal Survey*

   Indonesia's state geological agency routinely conduct geothermal surveys annually, the surveys covering geological, geochemical, geophysical, thermal gradient, and others exploration method. Most of the preliminary data available in Indonesia's Geothermal Potential book are sourced from the results of this investigation.

2. *Preliminary Survey Assignment (PSP & PSPE)*

   The government gives the opportunity to the private company to do PSP & PSPE (Preliminary Survey and Preliminary Survey + Exploration Drilling) in several green fields, report of this survey result become one of the sources of geothermal preliminary data.

3. *Existing Literature*

   Apart from surveys by government agencies and private companies, preliminary data also derived from previous literature studies, such as regional and detailed geological investigations by several institutions, as well as volcanology study from other government institutions.

Preliminary data accessibility

Besides from Indonesia's Geothermal Potential books published by EBTKE, to see preliminary data mentioned above investors or developers can access the IGIS website (http://igis.esdm.go.id/) which also managed by EBTKE. Although the data completeness of each field is differ, some fields have a very well presented technical data (see example above), while some others are very unrepresentative or incomplete.

In this IGIS portal, data reviewer can only see general and interpretative data as presented in the previous section. Reviewers can not see raw data groups, lab analysis results, processing data and post modeling data, that type of data can only be accessed by applying a special permit to the minister of Energy and Mineral Resources (MEMR Act. No. 33/2018). In addition, the IGIS portal does not provide a dynamic live data visualizer, so several maps and figures that have small digital resolution are not very informative because of the small text or symbols cannot be read clearly.

THE DOMINO EFFECT OF STRUGGLE CAUSED BY LACK OF QUALITY ASSURED PRELIMINARY DATA

The government claimed that Indonesia has around 28,597 MW of total geothermal resources potential, this resources potential is estimated from the state geological agency analysis (EBTKE, 2017). However, the basis for this resources estimation is still unclear yet over-rated as it generates wide spread perception that the number is (unrealistically) too large (ADB, 2015 p. 108). This over-rated resources potential has led disappointment from the investors because of the poor quality of data being offered in the geothermal concession tendering process, the big number presented on the tender release became meaningless as the database and information are vague, unclear, inconsistent, and inconclusive. Moreover, the developer that wins the tender has to pay preliminary data compensation prior to acquiring the concession area, this is actually an additional burden for the developer if the quality of data obtained does not match the expectations.

In addition, the data provided by the government is relatively dominant only from the technical side (although the quality is debatable). This is not enough because other aspects such as; social, economic, as well as political, must also be taken into account to showcase the business viability of any geothermal concession area. The lack of such information has caused real problems in Indonesia's geothermal development campaigns such as; resistance from the local communities and local government, land use overlap, unanticipated natural hazard, difficulties in finding financial support, as well as an unpredicted technical problem such as; acid hydrothermal fluid.

The lack of quality geothermal preliminary data and information is a serious but un-seen issue by the stakeholders in Indonesia. The following facts give clues of how a preliminary data with no quality assurance has been creating a domino effect of

struggle in current Indonesia's geothermal development:

23 concession areas are left un-owned due to low private enterprise interest in concession area tender

The quality of preliminary data is related to the success of geothermal field exploration. There is a widespread perception in Indonesia where preliminary data shows too much ambiguity and inconsistency. It happens due to lack of data quality assurance throughout the data life-cycle which force the operator to bear a big risk during the exploration drilling stage. Such big exploration risk is putting down the private enterprise interest in concession area tender participation, at least 23 from the 71 concession areas have no owner (see Table 1).

The low participation from the private enterprise side is reflected from the fact that 29 concession areas are managed by state-owned enterprises (12 of them are granted without open tender, and 16 others are inheritances of non-tender concession areas before 2003, 1 area from open tender is Mt. Lawu which recently face public refusal). On the other hand, only 4 areas from 21 areas managed by the private companies that have been running online (all 4 areas are under joint operation contract (JOC) with Pertamina Geothermal Energy). It means that besides the old projects by state-owned enterprises and those under JOC with private enterprise, other concession areas are still facing challenging situations that need to be solved.

Low development progress from several concession areas under-development

From the 48 concession areas that have been acquired by developers, only 11 geothermal plants that have been running online since Kamojang was first drilled back in the 1920's (Fauzi et al, 2000). The lack of preliminary information about the area offered during the tender seems to be a trap for developers; as some unexpected problems arise after the concession area is further explored. Some of the issues that led to the development become sluggish, include:

1. The lack of initial information to confirm the reserves makes several banks (especially local bank) reluctant to lend because of the high exploration risk at the beginning of the project.
2. The power generation capacity expected during the tender is difficult to be achieved due to the unanticipated technical problem, such as; acid hydrothermal fluid, low reservoir permeability, unproductive well, etc. Thus, the selling price of electricity (from the initial power purchase agreement) with a smaller power generation capacity becomes unprofitable for the developer.
3. Lack of information from environmental, social, economic, and political aspects have caused several non-technical obstacles that require unexpected cost and time for the problem-solving. Several case examples include; the resistant of mt. Lawu locals resident to the geothermal project due to its potential of destroying the cultural site located inside the concession, another example is the unexpected landslide that happened to several geothermal power plant facilities.

73% (21,058 MW) of the total resources potential claimed by the government is not yet registered as a concession area.

Due to the limited resources information, of 21,058 MW geothermal resources from 28,597 MW of the geothermal potential that spread over 330 fields has not been established as a concession area. This has an impact on the lack of options that can be chosen by the developer in determining the area for investment because the concession area offered at this time is not interesting enough.

UPGRADING THE STANDARD OF GEOTHERMAL PRELIMINARY DATA AND INFORMATION IN INDONESIA

Access to concession area information in Indonesia is severely limited to IGIS and the geothermal potential books. When comparing with other industries in Indonesia such as oil and gas, data and information are so easily accessible. Although it involves paid services, potential developers still keen to access data that includes all data types (general data, raw data, processing data, interpretative data) to be able to perform independent analysis and interpretation.

They did that to increase confidence in the resource prospects while comprehensively analyzing the future development risks before applying for bid. In fact, New Zealand enforces the same policy, in which enterprise data users pay for data access fees that are used to improve the quality of the geothermal preliminary data (ESMAP, 2016, p. 12). By considering higher risks in the geothermal energy business, the Government of Indonesia should give more vigorous and open access to its geothermal data. So developers have the flexibility to do initial study and gain more comprehensive knowledge about the offered geothermal prospect. Besides attracting more investors to join the tender, it will also encourage check and balances from the investor side to anticipate risks that previously may not be found by the study of Government agencies.

In the effort to improve the quality and expand the scope of preliminary data of a geothermal field to mitigate the upstream development risk, a comprehensive and multi-dimensional study has to be performed to certain geothermal prospect area

before being offered on the tender. The study should not only covers technical aspect but also includes land-use assessments, supporting infrastructure, the social community near the site, economic viability, as well as the political situation in the region. Furthermore, the data and information integrity resulted from the survey and the study activity has to be well maintained so that the future data user will get the best benefits from using such data and information.

Followings are several recommendations that could be executed to overcome the current obstacles in Indonesia's geothermal preliminary data quality:

Applying standards for concession area and geothermal field data presentation.

ADB research on "Unlocking Indonesia's Geothermal Potential" (2015) shows that Indonesia uses a less clear standard in determining the value of its geothermal potential. This standard has not been tested at the international level, prompting investor hesitation. It is unfortunate that potential renewable energy investors mostly come from outside Indonesia, and setting internationally recognized standards is an option that must be implemented. Some standards of geothermal resource information reporting and presentation can be used as a reference to ensure the quality of resources information, such as:

1. The Canadian Geothermal Code for Public Reporting; Reporting of Exploration Results, Resources and Geothermal Reserves by The Canadian Geothermal Code Committee (2010).
2. Geothermal Exploration Best Practice; A Guide to Resources Data Collection, Analysis, and Presentation for Geothermal Projects by International Geothermal Association – IGA GmbH (2013).

By applying transparent and accountable standards in assessing the geothermal fields potential, as well as establish a comprehensive report from it, the future developer will get clear insight to make a wise decision of investing their capital to the project. With more accountable information being offered before the tender, the risk of the development could be detected earlier and the strategy to mitigate such risk has to be clearly taken into account in every geothermal development proposal.

Applying data acquisition and data submission standards for surveyors

Several geothermal developers just hardly accept data interpretation or scientific models offered in the Government preliminary data without seeing or processing the raw data on their own. Therefore, it is important to make sure that every piece of information taken from the geothermal field is at its best quality. To maintain such quality field data, the Government needs to set a standard or best practice for geothermal data acquisition that covers the common methodology used in geothermal exploration.

Those preliminary data derived from government, private and academic investigations shall be submitted to the government as such data are considered state property. The best practice in data acquisition could also be the basis for establishing checking parameters of the survey data submitted by surveyors. Here are some examples of parameter that needs to be ensured when the survey results are submitted to the government:

Data type

Assessing geothermal fields requires collection of multiple preliminary data types. At a minimum, a preliminary data of such field should contains the following data type: Technical (geology, geochemistry, geophysics, thermal gradient, etc), Environmental Assessment (EIA, hydrology, natural hazard potential), Socio-cultural Assessment (Awareness of the local citizen to the project, existence of important cultural sites inside the field, analysis of potential rejection by the local residence) Economic Assessment (regional electricity demand/market analysis, regional supporting infrastructure, development cost estimation), Regional Politic Assessment (regional and local government commitment on geothermal development, easiness of applying permits in local Government, analysis of potential threat from local political situations).

Completeness of data attributes

Technical data taken from methods such as geology and geophysics may include a big set of data attributes. It is necessary to define data attributes that are essentially required in specific data sets. The geothermal geosciences content model from The U.S. Geoscience Information Network (USGIN) and the Professional Petroleum Data Model from the PPDM Association could be adapted to establish a suitable standard for Indonesia's geothermal data model.

By applying standard of data attributes, a comprehensive check can be performed to such data coming from any field survey such as; the availability of metadata regarding the rock and fluid samples, the complete report of laboratory analysis result, information on tools used for data acquisition, as well as profiles of the surveyor and the team that responsible for acquiring, processing, and interpreting those data.

Data format and storage media (physical and digital data)

Various kinds of data with different digital format are produced during the geothermal exploration.

With a common standard on this data format being set, the future user will be easy to reuse those data in the appropriate software. Nevertheless, maintaining data to be reusable for a long period of time also requires concern to the media where those data are stored. There are currently many different options of media to store digital data, as long as the media comply with the data back-up and security standard.

Storing physical data taken from geothermal fields such as rock and fluid samples may be challenging. However, technology from mining and oil and gas industry are definitely applicable to handle those physical data from the geothermal fields.

Providing more open data access to investors

Good and quality data will not have value if it cannot be utilized by the geothermal stakeholders. Therefore, access to geothermal data and information must be improved so that potential developers are more flexible in accessing, obtaining and using preliminary data to assess the geothermal prospects. The current system (IGIS) can adapt existing technology from several data dissemination systems in other countries or in other industries, such as the following examples:

South Australia Resources Information Gateway (SARIG)

The Government of South Australian's natural resources data portal not only presents administrative information regarding geothermal or other resources working area, users can also access and review live data including the digitalized rock sample from well core as well as the laboratory analysis results directly from the SARIG web-based application (https://map.sarig.sa.gov.au/).

US Geothermal Data Repository (GDR)

US Department of Energy - Geothermal Technologies Office (DOE GTO) is providing access to its geothermal project information through the GDR (https://gdr.openei.org/). The GDR is one of many data nodes on the National Geothermal Data System (NGDS) that gives access to data and information related to geothermal energy. In this portal, the user can download and use even the raw data from several geothermal fields.

Establishing Clear Regulation on Geothermal Data

Finally, considering that data is a state asset that is worth protecting, the government needs to make clear regulations related to the management of the geothermal data. And the good news is that a regulation on geothermal data (MEMR Act. 33/2018) is being published by the Government as this paper is written. This data management effort is to give a guarantee to the quality and benefits of the geothermal data. This regulation covers data confidential status, the stakeholders that responsible for data acquisition, data storage, and data dissemination, as well as the procedure to access those data. Hopefully, this regulation will form the basis of rights and responsibilities both from the government and developer side to maintain the quality of geothermal data so that it can provide maximum benefits and help reduce the risk of geothermal development in Indonesia.

CONCLUSION

Preliminary data is an important element in any geothermal energy development project. This set of data and information are used to make critical decisions such as determining the boundaries of the concession area, determining the magnitude of the potential, placing the first exploratory drill hole, as well as anticipating the future development risks. Quality assurance for preliminary data needs to be done so that high development risks in the upstream side can be mitigated through appropriate decision making and more detailed analysis with a basis of quality data. Maintaining good preliminary data quality must begin by setting a good standard in the data acquisition process in the field, data reporting, data storage and management, as well as data dissemination system to data users. The type of resources information provided for the developer has to be balance between technical and non-technical, as the development risk in Indonesia could come from multi-dimensions including technical, economic, social, environmental and political aspects. Nevertheless, good data and information alone are not enough to ensure geothermal development in Indonesia runs smoothly, it also needs improvement in other elements such as professional geothermal institutions, effective regulations, and sufficient financial support.

REFERENCES

Asian Development Bank/ADB. (2015), "Unlocking Indonesia's Geothermal Potential", *Asian Development Bank and The World* Bank. Metro Manila, Philippines.

Deibert, L., Hjartarson, A., McDonald, I., Mcllveen, J., Thompson, A., Toohey, B., and Yang, D. (2010), "The Canadian Geothermal Code for Public Reporting; Reporting of Exploration Results, Geothermal Resources and Geothermal Reserves". *The Canadian Geothermal Code Committee (CGCC), Canadian Geothermal Energy Association*. Calgary, Alberta, Canada.

Directorate General for New and Renewable Energy and Energy Conservation/DGNREEC. (2016), "Announcement of Graho Nyabu Geothermal Working Area Tender". *Ministry of Energy and Mineral Resources*, Jakarta, Indonesia.

Directorate General for New and Renewable Energy

and Energy Conservation/DGNREEC . (2017), "Doing Business in Geothermal". Jakarta, Indonesia.

Directorate of Geothermal – Directorate General for New and Renewable Energy and Energy Conservation/DGNREEC. (2017), "Indonesia Geothermal Potential", 1st copy, *Jakarta, Indonesia.*

Fauzi, A., Bahri, S., and Akuanbatin, H. (2000), "Geothermal Development in Indonesia: An Overview of Industry Status and Future Growth", *Proceedings: World Geothermal Congress 2000*, p. 1109-1114, Kyushu, Japan.

Gehringer and Loksha. (2012), "Geothermal Handbook: Planning and Financing Power Generation". *Energy Sector Management Assistance Program (ESMAP)*, Technical Report 002/12, Washington DC, USA.

GeothermEx Inc., and Harvey, C. (2013), "Geothermal Exploration Best Practices: A Guide to Resources Data Collection, Analysis, and Presentation for Geothermal Projects". *IGA Service GmbH*, Bochum, Germany.

MEMR regulation number 17 year 2014 on the Purchase of Electricity from Geothermal Power Plants and Geothermal Steam for Geothermal Power Plants by PT PLN (PERSERO).

MEMR regulation number 33 year 2018 on The Management and Utilization of Geothermal Data and Information for Indirect Use.

MEMR regulation number 36 year 2017 about Procedure of Assignment for Preliminary Survey and Assignment for Geothermal Survey and Exploration.

Sanyal, S. K., Robertson-Tait, A., Jayawardena, M. S., Huttrer, G., and Berman, L. (2016), "Comparative Analysis of Approaches to Geothermal Resources Risk Mitigation, a Global Survey". *Energy Sector Management Assistance Program (ESMAP)*, Knowledge Series 024/16, Washington DC, USA.

Setiawan, H. (2014), "Geothermal Energy Development in Indonesia: Progress, Challenges and Prospect". *Proceedings: International Journal on Advanced Science Engineering Information and Technology*, Vol. 4, p. 21-25.

Umbara, I. G. A. H. J., Hadi, T., Gunawan, H., and Widodo, A, P. (2016). "Building Web-Based Data-Information-Knowledge Application to Support Geothermal Energy Development in Indonesia", *Proceedings: 38th New Zealand Geothermal Workshop*, Auckland, New Zealand.

Internet Reference:

DGNREEC Media Center, (2018), "Kini Indonesia Menjadi Produsen Listrik Panas Bumi Terbesar ke Dua Dunia". *Ministry of Energy and Mineral Resources*. Retrieved from https://www.esdm.go.id/id/media-center/arsip-berita/kini-indonesia-menjadi-produsen-listrik-panas-bumi-terbesar-kedua-dunia.

Geothermal Data Repository (GDR), Retrieved from: https://gdr.openei.org.

Indonesia Geothermal Information and Services (IGIS), Retrieved from: igis.esdm.go.id.

South Australia Resources Information Gateway (SARIG), Retrieved from: https://map.sarig.sa.gov.au.

US Geosciences Information Network (USGIN), Retrieved from: schemas.usgin.org.



Resources and Management



THE URGENCY OF PROPER GEOTHERMAL RESERVOIR MANAGEMENT IN INDONESIA – A LITERATURE REVIEW

Yuniar Zhafira Abdillah and Qanitah

Institut Teknologi Bandung (ITB)
Jl. Ganesha 10, Bandung, Indonesia
Email: yzhafiraabdillah@gmail.com

ABSTRACT

Geothermal energy is the epitome of renewable and sustainable energy. With proper management, this energy could last through generations. Indonesia has recently increase its installed capacity count to 1,925 MW and become the second highest geothermal generating country in the world. Looking past through this great achievement, the responsibility of maintaining producing reservoirs awaits. This research aims to review and point out the urgency of proper reservoir management of geothermal fields in Indonesia and to study lessons learned from challenging and more experienced geothermal fields. Reservoir declines are reported in each producing field with causes that seem to be similar. Cold water and injection brine breakthrough, scaling and corrosion are the main problems that are shared by geothermal fields throughout Indonesia. Due to production activity, changes of pressure and temperature in reservoir, or reservoir condition in general, are expected and may trigger several side effects in a long run. Alongside natural causes, decisions made by the developers may alter the life of a reservoir. Although decline of production is inevitable, countermeasure must be done to maintain the longevity of our tapped resources, so the next generations to come could have more secure energy supply.

Keywords: Reservoir management, production activity, Indonesia Geothermal Field.

INTRODUCTION

Reservoir management in geothermal is the key to sustainable electricity production. It initiates as early as the time of reservoir discovery and ready for development. By definition, Management is the process of planning, organizing, leading and controlling the effort of organization members and of using all other organizational resources to achieve stated organizational goals (Stonner, 2012). This definition suggests that management is a continuous process as a team and aims at achieving the organization's goal by ensuring effective use of the resources. Therefore, reservoir management may be defined as a continuous process of planning, organizing, and controlling the reservoir to ensure sustainability of production and the reservoir itself. The aim of this paper is to review and point out the urgency of proper reservoir management of geothermal fields in Indonesia and to study lessons learned from challenging and more experienced geothermal fields. More importantly, to raise awareness towards proper reservoir management in geothermal fields, whether pre-existing or new, in Indonesia.

THE IMPORTANCE OF RESERVOIR MANAGEMENT

Production of geothermal reservoir may change the condition of reservoir. Continuous fluids extraction from below may trigger decline in pressure when the extracted amount is not recharged adequately. Recharge of geothermal reservoir, if the condition is favorable, occurs naturally. However, since the production of geothermal fluid occurs in relatively short time but huge amount of extracted mass, natural recharge cannot be the only way. Thus, injection wells are used to aid in channeling the fluid into the reservoir.

Vapour-dominated and liquid-dominated geothermal system respond differently to pressure decline, therefore requires different focus of reservoir management. Grant et al. (1982) explained that fluid extraction from vapour-dominated reservoir causes local pressure declines that only occur around the production well. This event will trigger superheated steam to be developed in the affected area. Overtime, less fluid mass will be available for production and the reservoir might dried out. On the other hand, on liquid-dominated system, when pressure drawdown will cause boiling to occur and may add steam ratio to liquid. This condition may become appealing to developer at first since steam production will increase. However, profound difference of pressure will later cause cold water from the formation to breakthrough to the reservoir and trigger decline of temperature. Problems from both reactions will affect the longevity of production and generation, therefore proper management is greatly required to monitor and accommodate every change of response from the reservoir throughout production period.

Reservoir sustainability is a topic that needs synergy from various discipline. Before the discussion get any further, the term sustainability must be defined. Sanyal (2005) defines sustainability as the ability to economically maintain the installed capacity, over the amortized life of a power plant, by taking practical steps (such as, make-up well drilling) to compensate for resource degradation (pressure drawdown and/or cooling). In Indonesia, normal amortized life of a geothermal powerplant according

to Government Regulation No.7/2017 is 25 to 30 years. However, according to Steingrímsson, Axelsson, & Stefánsson (2006), sustainable geothermal utilization involves energy production at a rate, which may be maintained for a very long time (100-300 years). The difference in these definitions are due to the understanding of resource renewability. According to Sanyal (2005), exploitation for over 30 years at sustainable level should not leave any permanent impact on the resource base, as any resource degradation and reservoir pressure will replenish within 100 to 300 years' time frame. To accomplish the renewability, overproduction must be avoided at any cost. The most appropriate way to make sure this would not happen is trough reservoir management.

According to Grant et. al. (1982), there are four most important elements of geothermal reservoir management, which are:

(1) Control and monitoring of the energy extraction from the reservoir so as to avoid over-exploitation.
(2) Careful monitoring of the actual response of the reservoir to long-term production.
(3) Modelling of the reservoir and its response history for making prediction of future response for different production scenarios.
(4) Deciding courses of action in the exploitation of the resource.

RESERVOIR MANAGEMENT IN INDONESIA

Indonesia has been utilizing geothermal power to generate electricity for 35 years, since the first power plant operated in 1983. At the end of 2017, installed capacity of geothermal is reported to be 1,808.5 MW and in 2018 additional 140MW was finalized through Sarulla Unit-3 (110MW) and Karaha (30MW) (ESDM, 2018). The goal is to expand the geothermal installed capacity to 7,241.5 MW in 2025. This high, yet achievable target requires geothermal field, whether pre-existing or new, to maintain the best condition to ensure maximum sustainable production. Developers must figure out the most suitable method to manage reservoir in respect to their field, due to differences of each.

In this review, six geothermal fields will be discussed, namely Kamojang, Darajat, Wayang Windu, Salak, Dieng and Ulubelu. Most of the field have gone through changes in geothermal industry of Indonesia and strived to provide steams throughout long production period.

Kamojang

Kamojang geothermal field is the oldest geothermal field in Indoneisa. Since the first exploration in 1926, Kamojang geothermal field has gone through several changes of Indonesia's geothermal regulations, including Indonesia's independence from Netherland. Owned by PT Pertamina Geothermal Energy, this field is currently working with 5 units with total 235 MWe installed capacity. The first three unit (Unit I, Unit II and Unit III) are operated by PT Pertamina Geothermal Energy (upstream) and PT Indonesia Power (downstream) while the latest two (Unit IV and Unit V) are fully operated by PT Pertamina Geothermal Energy. These three units belong to PT Indonesia Power were established in the 1980s under Steam Sales Agreement (SSA), which means the upstream developer is required to sell steam produced by the wells to the downstream developer, in this case PT PLN / PT Indonesia Power is the powerplant owner (downstream). Meanwhile, Unit IV and Unit V were established almost 20 years after the first three units. Unit IV was inaugurated in 2008 and Unit V was inaugurated in 2015. Total project agreement requires PT Pertamina Geothermal Energy to sell electricity by kilowatt hour (kwh) to PLN.

Located in Mount Guntur in Garut, West Java, Kamojang geothermal field the famous for its two-phase, vapour dominated system. The reservoir temperature is 235–245OC, and pressure of 31–38 kg/cm2, with fluids average enthalpy of 2792 kJ/kg (Utami, 2000; Kaya et al, 2011; Pambudi, 2018). This condition made dry steam power plant is possible to be utilized. According to Suryadarma et al. (2010), in order to generate 200 MWe, up to 1,575 to 1,600 ton/hour of steam need to be produced. Statistics made by EBTKE in 2016 reveals that at the year 2015 alone Kamojang geothermal field has produced 11,974,084 ton of steam. The steam production was peaked in 2009, with 12,612,255 ton of steam produced before Unit I were down for maintenance and finally shut down in April 2014 until October 2017 (Thalib, 2016).

Suryadarma et al. (2010) reported that from 1982 to 2008, to supply the 140 MWe plants, the productivity of individual wells has declined about 2–7%/year, with average decline of 3% per year. Three make-up wells were drilled every 2 to 3 years to stabilize production. After operating for 27 years, the reservoir pressure declined about 17–25% from the initial condition, or about 9.5 kg/cm2 in average. Meanwhile, temperature decline over 27 years utilization period are about 2–7% from initial conditions, or 19^{O}C in average. The report also noted that the eastern sector of the field no significant changes were observed during the period when only Unit I, Unit II and Unit III were on-line. However, some decline has become more notable since the production of Unit 4 started.

To overcome the problem, Kamojang has established three components of reservoir management – reservoir monitoring, reservoir modeling, and production and reinjection strategy. The Kamojang database system is called Integrated

Reservoir Information System (IRIS). The database holds all data including exploration, reservoir monitoring and exploitation data, production history and chemical sampling. According to Moeljanto (2004), Kamojang has adapt to the Environmental Management System (EMS) of ISO 14001.

With steam input needed as mentioned above, only 30% of steam is recovered as condensate and re-injected, which is disproportionate (Sofoyan et al., 2010). Natural recharge also low due to insufficient fractures that reach to reservoir. This condition leads to a decline trend of produced mass in the field and therefore an unsustainable production.

Reinjection strategy that is used in Kamojang geothermal field is total inflield injection. Aside from condensates, river water around the area is used for reinjection. Unproductive wells with low to medium permeability are used as injection wells. Overtime, the injection strategy has been updated by repositioning injection wells and changing the rate. From 1983 to 2003, little injection breakthrough is observed in production wells. When monitored by gravity, little positive gravity changes are visible near reinjection wells. Positive and negative effects are also seen depending on the location of wells with respect to reinjection. Overall, although the reinjection program has not shown a good effect in restoring the production rate, it gives a positive impact in delaying the steam decline.

Darajat

Darajat geothermal field is located at Garut, West Jawa and at the southwest of Kamojang geothermal field, approximately 10km. Previously, Darajat geothermal field was owned by Chevron Geothermal Indonesia and currently owned by Star Energy. Exploration in Darajat started in 1984, and currently generates a total of 270 MWe. This field went through the Asian Financial Crisis 1997, that stopped the development progress and was resumed in 2000. The first unit was operated 6 years after the exploration, which is in 2000 and produces 55 MW. The second unit was operated in 2007 with 95 MW and the third unit in 2009 with 121 MW.

Similar to Kamojang, Darajat has vapour-dominated system, thus employs dry-steam power plant to generate electricity. Darajat has the larget reported conversion efficiency with approximately 20%, whereas the worldwide average is 12%. The reservoir temperature is 245^{O}C, and pressure of 35 bar, with fluids average enthalpy of 2783 kJ/kg (Pambudi, 2018). In order to generate 260 MWe, according to Rejeki et al (2008), 1,563.1 ton per hour must be produced. Statistics from EBTKE in 2016 reported that Darajat field produces steam as much as 13,916,103 ton in 2015. The production peaked in 2012 with 14,282,785 ton before declining the following year to only 10,678,225 ton. Scaling issues in some wells are reported due to superheating condition and meteoric water influx. These affected wells are decreased in productivity, some up to zero. Production decline of these wells are reported to be 1 to 10%.

Darajat has also established three components of reservoir management – reservoir monitoring, reservoir modeling, and production and reinjection strategy. Darajat employs strict and scheduled monitoring procedure, allowing better understanding of the reservoir. Parameters that are directly in contact with reservoir such as gas chemistry and steam condensate are monitored tri-annually. Whereas superheat activity and total NCG are monitored monthly. Aside from regular monitoring, there are other parameters such as Microearthquake (MEQ) survey and other physical aspects that are not monitored regularly.

Injection strategy of Darajat changes overtime. Darajat has three infield reinjection wells at first, two (DRHJ-3 and DRJ-15) in the production area where the main natural recharge area is located and one (DRJ-12) in the condensate cell. Fluids that are used are condensates plus additional water with some NCG. As a result, thermal breakthrough and increase in NCG content are reported in some wells (Martiady et al., 2011; Rivera Diaz et al., 2016). Reinjection dampens the ability of production water to superheat. MEQ triggering mechanism is related to the increase of pore pressure in the reservoir through fluid reinjection (Pramono, 2005; Rivera Diaz et al., 2016). In December 2011, another strategy is established. Instead of adding an infield well, a well located in peripheral of the reservoir (DRJ-19) is suggested to replace the condensate injection wells. As a result, the injection well could accommodate partial production decline of all three units.

Gunung Salak

Gunung Salak geothermal field, or also known as Awi Bengkok geothermal system, is located within the Halimun Salak National Park. Administratively located in two districts, Sukabumi and Bogor, and approximately 100 km from Jakarta. The development project at Gunung Salak started in 1982 by Unocal Geothermal Indonesia with Pertamina. After the exploration phase was completed, two power plant units were built, generating 2 × 55 MW. The plant operated in this way until 1994. From 1995 to 1997, additional units 3, 4, 5 and 6 were constructed with a capacity of 55MW each, thereby providing a total capacity increase to 330MW. Currently, after upgrades to all 6 units, the total capacity of Gunung salak has reached 377MW. Unit 1, 2 and 3 were operated by PLN, whereas Unit 4, 5 and 6 were operated by Unocal, which acquires by Chevron Geothermal

Indonesia in 2005. Similar to Darajat, Gunung Salak is currently owned by Star Energy.

Gunung Salak has two-phase, high-enthalpy, liquid dominated system with reservoir temperature of 240^{O} to 310^{O}C and average enthalpy of 1842 kJ/kg. This condition requires single flash powerplant. According to Kaya, Zarrouk, & O'Sullivan (2011), to generate 330MWe the six units have to produce 11,520 ton of steam. Statistics from EBTKE in 2016 reported that Gunung Salak continuously provides approximately 24,000,000 ton of steam per year.

Reservoir management in Gunung Salak consists of three components – reservoir monitoring, reservoir modeling, and production and reinjection strategy. Current production strategy is targeting steam cap that is developed at the eastern part of the field, by using low-angle trajectories. Awi 16-7 was drilled in 2006 reached a deviation angle of ~60^{O}. This well produces more than 40 kg/s of steam without penetrating beneath the liquid level of the reservoir. Monitoring program of Awibengkok is supposedly similar to the program at Darajat, although focusing on fluid-based properties.

Gunung Salak is using initial infield reinjection strategy. However, there is a mix of infield and outfield injection. Brine is mostly injected within the reservoir and condensates out of the reservoir boundary (2km from production area) (Julinawati and Molling, 2013). Gunung Salak also use deep reinjection strategy (Pasiki et al., 2013). Faults play an important role as flow barriers between production and injection wells. Periodic changes in injection strategy are made based on well performance and trends in the well chloride concentration and enthalpy (Acuña, Stimac, Sirad-Azwar, & Pasikki, 2008).

As a result, the is an increased in energy recovery by periodic changes in reinjection strategy. However, this strategy also decreases temperature and enthalpy of the reservoir fluids over time (Pasiki et al., 2013). Infield reinjection is the major cause of chemical and thermal breakthrough. There is a direct correlation between injectate concentration in production and injection rates (Julinawati and Molling, 2013). Reservoir modelling suggests that reservoir performance would improve by moving injection from current infield location to more distant areas (Pasiki et al., 2013).

Wayang Windu

Located in Pangandaran, West Java, Wayang Windu geothermal field is operated by Star Energy. Geothermal activity in this field is manifested in the forms of hot springs, fumaroles, and steaming ground, and arise naturally from fractures over the reservoir. The temperature is approximately 260^{O} to 325^{O}C, with average enthalpy of 2700 kJ/kg. Although bearing high enthalpy, the system of this field is two-phase, liquid dominated system. This condition requires single-flash powerplant to generate electricity. Started exploration in 1985, Wayang Windu currently operates two generating units with total generation of 277 MW. The construction of the unit-1 completed in 1999 and Unit 2 was operated in 2009. The Unit-1 geothermal power plant has generating capacity of 110MW and is supplied by 13 production wells. Whereas, Unit-2 has generating capacity of 117MW with 6 production wells (Purnanto and Purwakusumah, 2015). There are additionally 5 injection wells.

According to Rivera Diaz et al. (2016), steam that required to generate 277MW is 1,528.1 ton per hour. Statistics from EBTKE in 2016 reported that Wayang Windu produces only 7,850,235 ton of steam in 2015 due to landslide that stopped power generation for four months (May 2015–September 2015). The steam production doubled in 2009 to accommodate additional unit, and the production peaked in 2010 with 13,675,168 ton.

Reservoir management strategy in Wayang Windu includes regular monitoring, reinjection, well cleaning and acidizing (Hermawan and Situmorang, 2013). The main problem of Wayang Windu is scaling. It declines the production up to 1% to 2% year from 2000 to 2012. Reinjection is done close to reservoir boundary (peripheral), at 2km from nearest production well to avoid interference and performed by gravity (Mulyadi and Ashat, 2011). Result from 2009 shows that the injection seems to bring the steam production back to 51 kg/s (Hernawan and Situmorang, 2013). To enhance the permeability of injection well and connectivity to reservoir, hydraulic fracturing with cold water were performed. The injected mass is reported to be 576 ton per hour.

Dieng

Dieng Plateu is a complex of voncanoes, with manifestations such as hot spring and fumaroles (Pambudi, 2018). Geothermal development in Dieng has been carried out since 1918, similar to the starting time of Kamojang. In 1964 to 1965, Dieng is recognized by UNESCO as a geothermal resource that has a very good prospect in Indonesia. By 1970, geophysical surveys were performed, and six shallow wells were drilled. Both were done by USGS. The temperature recorded at 1973 shallow wells was ranging from 92^{O} to 173^{O}C. In 1993, Dieng began to produce electricity through operation of 2MW monoblock powerplant in 1993. Himpurna-California Association of Energy (HCL) and Pertamina held Joint Operating Contract (JOC) in operating Dieng geothermal field. Currently Dieng geothermal field is owned by Geodipa.

Dieng geothermal system is two-phase, high-enthalpy, liquid-dominated system. The reservoir temperature is 280O to 330^{O}C with enthalpy of 2560kJ/kg (Kaya et al., 2011). This condition requires Dieng geothermal field to use single flash power plant. Current power generation of Dieng is 60MW with only 1 unit. Decline rate of production was 1,25MW per year, from the beginning of production up to 2008. However, in 2008, the installed capacity dropped significantly by 20 MW, therefore only produced 40MW. The drop of production continued to 2010 and left only 20MW to be supplied to the grid. This immediate and significant decrease was caused by silica scaling up to 1000 ppm (Pambudi et al, 2015). Based on statistics from EBTKE in 2016, Dieng produces 1,769,566 ton of steam, the highest ever produced. To overcome this problem, workover of production wells, well cleaning, acidizing and pH control were done regularly.

Dieng geothermal field currently employs infield reinjection (Kaya et al., 2011). Hot water and condensates are streamed to cooling pond before being reinjected to mitigate silica precipitation in the system. Previously, hot reinjection strategy was performed and resulting in development of continuous scaling problem (Rivera Diaz et al., 2016).

Ulubelu

Ulubelu geothermal field is located in Pagaralam and Muaradua, Lampung, and approximately about 125km from Bandar Lampung. Ulubelu geothermal field is operated by PLN and PGE. Exploration drilling activities began in 2007. However, the preliminary survey was conducted in 1986, when survey of geothermal energy was done throughout Sumatra. Further exploration activities were done in 1991 under coordination with Pertamina Unit II Plaju, and in 1994 the first slimhole exploration drilling was carried out.

The powerplant began operating in 2012 and currently producing 220MW with four generating units. The latest unit was completed and operated in 2017. The system of Ulubelu geothermal field is two-phase, medium-enthalpy, and liquid-dominated. The average temperature is 265^{O}C with average enthalpy of 1160 kJ/kg. Single-flash technology is used in four plants to generate electricity. In 2015, Ulubelu produced 6,044,075 ton of steam, according to statistics from EBTKE (2016), to supply steam to 2 operating units.

Although fairly new, compared to other fields discussed in this paper, decline rate based on calculated model by Hidayat (2016) are above the normal decline rate that is considered sustainable. The 30 years model proposed 9.4% decline per year. Management strategy that is established in Ulubelu includes reservoir monitoring (surface data, physical and chemical), daily well and surface facilities monitoring (pressure, temperature, valve opening, well head pressure and separator flow rate), and tracer dilution test (Yuniar et al., 2015).

Five reinjection wells in Ulubelu are located 1.5 to 2 km from the nearest production wells. The strategy that is used is injection at lower elevation than the production wells. However, Yuniar et al. (2015) also stated that several problems have started to rise, such as chemical breakthrough of reinjected fluids that might cause decline and intrusion of lower temperature fluid into well from shallow zone due to casing problem.

RECOMMENDATION

Reservoir declines are reported in each producing field with causes that seem to be similar. Cold water and injection brine breakthrough, scaling and corrosion are the main problems that are shared by geothermal fields throughout Indonesia.

Proper reservoir management is very urgent to overcome problem similar to the aforementioned. Based on the review of the six geothermal fields, recommendations are pointed out below:

1. Wells shall be used according to the initial purpose. In most fields, unproductive wells with medium to low permeability are transformed into injection and monitoring wells. Unproductive wells are those that are close or does not reach reservoir, thus do not represent the real reservoir condition. When transformed into injection well, injected fluids have higher possibility to flow to out of the reservoir, having very little connectivity.
2. Application of peripheral reinjection instead of infield reinjection at correct depth. Infield reinjection, at incorrect depth, have very high tendency to decrease the temperature of reservoir and change is condition. Infield reinjection, or reinjection in general, may cause injection brine breakthrough when located very near to production well. Peripheral reinjection strategy has proven to come up with better result.
3. If unproductive wells are obliged to be used as injection well, application of hydraulic fracturing may help in creating better connectivity.
4. Production rate must be controlled in order to maintain production in the long run.
5. Reservoir monitoring must be scheduled within adjacent time to have better visualization of reservoir response.

CONCLUSION

Sustainable utilization of geothermal energy is very much affected by the reservoir management. Good management may lengthen the life of the geothermal production. Reservoir management are commonly

done through monitoring, modelling and reinjection. Reinjection strategy should not cause any decrease in reservoir temperature but adequate enough to overcome the impact of pressure decline due to maximum fluid production.

REFERENCES

Acuña, J. A., Stimac, J., Sirad-Azwar, L., & Pasikki, R. G. (2008), "*Reservoir management at Awibengkok geothermal field, West Java, Indonesia"*. Geothermics, 37(3), 332–346. https://doi.org/10.1016/j.geothermics.2008.02.005

Grant, M., Donaldson, I., & Bixley, P. (1982), "*Geothermal reservoir engineering"*. New York: Academic Press.

Julinawati, T., Molling, P. (2013), *"Multi-species mixing models used to determine the amount of Awibengkok recharge liquids"*. In: Proceedings of the 35th New Zealand Geothermal Workshop; 2013 November 17–20: Rotorua, New Zealand.

Kaya, E., Zarrouk, S. J., & O'Sullivan, M. J. (2011), *"Reinjection in geothermal fields: A review of worldwide experience"*. Renewable and Sustainable Energy Reviews, 15(1), 47–68. https://doi.org/10.1016/J.RSER.2010.07.032

Martiady K, Pasaribu HAD, Roberts F, Sugandhi J. A. (2011), *"Managing the Decline Rate at the South Sector Production Area of Darajat geothermal field, Indonesia"*. GRC Trans 2011:35.

Mulyadi, Ashat A. (2011), *"Reservoir modeling of the northern vapor-dominated two- phase zone of the Wayang Windu geothermal field, Java, Indonesia"*. In: Proceedings of the Thirty-Sixth Workshop on Geothermal Reservoir Engi- neering; 2011 January 31−February 2: Stanford University, Stanford, California, USA.

Moeljanto. (2004), "Evaluation of the environmental impact at the kamojang geothermal field in indonesia". applying the ems of iso 14001. *Nation University, Report of Geothermal Training Programme*, 209–238.

Pambudi, N. A. (2018), "Geothermal power generation in Indonesia", a country within the ring of fire: Current status, future development and policy. Renewable and Sustainable Energy Reviews, 81, 2893–2901. https://doi.org/10.1016/J.RSER.2017.06.096

Pasikki, R.G., Maarif, J., Joeristanto, A., Libert, F., Kay, N. (2011), *"Studies and implementation of injector well conversion during Salak field operation"*. In: Proceedings of the Thirty-Sixth Workshop on Geothermal Reservoir Engineering; 2011 January 31−February 2: Stanford University, Stanford, California, USA

Pramono, B., Colombo, D. (2005), *"Microearthquake characteristics in Darajat geothermal field, Indonesia"*. In: Proceedings of the World Geothermal Congress; 2005 April 24−29: Antalya, Turkey

Purnanto MH, Purwakusumah A. (2015), *"Fifteen Years (Mid-Life Time) of Wayang Windu Geothermal Power Station Unit-1"*. An Operational Review, in World Geothermal Congress 2015; 2015

Rivera Diaz, A., Kaya, E., & Zarrouk, S. J. (2016), *"Reinjection in geothermal fields − A worldwide review update"*. Renewable and Sustainable Energy Reviews, 53, 105–162. https://doi.org/10.1016/J.RSER.2015.07.151

Sanyal, S. K. (2005), "Sustainability and Renewability of Geothermal Power Capacity". *Geothermal Energy*, (April), Retrieved from http://repository.usgin.org/sites/default/files/dlio/files/2011/u19/sustainability__renewability_of_geothermal_power_capaciity.pdf

Suryadarma, Dwikorianto, T., Zuhro, A. A., & Yani, A. (2010), *"Sustainable development of the Kamojang geothermal field"*. Geothermics, 39(4), 391–399. https://doi.org/10.1016/j.geothermics.2010.09.006

Sofoyan, Y., Daud, Y., Kamah, Y., Saibi, H., Nishijima, J., Fujimitsu, Y., et al. (2010), *"Monitoring of mass balance model during production capacity increase at Kamojang geothermal field, Indonesia"*. In: Proceedings of the Thirty-Fifth Workshop on Geothermal Reservoi Engineering; 2010 February 1−3: Stanford University, Stanford, California, USA.

Stonner, F. (2012), Gilbert (Jr.) 2000. "*Management"*.

Thalib, F. (2016), *"Unit I PLTP Kamojang Beroperasi Kembali Oktober 2017"*. Kementerian ESDM Republik Indonesia. Ebtke.Esdm.Go.Id. Retrieved from http://ebtke.esdm.go.id/post/2016/12/01/1462/unit.i.pltp.kamojang.beroperasi.kembali.oktober.2017

Utami, P. (2000), *"Characteristics of The Kamojang Geothermal Reservoir (West Java) As Revealed by Its Hydrothermal Alteration Mineralogy"*.



Social, Politics, Economics and Community



FRAMINGHAM'S SCORE IMPROVEMENT OF GEOTHERMAL EMPLOYEES AT DARAJAT THROUGH HEALTH PROMOTION AND HEALTH COMPETITION PROGRAM

Muhyidin and Indra Rohim

Star Energy Geothermal Darajat II, Limited
Sentral Senayan II, 25th floor. Jl.Asia Afrika No.8, Jakarta 10270. Indonesia
Email: muhyidin@starenergy.co.id and iroh@starenergy.co.id

ABSTRACT

In 2015, Star Energy Geothermal Darajat II, Limited initiated worksite wellness program to promote healthy lifestyle through voluntary health competition program for their employees. The baseline data based on previous Medical Check Up (MCU) result showed the average of Framingham's Score (FS) was 6.36%. It means in average, the estimation of 10-year of employees at Darajat to get cardiovascular risk (coronary heart disease) was 6.36 %. Some improvement plans taken during the activity such as conducted training & coaching from the health expert; health promotion through sport competition & aerobic, one day healthy menu within a week during lunch time at the workplace, and sharing healthy tips to participants. Total 106 employees participated in this voluntary program within consecutive 6 months program period. Monthly measurement was conducted to all partipants by company doctor. All participants are reviewed on their body weight to calculate body mass index (BMI), exercise / sport program implementation, ratio cholesterol and HDL (high density lipoprotein), fasting blood sugar, waist to hip ratio, blood pressure, and smoking behavior. Result of this program showed FS decreased from 6.36% to 5.71% by the end of program. The FS criteria was divided into 4 namely very low risk (<1%), low risk (1-<10%), intermediate risk (10-20%) and high risk (>20%). High risk employees reduced 2% to intermediate risk and 25% shifting of FS from low risk to very low risk.

Keywords: Framingham's Score, MCU, health improvement.

INTRODUCTION

Cardiovascular diseases (CVD) currently become a big problem globally. It become the leading cause of death worldwide and resulted in 17.6 million deaths in 2015 or 31.3% of total deaths. CVD is the leading of noncommunicable disease (NCD); nearly half of the 39 million deaths due to NCDs are caused by CVDs. (WHO, 2016).

The cause of death due to CVD is increasing from 14,4 million (27,7%) in 2000 to 17,6 million (31,3%) in 2015 and become number one cause of death worldwide (WHO, 2016). Global health estimates death by cause summary is shown in the Table 1 below.

Tabel 1: Global health estimates death by cause

No.	Cause of Death	2015		2000	
		Deaths (000s)	% of Total	Deaths (000s)	% of Total
1	Communi-cable disease	11.959	21	16.160	31
2	Non Communi-cable Disease	39.544	70,1	31.391	60,2
	Cardiovas-cular Diseases	17.689	31,3	14.425	27,7
3	Injuries	4.939	8,8	4.583	8,8
Total All Causes		56.441	100	52.135	100

Source: WHO, 2016

The different types of CVDs are listed below:

1. CVDs due to artherosclerosis. Arherosclerosis is the underlying disease process in the blood vessel that result in coronary heart disease (heart attack) and cerebrovascular disease (stroke): ischaemic heart disease or coronary artery disease, cerebrovascular disease, and disease of the aorta and arteries including hypertension and peripeheral vascular disease.
2. Other CVDs such as disorders of the heart muscle, disorder of the electrical conduction system of the heart and heart valve disease: congenital heart disease, rheumatic heart disease, cardiomyopathies, and cardiac arrhythmias (WHO, 2011).

A large percentage of CVD is preventable through the reduction of behavioral risk factors. Prevention of artherosclerosis involves improving risk factors through: healthy eating, exercise, avoidance of tobacco smoke and limiting alcohol intake. Treating risk factors, such as high blood pressure, blood lipids and diabetes is also beneficial. Unhealthy behavior lead to metabolic changes: raised blood sugar (hypertension); overweight/obesity; raised blood sugar (diabetes); and raised blood lipids. In terms of attributable deaths, the leading cardiovascular risk factor globally is high blood pressure result in 13% of CVD death, while tobacco result in 9%, diabetes 6%, lack of exercise 6% and obesity 5% (WHO, 2011).

In USA, heart disease is the leading cause of death, costing the country about $200 billion each year in health care services, medications, and lost productivity (CDC, 2017). In Indonesia, CVD is contributing 37% and become the number one leading cause of death (WHO, 2014).

Cardiovascular risk can be predicted with scientific prediction models that been developed to estimate the risk of developing CVD such as Framingham Risk Score (FRS) model. The FRS is a gender-specific algorithm used to estimate the 10-year cardiovascular risk of an individual. It was first developed based on data obtained from the Framingham Heart Study, to estimate the 10-year risk of developing CVD (Wilson et al, 1998). The FRS has been validated in the USA, both in men and women, both in European Americans and African Americans (D'Agostino et al, 2001).

The first FRS included age, sex, LDL (low density lipoprotein) cholesterol, HDL cholesterol, blood pressure (and also whether the patient is treated or not for his/her hypertension), diabetes and smoking. The updated version include dyslipidemia, age range, hypertension treatment, smoking and total cholesterol. It excluded diabetes because Type 2 diabetes meanwhile was considered to be a corronary heart disease (CHD) Risk Equivalent, having the same 10-year risk as individuals with prior CHD. (NIH, 2002).

At the workplace, cardiovascular risk can be prevented through health promotion program. According to the American Journal of Health Promotion (O'Donnell, 2009), health promotion defined as "the science and art of helping people discover the synergies between their core passion and optimal health, enhancing their motivation to strive for optimal health and supporting them in changing their lifestyle to move toward a state of optimal health. Optimal health is a dynamic balance of physical, emotional, social, spiritual, and intellectual health. Lifestyle change can be facilitated through a combination of learning experiences that enhance awareness, increase motivation, and build skills ad, most important, through the creation of opportunities that open access to environments that make positive health practices the easiest choice".

The health promotion through competetition program among employees at geothermal company at Darajat is a voluntary basis. Company, through Fight to Fit committees consist of some departments, collaborated in planning & organizing this program within 6 months period from April – October 2015. The purpose & objective of this programs are to improve healthy lifestyle, improve team building within Darajat employees and change paradigm from curative to preventive, and reduce the cardiovasular risk. Previous year, the initial program was launched, but in 2015 there are some improvements taken with more systematic approach and measurement.

The program was run by Health & Medical (HM) department and Health, Safety and Environment (SHE) department with sharing budget. The committee consist of several departments and management team to support the program. HM department absorbed the cost related to MCU, laboratory analysis and health talk. SHE absorbed the cost related to prizes, souvenir, and meals during the program.

This health promotion program also involved family & their spouse especially during supporting activities such as health talk about nutrition, sport, and medical sport topic from the experts. The spouse's involvement during health cooking competition & aerobic dance for all families are made to make the program more attractive and support the employees who involved in this program. Support from spouse is very important especially in serving health menu at home and keep healthy life style both at the workplace and at home. Spouse verified the implementation of employee health program by signing the form before submission to committee.

The health competition at Darajat was divided into some teams. Each team consist of 4 employees. There are 24 teams and 10 employees with individual categories as per company doctor recommendation. Total 106 of 127 employees or 83% of total employees involved in this program.

Baseline Framingham score data from participants was taken from 2014 MCU record. Medical team has divided the Framingham score into 4 criteria as shown in Table 2.

Tabel 2: Baseline Framingham score criteria

Framingham Score Criteria	Total Participants
Very low risk (<1%)	0
Low risk (1 - <10%)	82
Intermediate risk (1- 20%)	21
High risk (>20%)	3

Baseline average body mass index (BMI), cholesterol/HDL, and fasting sugar is shown in Figure 1. Total participants of men are 103 and women are 3 persons. The average of fasting sugar and BMI of women participants were higher compare to men participants.

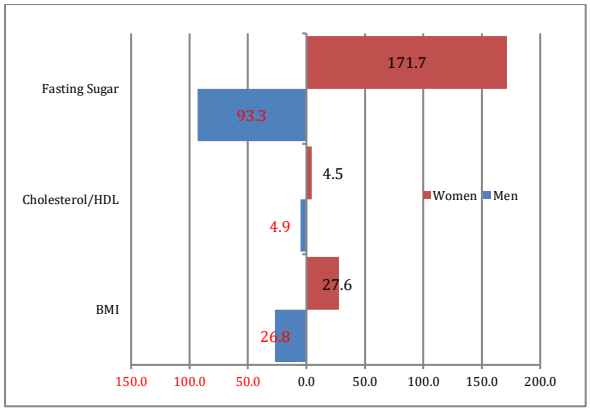


Figure 1: Baseline average BMI, cholesterol/HDL and fasting sugar.

METHOD

The FS baseline data of the Darajat employees are taken from previous MCU data on year 2014. Company doctor compile some employees' MCU data to calculate the FS such as age, sex, LDL cholesterol, HDL cholesterol, blood pressure, Body Mass Index (BMI), and smoking behavior.

The monthly measurement is conducted to all participants to monitor their BMI progress and waist to hip circumference ratio. Laboratory analysis on cholesterol and HDL cholesterol and fasting blood sugar were conducted every three months. Participants have to attend the approved laboratory based on the schedule. All the result from laboratory then sent to medical team.

The last measurement is conducted during annual MCU that conducted on October 2015 which is the last period of the program. Medical team will collect all the required data to count Framingham score of all participants.
The scoring criteria to select the winner of this competition program based on the program and implementation of healthy life style program (exercise, healthy food and rest time), BMI improvement result, cholesterol total and HDL ratio, fasting blood sugar, waist to hip circumference ratio, blood pressure, smoking behavior, and team compliance in submiting program & mothly report and measurement.

The weighting of scoring was 25% from healthy life style, 15% from BMI result (target BMI is 23 kg/m^2), 15% from cholesterol total and HDL ratio, 10% from fasting blood sugar, 10% from waist to hip circumference ratio, 10% from blood pressure, 5% from smoking behavior, and 10% from team compliance report.

On the beginning of competition, each team are required to present to committees on their specific program. Every month, each team shall submitted their program implementation evidences through report and pictures as part of scoring criteria.

Every team will have their own program based on their commitment. They will have their own exercise program such as play table tennis or badminton together and personnal exercise program such as daily push up / sit up, jogging and running. Team have to submit the implementation and it's evidence to Medical team to be reviewed and verified.

RESULT & DISCUSSION

During the program, committee conducted some monitoring & measurement. Interim complete measurement was conducted after 3 months program while monthly measurement such as body weight and team exercise program implementation keep monitored periodically. Medical team reminded all participants to conduct the measurement as per schedule.

The interim result of the program is shown in Figure 2. There is a shifting participants' FS criteria from low risk to very low risk, from intermediate risk to low risk and from high risk to intermediate risk. Very low risk criteria increased to 26% (28 of 106 participants), low risk criteria reduced to 13%, intermediate risk criteria reduce to 11% and high risk criteria reduce to 2%

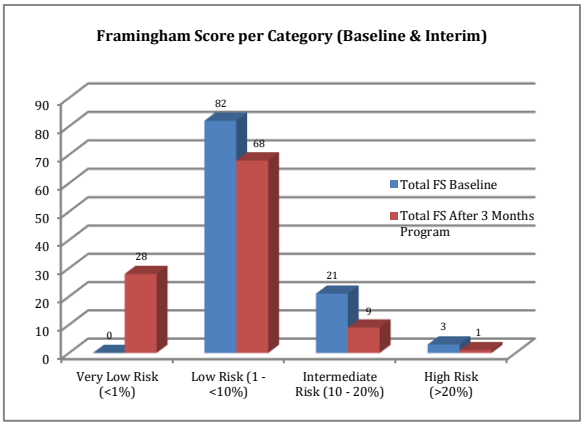


Figure 2: Interim result of Framingham score per category.

Comparison of Framingham score baseline and interim result from can be seen clearly through box and whisker plot (box plot) below in Figure 3. There are changes of data distribution such as median, Q1, Q3 and min and max data of Framingham score. The result showed improvement of Framing score, the lower score the lower possible risk of getting cardiovascular disease.

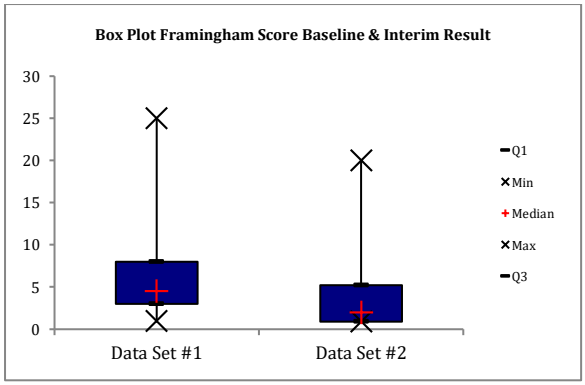


Figure 3: Box Plot Framingham score baseline & interim result.

The detail data showed there was reduction of total cholesterol per HDL with mean from 4.87 to 4.73. In the baseline data, there are 53 participants with total cholesterol per HDL >5. Total cholesterols are a measure of HDL, LDL and other lipoproteins that present in the blood. HDL often referred as good cholesterol while LDL known as bad cholesterol. The desired level of total cholesterol is 200 mg/dl or below. Since HDL protects the heart and vessel, increasing the HDL might be as important as decreasing of the total cholesterol. HDL may protect the body against narrowing blood vessel (AHA, 2018).
On October 2015, annual MCU was conducted for all employees (include participants). The parameters to count Framingham score already included in the MCU package. The final result comparison of FS baseline and FS after 6 months program is shown in the figure 4. It showed the reduction of FS from participants.

In this study we found that 3 of 106 (2,8%) total participants have high risk to get CVD. It was common for employees to have the condition or other risk factors to get CVD due to tobacco use, unhealthy weight (obesity) and lack of exercise. During the program, these high risk employees was implementing their specific team healthy program. Each participants has their own specific exercise program, diet program and specific team program that they need to implement. From the high risk participants, 2 of 3 (66,7%) improved their Framingham score and become intermediate risk.

The impact of workplace health promotion and competition at Darajat has led to change at both the employee and the organization levels. For employees, this program has impact to their health such as Framingham score and for organization this program has impact to reduction of medical cost. Average of Framingham score was reduced from 6.36% (year 2014) to 5.71% (during the program in year 2015).

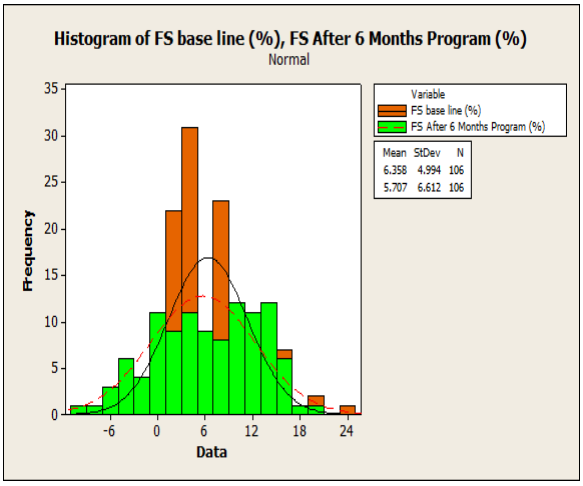


Figure 4: Histogram of FS baseline and FS after 6 months program.

On the other criteria, we found that 13 of 21 (61.9%) participants categorized as intermediate risk employees was shifted to low risk criteria. Total 37 of 82 (45.1%) was shifted to very low risk criteria. Detail data shown in the Table 3.

Tabel 3: Comparison of baseline Framingham score and after 6 months of program

Framingham Score Criteria	Baseline	After Program
Very low risk (<1%)	0	26
Low risk (1 - <10%)	82	45
Intermediate risk (1- 20%)	21	34
High risk (>20%)	3	1

The medical cost saving during this program was USD 7.430 from total participants or reduced 21% from total medical cost from previous year. There are 68 of 106 (64.15 %) of participants have reduced their medical cost. This comparison was conducted to the same participants on their medical cost.

The health promotion and competition program at Darajat was run through lean sigma approach which is divided into several stages:

Define phase

During this phase, lean sigma project contract and team was established. All team member from several departments, project champion and sponsor from management signed the contract as a commitment to succeed the program. Team committed to contributing to the successful completion of the project by using kaizen technique and contributing process knowledge, ideas and experiences, give time and priority in join meeting, do action items on time and communicating project progress to the champion and sponsor. Champion committed in coordinating available resources and conducting frequent review of the team progress.

Sponsor as management representative committed to ensure that the project was aligned with overall organization goals and regularly asking for project progress and help remove the barrier including in providing required resources.

Problem/opportunity statement, objective and scope was explored during this phase. Timeline and resources of the project was also defined to make it well planned.

Measure phase

In measure phase, team measured the as-is performance which is Framingham score of Fight to Fit participants at Darajat from MCU previous year data. Team from medical department measuring this data and divided into 4 criteria which are very low risk, low risk, intermediate risk and high risk. Due to confidentiality of the MCU data, medical team only provided the Framingham score and required data without showing detail data of each participants.

Medical team also provided medical cost of participants from previous year as baseline and then it will be compared after the program completed. Team targeted the medical cost reduction to 20% from this program.

Analyze phase

Causes and effect diagram was established during analyze phase. From brainstorming result, team divided into 4 aspects which are supporting program, people, method and monitoring. Figure 5 show the detail of causes and effect to run the program smoothly.

Possible solution from the causes was explored and some recommendation actions were formed. Alternative solution of the causes was also generated in case any barrier during the implementation. Some of recommendation actions during this phase such as conduct monthly formal review of participants' progress update and coaching to participants especially who did not meet the target. The face to face coaching was delivered by medical team.

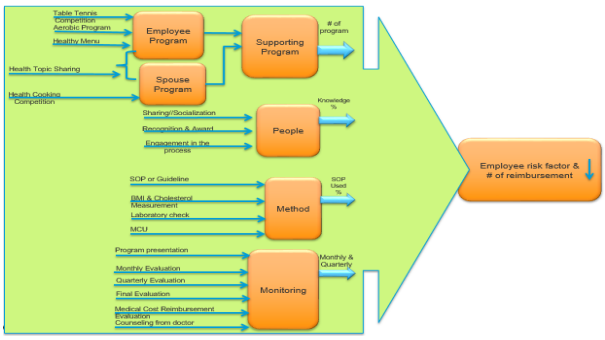


Figure 5: Causes and effect of program.

Improve phase

During improve phase, some detail improvement plans were made with person in charge and due date included in the plan. Here are the improvement plans during this phase:

Monthly review of measurement result

Each month, all participants are required to measure their body weight, waist to hip ratio, and blood pressure. If the participants did not conduct the monthly measurement, medical team will deduct the total score. The participants also submit their team program implementation with its evidences to get score. The incomplete of measurement data and program implementation will reduce their score. That's why, the participants remind each other of their team to ensure all members did it in timely manner.

Training and coaching from the health expert

During the program, committee provided special training and coaching from the health expert. The training was scheduled every 2 months with the topics on exercise specialist, nutrition specialist, and cardiologist. This event was conducted at Garut office and attended by participants and their spouse. The purpose in involving spouse due to family is very important in the implementation of healthy life style at home and to get support from their spouse.

Health promotion

Some health promotion program such as sport competition (table tennis and badminton), aerobic, health cooking competition for spouse, and one-day healthy menu in weekly at canteen. Table tennis and badminton competition was conducted per department team. The competition attended by most of the participants during the program period.

Aerobic and health cooking competition involving spouse. The spouse of participants' team competed in cooking and serving healthy food. Committee conducted assessment on this competition as per guidelines in healthy food cooking criteria and its hygiene process.

At Darajat, all employees were provided with lunch. To align this program, committee asked canteen personnel to have healthy menu in a week. During healthy menu, there was no fried food (only steam food processed). Participants who took healthy menu with certain portion as per nutritionist advice will have additional score. The amount of food was also controlled so participants cannot eat more.

CONCLUSION

The risk of CVD can be reduced through integrated health promotion and competition. The risk reduction can be seen from Framingham score

improvement of all participants from baseline and end of the program. The improvement of Framingham score could lead the reduction of medical reimbursement cost as one of the result of participants wellbeing improvement.

The health promotion and competition at Darajat can be adopted by other geothermal company. The detail program can be modified based on the organization culture and specific goal. Support from top management is one key of successes of this program.

REFERENCES

American Heart Association/AHA. (2018), *"What Your Cholesterol Level Mean"*. Retrieved from http://www.heart.org/HEARTORG/Conditions/Cholesterol/AboutCholesterol/What-Your-Cholesterol-Levels-Mean_UCM_305562_Article.jsp#.Wyys4uQcQaI.

Centers for Disease Control and Prevention/CDC, (2017). "Multiple Cause of Death 1999-2015". National Center for Health Statistics, December 2016. Data are compiled from data provided by the 57 vital statistics jurisdictions through the Vital Statistics Cooperative Program. Retrieved from http://wonder.cdc.gov/mcd-icd10.html.

D'Agostino, R. B. S., Grundy, S., Sullivan, L. M., and Wilson, P. (2001), *"Validation of the Framingham coronary heart disease prediction scores: results of a multiple ethnic groups investigation"*. JAMA. 2001;286(2):180-187. Retrieved from http://jamanetwork.com/journals/jama/fullarticle/193997.

National Institute of Health/NIH. (2002*), "Third Report of the National Cholesterol Education Program (NCEP) Expert Panel on Detection, Evaluation, and Treatment of High Blood Cholesterol in Adults (Adult Treatment Panel III) final report".* NIH Publication No.02-5215, September 2002. Retrieved from https://www.nhlbi.nih.gov/files/docs/resources/heart/atp-3-cholesterol-full-report.pdf.

O'Donnell, M. P. (2009), "Definition of Health Promotion 2.0: Embracing Passion, Enhancing Motivation, Recognizing Dynamic Balance, and Creating Opportunities". *American Journal of Health Promotion: September/October 2009, Vol. 24, No. 1, pp. iv-iv, updated from* Michael P. O'Donnell (1986), Definition of Health Promotion, *American Journal of Health Promotion, June 1986; vol. 1, 1: pp. 4-5.* Retrieved on 4 Sep 2017 from http://www.healthpromotionjournal.com.

Wilson, P. W. F., D.Agostino, R. B., Levy, D., Belanger, A. M., Silbershatz, H., and Kannel, W. B. (1998), "Prediction of Coronary Heart Disease Using Risk Factor Categories". *Circulation. 1998;97:1837-1847*. Retrieved from https://www.ahajournals.org/doi/full/10.1161/01.CIR.97.18.1837.

World Health Organization/WHO. (2011*), "Global Atlas on Cardiovascular Disease Prevention and Control".* pg.3-18. Retrieved from http://whqlibdoc.who.int/publications/2011/9789241564373_eng.pdf?ua=1.

World Health Organization/WHO. (2014), *"Noncommunicable Disease Country Profiles 2014"*. Geneva, Switzerland. Retrieved from https://apps.who.int/iris/bitstream/handle/10665/128038/9789241507509_eng.pdf;jsessionid=2D5C34BA59F4D1593ABFBD0240B45EC4?sequence=1., page 92.

World Health Organization/WHO. (2016), *"Global Health Estimates 2015: Deaths by Cause, Age, Sex, by Country and by Region, 2000-2015"*. Geneva, Switzerland. Retrieved from http://www.who.int/healthinfo/global_burden_disease/en/.

UPDATED LITHOLOGICAL AND TEMPERATURE MODEL IN SORIK MARAPI GEOTHERMAL FIELD, INDONESIA

S. Mulyani[1], Z.F. Sarmiento[3], A.C. Licup, Jr.[2], V.R. Chandra[2], R. Hendry[2], S. Nasution[2], R. Hidayat[2], P.P. Sari[1], Jhonny[1], and D. Juandi[1]

[1]Schlumberger
[2]PT Sorik Marapi Geothermal Power
[3]KS Orka Renewables PT Ltd
Email: smulyani@slb.com; zammy.sarmiento@ksorka.com; armando.licup@ksorka.com; vicky.chandra@ksorka.com; ridha.hendry@ksorka.com; syukri.nasution@ksorka.com; ryan.hidayat@ksorka.com; psari2@slb.com; jjhonny@slb.com; djuandi@slb.com

ABSTRACT

Sorik Marapi is one of geothermal field in Indonesia that has been drilled, with results indicating the existence of a high temperature-neutral resource. To achieve the target 240 MW installed capacity, understanding reservoir condition of this field at exploration stage is the key. In this case, lithology and temperature values in geothermal can be used as parameters for reservoir characterization and creating dynamic reservoir model. Initial modeling works in the field has been completed and discussed in previous study to create 3D conceptual subsurface model, including structural, lithology, resistivity and temperature distribution. This paper deals with the 3D modeling studies conducted in the same field, based on available data from surface exploration (3G-geological, geochemical & geophysical) surveys, and additional data from deep drilling in several wells path. The objective of this new paper is to build updated geological and temperature models with additional 10 wells data and give explanation about reservoir characterization in Sorik Marapi geothermal field, including new reservoir delineation based on the new model. The 3D subsurface modeling uses Petrel® software from Schlumberger which allows multidiscipline data integration. The 3D model containing structural, lithology, resistivity and temperature model from the 14 wells in the area. The workflow in the models starts with data loading and quality control, prepare structural model and 3D grid for reservoir property modeling, create 3D model of lithology, resistivity and temperature. The result of this study will be the 3D subsurface static model defining the vertical and lateral resource boundaries as well as the prime resource areas which would be the basis of designing next well targets. This model can be expanded to build updated numerical model, as parameter for reservoir simulation of geothermal field in the next stage.

Keywords: Updated model, updated wells, lithology model and temperature model, Petrel, Sorik Marapi, Indonesia

INTRODUCTION

This project reference field is Sorik Marapi that located in North Sumatra, Indonesia (Hochstein and Sudarman,1993). Sorik Marapi geothermal power plant unit 1 has ready for their production stage in March 2018, with capacity 20 MW (www.industri. bisnis.com). Meanwhile, the production of Sorik Marapi power plant unit 2 has been targeted at September 2018. The total capacity that will be produced by this field is 240 MW by 2022 (Filtech Energy Drilling Company, 2017).

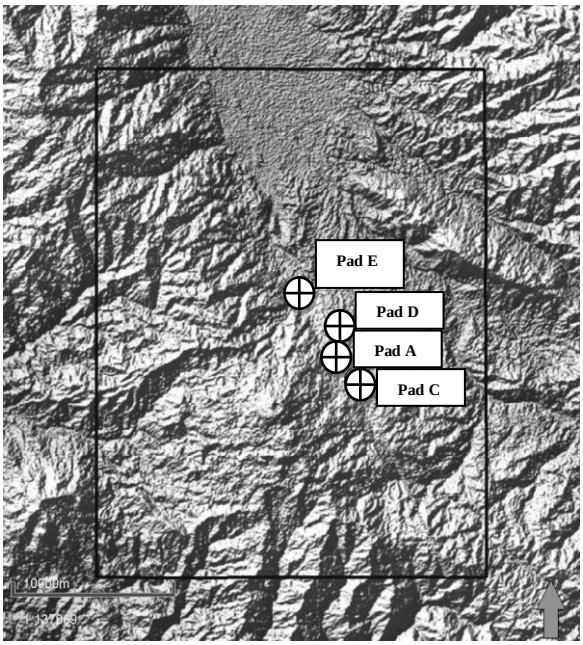


Figure 1: Project boundary (black square) of study area, with well pads from North are E, D, A and C.

The model boundary used in this project same with the previous study, as shown in Figure 1. The study area is 7.37 km^2 that cover 23.9 km x 31 km in length. Coordinate position of that area is 11069749-11093602 for x-axis and 65186-96200 for y-axis.

A conceptual 3D subsurface model built in the previous study based on 2 well pads data (A and E)

(Sagala et al, 2018). The model was built sequentially from structural model, lithology model, resistivity model and temperature model. Since they are built in the same 3D grid, all of results should be compatible with each other (Licup et al, 2017). Now on its exploration drilling and production stage, Sorik Marapi Geothermal Power get additional wells data from pad C and pad D that used to calibrate and update the previous model. The updated model includes lithology and temperature models which built by using Petrel® software.

EXISTING 3D SUBSURFACE MODEL

The Existing 3D model was built based on surface data such as topography points, faults lineament and formation boundaries (Akar et al, 2011). The vertical range of 3D model is -3000 to 2000m from sea level datum. The lateral dimension of cell grid which construct entire 3D model is 25 x 25m, with cell thickness 45m. Based on the information provided by the model, it consists of structural, lithology, resistivity and temperature distribution.

Structural Model

The structural model of previous study (Hamilton, 1979; Sieh and Natawidjaja, 2000; Cattin et al, 2009; Muraoka et al, 2010; Weller et al, 2012; Blanco et al, 2016), gave information about the faults plane position in the subsurface. Several faults plane with major direction Southwest – Northeast (SW-NE) shown by Figure 2. The trace of those faults influenced the topography at the surface with some clear lineament.

Lithology Model

The existing lithology model built based on the conceptual delineation from available well data (pad A and E). There are four main unit formation of lithology in Sorik Marapi field, they are: dacitic dike, sibanggor volcanic, roburan volcanic, and sorik volcanic. The stratigraphic relationship between three volcanic formations showing conformable contact, with intrusion by dacitic dike (Figure 3).

This model used as reference for updated lithological model, based on additional information of lithology from well pad A, C and D.

Resistivity Model

The resistivity model was built based on resistivity point values which derived from magneto telluric data. The interpolation method used kriging algorithm, that good for dense data modeling. Basically, this algorithm will assign all cells without resistivity value, based on the interpolation of values from neighboring cells. This algorithm and its modification mainly used for creating updated model.

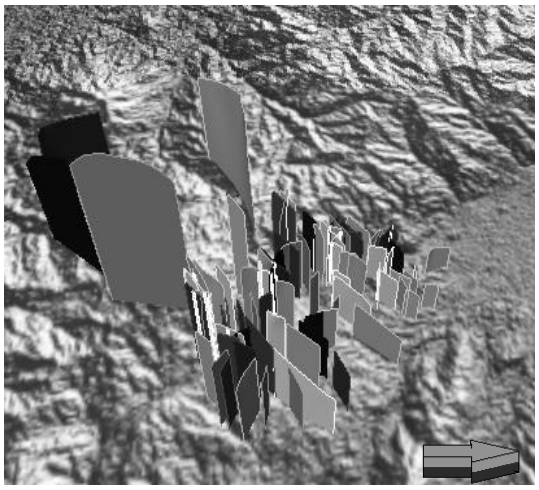


Figure 2: Faults plane at structural model with major direction SW-NE (Licup et al, 2017)

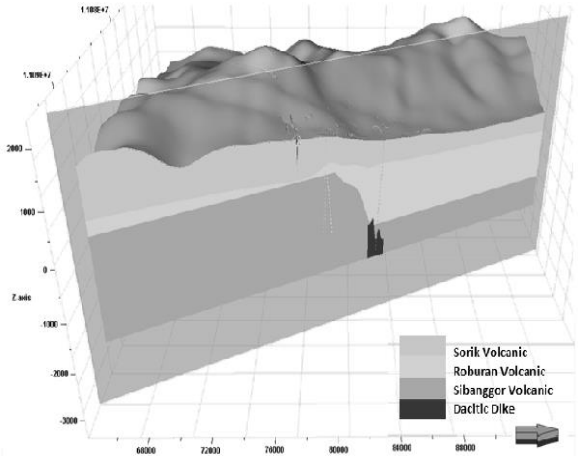


Figure 3: Lithological distribution of Sorik marapi field with conformable contact between sibanggor, roburan and sorik volcanics, and intrusion contact by dacitic dike.

Result of resistivity modeling gave information about the resistivity value distribution for entire area. Based on the existing data, the range value of resistivity is 0-500 ohm.m (Figure 4). As product of geophysical method (magneto telluric) done in the surface, there is no update for this model. Even though, this soft data will be used in the further analysis while doing update temperature modeling.

Temperature Model

One of the main objectives of this entire study is updating temperature model. Existing model built based on the correlation function between resistivity values and temperature well point data. With limited available data which came from Pad

A and Pad E, the result shown distribution of temperature value with high deviation at certain well path (well E201).

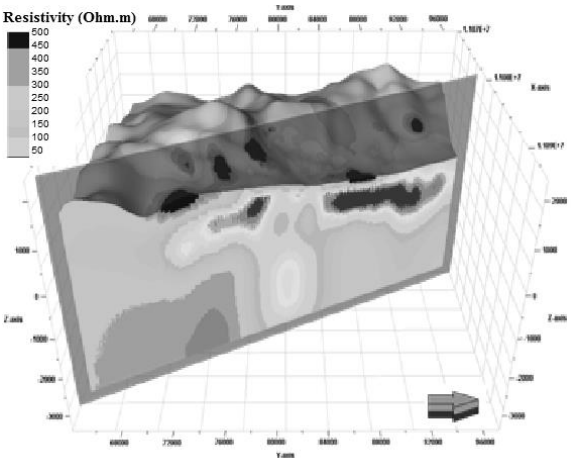


Figure 4: Resistivity model based on points with resistivity attribute which derived from magneto telluric data in Sorik marapi field (Licup et al, 2017)

Figure 5 show the temperature distribution from previous study, with range values 25-270ºC. By having additional well temperature data, the Existing model can be calibrated and updated to get better understanding of subsurface temperature.

DATA AND METHODOLOGY

To update the existing model, additional well data that consisted of lithology and temperature were given. The summaries of additional well data shown at table 1 below. By including four Existing well path data, there are total 17 wells path from 4 pads that used for this project.

Lithology data of several well path provided as stratigraphic marker (well tops). They gave information about the position of formation's contact along well path. Identification and classification of lithology formations done by using well data, based on characterization of each formation lithology units. Temperature data available for nine well path as continues log data. With small increment, this data gave more detail information of temperature, rather than temperature point well data that has been used in the previous study.

Methodology done in this project is 3D modeling by using Petrel® software. Workflow for this study consist of four main steps: model preparation, data analysis, updating model, and results validation. The flow chart for this workflow shown in Figure 6. Data preparation is the first step done in this project by having Existing model of structural, lithology, resistivity and temperature data from previous study. This step includes loading additional well data into existing project. Data importing process started from well head information that have the coordinate location of wells, followed by well path, well log temperature, and lithology as well tops. Quality control of those data applied by displaying them at 3D window and checking for their values.

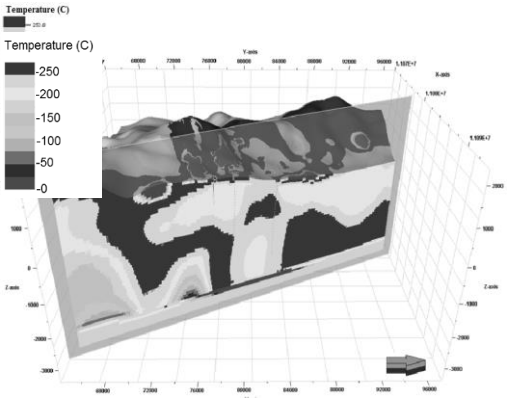


Figure 5: Existing temperature model based on resistivity & temperature function, with range values 25-270ºC.

Table 1: Summaries of Existing and additional wells data with the available information to be used in this project.

Data	Wells	Lithology	Temp. Points	Temp. Log
Existing	SM E-201	-	Yes	-
	SM E-202	-	-	-
Additional	SM A-101	Yes	-	Yes
	SM A-102	Yes	Yes	-
	SM A-103	Yes	Yes	Yes
	SM A-104	Yes	Yes	Yes
	SM A-105	Yes	-	-
	SM A-106	Yes	-	Yes
	SM A-107	Yes	-	Yes
	SM C-109	Yes	-	Yes
	SM C-111	Yes	-	Yes
	SM C-113	Yes	-	Yes
	SM C-114	Yes	-	Yes
	SM C-115	Yes	-	-
	SM D-108	Yes	-	-
	SM D-110	Yes	-	-
	SM D-112	Yes	-	-

Data Analysis is the second step which done by comparing the result of existing lithology and temperature model with the lithology and temperature data from additional wells. If the existing model is match, there is no need to rebuild the model. Those result will become calibrated model based on the update data. If the existing model is not match, rebuilding is needed. The modeling process could be similar with the previous study, with more information from additional well data.

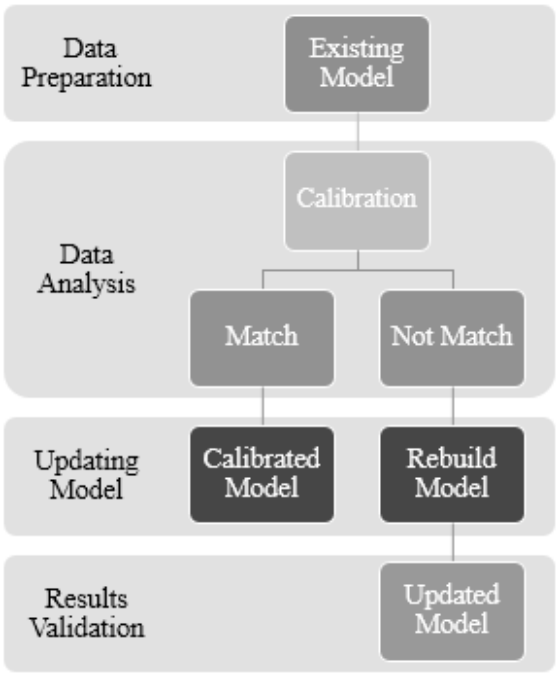


Figure 6: Workflow for calibrating and updating the Existing 3D Subsurface Model by using Petrel® software.

Results validation is the last step that needed to check the compatibility of updated model. This process can be done qualitatively based on the models' values at histogram or statistic information. To validate the last results, some blind well test which excluded during modeling process was used to do cross check with results value at their location. Similar values are a proof that the updated model is accurate, and vice versa.

RESULTS MODEL

There are two updated models that will be discussed in this project, they are lithology and temperature model. Each result used different approach to calibrate and rebuild the model. Both results analyzed at the same 3D grid structural model that consist of faults plane and properties information.

Lithology Model

Based on the workaround for this project, first step to be implemented is data calibration. The comparison between existing lithology model and additional lithology data done by displaying them at well section window.

The existing lithology model can be extracted along well path as discrete log. New lithology data displayed as marker (well top) that show the position of formation's contact and correlation for all wells.

Based on those contact, zone logs created by having formation's information at certain thickness. Figure 7 displaying several wells with discrete log from existing lithology model at the second column, and zone log from additional data at the third column. The connected lines are the contact position from three formations, they are sorik, roburan, and sibanggor volcanic. There is no information for dacitic dike formation from additional wells.

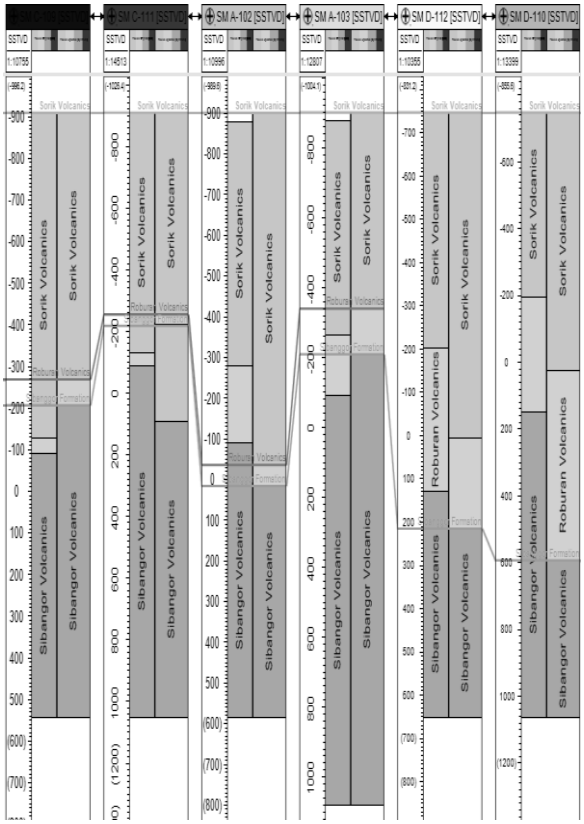


Figure 7: The comparison between discrete log from existing lithology model and zone log from additional data.

Based on those comparison, it clearly shows the deviation between existing lithology model with the well marker from additional data. For the example at well SM C-109, SM C-111, and SM A-103, the contact position between roburan and sibanggor are approximately 100m higher than the contact position based on existing lithology model. At well SM A-102, those contact position is 100m lower, and the roburan volcanic thickness is thinner compared with the existing model. Since there are many un-match results, rebuilding the lithology model is needed.

To rebuild the new lithology model, the surfaces contact used as input for 3D grid were updated based on the correct position of well tops data. The surface editing done for sorik, roburan and sibanggor formations. Figure 8 show the difference

surfaces of sibanggor before (above) and after (below) editing.

By using updated surfaces, the new 3D grid was built to get new lithology model (Figure 9). The distribution of formation's information done by using geometrical modelling with method assign value between surfaces and polygon.

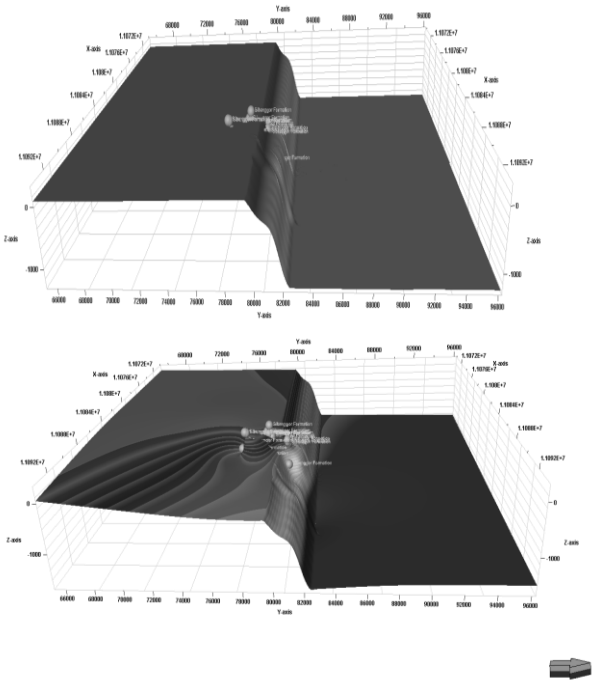


Figure 8: Sibanggor surface used for rebuilding 3D grid lithology (below) and the original surface used for creating existing lithology model (above).

Updated lithology model can be validated based on histogram results (Figure 10). The formation distribution shows largest proportion for sibanggor volcanic (51.8%), followed by roburan volcanic (36.2%), sorik volcanic (11.9%) and the smallest proportion is dacitic dike (0.2%).

Interpretation for lithology results done based on updated model. Overall there is no specific change in formation's classification. However, this new lithology model shows different thickness for each formation (excluded dacitic dike which kept as original). This model also gave new information related with the stratigraphic contact between three volcanic formations. In the existing model from previous study, those contacts are conformable for each of them. The additional data showing direct contact between sorik and sibanggor volcanic as shown in well SM C-111 (Figure 7) and intersection at Figure 9 where we found at depression morphology.

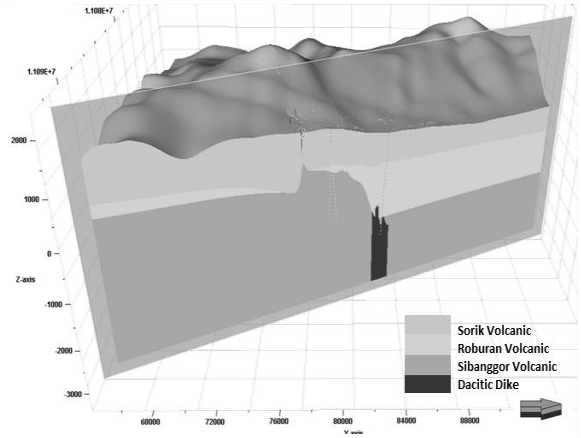


Figure 9: Updated lithology model in Sorik marapi field.

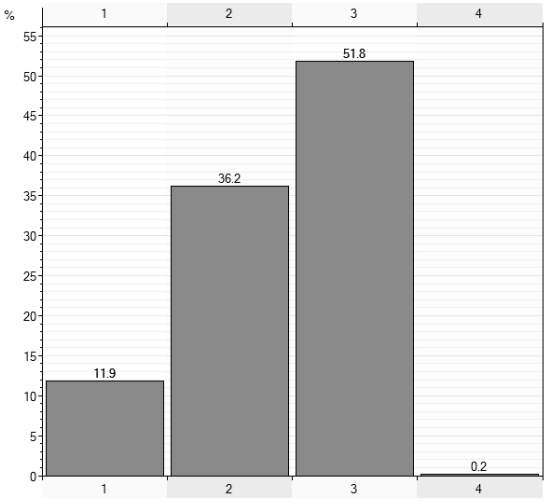


Figure 10: Histogram chart of lithological properties from updated model with information of formation's proportion for sorik volcanic (1), roburan volcanic (2), sibanggor volcanic (3) and dacitic dike (4).

There are some possibilities for that contact, whether the roburan volcanic was not deposited at entire area due to topography level so the young sorik volcanic was deposited directly above sibanggor volcanic, or the young sorik volcanic have erosional contact with roburan volcanic. The contact morphology of sorik and roburan volcanic found at some location at certain intersection. Figure 11 taken from cross section between well pad A and pad D. The lithology distribution near one of well path from pad A showing the direct contact between sorik volcanic (highest zone) and sibanggor volcanic (lowest zone) even though they are at relatively flat topography. It shows an evidence that the possibility of erosional contact below sorik volcanic is bigger. This new information can update the geological model in sorik marapi geothermal field.

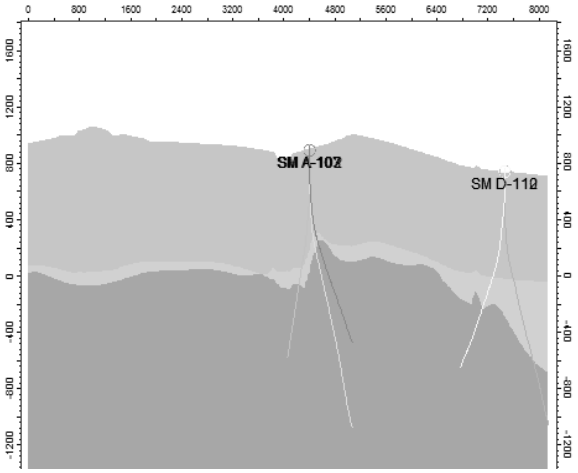


Figure 11: Intersection between pad A and pad D with lithology distribution that show small direct contact between sorik (1st zone) and sibanggor (2nd zone) volcanic, where there is possibility of erosional contact of sorik and roburan (3rd zone) volcanic.

Temperature Model

As the updating process for lithological model, data comparison for temperature was done to calibrate the existing model. The temperature data was imported as log ASCII and displayed as continues well log. The existing temperature model from previous study was extracted along well path the displayed as discrete log based on cell thickness of the grid. Figure 12 below shows some well path at well section window with temperature continues log fromnew well data in the second column, and temperature discrete log from existing model in the third column.

The data comparison gave visualization of how difference the existing temperature model compared with new additional data. One of good example for the comparison results is temperature model along well SM A-107 which has relatively similar range with temperature value from additional data. However, most of existing temperature model from previous study couldn't captured low resistivity at shallow area. Since the existing model is not match with the new data, so it needs to be updated.

To rebuild the update temperature data, the first process is upscaling the temperature continues logs for all of wells data. This process implemented to get the temperature value for cells penetrated by wells path, based on available temperature logs data. Algorithm to be used while upscaling the log data into cells is arithmetic calculation. The result of upscaled log shown at Figure 13 as below.

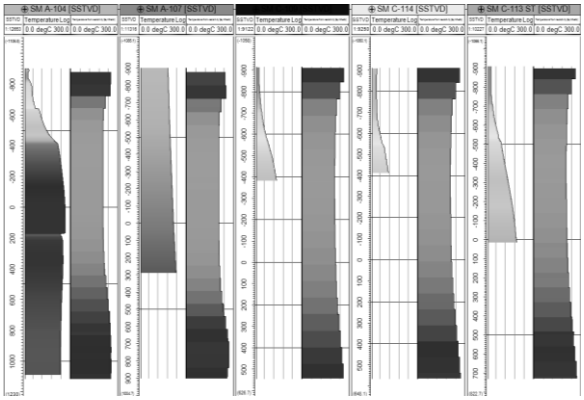


Figure 12: The comparison between temperature log from new wells data (second column) and temperature from existing model (third column).

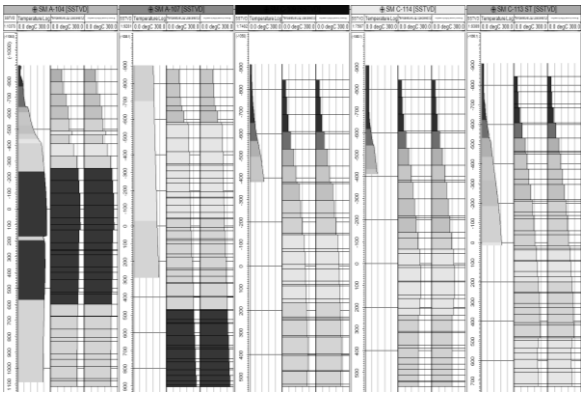


Figure 13: The temperature log data from additional wells (second column) and upscaled temperature data from 3D grid (third column) at well section window.

Available upscaled temperature log then used as main input for petrophysical modeling to interpolate them for entire cube. Due to limited data of wells, additional data can be used as secondary variable while modeling the temperature. In this case we tried to use available resistivity model. To see correlation between resistivity values from existing model, the resistivity model has been extracted into well log then used to create cross plot with temperature logs, as shown at Figure 14.

The cross-plot result show general trend which is at low resistivity, the temperature value can have very big range. While at medium to high resistivity, each well have relatively stable temperature (small range values) with certain trends as shown by connected lines. The correlation function created based on all available data as shown at Figure 15.

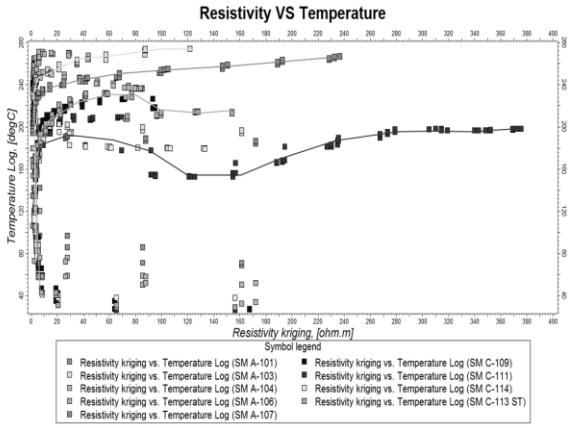


Figure 14: The cross plot between resistivity and temperature log from additional wells data, each point represents specific value at certain wells.

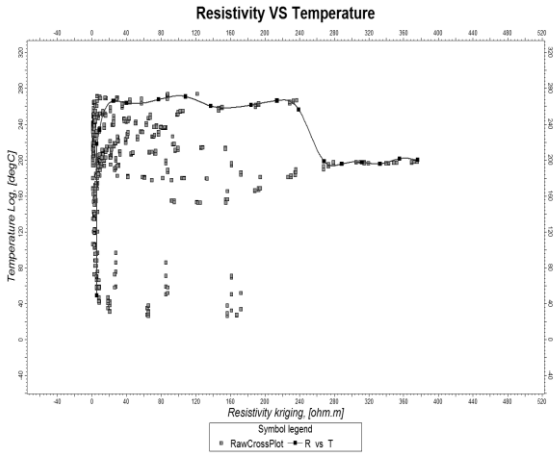


Figure 15: Nonlinear function graph based on the relationship between resistivity and all available temperature logs data.

The function formula derived based on those graphic is:

$$y = 196.249 + 0.1238x - 0.002x^2 + 4.9\ 10^6\ x^3$$

Those function is used for secondary variable while modeling temperature model. This model built by using upscaled temperature log as main input, and kriging algorithm as the method. The updated temperature model result is shown at Figure 16.

Values range of temperature result is 27-274^{o}C, with average temperature value in the surface around 25^{o}C. High temperature zone can be found under well pad A, B and D. To validate this result, quality control can be done by displaying all values at histogram window and see their comparison. The information consists of the proportion of temperature values from original well logs, upscaled cells, and the model results (Figure 17).

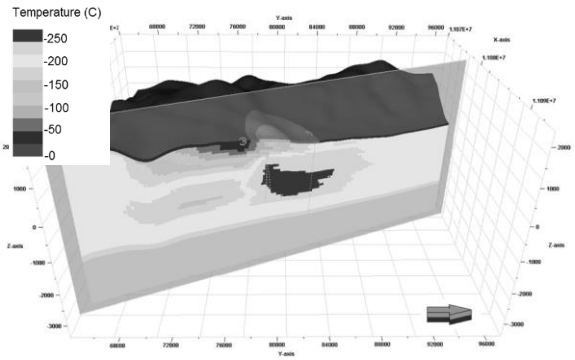


Figure 16: The updated temperature model based new additional data and nonlinear function.

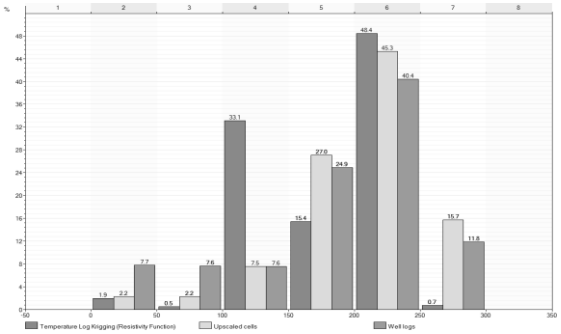


Figure 17: Histogram window to see the comparison of temperature values from well logs, upscaled and model.

Based on the updated temperature results, the model couldn't capture very high and very low temperature values, while medium temperature values proportion was being overestimated. The reason of this results could be caused by large volume and very thick grid cell. To increase the quality of this process, temperature model should be created by using finer 3D grid with small grid cell.

Another method to validate the result is by using blind well test which is excluded during modeling process. The wells used are well SM E-201 and SM A-102 that don't have temperature logs data. The validation done by displaying those wells with temperature well point value and updated temperature model extracted along well path. Based on the comparison, the updated temperature model at well SM E-201 has big deviation, while the values at well SM A-102 relatively match with the temperature well point data (Figure 18).

Wells position could be the reason of different results between both wells. Since well SM A-102 located near other well path at pad A, the accuracy is higher rather than well SM E-201 that located very far from other wells used for modeling. The temperature results and well position could be seen at Figure 19.

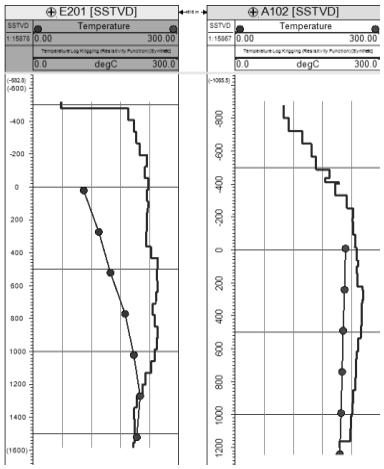


Figure 18: The comparison between extracted value of updated temperature model (line) with temperature point well data (dots) at well SM E-201 and SM A-102.

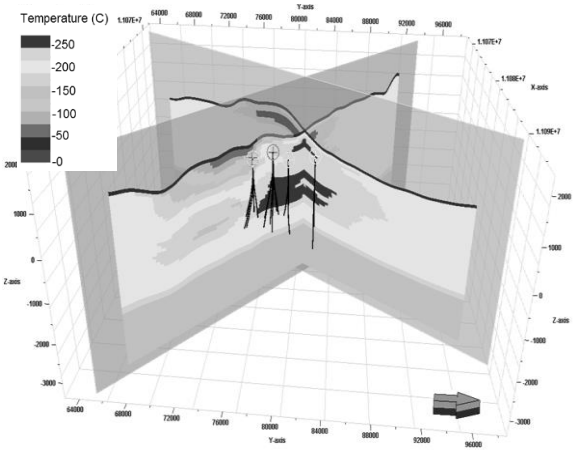


Figure 19: Updated temperature model and the wells position, from North (arrow direction) the well orders are pad E, D, A and C.

The hottest zone in sorik marapi geothermal field can be filtered for certain values (245-275ºC) to see their distribution a shown at Figure 20. The first hottest zone with shallower position is representative of volcanic area near Sorik Marapi Volcanoes. Deeper hottest zone with many wells could be identified as reservoir area.

Distribution of reservoir zone is located in the east of Sorik volcanoes. That zone has nearly ball shape with some lateral boundaries that separate the zone from cooler area. Figure 21 show the location of hottest zone and lower temperature zone at the same elevation. Based on the structural data in the sorik marapi field, there are two faults called Tobelirang and Sibanggor Besar which located at east boundary. Both faults may act as seal of hot temperature zone in the east part. So, the area in the east of those faults has lower temperature (130-190ºC) which shown by green color area. For the west boundary of high temperature zone is more controlled by the distribution of Sibanggor volcanic, which is the formation where the reservoir zone located.

DISCUSSION

Updated model based on additional well data in Sorik marapi field can be used to get new information about reservoir boundary and condition. To get better result for this model, any additional well data of lithology and temperature can be very helpful. Other parameters that have certain trend with temperature values could be added as secondary parameter for modeling those values.

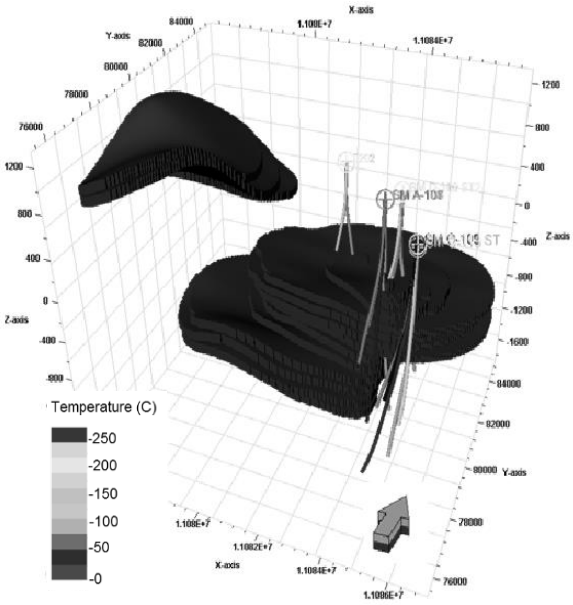


Figure 20: Hottest (245-275ºC) zone delineation based on updated temperature model that demonstrates the location or reservoir area.

CONCLUSIONS

1. The challenges to update the existing model is the limited data as some area.
2. Most of results at existing model from previous study need to be updated because they show noncompliance with additional new data.
3. Rebuilding process done for lithology and temperature model by using kriging method from lithological zone log and upscaled value.
4. The updated lithology model shows the same formations distribution, with additional information for the stratigraphic relationship and those area.

5. The updated temperature model shows delineation of hottest zone, with faults and formation distribution as boundaries. This information can be used for reservoir characterization, parameter in simulation model and drilling strategy.

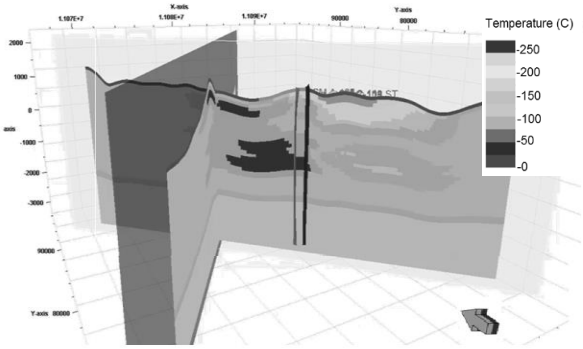


Figure 21: Tolbelirang fault (bold vertical line) and Sibanggor Besar fault (light vertical line) that separate high temperature (red zone) and lower temperature (green zone) in the same elevation and formation.

ACKNOWLEDGEMENTS

The authors would like to thank you for the managements of KS Orka, PT SMGP and Schlumberger who allowing us to use the data and software in the preparation of this manuscript.

REFERENCES

Akar, S., Atalay, O., Kuyumcu, C., Solaroğlul, U.Z.D., Colpan, B., and Arzuman, S. (2011), "3D Subsurface Modeling of Gümüşköy Geothermal Area, Aydın, Turkey". *GRC Transactions*,Vol. 35.

Blanco, D.F., Philippon, M., and Hagke, C.V. (2016), "Structure and Kinematics of the Sumatran Fault System in North Sumatra (Indonesia)". *Tectonophysics*. pp 1-12.

Cattin, R., Chamot-Rooke, N., Pubellier, M., Rabaute, A., Delescluse, M., Vigny, C., Fleitout, L., and Dubernet, P. (2009), "Stress change and effective friction coefficient along the Sumatra-Andaman-Sagaing fault system after 26 December 2004 (Mw = 9.2) and the 28 March 2005 (Mw = 8.7) earthquakes". *Geochemistry, Geophysics, Geosystems* Vol. 10, Q03011.

Filtech Energy Drilling Company. (2017), **"**Sorik Marapi Geothermal Power Plant ("PLTP Sorik Marapi") 240 MW", *Notice of Resources Confirmation*, Unpublished Technical Report.

Hamilton, W. (1979), "Tectonics of The Indonesia" Region. *US Geological Survey Numbered Series, Professional Paper* 1078. pp. 18-38.

Hochstein, M.P., and Sudarman, S. (1993), "Geothermal resources of Sumatra". *Geothermics Vol. 22*, pp 181–200.

Licup, A. C. Jr., Sarmiento, Z. F., Omac, X. L., Maneja, F. C., Chandra, V. R. M. B., Esberto, M. J. Z., Villareal, Baltasar, A. S. J., Mulyani, S., Sari, P. S., Jhonny, P. P., and Juandi, D. (2017), "Geothermal 3D Subsurface Modeling – A Case Study from Sorik Marapi Field, Indonesia". *PROCEEDINGS from The 5th Indonesia International Geothermal Convention & Exhibition 2017*.

Muraoka, H., Takashi, M., Sundhoro, H., Dwipa, S., Soeda, Y., Momita, M., and Shimada, K. (2010), "Geothermal systems constrained by the Sumatra Fault and its pull-apart basins in Sumatra, Western Indonesia". *Proceedings World Geothermal Congress* – Bali, Indonesia, pp. 1–9.

Petrel®. (2010), Schlumberger Information Solution, Petrel Software Online.

Sieh, K., and Natawidjaja, D. (2000), "Neotectonics of Sumatra fault, Indonesia". *Journal of Geophysical Research:Solid Earth* Vol. 105, Issue B12, pp. 1-30.

Sagala, B. D., Chandra, V. R., and Purba, D. P. (2018), "Conceptual Model of Sorik Marapi Geothermal System Based On 3-G Data Interpretation". Retrieved from https://www.researchgate.net/publication/323027498_CONCEPTUAL_MODEL_OF_SORIK_MARAPI_GEOTHERMAL_SYSTEM_BASED_ON_3-G_DA TA_INTERPRETATION

Weller, O., Lange D., Tilmann F., Natawidjaja D., Rietbrock A., Collings R., and Gregory L. (2012), "The Structure of the Sumatran Fault revealed by local seismicity". *Geophysical Research Letters*, Vol. 39, Issue 1, pp. 1-7

www.industri.bisnis.com/read/20180225/44/742878/pltp-sorik-marapi-siap-beroperasi-maret-2018

GEOTHERMAL POLICY OF INDONESIA: CHRONOLOGY, EFFECTIVENESS, AND THE LATEST CONDITION

Desy Caesary[1], Eko Hari Purwanto[2], Seo Young Song[1], Huieun Yu[1], and Myung Jin Nam[1]

[1]Department of Energy and Mineral Resource Engineering, Sejong University, Seoul.
[2]Directorate General of New, Renewable, and Conservation Energy,
Ministry of Energy and Mineral Resource, Indonesia
Email: nmj1203@gmail.com/nmj1203@sejong.ac.kr

ABSTRACT

The geothermal law, which was first established in 2003 as the highest degree of geothermal regulation in Indonesia, has been revised in 2014 to revoke the status of geothermal as mining activity. Subsequently, the government regulations and ministerial regulations related to detailed procedures of geothermal development activities have been accordingly revised by The Government of Indonesia to accelerate geothermal development whose utilization is mostly concentrated for electricity generation. Note that the installed capacity of geothermal power plant up to 2017 in Indonesia was only 1.8 GW, which is only around 6% of the total geothermal potential of Indonesia (that is about 28 GW being about 40% of total geothermal resource potential of the World). Further, Indonesia national energy plan of 2025 claims its goal to increase the amount of renewable energy; thus, geothermal sector is expected to contribute for the increase in geothermal utilization up to around 7.2 GW until 2025. This study will present a chronology of geothermal regulations in Indonesia while pointing out significant changes in the revised regulation. Effective indicator of Indonesia geothermal energy policy, which is modified from the International Renewable Energy Agency (IRENA) and International Energy Agency (IEA), is also be presented. Furthermore, the latest geothermal energy price regulation will be analyzed in comparison with the levelized cost of electricity (LCOE) estimation based on the literature data. At the end, future geothermal development will be discussed to not only understand the latest geothermal development condition in Indonesia but also foresee obstacles in geothermal target realization.

Keywords: Indonesi geothermal policy, revised regulation, geothermal utilization.

INTRODUCTION

Geothermal explorations in Indonesia have been conducted since 1970 and successfully constructed the first power plant of approximately about 800 MW by the year of 2000 (Hochstein & Sudarman, 2008). By the end of 2017, the geothermal installation is 1,808.5 MW, thus the average of additional geothermal utilization is about 59 MW per year, while the total potential of Indonesia's abundant geothermal energy is about 28,910 MW.

The geothermal law was first established in 2003 as the highest degree of geothermal regulation in Indonesia with its derivative policies of government regulation and ministerial regulation. However, up to 2011, the geothermal activities were only conducted in the existing area since 2004, hence there was no utilization in new areas. Due to this stagnant process, The Government of Indonesia (GOI) revised the geothermal law in 2014.

In this paper, each subject of the study will be discussed along with its results and analysis. First, chronology of Indonesian geothermal policy is presented along with analysis on significant changes of policy's revisions. Then, policy's effectiveness indicator methodology from IRENA is described and the result of Indonesian geothermal policy's effectiveness indicator is presented. Furthermore, levelized cost of electricity/energy (LCOE) from geothermal power plant is calculated based on previously-proposed model, and its results is compared and analyzed with the latest Ministry of Energy and Mineral Resource (MEMR) regulation on geothermal price. In addition, future geothermal development is discussed with consideration of Indonesian energy mix policy and power plant business plan of State Electricity Company of Indonesia (PLN) as a single buyer for electricity generation. In the end, several potential obstacles are further discussed to foresee what solution can be implemented to maintain geothermal development acceleration in Indonesia.

CHRONOLOGY OF GEOTHERMAL POLICY IN INDONESIA

Generally, the geothermal law explains about purpose of geothermal utilization, procedure of geothermal utilization activity, authority of each government parties; central and local government, and geothermal permit holder's responsibilities and rights. The details of each procedure are defined comprehensively in derivative policies the government regulations and ministerial regulations.

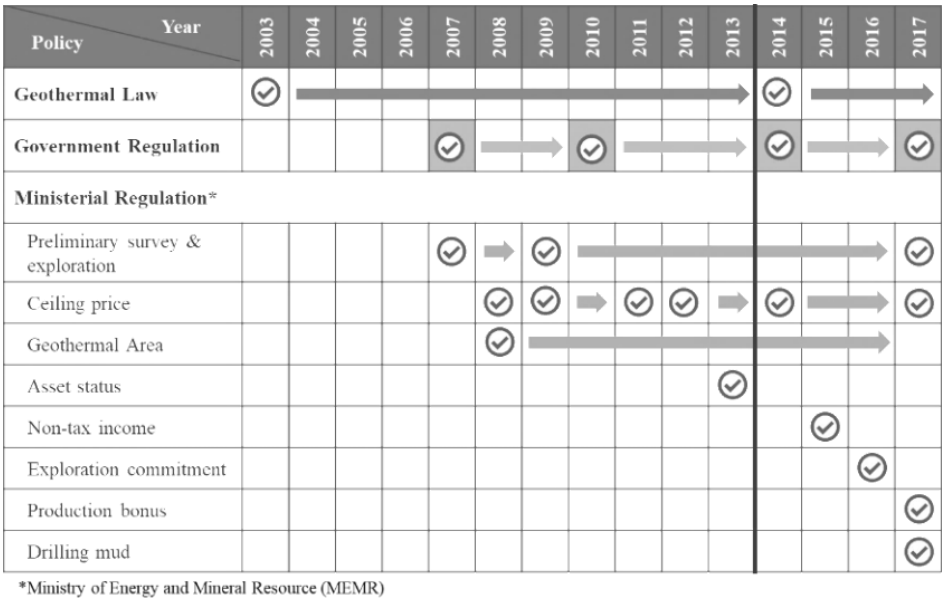


Figure 1: Chronology of geothermal policy in Indonesia, black line is represented of geothermal law revision in 2014 (compiled from MEMR's regulations)

Table 1: Significant differences between Geothermal Law No. 27 of 2003 and No. 21 of 2014.

Law	No. 27 of 2003	No. 21 of 2014
"Mining" terms	Geothermal was included as mining activity → conservation forest NO.	Geothermal is not included as mining activity → conservation forest OK.
Geothermal direct utilization	Not well explained	Explained more detail
Authority	Regional Government was given authorities to: • Tender geothermal area • Give geothermal permit • Conduct guidance and supervision	• Regional Government is only given an authority for geothermal direct utilization activity. • Tender, permit and guidance and supervision in geothermal indirect/electricity utilization are under Central Government.

The chronology of Indonesian geothermal policy is presented in Figure 1. Due to revision of the geothermal law in the 2014, its derivative geothermal regulations and ministerial regulations were also revised.

Analysis on Significant Changes of Geothermal Regulations

In this section, the revisions of geothermal law, government regulation, and MEMR's regulation on geothermal price were analyzed. The significant modification for the geothermal law was on general definition of geothermal activity, separation between regulation for direct utilization and indirect utilization, and authority changes of central government and local government. Detail results on significant changes of geothermal law and government regulation on geothermal development activity are listed in Table 1 and Table 2, respectively.

Moreover, a new scheme for geothermal development was introduced in the latest government regulation, which was an option for conducting preliminary survey and exploration before tender and will be carried with limited mechanism (Figure 2). The geothermal developers may choose one from these options.

For the ministerial regulation, only geothermal price regulation is discussed in this study, and comparison result to the latest pricing policy is shown in the Table 3. The first policy was based on Biaya Pokok Penyediaan Pembangkitan (BPP) or cost of generating power; not include the transmission and distribution cost, and it is calculated annually by PT PLN. Through the period, it was modified to be based on fixed price (research study from Indonesian Geothermal Association), then changed to feed-in tariff (FIT) mechanism which based on combination of several parameters; voltage, area, and/or year of commercial operation date (COD). Then for the latest one, it was back again to be based on BPP.

Table 2: Significant differences between Government Regulation No. 59 of 2007 and No. 7 of 2017.

Govt. Regulation	No. 59 of 2007	No. 7 of 2017
General	Indirect and direct utilization	• Indirect utilization (for electricity). • Direct utilization → separate Govt. Regulation • Additional data in the Working Area by the Central Govt.
Preliminary Survey	• Only preliminary survey • Assignment to the 3rd party: → Regional Govt. could propose the area → Mechanism: tender with first comes first served	• Preliminary survey: → Research institution or university • Preliminary survey and exploration: → Geothermal enterprise → Exploration commitment • Assignment to the 3rd party: → Only done by the Minister → Mechanism: contest/evaluation
Tender Process	• Central Govt or Regional Govt. • Based on the lowest tender price.	• Only Central Govt. • Based on the exploration commitment.

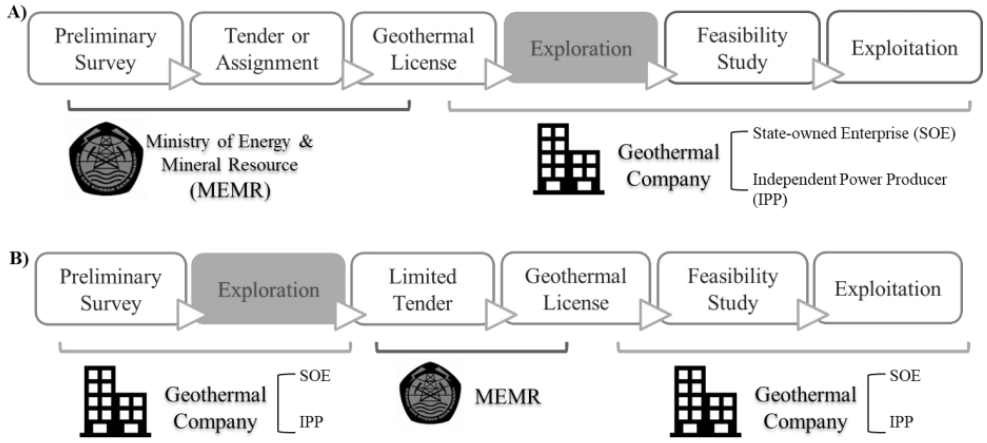


Figure 2: a) General geothermal development procedure, and b) new procedure of preliminary survey and exploration before tender process (illustrated from MEMR's regulations).

Table 3: Significant differences between Ministerial Regulation on Geothermal Price (summarized from MEMR's regulations)

	No. 14 of 2008	No. 32 of 2009	No. 02 of 2011
Principle	BPP	Correlated to PLN's Power Supply Business Plan.	
Ceiling price	• For 10 – 55 MW → 85% of BPP • For >55 MW → 80% of BPP	9.70 cents USD/kWh	

	No. 22 of 2012		No. 17 of 2014				No. 50 of 2017
Principle	Based on voltage and area section		Based on area and COD				BPP
Ceiling price		High Voltage	Medium Voltage	COD	Sumatera, Java, Bali	Others	Isolated	• Local BPP > National BPP: Local BPP • Local BPP < National BPP: Negotiation
	Sumatera	10	11.5	2015	11.8	17	25.4	
	Java & Bali	11	12.5	2016	12.2	17.7	25.8	
	Sulawesi	12–14	13.5–14.5	2017	12.6	18.2	26.2	
	Nusa Tenggara	15	16.5	…	…	…	…	
	Maluku & Papua	17	18.5	2025	15.9	23.3	29.6	

Effectiveness Indicator of Geothermal Policy

The effectiveness indicator of renewable policy is measured by achievement progress toward the International Energy Agency (IEA) World Energy Outlook (WEO) for 2030, and it is called as Policy Impact Indicator (PII) (Nicholls et al., 2014).

$$PII_n^i = \frac{G_n^i - G_{n-1}^i}{WEO_{2030}^i - G_{2005}^i} \text{ ... Equation i}$$

PII_n^i is policy impact indicator of renewable generation *i* in year of *n* and *G* is the electricity generation from *i*.

Result on Effectiveness Indicator for Indonesian Geothermal Policy

For assessing the effectiveness indicator of Indonesian geothermal policy, adaptation from IRENA (Equation i) is implemented as in the Equation ii $PII_n = \frac{G_n - G_{2004}}{Geo_{2025} - G_{2004}}$ … Equation ii; the indicator measures comparison between how much additional of installed geothermal on the year *n*, to the capacity requirement for achieving the energy mix target of 2025. The baseline is set to 2004 data as it is on available data and a remark of the first Geothermal Law of 2003. The Indonesian energy mix policy is referred to the Government Regulation No. 79 of 2014 and Presidential Decree No. 22 of 2017, which target for geothermal is about 7.2 GW in 2025. The result of policy impact indicator for geothermal policy in Indonesia is shown in Figure 3.

$$PII_n = \frac{G_n - G_{2004}}{Geo_{2025} - G_{2004}} \text{ ... Equation ii}$$

After the first Geothermal Law was established in 2003, there were not many of additional installed power plant, especially during 2009 and 2011, resulting low value of effectiveness indicator. Moreover, the developments were concentrated only on the existing area.

In comparison, after the year of 2014, the additional power plant had increased, the highest increase took place between 2015 and 2016. This was all due to additional units in the existing area in which took about 4 – 5 years from development drilling phase until COD. For example, additional units for Ululbelu unit 3 & 4, and Lahendong unit 5 & 6 were taken about 5 years, while Sarulla unit 1 & 2 were taken about 4 years. Based on observation, recently developed area which has started the exploration in the early 2010; such as Sorik Marapi, Muaralaboh, and Rantau Dedap field, will require at least 8 – 10 years to reach COD. Nevertheless, up to 2017, the policy impact indicator's result has achieved 17.74%, meaning that Indonesia still has a lot of tasks for future geothermal development.

LEVELIZED COST OF ELECTRICITY (LCOE) ANALYSIS

LCOE of geothermal power plant is defined as a ratio between total cost of power plant and possible amount of its electricity generation throughout power plant's lifetime:

$$LCOE = \frac{\sum_{t=1}^{n} \frac{C_{t=0} + O\&M_t + F_t}{(1+r)^t}}{\sum_{t=1}^{n} \frac{E_t}{(1+r)^t}} \text{ ... Equation iii}$$

Where:

$E_t = G \; x \; CF$ *Equation iv*

The numerator part or total cost consists of capital cost (*C*), operation and maintenance cost (*O&M*), and fuel cost (*F*). The capital cost itself includes such as engineering, procurement and construction (EPC) cost of power plant facility, road, land-use, and owner's project financing cost (U.S Energy Information Administration, 2016). The O&M cost is categorized into fixed O&M and variable O&M. Fixed O&M includes employees' salary, administration, tax, routines maintenance, and requirement of plant support equipment. Variable O&M includes materials that will be needed during power plant operations; hence the amount needed are necessary. The materials are for example raw water, water disposal expenses, chemicals or catalysts, lubricants, etc. The fuel cost is defined as amount of cost to purchase the fuel material for the power plant, noted that geothermal power plant has no fuel cost.

For denominator part, electricity generation in a *t* year, E_t, is defined as power plant's capacity, *G*, times its capacity factor throughout a year. Capacity factor, *CF*, is related to power plant's performance in generating the electricity. The discount rate, *r*, is used to calculate present value of the total cost over the lifetime of power plant (US Department of Energy, 2015).

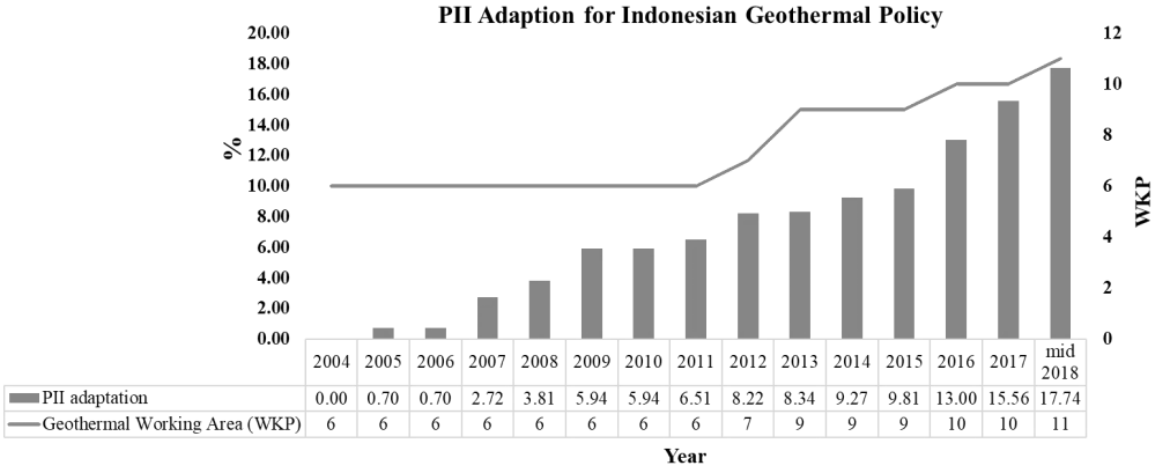


Figure 3: Result on policy impact indicator (PII) for Indonesian geothermal policy from Equation ii; analysis on progress condition of installed geothermal power plant toward requirement of fulfilling the geothermal target of 2025.

Result and Analysis on LCOE Calculation of Geothermal Power Plant

For understanding several conditions of power plant, variety value for each LCOE component will be analyzed based on several literature reviews as shown in Table 4. The calculation was done by implementing Equation iii using Microsoft Excel. The result is shown in Figure 4 with capacity factor is decreasing along the x-axis (ranging from 60% - 90%), and the result of estimated LCOE is in the y-axis is. For discount rate, it is determined and range from 10% to 14%. The result is categorized into 4 cases (a to d). Analyzing of Equation iii, high capacity factor with low discount rate value will lead to high value of denominator, resulting cheaper LCOE. Further, the lower capital and O&M cost; hence small value in the nominator, will result even to the smallest LCOE (see Figure 4 case a).

In addition, the capacity factor has more impacts as it is seen that variation in capacity factor caused more changes in LCOE, rather than the variation of discount rate. Moreover, comparing case a) & b) with case c) & d), shows that high capital cost (case c and d) will have higher range of LCOE with the increased of discount rate. For summary, the LCOE result for this study is in the range of 4.3 to 25.1 cents per kWh.

Analysis on Geothermal LCOE comparison with the latest Geothermal Price Policy

For comparison between BPP of 2017, established in MEMR Decree No. 1772 K/20/MEM/2018 (Table 5) and LCOE result (Figure 4), geothermal development will have more flexibility in Sumatera (some part), Kalimantan, Sulawesi, Nusa Tenggara, Maluku and Papua as the estimated LCOE are in the range of those regions' Local BPP (note: for case d is only with high capacity). In the other hand, geothermal price for Java, Bali, and some part of Sumatera, in which the Local BPP is lower than the National BPP, will determined by negotiation mechanism.

Table 4: Cost components of geothermal power plant based on several literature reviews.

Parameter	Unit	(LAZARD, 2017)	(IRENA, 2018)	(Schröder et al. 2013)
I. Capital Cost*	$/kW	4000 – 6400	2500 – 4500	4956 – 23,600***
II. O&M**	$/kW	262.8 – 350.4	110	187.9 – 594.8
III. Capacity Factor	%	85 – 90	60 - 80	

*including EPC cost, other construction cost, and Owner's other expenses
**including fixed O&M and variable O&M
*** >8000 : EGS technology

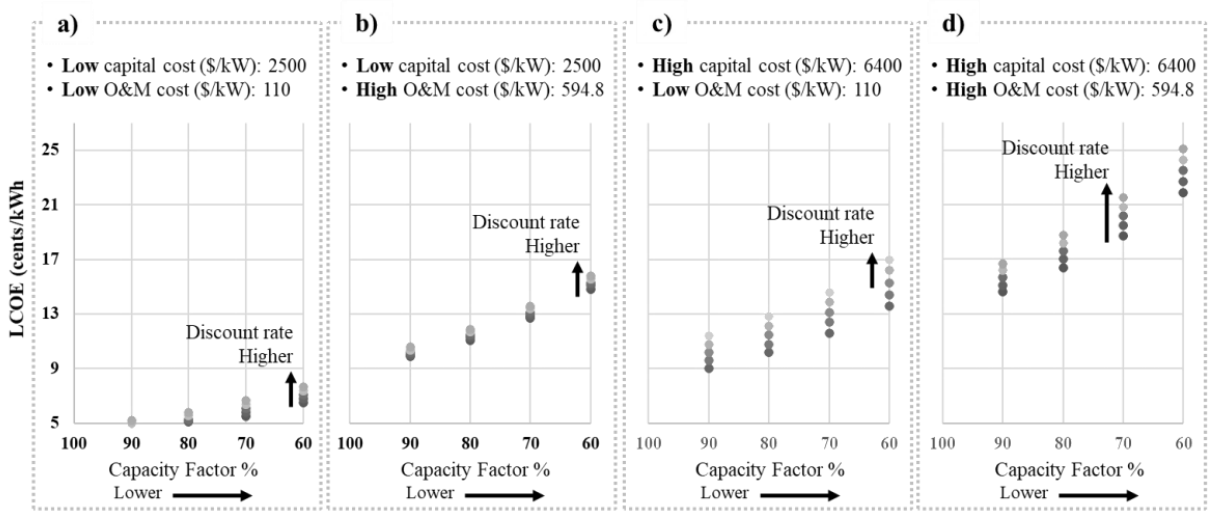


Figure 4: LCOE calculation results with variation of capacity factor (x-axis), capital and O&M cost (case a to d). Different value of discount rate is shown in LCOE result's color gradation; higher and lighter color of LCOE meaning higher discount rate value.

Table 5: List of BPP 2017; Local BPP and National BPP (MEMR Decree No. 1772 K/20/MEM/2018)

Region	BPP of 2017	
	Main Land	Islands or Sub-system
	cents/kWh	
Sumatera	7 – 11.1	12 – 20
Java – Bali	6.81	12.7 – 20
Kalimantan	8.6 – 12.6	20
Sulawesi	7.3 – 16.6	
Nusa Tenggara	13.9 – 18.1	
Maluku & Papua	13.1 - 20	
National	7.66	

FUTURE GEOTHERMAL DEVELOPMENT IN INDONESIA

Latest Development until Early 2018

In the last decade, geothermal power development in Indonesia has been actively expanded. The statistic shows that Indonesia's geothermal installed capacity at the end of 2017 is 1808.5 MW, doubled from installed capacity in 2004 (Figure 5). The largest development was occurred within 2016-2017 whereas details of additional capacity are presented below. Lists of additional power plants in 2016 is as follow:

1. Pertamina Geothermal Energy (PGE) had constructed and operated Ulubelu power plant unit 3 of 55 MW which delivering almost 380 GWh of electricity annually.
2. In Tompaso, Lahendong Field, unit 5 & 6 of 2 x 20 MW were built and commercially operated at the end of 4th quarter of 2017 by PGE and delivering 310 GWh annually.
3. In Sarulla, North Sumatera, a-110 MW of Geothermal Combined Cycle Unit (GCCU) was built and operated in Silangit Field by Sarulla Operations Ltd. (SOL). The GCCU unit consists of 1 Steam 60 MW turbine generator, 4 x 7 MW bottoming units and 2 x 11 MW brine units.

For the following is list of additional power plants in 2017:

1. Ulubelu unit 4 of 55 MW was commercially operated by PGE.
2. SOL had continued development northern field in Namora-i-Langit, Sarulla, where unit 2 (110 MW) of GCCU was commercially operated utilizing less similar scheme.

Up to early 2018 is listed as below:

1. SOL had completed final unit (unit 3) of 110 MW, resulting the total of 330 MW (unit 1, 2 &3) contract with PLN, and
2. 35 MW of Karaha Power Plant in West Java had also commercially operated by PGE.

Those power plants are contributed to 1948,5 MW installed capacity at the end of 1st semester 2018. The installed capacity plan by the end of 2018 is expected to reach 2043.5 MW, leaving the needs of 95 MW for another additional power plant.

Target of Geothermal Development in Indonesia

GOI has an optimistic updated target of geothermal development which has been mandated by Government Regulation No. 79 of 2014 which states that renewable energy mix should be increases from

7.7% in 2017 to 23% at the end of 2025. To fulfill this task, MEMR has elaborated geothermal roadmap which has been updated recently with the aims of achieving 7,241 MW in 2025.
Further in 2018, geothermal utilization is expected to increase by addition of:

1. 50 MW from geothermal wellhead power plant in Sorik Marapi using screw expander and binary power plant technology which currently is constructed by Sorik Marapi Geothermal Power,
2. 55 MW flash condensing power station in Lumut Balai, currently is built by PGE, and
3. 5 MW from Sokoria Field in Eastern Indonesia.

For 2019 plan, it is expected for additional power plant such as:

1. New technology of a built a-80 MW double flash condensing power station in Muaralaboh, expecting to be commercially operated in 2019 by Supreme Energy,
2. Jaboi power plant of 5 MW, and
3. Additional 50 MW from Sorik Marapi.

Further geothermal roadmap up to 2025 is shown in Figure 6, which is also compared with PLN's power supply business plan (PLN - RUPTL). In general, geothermal roadmap target is a bit higher than the RUPTL – PLN as it is optimistic target of the GOI. Significant additional development is indicated in the year of 2025 as the expectation of more commercially operated areas for achieving the Energy Mix Policy's target.

Potential Obstacles in Future Geothermal

Project Financing

The exploration cost will mainly be borne by the geothermal developers as they are not able to submit a loan proposal to the Bank due to requirement of feasibility study results which is which related to the certainty of geothermal resource capacity (Serdjuk et al, 2013). Thus, Bank's loan can only be utilized for the exploitation stage. Moreover, from view point of technology, drilling in higher temperature geothermal field is not the same as in conventional oil and gas. For this consideration, the beginning phase of geothermal development is categorized as high risk for both technologically and economically.

In effort to overcome this problem, GOI through the Ministry of Finance (MOF) had established geothermal fund policy, aiming to provide interesting investment condition for geothermal sector. The interest rate for the geothermal fund is differ from the usual high interest rate of the Bank. Further, its support types include loan, equity injection, and data provision for exploration phase conducted by the GOI or Geothermal SOE. For more details procedure, please refer to MOF regulation No. 62 of 2017.

As the latest geothermal fund policy was recently established in 2017, its implementation may not fully utilize yet, especially for loan to the IPP. However, this funding scheme is a high hope to become an accelerator for future geothermal development in Indonesia.

Price Determination

From comparison between geothermal LCOE result and BPP of 2017, further development should be carried out toward the outside of Java and Bali, as its low Local BPP might be found to be hard for geothermal developer to conduct geothermal power plant project. Although the negotiation can be done as it is written in the latest MEMR Regulation, uncertainty from negotiation period will still increase the project's risk.

One of possible solutions is to involve PLN during the tender process such as forming an early agreement, or head of agreement (HoA) regarding the price determination. The key purpose of this HoA is for balancing the needs for both PLN and geothermal developer; PLN as a single buyer of electricity will need confirmation of an adequate geothermal resource capacity, and on other hand, geothermal developer will need price guarantee especially regarding the negotiation mechanism for price determination. Moreover, MEMR (in this case Directorate of Geothermal) should take supervisor and facilitator role in case for any unexpected results or disputes occurred during the implementation phase.

Geothermal Power Plant Owned by PLN

In Indonesian electricity market, PLN which acts as single buyer for all electricity generation has also owned some geothermal power plants. This condition may be seen to have easier way to determine the geothermal price, but concern of monopoly issue will be raised.

The electricity sector mostly requires high investment cost which not any company or people could be the market player. Therefore, dominant player will naturally have more power than the others. However, vertically integrated electricity company will lead to fully monopolistic from supplier up to the seller to consumers, causing

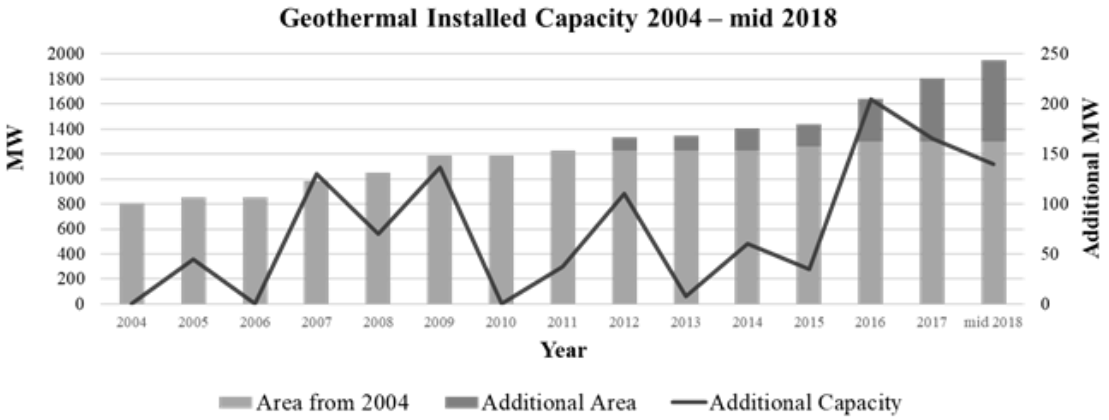


Figure 5: Geothermal Installed capacity from 2004 up to mid-2018. The darker grey color is new additional area, apart from the 2004 area (lighter grey color). The black line represents additional capacity value from the previous year (compiled from MEMR's data).

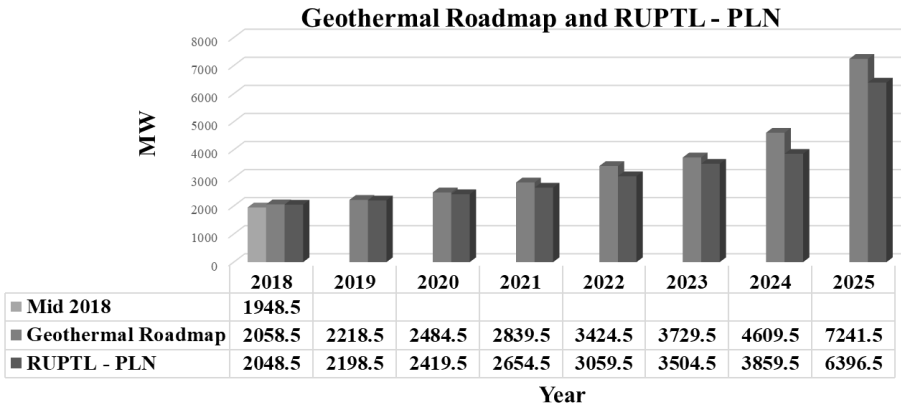


Figure 6: Comparison between geothermal roadmap (issued by MEMR) with RUPTL (power supply business plan) of PLN up to year of 2025 (compiled from MEMR's data).

several de-merits such as:

1. Price monopoly → may set higher price and price mechanism transparency will be concerned.
2. No flexibility in consumers; no other choice although if the consumers want to use electricity which generated from environmentally friendly technology.
3. Inefficient market → for long period, the market tends to be not able to grow.

CONCLUSIONS

1. The significant different for geothermal law is the revision of geothermal definition in which it was included with mining activity statement in the previous law. As mining terminology is revoked, the geothermal development can be conducted in conversion forest whereas some of geothermal potentials are located; thus, it may increase geothermal utilization. For consideration, cooperation with Ministry of Environment and Forestry should also be done in regards of policy view and permits for solid and comprehensive legalization.
2. Up to 2017, Indonesia has reached 17.74% of its geothermal policy impact indicator, which is comparing the additional installed power plant from the year 2004 to the Indonesia Energy Mix target of 2025.
3. For LCOE analysis, high capacity factor will have significant impact to lower the calculation result. As in Figure 4, high total cost with higher capacity factor (case d) will have similar LCOE with low total cost with low capacity factor (case b). Moreover, the 10% decreased of capacity factor will produce even lower LCOE rather than 1% decreased of discount rate. To be noted that, in this study, LCOE calculation does not yet considerate of financing cashflow (equity and debt) and the discount rate value is one of the input into the calculation.
4. Analysis between the latest BPP and LCOE calculation of geothermal power plant explains that development of new GWA will be more feasible in outside Java, hence expansion toward the Eastern and some are in Sumatera.

Further study to foreseen feasibility of new geothermal utilization in outside Java should be considered in correlation with its area's electricity demand.

5. For future geothermal development, geothermal roadmap which is estimated by the GOI (in this case is MEMR) and PLN's power supply business plan are quite match. The higher target of geothermal roadmap is based the optimistic plan from GOI to achieve Energy Mix Target of 2025.
6. Some potential obstacles during geothermal development are discussed, such financing project risk in term of geothermal developers will bear the upfront exploration cost and price determination based on negotiation. Some possible solutions are also presented; expecting that mutual understanding and good cooperation could be obtained, then later could provide benefit for all related parties.
7. In the end, GOI had issued several regulations aiming to accelerate geothermal development and to achieve Indonesia Energy Mix Target. The important task for now and further is how to implement the procedure of those regulation efficiently, taking consideration for all aspects and all parties. For that condition, the GOI in here MEMR, has crucial role as supervisor and facilitator. Furthermore, the policy consistency will result more certainty for both geothermal developer and Investors to have high interest and start developing geothermal in Indonesia.

ACKNOWLEDGEMENT

This work was supported by the Energy Efficiency & Resources of the Korea Institute of Energy Technology Evaluation and Planning (KETEP) granted financial resource from the Ministry of Trade, Industry & Energy, Republic of Korea (No. 20164010201120) and the "R&D Project on Environmental Management of Geologic CO2 Storage" from the KEITI (Project Number: 2018001810002).

REFERENCES

Government Regulation Number 59 year 2007 concerning Geothermal Business Activity.

Government Regulation Number 79 of 2014 on National Energy Policy.

Hochstein, M. P., and Sudarman, S. (2008), "History of geothermal exploration in Indonesia from 1970 to 2000". *Geothermics*, Volume *37*, Issue 3, 220–266.

IRENA. (2018), "Renewable power generation costs in 2017". *International Renewable Energy Agency, Abu Dhabi.*

Law of The Republic of Indonesia Number 21 year 2014 about Geothermal.

Law of The Republic of Indonesia Number 27 year 2013 concerning Geothermal.

LAZARD. (2017), "Lazard's levelized cost of energy analysis - version 11.0". Retrieved from https://www.lazard.com/media/450337/lazard-levelized-cost-of-energy-version-110.pdf.

MEMR Regulation Number 7 of 2017 concerning Procedure for Setting Benchmark Selling Prices of Metallic and Coal.

MEMR Regulation Number 17 year 2014 concerning Purchase of Electricity from Geothermal Power Plant and Geothermal Steam for Geothermal Power Plant by PT Perusahaan Listrik Negara (PERSERO).

MEMR Regulation Number 1772 K/20/MEM/2018 about Amount of Basic Cost of Provision of Generation for PT Perusahaan Listrik Negara (PERSERO) for 2017.

MEMR Regulation Number 50 of 2017 on Utilization of Renewable Energy Sources for Power Supply.

Nicholls, J., Mawhood, R., Gross, R., and Castillo, A. (2014), "Evaluating renewable energy policy: a review of criteria and indicators for assessment". *International Renewable Energy Agency (IRENA)*

Peraturan Menteri Energi dan Sumber Daya Mineral (MEMR) Nomor 2 tahun 2011 tentang Penugasan kepada PT Perusahaan Listrik Negara (PERSERO) untuk Melakukan Pembelian Tenaga Listrik dari Pembangkit Listrik Tenaga Panas Bumi dan Harga Patokan Pembelian Tenaga Listrik oleh PT Perusahaan Listrik Negara (PERSERO) dari Pembangkit Listrik Tenaga Panas Bumi.

Peraturan Menteri Energi dan Sumber Daya Mineral (MEMR) Nomor 14 tahun 2008 tentang Harga Patokan Penjualan Listrik Tenaga Panas Bumi.

Peraturan Menteri Energi dan Sumber Daya Mineral (MEMR) Nomor 22 tahun 2012 tentang Penugasan kepada PT Perusahaan Listrik dari Pembangkit Listrik Tenaga Panas Bumi dan Harga Patokan Pembelian Tenaga Listrik oleh PT Perusahaan Listrik Negara (PERSERO) dari Pembangkit Listrik Tenaga Panas Bumi.

Peraturan Menteri Energi dan Sumber Daya Mineral (MEMR) Nomor 32 tahun 2009 tentang Harga PAtokan Pembelian Tenaga Listrik oleh PT PLN (PERSERO) dari Pembangkit Listrik Tenaga Panas Bumi.

Schröder, A., Kunz, F., Meiss, J., Mendelevitch, R., & Hirschhausen, and C. von. (2013), "Data Documentation - Current and Prospective

Cost of Electricity Generation until 2050". *Deutsches Institut für Wirtschaftsforshung, Berlin.*

Serdjuk, M., Reif, T., Dumas, P., Angelino, L., and Tryggvadóttir, L. (2013), "Geothermal Investment Guide". *GeoElec PRoject Deliverable 3.4.* Retrieved from http://www.geoelec.eu/wp-content/uploads/2011/09/D3.4-Investment-guide.pdf

U.S Department of Energy. (2015), "Levelized cost of energy (LCOE)". *DOE Office of Indian Energy.* Retrieved from https://www.energy.gov/sites/prod/files/2015/08/f25/LCOE.pdf

U.S Energy Information Administration. (2016), "Capital Cost Estimates for Utility Scale Electricity Generating Plants". *Independent Statistics & Analysis U.S. Departement of Energy, Washington, DC*

SEEKING THROUGH THE POTENTIAL OF GEO-TOURISM AT IJEN, EAST JAVA, INDONESIA FOR FURTHER DEVELOPMENT

Dhara Adhnandya Kumara[1], Farhan[1], Faris Maulana Yunus[1], Haidar Firdaus Avicienna[1], and Yunus Daud[2]

[1]Study Program of Geophysics, Faculty of Mathematics and Natural Sience, UI
[2]Master Program in Geothermal Exploration, Graduate Program of Physical Science, UI
Email: dhara.adhnandyak@gmail.com

ABSTRACT

Ijen is a sub-district located in Bondowoso, East Java, Indonesia which now focused for geothermal exploration because of the enormous potential. Geologically, Ijen located in a huge ancient caldera that only remains in the northern while the southern has been replaced with new volcanoes, more than 10 volcanoes. Furthermore, there also preserve a huge fault crossing along the caldera from north to south which can be seen cutting in the middle of the northern caldera. Along the fault, there are also spotted several geothermal hot spring manifestations. Geo-tourism not only focuses on the geological aspect but also focus on the fauna, flora and the tradition in the site. The villager of Ijen has several interesting daily activities which potential to be developed as an educational tourism. Most of the Ijen's villager's works as a farmer have coffee and cabbage farm, also other herbs. This research has done by observing the activities of the people around and by visiting several objects that have potential to be developed as geo-tourism site. The diversity of flora and fauna also can be found at Ijen. Dominant flora which can be found at mountain slope is pine, while near the crater Mentigi and Edelweiss dominate. *Kumbang*, *lutung jawa*, *babi hutan*, *garangan*, and *luwak* are the endemic fauna in this site, also several endemic birds such as *Kepala ungu*, *cekaka jawa*, *sepah gunung*, *cucak gunung*, and *kipasan bukit*. The aim of this research is to introduce the potency of Geo-Tourism at Ijen, focused in the geological condition with an outlook to be able to help the development of tourism at Ijen and help to increase the local income. Furthermore, hopefully this site also can be developed as a geothermal educational field along with geological educational field.

Keywords: Geo-Tourism, geothermal educational, local tourism, Ijen.

INTRODUCTION

Geo-tourism can be defined as a concept of tourism activities that visit interesting geological spots (Hendratno, 2002). Geo-tourism is one of geopark aspect that has economic value which can develop the economy of local communities. This term was first introduced by a geologist from Buckinghamshire Chilterns University in England named Tom Hose. Geo-tourism has two important elements; there are conservations and educations (Kubalíkova and Kirchner, 2016).

This study focused on the introduction of geo-tourism potency at Ijen, East Java. The study takes place at sub-district of Ijen which located at Bondowoso district, East Java province, Indonesia. This site has high geo-diversity. Geologically Ijen Volcanic Complex (IVC) was form around the Pleistocene while the ancient caldera itself was formed by Plinian eruption in 0.2 – 0.05 Ma. Currently only the northern caldera left while the southern has been replaced by younger volcanoes. Several hills can be found at the center and southern site of this caldera where these hills have wonderful view and potential to be geo-tourism site.

This area is known for having abundant potency of geothermal energy. The geothermal potency was shown by the presence of several manifestations in the northern such as hot spring, also acidic lake at Ijen crater. Some of these manifestations have been utilized and developed as tourism area, however based on the observation done, the facility that was build left abandoned with bad condition.

The aim of this study is to introduce the high geo-diversity, potential ecotourism, and educational tourism at Ijen. However, this study mostly focused on the geo-diversity only while the other aspect needs more understanding in the future.

METHODS

The methods used to complete this study are literature study and observation by visiting several sites around the study area. Study literature was conducted to understand the basic principal of geo-tourism site and how a site can be accepted as tourism site. Due to the potency of geothermal at Ijen, literature study related with geo-tourism at geothermal area also conducted to get better understanding. Interview with local wisdom and observation at several sites has been done to find out what is needed the most for further development on these geo-tourism sites. By those analyses, the summary of potential geo-tourism site is made as introduction of geo-tourism at Ijen, East Java.

GEOLOGICAL SETTING

Tectonic activity at Java Island cannot be separated from Indo-Australian plate below it. This plate extends from Sumatra to Nusa Tenggara Timur. Ijen itself located at the margin between Java block and Sumba block (Smyth et al, 2008). According to Smyth et al, Java block and Sumba block have counterclockwise movement, however Sumba block movement is faster than java block. The different movement speed of two block make this area an active margin. Furthermore, as an active margin, it can generate major fault structure that affect Ijen area.

The study area is old Ijen volcanic complex (IVC) marked by a large caldera at northern part. Old Ijen Volcanic Complex was formed around pleistocene (Bemmelen, 1949). IVC is estimated has 15 times eruptions center (Caudron et al, 2015; Sujanto et al, 1988). Big pilinian eruption at 200,000-50,000 years ago ejected 80km^3 volcanic material and produce huge caldera. As seen today, the remaining of caldera is presence only left in the northern whereas the southern region has been replaced by new small volcanoes formed by intrusion. These younger mountains divided into 2 groups: Intra Caldera and Caldera Rim (Handley et al, 2007). Alignment river or mountains can indicate fault structure, such as Blawan fault at northern area. This Blawan fault was thrown down the wall caldera at northern part into waterfall. Fault structures at IVC can turn out as pathway to occurrence of geothermal manifestation in this area (Figure 1).

SOCIAL CONDITION AT STUDY AREA

The major livelihoods of the local resident are having coffee farm, cabbage farm, strawberry farm, and others plant that growth at plateau. The products of their farm will be distributed either for the local resident or for the citizens at Bondowoso, Banyuwangi, and others. The resident also has husbandry with major animals are cow and goat. There is a unique habit where people build the barnyard far away from the village to avoid theft.

Economic activity at the study area mostly depends on selling plantation products (other than coffee). While the coffee farms are owned and managed by PTPN (PT Perkebunan Nusantara) so that the residents who take care of these farms will be paid by PTPN. Tourism activities also have huge potency to be the source of economic activity here (Suryandari, 2005). However, it's not well managed yet. While around Ijen crater, sulfur mining becomes another source of local income.

Motorcycle dominates the local transportation around study area because it's easier to use around the farm, instead of using car. Public transportation also available but only has route to the town (not for short term travel).

Education of the resident at study area mostly graduates from Junior High School or Vocational High School. Sub-district of Ijen only has 13 schools there are 10 elementary school, 2 Junior High School, and 1 Vocational High School while no Senior High School available, except at Bondowoso city.

INTERESTING GEOLOGICAL SITE AT STUDY AREA

Description of the condition for each potential site can be shown below. These descriptions will include the geological condition, activities that can be done, and the condition in the site which make the site considerable as a geo-tourism object.

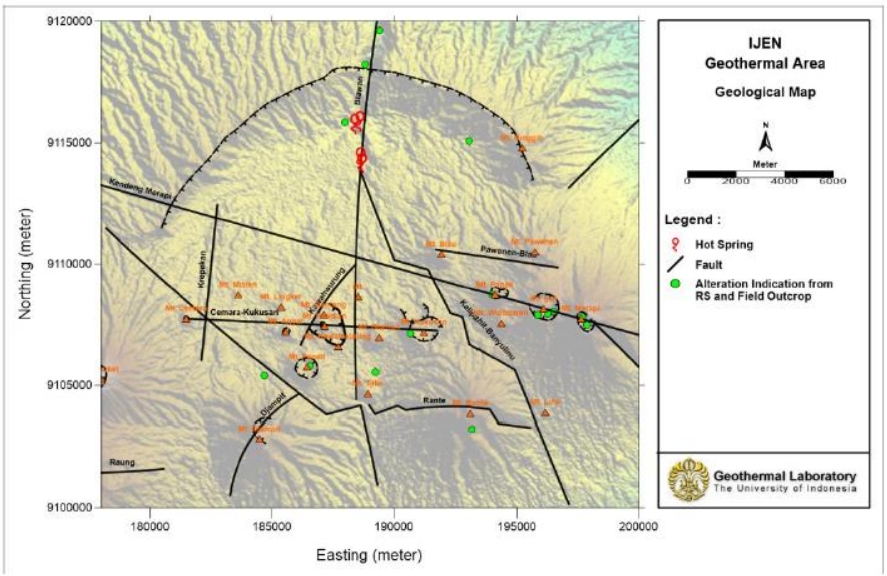


Figure 1: Geological map of Ijen Geothermal Area.

Ijen Crater

Ijen crater is a part of Ijen volcano which located at the administrative border between Bondowoso and Banyuwangi regency. The elevation of Ijen volcano is 2799 meters above the mean sea level. In the middle of crater spotted a lake which has a unique color. The color of the lake can be switch between blue or green (Riyadi et al, 2012), (Figure 2). Moreover, a rare blue flame or blue fire presence in the crater that becomes an interesting tourism object (Figure 3). The blue fire can be found either at Ijen or at Iceland only, it is a rare event.



Figure 2: Ijen crater with blue-green acid like.

Ijen crater was denoted as a nature preserve in 1920, while based on Indonesia's minister of algaculture decree Ijen was denoted as nature tourism park of Ijen Crater in 1981 (Taman Wisata Alam Kawah Ijen).

Considering the geological condition and the fact that Ijen crater is currently a tourism site, developing Ijen crater as a geo-tourism site would be possible and beneficial. Not only a tourism site, Ijen can be made as an educational tourism site for learning the origin of geology at Ijen. Several geo-tourism activities that can be done here are:

1. Beautiful blue-green color acid lake.
2. Good place to learn the geologic origin of Ijen crater and Ijen volcano.
3. Good place for photo shooting, either for family or pre-wedding shot.
4. Seeing blue flame which only can be found either at Ijen or Iceland.
5. Others.

Wurung Crater

Wurung crater located at Jampit village, sub-district of Sempol, Bondowoso, East Java or in the western side of Ijen crater. This crater is surrounded by hills which covered with grass forming a meadow (usually called savanna) (seen Figure 5 and Figure 6).



Figure 3: Blue Fire at Ijen (Triphobo, n/d).



Figure 4: Geo-tourism activity at Ijen Crater.

The place can be reach by car or motorcycle, however motorcycle would be recommended instead of car due to the condition of the road which can accommodate one car only. But to reach the peak the site can be reach by walk only. The road has not been paved yet, so when there is vehicle passing through there will be dust disperse.



Figure 6: Savanna at Wurung Crater.



Figure 6: View at Wurung Crater.

The beautiful scenery made this place worthy develop as a tourism site. Several cows owned by the local resident usually spotted here which made the view more wonderful (Figure 7) Moreover, educational tourism of geological condition also can be conducted here because the place itself has interesting geologic origin. Several geo-tourism potencies in this site are:

1. Good place to learn geologic origin of Kawah Wurung.
2. Good place for photo shooting, either for family or pre-wedding shot.
3. Others.

Further development that can be done in the site:

1. Improvement of facilities for the visitors.
2. Maintenance of the facilities need to be considered.
3. The place need keepers for the maintenance.



Figure 7: Several cows owned by the resident at Wurung Crater.

Kali Pahit

Kalipahit is one of the waterfalls located at the foot of ijen volcano. Kalipahit comes from Ijen crater directly. The color of the water flow is green because there is a high contain of sulfur. Named Kalipahit because the taste of the water is not fresh but bitter. The view around this mini waterfall is very beautiful and this little waterfall used as medicine for various skin diseases.

Visitors can use either motorcycle or car because the location is located on the roadside to the crater of ijen. Public transportation also can be used from terminal Bondowoso.

A lot of volcanic rock outcrops exist in Kalipahit. Geotourism potential in this place include:

1. A good place to see the beautiful views of volacanic lakes.
2. A good destination for nature and community lovers.
3. Others.

Development of Kalipahit area include:

1. Improvement of facilities for the visitors.
2. Build toilets for the visitors.
3. Build rest area or canteen for the visitors.



Figure 8: Kalipahit river flow.



Figure 9: Geo-tourism activity at Kalipahit.

Blawan Waterfall

In addition to the Kalipahit there is also a waterfall in Blawan area. Blawan waterfall is located at Kamuyar village, sub-district of sempol

Bondowoso. Blawan waterfall is the "downstream" of Kalipahit which is a flow from Ijen crater that has sulfur content. One of the unique things in this waterfall is the flow of the river fall directly into the land like Niagara Falls in America. Debit flow of the waterfall is very heavy, so the atmosphere around the waterfall Blawan sounds rumble. The plants grow very fertile and lush (seen Figure 10 and Figure 11).

Blawan Hot-spring

In the blawan area there is also a source of hot water containing sulfur and natural awake, visitors can usually soak their feet. Access the journey to blawan waterfall using stairs about 5 minutes and continued down the same stairs (Figure 12).

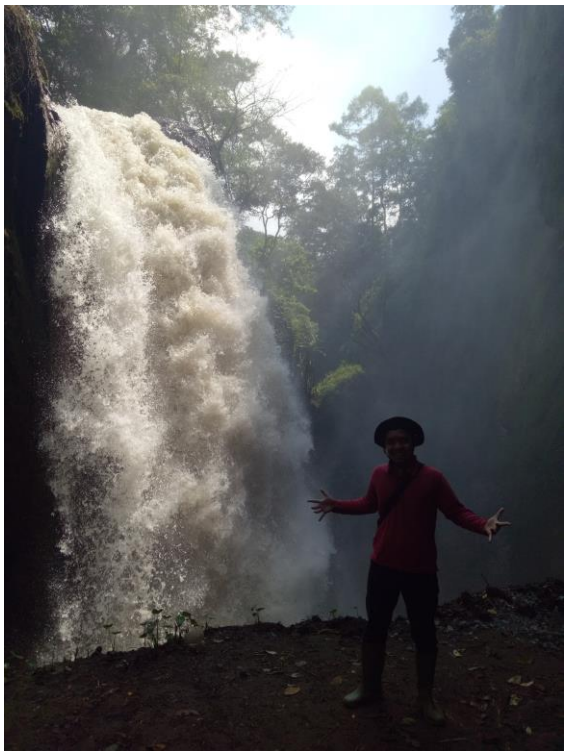


Figure 10: Blawan waterfall.

Teletubbies Hills

Teletubbies hills (the local resident called it so) located around the middle and southern part of Kendeng Caldera (Figure 15). At this point, several hills which growth with grass and weeds can be seen. The fault trace which separate northern part of Kendeng Caldera can be seen at this site too (Figure 13).

This place can be reached by motorcycle or car, however the peak of the hills can be reach by walk only with a bit effort. Geo-tourism activity that can be done here are:

1. Light hiking adventure.
2. Good spot for photo shooting.
3. Good place to enjoy beautiful scenery.
4. Good place to learn geological history of Ijen, because from the peak of the hills a lot of geological story can be told.



Figure 11: View at Blawan Waterfall.

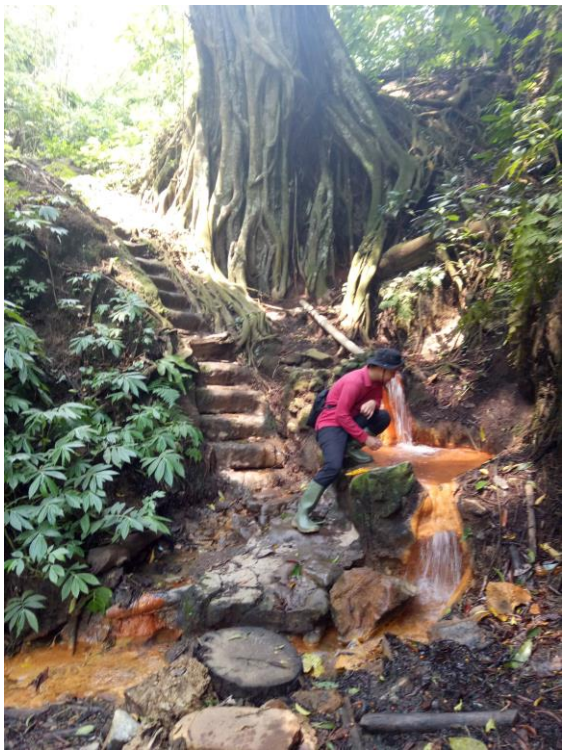


Figure 12: Geo-toruism activity at Blawan Hot-Spring.



Figure 13: Trace of fault at nothern caldera can be seen from Teletubbies hills.



Figure 14: Hills covered with grass and weeds

Mini Niagara

Mini Niagara located at Kalianyar village, sub-district of Sempol, Bondowoso (Figure 15). It is called mini Niagara because the waterfall has wonderful view exactly like Niagara waterfall has but with smaller size. The site has been managed by several people (mostly local resident), however it's not well managed yet.

It's located near Arabica Coffee factory which managed by PTPN, so that the visitors can reach this place by car or motorcycle because the road is huge and already being paved. Several geo-tourism activities that can be done here are:

1. Good place to learn about geological history and learning about the source of the river flow.
2. Good place to take picture.
3. Family recreation site.
4. Place to feel clean and fresh water.
5. Others.

ECOLOGICAL DIVERSITY AT STUDY AREA

As a nature preserve or nature tourism park, Ijen has high biodiversity. Various flora and fauna can be found at Ijen and would become valuable for a tourism object. There are two important parameters which support ecotourism for a site, the first one is related with natural resources which can be the object or subject for tourism and get a good acknowledgement from the local government, supported by the local community. The second one is the presence of endemic fauna.

In this study, Ijen is proposed to get more recognition for ecotourism. Dominant flora which can be find at mountain slope is pine, while near the crater Mentigi and Edelweiss dominate. Meanwhile, dominant fauna that has been identified around Ijen are divided in two classes there are mammals and birds. There were 16 species of mammals in the site, for example *macan kumbang (Panthera pardus melas), kucing hutan (Felis chaus), ajag (Cuon alpinus javanicus), lutung jawa merah (Trachypithecus auratus), tupai terbang (Pteromyini), kijang (Muntiacus), babi hutan (Sus Scofra*), and *luwak*. While the endemic birds are *elang, cekaka jawa, walik kepala ungu, ayam hutan hijau, cucak gunung, kipasan bukit* and *sepah gunung.*

EDUCATIONAL TOURISM POTENCY

The site also potential to be developed as educational tourism site. The role of educational tourism is expected to connect the related aspects of environmental concepts and geosciences knowledge values so that the information can be delivered to the community. Educational tour can be done with various creative and innovative programs such as gardening program, particularly comprehensive learning of gardening management for plantation products such as strawberry, cabbage, coffee, etc. A collaboration with PTPN (PT Perkebunan Nusantara) who is currently owned mostly all plantation at Ijen (specifically coffee) and local resident can be done in order to develop this agritourism. Moreover, by this educational tourism hopefully it can help encourage the communication between the tourist who want to understand gardening management with the local resident. In addition to the program, there are still handicraft programs from Sulfur at Ijen Crater Area. Miners who also have the ability to make handicrafts from sulfur can be empowered within the scope of educational tourism.



Figure 15: Mini Niagara Waterfall

CONCLUSION

The conclusions of this study are Ijen area has a lot of potency to be developed as geo-tourism site. There is Ijen crater which already has a good management, also several sites which not well manage yet tough it has great view like Wurung Crater, Blawan Waterfall, Blawan Hot-Spring, Telletubies Hills, and Mini Niagara. Collaboration between local government, local residents, investor, and society needed for further development. Furthermore, further geological study also needed to understand the geological history at the study area for geo-educational purpose.

REFERENCES

Bemmelen, R. W. V. (1949), "The Geology of Indonesia Vol. IA General Geology of Indonesia and Adjacent Achipelagoes". *Government Printing Office: The Hague 1949*.

Caudron, C., Syahbana, D. K., Lecocq, T., Hinsberg, V. V., McCausland, W., Triantafyllou, A., Camelbeeck, T., Bernard, A., and Surono. (2015), "Kawah Ijen volcanic activity: A review". *Bull Volcanol*. 77:16.

Handley, H. K., Macpherson, C. G., Davidson, J. P., Berlo, K., and Lowry, D. (2007), "Constraining Fluid and Sediment Contributions to Subduction-Related Magmatism in Indonesia: Ijen Volcanic Complex". *Journal of Petrology*, volume 00, number 0, p.1-29.

Hendratno, A. (2002), "Perjalanan Wisata Minat Khusus Geowisata Gunung Merapi (Studi di Lereng Merapi Bagian Selatan, Yogyakarta)", *Jurnal Nasional Pariwisata*, vol. 2, no. 2.

Kubalíková, L., and Kirchner, K. (2016), "Geosite and Geomorphosite Assessment as a Tool for Geoconservation and Geotourism Purposes: a Case Study from Vizovická vrchovina Highland (Eastern Part of Czech Republic)", *Geoheritage*, 8:5-14.

Riyadi, S., Hadiwidjojo, D., Djumahir., and Hakim, L. (2012), "Daya Saing Daerah Tujuan Wisata (Studi Kasus Rendahnya Daya Saing Taman Wisata Alam Kawah Ijen Banyuwangi)". *Jurnal Aplikasi Manajemen Universitas Brawijaya*. Vol 10, No 3 (2012).

Smyth, H. R., Hall, R., and Nichols, G. J. (2008), "Cenozoic volcanic arc history of East Java, Indonesia: The stratigraphic record of eruptions on an active continental margin". *The Geological Society of America*, Special Paper 436.

Sujanto, M., Syarifuddin. Z., and Sitorus, K. (1988), "Geological Map of the Ijen Caldera Complex, East Java". *Volcanology Survey of Indonesia*: Bandung, Indonesia.

Suryandari, E. Y. (2005), "Peluang Usaha Ekowisata Cagar Alam/Taman Wisata Alam Kawah Ijen di Kawasan Taman Nasional Alas Purwo". *Jurnal Analisis Kebijakan Kehutanan*, 2.1. 13-26.

COMPARISON BETWEEN AUTOMATIC LINEAMENTS EXTRACTION AND MANUAL LINEAMENTS EXTRACTION METHODS FOR GENERATING FAULT AND FRACTURE DENSITY MAP: A CASE STUDY FROM CANDI UMBUL TELOMOYO GEOTHERMAL FIELD, MAGELANG, CENTRAL JAVA

Albertus Ivan[1] and Jason[2]

[1]Geothermal Engineering Department, Bandung Institute of Technology, Bandung, Indonesia
[2]Geological Engineering Department, Trisakti University, Jakarta, Indonesia
Email: albertusivanw@gmail.com; jasonkartasasmita@yahoo.com

ABSTRACT

Fault and Fracture Density (FFD) method is one of the method that can be utilized to delineate geothermal prospective area by extracting and analysing lineaments from various data sources, such as DEM or satellite image. This method is used to aid and simplify early geothermal exploration stage because it is relatively cheap and less time consuming. Lineaments extraction is a crucial part to generate the FFD map. Manual lineaments extraction is the common method that is usually used, but it is a tedious process and the quality of the extracted lineaments depends on the skills and the objectivity of the interpreter. This paper aims to extract lineaments automatically by using panchromatic band (8) satellite image from Landsat-8 on the study area of Candi Umbul Telomoyo geothermal field, Magelang, Central Java and compare it with the result generated from manual lineaments extraction. Four (4) applications were used in this study: ENVI 5.1, PCI-Geomatica 2015, ArcGis 10.3, and RockWorks 16. Before starting the extraction processes, the satellite image was processed with several methods, such as layer stacking and forward PC rotation to obtain a better image quality. Automatic lineaments extraction can be done by adjusting the algorithm parameter of 'Line: Lineament Extraction" module on PCI-Geomatica 2015. The result from the automatic lineaments extraction method, which is the length of the lineaments, the FFD map, and the rose diagram, shows more or less similar result as compared to the manual lineaments extraction that had been done by the team from Pusat Sumber Daya Geologi (PSDG) Bandung on 2011.

Keywords: Automatic Lineament Extraction, Candi Umbul Telomoyo, FFD, Landsat-8, Rose Diagram.

INTRODUCTION

In the geothermal exploration process, one of the method that is used to deliniate the prospect zones is lineament analysis from satellite image. From this analysis, the highest geological structures density zones can be detected. These geological structures are potentially permeable zone that can act as paths for thermal fluid to flow from the reservoir at depth to the shallower level (Suryantini and Wibowo, 2010). At some geothermal exploitation activity, it has been proven that these permeable zones are significant drilling targets to place production wells (Soengkono, 1999a and 1999b).

The lineament analysis method have been used many times for geothermal exploration. However, the method that is used until today is manual lineament extraction. Meanwhile, there is another method, which is automatic lineament extraction method by using several software that is faster and shows more or less similar result as compared to the manual lineament extraction. Therefore, this paper aims to show that automatic lineament extraction can be used and more efficient compared to the manual lineament extraction.

This case study was held at Candi Umbul Telomoyo geothermal field, which covers Temanggung Regency, Magelang Regency, Boyolali Regency, Semarang Regency, and Salatiga City, Central Java Province, Indonesia (Figure 1).



Figure 1: Location of the study area.

GEOLOGICAL SETTING

Tectonic Setting

Java Island is located at the active margin plates between Eurasia continental plate and Indian oceanic plate which has been colliding since Late Cretaceous. The major tetonic elements as an effect of Eurasian and Indian plate interaction are subduction zone, magmatic-volcanic belt, accretionary crust, back-arc basin, and fore-arc basin (Figure 2). As the result, Java Island is composed by the combination between Eurasia continental crust (mostly West Java and northern part of Central Java), accretionary crust between two

plate (southern part of West and Central Java and mostly East Java), magmatic and volcanic igneous rock of Java volcanoes belt, and all the sedimentary rock derived from it. In this case, Central Java position becomes unique because this area is a transition zone between continental crust and accretionary crust (Satyana and Purwaningsih, 2002).

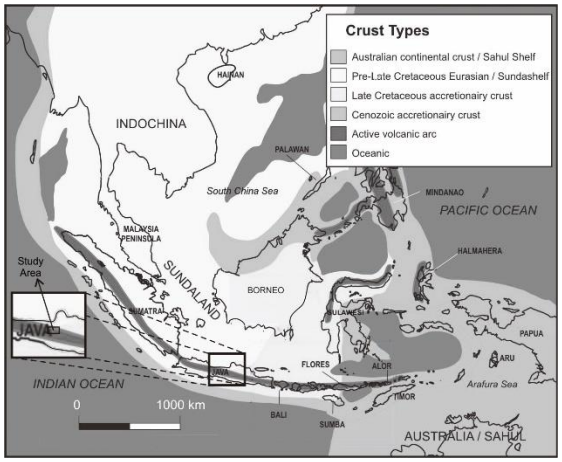


Figure 2: Map of Southeast Asia showing the different crustal type in the region (Doust and Lijmbach, 1997).

Physiography

Physiographically, Candi Umbul Telomoyo geothermal field is located in the North Serayu mountain range zone (Figure 3). In these zone, a volcanic complex were formed in NW-SE trend, which is Mount Ungaran-Telomoyo-Merbabu-Merapi ranges that is located at quarternary volcanic environment. The products of the volcano are pyroclastic rocks and lava with andesit-basaltic composition (Hermawan and Rezky, 2011).

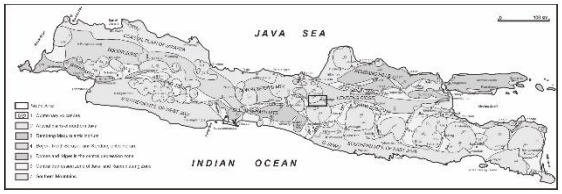


Figure 3: Physiographic sketchmap of Java and Madura island (Van Bemmelen, 1970).

Stratigraphy

Stratigraphy of the study area was arranged based on the relative connection between each lithology unit. The naming of it is based on the eruption center, mechanism, and the genesis of the lithology. Based on the field research (Hermawan and Kholid, 2010), the lithology of the study area can be separated into 18 units, which consists of one sedimentary rock, 16 volcanic rocks, and one surface deposit (Figure 4).

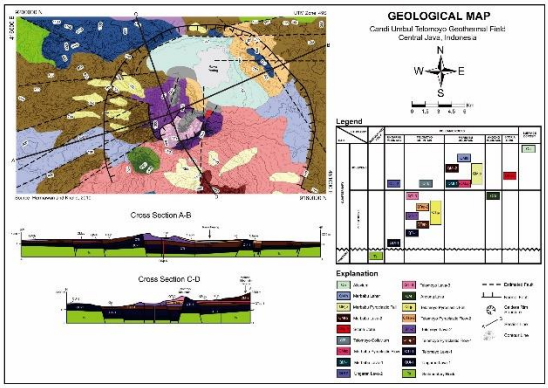


Figure 4: Geological map of Candi Umbul Telomoyo geothermal field (Hermawan and Kholid, 2010).

Structure

There are two types of geological structures that develops at the study area, the volcanic structures and tectonic structures. This volcanic structures were formed because of the Telomoyo Mountain volcanic activity, so it created caldera rim structure and the normal faults with NW-SE trend (Figure 4). These structures also provides the presence of Candi Umbul and Pakis Dadu geothermal manifestations (Hermawan and Kholid, 2010).

DATA

The data used in this study is Landsat 8 OLI/TIRS image (Path 120 Row 65). There are 11 spectral bands. Band 1 until 9 are Operational Land Imager (OLI) spectral bands and band 10 and 11 are Thermal InfraRed Sensor (TIRS) spectral bands (Table 1) (Loyd, 2013). Band 8 was chosen for this study because band 8 is a panochromatic band with 15 meters resolution so it is useful in the extraction of geological formations and rock features (El-Sawy et al. 2016) (Figure 5).

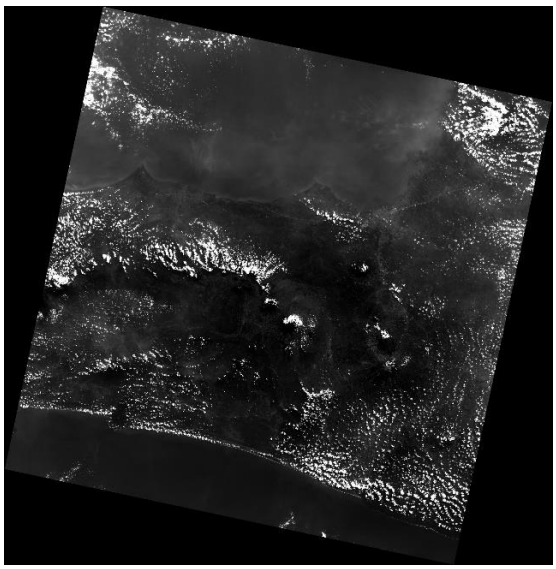


Figure 5: Satellite image of band 8 from Path 120 Row 65, acquisition date on June 6, 2018 (EarthExplorer, 2018).

Table 1: Landsat 8 OLI/TIRS bands (Loyd, 2013)

Band Number	Length (µm)	Resolution
1	0.433 – 0.453	30 m
2	0.450 – 0.515	30 m
3	0.525 – 0.600	30 m
4	0.630 – 0.680	30 m
5	0.845 – 0.885	30 m
6	1.560 – 1.660	30 m
7	2.100 – 2.300	30 m
8	0.500 – 0.680	15 m
9	1.360 – 1.390	30 m
10	10.6 – 11.2	100 m
11	11.5 – 12.5	100 m

METHODOLOGY

The aim of this paper is to compare automatic lineament extraction method and manual lineament extraction to show that the automatic method is more effective than the manual method because it takes less time to generate. There are four applications that are used in this study, which is ENVI 5.1, PCI-Geomatica 2015, ArcGis 10.3, and RockWorks 16. The flowchart of the automatic lineament extraction are shown in (Figure 6).

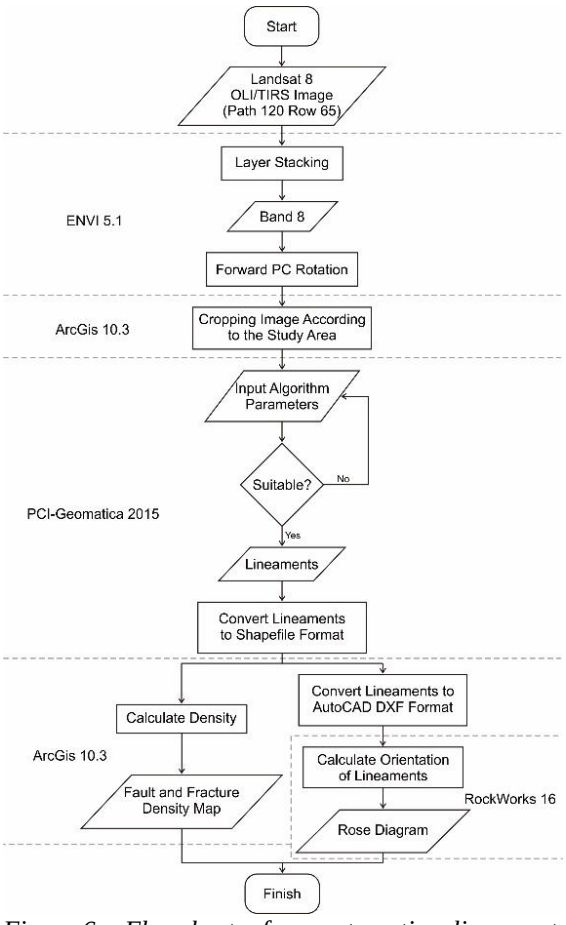


Figure 6: Flowchart for automatic lineament extraction.

The first step is layer stacking. This process aims to combine all the bands into one single file. Second, apply the forward PC rotation process to band 8. This process was done to remove the noises from the satellite image (Figure 7). After the noises are removed, the image is cropped according to the study area (Figure 8).

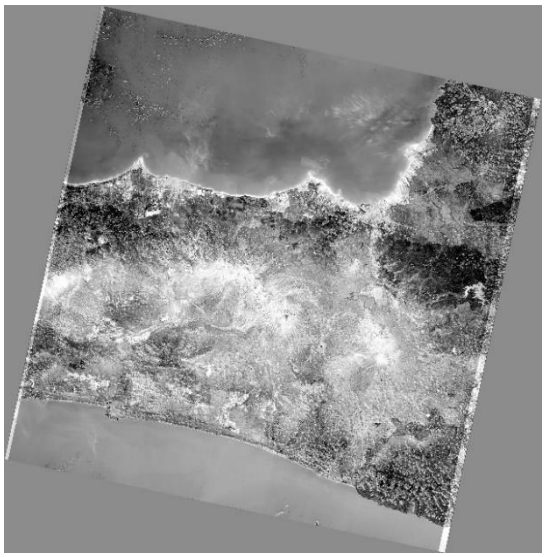


Figure 7: Satellite image of band 8 after applied by forward PC rotation.

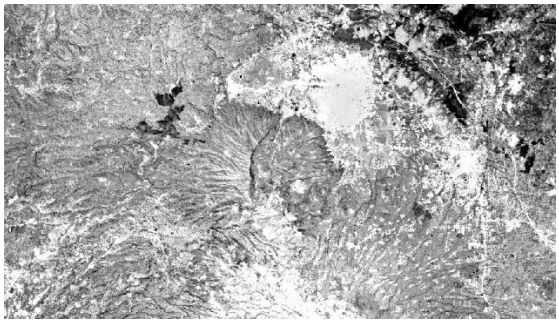


Figure 8: Satellite image of band 8 after applied by forward PC rotation and cropped according to the study area.

The next step is extracting the lineament using algorithm parameters. These parameters are explained briefly according to the Sarp (2005). There are six parameters used in the algorithm:

RADI (Filter radius): This parameter specifies the radius of the edge detection filter (in pixels). It roughly determines the smallest-detail level in the input image to be detected. The data range for this parameter is between 0 and 8192.

GTHR (Gradient threshold): This parameter specifies the threshold for the minimum gradient level for an edge pixel to obtain a binary image. The data range for this parameter is between 0 and 255.

LTHR (Length threshold): This parameter specifies the minimum length of curve (in pixels) to be considered as lineament or for further consideration (e.g., linking with other curves). The data range for this parameter is between 0 and 8192.

FTHR (Line fitting error threshold): This parameter specifies the maximum error (in

pixels) allowed in fitting a polyline to a pixel curve. Low FTHR values give better fitting but also shorter segments in polyline. The data range for this parameter is between 0 and 8192.

ATHR (Angular difference threshold): This parameter specifies the maximum angle (in degrees) between segments of a polyline. Otherwise, it is segmented into two or more vectors. It is also the maximum angle between two vectors for them to be linked. The data range for this parameter is between 0 and 90.

DTHR (Linking distance threshold): This parameter specifies the minimum distance (in pixels) between the end points of two vectors for them to be linked. The data range for this parameter is between 0 and 8192.

To acquire the best result for the lineaments, it is necessary to do several experiments by changing the number of the six controlling parameters above. There are some researchers who gave recommendation for the algorithm such as Kocal (2004), Sarp (2005), Abdullah et al. (2010), Ibrahim and Mutua (2014), and El-Sawy et al. (2016). After that, the lineaments were converted into shapefile format (.shp) to generate the fault and fracture density (FFD) map. The lineaments was also converted into autocad dxf format (.dxf) for the purpose of generating the rose diagram. After all the steps above were done, the result were compared with the manual lineament extraction report (Hermawan and Rezky, 2011).

RESULTS

Lineaments

The lineaments were generated using a module from PCI-Geomatica 2015 software called Line: Lineament Extraction. The extraction process was done by changing the six parameters several times. Several lineament maps were generated using different parameters values until it got the most suitable values (Table 2) these lineaments are considered as fault lines according to the satellite image view (Figure 8).

Table 2: Suggested parameters values

Parameters	Value
RADI	5
GTHR	5
LTHR	15
FTHR	3
ATHR	15
DTHR	10

The result from automatic lineament extraction (Figure 9) shows that the extracted lines are shorter than the manual lineament extraction (Figure 10), it goes to show that the automatic method is more specific The distribution of the lines are more or less similar.

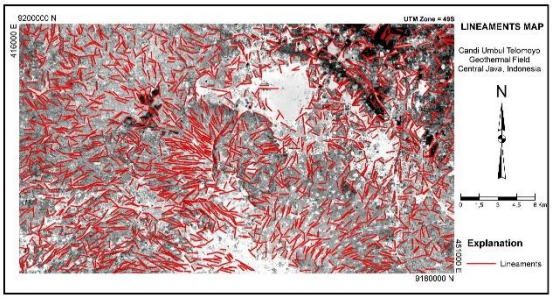


Figure 9: Lineaments map generated from automatic lineament extraction method.

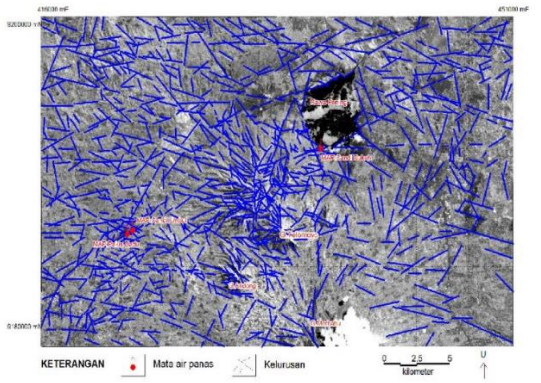


Figure 10: Lineaments map generated from manual lineament extraction method (Hermawan and Rezky, 2011).

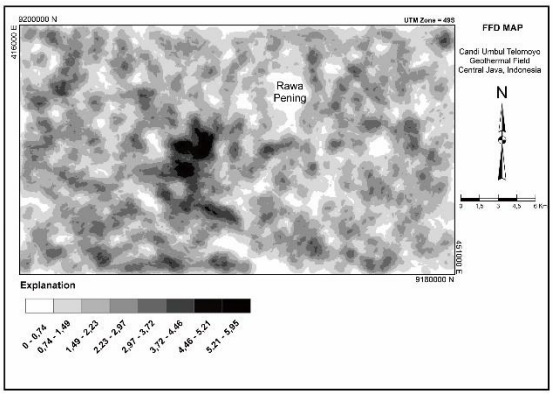


Figure 11: FFD map generated from automatic lineament extraction method.

Fault and Fracture Density (FFD) Map

The FFD map was generated using ArcGis 10.3 software. This map shows the density anomaly of the lineaments that is assumed as the recharge area, which have the highest permeability. The result from automatic method shows that the highest density area is located around southwest Rawa Pening (darkest area) (Figure 11). Meanwhile, the manual method show that the highest density area is larger than the automatic method but still at the same area, which is also at the southwest Rawa Pening (Figure 12). Compared to the manual method, the automatic method generates the density value that is a little bit lower, but more or less similar with the

manual method. The automatic method generates between 0 – 5.95 Km/Km^2 and the manual method generates between 0 – 7 Km/Km^2.

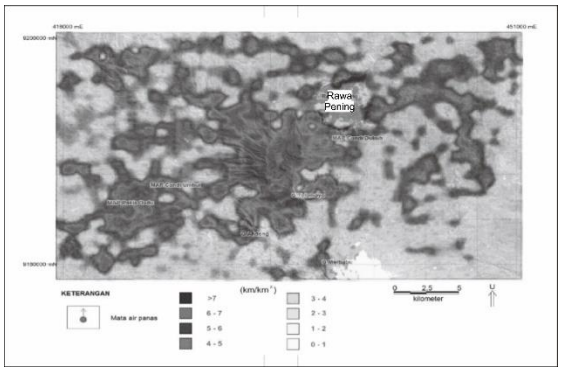


Figure 12: FFD map generated from manual lineament extraction method (Hermawan and Rezky, 2011).

Rose Diagram

The rose diagram was generated using RockWorks 16 software. The result from the diagram shows that there are four main structural trends generated from the automatic method (Figure 13). Compared with the manual method (Figure 14), the main trends shows the almost similar trends with about 10º to 40º difference but still a the same trends (Table 3).

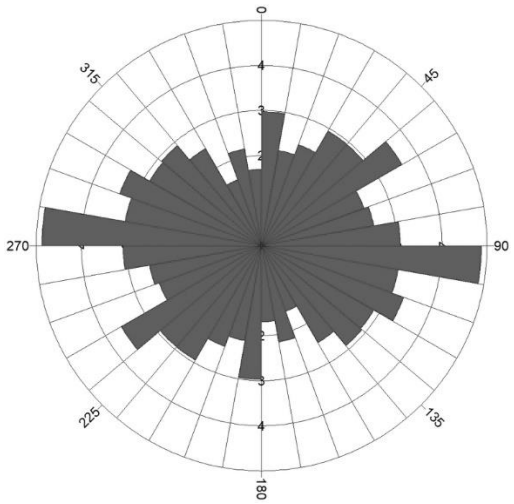


Figure 13: Rose diagram generated from automatic lineament extraction method.

CONCLUSIONS

This study has shown that the result from the automatic method is more or less similar with the manual method. The lineaments are shorter but it have the same distribution area. The FFD map has a lower density value, but shows the same prospect area, althougth the manual method shows the larger density area and the automatic method shows the more specific area. The rose diagram shows almost similar main structural trends with about 10º to 40º difference. In conclusion, the automatic method is more efficient compared to the manual method because it takes less time to generate and the results are accountable.

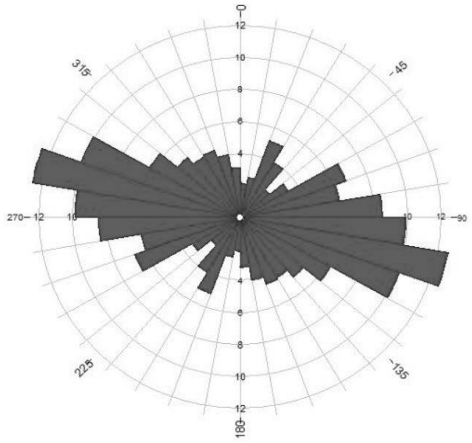


Figure 14: Rose diagram generated from manual lineament extraction method (Hermawan and Rezky, 2011).

Table 3: Result of rose diagram from automatic method and manual method showing the main structural trends

Trends	Automatic	Manual
N-S	N0º–10ºE or N170º–180ºW	N20º–30ºE or N150º–160ºW
NE-SW	N50º–60ºE or N120º–130ºW	N60º–70ºE or N110º–120ºW
E-W	N90º–100ºE or N80º–90ºW	N100º–110ºE or N70º–80ºW
NW-SE	N110º–120ºE or N60º–70ºW	N150º–160ºE or N20º–30ºW

REFERENCES

Abdullah, A., Akhir, J. M., and Abdullah, I. (2010), "Automatic Mapping of Lineaments Using Shaded Relief Images Derived from Digital Elevation Model (DEMs) in the Maran – Sungai Lembing Area, Malaysia", *Electronic Journal of Geotechnical Engineering*, **15**, 949-957.

Doust, H. and Lijmbach, G. (1997), "Charge Constraints of the Hydrocarbon Habitat and Development of Hydrocarbon Systems in Southeast Asia Tertiary Basins", *Proceedings of an International Conference on Petroleum Systems of SE Asia and Australasia*.

EarthExplorer. (2018), "Path 120 Row 65 [Satellite Image]", Retrieved June 6, 2018 From https://earthexplorer.usgs.gov/.

El-Sawy, K., Atef, M. I., El-Bastawesy, M.A., and El-Saud, W.A. (2016), "Automated, Manual Lineaments Extraction and Geospatial Analysis for Cairo-Suez District (Northeastern Cairo-Egypt), Using Remote Sensing and GIS", *International Journal of Innovative Science, Engineering & Technology*, **3**, 491-500.

Hermawan, D. and Kholid, M. (2010), "Penyelidikan Terpadu Daerah Panas Bumi Candi Umbul-Telomoyo, Provinsi Jawa

Tengah", *Prosiding Hasil Kegiatan Pusat Sumber Daya Geologi*.

Hermawan, D. and Rezky, Y. (2011), "Delineasi Daerah Prospek Panas Bumi Berdasarkan Analisis Kelurusan Citra Landsat di Candi Umbul – Telomoyo, Provinsi Jawa Tengah" *Buletin Sumber Daya Geologi*, **6**, 1-10.

Ibrahim, U. and Mutua, F. (2014), "Lineament Extraction Using Landsat 8 (OLI) in Gedo, Somalia", *International Journal of Science and Research*, **3,** 291-296

Kocal, A. (2004), "*A Methodology for Detection and Evaluation of Lineaments from Satellite Imagery*", Master's Thesis: Middle Easth Technical University.

Loyd, C. (2013), "Landsat 8 Bands", Retrieved July 7, 2018 From https://landsat.gsfc.nasa.gov/.

Sarp, G. (2005), "*Lineament Analysis from Satellite Images, North-West Ankara*", Master's Thesis: Middle East Technical University.

Satyana, A.H. and Purwaningsih, M.E.M. (2002), "Lekukan Struktur Jawa Tengah: Suatu Segmentasi Sesar Mendatar", *Proceedings Indonesian Association of Geologist (IAGI)*, Yogyakarta – Central Java Section.

Soengkono, S. (1999a), "Te Kopia Geothermal System (New Zealand) – The Relationship Between Its Structure and Extent", *Geothermics*, **28**, 767-784.

Soengkono, S. (1999b), "Analysis of Digital Topographic Data for Exploration and Assessment of Geothermal System", *Proceedings 21st New Zealand Geothermal Workshop*.

Suryantini and Wibowo, H.H. (2010), "Application of Fault and Fracture Density (FFD) Method for Geothermal Exploration in Non-Volcanic Geothermal Systems; A Case Study in Sulawesi-Indonesia", *Proceedings World Geothermal Congress*, Bali, Indonesia.

Van Bemmelen, R. W. (1970), "*The Geology of Indonesia, 1A: General Geology of Indonesia and Adjacent Archipelagoes*", 2nd ed.: The Hague.

OPPORTUNITY AND CHALLENGES OF CLEAN DEVELOPMENT MECHANISM GEOTHERMAL PROJECTS IN INDONESIA TO CONTRIBUTE IN NATIONAL EMISSION REDUCTION

Muhyidin

Star Energy Geothermal Darajat II, Limited
Sentral Senayan II, 25th floor. Jl.Asia Afrika No.8, Jakarta 10270. Indonesia
Email: muhyidin@starenergy.co.id

ABSTRACT

Indonesia has renewable resources with potential more than 443 GW. Its potential such as hydro energy 75 GW, geothermal 29 GW, solar energy 207 GW, wind energy with 60.6 GW, and bioenergy with more than 102 GW. Indonesia is also known as a biggest geothermal resources in the world with total potential 29 GW at 312 areas in the ring of fire Sumatera, Java, Bali, Nusa Tenggara, North Sulawesi and Maluku. The government of Indonesia has commitment through Presidential Decree No.79/2014 on National Energy Policy to increase renewable energy. Renewable energy (include geothermal) currently only 7.7 % from the primary energy mix and targeted to minimum 23% or equal to 45 GW on 2025 (geothermal targeted to 7% by 2025). Geothermal sector has contributed in national emission reduction from Clean Development Mechanism (CDM) projects with total 9,630,199 ton CO_2e or 29,94% of total certified emission reduction (CER). There are 13 CDM projects registered at United Nations Framework Convention on Climate Change (UNFCCC) secretariat and only 4 of them with CERs issued status. The biggest CERs issuance is from Darajat Unit 3 CDM project with total 6,260,609 ton CO_2e or 65% of total CERs issuance from geothermal project in Indonesia. There are potential emission reduction 7,437,880 ton CO_2e / year from registered geothermal CDM project in Indonesia. Some improvement plan to be implemented to increase the amount of CERs from geothermal CDM project in Indonesia such as sharing best practice & knowledge among project participants to discuss the opportunity and challenges in CDM implementation.

Keywords: CDM, emission reduction, goethermal, Indonesia.

INTRODUCTION

Indonesia, a country within the Southeast Asia countries, covers 790 million hectares (ha) with a total coastline of 81,000 km and land territory of about 200 million ha. It has approximately 13,667 islands which 56% of it are nameless and only 7% are permanently inhabited. The country population is the fourth most populous nation in the world, following China, India and the United States. The population grew from 119 million in 1971 to 219 million in 2005. It is projected that Indonesia's population will reach 300 million in 2030 (Kementerian Lingkungan Hidup, 2010).

The increasing growth of population has led to the increase of energy consumption. Increasing of energy consumption shall provide energy sources to meet the energy needs whether from renewable or non-renewable energy sources (Prihantono, 2006). The use of non-renewable energy especially from fossil fuel energy has increased the potential of global warming.

Climate change is largely result of anthropogenic greenhouse gas (GHG) emission. Under the most pessimistic emission scenario developed in IPCC 2000, by the end of this century temperature could rise to more than 4 ^{0}C above 1980-1999 levels (DJPPI, 2015). This would have serious consequences for the world's growth and development (ADB, 2009).

Southeast Asia with 563.1 million people is the most vulnerable region to climate change. Increasing trend in mean surface air temperature with a 0.1-0.3 ^{0}C increase per decade recorded between 1951 and 2000. Rainfall has been trending down and sea levels up (at the rate of 1-3 millimeters per year), and the frequency of extreme weather events has increased such as heat waves are more frequent; heavy precipitation events rose significantly; and the number of tropical cyclones was higher during 1990-2003. These climatic changes have led to massive flooding, landslides, and droughts in many parts of the region, causing extensive damage to property, assets and human life. Climate change is also exacerbating water shortages in many areas, constraining agricultural production and threatening food security, causing forest fires and degradation, and increasing the risk of outbreaks of infectious diseases. In 2000, Southeast Asia contributed 12% of the world's GHG emissions, amounting to 5,187 $MtCO_2$e, an increase of 27% from 1990 and it is faster than the global average (ADB, 2009).

According to Indonesia's Second National Communication of 2010, GHG emission in Indonesia were estimated to be 1.8 $GtCO_2$e in 2005. This represents an increase of 0.4 $GtCO_2$e compared to 2000. Most emissions (63%) are the result of land

use change and peat and forest fires while combustion of fossil fuels contributing approximately 19% of total emission (KLH, 2016)

Mitigation strategies are available in both the energy supply and demand sectors. On supply side, major options such as by using of renewable energy including biomass, solar, wind, hydro and geothermal resources. On the demand side, implementing energy efficiency is the key such as use of more efficient lighting and electrical appliances in residential and commercial building sector; use of more efficient boiler, motors and furnaces, fuel switching and material recycling and substitution in industry sector; switching to cleaner fuels, use of fuel-efficient vehicle and better traffic management in transport sector (ADB, 2009).

Indonesia has voluntary pledged to reduce emission by 26% on its own efforts and up to 41% with international support against the business as usual scenario by 2020. To meet these objectives, Indonesia has set up various programs to reduce its emission in energy sector, industry sector, forestry sector, peatland, agriculture sector and waste. In energy sector, Indonesia has established the development of clean energy sources as a national policy directive to put this country on the path to de-carbonization in line with GHG reduction (Spalding-Fecher et al, 2012). Government Regulation No.79/2014 on National Energy Policy, set out the ambition to transform, by 2025 and 2050, the primary energy supply mix with shares as follows: a) new and renewable energy at least 23% in 2025 and at least 31% in 2050; b) oil should be less than 25% in 2025 and less than 20% in 2050; c) coal should be minimum 30% in 2025 and minimum 25% in 2050; and d) gas should be minimum 22% in 2025 and minimum 24% in 2050 (KLH, 2016).

Indonesia has signed the United Nations Framework Convention on Climate Change in Rio de Janeiro on 1992 which was then ratified in 1994 through Law No.6/1994. In this framework, the countries divided into 2 groups which are Annex I and Non-Annex I countries. Annex I countries are the developed countries contributed to GHG emission since industrial revolution. Non-Annex I countries are developing countries excluded in the Annex I which less contribution to GHG emission. Indonesia is part of Non-Annex I countries. Under this framework, Indonesia has committed to fully implementing the framework and have the right and obligation to get support offered by UNFCCC to achieved its goal. To run the framework, UNFCCC formed the highest decision board which is Conference of Parties (COP). COP has annual meeting for all UNFCCC members and serving as meeting of parties to the Kyoto Protocol (CMP). In the third session of the COP (COP-3) at Kyoto, Japan, on 1997, there was consensus to adopt Kyoto Protocol as a framework for climate change. In Kyoto Protocol, Annex I countries legally binding to reduce their GHG emission at least 5% from emission level on 1990. Indonesia also signed the Kyoto Protocol and ratified it through Law No.17/2004. Under Kyoto Protocol, there are three flexible mechanism to reduce emission: Emission Trading (ET), Joint Implementation (JI) and CDM. Through this ratification, Indonesia able to participate in one of Kyoto Protocol mechanism which is CDM (Ridha et al, 2016).

In COP-21 UNFCCC conducted meeting at Paris on 30 November – 12 December 2015. Total 196 countries agreed to adopt the Paris Agreement. Paris Agreement goal is to mitigate the global temperature below 2 ^{0}C from pre-industrialization and effort to reduced it until below 1.5 ^{0}C, and to improve the adaptation ability of negative climate change for low emission development (Ridha et al, 2016).

Energy supply mix is still dominated by coal (57.22%), gas (24.82%), hydro (7.06%), fossil fuel (5.81%) and geothermal & other renewable resources (5.09%). Electrical consumption in 2017 was 1,012 kWh per capita or increase compared to 2016 with 956 kWh per capita. For the first time, Indonesia reached electrical consumption above 1,000 kWh per capita. It is one of indicator on economic growth (Kementerian ESDM, 2018).

Indonesia has renewable resources with potential more than 443 GW. Its potential such as hydro energy 75 GW, geothermal 29 GW, solar energy 207 GW, wind energy with 60.6 GW, and bioenergy with more than102 GW (Kementerian ESDM, 2018). Indonesia is also known as a biggest geothermal resources in the world with total potential 29 GW at 312 areas in the ring of fire Sumatera, Java, Bali, Nusa Tenggara, North Sulawesi and Maluku. Geothermal is clean, environmental friendly and sustainable energy resources (Dirjen EBTKE, 2015). Table 1 show installed capacity per December 2016 per island location (Dirjen EBTKE, 2016).

Total installed capacity of geothermal plant in Indonesia in 2017 is 1,808.5 MW which came from additional installed capacity of geothermal plant of Ulubelu 4 with 55 MW and operational start of Sarulla 2 with 110 MW. On 2018, additional install capacity from geothermal was targeted to 2,058.5 MW (Kementerian ESDM, 2018).

CDM project from geothermal projects in Indonesia has contributed in national GHG emission reduction. It has reduced 9,630,199 ton CO_2e (29.94%) from total CERs issuance from UNFCCC secretariat. Table 2 showed CDM register status from geothermal projects in Indonesia. There are 13 CDM

projects registered with total amount of reduction is 7,437,880 ton CO_2e / year (UNFCCC, 2018).

Only 4 of 13 (30.77%) from registered CDM projects have got CER issuances from UNFCCC secretariat. It means those CDM projects have been run and verified by Designated Operational Entity (DOE) as per approved Project Design Document (PDD). The CER issuance amount of CDM project from geothermal sector is described in the Table 3.

Darajat Unit 3 geothermal project is a pioneer of CDM project in Indonesia. Its initial registration request was on 26 September 2006. The second CDM registration was from Lahendong II-20 MW Geothermal Project with the initial registration request was on 4 August 2009 and then followed by registration of CDM project from Kamojang Geothermal Project and Wayang Windu Phase 2 Geothermal Power Project on 2009.

Table 1: Distribution of geothermal installed capacity.

No	Island	Quantity of location	Total poten-tial (MW)	Installed capacity
1	Sumatera	97	12,912	122
2	Java	73	9,795	1,274
3	Bali – Nusa Tenggara	33	1,920	12.5
4	Kalimantan	27	182.5	0
5	Sulawesi	14	3,208	80
6	Maluku	77	1,451	0
7	Papua	33	75	0
	Total	330	29,543.5	1,438.5

Source: Dirjen EBTKE, 2016

Table 2: CDM register status from geothermal projects in Indonesia

No.	CDM project reference number	Registration project title	Initial registration request	Registered	Start of first crediting period	End of first crediting period	Amount Of Reductions (PDD ex-ante) per year
1	673	Darajat Unit 3 Geothermal Project	26sep2006	11dec2006	14jun2007	13jun2014	652,173
2	2,876	Lahendong II-20 MW Geothermal Project	04aug2009	19dec2009	19dec2009	18dec2016	66,713
3	3,028	Kamojang Geothermal	12oct2009	16dec2010	16dec2010	15dec2017	402,780
4	3,193	Wayang Windu Phase 2 Geothermal Power Project	07dec2009	02dec2010	02dec2010	01dec2017	794,832
5	3,637	Patuha Geothermal Project	20dec2012	21dec2012	01jan2014	31dec2020	263,851
6	5,773	Project Ulubelu Unit 3 - 4 PT. Pertamina Geothermal Energy	07feb2012	15may2012	21jun2014	20jun2021	581,784
7	5,785	Project Lumut Balai Unit 1 - 2 PT. Pertamina Geothermal Energy	10feb2012	22may2012	01jan2015	31dec2021	581,784
8	6,305	Gunung Rajabasa Geothermal Power Plant	30may2012	18sep2012	01jan2016	31dec2022	1,105,668
9	6,307	Liki Pinangawan Muaralaboh Geothermal Power Plant	30may2012	31oct2012	18sep2015	17sep2022	993,428
10	6,834	Rantau Dedap Geothermal Power Plant	24jul2012	21nov2012	18may2016	17may2023	1,099,745
11	7,315	Project Lumut Balai Unit 3 - 4 PT. Pertamina Geothermal Energy	17sep2012	19sep2012	01jan2017	31dec2023	581,784
12	7,430	Project Kamojang Unit 5 PT. Pertamina Geothermal Energy	23nov2012	28nov2012	01jan2014	31dec2020	156,669
13	7,431	Project Karaha Unit 1 PT. Pertamina Geothermal Energy	23nov2012	27nov2012	01jan2014	31dec2020	156,669
						Total	7,437,880

Source: UNFCCC, 2018

The next CDM registration was on 2012 starting from Patuha Geothermal Project, Project Ulubelu Unit 3-4 PGE and lastly Project Karaha Unit I PGE. Lahendong Unit 5 & Unit 6 Geothermal Project, the registration request was on 11 Jan 2013 but until July 2018 the status is still Pending Publication and was not registered yet as CDM project. Another CDM project is Sibayak Geothermal Power Plant, the start validation was on 27 August 2008 and the current status is Validation Terminated. It means the total registered CDM project from geothermal sector in Indonesia is 13 projects.

METHOD

This research is descriptive qualitative method to describe and explain the opportunity and challenges of CDM geothermal project in Indonesia by data collection method, review of literature, and interview & discussion. The rationale of this qualitative approach was to explore and describe the experiences and perspective of some CDM projects participants to contribute in national emission reduction.

Best practice sharing session among CDM participants already conducted in April 2018. This session was coordinated by Pertamina Geothermal Energy (PGE) and attended by geothermal company under PGE joint operation contract. There was no competition in this CDM project, and some of companies share their best practice and CDM update. Star Energy Geothermal Darajat II, Limited (SEGD) sharing on Darajat Unit 3 CDM project while Star Energy Geothermal (Wayang Windu) Ltd sharing on Wayang Windu Unit 2 CDM project experience including their Voluntary Emission Reduction (VER) program and PGE sharing on progress of all CDM project under PGE.
This study will contribute to the literature on the sources of geothermal project as a lower emission energy sources and its initiative GHG emission reduction program implementation & best practices in contribution to national GHG emission reduction.

RESULT & DISCUSSION

Even though there are 13 registered CDM project from geothermal power plant in Indonesia, but only 4 of them already got CER issuance from UNFCCC secretariat. The highest CDM project was from Darajat Unit 3 project with 65% of total CER issuance from geothermal sector. The second highest is from Wayang Windu Phase 2 Geothermal Power Project with 32% from total CER issuance. The detail CER issuance from geothermal sector is described in Table 3.

Table 3: CER issuance of CDM project from geothermal sector in Indonesia.

CDM Project Title	Total CERs	Percentage
Darajat Unit III	6,260,609	65%
Lahendong II-20 MW Geothermal Project	216,304	2%
Kamojang Geothermal	92,691	1%
Wayang Windu Phase 2 Geothermal Power Project	3,060,595	32%
Total	9,630,199	100%

Source: UNFCCC, 2018

There are some reasons why CDM project from geothermal sectors in Indonesia were not run smoothly mainly due to some projects have not been implemented and some registered project have not completed verification audit on their CDM monitoring report. There are 3 CDM project with status those projects have not been implemented which are: Gunung Rajabasa Geothermal Power Plant, Liki Pinangawan Muaralaboh Geothermal Power Plant and Rantau Dedap Geothermal Power Plant.

Kamojang Geothermal CDM project with installed capacity 60 MW, the current status is that verification contract has been terminated since 12 August 2015. Last day of the las monitoring period was on 28 February 2011 with total CERs issuance was 92,691 ton CO_2e with latest issuance on 18 November 2011.

The first crediting period of Darajat Unit 3 CDM project end was on 13 Jun 2014 and has been renewed to UNFCCC secretariat. Its second crediting period currently renewed become 14 Jun 2014 – 5 Oct 2019 with amount of emission reduction based on approved PDD is 753,136 ton CO_2e / year. The last day of the last monitoring period was 30 June 2016 with total CERs issuance 801,111 ton CO_2e (period 1 Jul 2015 – 30 June 2016). The CERs issuance on 18 August 2017.

Darajat Unit 3 first CERs issuance 90,804 tonnes CO_2 equivalent was on 11 June 2009 for the Monitoring Report (MR) #1 period 14 June 2007 – 31 August 2007. Then on 25 May 2011, CERs of MR #2 and MR #3 were issued for period 1 September 2007 – 1 November 2008 and period 2 November 2008 – 31 July 2009. Starting MR #6 until MR #10 (end of MR of 1st crediting period), MR verification audit by DOE were conducted every 6 months basis (semi annual). Since MR #11, monitoring report verifications audit were conducted on annual basis with first CERs issuance 761,593 ton CO_2 equivalent on the beginning of MR of 2nd crediting period (Muhyidin, 2017). Summary

of Darajat Unit 3 CERs issuance can be seen in the Table 4 below.

Wayang Windu Phase 2 Geothermal Power Project with total CERs issuance was 3,060,595 ton CO_2e or 32% from total CER issuance in Indonesia from geothermal sector currently is still in progress of renewal of second crediting period. MR #6 with total CERs 1,678,445 ton CO_2e is currently awaiting issuance request. Table 5 showed summary CERs issuance from MR #1 – MR #6. Commercial Operation Date (COD) of Wayang Windu Phase 2 is on 4 Mar 2009 while their CDM registration was on 2 December 2010, so during that period the CERs cannot be claimed into CDM project under UNFCCC. Carbon credits developed by carbon offset which are not yet certified called Voluntary Emission Reduction (VER). The opportunity to commercialize the real and verifiable reductions for project which have not been operational prior the successful registration at UNFCCC secretariat. In this case, emission reduction from the COD to the registered date was under VER. The VER has been verified by external parties so it can be commercialized as carbon trading (World Bank and Ecofys, 2015).

Lahendong II-20 MW Geothermal Project already 3 MR that have been verified by DOE with total CERs issuance are 216,304 ton CO_2e. MR period 1 January 2013 – 18 December 2016 (first crediting period) has not been verified by DOE. Estimated total CERs as per approved PDD from Lahendong CDM project is 66,713 ton CO_2e / year.

Table 4: Summary of Darajat Unit 3 CER Issuance

Category	Cover Period	CERs (tCO_2e)
Monitoring Report #1 (CERs issued on 11 Jun 2009)	14 Jun 2007 – 31 Aug 2007	90,804
Monitoring Report #2 (CERs issued on 25 May 2011)	1 Sep 2007 – 1 Nov 2008	737,846
Monitoring Report #3 (CERs issued on 25 May 2011)	2 Nov 2008 – 31 Jul 2009	501,310
Monitoring Report #4 (CERs issued on 17 Apr 2012)	1 Aug 2009 – 31 Oct 2010	889,337
Monitoring Report #5 (CERs issued on 11 Dec 2012)	1 Nov 2010 – 31 Dec 2011	838,969
Monitoring Report #6 (CERs issued on 15 Apr 2013)	1 Jan 2012 – 30 June 2012	362,546
Monitoring Report #7 (CERs issued on 16 Jun 2013)	1 July 2012 – 31 Dec 2012	345,420
Monitoring Report #8 (CERs issued on 13 Jun 2014)	1 Jan 2013 – 30 Jun 2013	346,094
Monitoring Report #9 (CERs issued on 15 Aug 2014)	1 Jul 2013 – 31 Dec 2013	263,040
Monitoring Report #10 (CERs issued on 4 Dec 2015)	1 Jan 2014 - 13 Jun 2014	322,539
Monitoring Report #11 (CERs issued on 5 Jan 2017)	14 Jun 2014 - 30 Jun 2015	761,593
Monitoring Report #12 (CERs issued on 18 Aug 2017)	1 Jul 2015 - 30 Jun 2016	801,111
Total CERs		**6,260,609**

Source: UNFCCC, 2018

Table 5: Summary of Wayang Windu Phase 2 Geothermal Power Project CERs Issuance

Category	Cover Period	CERs (tCO_2e)
Monitoring Report #1 (CERs issued on 2 Feb 2012)	2 Dec 2010 – 22 May 2011	379,773
Monitoring Report #2 (CERs issued on 27 Apr 2012)	23 May 2011 – 31 Oct 2011	329,762
Monitoring Report #3 (CERs issued on 28 Dec 2012)	1 Nov 2011 – 31 May 2012	444,255
Monitoring Report #4 (CERs issued on 21 May 2013)	1 Jun 2012 – 31 Dec 2012	401,492
Monitoring Report #5 (CERs issued on 15 May 2015)	1 Jan 2013 – 31 Dec 2014	1,505,313
Monitoring Report #6 (*awaiting issuance request*)	1 Jan 2015 – 1 Dec 2017	1,678,445
Total CERs		**4,739,040**

Table 6: Summary of Lahendong II-20 MW Geothermal Project CERs Issuance

Category	Cover Period	CERs (tCO_2e)
Monitoring Report #1 (CERs issued on 14 Mar 2014)	19 Dec 2009 – 31 Dec 2010	84,960
Monitoring Report #2 (CERs issued on 14 Mar 2014)	1 Jan 2011 – 31 Dec 2011	63,817
Monitoring Report #3 (CERs issued on 14 Mar 2014)	1 Jan 2012 – 31 Dec 2012	67,527
Total CERs		**216,304**

Source: UNFCCC, 2018

Even though CDM project from geothermal sector have opportunity to get some fund from carbon trading and can contribute to national emission reduction, some challenges to run this project shall be handled properly. Some challenges of CDM geothermal project in Indonesia were: a) financial barriers, b) carbon market, c) international CDM regulation and policy, d) capacity building and knowledge, e) local regulation and policy, and f) unspecific domestic policy related to CDM (DNPI, 2014).

Current situation of registered CDM project from geothermal sectors are described to explore the challenges and figure out the best practice to solve it. There are 3 of registered CDM project from geothermal sectors which have not been implemented. They are Gunung Rajabasa Geothermal Power Plant, Liki Pinangawan Muaralaboh Geothermal Power Plant, and Rantau Dedap Geothermal Power Plant.

Gunung Rajabasa Geothermal Power Plant was operated by PT Supreme Energy Rajabasa (SERB) (Supreme Energy, 2018). This CDM project was registered since 30 May 2012 same with Liki Pinangawan Muaralaboh Geothermal Power Plant. SERB has started the engineering design for civil constructed since August 2012. On April 2014, SERB just receive Borrow Use Permit of Protection Forest (IPPKH) permit from the Ministry of Forestry. This permit is a final requirement for the commencement of construction work in the area of the protection forest (Supreme Energy, 2018)

Liki Pinangawan Muaralaboh Geothermal Power Plant was operated by PT Supreme Energy Muara Laboh (SEML) (Supreme Energy, 2018). By the end of 2013, SEML has completed the exploration drilling program covering 6 wells. In 2014, construction of admin and accommodation building was completed on September 2014. By the end of 2015, SEML has completed the Engineering, Procurement, and Construction (EPC) tender process, and construction of geothermal power plants began in 2016 and estimated electricity production in 2019 (Supreme Energy, 2018).

Rantau Dedap Geothermal Power Plant was operated by PT Supreme Energy Rantau Dedap (SERD) (Supreme Energy, 2018). This CDM project has been registered since 24 July 2012. By the end of 2013, about 14 kilometers of road has already been opened and civil construction has been finished its original scope on July 2014. In November 2014, SERD reached financial closing to get USD 50 million facility agreement from the Asian Development Bank (ADB) supported by the Clean Technology Fund, for the exploration of Rantau Dedap geothermal project. The exploration drilling continued until early 2015 and completed 6 wells. In 2016, SERD completed the feasibility study report, and EPC tender.

The current challenges of Darajat Unit 3 Geothermal Project are on the transition of project participant names due to divestation process. Formerly the project participants from the host party (The Government of Indonesia) are Chevron Geothermal Indonesia, ltd and PT Darajat Geothermal Indonesia. After divestation, the project participant become Star Energy Geothermal Darajat II, limited (SEGD). While project participants from other party (The Government of the United Kingdom of Great Britain & Northern Island) (Chevron Geothermal Indonesia, 2015), are Chevron Limited and Chevron Products.

Since April 2017, SEGD as new operator of Darajat Unit 3 Geothermal Project was in progress of changing the project participant name including coordinated with UNFCCC, Government of Indonesia and Chevron. The MR #13 and MR #14 currently cannot be submitted to DOE for verification, due to the participant name has not been changed formally.

Lahendong II-20 MW Geothermal Project and Wayang Windu Phase 2 Geothermal Power Project are currently in progress of renewal for second crediting period in its CDM project. The end of first crediting period of Lahendong II-20 MW Geothermal Project was on 18 December 2016 while Wayang Windu Phase 2 Geothermal Power Project ended its first crediting period on 1 December 2017. Past experience from Darajat Unit 3 Geothermal Project on its journey of second crediting period approval, it takes about 2 years since formal notification to UNFCCC secretariat on 10 December 2013 until renewal date of PDD approval from UNFCCC secretariat on 5 September 2015. It took

time especially on preparing contract for consultant service, interview validator with CDM members, Ministry of Energy and Mineral Resources and National Council for Climate Change (DNPI) until supporting document and submit renewal of PDD report to DOE.

Patuha Geothermal Project was operated by PT Geo Dipa Energi. This project was registered since 12 December 2012. The estimated CERs from this CDM project based on approved PDD was 263,851 ton CO_2e. Currently there is no CERs issuance from this project that has been verified by DOE.

The rest of registered CDM projects under PT Pertamina Geothermal Energy (Project Ulubelu Unit 3 – 4, Project Lumut Balai Unit 1 – 2, Project Lumut Balai Unit 3 – 4, Project Kamojang Unit 5, and Project Karaha Unit 1) have not got CERs issued due to those project have not been verified by DOE. These projects have been upgraded to Gold Standard CDM project since February 2013. The Gold Standard is a standard for creating high quality emission reduction projects in the CDM, Joint Implementation (JI) and Voluntary Carbon Market. Its objective is to add branding, a label to existing and new carbon credits generated by projects which can then be brought and traded by countries that have a binding legal commitment according to the Kyoto Protocol.

Sarulla Operation, one of the geothermal project that already reached full commercial operation of its 3x110 MW, have not been registered yet as CDM project at UNFCCC secretariat. The commercial operation of the first unit was operated on 18 March 2017, the unit 2 in November 2017 and unit 3 in May 2018. The potential of CERs from this geothermal project will be more contribute in national emission reduction.

CONCLUSION

CDM project from geothermal sectors in Indonesia has significant contribution to national emission reduction. Current CERs from all geothermal sectors was 9,630,199 or 29.94% of all total CERs from all sector include biomass, cement, fossil fuel switch, hydro, methane avoidance, etc.

Only 30.77% of registered CDM projects achieved CERs issuances from UNFCCC secretariat. It means still have opportunity from all registered CDM project from geothermal sector to get more CERs to contribute in national emission reduction program.

Regular best practice sharing and discussion among CDM project participants need to be conducted to update and share best practice among participants so that CDM project implementation can be run smoothly and higher CERs can be achieved.

REFERENCES

Asian Development Bank/ADB. (2009), "The Economics of Climate Change in Southeast Asia: A Regional Review", Asian Development Bank, Manila, Philippines, pg.4-50, 134. Retrieved from https://www.adb.org /sites/default/files/publication/29657/economics-climate-change -se-asia.pdf.

Chevron Geothermal Indonesia. (2015), "Project Design Document 0673: Darajat Unit III Geothermal Project", *Clean Development Mechanism (CDM), United Nation Climate Change (UNCC),* pg.4. Retrieved from https://cdm.unfccc.int/filestorage/P/D/E/PDEI58VK09H1ZJMGU7RBSOAFTLCWQ4/Revised_PDD_0673_Clean.pdf?t=UXl8cHNkcWQ1fDAamC7becjquKtRzhopmdgh.

Dewan Nasional Perubahan Iklim. (2014), "Bunga Rampai Mekanisme Pembangunan Bersih (CDM) di Indonesia 2005 – 2014", pg.26-76. Retrieved from http://www.mitrahijau.or.id /mh_content/uploads/2015/05/Bunga-Rampai-CDM-Indonesia.pdf. Accessed on 12 Jun 2017.

Direktorat Jenderal Pengendalian Perubahan Iklim/DJPPI. (2015), "Rencana Strategis Tahun 2015-2019", *Direktorat Jenderal Pengendalian Perubahan Iklim Kementerian Lingkungan Hidup dan Kehutanan*, pg.26. Retrieved from http://ditjenppi.menlhk.go.id/ reddplus/images/resources/renstra/renstra_for_web.pdf.

Dirjen EBTKE. (2015), "Potensi dan Peluang Investasi Energi Baru, Terbarukan dan Konservasi Energi (EBTKE)", pg.8. Jakarta: Indonesia. Retrieved from http://ebtke.esdm.go.id/post/2015/03/26/818/potensi.dan.peluang.investasi.ebtke.

Dirjen EBTKE. (2016), "Statistik EBTKE 2016", pg.3. Jakarta, Indonesia. Retrieved from http://ebtke.esdm.go.id/post/2017/03/07/1583/statistik.ebtke.2016.

Kementerian ESDM. (2018), "Capaian 2017 dan Outlook 2018 Subsektor Ketenagalistrikan dan EBTKE", pg.2. Retrieved from https://www.esdm.go.id/en/media-center/arsip-berita/capaian-2017-dan-outlook-2018-subsekt or-ketenagalistrikan-dan-ebtke-.

Kementerian ESDM. (2018), "Kembangkan Energi Lestari Wujudkan Energi Berkeadilan", *Buletin Hijau edisi 1 tahun 2017*, pg. 9. Retrieved from http://ebtke.esdm.go.id/post/2

018/04/16/1936/energi.hijau.edisi.1.tahun.2017.kembangkan.energi.lestari.wujudkan.energi.berkeadilan.

Kementerian Lingkungan Hidup. (2010), "Indonesia Second National Communication Under the United Nations Framework Convention on Climate Change (UNFCCC)", pg.ix - V-12. Retrieved from http://unfccc.int/files/national _reports/non-annex_i_natcom/submitted_natcom/application/pdf/indonesia_snc.pdf.

Kementerian Lingkungan Hidup. (2016), "First Nationally Determined Contribution Republic of Indonesia", pg. 4. Retrieved from http://ditjenppi.menlhk.go.id/reddplus/images/resources/ndc/First_NDC.pdf.

Muhyidin. (2017), "Darajat Unit 3 Geothermal Clean Development Mechanism (CDM) Program Contribution in National Greenhouse Gas (GHG) Emission Reduction". *Proceedings from The 5th Indonesia International Geothermal Convention & Exhibition (IIGCE) 2017*.

Prihantono, D. S. (2006), "Renewable Energy / Energy Efficiency and the CDM", *Chevron, DNA Tech Team Presentation*, pg. 10. Retrieved from http://siteresources.worldbank.org/INTINDONESIA/Resources/Environment/279303-1158132387452/2930926-115813749 7813/2930959-1158137636671/2930961-1158759403410/DwitaPrihantono.pdf.

Ridha, D. M., Purbo, A., Wibowo, A., Tobing, L. B., Widyaningtyas, N., Widayati, T., Bagiyono, R., Anwar, S., and Farid, M. (2016), "Perubahan Iklim, Perjanjian Paris dan Nationally Determined Contribution", *Direktorat Jenderal Pengendalian Perubahan Iklim Kementerian Lingkungan Hidup dan Kehutanan* pg. 9-22.

Spalding-Fecher, R., Achanta, A. N., Erickson, P., Haites, E., Lazarus, M., Pahuja, N., Pandey, N., Seres, S., and Tewari, R. (2012), "Assessing the Impact of the Clean Development Mechanism", *Report Commissioned by The High-Level Panel on The CDM Policy Dialogue*, pg. 23-56. Retrieved from http://www.cdmpolicydialogue.org/research/1030_impact.pdf.

Supreme Energy. (2018), "Company PT Supreme Energy Muara Laboh, PT Supreme Energy Rajabasa, and PT Supreme Energy Rantau Dedap". Retrieved from http://www.supreme-energy.com/company/se-muara-laboh/; http:// www.supreme-energy.com/company/se-raja-basa/; http://www.supreme-energy.com/company/se-rantau-dedap/. Accessed on 23 July 2018.

United Nations Framework Convention on Climate Change/UNFCCC. (2018), "CDM Insights: Database for PAs and PoAs". Retrieved from http://cdm.unfccc.int/Statistics/Public/files/Database%20for%20PAs%20and%20PoAs.xlsx. Accessed on 23 Jul 2018.

United Nations Framework Convention on Climate Change/UNFCCC. (2008), "Kyoto Protocol Reference Manual on Accounting of Emissions and Assigned Amount", pg.12-13. Retrieved from https://unfccc.int/resource/docs/publications/08_unfccc_kp_ref_manual.pdf.

United Nations Framework Convention on Climate Change/UNFCCC. (2018), "Project 0673: Darajat Unit III Geothermal Project". Retrieved from https://cdm.unfccc.int/Projects/DB/KPMG1159285050.32/view?cp=1. Accessed on 23 Jun 2018.

United Nations Framework Convention on Climate Change/UNFCCC. (2018), "Project 2876: Lahendong II-20 MW Geothermal Project". Retrieved from https://cdm.unfccc.int/Project s/DB/TUEV-SUED1249404911.81/view. Accessed on 23 Jul 2018.

United Nations Framework Convention on Climate Change/UNFCCC. (2018), "Project 3193 : Wayang Windu Phase 2 Geothermal Power Project". Retrieved from https://cdm.unfccc.int/Projects/DB/TUEV-SUED1260194062.48 /view. Accessed on 23 Jul 2018.

World Bank and Ecofys. (2015), "State and Trends of Carbon Pricing 2015", pg. 34, Washington DC. Retrieved from http://documents.worldbank.org/curated/en/636161467995665933/pdf/99533-REVISED-PUB-P153405-Box393205B.p df. Accessed on 10 Jul 2018.

NUMERICAL INVESTIGATION FOR ESTIMATION OF ROCK TEMPERATURE IN ENHANCED GEOTHERMAL SYSTEM

Muhammad Qarinur, Hideaki Yasuhara, and Naoki Kinoshita

Department of Civil and Environmental Engineering, Ehime University
Matsuyama 790-8577, Japan
Email: mqarinur@gmail.com

ABSTRACT

Numerical modeling was used to estimate rock temperature in the geothermal reservoir. It is important to develop a new geothermal resource and improve production performance probably by Enhanced Geothermal System (EGS). In this research, we have used COMSOL Multiphysics (COMSOL 5.3a, 2017) to simulate the coupled thermal and hydraulic (TH) processes in the geothermal reservoir by using the local thermal non-equilibrium theory. The reservoir is treated as a fractured porous medium by adopting discrete fractured model (DFM). A geothermal field in Lahendong, Indonesia is simulated to study the characteristics of fluid flow and heat transfer. Based on the results, the rock temperature in the production well LHD-5 will decrease faster because of close to the injection wells. The rock temperature in the production well LHD-23 shows almost no change and the system can maintain a stable running condition. It is found that the distance between injection wells and production wells is crucial to the performance and service life of the geothermal reservoir.

Keywords: Numerical modeling, rock temperature, EGS, Lahendong.

INTRODUCTION

Geothermal energy is the one of renewable energy for reducing dependence on gas and other fossil fuels. Based on the origins and conditions of production, geothermal resource are divided into hot dry rock (HDR) and hydrothermal (Qu et al, 2017). The temperature-depth relationship (i.e., geothermal gradient), permeability, porosity and the amount of fluid saturation in the geothermal reservoir are important in assessing geothermal resources potential (Massachusetts Institute of Technology, 2006). High average thermal gradients, high rock permeability and porosity, sufficient fluids in place, and an adequate reservoir recharge of fluids are the characteristics of the hydrothermal reservoir. Compared to the hydrothermal resources, HDR resources may have higher temperature potential, but may not produce energy sufficiently because of deeply buried, low permeability, low porosity, insufficient reservoir volume, and the absence of naturally contained fluids. Therefore, Enhanced Geothermal System (EGS) can be used to stimulate fractures in the rock to create a connected path through which fluids can be induced to flow and extract heat (Xu et al, 2015).

Currently, several useful models have been developed for modeling flow and temperature of EGS. Jiang et al (2014) simulated long-term heat extraction using three-dimensional transient model for EGS subsurface thermo-hydraulic processes. Xu et al. (2015) studied coupled hydro-thermal model for EGS by using equivalent pipe network (EPN). Yao et al (2018) used thermal-hydraulic-mechanical (THM) coupling to simulate and analyze the heat extraction in EGS based on discrete fracture model. The modeling method and procedure aforementioned may be provided for the current study.

In this study, a mathematical model incorporating thermal and hydraulic coupling is adopted to estimate the rock temperature in the geothermal reservoir by using the local thermal non-equilibrium theory. Adopting discrete fracture model (DFM), the geothermal reservoir is treated as a fractured porous medium that consists of the rock matrix and discrete fractures. Finally, the 3D numerical model of the Lahendong geothermal field is created in COMSOL Multiphysics 5.3a to predict the evolution of rock temperature in the geothermal reservoir.

METHODOLOGY

Model Overview

Thermal and hydraulic coupling method in this study based on discrete fracture model (DFM) consists of two parts (i.e., the rock matrix and discrete fractures) (Figure 1). The discrete fracture model (DFM) uses grid nodes to represent flow relationship between fracture to fracture, fracture to matrix, and matrix to matrix (Liang et al, 2016).

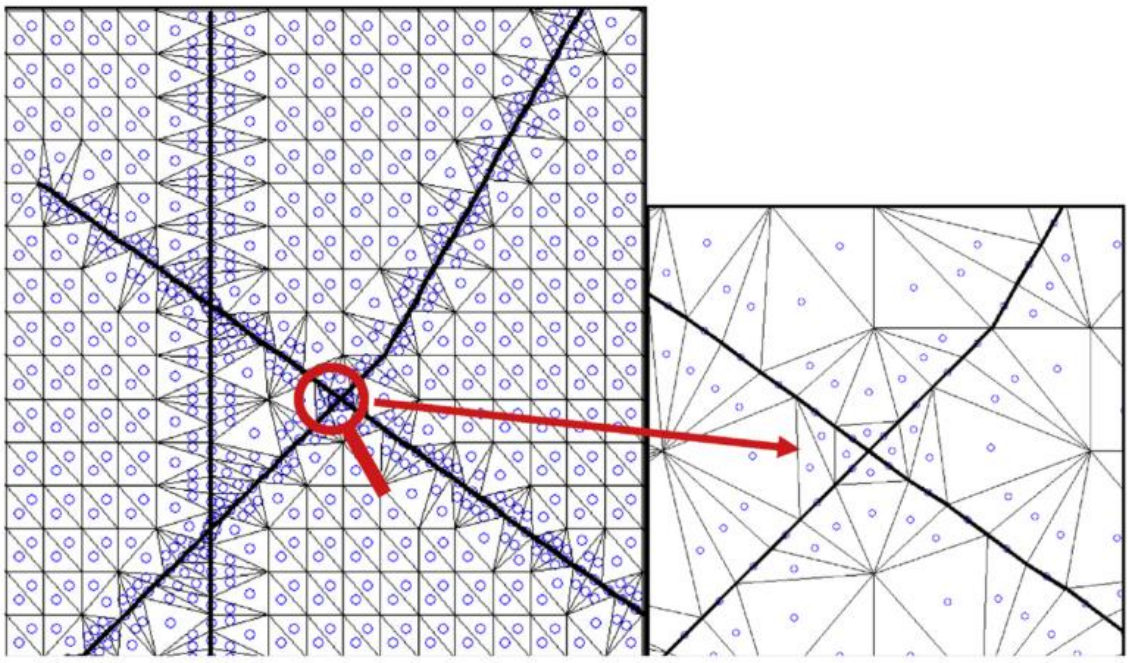


Figure 1: The unstructured grid and the node of DFM (Liang et al, 2016).

Governing Equations

The governing equations of thermal and hydraulic coupling model are described as follows:

Rock mass flow

The rock matrix permeability is less than that of the discrete fractures. Because of that, flow in the rock matrix is calculated by Darcy's law and that in the discrete fractures is done by the modified Darcy's law. The equations for the rock matrix and discrete fracture flow are expressed by (Liang et al, 2016; Yao et al, 2018).

$$S\frac{\partial p}{\partial t} + \nabla\left(-\frac{\kappa}{\eta}(\nabla p + \rho_w g \nabla z)\right) = -\frac{\partial e}{\partial t} + Q \qquad (1)$$

$$d_f S_f \frac{\partial p}{\partial t} + \nabla_\tau\left(-d_f \frac{\kappa_f}{\eta}(\nabla_\tau p + \rho_w g \nabla_\tau z)\right) = -d_f \frac{\partial e_f}{\partial t} + Q_f \qquad (2)$$

where S is the rock matrix storage coefficient [1/Pa], p is the hydrostatic pressure [Pa], t is the time [s], κ is the rock matrix permeability [m^2], η is the dynamic fluid viscosity [Pa·s], ρ_w is the fluid density [kg/m^3], g is the gravitation [m/s^2], e is the volumetric strain of rock matrix [-], Q is the source-sink term of the seepage process [s^{-1}], d_f is the discrete fracture thickness [m], S_f is the discrete fracture storage coefficient [1/Pa], ∇_τ is the gradient operator restricted to the fracture's tangential plane, κ_f is the discrete fracture permeability [m^2], e_f is the volumetric strain of discrete fracture [-], Q_f is the flow exchange between rock matrix and discrete fracture [s^{-1}].

Rock mass temperature

Energy conservation in rock matrix is described as (Saeid et al, 2013):

$$\rho C_s \frac{\partial T_s}{\partial t} + \nabla \cdot (-\lambda \nabla T_s) = 0 \qquad (3)$$

where ρ is the rock density [kg/m^3], Cs is the specific heat capacity of rock matrix [J/kg/K], Ts is the rock temperature [°C], λ is the thermal conductivity of rock [W/m/K].

Energy conservation in the discrete fracture is defined as (Chen and Raghavan, 2013; Yao et al, 2018):

$$d_f \rho_w C_w \frac{\partial T_f}{\partial t} + d_f \rho_w C_w \cdot u_f \nabla_\tau T_f = \nabla_\tau \cdot \left(d_f \lambda_f \nabla_\tau T_f\right) + h(T_s - T_f) \qquad (4)$$

where C_w is the specific heat capacity of fluid [J/kg/K], T_f is the water temperature in the discrete fracture [°C], u_f is the fluid flow velocity in the discrete fracture, λ_f is the thermal conductivity of fluid [W/m/K], h is the convection efficiency [$W/m^2/K$].

Coupling effects

TH coupling effect

One of the most important factors that affect the coupling is the properties of the work fluid in the reservoir. The density of water is no longer a constant value due to the influence of high pressure and high temperature in the reservoir. The effects can be expressed in the function of pressure and temperature as follows (Zhao et al, 2015):

$$\frac{1}{\rho_w} = 3.086 - 0.899017(4014.15 - T)^{0.147166} - 0.39(658.15 - T)^{-1.6}(p - 225.5) + \delta_w \quad (5)$$

where T is the water temperature [K], p is the absolute water pressure [Pa], and δ is a function of "p" and "T"; in general, the value of δ does not exceed 6% of $1/\rho_w$.

Dynamic viscosity (η) is also affected by the temperature of water, $\eta = v\rho_w$ in which v is the kinematic viscosity of water. A commonly used empirical formula for the kinematic viscosity can be expressed as follows:

$$v = \frac{0.01775}{1+0.033T_f+0.000221T_f^2} \quad (6)$$

The density and the viscosity of water are greatly affected by the temperature. Therefore, they are important in the process of seepage and heat transfer in the geothermal reservoir.

RESEARCH AREA

The Lahendong geothermal field is located in Tomohon, North Sulawesi, Indonesia. Currently, the Lahendong geothermal field has six units with a total production capacity of 120 MW (Pambudi, 2018). In this study, five wells in Cluster-5, Lahendong Unit III Geothermal Power Plant, comprising three injection wells (LHD-19, LHD-20, LHD-21) and two production wells (LHD-5, LHD-23) are simulated to evaluate geothermal reservoir temperature. The research area and the well locations are shown in Figure 2.

Computational Model

Based on the actual conditions (Koestono, 2010), the locations of injection and production wells are shown in Figure 2. The 3D computational model in the current study is also shown in Figure 3. It is assumed that the reservoir is located at 2,450 m below the ground surface with a domain of 1500m x 1500m x 1200 m (Figure 3 and Figure 4). The reservoir rock is assumed to be homogenous and the fault zone is assumed as the fracture area.

According to the drilling well design in the well LHD-23, the length of each slotted liner pipe in the injection and production wells in Cluster-5 is assumed to be 300 m with diameter 7 inch. The finite element mesh used in the calculation is shown in Figure 5.

Initial and boundary conditions

In the simulations using the present model, the total heat extraction period is 100 years with each time step of 1 year. The influence of temperature gradient is not considered in the domain. Therefore, the temperature variation along the depth is ignored. A thermal insulated boundary is selected for the external conditions. The initial temperature of the reservoir is 230 °C with the hydrostatic pressure of 12 MPa. In the injection wells, 83.3 kg/s of cold water at the temperature of 40 °C is injected, and 31.7 kg/s production rate in the production well has been determined (Prabowo et al, 2015). For the other external conditions, an impermeable boundary is selected, and it is assumed that reservoir pressure has reached a steady state before water injection.

Model parameters

The accuracy of obtaining results that match the actual conditions in numerical simulations depends on the selection of computational parameters. Due to lack of several data to perform numerical simulations, several parameters are selected by assumptions and references of the existing numerical simulations. The parameters used in the numerical model are listed in Table 1 (Khasani et al, 2001; Utami, 2011; Brehme et al, 2016; Yao et al, 2018).

Table 1: Model parameters in reservoir

Parameter	Value	Unit
$\boldsymbol{\rho_w}$	1,000	[kg/m^3]
$\boldsymbol{\eta}$	9.54 x 10^{-5}	[Pa·s]
C_w	4,200	[J/kg/K]
C_s	1000	[J/kg/K]
λ_f	1.8	[W/m/K]
λ_s	2.5	[W/m/K]
h	3000	[W/m^2/K]
ρ_s	2740	[kg/m^3]
κ	2.3 x 10^{-14}	[m^2]
κ_f	1.3 x 10^{-11}	[m^2]
S	1.0 x 10^{-8}	[1/Pa]
S_f	1.0 x 10^{-9}	[1/Pa]
α_T	2.0 x 10^{-6}	[1/K]
ϕ_s	0.105	[-]
ϕ_f	0.3	[-]
d_f	0.001	[m]
g	9.81	[m/s^2]

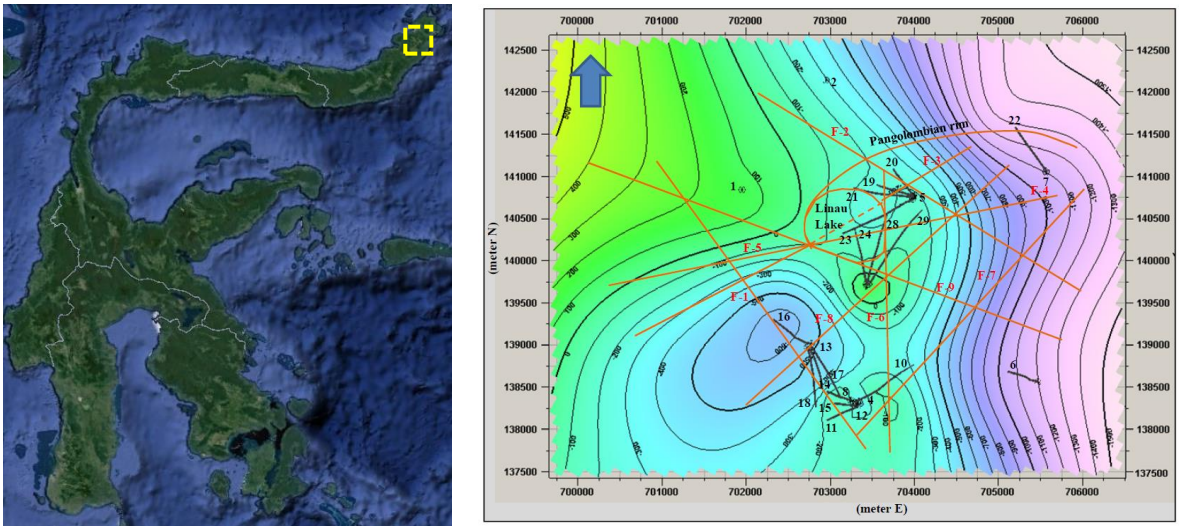


Figure 2: Location of the research area and wells at Lahendong geothermal field (Koestono, 2010).

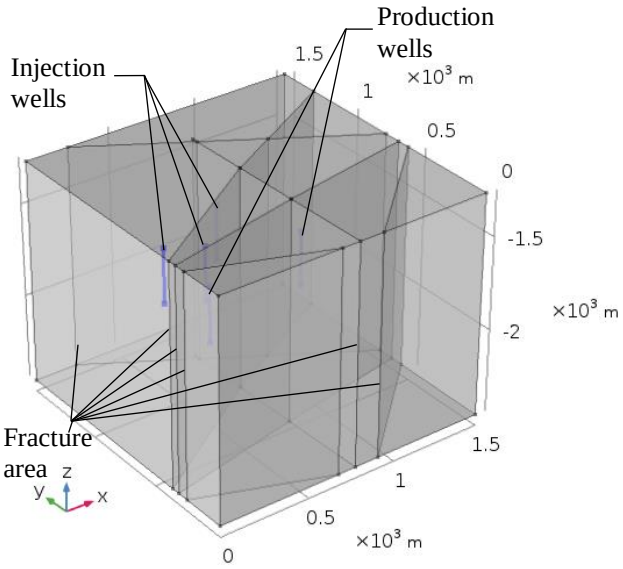


Figure 3: The 3D model geometry of Lahendong geothermal field.

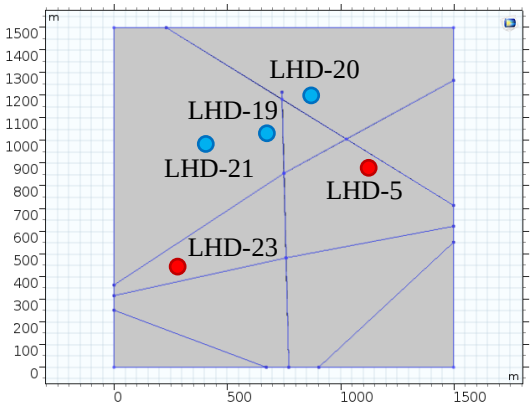


Figure 4: A cut plane at Z = 1750 m.

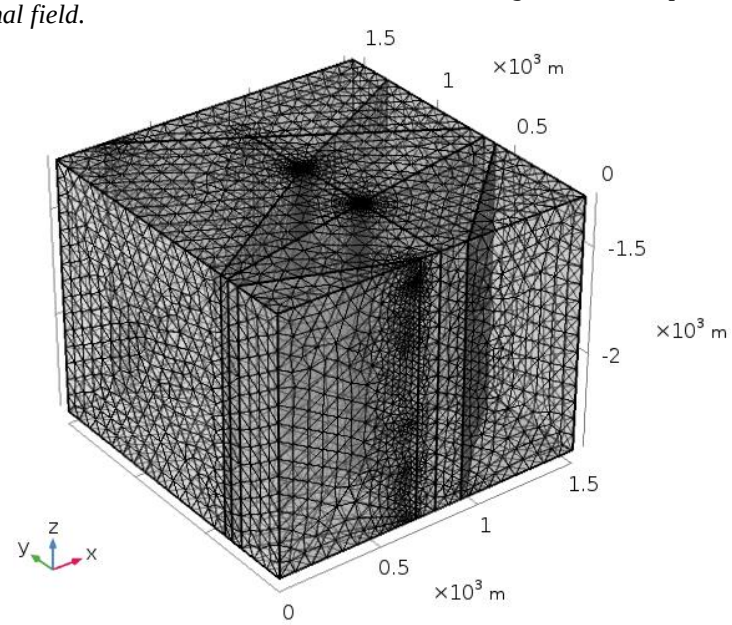


Figure 5: Mesh system of Lahendong geothermal field (tetrahedra elements 182597).

RESULTS

Fluid Production Temperature

The evolution of the fluid production temperature is shown in Figure 6. The average outlet temperature remains constant at 230 °C for about 20 years. After 20 years, the temperature of the production well especially in LHD-5 began to decline. The outlet temperature decreases from 230 °C to 216 °C for about 100 years. In the production well LHD-23 the temperature little changes because the system can maintain a stable running condition for about 100 years. This is because the production well LHD-23 position is farther from the injection well than the production well LHD-5, so the time required in the process of decreasing the reservoir temperature is longer.

From these results, it can be concluded that the determination of the distance of the injection wells with the production well becomes important in determining the service life of the geothermal reservoir.

Injection Pressure

The evolution of the injection well pressure is shown in Figure 7. In the beginning, the injection well pressure in the injection well LHD-19, LHD-20, and LHD-21 increases quickly from 12 MPa to 13.7 MPa, 13 MPa, and 12.8 MPa respectively. The pressure in the injection well LHD-19 is higher than the others because the position is between LHD-20 and LHD-21 and the injections from the two wells should affect the injection pressure of LHD-19. On the other hand, the pressure on the injection well LHD-21 is lower than the others because it is relatively further than the other injection wells.

After one-year production time, the injection pressure increases more gently. In the 100-year production time, the pressures in the injection well LHD-19, LHD-20, and LHD-21 increase to 21.5 MPa, 20.8 MPa, and 20.5 MPa respectively. It can be concluded that the injection pressure should maintain a high level, to achieve the requirement of constant injection and production rates of 83.3 kg/s and 31.7 kg/s, respectively.

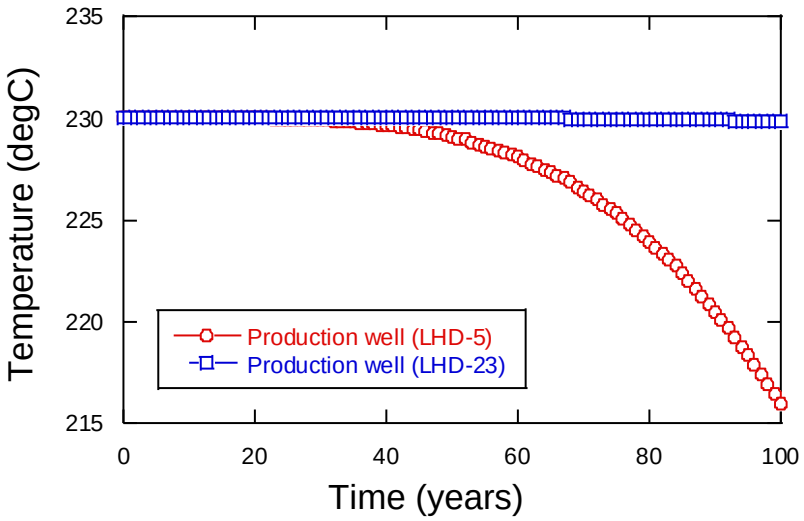


Figure 6: Evolution of rock temperature in production wells.

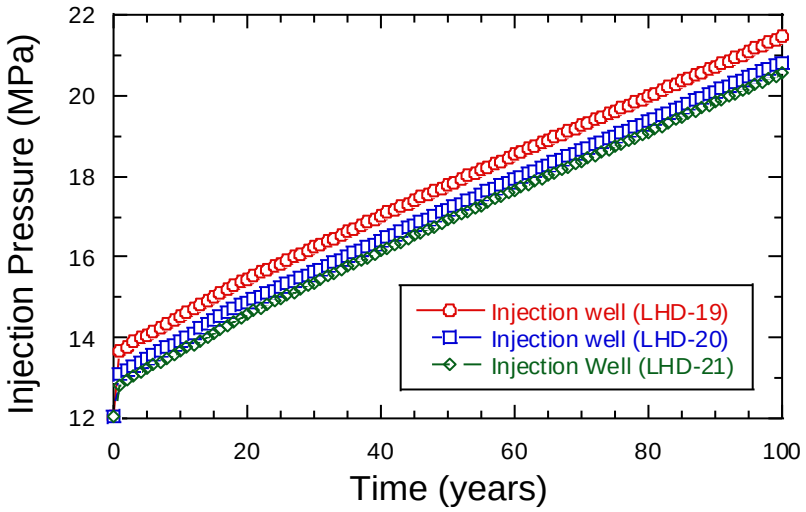


Figure 7: Evolution of the injection well pressure.

Distribution of Rock Temperature

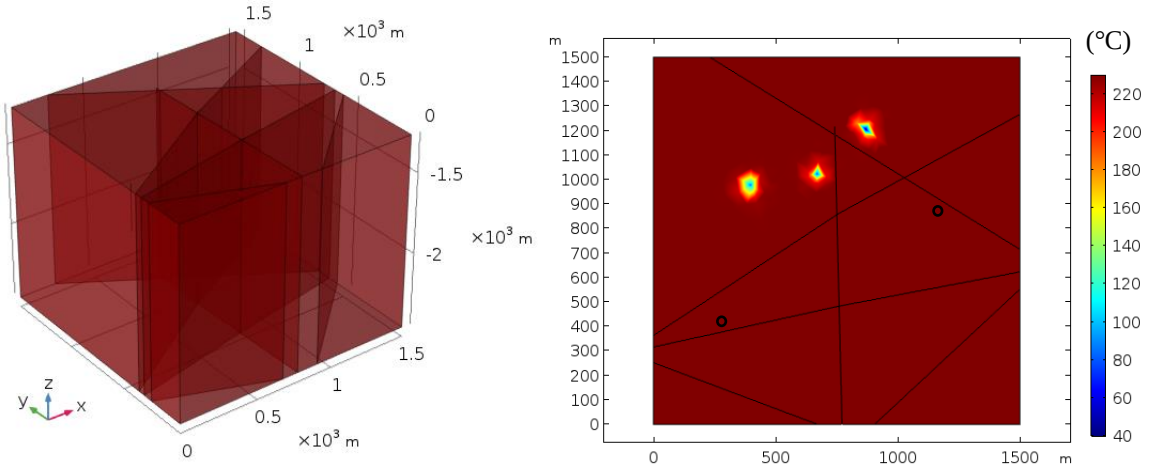
The rock temperature distribution in the reservoir with time is shown in Figure 8. In the initial stage (Figure 8(a)) with the injection of 40 °C water temperature, the rock temperature exchange occurs in the rock matrix. The temperature in the rock matrix decreases gradually by forming the low-temperature zone. However, the rock temperature close to the production wells almost has no change, and the system can maintain the sustained and stable output of heat production.

As shown in Figure 8, the production wells begin to undergo a temperature change gradually. It is indicated that the steady and continuous heat output is beginning to decline. Finally, the low-temperature zone in the reservoir will expand and reach the production well (Figure 8(c) and (d)). Because of that, the water temperatures in the production wells gradually decrease with time.

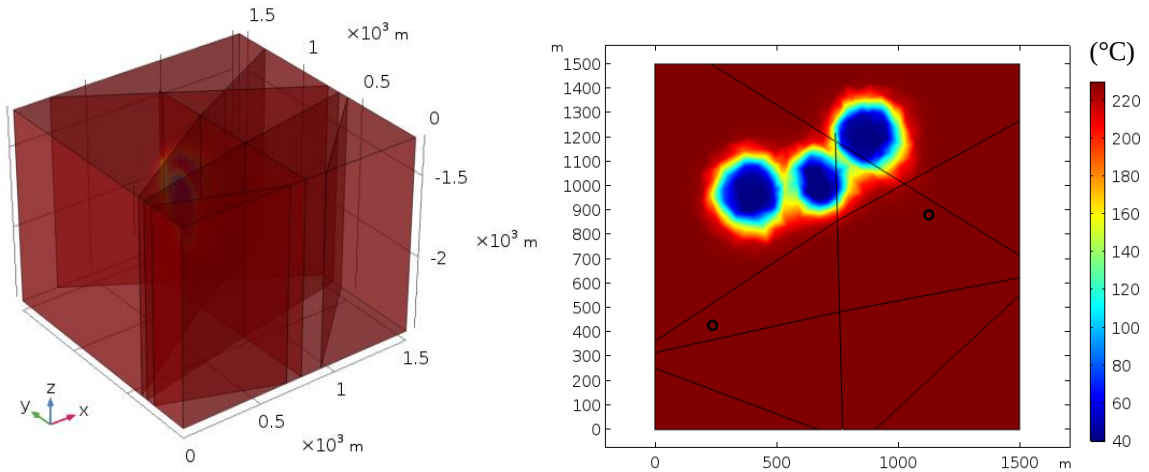
CONCLUSIONS

Thermal and hydraulic (TH) coupling by adopting discrete fracture model was established to estimate the rock temperature of the Lahendong geothermal reservoir. The rock temperature in the production well LHD-5 decreases faster than that in the production well LHD-23. It is because the location of LHD-5 is closer to the injection wells. The rock temperature in the production well LHD-23 little change for 100 years, and the system can maintain a stable running condition throughout the simulation period.

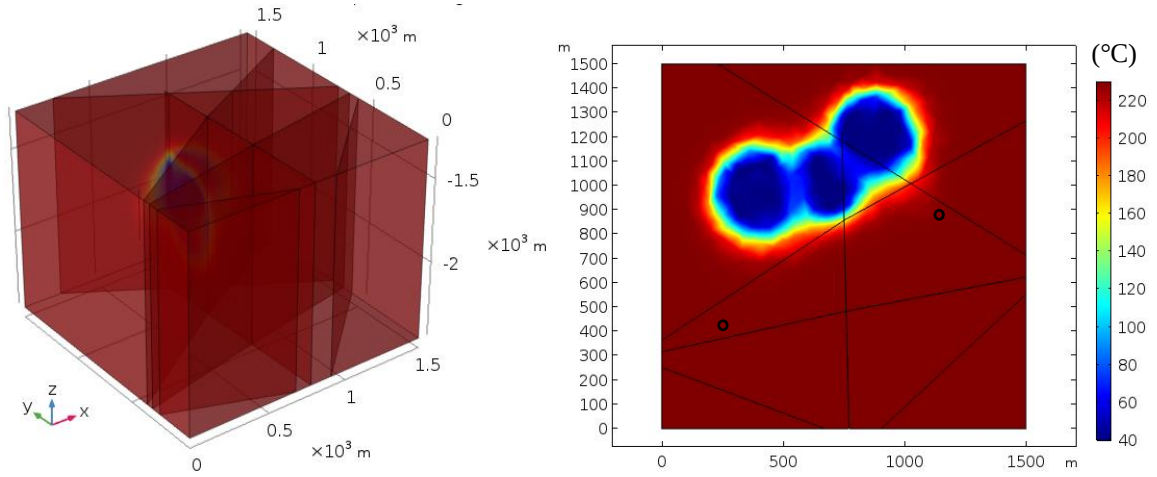
However, due to lack of in-situ data and specific research in this reservoir area, the results shown in the current work cannot be well validated yet, and the validation must be accomplished by actual measurements and/or experiments under in-situ conditions. Furthermore, the effects of mechanical and chemical processes are not considered in this work, and should be considered in the future work to obtain more plausible estimation of the energy production.



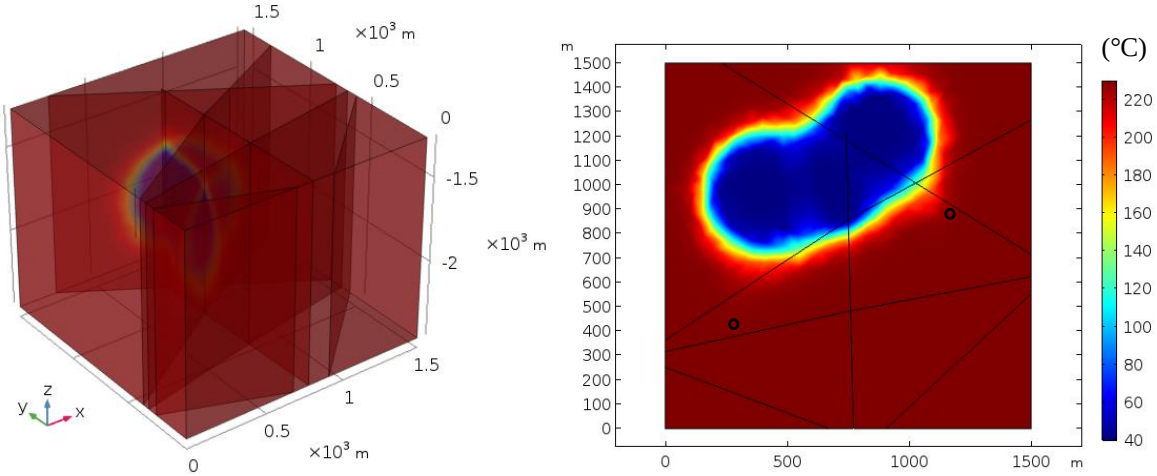
(a) lifespan 1 year



(b) lifespan 25 years



(c) lifespan 50 years



(d) lifespan 100 years

Figure 8: Temperature evolution in the fracture and a cut plane at z = 1750 m.

REFERENCES

Brehme, M., Blöcher, G., Cacace, M., Kamah, Y., Sauter, M., and Zimmermann, G. (2016), "Permeability distribution in the Lahendong geothermal field: A blind fault captured by thermal – hydraulic simulation", Environmental Earth Sciences, 75:1088. Springer-Verlag Berlin Heidelberg.

Chen, C., and Raghavan, R. (2013), "On The Liquid-Flow Analog to Evaluate Gas Wells Producing in Shales", Society of Petroleum Engineers, SPE Reservoir Evaluation & Engineering. Vol. 16, Issue 02.

COMSOL 5.3a. (2017), "COMSOL Multiphysics Reference Manual", p. 1150. Available at: www.comsol.com.

Jiang, F., Chen, J., Huang, W., and Luo, L. (2014), "A three-dimensional transient model for EGS subsurface thermo-hydraulic process", Energy. Elsevier Ltd, 72, pp. 300–310.

Khasani, Itoi, R., Fukuda, M., and Sudarman, S. (2001), "Interpretation of Well Logging Data on Lahendong Geothermal Field, Indonesia", Proceeding of the 5th INAGA Annual Scientific Conference & Exhibitions. Yogyakarta.

Koestono, H. (2010), "Lahendong Geothermal Field , Indonesia : Geothermal model based on wells LHD-23 and LHD-28". United Nations University, GEOTHERMAL TRAINING PROGRAMME Reykjavik, Iceland.

Liang, B., Jiang, H., Li, J., and Gong, C. (2016), "A systematic study of fracture parameters effect on fracture network permeability based on discrete-fracture model employing Finite Element Analyses", Journal of Natural Gas Science and Engineering, 28, pp. 711–722.

Massachusetts Institute of Technology. (2006), "The Future of Geothermal Energy, Impact of Enhanced Geothermal Systems (EGS) on the United States in the 21st Century", Idaho National Laboratory". Retrieved from

http://www.eere.energy.gov/geothermal/pdfs/structure_outcome.pdf.

Pambudi, N. A. (2018), "Geothermal power generation in Indonesia , a country within the ring of fire : Current status, future development and policy", Renewable and Sustainable Energy Reviews, 81, part 2, pp. 2893–2901.

Prabowo, T., Yuniar, D. M., Suryanto, S., and Silaban, M. (2015), "Tracer Test Implementation and Analysis in Order to Evaluate Reinjection Effects in Lahendong Field", World Geothermal Congress 2015, (April), pp. 1–6.

Qu, Z. Qing., Zhang, W., and Guo, T. (2017), "Influence of different fracture morphology on heat mining performance of enhanced geothermal systems based on COMSOL", International Journal of Hydrogen Energy. Elsevier Ltd, 42(29), pp. 18263–18278.

Saeid, S., Al-Khoury, R., and Barends, F. (2013), "An efficient computational model for deep low-enthalpy geothermal systems", Computers & Geosciences, 51, pp. 400–409.

Utami, P. (2011), "Hydrothermal Alteration and The Evolution of The Lahendong Geothermal System, North Sulawesi, Indonesia". University of Auckland.

Xu, C., Dowd, P. A., and Tian, Z. F. (2015), "A simplified coupled hydro-thermal model for enhanced geothermal systems", Applied Energy, 140, pp. 135–145.

Yao, J., Zhang, X., Sun, Z., Huang, Z., Liu, J., Li, Y., Xin, Y., Yan, X., and Liu, W. (2018), "Numerical simulation of the heat extraction in 3D-EGS with thermal-hydraulic-mechanical coupling method based on discrete fractures model", Geothermics, 74, pp. 19–34.

Zhao, Y., Feng, Z., Feng, Z., Yang, D., and Liang, W. (2015), "THM (Thermo-hydro-mechanical) coupled mathematical model of fractured media and numerical simulation of a 3D enhanced geothermal system at 573 K and buried depth 6000–7000 M", Energy, 82, pp. 193–205.

HYDROTHERMAL ALTERATION CHARACTERISTIC OF CEMENT CONSTRUCTION CHANGES: A CASE STUDY OF BUKIT KASIH GEOTOURISM AREA

Listiana Alifia Nurlaely, I Wayan Warmada, and Ilham Dharmawan Putra

Geological Engineering Department, Faculty of Engineering, Universitas Gadjah Mada
Grafika St.2 Bulaksumur, Sinduadi, Mlati, Sinduadi, Sleman, D.I. Yogyakarta 55284
Email: listiana.alifia.n@mail.ugm.ac.id

ABSTRACT

Bukit Kasih geotourism area is one of essential elements of geothermal education in Minahasa District, North Sulawesi. Bukit Kasih is a place that include various aspects, such as geothermal, aesthetical, and cultural as the supporting values of society education for locals and tourists. In the first decade of 2000 until now, the damaged cement constructions and geothermal manifestations are parts of many issues that can be seen in Bukit Kasih, as it held important role to serve an enjoyable and safety geotourism activities. This research is conducted as preliminary approach by knowing the hydrothermal alteration characteristics present in cement construction at Bukit Kasih geotourism area to support other advance future research in order to build a better cement construction for geotourism activities. Several samples from cement constructions and rocks are analyzed thorough petrography and X-ray diffraction (XRD) as the methods in this research. The results show that several neutral pH and low temperature hydrothermal alteration suite mineral such as smectite, chlorite, calcite, sericite, anhydrite, and secondary silica minerals are identified, as well as the presence of acid pH and low temperature hydrothermal alteration minerals such as kaolinite and alunite are also identified. The hydrothermal alteration minerals in this study are mainly found present as replacement minerals of primary constituents and depositional minerals from geothermal fluids. The weakening of cement constructions is believed happen due to the replacement of primary constituent by secondary hydrothermal alteration minerals. This study also suggest further research to find the mixed cementing materials for construction as well as the geotechnical aspects experiment in order to creates education, so that geothermal energy can be accepted by locals and tourist.

Keywords: Bukit Kasih, cement construction, geothermal manifestation, hydrothermal alteration, weakening

INTRODUCTIONS

Backgrounds

Bukit kasih is one of geotourism sites in Tompaso Geothermal Field, Minahasa District, North Sulawesi. This area is composed by several geothermal manifestation such as fumaroles, steaming grounds, hot and boiling springs, solfataras, and altered rocks. Survey in this area shows that the presence of steaming grounds in Bukit Kasih are disseminated widely in the slope and peak of the hills, meanwhile the presence of hot springs in mainly found in lower parts of the slope. Altered rock are present due to hydrothermal fluid activity, i.e. in the surface where hot water and steam from steaming and fumarole activity can be seen affecting the formation of altered rocks. Bukit Kasih geotourism area not clearly free from problems. The damaged cement constructions are one of the problems appear in this area, as can be seen that stairs and building in this area are damaged because of the reactions between hydrothermal fluids came from geothermal manifestation with cement materials. Based on those backgrounds, the research about the characteristics of damaged cement construction are need to be done. This research plays important role as preliminary method in findings the solutions for the damaged cement problems, which can support further research in the future. In the end, this research can be counted as one of effort in creating safe an enjoyable geothermal geotourism education in Bukit Kasih area.

Goals

Based on point of backgrounds above, the goals of this research is aimed to:

1. Understand the characteristics of hydrothermal alteration happened in cement materials from infrastructure at Bukit Kasih geotourism area
2. Identify the presence of secondary hydrothermal alteration minerals in the cement constructions at Bukit Kasih geotourism area.

REGIONAL GEOLOGY

Physiography

Based on literature study, study area location is abutting with the remnants of collapsing volcanic edifices of Mt Rindengan. Geomorphological condition of the study area mainly composed by cone-shaped mountainous terrain with average elevation of 970 masl. This area is consist of several geothermal manifestation, appear as past processes of volcanism in this area (Savitri, 2016).

Physiography

The study area can be divided into two (2) main stratigraphic groups, the tertiary pre-caldera group and quaternary post-caldera group. Tertiary-aged units are consist of basement rock (Tb), and Tondano Tuff (Tf). Quaternary-aged unit (oldest-youngest) are consist of lengkoan volcanic rock (Qlk), Rindengan volcanic 1 (Qrd 1), Rindengan volcanic 2 (Qrd 2), Rindengan volcanic 3 (Qrd 3), Sempu volcanic 1 (Qsp 1), Sempu volcanic 2 (Qsp 2), Soputan volcanic (Qst), and Tondano lake sedimentary deposit (Qal). Bukit kasih is composed by Rindengan volcanic 3 unit, which consist of andesitic lavas, bomb, lapilli, and tuff.

Physiography

Bukit kasih area is passed by Soputan sinistral fault with orientation of East/ Northeast to West/ Southwest. Soputan fault are located in the center of Tompaso geothermal field and extends from east flank of Rindengan to Mt. Luuk - Umeh in about 17 kilometers length. Sardiyanto and Nurseto (2013) in Sardiyanto et al. (2015) stated that Soputan fault is main controlling structure in Tompaso geothermal field, together with other minor structure relatively directed northeast to southwest. This faults later controls the flow of hydrothermal fluid and the distribution of geothermal manifestation in the study area.

Geothermal Manifestation of Bukit Kasih

Geothermal manifestations present in Bukit Kasih consist of fumaroles, solfatara, hot and boiling water springs, steaming grounds, and altered rocks. Fumaroles presence indicate that this area act as upflow zone. Hot and boiling springs are showing the temperature of 50^{O} C with pH about 6, meanwhile boiling springs show temperature of 94^{O} to 97^{O} C. Steaming ground are found with the temperature ranged from 52 to 97^{O} C. Altered rock in Bukit Kasih can be divided into three characteristics, the reddish brown colour that present due to ferric ion oxidation, the yellow colour due to its H2S content, and white colour rock which contain clay minerals (PT PGE, 2013 in Siahaan, 2017).

METHODS

Sample collected from the field (cement and rocks) are analyzed using megascopic, petrography, and XRD methods. Samples of cement are taken in 7 location points, and rock are taken in 1 location point (see figure 1). In this study, petrographic observation and XRD analysis will be done by using standard guide, such as Barker (2014) for petrographic observation and Chen (1977) for XRD analysis.

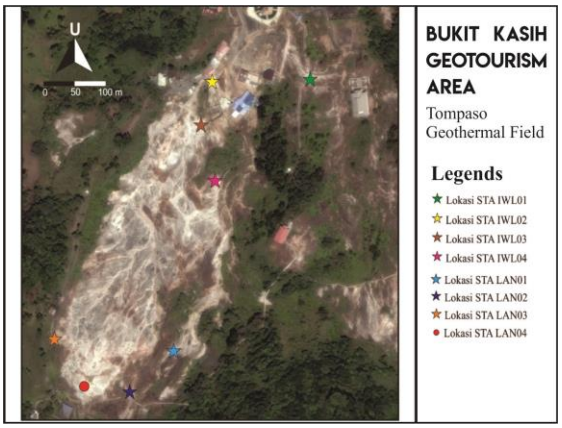


Figure 1: Point of sampling locations in Bukit Kasih geotourism area

RESULTS AND DISCUSSIONS

Megascopic and Petrographic Observation

Three representative samples are taken to be discussed in this study, they are LAN01, LAN02, and LAND 03. The megascopic observation results are discussed as:

- Megascopic observation of LAN01 shows brownish white color, this sample is mainly consist of sulfur and clay minerals (figure 2). This sample is heavily damaged, that made primary minerals are hard to be observed.
- Megascopic observation of LAN02 sample shows whitish red color, this sample consist of carbonate, sulfur, iron oxides, and clay minerals (figure 2). This sample also show characteristic of heavily damaged by the process of hydrothermal alteration, make it hard to observe the primary minerals.
- Megascopic observation of LAN03 sample shows that carbonate minerals, sulfur, and clay minerals are present composed the sample. This sample is also has been damaged, makes it hard to be observed only thorough megascopic observation (see figure 2)



Figure 2: LAN01 (a), LAN02 (b), and LAN03 (c) that showing different charateristics in hand specimen.

The petrographic observation results are discussed as:

- Petrographic observation of LAN01 sample show brownish white color at plane polarized light (PPL) and grayish black at cross polarized (XPL). The mineral present in this cement as mixed materials are plagioclase and pyroxene, which has been partly/ fully replaced by clay minerals (figure 3). The observation of intensity of alteration shows that LAN01 sample has experienced moderate to high intensity of alteration, with the style of alteration is dominantly selective replacement. The presence of clay minerals and quartz are expected as the product of plagioclase and pyroxene replacement, meanwhile, the presence of carbonate minerals, i.e. calcite, also present, expected as the product of dissolution and precipitation processes of cementing materials (see figure 3)
- Petrographic observation of LAN02 sample shows whitish brown/ whitish red color in PPL, and grayish black in XPL. Cement materials shows change in texture because of alteration, along with the presence of plagioclase and pyroxene as mixed materials that has been replaced by hydrothermal alteration process into iron oxide, quartz and clay minerals (see figure 3)
- Petrographic observation of LAN03 sample shows brownish white color of sample in PPL, and brownish black color in XPL. The texture of cement materials are totally altered, along with the presence of secondary hydrothermal alteration minerals, such as clay minerals and quartz as the replacement product of plagioclase and pyroxene. Observation of intensity of alteration also show high intensity of alteration, with pervasive style of alteration (see figure 3).

X-Ray Diffraction Analysis

XRD method is used to identify the presence of secondary hydrothermal alteration minerals, especially from clay minerals group. In this study, 4 samples of altered rock (IWL01 – IWL04) are analyzed thorough bulk and clay (multiple treatment), and other 4 sample of altered rock (LAN00-LAN03) also have been analyzed, but only to identify the presence of clay minerals, due to intensive alteration. Several hydrothermal alteration minerals are identified (see table 1), such as quartz, plagioclase, pyrite, alunite, calcite, gypsum, hematite, sericite, and cristobalite (bulk), and kaolinite, smectite, and chlorite (clay analysis). Several representative XRD samples can be seen in figure 4, 5, and 6.

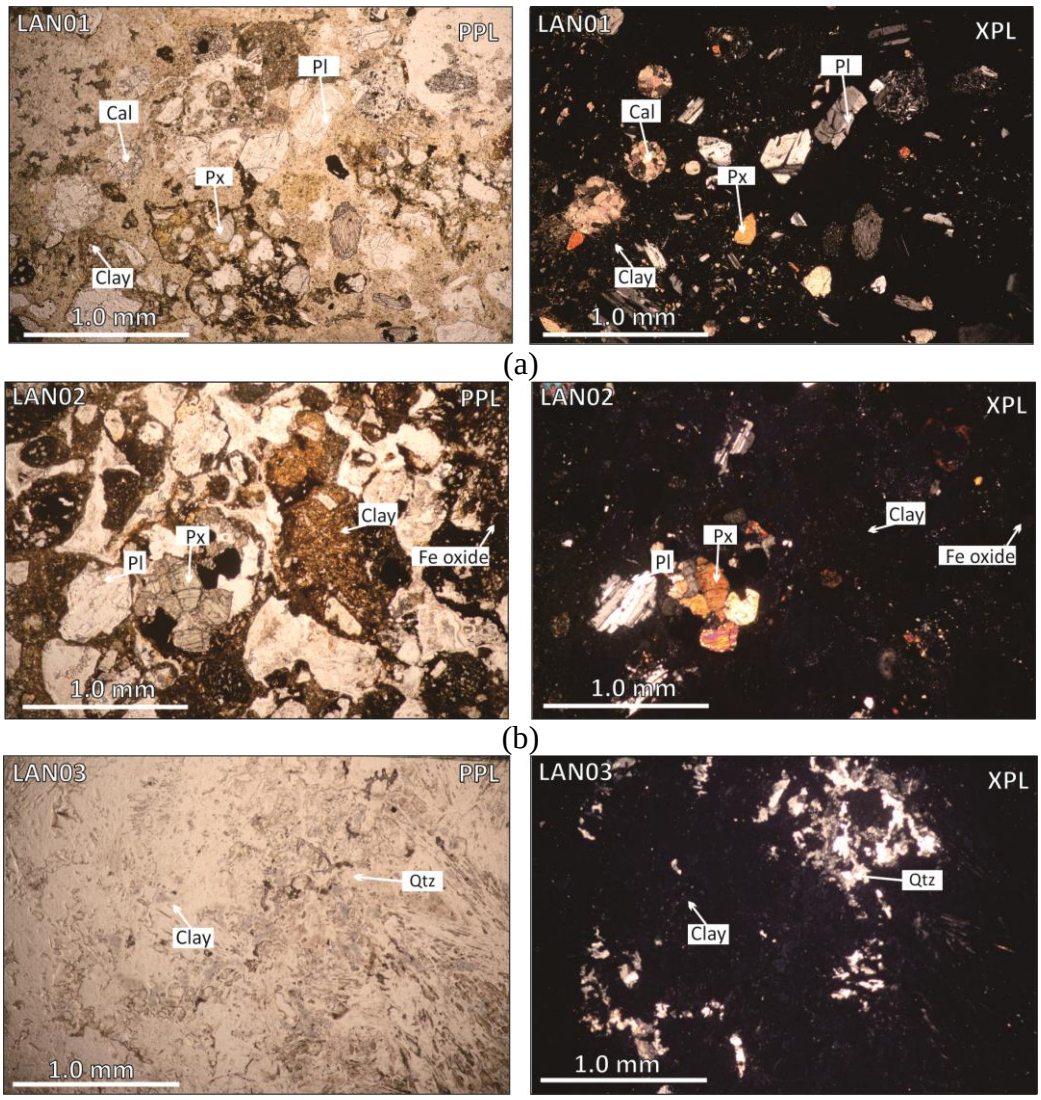


Figure 3: LAN01 (a), LAN02 (b), and LAN03 (c) samples in thin section

Table 1: Summary of XRD analysis conducted for 8 sample of altered rock from Bukit Kasih

No	Sample ID	Bulk*	Clay*
1	IWL 01	Gp, sec. qz, chl, and cal	Sme and chl
2	IWL 02	Gp, ser, chl, cal, crs, and hem	Kao and chl
3	IWL 03	Gp, alu, chl, sec. qz, and hem	Kao and chl
4	IWL 04	Gp, sec. qz, chl, and cal	Sme and chl
5	LAN 01	-	Kao and chl
6	LAN 02	-	Sme and chl
7	LAN 03	-	Chl
8	LAN 00	-	Chl

*Abbreviation of mineral name based on Whitney and Evan (2010)

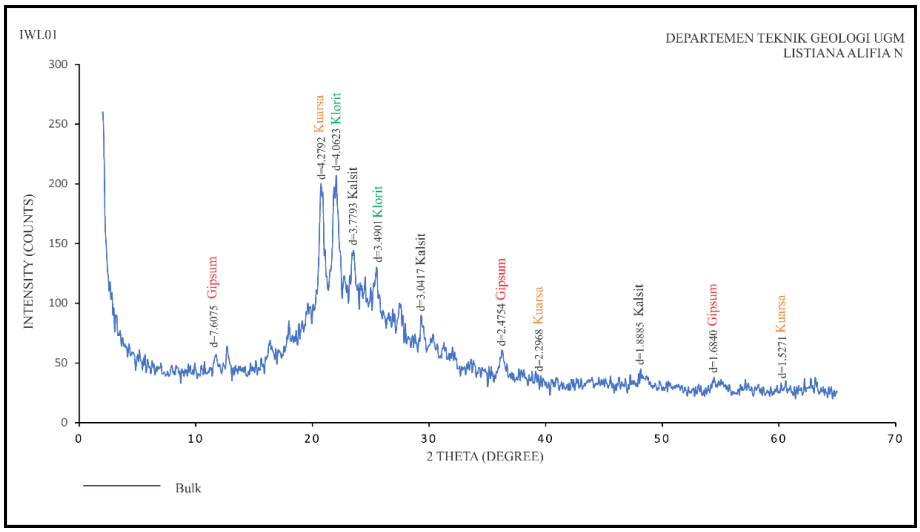


Figure 4: Bulk analysis from IWL01

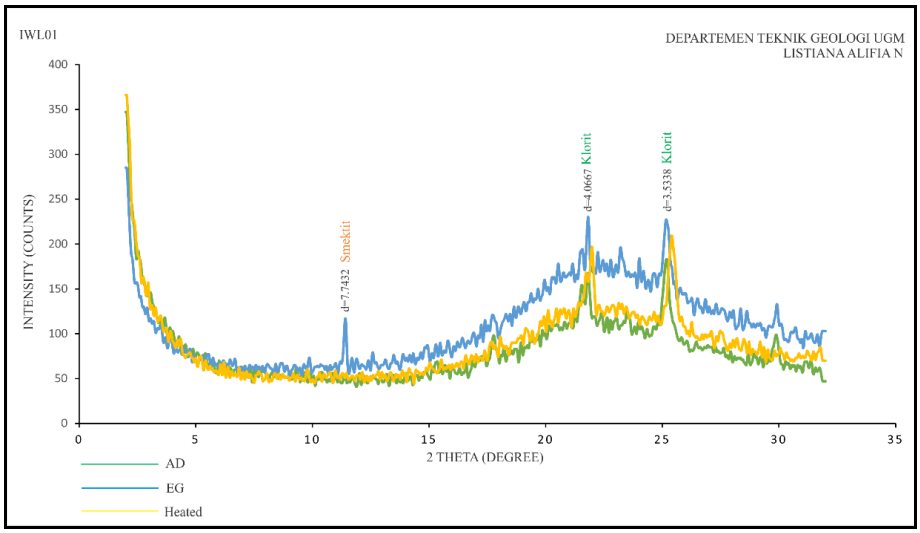


Figure 5: Clay analysis from IWL01

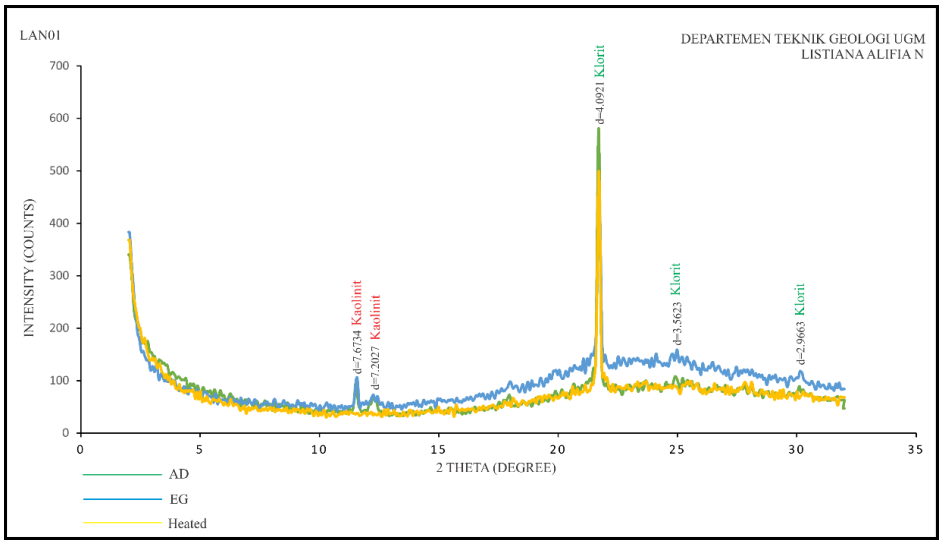


Figure 6:. Clay analysis from LAN01

Based on observation and analysis above, can be seen that the changes in cement construction are happened due to hydrothermal activity of geothermal manifestations. The changes occur in cement material consist of replacement (selective and pervasive), and dissolution process, that increasing the porosity of the cement materials. The minerals found in this research are mainly formed at low temperature (<200^{O} C), or have long temperature range, such as smectite, kaolinite, chlorite, sericite, and secondary quartz. The presence of kaolinite and alunite in several sample also indicate acid pH (Reyes, 2000).

The weakening of cement materials are expected happen because of the presence of the clay minerals that replaced cement materials, Winarti et al (2016) mentioned that clay minerals have swelling properties, especially smectite. On the other hand, the presence of high intensity of hydrothermal alteration also indicate that the changes in rocks are intensively happened. Further/ advanced treatments are need to be conducted in Bukit Kasih, i.e. using new

CONCLUSIONS

1. Hydrothermal alteration characteristics of cement construction in Bukit Kasih geotourism area are consist of high degree/ intensity of alteration, selective style of alteration, and characterized by the presence of alunite group minerals and sulphate minerals, dominantly composed by sulfur.
2. Hydrothermal alteration minerals identified from megascopic, petrography, and XRD method in this study are kaolinite, chlorite, smectite, calcite, gypsum, sericite, alunite, pyrite, cristobalite, and secondary silica minerals, which are mainly formed at low temperature (<200^{O} C), in neutral to acid (low pH) environtment.

REFERENCES

A. G. Reyes, (2000), Petrology and mineral alteration in hydrothermal systems: From diagenesis to volcanic catastrophes, *UNU GTP Lecture notes.*

Barker, A. J., (2014), *A Key for Identification of Rock-forming Minerals in Thin-Section, United Kingdom, CRC Press, 181p*

Chen, P. Y., (1977), *Table of key lines in X-ray powder diffraction patterns of minerals in clays and associated rocks.*

Sardiyanto, Nurseto, S.T., Prasetyo, I. M., Thamrin, M. H., Kamah, M. Y., (2015). Permeability Control on Tompaso Geothermal Field and Its Relationship to Regional Tectonic Setting. *Proceedings World Geothermal Congress 2015. Melbourne.*

Savitri, K.P., (2016), Geology and Geothermal Setting of Tompaso Geothermal Sistem, Indonesia, with Comparisons of Andesite Alteration Patterns with Wairakei, New Zealand, *M.Sc. Thesis.* Victoria University of Wellington. Australia.

Whitney, D. L. and Evans, B. W., (2010), Abbreviations for names of rock-forming minerals, *journal of American mineralogist, **95,** pp 185- 187.*

Winarti, D., Karnawati, D., Hardiyatmo H.C., and, Srijono, (2016), Mineralogical and Geochemical Control of Altered Andesitic Tuff upon Debris Slide Occurences at Pelangan Area, Southern Mountain of Lombok Island, Indonesia, *Journal of Applied Geology*, **1,** 19 – 28

Yeftamikha, (2017), Aplikasi Studi Alterasi Hidrotermal dalam Pengembangan Lapangan Panas Bumi "YMS", Kabupaten Minahasa, Sulawesi Utara. *Skripsi.* Universitas Gadjah Mada. Yogyakarta



ISBN 978-602-52132-1-2

Asosiasi Panasbumi Indonesia (API)
Apartemen Menteng Square, BR-9 Tower B
Jl. Matraman No 30 E, Jakarta Pusat - 10320 Indonesia
Email: api.inaga@yahoo.co.id